Appendix 1
Soil Data Report for 17th Street Canal

Introduction

This is a data report detailing the data collected by the Interagency Performance Evaluation Task Force (IPET) to support the analysis of the I-wall section that breached at the 17th Street Canal as a result of Hurricane Katrina on August 29, 2005. The location of the 17th Street Canal is shown in Figure 1-1. The site of the breach, located on the east bank near the north end of the canal, is also noted on Figure 1-1.

The data will be used in the Floodwall and Levee Performance Analysis task as part of its effort to determine how the flood protection structures performed in the face of the forces to which they were subjected by Hurricane Katrina, and to compare this performance with the design intent, the actual as-built condition, and observed performance. This effort includes understanding why certain structures failed catastrophically and why others did not. The effort will determine, in detail, how the levees and floodwalls performed during Hurricane Katrina. These studies will be documented in a series of reports. The series of reports will start with data reports detailing the data collected on the site conditions at 17th Street Canal, London Avenue Canal, Orleans Canal, and Inner Harbor Navigation Canal, as noted on Figure 1-1.
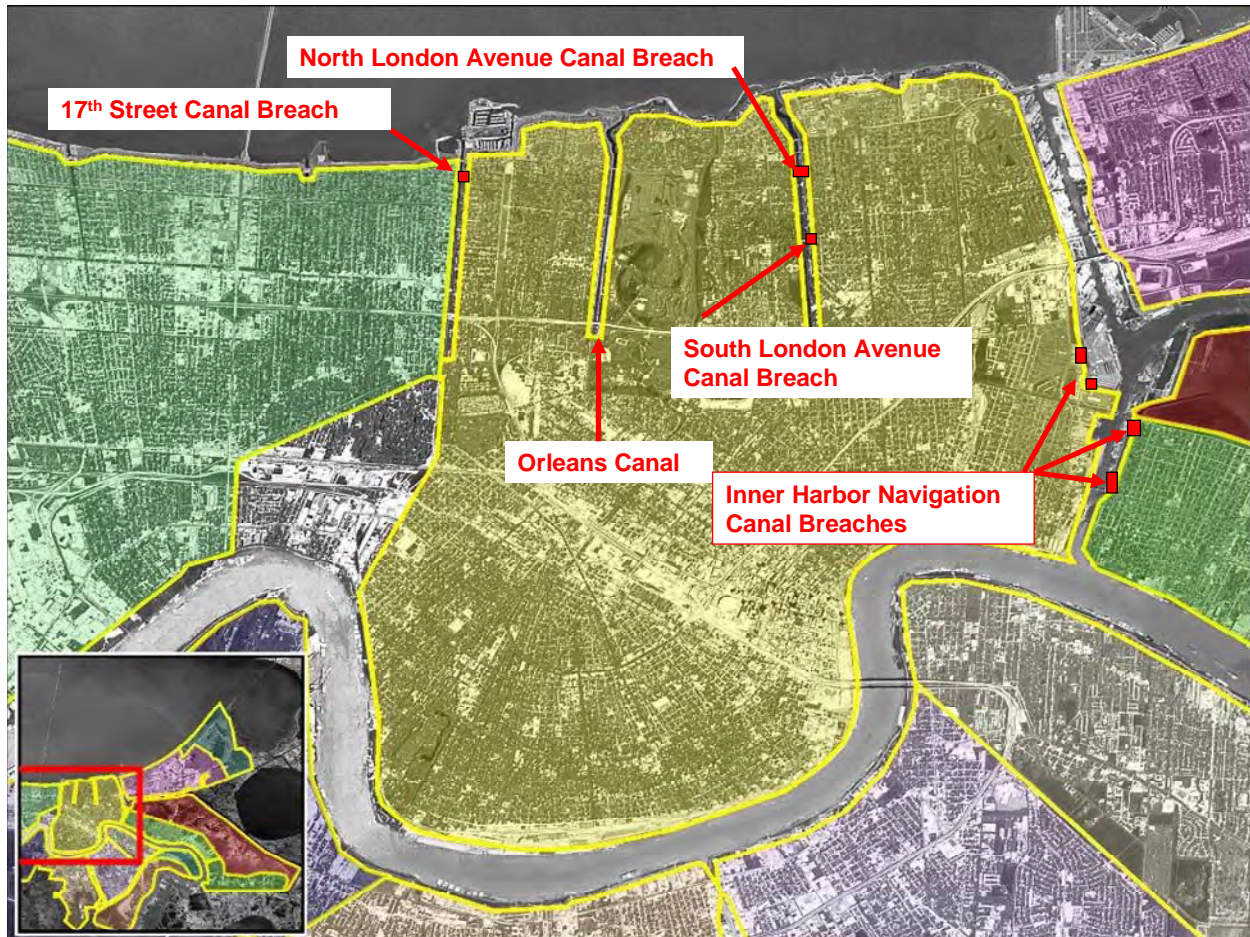
Figure 1-1. Location of Orleans Parish canals

The key data obtained for the breach site and documented as part of this report include:

a. Geology of the area.

b. Description of soil stratigraphy.

c. Representative pre-Katrina cross section through the breach area.

d. Soil undrained shear strength profiles.

These data were obtained from a variety of sources, including the project's General Design Memorandum, design documents, and surveys prepared prior to Katrina. In addition, this report contains information obtained from field and laboratory investigations and surveys conducted after the Hurricane Katrina event. This report was prepared with the intent to provide numerical and physical modelers with the information needed to build their models.

Geology

Introduction

Before examining the individual failure areas at the 17th Street Canal, a review of the geology is presented to familiarize the reader with the broader context of the geology of the delta plain, its stratigraphy, and the soils comprising the foundations at the different failure areas. For comparison purposes, the general geology of the 17th Street, Orleans, and London Avenue Canals levee breaches is reviewed. The geology of the New Orleans area has been determined from detailed mapping studies of the Louisiana Coastal Plain (LCP), from a review of the published literature, from data collection activities at each of the failure sites by an IPET study team, and from an evaluation of preexisting and recently drilled engineering borings from each of the failure areas.

Previous Studies

A review of the past geologic literature from the New Orleans area identifies the US Army Corps of Engineers (USACE) as being actively involved with much of the regional and focused geologic studies that have been performed in the eastern LCP or deltaic plain (Dunbar and others, 1994 and 1995; Dunbar, Torrey, and Wakeley, 1999; Fisk, 1944; Kemp and Michel, 1967; Kolb, Smith, and Silva, 1975; Kolb, 1964; Kolb and Van Lopik, 1958a and 1958b; Kolb and Schultz, 1954; Kolb and Saucier, 1982; May and others, 1984; Michel, 1967; Saucier, 1963, 1984, and 1994; and Schultz and Kolb, 1950). Many of these studies and associated geologic maps are available from a USACE-sponsored website on the geology of the Lower Mississippi Valley that is accessible to the public at lmvmapping.erdc.usace.army.mil.

Geologic History and Principal Physiographic Features of the New Orleans Area

To better understand the soils beneath the 17th Street, Orleans, and London Avenue Canals, and the engineering properties of these soils, a brief summary of the geologic history of the New Orleans area is presented. Detailed descriptions of the geologic history are presented in Saucier (1964 and 1994); Kolb, Smith, and Silva (1975); Kolb and Saucier (1982); and Kolb and Van Lopik (1958).

The geology and stratigraphy of the New Orleans area are young in terms of its age. Generally, sediments comprising the New Orleans area are less than 7,000 years old. Formation of the present day New Orleans began with the rise in global sea level, beginning about 12,000 to 15,000 years before the present. The rise in sea level was caused by melting of continental glaciers in the Northern Hemisphere and the release of ice-bound water to the oceans. At the maximum extent of continental glaciation, eustatic sea level was approximately 300 ft (~100 m) lower that the present level. In addition, the ancestral coastal shoreline was much farther south of its current location, probably near the edge of the continental shelf.

The underlying Pleistocene surface throughout much of coastal Louisiana was subaerial, and exposed to oxidation, weathering, and erosion. These conditions led to the development of a well-developed drainage network across its surface, and created a distinct soil horizon in terms of its

engineering properties. The Pleistocene horizon is easily recognizable in borings because of its distinct physical properties as compared to the overlying Holocene fill (i.e., oxidized color, stiffer consistency, higher shear strength, lower water content, and other physical properties.). The axis of the main valley or entrenchment of the Mississippi River was located west of New Orleans, in the vicinity of present day Morgan City, LA (Figure 1-2). Consequently, development of the early Holocene deltas was concentrated near the axis of Mississippi entrenchment when sea level rise began to stabilize sometime between 5,000 to 7,000 years before the present. New Orleans is located on the eastern edge of this buried entrenchment or alluvial valley.

The Pleistocene surface in the New Orleans area is variable, but generally ranges between 50 and 75 ft below sea level as determined from detailed mapping and examination of boring data (Kolb and Van Lopik 1958; Kolb, Smith, and Silva 1974; Saucier 1994; and Dunbar and others 1994 and 1995). Various sea level curves for the Louisiana coast are presented and discussed in Kolb, Smith, and Silva (1975) and Tornquist and Gonzalez (2002). These curves generally indicate that sea level transgression in the New Orleans area generally occurred between 6,000 to 9,000 years before the present, based on the mapped depths to the top of the Pleistocene surface.

As the rate of the sea level rise declined and stabilized, it led to the development of five, short-lived delta complexes across the Louisiana coast by deposition of Mississippi River sediments (Figure 1-2). Individual delta complexes are composed of numerous, branching distributary channels. These channels transport and deposit fluvial sediments along the margin of the delta and build land seaward into shallow coastal water. Distributary channels from the St. Bernard delta are responsible for filling the shallow Gulf waters in the greater New Orleans area (Frazier 1967).

Bayou Sauvage is a major distributary involved in the filling of the shallow Gulf waters in the New Orleans area (Figure 1-3). This channel extends eastward from the Mississippi River and is composed of Bayous Metairie, Gentilly (or Gentilly Ridge), and Sauvage. Natural levees of this distributary channel form a pronounced physiographic feature in the northern New Orleans area (Figure 1-3). Similarly, Mississippi River's natural levees are some of the highest land elevations found in New Orleans, and these were the first areas to be settled by the early inhabitants in the 1700s. Distributary channels in New Orleans are pronounced physiographic features, and are associated with the St. Bernard delta complex as determined from radiocarbon dating of organic sediments (Frazier, 1967; Kolb and Van Lopik 1958; McFarlan 1961; Britsch and Dunbar 1999; and Smith, Dunbar, and Britsch 1986).

Equally important to the development and filling history of the New Orleans area is the presence of a buried, barrier beach ridge which formed approximately 4,500 to 5,000 years before the present. This beach extends northeast in the subsurface along the southern shore of Lake Pontchartrain (Figure 1-4). Sea level was 10 to 15 ft lower than the current level when the beach ridge formed. A stable sea level permitted sandy sediments from the Pearl River to the east to be concentrated by longshore drift, and formed a sandy spit or barrier beach complex in the New Orleans area as shown by Figure 1-3 (Saucier 1994).
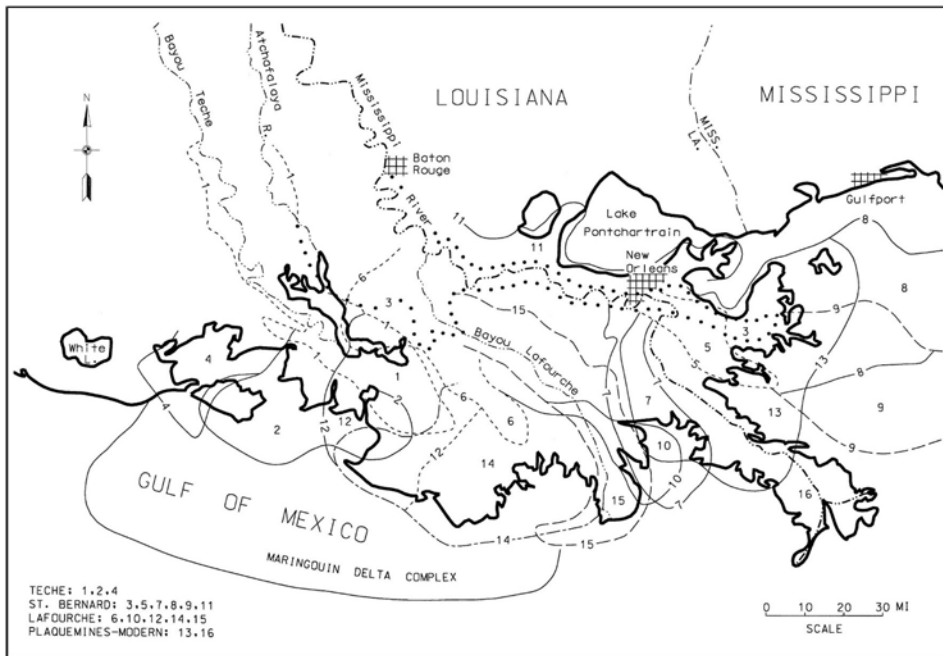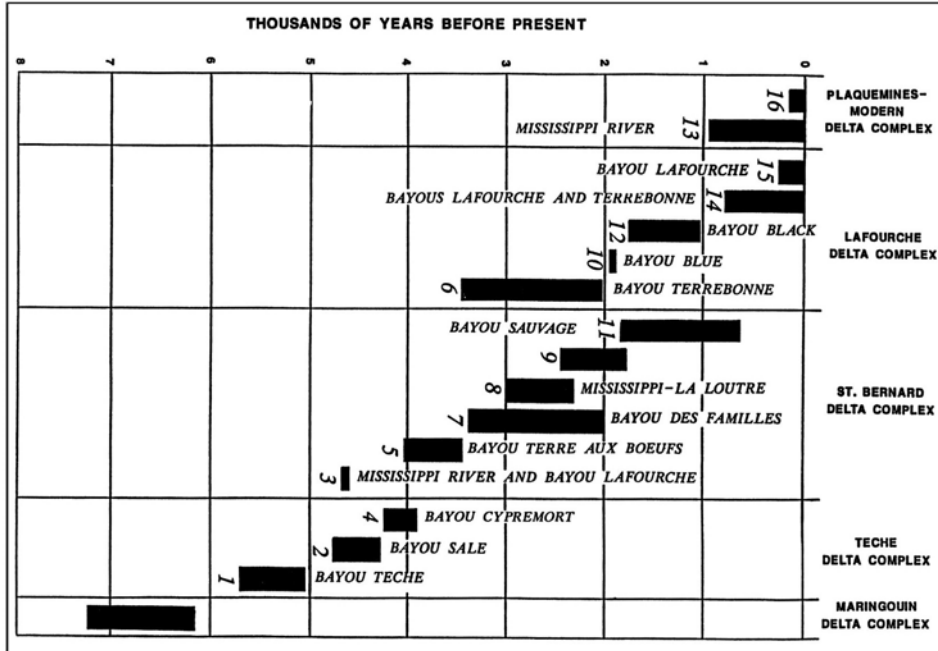
Figure 1-2.   Location and approximate chronology of the Mississippi River
                Deltas, major distributary channels are numbered, note Bayou
                Sauvage (No. 11) which extends across the New Orleans area and
                forms the Bayou Metairie/Gentilly Ridge (after Frazier, 1967).
                Morgan City, LA, located along axis of maximum Mississippi River
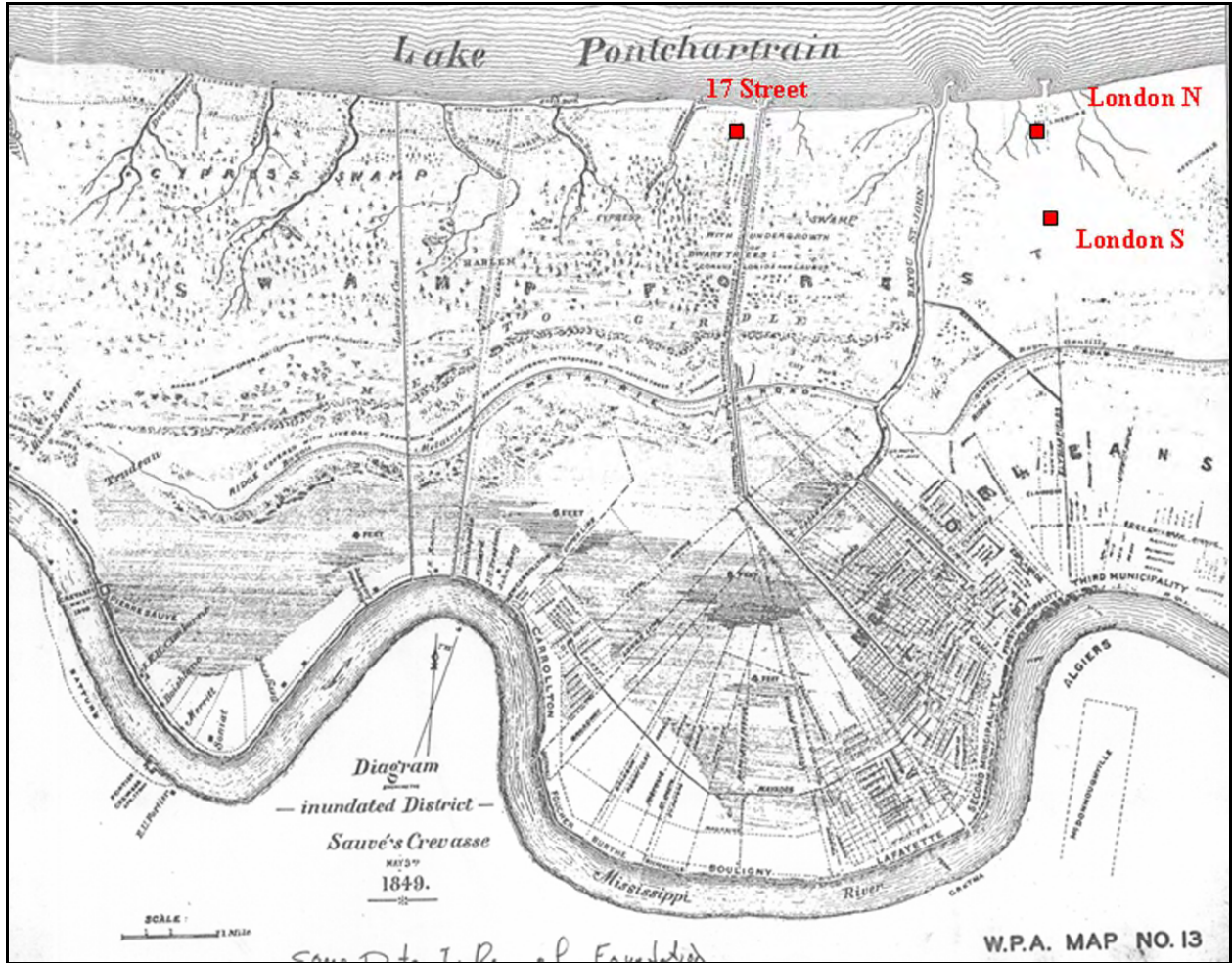   entrenchment

Figure 1-3.   New Orleans area map from 1849 showing city limits and topography. Note the location of Bayous Metairie and Gentilly (i.e., Bayou Sauvage) and the identified cypress swamp north of the city at this time (Work Projects Administration 1943).

The presence of the barrier beach affected sedimentation patterns and the subsequent locations for advancing distributary channels in the New Orleans area. The beach complex likely prevented the Mississippi River and later St. Bernard distributaries from completely filling Lake Pontchartrain with sediment. Consequently, foundation soils beneath the 17th Street, Orleans, and London Avenue Canal breaches are affected by their proximity to the buried beach complex. As shown by Figure 1-4, the breach at the 17th Street Canal is located on the protected or land side of the beach ridge, while both of the London canal breaches are located over the thickest part or axis of this ridge complex. The beach ridge cuts across the Orleans Canal with the north portion on the landside and south portion over the axis of this ridge complex.
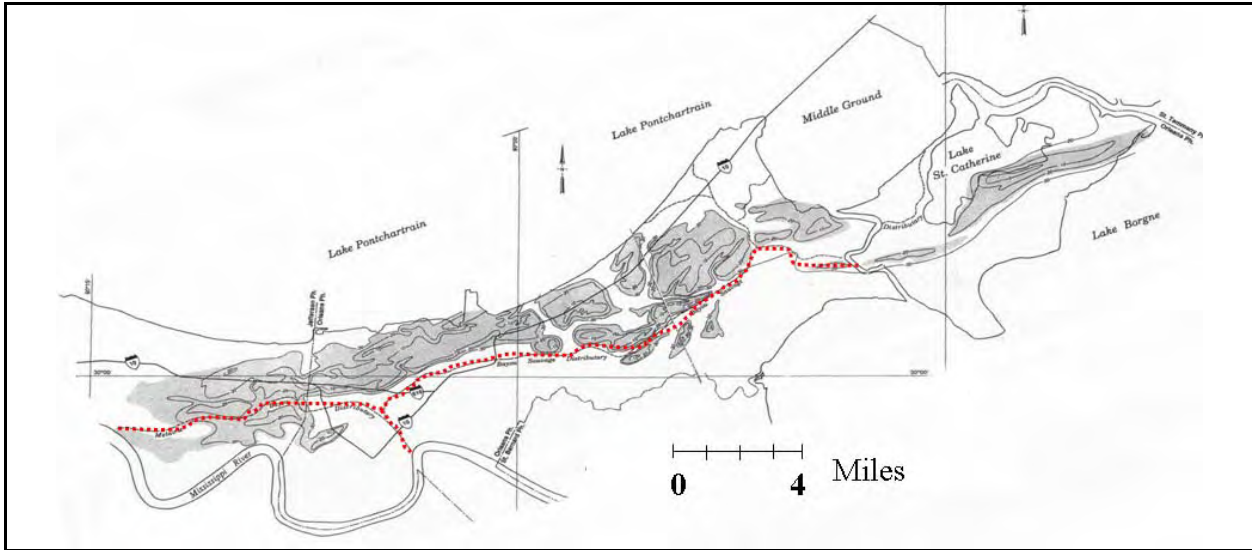
Figure 1-4a. Pine Island buried beach complex in the New Orleans Area (from Saucier 1994). Course of Bayou Sauvage (i.e., Bayous Metairie and Gentilly) identified in red. Note the presence of the barrier beach prevented this distributary course from extending northward into present day Lake Pontchartrain and filling the lake. Canal breaches are identified in blue with 17th Street breach behind the thickest part of the beach ridge, while both the London North and South breaches are on the axis of the barrier. See Figure 1-3b for close-up of canal areas.
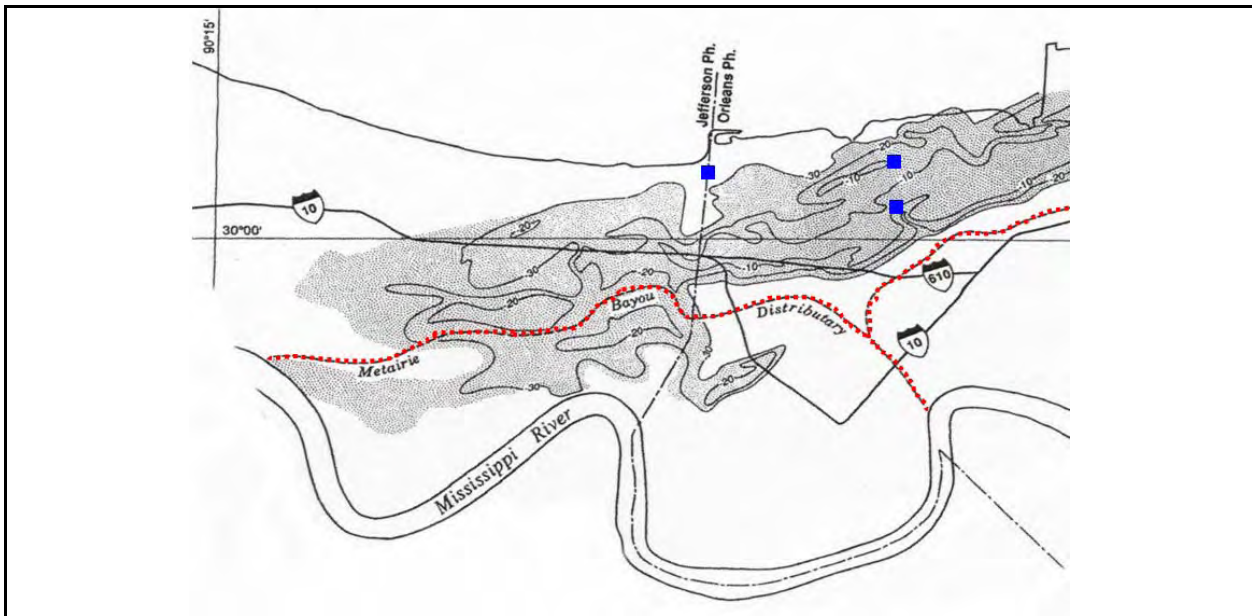

Figure 1-4b. Close-up view of the buried beach ridge, and the locations of the canal breaches to the buried beach (after Saucier 1994). The 17th Street breach is located behind the axis of the beach ridge while the London Canal breaches are located on the axis of the ridge. Bayou Metairie is identified in red and forms the Bayou Sauvage distributary course (No. 11) in Figure 1-2.

Surface and Subsurface Geology of the New Orleans Area

A geologic map of the New Orleans area is presented in Figure 1-5 and identifies the major environments of deposition at the surface in the vicinity of the 17th Street, Orleans, and London Avenue Canals. Located on the surface of the New Orleans area are natural levee and point bar deposits adjacent to the Mississippi River, abandoned distributary courses (Bayou Sauvage-Metairie north of the Mississippi River and Bayou des Families south of the Mississippi River, respectively), and extensive marsh-swamp deposits at the surface (see also Figure 1-3). Land reclamation occurred in the 1920's along the shore of Lake Pontchartrain by dredging, and this area is identified as spoil deposits.
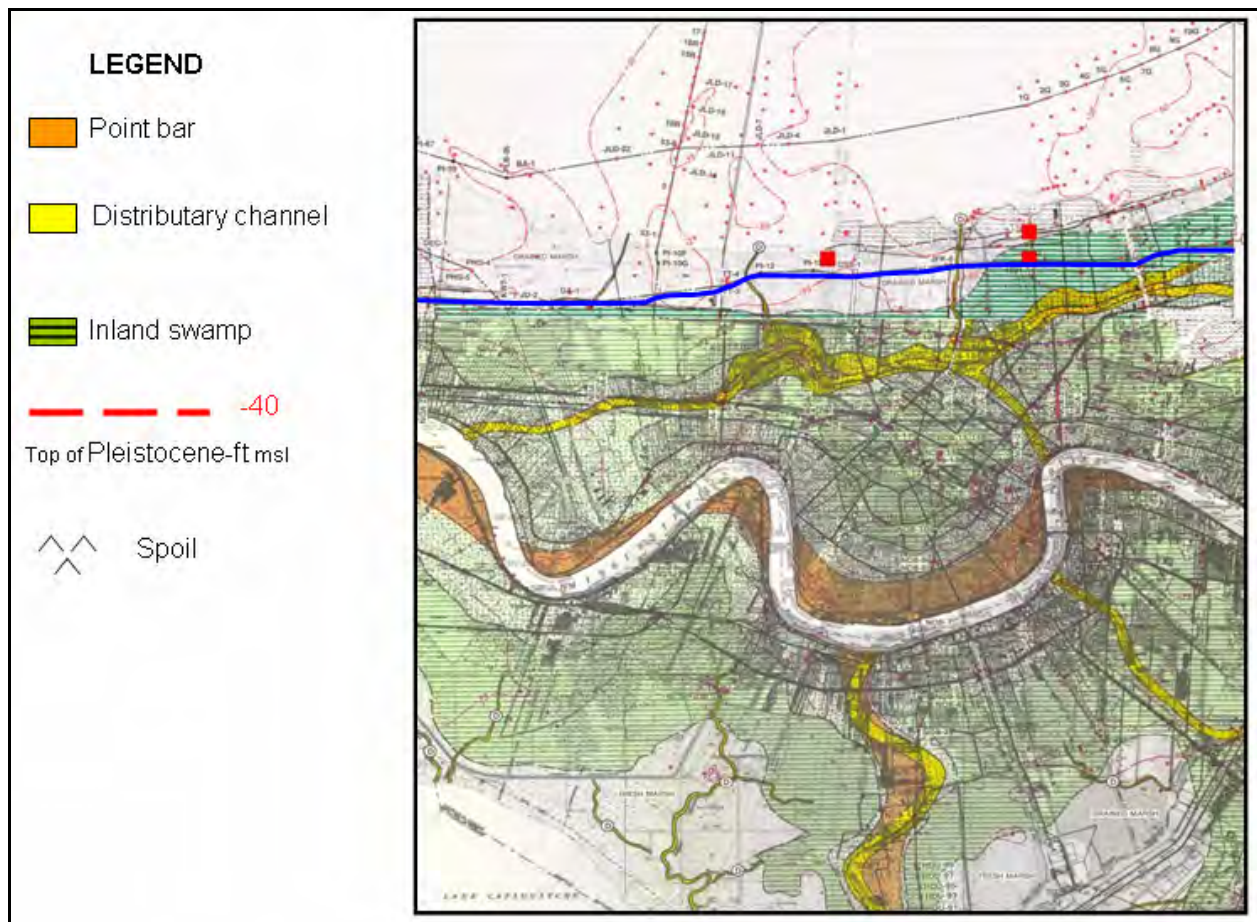

Figure 1-5.   Geology map of the New Orleans and Spanish Fort Quadrangles showing the distribution of environments at surface. Elevation of the Pleistocene surface shown in red along with borings used to map this surface. Cross-section C-C' in blue extends through 17th Street and London Canal Areas (areas identified in red). See website lmvmapping.erdc.usace.army.mil for nearby maps and other cross-sections identified. Portion of cross-section C-C' above is presented as Figure 1-6 (from Dunbar and others 1994 and 1995).

A portion of cross-section C-C from the Spanish Fort Quadrangle is presented as Figure 1-6 to identify the general subsurface stratigraphy beneath the 17th Street and London canal breaches. Boring data from this section identify distinct depositional environments in the

subsurface that are stacked vertically and form a stratigraphic record of the filling history during the Holocene period. Major stratigraphic units in the subsurface, beginning with the oldest, include the Pleistocene (older fluvial and deltaic deposits), bay sound/estuarine, relic beach (Pine Island Beach ridge) lacustrine/interdistributary, and marsh/swamp deposits. A summary description of the different depositional environments in the New Orleans area is presented in Appendix 2 (from Dunbar, Torrey, and Wakeley, 1999). Additionally, detailed descriptions of the different depositional environments are contained in Saucier (1994), Kolb (1962), and Kolb and Van Lopik (1958).
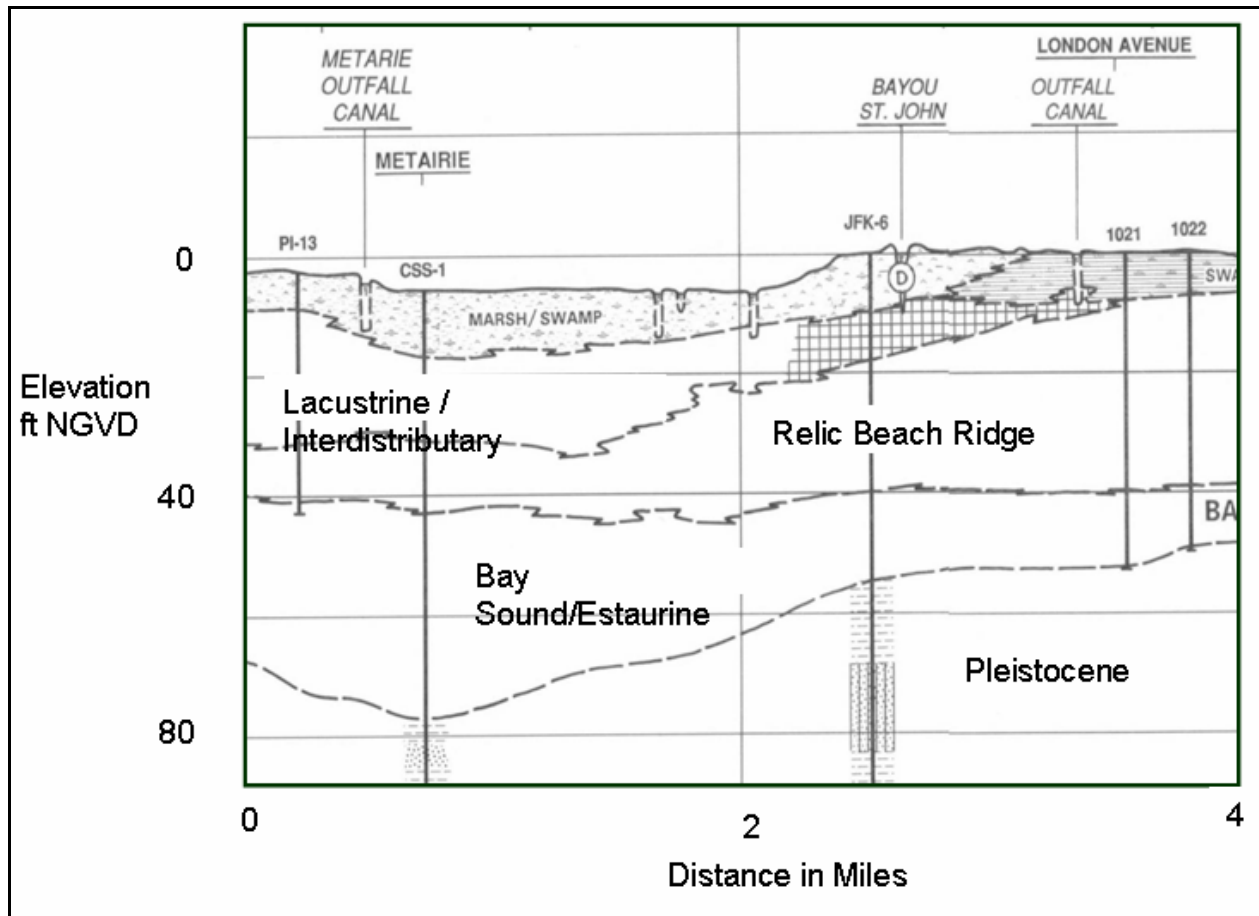

Figure 1-6.   Portion of cross section C-C" from the Spanish Fort Quadrangle which extends through the 17th and London Canal breaches and identifies the stratigraphic environments in the subsurface (from Dunbar and others 1995)

Besides mapping the horizontal and vertical limits of the various environments of deposition, relationships between these environments and key engineering properties of the respective soils have been developed. These relationships have been tabulated and are published in Kolb (1962), Montgomery (1974), and Saucier (1994). A summary of these engineering relationships is presented in Appendix 2. Similarly, relationships have been developed from the engineering properties and laboratory soil test data from 17th Street, Orleans, and London Avenue Canals. These data are presented in later sections of this summary as related to discussions of their engineering significance.

Geologic information from the New Orleans area helped the IPET focus its investigation and collection of data for the 17th Street, Orleans, and London Avenue Canal breaches. An understanding of the geology was an important first step to systematically collecting and evaluating stratigraphic and engineering data from these breach areas.

Development of Cross Sections

Pre-Katrina Sections

A significant amount of information was obtained from General Design Memorandum No. 20 – 17th Street Outfall Canal – Volume 1 (GDM No. 20) in the development of pre-Katrina cross sections. This document was completed in March 1990 in preparation for upgrading the New Orleans levee system to provide increased flood protection against a stronger revised design hurricane.

Figures 1-7 and 1-8 show longitudinal profiles of the east and west bank levees of the northern half of the 17th Street Outfall canal, respectively. These figures, obtained from GDM No. 20, show boring locations and the soil types obtained during the explorations for the project upgrade. It is noted that odd numbered borings are located on the west bank, and even numbered borings are located on the east bank. Noted on the figures is the location of the breach site which is situated on the east bank of the canal between Stations 560+50 and 564+50.

A more detailed representation of the soil stratigraphy profile along the centerline in the breach area is shown in Figure 1-9. This profile was constructed using additional soil data acquired during the post-Katrina soil exploration conducted during September through October 2006. The additional borings included B1, B2, B3, B4, B5, NO-1-05U, and NO-2-05U. A plan view showing the locations of both old and new borings is shown in Figure 1-10. The new borings were needed because only the two old borings, B62 and B64 (reported in GDM No. 20), were in the immediate vicinity of the breach. The new borings extended the depth of the investigation in this area from approximately Elevation -50 ft NGVD to Elevation -115 ft NGVD. Additionally, data from cone penetration testing, from the new exploration program, were used to supplement soil data from the old and new borings and refine the stratigraphy in the breach area. Since the levee was destroyed in the breach area during the storm, the new borings, B1 through B4, were drilled from a barge in the canal and were offset from the centerline. Data acquired from these borings were projected back to the centerline in an effort to improve the interpretation of the stratigraphy.
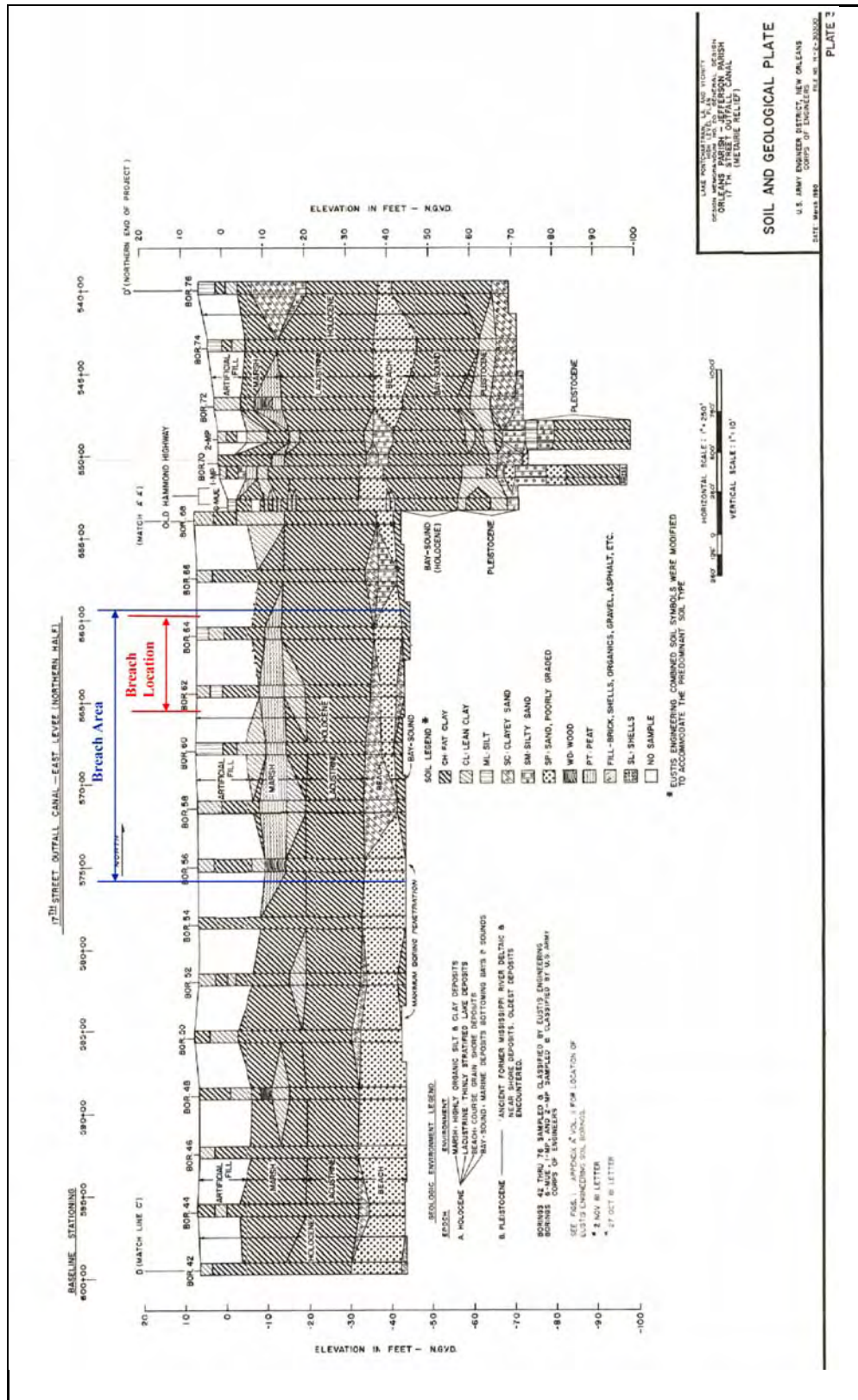
Figure 1-7. Geological Profile showing Breach Area (East Levee)

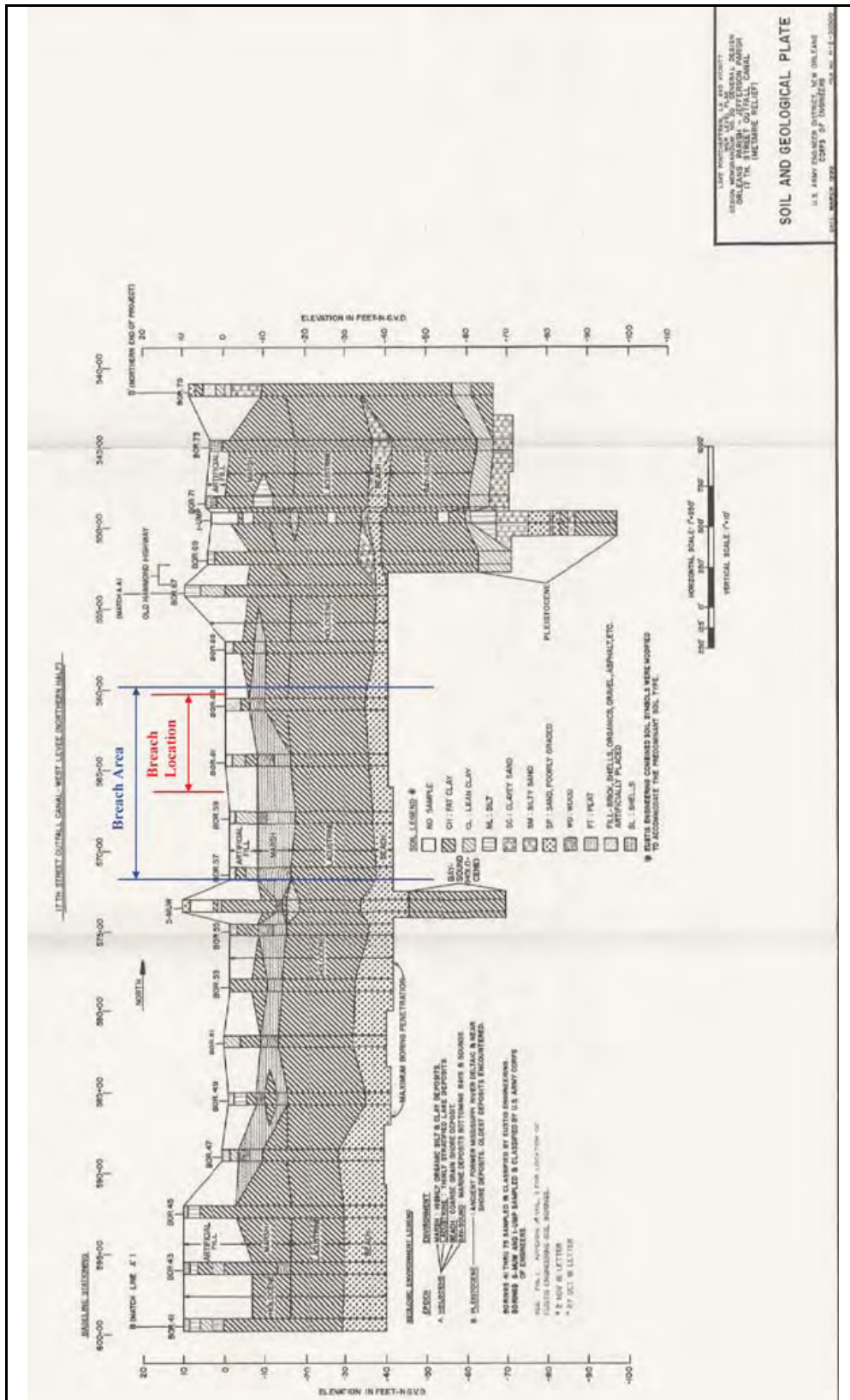Figure 1-8.   Geological Profile showing Breach Area (West Levee)

This is a preliminary report subject to revision; it does not contain final conclusions of the United States Army Corps of Engineers.
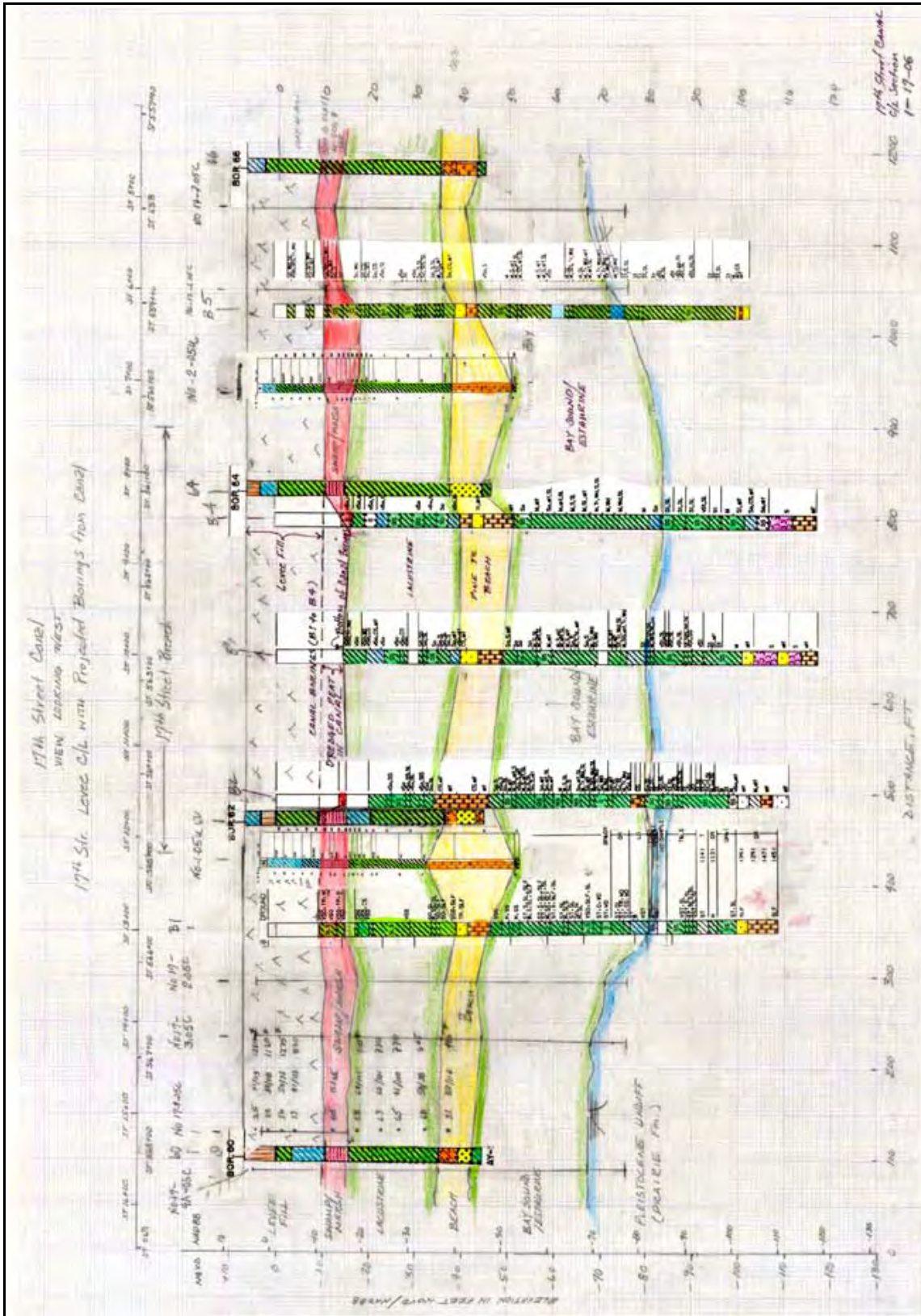
Figure 1-9. Centerline (CL) Cross-section of Breach

Figure 1-10.   Boring and CPT Location Map

The information presented on Figure 1-9 yielded the following interpretation of the subsurface stratigraphy in the breach area. The subsurface in the breach area was simplified into six basic groups of soil types over the depth of the investigation:

Table 1-1
Major Soil Groups at the 17th Street Outfall Canal Breach Site

Layer	Approximate Elevation of Top of Layer, ft (NGVD)	Approximate Elevation of Bottom of Layer (NGVD)	Soil Type	Consistency
Embankment	6.5	-10	Clayey (CL's and CH)	Stiff
Marsh	-10	-15	Organic/Peat	Very Soft
Lacustrine	-15	-35	Clays (CH)	Very Soft
Beach Sand	-35	-45	Sand	
Bay Sound/Estuarine	-45	-75	Clayey (CH)	Stiff to V. Stiff
Pleistocene (Undifferentiated) Prairie Formation	-75		Clays – Generally CH with some sand	Stiff

An additional word about the Marsh deposit may be useful. The marsh is represented as an organic soil and a peat-type material. Examination of the drilling logs suggests that since wood was encountered at the top part of the layer, this layer may be more fibrous near the top and more amorphous at the bottom of the layer. Further investigation of the peat layer may be necessary to better quantify the differences between the top and bottom of the layer.

Transverse Cross Sections through the Breach Site

Three representative transverse cross sections through the levee breach site were prepared from the data at hand. These three sections were developed from Station 8+30, Station 10+00, and Station 11+50. Station 8+30 is the most northerly station of the three. These cross sections were prepared with the intent that they represent the conditions that existed *immediately before* the arrival of Katrina. Data from a pre-Katrina airborne LIDAR (Light Detection and Ranging) survey on the New Orleans Levee System that was conducted during the year 2000 were used to improve the surface topography in the breach area from that presented in the GDM No. 20 and the design documents. The LIDAR data is the best data available for establishing the cross sections before Katrina, because accurate ground survey data were not available during the preparation of this report. The surveys generate points of X, Y, and Z data that are accurate to the nearest foot. A typical LIDAR section is shown in Figure 1-10. The LIDAR surveys were particularly useful in establishing the levee dimensions, slope, and toe elevations on the protected side of the floodwall. Unfortunately, the LIDAR system cannot penetrate through water, so it was not possible to use this technology to acquire the ground topography in the canal. A hydrographic survey was obtained *immediately after* Katrina, on August 31, 2006, to obtain the surface elevations of the canal between the floodwalls on the east and west banks. The data obtained from the hydrographic surveys are reflected in the cross-sections described in the next paragraph.

The three representative cross sections for Station 8+30, Station 10+00, and Station 11+50 are shown in Figures 1-11, 1-12, and 1-13, respectively. Three sections were prepared because the levee dimensions are variable in the breach area on the east bank. Each cross section shows the conditions across the entire canal from the west bank to the east bank where the breach site is located. A degree of interpretation was necessary, particularly pertaining to the east bank

protected side, to complete the cross sections because of the lack of soil boring data in this area. Thus, the marsh/peat layer was interpreted to be thinner under the centerline of the levee than at the toe due to consolidation from the surcharge caused by the weight of the levee. Also, an interpretation was made to include a 2- to 3-ft layer of topsoil over the top of the peat in this area. This effect may be cultural in nature because the protected side of the east bank was located in a residential area with houses having well-kept lawns.

It is also noted that the levee cross section at Station 11+50, the southernmost section of the three and shown in Figure 1-13, is the location where the post-Katrina surveys showed that the most scour occurred while water was flowing through the breach.

Uncertainties

Many uncertainties pertaining to the subsurface in the breach area will be difficult, if not impossible, to resolve because the levee in this area was destroyed and drastically changed due to emergency relief efforts. There was a lack of subsurface information on the protected side of the levee during the 1990 levee raising project described in GDM No. 20. There are efforts planned by the IPET to obtain more information in the vicinity immediately north and south of the breach area to better define soil strengths and thickness of the top soil and peat layers.
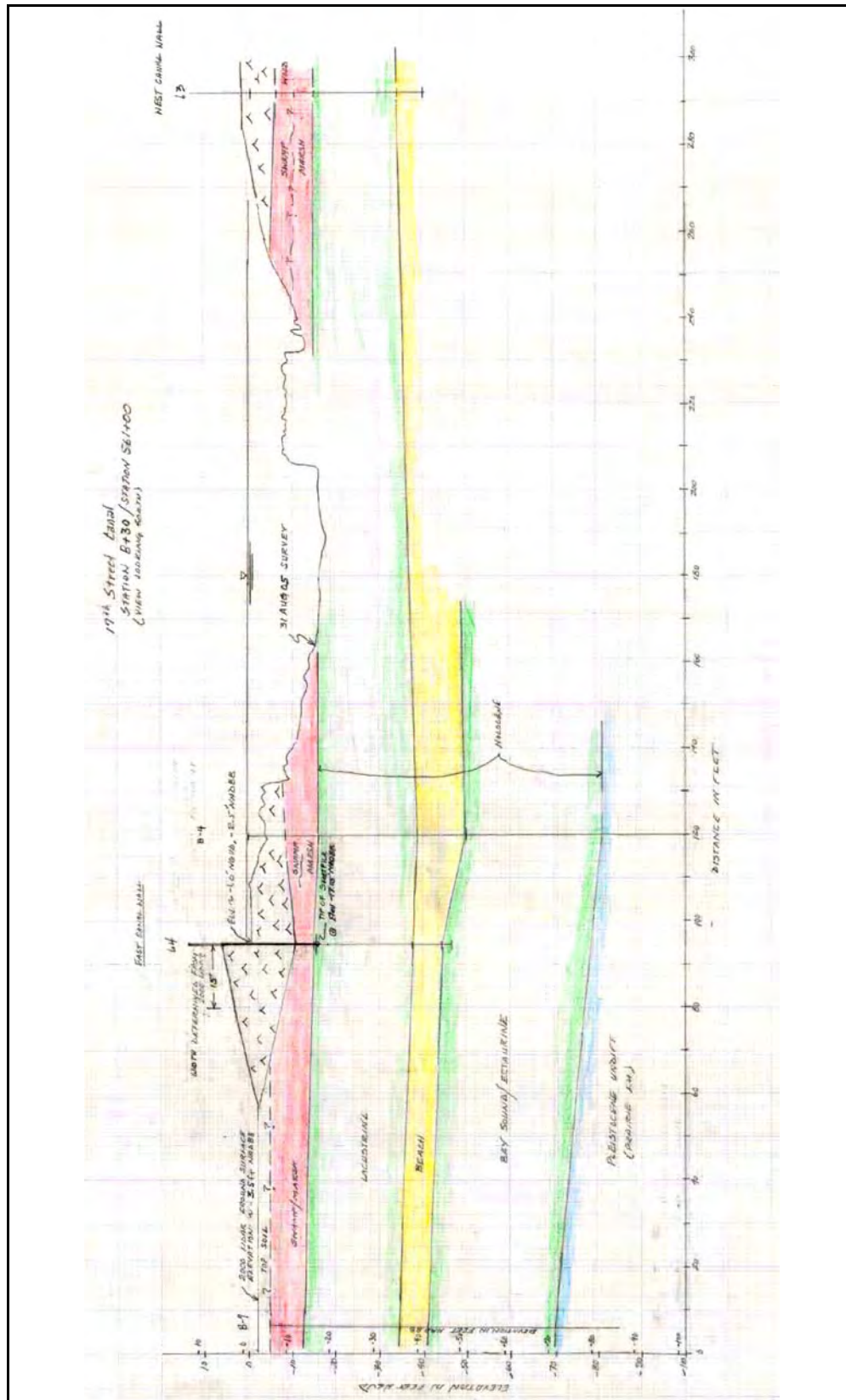
Figure 1-11. Prefailure Cross-Section at Sta 8+30 (New Stationing)/ Sta. 561+00 (GDM Stationing)
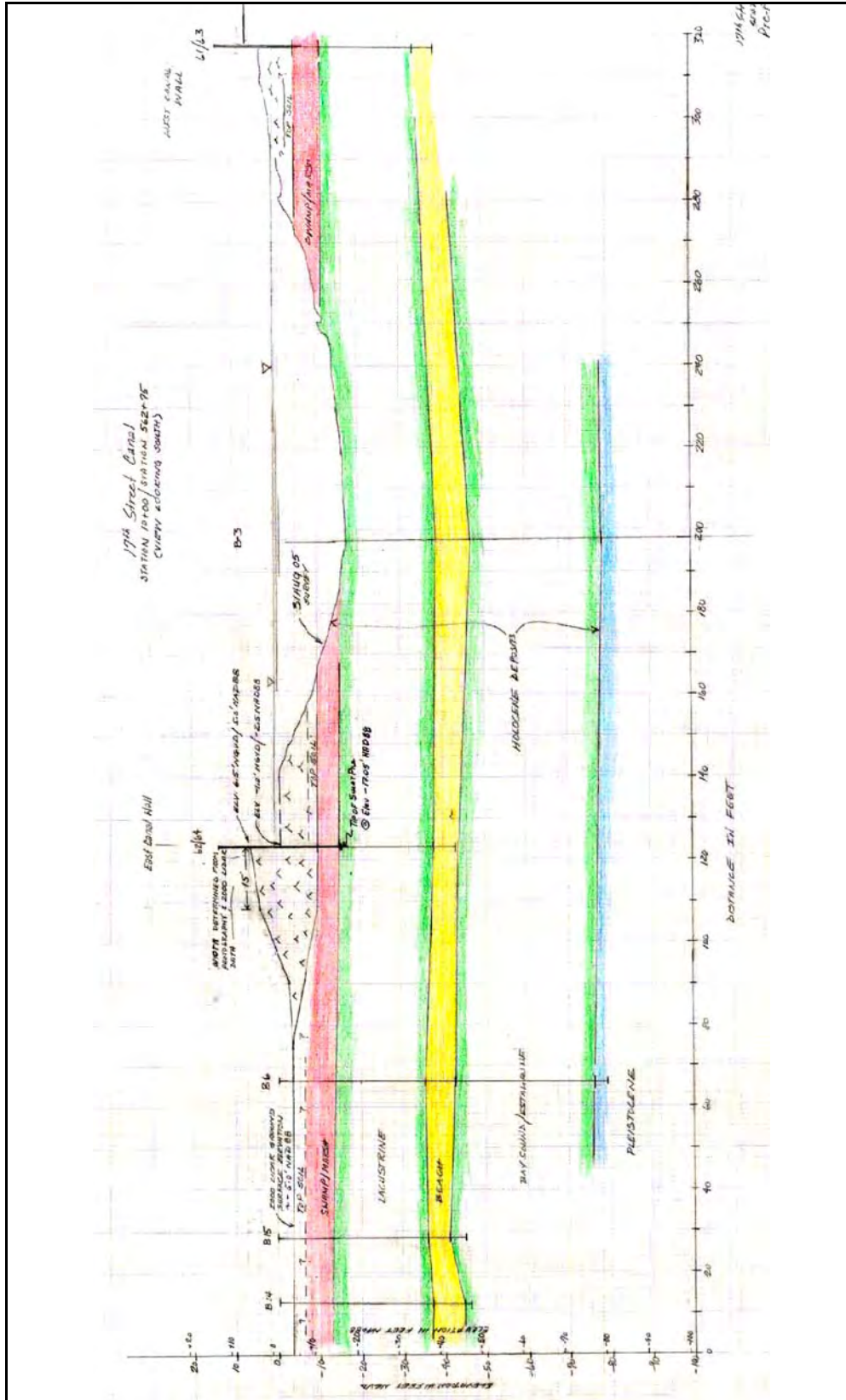
Volume V The Performance – Levees and Floodwalls – Technical Appendix

V-1-17

This is a preliminary report subject to revision; it does not contain final conclusions of the United States Army Corps of Engineers.

Figure 1-12. Prefailure Cross-Section at Sta 10+00 (New Stationing)/ Sta. 562+75 (GDM Stationing)

Volume V The Performance – Levees and Floodwalls – Technical Appendix
This is a preliminary report subject to revision; it does not contain final conclusions of the United States Army Corps of Engineers.
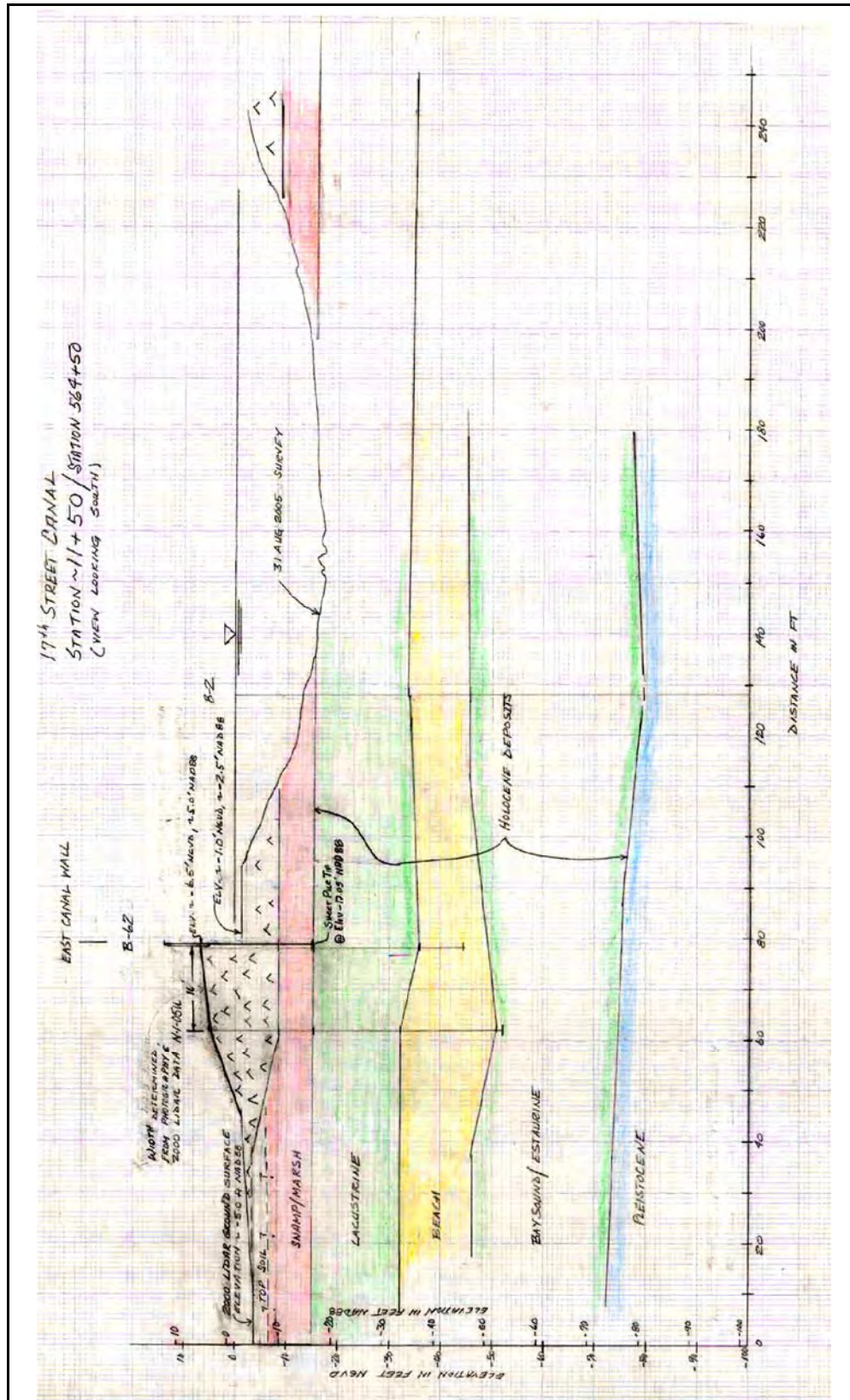
Figure 1-13. Prefailure Cross-Section at Sta 11+50 (New Stationing)/ Sta. 564+50 (GDM Stationing) (Note: Most scour occurred near this station)

Soil Properties

Introduction

The following is a summary of the current soil data available in the breach area of the 17th Street Canal. The soil's data for the breach include all borings and cone penetrometer tests (CPT) in the breach area. This area was chosen because the geology and soil types are very similar to the soil types and geology found at the breach area. The breach area and breach location are shown in Figure 1-7. In addition, some soil data from the west levee will be used for the breach area because of similar geology and soil types. This area is shown in Figure 1-8.

The stratigraphy in the breach area is divided into Levee Embankment, Marsh Stratum, Lacustrine Stratum, and Beach Sand Stratum. The data for each stratum are presented below. These data consist of GDM borings, new borings (taken in 2005), and CPTs. Testing is not complete on all of the samples from new borings. In addition, field vane shear tests and CPTs are scheduled to occur in the next couple of weeks, which will provide more data in the breach area.

Levee Embankment

Data on the levee embankment consist of five borings shown in the 1990 General Design Memorandum (GDM) and four cone penetrometer tests (CPT). Of the five GDM borings, four borings collected 3-in. (diameter) undisturbed samples, and one boring collected 5-in. (diameter) undisturbed samples. From the 3-in. samples, four unconfined compression (UC) tests were performed, and five one-point unconsolidated-undrained triaxial compression tests (UU-1), confined at existing overburden pressure, were performed. From the 5-in. samples, four one-point unconsolidated-undrained triaxial compression tests (UU-1), confined at existing overburden pressure, were performed. From these laboratory tests, moisture content and wet unit weights were determined. The moisture contents (%w) in the breach area are shown in Figure 1-14. In addition, these moisture content data were also plotted (Figure 1-15) with the moisture content data collected for the entire east levee on the canal. Also, the moisture content data for the entire west levee on the canal are shown in Figure 1-16.

The wet unit weight data in the breach area are shown in Figure 1-17. Wet unit weight data from the breach area plotted with wet unit weight data for the entire east levee are shown in Figure 1-18. Wet unit weight for the entire west levee on the canal is shown in Figure 1-19.

The undrained shear strength determined from the laboratory tests conducted on samples in the breach area is shown in Figure 1-20. Interpretation of the undrained shear strength from the CPTs using Mayne's method is plotted with laboratory test results in Figure 1-21. Interpretation of the undrained shear strength from the CPTs using the bearing capacity equation ($Nk=15$) is plotted with laboratory test results in Figure 1-22. These interpretations were provided by Dr. Thomas Brandon (Virginia Tech). Undrained shear strength data in the breach area plotted with undrained shear strength data for the entire east levee are shown in Figure 1-23. Undrained shear strength data for the entire west levee are shown in Figure 1-24.

Marsh Stratum

The data for the marsh stratum will be divided into two groups: Data on the marsh stratum under the levee embankment, and data on the marsh stratum at the toe of the levee.

Under the Levee Embankment

Data on the marsh stratum under the levee embankment consist of five borings shown in the 1990 General Design Memorandum (GDM) and four cone penetrometer tests (CPT) taken on the east levee. Of the five GDM borings, four borings collected 3-in. (diameter) undisturbed samples and one boring collected 5-in (diameter) undisturbed samples. From the 3-in. samples, five unconfined compression (UC) tests were performed. From the 5-in. samples, no shear strength data were available. From these laboratory tests, moisture content and wet unit weights were determined. The moisture contents (%w) in the breach area are shown in Figure 1-25. In addition, this moisture content data were also plotted (Figure 1-26) with the moisture content data collected for the entire east levee on the canal. Also, the moisture content data for the entire west levee on the canal are shown in Figure 1-27.

The wet unit weight data in the breach area are shown in Figure 1-28. Wet unit weight data from the breach area plotted with wet unit weight data for the entire east levee are shown in Figure 1-29. Wet unit weight for the entire west levee on the canal are shown in Figure 1-30.

The undrained shear strength determined from the laboratory tests conducted on samples in the breach area is shown in Figure 1-31. Interpretation of the undrained shear strength from the CPTs using Mayne's method is plotted with laboratory test results in Figure 1-32. Interpretation of the undrained shear strength from the CPTs using the bearing capacity equation (Nk=15) is plotted with laboratory test results in Figure 1-33. These interpretations were provided by Dr. Thomas Brandon (Virginia Tech). Undrained shear strength data in the breach area plotted with undrained shear strength data for the entire east levee are shown in Figure 1-34. Undrained shear strength data for the entire west levee are shown in Figure 1-35.

At the Toe of Embankment

Data on the marsh stratum under the toe of the levee embankment consist of five borings taken in 2005 on the protected side, four borings taken in 2005 on the canal side, three borings on the west levee toe shown in the 1990 GDM. Of the borings on the protected side of the east levee, four borings collected 5-in. (diameter) undisturbed samples, and one boring collected 3-in. (diameter) undisturbed samples. Of the borings on the canal side of the east levee, three borings collected 5-in. (diameter) undisturbed samples, and one boring collected 3-in. (diameter) undisturbed samples. Of the three GDM borings taken on the protected side of the west levee, two borings collected 3-in. (diameter) samples, and one boring collected 5-in. (diameter) undisturbed samples. From the 3-in. samples, four unconfined compression (UC) tests were performed, and two one-point unconsolidated-undrained triaxial compression tests (UU-1), confined at existing overburden pressure, were performed. From the 5-in. samples, 14 UC tests were performed, and six unconsolidated-undrained triaxial compression tests (Q) were

performed. From these laboratory tests, moisture content and wet unit weights were determined. The moisture contents (%w) in the breach area are shown in Figure 1-36. In addition, this moisture content data were also plotted (Figure 1-37) with the moisture content data collected for the entire east levee on the canal. Also, the moisture content data for the entire west levee on the canal are shown in Figure 1-38.

The wet unit weight data in the breach area are shown in Figure 1-39. Wet unit weight data from the breach area plotted with wet unit weight data for the entire east levee are shown in Figure 1-40. Wet unit weight for the entire west levee on the canal is shown in Figure 1-41.
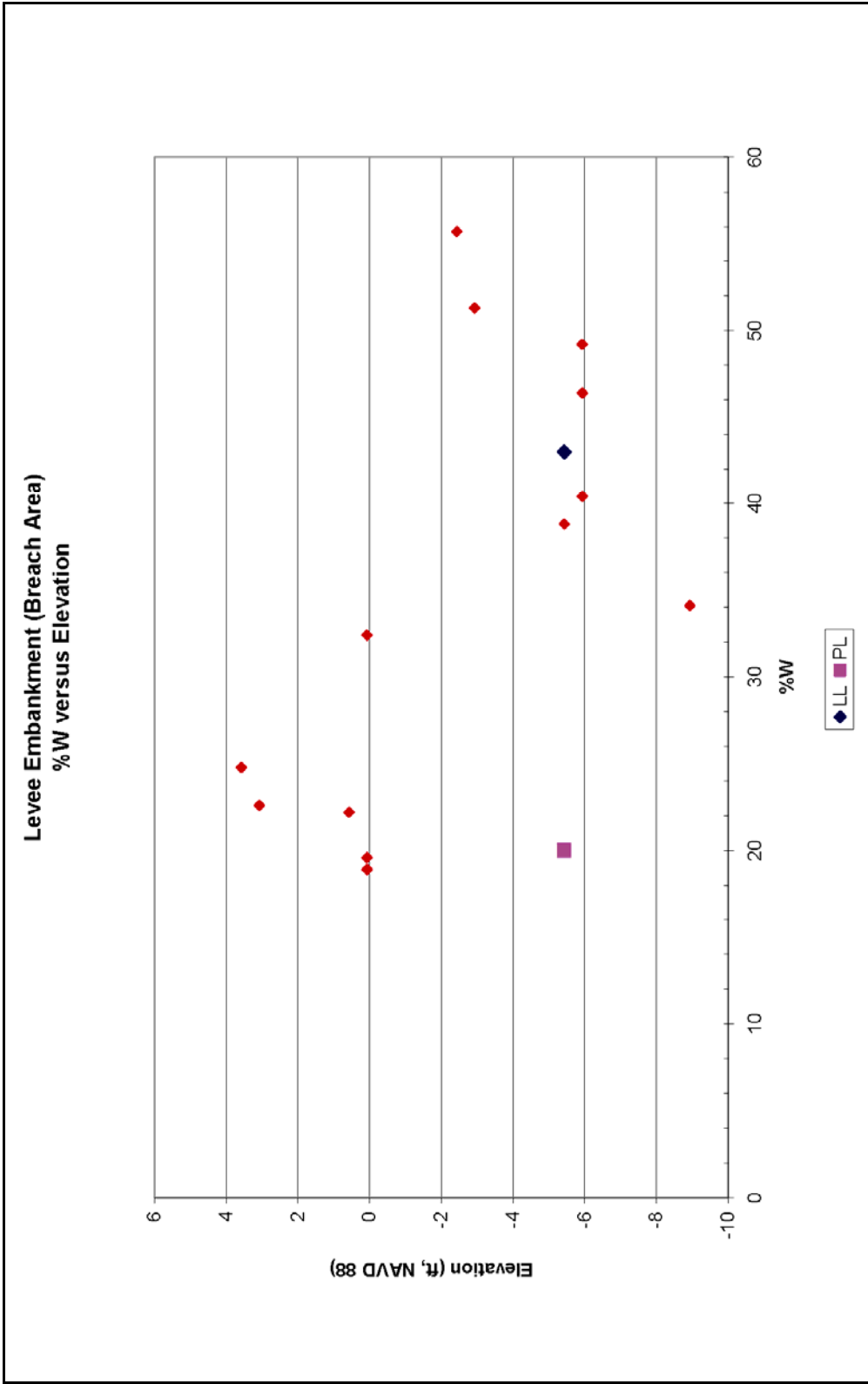
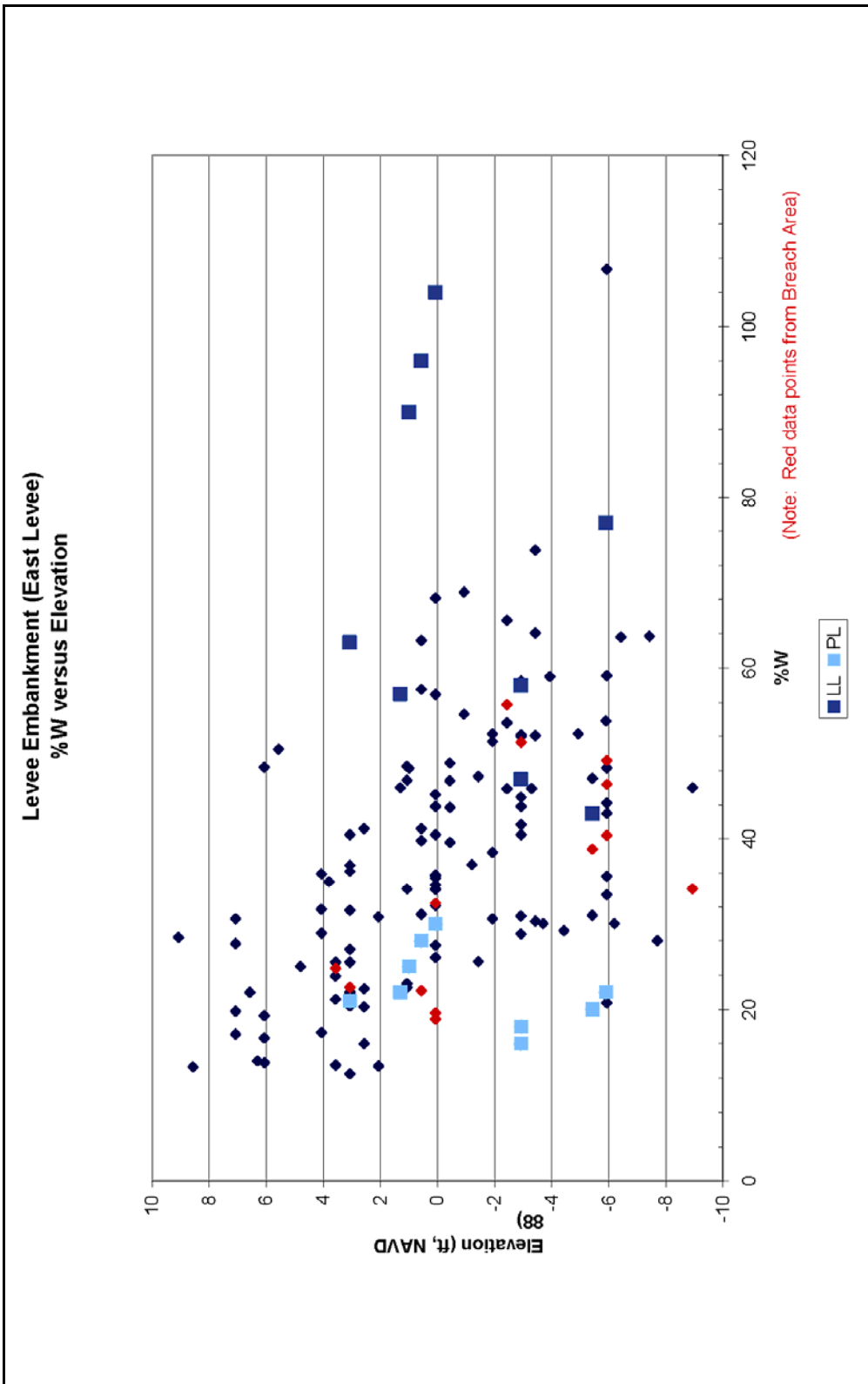Figure 1-14. Levee Embankment (Breach Area), %w versus Elevation

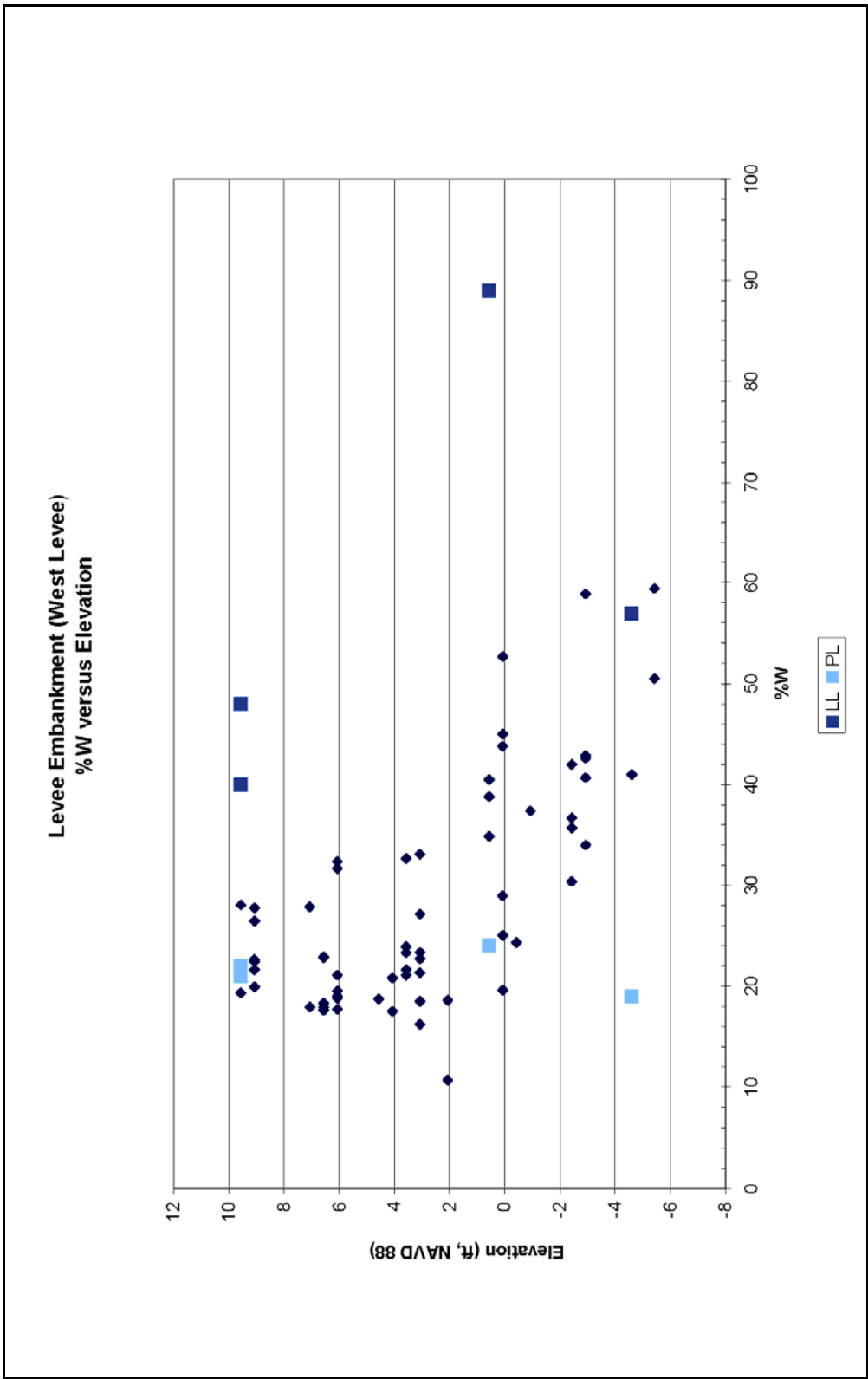Figure 1-15.   Levee Embankment (East Levee), %w versus Elevation

Volume V The Performance – Levees and Floodwalls – Technical Appendix
This is a preliminary report subject to revision; it does not contain final conclusions of the United States Army Corps of Engineers.

Figure 1-16. Levee Embankment (West Levee), %w versus Elevation

Figure 1-17.   Levee Embankment (Breach Area), Wet Unit Weight versus Elevation

This is a preliminary report subject to revision; it does not contain final conclusions of the United States Army Corps of Engineers.
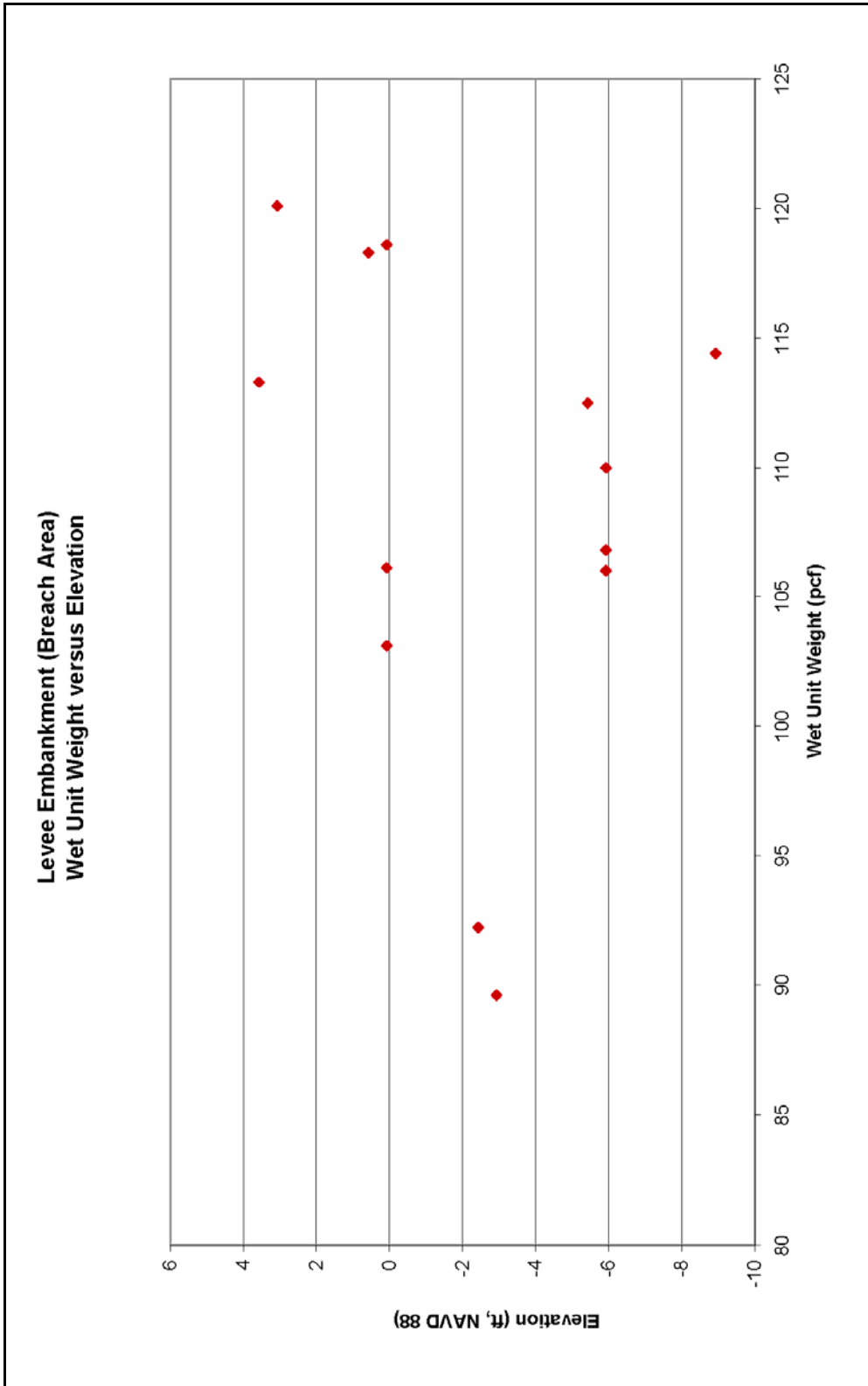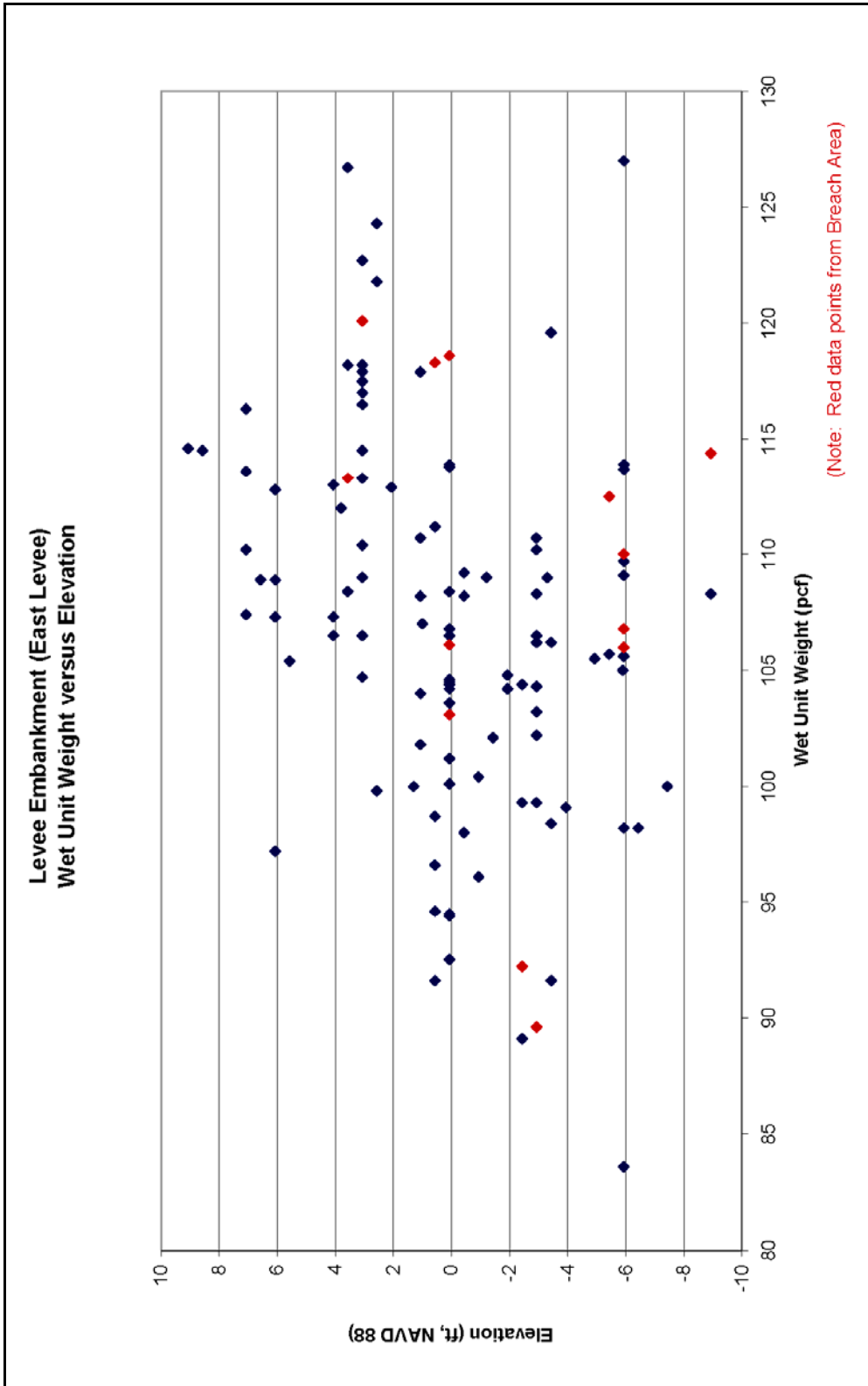
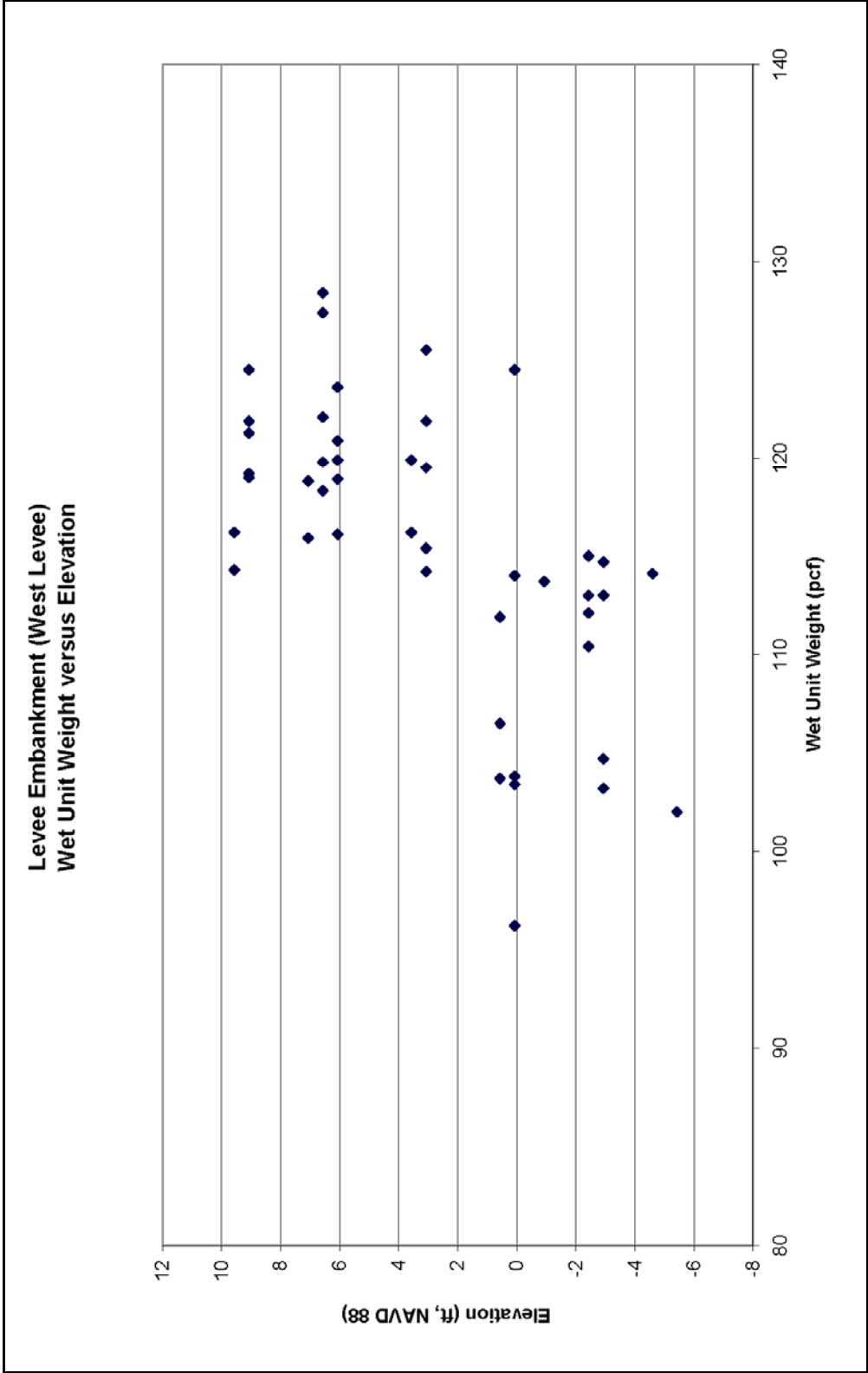Figure 1-18.   Levee Embankment (East Levee), Wet Unit Weight versus Elevation

Figure 1-19.   Levee Embankment (West Levee), Wet Unit Weight versus Elevation

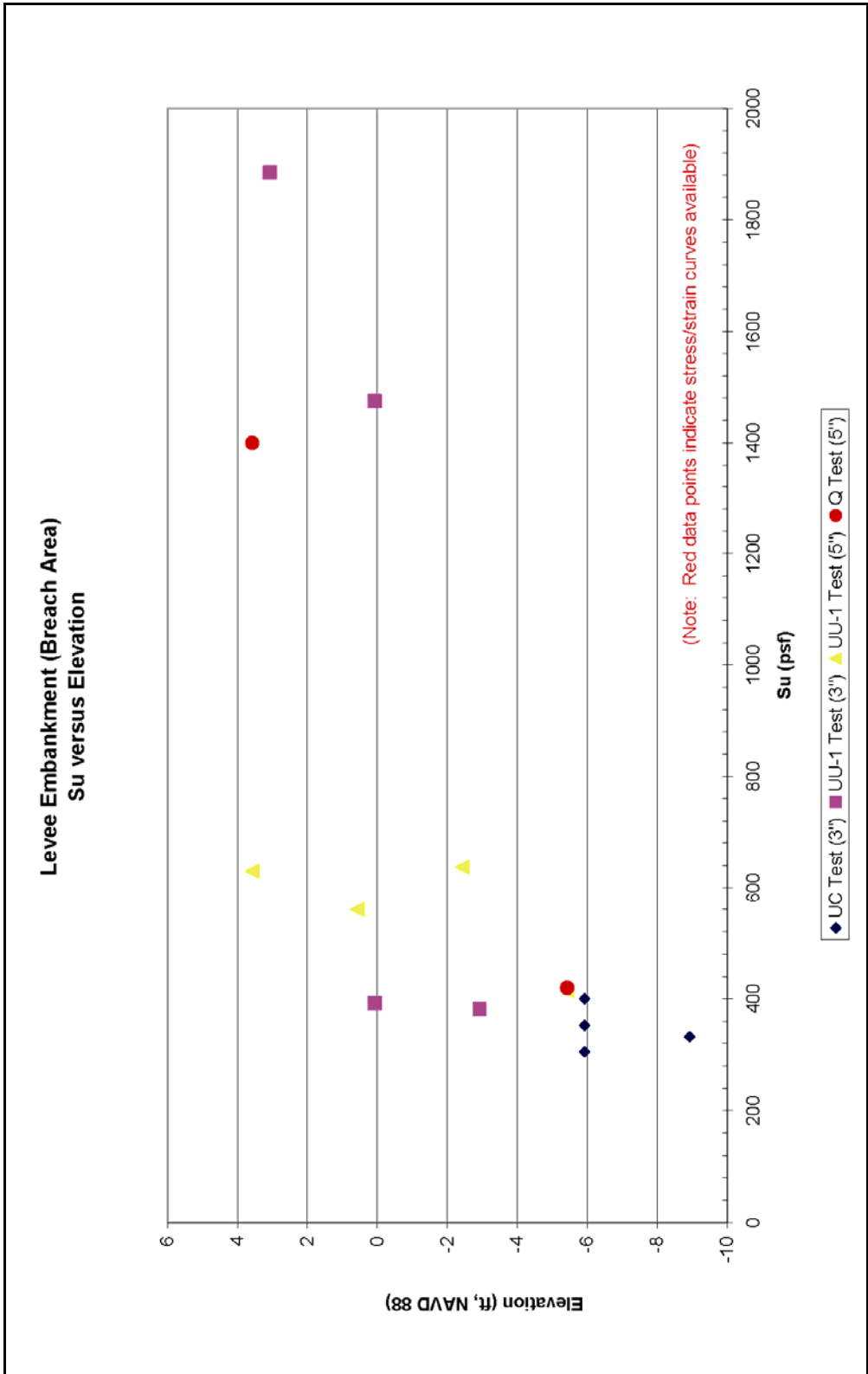Figure 1-20. Levee Embankment (Breach Area), Su versus Elevation

Volume V The Performance – Levees and Floodwalls – Technical Appendix

V-1-29

This is a preliminary report subject to revision; it does not contain final conclusions of the United States Army Corps of Engineers.
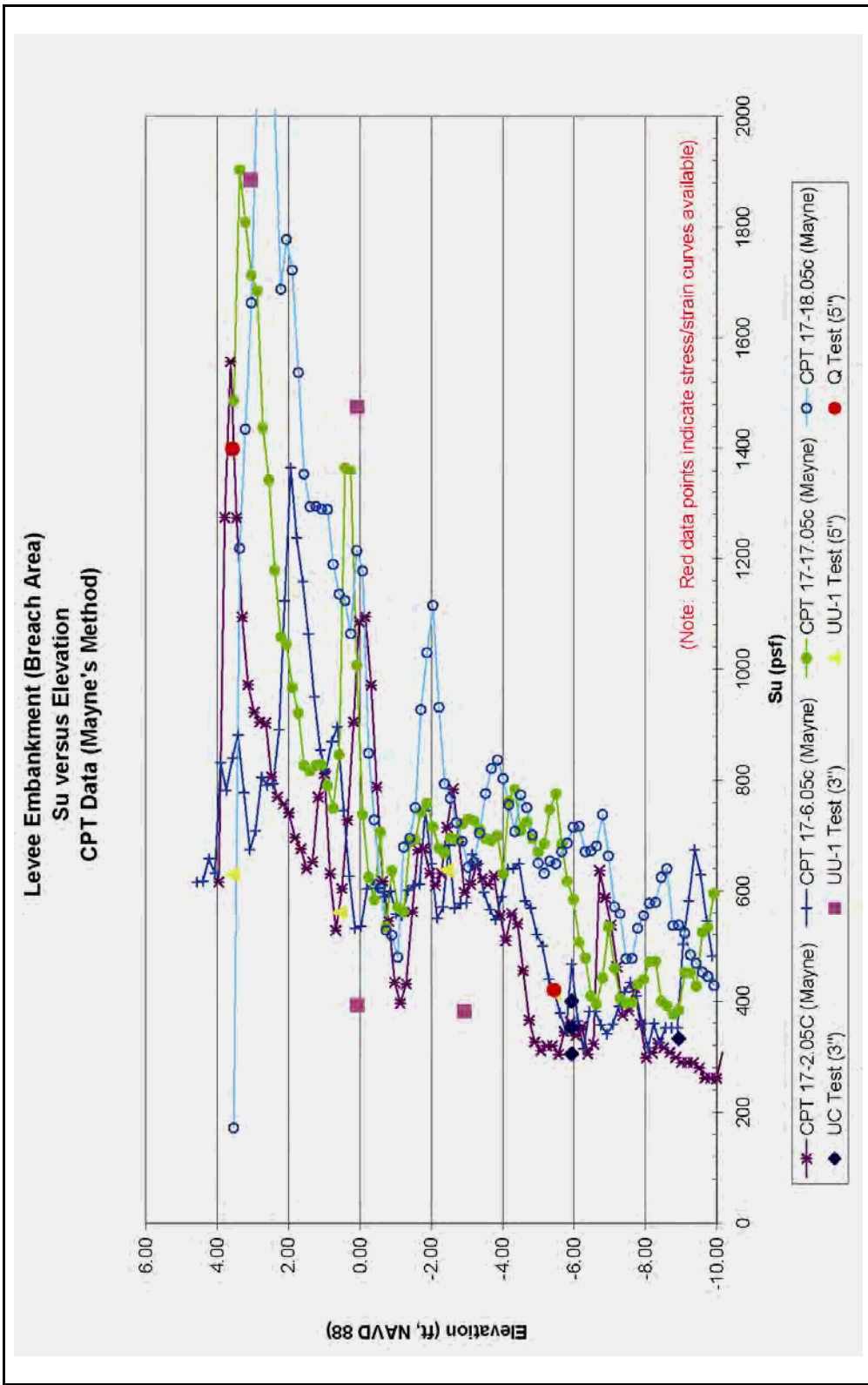
Figure 1-21. Levee Embankment, Su versus Elevation (CPT Data – Mayne's Method)

This is a preliminary report subject to revision; it does not contain final conclusions of the United States Army Corps of Engineers.
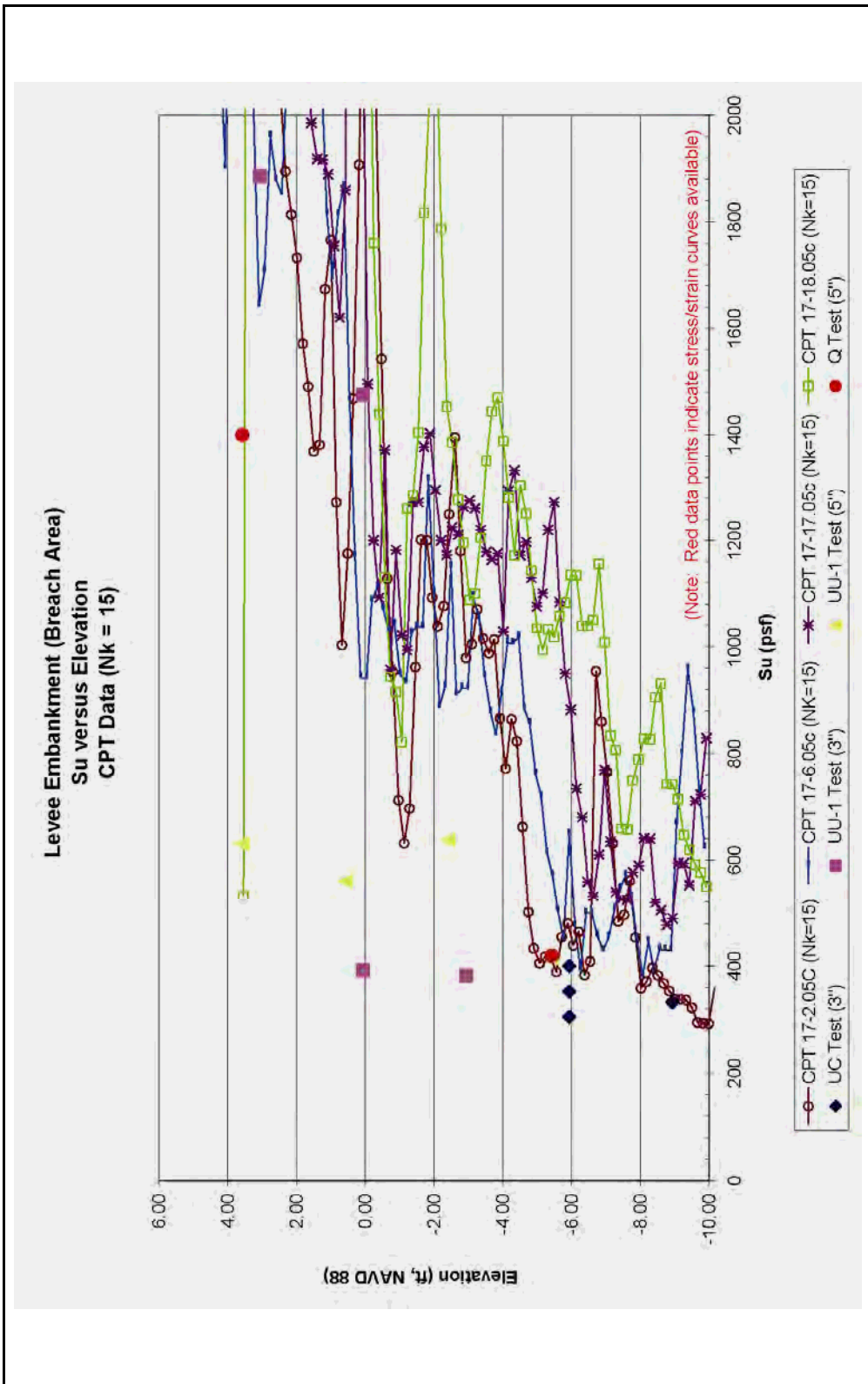
Figure 1-22. Levee Embankment (Breach Area), Su versus Elevation (CPT Data – Nk=15)
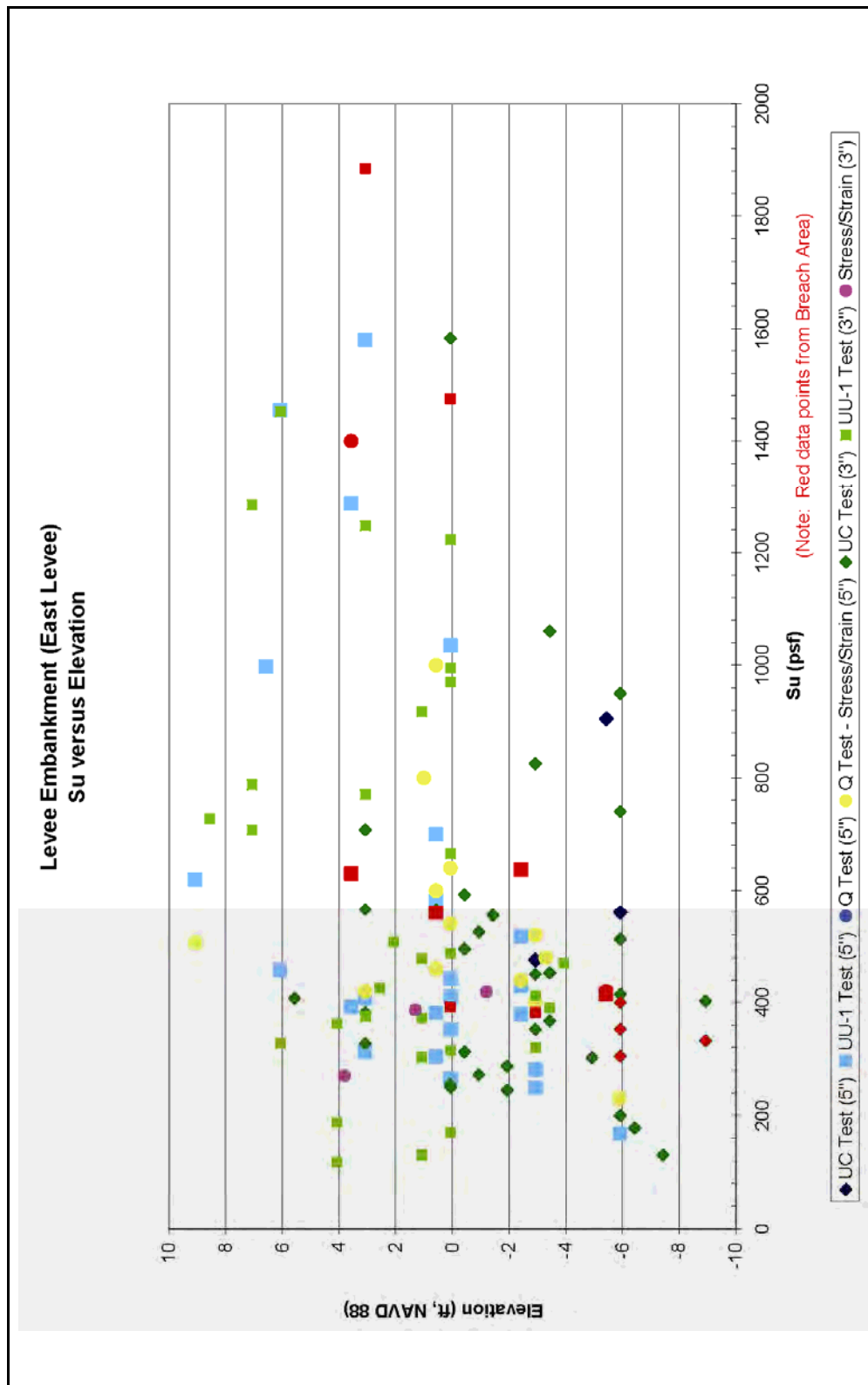
Figure 1-23.   Levee Embankment (East Levee), Su versus Elevation

This is a preliminary report subject to revision; it does not contain final conclusions of the United States Army Corps of Engineers.
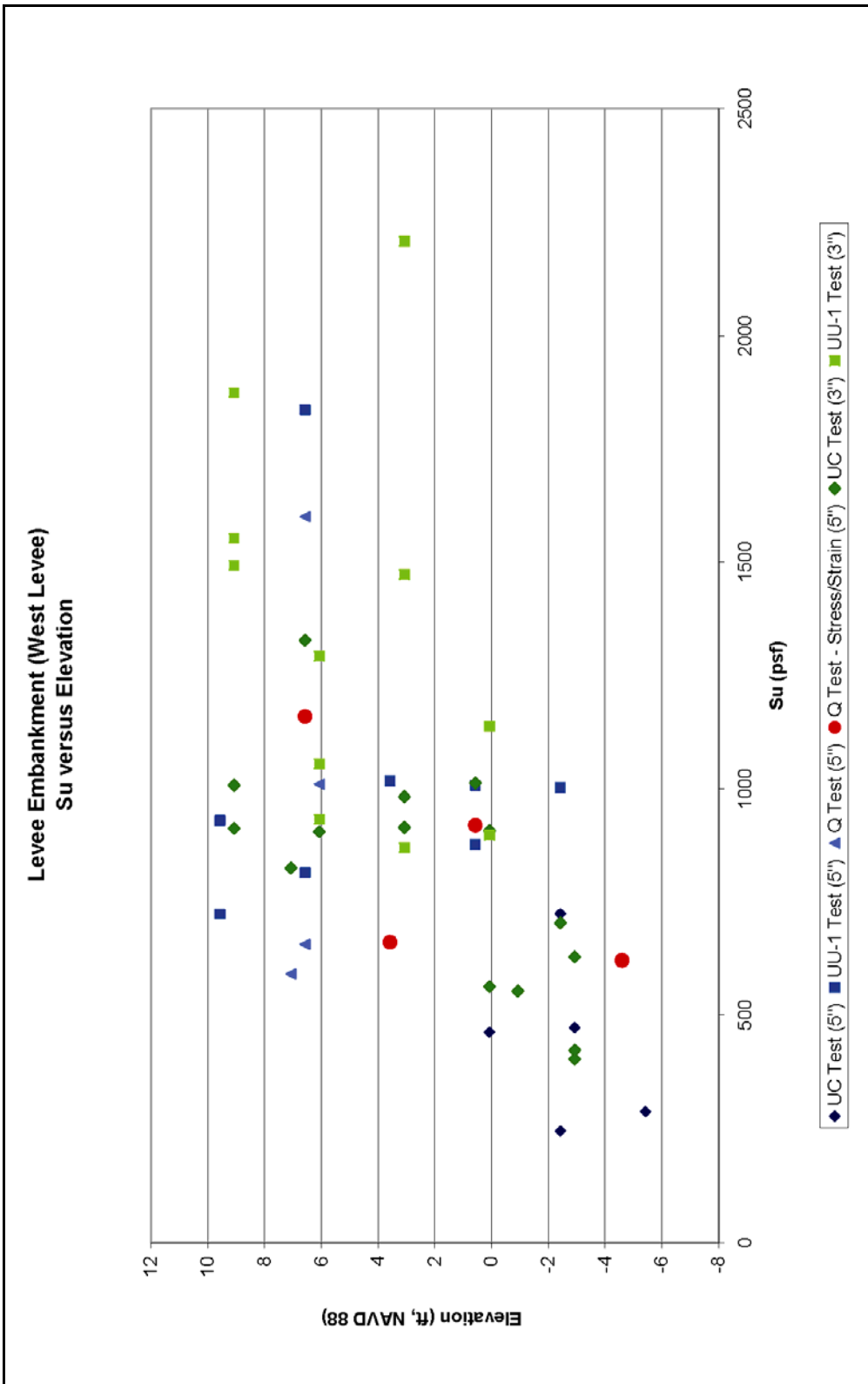
Figure 1-24. Levee Embankment (West Levee), Su versus Elevation

Figure 1-25.   Marsh Stratum (CL of East Levee – At Breach Area), %w versus Elevation

This is a preliminary report subject to revision; it does not contain final conclusions of the United States Army Corps of Engineers.

Figure 1-26. Marsh Stratum (CL of East Levee), %w versus Elevation

Figure 1-27.   Marsh Stratum (CL of West Levee), %w versus Elevation

Figure 1-28.   Marsh Stratum (CL of East Levee – At Breach Area), Wet Unit Weight versus Elevation

Figure 1-29.   Marsh Stratum (CL of East Levee), Wet Unit Weight versus Elevation

This is a preliminary report subject to revision; it does not contain final conclusions of the United States Army Corps of Engineers.

Figure 1-30. Marsh Stratum (CL of West Levee), Wet Unit Weight versus Elevation

Figure 1-31.   Marsh Stratum (CL of East Levee – At Breach Area), Su versus Elevation

This is a preliminary report subject to revision; it does not contain final conclusions of the United States Army Corps of Engineers.

Figure 1-32.   Marsh Stratum (CL of East Levee – At Breach Area), Su versus Elevation (CPT Data – Mayne's Method)
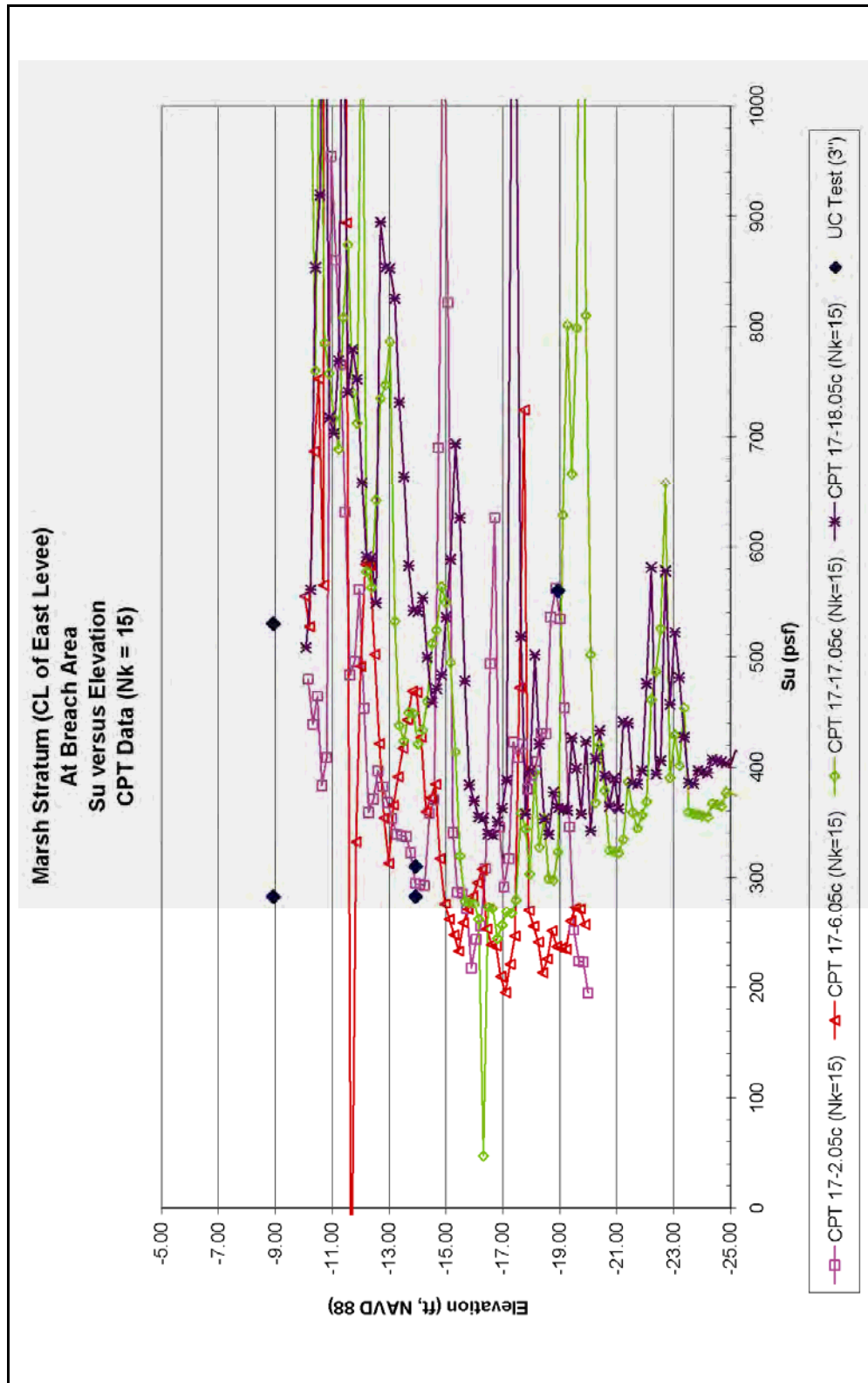
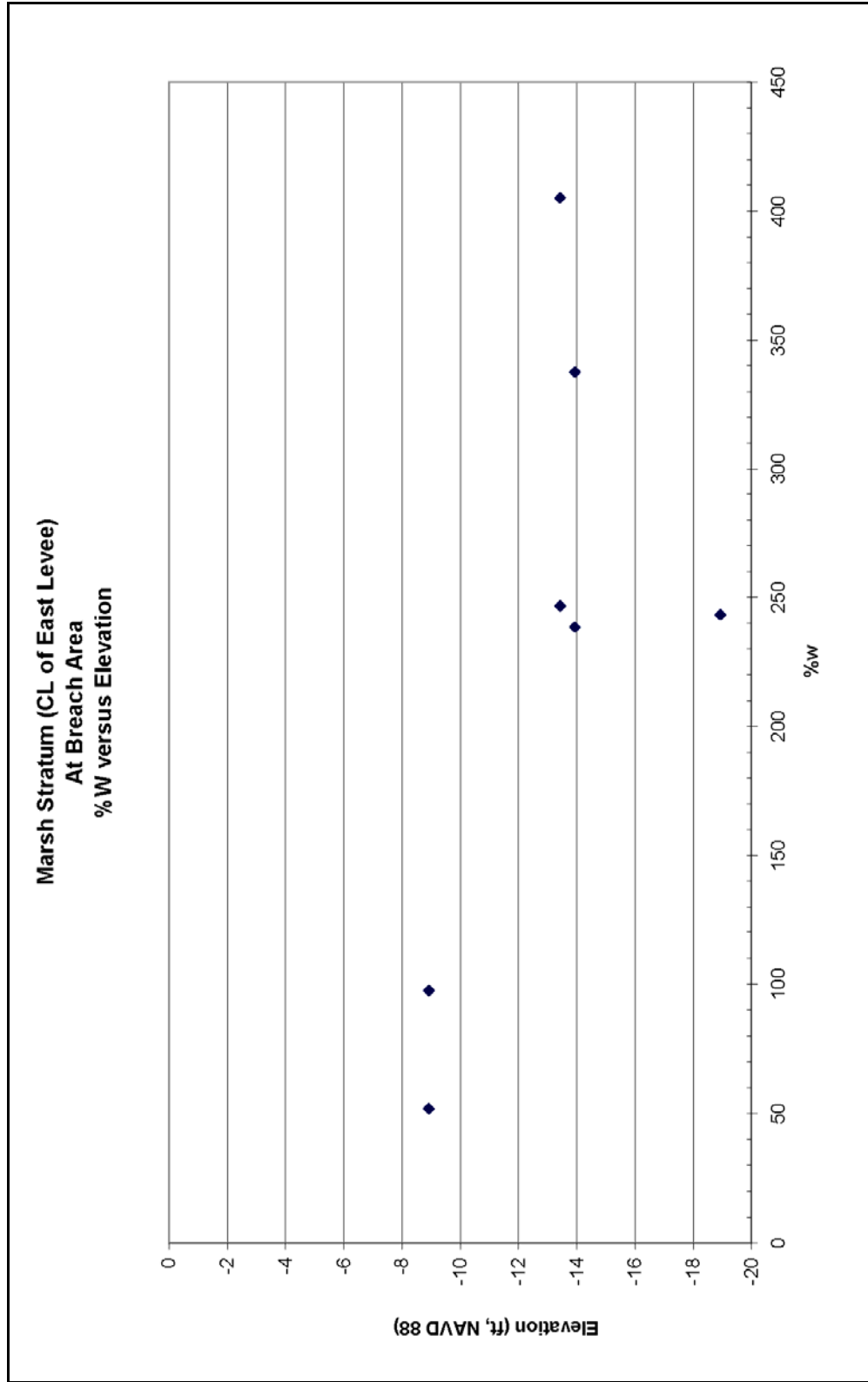Figure 1-33. Marsh Stratum (CL of East Levee), Su versus Elevation (CPT Data – Nk=15)
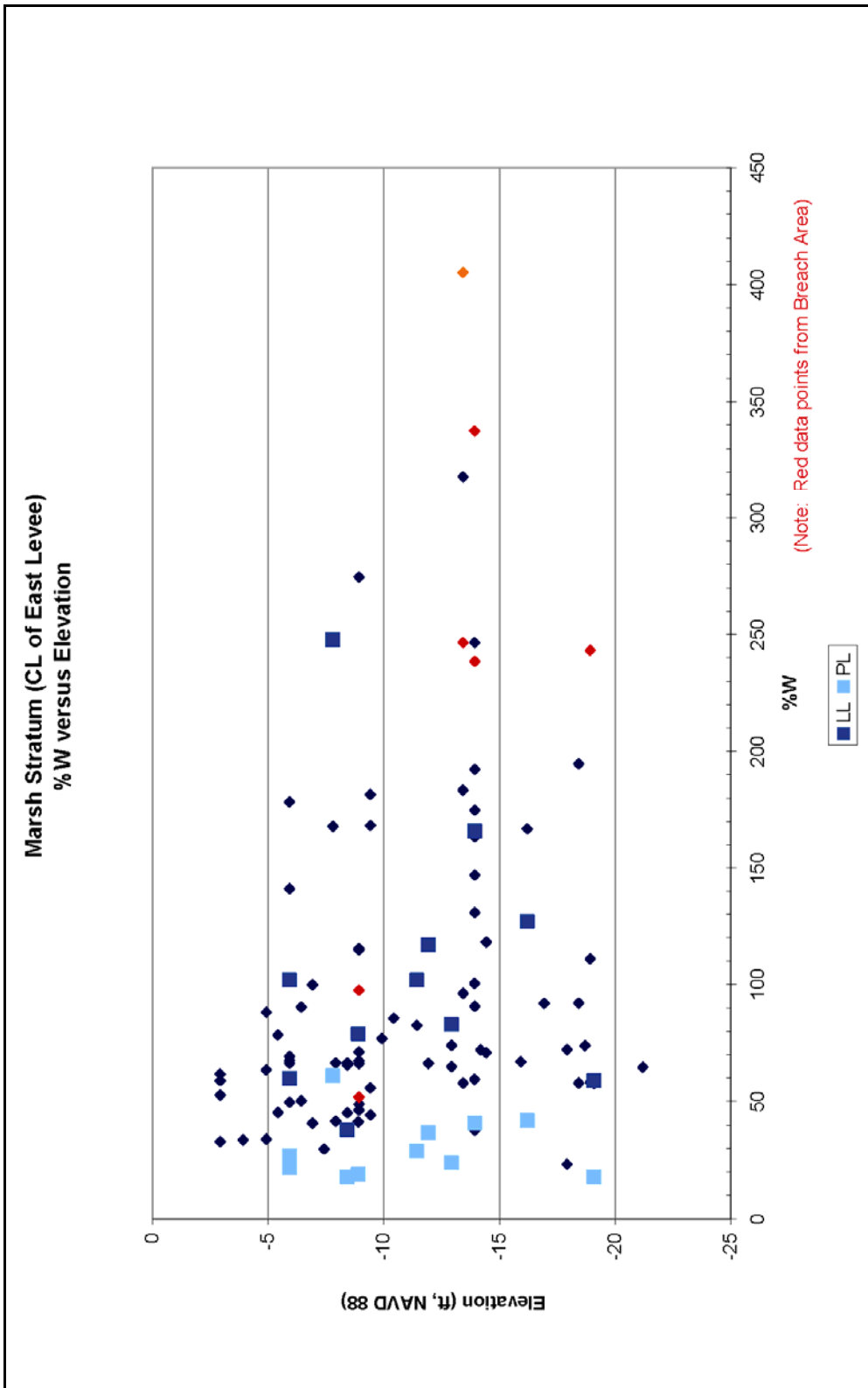
Figure 1-34. Marsh Stratum (CL of East Levee), Su versus Elevation

Figure 1-35.   Marsh Stratum (CL of West Levee), Su versus Elevation

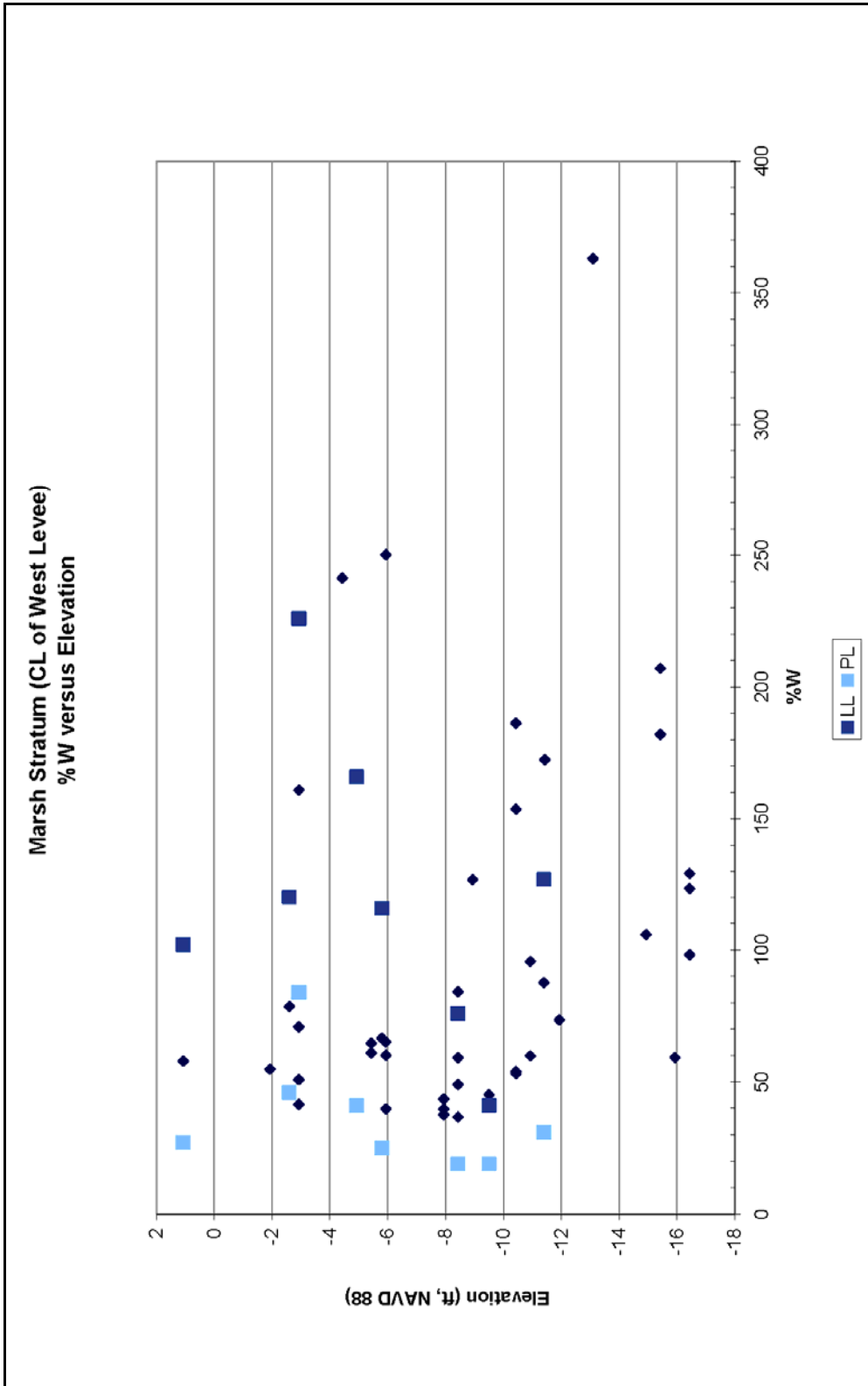Figure 1-36. Marsh Stratum (Toe of East and West Levee – At Breach Area), %w versus Elevation

Volume V The Performance – Levees and Floodwalls – Technical Appendix
V-1-45

This is a preliminary report subject to revision; it does not contain final conclusions of the United States Army Corps of Engineers.

Figure 1-37.   Marsh Stratum (Toe of East Levee), %w versus Elevation

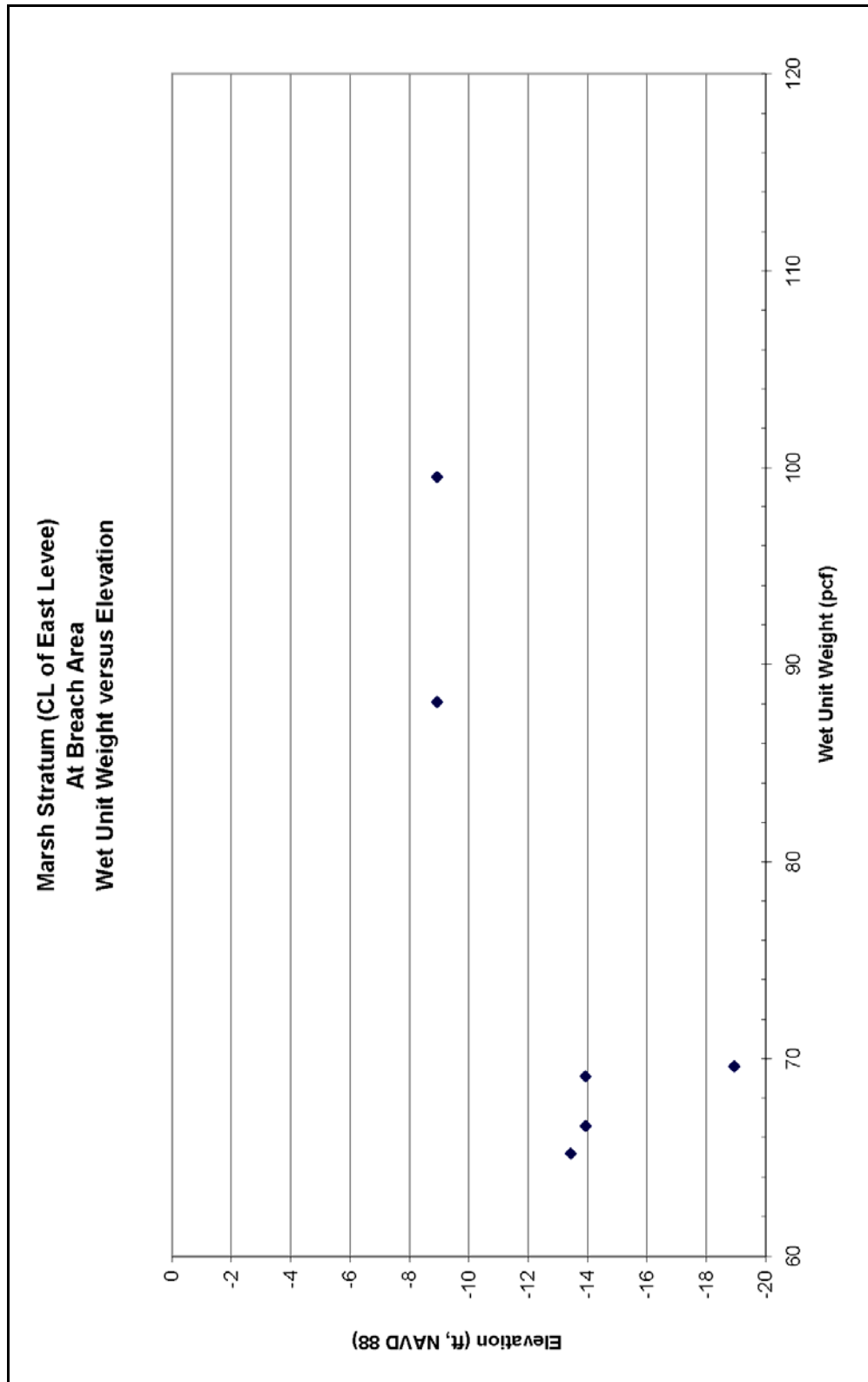Figure 1-38.   Marsh Stratum (Toe of West Levee), %w versus Elevation

Figure 1-39. Marsh Stratum (Toe of East and West Levee – At Breach Area), Wet Unit Weight versus Elevation

This is a preliminary report subject to revision; it does not contain final conclusions of the United States Army Corps of Engineers.
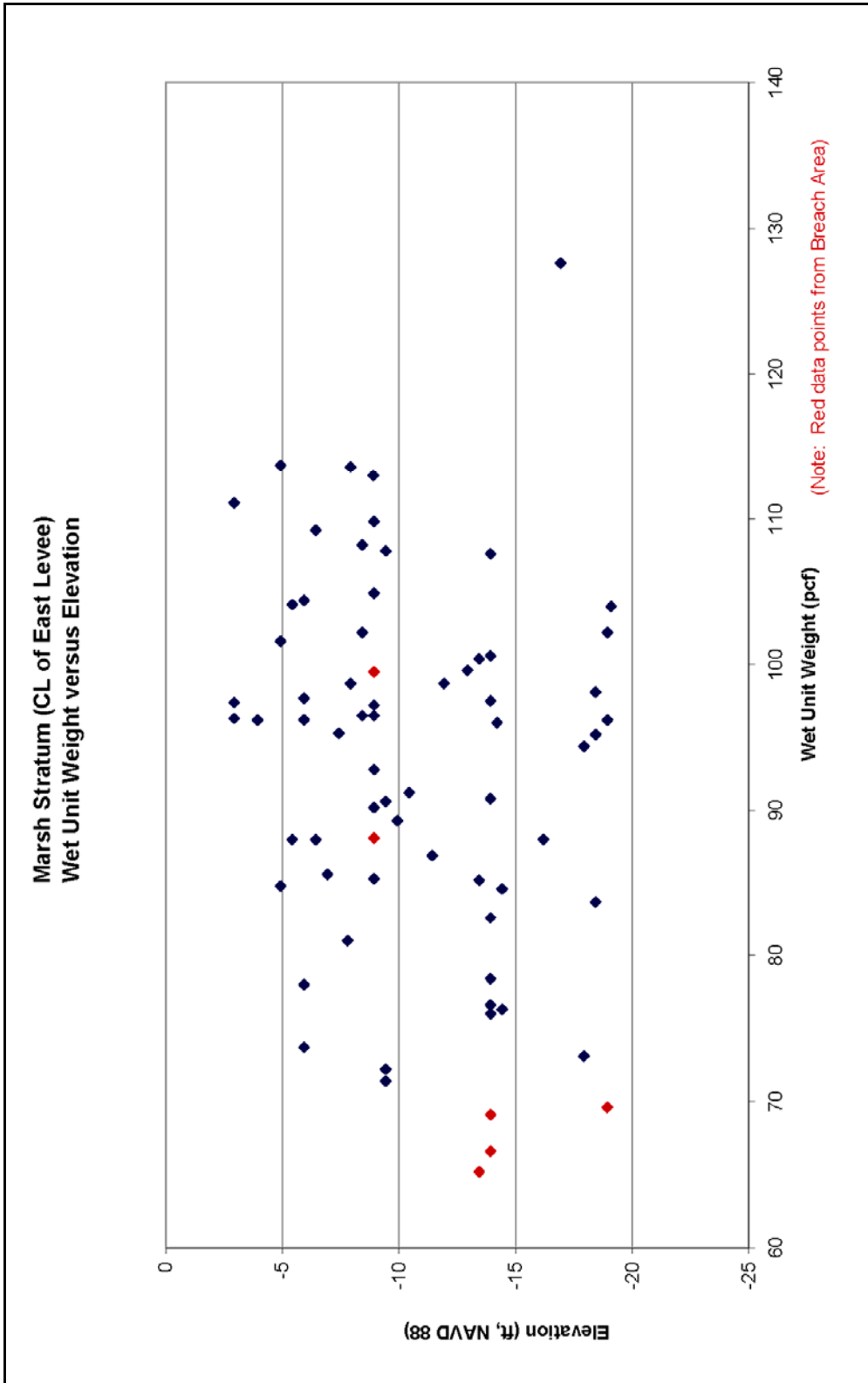
Figure 1-40.   Marsh Stratum (Toe of East Levee), Wet Unit Weight versus Elevation

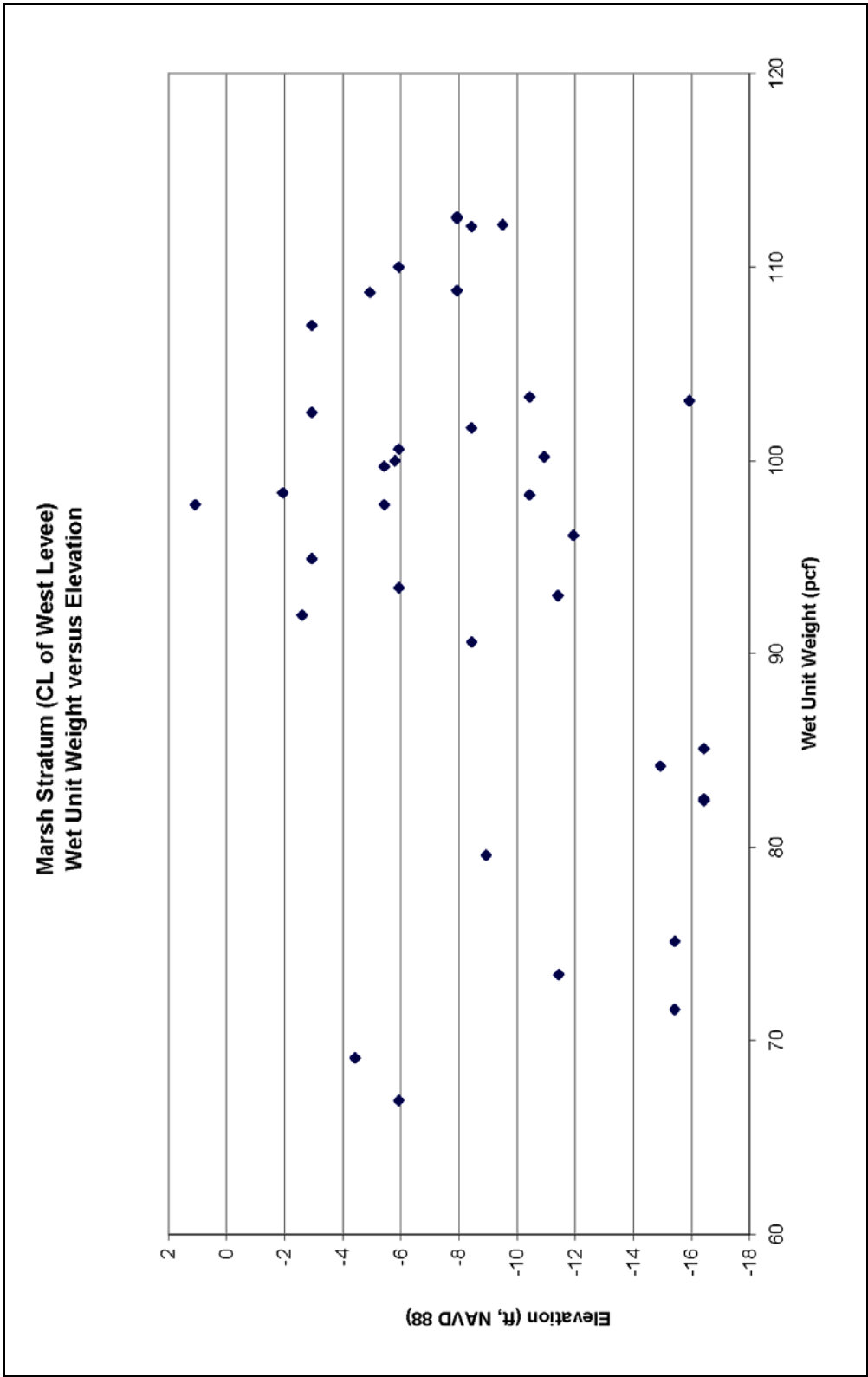Figure 1-41.   Marsh Stratum (Toe of West Levee), Wet Unit Weight versus Elevation
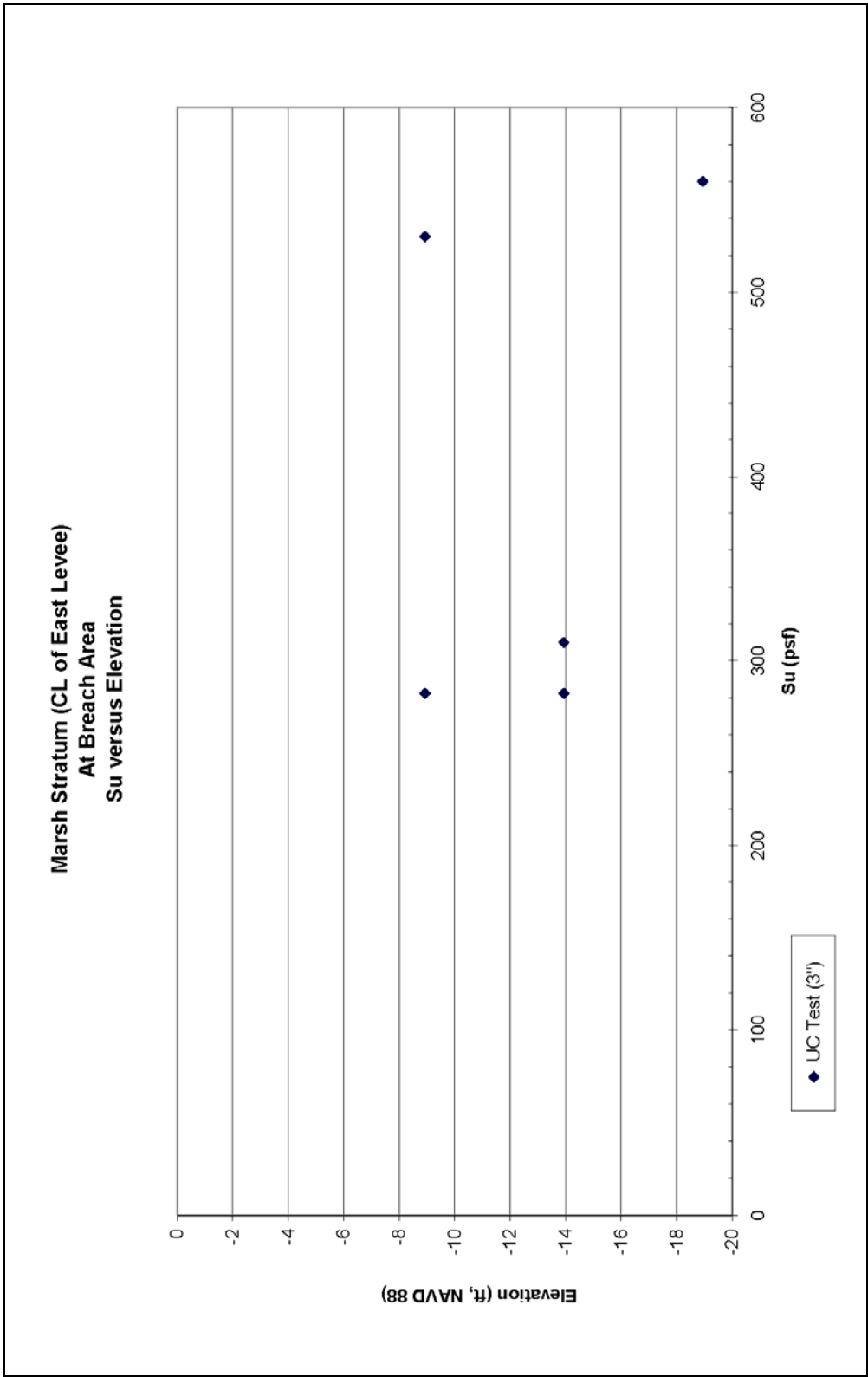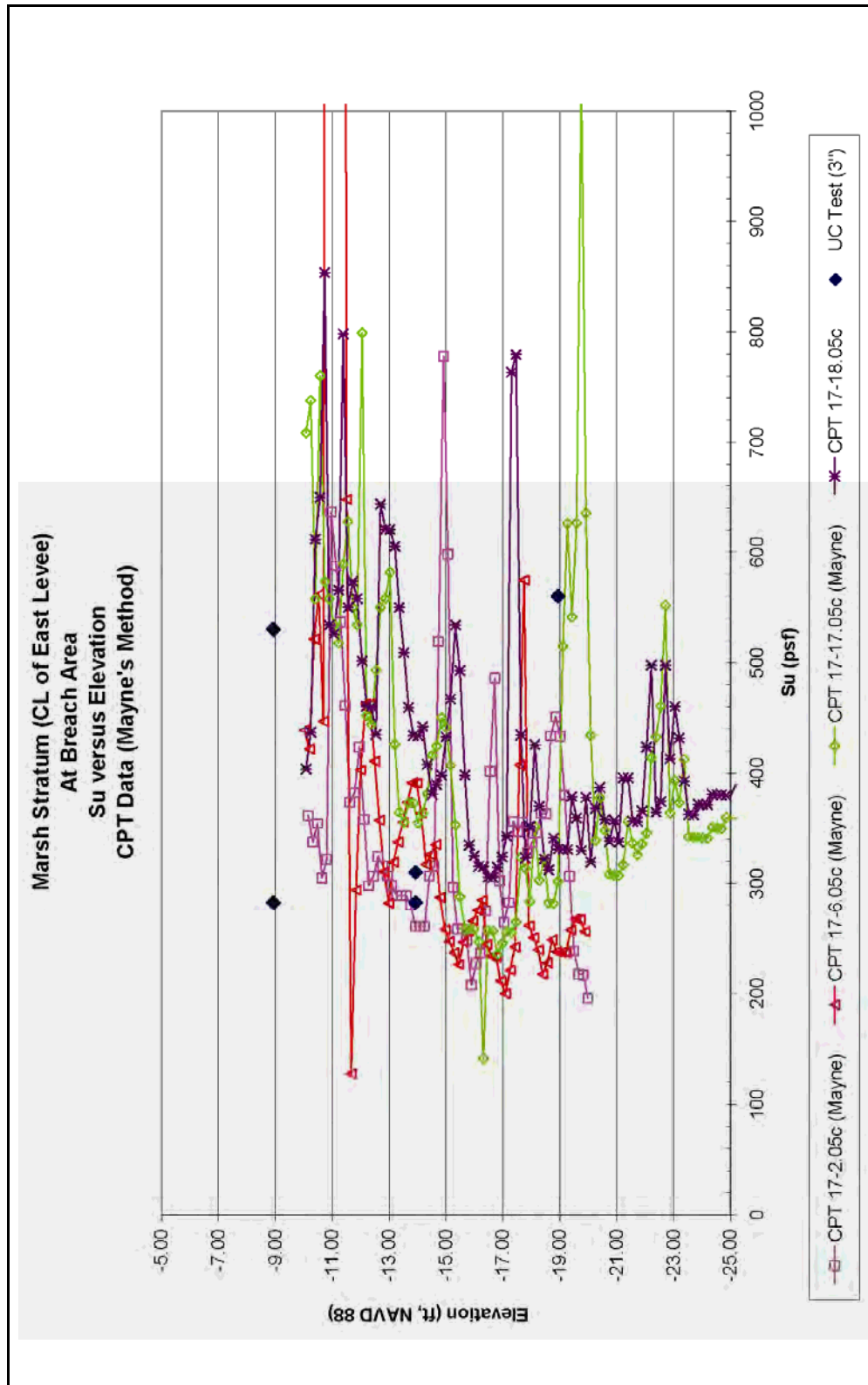
This is a preliminary report subject to revision; it does not contain final conclusions of the United States Army Corps of Engineers.

The undrained shear strength determined from the laboratory tests conducted on samples in the breach area is shown in Figure 1-42. Undrained shear strength data in the breach area plotted with undrained shear strength data for the entire east levee are shown in Figure 1-43. Undrained shear strength data for the entire west levee are shown in Figure 1-44.

Lacustrine Stratum

The data for the lacustrine stratum will be divided into two groups: data from under the levee embankment, and data from the toe of the levee.

Under the Levee Embankment

Data on the lacustrine stratum under the levee embankment consist of five borings shown in the 1990 GDM, and four cone penetrometer tests (CPT) taken on the east levee. Of the five GDM borings, four borings collected 3-in. (diameter) undisturbed samples, and one boring collected 5-in. (diameter) undisturbed samples. From the 3-in. samples, ten unconfined compression (UC) tests were performed. From the 5-in. samples, four UC tests were performed, and two one-point unconsolidated-undrained triaxial compression tests (UU-1), confined at existing overburden pressures, were performed. From these laboratory tests, moisture content and wet unit weights were determined. The moisture contents (%w) in the breach area are shown in Figure 1-45. The wet unit weight data in the breach area are shown in Figure 1-46.

Interpretation of the undrained shear strength from the CPTs using the bearing capacity equation (Nk=15) is plotted with laboratory test results in Figure 1-47. These interpretations were provided by Dr. Thomas Brandon (Virginia Tech).

At the Toe of Embankment

Data on the marsh stratum under the toe of the levee embankment consist of five borings taken in 2005 on the protected side, four borings taken in 2005 on the canal side, and three borings on the west levee toe shown in the 1990 GDM. Of the borings on the protected side of the east levee, four borings collected 5-in. (diameter) undisturbed samples, and one boring collected 3-in. (diameter) undisturbed samples. Of the borings on the canal side of the east levee, three borings collected 5-in. (diameter) undisturbed samples, and one boring collected 3-in. (diameter) undisturbed samples. Of the three GDM borings taken on the protected side of the west levee, two borings collected 3-in. (diameter) samples, and one boring collected 5-in. (diameter) undisturbed samples. From the 3-in. samples, 14 UC tests were performed, and five one-point unconsolidated-undrained triaxial compression tests (UU-1), confined at existing overburden pressure, were performed. From the 5-in. samples, 25 UC tests were performed, 19 unconsolidated-undrained triaxial compression tests (Q), and 7 one-point unconsolidated-undrained triaxial compression tests (UU-1), confined at existing overburden pressure, were performed. From these laboratory tests, moisture content and wet unit weights were determined. The moisture contents (%w) in the breach area are shown in Figure 1-48. The wet unit weight data in the breach area are shown in Figure 1-49.

Figure 1-42. Marsh Stratum (Toe of East and West Levee – At Breach Area), Su versus Elevation

This is a preliminary report subject to revision; it does not contain final conclusions of the United States Army Corps of Engineers.
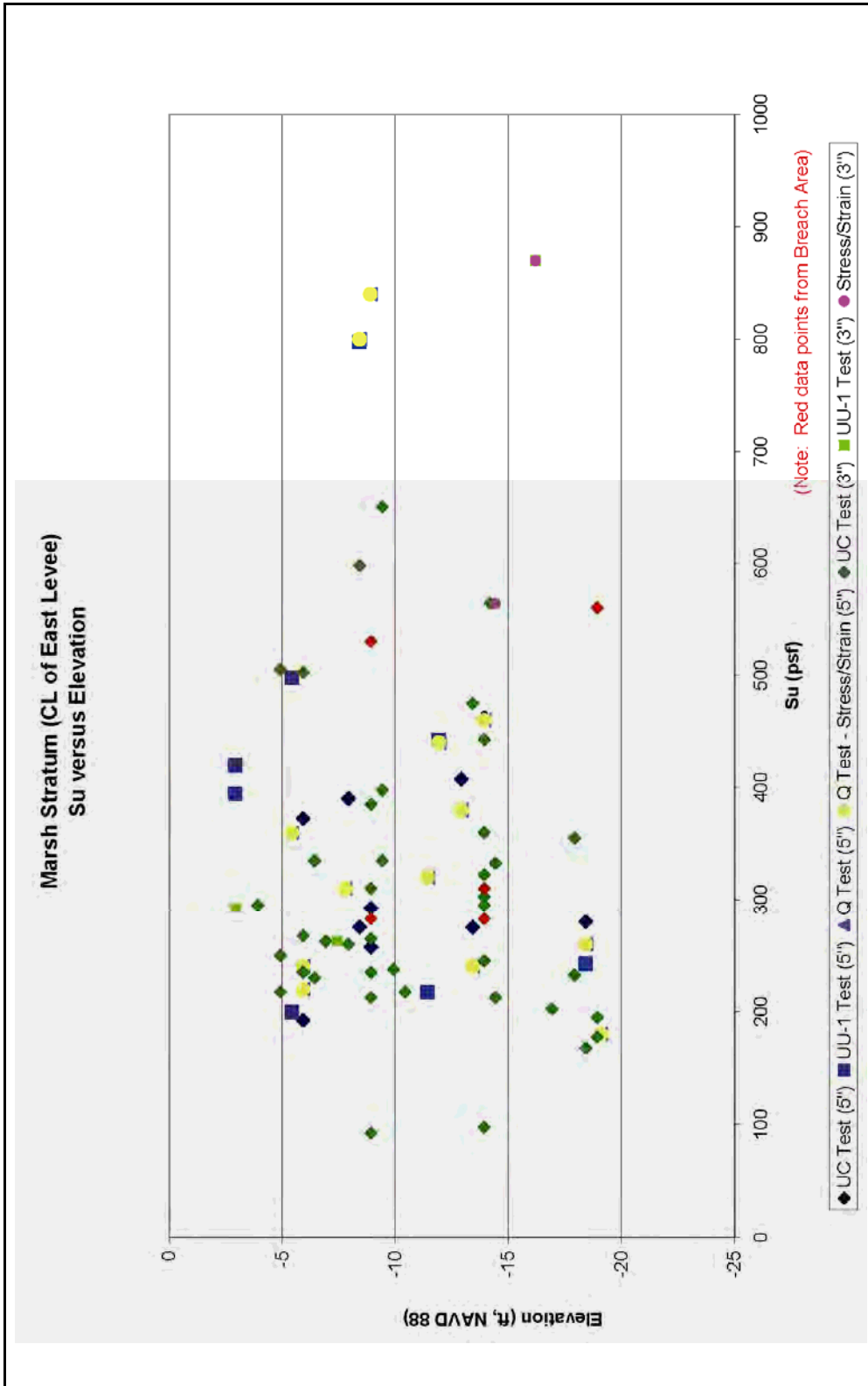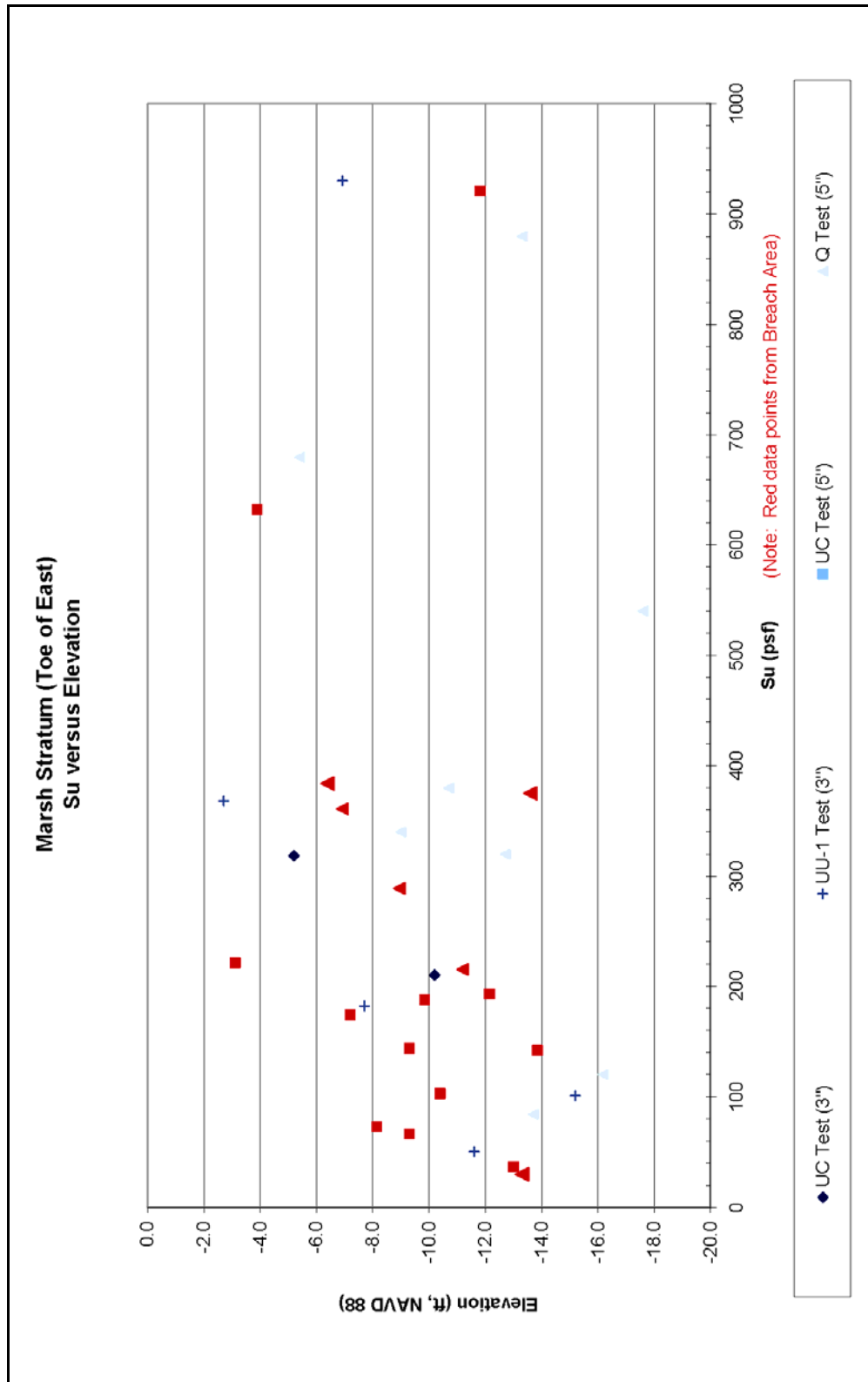
Figure 1-43.   Marsh Stratum (Toe of East Levee), Su versus Elevation

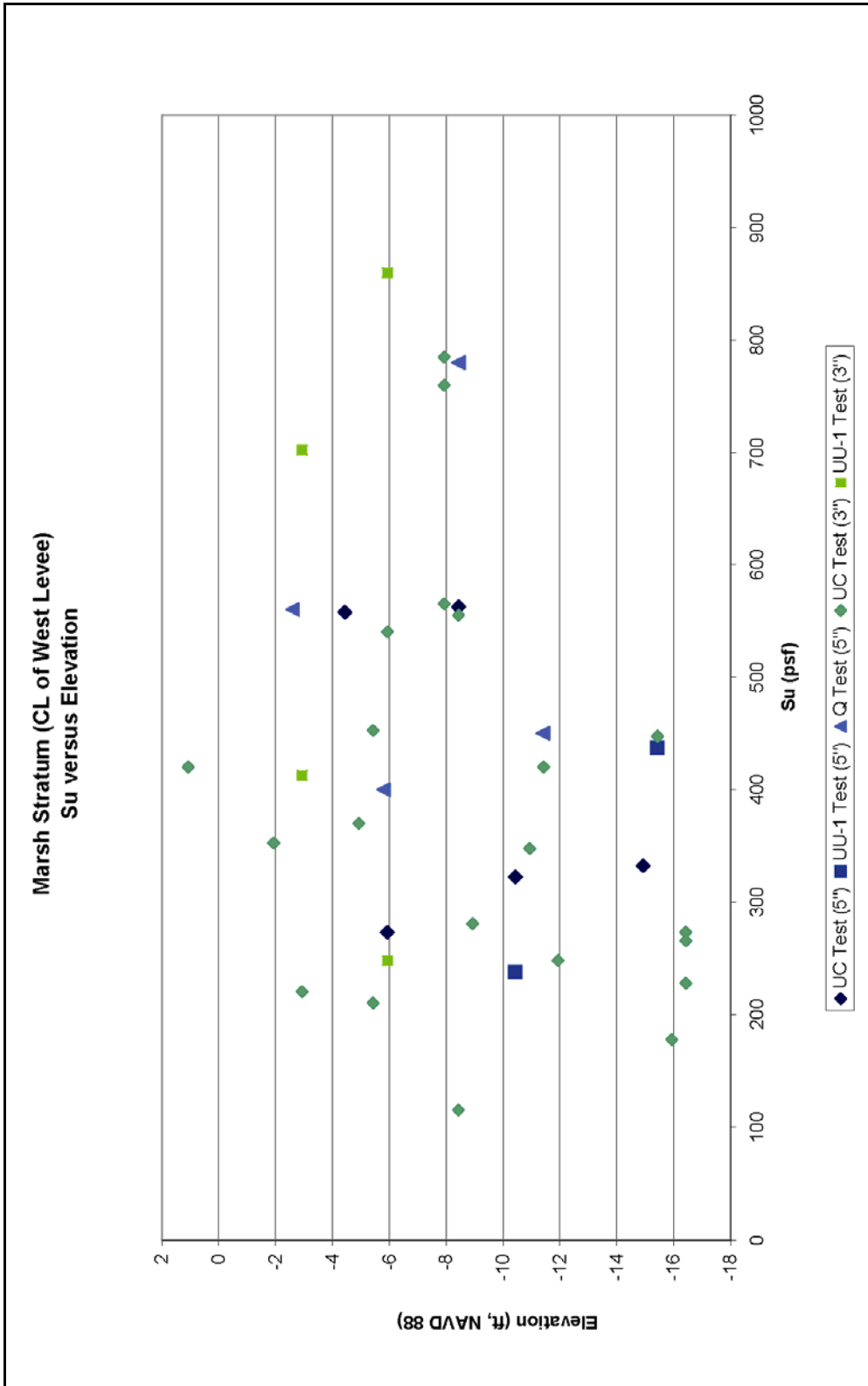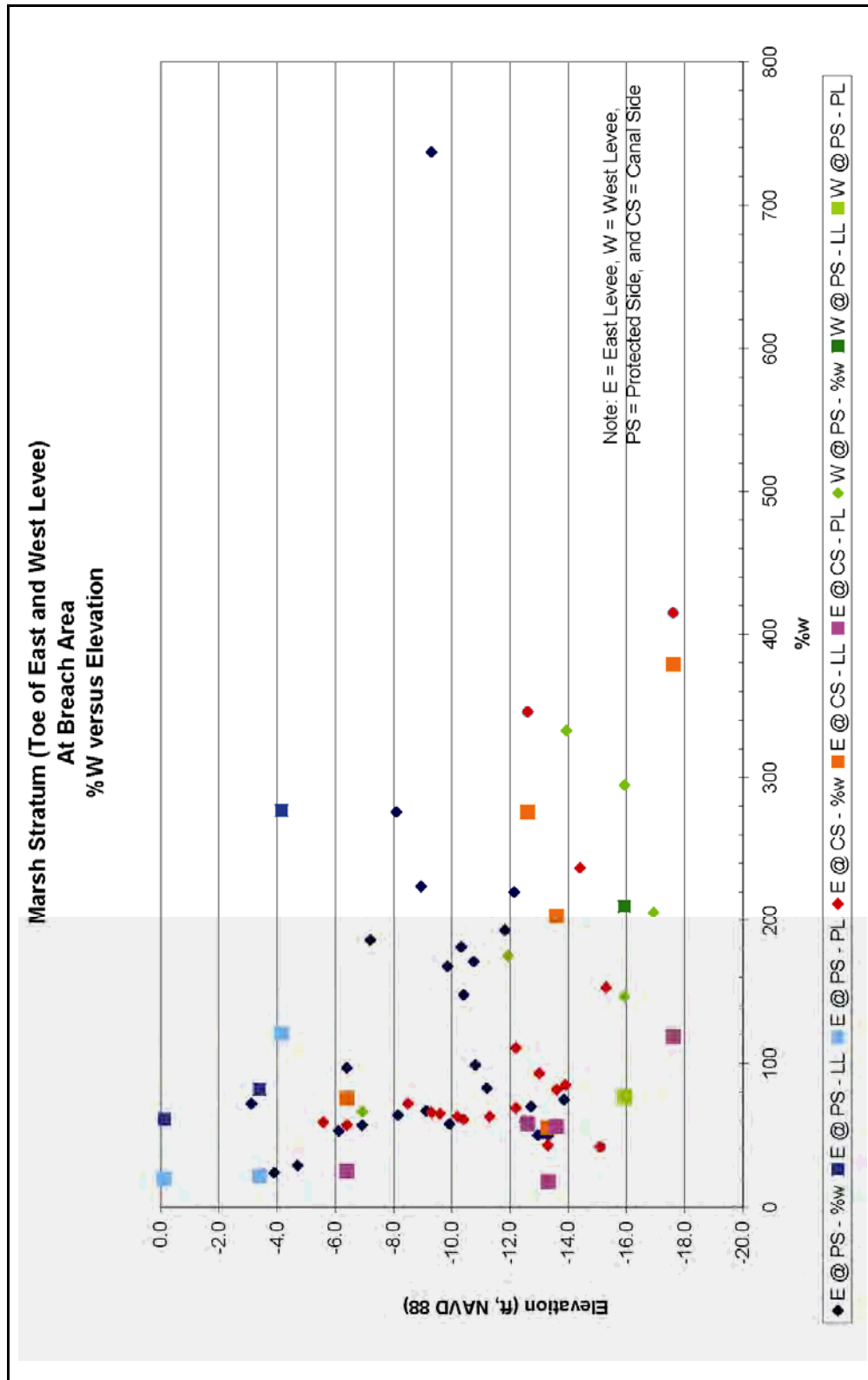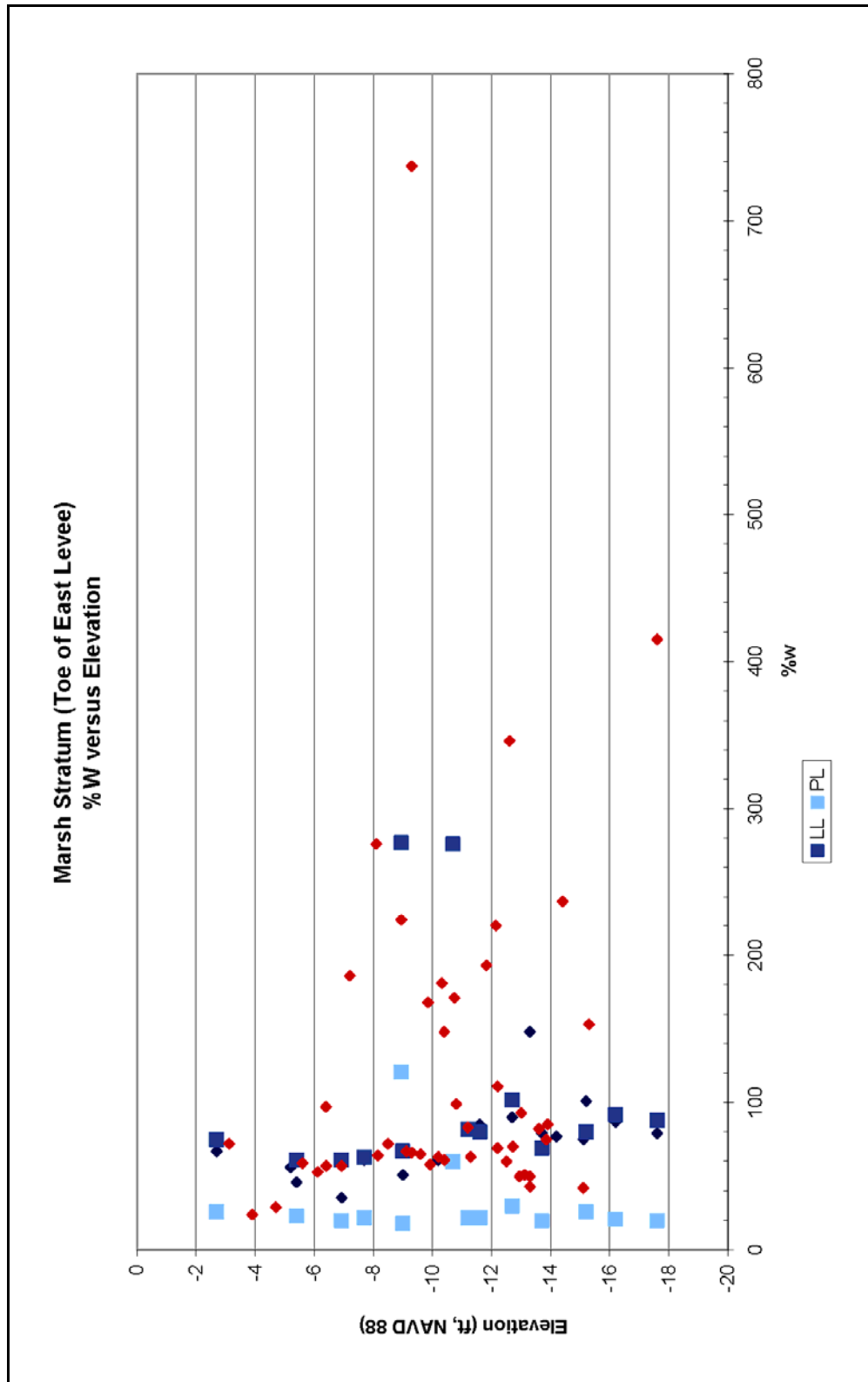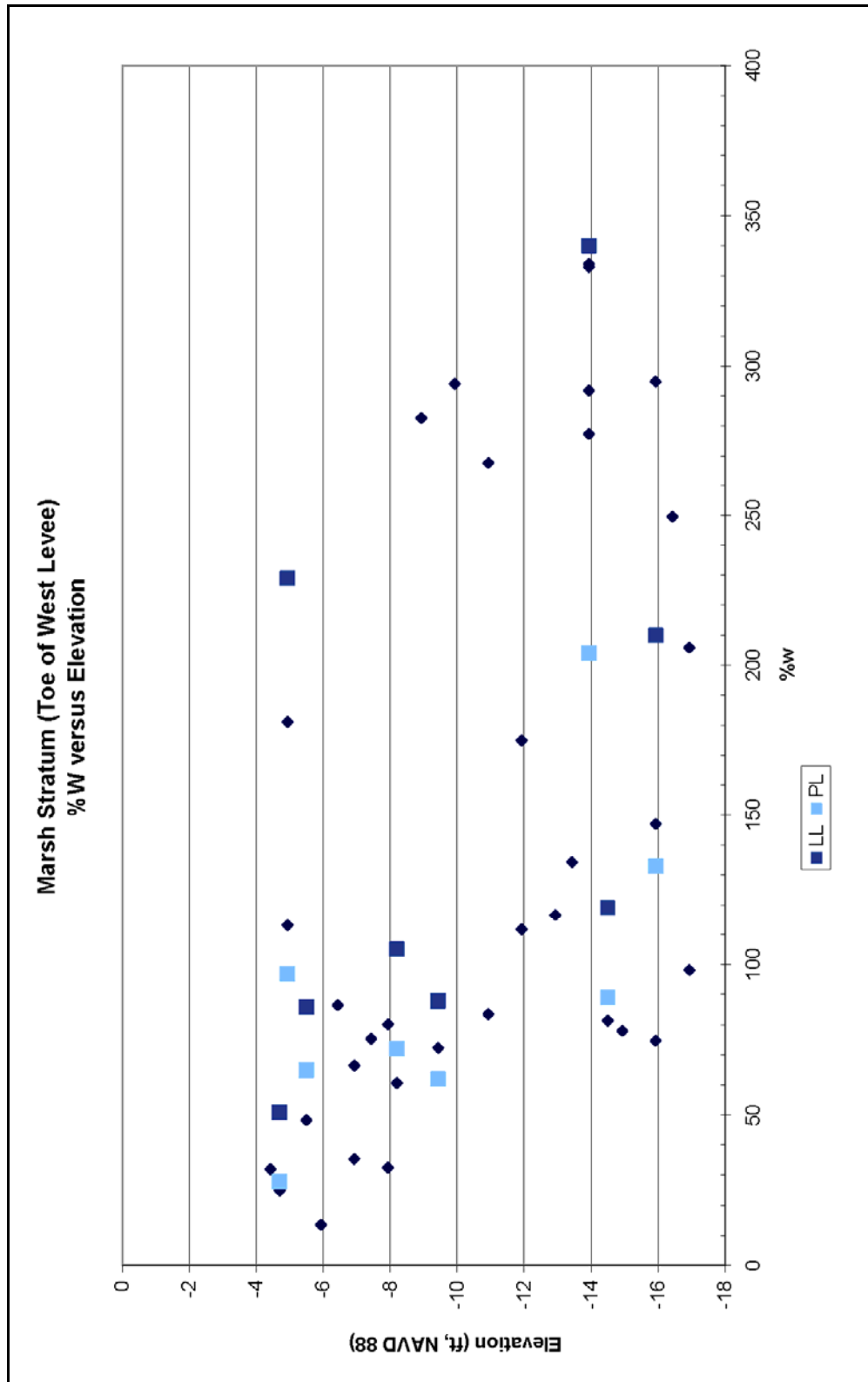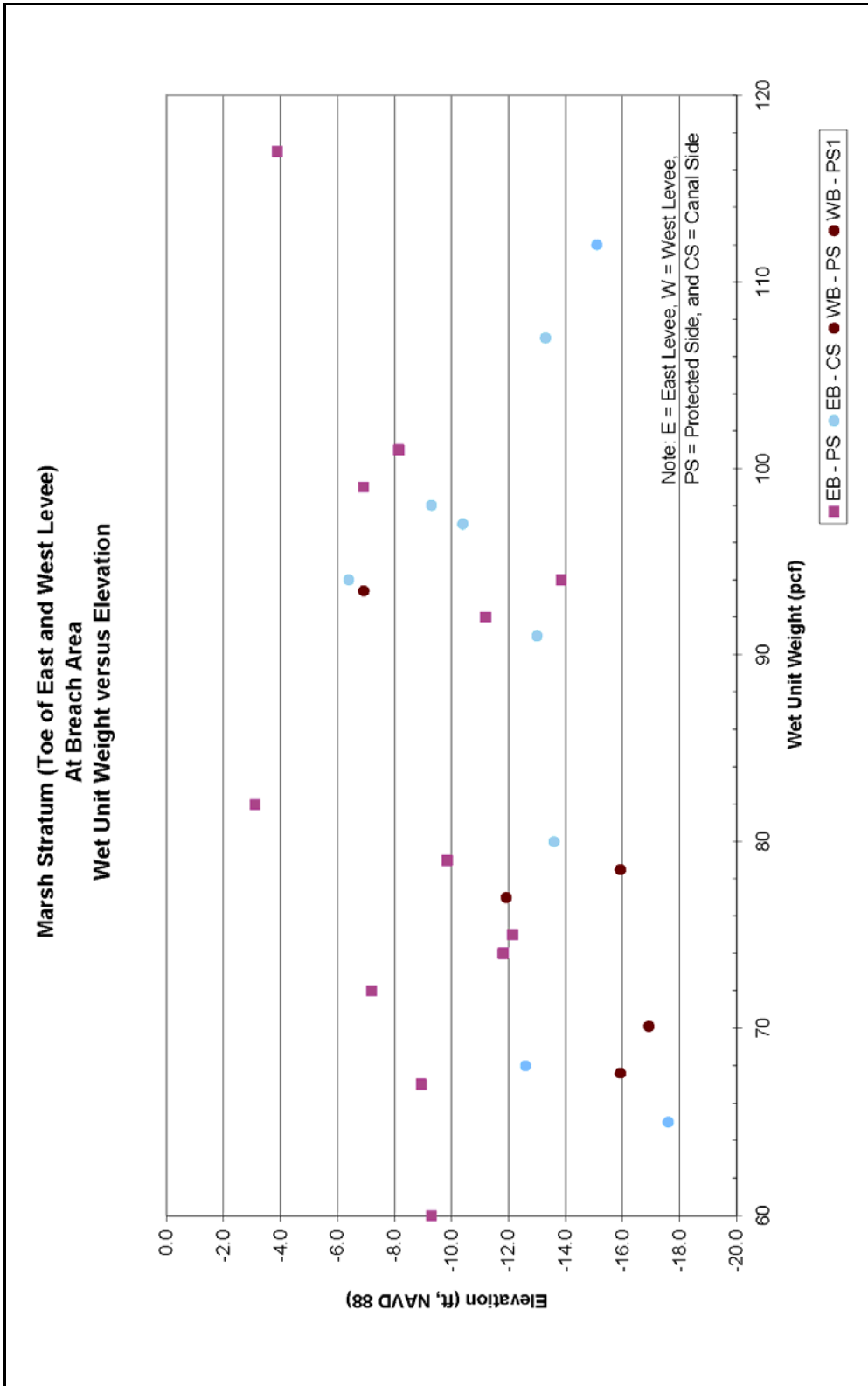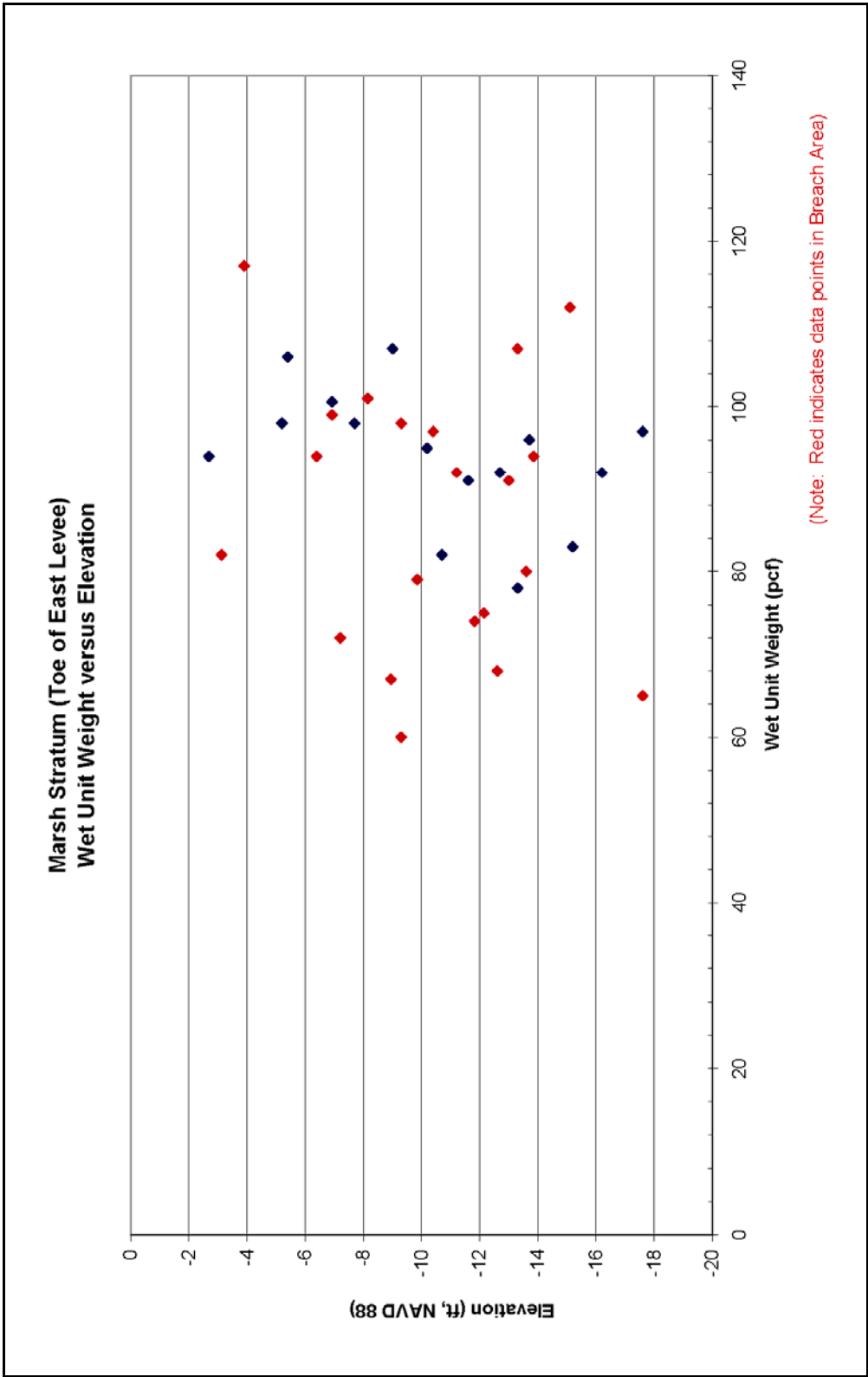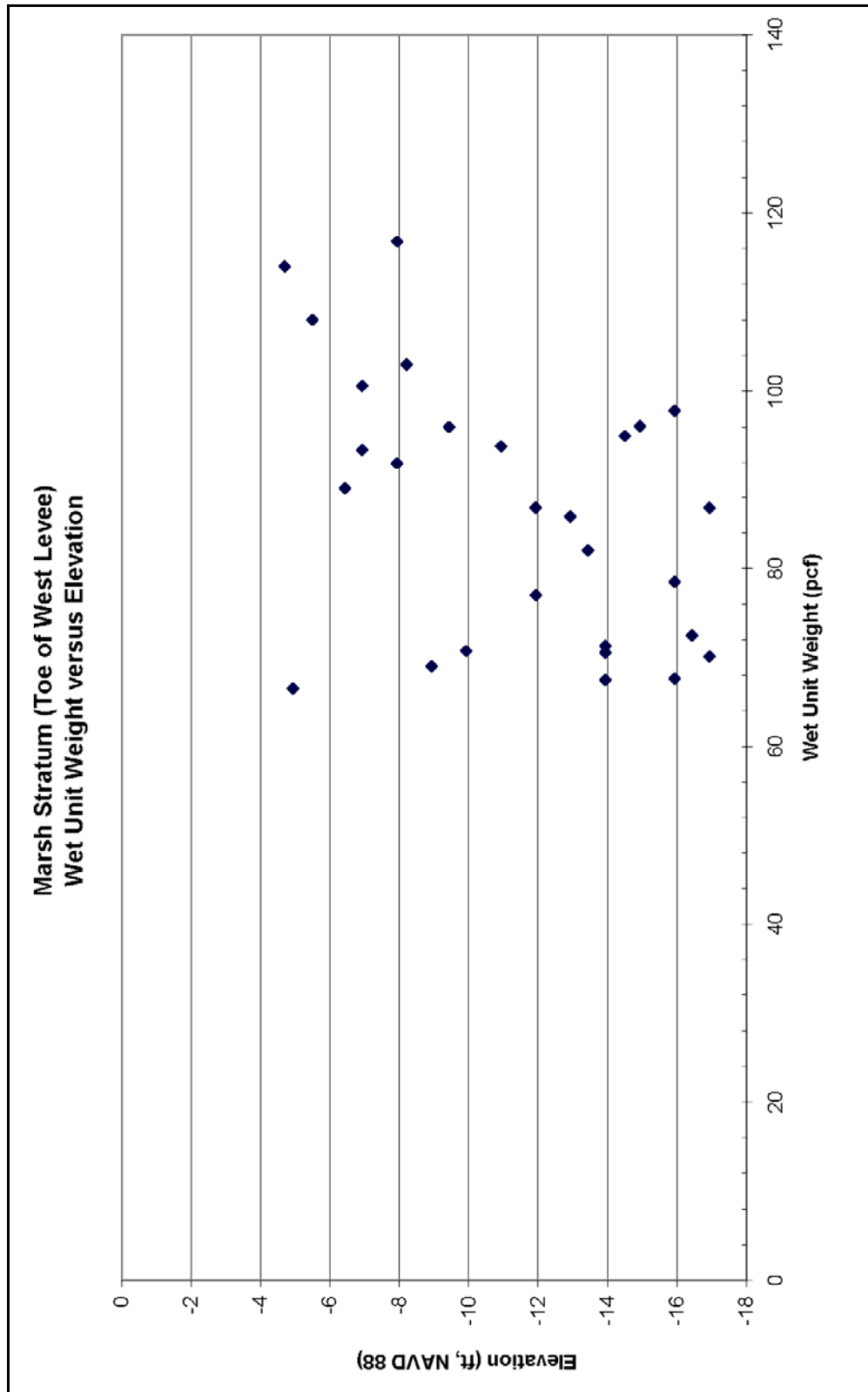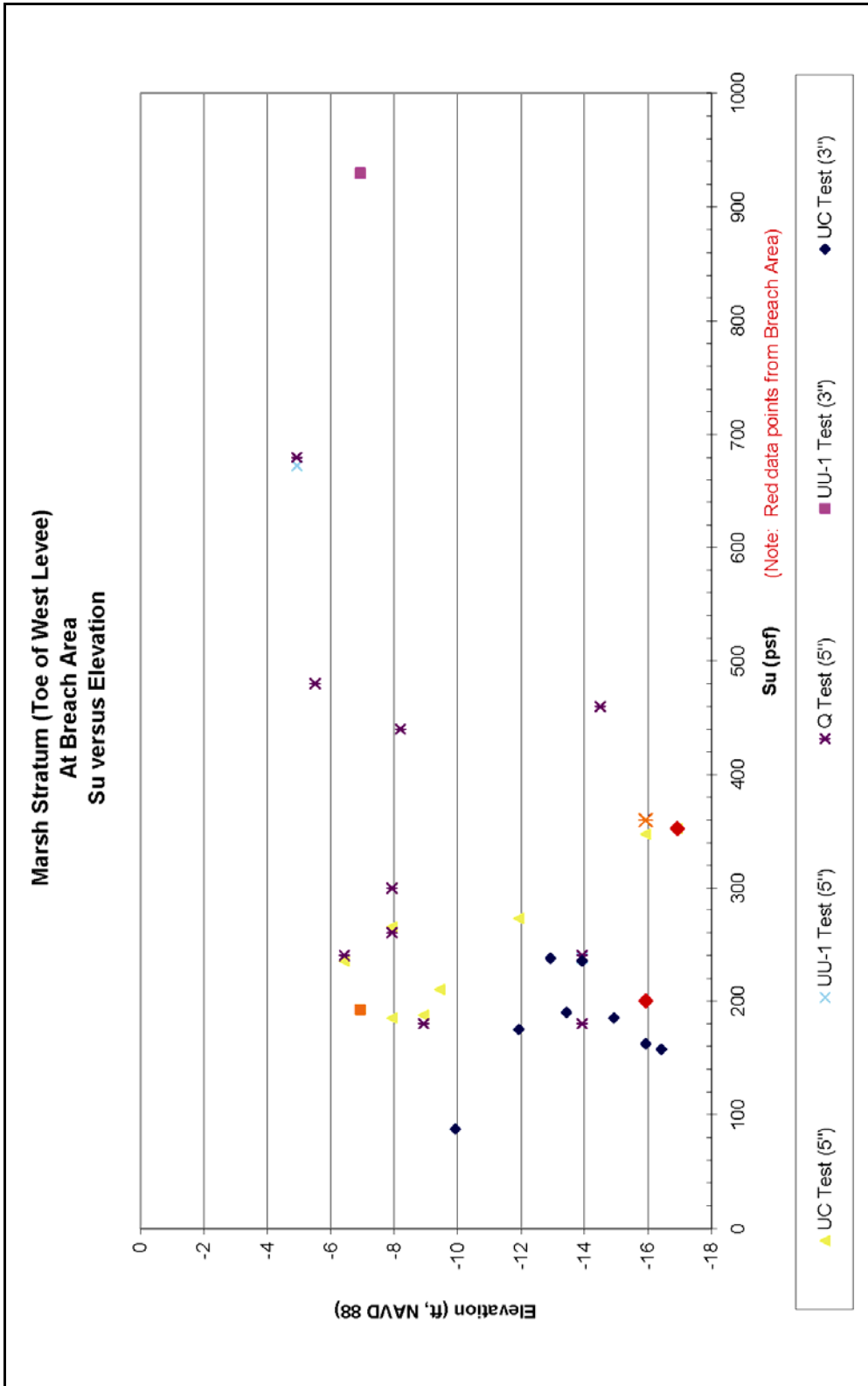Figure 1-44.   Marsh Stratum (Toe of West Levee), Su versus Elevation

    This is a preliminary report subject to revision; it does not contain final conclusions of the United States Army Corps of Engineers.
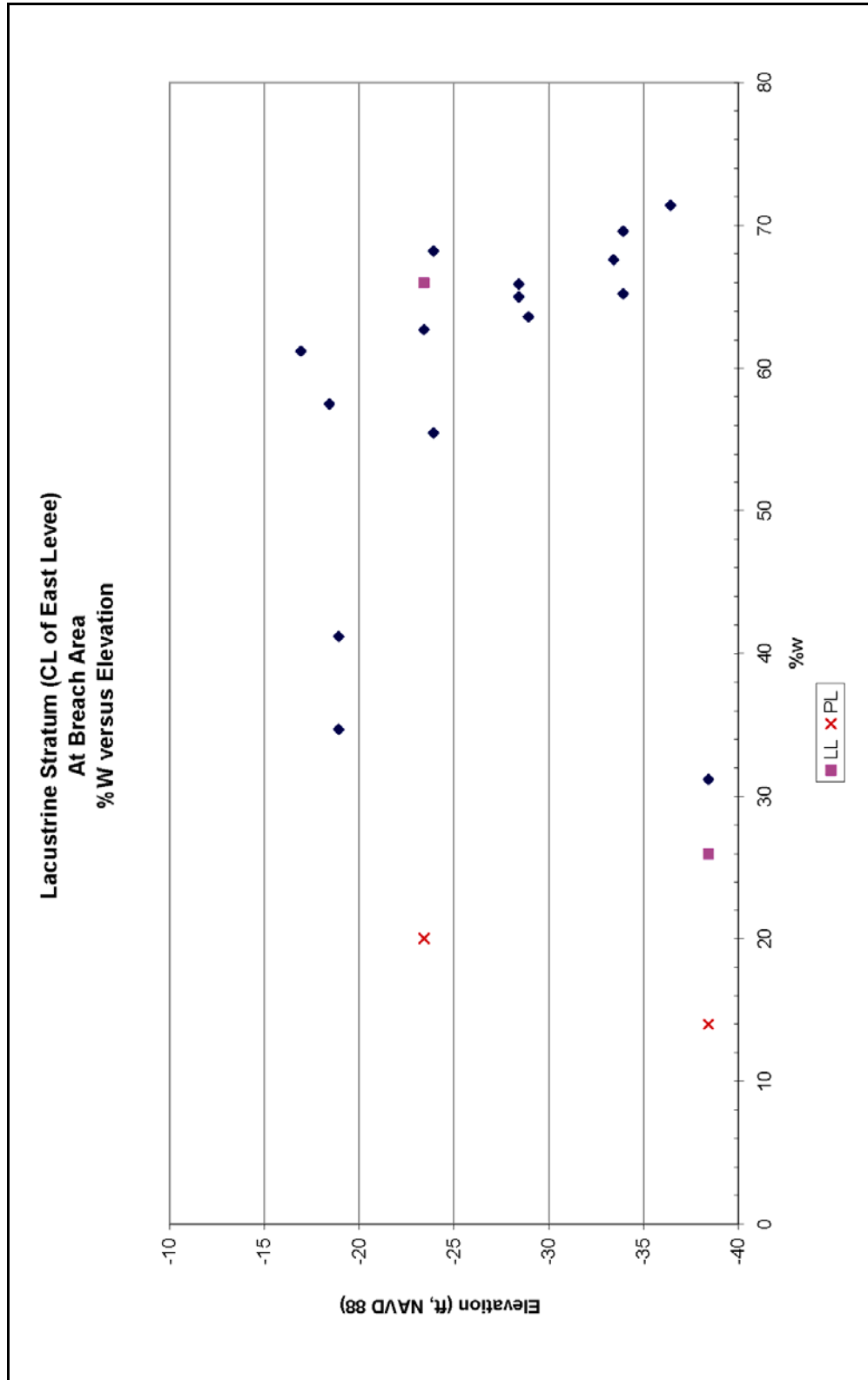
Figure 1-45.   Lacustrine Stratum (CL of East Levee – At Breach Area), %w versus Elevation
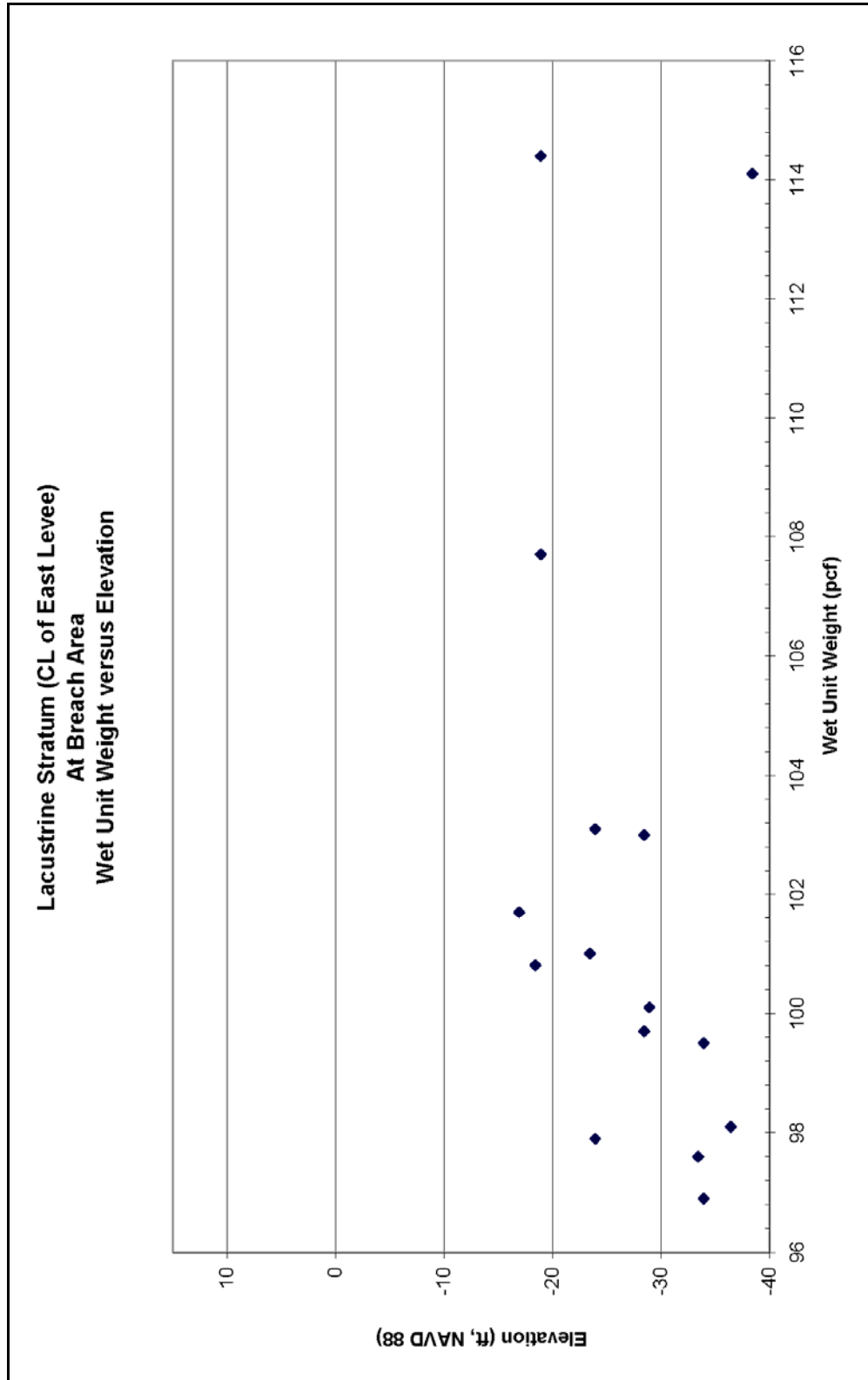
Figure 1-46.   Lacustrine Stratum (CL of East Levee – At Breach Area), Wet Unit Weight versus Elevation
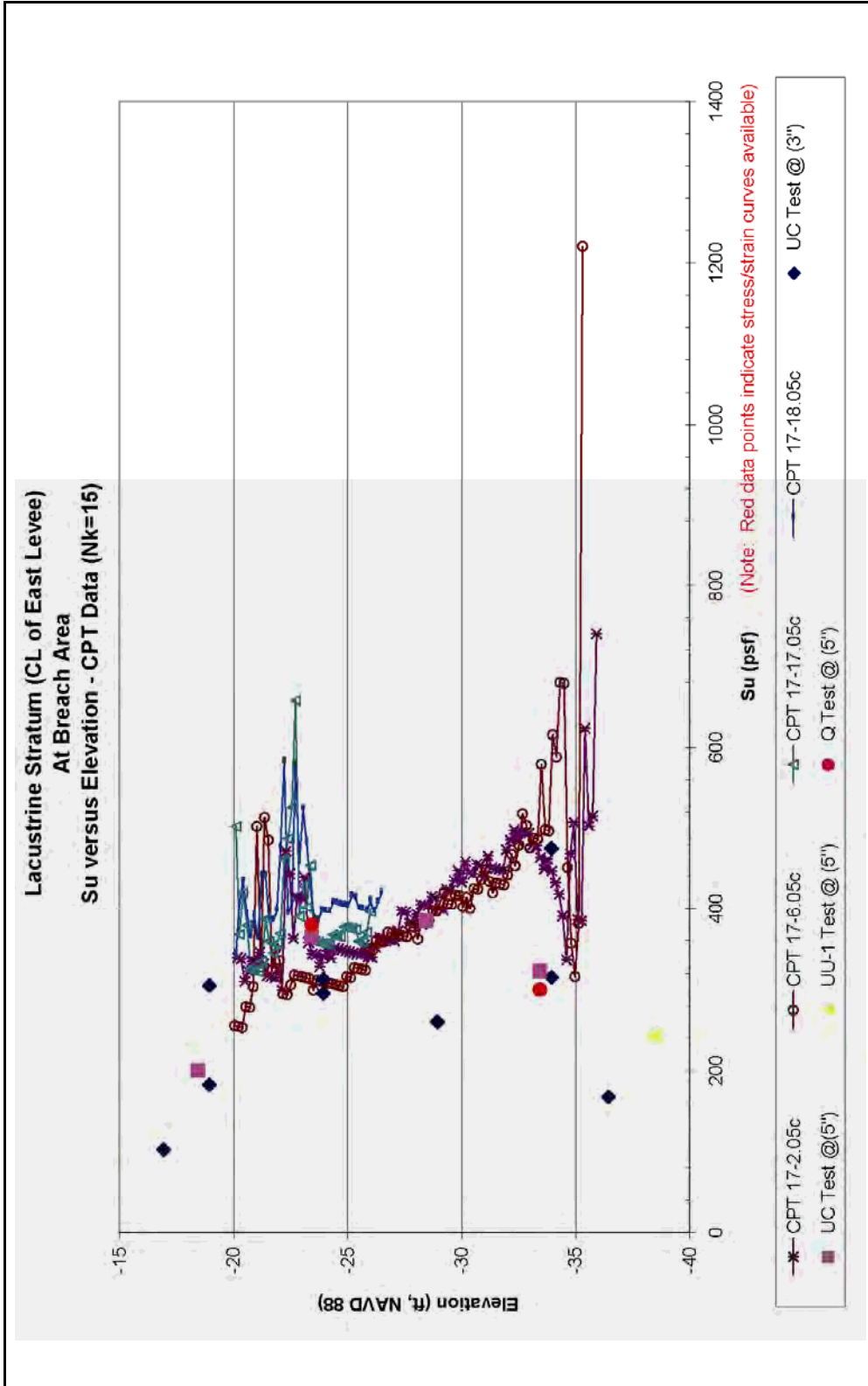
Figure 1-47.   Lacustrine Stratum (CL of East Levee – At Breach Area), Su versus Elevation (CPT Data – Nk=15)
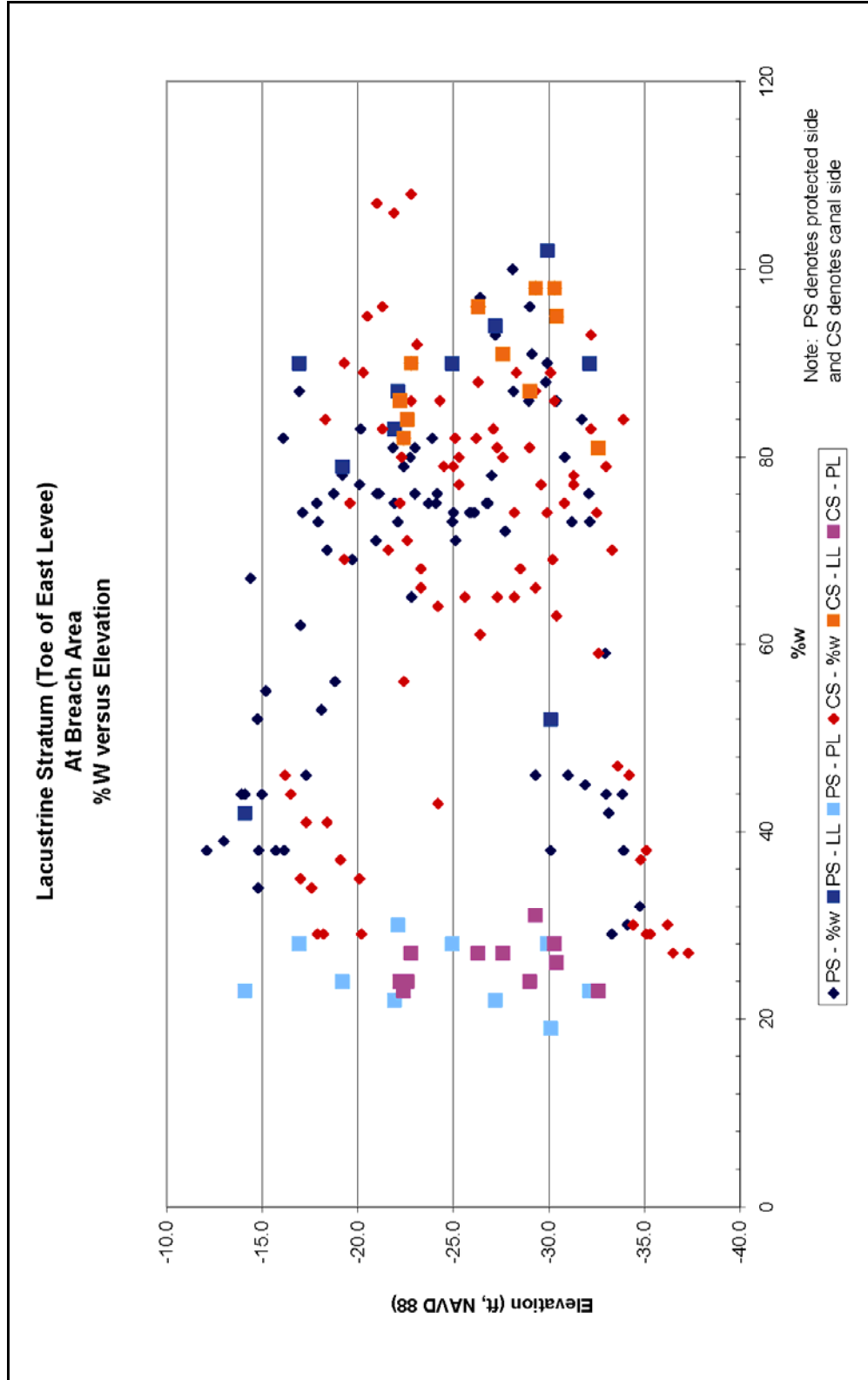
Figure 1-48. Lacustrine Stratum (Toe of East Levee – At Breach Area), %w versus Elevation

This is a preliminary report subject to revision; it does not contain final conclusions of the United States Army Corps of Engineers.
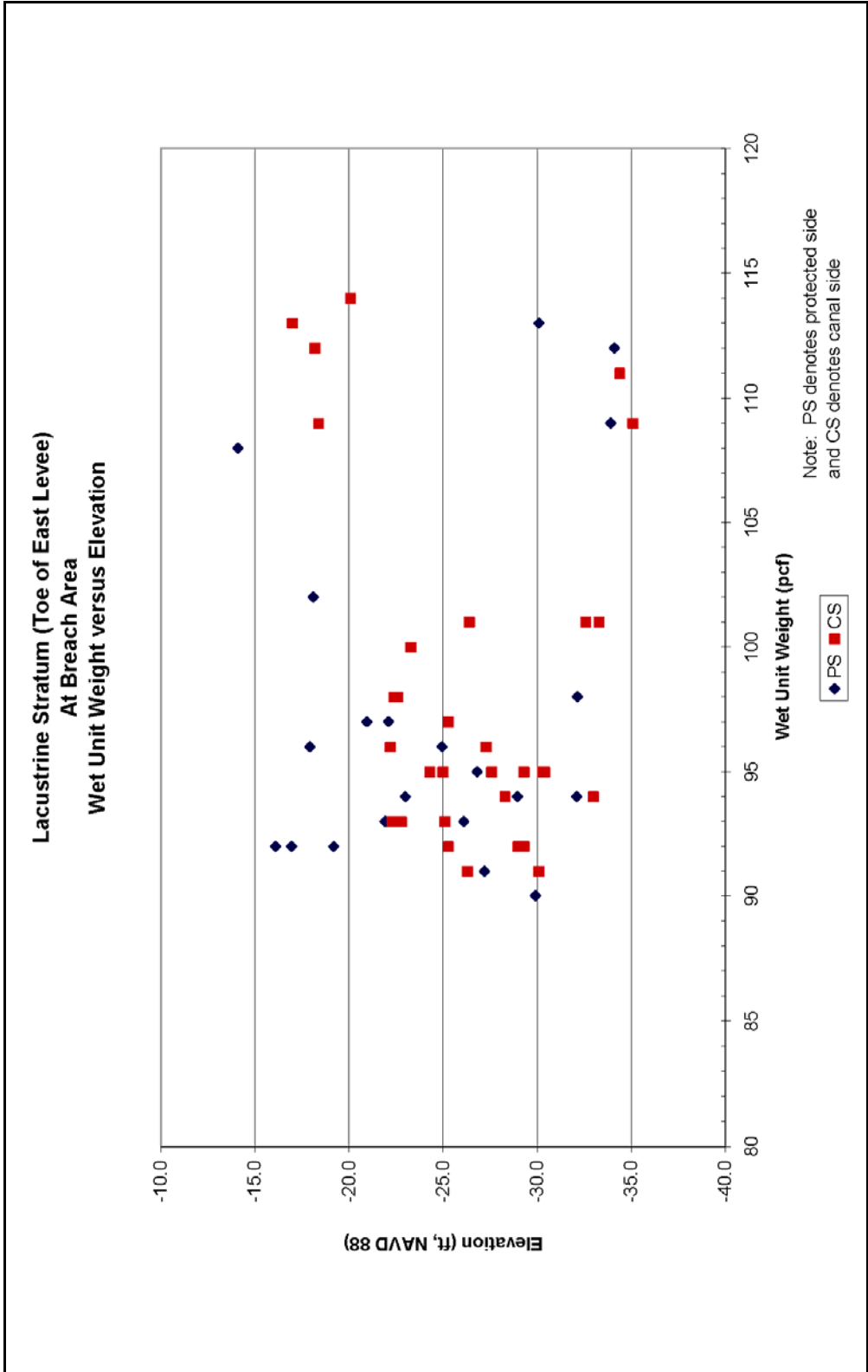
Figure 1-49. Lacustrine Stratum (Toe of East Levee – At Breach Area), Wet Unit Weight versus Elevation

Volume V The Performance – Levees and Floodwalls – Technical Appendix

V-1-59

This is a preliminary report subject to revision; it does not contain final conclusions of the United States Army Corps of Engineers.

The undrained shear strength determined from the laboratory tests conducted on samples in the breach area is shown in Figure 1-50. The Su/P ratio for the shear strengths samples is shown in Figure 1-51.

Beach Sand Stratum. Forty standard penetration tests (SPT) were conducted in the beach sand stratum in the breach area. The field (uncorrected) standard penetration number for the beach sand stratum is shown in Figure 1-52. Interpretation of the SPT number from the CPTs will be provided later. Dissipation tests with the CPT were conducted at this stratum at 17-2.05c and 17-6.05c. At 17-2.05c, the head in the sand was about 7.8 ft below the top of the hole or at elevation -3.68 (NAVD 88). At 17-6.05c, the head in the sand was about 6 ft below the top of the hole or at elevation -1.3 (NAVD 88).

Figure 1-50.   Lacustrine Stratum (Toe of East and West Levee – At Breach Area), Su versus Elevation

Figure 1-51. Lacustrine Stratum (East and West Levee), Su/P ratio versus Elevation

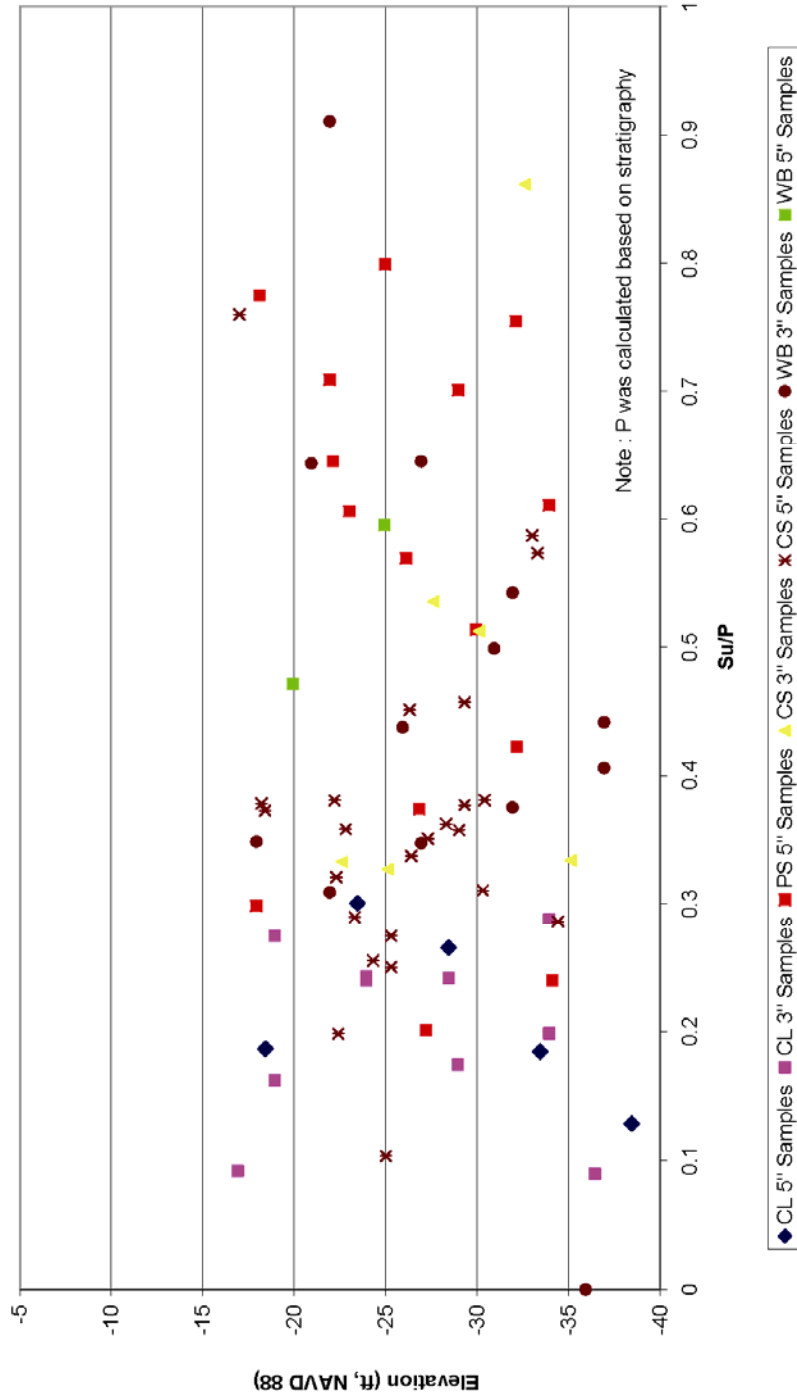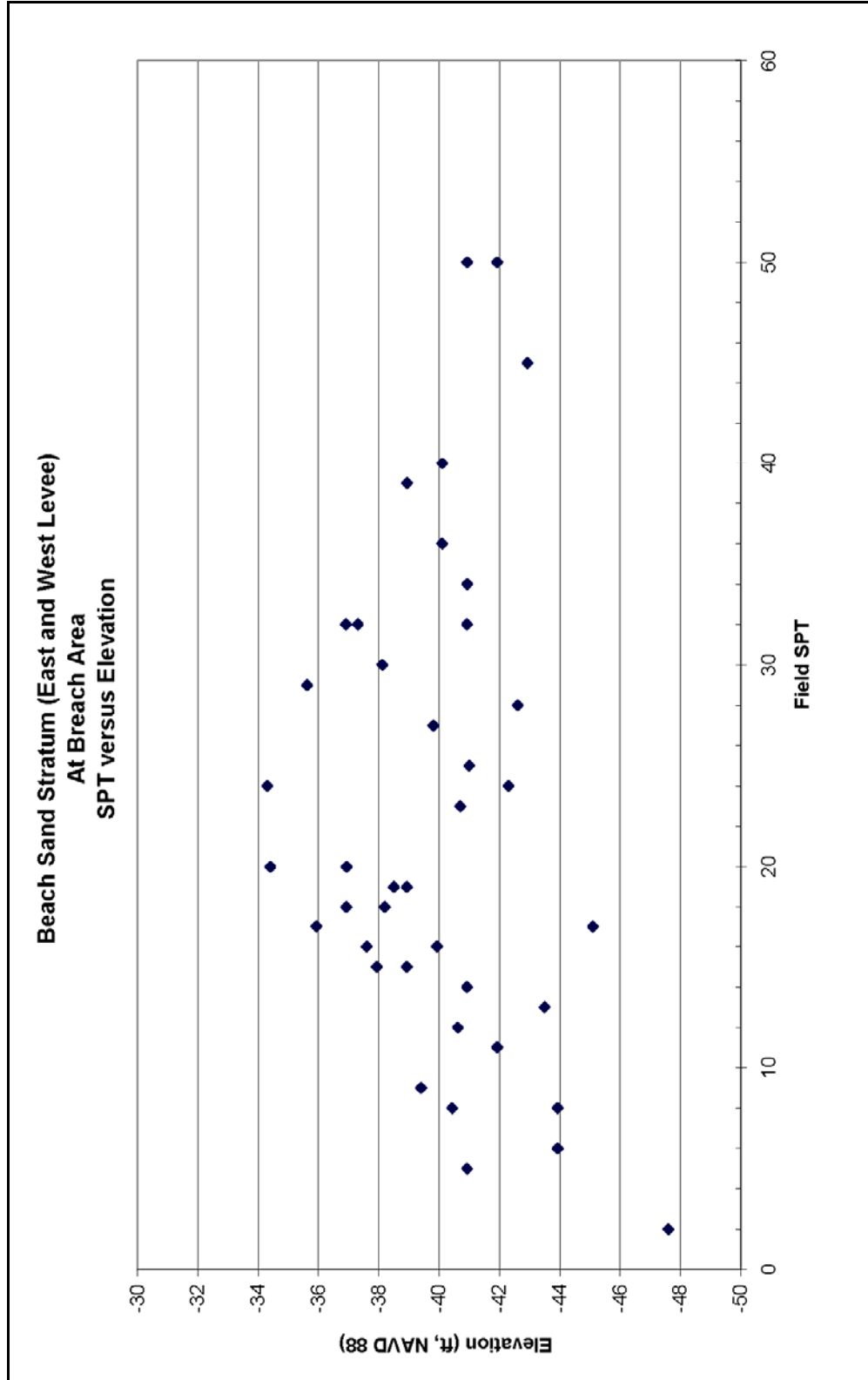Figure 1-52.   Beach Sand Stratum (East and West Levee – At Breach Area), Field SPT versus Elevation

Appendix 2
Description of New Orleans Area Geology, Environments of Deposition, and General Engineer Properties of these Environments

1   Introduction[1]

The following summary describes the geology and the Holocene history of the New Orleans area, and the relationships between the associated environments of deposition and general engineering properties. This information has been extracted from a technical report on the geological and geotechnical aspects of the Celotex Levee failure, which occurred along the west bank of the Mississippi River in 1985 in the greater New Orleans area (Figure 2-1). Only the geology sections are presented in this Appendix. This information serves as background information for evaluation of the various canal failures during Hurricane Katrina.

The geologic portions of the Celotex Report are presented in Chapter 2 and Appendix A. Chapter 2 describes the geologic history and geology of the New Orleans area as determined from a review of the technical literature, an evaluation of numerous engineering borings, aerial photo interpretation, and preparation of several detailed cross-sections (Figures 2-2 through 2-5 of Chapter 2, see enclosed). Appendix A of this same report provides detailed descriptions and information about the engineering properties of the depositional environments that are present at the surface and in the subsurface. Chapter 2 and Appendix A are presented here in their original order of presentation because of their logical arrangement in the text. The descriptions of the environments are important when examining soil types and physical properties from the respective environments.

Additionally, various references are identified in the text and are presented at the end of this summary appendix. Many of the Corps of Engineer cited publications and maps for the New Orleans area are now presented at the ERDC website on the Geology of the Lower Mississippi Valley (see lmvmapping.erdc.usace.army.mil)

A final note, the lacustrine environment is not identified in the summary description and is an important lithostratigraphic unit. This environment is unique to this area because of the protection afforded by the now buried Pine Island beach complex during the filling of the New Orleans area with subsequent sediment by the various Mississippi River distributary channels during the Middle to Late Holocene. The lacustrine environment has been mapped for the back or northern side of the beach ridge in various GDMs, while the front or seaward side has been mapped as being interdistributary. This distinction is primarily a matter of semantics, as opposed

---

[1] This appendix was extracted from Dunbar, J. B., Torrey, V. H., III, Wakeley, L. D., 1999. "A Case History of Embankment Failure, Geological and Geotechnical Aspects of the Celotex Levee Failure, New Orleans, Louisiana," Technical Report GL-99-11, Engineer Research and Development Center, Waterways Experiment Station, Vicksburg, MS.

to any significant differences between lithology and/or engineering properties of these respective two environments. For purposes of this discussion and overall context, these two environments are nearly identical. The discussion of the interdistributary environment will be representative for the lacustrine environment identified throughout many of the GDMs.
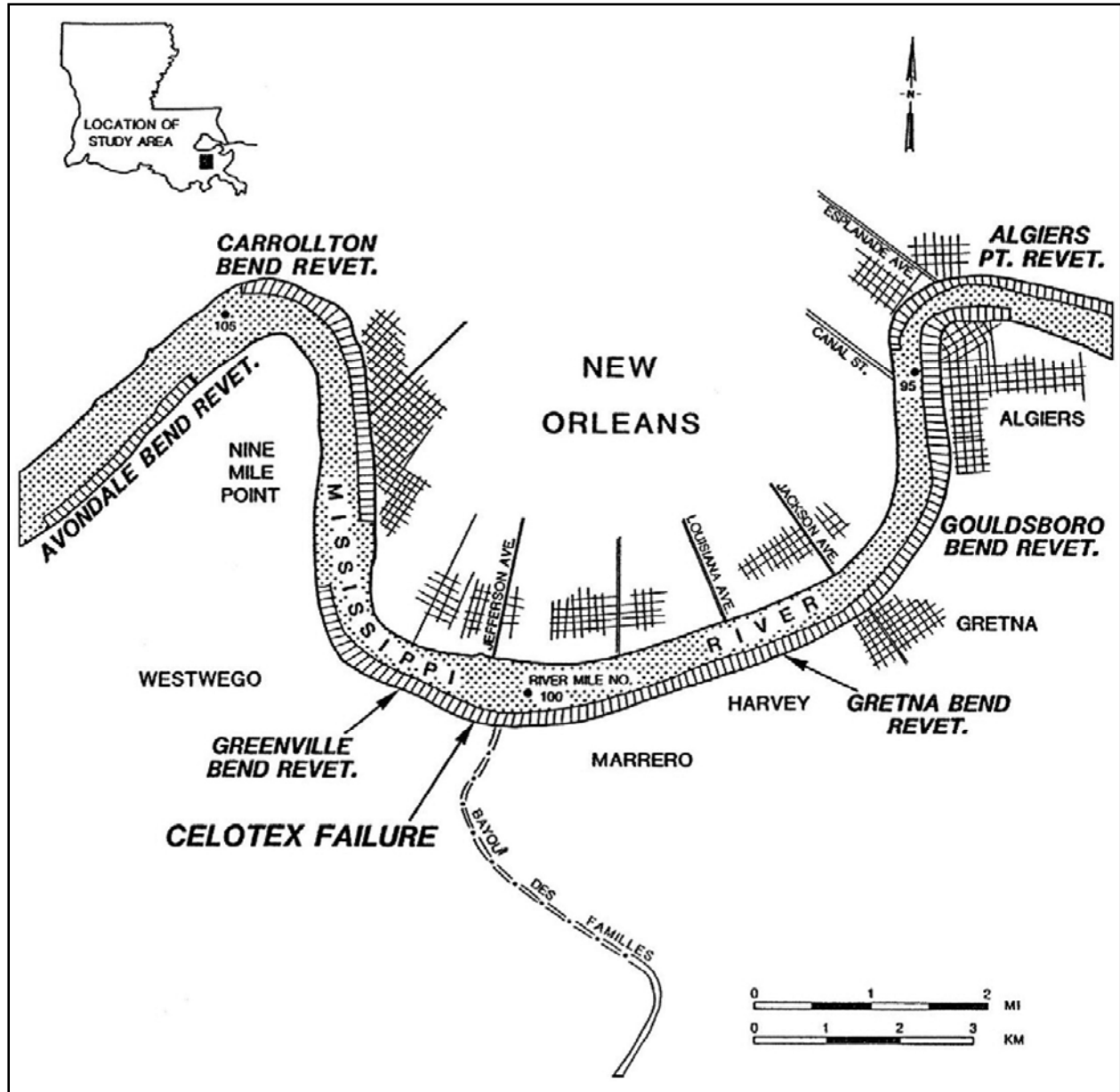
Figure 2-1. Map of study area showing location of the Celotex levee failure

2   Geology

Physiography

The study area is located in the southern portion of the lower Mississippi Valley and is a part of the Mississippi River's deltaic plain. Broad natural levees associated with the Mississippi River and Bayou des Familles, a prehistoric distributary channel, are the most prominent physiographic features in this area. Surface topography is generally of low relief with surface elevations ranging from approximately 25 ft (7.6 m) NGVD along the levee crests to sea level throughout much of the study area. Over a significant part of the New Orleans Metropolitan area the surface elevation is at or below sea level.

In the New Orleans area, the meander pattern of the Mississippi River is distinctive, making four nearly right angle turns which have changed very little during the past 100 years (Figure 2-1). The width of the Mississippi River within the study area (river mile 91.0 to 106.0 (146.45 to 170.59 km)) varies from 1,750 to 2,700 ft (533 to 823 m). The river thalweg elevations through this reach range from -70 ft (-21 m) to about -190 ft (-58 m) NGVD. The top of the bank elevation through the study reach averages about 10 ft (3 m) NGVD. Channel bendways are characterized by deep "permanent" scour pools separated by shallower crossings. Revetment protection along the river corresponds to the deeper scour pools at Avondale, Carrollton, Greenville, Gretna, Gouldsboro, and Algiers (Figure 2-1).

Geologic Setting and History

The scope of this study permits a summary of the major events to explain the significance of the engineering geology in the study area. The general geologic chronology that has been defined for the Mississippi River's deltaic plain is based upon thousands of engineering borings drilled during the past 50 years, hundreds of radiometric age determinations of organic deltaic sediments, and numerous geologic studies conducted in this region (Fisk 1944; Kolb and Van Lopik 1958a and 1958b; Kolb 1962; Kolb, Smith, and Silva 1975; Autin et al. 1991; Frazier 1967; Saucier 1969 and 1974; May et al. 1984; Dunbar et al. 1994 and 1995; Smith, Dunbar, and Britsch 1986). Boring data identify a diverse surface and subsurface geology that is related to the different course shifts by the Mississippi River and associated deltaic advances during the Holocene (last 10,000 years).

To better understand the geology of the area, it is first necessary to briefly review the geologic history of coastal Louisiana since the late Pleistocene (17,000 to 10,000 years ago). Approximately 17,000 years ago, glaciers covered much of North American and sea level was approximately 300 ft (91 m) below the present level (Kolb, Smith, and Silva 1975). The Gulf shoreline was much farther seaward than at its present location.

The ancestral Mississippi River and its tributaries below Baton Rouge, LA, were entrenched into the underlying Pleistocene surface and had developed a broad drainage basin, approximately 25 miles (40 km) wide, which extended southeasterly beneath the present deltaic plain (Kolb and Van Lopik 1958a). Geologic mapping (Kolb and Van Lopik 1958a and 1958b; May et al. 1984) indicates that the axis of the valley entrenchment occurs in the vicinity of Houma, LA, approximately 45 miles (72 km) southwest of New Orleans.

The underlying Pleistocene surface represents deposits from a much older Mississippi River deltaic plain sequence and associated nearshore environments. These sediments were deposited during the previous interglacial cycle (Sangamon interglacial period), approximately 125,000 to 70,000 years ago. Fisk (1944) collectively called these Pleistocene sediments the Prairie Formation. Sediments of the Prairie Formation outcrop at the surface just north of Lake Pontchartrain.

Sea level began rising approximately 17,000 years ago because of glacial melting and reached its present level between 4,000 and 6,000 years before the present. Rising sea level corresponds to a period of valley-wide aggrading of the ancestral alluvial valley by the existing fluvial systems. Melting glaciers released large quantities of sediment to the Pleistocene drainage system and filled the entrenched valley with coarse sediments (sand and gravel). A dense network of shallow and swiftly flowing braided stream courses formed within the ancestral alluvial valley because of overloading by the massive influx of glacial outwash. Along the length and width of the Lower Mississippi Valley, basal substratum sands are present in the subsurface which represent the relic braided stream or outwash plain sediments from glacial melting (Fisk 1944; Kolb et al. 1968; Krinitzsky and Smith 1969; Saucier 1964 and 1967; Smith and Russ 1974). The change in deposition from a braided system to a meandering Mississippi River system occurred approximately 12,000 years before the present (Saucier 1969; and Krinitzsky and Smith 1969).

Advent of the modern sea level began creation of the modern deltaic plain and led to the present land surface. Present day coastal Louisiana is the product of numerous, but generally short lived, seaward prograding delta systems. These deltas are subsequently reworked by coastal transgressive processes and modified. Five major deltaic systems have been built seaward during the past 6,000 years as shown by Figure 2-2 (after Frazier 1967). Each delta system consists of several major distributary channels and numerous individual delta lobes (Figure 2-3). The relative ages of these delta systems are generally well established by radiocarbon dating techniques. Limits of the different delta systems and the chronology of the major distributary channels associated with each system are summarized in Figures 2-2 and 2-3 (after Frazier 1967).

The first advance of a major delta system into the New Orleans area occurred with the St. Bernard system. The present course of the Mississippi River through the New Orleans area

was established during the active St. Bernard delta. Partial Mississippi River flow continued to pass through the New Orleans reach following abandonment of the St. Bernard system for the Lafourche delta complex. During the active Lafourche system, the Mississippi River flowed southward at Donaldsonville, through Bayou Lafourche, and to the Gulf of Mexico. After abandonment of the Lafourche system approximately 500 years ago, nearly full Mississippi River flow returned to the present day course.
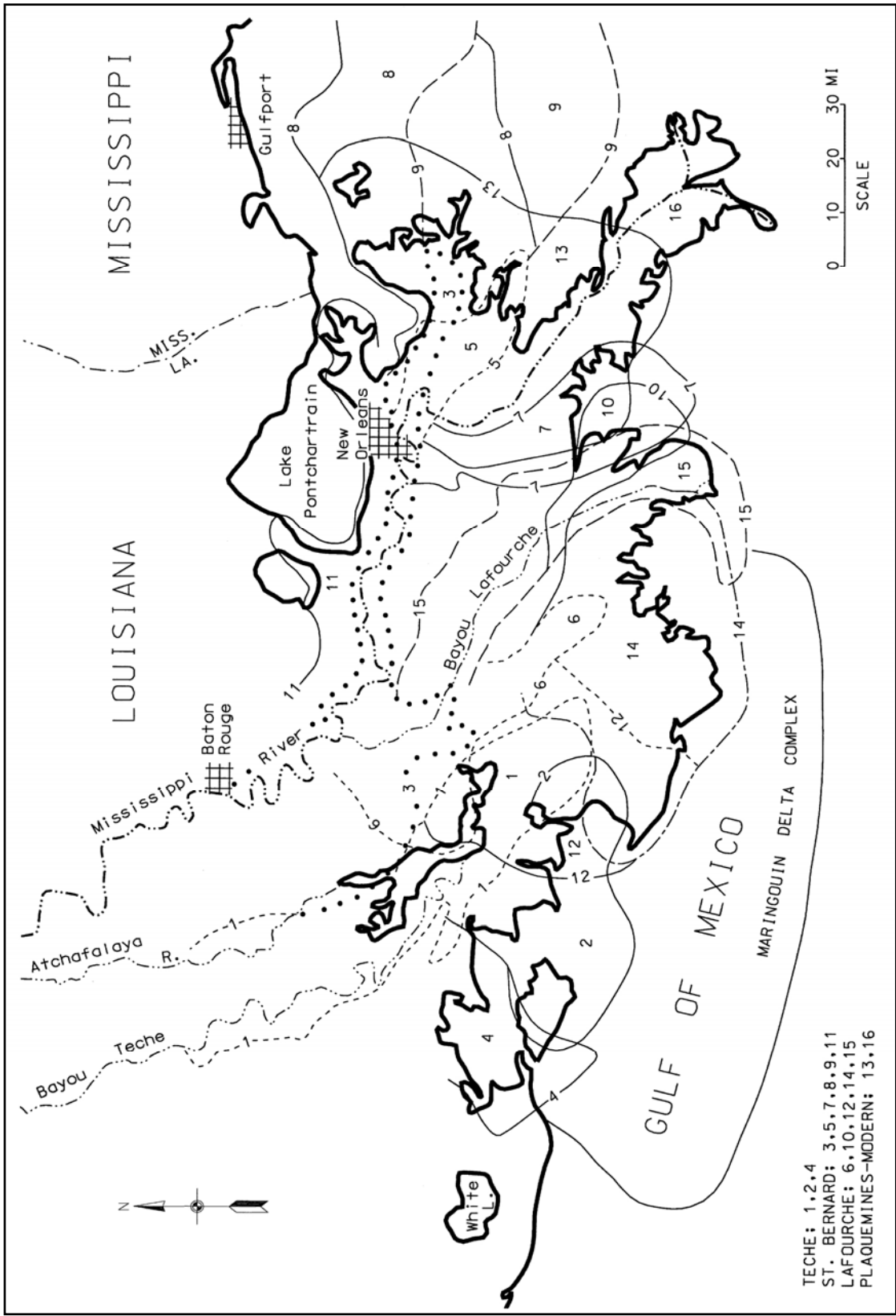
Figure 2-2. Holocene delta and distributary systems (after Frazier 1967)

TECHE: 1,2,4
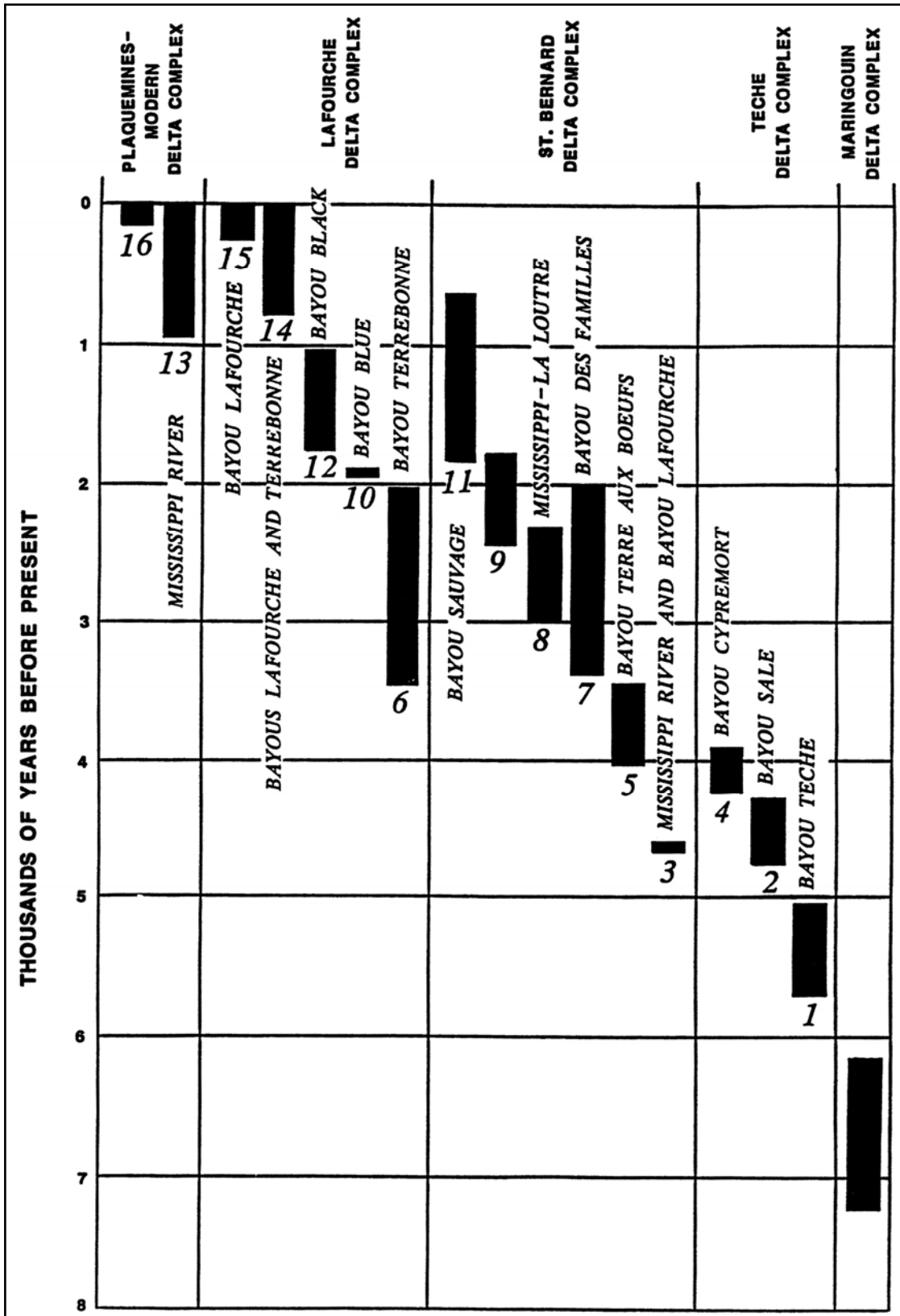ST. BERNARD: 3,5,7,8,9,11
LAFOURCHE: 6,10,12,14,15
PLAQUEMINES-MODERN: 13,16

Figure 2-3. General chronology of Mississippi River delta and distributary systems (after Frazier 1967)

Volume V The Performance – Levees and Floodwalls – Technical Appendix

Geologic Structure

The study area is part of the seaward thickening wedge of Quaternary sediments which dip gently gulfward and fill the Gulf of Mexico geosyncline. Major structures within this sedimentary prism are piercement salt domes and growth faults. In the study area there are no buried salt domes. The vast majority of Louisiana's salt domes are located south and west of the New Orleans area (New Orleans Geological Society 1962 and 1983; and Halbouty 1967).

Faulting has been identified in the subsurface throughout the deltaic plain and in the Pleistocene deposits exposed at the surface north of Lake Pontchartrain (Wallace 1966; and Snead and McCulloh 1984). These faults are not tectonically active. Instead, they are related to sedimentary loading of the Gulf of Mexico basin. Faulting has been identified in the Pleistocene sediments beneath Lake Cataouatche (approximately 8 miles (12.8 km) southwest of New Orleans) and beneath Lake Pontchartrain (Wallace 1966; and Kolb, Smith, and Silva 1975). Fisk (1944) identified several normal faults in the buried Pleistocene sediments beneath New Orleans. He interpreted these faults based on the orientation of stream courses, lake shores, and the Mississippi River. The presence of these faults based solely on this type of evidence is speculative without more detailed stratigraphic evidence to support their existence. Non-tectonic geomorphic and stratigraphic processes can produce these types of linear features without faulting as the underlying mechanism. A detailed engineering study of Pleistocene sediments in the New Orleans area by Kolb, Smith, and Silva (1975) did not identify subsurface faults near the Celotex failure site or for the general New Orleans area. Their study identified only one fault in the New Orleans area (in Lake Pontchartrain) and was based on combined boring and geophysical (subbottom profiling) data.

No faults were identified during this investigation in the study area. Surface faults in Holocene sediments are difficult to detect, because unconsolidated sediments tend to warp rather than shear. Geologic mapping and boring data evaluated during the course of this study did not identify any surface or subsurface faulting in the study area.

Geology and Environments of Deposition

Surface geology

The first objective of this investigation was to map and define the surface and subsurface geology of the study area. Definition of the geology was accomplished by examination and interpretation of historic aerial photography, subsurface data (engineering borings and electrical logs), different hydrographic survey periods, historic maps, and by review of the available geologic literature (Autin et al. 1991; Eustis Engineering Company 1984; Frazier 1967; Kemp 1967; Kolb 1962; Kolb and Van Lopik 1958a and 1958b; Kolb, Smith, and Silva 1975; Kolb and Saucier 1982; Miller 1983; Saucier 1963; Self and Davis 1983). A map of the surface geology for the study area is presented in Figure 2-4.
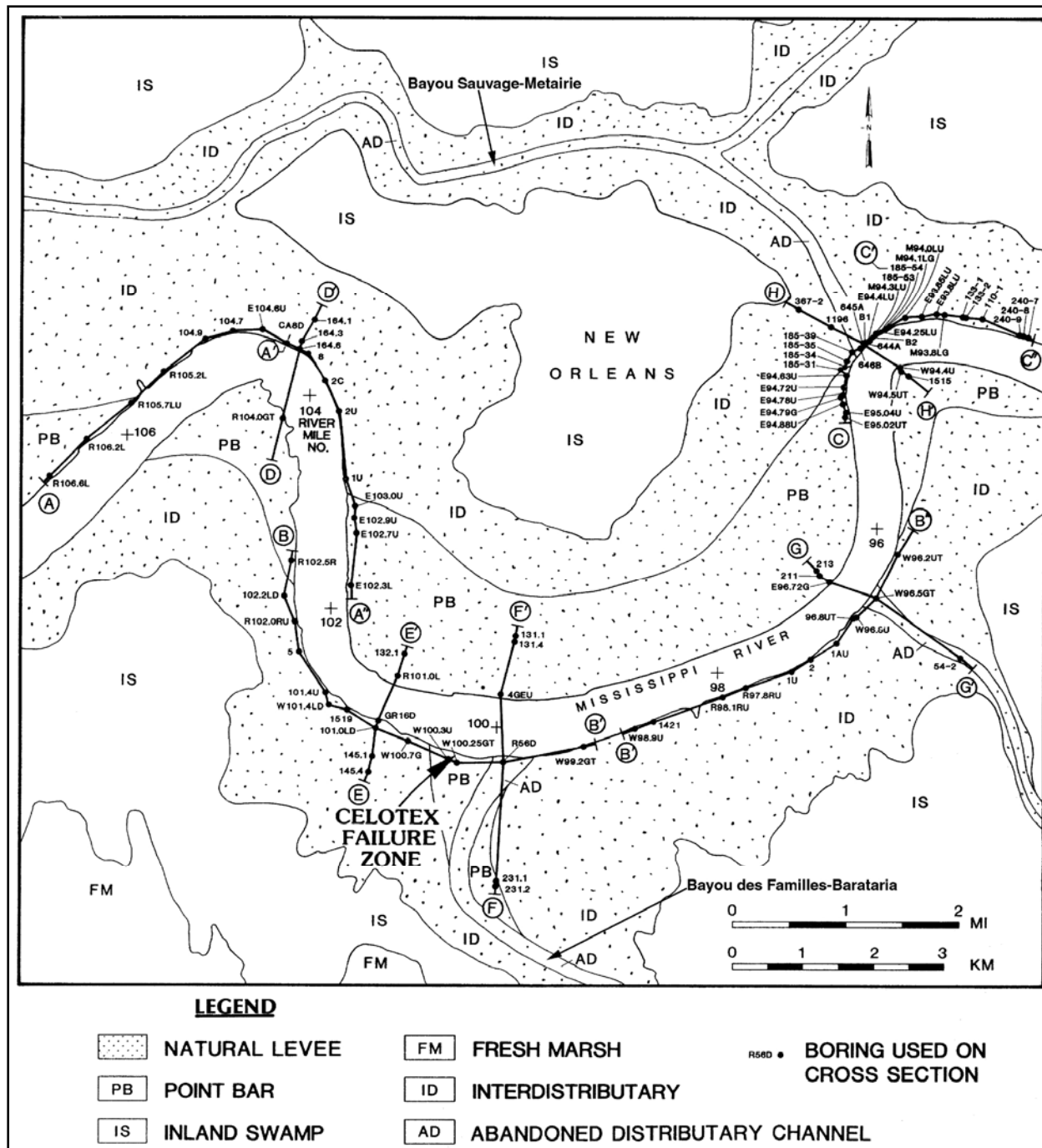
Figure 2-4. Geologic map of the study area showing boring and cross section locations

Environments of deposition mapped at the surface in Figure 2-4 include natural levee, point bar, inland swamp, fresh marsh, and several abandoned distributary channels. A complete description of the different environments of deposition present in the study area is contained in Appendix A. Natural levee deposits identified on the geologic map in Figure 2-4 are shown with the underlying environment of deposition. The surface geology consists primarily of Mississippi

River natural levee and point bar deposits, several abandoned distributary channels, and their associated fluvial and deltaic deposits.

Formation of the study area is directly related to the past and present courses of the Mississippi River and its abandoned distributary channels. Abandoned distributary channels within the study area are associated with two major distributary systems, Bayou des Familles-Barataria and Bayou Sauvage-Metarie Bayou (Figure 2-4). Bayou Des Familles-Barataria is a major St. Bernard distributary channel or Mississippi River course which extends due south from the Mississippi River at the Celotex failure site to Barataria, LA. This distributary system was active from approximately 2,000 to 3,400 years before the present (Frazier 1967).

The second major distributary course mapped in the study area is Bayou Sauvage-Metarie Bayou. According to Frazier (1967), this course was active from about 800 to 1,800 years before the present (Figure 2-3). However, Saucier (1963) and Kolb and Van Lopik (1958a) indicate that this system may have been active even earlier. Radiocarbon dates from organic sediments beneath the natural levees of Metarie Bayou range from 2,300 to 2,600 years before the present and indicate that a marsh surface was developed within this area. Metarie Bayou intersects the Mississippi River at Kenner and extends eastward, branching into two segments north of Algiers Point. The northern branch extends northeast toward Chef Menteur, Louisiana, as Bayou Sauvage. The southern branch, labeled Unknown Bayou by Saucier (1963), intersects the Mississippi River at Algiers Point (Figures 2-1 and 2-4), follows the Mississippi River between Algiers Point and Gretna, and then extends due southeast where it intersects the Mississippi River at 12 Mile Point.

Subsurface geology

Eight geologic cross sections were constructed from borings collected and evaluated during this study. The locations of the cross sections are shown on the geologic map in Figure 2-4. Cross sections A through H are presented as Figures 2-5a through 2-5k, respectively. The longer cross sections are presented as two separate sections or figures for illustration purposes. A legend of symbols and soil types identified on the sections is presented in Figure 2-5l. Sections were constructed such that each revetment reach includes sections parallel and perpendicular to the river bank. Parallel sections were constructed for only the cutbank or concave side as this is the side for maximum erosion and potential bank instability. The majority of soil types shown on the geologic sections are classified according to the Unified Soil Classification System (USCS). Borings not using the USCS (e.g., borings from private engineering companies) are shown with their textural soil types identified. The geologic cross sections show the vertical and horizontal limits of the various environments of deposition adjacent to the river as well as the soil types that form these different environments. Depositional environments present in the subsurface include interdistributary, intradelta, and nearshore gulf. A general description of these environments is contained in Appendix A. For readers desiring further engineering soils data beyond what is presented in this report, a detailed summary of soil engineering properties for the various environments of deposition is presented by Kolb (1962) and Montgomery (1974).
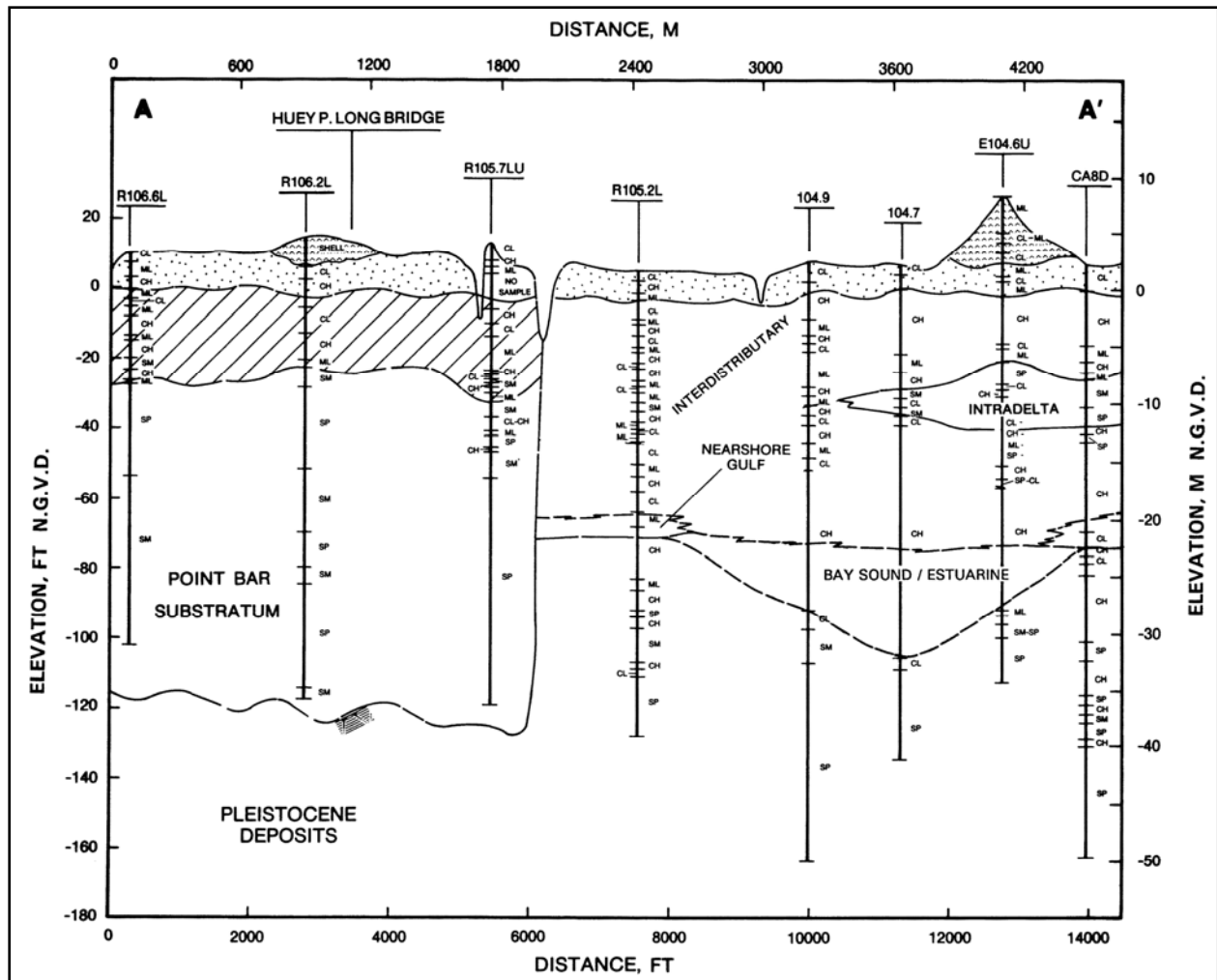
Figure 2-5a. Geologic cross section A-A' (see Figure 2-5l for symbol legend)
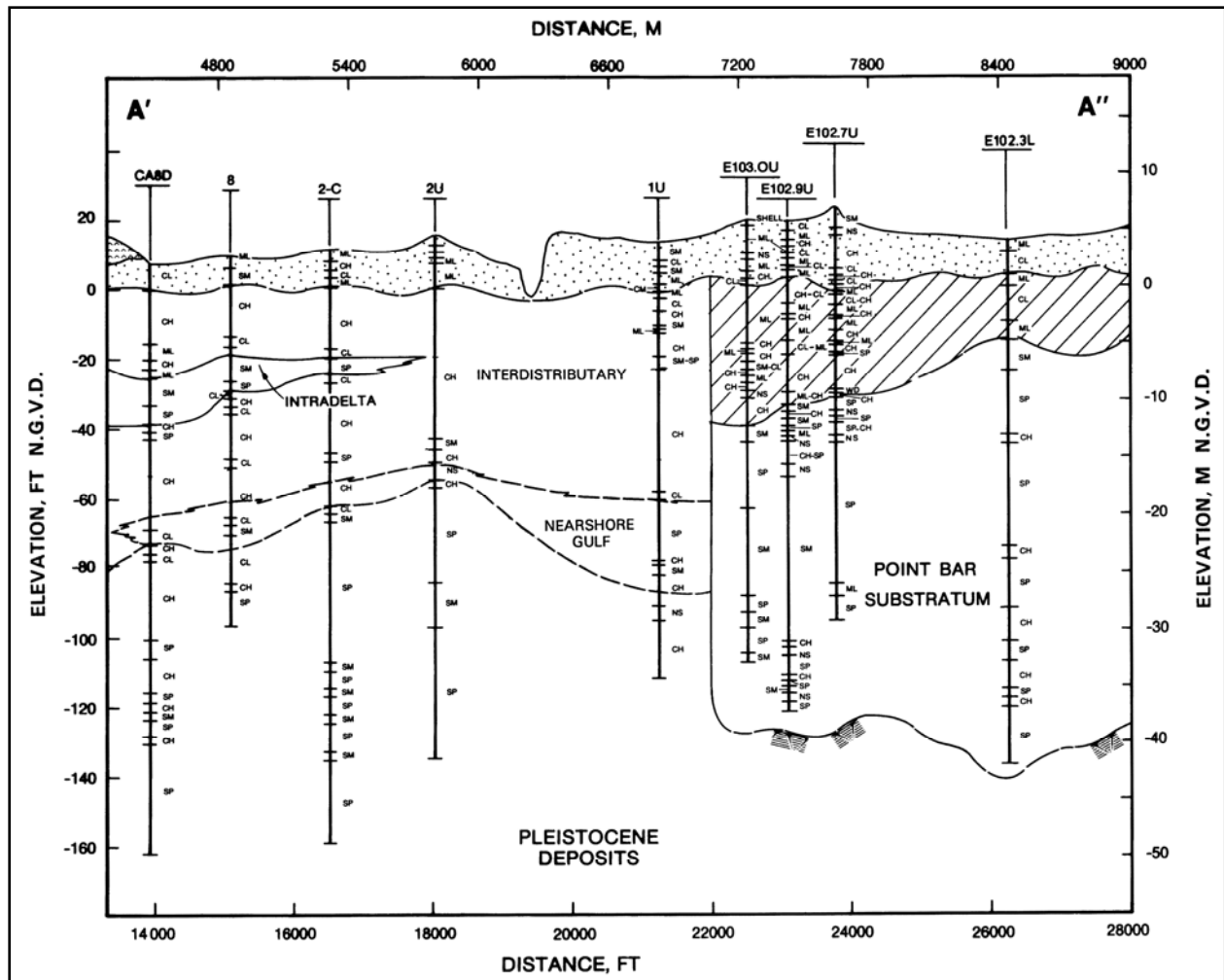
Figure 2-5b. Geologic cross section A'-A" (see Figure 2-5l for symbol legend)
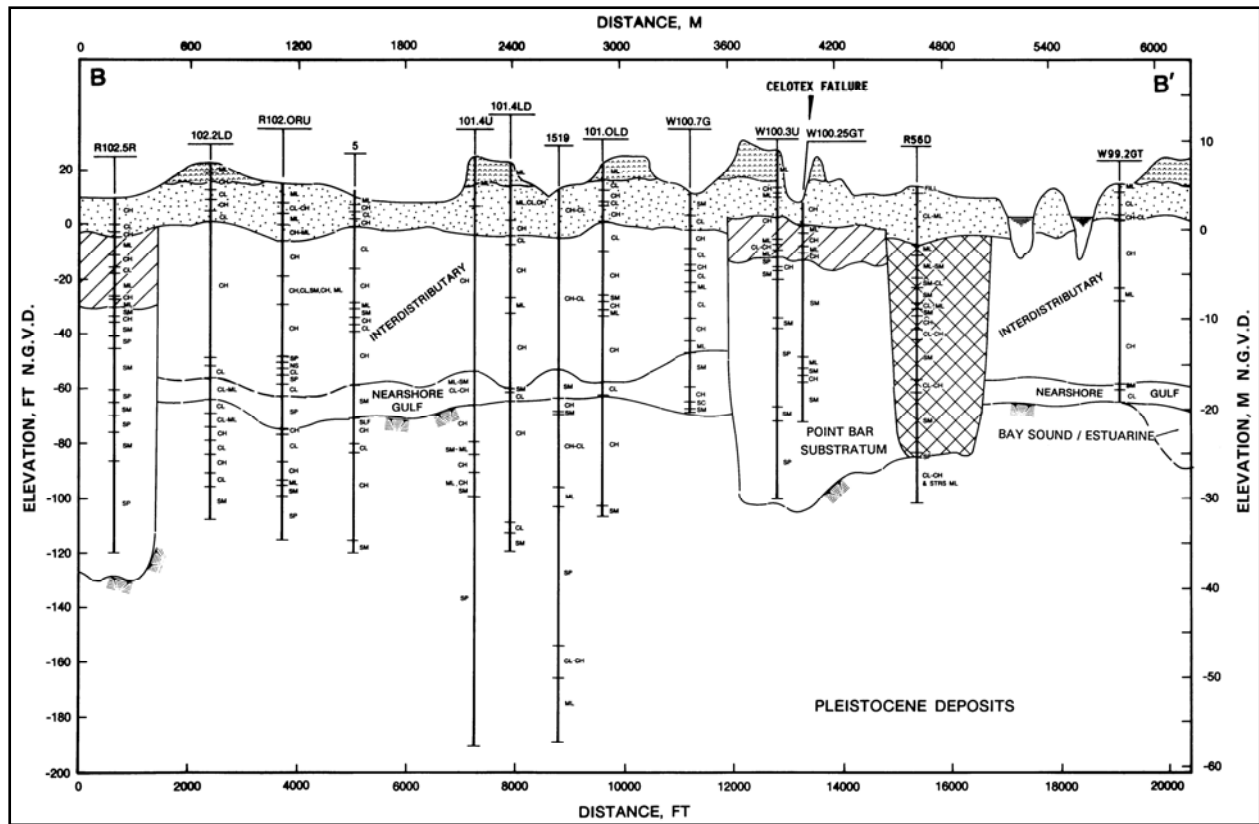
Figure 2-5c. Geologic cross section B-B' (see Figure 2-5l for symbol legend)
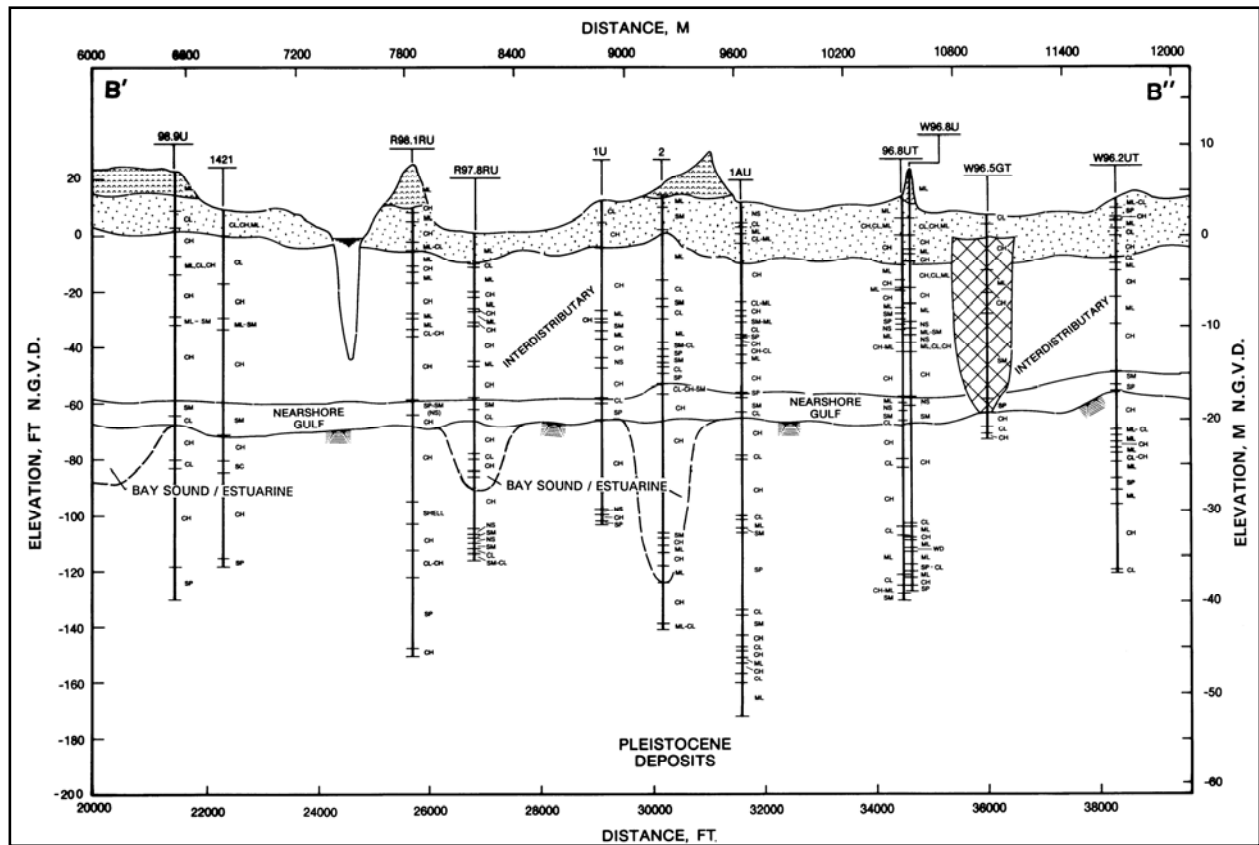
Figure 2-5d. Geologic cross section B'-B" (see Figure 2-5l for symbol legend)

Volume V The Performance – Levees and Floodwalls – Technical Appendix

V-2-15

This is a preliminary report subject to revision; it does not contain final conclusions of the United States Army Corps of Engineers.

Figure 2-5e. Geologic cross section C-C' (see Figure 2-5l for symbol legend)

Figure 2-5f. Geologic cross section C'-C" (see Figure 2-5l for symbol legend)
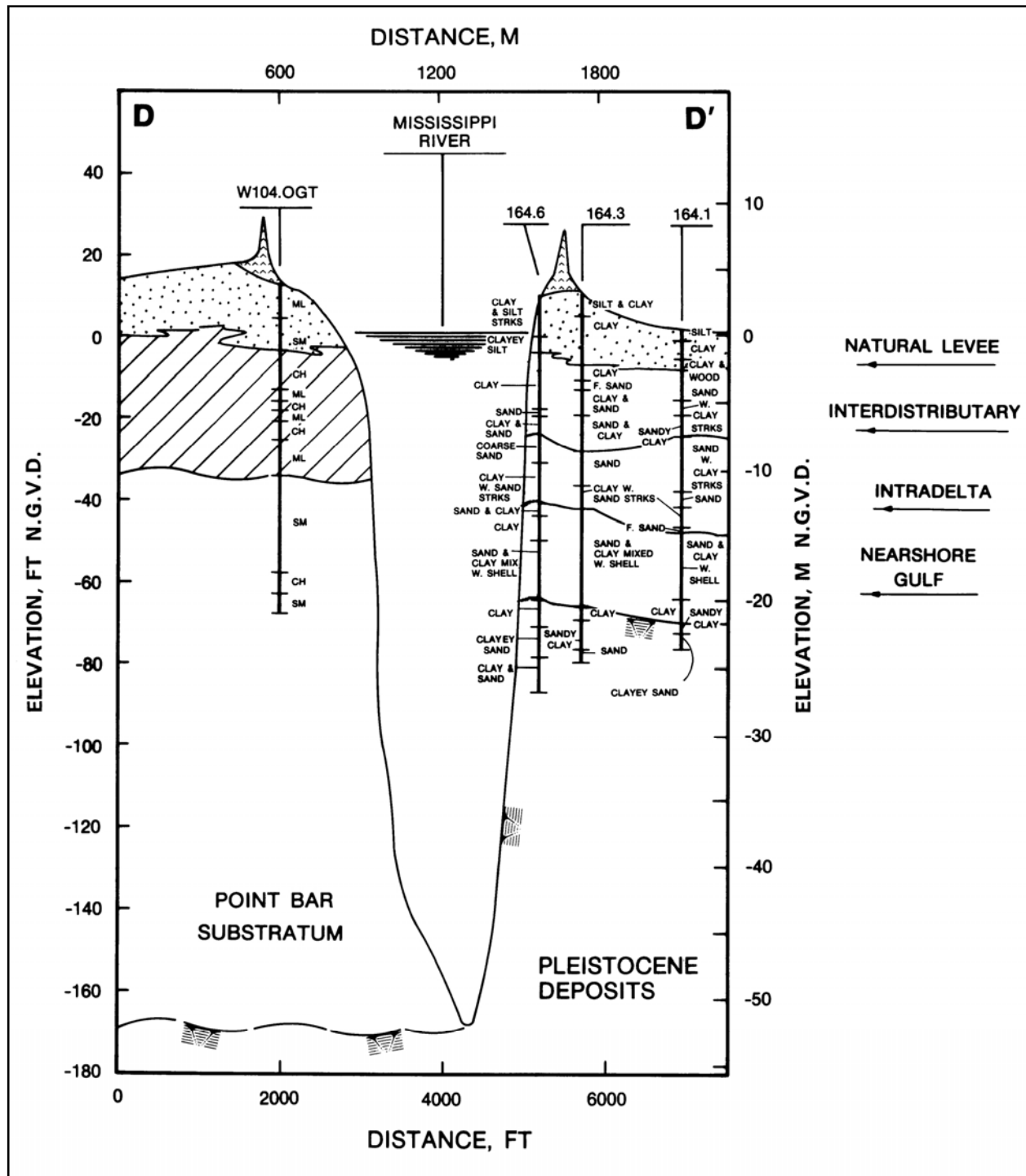
Figure 2-5g. Geologic cross section D-D' (see Figure 2-5l for symbol legend)
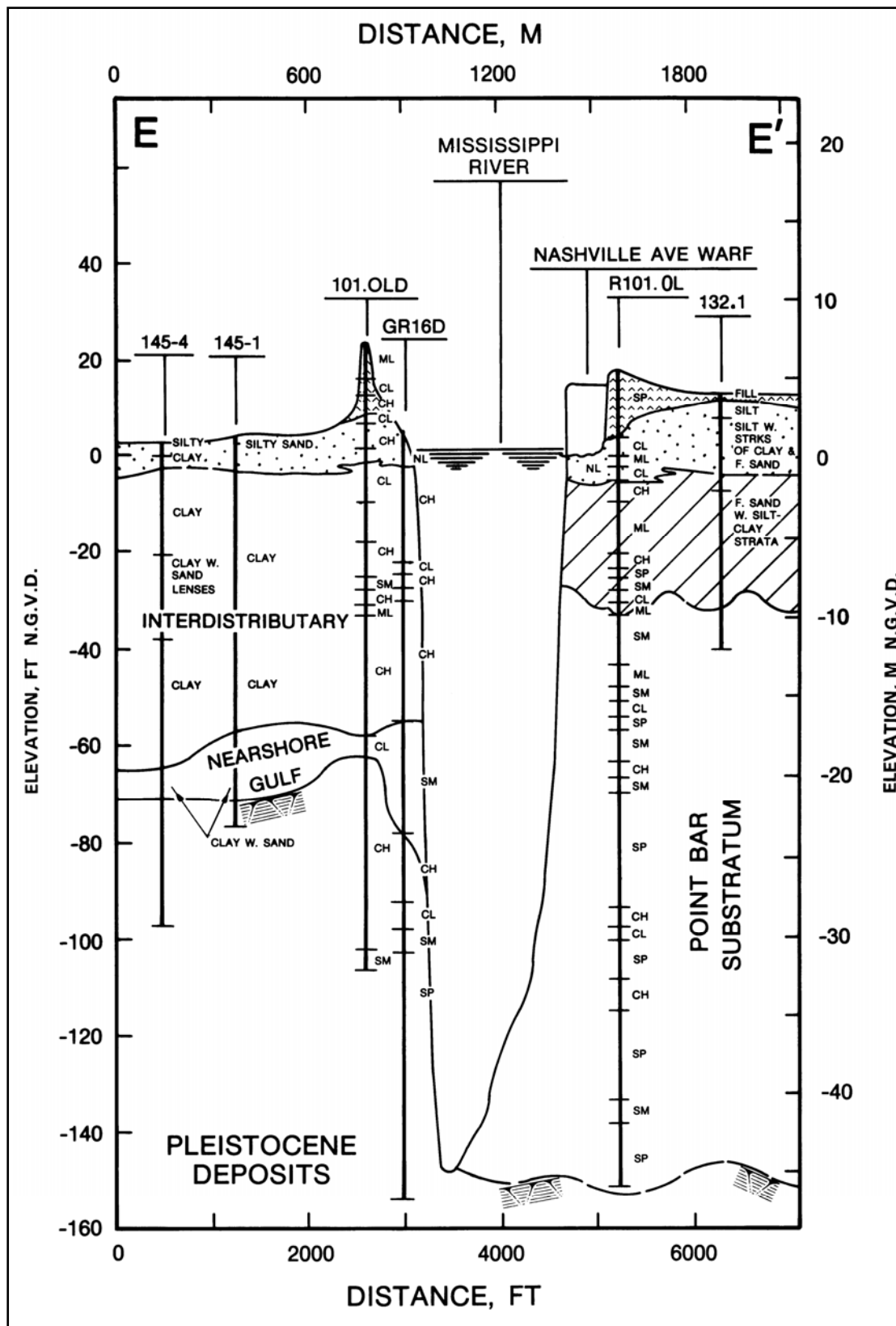
Figure 2-5h. Geologic cross section E-E' (see Figure 2-5l for symbol legend)
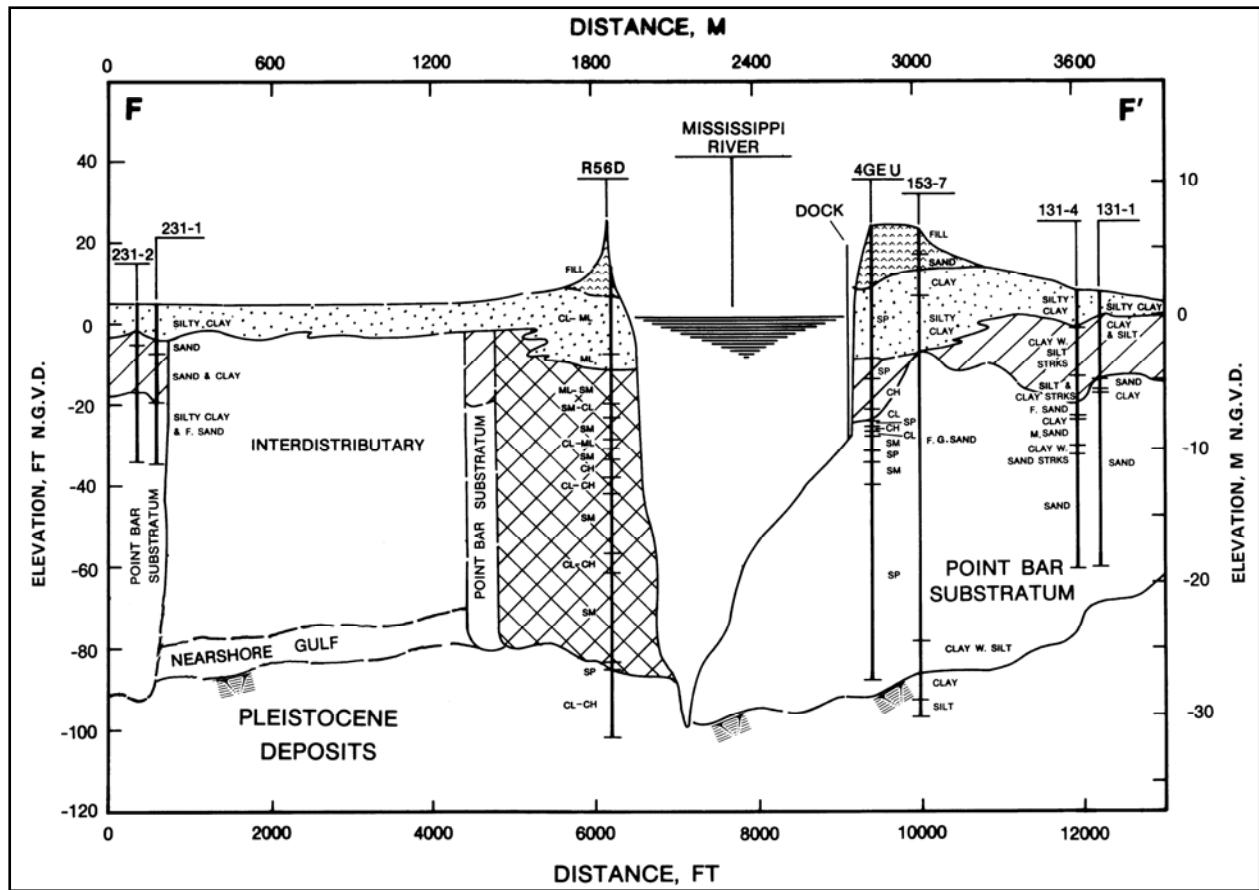
Figure 2-5i. Geologic cross section F-F' (see Figure 2-5l for symbol legend)
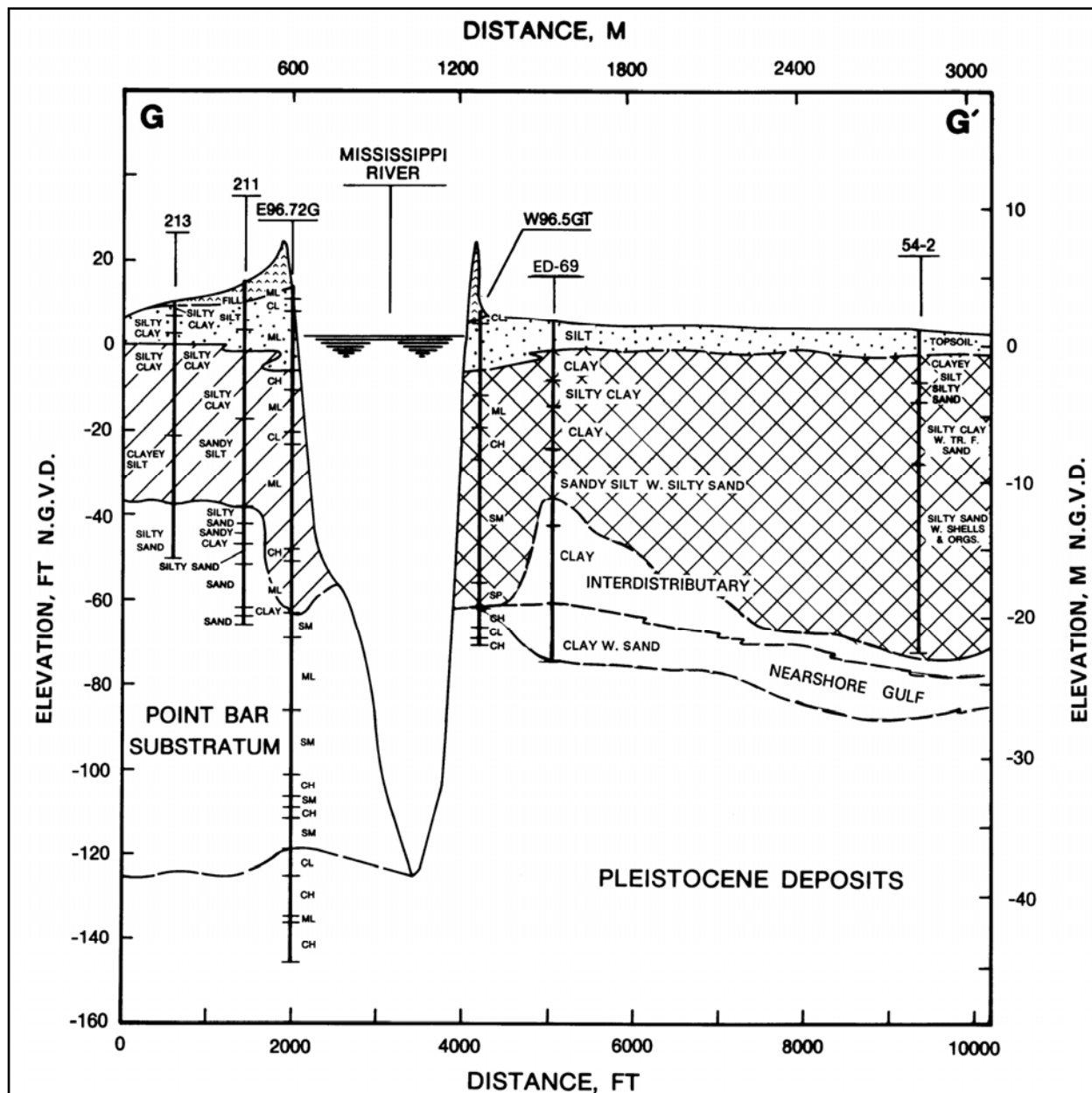
Figure 2-5j. Geologic cross section G-G' (see Figure 2-5l for symbol legend)
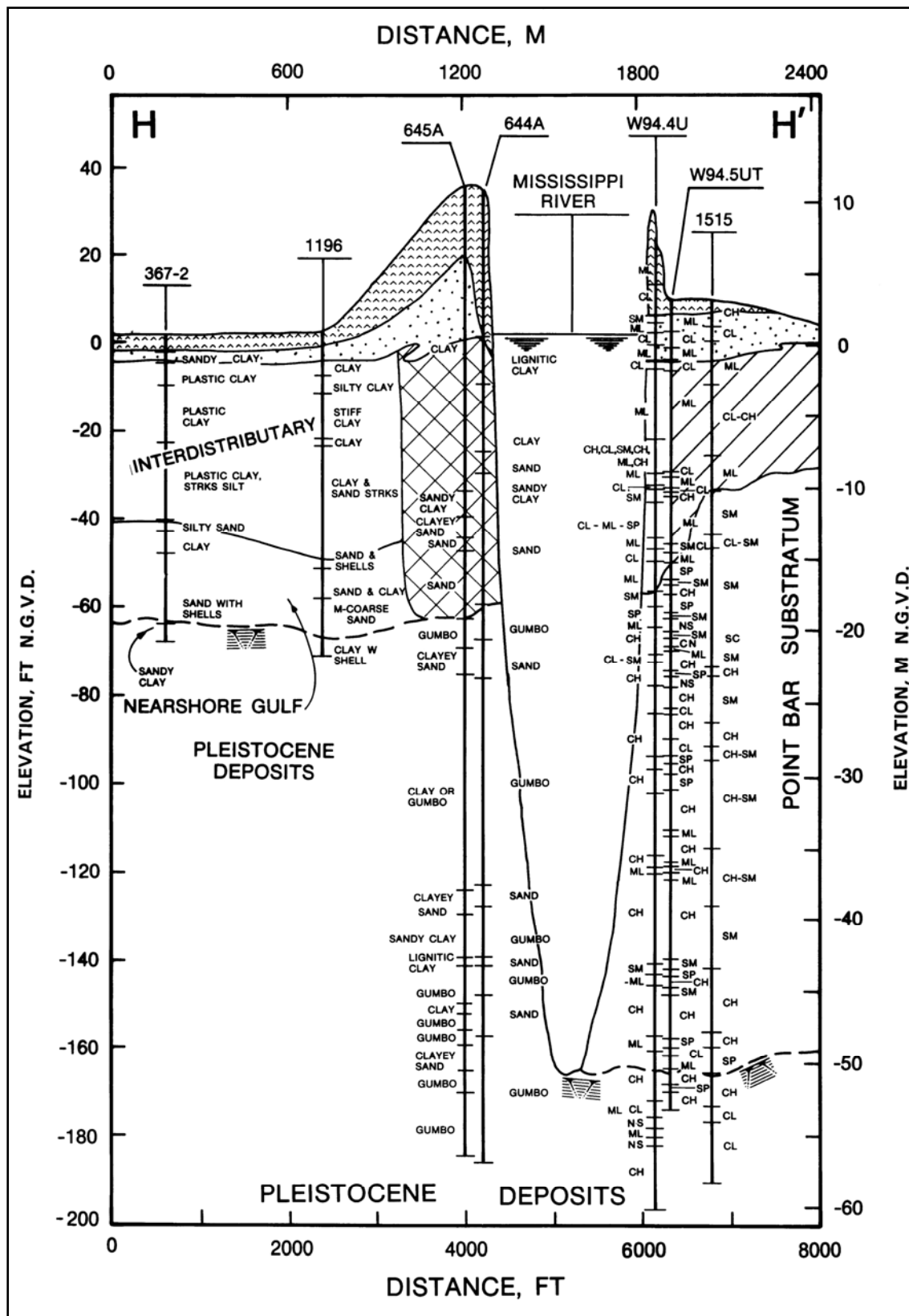
Figure 2-5k. Geologic cross section H-H' (see Figure 2-5l for symbol legend)
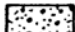
LEGEND

ENVIRONMENTS OF DEPOSITION

TOPSTRATUM DEPOSITS

LEVEE FILL

NATURAL LEVEE

POINTBAR

BACKSWAMP

ABANDONED COURSE

SUBSTRATUM DEPOSITS

UNDIFFERENTIATED SAND AND GRAVEL

UPPER FINE-GRAINED PLEISTOCENE SURFACE

SOIL TYPES (USCS)

CH — CLAY

CL — SILTY CLAY, SANDY CLAY

ML — SILT, SANDY SILT, CLAY SILT

SC — CLAYEY SAND

SM — SILTY SAND

SP — POORLY GRADED SAND

SW — WELL-GRADED SAND

GM — SILTY SAND-GRAVEL

GW — WELL-GRADED SAND-GRAVEL

GP — POORLY GRADED SAND-GRAVEL

Figure 2-5l. Legend for the geologic sections of Figures 2-5a through 2-5k

Beneath the nearshore gulf sequence is the Pleistocene surface. The nearshore gulf sediments represent the deposits formed by the transgression of sea level onto the Pleistocene surface. These sediments were deposited under shallow-water conditions, before the advancement of the two major St. Bernard distributary systems into the study area. Establishment of the St. Bernard distributary systems into the study area produced the interdistributary sediments that were deposited into shallow-water, freshwater areas between the active distributary channels. Interdistributary sediments over time filled these shallow areas, and emergent vegetation in the form of fresh marsh began developing when interdistributary filling approached sea level. Closer to the active distributary systems, overbank deposition from the active distributary channels developed well drained natural levees and inland swamps.

A generalized contour map of the Pleistocene surface is presented in Figure 2-6 (Kolb, Smith, and Silva 1975). In general, the Pleistocene surface throughout the study area dips to the south and southwest at approximately 3 ft per mile (1 m per 1.6 km). Surface elevations on this surface are variable due to erosion by the preexisting Pleistocene drainage system and later Holocene scouring by past and present courses of the Mississippi River and its distributaries. Elevations of the Pleistocene surface range from -50 ft (-15 m) NGVD to greater than -150 ft (-46 m) NGVD in the bendways of the present Mississippi River channel.

Pleistocene deposits are characterized by a significant increase in stiffness and shear strength as compared to the overlying Holocene sediments. Pleistocene soils are fairly resistant to erosion from fluvial scouring. Where these soils occur in the riverbank, they represent a "hard point" which restrains the river's migration and deepening. Pleistocene deposits in the bed and bank of the river have had a significant influence on the river's ability to meander through the study area. There has been very little migration of the channel during the past 100 years as determined from comparison of old hydrographic surveys in Chapter 3 of this report.

Each of the different depositional environments present in the study area has distinct physical characteristics reflected by differences in soil types and associated engineering properties. Therefore, the geology of the study area will have a major influence on river scouring, lateral migration, and bank stability.
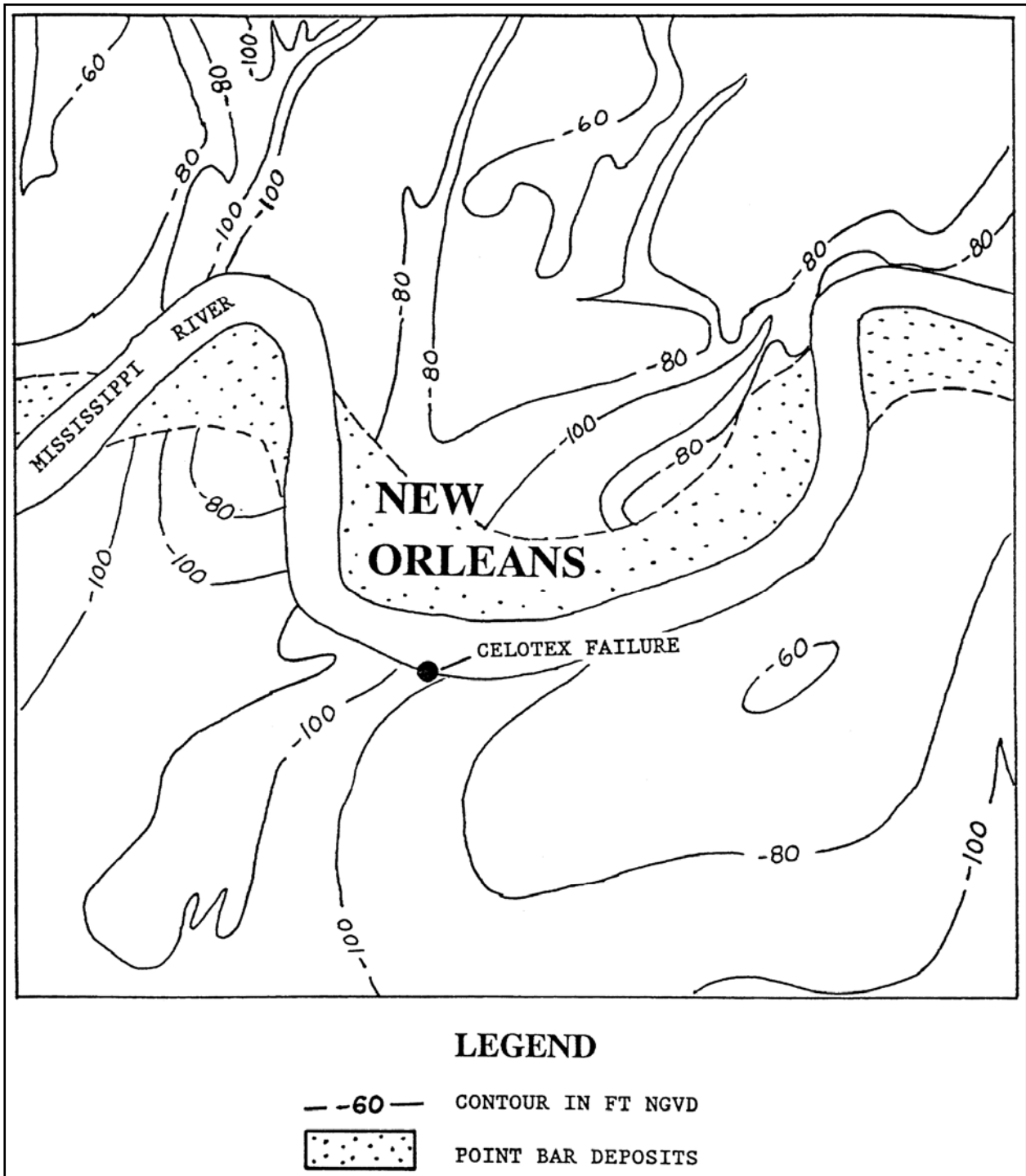
Figure 2-6. Generalized contour map of the Pleistocene surface (modified after Kolb, Smith, and Silva 1975)

Geology of Selected Revetment Reaches

Celotex failure site and Greenville Bend revetment

This riverbank reach extends from river mile 98.3 to 102.0 (158.2 to 164.1 km) on the right descending bank. The subsurface geology of the Celotex failure site is shown by cross sections B-B' (Figure 2-5c) and F-F' (Figure 2-5i). The locations of these sections are shown in Figure 2-4. Areal photography and boring data identify a point bar sequence (Figure 2-4 and 2-5c) associated with Bayou des Familles (Figure 2-5i). This distributary channel was a major course of the Mississippi River during the active St. Bernard delta complex.

The exact intersection and lateral limits of Bayou des Familles at the Mississippi River are not well defined from areal photography because this area has been extensively developed by industrial and residential construction. The position and lateral extent of the Bayou des Familles channel at the Mississippi River was interpreted from available historic charts, maps, and boring data.

Soil types within the point bar-abandoned distributary sequence are primarily coarse-grained, consisting mainly of silty sands (SM) and well sorted or poorly graded sands (SP). The available boring data indicate that the point bar-abandoned distributary sequence extends approximately 100 ft (30.5 m) below the ground surface before encountering the oxidized and erosion-resistant Pleistocene surface.

The geology immediately upstream and downstream from the Bayou des Familles point bar sequence consists of interdistributary deposits underlain by a generally coarser nearshore gulf sequence (CL, ML, SM, and SC). Soil types are variable within these two depositional environments. Interdistributary sediments consist primarily of clay (CL and CH) with disseminated organics.

Carrollton Bend and Carrollton Bend revetment

This bank reach extends from about river mile 102.0 to 105.0 (164 to 169 km) and encompasses the Carrollton Bend revetment which is on the left descending bank. The subsurface geology of the Carrollton Bend reach is shown on cross sections A-A' (Figure 2-5a), A'-A" (Figure 2-5b), and D-D' (Figure 2-5g) (see Figure 2-4 for section locations). The geology consists of natural levee, interdistributary, intradelta, and nearshore gulf sediments. Soil types are variable within the individual environments as shown by the cross sections. The Pleistocene surface ranges between elevations -50 to -75 ft (-15.2 to -22.9 m) NGVD. Where the Mississippi River has entrenched itself into the Pleistocene, the river has formed thick point bar sediments in excess of 120 ft (36.6 m) deep.

Gretna Bend and Gouldsboro revetments

This revetted bank lies between river miles 95.5 and 98.3 (153.6 and 158.2 km). The Gretna Bend and Gouldsboro revetments are contiguous from upstream to downstream, respectively, along the right descending bank. The subsurface geology of the Gretna Bend and Gouldsboro Revetment reach is shown by cross sections B′-B″ (Figure 2-5d) and G-G′ (Figure 2-5j) (see Figure 2-4 for section locations). The geologic sequence is similar to the two upstream revetment reaches already described. The Pleistocene surface ranges between elevations -55 to -70 ft (-16.8 to -21.3 m) NGVD and is overlain by nearshore gulf, interdistributary, and natural levee sediments.

As shown by the surface geology map in Figure 2-4, there is an abandoned distributary channel which intersects the Mississippi River and extends southeast at approximately river mile 96.5 (155.3 km). The existence of this former distributary channel is indicated by the presence of well-developed natural levees several miles southeast of the Mississippi River. The intersection of this distributary channel with the present Mississippi River is indicated by boring W96.5GT. At this location, a thick sand sequence was encountered in the subsurface.

Algiers Point revetment

This revetment reach lies between river mile 93.7 and 95.5 (150.8 and 153.7 km) on the right descending bank. The subsurface geology of Algiers Point is shown by cross sections C-C′ (Figure 2-5e), C′-C″ (Figure 2-5f), and H-H′ (Figure 2-5k). The permanent scour pool along Algiers Point is one of the deepest of the Mississippi River entrenchment below Baton Rouge. River thalweg elevations have historically been between -175 and -200 ft (-53.3 and -61 m) NGVD. At Algiers, along the point bar side of the river, fluvial scouring has created a 170-ft (51.8-m) thick point bar sequence (see cross section H-H′ of Figure 2-5k). Soil types are variable within this thick sequence, but are primarily coarse-grained.

Along the concave or left bank of the river, the subsurface geology at Algiers Point consists of interdistributary sediments, separated by point bar deposits and an abandoned interdistributary channel (see Figure 2-4 and cross section C-C′ of Figure 2-5e). These sediments are underlain by the Pleistocene surface. The lateral and vertical limits of the different depositional environments are shown by the surface geology map and the respective geologic cross sections. Soil types are highly variable as defined by the sections.

The abandoned distributary channel shown in Figure 2-4 is a former St. Bernard distributary which branches from the main Bayou Sauvage-Metarie Bayou course northwest of Algiers Point. The intersection of this distributary channel at the Mississippi River is defined by coarse-grained sediments in the subsurface in borings located within the former distributary channel (see sections C-C′ of Figure 2-5e and H-H′ of Figure 2-5k).

References

Autin, W. J., Burns, S. F., Miller, B. J., Saucier, R. T., and Snead, J. I. (1991). "Chapter 18: Quaternary geology of the Lower Mississippi Valley." Vol K-2, The Geology of North America. The Geological Society of North America, Boulder, CO, 547-581.

Bates, R. L., and Jackson, J. A. (1987). Glossary of Geology, 3rd ed., American Geological Institute, Alexandria, VA.

Clough, G. W. (1966). "Ground water level in silty and sandy Mississippi River upper banks," Mississippi River Commission, Corps of Engineers, Vicksburg, MS. (Mr. F. J. Weaver, Lower Mississippi Valley Division, was a principal assistant in this study).

Cullinan, T. A. (1969). "Contributions to the geology of Washington and St. Tammany Parishes, Louisiana," U.S. Army Engineer District, New Orleans, LA.

Dunbar, J. B., Blaes, M. Dueitt, S., and Stroud, K. (1994). "Geological investigation of the Mississippi River deltaic plain, Report 2 of a Series," Technical Report GL-84-15, U.S. Army Engineer Waterways Experiment Station, Vicksburg, MS.

Dunbar, J. B., Blaes, M., Dueitt, S., and May, J. (1995). "Geological investigation of the Mississippi River deltaic plain, Report 3 of a Series," Technical Report GL-84-15, U.S. Army Engineer Waterways Experiment Station, Vicksburg, MS.

Dunbar, J. B., and Torrey, V. H. (1991). "Geologic, geomorphological and geotechnical aspects of the Marchand Levee failure, Marchand, Louisiana," Miscellaneous Paper GL-91-17, U.S. Army Engineer Waterways Experiment Station, Vicksburg, MS.

Eustis Engineering Company. (1984). "Geotechnical investigation: Soil stratification and foundation conditions for residential development," Report for City of New Orleans, Sewerage and Water Board of New Orleans, New Orleans, LA.

Fisk, H. N. (1944). "Geological investigation of the alluvial valley of the Lower Mississippi River," U.S. Army Corps Engineers, Mississippi River Commission, Vicksburg, MS.

Frazier, D. E. (1967). "Recent deltaic deposits of the Mississippi River: Their development and chronology." Gulf Coast Association of Geological Societies. Transactions 17th annual meeting. San Antonio, TX.

Halbouty, M. T. (1967). Salt Domes, Gulf Region, United States and Mexico. Gulf Publishing Company, Houston, TX.

Hvorslev, M. J. (1956). "A review of the soils studies," Potamology Investigations Report No. 12-5, U.S. Army Engineer Waterways Experiment Station, Vicksburg, MS.

Kemp, E. B. (1967). "Geologic setting of New Orleans." Guidebook New Orleans, LA and vicinity field trip. The Geological Society of America and Associated Societies, Annual meetings.

Kolb, C. R. (1962). "Distribution of soils bordering the Mississippi River from Donaldsonville to Head of Passes," Technical Report No. 3-601, U.S. Army Engineer Waterways Experiment Station, Vicksburg, MS.

Kolb, C. R., and Saucier, R. T. (1982). "Engineering geology of New Orleans," Geological Society of America, Reviews in Engineering Geology 5, 75-93.

Kolb, C. R., Smith, F. L., and Silva, R. C. (1975). "Pleistocene sediments of the New Orleans-Lake Pontchartrain area," Technical Report S-75-6, U.S. Army Engineer Waterways Experiment Station, Vicksburg, MS.

Kolb, C. R., Steinriede, W. B., Krinitzsky, E. L., Saucier, R. T., Mabrey, P. R., Smith, F. L., and Fleetwood, A. R. (1968). "Geological investigation of the Yazoo Basin, Lower Mississippi Valley," Technical Report 3-480, U.S. Army Engineer Waterways Experiment Station, Vicksburg, MS.

Kolb, C. R., and VanLopik, J. R. (1958a). "Geology of the Mississippi River Deltaic Plain," Technical Report No. 3-483, Vol 1 and 2, U.S. Army Engineer Waterways Experiment Station, Vicksburg, MS.

_____. (1958b). "Geological investigation of the Mississippi River-Gulf Outlet Channel," Miscellaneous Paper No. 3-259, U.S. Army Engineer Waterways Experiment Station, Vicksburg, MS.

Krinitzsky, E. L. (1965). "Geological influences on bank erosion along meanders of the Lower Mississippi River," Potamology Investigations, Report 12-15, U.S. Army Engineer Waterways Experiment Station, Vicksburg, MS.

Krinitzsky, E. L., and Smith, F. L. (1969). "Geology of backswamp deposits in the Atchafalaya Basin, Louisiana," Technical Report S-69-8, U.S. Army Engineer Waterways Experiment Station, Vicksburg, MS.

Krinitzsky, E. L., Turnbull, W. J., and Weaver, F. J. (1966). "Bank erosion in cohesive soils of the Lower Mississippi Valley," Vol 92, No. SM1, Journal of Soil Mechanics and Foundations Division, Proceedings American Society of Civil Engineers, 121-136.

May, J. R., Britsch, L. D., Dunbar, J. B., Rodriguez, J. P., and Wlosinski, L. B. (1984). "Geological investigation of the Mississippi River Deltaic Plain," Technical Report GL-84-15, U.S. Army Engineer Waterways Experiment Station, Vicksburg, MS.

Miller, W. (1983). "Stratigraphy of newly exposed quaternary sediments, Eastern Orleans Parish, Louisiana," Tulane Studies in Geology and Paleontology 17(3, 4), 85-104.

Montgomery, R. L. (1974). "Correlation of engineering properties of cohesive soils bordering the Mississippi River from Donaldsonville to Head of Passes, LA," Miscellaneous Paper S-74-20, U.S. Army Engineer Waterways Experiment Station, Vicksburg, MS.

New Orleans Geological Society. (1962). "Salt domes of South Louisiana," Vol 1 and 2, J. C. Stipe and J. P. Spillers, ed., New Orleans, LA.

_____. (1983). "Salt domes of South Louisiana," Vol 3, S. J. Waguespack, ed., New Orleans, LA.

Padfield, C. J. (1978). "The stability of riverbanks and flood embankments," Final Technical Report, U.S. Army European Research Office, London, England.

Saucier, R. T. (1963). "Recent geomorphic history of the Pontchartrain Basin, Louisiana," Technical Report 16, Part A, United States Gulf Coastal Studies, Coastal Studies Institute, Contribution No. 63-2, Louisiana State University, Baton Rouge, LA.

_____. (1964). "Geological investigation of the St. Francis Basin," Technical Report 3-659, U.S. Army Engineer Waterways Experiment Station, Vicksburg, MS.

_____. (1967). "Geological investigation of the Boeuf - Tensas Basin Lower Mississippi Valley," Technical Report 3-757, U.S. Army Engineer Waterways Experiment Station, Vicksburg, MS.

_____. (1969). "Geological investigation of the Mississippi River area, Artonish to Donaldsonville, Louisiana," Technical Report S-69-4, U.S. Army Engineer Waterways Experiment Station, Vicksburg, MS.

Saucier, R. T. (1974). "Quaternary geology of the Lower Mississippi Valley," Arkansas Archeological Survey, Research Series No. 6, Fayetteville, AR.

_____. (1977). "The Northern Gulf Coast during the Farmdalian Substage: A search for evidence," Technical Report S-69-4, U.S. Army Engineer Waterways Experiment Station, Vicksburg, MS.

Saucier, R. T., and Kolb, C. R. (1967). "Alluvial geology of the Yazoo Basin, Lower Mississippi Valley," 1:250,000 map, U.S. Army Engineer Waterways Experiment Station, Vicksburg, MS.

Self, R. P., and Davis, D. W. (1983). "Geology of the New Orleans area," The Compass of Sigma Gamma Epsilon 60(2), 29-38.

Smith, F. L., and Russ, D. P. (1974). "Geological investigation of the Lower Red River-Atchafalaya Basin area," Technical Report S-74-5, U.S. Army Engineer Waterways Experiment Station, Vicksburg, MS.

Smith, L. M., Dunbar, J. B., and Britsch, L. D. (1986). "Geomorphological investigation of the Atchafalaya Basin, Area West, Atchafalaya Delta, and Terrebonne Marsh, Vol 1 and 2," Technical Report GL-86-3, U.S. Army Engineer Waterways Experiment Station, Vicksburg, MS.

Snead, J. I., and McCulloh, R. P. (1984). "Geologic map of Louisiana, scale 1:500,000, Baton Rouge, LA."

Torrey, V. H., III. (1988). "Retrogressive failures in sand deposits of the Mississippi River, Report 2, Empirical evidence in support of the hypothesized failure mechanism and development of the levee safety flow slide monitoring system," Technical Report GL-88-9, U.S. Army Engineer Waterways Experiment Station, Vicksburg, MS.

Torrey, V. H., III, Dunbar, J. B., and Peterson, R. W. (1988). "Retrogressive failures in sand deposits of the Mississippi River, Report 1, Field investigations, laboratory studies and analysis of the hypothesized failure mechanism," Technical Report GL-88-9, U.S. Army Engineer Waterways Experiment Station, Vicksburg, MS.

Torrey, V. H., III, and Weaver, F. J. (1984). "Flow failures in Mississippi riverbanks." Proceedings IV International Symposium on Landslides. Vol 2, Toronto, Canada, 355-360.

Turnbull, W. J., Krinitzsky, E. L., and Weaver, F. J. (1966). "Bank erosion in soils of the Lower Mississippi Valley." Proceedings of the American Society of Civil Engineers, Journal of the Soil Mechanics and Foundation Division, 92(SM1), 121-136.

U.S. Army Corps of Engineers. (1909). "Survey of the Mississippi River, Chart Nos. 69 and 70," Mississippi River Commission, Vicksburg, MS.

U.S. Army Corps of Engineers. (1921). "Survey of the Mississippi River, Chart Nos. 69 and 70," Mississippi River Commission, Vicksburg, MS.

_____. (1950). "Piezometer observations at Reid Bedford Bend and indicated seepage forces," Potamology Investigations Report No. 5-4, Vicksburg, MS.

U.S. Army Corps of Engineers. (1975). "Master index, upper and lower Mississippi River surveys for period 1879-80 to 1928 and some historic maps prior to this period," Vol 2, Mississippi River Commission, Vicksburg, MS.

U.S. Army Engineer District, New Orleans. (1938). "Maps of the Mississippi River, Angola, La., to the Head of Passes," New Orleans, LA.

_____. (1952). "Mississippi River hydrographic survey, 1949-1952, Angola, La., to Head of Passes and South and Southwest Passes and Pass A Loutre," New Orleans, LA.

_____. (1965). "Mississippi River hydrographic survey, 1961-1963, Black Hawk, La., to Head of Passes and South and Southwest Passes and Pass A Loutre," New Orleans, LA.

_____. (1976). "Mississippi River hydrographic survey, 1973-1975, Black Hawk, La., to Head of Passes and South and Southwest Passes and Pass A Loutre," New Orleans, LA.

_____. (1984). "Mississippi River levees, Item M-181.1 to 180.2-L, Marchand Levee setback, final report," New Orleans, LA (internal report, unpublished).

_____. (1986). "Mississippi River levees, Item M-100.4-R, Celotex Levee and Batture restoration, final report," New Orleans, LA (internal report, unpublished).

_____. (1988). "Mississippi River hydrographic survey, 1983-1985, Black Hawk, La., to Head of Passes and South and Southwest Passes and Pass A Loutre," New Orleans, LA (internal report, unpublished).

Wallace, W. E. (1966). "Fault and salt map of South Louisiana," Gulf Coast Association of Geological Societies, Vol 16.

Appendix A
Environments of Deposition

General

This appendix provides a general description of the environments of deposition which produced the surface and subsurface geology encountered in the study reach. The distribution of surface deposits is shown by the geologic map in Figure 2-4 of the main text. Subsurface limits of the various depositional environments are shown by the cross sections in Figures 2-5a through 2-5k. A geologic legend is presented in Figure 2-5l that identifies symbols used in the geologic cross sections.

In addition to the general descriptions of the individual environments of deposition, this appendix also provides a very generalized indication of the engineering properties for each environment. Correlation of engineering properties and soil types to the different environments of deposition is based primarily on work by Kolb (1962)[1] and is summarized in Table A1. Additionally, Montgomery (1974) expanded upon Kolb's original work for several of the major depositional environments which form the bulk of the land area in the deltaic plain. Montgomery's work is summarized in Table A2 and provides further engineering data on the following selected environments of deposition: natural levee, point bar, backswamp, prodelta, intradelta, and inter-distributary deposits.

In terms of their engineering significance, the biggest contrast occurs between the Pleistocene and Holocene age sediments as shown by the engineering data in Table A1. Pleistocene sediments have higher cohesive strengths, lower water contents, and are much denser than Holocene soils. Holocene deposits in contrast are less consolidated, have higher water contents, and are more variable in density.

---

[1] References are listed following the main text.

Volume V The Performance – Levees and Floodwalls – Technical Appendix

V-2-33

This is a preliminary report subject to revision; it does not contain final conclusions of the United States Army Corps of Engineers.

Table A1. Engineering Properties of Depositional Environments from the Mississippi River Deltaic Plain (from Kolb 1962)

V-2-34

Volume V The Performance – Levees and Floodwalls – Technical Appendix
This is a preliminary report subject to revision; it does not contain final conclusions of the United States Army Corps of Engineers.

Table A2. Engineering properties of selected depositional environments from the Mississippi River deltaic plain (from Montgomery, 1974)

Deposit	Grain Size and Organic Content	Natural Water Content %	Liquid Limit %	Plasticity Index %	Dry Density pcf	Specific Gravity	Void Ratio e_o	s_u/p_o Ratio	Shear Strength Q c T/sq ft	Shear Strength R c T/sq ft	Shear Strength R φ deg	Shear Strength S φ deg
Natural levee		18-83 (45)	29-129 (66)	2-90 (42)	50-92 (76)	2.62-2.74 (2.69)	0.82-6.16 (1.46)	--	0.08-0.68	0.01-0.50 (0.20)	8-22 (13)	16-31 (24)
Point bar (silty)		26-79 (44)	31-87 (54)	7-63 (33)	54-98 (78)	2.65-2.77 (2.69)	0.70-2.12 (1.12)	0.14-0.37 (0.27)	0.11-1.24	0.01-0.50 (0.20)	8-22 (13)	16-31 (24)
Backswamp (organic)	Insufficient data	42-367 (127)	58-397 (152)	43-218 (106)	16-73 (43)	2.10-2.74 (2.46)	1.36-6.73 (3.11)	--	0.03-0.27	0.00-0.40 (0.14)	7-20 (13)	13-35 (22)
Backswamp (inorganic)		31-98 (59)	27-148 (83)	19-86 (56)	48-91 (65)	2.52-2.75 (2.68)	0.85-2.57 (1.62)	0.07-0.76 (0.26)	0.1-0.72	0.00-0.50 (0.13)	4-27 (12)	13-36 (21)
Prodelta		31-70 (53)	39-100 (79)	16-72 (51)	49-90 (72)	2.67-2.80 (2.72)	0.84-2.06 (1.32)	0.11-0.39 (0.22)	0.18-0.85	0.01-0.50 (0.20)	2-22 (13)	16-31 (24)
Intradelta		24-132 (58)	25-212 (77)	5-164 (52)	33-98 (67)	2.57-2.76 (2.70)	0.64-2.84 (1.57)	0.07-0.65 (0.29)	0.05-0.4	0.01-0.50 (0.20)	8-22 (13)	16-31 (24)
Inter-distributary		24-113 (57)	38-179 (82)	19-162 (59)	45-94 (66)	1.59-2.74 (2.64)	1.01-2.59 (1.58)	0.22-0.85 (0.37)	0.2-0.5	0.01-0.50 (0.20)	8-22 (13)	16-31 (24)

Row groupings (left margin): Fluvial (Natural levee, Point bar, Backswamp organic, Backswamp inorganic); Fluvial-Marine (Prodelta, Intradelta, Inter-distributary); overall: Mississippi River Deltaic Plain

LEGEND

▨ Clay (0.005 mm)   ▥ Silt (0.05-0.005 mm)

▦ Sand (2.0-0.05 mm)   ■ Organic material

Notes:

(1) Numbers in parentheses are average values.

(2) Insufficient consolidated-undrained and drained shear strength data were available for the natural levee, point bar, prodelta, intradelta, and interdistributary deposits. The data shown represent all five deposits.

(3) Insufficient data were available to clearly establish the amount of organic matter typically occurring in each deposit.

(4) Shear strengths are given in cohesion (c), tons per square foot and angle of internal friction (φ) in degrees.
   Q denotes unconsolidated-undrained triaxial compression tests.
   R denotes consolidated-undrained triaxial compression tests.
   S denotes consolidated drained direct shear tests.

(5) Grain-size characteristics based on references 2 and 10.

Volume V The Performance – Levees and Floodwalls – Technical Appendix

V-2-35

This is a preliminary report subject to revision; it does not contain final conclusions of the United States Army Corps of Engineers.

The biggest contrast in Holocene soils occurs between the high- and low- energy depositional environments. High-energy environments are generally associated with maximum fluvial and/or wave activity and are mainly composed of coarse-grained sediments. These environments include point bar, substratum, abandoned course, abandoned distributary, beach, nearshore gulf, estuarine/bay sound, and intradelta deposits (Table A1). Low-energy environments are composed primarily of fine-grained sediments and include marsh, swamp, natural levee, prodelta, and interdistributary. Only the environments of deposition that are present in the study area are examined in the following section. The environments are presented and described by their order and distribution of occurrence. Deltaic environments not present in the study area but identified in Table A1 are described in further detail by Kolb (1962) or Kolb and Van Lopik (1958a,b) for readers desiring further information.

Surface Environments of Deposition

Natural levee

Natural levees are vertical accretion deposits formed when the river overtops its banks during flood stage and sediment suspended in the flood flow is deposited immediately adjacent to the channel. The resulting landform is a low, wedge-shaped ridge decreasing in thickness away from the channel. The limits of natural levee deposits in the study area are shown in Figure 2-4 of the main report. Natural levee deposits are mapped in Figure 2-4 with the underlying environment of deposition (i.e., interdistributary, point bar, or inland swamp). Natural levee deposits cover approximately 40 percent of the study area and involve the Mississippi River and abandoned distributary channels from the active St. Bernard delta complex (i.e., Bayou des Familles-Barataria, Metairie Bayou, Bayou Sauvage, and two unnamed bayous).

Natural levee widths in the study area vary from about 3/4 to approximately 2 miles wide along the Mississippi River, and between 1/4 and 1/2 mile wide along the abandoned St. Bernard distributary channels (Figure 2-4). Natural levees are thickest adjacent to the main channel, ranging from 10 to 20 ft in thickness (Figures 2-5a to 2-5k). Their thickness decreases away from the river, eventually merging with inland swamp deposits.

Natural levee deposits in the study area are composed primarily of clay and silt with minor sand lenses. Soils associated with natural levee deposits are identified in Figures 2-5a through 2-5k of the main report. These deposits are generally coarser-grained near the channel, composed of silt (ML) and silty clay (CL), and become finer-grained (i.e., CL and CH) further from the river. Color varies from reddish brown or brown near surface to grayish brown, and medium to dark gray with depth. Darker colored natural levee soils are due to the higher organic content. Organic content is generally low and is in the form of small roots and occasionally disseminated wood fragments. Larger wood fragments are uncommon as oxidation has reduced organic materials to a highly decomposed state. Frequently associated with natural levee deposits are small calcareous nodules, formed as a result of groundwater percolating through the permeable soils and precipitated from solution. Natural levee soils are well-drained, have low-water contents, and generally have a stiff to very stiff consistency (Tables A1 and A2).

Inland swamp

Before describing characteristics of inland swamps and their distribution in the study area, a clarification of terminology is in order. Usage of the term inland swamp is restricted to the deltaic plain, whereas the term backswamp is restricted to the Mississippi River alluvial valley. Mapping by May et al. (1984) adopted the usage of the term inland swamp and defined the upvalley margin of this environment. Inland swamps are not bounded by valley margins or older meander belt ridges as in the alluvial valley. Instead, inland swamps in the deltaic plain are areas of high ground and woody vegetation formed because of the high sediment rates from advancing distributary channels.

Kolb (1962) recognized that the term backswamp was inappropriate for the deltaic plain and had reservations about using this term to describe swamp sediments below Donaldsonville, LA. May et al. (1984) have placed the boundary between backswamp and inland swamp near the vicinity of Houma, LA. The boundary separating the two swamp types occurs at the junction of Bayou Teche and Bayou LaFourche, two former Mississippi River courses. Consequently, the summary descriptions and engineering properties in Tables A1 and A2 for backswamp are more appropriate to inland swamp as the samples were derived primarily from inland swamp sediments. The primary distinction here is in process and the ultimate nature of the sediments derived by these processes. In theory, inland swamp sediments are considered to be much finer-grained than backswamp sediments since they are transported by smaller-scale distributary channels to locations on the deltaic plain that are well removed from the main channel. As shown by Figure 2-3 in the main report, primary Mississippi River flow was not confined to a single main channel during the period of active Holocene delta building but rather was shared by several smaller major distributary courses.

Inland swamps are vertical accretion deposits that receive sediment during times of high-water flow, when the natural levees are crested and suspended sediment in the flood waters is deposited in areas well removed from the main distributary channel. Inland swamp environments are low, often poorly drained, tree-covered areas flanking the main distributary channel. Inland swamps are low areas that are settling basins for flood flow and sediment, and represent one of the final stages in land building by the passing delta front. Sediment supply is sufficient to elevate the land surface to above sea level and allow woody vegetation to develop and become stable.

Inland swamps are the dominant surface environment in the study area and comprise approximately 50 percent of the Holocene deposits depicted in Figure 2-4. The surface of the inland swamp environment begins at about the 0 ft NGVD elevation. These deposits are approximately 10 to 15 ft thick with the base of this sequence grading into marsh and interdistributary sediments between -10 to -15 ft NGVD (Dunbar et al. 1994).

Inland swamps are composed of uniform, very fine-grained soils, primarily silty clay (CL) and clay (CH). Sand (SM and SP) and silt (ML) may be present but is considered a minor constituent of the total depositional sequence (Table A1 and A2, and Figures 2-5a through 2-5k of the main report). These deposits typically contain moderate to high organic contents in the form of decayed roots, leaves, and wood. Disseminated pyrite is a common but a very minor

constituent of these soils and is commonly found in more poorly drained areas which promotes reducing conditions. Inland swamp soils may become well drained during times of low water and undergo short periods of oxidation, lending a mottled appearance to the soil. Inland swamp soils are gray, dark gray, or occasionally black. Inland swamp soils have generally high-water contents, between 30 and 90 percent, as shown by Tables A1 and A2 (backswamp environment).

Point bar

Point bar deposits are lateral accretion deposits formed as a river migrates across its flood plain. River channels migrate across their floodplain by eroding the outside or concave bank and depositing a sandbar on the inside or convex bank. With time the convex bar grows in size and the point bar is developed. Associated with the point bar are a series of arcuate ridges and swales. The ridges are formed by lateral channel movement and represent relic lateral bars separated by low lying swales. The swales are locations for fine-grained sediments to accumulate. Point bar deposits are as thick as the total depth of the river that formed them. These deposits become coarser-grained with increasing depth. Maximum grain size is associated with the river's bedload (coarse sand and fine gravel) while the fine-grained soils occur near the surface. The basal or coarse-grained portion of the point bar sequence is deposited by lateral accretion while the fine-grained or upper portion of the point bar sequence is deposited by vertical accretion.

Point bar deposits in the study area are considered to be young, generally less than 3,500 years old. They began forming along Bayou des Familles-Barataria when the St. Bernard delta system was active but did not fully develop along the main river until the present Mississippi River course began forming less than 1,000 years before the present.

Soil types in a point bar sequence grade upward from coarse-grained sands and fine gravels near the base to clays near the surface. These deposits are variable, but in the study area are generally composed of at least 50 percent poorly graded fine sand (Figures 2-5a through 2-5h and Tables A1 and A2). Point bar deposits are separated into two distinct units, a predominantly fine-grained upper sequence or point bar top stratum, and a coarse-grained lower sequence or point bar substratum. Soil types associated with each unit are identified in the geologic sections in Figures 2-5a through 2-5f of the main report.

Abandoned course

An abandoned course as the name implies is a relic fluvial course that is abandoned in favor of a more hydraulically efficient course. An abandoned course contains a minimum of two meander loops and forms when the river's flow path is diverted to a new position on the river's floodplain. This event usually is a gradual process that begins by a break or a crevasse in the river's natural levee during flood stage. The crevasse forms a temporary channel that may, over time, develop into a more permanent channel. Eventually, the new channel diverts the majority of flow and the old channel progressively fills. Final abandonment begins as coarse sediment fills the abandoned channel segment immediately downstream from the point of diversion. Complete

filling of the abandoned course is a slow process that occurs by overbank deposition. The complete filling process may take several hundreds or even thousands of years to complete.

The Bayou des Familles-Barataria abandoned course is a prominent physiographic feature that extends due south from the Mississippi River at approximately river mile 100 (Figures 2-1 and 2-4 of the report). The abandoned course extends well beyond the limits of the study area and continues south to Barataria Bay (May et al. 1984, Dunbar et al. 1994). It contains broadly developed natural levees which are easily identified on aerial photography and topographic maps. Well developed natural levees and a meandering plan form distinguish the abandoned course from its short lived predecessor, the crevasse channel.

Boring information from the greater New Orleans area indicates channel fill from the Bayou des Familles abandoned course consists primarily of thick sand deposits capped by a thin layer of silt and clay. Detailed boring information from the abandoned course at its confluence with the Mississippi River is presented in Figures 2-5c and 2-5i of the main report. Engineering properties of abandoned course sediments are not sufficiently categorized in Table A1 due to lack of boring data. However, these sediments are considered to be similar in composition to sandy point bar deposits for which data are present.

Abandoned distributary channel

Distributary channels are channels that diverge from the trunk channel dispersing or "distributing" flow away from the main course. By definition, distributary channels do not return flow to the main channel on a delta plain (Bates and Jackson 1987). Distributary channels originate initially as crevasse channels during high flow periods when the main channel is unable to accommodate the larger discharge. If the flood is of sufficient duration, a permanent distributary channel is soon established through the crevasse. Abandonment of a distributary channel or distributary network occurs either as a major course shift upstream or the distributary becomes over extended and loses its gradient advantage in favor of a much shorter distributary channel. Complete abandonment usually occurs because of an improved gradient advantage by the new distributary.

Distributary channel abandonment closely parallels the abandonment of a course. During abandonment, the base of the channel is filled with poorly sorted sands, silts, and organic debris. As the channel continues to fill, the flow velocities are decreased, and the channel is filled by clay, organic ooze, and peats. Abandoned distributaries in the study area are approximately their original width, but only a fraction of their original depth due to infilling. Abandoned distributary channels in the study area are Metairie Bayou, Bayou Sauvage, and two unnamed distributaries that intersect the Mississippi River on the east and west banks (Figure 2-4). These distributary channels have all been partially or completely filled with sediments.

Often the distal ends of abandoned distributaries have been buried due to subsidence, destroyed by coastal erosion, or closer to the trunk channel, buried by later natural levee deposits (Figure 2-4). Metarie Bayou in the northern portion of the study area has been buried by later Mississippi River natural levee deposits and altered by the historic activities of man north of the

river. Natural levees are ideal for urban development since these areas are topographically higher than the surrounding area.

Abandoned distributaries are recognized on aerial photographs by their natural levees and the urban development associated with these levees. In the subsurface, distributary sediments are recognized by soil types (Table A1) and sedimentary structures characteristic of channel fill deposits. Engineering properties of abandoned distributary sediments are not sufficiently categorized in Table A1 due to lack of boring data. Upper channel fill consists of parallel and wavy laminated silts and silty clays, interbedded with highly burrowed clays with high-water contents. Distorted bedding, slump structures, organic layers, and minor shell material are also common in abandoned distributary deposits.

Freshwater marsh

In the southwestern portion of the study area there is an area of freshwater marsh, a nearly flat expanse where grasses and sedges are the only vegetation. Organic sedimentation plays an important role in the formation of marsh deposits. Peats, organic oozes (mucks), and humus are formed as the marsh plants die and are buried. Decay is largely due to anaerobic bacteria in stagnant water. Vegetative growth and sedimentation maintain the surface elevation at a fairly constant level, and the marsh deposits thicken as a result of subsidence over time. When marsh growth fails to keep pace with subsidence, the marsh surface is eventually inundated by water.

Peats are the most common form of marsh strata remains, and they consist of black fibrous masses of decomposed plants. Detrital organic particles, carried in by marsh drainage, and vegetative tissues form the mucks. Mucks are watery oozes that can support little or no weight. Sedimentation occurs in the marsh when floodwater overtops the natural levees, depositing clays and silts onto the marsh surface. Sediments are also transported to the marsh during lunar tides, wind tides, and hurricane tides when sediment laden marine waters inundate the marsh surface.

Marsh sediments are found in the subsurface as peats (Figures 2-5b through 2-5k) and represent a time during the Holocene where the land surface was at sea level and supporting marsh vegetation. Often marsh deposits grade vertically upward in a prograding delta system into inland swamp, followed by natural levee deposits. The reverse sequence is also true (i.e., marsh, natural levee, inland swamp, marsh). Engineering properties of marsh sediments are identified in Table A1.

Subsurface Environments of Deposition

Interdistributary

Interdistributary deposits are sediments deposited in low areas between active distributary channels, usually under brackish water conditions. Sediment laden waters overtop the natural levees of distributary channels during flood stage and deposit the coarsest sediment (silt) near the channel. The finer sediment (silty clay and clay) is transported away from the active

distributary channel and settles out of suspension as interdistributary deposits. In this manner, considerable thicknesses of clay are deposited as the distributary builds seaward. Interdistributary clays often grade downward into prodelta clays and upward into the highly organic clays of swamp and marsh deposits.

Interdistributary deposits are found throughout the study area in the subsurface (Figures 2-5b through 2-5k of the main report). These deposits range in thickness from 30 to 60 ft and start between 0 to -10 ft NGVD as shown by the cross sections in Figures 2-5b through 2-5k. Interdistributary deposits consist of saturated gray clays which are highly bioturbated and contain some silt laminae. Shell fragments and minor amounts of organic debris are also commonly distributed throughout the interdistributary sequence as shown by Tables A1 and A2.

Buried beach

Interdistributary sediments associated with Metairie Bayou, an abandoned St. Bernard distributary in the northern edge of the study area, overlie and grade laterally with buried beach deposits. Buried beach deposits are part of the Pine Island Beach trend, an early Holocene beach trend associated with active sedimentation from the Pearl River (Saucier 1963). Approximately 5,000 years ago, when sea level was slightly lower than the present, longshore drift created a southwest to northeast trending offshore spit or barrier beach complex in the New Orleans area. Sediments forming the spit were derived from sandy fluvial sediments transported by the Pearl River. This spit originated at the river's mouth and extended southwest to the vicinity of New Orleans. This buried beach complex forms the southern shore of Lake Pontchartrain and acted as a natural barrier for filling of Lake Pontchartrain by advancing distributary channels during the active St. Bernard stage of delta growth.

Metairie Bayou (Figure 2-4) follows the seaward edge of the Pine Island Beach trend and was blocked from entering the main body of Lake Pontchartrain by the higher topography of the relic beach. Instead, Metairie Bayou follows the relic beach trend northeast toward the coastal mainland as the Bayou Sauvage distributary channel. Coastal drainage into Lake Pontchartrain from the Pleistocene uplands breached the beach ridge and formed "The Rigolets," a pass into Lake Pontchartrain at the eastern edge of the deltaic plain (Figure A1 from Saucier 1963).

The beach trend grades laterally into intradelta and abandoned distributary deposits (Figure A1). Boring data identifies the buried beach deposits as consisting of uniform, fine to medium grained, quartz sand, ranging in color from gray to tan, and white upon exposure at the surface (Saucier 1963). Beach sand is generally well sorted and contains shell fragments.
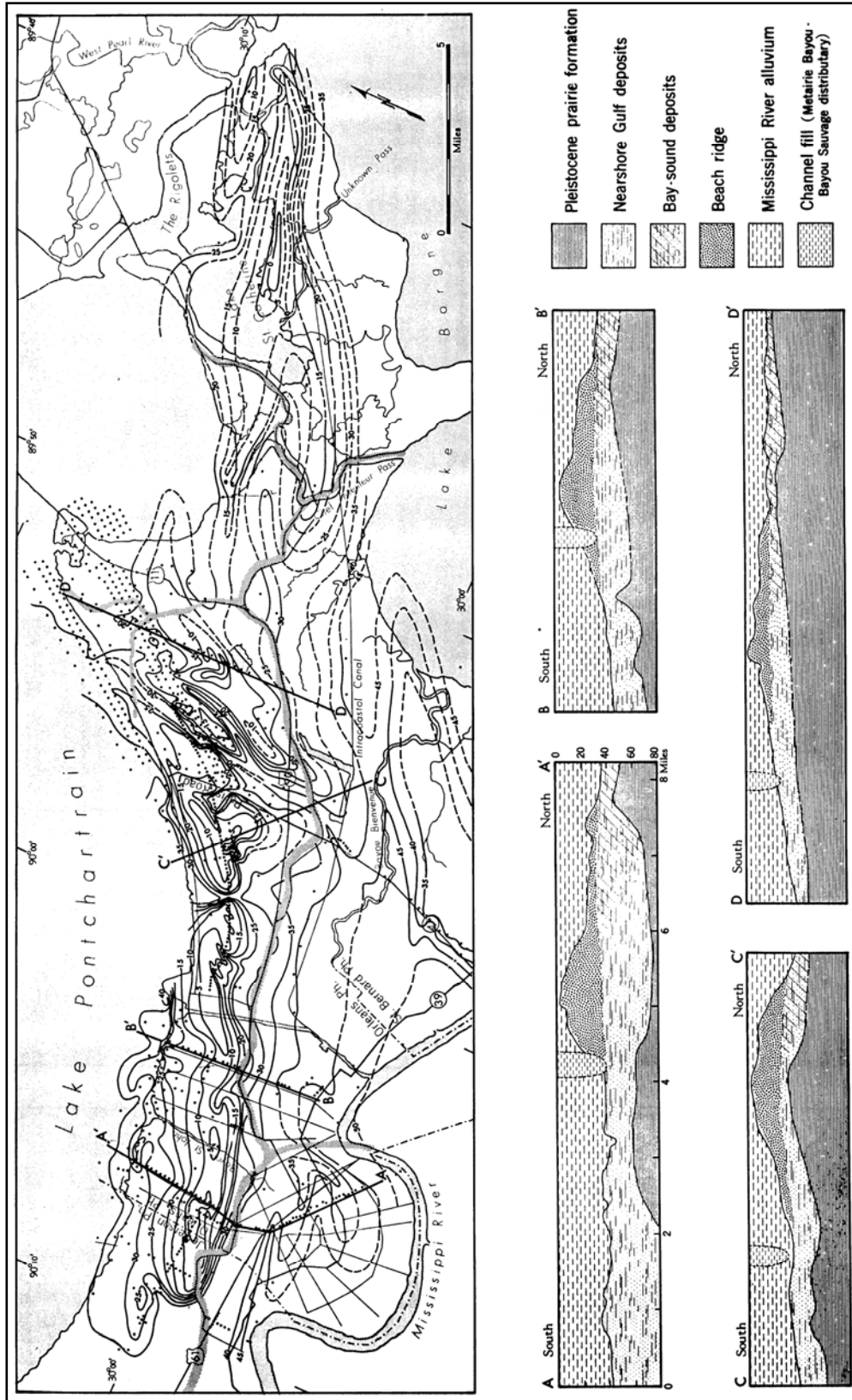
Figure A1. Topography of the buried Pine Island beach trend (Saucier 1963)

This is a preliminary report subject to revision; it does not contain final conclusions of the United States Army Corps of Engineers.

Intradelta

Intradelta deposits form at the mouth of distributary channels and consist of coarse-grained or sandy sediments. At the mouth of a distributary, the water velocity decreases upon entering open water, depositing coarse-grained sediments from suspension as distributary mouth bars. The coarse sediments are deposited on the bar crest or as fans along the sides of the bars. As the distributary is built seaward, it may cut through or split around the bar. The process is then repeated in each of the smaller, branching distributary channels. These deposits interfinger and merge with interdistributary clays.

Intradelta deposits are identified in the subsurface in borings near the Mississippi River (Figures 2-5a, 2-5b, 2-5e, and 2-5g). They consist primarily of clean sands and silty sands with some silts. Intradelta deposits are thickest nearer the distributary channels or channel source areas. Engineering properties of intradelta sediments are summarized in Tables A1 and A2.

Nearshore gulf

Nearshore gulf deposits are generally coarse-grained sediments formed by the transgression and interaction of the rising Holocene sea level with the drowned Pleistocene surface. Nearshore gulf deposits represent sediments eroded, transported, and deposited at the land/sea level interface, often at maximum wave energy and under storm conditions. These deposits generally consist of coarse-grained sediments and are primarily characterized by sand and shell hash. Available engineering data is presented in Table A1. The subsurface distribution of this depositional environment is shown by the cross sections in Figures 2-5a through 2-5k of the main report. Generally, this environment directly overlies the Pleistocene surface throughout the deltaic plain region.

Estuarine and bay sound

Both of these environments are marine and are a minor environment in the subsurface (see Figures 2-5a through 2-5l). Both of these environments directly overlie the Pleistocene surface. These two environments were formed early during the Holocene, or perhaps even Late Pleistocene, when sea level advanced onto the Pleistocene surface. As sea level advanced, it drowned the existing Pleistocene drainage network and created small estuaries and bays.

An estuary is a river valley where fresh water comes into contact with sea water (Bates and Jackson 1987). A bay sound is a partly enclosed brackish water body which is sheltered from direct access to the Gulf and is dominated by both fluvial and marine processes. Since the bay sound is partly restricted from the Gulf, the depositional energy and associated geomorphic processes are less severe than those associated with the nearshore gulf environment. Sediments deposited within an estuary or bay sound environment have a much greater range in grain size than sediments deposited within the nearshore gulf environment (Table A1). Silt and clay are usually more common within the estuarine and the bay sound environment than the nearshore gulf environment as shown by Table A1.

Volume V The Performance – Levees and Floodwalls – Technical Appendix

V-2-43

This is a preliminary report subject to revision; it does not contain final conclusions of the United States Army Corps of Engineers.

Substratum

Substratum or "braided stream/outwash plain" deposits related to glacial melting and sea level rise are not present in the study area. Substratum deposits as identified in this report are coarse-grained sediments associated with the point bar environment. The term substratum as used in this report and on the cross sections in Figures 2-5a through 2-5k is used in conjunction with and is a modifier of the point bar environment. Point bar substratum deposits are typically the lateral accretion or coarse-grained component of the point bar sequence. The upper boundary occurs at the base of the fine-grained or vertical accretion component of the point bar sequence and is defined by the first nearly continuous silty sand (SM) contact.

Pleistocene

Pleistocene deposits are present only in the subsurface and are correlative to the Prairie Formation. The Prairie Formation is the youngest of Fisk's (1944) four major interglacial fluvial and deltaic sequences and was deposited during Sangamonian time, approximately 70,000 to 125,000 years ago. The Prairie Formation is similar in origin to the Holocene age deposits which overlie the Prairie. They were both envisioned by Fisk (1944) as fining upward from a coarse-grained substratum to a fine-grained top stratum. Both are products of rising sea level and deposition following continental glaciation. However, detailed analysis of glacial chronology from the midwest, combined with detailed geologic mapping from the Lower Mississippi Valley in recent years, indicates that the four-cycle model of Pleistocene glaciation and the accompanying interglacial deposition are an oversimplification (Autin et al. 1991). Recent studies indicate that the geology of the Prairie Formation in the study area is highly complex (Cullinan 1969; Kolb, Smith, and Silva 1975; Saucier 1977; Dunbar et al. 1994).

Lithologic and stratigraphic data on the Prairie Formation are based on surface exposures north of Lake Pontchartrain in St. Tammy, St. Helena, Tangipahoa, and Washington Parishes, Louisiana, and foundation engineering borings from the greater New Orleans metropolitan area. Pleistocene age soils outcropping on the north shore of Lake Pontchartrain were mapped by Cullinan (1969) as being typically light gray, light brown, or yellowish orange in color and composed of muddy, fine sandstones or fine to very fine sandy siltstones. Beneath the Holocene sediments in the New Orleans area, numerous engineering borings drilled into the Pleistocene surface identify the Prairie as being composed primarily of clay and silty clay and having the following characteristics (Kolb and VanLopik 1958a,b, Kolb 1962): (a) oxidized tan, yellow, or greenish gray color, (b) a marked decrease in water content, (c) distinctive stiffening in soil consistency and a general increase in shear strength, and (d) the presence of concretions. Pleistocene age soils forming the subsurface in the New Orleans area are usually easily distinguished from Holocene age soils by their sharp contrast in engineering properties, lithology, and stratigraphy. Soil color, water content, and shear strength are the most diagnostic criteria distinguishing Pleistocene from Holocene soils (Table A1).

Between the fine-grained Pleistocene sediments beneath the New Orleans area and the more coarse-grained sediments that outcrop at the surface north of Lake Pontchartrain, there is a transition which may be due to variations within environments of deposition or stratigraphy during

the Late Pleistocene. The New Orleans area Pleistocene soils may have formed under several depositional settings, including inland swamp, interdistributary, bay sound, and/or estuarine environments, while the coarser-grained soils north of Lake Pontchartrain are perhaps related to mainland beach and terrestrial fluvial environments draining the Pleistocene uplands. The Prairie surface is a highly complex stratigraphic sequence that consists of multiple depositional facies which formed over a period of several tens of thousands of years, followed by thousands of years of subaerial oxidation and erosion during maximum glacial episodes and lowered sea levels, and then later burial by Holocene sediments.

The Pleistocene surface dips gently to the south and southwest at about 3 to 5 ft per mile (Figure 2-6 of the main report). Elevations on the Pleistocene surface range from approximately -60 ft NGVD in the northern portions of the study area to more than -100 ft NGVD south of the Mississippi River. The base of the Prairie Formation beneath the Celotex failure site occurs somewhere between elevation -500 and -600 ft NGVD (Cullinan 1969).

Appendix 3
17th Street Canal Strength Evaluation

Objectives

The analysis of strength data described in the following sections had three objectives:

1. To develop a "shear strength model" for use in stability analyses and soil-structure interaction analyses of the I-walls at the 17th Street Canal, using all data available as of April 7, 2006. This strength model includes strengths for the levee fill, the marsh layer, the clay, and the sand in the foundation.

2. To compare this strength model to the strengths that were used for design of the I-walls in the area where the breach occurred.

3. To compare the strengths in the breach area with strengths in other sections of the 17th Street Canal I-wall.

Stratigraphy

The northern section of the 17th Street Canal where the breach occurred encompasses Stations 8+30, 10+00, and 11+50, on which this strength evaluation focuses.

The levee fill is compacted CL and CH material, with an average Liquid Limit of about 45. The average moist unit weight of the fill is about 109 pcf.

Beneath the fill is a layer of "marsh" material (or peat) 5 ft to 10 ft thick. The marsh layer is composed of organic material from the cypress swamp that occupied the area, together with silt and clay deposited in the marsh. The average moist unit weight of the marsh layer is about 80 pcf. Water contents of the marsh layer are as high as 737%. The average water content is approximately 112%. The marsh layer is fibrous at the top, and more amorphous near the bottom, indicating more advanced decomposition of the older organic materials at depth.

Beneath the marsh layer is a layer of lacustrine clay with an average Liquid Limit of about 95%. The clay is normally consolidated throughout its depth, having been covered and kept wet

by the overlying marsh layer. The average moist unit weight of the clay is about 109 pcf, and the average water content is approximately 65%.

Beneath the clay is a layer of Pine Island Beach sand, a silty sand with Standard Penetration blow counts ranging from 2 to 50. This layer is not involved in observed or calculated mechanisms of instability, and its strength is therefore of little importance in stability analyses, except as a more resistant layer beneath the clay.

Sources of Information on Shear Strengths

A considerable number of borings were drilled in the breach area and in neighboring areas before the failure. Additional borings have been drilled, cone penetration tests have been performed, and test pits have been excavated since the failure.

Several hundred unconfined compression tests, UU tests performed using only one confining pressure rather than a range of confining pressures (called UU-1 tests), and conventional UU tests performed using a range of confining pressures have been conducted on the soils at the site. Tests were performed on specimens trimmed from three-inch and five-inch diameter samples. Statistical analyses have been performed on the data from these tests to compute minimum, maximum, and average values of strength for the levee fill, the marsh layer, and the clay.

Four cone penetration tests with pore pressure measurements (CPTU tests) were performed near the area of the breach after the failure. These have proven to be very useful for evaluating the undrained strength of the clay, and for distinguishing the clay from the overlying marsh layer and the underlying sand.

The evaluation described here focused on undrained shear strengths of the levee fill, the marsh layer and the clay. Because the water loads that resulted in failure of the I-walls increased over a period of hours, there is little doubt that the levee fill and the clay beneath the marsh layer were undrained during the event. Determining whether the marsh layer should be modeled as drained or undrained will require laboratory consolidation tests to determine how quickly it drains when subjected to changes in load. Those tests are being performed at this time. The discussion below considers only undrained strength of the marsh layer. If it is determined that the drained strength, or partially drained strength, is more appropriate for the marsh layer, additional strength tests and slope stability analyses will be needed.

Shear Strength of Levee Fill

Data is available from two borings in the breach area (Borings 62 and 64) and several more in the neighborhood of the breach. In all, about 125 strength tests were performed on the levee fill material. Much of the fill is below the static water table, and an $s_u = c$, $\phi_u = 0$ strength interpretation is therefore appropriate.

The measured shear strengths of the levee fill material scatter very widely, from about 120 psf to more than 5,000 psf. With such widely scattered values, an average value may not be

meaningful, and considerable judgment is needed to select a representative value. Placing greatest emphasis on data from UU tests on five-inch diameter samples, $s_u = 900$ psf appears to be a reasonable value to represent the levee fill strength. This strength can be compared to a value of 500 psf used in the design analyses.

Shear Strength of the Marsh Layer

The marsh layer is stronger beneath the levee crest where it had been compressed under the weight of the levee, and weaker at the toe of the levee and beyond, where it has not been compressed so heavily. The same types of tests were used to measure marsh layer strengths as were used for fill strengths, and tests were performed on three-inch and five-inch diameter samples. Tests were also performed on two-inch diameter samples, but these were not included in the evaluation described here, because it was considered that such small samples would likely be too disturbed to be representative of field conditions.

The measured shear strengths scatter very widely, from about 50 psf to about 920 psf. Values of $s_u = 400$ psf beneath the levee crest, and $s_u = 300$ psf beneath the levee toe appear to be reasonably representative of the measured values. These strengths can be compared to a value of 280 psf used in the design analyses.

Shear Strength of Clay

The clay is normally consolidated, and its undrained shear strength increases with depth. Figure 3-1 shows variations of undrained shear strength with depth determined using Mayne's method (Mayne 2003)[1] for determining undrained shear strength from CPTU test results. Mayne's method uses the relationship among undrained strength, effective overburden pressure, and preconsolidation pressure that was proposed by Ladd (1991)[2], and has been found to give more reasonable values of undrained shear strength than use of constant values of the cone factors N_k or N_{kt}.

Whereas other methods of interpreting undrained shear strength from cone results are based on bearing capacity theory, Mayne's method considers tip resistance in relation to pore pressure and overburden pressure. For this reason it does not correspond to a single value of N_{kt}.

With Mayne's method, the undrained shear strength is related to cone tip resistance by the equation

$$s_u = 0.091 \left(\sigma'_v \right)^{0.2} \left(q_t - \sigma_v \right)^{0.8} \tag{3-1}$$

---

[1] Mayne, P. W. (2003). "Class 'A' Footing Response Prediction from Seismic Cone Tests," Proceedings, Deformation Characteristics of Geomaterials, Vol. 1, Lyon, France.
[2] Ladd, C. C. (1991) "Stability Evaluation During Staged Construction," Terzaghi Lecture, ASCE Journal of Geotechnical Engineering, 117 (4), 540-615.

where s_u = undrained shear strength, σ'_v = effective vertical stress, q_t = total cone tip resistance adjusted for pore pressure effects, and σ_v = total vertical stress.

The undrained shear strength calculated with this method is based on that measured using Direct Simple Shear (DSS) tests. This strength is lower than that measured by conventional triaxial compression tests and greater than that measured by triaxial extension tests. Ladd (1991) has suggested that this is a reasonable average value for design purposes.

For the soft and very soft clay along the 17th Street Canal, the values of undrained shear strength are very close to values calculated using N_{kt} = 15, a value often used for computing undrained strengths of soft clays from CPTU test results.

As shown in Figure 3-1, the variations of undrained strength with depth within the clay computed using Equation 3-1 are very nearly the same for all four CPTU tests. The straight line representing the average undrained shear strength in the clay has a slope of 11 psf per foot of depth. This rate of strength increase with depth compares to values of 8.4 psf per foot to 13.5 psf per foot determined using laboratory strength test results for samples from borings B-1, B-2, B-3, B-4, and B-6, which appeared to have the most consistent test results.

The rate of increase of strength with depth is directly related to the s_u/p' ratio for the clay, and its buoyant unit weight, as follows:

$$\frac{s_u}{p'} = \frac{rate\ of\ increase\ of\ s_u\ with\ depth}{rate\ of\ increase\ of\ p'\ with\ depth} = \frac{\Delta s_u / \Delta z}{\gamma_{buoyant}} \qquad (3\text{-}2)$$

The value of $\gamma_{bouyant}$ for the clay is 109 pcf – 62.4 pcf = 46.6 pcf. Thus the value of s_u/p' is:

$$\frac{s_u}{p'} = \frac{11\ psf\ per\ ft}{46.6\ pcf} = 0.24 \qquad (3\text{-}3)$$

which is a reasonable value for this normally consolidated clay.

These values provide a good basis for establishing undrained strength profiles in the clay. The undrained strength at the top of the clay is equal to 0.24 times the effective overburden pressure at the top of the clay, and the undrained strength increases with depth in the clay at a rate of 11 psf per foot.

In the IPET strength model the undrained shear strength of the clay is equal to 0.24 times the effective overburden pressure. The clay strength thus varies with lateral position, being greatest beneath the levee crest where the effective overburden pressure is greatest, and varying with depth, increasing at a rate of 11 psf per foot at all locations.

This model does not consider details of the stress distribution beneath the levee, which would result in "load spread" effects. These effects would result in rotation of principal stresses beneath

V-3-4

Volume V The Performance – Levees and Floodwalls – Technical Appendix
This is a preliminary report subject to revision; it does not contain final conclusions of the United States Army Corps of Engineers.

the levee, and in the added stress due to the levee load that would decrease with depth. Including these complex effects would complicate the model considerably. In our opinion, such refinement would make the model impractical, and is not justified. The model described in the previous paragraphs uses a simple stress distribution beneath the levee that satisfies vertical equilibrium, and it reflects the fact that the undrained strength is proportional to consolidation pressure, certainly the most important aspect of the strength of the clay.

The computer programs SLIDE[3] and UTEXAS4[4] use two-dimensional interpolation to compute strengths that vary in both the horizontal and vertical direction, as is the case with the IPET strength model described above. This feature of these computer programs provides a convenient means for representing the New Orleans levee clay strengths in stability analyses. Provided that a sufficient number of interpolation points are used, the two computer programs give the same horizontal and vertical variations of shear strength.

Shear Strength of Sand

Correlations with Cone Penetration tip resistance were used to estimate a value of $\phi' = 35$ degrees for the silty sand beneath the clay. As noted previously, the sand layer is not involved in observed or computed failure mechanisms, and the value of ϕ' assigned to it therefore has no influence on computed factors of safety.

Comparison with Strengths Used in Design

The design analyses used undrained strengths for the levee fill, the marsh layer, and the clay, and a drained friction angle to characterize the strength of the sand layer beneath the clay, as does the strength model described above. Thus the design strengths are directly comparable to the IPET strengths discussed here.

The values of strength for the levee fill, the marsh layer, and the sand that were used in the design analyses for the 17th Street Canal I-wall, Stations 552+70 to 635+00 (new Stations 0+00 to 82+30) are shown in Table 3-1. This interval includes the breach area, which extends approximately from new Station 7+50 to new Station 12+20.

The design strength values shown in Table 3-1 are taken from Plate 56 of the 17th Street Canal Geotechnical Design Memorandum (GDM)[5]. Also shown in Table 3-1 are the values of strength from the IPET strength model.

It can be seen that the strengths for the levee fill, the marsh layer and the sand used in design are consistently lower that those estimated using all of the data available in April 2006.

---

[3] Available from Rocscience Inc., 31 Balsam Avenue, Toronto, Ontario, Canada M4E 3B5
[4] Available from Shinoak Software, 3406 Shinoak Drive, Austin TX 78731
[5] Design Memorandum No. 20, General Design, Orleans Parish – Jefferson Parish, 17th Street Outfall Canal, U.S. Army Engineer District, New Orleans, March 1990.

The values of strength for the clay vary with depth and laterally, as discussed above. The values of undrained strength used in design are compared with those described above in Figures 3-2, 3-3, and 3-4. These figures show the strengths for the IPET strength model discussed previously as dotted lines, superimposed on photocopies of the GDM figure. Minor variations in the strengths at Stations 8+30, 10+00 and 11+50 occur because the thicknesses of the levee fill and marsh layer are slightly different in the three cross sections, and the effective stresses at the top of the clay are therefore slightly different.

In each of the three cases the rate of increase of strength with depth (11 psf per foot) are essentially the same in the IPET strength model as for the design strengths. The GDM strength model assumed a maximum strength of 380 psf in the clay layer, while the IPET model allowed the strength to increase past 380 psf. Beneath the levee crest, the design strengths are very close to those determined from the IPET strength model. At the toe of the levee, however, the IPET strengths are considerably lower than those used in design. This is the most significant finding that has emerged from this evaluation of shear strengths.

Comparison of Strengths within the Breach Area
with Strengths Elsewhere

Field observations and preliminary analyses show that the shear strength of the clay has a greater effect on stability than the strengths of the levee fill, the marsh layer, or the sand. Critical slip surfaces intersect only small sections within the marsh layer and the levee fill, and do not intersect the sand layer beneath the clay at all. Therefore the strengths of these materials have small influence on stability, and minor variations in these strengths from section to section would not control the location of the failure. For this reason, the comparison of strengths in the breach area with strengths elsewhere has been focused mainly on the undrained strength of the clay.

Within the breach area, only two borings drilled before the failure (Borings 62 and 64) are available. The strengths measured on undisturbed specimens from these borings are listed in Table 3-2.

The strengths summarized in Table 3-2 can be compared with the strengths of specimens from borings to the north and south of the breach, which are summarized in Tables 3-3 and 3-4. For the purpose of comparing relative strengths, it was assumed that the strength was constant with depth.

The average strengths from Tables 3-2, 3-3, and 3-4 are compared in Table 3-5 and Figure 3-5.

Although the data is sparse, it is fairly consistent, and it appears that the clay strengths in the areas north and south of the breach are somewhat higher than those in the breach.

Based on the average values shown in Table 3-5 and Figure 3-5, the undrained strengths of the clay in the areas adjacent to the breach are 20% to 30% higher than those in the breach area.

Strength differences of this magnitude are significant. They indicate that the reason the failure occurred where it did is very likely that the clay strengths in the breach area were lower than in adjacent areas to the north and south.

At the time of completion of this report the results of some vane shear tests and cone penetration tests are not yet available. Those results will be reflected in a revision of this report if that is found necessary.

Table 3-1
Comparison of Strengths of Levee Fill, Marsh Layer and Sand Used in Design for Stations 552+70 to 635+00 with the IPET Strengths

Material	Strengths used for design	IPET strength model
Levee fill	$s_u = 500$ psf, $\phi = 0$	$s_u = 900$ psf, $\phi = 0$
Marsh layer	$s_u = 280$ psf, $\phi = 0$	$s_u = 400$ psf, $\phi = 0$ beneath levee crest $s_u = 300$ psf, $\phi = 0$ beneath levee toe
Sand	$\phi' = 30$ degrees	$\phi' = 35$ degrees

Table 3-2
Undrained Strengths of Clay for Specimens from the Breach

Boring 62			
Depth	**Test type**	**s_u**	**Average**
24 ft	UC	305 psf	
34 ft	UC	260 psf	280 psf
42 ft	UU-1	178 psf (very loose clayey sand – ignore)	
Boring 64			
Depth	Test type	s_u	Average
22 ft	UC	103 psf	
33.5 ft	UC	383 psf	240 psf
41.5 ft	UC	168 psf (likely disturbed – ignore)	

Table 3-3
Undrained Strengths of Clay for Specimens from Borings North of the Breach

Boring 66			
Depth	**Test type**	**s_u**	**Average**
28.5 ft	UC	235 psf	
38.5 ft	UC	398 psf	317 psf
Boring 68			
Depth	Test type	s_u	Average
33 ft	UC	340 psf	
33 ft	UU	360 psf	
39 ft	UU	360 psf	353 psf
42.5 ft	UU-1	250 psf (likely sand, not clay – ignore	
42.5 ft	UU	240 psf (likely sand, not clay - ignore	

Table 3-4
Undrained Strengths of Clay for Specimens from Borings South of the Breach

Boring 60			
Depth	**Test type**	s_u	**Average**
24 ft	UC	200 psf	326 psf
29 ft	UC	365 psf	
29 ft	UU	380 psf	
34 ft	UC	385 psf	
39 ft	UC	323 psf	
39 UU	UU	300 psf	
44 ft	UU-1	243 psf (loose clayey sand – ignore)	
Boring 58			
Depth	**Test type**	s_u	**Average**
24 ft	UC	183 psf	324 psf
29 ft	UC	313 psf	
39 ft	UC	475 psf	
Boring 56			
Depth	**Test type**	s_u	
29 ft	UC	295 psf	305 psf
39 ft	UC	315 psf	

Table 3-5
Comparison of Undrained Strengths from Breach Area Borings with Strengths from Borings North and South of the Breach

Area	Range of s_u	Average s_u
Breach (Borings 62 and 64)	240 psf to 280 psf	260 psf
North of breach (Borings 66 and 68)	317 psf to 353 psf	335 psf
South of breach (Borings 56, 58 and 60)	305 psf to 326 psf	318 psf
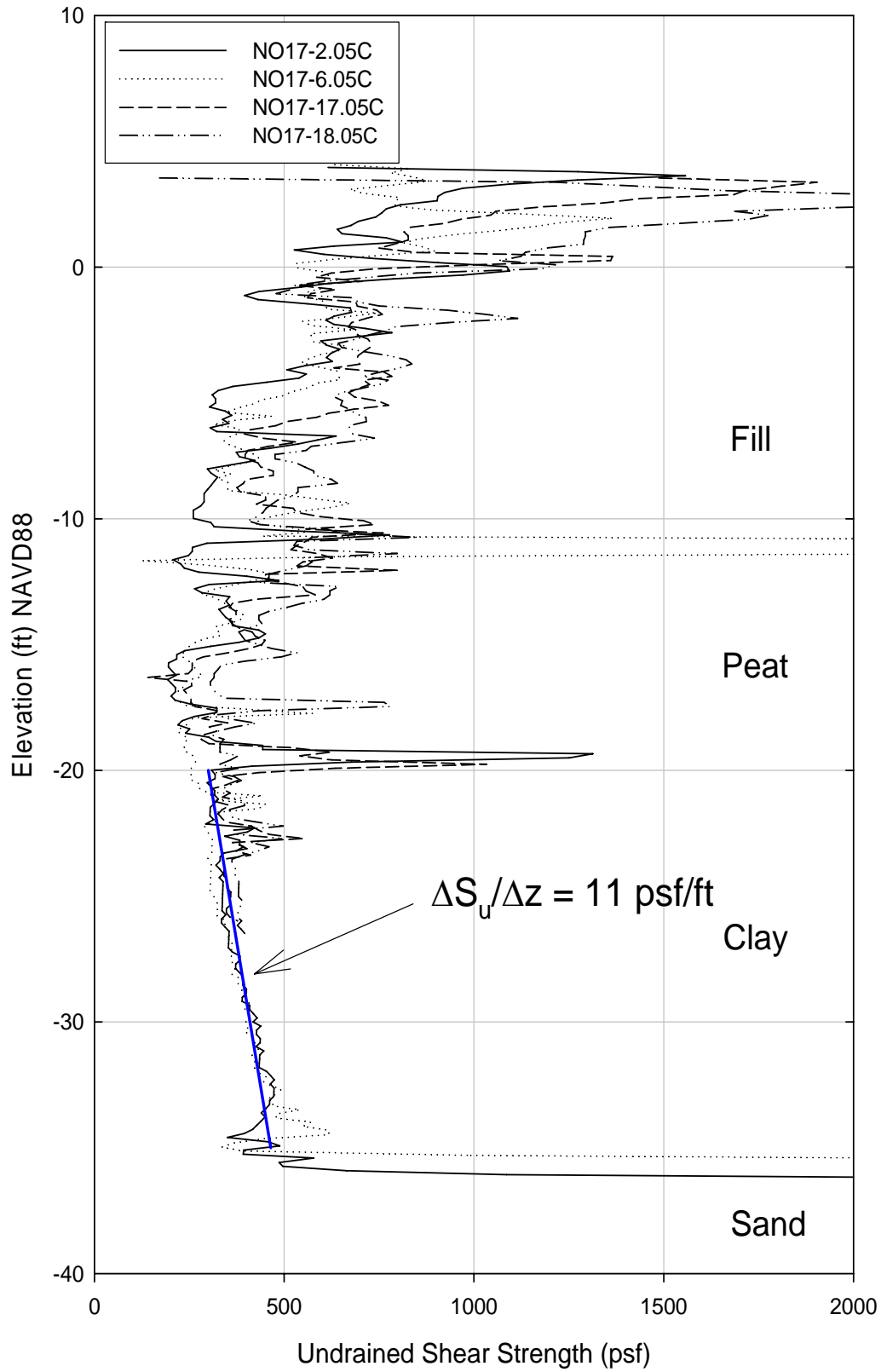
Figure 3-1. Undrained Shear Strength Calculated from CPTU Tests using Mayne's Method
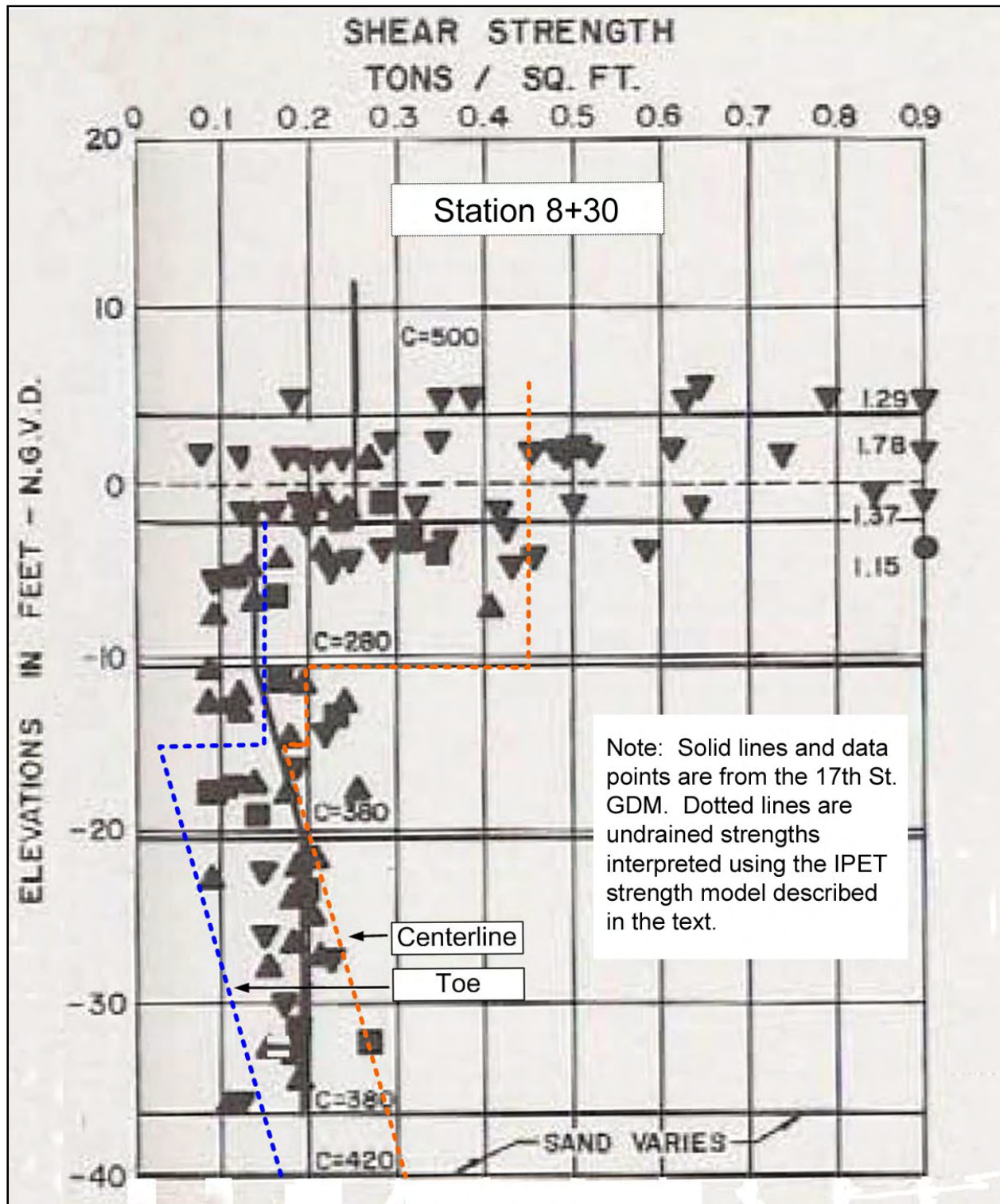
Figure 3-2. Comparison of Undrained Strength Profiles used for 17th Street I-Wall Design with Strength Profiles Interpreted from the IPET Strength Model for Station 8+30

This is a preliminary report subject to revision; it does not contain final conclusions of the United States Army Corps of Engineers.
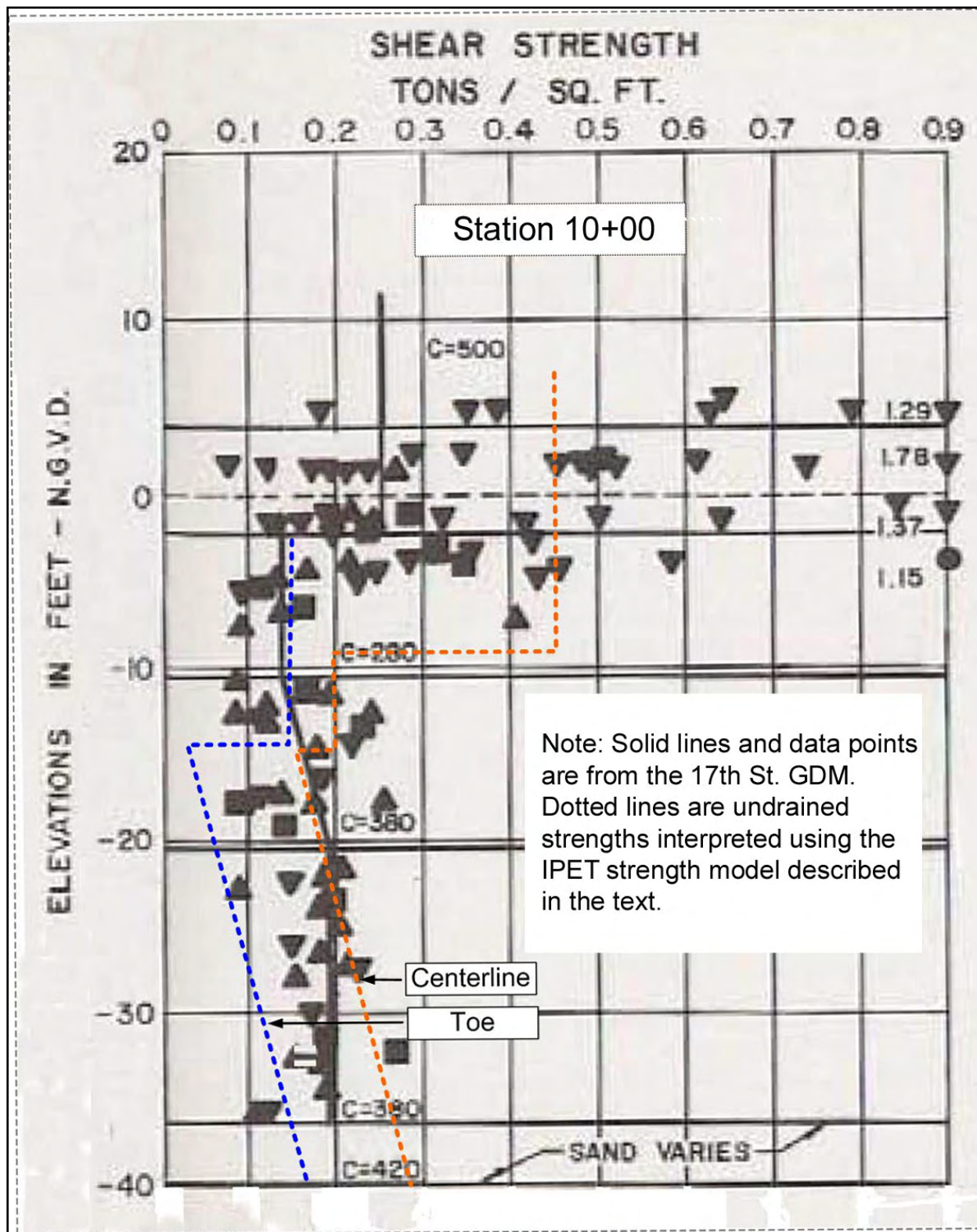
Figure 3-3. Comparison of Undrained Strength Profiles used for 17th Street I-Wall Design with Strength Profiles Interpreted from the IPET Strength Model for Station 10+00
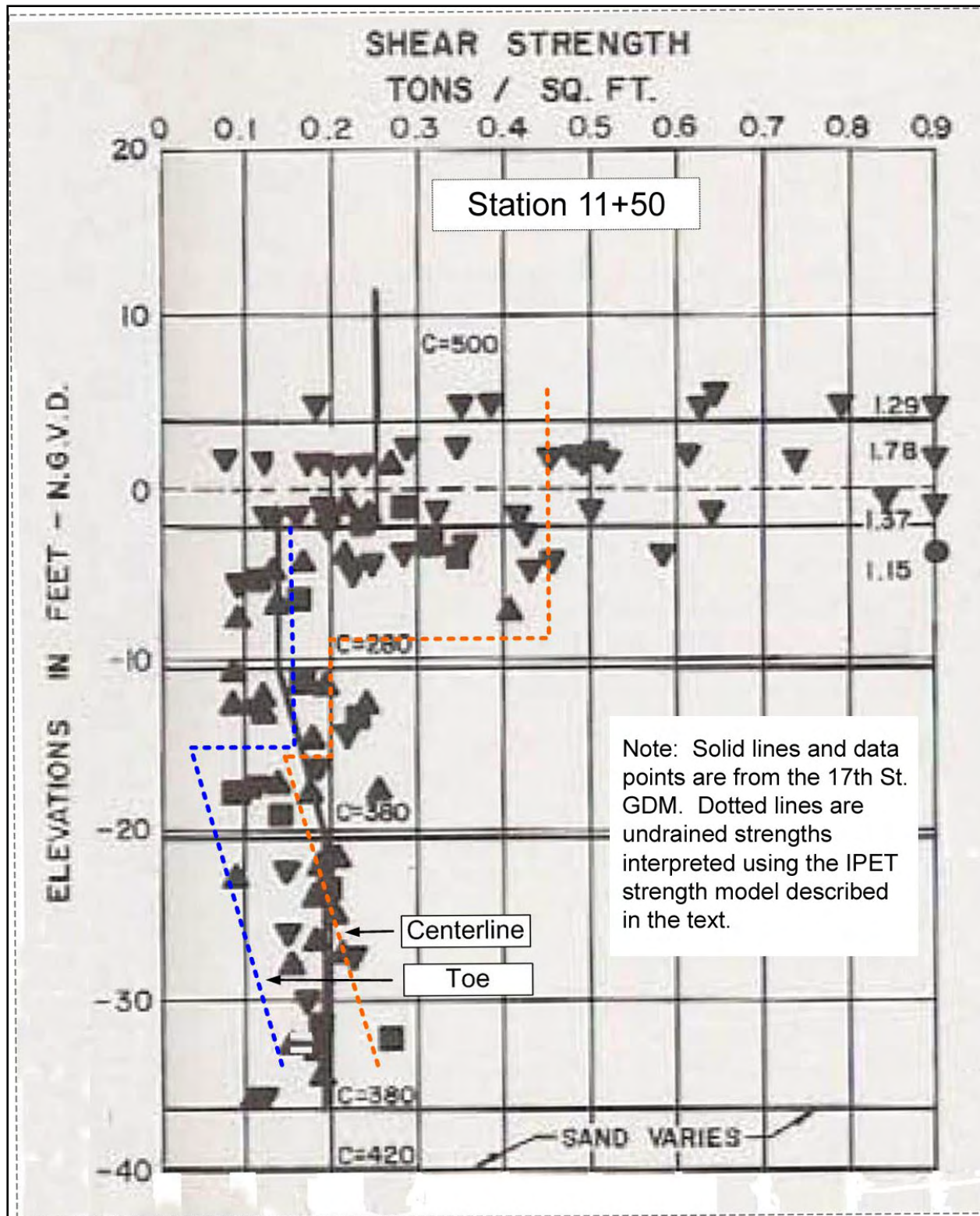
Figure 3-4. Comparison of Undrained Strength Profiles used for 17th Street I-Wall Design with Strength Profiles Interpreted from the IPET Strength Model for Station 11+50

This is a preliminary report subject to revision; it does not contain final conclusions of the United States Army Corps of Engineers.
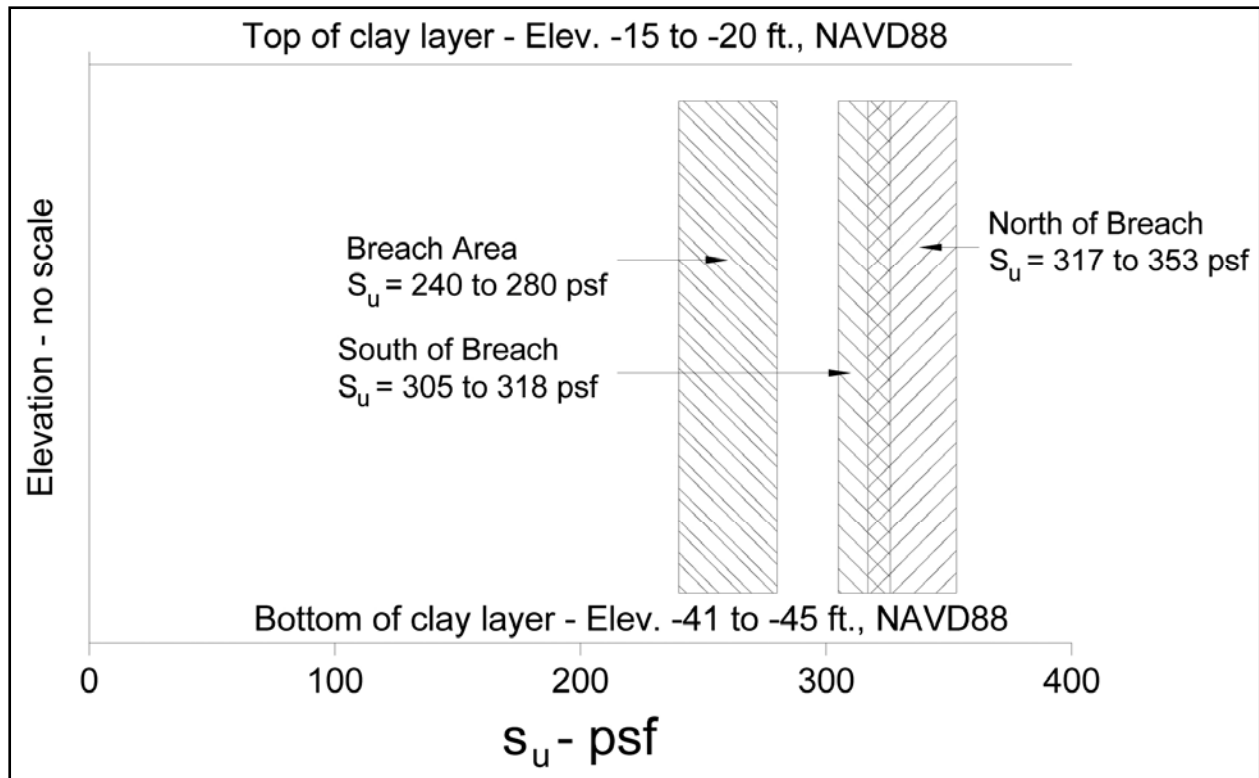
Figure 3-5. Comparison of Undrained Strengths from Breach Area Borings with Strengths from Borings North and South of Breach

Appendix 4
17th Street Canal
Slope Stability Analyses

Objectives

The analyses of stability described in the following sections were performed to answer these questions:

1. What are the factors of safety for the 17th Street Canal I-wall based on the IPET shear strength model, and how do the factors of safety vary with water level in the canal?

2. How are these factors of safety affected by assuming that a crack forms between the canal side of the wall and the levee fill, as the water level rises on the canal side of the wall?

3. What water level is needed for a factor of safety equal to 1.0, and how does this differ for Stations 8+30, 10+00, and 11+50?

4. How do factors of safety calculated using the New Orleans District Method of Planes compare to factors of safety calculated using Spencer's Method?

5. How do factors of safety calculated for design compare with those calculated using the IPET shear strength model and Spencer's Method?

6. How do factors of safety calculated for the breach area compare to factors of safety calculated for adjacent reaches of the I-wall, north and south of the breach area?

7. What are the probabilities of failure in the breach and adjacent areas?

Conditions Analyzed

Fifteen slope stability analyses (Cases 1 through 15 in Table 4-1) were performed for cross sections at Stations 8+30, 10+00, and 11+50. The shear strength profiles for these analyses are

shown in Figures 2, 3, and 4 of the shear strength evaluation report. These strengths are identified as "IPET" in Table 4-1.

Five slope stability analyses (Cases 16 through 20 in Table 4-1) were performed using the cross section and strength profile used in the 17th Street Canal design memorandum[1]. These are identified as "GDM 20" in Table 4-1.

Average values of moist unit weight were used in the analyses: $\gamma_{sat} = 109$ pcf for the levee fill, $\gamma_{sat} = 80$ pcf for the marsh layer, and $\gamma_{sat} = 109$ pcf for the clay beneath the marsh layer, based on values measured in laboratory tests on undisturbed samples.

The critical slip surfaces found in the analyses did not extend down to the sand beneath the clay, and the sand strength and unit weight therefore did not influence the results of the analyses.

The analyses were performed for undrained conditions in the levee fill, the marsh layer, and the clay beneath the marsh layer. Based on available information, it appears that the values of permeability of all three of these materials were low enough so that dissipation of excess pore pressures during the rise of the water level in the canal would have been negligible, and would have had at most a minor influence on stability.

Analyses were performed for two conditions regarding contact between the I-wall and the adjacent soil on the canal side of the wall. These are indicated by "yes" or "no" in the column labeled "Crack" in Table 4-1. The term "crack" as used in herein refers to a vertical separation between the wall and the canal-side levee fill, not a local failure of either the wall or the fill soil.

- For the "no crack" analyses, it was assumed that the soil on the canal side of the wall was in intimate contact with the wall. Water pressures were applied to the surface of the levee fill, and to the I-wall where it projected above the crown of the levee, but were not applied to the face of the wall below the crown of the levee.

- For the "crack" analyses, it was assumed that the I-wall was separated from the levee fill on the canal side of the wall as the water level in the canal rose and caused the wall to deflect away from the canal. Full hydrostatic water pressures were applied to the I-wall, from the water level in the canal to the bottom of the wall.

Analyses were performed for the following canal water levels:

- Elevation 7.0 ft, the approximate water level at the time of failure[2]. It is estimated that the water level in the 17th Street Canal at the time the I-wall began to fail was 6.7 ft to 7.7 ft.

- Elevation 10.0 ft, the water level used as the principal design loading condition (converted here to NAVD88 datum).

---

[1] General Design Memorandum #20 – 17th Street Outfall Canal – Volume 1 (GDM20).
[2] All elevations here are referred to NAVD88 datum.

- The elevations that resulted in computed factors of safety equal to 1.0 at 8+30, 10+00, and 11+50. These were different elevations for the three stations.

- Elevation 11.5 ft, the elevation that resulted in a computed factor of safety equal to 1.0 for the GDM20 cross section and strength. This was analyzed only for the GDM20 design cross section and strength model.

The analyses described here were performed using the computer program SLIDE[3], and factors of safety were checked using UTEXAS4[4]. Critical circular slip surfaces were located for each case, using the search routines available in SLIDE and UTEXAS4. The analyses were performed using Spencer's method[5], which satisfies all conditions of equilibrium. Methods that satisfy all conditions of equilibrium have been shown to result in values of factor of safety that are not influenced appreciably by the details of the assumptions they involve[6].

In all, 20 cases were analyzed. The conditions analyzed and results of these analyses are summarized in Table 4-1. The critical circles for these cases are shown in Figures 4-1 through 4-15, and 4-17 through 4-21.

Effect of Canal Water Level

The higher the water level in the canal, the lower was the calculated factor of safety, all other things being equal. This can be seen for the no crack condition by comparing Cases 1 and 3, for Station 8+30. Raising the canal water level from elevation 7.0 ft to elevation 10.0 ft results in a decrease in the computed factor of safety of 0.34, from 1.75 to 1.41. For Station 10+00, raising the water level from elevation 7.0 to 10.0 results in a decrease in factor of safety of 0.29 (Cases 6 and 8). For Station 11+50, the reduction is 0.31 (Cases 11 and 13).

Raising the water level also reduces the factor of safety for the cracked condition, as can be seen by comparing Cases 2 and 4, Cases 7 and 9, and Cases 12 and 14. The reduction in the value of F for these cases varies from 0.21 to 0.28.

Effect of a Crack on the Canal Side of the Wall

Assuming that a crack formed on the canal side of the wall, and that hydrostatic water pressure acted through the full depth of the crack, causes a very significant reduction in the value of the calculated factor of safety.

---

[3] Available from Rocscience Inc., 31 Balsam Avenue, Toronto, Ontario, Canada M4E 3B5
[4] Available from Shinoak Software, 3406 Shinoak Drive, Austin, TX 78731
[5] Spencer, E. (1967) "A Method of Analysis of the Stability of Embankments Assuming Parallel Inter-Slice Forces," *Geotechnique*, Institution of Civil Engineers, Great Britain, Vol. 17, No. 1, March, pp. 11-26.
[6] Duncan, J. Michael, and Wright, Stephen G. (2005), *Soil Strength and Slope Stability*, John Wiley and Sons, New York, 293 pp.

For Station 8+30, with the canal water level at elevation 7.0 ft, the calculated factor of safety for the cracked condition is 1.32, as compared to 1.75 for the uncracked condition. With the water level at 10.0 ft, introducing a crack reduces the factor of safety from 1.41 to 1.04.

For Station 10+00, with the canal water level at elevation 7.0 ft, the calculated factor of safety for the cracked condition is 1.21, as compared to 1.57 for the uncracked condition. With the water level at 10.0 ft, introducing a crack reduces the factor of safety from 1.28 to 0.98.

For Station 11+50, with the canal water level at elevation 7.0 ft, the calculated factor of safety for the cracked condition is 1.21, as compared to 1.60 for the uncracked condition. With the water level at 10.0 ft, introducing a crack reduces the factor of safety from 1.29 to 1.00.

The "no crack" and "full crack" conditions considered here represent the extremes that are possible. The centrifuge model tests of the 17th Street I-wall showed that a crack did form full-depth at the back of the wall, consistent with the "full crack" condition considered here.

It seems likely that the failure was progressive, with a gradual reduction in factor of safety as the water rose, followed by a more sudden further reduction in factor of safety when the crack formed and water filled it. This appears to be a key factor in the mechanism of failure.

For the canal water level at elevation 10.0 ft, the calculated factor of safety is lowest at Station 10+00. This is approximately the same location where an eyewitness report indicates the failure began at 7:00 AM to 8:00 AM on August 29. The eyewitness reported that failure began at Station 11+00. Subsequently, failure spread to other locations in the breach area.

A sequence of events consistent with the eyewitness report and the calculated results is this:

- As the canal water level rose, a crack did not form until the water reached an average elevation (not accounting for wave effects) of 6.7 ft to 7.7 ft, and the factor of safety before the crack formed was above 1.0.

- When the average water level reached elevation 6.7 ft to 7.7 ft, and the static water pressure force was increased by wave effects, a crack formed between the I-wall and the levee fill on the canal side of the wall, resulting in a reduction in the factor of safety, and the wall began to fail at the location where the factor of safety was lowest.

Static Water Level for Factor of Safety Equal to 1.0

The canal water level was varied to determine the static water level at which the calculated factor of safety would be equal to 1.0, with a crack. Calculated water levels for factors of safety equal to 1.0 for the cracked condition vary from 9.8 ft to 10.6 ft, as compared with a water level of 6.7 ft to 7.7 ft when failure began based on the eyewitness report. It appears that wave effects might raise the effective water level at the time of failure by as much as 2.0 ft, to 8.7 ft to 9.7 ft. In this case the water levels for $F = 1.00$ would exceed the observed water level at the time of failure by 0.1 ft to 1.9 feet.

An additional factor to be considered is the fact that the analyses discussed so far used circular slip surfaces. Additional analyses have been performed using noncircular slip surfaces with UTEXAS4. A comparison of the critical circular surface with the critical noncircular surface is shown in Figure 4-22. Although the critical noncircular surface is very similar in shape and position to the critical circle, the factor of safety for the noncircular surface is 6% lower. This 6% lower factor of safety corresponds to a water level for F = 1.00 that is 0.8 ft lower than the F = 1.00 water level found using circular slip surfaces.

These considerations can be summarized as follows:

- Static average water level at the time of failure = 6.7 ft to 7.7 ft.

- Effective water level at the time of failure, including 2.0 ft wave effects = 8.7 ft to 9.7 ft.

- Water level for F = 1.00 based on noncircular slip surfaces = 9.0 ft.

Considering the uncertainties involved in the time of failure and the magnitude of the wave effects, it appears that the best estimate of the water level at the time of failure is in good agreement with the water level for F = 1.00 determined using noncircular slip surfaces. As a result, it can be concluded that the IPET strength model is a reasonable characterization of the shear strengths in the 17th Street Canal breach area.

Comparison of Spencer's Method with the Method of Planes

Cases 16 through 20 of Table 4-1 used the design cross section and the shear strengths used in design. The cross section is shown in Figure 4-16, which is taken from Plate 62 of GDM20. The shear strengths are shown in Figures 2, 3, and 4 of the shear strength evaluation report (the design strength profile is the same in all three figures). This cross section and these shear strengths were used as the basis for design of the wall from Wall Stations 554+00 to 568+00, which includes the area where the breach occurred.

The factor of safety computed using the Method of Planes[7] for these conditions was 1.30, with the canal water level at 10.0 ft NAVD88 (11.5 ft NGVD29), and no crack on the canal side of the wall. The factor of safety for this same condition computed using Spencer's Method (Case 18 in Table 4-1) was 1.45.

Comparison of Design Analyses with Analyses Performed Using the IPET Strength Model and Spencer's Method

The design analyses were based on these conditions:

---

[7] A study of the Method of Planes, undertaken by IPET at the request of the New Orleans District Task Force Guardian, indicates that the Method of Planes gives lower factors of safety than more accurate methods of analysis, such as Spencer's method. The magnitude of the difference between the two varies from case to case.

1. The analyses were performed for the cross section shown in Figure 4-16.

2. The design strength profile shown in Figures 2, 3, and 4 of the shear strength evaluation report were used in the analyses. The same strengths were used under the embankment crest, under the slope, and beyond the toe of the levee.

3. The Method of Planes was used to calculate the factor of safety.

4. The wall was assumed to be in contact with the levee fill soil on the canal side (the no crack condition).

5. The water elevation was assumed to be at 10.0 ft NAVD88 (11.5 ft NGVD29).

As noted previously, for these conditions a factor of safety equal to 1.30 was calculated using the Method of Planes. Five variations on these conditions were analyzed using Spencer's Method. These are shown in Table 4-1 as Cases 16 through 20.

With the water level at 10.0 ft NAVD88, and a crack between the wall and the soil on the canal side, the factor of safety calculated using Spencer's Method is 1.24. The water level required to reduce the factor of safety to 1.0 is 11.5 ft NAVD88.

It appears that the most important difference between the conditions used as the basis for design and the conditions defined in this report is related to the strengths of the marsh layer and clay soils beneath the slopes and beyond the toe of the levee. The design strengths and the IPET strengths are very nearly the same beneath the crest of the levee. However, beneath the levee slopes, and beyond the toe, the design strengths were higher than the IPET strengths.

Comparison of Factors of Safety in the Breach Area with Those in Areas to the North and the South

In order to examine the effect on stability of the higher strengths in the sections north and south of the breach that were discussed in the strength evaluation report, stability analyses were performed using shear strengths for the clay and the marsh layer that were 20% higher than those estimated for the breach area. This 20% higher strength was based on the data available for the area south of the breach. North of the breach a greater difference in clay strength (about 30%) was indicated by the available strength data.

The analyses with higher strengths were performed for Station 10+00, with a crack at the canal side of the wall, full hydrostatic water pressure in the crack, and canal water levels at elevations 7.0 ft and 10.0 ft. The results of these analyses are shown in Table 4-2, together with the comparable results from Table 4-1.

For the canal water level at elevation 7.0 ft, a 20% increase in clay strength results in a 15% increase in factor of safety. A 20% increase in marsh layer strength results in 4% increase in factor of safety. For the canal water level at elevation 10.0 ft, a 20% increase in clay strength

results in a 13% increase in factor of safety. A 20% increase in marsh layer strength results in 5% increase in factor of safety.

The factors of safety shown in Table 4-2 for increased clay and marsh layer strengths are consistent with the fact that failure did not occur in these areas. However, it appears that the margin of safety was very small.

Probabilities of Failure

Probabilities of failure have been estimated using an approximate technique based on the Taylor Series method. The coefficient of variation of the average clay strength and the average marsh layer strength were estimated to be 20%. The data available is sparse, and the scatter in measured values is influenced significantly by sample quality as well as variations in properties from one location to another. The estimated values of COV = 20% is thus largely based on judgment. Even so, it is useful to examine what probabilities of failure would be associated with this level of uncertainty concerning shear strengths.

The Taylor Series numerical method[8,5] was used to estimate the standard deviation (σ_F) and the coefficient of variation of the factor of safety (COV$_F$), using these formulas:

$$\sigma_F = \sqrt{\left(\frac{\Delta F_{clay\,strength}}{2}\right)^2 + \left(\frac{\Delta F_{peat\,strength}}{2}\right)^2} \tag{4-1}$$

$$COV_F = \frac{\sigma_F}{F_{MLV}} \tag{4-2}$$

where $\Delta F_{clay\,strength}$ = difference between the values of the factor of safety calculated with the clay strength increased by one standard deviation and decreased by one standard deviation from its most likely value. $\Delta F_{marsh\,layer\,strength}$ is determined in the same way. F_{MLV} is the "most likely value" of factor of safety, computed using the IPET shear strengths.

Values of F_{MLV} and COV$_F$ have been calculated for Station 10+00 and for areas adjacent to the breach, which were assumed for this purpose to have strengths 20% higher than the IPET strength model. The results are listed in Table 4-3, together with the corresponding values of probability of failure based on an assumed lognormal distribution of factor of safety.

For Station 10+00, the calculated probabilities of failure are 12% for a water level of 7.0 ft, and 58% for a water level of 10.0 ft. These values are reasonable, considering that the water level (including wave effects) was 8.7 ft to 9.7 ft at the time of failure. For adjacent areas with

---

[8]Wolff, T. F. (1994). "Evaluating the reliability of existing levees." Report, Research Project: Reliability of Existing Levees, prepared for U.S. Army Engineer Waterways Experiment Station Geotechnical Laboratory, Vicksburg, Miss.

higher strengths, the probabilities of failure are lower, but still too high to offer confidence in the ability of the I-wall to survive water levels higher than about 7.0 ft.

Summary

The results of the analyses described in the preceding sections are consistent with the performance of the I-wall in the breach area, indicating that the IPET strength model and the mechanism of failure provide a suitable basis for evaluating the performance of the 17th Street Canal I-wall during Hurricane Katrina.

Calculated factors of safety are about 25% lower when it is assumed that a crack develops between the wall and the levee fill on the canal side of the wall. The results calculated assuming that a crack formed, and that full hydrostatic water pressure acted in the crack, are consistent with field observations and centrifuge test results, indicating a high likelihood that a crack did form in the areas where the wall failed. Centrifuge model tests of the 17th Street I-wall showed that a crack did form full-depth at the back of the wall, consistent with the "full crack" condition considered here.

The New Orleans District Method of Planes is a conservative method of slope stability analysis. A study of the Method of Planes undertaken by IPET at the request of the New Orleans District Task Force Guardian indicates that the Method of Planes gives lower factors of safety than more accurate methods of analysis, such as Spencer's method. The magnitude of the difference between the two varies from case to case

The factors of safety calculated in the design analyses were higher than the factors of safety calculated for the conditions that are believed to best represent the actual shear strengths, geometrical conditions, and loading at the time of failure. The principal differences between the design analyses and the conditions described in this report relate to (1) the crack between the wall and the levee soil on the canal side of the wall, and (2) the fact that the design analyses used the same strength for the clay and the marsh layer beneath the levee slopes, and for the area beyond the levee toe, as for the zone beneath the crest of the levee. The IPET strength model has lower strengths beneath the levee slopes and beyond the toe.

Factors of safety for areas adjacent to the breach, where clay strengths are higher, were about 15% higher than those calculated for the breach area. These differences in calculated factor of safety are not large, and it thus appears that the margin of safety was small in areas that did not fail. It is possible that cracks or gaps did not form in those areas.

Estimates of probability of failure for water a level of 7.0 ft NAVD88 are about 12% in the breach area, and 1% in adjacent areas with clay strengths 20% higher. For a water level of 10.0 ft, the estimated probability of failure is 58% in the breach area and 16% in adjacent areas.

Table 4-1
Results of Slope Stability Analyses for Stations 8+30, 10+00, and 11+50 of the 17th Street Canal Floodwall

Case	Section	Slip Surface	Method	Strength Model	Crack	Water Elev. Ft. NAVD88	F
1	8+30	Crit. Circle	Spencer's	IPET	no	7.0	1.75
2	8+30	Crit. Circle	Spencer's	IPET	yes	7.0	1.32
3	8+30	Crit. Circle	Spencer's	IPET	no	10.0	1.41
4	8+30	Crit. Circle	Spencer's	IPET	yes	10.0	1.04
5	8+30	Crit. Circle	Spencer's	IPET	yes	10.6	1.00
6	10+00	Crit. Circle	Spencer's	IPET	no	7.0	1.57
7	10+00	Crit. Circle	Spencer's	IPET	yes	7.0	1.21
8	10+00	Crit. Circle	Spencer's	IPET	no	10.0	1.28
9	10+00	Crit. Circle	Spencer's	IPET	yes	10.0	0.98
10	10+00	Crit. Circle	Spencer's	IPET	yes	9.8	1.00
11	11+50	Crit. Circle	Spencer's	IPET	no	7.0	1.60
12	11+50	Crit. Circle	Spencer's	IPET	yes	7.0	1.21
13	11+50	Crit. Circle	Spencer's	IPET	no	10.0	1.29
14	11+50	Crit. Circle	Spencer's	IPET	yes	10.0	1.00
15	11+50	Crit. Circle	Spencer's	IPET	yes	10.1	1.00
16	GDM 20	Crit. Circle	Spencer's	GDM 20	no	7.0	1.77
17	GDM 20	Crit. Circle	Spencer's	GDM 20	yes	7.0	1.60
18	GDM 20	Crit. Circle	Spencer's	GDM 20	no	10.0	1.45
19	GDM 20	Crit. Circle	Spencer's	GDM 20	yes	10.0	1.24
20	GDM 20	Crit. Circle	Spencer's	GDM 20	yes	11.5	1.00

Table 4-2
Factors of Safety Calculated for Stations 10+00 Geometry Using Clay Strength and Marsh Layer Strength 20% Higher than the IPET Strengths of these Materials

Case	Section	Slip Surface	Method	Strength Model	Crack	Water Elev. Ft. NAVD88	F
7	10+00	Crit. Circle	Spencer's	IPET	yes	7.0	1.21
7A	10+00	Crit. Circle	Spencer's	clay + 20%	yes	7.0	1.40
7B	10+00	Crit. Circle	Spencer's	clay - 20%	yes	7.0	1.02
7C	10+00	Crit. Circle	Spencer's	marsh + 20%	yes	7.0	1.26
7D	10+00	Crit. Circle	Spencer's	marsh - 20%	yes	7.0	1.16
9	10+00	Crit. Circle	Spencer's	IPET	yes	10.0	0.98
9A	10+00	Crit. Circle	Spencer's	clay + 20%	yes	10.0	1.12
9B	10+00	Crit. Circle	Spencer's	clay - 20%	yes	10.0	0.84
9C	10+00	Crit. Circle	Spencer's	marsh + 20%	yes	10.0	1.04
9D	10+00	Crit. Circle	Spencer's	marsh - 20%	yes	10.0	0.93

Table 4-3
Calculated Probabilities of Failure for Station 10+00 and Adjacent Areas

Area	Water level (ft) NAVD88	F_{MLV}	COV_F	Probability of failure
Sta. 10+00	7.0	1.21	16%	12%
Sta. 10+00	10.0	0.98	15%	58%
Adjacent	7.0	1.47	15%	1%
Adjacent	10.0	1.17	15%	16%
F_{MLV} = most likely value of factor of safety COV_F = coefficient of variation of factor of safety				

Figure 4-1. Critical Circle for 17th Street Canal Station 8+30 – Water Elevation 7.0 ft, No Tension Crack

Figure 4-2. Critical Circle for 17th Street Canal Station 8+30 – Water Elevation 7.0 ft, Tension Crack

Figure 4-3. Critical Circle for 17th Street Canal Station 8+30 – Water Elevation 10 ft, No Tension Crack

Figure 4-4. Critical Circle for 17th Street Canal Station 8+30 – Water Elevation 10 ft, Tension Crack

This is a preliminary report subject to revision; it does not contain final conclusions of the United States Army Corps of Engineers.

Figure 4-5. Critical Circle for 17th Street Canal Station 8+30 – Water Elevation 10.6 ft, Tension Crack.

Figure 4-6. Critical Circle for 17th Street Canal Station 10+00 – Water Elevation 7.0 ft, No Tension Crack

This is a preliminary report subject to revision; it does not contain final conclusions of the United States Army Corps of Engineers.

Figure 4-7. Critical Circle for 17th Street Canal Station 10+00 – Water Elevation 7.0 ft, Tension Crack
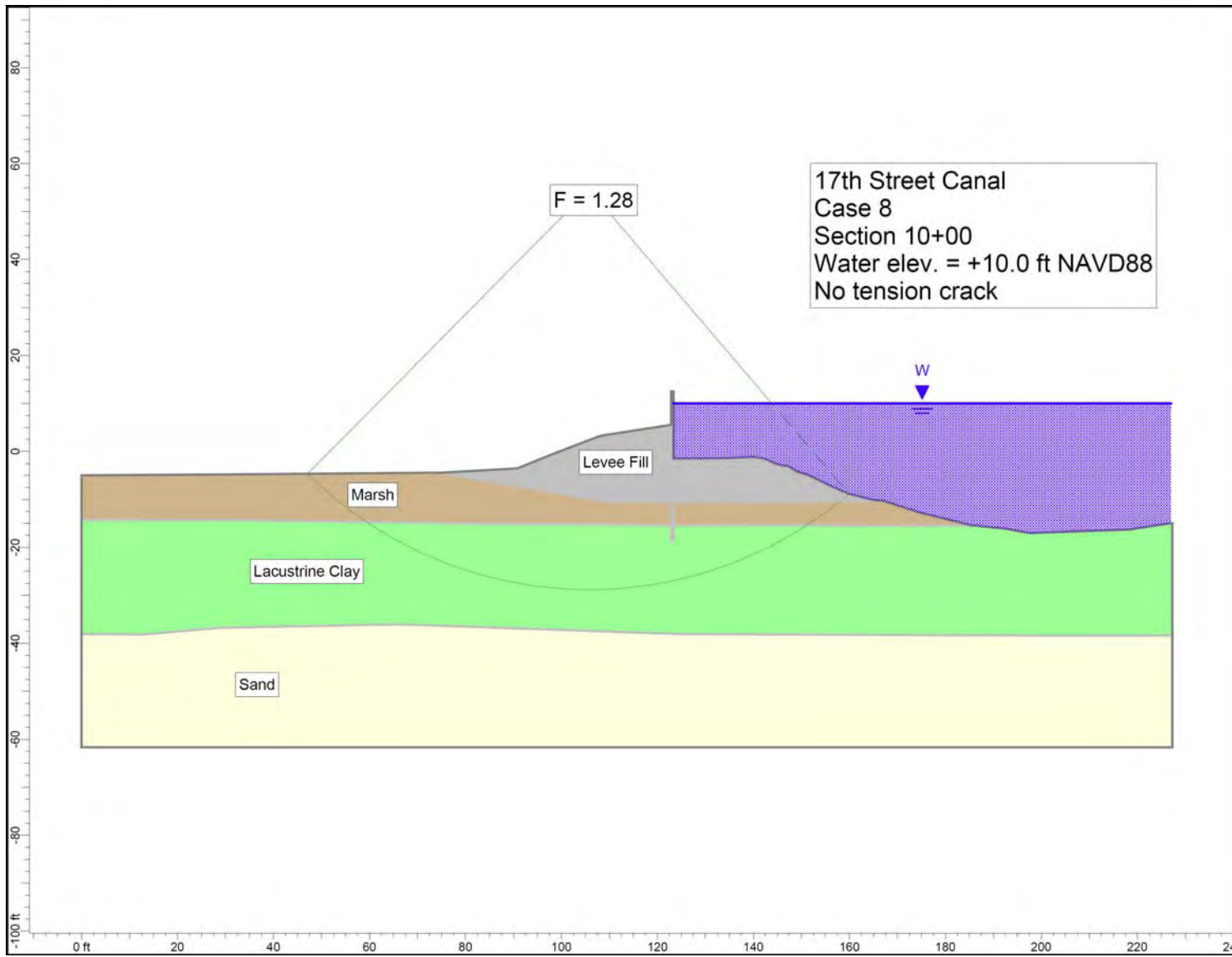
Figure 4-8. Critical Circle for 17th Street Canal Station 10+00 – Water Elevation 10 ft, No Tension Crack
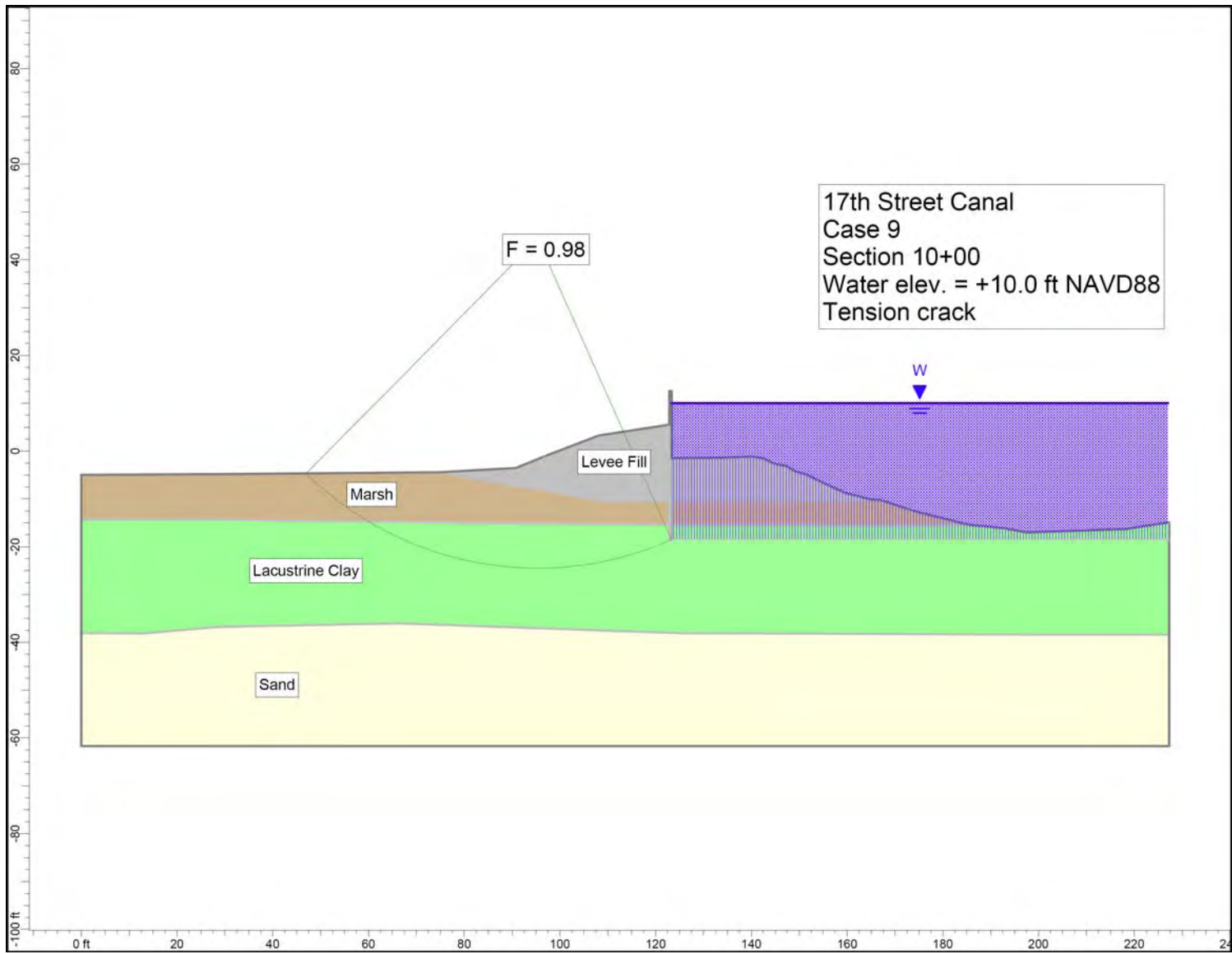
Figure 4-9. Critical Circle for 17th Street Canal Station 10+00 – Water Elevation 10 ft, Tension Crack

Volume V The Performance – Levees and Floodwalls – Technical Appendix
This is a preliminary report subject to revision; it does not contain final conclusions of the United States Army Corps of Engineers.

V-4-19
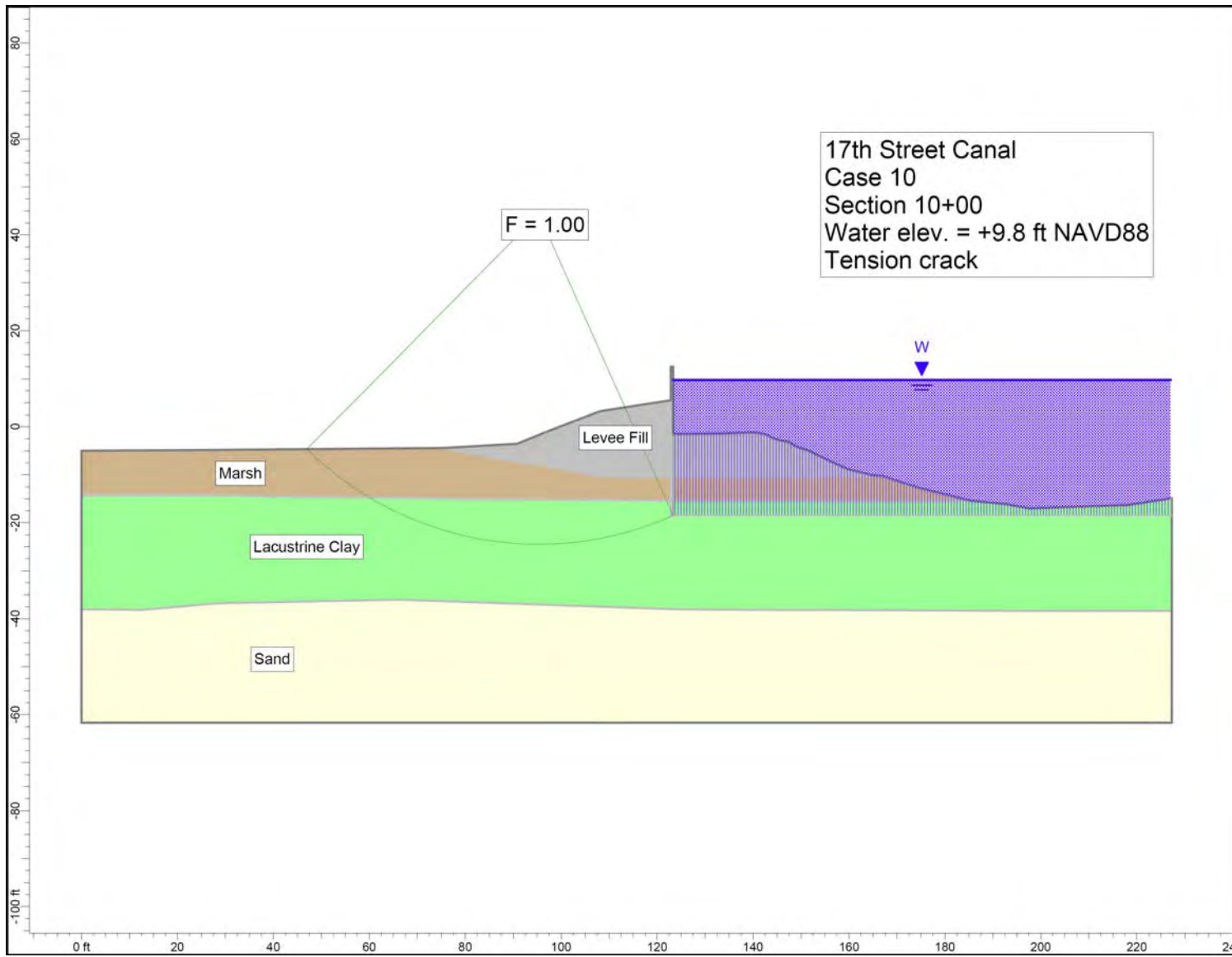
Figure 4-10.   Critical Circle for 17th Street Canal Station 10+00 – Water Elevation 9.8 ft, Tension Crack

This is a preliminary report subject to revision; it does not contain final conclusions of the United States Army Corps of Engineers.
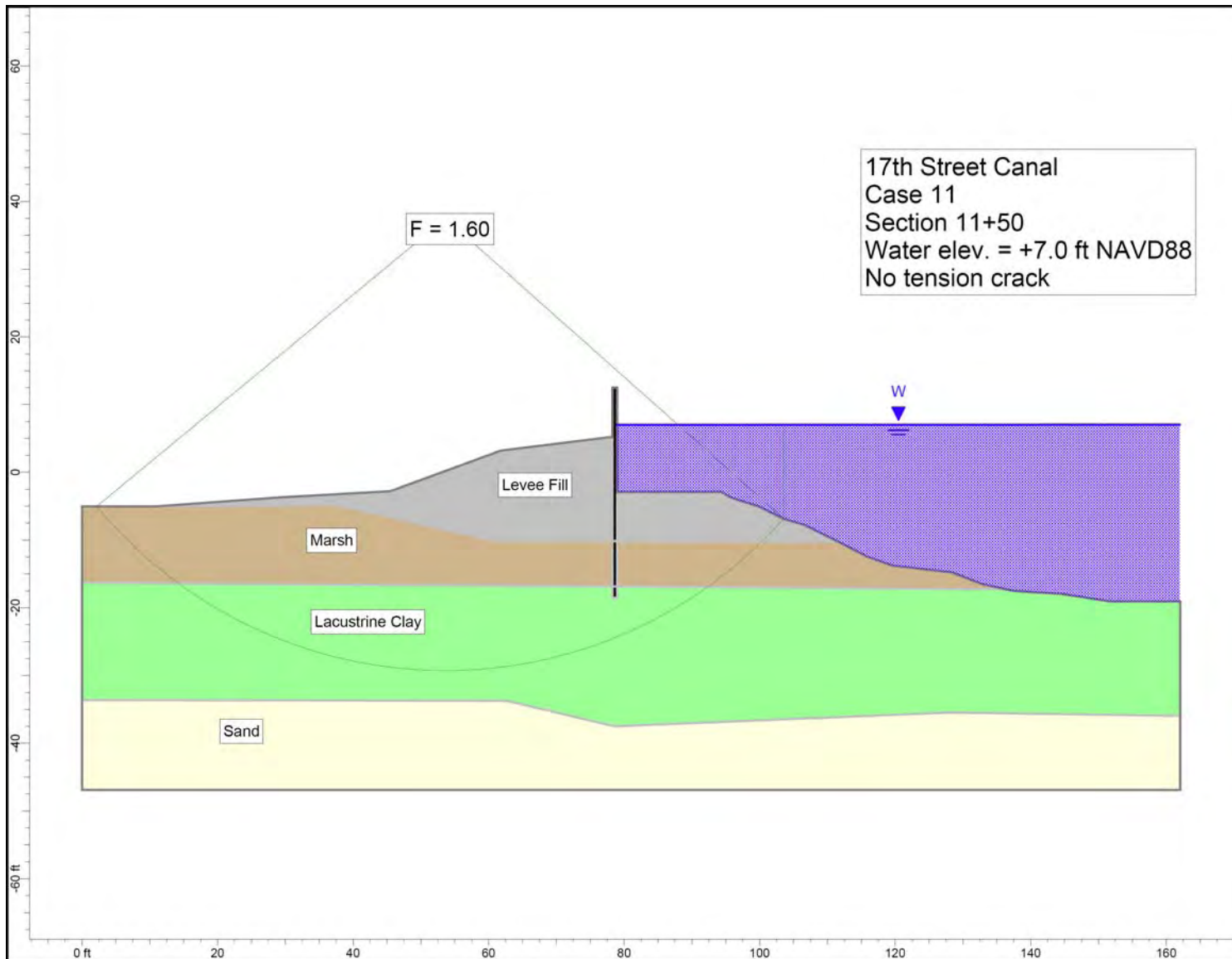
Figure 4-11.   Critical Circle for 17th Street Canal Station 11+50 – Water Elevation 7 ft, No Tension Crack
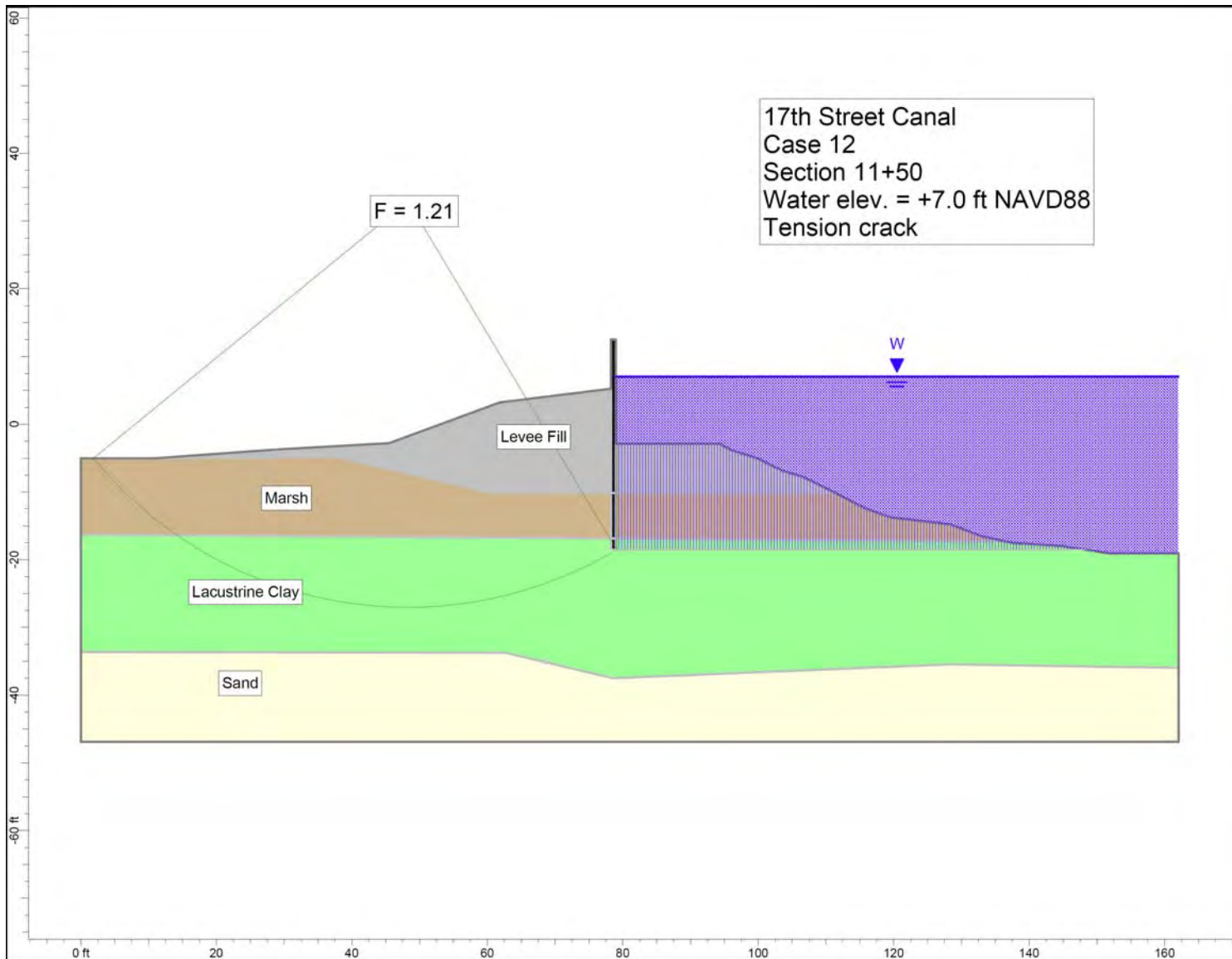
Figure 4-12.   Critical Circle for 17th Street Canal Station 11+50 – Water Elevation 7 ft, Tension Crack

This is a preliminary report subject to revision; it does not contain final conclusions of the United States Army Corps of Engineers.
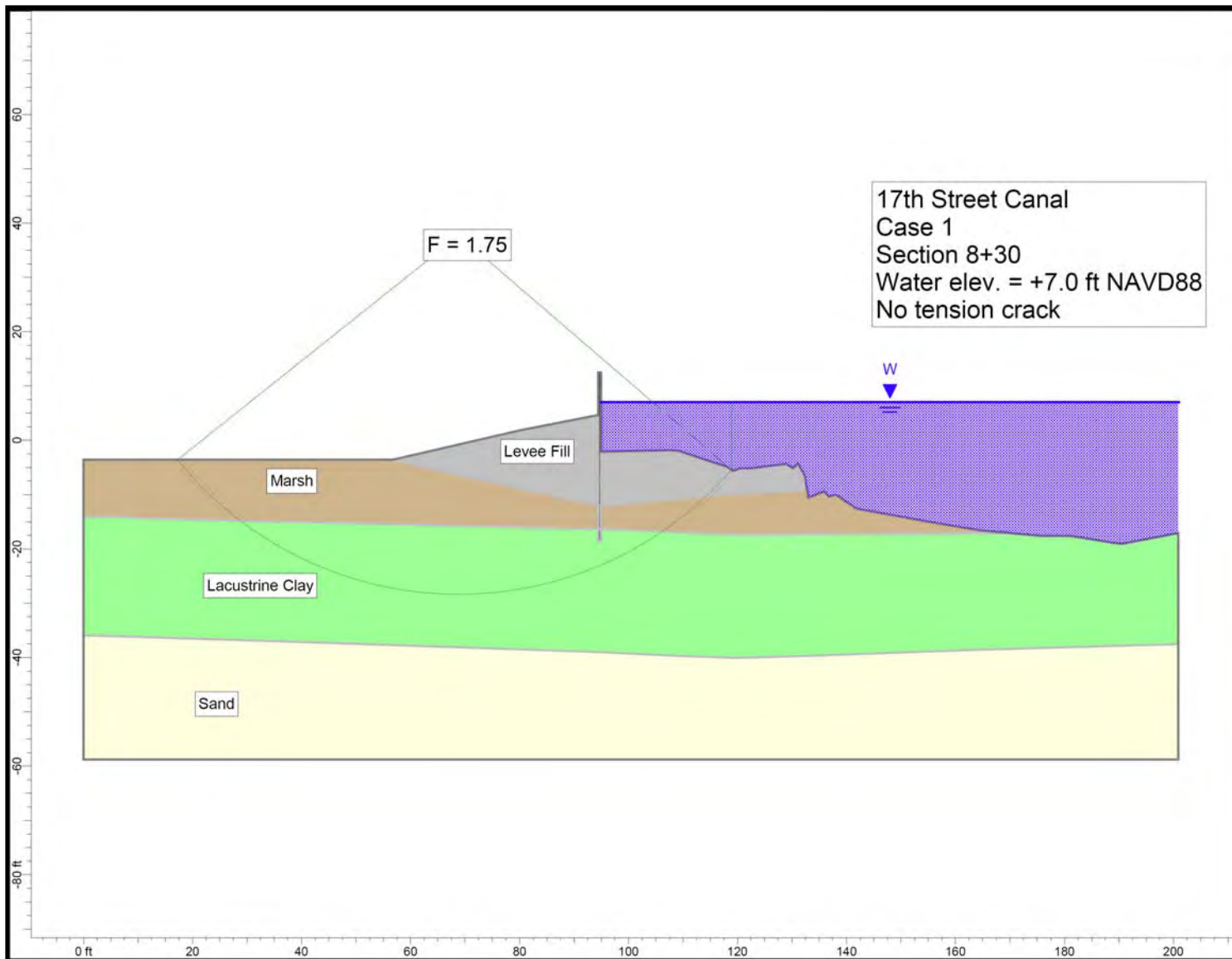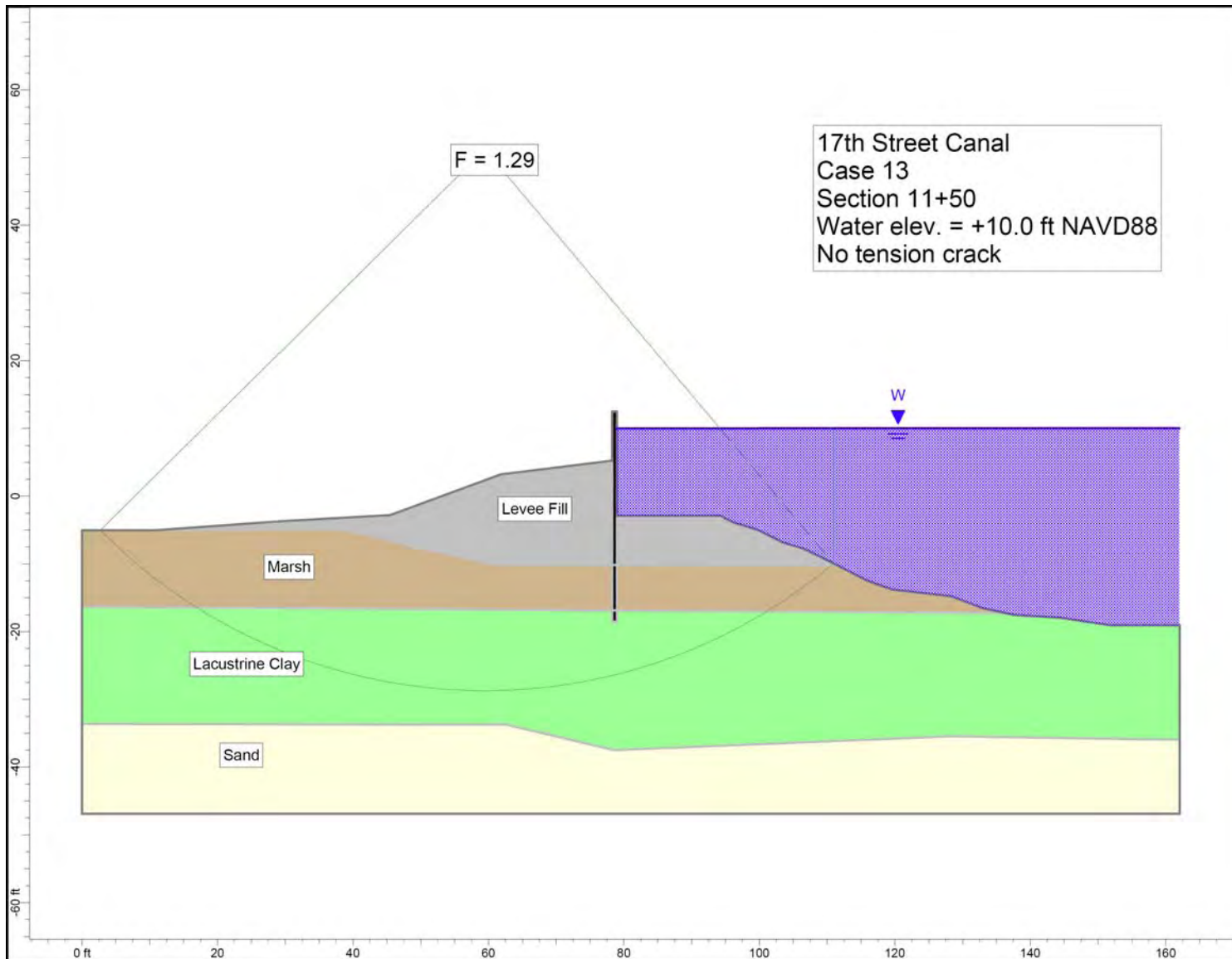
Figure 4-13. Critical Circle for 17th Street Canal Station 11+50 – Water Elevation 10 ft, No Tension Crack
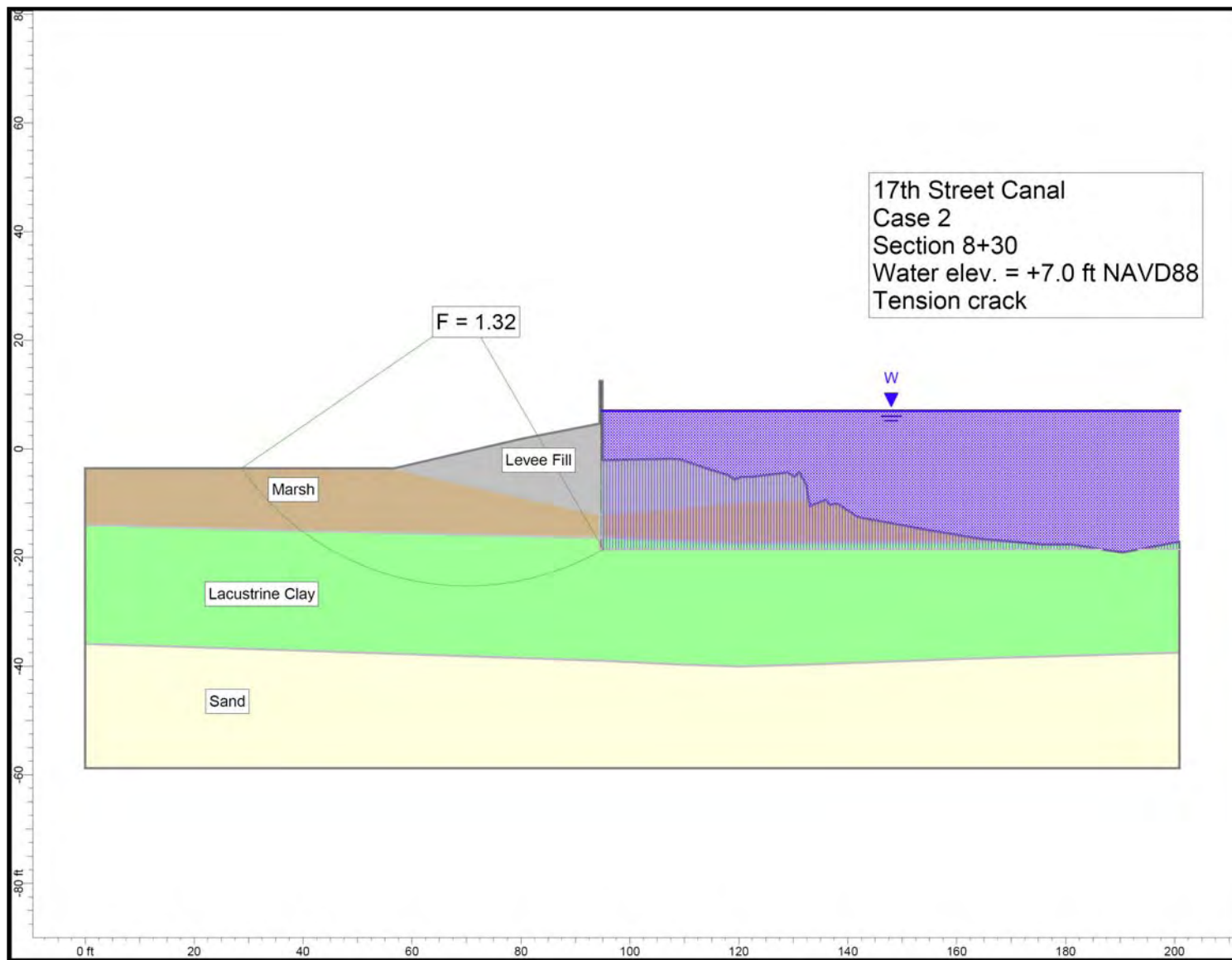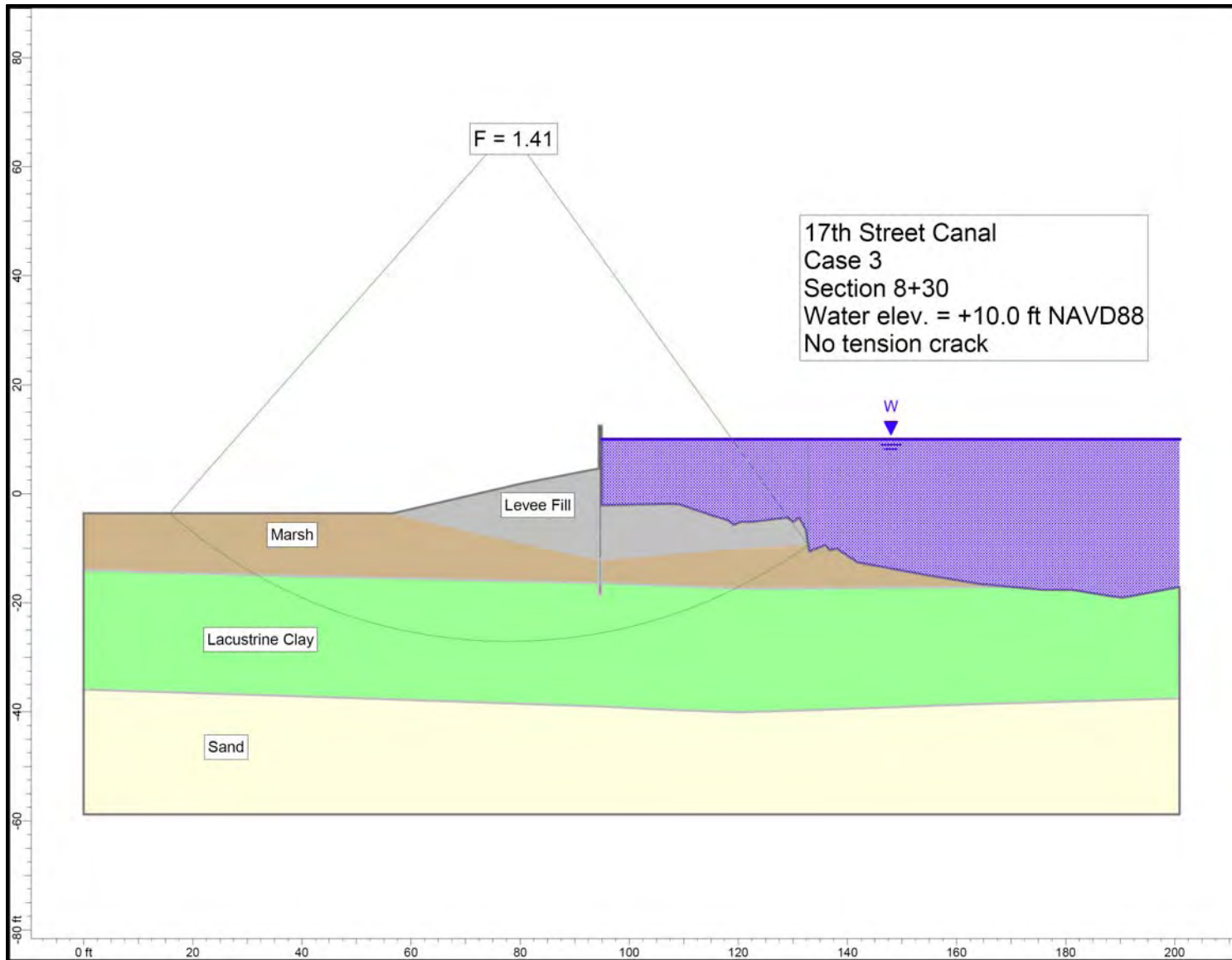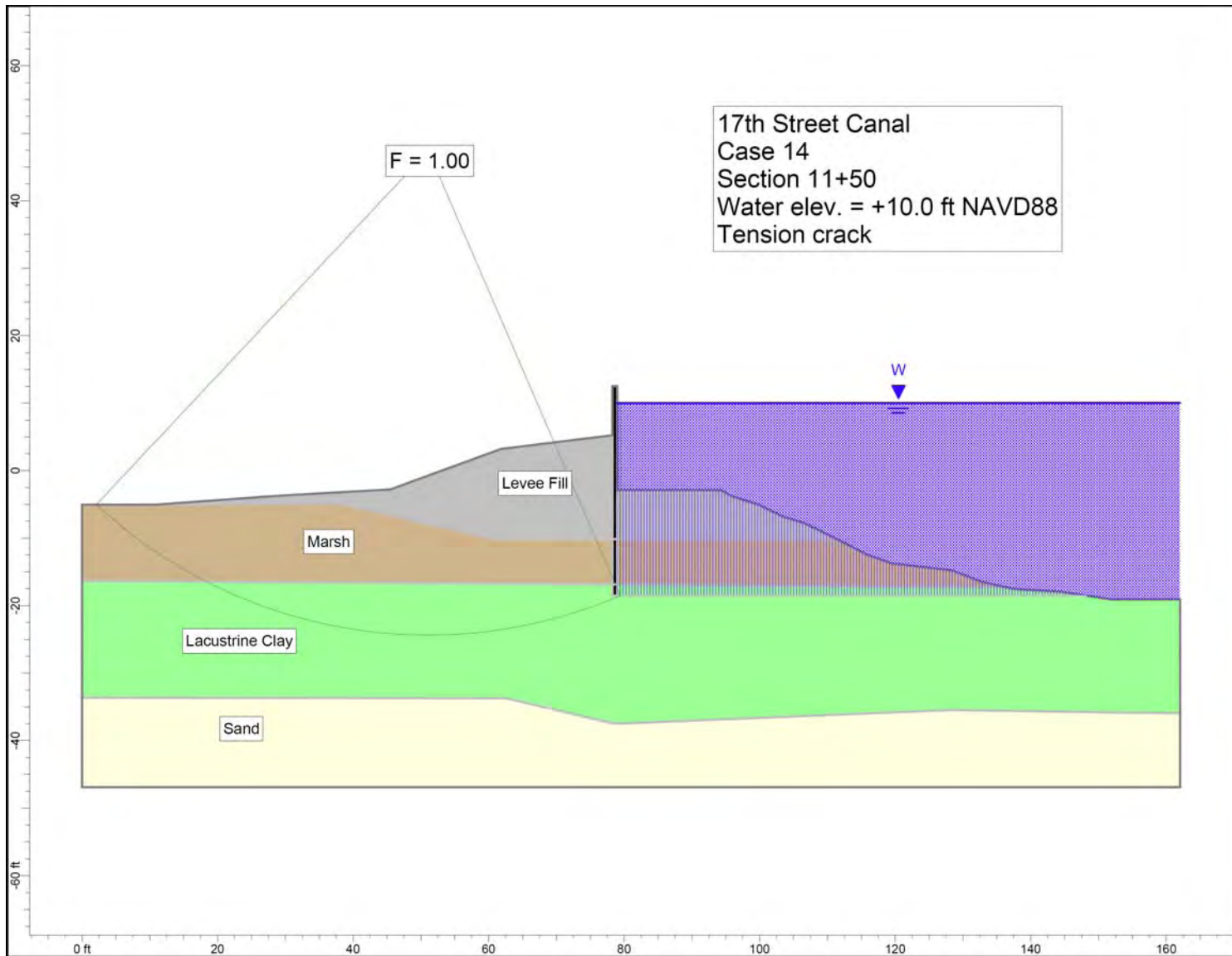
Figure 4-14.   Critical Circle for 17th Street Canal Station 11+50 – Water Elevation 10 ft, Tension Crack
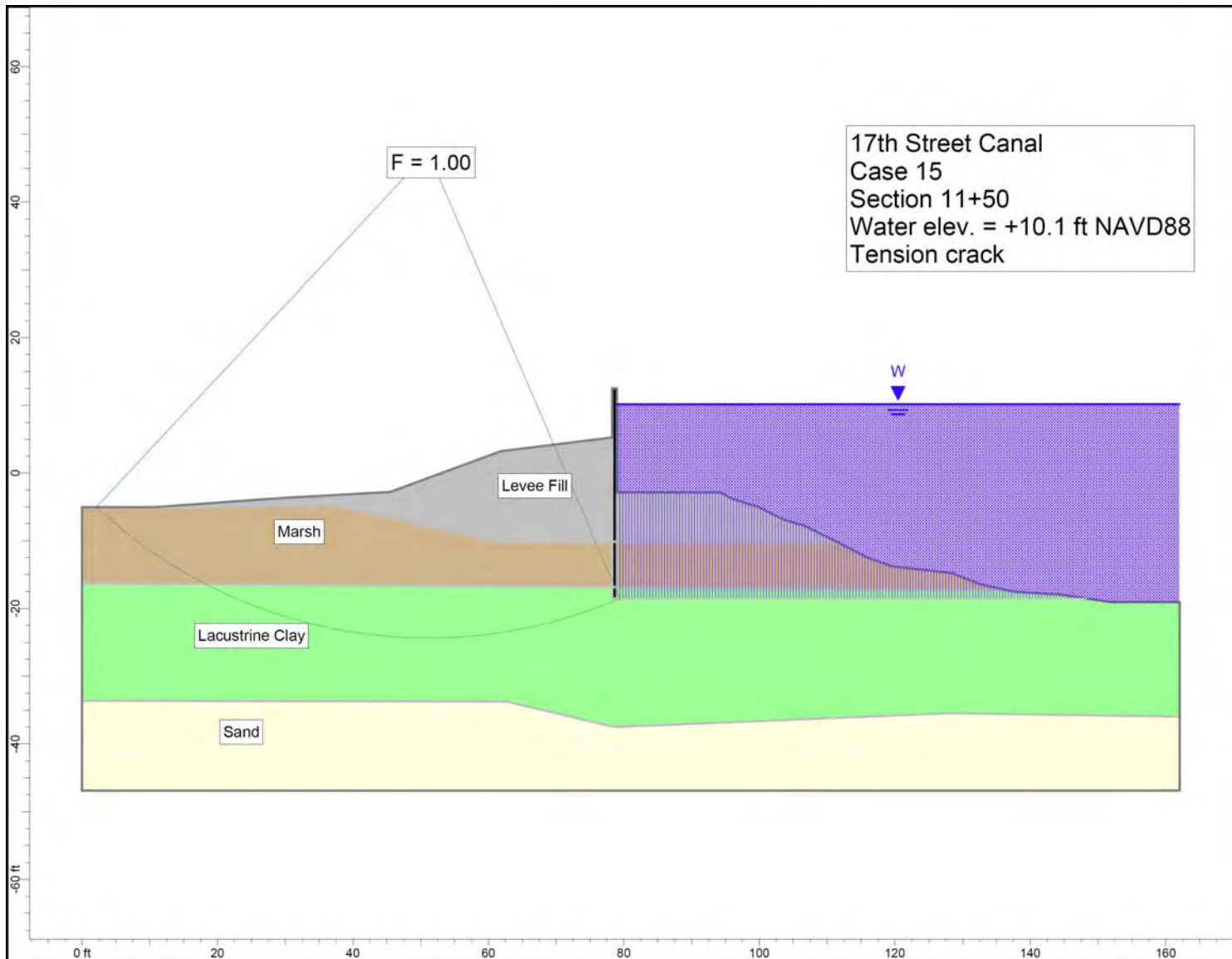
Figure 4-15.   Critical Circle for 17th Street Canal Station 11+50 – Water Elevation 10.1 ft, Tension Crack
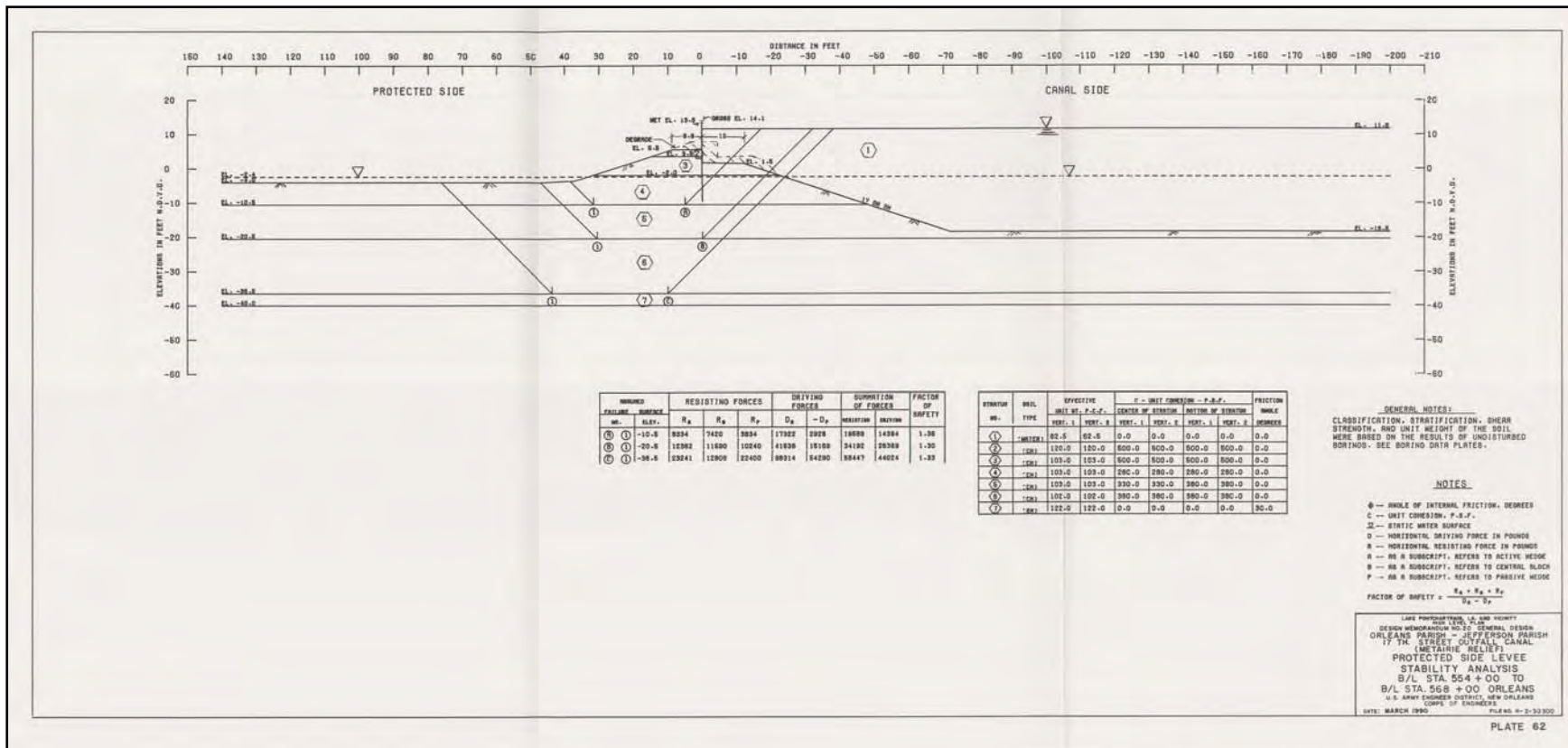
Figure 4-16.   Design Cross Section, from GDM 20, Plate 62

V-4-26

Volume V The Performance – Levees and Floodwalls – Technical Appendix
This is a preliminary report subject to revision; it does not contain final conclusions of the United States Army Corps of Engineers.
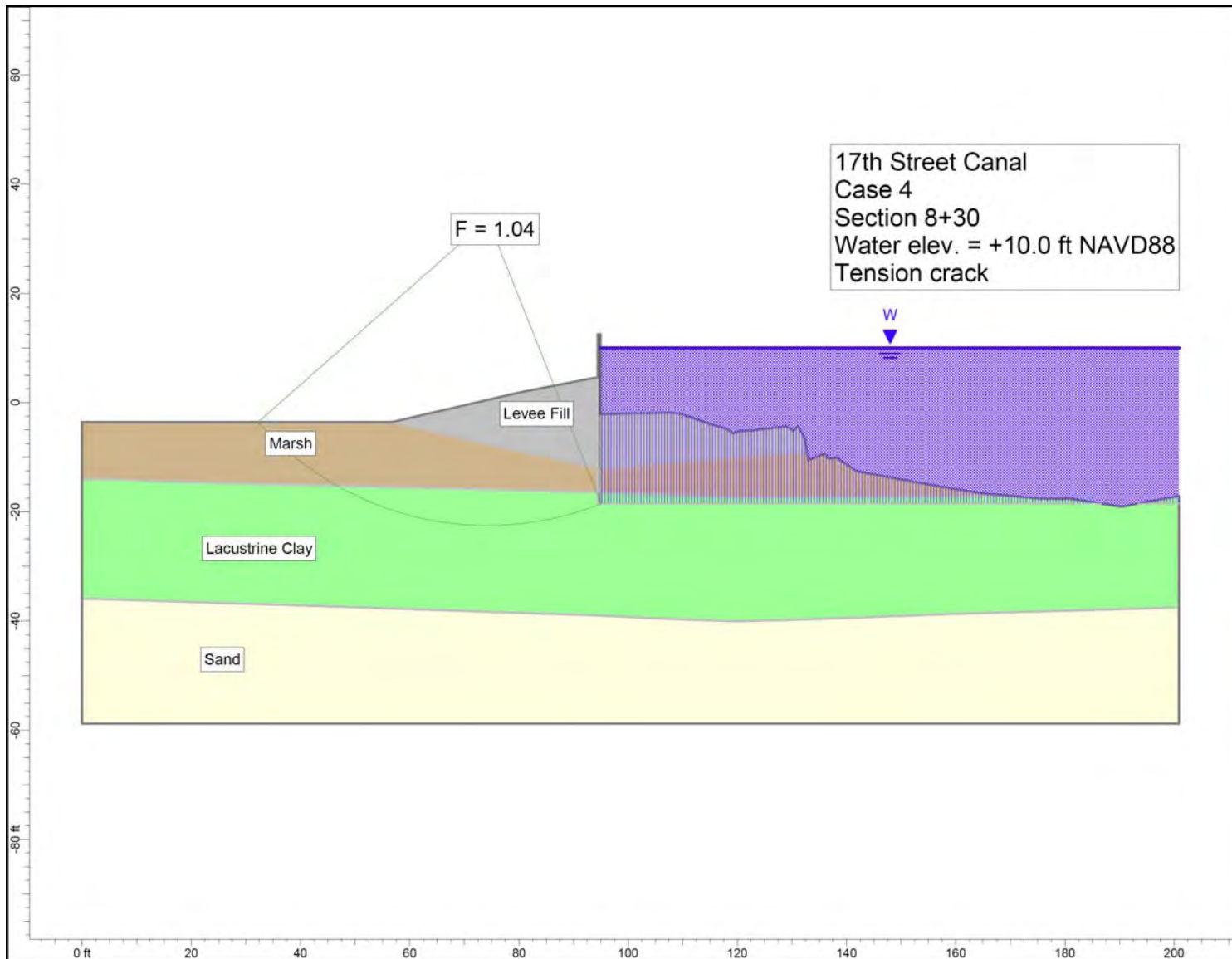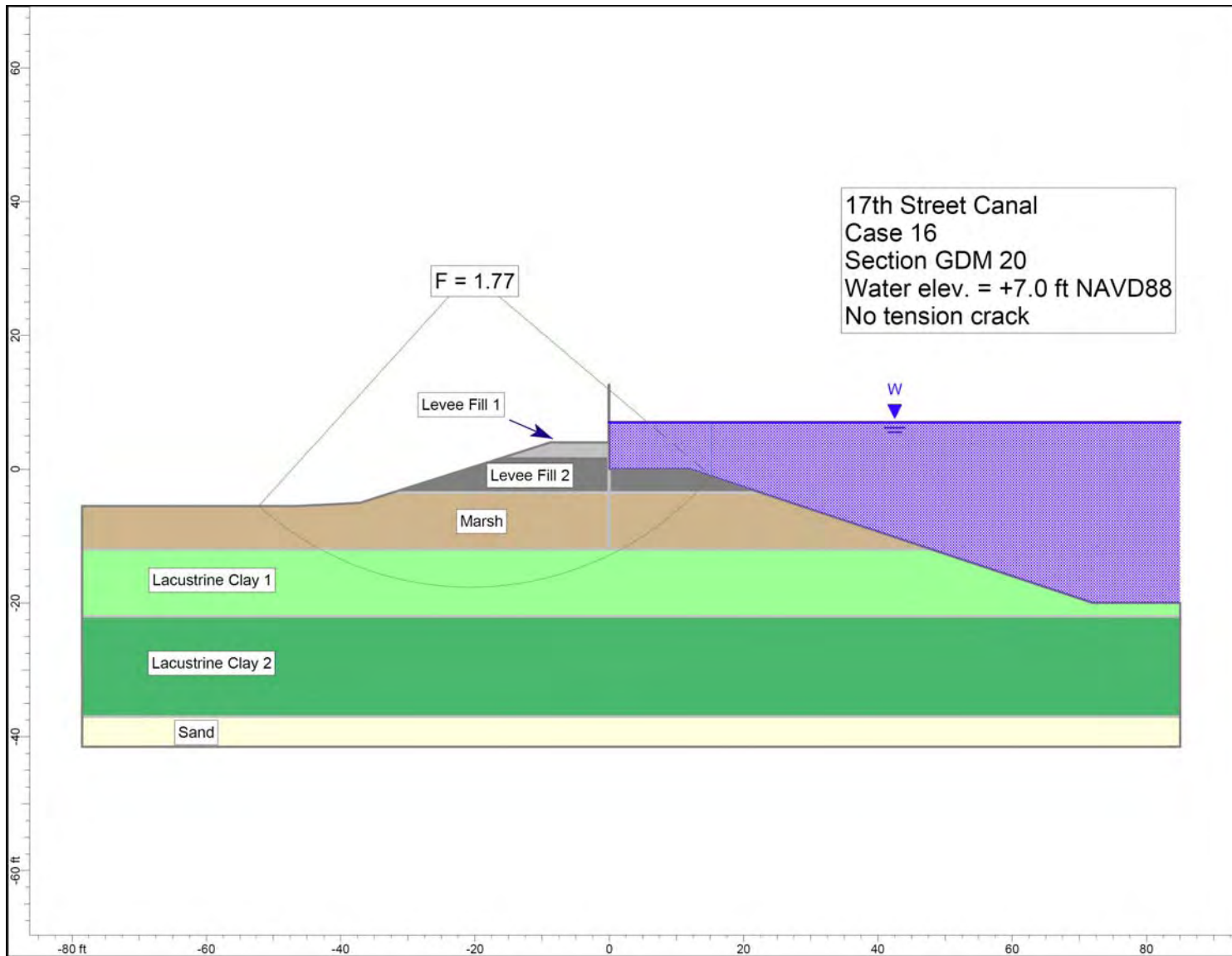
Figure 4-17.   Critical Circle for 17th Street Canal Design Cross Section – Water Elevation 7 ft, No Tension Crack
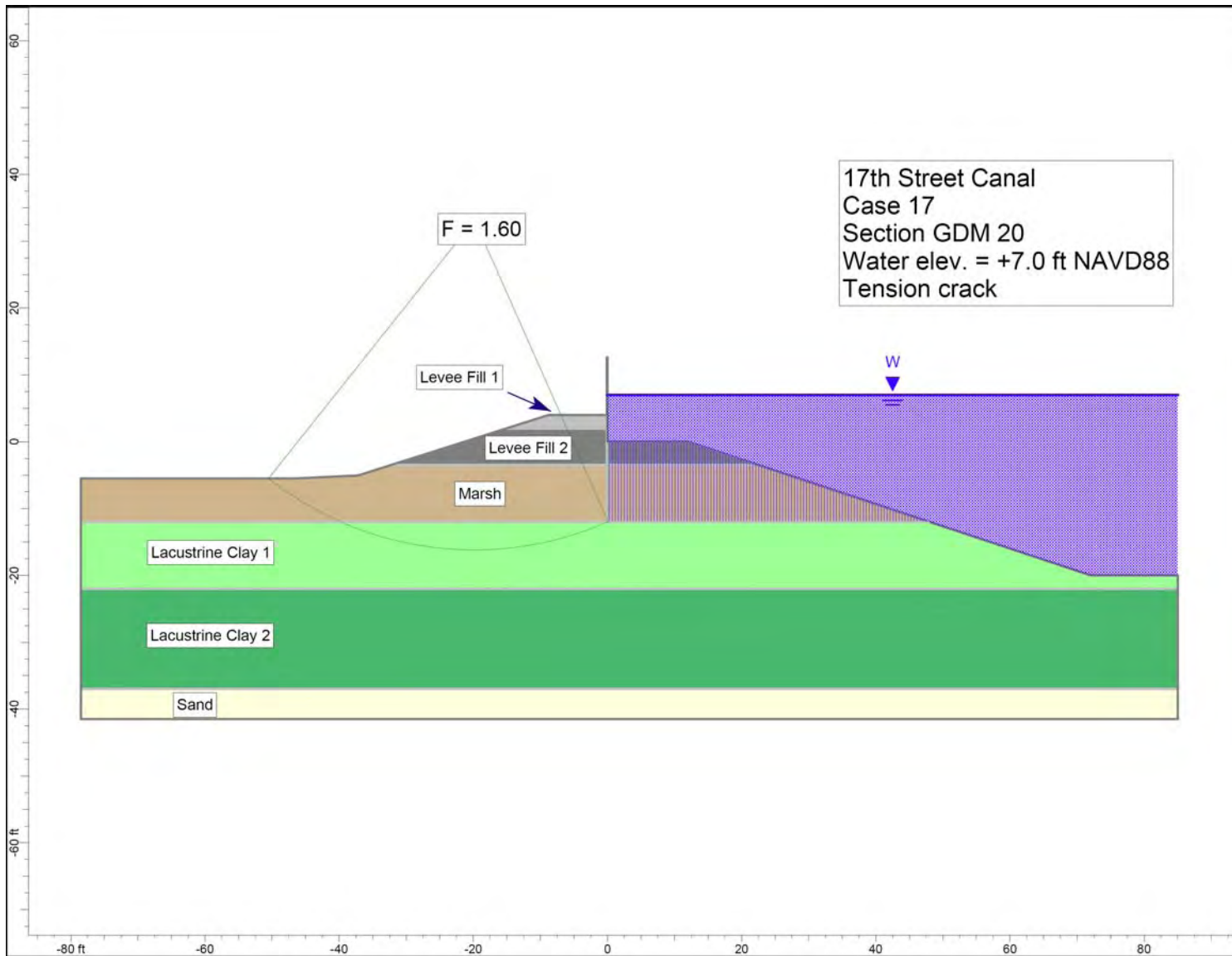
Figure 4-18.   Critical Circle for 17th Street Canal Design Cross Section – Water Elevation 7 ft, Tension Crack

This is a preliminary report subject to revision; it does not contain final conclusions of the United States Army Corps of Engineers.
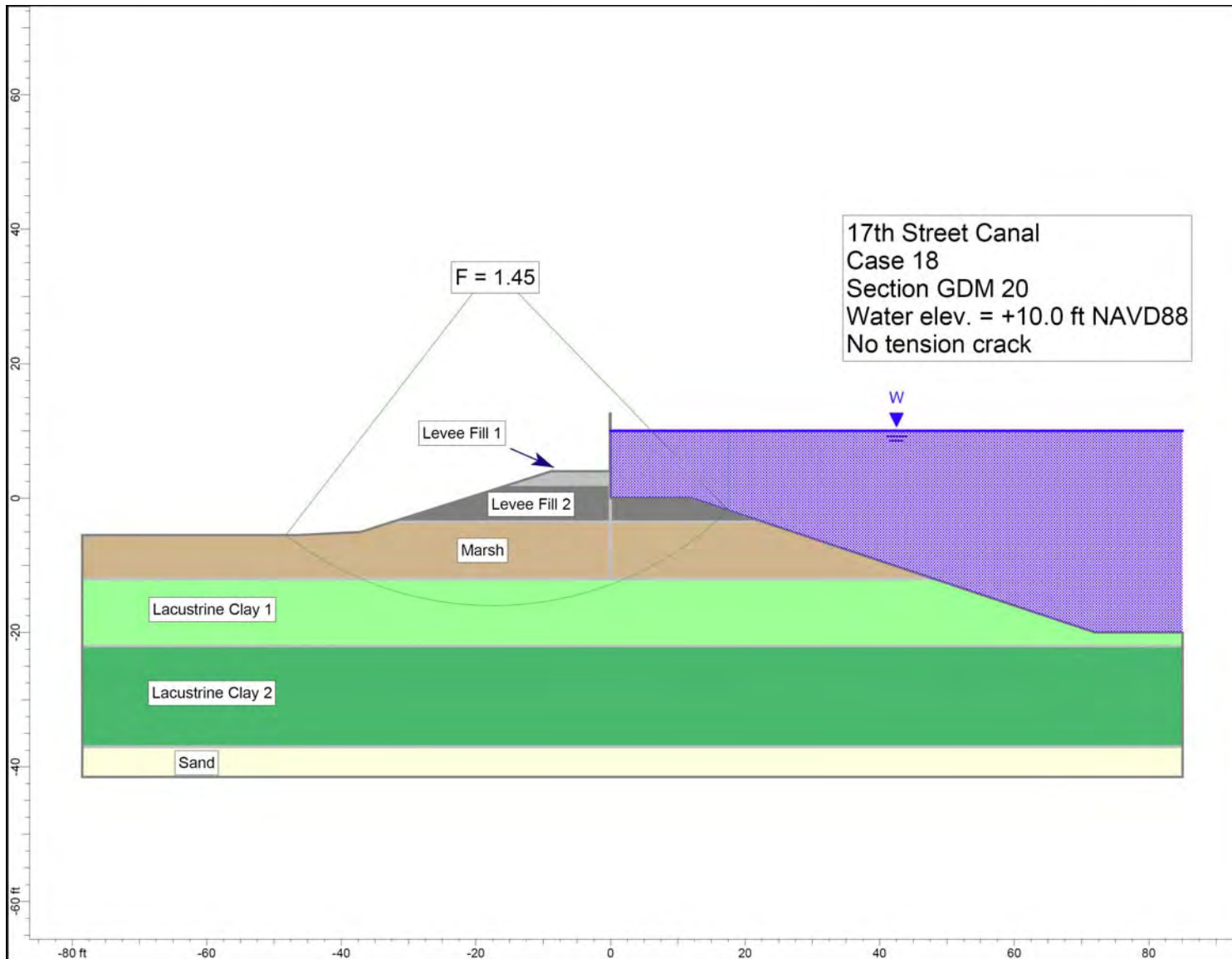
Figure 4-19.   Critical Circle for 17th Street Canal Design Cross Section – Water Elevation 10 ft, No Tension Crack
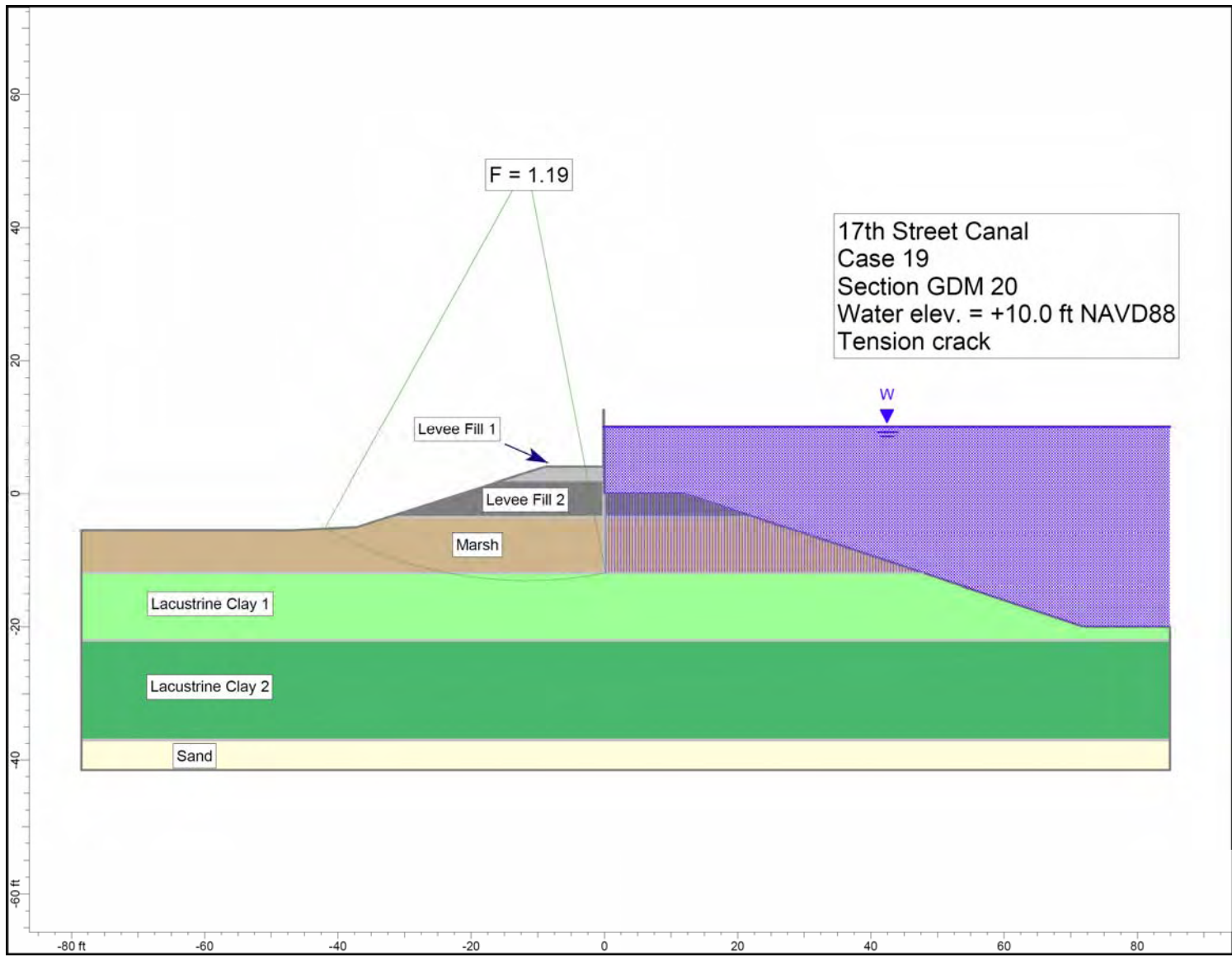
Figure 4-20.   Critical Circle for 17th Street Canal Design Cross Section – Water Elevation 10 ft, Tension Crack
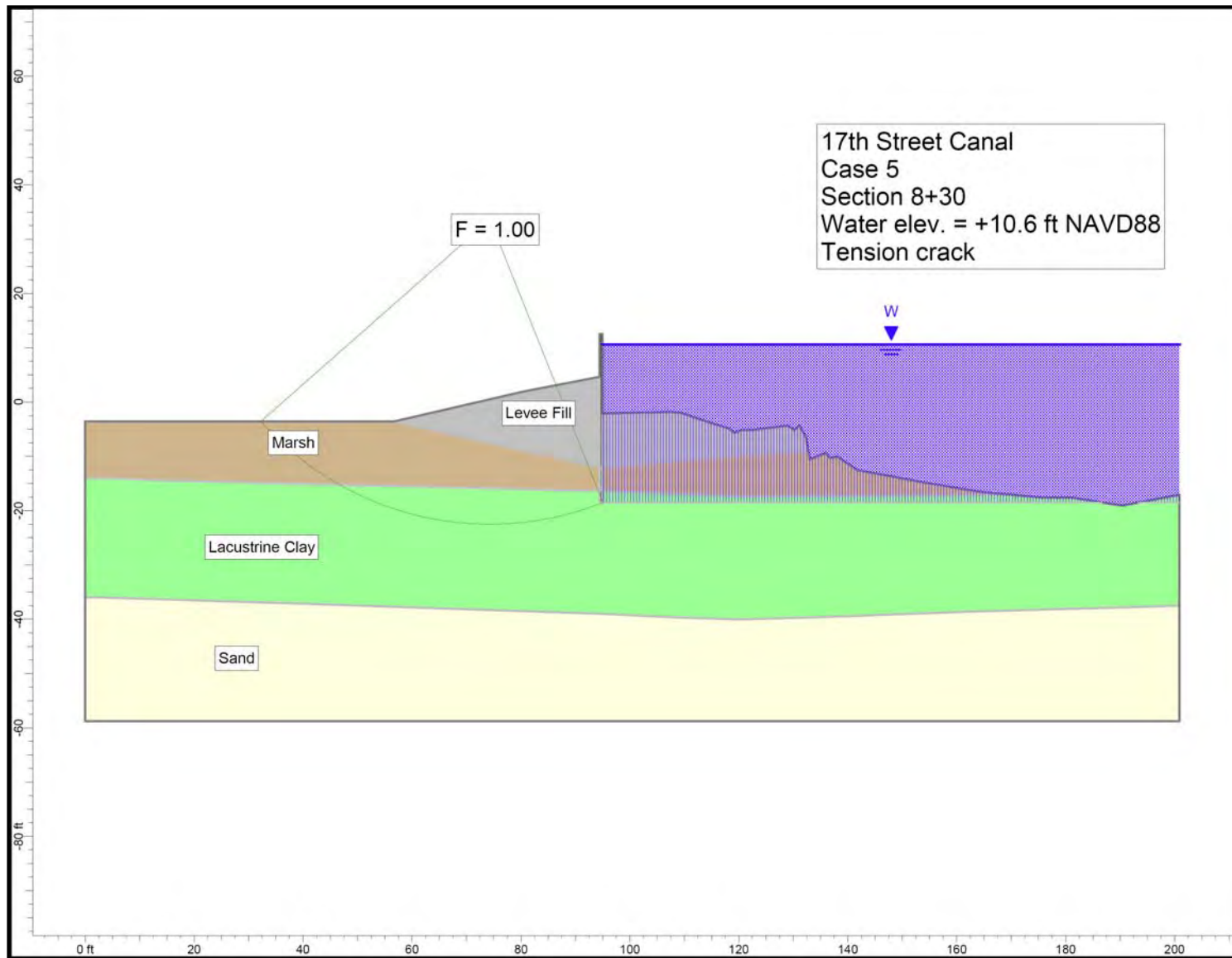
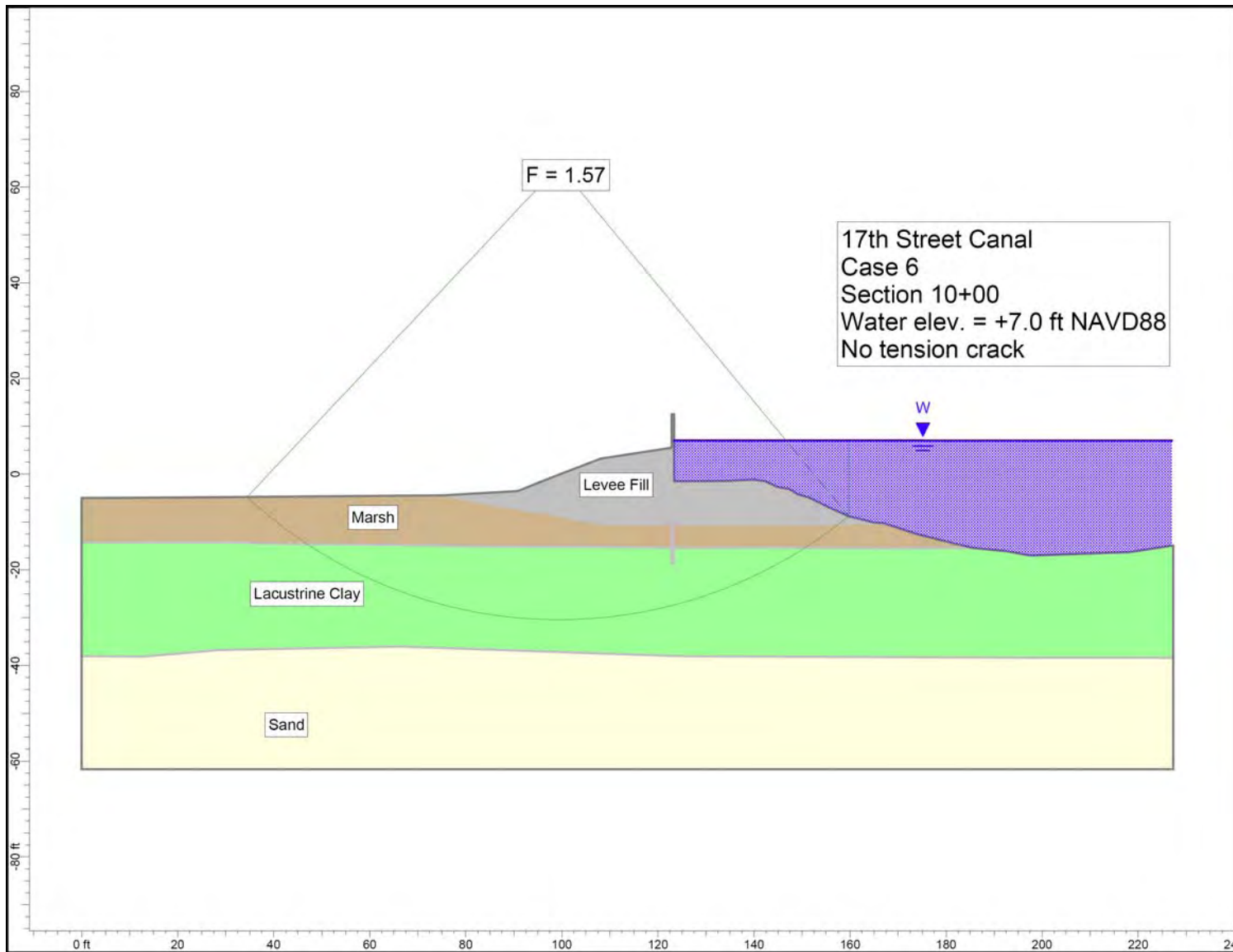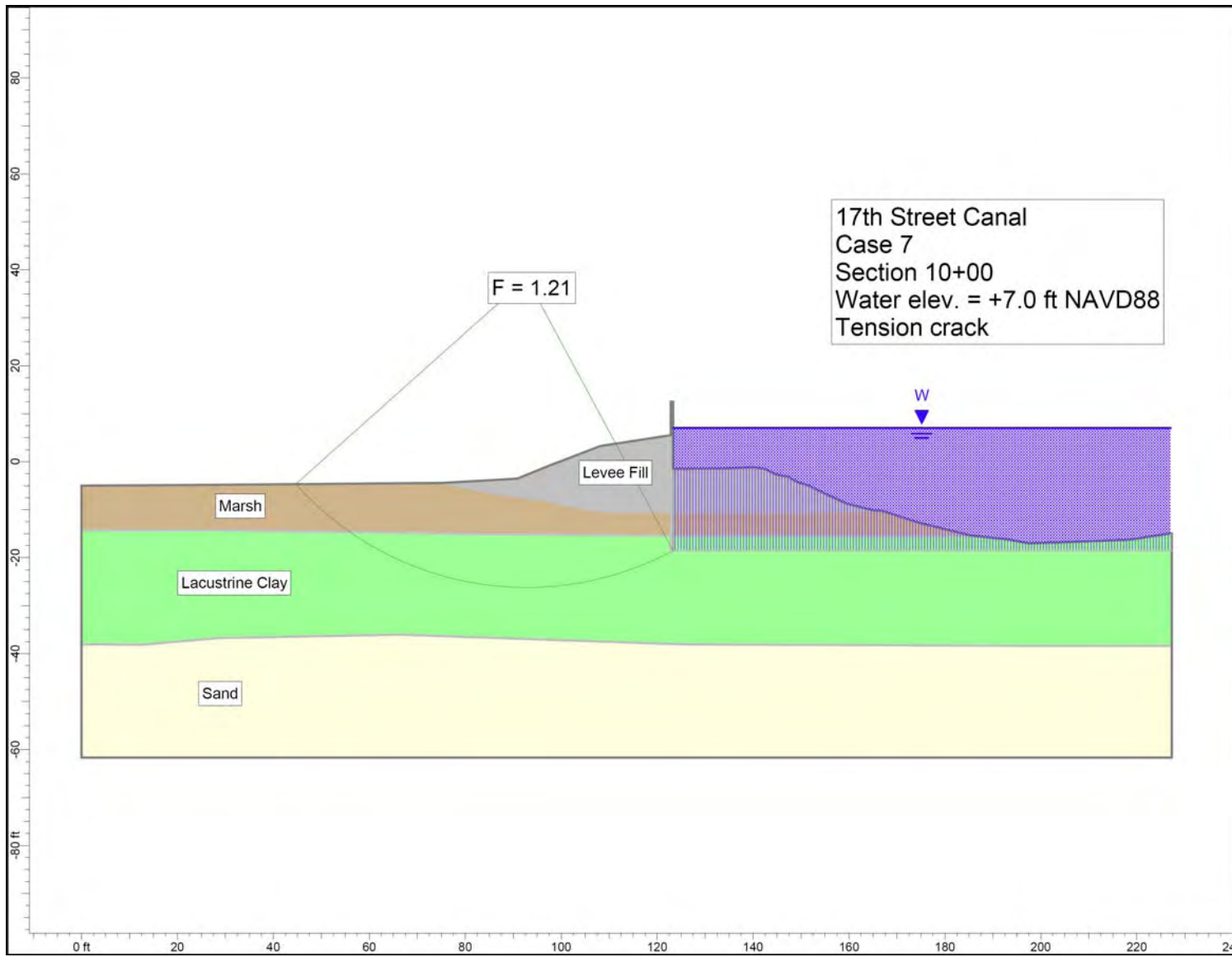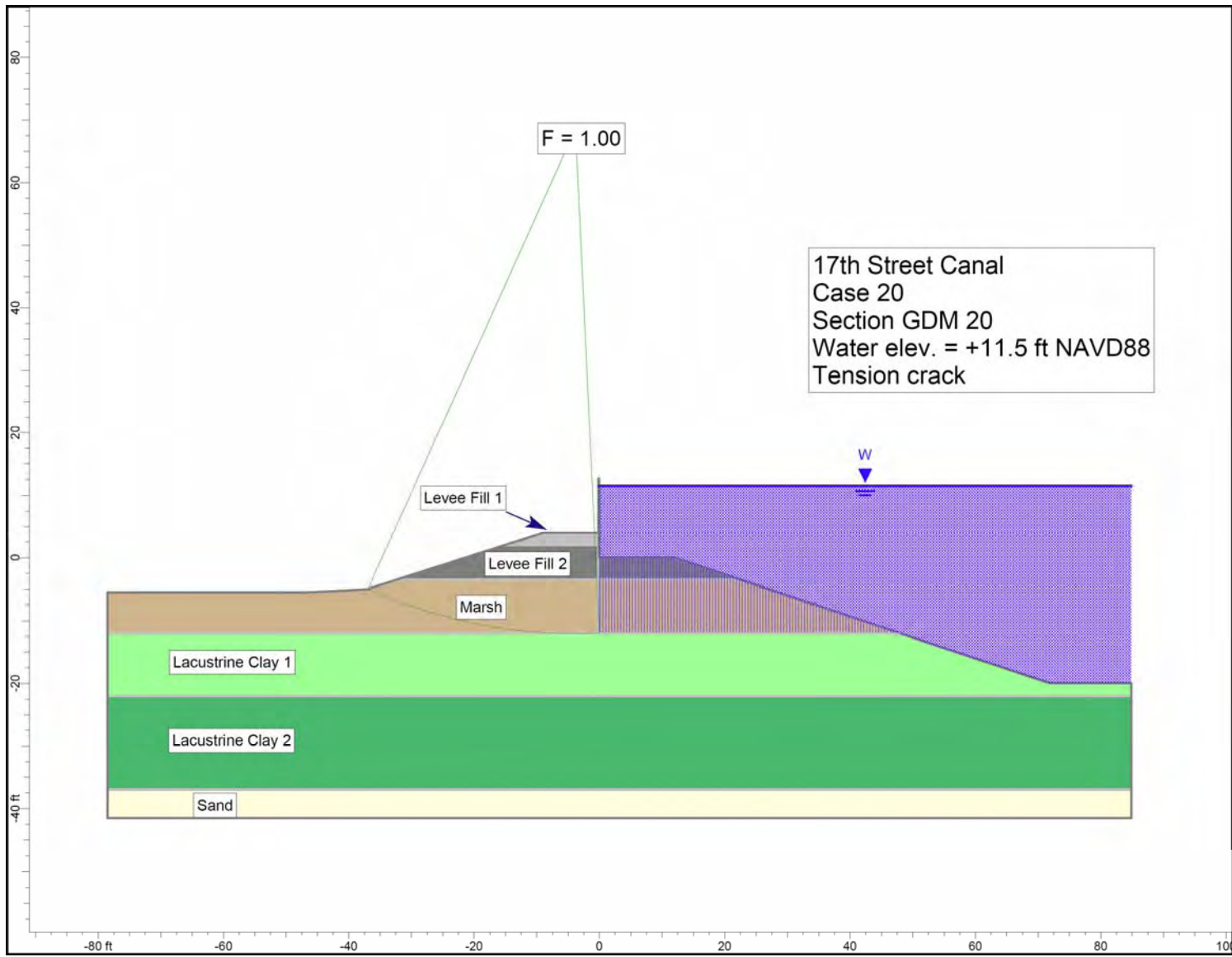Figure 4-21. Critical Circle for 17th Street Canal Design Cross Section – Water Elevation 11.5 ft, Tension Crack
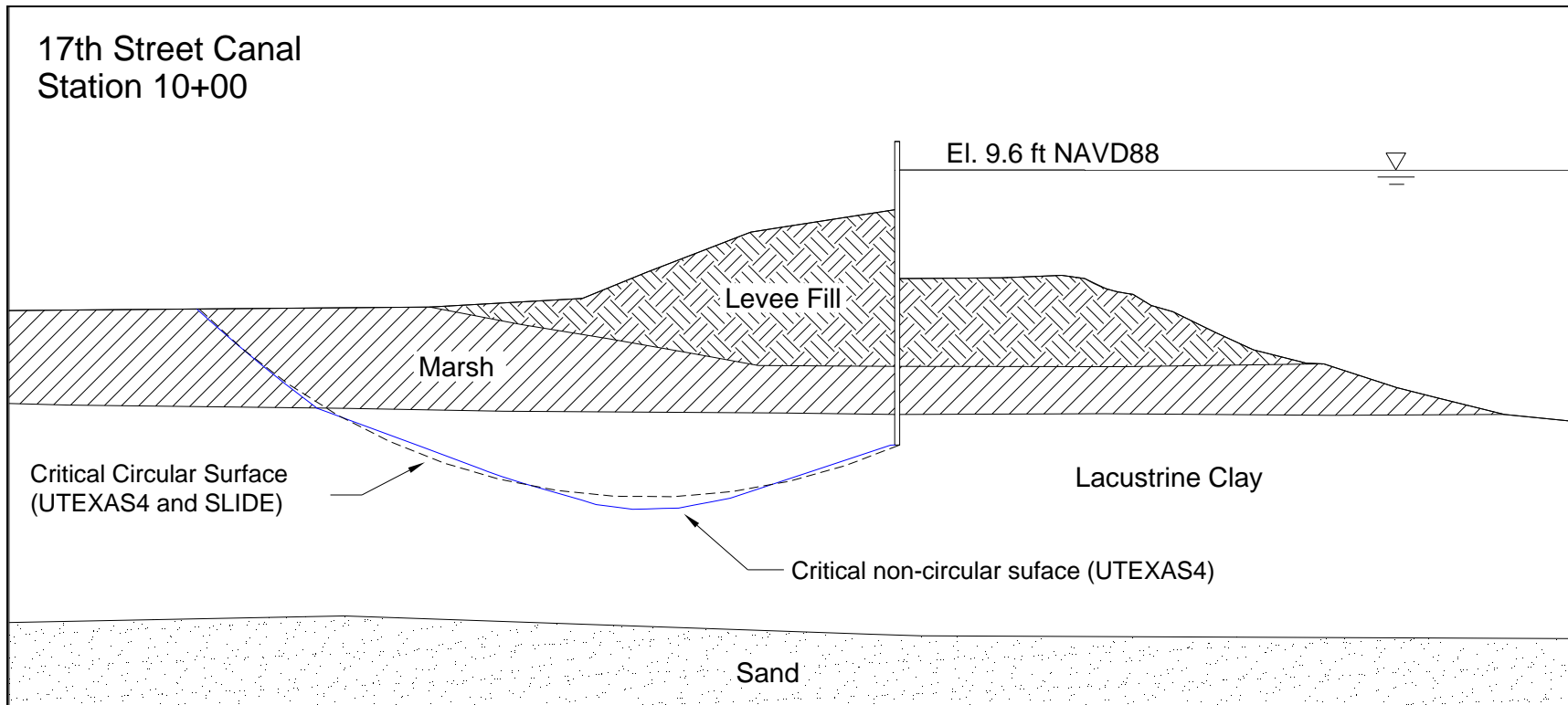
Figure 4-22.　　Critical Circular and Noncircular Slip Surfaces for 17th Street Canal, Station 10+00, Fully Cracked Condition

This is a preliminary report subject to revision; it does not contain final conclusions of the United States Army Corps of Engineers.

Appendix 5
IPET Centrifuge Model Test Report

Executive Summary

The physical (centrifuge) models of the levees on 17th Street, London Avenue and Orleans canals provided detailed insights into the mechanisms that led to the breaches in the outfall canals in the city. In this section of the report, the contribution of the centrifuge models towards the overall understanding of the performance of the outfall canal levees is presented.

Using a centrifuge is a well established technique for scale modelling of geotechnical phenomena and many facilities, large and small, exist around the world. The application of centrifuge modelling to the New Orleans levees has been described in detail in earlier reports in this series and will not be repeated here, although a general description is provided to assist the discussion of the results. The centrifuge models were carried out at ERDC, Vicksburg MS and at RPI, Troy NY with technical support from engineers at GeoDelft in the Netherlands, and from consultants Steedman & Associates in the UK.

The scale models of the levees relied on the same information used for the numerical modelling of the levee performance, typically the cross sections of the levees at the breach locations and the mechanical properties of the levee material, the floodwall and underlying deposits of sand, swampy marsh and clay. A summary of the scale model tests carried out for this investigation is presented below, together with a summary of relevant material properties and dimensional information.

Two mechanisms were observed in the scale models that could lead to breach, both of which stemmed from a water filled crack which formed in front of the flood wall as the water in the canal rose above the level of the levee. Depending on the foundation conditions and geometry of the flood wall and levee shoulders, the crack either led to a rotation of the flood wall landward with uplift and sliding on the top of the sand towards the landward toe of the levee, or to a translational (sliding) failure in the clay layer commencing from the bottom or toe of the flood wall. In other circumstances, no failure ensued and comparisons can therefore be drawn between the conditions that led to failure and those that did not.

These mechanisms and the supporting evidence from the scale models are described in the following sections using data from the model tests to explain how the mechanism was initiated and the sequence of events that followed.

Principles of Centrifuge Modeling

The use of a centrifuge is necessary to correct the distortion introduced in a scale model of a geotechnical field problem constructed 'on the laboratory floor'. As the behaviour of soil is stress dependant, it is crucial in studying the performance of a geotechnical system such as the New Orleans levees to ensure that the correct stresses are applied to each element in the levee and foundation. This is difficult to achieve in a scale model under earth's gravity alone as the weight of the model is not sufficient to bring the soil to the correct state. In a centrifuge, however, a model such as shown in Figure 5.1 at a scale of 1/N can be subjected to a steady acceleration field equivalent to N times earth's gravity. In this state, the same stress conditions as exist in the field can be effectively reproduced at all points in the model. An event such as rising water leading to the onset of foundation failure in a levee system can then be modelled in a highly realistic manner. Detailed information can be collected during the model test including measurements of water pressure in the ground at different locations, the movement of the flood wall and ground surface, and video imagery of the sequence of events. The history of centrifuge modelling and explanation of scaling principles is available in the literature. A detailed description of the principles of centrifuge modelling and its application to the model tests carried out for this investigation was presented in an earlier report, and is not repeated here.
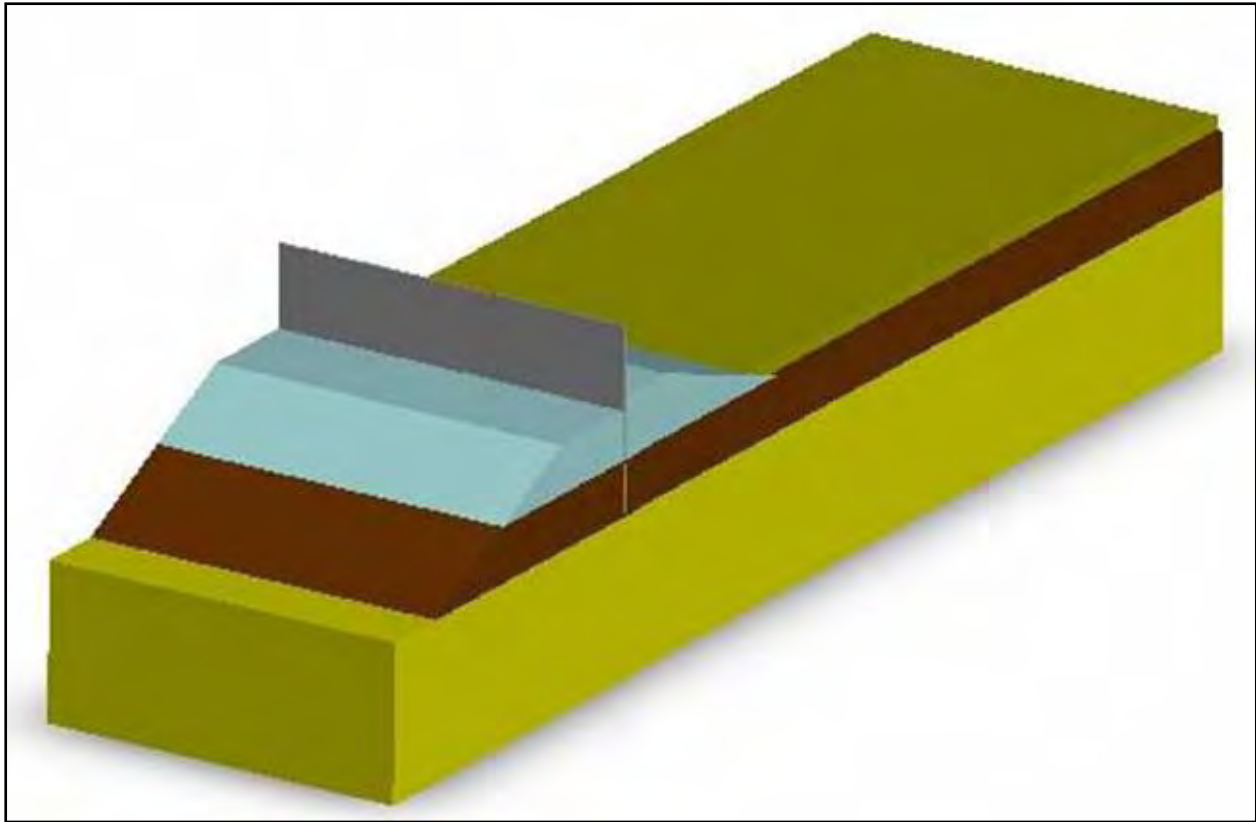
Figure 5-1. Typical geometry of scale model test (canal on the left hand side)

Summary of Model Tests

Model tests were carried out using the Army Centrifuge at ERDC, Vicksburg and at RPI, Troy. Table 5.1 summarises the models completed for this investigation.

Table 5-1 Model Tests completed for IPET			
Levee profile	Research center	Foundation	Mechanism
London North	ERDC	Swampy marsh over sand	Rotational failure of wall
London North	RPI	Swampy marsh over sand	Rotational failure of wall
London South	ERDC	Swampy marsh over sand	Rotational failure of wall
London South	RPI	Swampy marsh over sand	Rotational failure of wall
17th Street	RPI	Swampy marsh over clay	Translational failure in clay layer
17th Street	ERDC	Swampy marsh over clay	Translational failure in clay layer
17th Street	ERDC	Swampy marsh over clay	Translational failure in clay layer
Orleans South	RPI	Swampy marsh over sand	No failure
Orleans North	ERDC	Swampy marsh	No failure

The model tests generated large volumes of data for analysis. It was evident that in all cases failure of the levees was presaged by the opening of a water filled crack on the canal side of the

levee, which allowed full hydrostatic pressure to act on the flood wall over its entire submerged height. The flood water in the centrifuge models was raised steadily, without wave effects, and it was observed that once a crack had opened, then in the cases of London Avenue and 17th Street canal models, a failure soon followed, either by rotation of the flood wall (London Avenue) and uplift (sliding) on the top of the sand layer or by translational failure (sliding) in the clay stratum (17th Street), originating at the bottom (toe) of the sheet pile wall.

In this report, these data are used to illustrate the mechanisms of failure observed in the models, and to draw conclusions concerning the onset of failure in the field. Analysis of the mechanisms of failure provides insights into the Factor of Safety (FoS) as the water levels in the canals rise.

Material Properties

The levee and foundation in all of the models was constructed using three materials: sand, and clay to represent the natural sand, soft lacustrine clay and levee clay and natural material from the field to represent the swampy marsh deposits.

The sand used in all the models was a fine laboratory sand (Nevada sand), which is well characterized as a result of its widespread use by different research laboratories. Nevada sand has a specific gravity of 2.67 and maximum and minimum dry densities of 17.33 kN/m^3 and 13.87 KN/m^3 respectively at corresponding minimum and maximum void ratios of e_{min} = 0.511 and e_{max} = 0.887. The permeability of Nevada sand in a medium dense state is around 5.6 x 10-5 m/sec and its mean grain size (D_{50}) is 0.15mm.

The material selected to model the soft normally consolidated 'laucustrine' clay stratum and the stiffer clay that forms the levees was a speswhite kaolin clay, widely used in geotechnical research laboratories. Kaolin is coarse grained clay with a Specific Gravity of 2.58. For normally consolidated or lightly overconsolidated clays the ratio of undrained strength S_u to the effective overburden stress S_u/σ_v' has been shown empirically to lie in the range 0.2-0.25, and for kaolin clay a value of 0.22 is typical. For overconsolidated clays, this ratio depends on the overconsolidation ratio and is larger.

The water content, w at the Liquid Limit (LL) and Plastic Limit (PL) of the clay used in these model tests was measured using the Fall cone method (following BS1377) as 70% and 33% respectively, giving a Plasticity Index (PI) of 37%. The Fall cone method was used to determine the LL in preference to the percussion cup method (following ASTM) as, being a strength test, it enables a theoretical relationship between water content and undrained shear strength S_u to be derived directly. This was used in the model testing to help confirm the initial condition of the clay layer and levee.
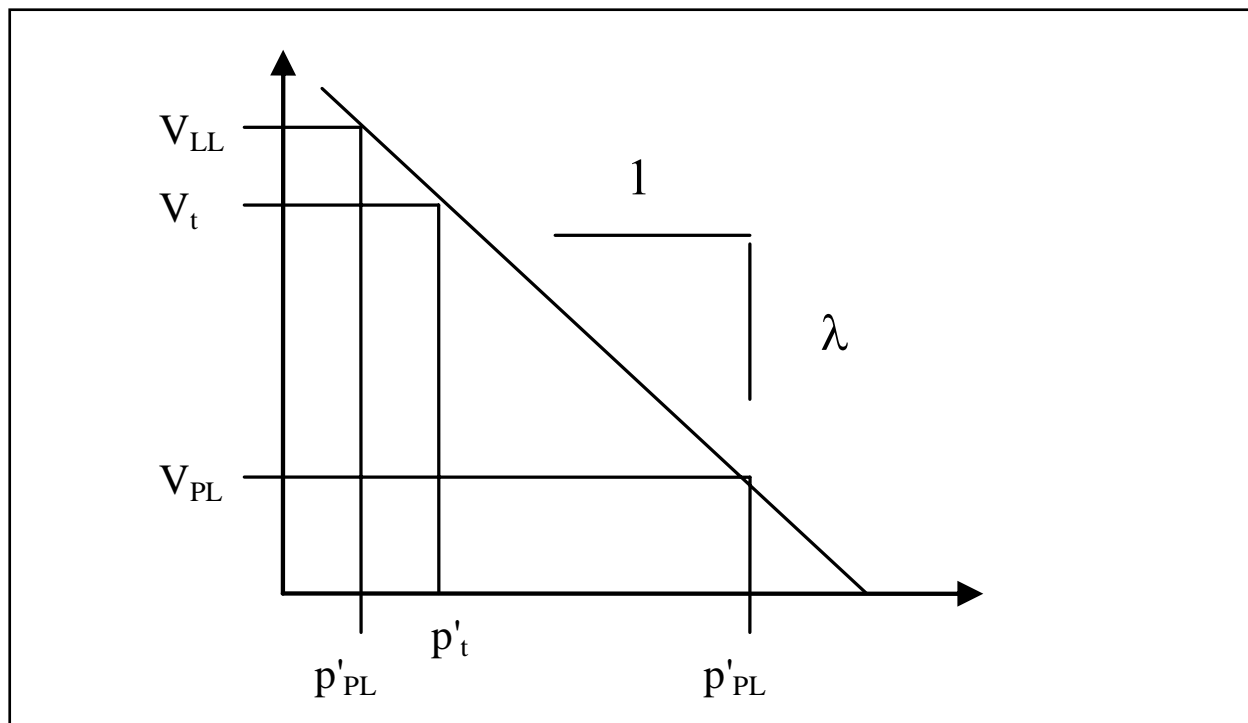
Figure 5.2. Normal consolidation curve in V – ln p' space

Assuming that the undrained shear strength S_u at a mean effective confining stress, p'_t may be related at the water content w_t via the Specific Volume (V)by a log-linear relation (Figure 5.2) of the form:

$$p'_{PL}/ p'_t = (Su)_{PL}/(Su) = \exp [(V_t - V_{PL})/\lambda]$$

where the subscript $_{PL}$ refers to the Plastic Limit, V is the Specific Volume and λ is the slope of the (linear) normal consolidation line in V – ln p' space, Figure 5.2, then λ may be deduced from the Plasticity Index, noting that

$$V = 1 + e = 1 + wGs$$

and

$$w_{LL} - w_{PL} (\%) = (\lambda/Gs) \ln R = PI/100$$

where e (= wGs for fully saturated soil) is the void ratio, R is the ratio between the strength of the clay at the plastic limit and the liquid limit and is related to the characteristics of the clay. This provides a relationship between the moisture content of the clay and the undrained shear strength, which is consistent with the empirical approach based on strength ratio Su/cv' outlined above.

The saturated unit weight of kaolin at a moisture content of around 43% is 109 pcf (17.1 KN/m^3).

The model tests used bulk samples of the natural material from the field to represent the swampy marsh stratum in the foundation of all the levee models. Undisturbed samples taken from borings have provided laboratory samples from which compression tests, moisture content and unit weights have been determined. These are reported elsewhere in this report. The saturated unit weight of peat was taken as 80 pcf (12.6 KN/m^3), consistent with the slope stability analyses. Site investigation reports show that the unit weight of the swampy marsh is variable, from a low of around 65 pcf (10.2 KN/m^3) to a high of around 80 pcf (12.6 KN/m^3). The stiffness of the swampy marsh varies but consolidated undrained direct simple shear laboratory tests on samples taken from the 17th Street breach area suggest that a value of Shear Modulus, $G/\sigma_v' \approx 10$, where σ_v' is the initial vertical effective stress may be appropriate for strains up to 2-3%.

In the field, the concrete flood wall is supported by a steel sheet pile wall that passes through the levee, terminating at a variable elevation. In the model tests, this wall element was scaled using an aluminium or steel plate, with a bending stiffness comparable to the bending stiffness of the sheet pile wall. A solid plate was used in the model tests as there was no evidence from the walls in the field that water leakage through the sheet piles was significant in the early stages of wall movement.

Further details of each of these materials, how they were used and placed in the models and the techniques for controlling their strength and stiffness with depth were reported in Report 2 of this series.

Establishing Initial Conditions

All centrifuge models completed for this study fall broadly in one of two categories: those with a clay sub-stratum (e.g 17th Street) and those with a sand layer beneath the swampy marsh (e.g. London Avenue). In each case, it was necessary to confirm that the correct initial conditions had been established prior to the flood stage.

In the sand models, seepage under the levee was driven by a differential head between the water in the canal and the ground water table on the landward side. Over time in the field, a steady state 'flownet' will develop governing the excess water pressure or head at different locations under the levee. Figure 3 shows a steady state flownet (calculated using the software programme SEEP-W) compared to piezometric head levels measured by pore pressure transducers at different locations under the levee at around the same depth in the sand.
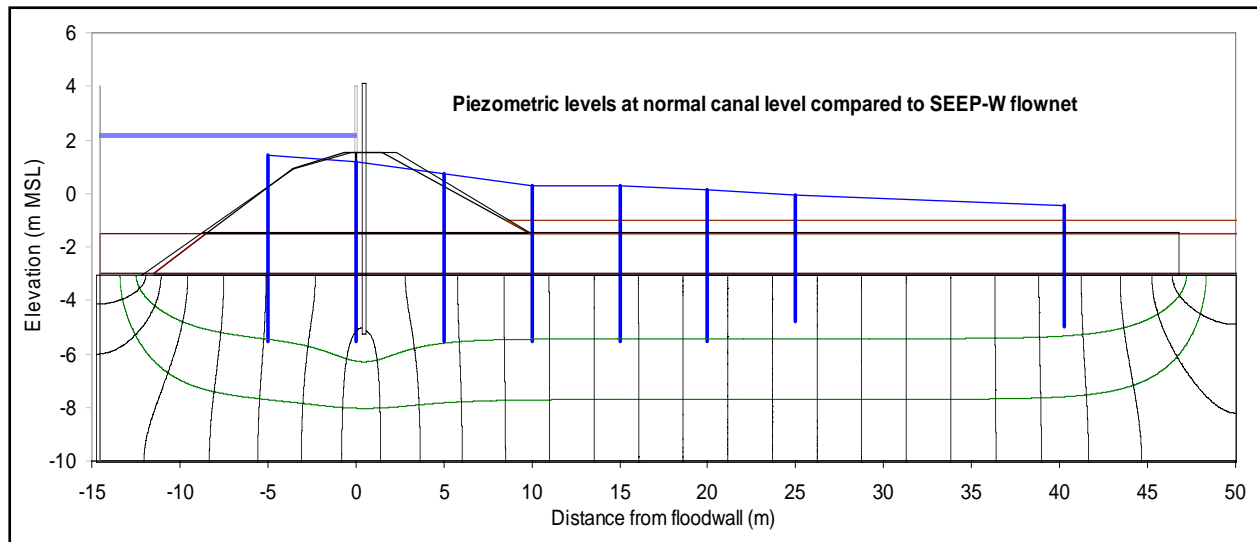
Figure 5.3. London south model, flownet and piezometric levels at different locations, typical canal level

The early stages of water rise in the model tests in all cases were characterised by rising water pressures in the soil layers beneath the levee. This was most apparent in the case of the London Avenue models, where the deep sand layer underlying the swampy marsh was connected hydraulically to the canal, and showed an immediate response as the canal water level changed, Figure 5.4.
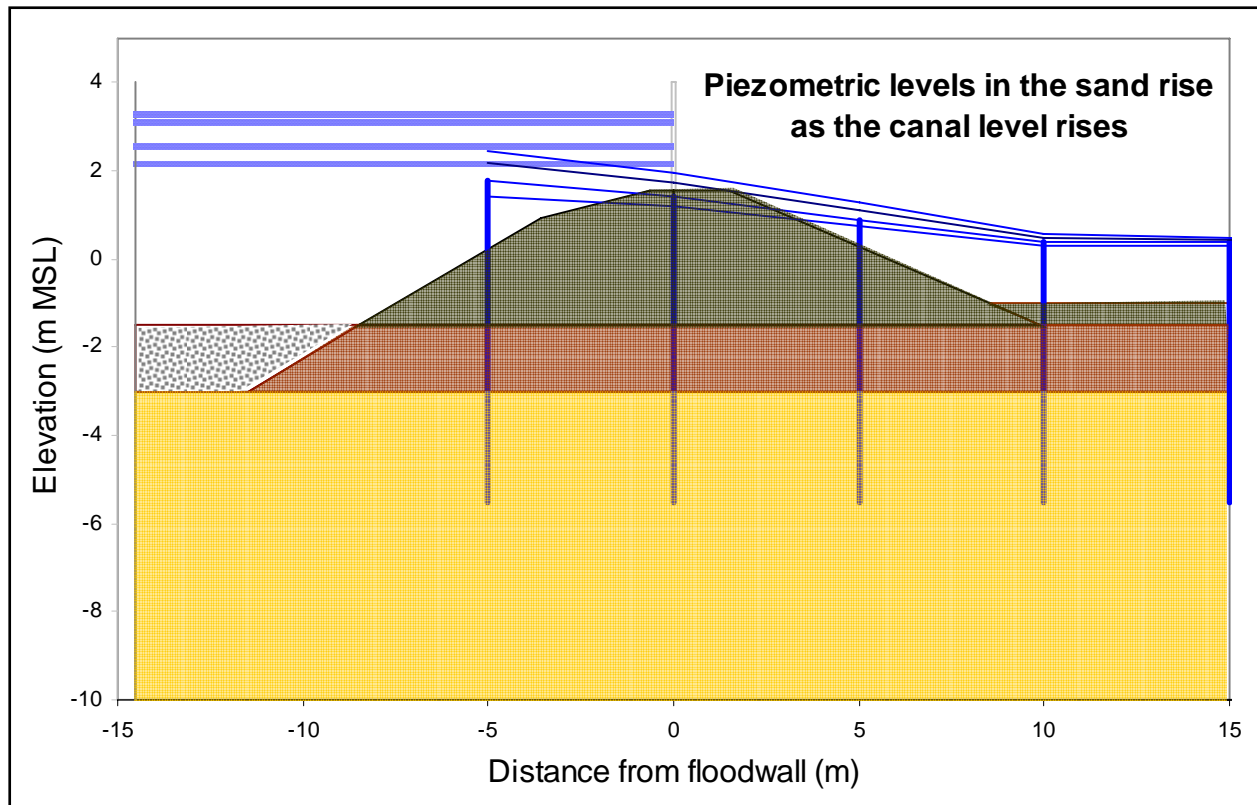
Figure 5.4. Rising canal levels lead to immediate rise in piezometric levels

In the sand layer, the increase of water pressure (head) was largest nearest to the canal and reduced with distance from the canal, landward. This is due to head loss in the sand layer as seepage through the sand layer developed from the flood side towards the land side drain and is seen clearly in the figures above.

The second class of centrifuge model were the clay models, simulating the ground profile below the 17th Street levee. Establishing initial conditions in the peat and clay layers requires confirmation that the swampy marsh and clay layers have reached a stress state comparable to that in the field. This is achieved by a process of consolidation in the centrifuge over time, using self weight and surcharging, to bring the clay forming the levee, the foundation sub-stratum and the shallow swampy marsh deposits into their required condition.

The consolidation process for a layer with vertical (one-way) drainage may be analysed using parabolic isochrones in the standard way. Two stages of consolidation are observed, Stage 1 and Stage 2, as the excess pore water pressures drain over time and a total stress increment is transferred from the pore water to the soil skeleton. The two stages are illustrated in Figure 5.5, which shows how excess pore water pressures at different depths through the layer decay with time, returning to a simple hydrostatic profile towards the end of the consolidation process. The units are at model scale as these are the units used to monitor the progress of the experiment. The length of time required for consolidation is independent of the stress increment.
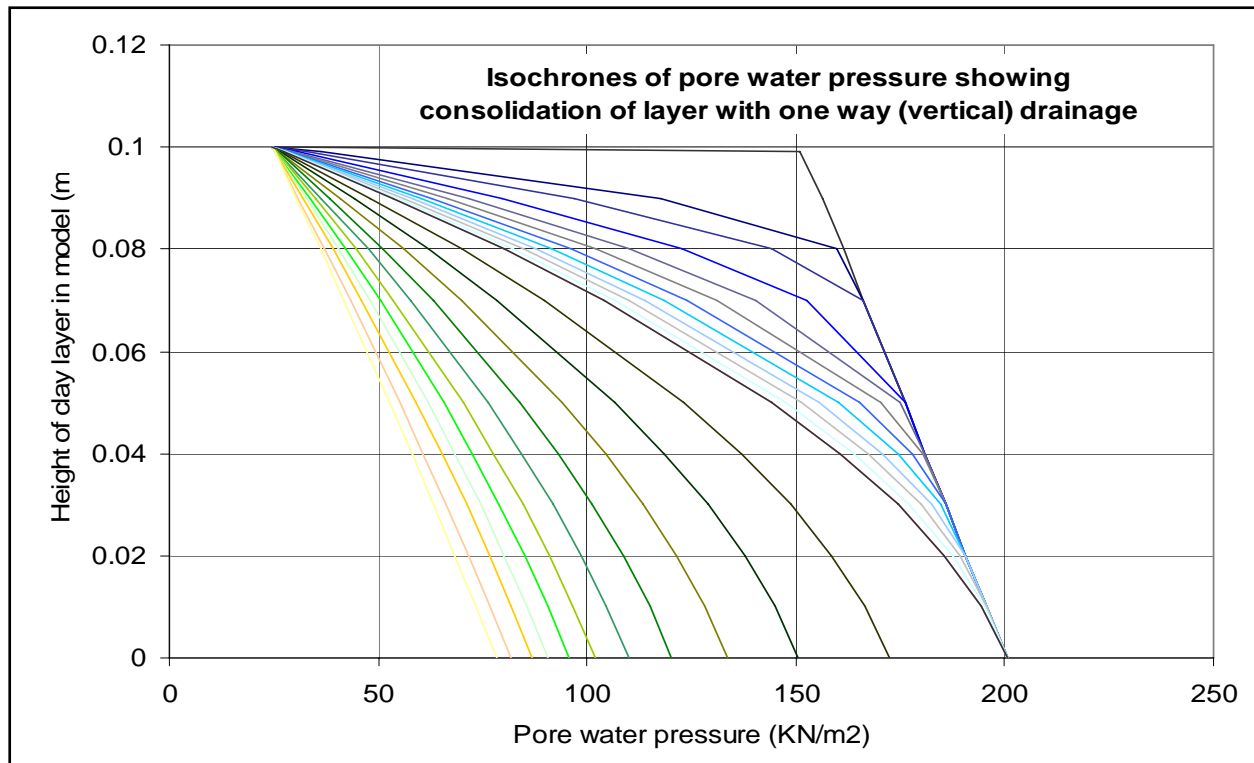
Figure 5.5. Theoretical isochrones for a clay layer in model units, draining upwards

Plotting the pore water pressure at different depths over time gives a prediction of the decay in pore water pressure at different depths which can be used to compare with the experimental data during the initial stage. For the clay layer beneath the levee and for and the swamp marsh the actual and predicted time histories of pore water pressure dissipation are shown in Figures 5.6 and 5.7 for two typical models, confirming that consolidation has been achieved and the initial conditions for the soil beneath the levee were established.

In both model and field conditions with a clay substratum layer, the flooding of the canal is too rapid a process to permit drained behaviour of the clay to take place, and hence the process may be considered as an undrained event. As water levels in the canal rise, the pore water pressures in the clay also rise due to the increase in total stress (the weight of the water in the canal) and not due to seepage, as in the sand foundation. Over time, if the canal water levels were held at a high water level then drainage would take place and the original profile of effective stress would ultimately be re-established. In practice, there was no time for drainage to take place and the models reflect this behaviour, exactly as in the field conditions. Figure 5.8 shows the rise in pore water pressure at four locations in the clay layer beneath the levee on the canal side as the canal water level is raised. The exact correspondence confirms that the clay layer is responding in an undrained manner, with the increment of total stress (due to the weight of water in the canal) exactly matched by the increment of pore water pressure, regardless of depth in the foundation, which means that the strength of the underlying clay is fully described by its undrained shear strength. (As the canal level rises higher, the additional load on the canal side of the levee will also alter the elastic stress distribution in the foundation beneath, and this adds a slight additional increment to the transducers under the levee shoulder.)
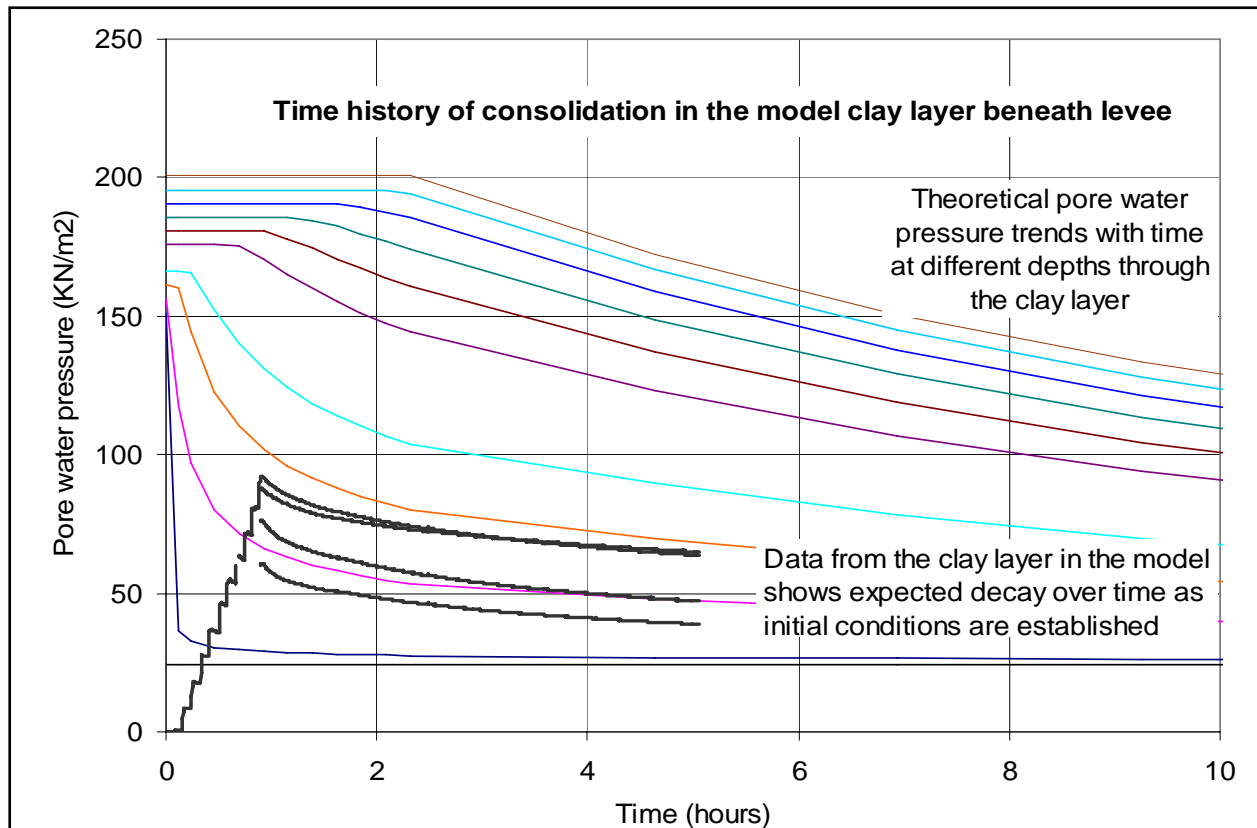
Figure 5.6. Trend of dissipating pore water pressure in the clay layer as initial conditions are established (time in model units)
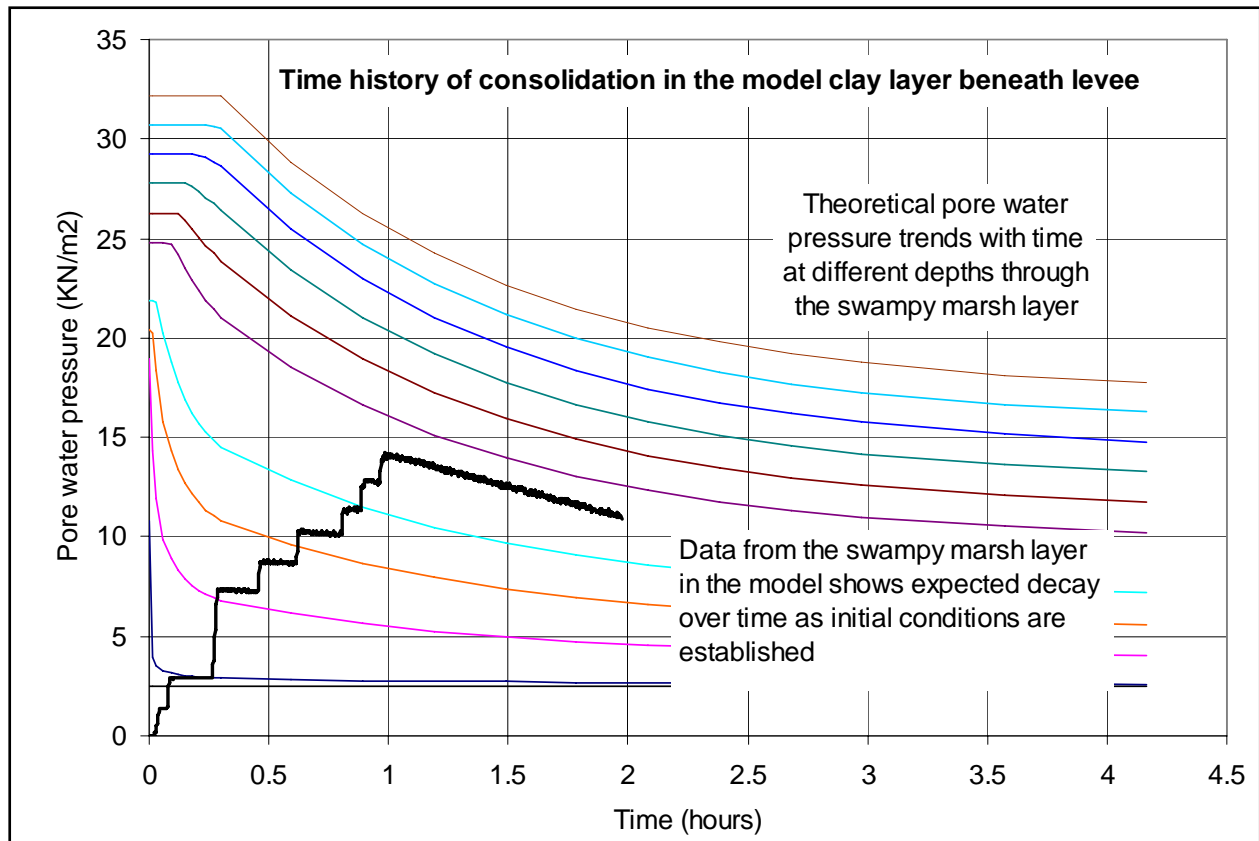
Figure 5.7. Trend of dissipating pore water pressure in the swampy marsh layer as initial conditions are established (time in model units)
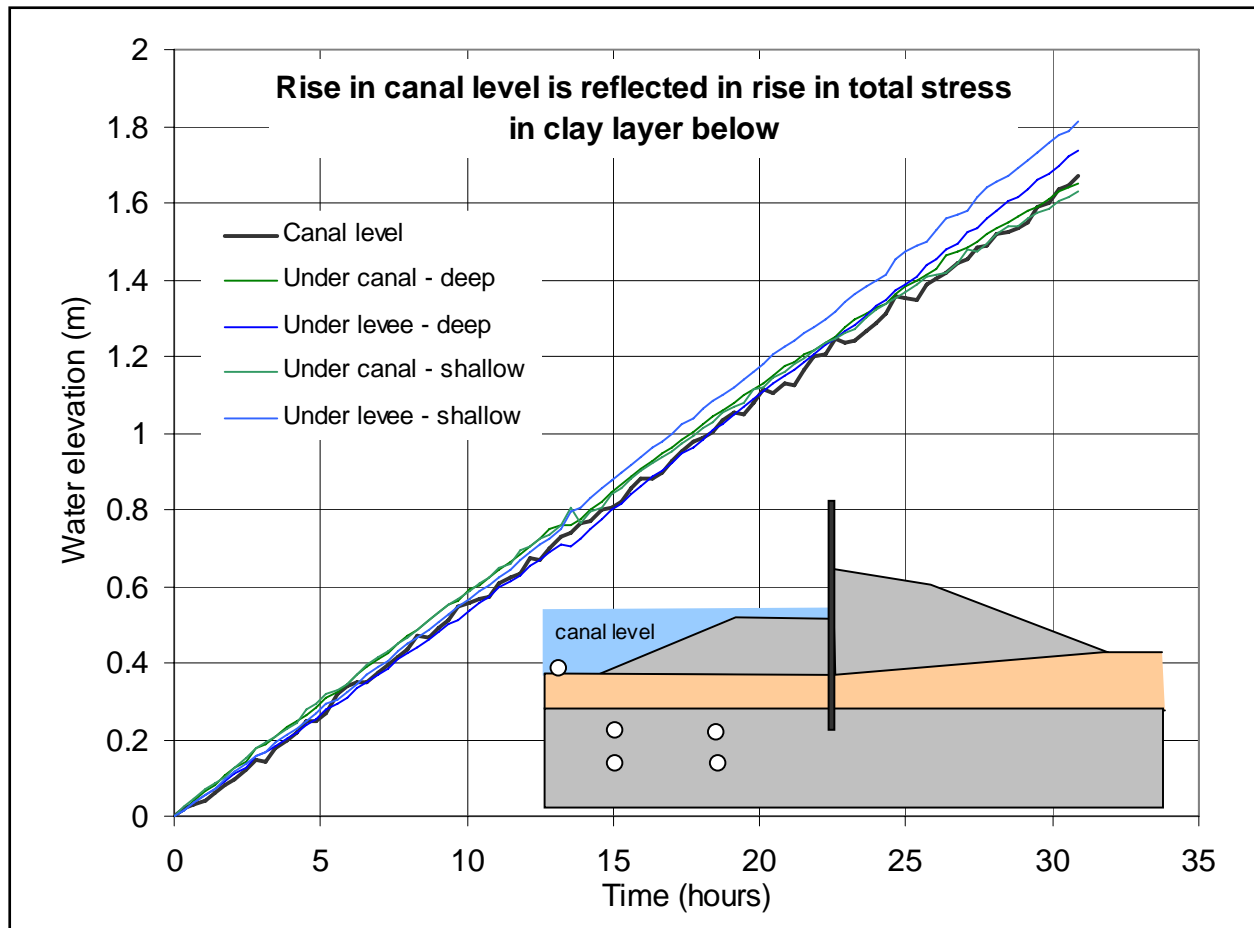
Figure 5.8. Water level in canal compared to incremental pore water pressure rise in clay layer beneath levee

Formation of a Water Filled Crack

In all of the centrifuge model tests on the London Avenue, 17th Street and Orleans levee profiles, with both sand and clay foundations, a crack or gap was observed to form on the flooded side of the flood wall once water had overtopped the canal side crest of the levee and the wall rotated slightly landwards. The gap permitted a full hydrostatic head of water to develop to the bottom of the crack, which in the case of the London South and North profiles, provided a hydraulic connection between the underlying sand layer and the canal above under the centre of the levee. In the case of the 17th Street profile, where the wall penetrated through the swampy marsh into the clay stratum beneath, the crack opened to near the toe of the wall. In the case of the Orleans South profile, where the wall did not penetrate through the swampy marsh layer, the swampy marsh continued to provide a hydraulic barrier to prevent high water pressures reaching the underlying sand.

The formation of the crack followed the rise in water level on the canal side. As the water level rose against the levee, the flood wall did not experience any increase in lateral load. Once the water reached the flood wall, however, a hydrostatic force started to build up on the wall,

pushing it landward. All of the flood walls in this study were un-propped (as in the field), and therefore the rising water on the flood wall is reacted by a small rotation of the wall, resisted by the embedment of the sheet pile wall, and the passive resistance of the levee material on the landward side of the flood wall.

In this condition, an un-propped wall is susceptible to the opening of a tension crack down the canal side of the flood wall which is immediately water filled.

The theoretical depth, z of a dry tension crack for an unpropped smooth wall retaining a cohesive clay material with undrained strength S_u, Figure 5.9, is simply derived following Rankine as:

$$z = (2 \, S_u - q) / \gamma$$

where q is a surcharge and γ is the unit weight of the clay. A similar depth of crack could occur through desiccation cracking. Where water is able to fill the crack and the clay responds in an undrained manner, the water is able to partially support the clay and the theoretical depth of the crack increases to:

$$z = (2 \, S_u - q) / (\gamma - \gamma_w)$$

where γ_w is the unit weight of water.
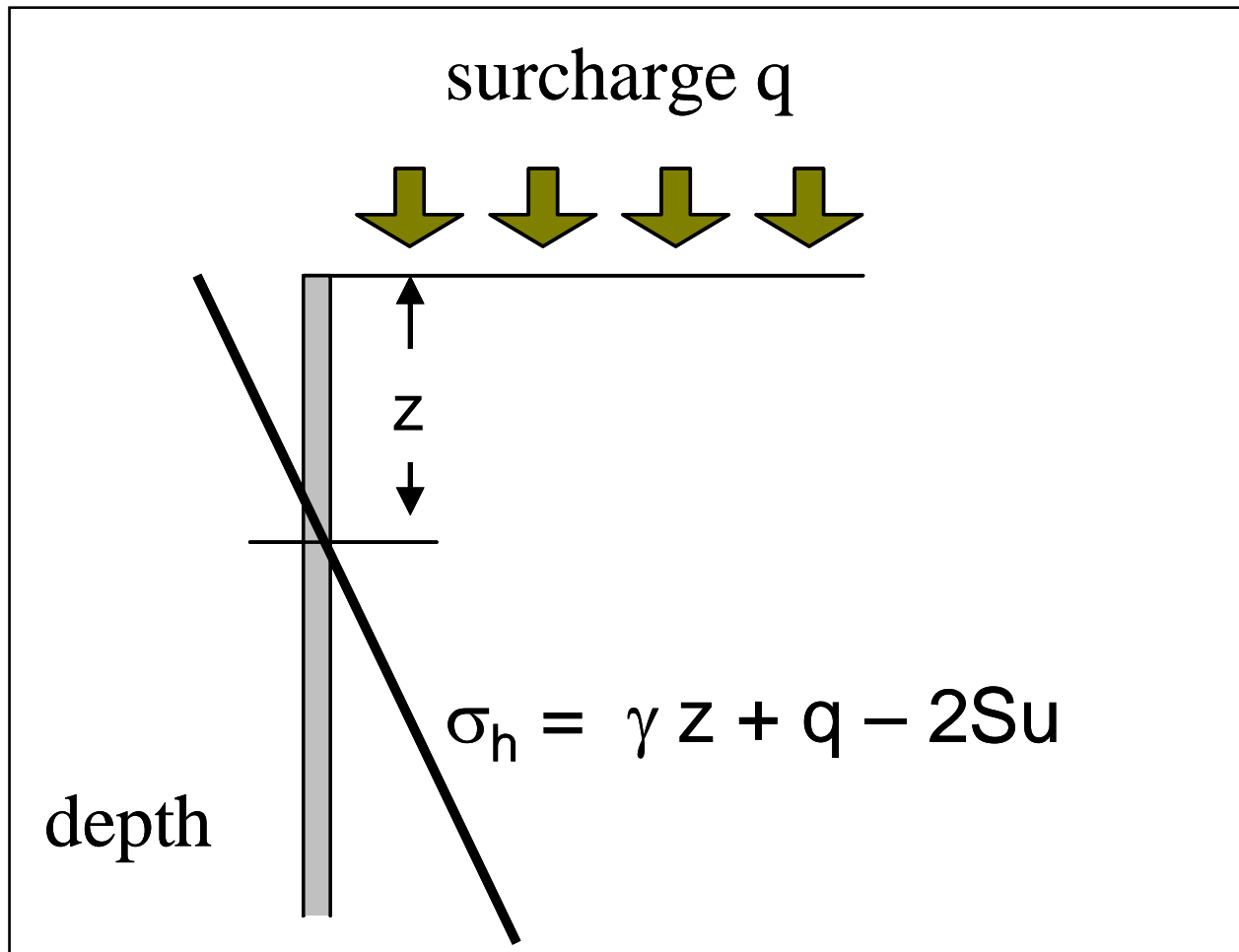
Figure 5.9. Depth z, of a dry crack behind an unpropped smooth retaining wall, limiting active Rankine
stress state

The analysis above is relevant to unpropped walls supporting soil in an undrained condition adjacent to an open excavation. In the case of a wall with support on the passive side, however, the theoretical depth of the crack will be less, provided that the strain required to mobilise the passive (or propping) resistance is small.
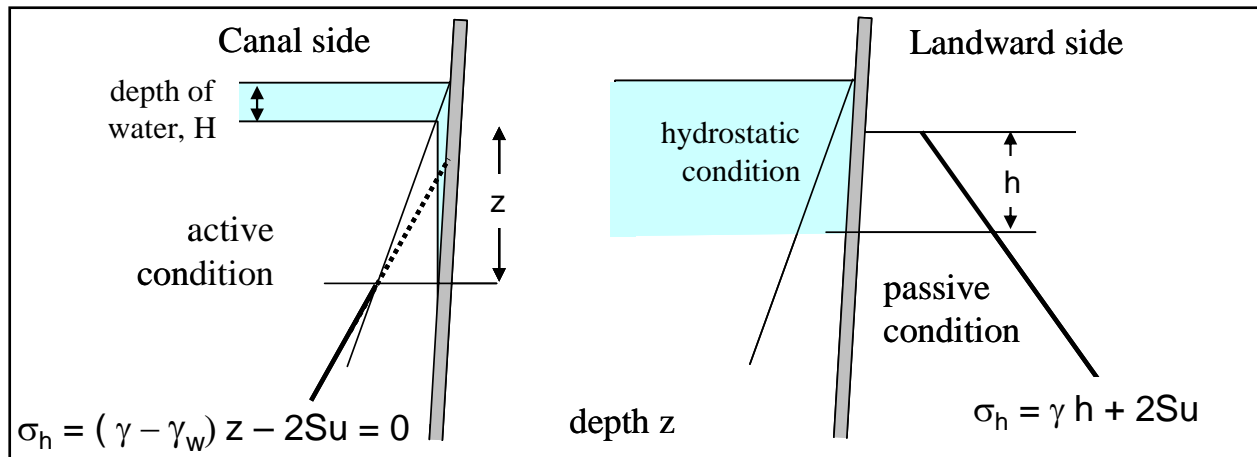
Figure 5.10. Limiting Active and Passive Rankine stress states on either side of a stiff wall with water filled crack

Figure 5.10 shows the canal side and land side conditions similar to those in the models carried out for this study. Water fills a gap between the wall and the clay on the 'active' side. The depth of the water filled crack in this active condition (without support) is unchanged from the simple equation above as the increase in total vertical stress is equal to the increase in hydrostatic pressure from the water in the gap. If limiting passive resistance can be mobilised on the landward side of the wall with negligible landward movement, then the theoretical depth of the crack (in almost all cases) will be controlled by the passive propping force that is mobilised to resist the hydrostatic force on the opposite side of the wall. The depth of the crack, z below the crest of the levee on the canal side (if any) would then be given by:

$$\gamma_w \, (\, z + H \,) = \gamma \, h + 2 \, S_u$$

Under the conditions of 17th Street or London Avenue, this 'rigid prop' approach does not suggest that a crack would form. However, this analysis takes no account of the actual movement required to mobilise passive resistance from the landward side of the levee. In practice, the geometry of the landward shoulder of the levees and the low shear stiffness of the swampy marsh beneath, mean that significant movement of the passive block on the landward side is required to mobilise any resistance to the crack formation.

Rotation of the floodwall under the additional hydrostatic load (and moment) caused by the water rising up the exposed face will therefore negate the potential benefit (in terms of reduced crack depth) of the passive resistance on the landward side opening a gap on the canal side of the wall as if there was no resistance from the landward side. Unlike the case of the rigid prop, which is infinitely stiffer than the soil, the passive soil block is only capable of resisting the lateral load by movement, and any movement landward at all of the wall will open a crack that is immediately water filled.

Figure 5-11 shows a typical example of the relationship between movement ΔH/H of a stiff retaining wall into or out of the backfill and the mobilisation of active and passive resistance (for a wall translating or rotating about the toe). It is seen that as much as 5% rotation is required to

mobilise full passive resistance, even in a condition where there is an extensive horizontal layer of soil beyond the wall.
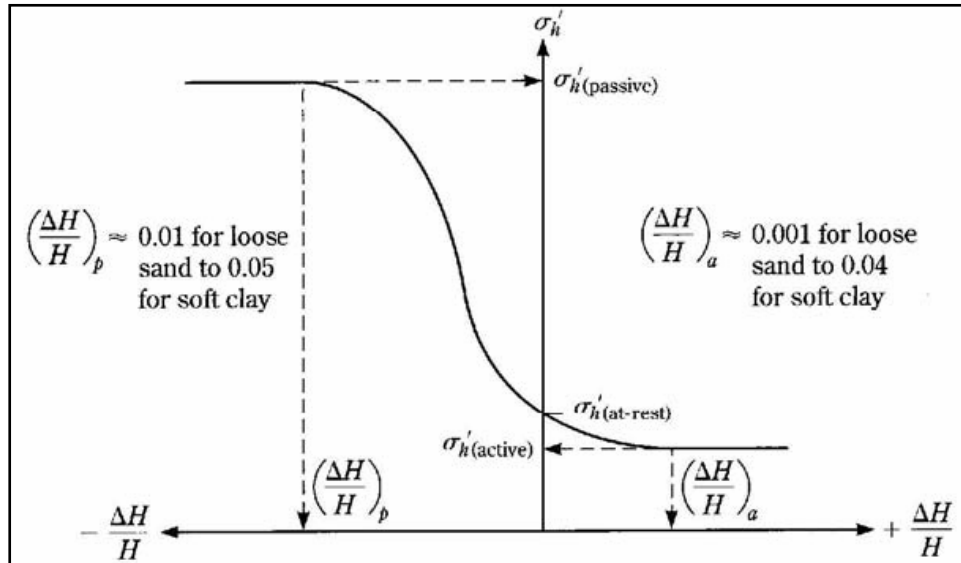
Figure 5-11. Rotation or movement required to mobilize active and passive resistance, from Principles of Foundation Engineering, BM Das

It is concluded that any rotation of the wall landward as it mobilises passive resistance against the flood condition will immediately open a water filled crack on the canal side, as the canal side acts in an undrained active manner, following the approach described above.

As the clay levee is saturated, it is sufficient to 'break the seal' on the canal side for full hydrostatic conditions to exist (in the case of the levee profiles considered) either to the base of the wall (where the wall does not reach an underlying sand layer), or to the top of the sand layer (where it does). (Note that following the approach outlined above, for an undrained strength $S_u = 500$ psf, the theoretical depth of a water filled crack will be over 21 feet.)

The evidence for the formation of the crack is clearly seen in the video imagery from the model tests, seen here in Figure 5.12, and also in the record of the pore pressure transducers located near the toe of the flood wall, Figure 5.13, which showed a rapid rise in water pressure to the full canal water level as the wall moved landward slightly.
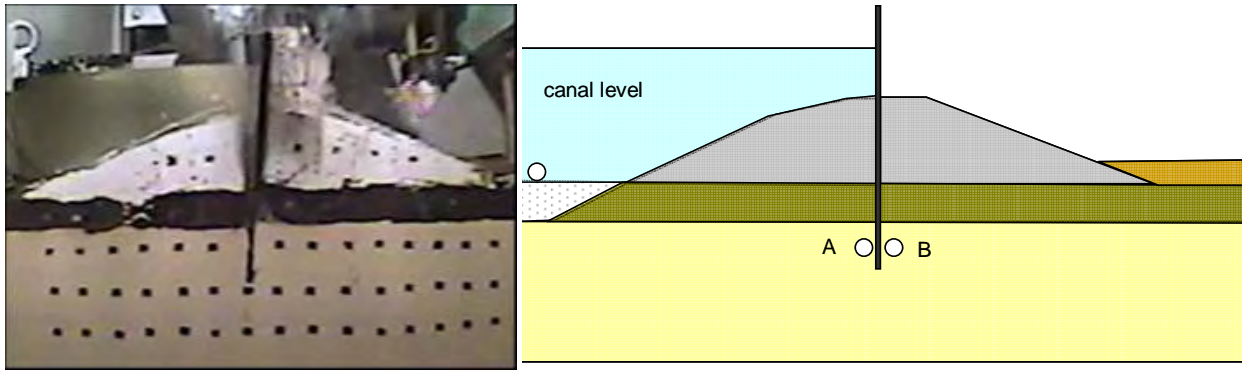
Figure 5.12. Early stage of crack formation in London South model
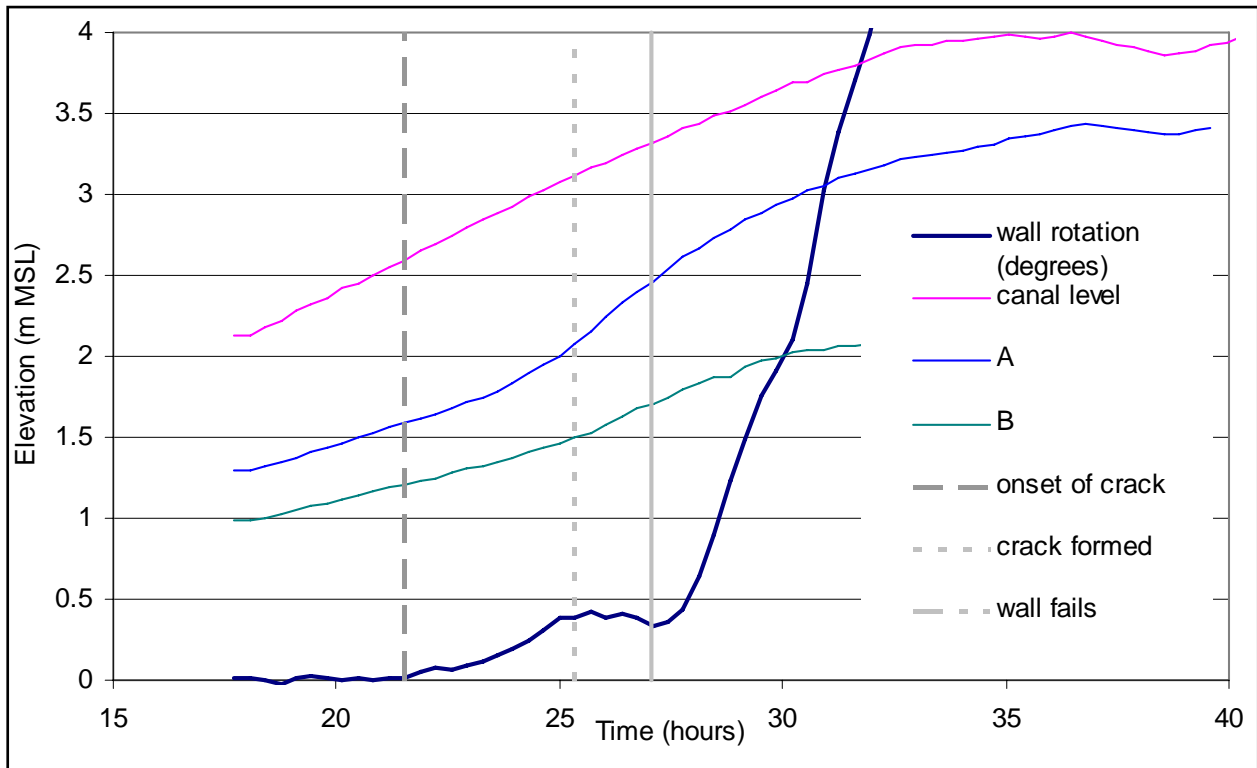
Figure 5.13. Comparison between canal level, water pressure at base of wall and wall rotation, London South Model 1, ERDC

The same sequence of crack formation, wall stabilisation and then wall failure was observed in a repeat model of London South, Model 2, carried out at RPI, Figures 5.14 and 5.15.
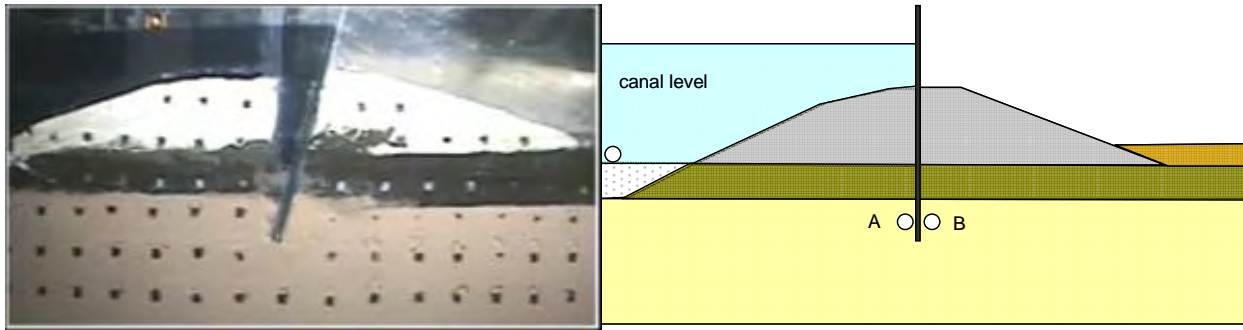
Figure 5.14. Early stage of crack formation in London South Model 2
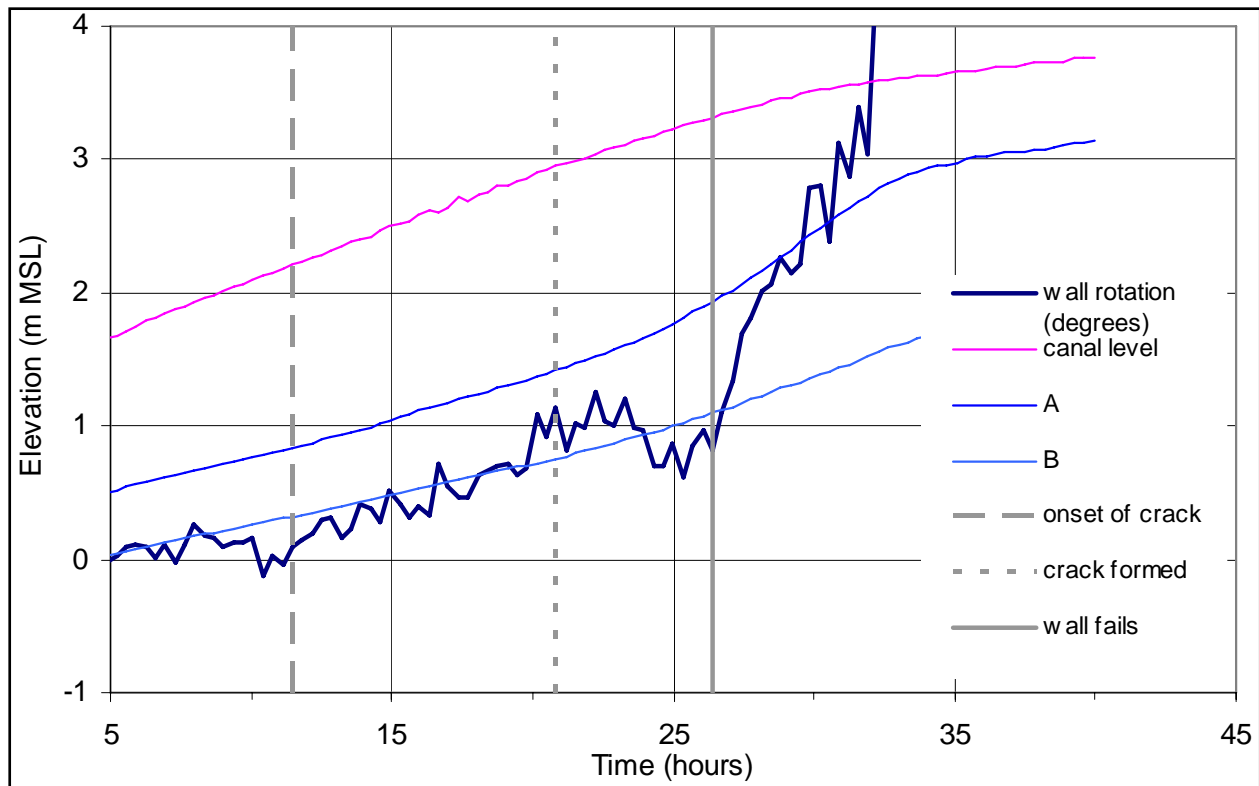
Figure 5.15. Comparison between canal level, water pressure at base of wall and wall rotation, London South Model 2

In the case of levees on clay foundations, a similar phenomenon was observed. Figure 5.16 shows the rotation of the wall followed by a brief period of stabilisation before the main failure ensued.

Model tests carried out on a cross section representative of the Orleans canal (Orleans South), which has a less deep flood wall that does not reach the underlying sand layer showed very small movements of the wall at flood levels up to Katrina. Beyond the Katrina flood level (over 1m higher) movement of the wall was observed indicative of crack formation. This is clearly seen in the video image, Figure 5.17. Plotting canal elevation against wall displacement, Figure 5.18, for Orleans South, shows the early time stiff response of the levee system up to the

Katrina flood level. At higher flood levels, the rate of landward movement of the wall increases sharply as the crack forms. The formation of the crack increased both the load and the moment on the wall. In this model test the flood wall remained in place and did not show the same unstable response to high flood levels as the levee sections on 17th Street and London Avenue though its performance did appear to be close to failure (discussed below).
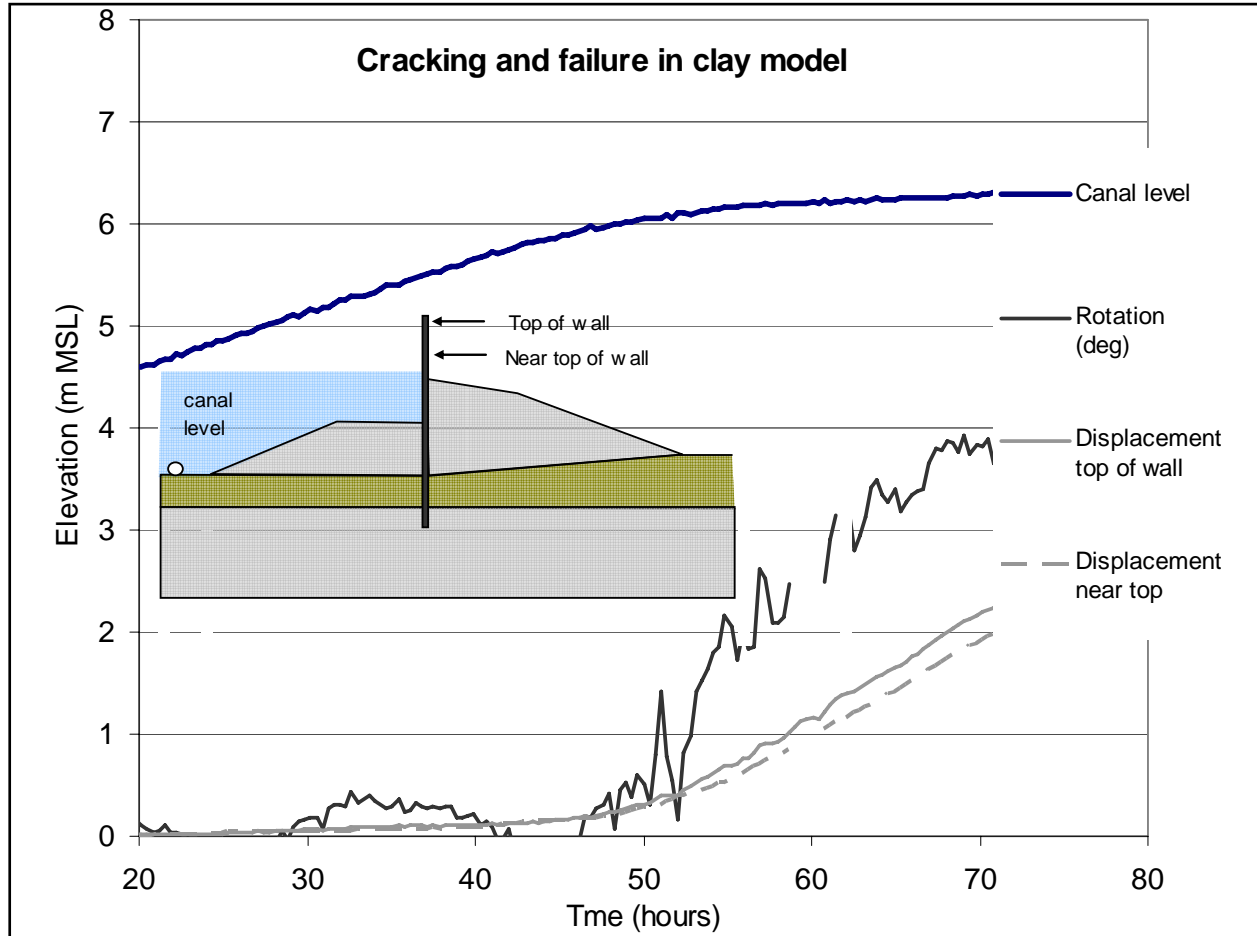
Figure 5.16. Rotation and translation evidence of crack formation prior to failure, 17th street model
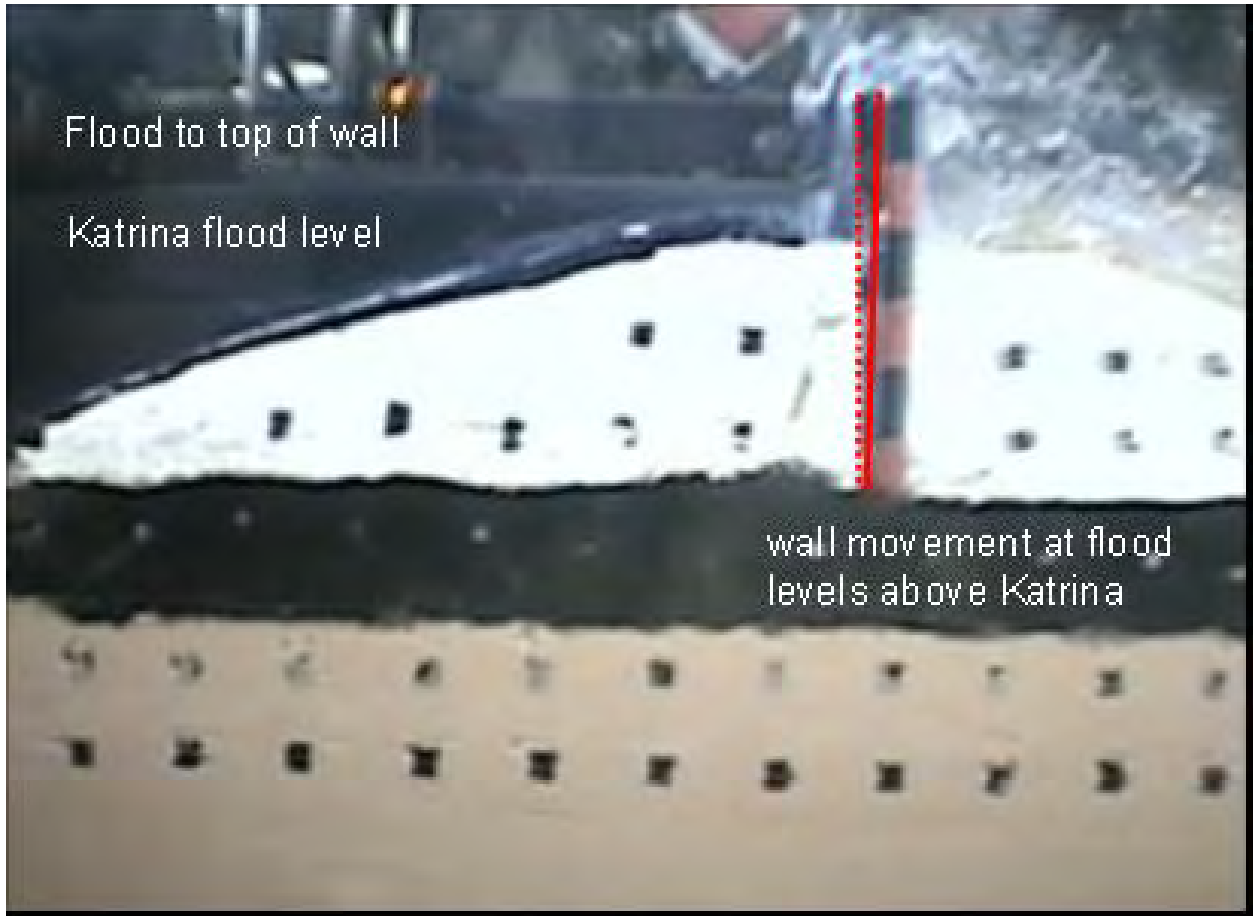
Figure 5.17. Crack forming at Orleans South levee section at flood level above Katrina
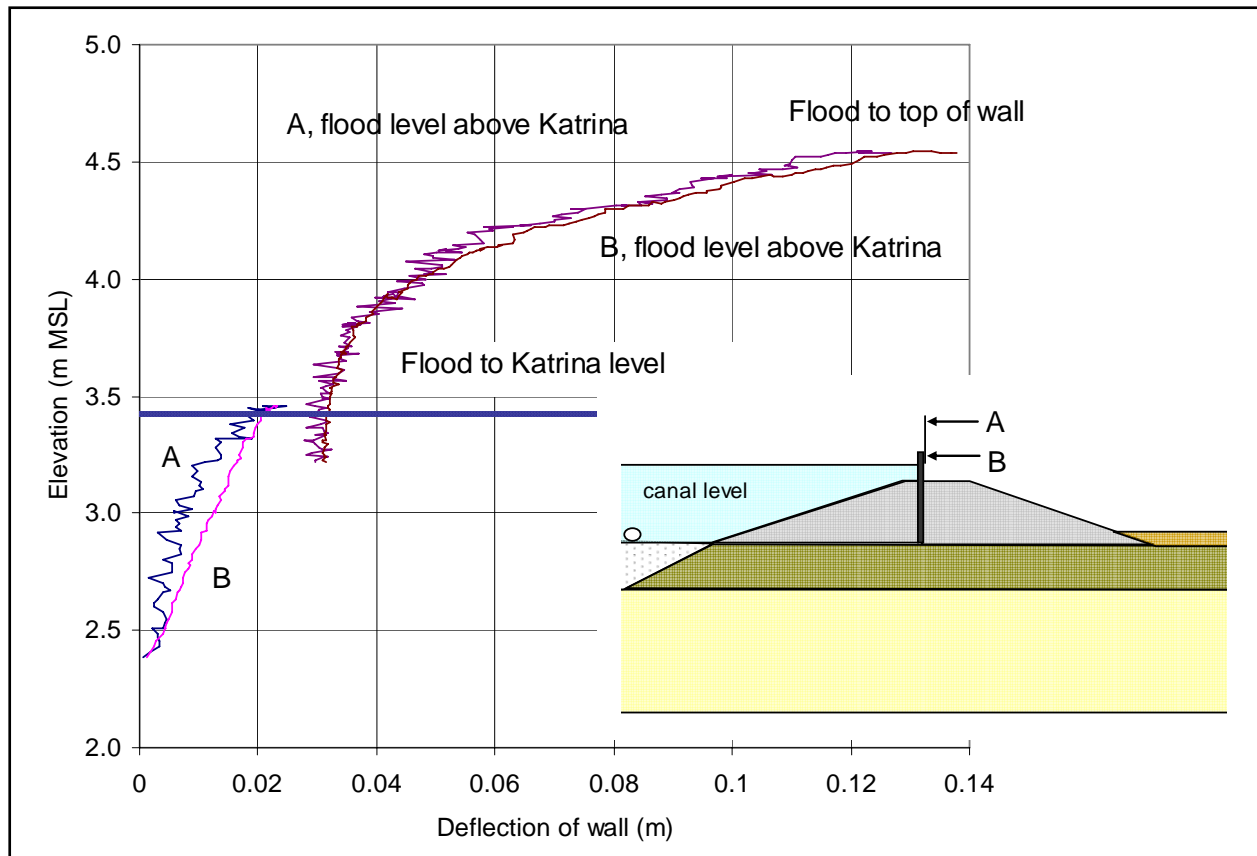
Figure 5.18. Small translation of wall at Orleans South at Katrina flood level, larger movement at higher flood levels indicative of crack formation

Rotation of the Wall

In the model tests where the toe of the sheet pile wall penetrated into the sand and was restrained from lateral movement, the opening of the crack on the canal side of the flood wall was followed by a rotation of the wall landward. Instruments on the wall recorded the horizontal movement, from which it may be seen that the wall rotated, consistent with the video imagery of the failure. In all of the model tests with sand foundations (London South and London North) that showed gross movements indicative of wall failure, the rotational movement was accompanied by a translational sliding of the landward part of the levee with the underlying swampy marsh, on top of the deeper sand layer.

Piezometric levels indicating the pore water pressure in the sand foundation show that the vertical stress on the foundation at the onset of failure was near zero towards the toe of the levee on the landward side.

Figure 5.19 shows rotation of the wall in a London South model and Figure 5.20 shows a sequence of video images of the rotational movement in progress. A similar sequence was found for the repeat model of London South, Model 2, Figure 5.21.
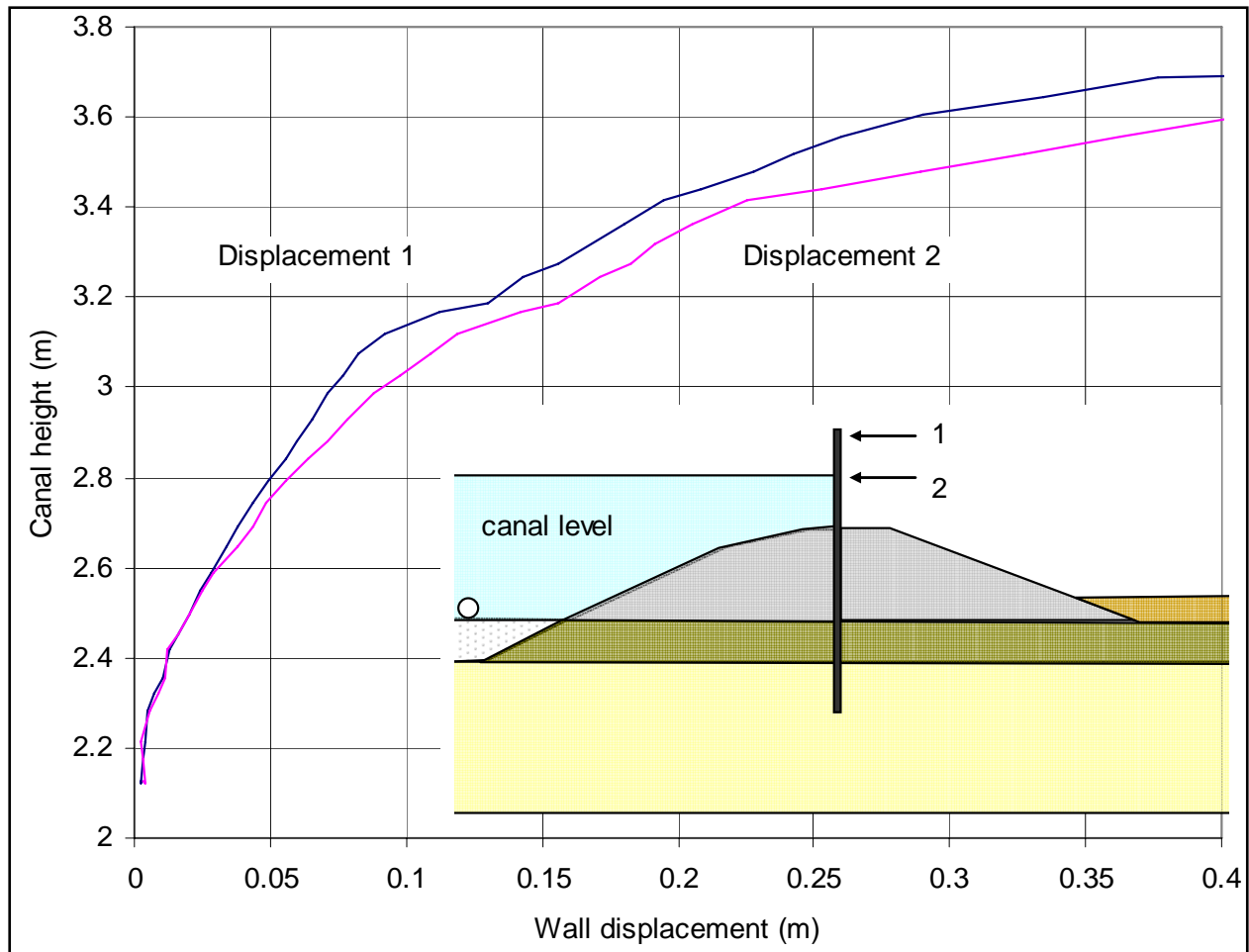
Figure 5.19. Rotation of the wall as canal level increases followed by failure, London South, Model 1

Figure 5.20. Wall failure follows crack formation, London South model, Model 1

Figure 5.21. Crack formation, wall rotation and sliding failure, London South Model 2

The rotation of the wall is linked to the reduction in effective confining stress in the sand layer beneath the landward shoulder of the levee. Once the crack was fully opened pore pressure transducers in the foundation sand layer show that the excess pore pressure in the sand rises to reflect the increase in pressure at the toe of the wall. The increase is seen to reduce linearly with distance from the toe of the wall. The increasing water pressure in the sand layer reduces the vertical effective stress under the swampy marsh.

The reduction in vertical effective stress has two effects: the first is to increase the likelihood of uplift of the swampy marsh (as the increasing water pressure in the foundation balances the weight of the levee and swampy marsh layer above) and the second is to reduce the stiffness of the sand surrounding the toe of the sheet pile wall, providing passive resistance.

The mechanism of failure in the sand models (London South, London North) was analysed as follows. Piezometric levels under the levee on the landward side rise, reducing the vertical effective stress on the swampy marsh – sand interface as the canal level rises, Figure 5.22. Rotation of the wall under the hydrostatic load on the exposed section of floodwall above the crest is resisted by the embedment of the wall in the sand layer, the elastic stiffness of the swampy marsh layer and the clay levee (landward side).
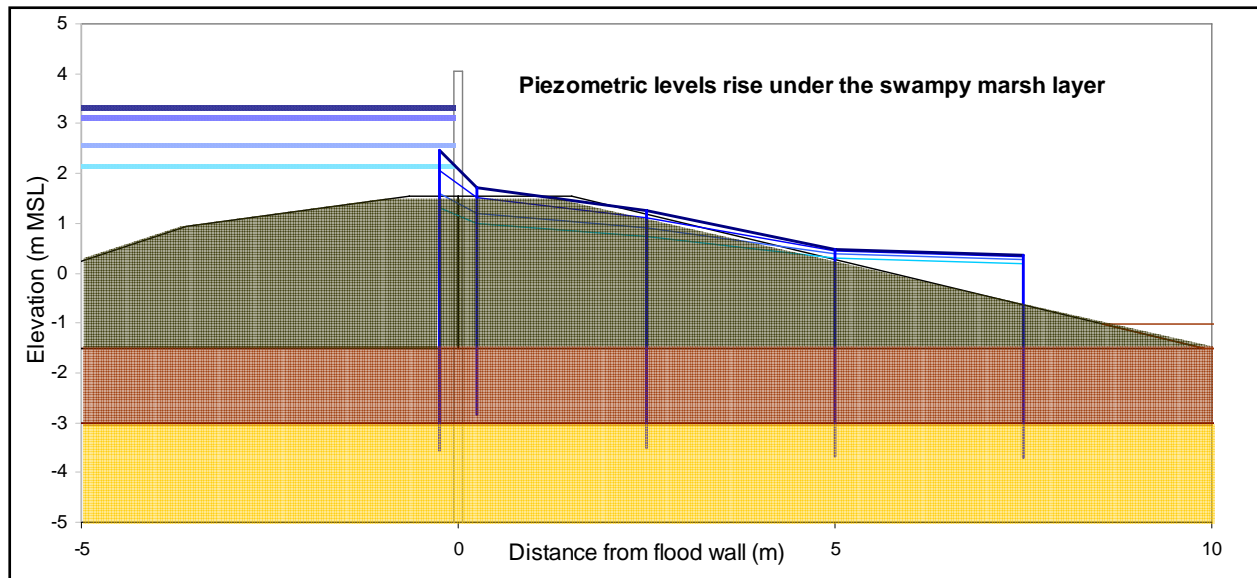
Figure 5.22. Piezometric levels immediately under the swampy marsh show increase under the levee as the wall rotates

Observations of the extent of crack rotation prior to failure show that the rotation reached around 0.5 degrees prior to a brief period of stabilisation, before the rising piezometric levels under the levee coupled with the rising canal level triggered the failure of the wall, Figure 5.13 above. As noted earlier, a passive rotation of less than 1% (around 0.5 degrees) in loose sand or less in dense sand (as at London South) is sufficient to mobilise the limiting passive resistance of sand.
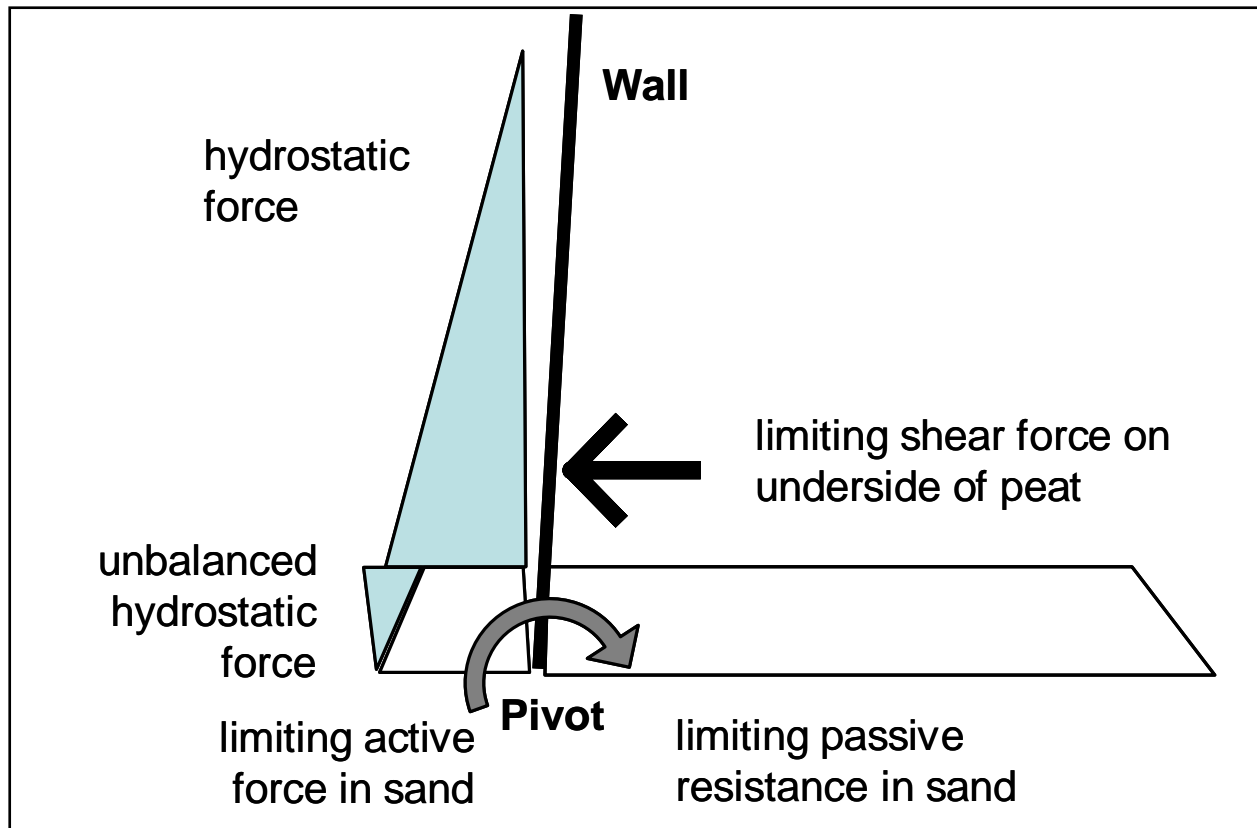
Figure 5.23. Equilibrium stress analysis for the collapse of the wall

Figure 5.23 shows an equilibrium stress analysis for the wall at the onset of failure used for the analysis of the London Avenue models. Hydrostatic pressure from the canal reaches the base of the swampy marsh. Below this level, an active stress condition exists to the base of the wall (for simplicity). Differences in the hydrostatic pressure on either side of the toe of the wall in the sand lead to a small resultant 'unbalanced' force landward. On the passive side, full passive pressure is mobilised in the sand, and a limiting shear stress is mobilised along the underside of the swampy marsh beyond the passive zone, where the vertical effective stress is greater than zero. Forces acting on the swampy marsh are discussed further below (Figure 5.25).

Figure 5.24 shows a superposition of three images at different stages of the levee failure, with two marker points highlighted in the passive zone and in the swampy marsh near to the levee toe. It is clear that the swampy marsh is moving laterally while a wedge shaped passive zone develops in the sand showing both a slip surface extending from near the toe of the wall and some heave at the top of the sand layer, below the levee crest.

Figure 5.24. Overlay of video images of the rotational failure of the London South model wall, Model 1

Figure 5.25 shows diagrammatically the forces acting on the swampy marsh towards the landward side of the levee and beyond the passive wedge in the sand layer at the toe of the wall (Figure 5.24). The compressibility of the swampy marsh landward of the levee means that no significant passive resistance from this layer can be mobilised in the 'crumple zone'. Near the toe of the levee, water pressures in the sand layer are sufficiently high that the vertical effective stress between the swampy marsh and the sand layer is near zero (Figure 5.27), and hence the shear stress that may be carried across this interface in this area is also near zero. Forces acting on the levee from the wall must be transferred through the swampy marsh to the sand below, and therefore the maximum horizontal force that may be applied from the wall is controlled by the maximum shear force that can be mobilised on the underside of the swampy marsh layer.
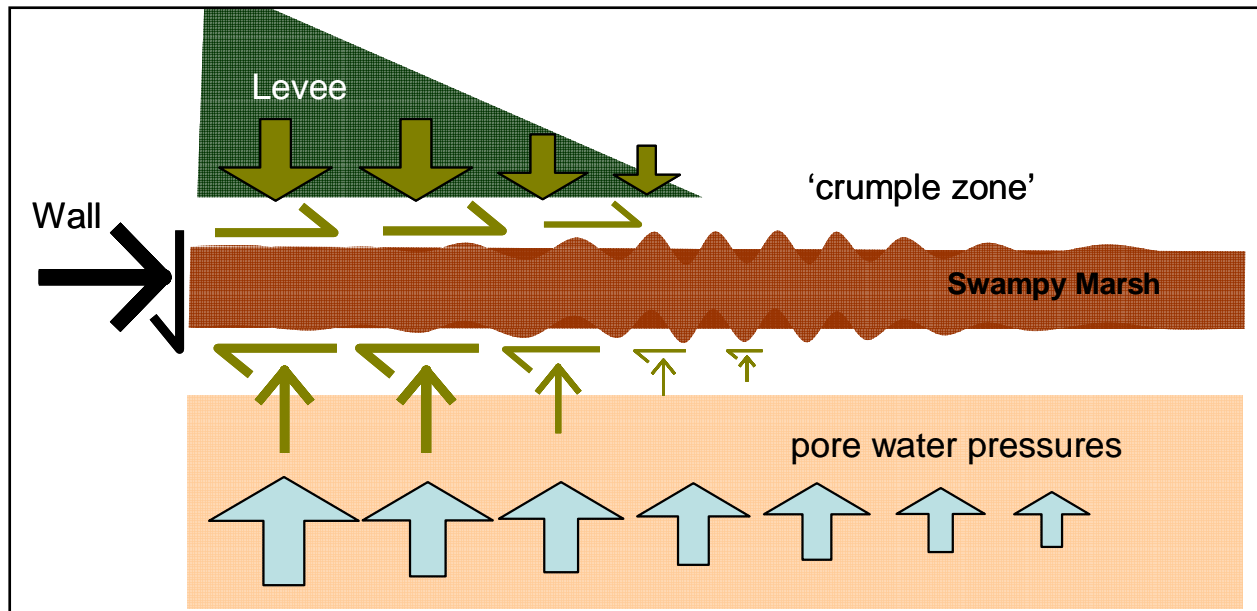
Figure 5.25. Diagram of forces acting on the swampy marsh towards the toe of the levee

The Factor of Safety for the London South models was analysed at a series of discrete instants when the water level in the canal was (a) normal or typical canal level (b) at the onset of crack formation (c) at the completion of crack formation and (d) at the onset of sudden failure. These instants are also shown in Figure 5.13 above entitled, 'Comparison between canal level, water pressure at base of wall and wall rotation, London South model'.

Figure 5.22 showed the piezometric levels under the swampy marsh at different canal levels. Figure 5.26 shows the reduction in vertical effective stress under the swampy marsh as the wall starts to fail. Near the wall, vertical effective stresses are slightly lower on the canal side of the levee, compared to the landward side. Towards the toe of the levee, the vertical effective stress falls to near zero.

The passive and active forces in the sand were calculated on the basis of a limiting angle of shearing resistance of 33 degrees, considered appropriate to the degree of strain that the wall had undergone. The limiting shear force on the underside of the swampy marsh was calculated on the basis of the average vertical effective stress acting over discrete lengths of the interface, outside the passive zone and where the effective stress was greater than zero. The unbalanced hydrostatic force was computed from the measured water pressures in the sand on either side of the wall (this force is due to seepage effects). Saturated unit weights of the levee clay, swampy marsh and sand were taken as 110 pcf, 80 pcf and 120 pcf respectively, appropriate to the unit weight of kaolin and Nevada sand. (The value for the saturated unit weight of the swampy marsh was the same value used for the slope stability analysis.)
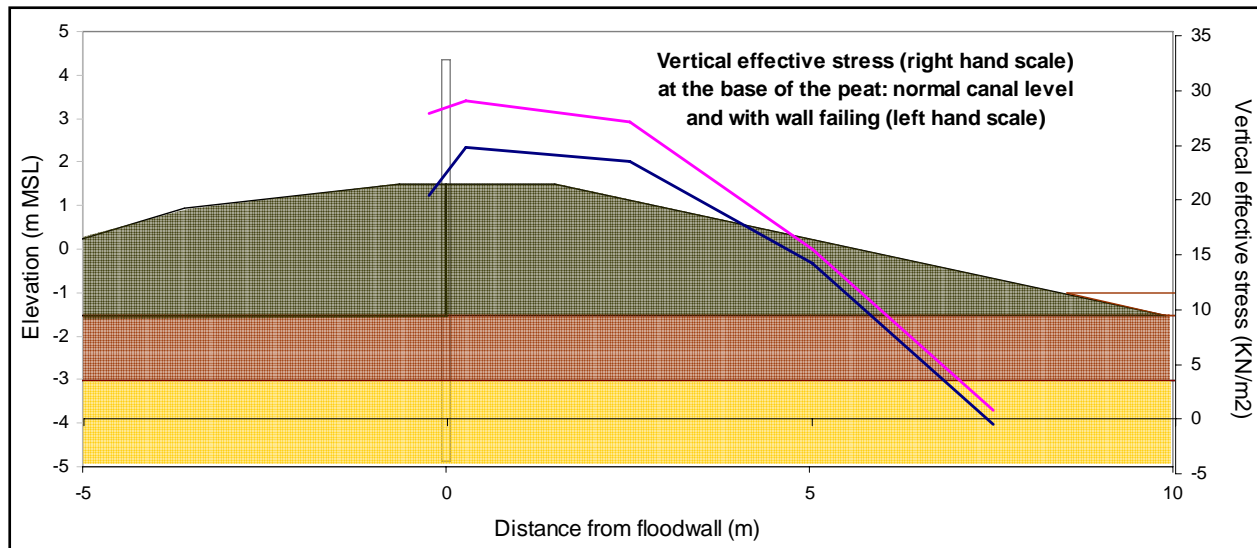
Figure 5.26. Reduction of vertical effective stress on landward side of flood wall at onset of failure

The results of the calculation for two different models were highly consistent, showing that this mechanism of failure was in a limiting condition at the instant of failure, based on the measured data from the model tests. Figure 5.27 shows the Factor of Safety calculated for the two models, at four different stages of normal (typical) canal level, crack opening, crack formed and the onset of wall failure.
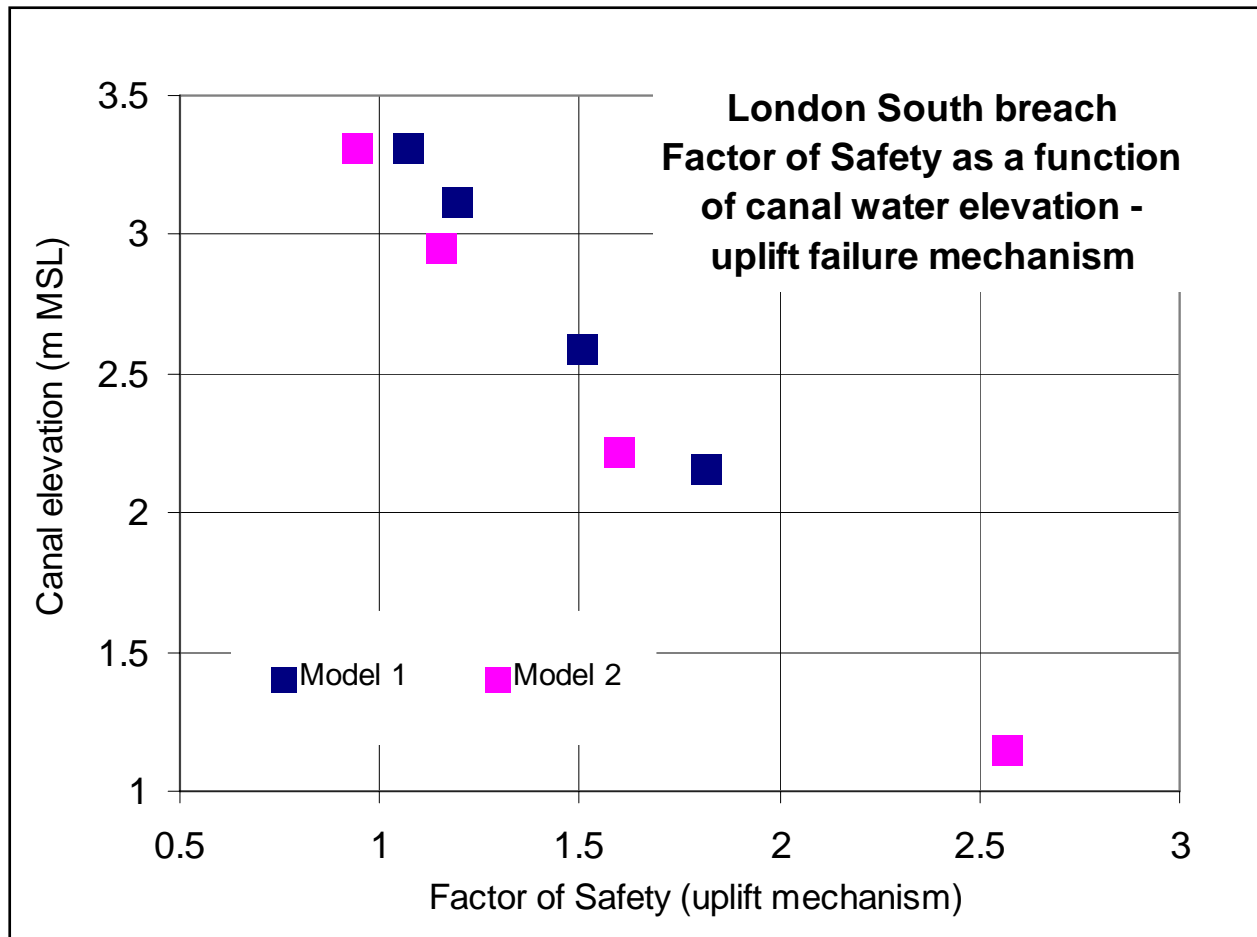
Figure 5.27. Factor of Safety for observed failure mechanism (uplift and rotation) for two London South models carried out at ERDC and RPI

The analysis is consistent with the observation from all the model tests that the formation of the crack and the re-adjustment of the wall to the new hydrostatic loading condition, with increased moment and lateral force, is a separate event from the failure that follows. In both models analysed here, the factor of safety remains above 1 at the completion of the crack formation, and falls to 1 at the onset of failure.

The rotation and uplift mechanism of failure observed in all the sand foundation models (London South and London North) is sensitive to the unit weight of the swampy marsh. In the analysis of the model tests presented above, the unit weight for this material was selected appropriate to the samples used in the experiments. Reducing the unit weight of the swampy marsh by 10 pcf (80 pcf to 70 pcf) reduces the FoS by around 0.1.

Because of the significance of the formation of the crack, the model tests show that shallow penetrations into the sand layer will have particularly low FoS. Following the analysis above, varying the depth of the bottom of the sheet pile wall by 1ft up or down changes the FoS by +/- 0.15.

Figure 5.28. Water emerging from toe of levee as failure progresses, London South Model 2

The high pore water pressures under the toe of the levee on the landward side and under the swampy marsh led to water being ejected from the ground at the toe of the levee. This may be deduced from the piezometric heads near the toe of the levee, and may be seen in the video images of the landward toe. Figure 5.28 shows a view of the levee and floodwall as seen from the 'backyard' of houses behind the levee showing 'black' water emerging from the toe of the levee as the flood wall rotates landward.

Translation of the Wall

In all of the scale models where the toe of the sheet pile wall terminated in the clay layer, then following the opening of the water filled crack a translational failure occurred through the clay, starting at the toe of the wall and progressing landwards. This is clearly seen in the instruments recording movement of the wall and in the video imagery, Figure 5.32.

The observation of crack formation in the 17th Street levee models has been described above and was shown in Figure 5.16 for one case. A second example is shown here, Figure 5.29, from 17th Street Model 1, which shows an early rotation that briefly stabilises before the main failure commences (Scale time 28 to 36). (Note time scales in the centrifuge models are unrelated to the actual time line of the Katrina flooding. Time in the centrifuge models is therefore referred to in the text here as 'Scale time' to distinguish the two time lines.) Video imagery of the phase between the initial opening of the crack and the onset of the main failure shows active slumping behind the wall, which may explain the increase in rotation between around Scale time 37 and 42 hours.
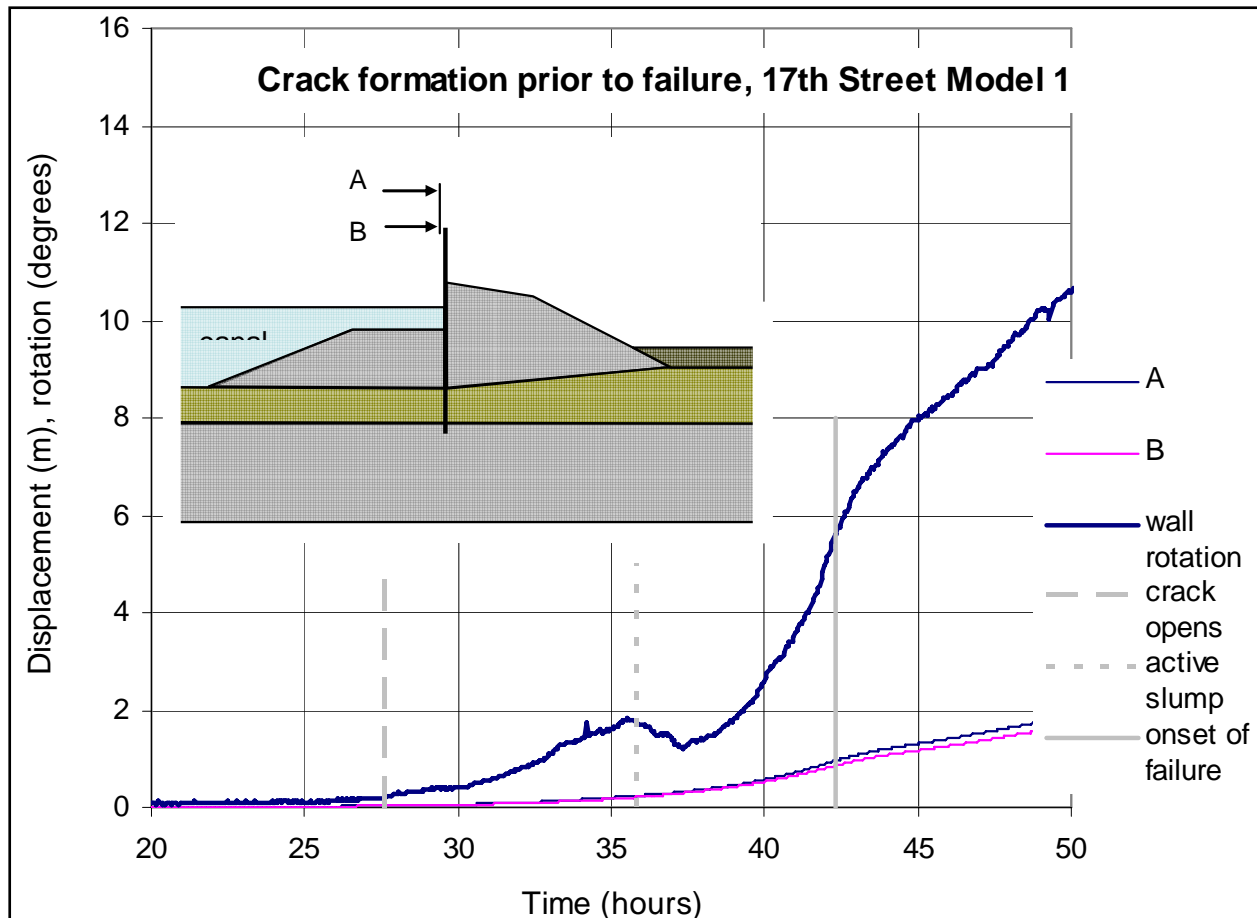
Figure 5.29. Crack formation prior to wall failure, 17th Street Model 1

The sliding surface developed near the top of the clay layer and progressed landwards until it was outside the levee, before it turned upwards to exit through the swampy marsh layer. This mechanism is similar to the observations in the field from 17th Street. The progression of the slip surface landwards can be identified from the pore pressure records, which show a progressively delayed reaction landwards to the translational movement.

Comparing the wall rotation with the pore water pressure measurements at locations in the clay on the canal side of the wall, at the toe of the wall and the canal level (expressed as head in m of water) with the wall rotation gives further insight into the mechanism of failure, Figure 5.30. The crack formation phase is marked by a small rotation, up to 2 degrees movement, following which the wall briefly stabilises. As noted above, active slumping starts towards the end of the crack formation phase, perhaps as early as Scale time 30, indicated by the change of slope and reduction in excess head near the toe of the wall on the canal side. During this period, the pore pressures beneath the levee on the canal side reflect the increase in total stress but show no evidence of the wall movement.

The reduction in excess head near the toe of the wall continues as the wall ceases to rotate but continues to translate (between Scale time 36 – 37.5) before rotation starts again, leading to a sharp transition in performance around Scale time 42 as the wall fails. At this moment, the canal

level drops due to the rapid lateral movement, the water pressure at the bottom of the wall changes slope again and rapidly rises (to reach and exceed the canal level), and the rate of rotation slightly decreases as the main translational movement commences.
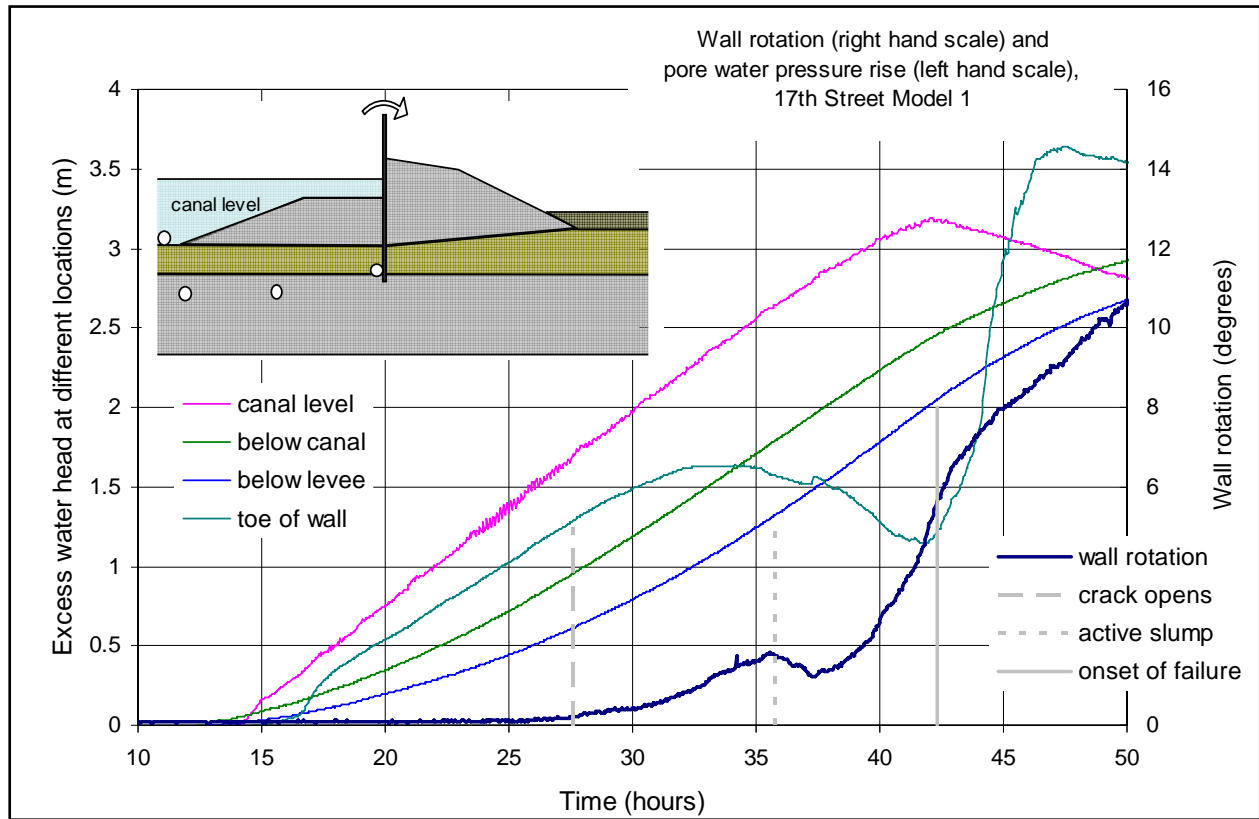
Figure 5.30. Comparison between wall rotation and excess head at onset of failure, 17th Street, Model 1

The sliding failure of the model wall was arrested before a full breach took place to capture the final state of the 17th Street model (Model 1), Figure 5.31. Despite the large lateral movement, there is minimal heave of the swampy marsh layer on the landward side.

Figure 5.31. Final state of 17th Street Model 1 showing lateral translation on sliding surface starting at the toe of the wall and progressing landwards.

All of the clay foundation models failed with a similar mechanism under the flood loading, commencing with a small rotation and crack formation, followed by further rotation and large translation associated with a shear plane the formed from the toe of the sheet pile wall and progressed landwards through the top of the clay layer. This was consistent with the field observations.

Other observations relevant to the site conditions on 17th Street were also noted from the centrifuge model tests. The very soft, normally consolidated clay beneath the levee experienced significant settlements as the weight of the levee was increased to full height. The swampy marsh layer also tended to be compressed below the levee, but predominantly through elastic compression.

In one model of the 17th Street levee, the weight of the levee on the landward side was sufficient to provoke bearing failure in the clay foundation, Figure 5.33, with the formation of inclined slip planes, prior to the flood condition. This is a situation analogous in the field to raising the height of the levee too rapidly, without allowing time for the high excess pore pressures in the foundation to dissipate and the strength of the clay to develop. On the surface, the only evidence is increased settlement. At depth, however, local slip surfaces form in the soft clay and swampy marsh
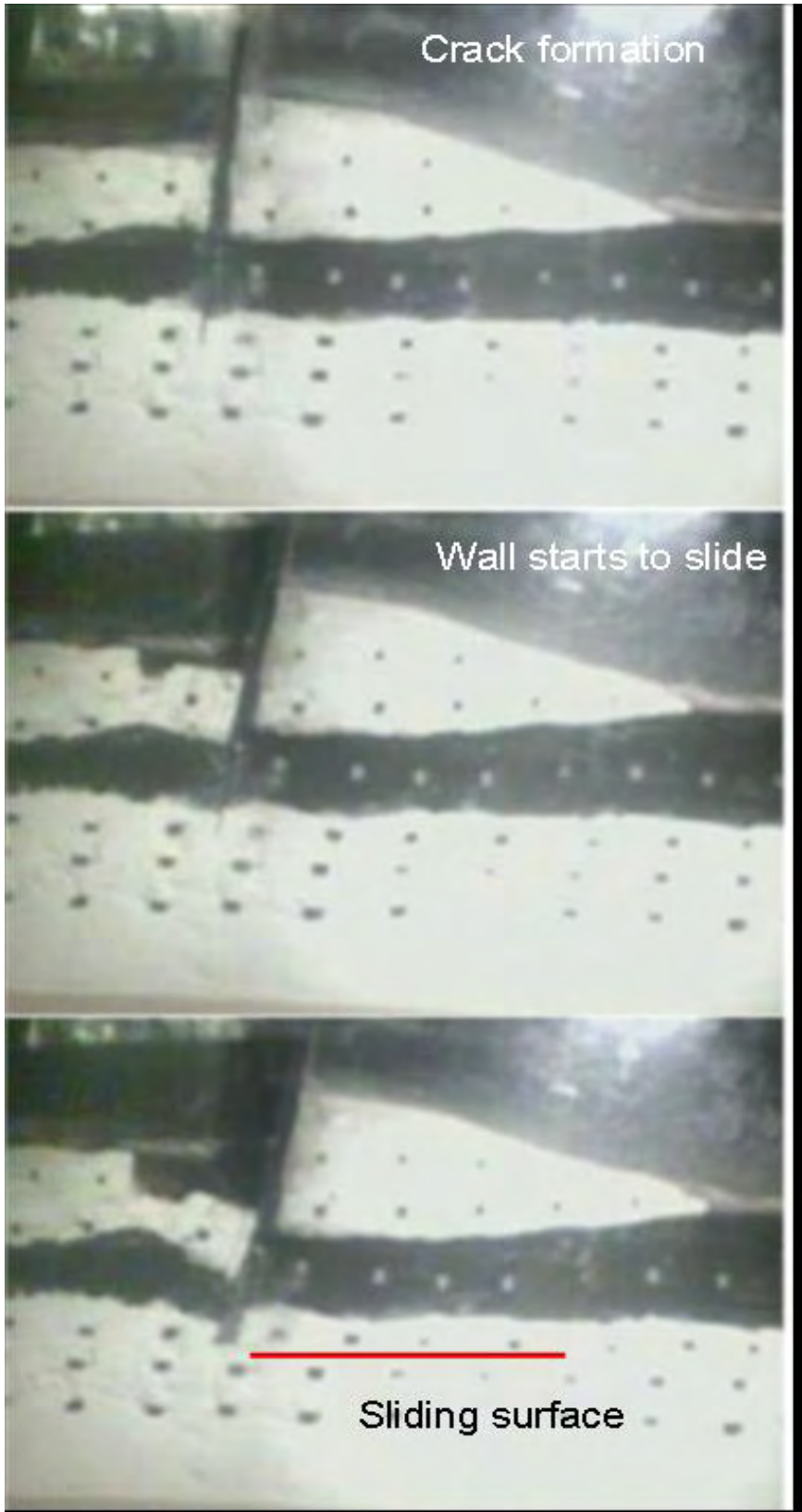
Figure 5.32. Sliding surface forms at top of clay layer in 17th Street Model 1

This is a preliminary report subject to revision; it does not contain final conclusions of the United States Army Corps of Engineers.

Figure 5.33. Bearing failure and multiple slip planes in the clay foundation caused by rapid construction on landward side, 17th Street Model 2

On flooding of this model, the same mechanism of translational failure was observed, independent of the initial disturbance in the clay foundation of the levee. The new sliding surface cut 'horizontally' through the pre-existing inclined surfaces along the top of the clay layer as in previous models. The new surface exited through the swampy marsh along the pre-existing surface, forming an up thrust on the ground surface. The bearing failure in the foundation had no significant effect on the height of flood water to cause translational failure.

No Failure Condition

Scale model tests were also carried out of levee sections on Orleans Avenue canal which did not fail, as part of a validation process. The cross section chosen to represent the southern portion of the Orleans Avenue levees is similar to the cross section at London Avenue, except that the levee is wider and higher, and the penetration of the flood wall is less (the toe of the wall is at the base of the levee/top of the swampy marsh layer).

As with the other levee sections, the instruments beneath the model levee responded to the rising water in the canal by an increased excess water pressures in the ground, reducing linearly

from a maximum near the canal to a minimum to the landward side of the levee, Figure 5.34. At the water level experienced in Orleans Avenue canal, the floodwall did not show any movement to indicate the opening of a crack, Figure 5.35.
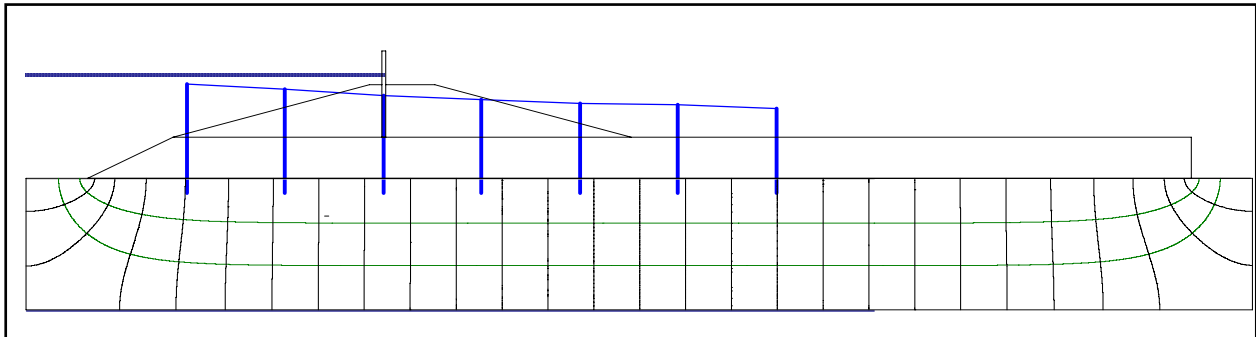
Figure 5.34. Seepage flow net for Orleans Avenue South with piezometric levels under the swampy marsh at Katrina flood level

Figure 5.35. Orleans South model at Katrina flood level

The piezometric levels below the swampy marsh in the Orleans South model showed a declining level from the canal side to the protected side of the levee, Figure 5.36. The additional height and width of the Orleans South levee, seen overplotted in the figure for both Orleans South and London South, significantly increase its capacity to resist the flood levels and no evidence was seen of a crack opening through the swampy marsh and providing a hydraulic

connection to the sand below. The London South piezometric levels, shown in the figure for comparison together with its cross section (aligned at the elevation of the top of the sand layer) show a more critical condition in terms of uplift under the landward side of the levee. Both models however show high piezometric levels near the toe of the levee on the landward side, sufficient to lead to hydraulic fracture.
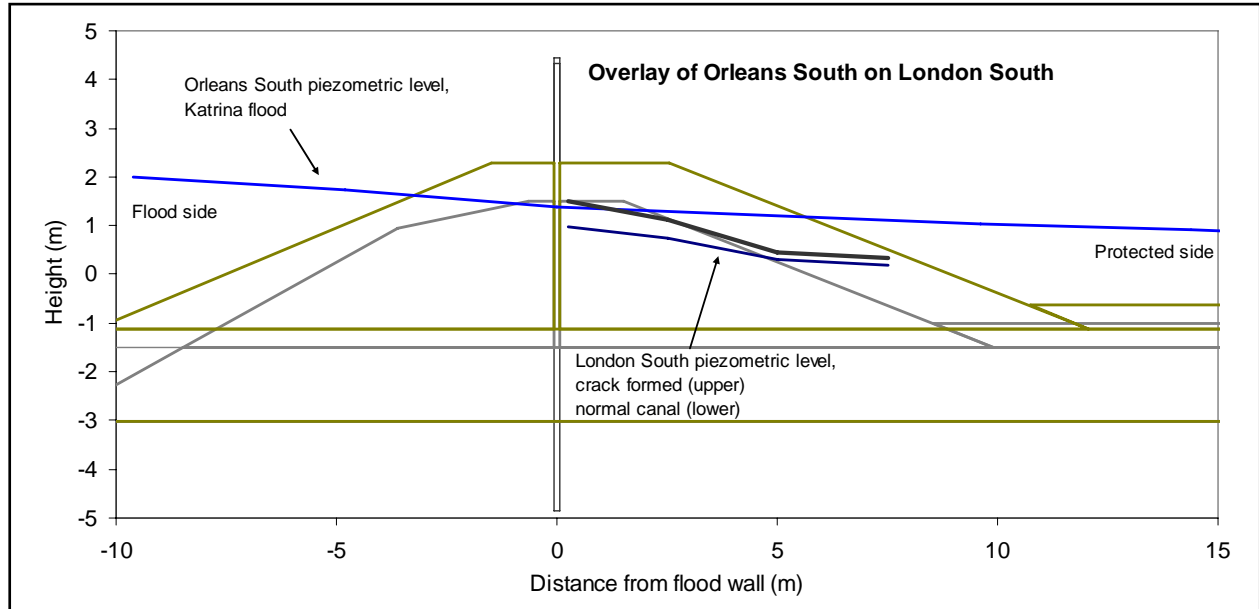
Figure 5.36. Comparison of piezometric levels in Orleans South (Katrina flood) and London South, with the base of the swampy marsh assumed to be at a common elevation

As the water level was increased above the Katrina flood level in the Orleans South model, a crack was seen to open to the toe of the flood wall, associated with small movements of the flood wall landward, as shown in Figure 5.37. Unlike the other models, this crack did not develop into a full failure condition; no unstable movement of the flood wall was observed, despite the water level reaching the top of the flood wall. Translational movements were observed to be controlled by compression of the swampy marsh layer. Relative movement between the top of the sand and the swampy marsh was apparent, in a similar manner to the uplift mechanism in the London Avenue models.

Figure 5.37. Sliding movement of swampy marsh as crack forms, Orleans South model

    Comparison between the geometry of Orleans and London Avenue shows that the vertical effective stress in the sand foundation below the levee was considerably higher under the Orleans levee than under the London Avenue levees. The capacity of the flood wall to rotate is reduced by the height and weight of the landward section of the Orleans levee. Figure 5.38 shows the vertical effective stress on the underside of the swampy marsh layer measured in the Orleans South and, for comparison, the London South models. Although the Orleans levee section is higher than London South, the piezometric levels near the landward toe are sufficiently high that a zero vertical effective stress condition is created near the landward toe of the Orleans South levee in both the Katrina flood and full flood condition.
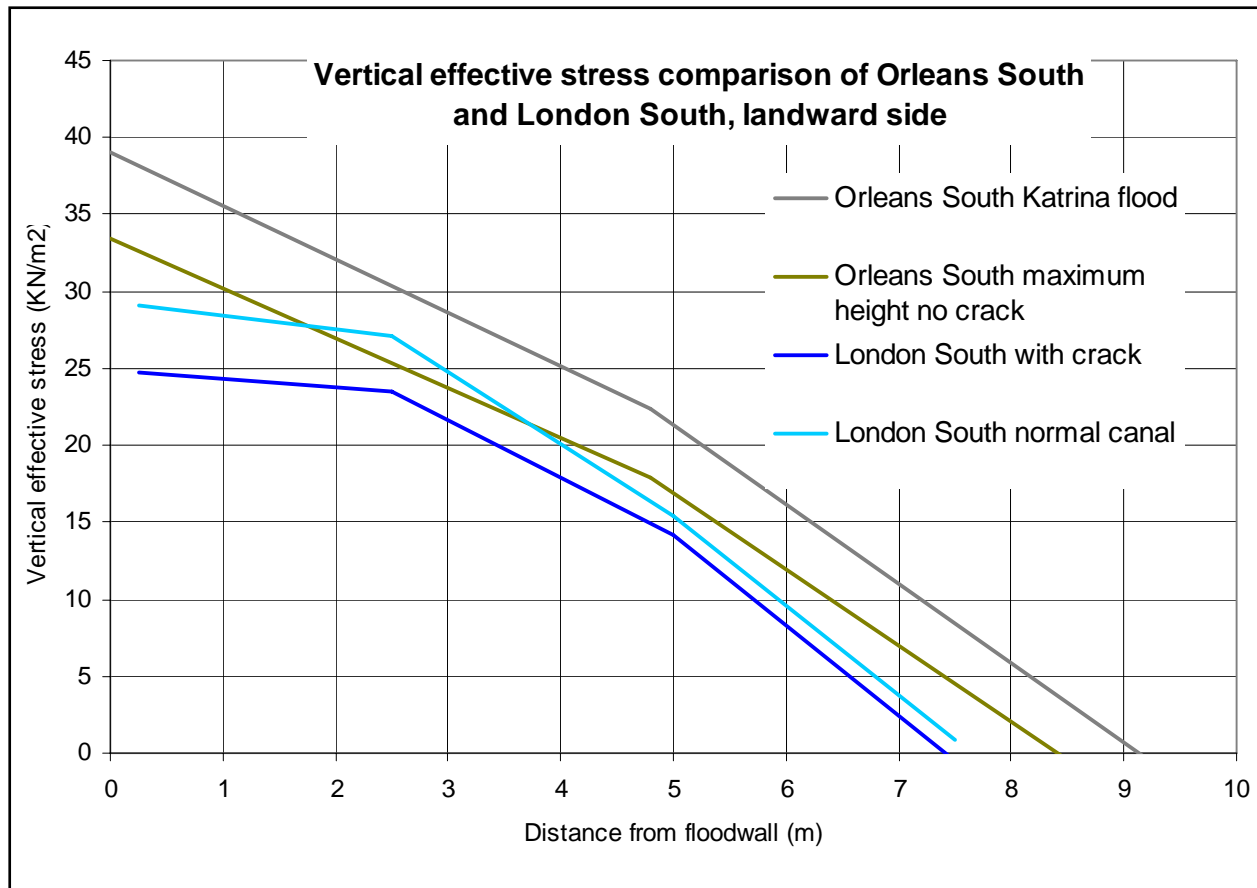
Figure 5.38. Vertical effective stress comparison between Orleans South and London South

Examining the stability of the Orleans South model, Figure 5.37 shows that the formation of the crack during the raising of the water level to the top of the wall was accompanied by lateral sliding or translation of the swampy marsh layer. The landward movement was small but noticeable and appeared uniform under the landward side of the levee, extending close to the canal side of the wall. A shearing zone appears to dip steeply downwards from the canal side toe of the wall landwards.

The stability of the landward section of the Orleans South levee may be analysed using the simple mechanism shown in Figure 5.39. Video imagery show sliding of the swampy marsh on the top of the sand layer. The sliding surfaces through the swampy marsh forming a triangular sliding block ABC are chosen to lie at angles of 60 degrees for simplicity. Assuming the levee block is free to move laterally with the swampy marsh, then work is only done on the lower surface of the swampy marsh, and on the internal sliding surfaces AB, BC and CA.
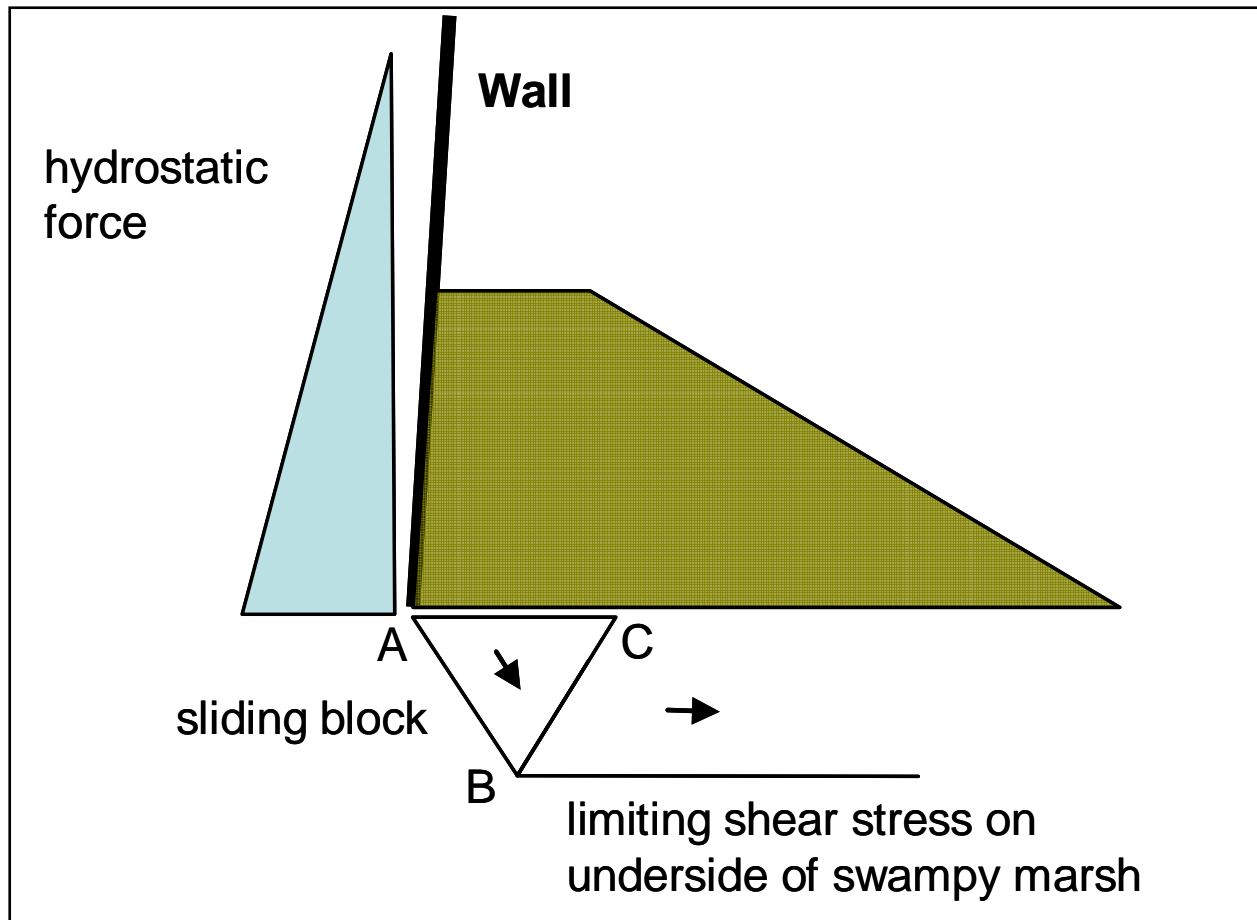
Figure 5.39. Possible upper bound mechanism for Orleans South

For infinitesimal lateral movements, a work balance gives an expression for the limiting height of water, H as a function of the depth of swampy marsh, D, its undrained shear strength S_u and the limiting shear stress mobilised on the top of the sand layer, σ_v'tan φ'.

$$\sigma_v D + \gamma_w H^2 = 6S_u\, D/\sqrt{3} + \sigma_v\text{'tan } \varphi\text{'}L$$

where σ_v is the vertical stress on the landward side of the flood wall, D is the depth of the swampy marsh, H is the height of water above the toe of the wall and L is the length of the shear surface along the top of the sand layer offering significant shear resistance.

Solving this equation for H, the critical depth of water in the crack, and using the actual measured excess pore water pressures in the Orleans South model (Figure 5.36) suggests that the Orleans South model was close to failure at full flood level. Using the value of undrained shear strength adopted for the slope stability calculations for the swampy marsh (S_u = 400psf) and a limiting angle of shearing resistance of 33 degrees in the sand, a Factor of Safety may be calculated of 1.50 under Katrina flood conditions (Figure 5.35) and 1.07 under full flood conditions (flood to the top of the wall, as seen in Figure 5.37). This is consistent with the

observations of small but continuing displacements of the wall under full flood conditions, Figure 5.18 above.

Onset of Failure

The transition from an initial condition prior to the rise in water level, through the development of a water filled crack in front of the wall to ultimate failure of the levee by rotation or sliding has been clearly demonstrated in the centrifuge models. The comparison with Orleans South has shown that a water filled crack does not necessarily lead to failure, and therefore the conditions that presage the onset of failure are of particular importance.

The models showed that following the formation of the crack on the canal side of the flood wall, there was a rapid re-adjustment of the levee and its foundation to the new loading conditions. In this state, the residual levee section on the canal side is isolated from the landward section and submerged. In the case of a sand foundation, the hydraulic connection between the sand layer and the canal through the centre of the levee means that water pressures in the ground on the canal side quickly re-establish a hydrostatic state with no landward seepage. The remaining material on the canal side provides some passive restraint to the toe of the flood wall.

Water in the crack creates a hydrostatic force on the floodwall over the height of the crack. One of three conditions was observed to follow. In the Orleans South model, at water levels higher than the Katrina flood level and sufficiently high to lead to the formation of a crack to the toe of the wall, the wall remains stable, though with creeping movements landwards indicative of a near failure condition. The failure mode that is seen to be developing (Figure 5.37 above) closely resembles London South (Figure 5.14, 5.20). Stability analysis confirms that the condition of the floodwall is near failure.

In the London Avenue models, the formation of the crack and resulting hydraulic connection between the canal and the sand layer is followed by an upsurge in the water pressure below the landward section of the levee, which is coincident with an increasing rotation of the flood wall and eventual failure. This is an unstable event, which once initiated, leads to a rapid collapse as the increasing water pressures under the swampy marsh further reduce the shear resistance on the sliding surface along the top of the sand.

In the 17th Street models, the formation of the crack is followed by the immediate development of a slip movement at the toe of the wall, and an increasing rate of landward movement. The absence of a time delay between these observations is notable. This mode of failure is also unstable. As the initial slip surface extends landwards towards the toe of the levee, the weaker clay further from the centreline of the levee is less and less able to resist the driving forces acting on the levee block.

The observations in the physical models have provided detailed insights into the mechanisms that lead to the onset of failure. The profile or geometry of the levee, flood wall and foundation was found to be critical to the development of the shallow failure mechanisms. Pre-existing

water pressures in the ground were seen to be key to the failure in all the sand foundation profiles.

The low shear stiffness of the swampy marsh and large passive strain (movement) required in the landward levee block to mobilise passive resistance controlled the mechanism of the crack formation in all models.

Summary of Physical Model Tests

Introduction

The preliminary observations of levee performance in and around N.O. indicate that foundation soils possibly played a large role in the performance. Evaluation of levee performance including the effects of the foundation in the overall behavior was conducted through scaled physical centrifuge modeling. The physical data collected from the centrifuge models was used for direct observations of levee performance and primarily to improve numerical model predictions. Results from centrifuge modeling of the failed levees in and around New Orleans resulted in a detailed set of well controlled data used to validate numerical models used in analysis, confirmation of the failure mechanisms, and additional insights of factors that may have played a part in the failure as of yet unrecognized.

The objectives of this task were to physically model selected sections of the N.O. levees to determine plausible mechanisms of failure and to provide data for use in validating and verifying the numerical modeling tools. Specifically, typical levee sections along the 17th Street Canal, London Avenue Canal, and Orleans Canal representative of the failed and non-failed sections were modeled. The specific objective for the 17th Street Canal levee models was to explore the foundation peat and clay layers and their role in the failure. For the London Avenue Canal levee models, the specific objective was to explore the role of the fine sand foundation material in the failures (North and South). The specific objective for the Orleans Canal levee models (North and South) was to explore the behavior in a canal where no failures occurred.

Physical Model Plan

A detailed plan for completing the required physical modeling tests was developed by the task research team prior to initiation of any testing. In order to complete the test in a timely manner and to provide redundancy and independence in the modeling effort, it was decided that two centrifuge facilities would perform the work. Those two facilities are the Centrifuge Research Center at ERDC, and the Geotechnical Centrifuge facility at Rensselaer Polytechnic Institute. The physical modeling plan consists of modeling the single breach at 17th Street Canal, the two breaches at London Avenue Canal, and two non-breached sections of the Orleans Canal (one on the north end and one on the south end). Each of these areas would have two models completed, one at ERDC and one at RPI.

The model tests generated large volumes of data for analysis. It was evident that in all cases failure of the levees was presaged by the opening of a water filled crack on the canal side of the

levee, which allowed full hydrostatic pressure to act on the flood wall over its entire submerged height. The flood water in the centrifuge models was raised steadily, without wave effects, and it was observed that once a crack had opened, then in the cases of London Avenue and 17th Street canal models, a failure soon followed, either by rotation of the flood wall (London Avenue) or by translational failure (sliding) in the clay stratum (17th Street), originating at the bottom (toe) of the sheet pile wall. In the following sections, synopsis of the test layout, instrumentation, and results for each test will be presented.

Physical Models of 17th Street Canal

Two models of a section at the breach location were completed. One of the models was performed at RPI and the other one at ERDC. This section of the report will present information relevant to each model. Thorough details of the levee geometry and material in addition to foundation materials were determined from field and laboratory data as highlighted in other sections of the performance evaluation report. Based on careful analysis of all that information a section representative of the breach area was developed and led to the physical models as described following. All of the models were constructed in the same container with dimensions 1.2 m in length and 44 cm in width. The models are a $1/50^{th}$ scale of the actual 17th street levee and foundation, therefore all model dimensions should be increased 50 times. Henceforth, all dimensions will be given in prototype scale. In all plots, the time is scaled time not field time.

ERDC 17th Street Canal Model

The model representative of a section through the breach at 17th Street Canal is shown in Figure 5.40. The layers consists of 1.5 m thick sand layer, 5 m thick clay layer, 1.5 m to 2.5 m thick swampy/marsh layer, 0.5 m thick overburden The levee is constructed of kaolin clay and the sheet pile of aluminium.
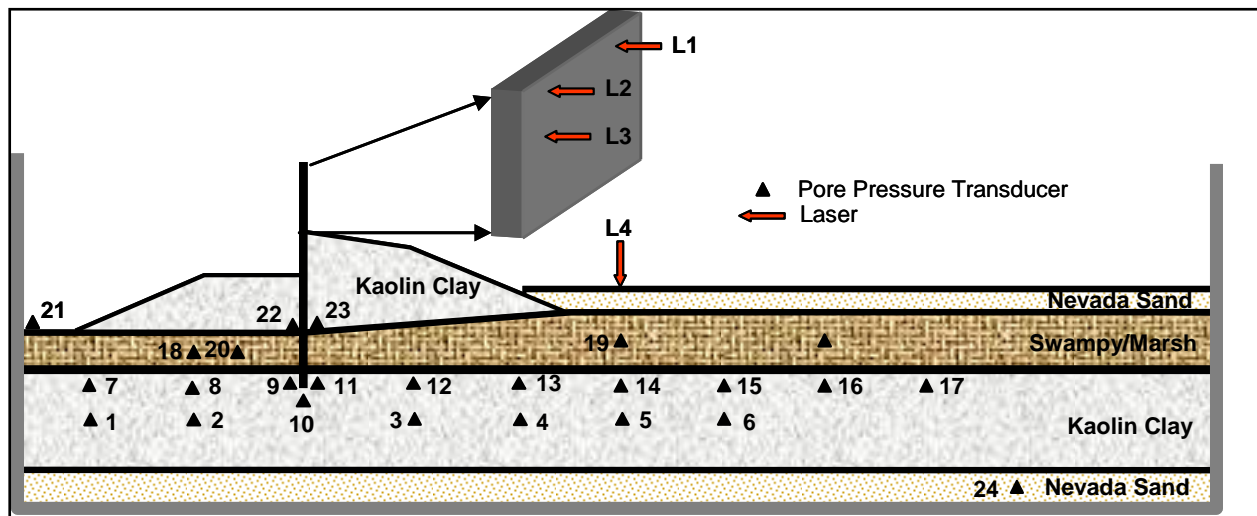
Figure 5.40. Schematic of ERDC 17th street physical model

The sequence of model construction proceeded as follows. The Nevada sand layer is rained in dry with instrumentation placed at the appropriate location. The model was then sealed, vacuumed, and the sand layer saturated. A view of the model at the end of this step is shown in Figure 5.41. At the conclusion of this step, the mixed kaolin clay was placed on top of the sand with instrumentation placed where appropriate. Figure 5.42 shows a photo of the clay mixing process and Figure 5.43 a view of the finished clay layer with markers clearly visible. The pre-mix water content was targeted to be 100%, with post-mix measurements giving moisture contents of 102%. Based on vane shear measurements the pre-consolidation strength of the clay was 48 psf.
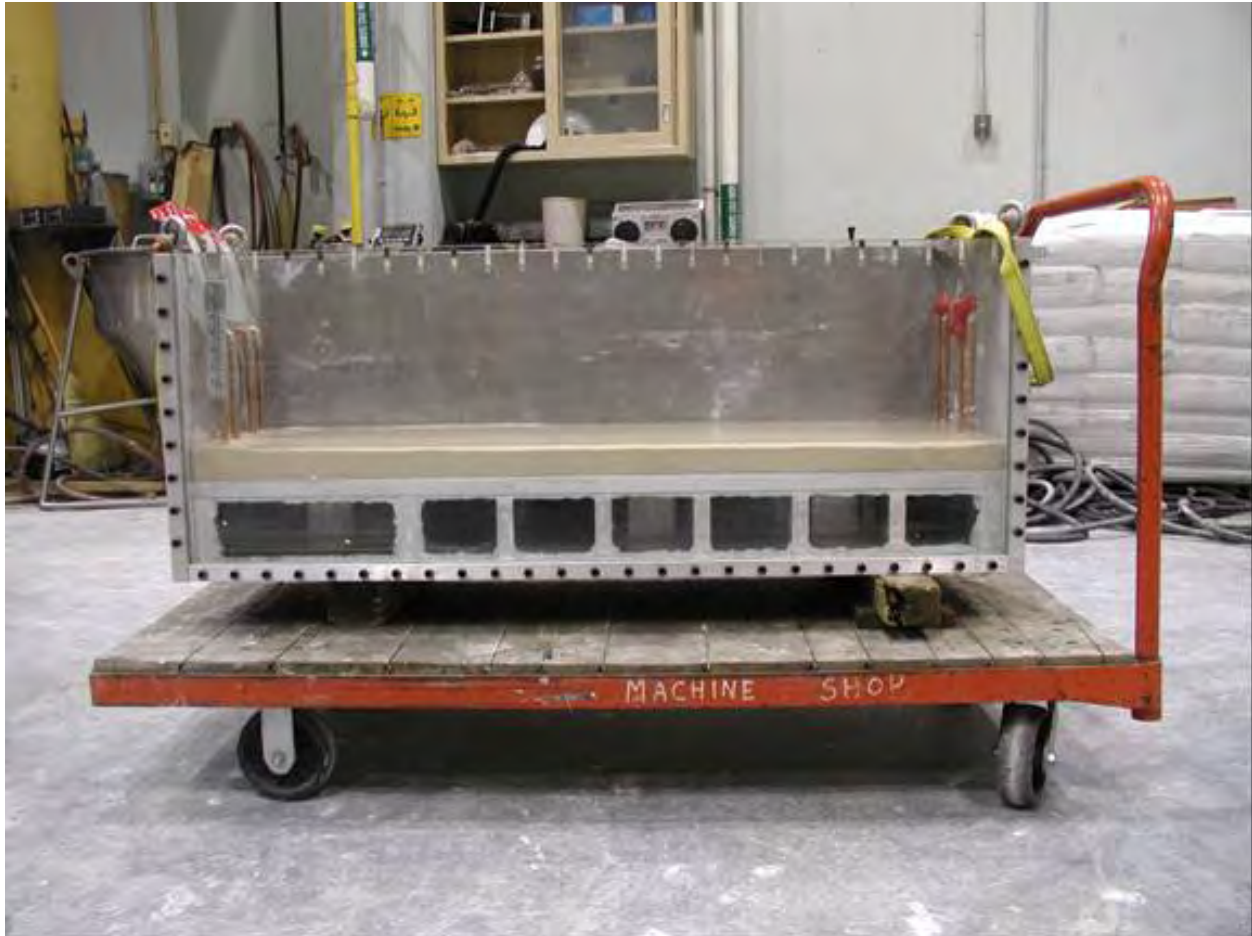
Figure 5.41. View of ERDC 17th street model at end of sand layer placement and saturation

Figure 5.42. View of the clay mixing process
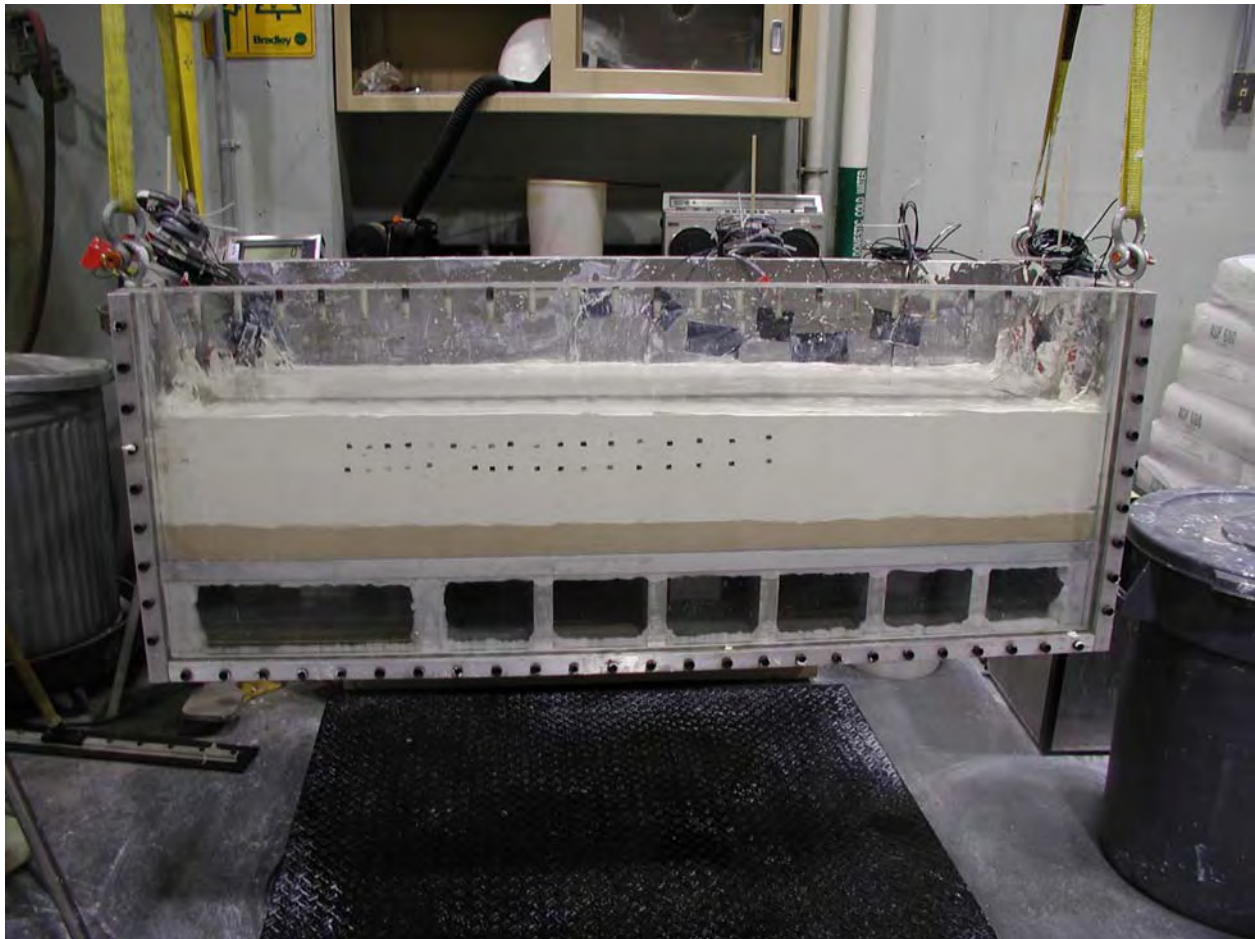
Figure 5.43. View of the completed clay layer for the ERDC 17th Street model

   After completion of the clay layer, the swampy/marsh layer was placed. This was material taken directly from the site collected in 40.5 cm cube undisturbed block samples. The material was stored in a humid room prior to use and sliced into segments of the appropriate thickness for use in the model. A view of the model with swampy/marsh layer in place is shown in Figure 5.44.
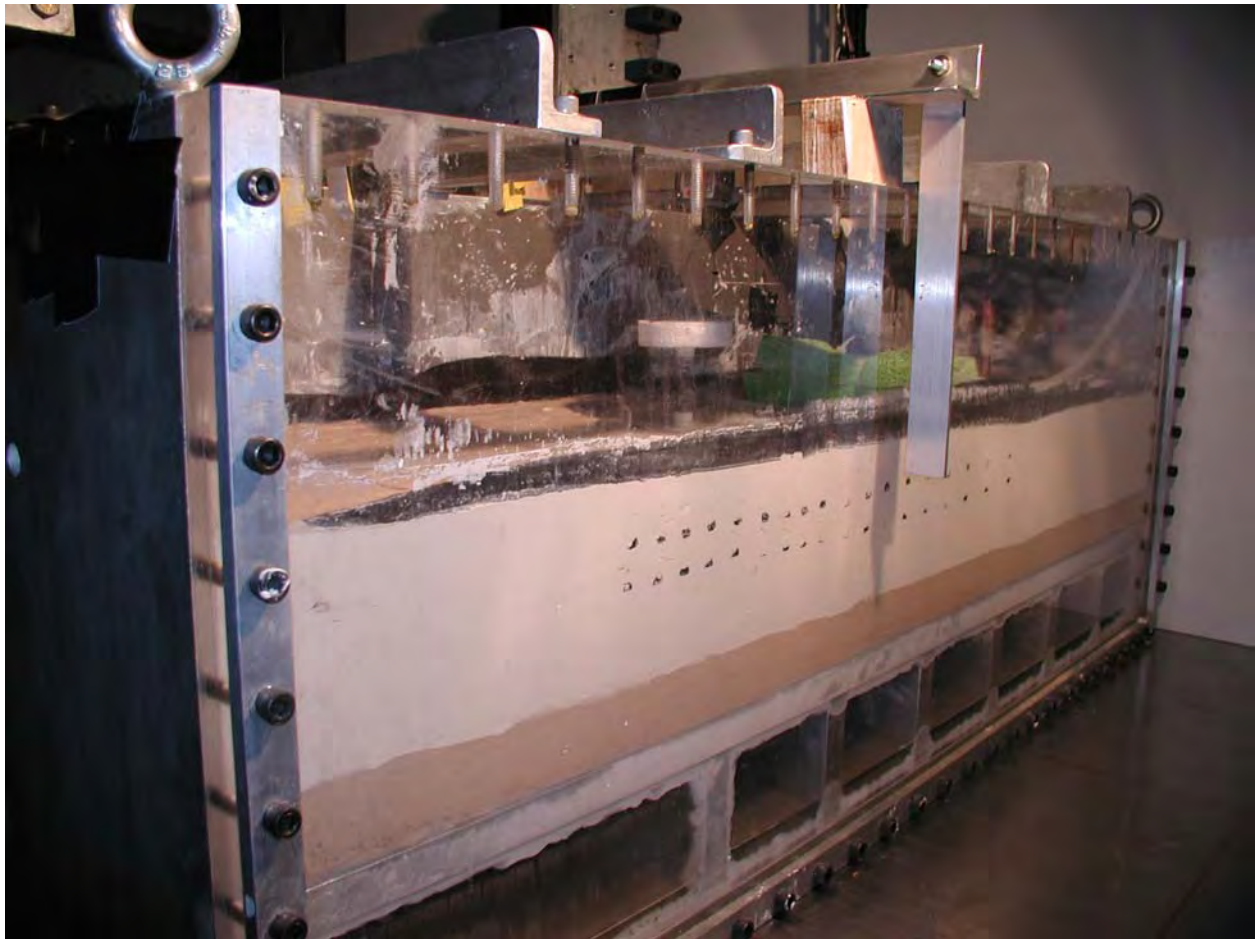
Figure 5.44. View of ERDC 17th Street model with swampy/marsh layer

This layer had markers similar to the clay layer placed for tracking movement and PPT's added for measuring pore pressure. Prior to placement of the swampy/marsh material both vane shear and moisture contents were obtained. Average values for the vane shear readings were 280 psf and the moisture contents 324%.

The clay layer was normally consolidated at 50 g. Additionally, gravel was added of a shape and weight simulating the levee to further consolidate the swampy/marsh layer. This material was removed and the consolidated clay levee added. Vane shear measurements of the clay levee material averaged 325 psf and moisture contents averaged 105%. Lasers to measure displacements were added and the model was placed on the centrifuge for testing at 50 g. The completed model is shown in Figure 5.45. The canal side is on the left of the model in the figure and the protected land side is on the right. The sheet pile wall on the canal side extends 4.6 m above the top of the levee.
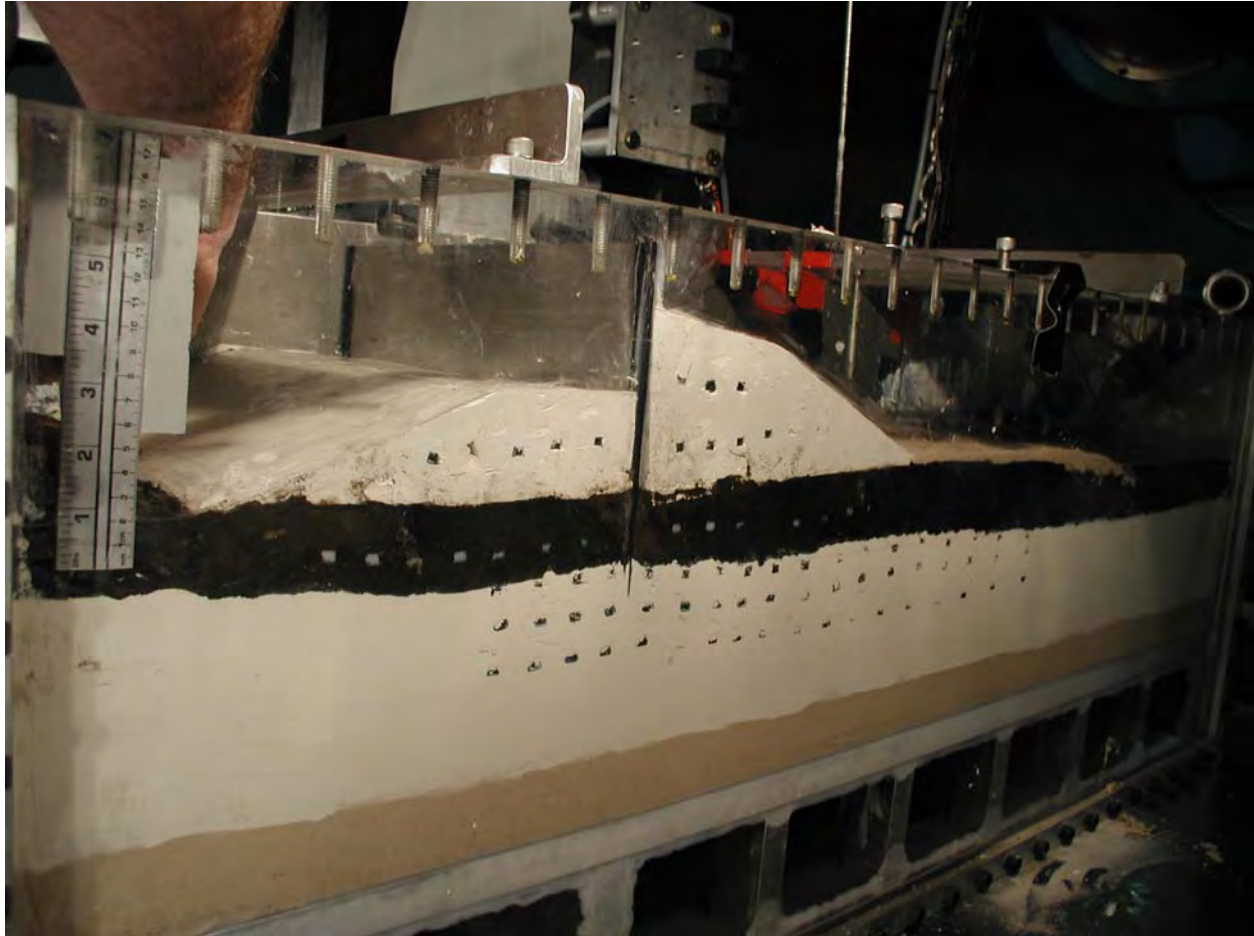
Figure 5.45. Completed ERDC 17th Street model

Once the model is completed and all instrumentation connected and zeroed, the package is slowly spun up to 50 g. Water is maintained in the canal at a depth of approximately 2.5 m until 50 g is reached. At 50 g, the model is properly scaled such that it has the correct weight, and pressure at all points in the model as would be the case in the field. The water level in the canal is increased to what it would be during normal canal operation level. In this case the normal canal level prior to hurricane Katrina was approximately 30 cm above the canal levee top elevation. The model is allowed to stabilize (pore pressures equalize) at 50 g, with the correct canal water elevation prior to addition of flood load.

The flood load is applied to the model in a steady increment. Figure 5.46 is a sequence of still shots taken from the video recording detailing the flood and failure event. The failure event is as highlighted following.

1. Water level increases to a point on the wall where initial movement of the wall begins to occur. This movement starts out as a rotation of the wall.
2. A crack begins to form between the sheet wall and canal side levee.

3. As the crack reaches the bottom of the sheet pile, hydrostatic pressure increases in the foundation soil. The low shear strength in the clay layer just beneath the swampy/marsh is not enough to resist the driving force of the flood load.
4. A near horizontal shear failure surface forms in the clay layer and the entire wall/land side levee begins to translate toward the land side.
5. As the flood load is maintained the translational failure continues.

Figure 5.46a. ERDC 17th street model at flood load just prior to development of crack

Figure 5.46b. ERDC 17th street model just after wall movement and crack formation

Figure 5.46c. ERDC 17th street model near end of failure

At completion of the test, sample tubes were pushed through the levee and foundation on the landside for laboratory testing. Average values of the moisture contents for the levee section were 53%, for the swampy/marsh 155%, and for the foundation clay layer 58%.

The next series of plots will show the recorded data during the actual flood event. Recall that the model is at 50 g such that everything is properly scaled to field weights and pressures, the water is held at normal canal operating elevation, and all instruments have equalized under those conditions prior to addition of the flood load. The data is presented in Figures 5.47 through 5.50. Figure 5.47 is a plot of the PPT's located mid-depth of the foundation clay layer. Detailed discussions related to the processes and mechanisms occurring during the flood load and subsequent failure were previously discussed. Figure 5.48 is a plot of the PPT's located near the top of the foundation clay layer, revealing a similar characteristic as the mid-depth PPT's. Figure 5.49 is a plot of the PPT's located in the swampy/marsh layer and the levee both canal and land side. Finally, Figure 5.50 is a plot of the lasers, three on the sheet pile wall and one on the land side surface away from the toe. Notice that there is some heaving of the foundation away from the toe on the land side as the failure occurs.
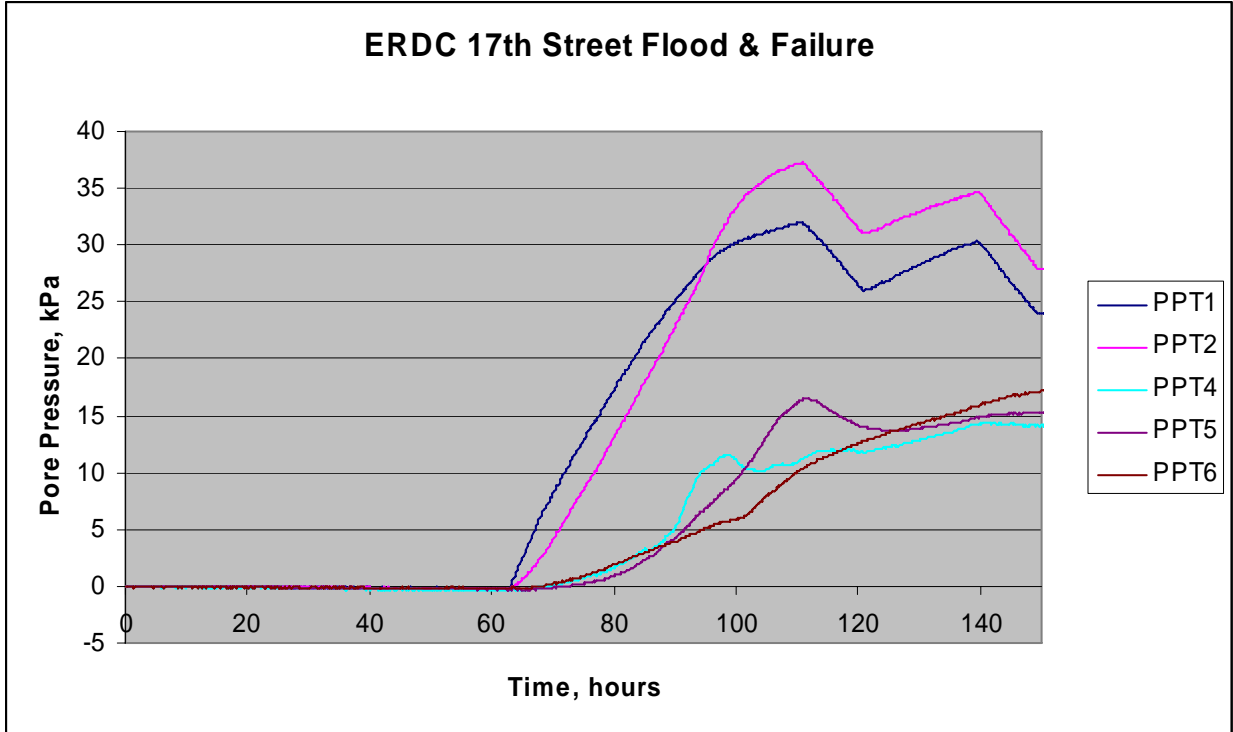
Figure 5.47. Data from mid-depth of foundation clay layer during flood loading
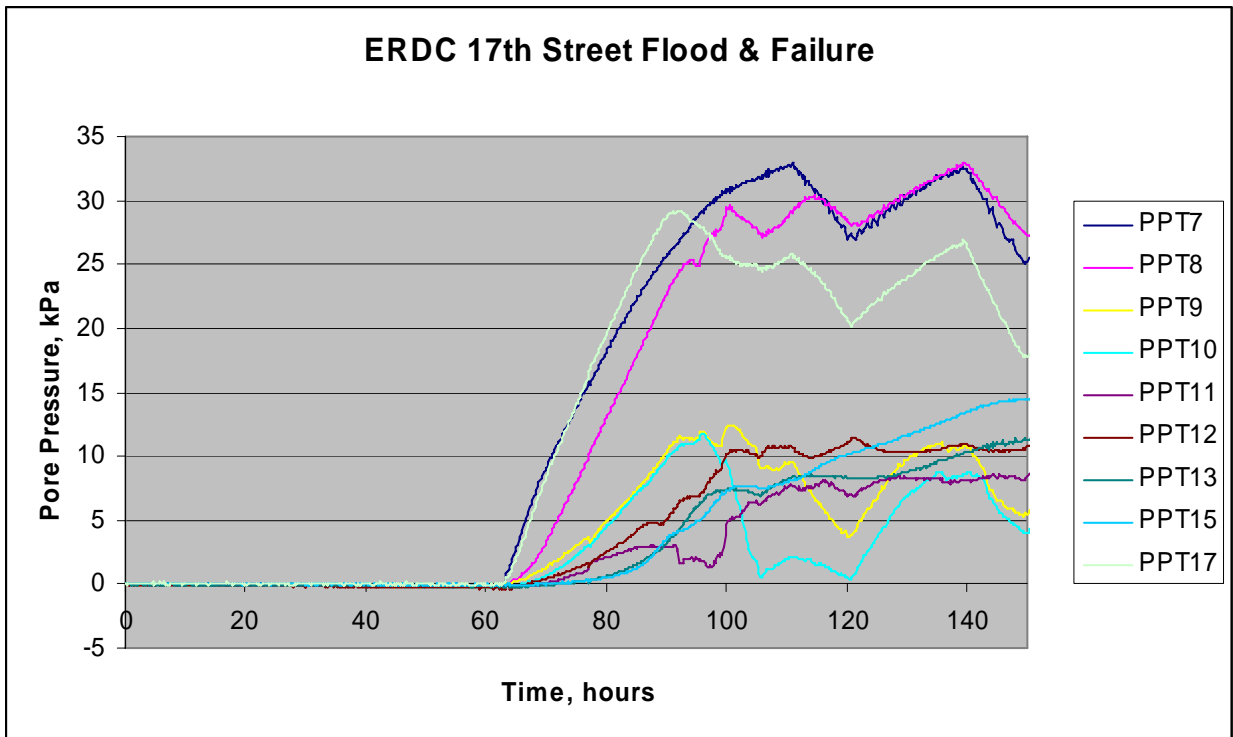
Figure 5.48. Data from top of foundation clay layer during flood loading

This is a preliminary report subject to revision; it does not contain final conclusions of the United States Army Corps of Engineers.
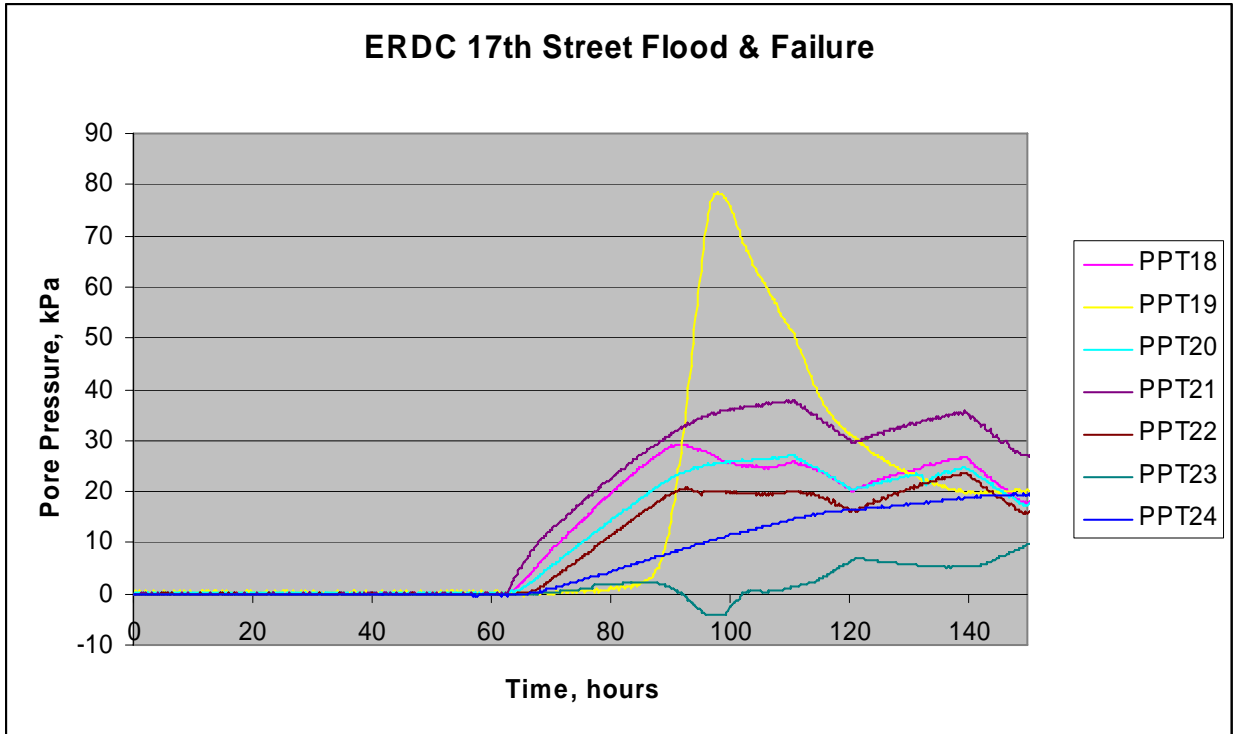
Figure 5.49. Data from levee and swampy/marsh during flood loading
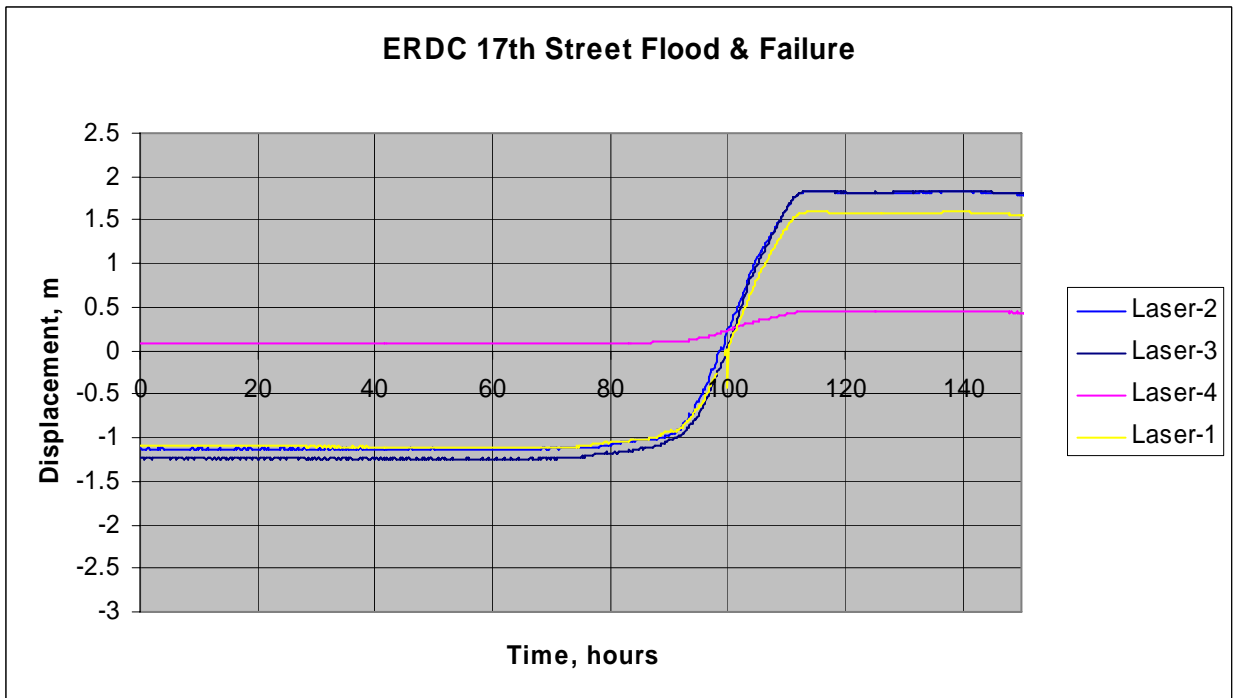
Figure 5.50. Displacement data from lasers during flood loading

RPI 17th Street Canal Model

A second model of the 17th Street canal breach was conducted at RPI. The model is shown in Figure 5.51. Material used in the model and construction sequence was exactly as described for the ERDC model above. Moisture content in the foundation clay layer averaged 61% with strength from the vane shear of 125 psf. For the levee the moisture content was average of 47% with vane shear strength of 355 psf. The swampy/marsh was consistent with the ERDC values since the material all came from the same area and was collected at the same time in the same manner.
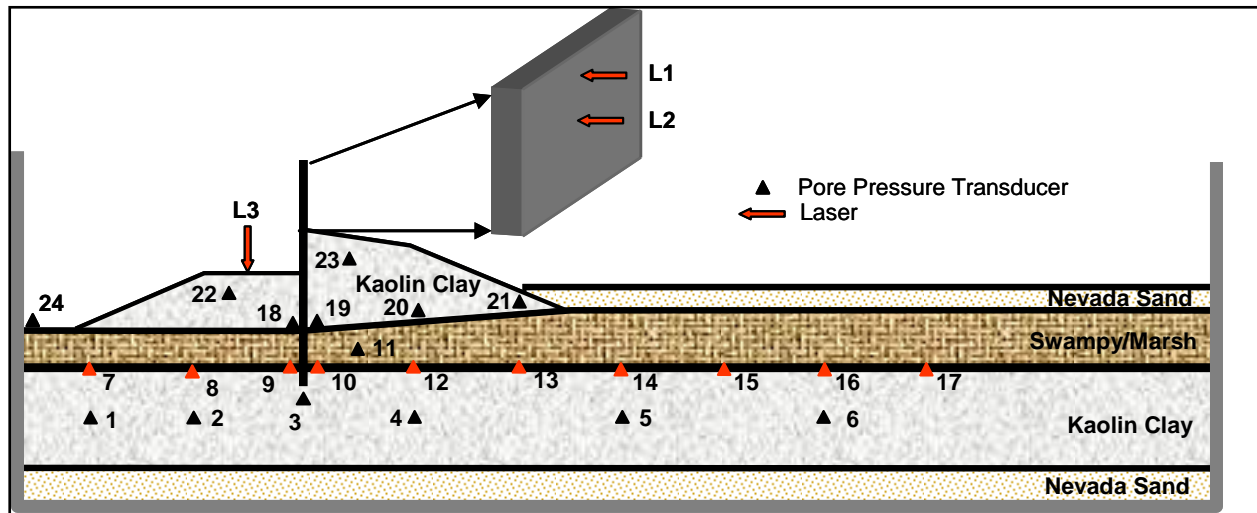
Figure 5.51. RPI 17th Street model

The following discussions and presentations focus on the flood and failure of the model. The model was spun to 50 g with water level held at a depth consistent with canal operating water level, instrumentation allowed to stabilize and ready for application of flood load. Results of the flood loading are presented in Figures 5.52 through 5.55. Figure 5.52 is a plot of the PPT data from series of transducers located in the foundation clay layer. The PPT shown in yellow on Figure 5.52 is attached to the bottom of the sheet pile wall in the clay layer. The sudden decrease and sharp increase in the reading is associated with development of the crack between the sheet pile wall and canal side levee.
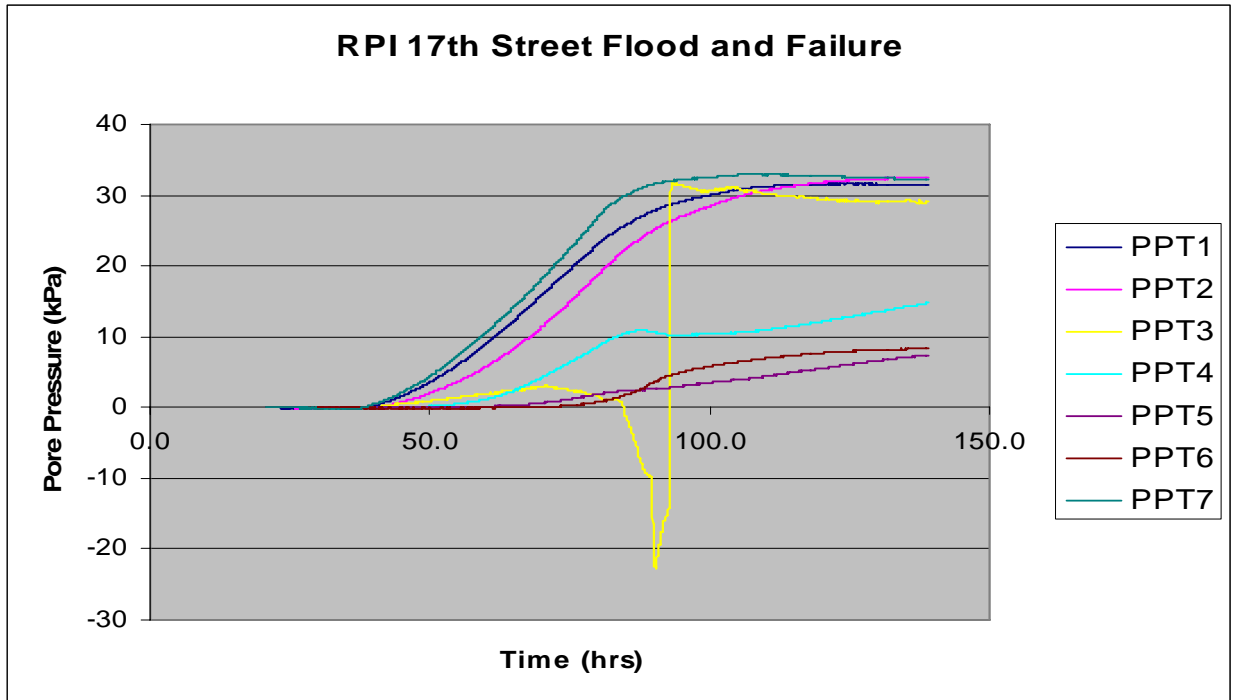
Figure 5.52. PPT data in foundation clay layer during flood and failure

Data from the PPT's located along the foundation clay swampy/marsh interface is shown in Figure 5.53. Notice that some of the PPT's show an initial rise in values followed by a drop in values then a sudden increase in values. These PPT's are located very near the sheet pile and are indicative of development of the crack. A second observation is the value of each PPT reading. The PPT values in Figure 5.53 from highest to lowest represent sensors located in the model moving from the canal side to the land side. So, the highest recorded values are in the material under the canal/land side with decreasing values under the land side levee and out into the free field. This is exactly as would be expected for this type of foundation material. Figure 5.54 is the recorded PPT data in the levee. Behavior is consistent with that previously discussed.

Figure 5.55 shows the recordings of the lasers on the sheet pile wall and top of the levee canal side. In the figure, the green and blue curves show movement of the wall with the two measurements on the same vertical plane of the wall but separated some distance apart. This arrangement allows determination of how the wall moved in terms of rotation, translation, etc. The data show that from start of movement until sometime thereafter, the wall movement was translational and at the very end became more rotational (the lines are diverging). This is an important point in confirming that the failure was translational. The red curve in the plot is the displacement of the canal side levee during the flood and failure.
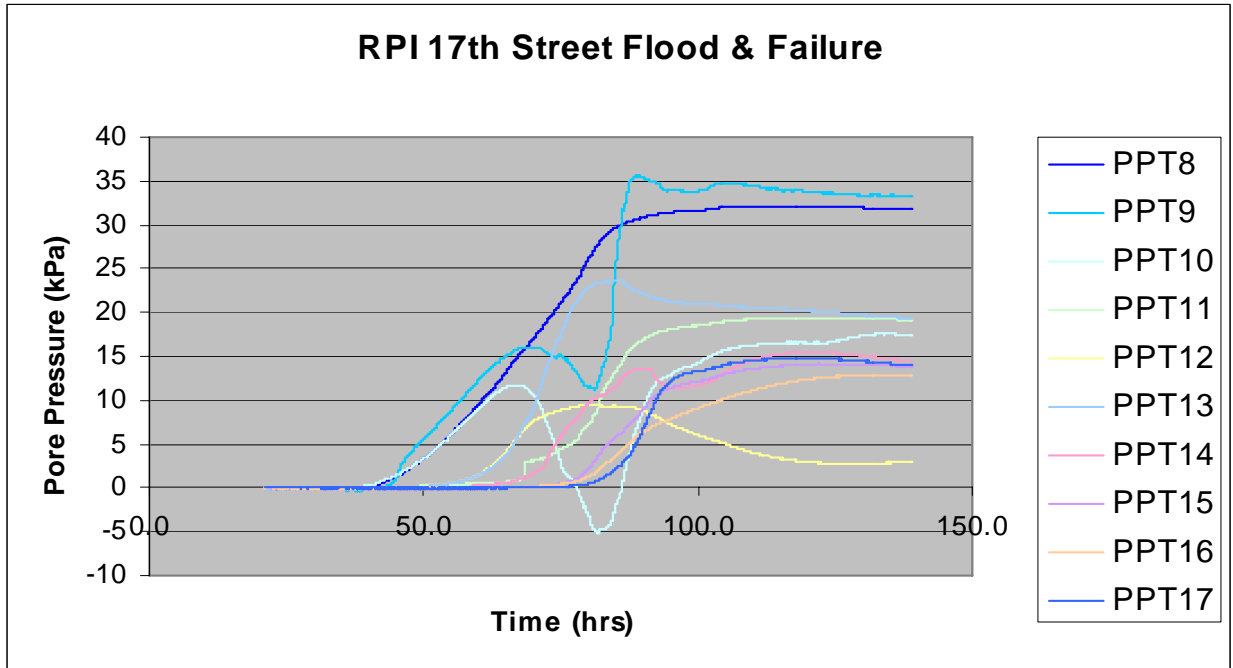
Figure 5.53. PPT data along the foundation clay swampy/marsh interface during flood and failure
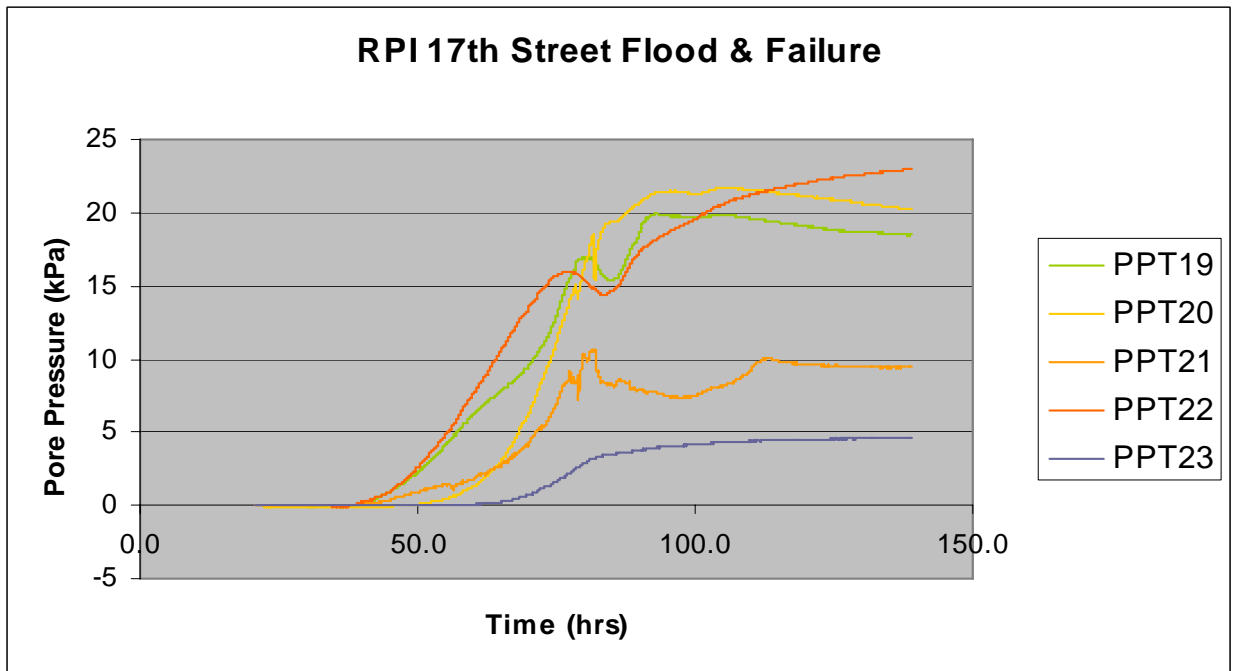
Figure 5.54. PPT data in the levee during flood and failure

This is a preliminary report subject to revision; it does not contain final conclusions of the United States Army Corps of Engineers.
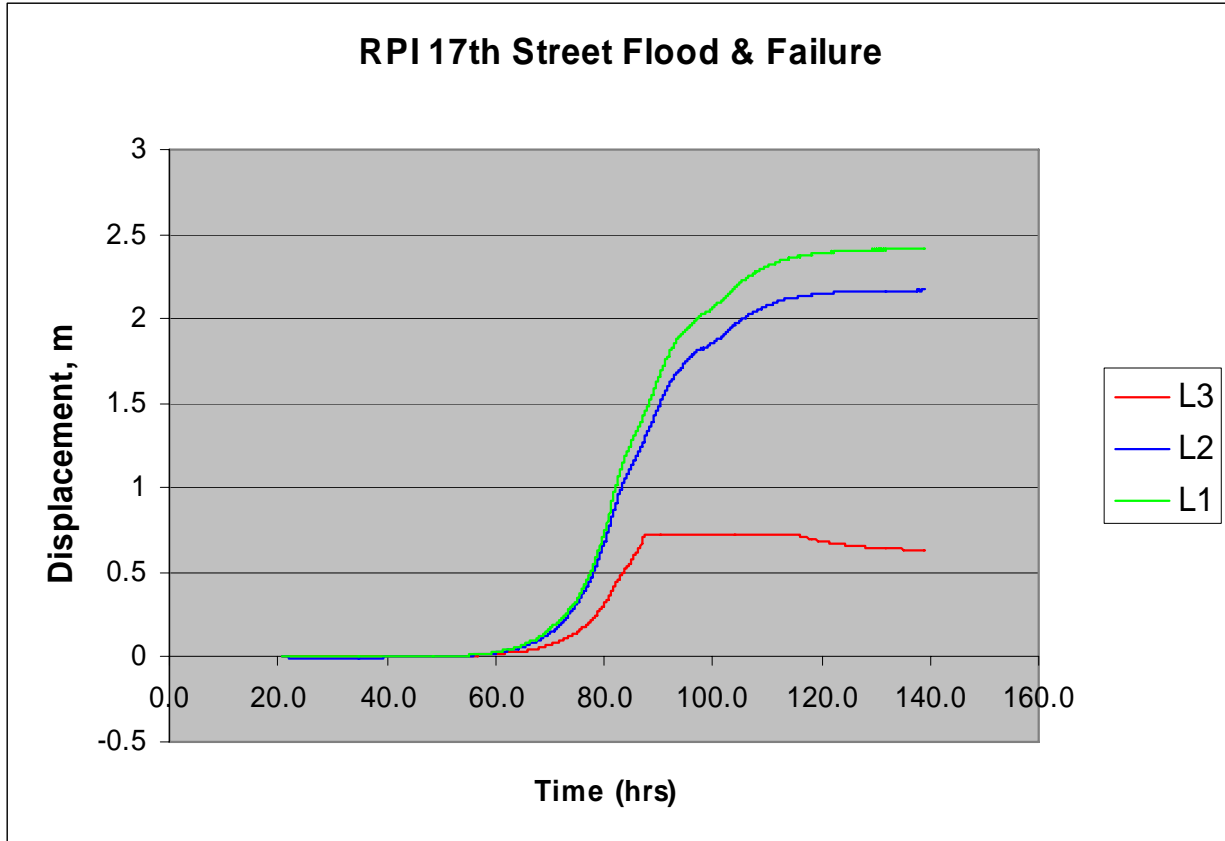
Figure 5.55. Displacement recordings of the sheet pile and canal side levee

The following series of pictures are still captures from the video recorded during flood and failure. Figure 5.56 is a shot captured with the water elevation at maximum level just prior to any wall movement. In the figures, the canal side is on the left and the protected side on the right. The sheet pile can be seen in the middle of the figure with the shorter canal levee on the left and the taller land side levee on the right.

Figure 5.56. RPI 17th street model during flood load

In Figure 5.57, the wall has moved toward the land side, a crack has formed between the sheet pile wall and canal levee. The crack has penetrated through the levee, through the swampy/marsh and into the top surface of the clay layer.

Figure 5.57. RPI 17th street model just after movement of wall and crack formation

Figure 5.58. RPI 17th street model in process of translational failure

Figure 5.58 shows the model at a time where the failure is well in progress. Attention should be given to the row of markers just below the swampy/marsh layer in the clay on the land side of the sheet pile. Notice that the entire row of markers has moved to the right while the row of markers below remains unmoved. Also notice that the wall has remained at a similar angle as in Figure 5.57. All of this information indicates that there is a horizontal failure plane in the clay and that the wall-land side levee-land side swampy/marsh is translating to the right. Figure 5.59 is a view near the end of failure. Notice the row of markers displaced well to the right and the non-rotated nature of the sheet pile wall. Again indications of translational failure along a horizontal failure plane in the foundation clay layer.

Figure 5.59. RPI 17th street model near end of flood failure

Discussion presented in the following section will highlight the agreement between the measured data in the foundation clay layer and basic soil mechanics predicted behavior. Focusing on the foundation clay layer material on the canal side before any failure, the following observations can be made.

Measured Δu on the upstream side before levee failure

$\Delta \sigma_1 = \Delta \sigma_w$ (weight of water) - levee weight near the toe

Assuming levee weight near the toe is small, then $\Delta \sigma_1 = \Delta \sigma_w$

$\Delta \sigma_3 = 0 \rightarrow$ | $\Delta \sigma_2$
$\varepsilon_2 = 0$
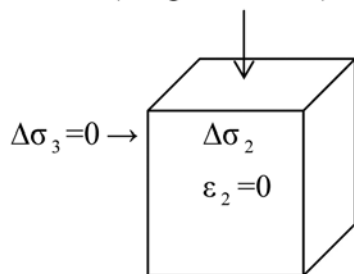
$$\varepsilon_2 = \frac{1}{E}[\Delta\sigma_2 - \mu(\Delta\sigma_1 + \Delta\sigma_3)]$$

$$0 = \frac{1}{E}[\Delta\sigma_2 - \mu\Delta\sigma_1]$$

$$0 = \Delta\sigma_2 - \mu\Delta\sigma_w \rightarrow \text{ for undrained condition. } \mu = 0.5$$

$$\Delta\sigma_2 = 0.5\,\Delta\sigma_w$$

$$\Delta u = A(\Delta\sigma_1 + \Delta\sigma_2 + \Delta\sigma_3) \quad A = \frac{1}{3}$$

$$\Delta u = \frac{1}{3}(\Delta\sigma_1 + \Delta\sigma_2)$$

$$\Delta u = \frac{1}{3}(\Delta\sigma_w + 0.5\,\Delta\sigma_w)$$

$$\Delta u = 0.5\,\Delta\sigma_w$$

As shown in Figure 5.60, in the early stages of water rise, with the canal level very low, the ratio between the increase in water pressure $\Delta\sigma_w$ (red line) and the increase in measured (blue and green lines) near the toe varies between 0.4-0.55 (comparing the slope of the lines). As the water rises higher, the rate of increase of water pressure Δu increases to match the rate of increase of total vertical stress, $\Delta\sigma_w$, indicating one dimensional loading in the clay layer at higher water levels.
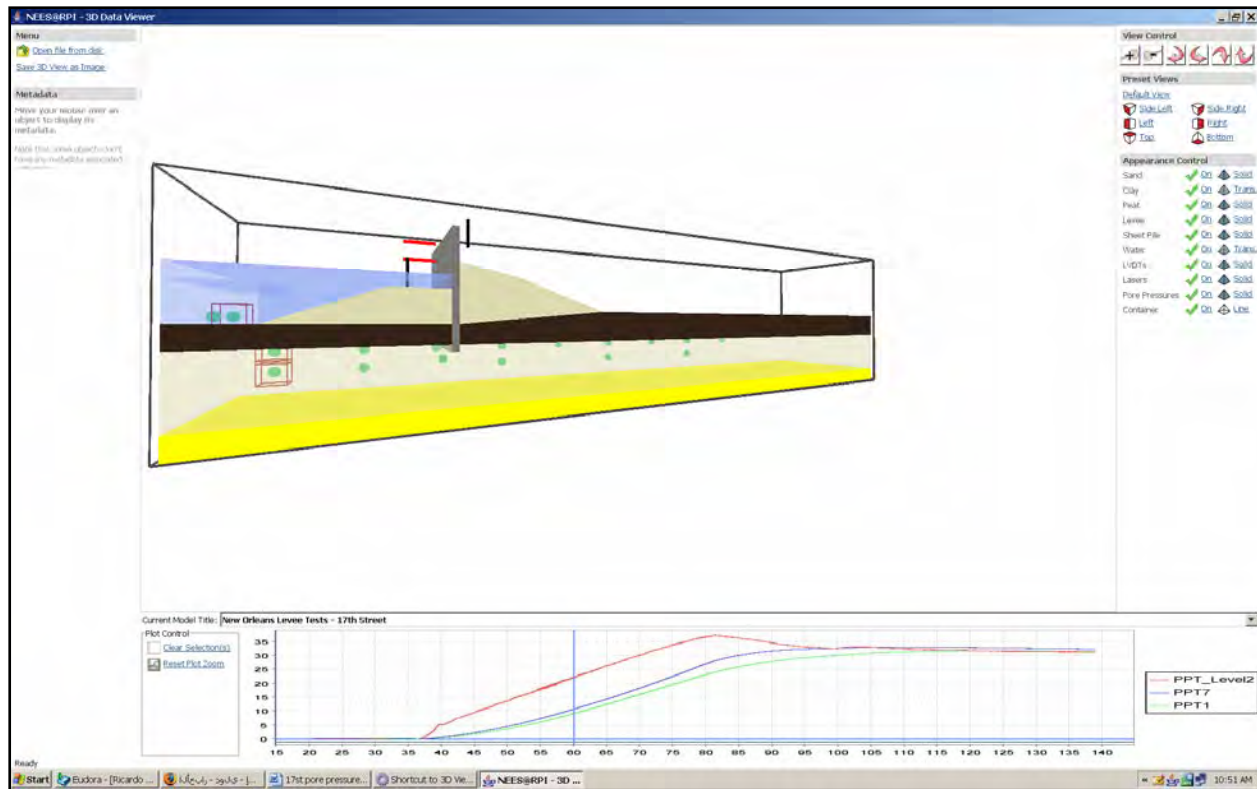
Figure 5.60. PPT data for transducers as indicated in the figure

Measured Δu on the downstream side due to levee failure

It is assumed that the soil outside the failure zone remains elastic (Figure 5.61). A soil element outside the failure zone will be subjected to an increase in the horizontal pressure while the vertical pressure remains constant. Thus $\Delta\sigma_1 = \Delta\sigma_h$ and $\Delta\sigma_3 = \Delta\sigma_v = 0$. For plain strain condition $\varepsilon_2 = 0$.
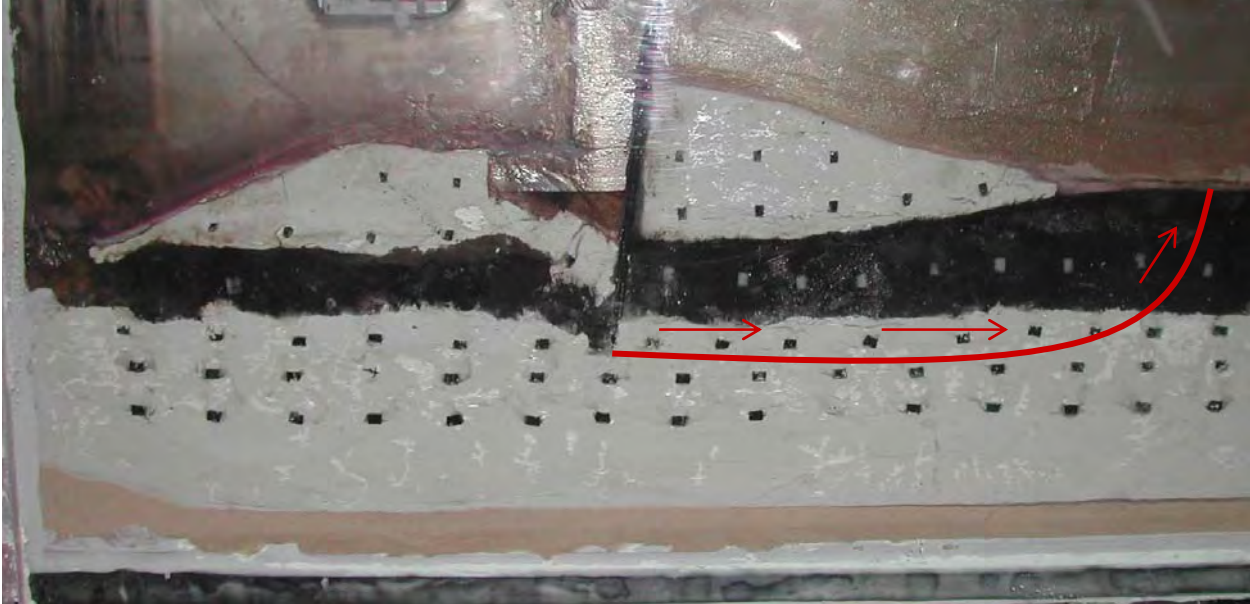
Figure 5.61. View of model after failure

$$\varepsilon_2 = \frac{1}{E} [\Delta\sigma_2 - \mu (\Delta\sigma_1 + \Delta\sigma_3)]$$

$$\Delta\sigma_2 - \mu (\Delta\sigma_1 + \Delta\sigma_3) = 0$$

$$\Delta\sigma_2 - \mu \Delta\sigma_1 = 0$$

$$\Delta\sigma_2 = \mu \Delta\sigma_1 \text{ for undrained condition. } \mu=0.5$$

$$\Delta\sigma_2 = 0.5 \Delta\sigma_1$$

$$\Delta\sigma_1 = \sum\gamma_t H (k_p\text{-}k_o) + 2 S_u$$

$$\Delta\sigma_1 = (12.5*2*0.5 + 17.5*0.75*0.5) + 2*5$$

$$\Delta\sigma_1 = 29 \text{ kpa}$$

$$\Delta\sigma_2 = 0.5 \Delta\sigma_1 = 0.5 (29) = 14.5 \text{ kpa}$$
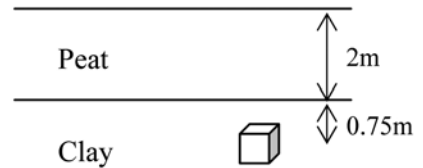
$$\Delta u = \ A\ (\Delta\sigma_1 + \Delta\sigma_2 + \Delta\sigma_3)\quad A = \frac{1}{3}$$

$$\Delta u = \ \frac{1}{3}\ (\Delta\sigma_1 + \Delta\sigma_2)$$

$$\Delta u = \ \frac{1}{3}\ (29 + 14.5) = 14.5\ \text{kpa}$$

As shown in Figure 5.62 the pore pressure measured by the three pore pressure sensors just outside of the failure zone recorded about 14kpa. It is important to note that the measured Δu indicate that it started to increase at the same time the levee started to fail.
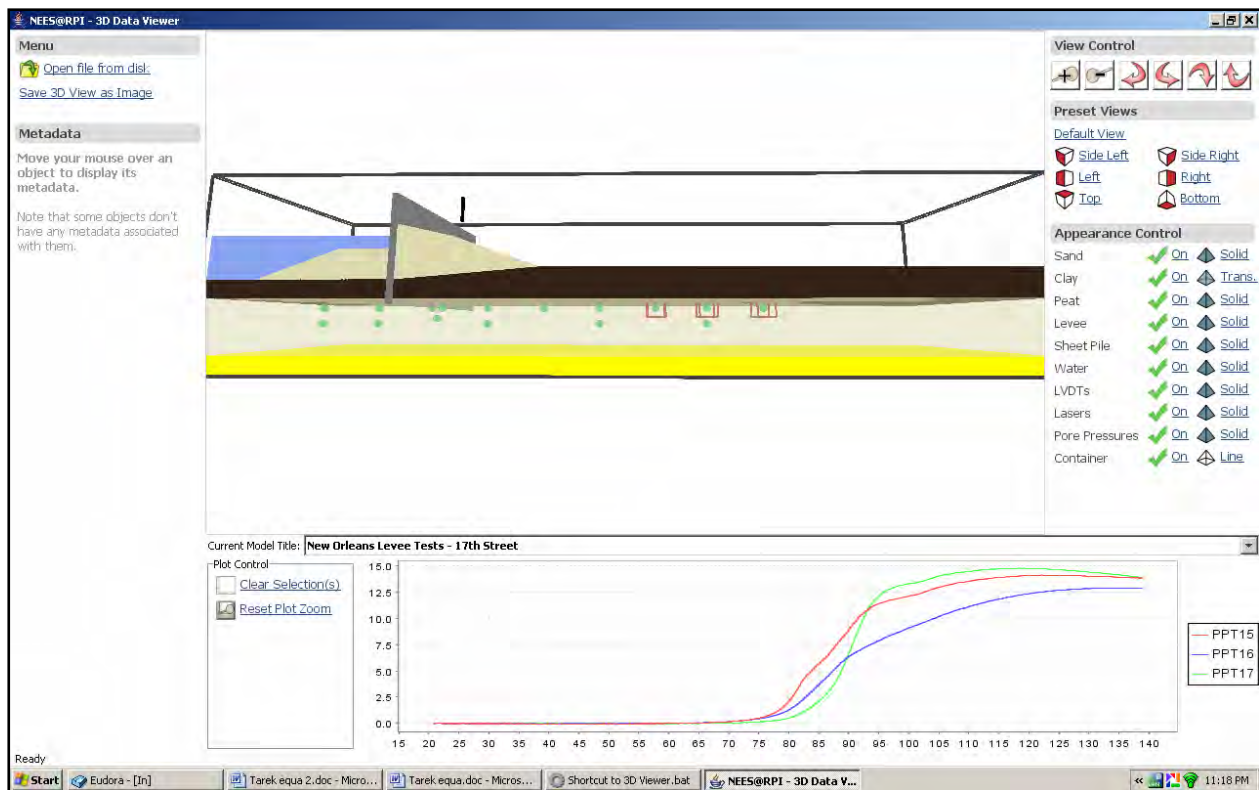
Figure 5.62. PPT data for the transducers as indicated in the figure

All of the information presented and discussed for the RPI 17th street model enforces the following observations about the model behavior.

1. At a certain time during rise in canal water elevation, the wall moved slightly to the land side and allowed the start of a crack forming.
2. This crack propagated down through the canal side levee, the swampy/marsh layer, and the top portion of the foundation clay layer to the end of the sheet pile.

3. This allowed full hydrostatic pressures to reach the underlying foundation material.
4. A horizontal failure surface forms in the foundation clay layer and the entire land side levee material translates along this surface to the land side.
5. This movement continues as the water load remains constant leading to total failure of the levee.

Physical Models of London Avenue Canal, South Breach

Two models of a section at the south breach location of London Avenue canal were completed. One of the models was performed at RPI and the other at ERDC. This section of the report will present information relevant to each model.

ERDC London Avenue Canal, South Breach Model

The model representative of a section through the south breach at London Avenue canal is shown in Figure 5.63.
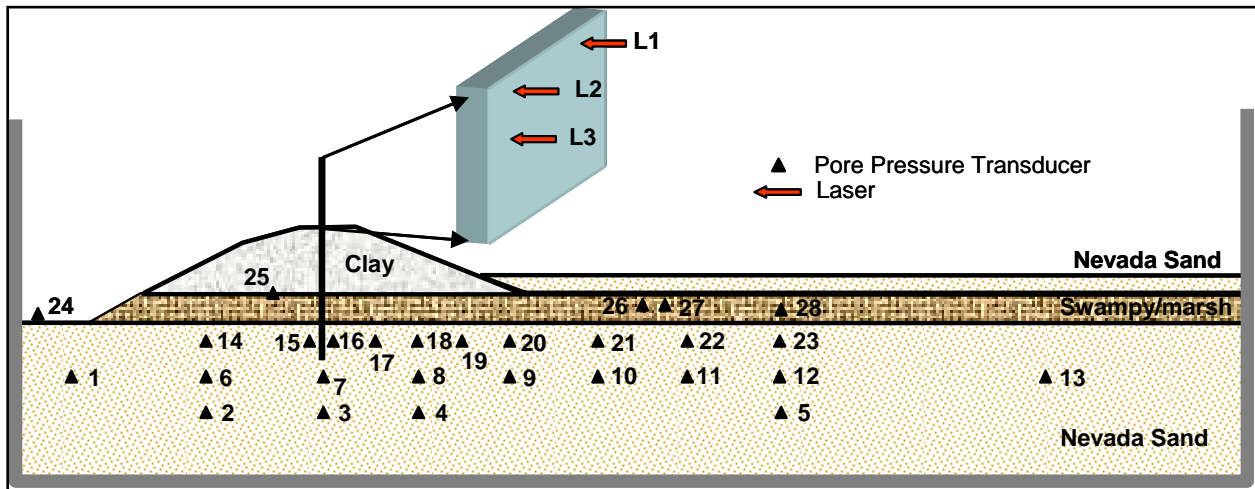
Figure 5.63. Physical model of ERDC London Avenue canal, south breach area

The sequence of model construction and testing were as previously discussed for other models. Prior to placement of the swampy/marsh material both penetrometer and moisture contents were obtained. Average values for the penetration testing were 400 psf and the moisture contents 357%. Penetration measurements of the levee material after consolidation averaged 360 psf and moisture contents averaged 61%. A view of the model with saturated sand layer and swampy/marsh layer in place is shown in Figure 5.64.

Figure 5.64. View of the ERDC model with sand and swampy/marsh layer

Figure 5.65. Completed ERDC London Avenue south model

The completed model is shown in Figure 5.65. The canal side is on the left of the model in the figure and the protected land side is on the right. The canal side and land side levees were nearly identical in height. The sheet pile wall extends 2.5 m above the top of the levee.

Once the model is completed and all instrumentation connected and zeroed, the package is slowly spun up to 50 g. Water is maintained in the canal at a depth of approximately 1 m until 50 g is reached. At 50 g, the model is properly scaled such that it has the correct weight, and pressure at all points in the model as would be the case in the field. The water level in the canal is increased to what it would be during normal canal operation level. In this case the normal canal level prior to hurricane Katrina was approximately 30 cm above the canal levee top elevation. The model is allowed to stabilize (pore pressures equalize) at 50 g with the correct canal water elevation prior to addition of flood load.

Figure 5.66 is a sequence of still shots taken from the video recording detailing the flood and failure event. The failure event is as highlighted following.

1. Water level increases to a point on the wall where initial movement of the wall begins to occur. This movement starts out as a rotation of the wall.

2. A crack begins to form between the sheet wall and canal side levee and propagates downward.
3. The crack extends all the way through the levee and the swampy/marsh layer to the top of the sand layer.
4. Full hydrostatic pressure is allowed to reach the foundation sand layer causing a sudden increase in pore water pressure.
5. This increase in pore water pressure reduces the vertical effective stress of the overlying swampy/marsh and levee material. Effectively the land side material approaches zero effective stress and begins to 'float'.
6. Load from the flood pushes the wall over in a rotational manner with no resisting force form the land side material.

This failure mechanism will be shown through the recorded data to be presented and discussed following. Post test measurements of the swampy/marsh and levee material were taken and produced these results. Moisture contents in the swampy/marsh on the canal side were 301% and on the land side 217%. For the clay levee, canal side moisture contents were 64% and land side 61%.
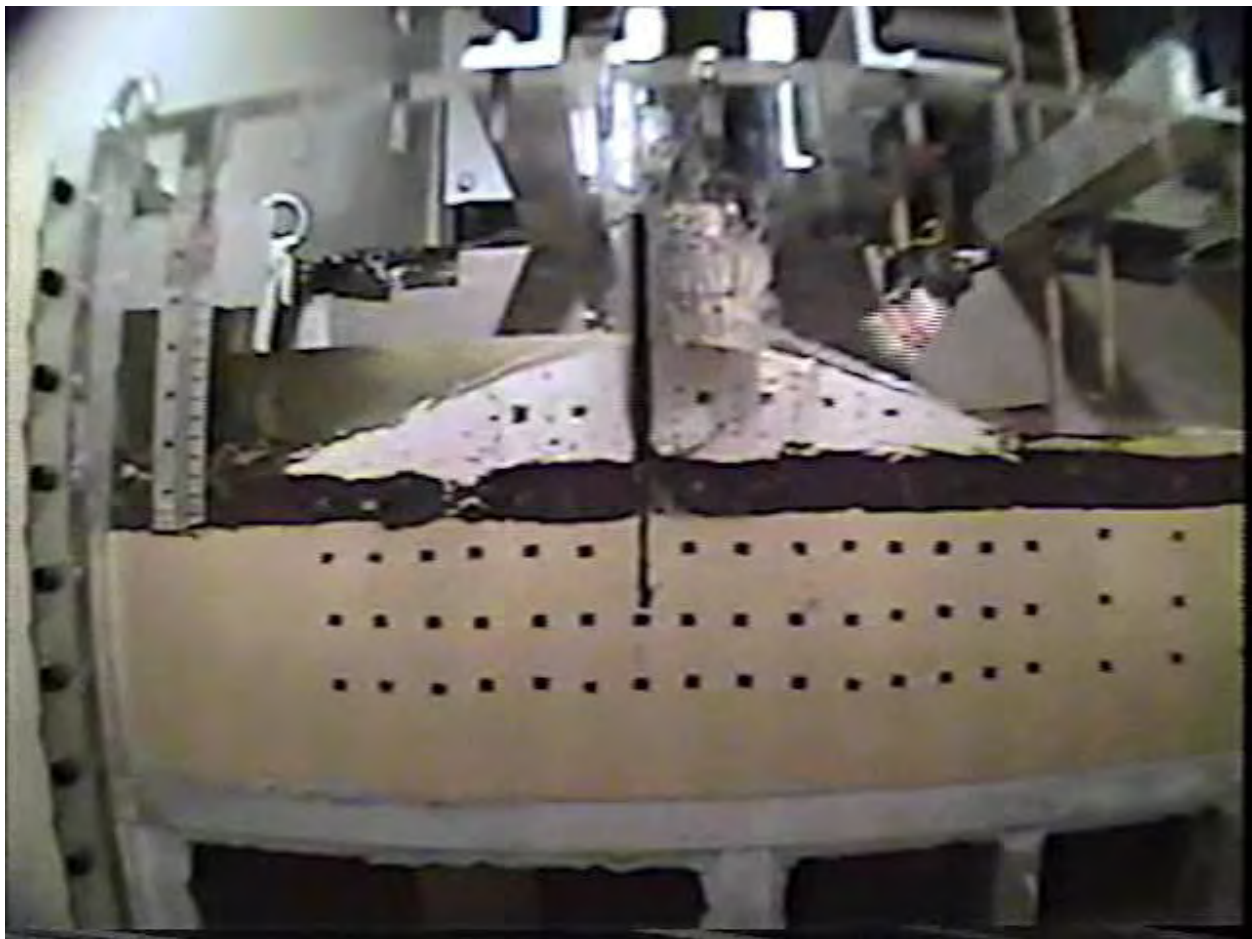
Figure 5.66a. ERDC London Avenue south model at normal canal water level

Figure 5.66b. ERDC London Avenue south model at flood level just prior to any wall movement
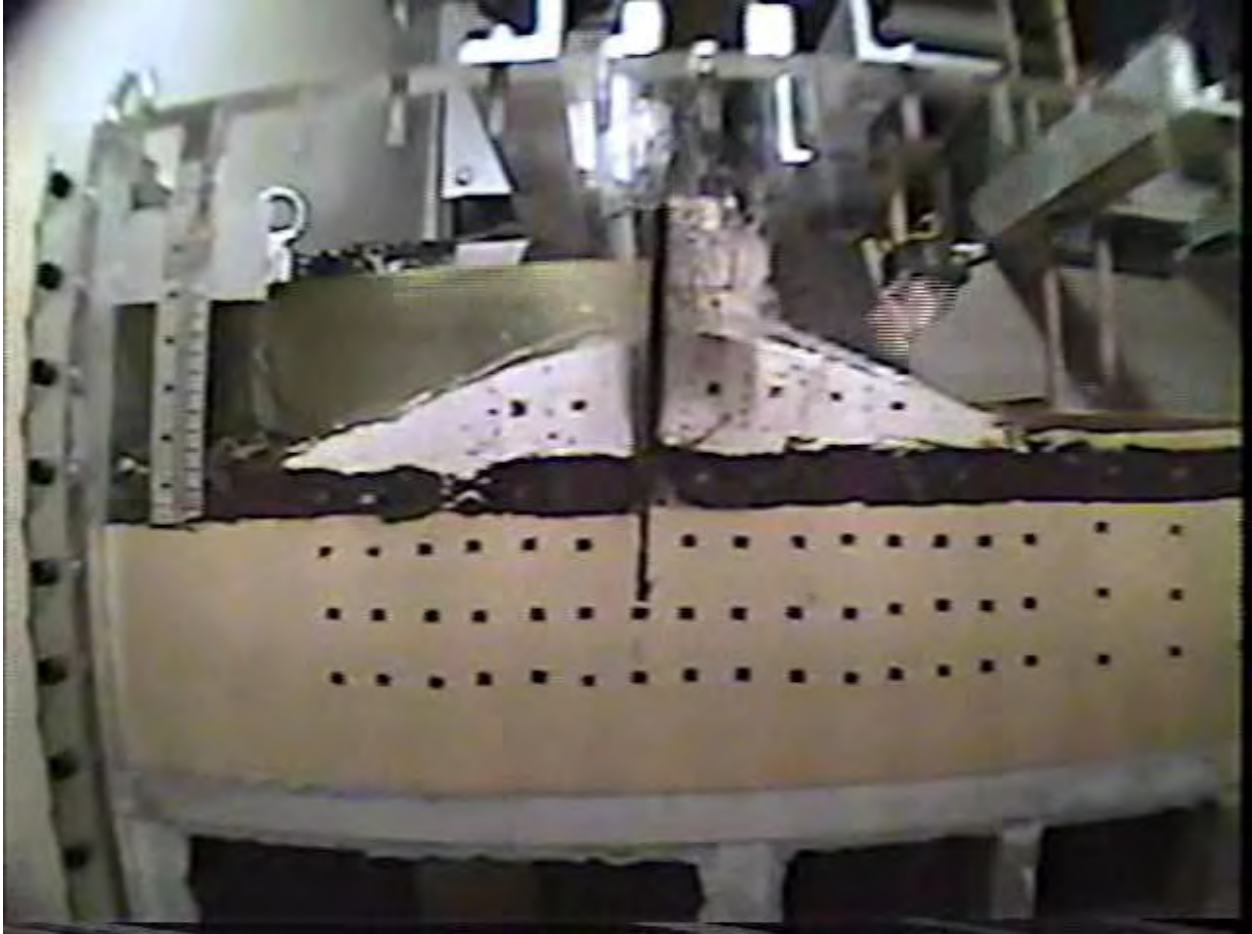
Figure 5.66c. ERDC London Avenue south model after wall movement and crack formation
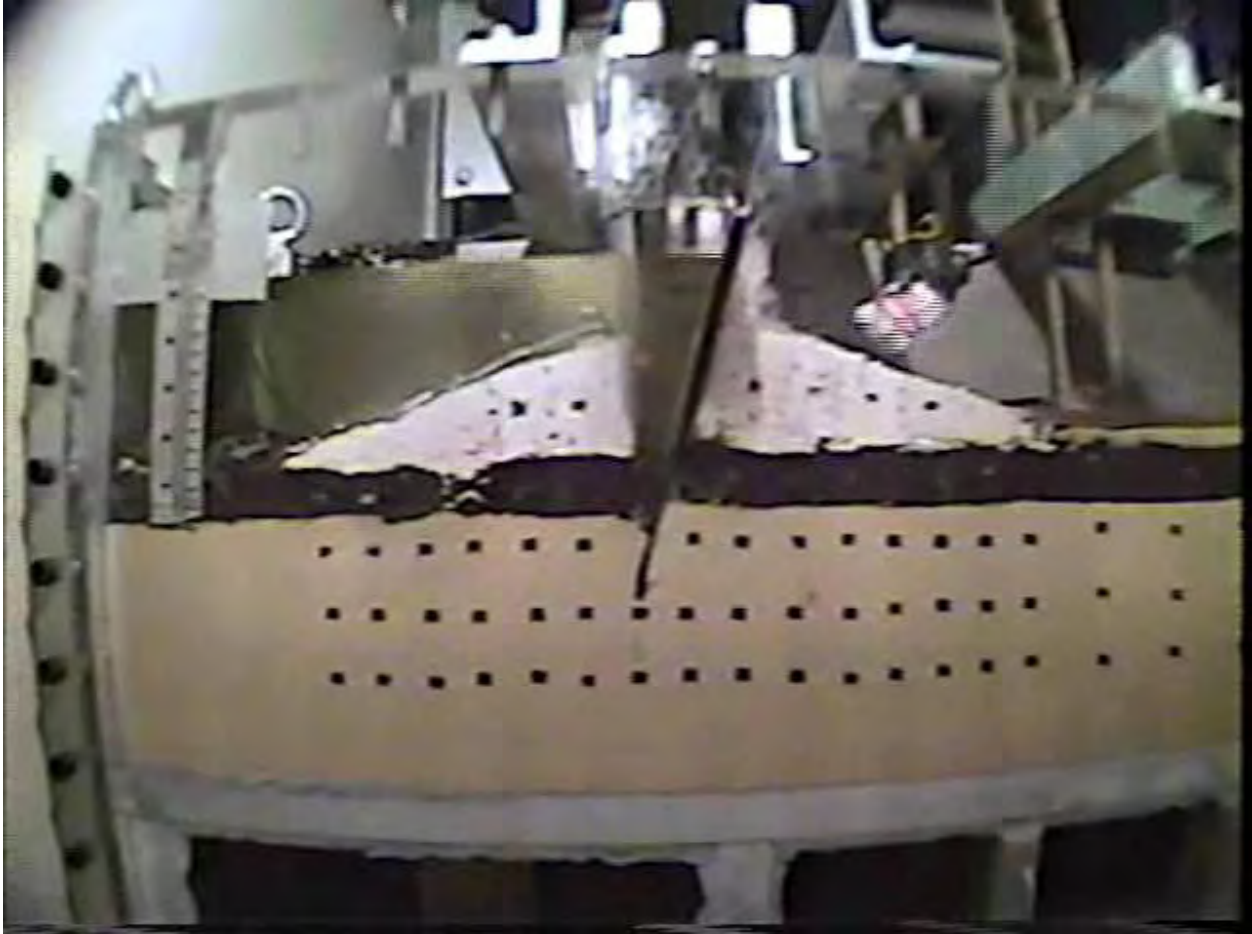
Figure 5.66d. ERDC London Avenue south model well into failure model

Figure 5.66e. ERDC London Avenue south model at end of test

The data recorded during the flood loading are presented in the following figures. The model is at 50 g, water level in the canal is at normal operating levels, and the flood load is steadily applied. Figure 5.67 presents the results of the PPT's at depth in the sand layer. Figure 5.68 is a plot of PPT data from the top of the sand layer with behavior as shown in Figure 5.67. Notice the change in character of the data indicated by a very short plateau, this is the onset of crack formation and the wall really rotating. This is most evident in PPT's 15 and 16 which are located very close to the wall.
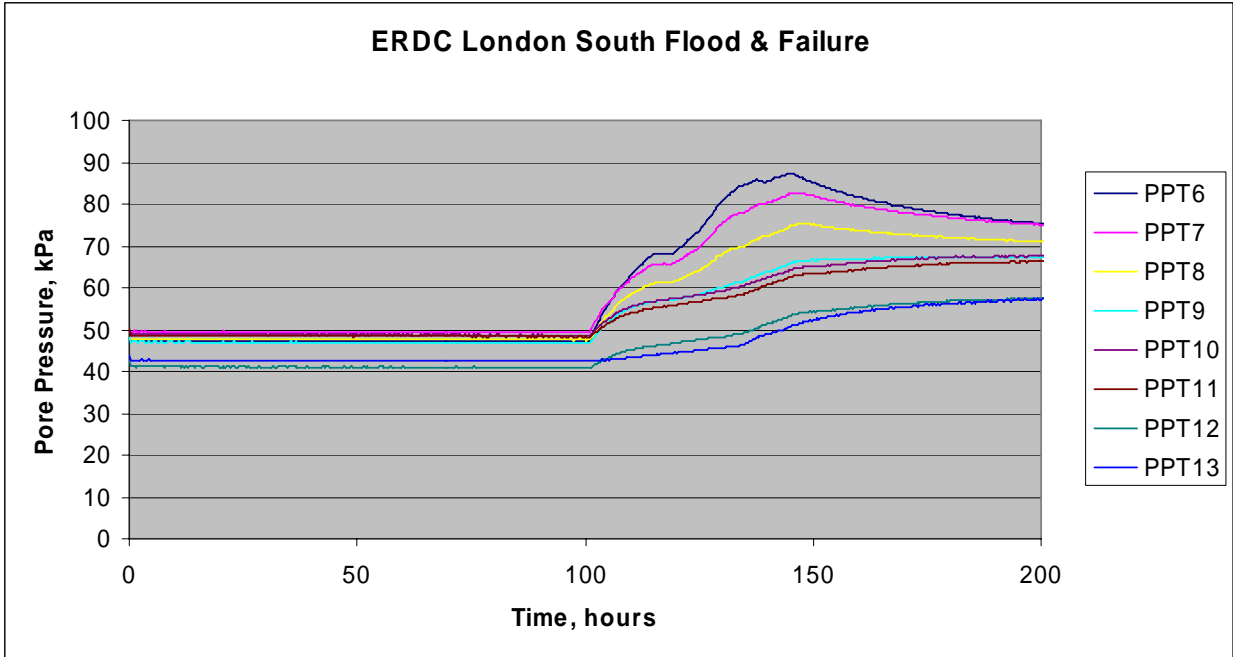
Figure 5.67. PPT data at depth in the sand layer during flood load
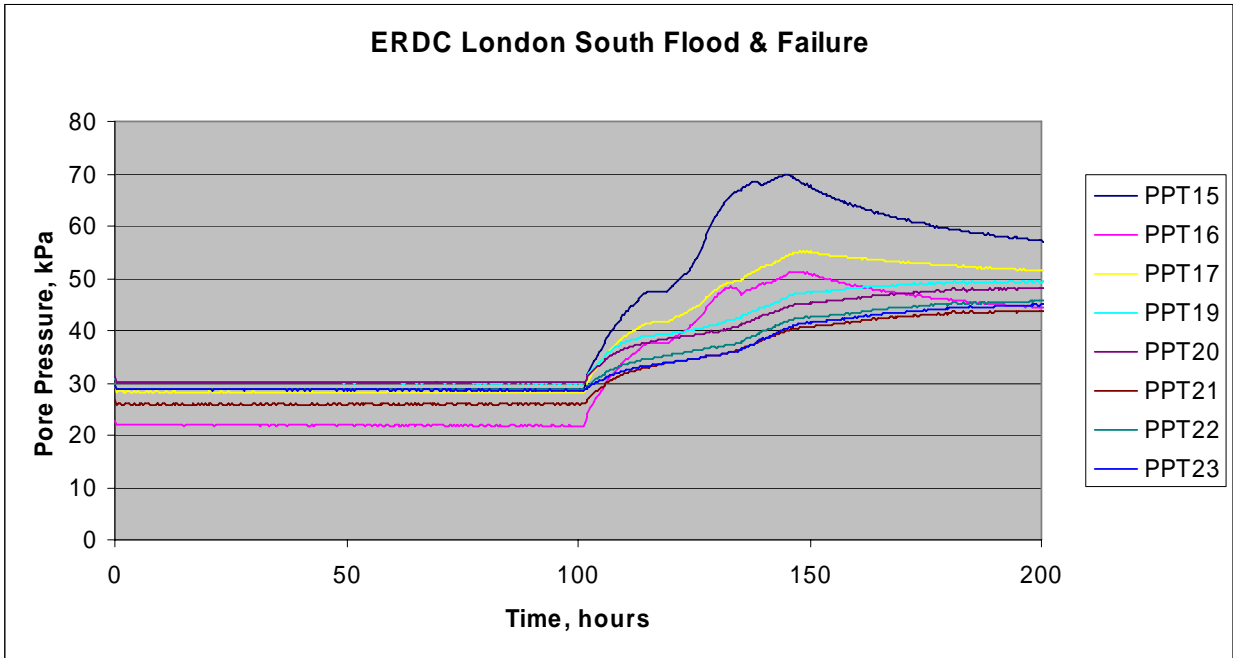
Figure 5.68. PPT data near the top of the sand layer during flood load

Data from the PPT's located in the levee and swampy/marsh is shown in Figure 5.69. Instrument 24 is located in the canal and tracks the increase in pore pressure associated with increase of water depth in the canal. As can be seen in data from the previous plot, there is a slight delay in reaction of the PPT data in the soil and that in the canal. Figure 5.70 shows the

displacement of the wall during the flood load. Notice that laser one and two are perfectly in sync. These are at the same elevation on the wall and reveal that wall movement remains constant along the plane of the wall (there is no twisting from front side to back side of the model). Secondly, notice that all lasers are moving together until later in time where laser three begins to change slope. This is an indication that the movement is becoming much more rotational in nature as the failure proceeds.
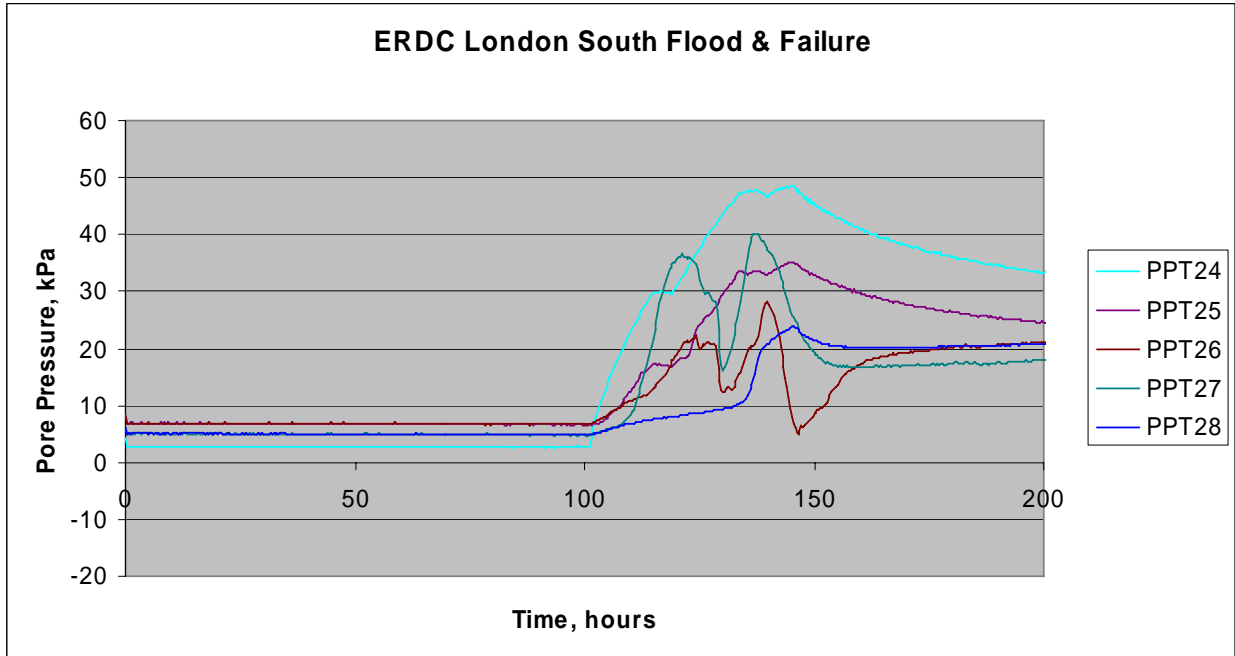
Figure 5.69. PPT data in the levee and swampy/marsh layer during flood load
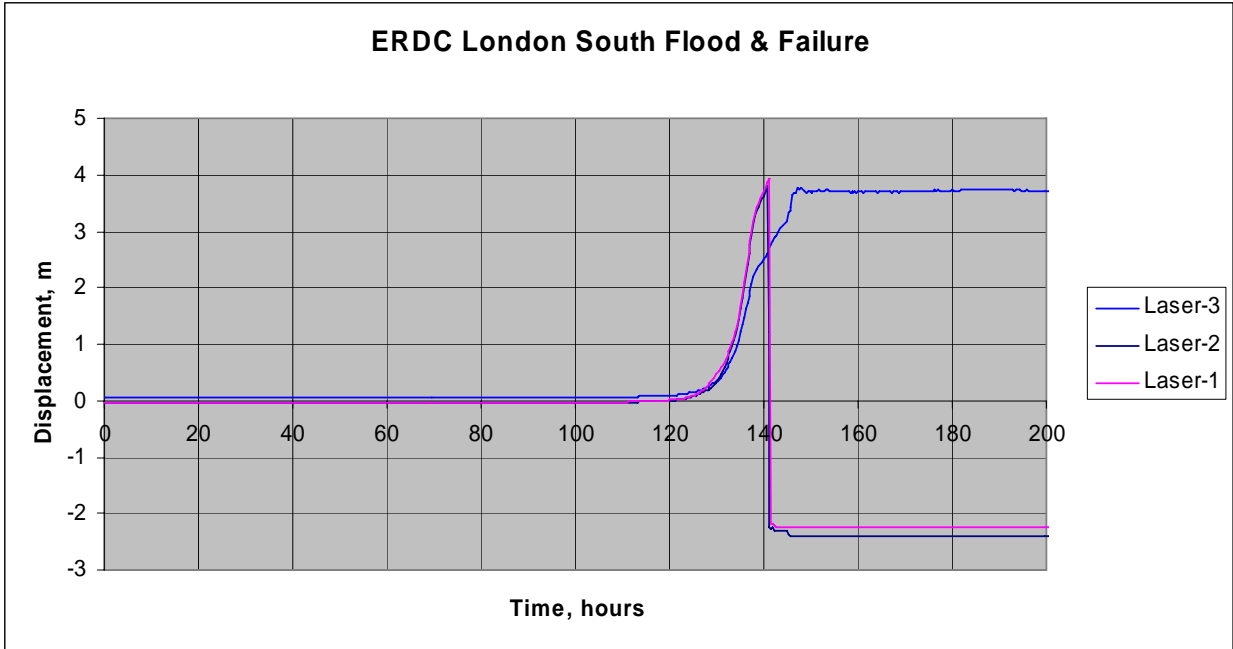
Figure 5.70. Displacement of the wall during flood load

RPI London Avenue Canal, South Breach Model

The second model representative of a section through the south breach at London Avenue canal tested at RPI is shown in Figure 5.71. The model has the same dimensions and makeup as described for the ERDC model.
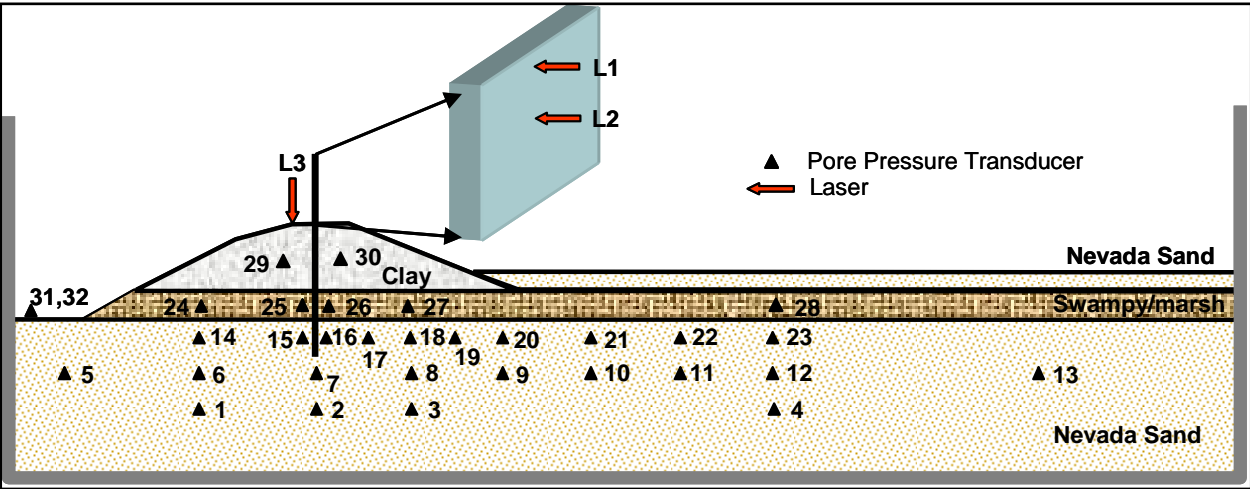
Figure 5.71. RPI London Avenue canal, south breach area model

The sequence of model construction and testing were as previously described for the ERDC model and will be briefly highlighted following. Measurements of water content in the clay

material after consolidation prior to forming the levee averaged 43% and vane shear measurements averaged 525 psf.

The model was slowly spun up to 50 g to prevent any sudden increase in pore pressure. Water elevation was maintained in the canal until reaching 50 g. At this point the water level was brought to normal canal elevation and the instruments allowed to equalize. Once this was accomplished the flood load could be applied. Data recorded during the flood and failure event will be presented in Figures 57.2 through 5.75. Figure 5.72 is a plot of PPT data recorded in the sand layer at approximated mid-depth.
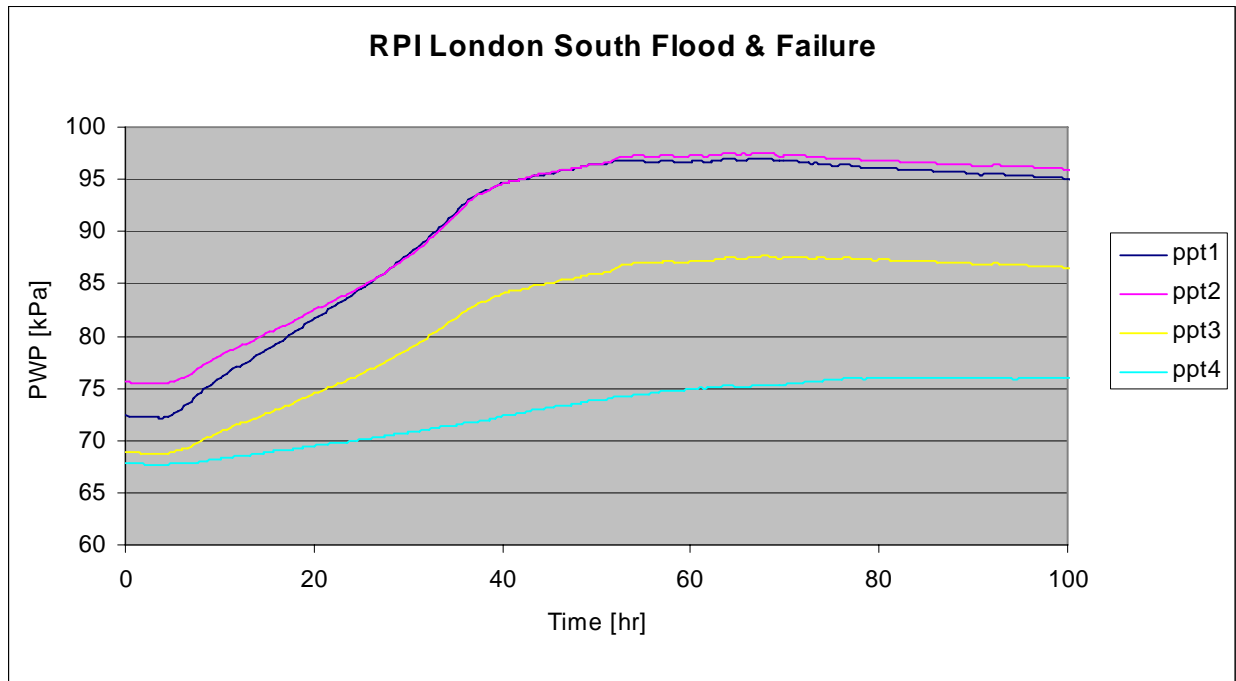
Figure 5.72. PPT data in the sand layer, mid-depth during flood.

It is seen in the data of Figure 5.72 that water pressure is highest closer to the canal (source of water) and reduces through the sand layer moving away from the canal. This is indicative of the transient flow situation that was created in the model by allowing water to move through the sand layer from the canal under the levee and then be collected and disposed of on the land side at the far end of the levee. Figure 5.73 shows data for the PPT's located in the sand layer at a higher elevation. PPT's 5, 6, and 7 are responding to more hydrostatic pressure than are any of the other instruments. This is also a consequence of the fact that after the crack forms, this material now has two sources for water, the canal and the crack.
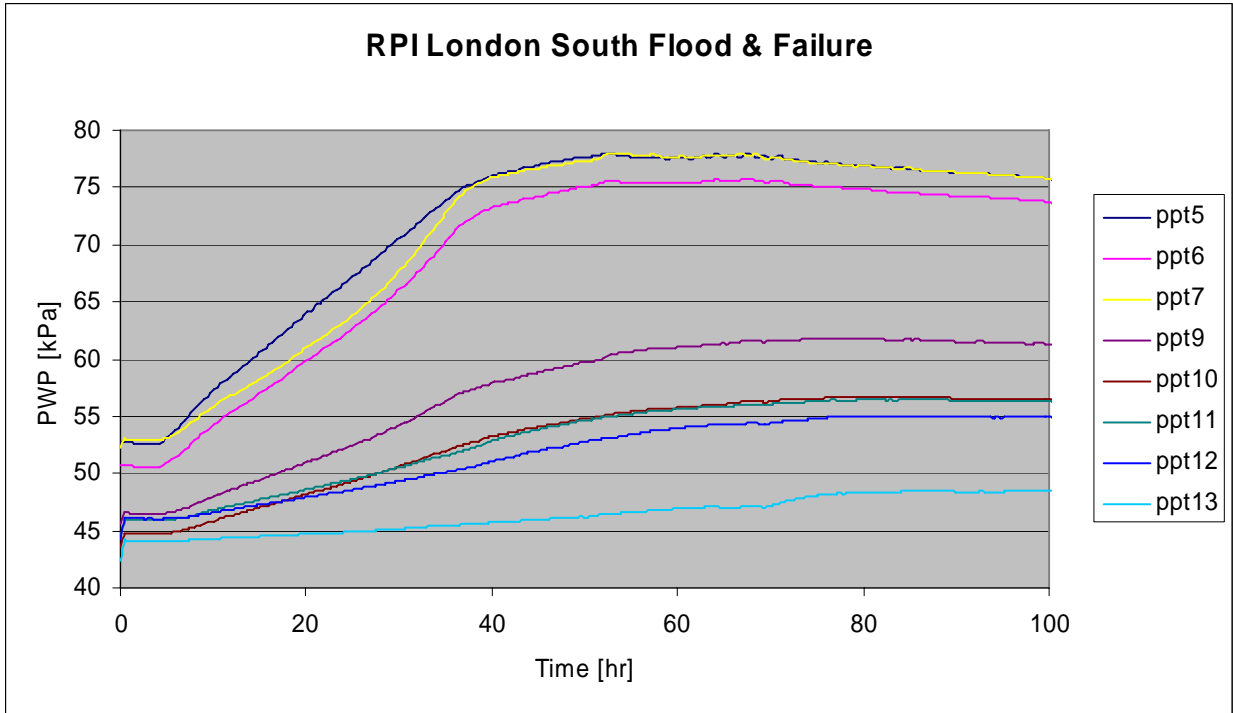
Figure 5.73. PPT data at higher elevation in the sand layer during flood

Figure 5.74 is a plot of the PPT data in the sand layer just at the interface of the sand layer and the swampy/marsh layer. Notice that PPT 15 has nearly reached full hydrostatic pressure as the crack has formed all the way to this elevation. This is true for PPT 7 in Figure 5.73 also. Figure 5.75 is a plot of the PPT data in the levee and swampy/marsh layer during the flood event. Measurement of displacement data of the sheet pile wall is presented in Figure 5.76.
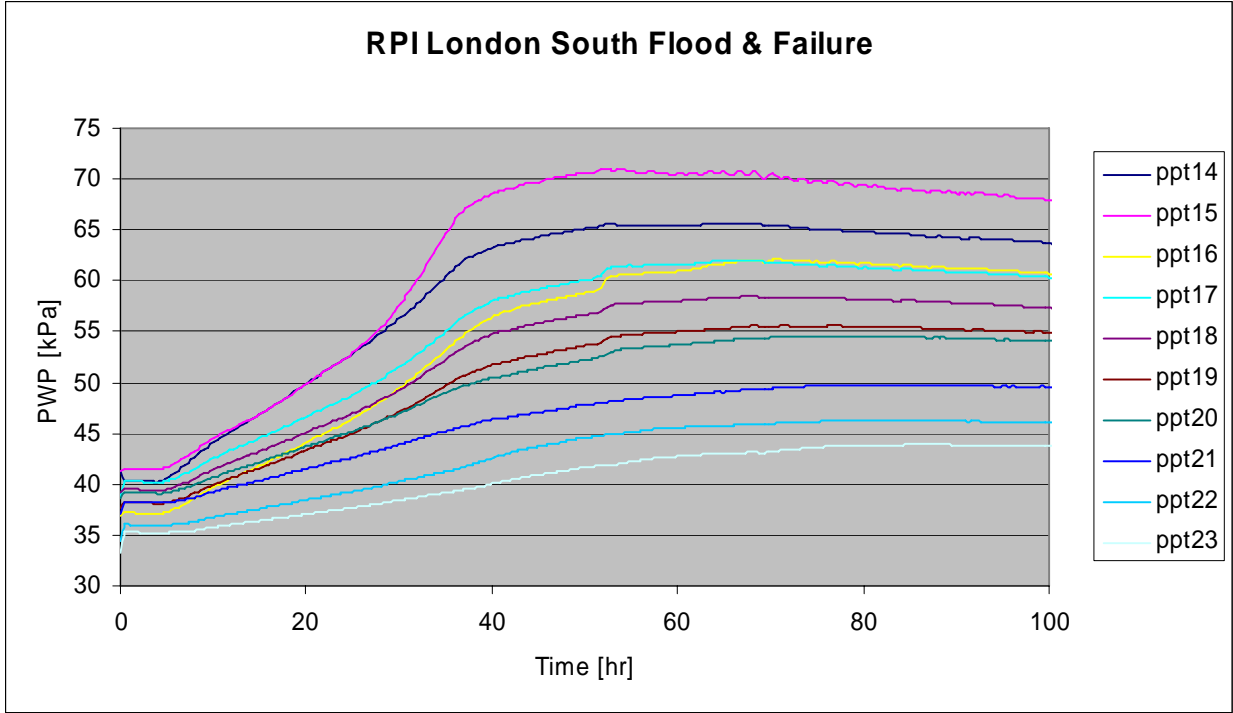
Figure 5.74. PPT data at the interface of the sand layer and the swampy/marsh layer during flood
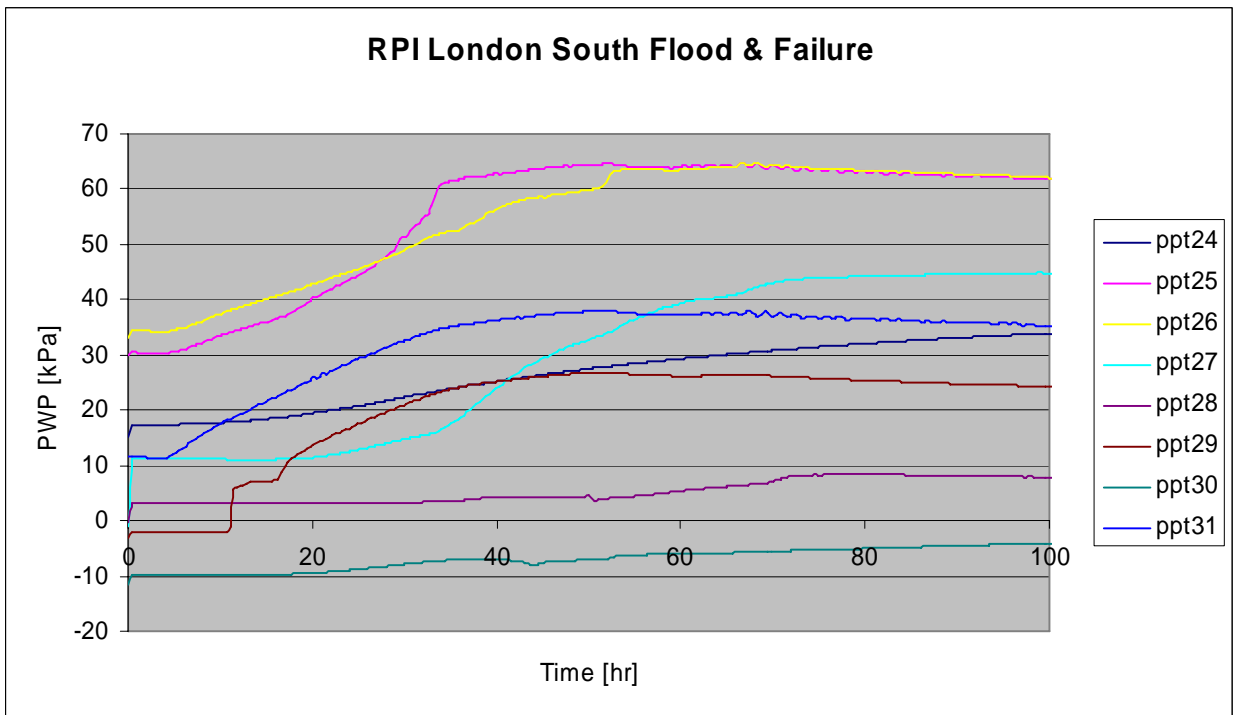
Figure 5.75. PPT data in the levee and swampy/marsh layer during flood
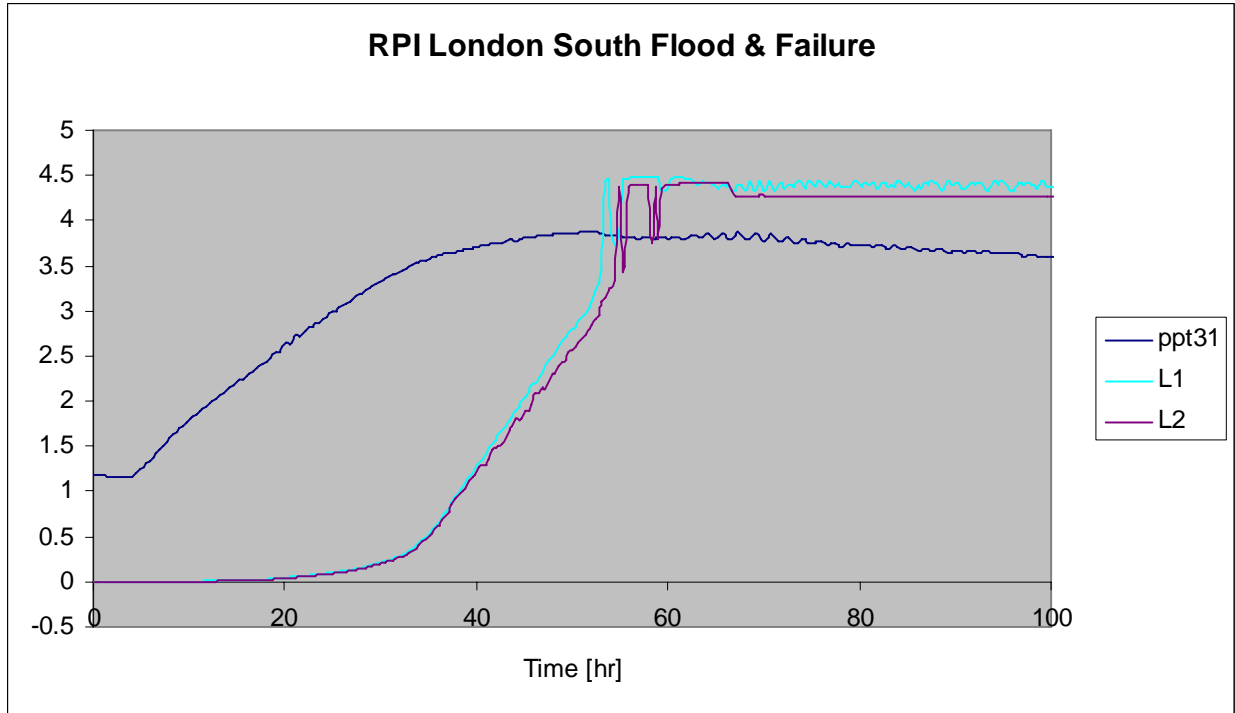
Figure 5.76. Displacement of the sheet pile wall during flood load

The increase in water level is shown to occur at time five hours and steadily increase to a depth of around 4 m (y-axis is water depth, m and displacement, m). The movement of the wall begins at around time ten hours with a small initial movement that is associated with the crack. At time 30 hours, the wall movement is seen to greatly increase, which is associated with failure of the wall. The two readings are parallel for most of the recorded time indicating that the wall is failing in a rotational manner. The following sequence of images shown in Figure 5.77 are stills taken from the video recording during the flood event. In the sequence the entire flood and failure event is shown.

Figure 5.77a. RPI London south model at normal canal water elevation
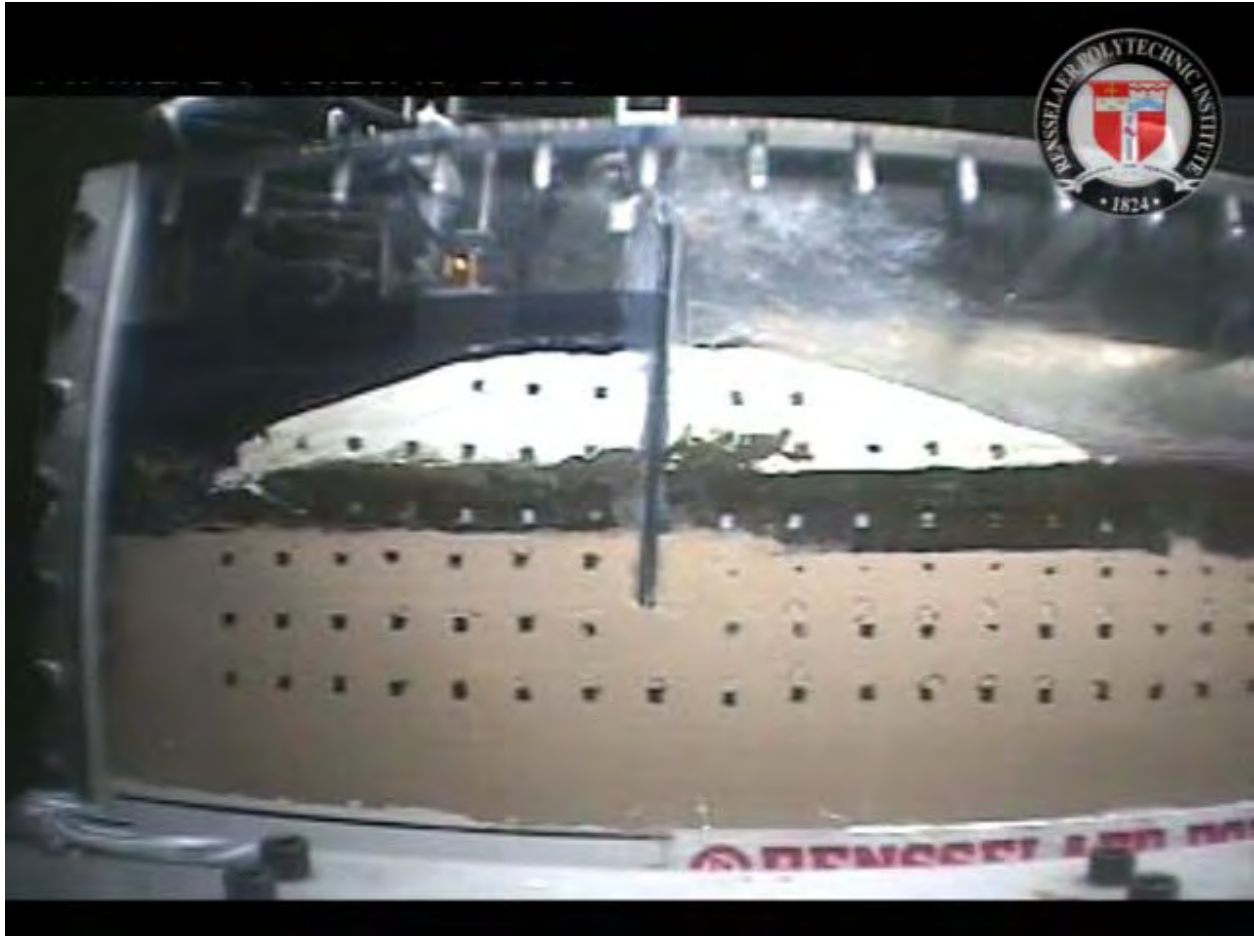
Figure 5.77b. RPI London south model flood level prior to any wall movement
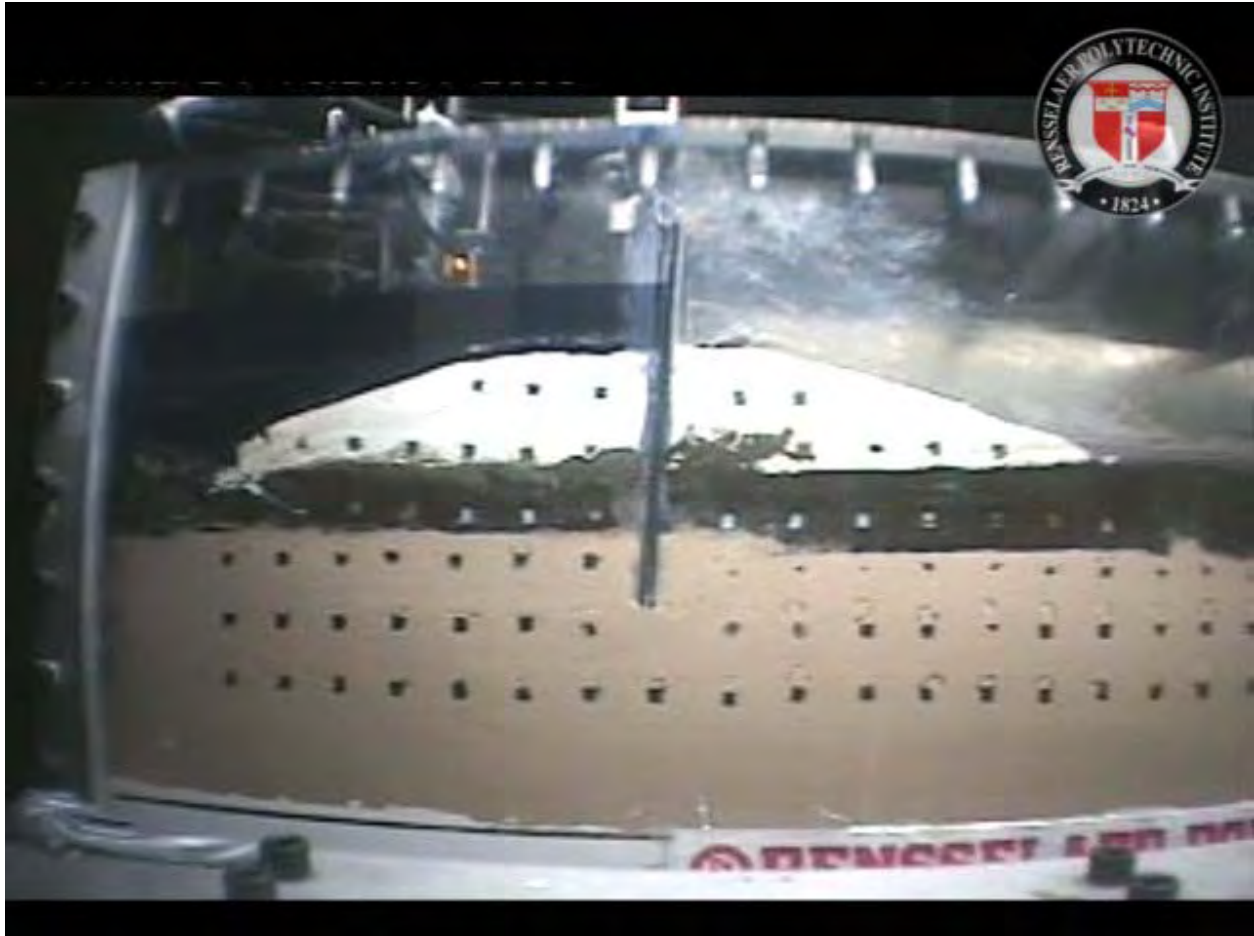
Figure 5.77c. RPI London south model just after wall movement and crack formation

Figure 5.77d. RPI London south model in process of failure

Figure 5.77e. RPI London south model in failure showing rotation of wall

Figure 5.77f. RPI London south model during failure, note how the swampy/marsh layer is moving as evidenced by the white markers

Figure 5.77g. RPI London south model at end of failure

A synopsis of the failure event that occurred in the RPI London south model is as highlighted following. This is exactly the same failure event as was observed in the ERDC London south model and confirms the event.

1. Water level increases to a point on the wall where initial movement of the wall begins to occur. This movement starts out as a rotation of the wall.
2. A crack begins to form between the sheet wall and canal side levee and propagates downward.
3. The crack extends all the way through the levee and the swampy/marsh layer to the top of the sand layer.
4. Full hydrostatic pressure is allowed to reach the foundation sand layer causing a sudden increase in pore water pressure.
5. This increase in pore water pressure reduces the vertical effective stress of the overlying swampy/marsh and levee material. Effectively the land side material approaches zero effective stress and begins to 'float'.
6. Load from the flood pushes the wall over in a rotational manner with no resisting force fr0m the land side material.

Physical Models of London Avenue Canal, North Breach

Two models of a section at the north breach location of London Avenue canal were completed. One of the models was performed at RPI and the other at ERDC. This section of the report will present information relevant to each model.

ERDC London Avenue Canal, North Breach Model

The model representative of a section through the north breach at London Avenue canal is shown in Figure 5.78. The main difference between the London south model previously discussed and the north model to be discussed following is the levee geometry and depth of sheet pile embedment in the sand layer, also the density of the sand deposit. In London south the sheet pile is into the sand seven feet while in London north it extends into the sand four feet. Density of the sand at the London south area was 75% while at London north 60%.
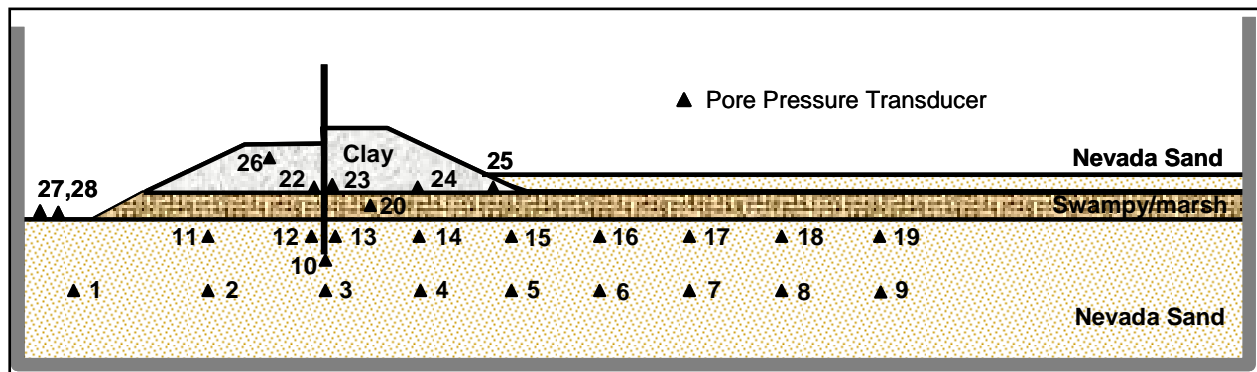
Figure 5.78. ERDC London north breach area model

Prior to placement of the swampy/marsh layer into the model vane shear measurements were made and averaged 275 psf. A view of the swampy/marsh layer and vane shear testing is shown in Figure 5.79. A view of placement of the swampy/marsh layer into the model is shown in Figure 5.80. Great care is taken to insure that the material remains intact during placement and that there is a good tight seal along the edges where the material contacts the container.

Figure 5.79. Swampy/marsh layer and taking vane shear measurements

Figure 5.80. View of placement of swampy/marsh layer

A view of the completed model ready for testing is shown in Figure 5.81. The model was slowly spun up to 50 g. As mentioned in the previous models, this slow spin up prevents any pre-failure associated with sudden increase in pore pressure but it also serves to allow the clay levee

to further consolidate and mold itself against the container side walls and the aluminum plate. Evidence of the effectiveness of this lies in the fact that no water was seen to move between the levee and container side walls nor between the aluminum plate and side walls. All movement of water was confined to the foundation material. Once the model had reached 50 g, water was raised to the level of normal canal operating elevation (just over the canal side levee crest) and time was given to allow the model and instrumentation to stabilize. When all recordings from PPT's indicated that the pore pressures were stable (not increasing or decreasing) then the actual flood event was initiated. The results of the recorded data will be presented and discussed in the next section. Typically the water was maintained on the wall until full movement had concluded.
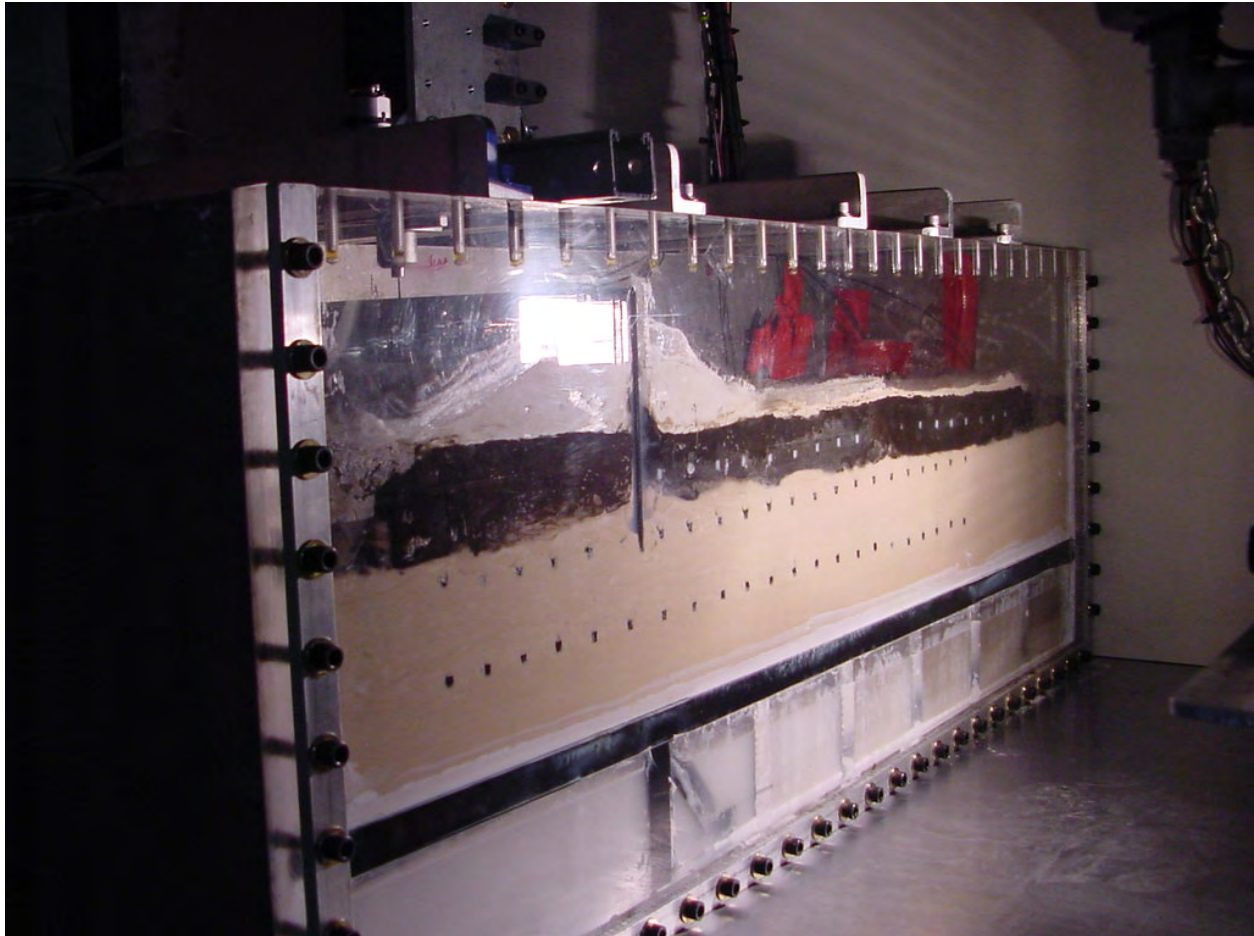
Figure 5.81. View of completed model prior to testing

This section will present the data recorded during the flood and failure event. As mentioned previously the displacement transducers on the wall failed to operate, therefore only PPT data will be shown. That data is given in Figures 5.82 through 5.84. Figure 5.82 is the PPT data in the sand layer about mid-depth. The small short plateau is associated with wall movement forming a crack that leads to eventual failure.
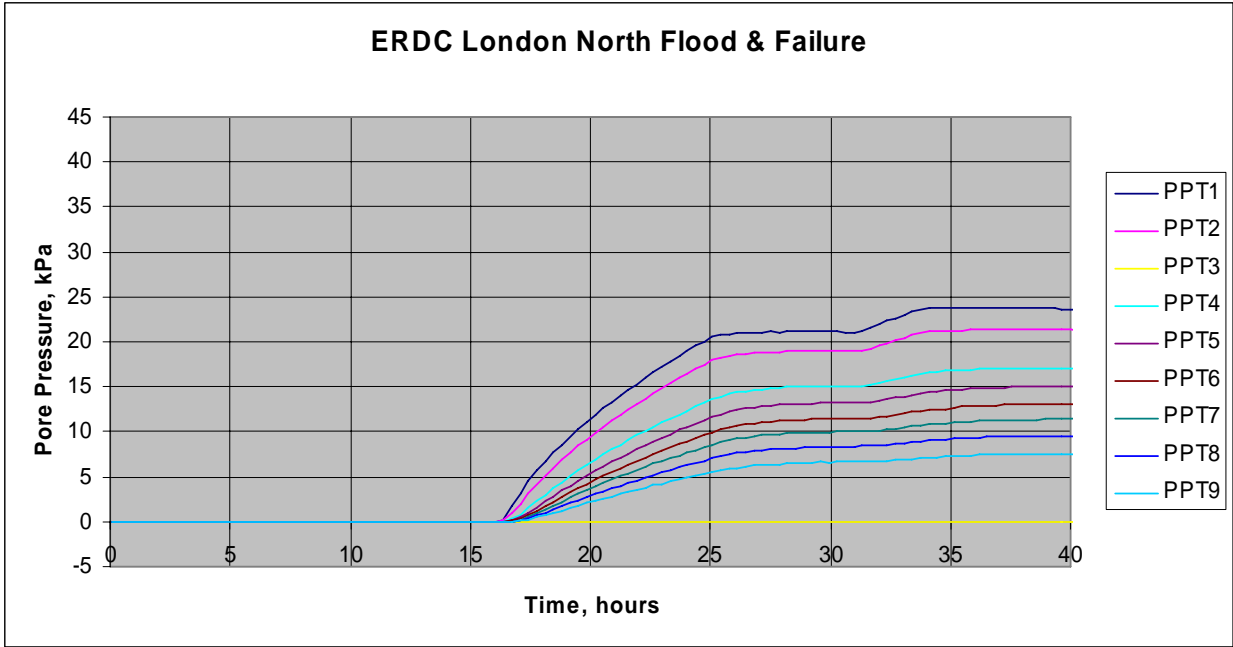
Figure 5.82. PPT data in the sand layer, mid-depth during flood event

Figure 5.83 is a plot of PPT data in the sand layer just near the top of that layer. The behavior is exactly as described above. Finally, the PPT data from the levee and swampy/marsh recorded during the flood are shown in Figure 5.84. The PPT's in the clay are very erratic. This response is attributed to a combination of the clay material drying out during the long spin time and to changes in the clay geometry as the failure is occurring.
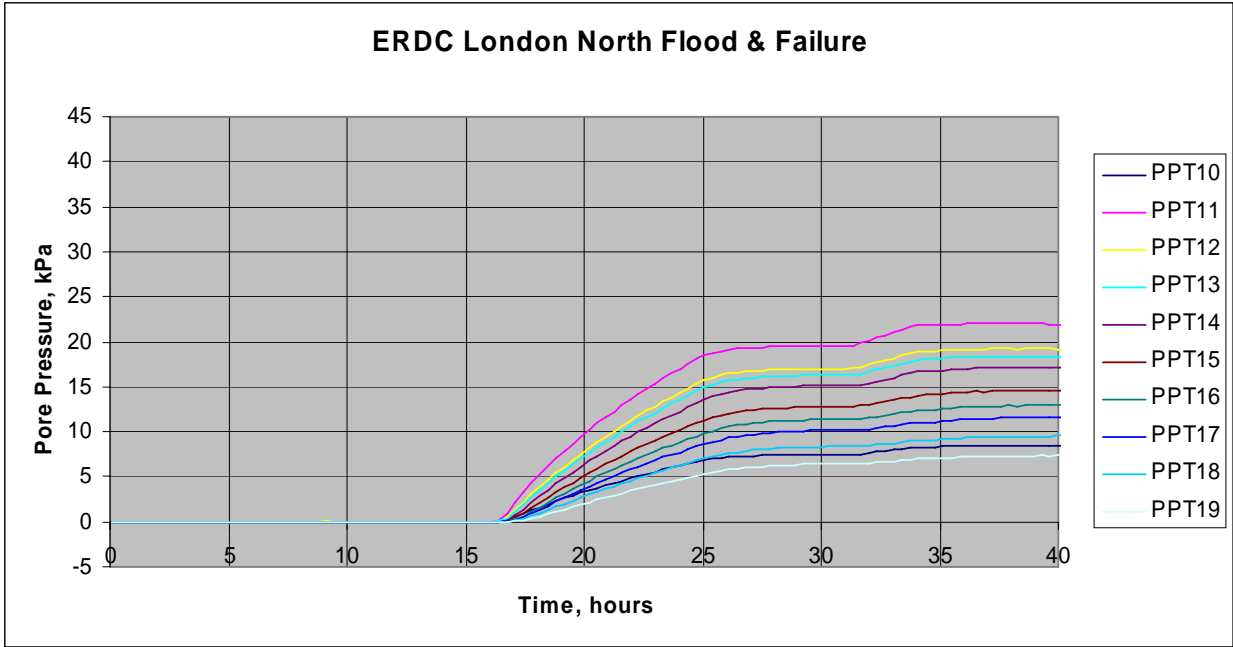
Figure 5.83. PPT data in the sand layer, near top, during flood
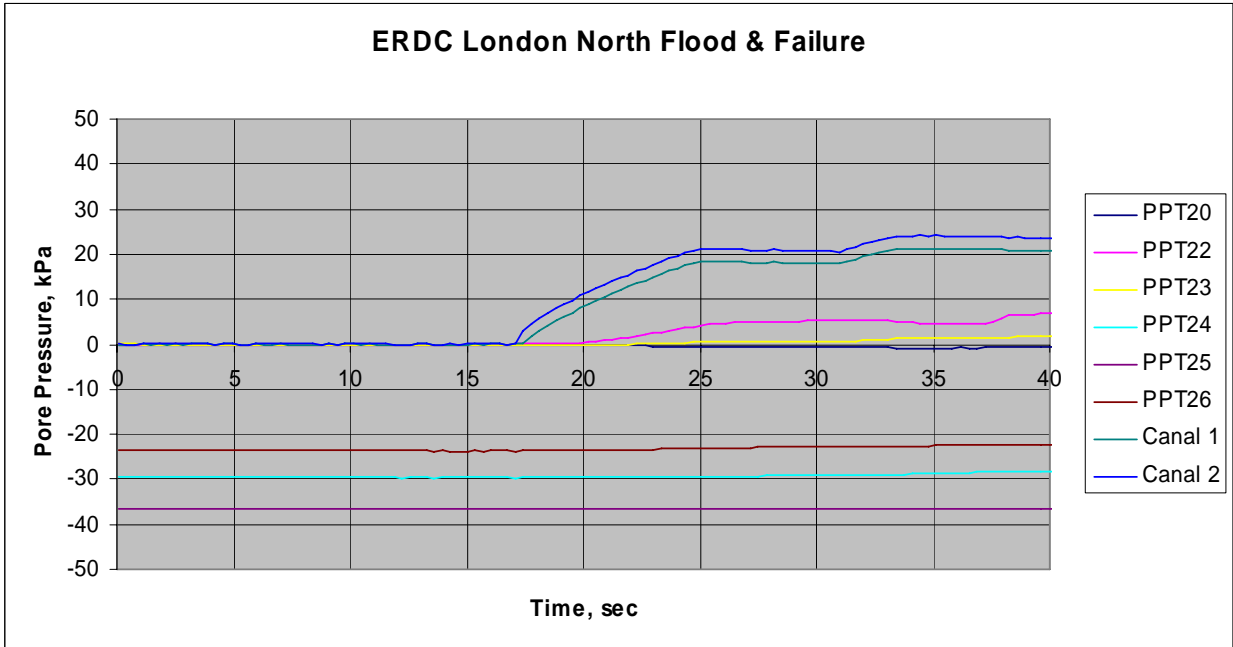
Figure 5.84. PPT data in the levee and swampy/marsh layer during flood

Finally, this section will present still shots taken from the video during flood and failure to highlight the event. Those views are shown in Figure 5.85, and clearly indicate the failure mechanism.

Figure 5.85a. View of ERDC London north model at normal canal water elevation

Figure 5.85b. View of ERDC London north model at flood level prior to wall movement

Figure 5.85c. View of ERDC London north model at flood level just after wall movement and opening of crack between wall and canal side levee

Figure 5.85d. View of ERDC London north model at flood level well into failure

This is a preliminary report subject to revision; it does not contain final conclusions of the United States Army Corps of Engineers.

Figure 5.85e. View of ERDC London north model at flood level end of failure

In a manner very similar to what was revealed in the two London south models, the description of failure mechanism for this London north model follows.

1. Water level increases to a point on the wall where initial movement of the wall begins to occur. This movement starts out as a rotation of the wall.
2. A crack begins to form between the sheet wall and canal side levee and propagates downward.
3. The crack extends all the way through the levee and the swampy/marsh layer to the top of the sand layer.
4. Full hydrostatic pressure is allowed to reach the foundation sand layer causing a sudden increase in pore water pressure.
5. This increase in pore water pressure reduces the vertical effective stress of the overlying swampy/marsh and levee material. Effectively the land side material approaches zero effective stress and begins to 'float'.
6. Load from the flood pushes the wall over in a rotational manner with no resisting force from the land side material.

RPI London Avenue Canal, North Breach Model

A second model representative of a section through the north breach at London Avenue canal was conducted at RPI and shown in Figure 5.86. The model was exactly as previously described for the ERDC London north model.
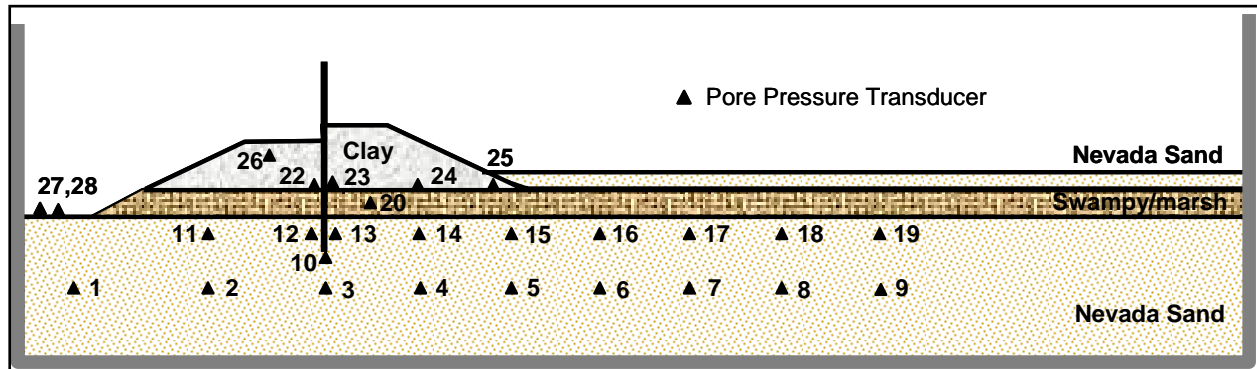
Figure 5.86. RPI London north model

The sequence of construction and testing has already been described for the ERDC model. At the conclusion of the consolidation process, moisture contents and shear strengths of the levee material were taken. Average moisture contents 47% and vane shear 375 psf.

The model was slowly spun up to 50 g in a manner previously described. At 50 g the water in the canal was brought to an elevation consistent with normal canal operating levels. All instrumentation was allowed to stabilize prior to the addition of any flood loading. The next section will present data recorded during the flood and failure event.

Results of the flood event are shown in Figures 5.87 through 5.90. Figure 5.87 is a plot of the rise in water during the flood event. Figure 5.88 is a plot of the PPT data in the sand layer mid-depth during the flood event. The data has a character as described for the ERDC model. The curves show a steady increase in pressure then a marked change in slope. This is associated with the crack formation and ultimate failure of the levee. Also, the pressure are higher under the canal and canal side levee reducing as you move through the foundation to the land side, as would be expected for the flow conditions of the model. Figure 5.89 is a plot of the PPT data in the sand layer near the top of that layer during the flood event. Finally, Figure 5.90 shows the PPT data in the levee and swampy/marsh during the flood. The data are erratic as discussed in the ERDC model but do show a change in character of the curves at a time near 50 hours
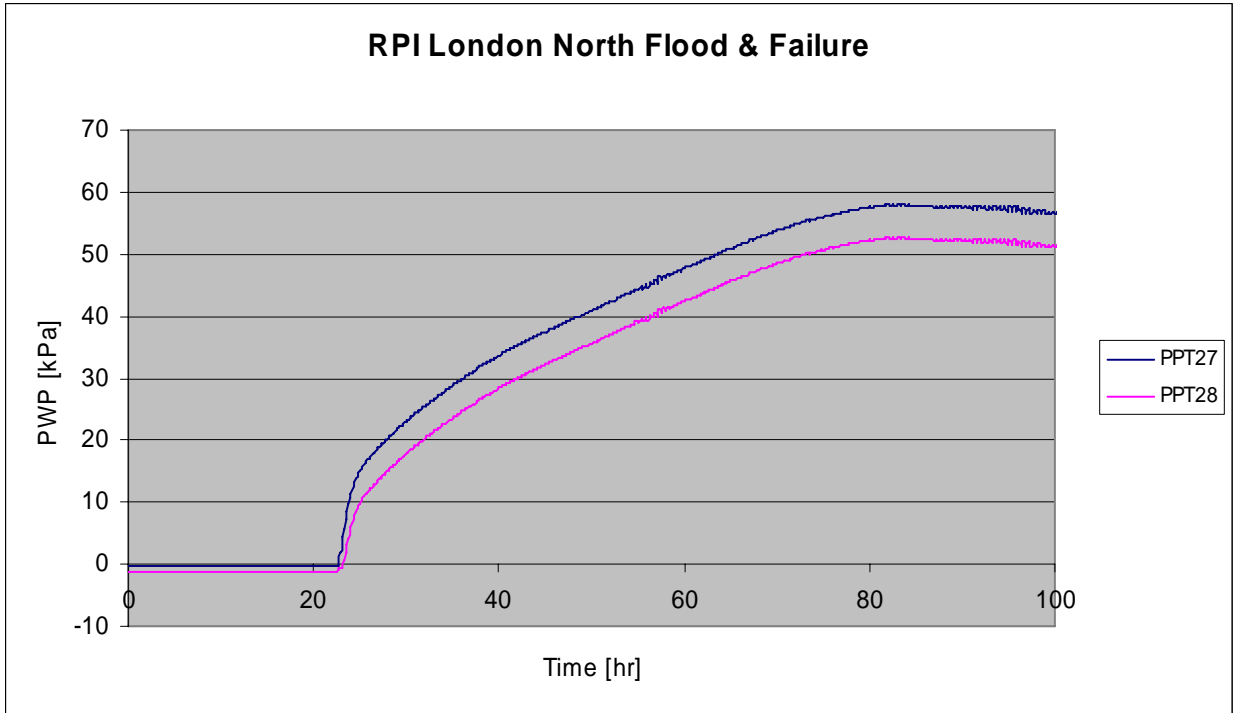
Figure 5.87. PPT data showing the rise in canal water elevation
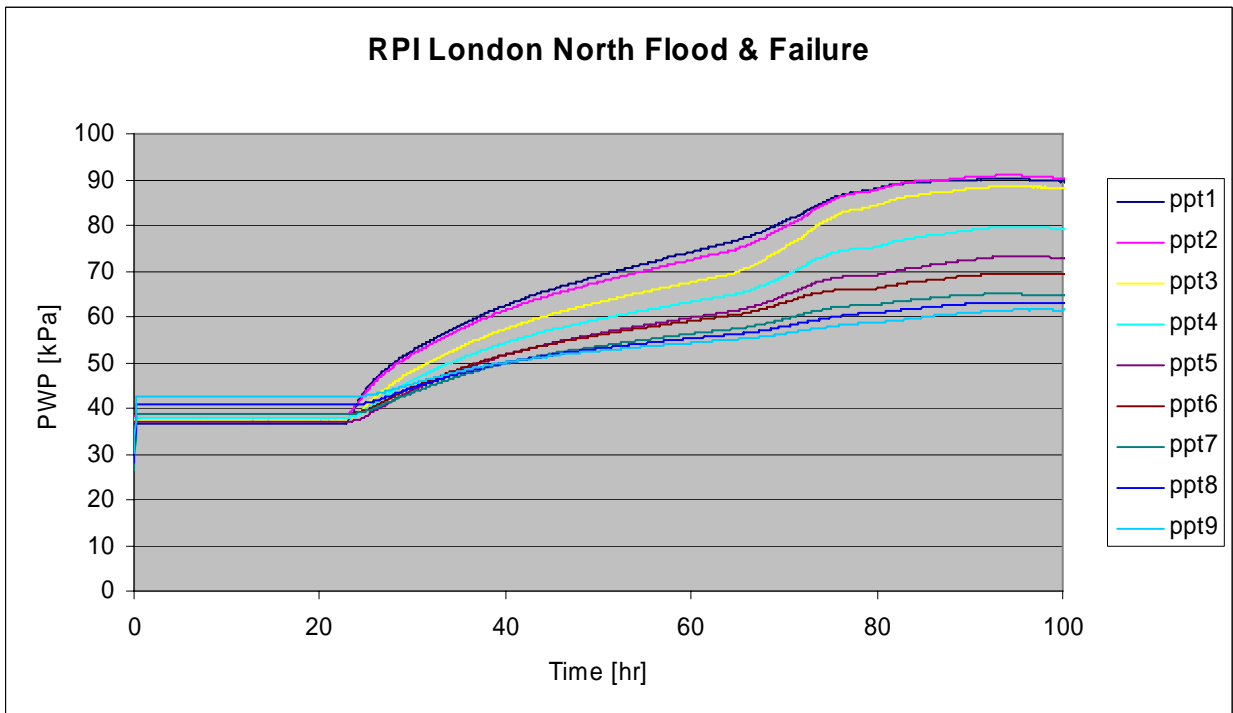
Figure 5.88. PPT data in the sand layer mid-depth during flood
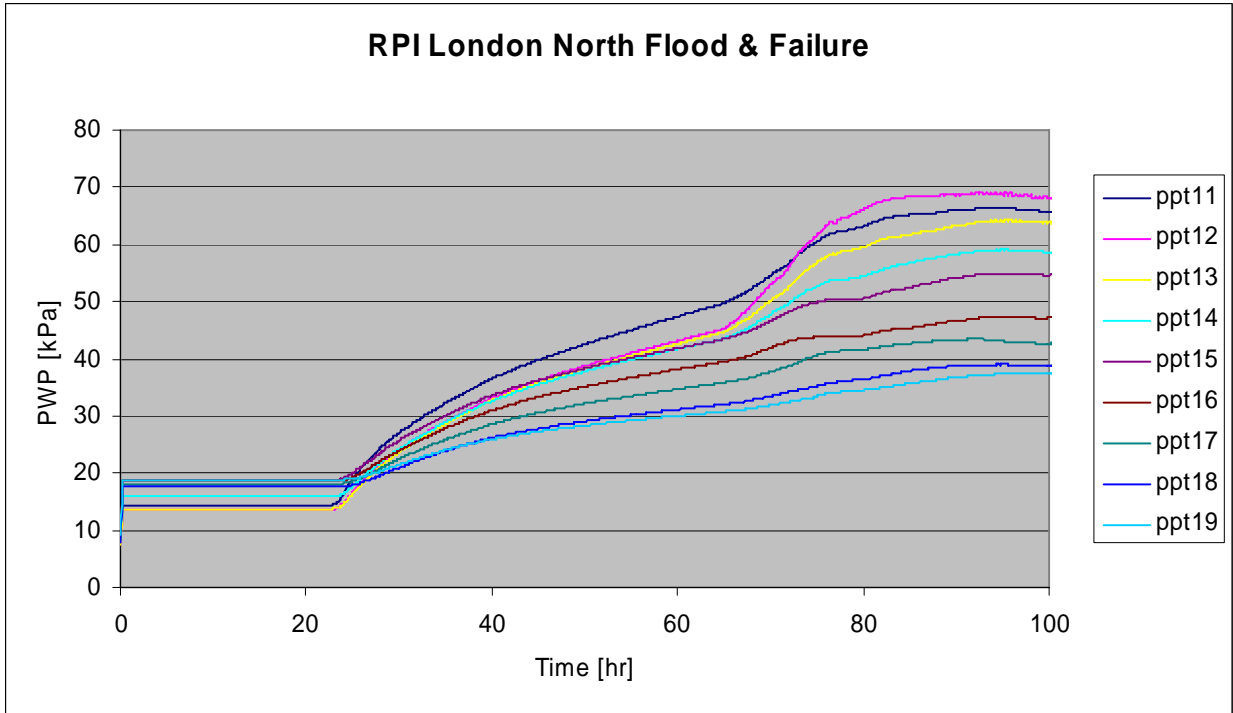
Figure 5.89. PPT data in the sand layer near top during flood
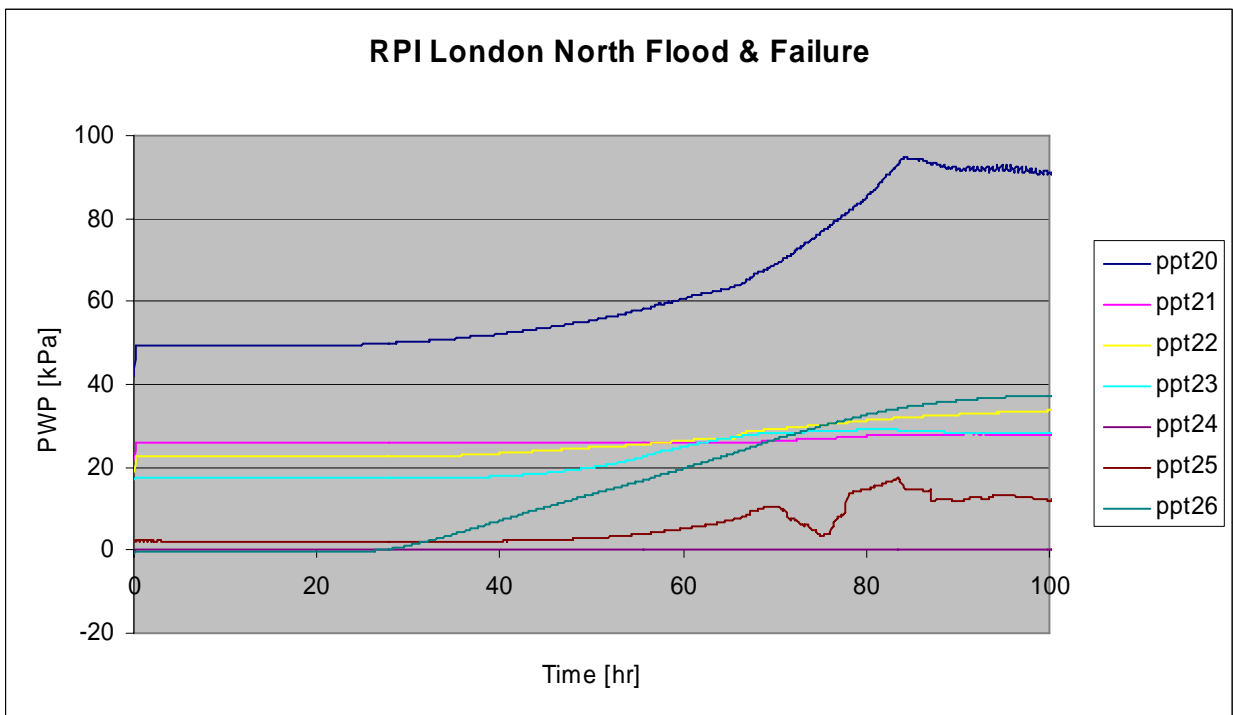
Figure 5.90. PPT data in the levee and swampy/marsh during flood

The following sequence of views, shown in Figure 5.91, are stills taken from the video recording of the flood and failure event. These shots clearly show the mechanism of failure. The vertical striations in the model are markers placed to determine deformations in the clay levee and foundation (this is similar to the "dots" used in previous models).
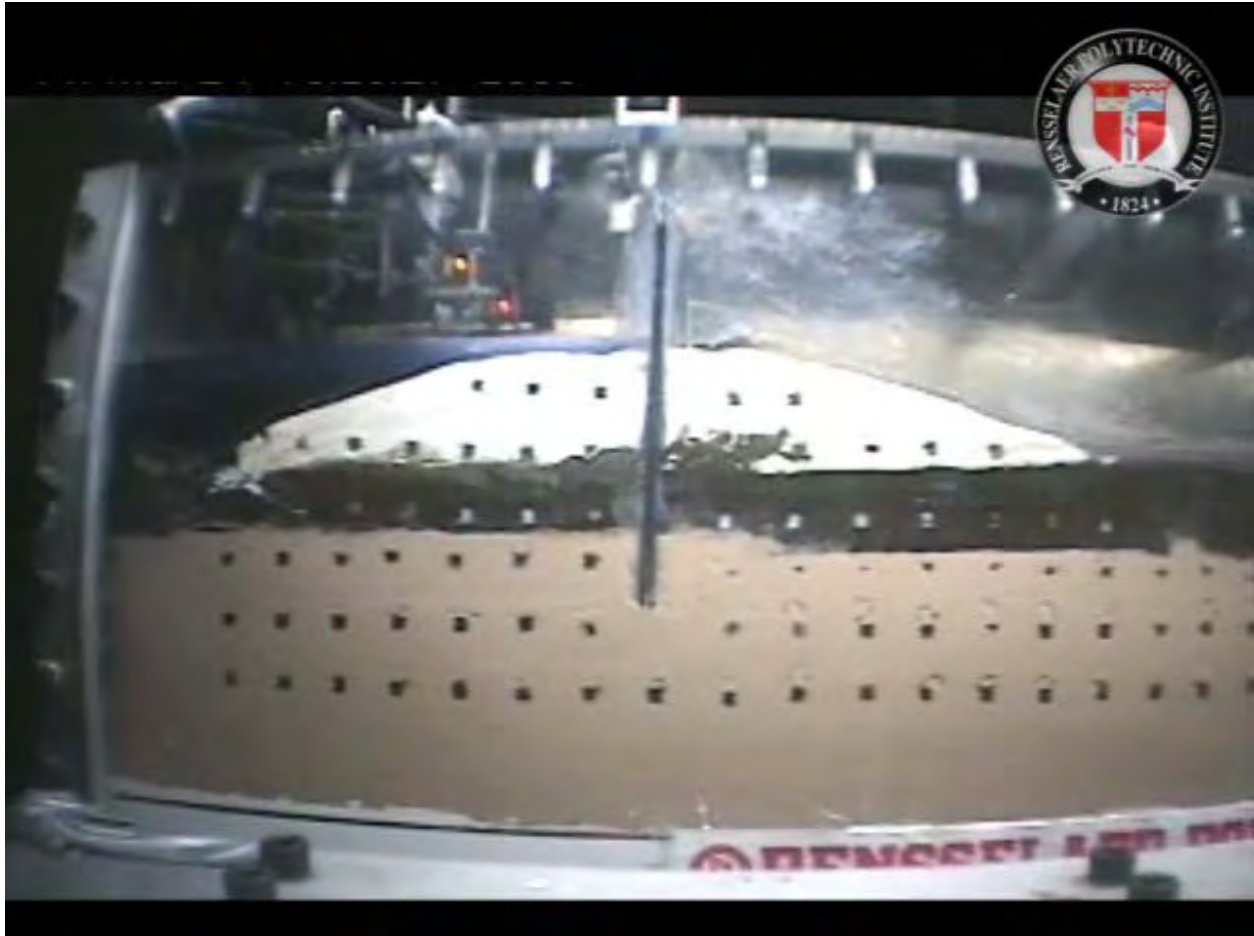

Figure 5.91a. RPI London north model at normal canal water elevation

Figure 5.91b. RPI London north model at flood level just prior to any wall movement

Figure 5.91c. RPI London north model at flood level just after wall movement when crack has opened

Figure 5.91d. RPI London north model at flood level well into failure

Figure 5.91e. RPI London north model at flood level end of failure

A synopsis of the failure event that occurred in the RPI London north model is as highlighted following. This is exactly the same failure event as was observed in the ERDC London north model and confirms the event.

1. Water level increases to a point on the wall where initial movement of the wall begins to occur. This movement starts out as a rotation of the wall.
2. A crack begins to form between the sheet wall and canal side levee and propagates downward.
3. The crack extends all the way through the levee and the swampy/marsh layer to the top of the sand layer.
4. Full hydrostatic pressure is allowed to reach the foundation sand layer causing a sudden increase in pore water pressure.
5. This increase in pore water pressure reduces the vertical effective stress of the overlying swampy/marsh and levee material. Effectively the land side material approaches zero effective stress and begins to 'float'.
6. Load from the flood pushes the wall over in a rotational manner with no resisting force from the land side material.

Physical Models of Orleans Avenue Canal

Two models of sections of the Orleans Avenue canal were completed. One of the models was performed at RPI representing a section at the south end of the canal and the other at ERDC representing a section at the north end of the canal. There were no failures of any of the walls in the Orleans canal and the two sections were selected to be representative of the canal in general. Only sections of the east levee were modeled since this levee contains I-walls while the west levees have T-walls. The south section of the canal is similar in foundation material to that of the London Avenue canal south breach area. The north section of the canal has foundation conditions similar to those of the 17th Street canal breach area. This section of the report will present information relevant to each model.

ERDC Orleans Avenue Canal, North Area Model

The model representative of a section through the north end of the Orleans Avenue canal is shown in Figure 5.92. The sheet pile extends through the swampy/marsh layer almost to the bottom. The height of the wall above the levee crest on the canal side is approximately 1.5 m, and the normal canal elevation does not reach the top of the levee.
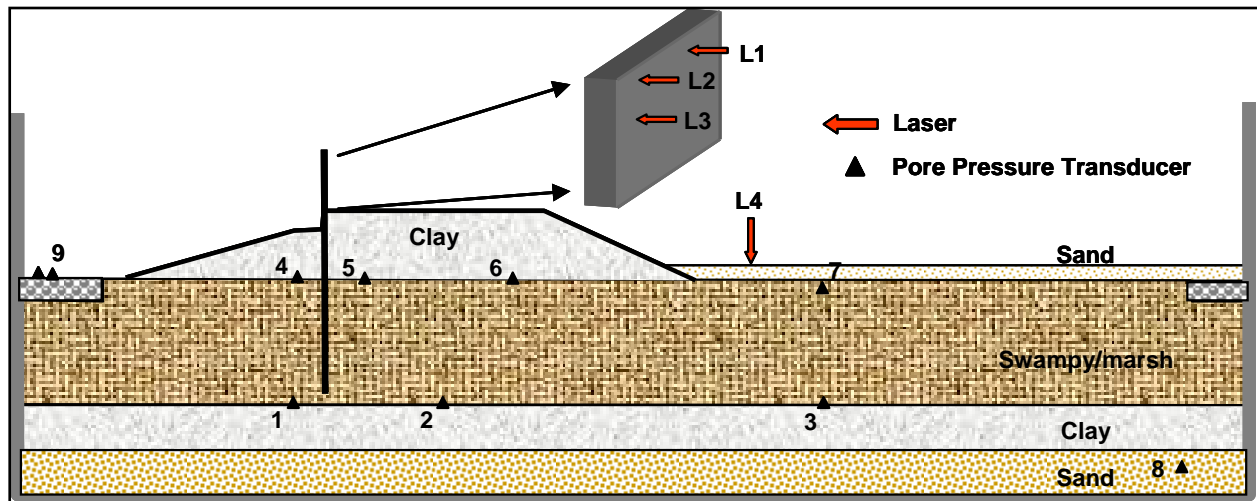
Figure 5.92. ERDC model of Orleans Avenue canal, north area

Post consolidation moisture content of the levee was 54%. The swampy/marsh layer had an average vane shear of 350 psf. The model was slowly spun up to 50 g and readied for testing. Water was maintained in the canal during spin up to 50 g, where it was increased to normal canal water elevation. The model and instrumentation were allowed to stabilize prior to increasing the water level from normal canal level to flood level. The following section will present data and discussions recorded during the flood and failure process.
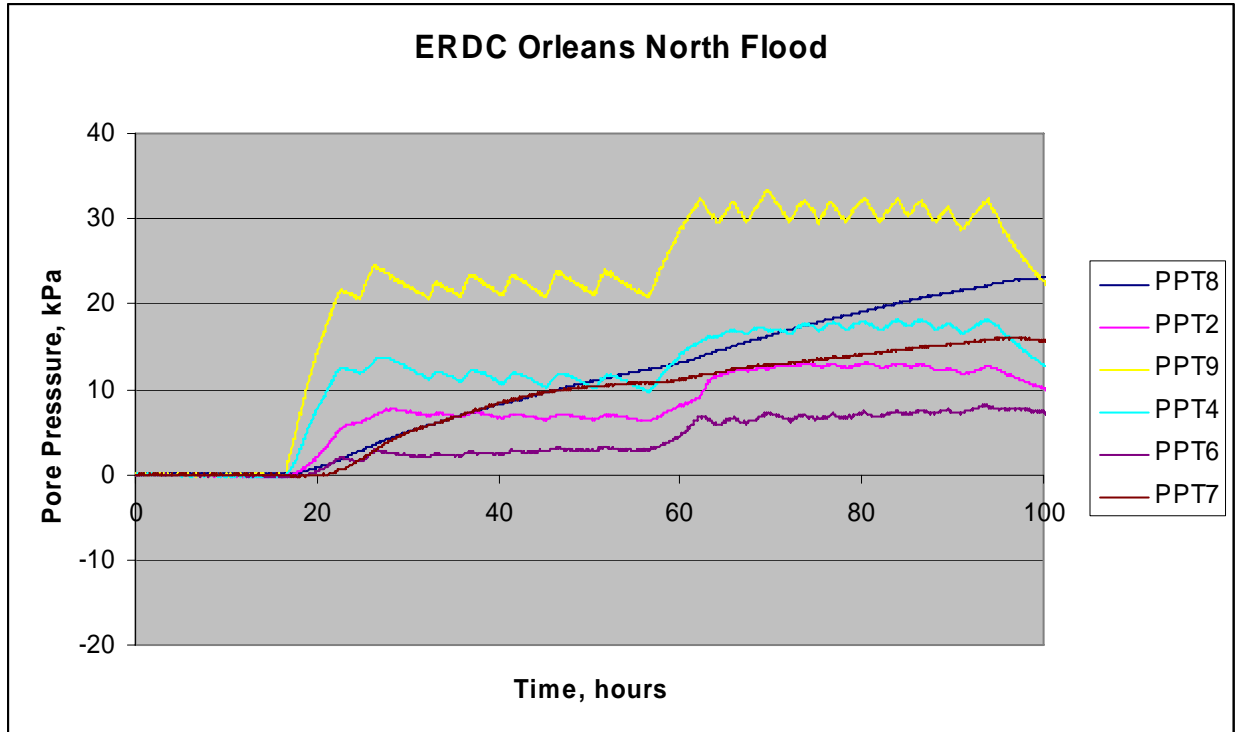
Figure 5.93. PPT data recorded in the ERDC Orleans North model during the flood

There is a step in the PPT data from shortly after the flood event associated with the rise in water level from the normal canal elevation to that at hurricane Katrina. Starting at time 20 hours until approximately 55 hours is the water level being held at the Katrina flood level. A second increase in pressure that is associated with increase in water level to the top of the wall occurs between time 60 hours and 95 hours. This was done to explore the behavior of the wall should the water elevation have gone up to a higher level.

Displacement of the wall as recorded during the flood event is shown in Figure 5.94. As the water level increases there is a point where the wall moves slightly, this is seen as a movement of less than 0.1 m that quickly stops and remains constant for the period of water being held at flood level. At a time of approximately 25 hours the water level was increased to the top of the wall. The displacement data shows that the wall moved an additional 0.2 m. At this point the wall continued a slow movement of an additional 0.1 m. In the video to be shown following, there was a clear formation of a crack at the increased water elevation but this did not develop into a failure of any type.
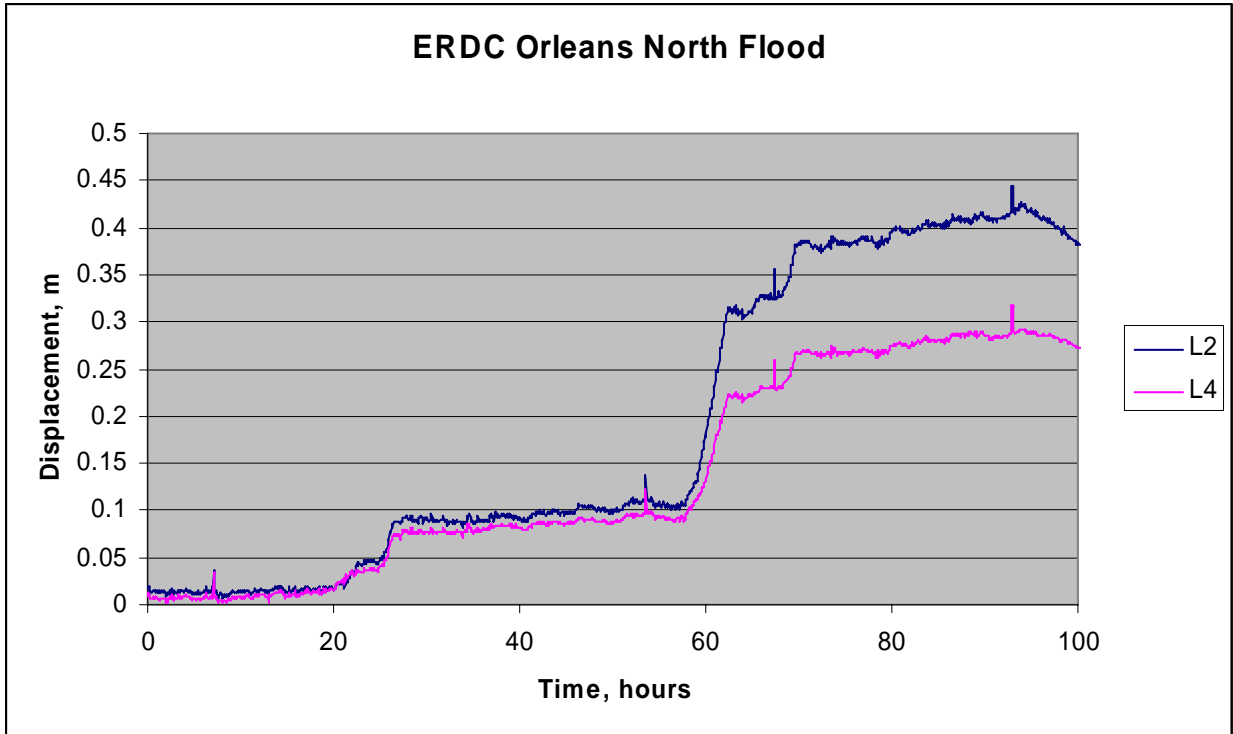
Figure 5.94. Displacement of wall during flood event, Katrina level and additional flood to top of wall

The following sequence of images shown in Figure 5.95 are stills taken from the video recording of the flood and failure event.

Figure 5.95a. View of model at normal canal elevation prior to flood

Figure 5.95b. View of model at hurricane Katrina flood level

Figure 5.95c. View of model at hurricane Katrina flood level, extended time at flood

Figure 5.95d. View of model where water has been increased above hurricane Katrina level to explore wall behavior

Figure 5.95e. View of model at flood level greater than hurricane Katrina, wall has moved

A synopsis of the model results is presented following for both conditions of hurricane Katrina flood level and the increased flood level.

1. The canal water elevation was increased from normal elevations to those of hurricane Katrina where a very small movement in the wall occurred.
2. Water was held at this level for a long period of time and no further movement of the wall occurred, and the levee was completely stable.
3. Water level was increased from hurricane Katrina level to near top of wall. The wall had an additional movement that formed a crack between the wall and canal side levee.
4. The wall continued to move a very small amount toward the land side but did not lead to failure of any kind in the levee.

RPI Orleans Avenue Canal, South Area Model

The model representative of a section through the south end of the Orleans Avenue canal is shown in Figure 5.96. The sheet pile extends through the levee to the top of the swampy/marsh

layer. The height of the wall above the levee crest on the canal side is approximately 1.5 m, and the normal canal elevation does not reach the top of the levee.
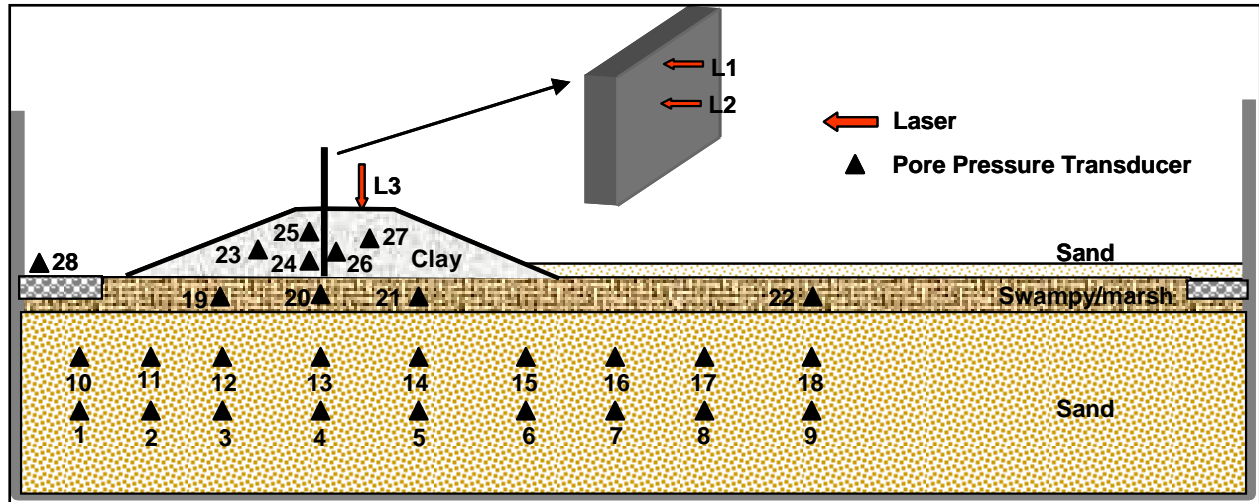
Figure 5.96. RPI model of the Orleans Avenue canal, south area

At the conclusion of consolidation moisture content and vane shear measurements of the levee were taken. Those values indicate moisture contents of 47% and vane shear readings of 505 psf.

The model was slowly spun to 50 g, water level increased to that at normal canal operation and all instrumentation allowed to stabilize. Once this was accomplished, the flood load was applied. Results of the flood loading are presented in Figures 5.97 through 5.100. Figure 5.97 is a plot of the PPT data recorded in the sand layer at mid-depth. Notice that there is a steady increase in the pore pressures reaching a level where they remain constant through the flood load.
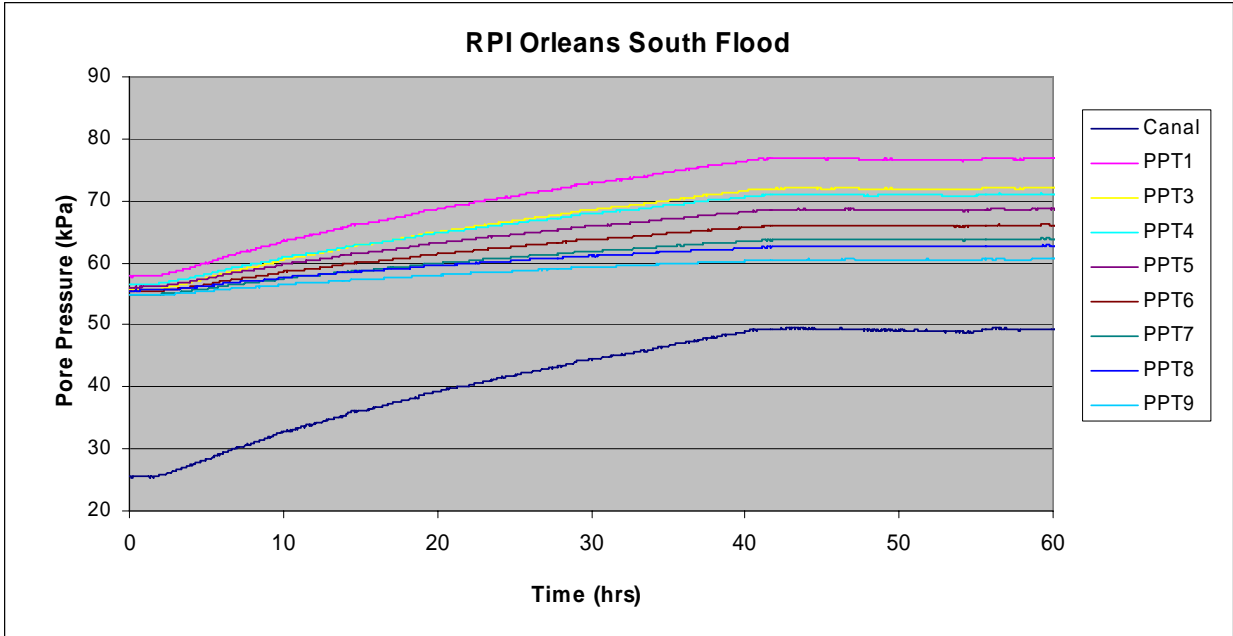
Figure 5.97. PPT data recorded in the sand layer, mid-depth during flood

Figure 5.98 is a plot of the PPT data in the sand layer near top during flood event. The character is very much like that of the data in Figure 5.97. Figure 5.99 is the PPT data recorded in the levee and swampy/marsh layer during the flood. There is very little to no response from any of the PPT's located in the swampy/marsh layer. This is not an unexpected event since increase in canal water level would have little effect on these readings over the relatively short duration of the flood event. Notice that there is an increase in PPT's 24, 25 and 26. Instruments 24 and 25 are located near the wall on the canal side and are feeling the load of the increased water level. There is a delayed response in the rise of pressure recorded by PPT 26 which would be expected.
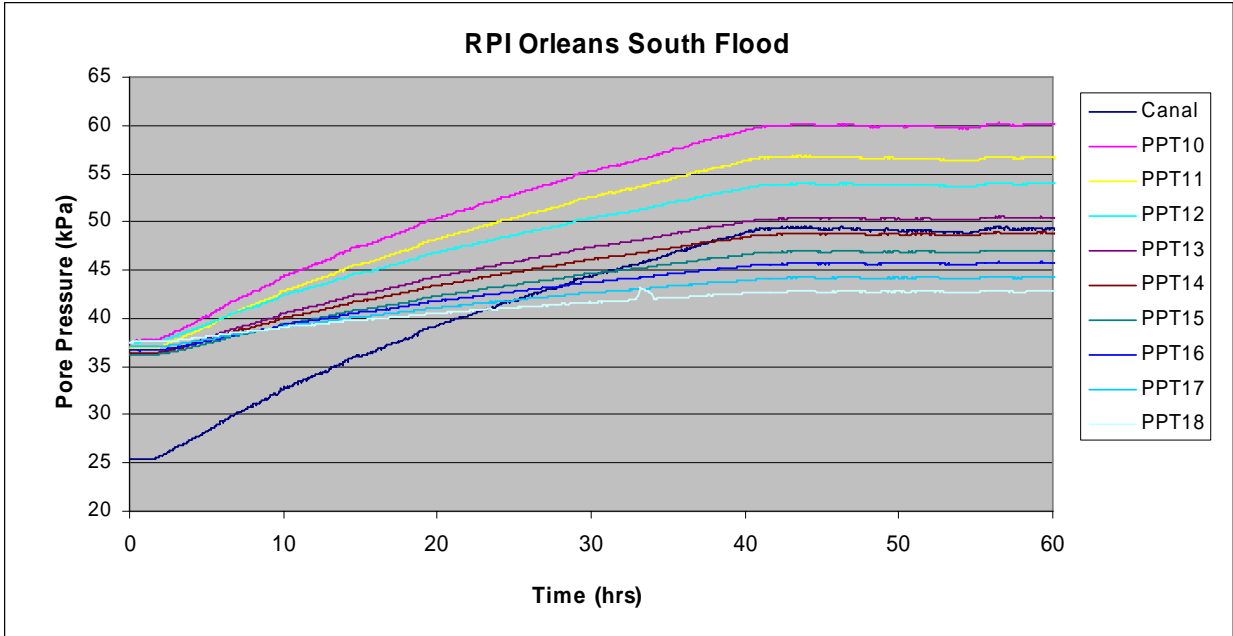
Figure 5.98. PPT data in the sand layer, near top during flood event
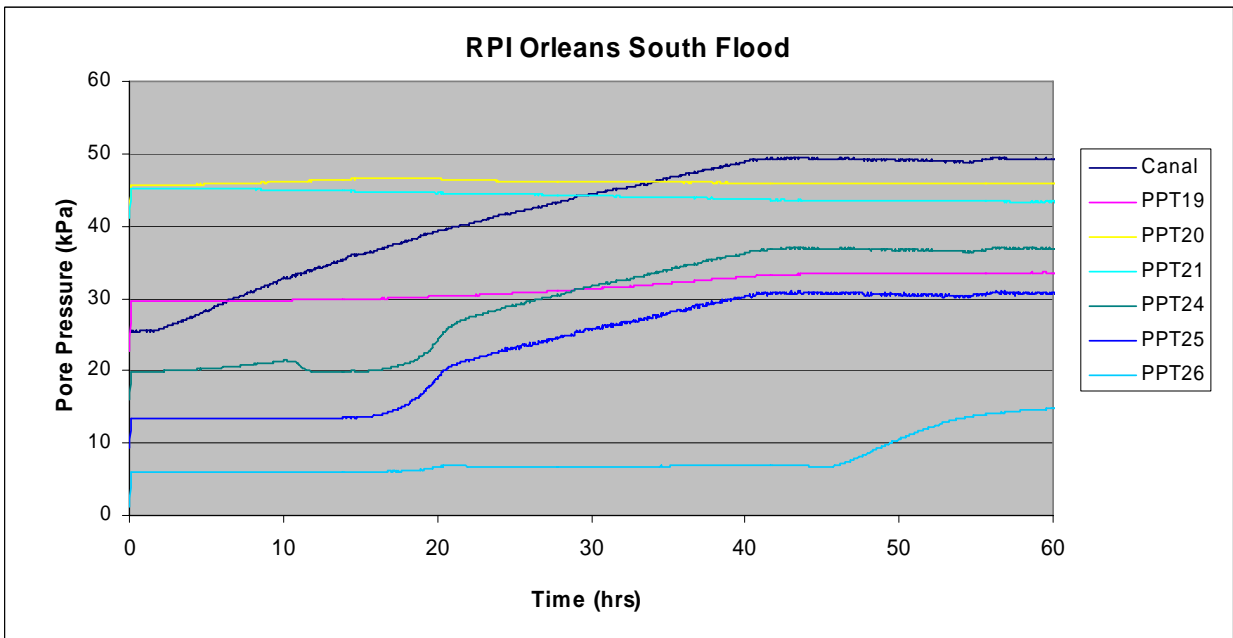
Figure 5.99. PPT data in the levee and swampy/marsh layer during flood

Measurement of wall movement is shown in Figure 5.100. There is a very small movement in the wall of only 0.03 m but the wall remains constant with no movement thereafter. Although this movement may have opened a very small crack behind the wall, this did not lead to any further movement of the wall or failure of the levee.
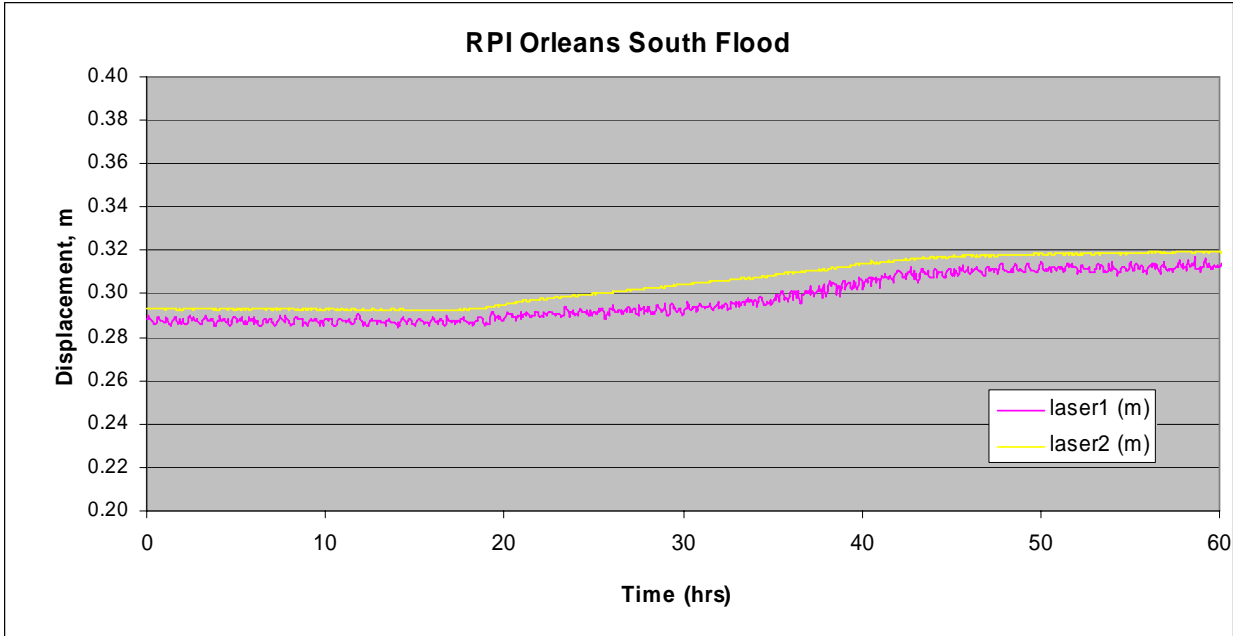
Figure 5.100. Displacement of the wall during flood loading

After the model was held at the hurricane Katrina level for a period sufficient to show that no failure of the levee would occur, the water elevation was increased to near the top of the wall to explore the behavior of the levee. This was done simply as an exercise to determine what would have happened had the flood level actually reached that high. Just showing the movement of the wall, Figure 101, is enough to show the behavior. The zero time on the plot corresponds to the time when the water elevation is at hurricane Katrina level and risen to the top of the wall. Therefore, all wall movements were as a result of the increased water load above hurricane Katrina level. Notice that the wall starts to move immediately and continues on a fixed slope until about 50 hours. This movement is associated with opening of a crack behind the wall. From this point on, there is a slow steady movement of the wall amounting to about 0.2 m total. This movement would have been enough to cause concern about future stability of the wall.
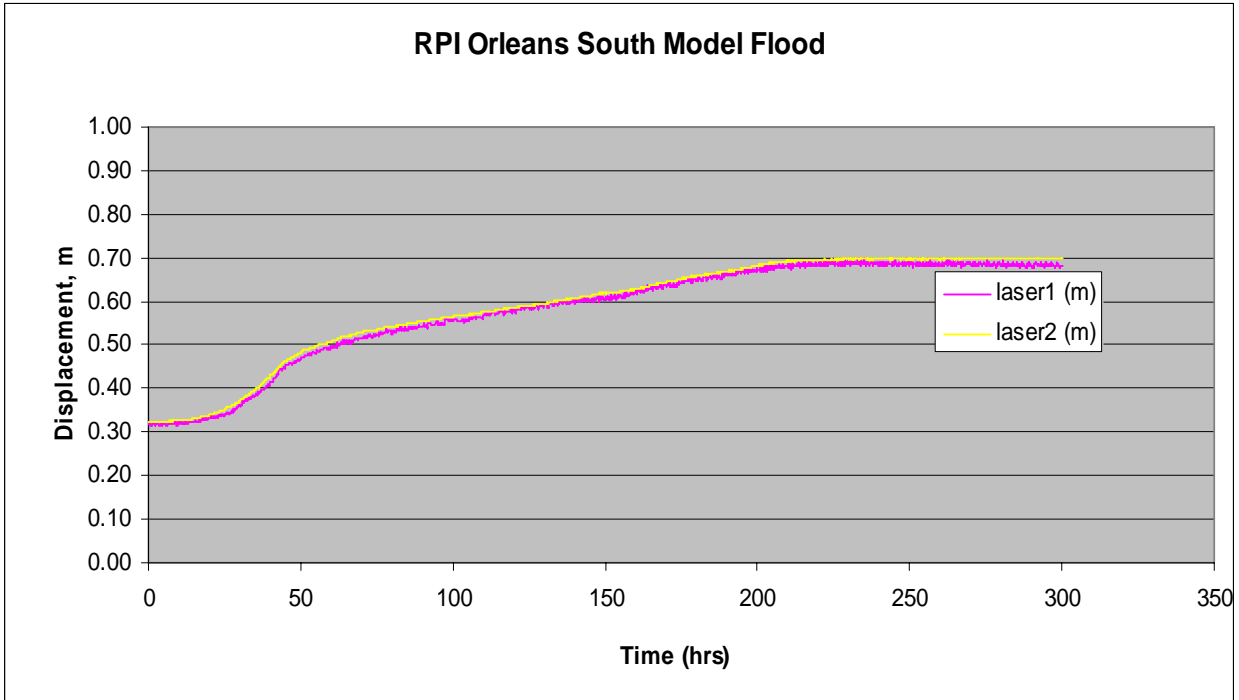
Figure 5.101. Displacement of wall during increased flood load above hurricane Katrina level

The sequence of images shown in Figure 5.102 are stills taken from the video recording of the flood event. The images clearly show the behavior of the levee during the flood load.

Figure 5.102a. View of RPI Orleans south model at normal canal elevation

Figure 5.102b. View of RPI Orleans south model at hurricane Katrina flood level

Figure 5.102c. View of RPI Orleans south model at hurricane Katrina flood level, held here for long period

Figure 5.102d. View of RPI Orleans south model with water elevation raised above hurricane Katrina level to near top of wall

Figure 5.102e. View of RPI Orleans south model with water elevation raised above hurricane Katrina level showing movement of wall

The sequence of events in the Orleans south model are as highlighted following. These events are very similar to those as described for the north section of the levee.

1. Water was raised to the level of hurricane Katrina and allowed to remain there for an extended period of time
2. The wall moved slightly but did not lead to any failure of the levee or subsequent movement in the wall.
3. Water elevation was then taken to the top of the wall, above hurricane Katrina level. The wall moved an additional amount forming a crack behind the wall as was observed in the other canal walls.
4. This crack opening was preceded by slow steady movement of the wall that did not lead to catastrophic failure, but would have placed the stability of the levee in jeopardy.

Appendix 6
Soil-Structure Interaction Analysis of the Floodwall at 17th Street

Introduction

This section describes a complete soil-structure interaction (SSI) analysis of an existing floodwall within 17th Street Canal using the PC-based finite-element program, Plaxis (2004). A two-dimensional (2-D) cross section within the section of the east side of the 17th Street Canal that failed during hurricane Katrina is the subject of this evaluation. Results of a complete nonlinear finite-element analysis of a 2-D cross section at Station 10+00 during simulated flood loading are described.

Plaxis is a complete nonlinear finite-element package geared towards geotechnical engineering applications that include SSI issues such as those that occur between a sheet pile and the soils in which it is embedded. It allows for the nonlinear response of soils to flood loading as occurred at the 17th Street Canal with an I-wall along the centerline of the soil-founded levee. The Plaxis PC-based software comprises a visual pre-processor, a nonlinear finite-element engineering analysis module, and a visual post-processor. All software components are combined into a single package. Computed results include not only soil stresses, but also structural (e.g. sheet pile and I-wall) bending moments, interaction stresses between sheet piling, the soil in which it is embedded, as well as soil (e.g., levee) and structural deformations. A complete SSI analysis is considered to provide the most reasonable estimate for deformation response of a soil-structural system involving nonlinear material behavior. In a complete SSI analysis, loads exerted by the canal water acting on the soils of the levee and then onto the sheet pile wall (below the I-wall) by means of a load transfer through the levee and foundation soils are generated automatically during the analysis (i.e., predetermined earth pressure force distributions between the soil and the embedded sheet pile are not specified).

Section Analyzed

The 2-D cross section within the failed section of the east side of the 17th Street Canal at Station 10+00 analyzed for flood loading is shown in Figure 6-1.[1] The 2-D section is 247-ft wide and extends from x-coordinate equal to -27 ft to the centerline of the canal at x equal to 220 ft. The top of the I-wall is at El 12.5. The crest of the earthen levee on the protected (east) side of the I-wall is at El 5, with a crest width of approximately 15 ft. Note that the I-wall extends above the crest of the soil-founded levee. The protected side of the levee has a 1 on 3 side slope to approximately El -4.5. The protected side ground surface is assigned El -5 for this section. A bench exists at El -2.5 on the canal side of the I-wall. This bench is submerged for the normal water level in the canal, El 1. In the canal and beyond the end of the bench, the submerged levee face has a 1 on 3 side slope to approximately El -11.5. Between El -11.5 and El -16.5, the face of the peat soil layer is exposed to canal water. Below El -16.5, the Lacustrine clay soil layer is exposed to water in the canal. The deepest point in the canal is at the canal centerline (i.e., x = 220 ft in Figure 6-1), with a top of Lacustrine clay at El -18.5 at this location.
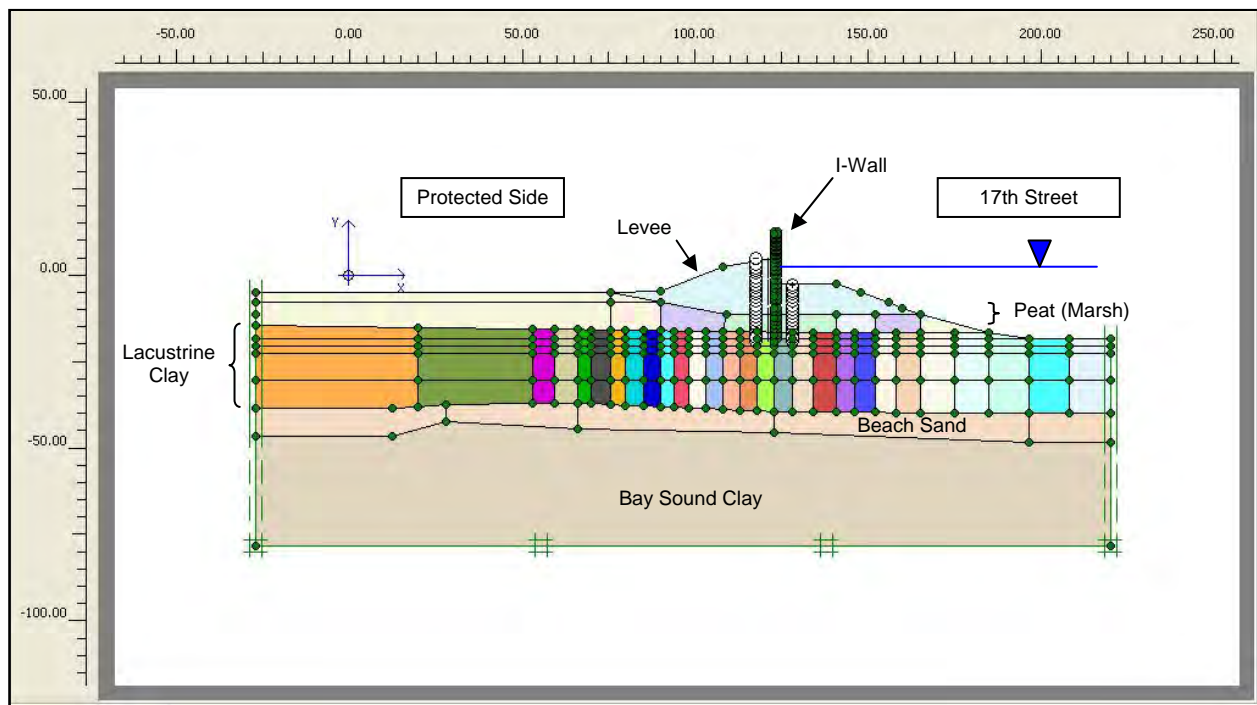
Figure 6-1. Two-Dimensional Cross-Section Model used in the Complete SSI Analysis of Station 10+00 at the 17th Street Canal – East Side

Proceeding from top to bottom in Figure 6-1, this cross section contains layers of levee fill (clay), peat (also referred to as marsh), lacustrine clay, beach sand, and Bay Sound clay. The top of the I-wall is at El 12.5, and the base of the Figure 6-1 cross section is assigned to El -78.5. El -78.5 corresponds (approximately) to the bottom of the Bay Sound clay at Station 10+00. The soil layering is consistent with that used in the slope stability evaluations made for this cross section.

---

[1] All elevations cited are according to NAD88.

Volume V The Performance – Levees and Floodwalls – Technical Appendix

The regions of uniform color in Figure 6-1 reflect the Plaxis "soil clusters" used to define the mesh and to assign soil regions with common properties.

Finite-Element Mesh

Key Plaxis modeling features used in the plane strain analysis of the 17th Street include the use of 15-node triangular elements to model the soil, plates (i.e., special beam elements) to model the bending of the I-wall and the sheet pile wall, and interface elements to model SSI between the sheet pile wall and the adjacent soil elements. A total of 26,858 nodes and 3,374 elements, containing 39,492 stress points, were used to define the Figure 6-2 mesh. Details regarding the quantity of each of the three types of plane strain elements used in the finite-element model, as well as select characteristics of each type of element, are summarized in Table 6-1.
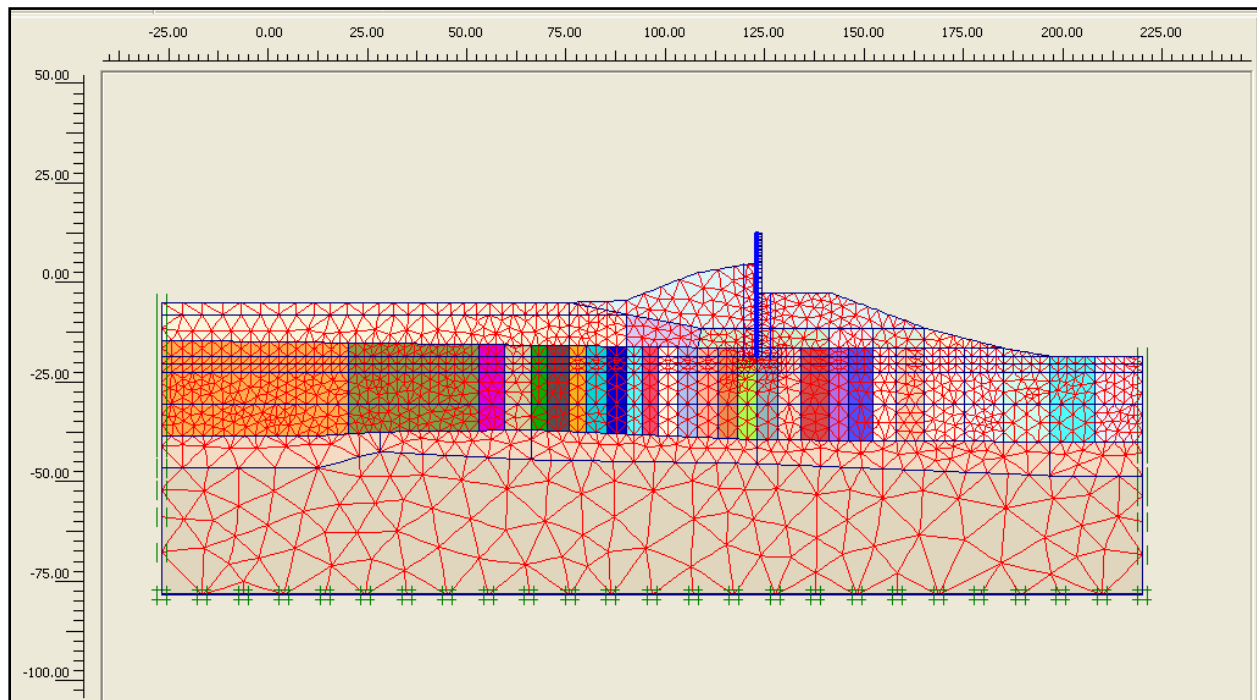
Figure 6-2. Finite-Element Mesh used in the Complete SSI Analysis of Station 10+00 at 17th Street Canal – East Side

Table 6-1
Mesh Data Summary of Elements Used

Type	Type of element	Type of integration	Total No.
Soil	15-noded	12-point Gauss	3291
Plate	5-node line	4-point Gauss	39
Interface	5-node line	4-point Newton-Cotes	44

A zero horizontal displacement is specified along the left- and right-hand side vertical boundaries of the Figure 6-2 finite-element mesh. However, these nodes are free to displace in the vertical direction. Along the bottom boundary of the mesh, zero horizontal and vertical displacements are specified at these nodes.

Material Properties for the Soils and Floodwall in the Complete Soil-Structure Interaction Analysis

The soil material properties used in this complete SSI analysis are the same as those used in the slope stability analyses of this cross section. Figure 6-3 shows the 219 soil clusters used to define the regions of common soil properties for the five categories of soil within the mesh (i.e., the levee clay, peat (or marsh), lacustrine clay, beach sand, Bay Sound clay). Note that each soil layer comprises many clusters, each of which is designated by a different color. Spatially varying soil properties are assigned in the slope stability analyses. Accordingly, multiple soil clusters are used in the nonlinear finite-element mesh to assign material properties within each soil layer to accommodate the spatially varying (i.e., vertically as well as horizontally) soil properties. Table 6-2 summarizes the engineering material properties and, for some layers, the range in assigned engineering soil properties used in the complete SSI analysis.
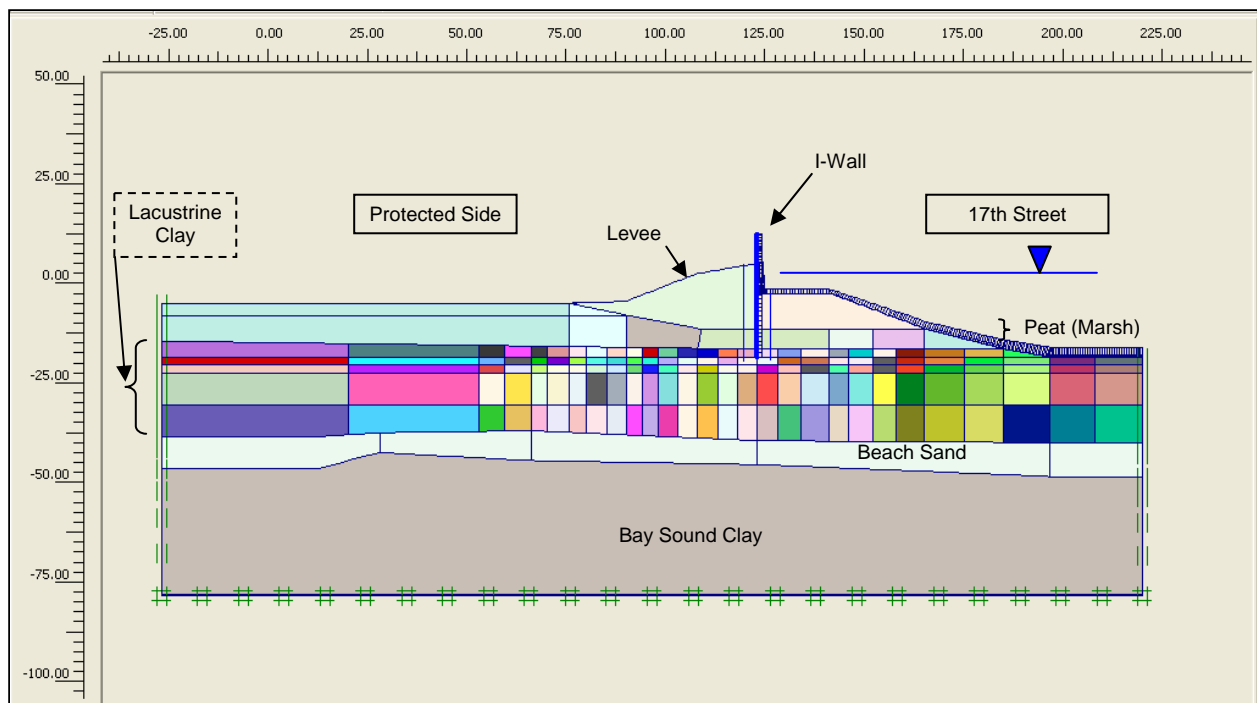
Figure 6-3. The 219 Soil Clusters used in the SSI Analysis of Station 10+00 at 17th Street Canal – East Side

Table 6-2
Material Characterization for Soils

Soil type	Total unit weight (pcf)	S_u Constant value in soil cluster (psf)	S_u @ top of soil layer (psf)	ΔS_u per ft of depth (psf)	ϕ' (deg)	Young's Modulus E^{ref}/S_u	Young's Modulus E^{ref} (psf)	m	$R_{interface}$
Levee clay	110	900	–	–	–	48	–	0.5	0.8
Peat (marsh)	80	300 to 400	–	–	–	48	–	0.5	0.8
Lacustrine clay	109	–	45 to 300	11	–	92	–	1.0	0.8/1.0
Beach sand	120	–	–	–	36	–	477,725	0.5	–
Bay Sound clay	102	779	–	–	–	68	–	1.0	–

Note:$(E^{ref})_{50} = (E^{ref})_{oed} = E^{ref}$; $(E^{ref})_{ur} = 3*E^{ref}$; $\psi = 0$ deg; $p_{ref} = 2116$ psf; $_{ur} = 0.2$; $R_f = 0.9$

   Levee clay: A total unit weight of 110 pcf is assigned to the levee clay soil clusters. Stress-strain data for levee clay specimens tested in an undrained shearing (mode) to failure in laboratory triaxial tests leads to the assignment of a value for Young's modulus, E^{ref}, expressed in terms of (E^{ref}) normalized by S_u and equal to 48. A value for E^{ref}/S_u of 48 corresponds to the mean value from the stress-strain results of 15 triaxial tests conducted on levee clay. Note that a secant value definition for Young's modulus (for a secant line originating at a strain of zero and passing through the point on the nonlinear stress-strain curve corresponding to 50% of the principal stress difference for the soil specimen) is used to assign a value for E^{ref}. Based on this and other shear strength test data, the undrained shear strength (S_u) is set equal to 900 psf for the levee clay (average value).

   For the Plaxis nonlinear Hardening Soil (HS) model, the parameters (E^{ref})$_{50}$ and (E^{ref})$_{oed}$ are set equal to [E^{ref}/S_u times S_u]. Additional HS parameters assigned are reference stress for stiffness, p_{ref}, equal to 2,116 psf, failure ratio $R_f = 0.9$, and the exponent m = 0.5. For unload reload HS parameters, (E^{ref})$_{ur}$ is set equal to 3 times (E^{ref})$_{50}$ and ν_{ur} equals 0.2. For Hoesch 12 steel sheet piles to levee clay, the interface strength parameter, $R_{interface}$, is set equal to 0.8 for levee clay-to-steel interfaces (by the Potyondy, 1961, data).

   Peat (or marsh): A total unit weight of 80 pcf is assigned to the peat (or marsh) soil clusters. Stress-strain data for peat specimens tested in an undrained shearing (mode) to failure in laboratory triaxial tests leads to the assignment of a value for Young's modulus (E^{ref}) normalized by S_u equal to 48. A value for E^{ref}/S_u of 48 corresponds to the mean value for 27 triaxial tests conducted on peat/marsh, with a 50% stress level secant value definition being used for E^{ref}. Based on this and other test data, the undrained shear strength (S_u) is set equal to between 300 and 400 psf for the peat, depending on overburden and/or location. Strength test results indicate that peat regions located below overburden, such as below the levee, have higher shear strengths. The region of peat immediately below the centerline region of the levee, the location of greatest overburden, is assigned $S_u = 400$ psf. The peat on the protected side and immediately beyond the toe of the levee (i.e., x < 75 ft) is assigned Su = 300 psf, as is the peat at the toe of the canal side (x = 185 ft). A shear strength value is assigned to each peat cluster based on the magnitude of the

overburden for the center position of each peat cluster below the levee. There is an approximate linear variation in Su with position between the centerline and the toe on the protected side and the centerline and the toe on the canal side. There is no vertical variation in undrained shear strength for the peat layer.

For the Plaxis nonlinear Hardening Soil (HS) model, the parameters $(E^{ref})_{50}$ and $(E^{ref})_{oed}$ are set equal to $[E^{ref}/S_u$ times $S_u]$. Additional HS parameters assigned are reference stress for stiffness, p_{ref}, equal to 2,116 psf, failure ratio $R_f = 0.9$, and the exponent m = 0.5. For unload reload HS parameters, $(E^{ref})_{ur}$ is set equal to 3 times $(E^{ref})_{50}$, and ν_{ur} equals 0.2. For Hoesch 12 steel sheet piles to peat/marsh interface, $R_{interface}$ is set equal to 0.8.

Lacustrine clay: A total unit weight of 109 pcf is assigned to lacustrine clay soil clusters. Stress-strain data for Lacustrine clay specimens tested in an undrained shearing (mode) to failure in laboratory triaxial tests leads to the assignment of a value for Young's modulus (E^{ref}) normalized by S_u equal to 92. A value for E^{ref}/S_u of 92 corresponds to the mean value for 57 triaxial tests conducted on lacustrine clay, with a 50% stress level secant value definition being used for E^{ref}. Consolidation test data results show the lacustrine clay to be normally consolidated below the protected side and below the levee. Based on this data, as well as other laboratory and field test data, including interpreted cone data results, the undrained shear strength at the top of the lacustrine clay layer is defined in terms of an S_u/σ_v' equal to 0.24. The value of S_u at any point along the top of the lacustrine clay layer is equal to 0.24 times the effective overburden pressure. At the top of the lacustrine clay layer on the protected side, S_u ranges in value from 44 psf beyond the toe of the levee, to 53 psf below the toe of the levee. The value for Su at the top of the lacustrine clay increases from 53 psf below the toe of the levee (on the protected side) to a maximum value of 300 psf below the I-wall, with a distribution for Su that approximately mirrors the shape of the ground surface between these two points (refer to Figure 6-3). The value for Su at the top of the lacustrine clay decreases from a maximum value of 300 psf below the I-wall to a value of 76 psf below the toe of the submerged peat layer on the canal side, with a distribution for Su that mirrors the shape of the ground surface between these two points. At the top of the lacustrine clay layer below the canal, Su is set equal to a value of between 82 and 96 psf. This zone of levee clay is overconsolidated as a result of the removal of overburden during the canal excavation process that has taken place over the years.

There are five rows of soil clusters used to define the lacustrine clay layer (refer to Figure 6-3). Shear strengths for the top row of soil clusters are assigned undrained shear strength values using the data discussed in the previous paragraph and based on its center x-coordinate. Interpretation of cone test results shows an increase in undrained shear strength with depth equal to 11 psf per ft depth. Undrained shear strengths for the lower four rows of lacustrine clay are assigned based on the value for Su at the top of the lacustrine clay, plus the product of 11 psf per ft depth times the vertical distance between cluster center and the top of the lacustrine clay layer.

For the Plaxis nonlinear Hardening Soil (HS) model, the parameters $(E^{ref})_{50}$ and $(E^{ref})_{oed}$ are set equal to $[E^{ref}/S_u$ times $S_u]$ for each soil cluster. Additional HS parameters assigned are reference stress for stiffness, p_{ref}, equal to 2,116 psf, failure ratio $R_f = 0.9$, and the exponent m = 1. For unload reload HS parameters, $(E^{ref})_{ur}$ is set equal to 3 times $(E^{ref})_{50}$ and ν_{ur} equals 0.2. For

Hoesch 12 steel sheet piles to lacustrine clay interface, $R_{interface}$ is set equal to 0.8. $R_{interface}$ is set equal to 1.0 for all soil-to-soil interfaces.

Beach sand: A total unit weight of 120 pcf is assigned to the beach sand soil clusters. Standard Penetration Test results in this layer indicate an average value of 21 blows per ft depth for 60% of free-fall energy (i.e., $N_{60} = 21$). Correcting these results to an effective overburden pressure of 1 ton/ft^2 results in $(N_1)_{60}$ equal to 25 blows per ft depth. For a fine sand with $(N_1)_{60} = 25$, the relative density (D_r) is 63% by Skemption's (1986) correlation. For fine sand with a D_r of 63%, the effective angle of internal friction is equal to 36 degrees by Schmertman's (1978) correlation. For $N_{60} = 21$ and using the Kulhawy and Mayne (1990) equation, 5-26b, the value of Young's modulus E^{ref} is set equal to 477,725 psf.

For the Plaxis nonlinear Hardening Soil (HS) model, the parameters $(E^{ref})_{50}$ and $(E^{ref})_{oed}$ are set equal to 477,725 psf. Additional HS parameters assigned are reference stress for stiffness, p_{ref}, equal to 2,116 psf, failure ratio $R_f = 0.9$, and the exponent m = 0.5. For unload reload HS parameters, $(E^{ref})_{ur}$ is set equal to 3 times $(E^{ref})_{50}$, and ν_{ur} equals 0.2. For Hoesch 12 steel sheet piles to beach sand, the interface strength parameter, $R_{interface}$, is set equal to 0.8.

Bay Sound clay: A total unit weight of 102 pcf is assigned to the Bay Sound clay soil cluster. Stress-strain data for Bay Sound clay specimens tested in an undrained shearing (mode) to failure in laboratory triaxial tests leads to the assignment of a value for Young's modulus, E^{ref}, expressed in terms of (E^{ref}) normalized by S_u and equal to 68. A value for E^{ref}/S_u of 68 corresponds to the mean value for 54 triaxial tests conducted on Bay Sound clay, with a 50% stress level secant value definition being used for E^{ref}. Based on this and other shear strength test data, the undrained shear strength (S_u) is set equal to 779 psf for the Bay Sound clay (average value).

For the Plaxis nonlinear Hardening Soil (HS) model, the parameters $(E^{ref})_{50}$ and $(E^{ref})_{oed}$ are set equal to $[E^{ref}/S_u$ times $S_u]$. Additional HS parameters assigned are reference stress for stiffness, p_{ref}, equal to 2,116 psf, failure ratio $R_f = 0.9$, and the exponent m = 1.0. For unload reload HS parameters, $(E^{ref})_{ur}$ is set equal to 3 times $(E^{ref})_{50}$, and ν_{ur} equals 0.2.

Floodwall: The floodwall comprises an exposed reinforced concrete I-wall, a reinforced concrete cap, and Hoesch 12 hot-rolled sheet pile. The 12-in.-thick reinforced concrete I-wall extends from the top of protected levee (El 5) to El 12.5. At Station 10+00, the sheet pile tip is at El -18.5. The upper reach of pile is encased in a 2-ft-thick reinforced concrete cap, extending below the surface of the protected side of the levee. Linear-elastic material response was assumed in the complete SSI analysis. Engineering properties for the I-wall, cap, and sheet pile are summarized in Table 6-3 for the zero thickness plate elements used in the finite-element model.

Table 6-3
Material Characterization for the Floodwall

Identification	EA [lb/ft]	EI [lbft²/ft]	Weight [lb/ft/ft]	v [-]
Reinforced Concrete I-wall	4.32E8	3.6E7	150.00	0.20
Reinforced Concrete Cap	8.64E8	2.88E8	190.00	0.20
Sheet Pile (Hoesch 12)	1.88E8	1.83E7	17.64	0.30

Complete Soil-Structure Interaction Analysis

Introduction: A complete SSI analysis of the Figure 6-1 2-D cross section of Station 10+00 at the 17th Street Canal from canal water at El 1.0, on through a series of incremental 0.5- to 1-ft raises in canal elevation to model flood loading is conducted in a staged analysis using Plaxis. Table 6-4 summarizes the calculation phases of the analysis. More than 25 phases of calculations are used in the complete SSI analysis.

Table 6-4
Calculation Phases of the Nonlinear Finite-Element Analysis

Phase	Phase No.	Calculation type	Load input
Initial Phase	0		-
Place Wall & Interface	1	Plastic analysis	Staged construction
Gravity (0.15)	2	Plastic analysis	Total multipliers
Water Table El -11.5	3	Plastic analysis	Staged construction
Gravity (0.3)	4	Plastic analysis	Total multipliers
Water Table El -8	5	Plastic analysis	Staged construction
Gravity (0.45)	6	Plastic analysis	Total multipliers
Water Table El -5.0	7	Plastic analysis	Staged construction
Gravity (0.60)	8	Plastic analysis	Total multipliers
Water Table El -2.5	9	Plastic analysis	Staged construction
Gravity (0.75)	10	Plastic analysis	Total multipliers
Water Table 0.0	11	Plastic analysis	Staged construction
Gravity (1.0)	12	Plastic analysis	Total multipliers
Water Table El +1	13	Plastic analysis	Staged construction
Canal Water El +1.5	14	Plastic analysis	Staged construction
Canal Water El +2.5	15	Plastic analysis	Staged construction
Canal Water El +3.5	16	Plastic analysis	Staged construction
Canal Water El +4.5	17	Plastic analysis	Staged construction
Canal Water El +5.5	18	Plastic analysis	Staged construction
Canal Water El +6.5	19	Plastic analysis	Staged construction
Crack to El -16.5	20	Plastic analysis	Staged construction
Crack to El -18.5	21	Plastic analysis	Staged construction
Canal Water El +7.5	22	Plastic analysis	Staged construction
Canal Water El +8.5	23	Plastic analysis	Staged construction
Canal Water El +9	24	Plastic analysis	Staged construction
Phi-C Reductions	25[+]	Phi/c reduction	Incremental multipliers

Loading phases 0 through 13 are used in the complete SSI analysis to establish the initial total stress state condition existing prior to flooding. Loading phase 13 concludes with canal water at El 1, a steady state water elevation in the canal.

Loading phases 14 through 24 are used in the complete SSI analysis to perform an incremental raise in the canal water to El 9, modeling the flood loading of the levee/I-wall system and the introduction of a crack along the canal-side face of the sheet pile in the levee clay, the peat/marsh, and the 2 ft of lacustrine clay.

The last of the loading phases is used to compute the reserve capacity of the levee/I-wall system for different canal water elevations. This reserve capacity is expressed in terms of a factor of safety and is computed in a series of Plaxis phi/c reduction loading phases.

Initial steady state condition for canal water at EL 1: Loading phases 0 through 13 are used in the complete SSI analysis to establish the initial total stress state within the finite-element mesh with a steady state canal water elevation at El 1. An alternating series of incremental applications of gravity loading followed by incremental raises of the water table is conducted. In the beach sand layer, the water table is established at El -6.33 by analysis phase 5 and is maintained at this elevation in all subsequent computation phases. This elevation is established by piezometric readings taken in the beach sand layer. Load input for gravity loading is specified in Plaxis by means of the total multiplier method, and changes in water table are accomplished by staged construction.

The initial steady-state, total stress condition for the usual canal water elevation of 1 is established by adjusting modulus values for the Mohr-Coulomb soil model until a suitable total stress regime is obtained within the mesh for loading phases 0 through 13. The results from the IPET Task 7 slope stability analyses for this usual canal elevation indicate a stable cross section with an ample factor of safety, i.e., above 1.5. Consequently, an important aspect of the total stress regime achieved within the Figure 6-2 finite-element mesh is that the mobilized shear stress at the strain integration points within the finite-elements contained in the soil clusters shown in this figure be less than the shear strength of the soil. The resulting computed fraction of mobilized shear strength (referred to as relative shear stress in Plaxis output) from the resulting initial total stress condition is shown in Figure 6-4. The fraction of mobilized shear strength is less than or equal to 0.95 at the stress integration points for the five soil types.
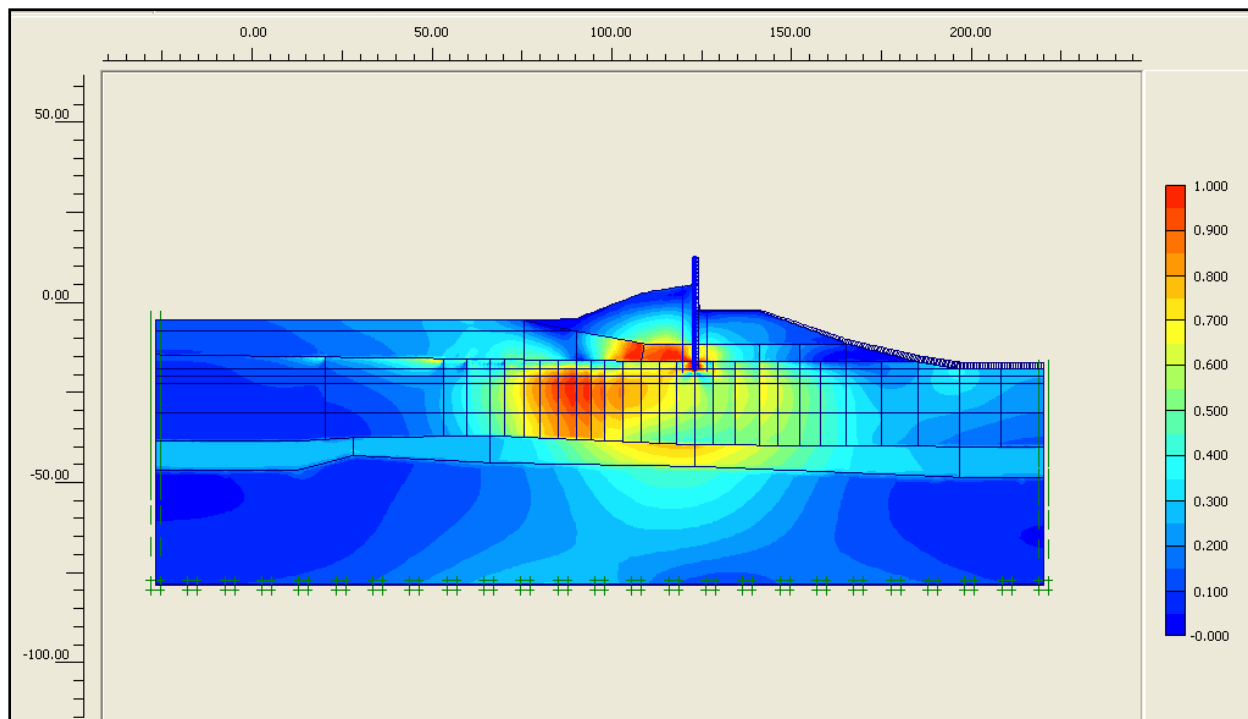
Figure 6-4. Fraction of Mobilized Shear Strength for Canal El 1

Flood loading: Modeling of flood loading commenced in the complete SSI analysis after the total initial stress state is established within the finite element mesh for steady state canal elevation (i.e., El 1). The hardening soil model with the Table 6-2 material property values is assigned to each of the five types of soil regimes. Loading phases 14 through 24 are used in the complete SSI analysis to perform an incremental raise in the canal water to El 9, modeling the flood loading of the levee/I-wall system. Load input for changes in canal water elevation is specified by staged construction.

Canal El 1.5: The first increment in flood loading, designated loading phase 14, corresponds to a 0.5-ft increase in canal water, i.e., from canal steady state El 1 to El 1.5. Hydrostatic canal water pressures are applied as boundary water pressures normal to the wetted side of the I-wall and normal to the wetted exposed face of the levee and clays below the canal. The deformed mesh is shown in Figure 6-5. Note that the nodal deformations are increased by a factor of 100 in order to show the deformed mesh relative to its position at a canal water elevation of 1.0 (shown as a blue outline in this figure). The general trend of deformations is downward and towards the protected side due to the boundary water pressure loading applied within the canal. The maximum (relative) displacement within the mesh is 0.028 ft (< 3/8 in.). There is no indication of a fully developed failure mechanism occurring at this flood stage.
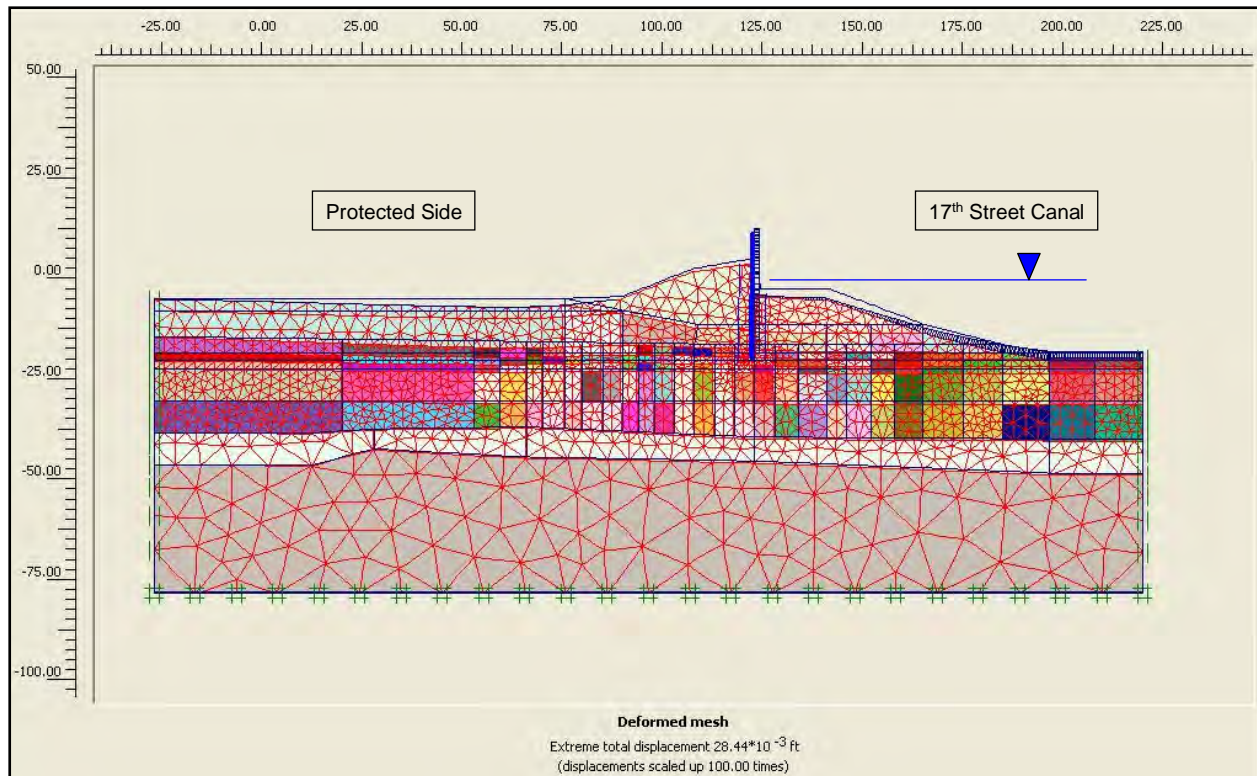
Figure 6-5. Deformed Mesh, Exaggerated by a Factor of 100, for Canal El 1.5 (Note: Canal El not to scale in figure)

The mobilized shear stress at the strain integration points within the finite elements contained in the soil clusters is shown in Figure 6-6 to be less than the shear strength of the soil. The resulting computed fraction of mobilized shear strength is less than or equal to 0.96 at the stress integration points for the five soil types. The horizontal total stress state at the top of the submerged levee berm on the canal side and adjacent to the sheet pile does not indicate that a crack will open at this canal water elevation.
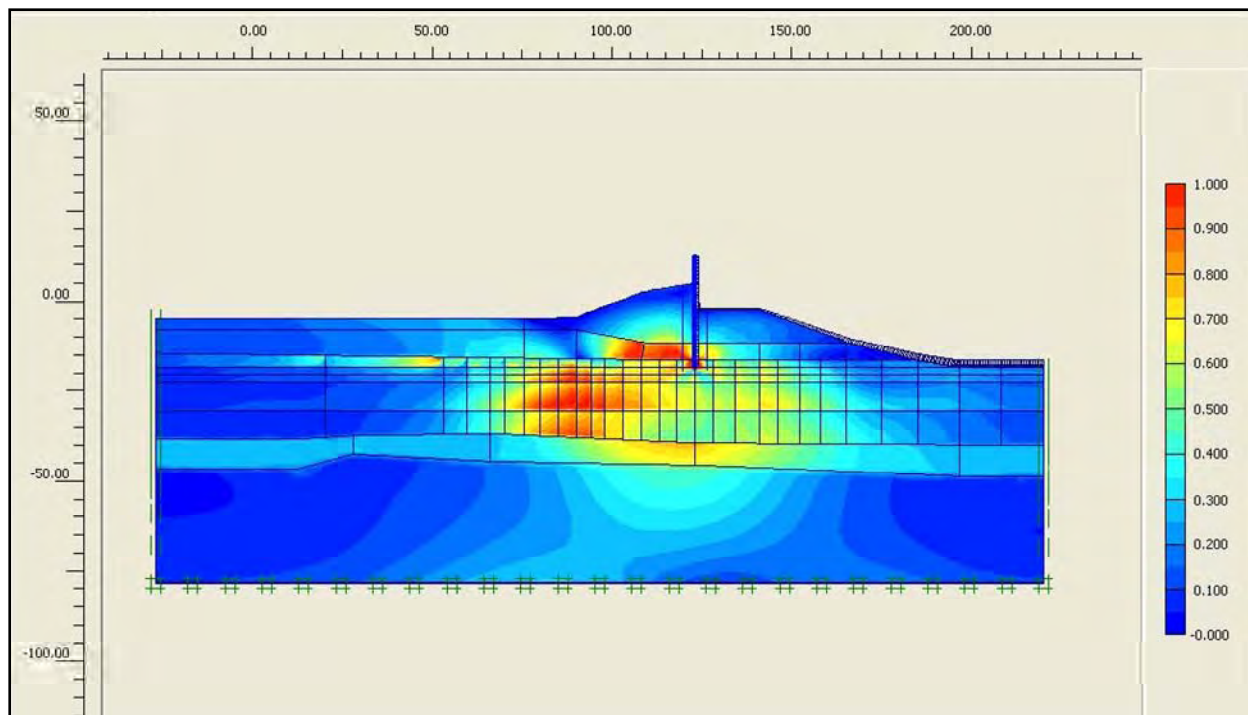
Figure 6-6. Fraction of Mobilized Shear Strength for Canal El 1.5

Canal El 2.5: The second increment in flood loading, designated loading phase 15, raises the canal water to El 2.5. This is a 1.5-ft increase in canal water relative to canal steady state El 1 or, equivalently, a 1-ft increase in canal flood water elevation from canal El 1.5 of loading phase 14. The loading applied to the mesh is again solely due to hydrostatic canal water pressures applied as boundary water pressures normal to the wetted side of the I-wall and normal to the wetted exposed face of the levee and clays forming the sides and base of the canal. The deformed mesh is shown in Figure 6-7. Note that the nodal deformations are increased by a factor of 50 in order to show the deformed mesh relative to its position at a canal water elevation of 1.0 (shown as a blue outline in this figure). The general trend of deformations is downward and towards the protected side due to the boundary water pressure loading applied within the canal. The maximum (relative) displacement within the mesh is 0.093 ft (< 1-1/8 in.). There is no indication of a fully developed failure mechanism occurring at this flood stage.
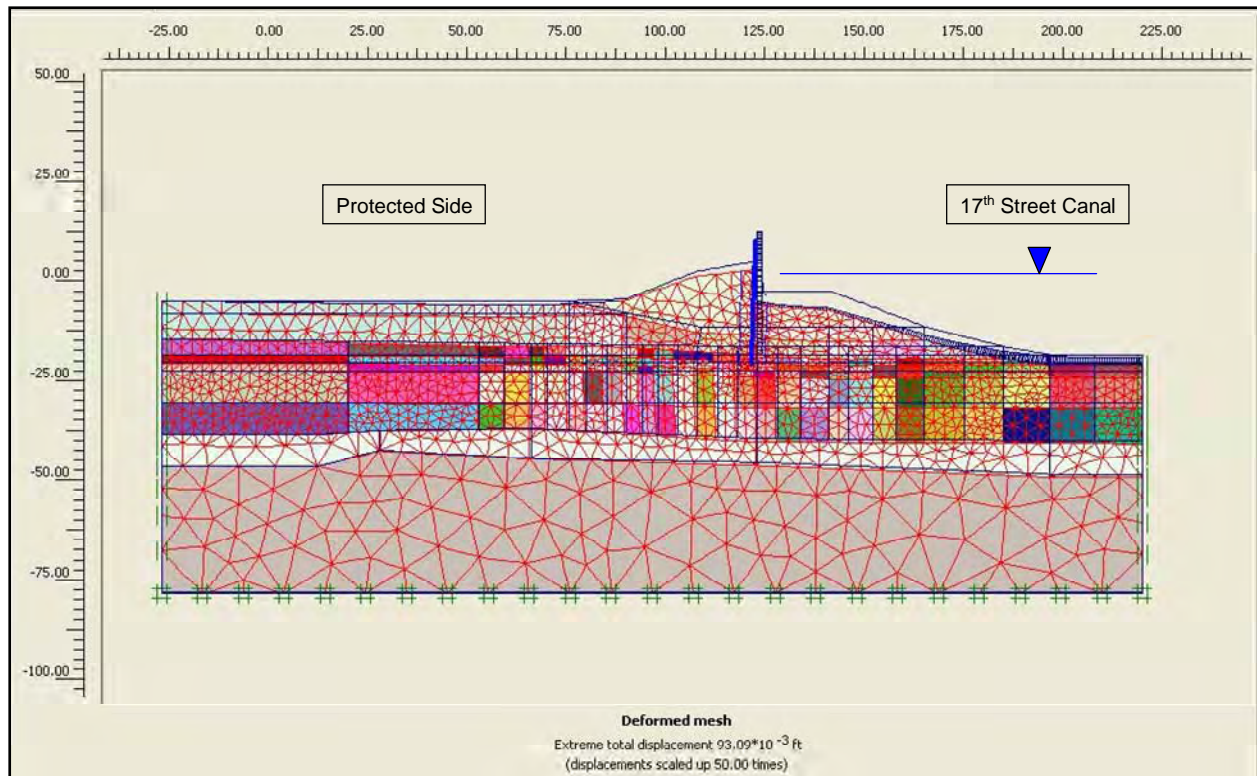
Figure 6-7. Deformed Mesh, Exaggerated by a Factor of 50, for Canal El 2.5 (Note: Canal El not to scale in figure)

The mobilized shear stress at the strain integration points within the finite elements contained in the soil clusters is shown in Figure 6-8 to be less than the shear strength of the soil. The resulting computed fraction of mobilized shear strength is less than or equal to 0.96 at the stress integration points for the five soil types. The horizontal total stress state at the top of the submerged levee berm on the canal side and adjacent to the sheet pile does not indicate that a crack will open at this canal water elevation.
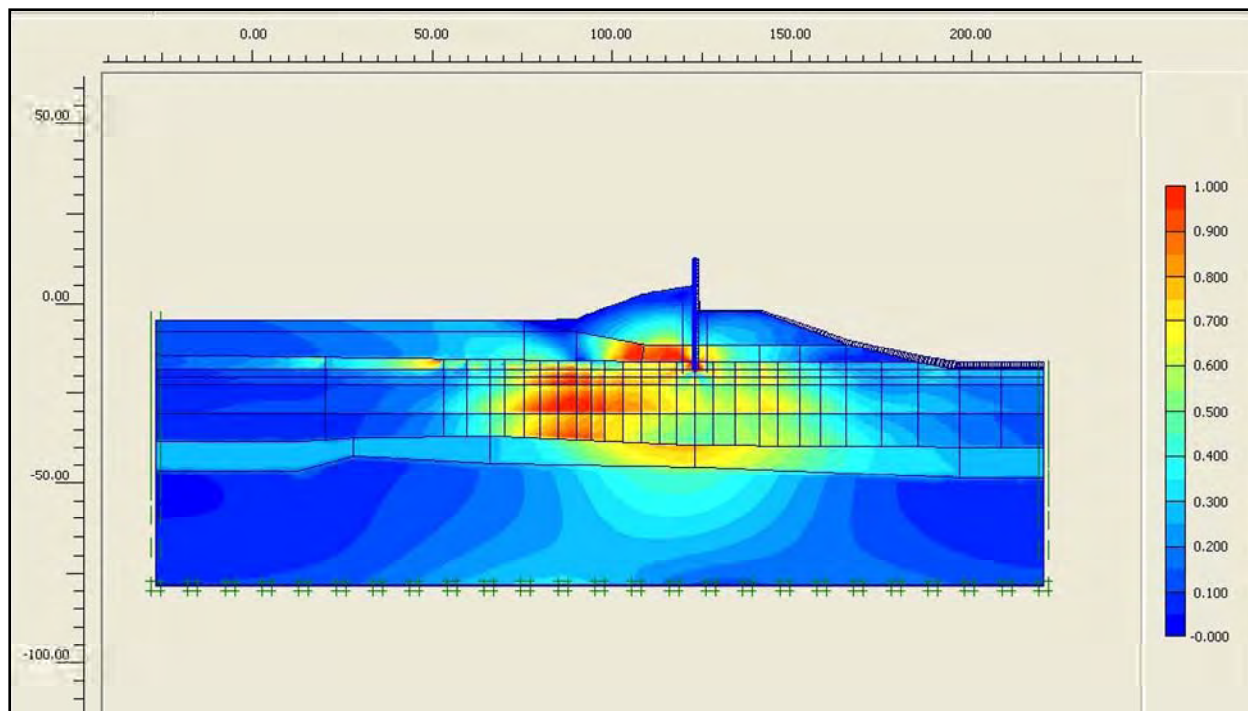
Figure 6-8. Fraction of Mobilized Shear Strength for Canal El 2.5

Canal El 3.5: The third increment in flood loading, designated loading phase 16, raises the canal water to El 3.5. This is a 2.5-ft increase in canal water relative to canal steady state El 1 or, equivalently, a 1-ft increase in canal flood water elevation from canal El 2.5 of loading phase 15. The loading applied to the mesh is again solely due to hydrostatic canal water pressures applied as boundary water pressures normal to the wetted side of the I-wall and normal to the wetted exposed face of the levee and clays forming the sides and base of the canal. The deformed mesh is shown in Figure 6-9. Note that the nodal deformations are increased by a factor of 25 in order to show the deformed mesh relative to its position at a canal water elevation of 1.0 (shown as a blue outline in this figure). The general trend of deformations is downward and towards the protected side due to the boundary water pressure loading applied within the canal. The maximum (relative) displacement within the mesh is 0.176 ft (< 2-1/8 in.). There is no indication of a fully developed failure mechanism occurring at this flood stage.
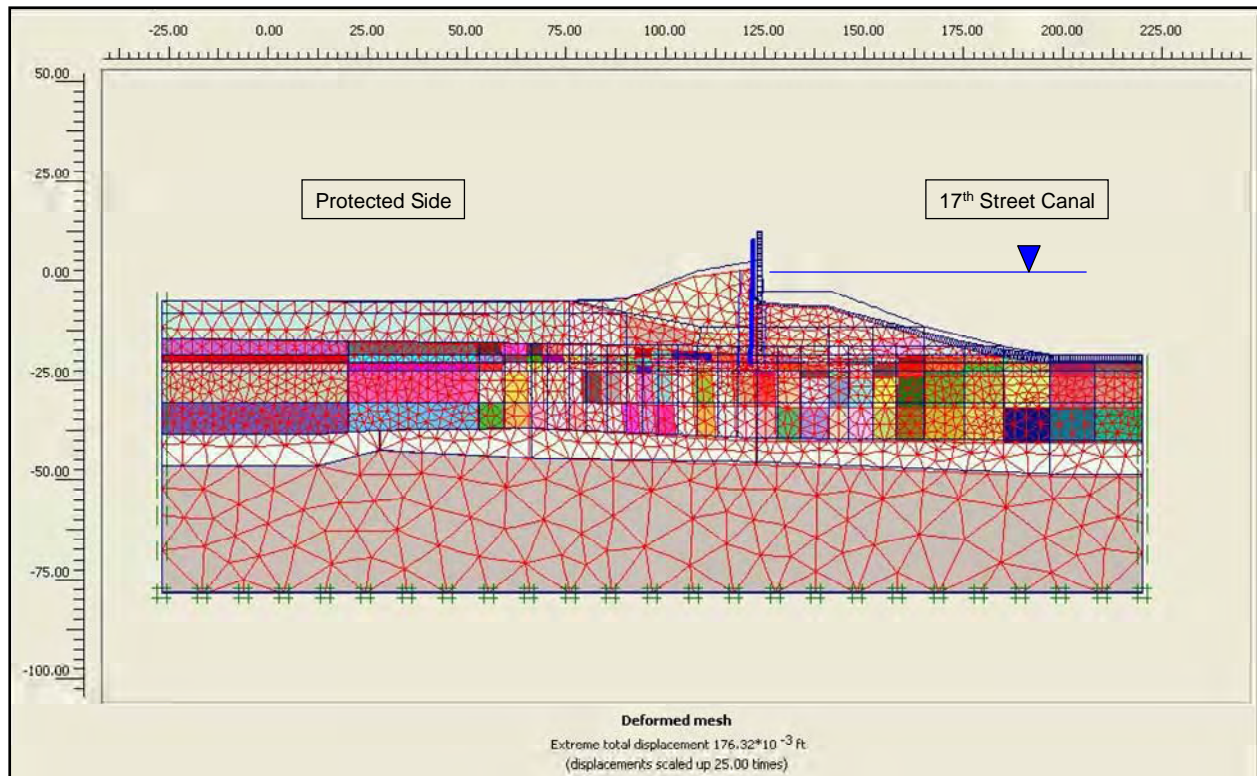
Figure 6-9. Deformed Mesh, Exaggerated by a Factor of 25, for Canal El 3.5 (Note: Canal El not to scale in figure)

The mobilized shear stress at the strain integration points within the finite elements contained in the soil clusters is shown in Figure 6-10 to be less than the shear strength of the soil. The resulting computed fraction of mobilized shear strength is less than or equal to 0.96 at the stress integration points for the five soil types. The horizontal total stress state at the top of the submerged levee berm on the canal side and adjacent to the sheet pile does not indicate that a crack will open at this canal water elevation.
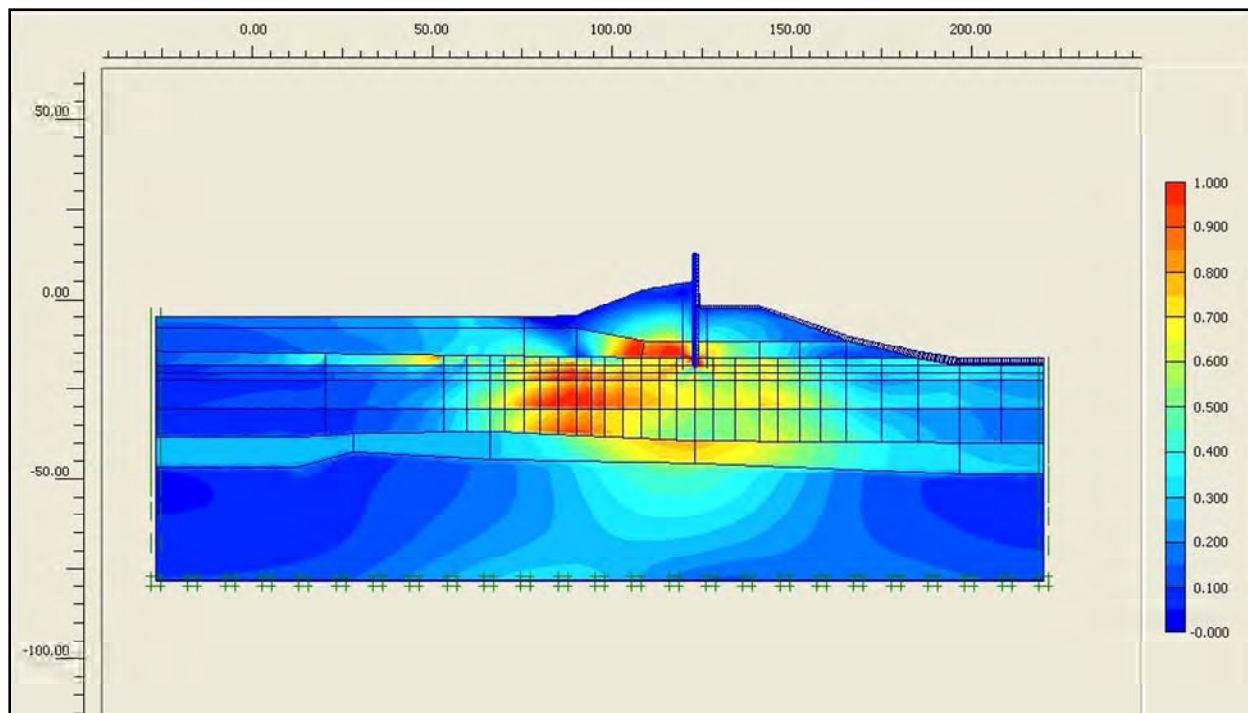
Figure 6-10. Fraction of Mobilized Shear Strength for Canal El 3.5

Canal El 4.5: The fourth increment in flood loading, designated loading phase 17, raises the canal water to El 4.5. This is a 3.5-ft increase in canal water relative to canal steady state El 1 or, equivalently, a 1-ft increase in canal flood water elevation from canal El 3.5 of loading phase 16. The loading applied to the mesh is again solely due to hydrostatic canal water pressures applied as boundary water pressures normal to the wetted side of the I-wall and normal to the wetted exposed face of the levee and clays forming the sides and base of the canal. The deformed mesh is shown in Figure 6-11. Note that the nodal deformations are increased by a factor of 20 in order to show the deformed mesh relative to its position at a canal water elevation of 1.0 (shown as a blue outline in this figure). The general trend of deformations is downward and towards the protected side due to the boundary water pressure loading applied within the canal. The maximum (relative) displacement within the mesh is 0.273 ft (approximately 3-1/4 in.). There is no indication of a fully developed failure mechanism occurring at this flood stage.
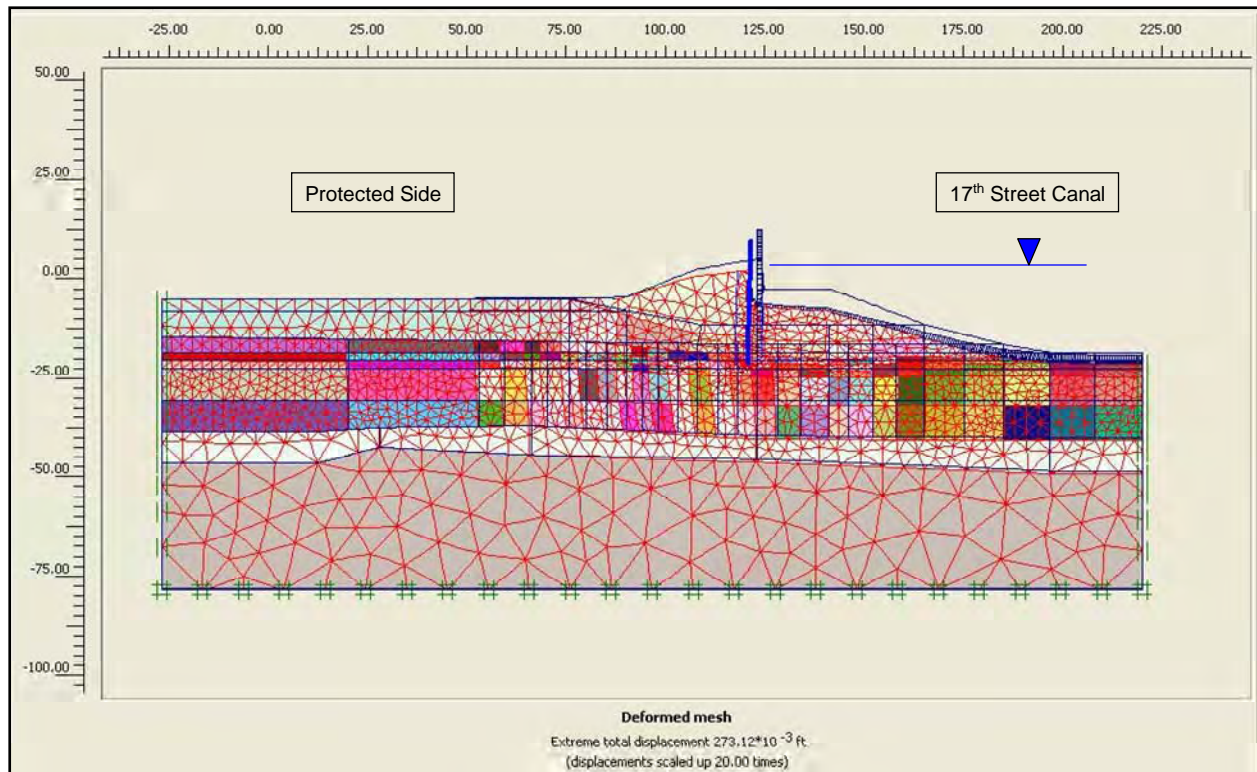
Figure 6-11. Deformed Mesh, Exaggerated by a Factor of 20, for Canal El 4.5 (Note: Canal El not to scale in figure)

The mobilized shear stress at the strain integration points within the finite elements contained in the soil clusters is shown in Figure 6-12 to be less than the shear strength of the soil. The resulting computed fraction of mobilized shear strength is less than or equal to 0.96 at the stress integration points for the five soil types. The horizontal total stress state at the top of the submerged levee berm on the canal side and adjacent to the sheet pile does not indicate that a crack will open at this canal water elevation.
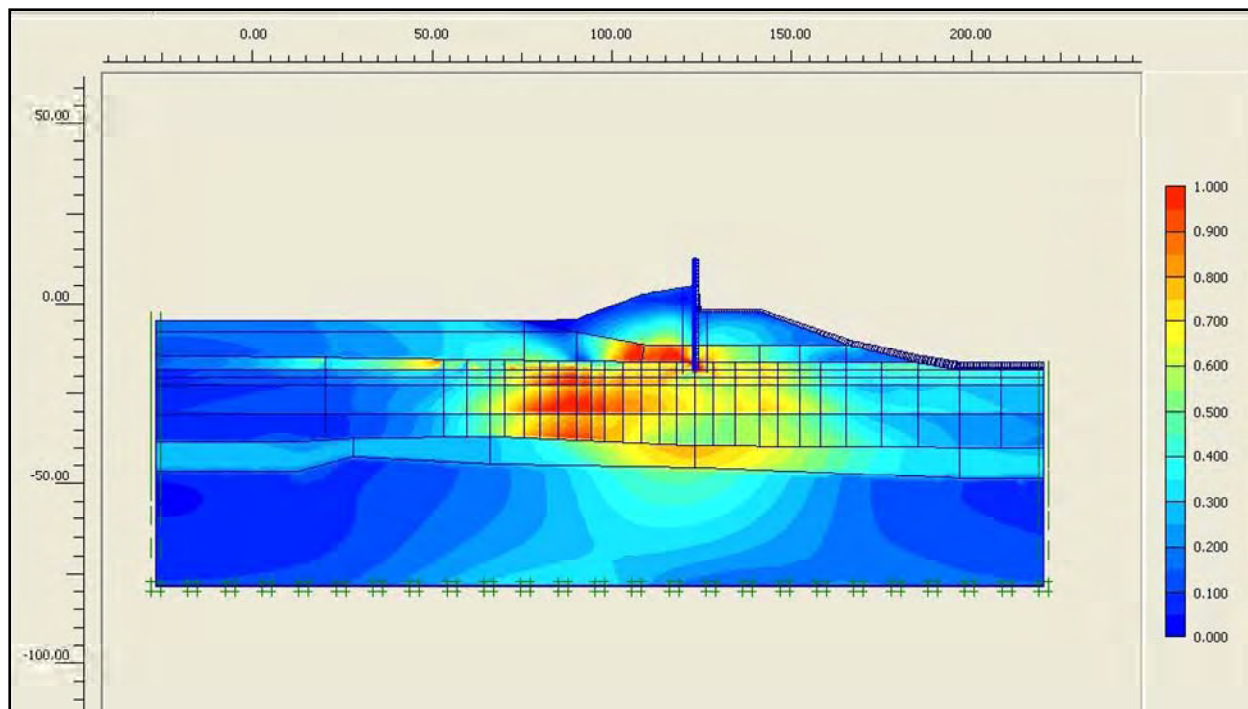
Figure 6-12. Fraction of Mobilized Shear Strength for Canal El 4.5

   Canal El 5.5: The fifth increment in flood loading, designated loading phase 18, raises the canal water to El 5.5. This is a 4.5-ft increase in canal water relative to canal steady state El 1 or, equivalently, a 1-ft increase in canal flood water elevation from canal El 4.5 of loading phase 17. The loading applied to the mesh is again solely due to hydrostatic canal water pressures applied as boundary water pressures normal to the wetted side of the I-wall and normal to the wetted exposed face of the levee and clays, forming the sides and base of the canal. The deformed mesh is shown in Figure 6-13. Note that the nodal deformations are increased by a factor of 13 in order to show the deformed mesh relative to its position at a canal water elevation of 1.0 (shown as a blue outline in this figure). The general trend of deformations is downward and towards the protected side due to the boundary water pressure loading applied within the canal. The maximum (relative) displacement within the mesh is 0.383 ft (< 4-5/8 in.). There is no indication of a fully developed failure mechanism occurring at this flood stage.

Figure 6-13. Deformed Mesh, Exaggerated by a Factor of 13, for Canal El 5.5 (Note: Canal El not to scale in figure)

The mobilized shear stress at the strain integration points within the finite elements contained in the soil clusters is shown in Figure 6-14 to be less than the shear strength of the soil. The resulting computed fraction of mobilized shear strength is less than or equal to 0.96 at the stress integration points for the five soil types. The horizontal total stress state at the top of the submerged levee berm on the canal side and adjacent to the sheet pile does not indicate that a crack will open at this canal water elevation.
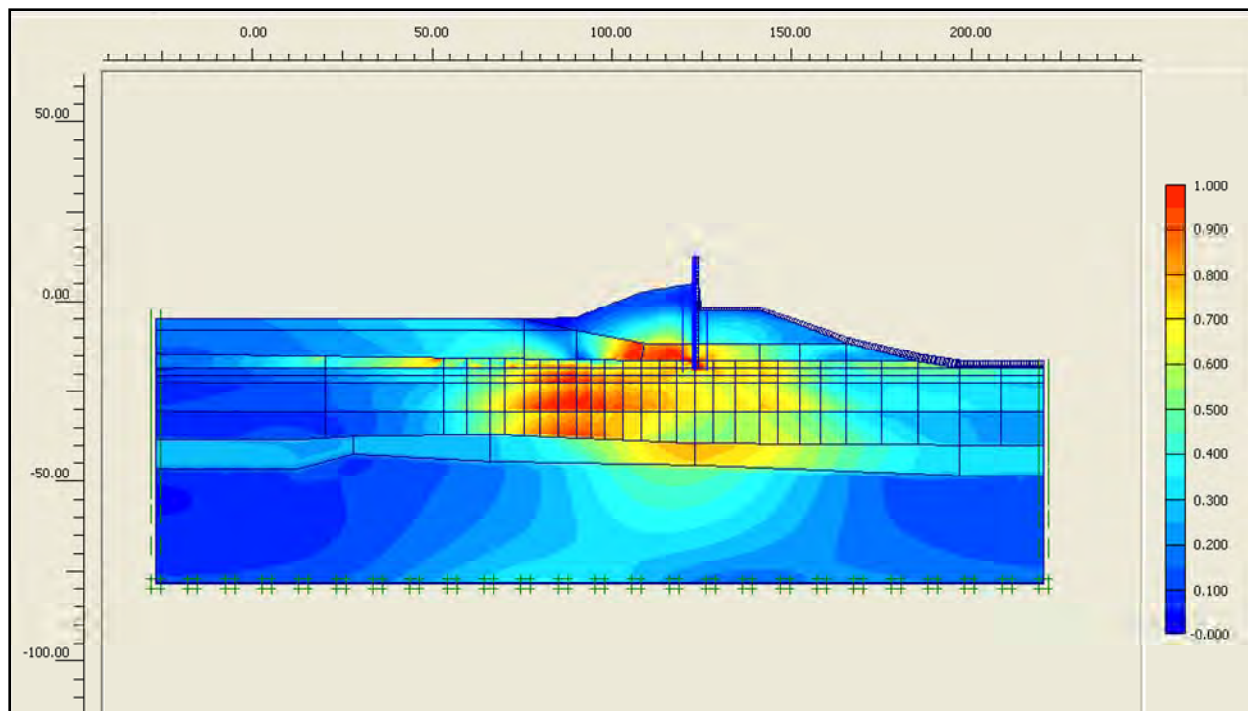
Figure 6-14. Fraction of Mobilized Shear Strength for Canal El 5.5

Canal El 6.5: The sixth increment in flood loading, designated loading phase 19, raises the canal water to El 6.5. This is a 5.5-ft increase in canal water relative to canal steady state El 1 or, equivalently, a 1-ft increase in canal flood water elevation from canal El 5.5 of loading phase 18. The loading applied to the mesh is again solely due to hydrostatic canal water pressures applied as boundary water pressures normal to the wetted side of the I-wall and normal to the wetted exposed face of the levee and clays forming the sides and base of the canal. The deformed mesh is shown in Figure 6-15. Note that the nodal deformations are increased by a factor of 10 in order to show the deformed mesh relative to its position at a canal water elevation of 1.0 (shown as a blue outline in this figure). The general trend of deformations is downward and towards the protected side due to the boundary water pressure loading applied within the canal. The maximum (relative) displacement within the mesh is 0.479 ft (approximately 5-3/4 in.). There is no indication of a fully developed failure mechanism occurring at this flood stage.
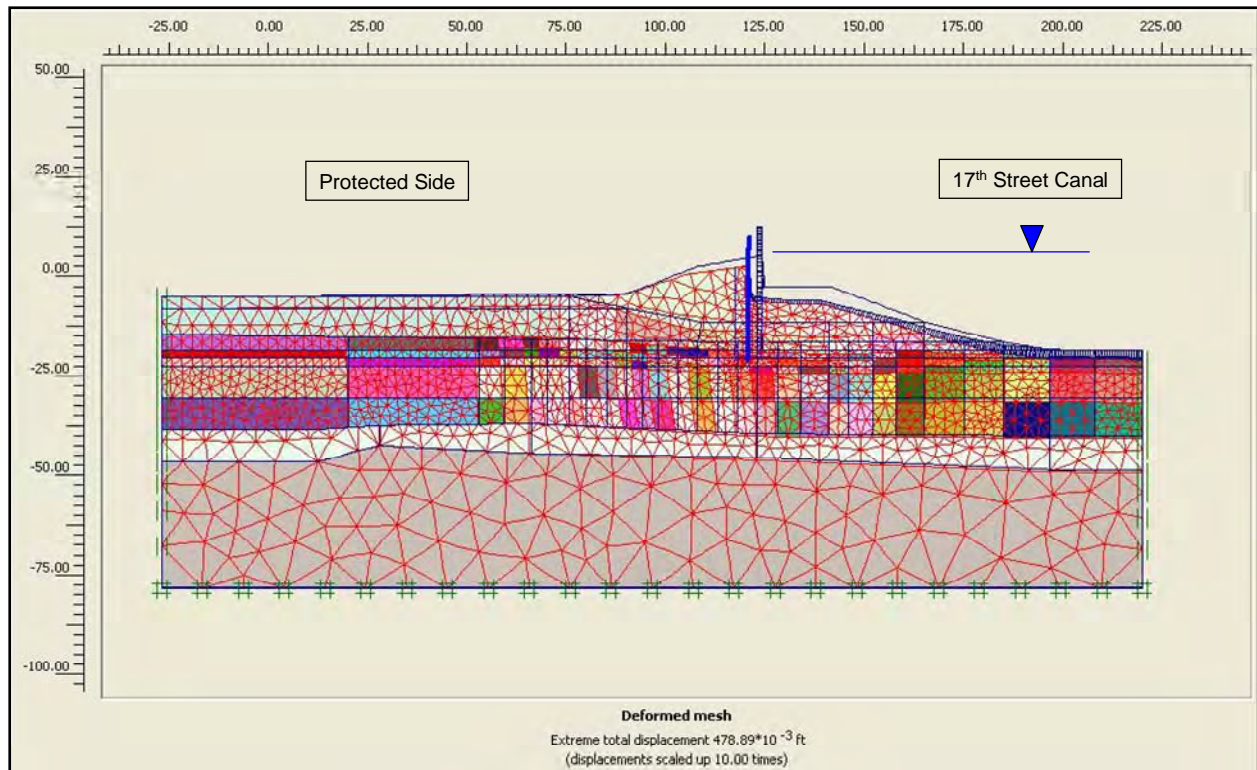
Figure 6-15. Deformed Mesh, Exaggerated by a Factor of 10, for Canal El 6.5 (Note: Canal El not to scale in figure)

The mobilized shear stress at the strain integration points within the finite elements contained in the soil clusters is shown in Figure 6-16 to be less than the shear strength of the soil. The resulting computed fraction of mobilized shear strength is less than or equal to 0.96 at the stress integration points for the five soil types. The horizontal total stress state at the top of the submerged levee berm on the canal side and adjacent to the sheet pile indicates that a crack will open at this canal water elevation.
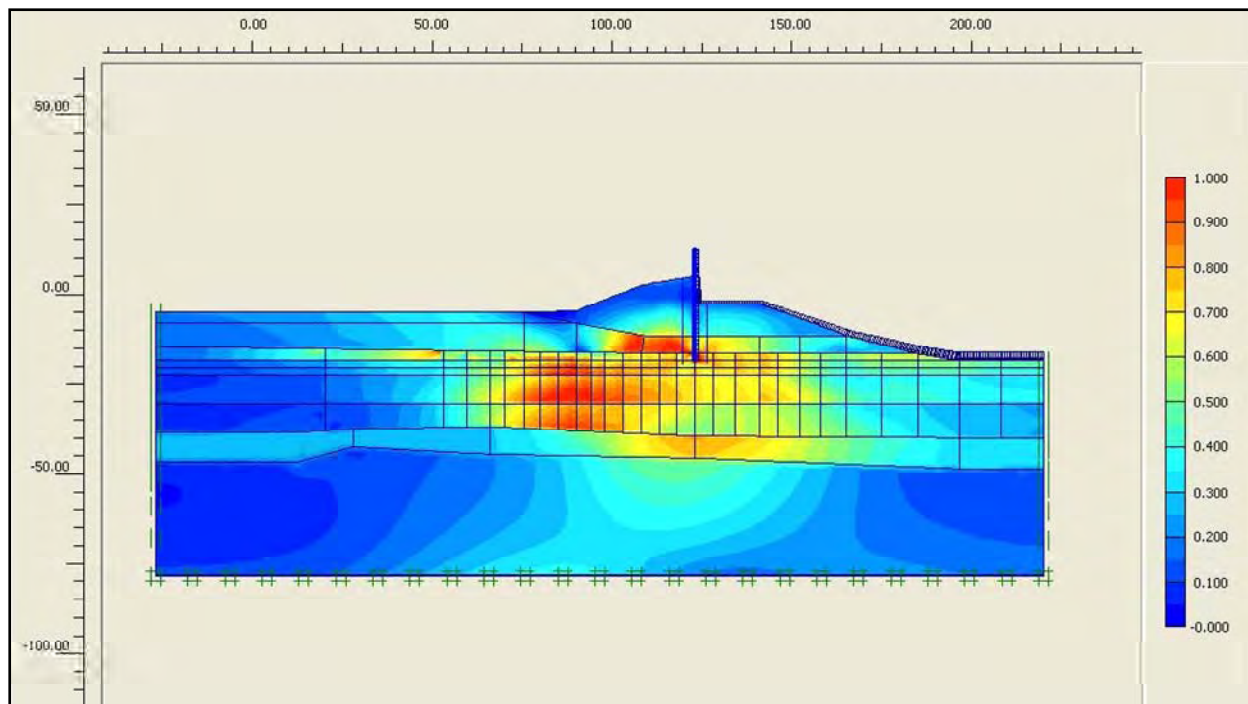
Figure 6-16. Fraction of Mobilized Shear Strength for Canal El 6.5

Crack initiation occurs at the top of the levee clay, on the canal side (at El -2.5) of the sheet pile wall when the total horizontal stress in the clay is less than the value for hydrostatic water pressure (i.e., γ_{water} times depth below canal water surface). This first occurs after raising canal water to El 6.5 (i.e., loading phase 19). Comparisons of values for hydrostatic water pressure, generated by hand computation, with the total horizontal stresses computed in the compete SSI analysis, indicate a crack will extend from El -2.5 down to EL -16.5, the elevation of the peat (or marsh) to lacustrine clay interface. For reference, the levee clay to peat (or marsh) interface is at EL -11.5. A 14-ft-long crack is introduced along the canal side interface of the sheet pile wall in the next loading phase.

Canal El 6.5: In the seventh increment in loading, designated loading phase 20, a crack is introduced at the top of the levee soil (El -2.5) on the canal-side face of the sheet pile. This crack extends from the top of the canal side submerged levee to El -16.5. For reference, the sheet pile tip is at El -18.5. The development of the crack in loading phase 20 is accomplished by means of staged excavation of a narrow (i.e., 1-ft-wide) column of vertical clusters of levee and peat soils along this canal side face of the sheet pile wall to El -16.5. Additionally, loading phase 20 differs from loading phase 19 in that hydrostatic water pressures, corresponding to canal water at El 6.5, are applied to the now exposed canal-side sheet pile face, as well as the now exposed levee clay face that form the sides of the crack in these 1-ft-wide (excavated) vertical soil clusters. The deformed mesh is shown in Figure 6-17. Note that the nodal deformations are increased by a factor of 10 in order to show the deformed mesh relative to its position at a canal water elevation of 1.0 (shown as a blue outline in this figure). The general trend of deformations is downward and towards the protected side due to the boundary water pressure loading applied within the

canal and the crack. The maximum (relative) displacement within the mesh is 0.88 ft (approximately 10.5 in.).


Figure 6-17. Deformed Mesh, Exaggerated by a Factor of 10, for Canal El 6.5 and Crack to El -16.5 (Note: Canal El not to scale in figure)

The mobilized shear stress at the strain integration points within the finite elements contained in the soil clusters is shown in Figure 6-18 to be less than the shear strength of the soil. The resulting computed fraction of mobilized shear strength is less than or equal to 0.96 at the stress integration points for the five soil types. Introduction of the crack to El -16.5, as well as application of hydrostatic water pressures within the crack, results in more of the lacustrine clay being loaded, as indicated by comparison of Figure 6-18 fraction of mobilized shear strength results to the Figure 6-16 pre-crack results.

Figure 6-18. Fraction of Mobilized Shear Strength for Canal El 6.5 and Crack to El -16.5

There is no indication of a fully developed failure mechanism at this flood stage for a crack to El -16.5. However, Figure 6-19 shows four distinct reaches of high shear strains (that may, with additional applied loadings, develop into a complete failure mechanism). Evaluation of the computed horizontal total stress state immediately below the El -16.5 crack tip region on the canal side of the sheet pile indicates that this crack will extend to the sheet pile tip, El -18.5. Consequently, in the next loading phase (21), the crack is extended by means of staged excavation of a narrow cluster of lacustrine clay from El -16.5 to El -18.5 and with hydrostatic water pressures applied along the exposed sheet pile and clay faces that form the sides of the crack.
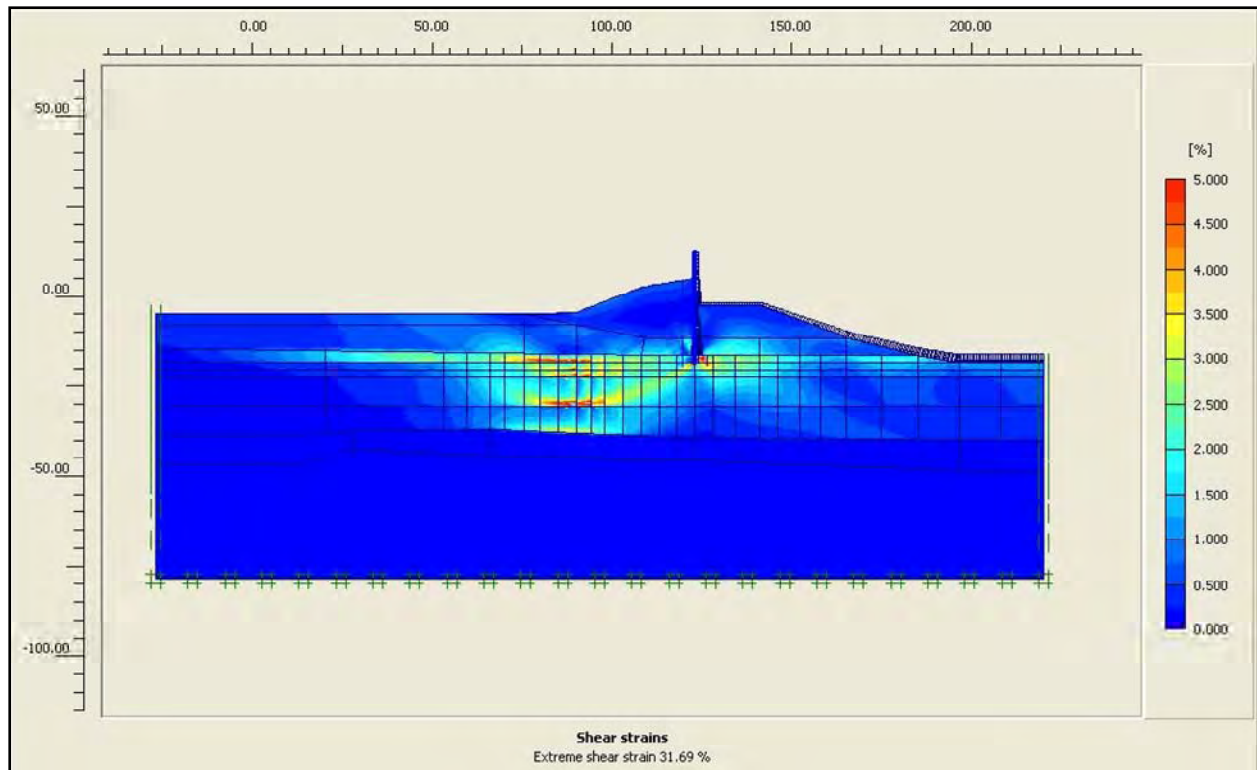
Figure 6-19. Reaches of Large Shear Strains for Canal El 6.5 and Crack to El -16.5

Canal El 6.5: In the eighth increment in loading, designated loading phase 21, the crack is extended to the sheet pile tip (El -18.5) on the canal-side face of the sheet pile. The development of the crack in loading phase 20 is accomplished by means of 2 ft of additional staged excavation of a narrow (i.e., 1-ft wide) column of vertical clusters of lacustrine clay soil along this canal-side face of the sheet pile wall. Additionally, loading phase 21 differs from loading phase 20 in that hydrostatic water pressures, corresponding to canal water at El 6.5, are applied along this additional 2 ft of newly exposed canal-side face of sheet pile, as well as the now exposed 2-ft-high lacustrine clay face that form the sides of this last segment of crack. The deformed mesh is shown in Figure 6-20. Note that the nodal deformations are increased by a factor of 10 in order to show the deformed mesh relative to its position at a canal water elevation of 1.0 (shown as a blue outline in this figure). The general trend of deformations is downward and towards the protected side due to the boundary water pressure loading applied within the canal and the 14-ft-deep crack. The maximum (relative) displacement within the mesh is 0.888 ft (approximately 10-5/8 in.).

Figure 6-20. Deformed Mesh, Exaggerated by a Factor of 10, for Canal El 6.5 and Crack to El -18.5 (Note: Canal El not to scale in figure)

The mobilized shear stress at the strain integration points within the finite elements contained in the soil clusters is shown in Figure 6-18 to be less than the shear strength of the soil. The resulting computed fraction of mobilized shear strength is less than or equal to 0.96 at the stress integration points for the five soil types.
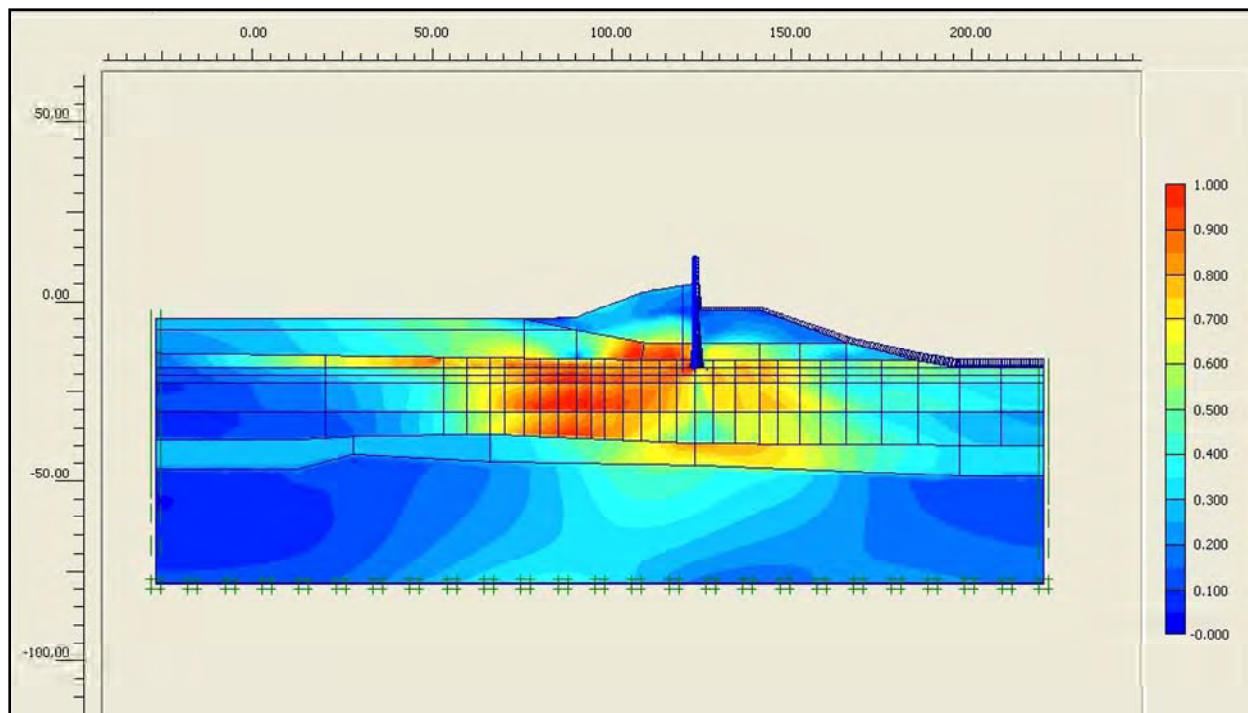
Figure 6-21. Fraction of Mobilized Shear Strength for Canal El 6.5 and Crack to El -18.5

There is no indication of a fully developed failure mechanism at this flood stage for a crack to El -16.5. However, Figure 6-19 shows that at this stage of flood loading, there are four distinct reaches of high shear strains (that may, with additional applied loadings, develop into a complete failure mechanism).

Volume V The Performance – Levees and Floodwalls – Technical Appendix

V-6-27

This is a preliminary report subject to revision; it does not contain final conclusions of the United States Army Corps of Engineers.
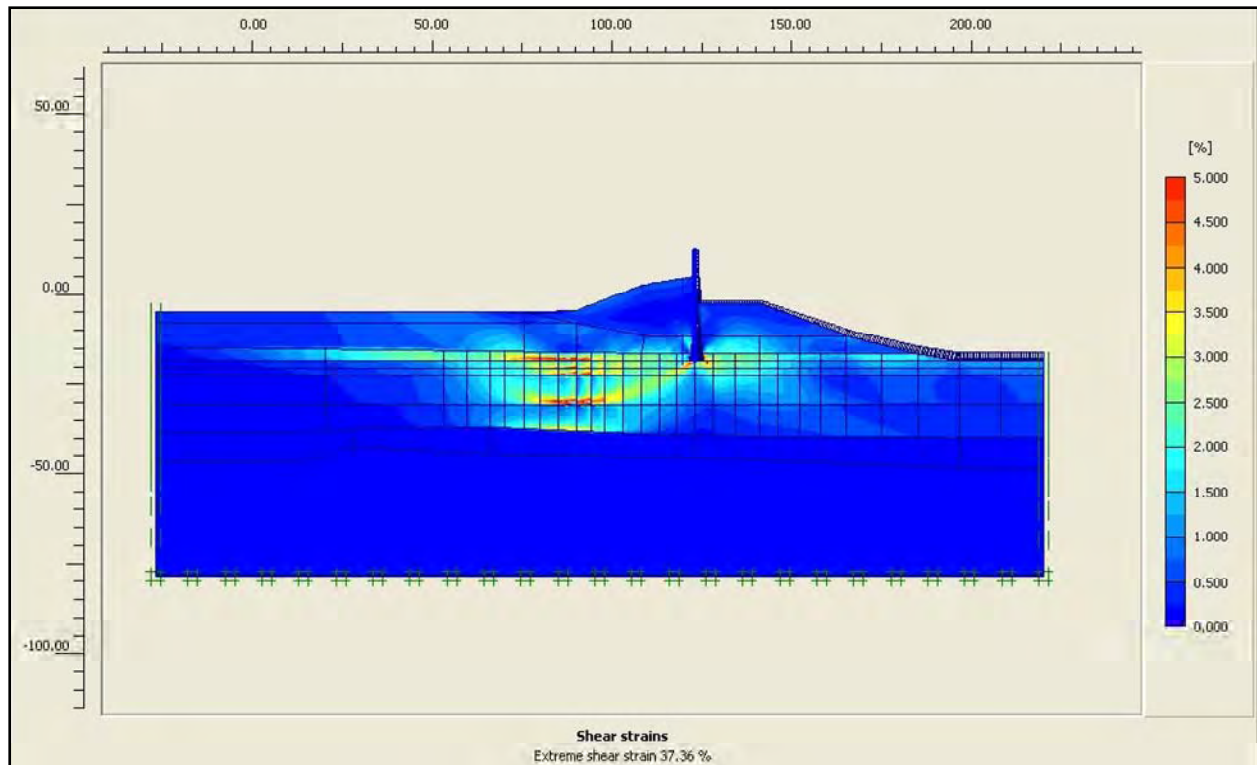
Figure 6-22. Reaches of Large Shear Strains for Canal El 6.5 and Crack to El -18.5

Figure 6-23 shows the horizontal displacements of the soil regions within the mesh, relative to their position at a canal water elevation of 1.0. This figure shows the deformation of the protected side levee, the peat below the levee, and the top layer of the lacustrine clay, all to be moving away from the canal with a displacement of between -0.6 to -0.8 ft under an El 6.5 flood loading and including a full crack. (Note negative Ux values denote movement towards the protected side.)

Figure 6-24 shows the horizontal displacements of three points within the flood wall, relative to its position at a canal water elevation of 1.0. The points monitored through the analyses are at the top of the I-wall, at El 5 (top of levee), and at sheet pile tip (El -18.5). This figure shows that prior to the crack opening at canal water El 6.5, the deformation of the sheet pile is uniformly translational. At canal water El 6.5 and prior to cracking, the flood wall translates towards the protected side by 0.21 ft (2.5 in.). After the crack opens to sheet pile tip and with the flood loading maintained at El -6.5, the horizontal deformation at the top of the I-wall and at the base of the I-wall (El 5) is identical, implying uniform translation of the I-wall by 0.79 ft (9.5 in.). However, the tip of the sheet pile undergoes less than half as much horizontal deformation as the I-wall, 0.44 ft (5-¼ in.).
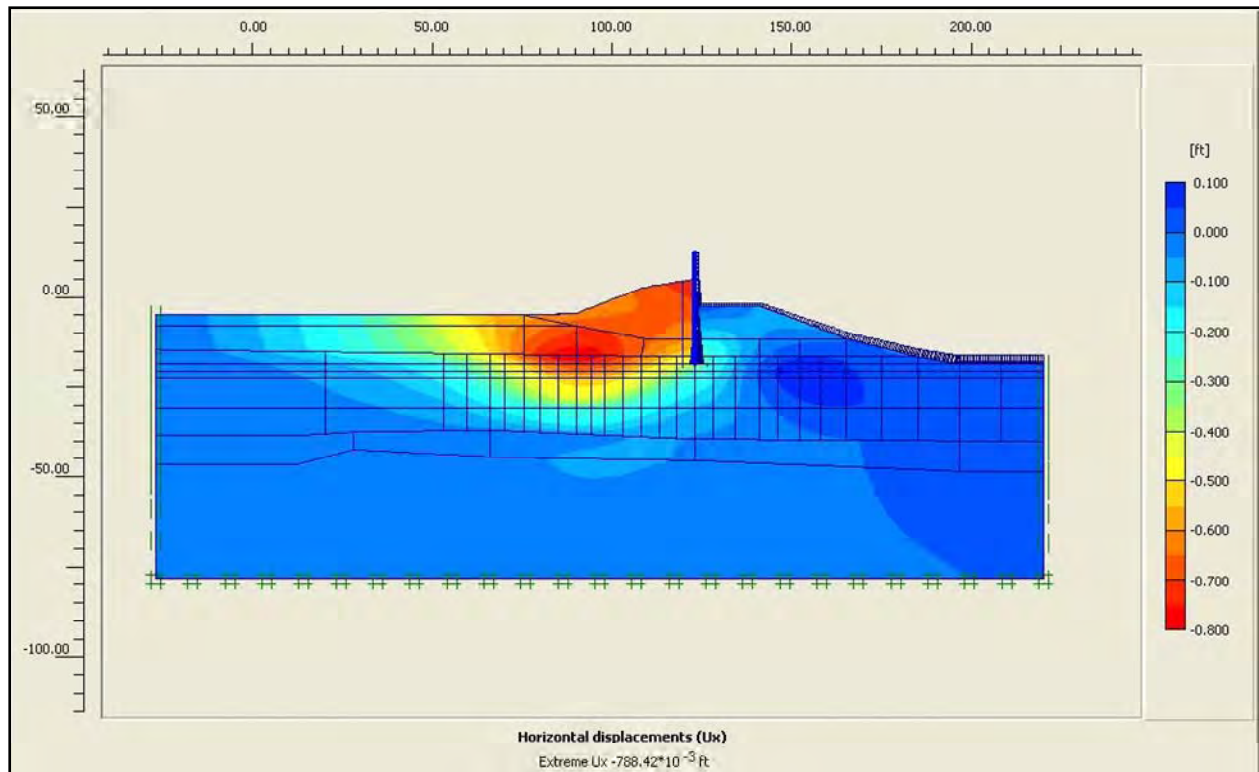
Figure 6-23. Horizontal Deformation Shadings for Canal El 6.5 and Crack to El -18.5
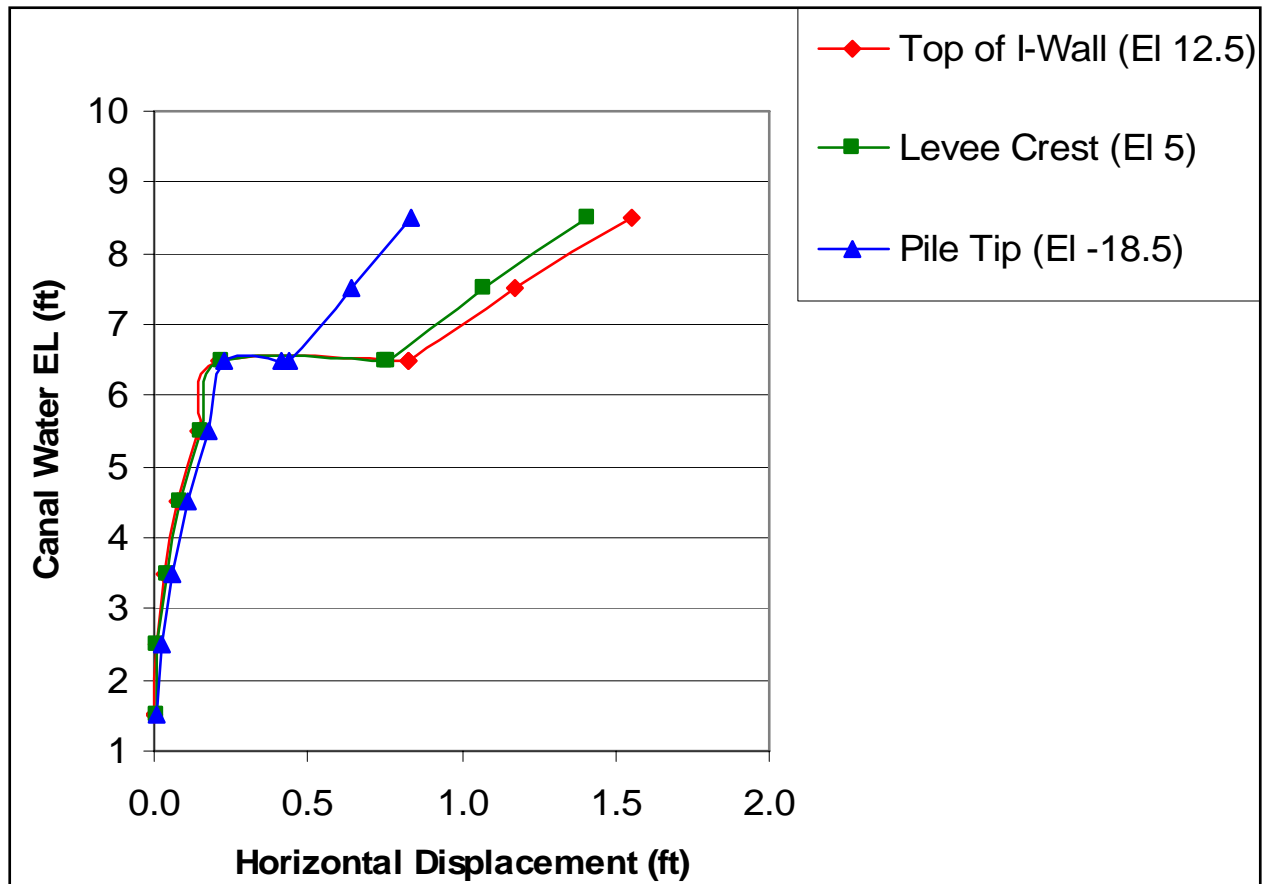
Figure 6-24. Horizontal Sheet Pile Deflections versus Canal Water El

Figure 6-25 shows the vertical displacements of the soil regions within the mesh for canal El 6.5 and with full crack, relative to its position at a canal water elevation of 1.0. This figure shows the deformation tendency of the peat to rise up (i.e., positive displacements) just beyond the toe of the levee on the protected side, and the levee berm to move downwards (i.e., negative displacements).
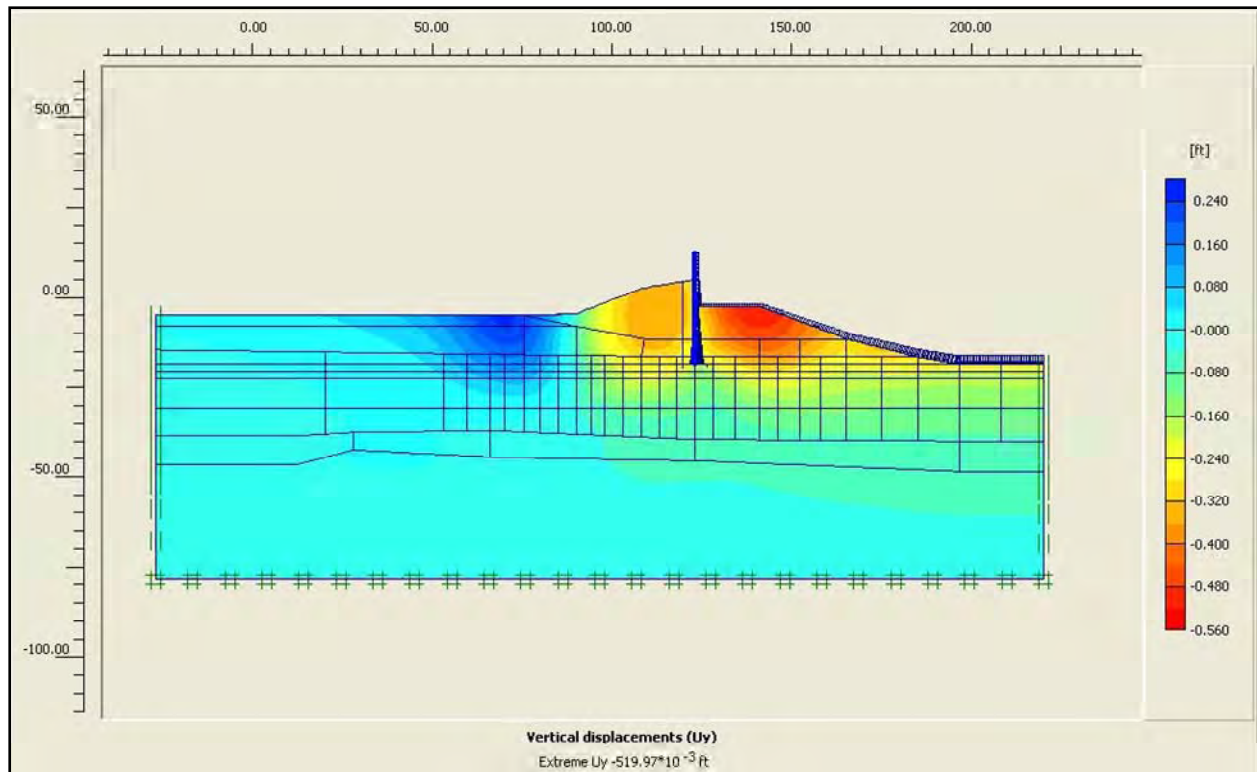
Figure 6-25. Vertical Deformation Shadings for Canal El 6.5 and Crack to El -18.5

Crack propagation concludes with a 16-ft-deep crack extending from the top of the submerged levee berm at El -2.5 to the sheet pile tip. This crack is maintained with subsequent rises in canal water, with water pressures within the crack increased accordingly.

Canal El 7.5: The ninth increment in loading, designated loading phase 22, raises the canal water to El 7.5. This is a 6.5-ft increase in canal water relative to canal steady state El 1 or, equivalently, a 1-ft increase in canal flood water elevation from canal El 6.5 of loading phases 19, 20, and 21. The loading applied to the mesh is again solely due to hydrostatic canal water pressures applied as boundary water pressures normal to the wetted side of the I-wall, normal to the wetted exposed face of the levee and clays forming the sides and base of the canal, and normal to the sheet pile and soil that form the crack. The deformed mesh is shown in Figure 6-26. Note that the nodal deformations are increased by a factor of 8 in order to show the deformed mesh relative to its position at a canal water elevation of 1.0 (shown as a blue outline in this figure). The general trend of deformations is downward and towards the protected side due to the boundary water pressure loading applied within the canal. The maximum (relative) displacement within the mesh is 1.22 ft (approximately 14-5/8 in.). There is no indication of a fully developed failure mechanism occurring at this flood stage.
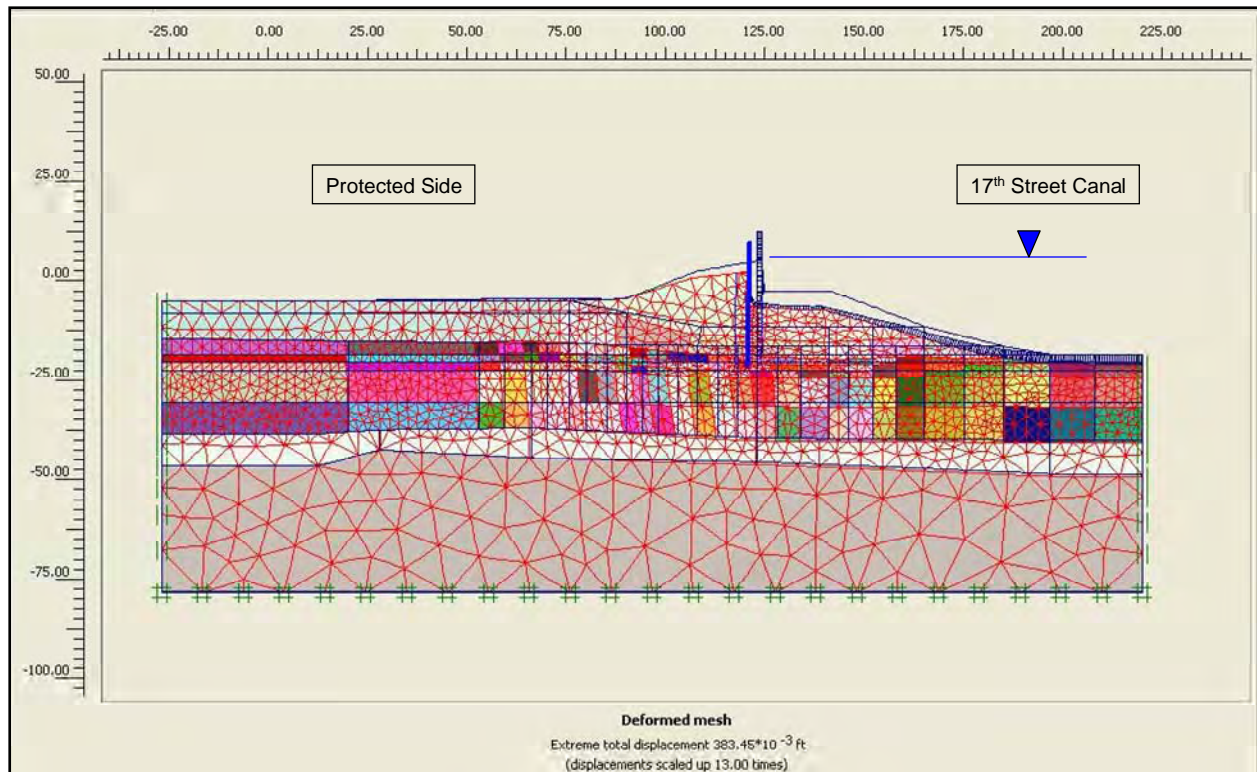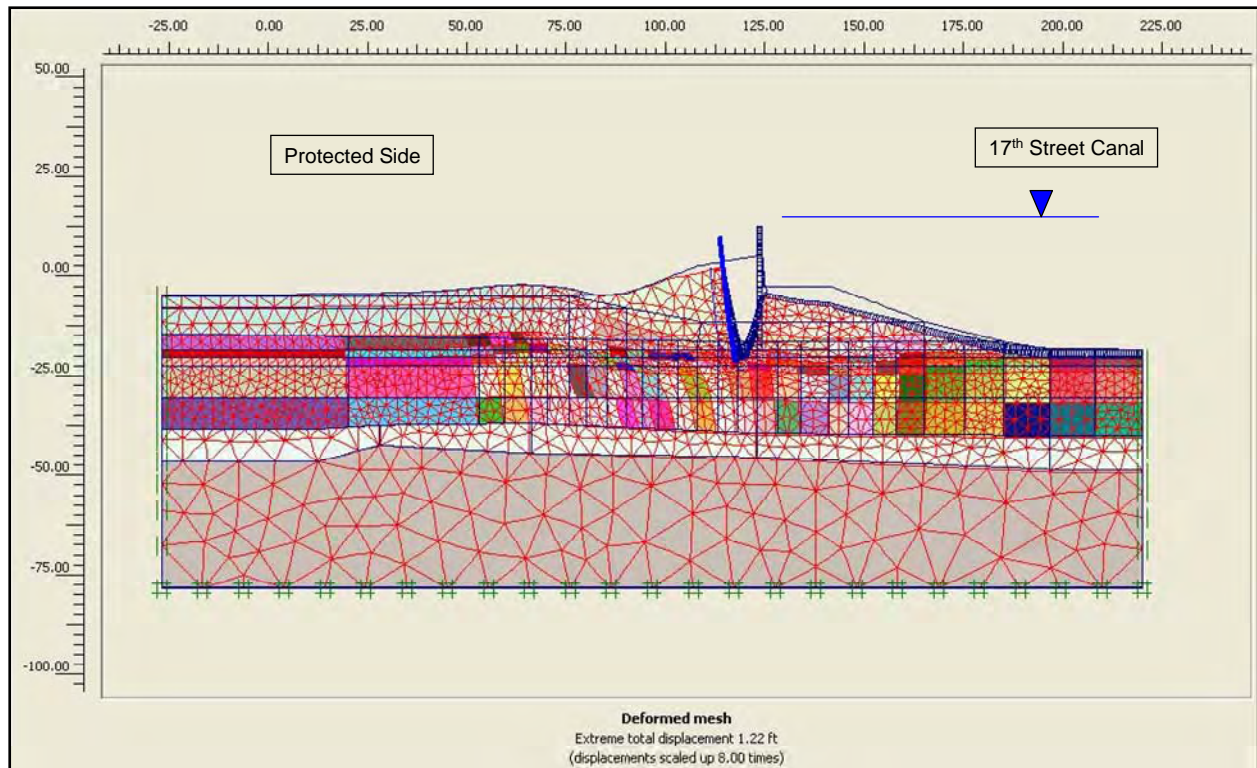
Figure 6-26. Deformed Mesh, Exaggerated by a Factor of 8, for Canal El 7.5 and Crack to El -18.5 (Note: Canal El not to scale in figure)

The mobilized shear stress at the strain integration points within the finite elements contained in the soil clusters is shown in Figure 6-27 to be less than the shear strength of the soil. The resulting computed fraction of mobilized shear strength is less than or equal to 0.96 at the stress integration points for the five soil types.
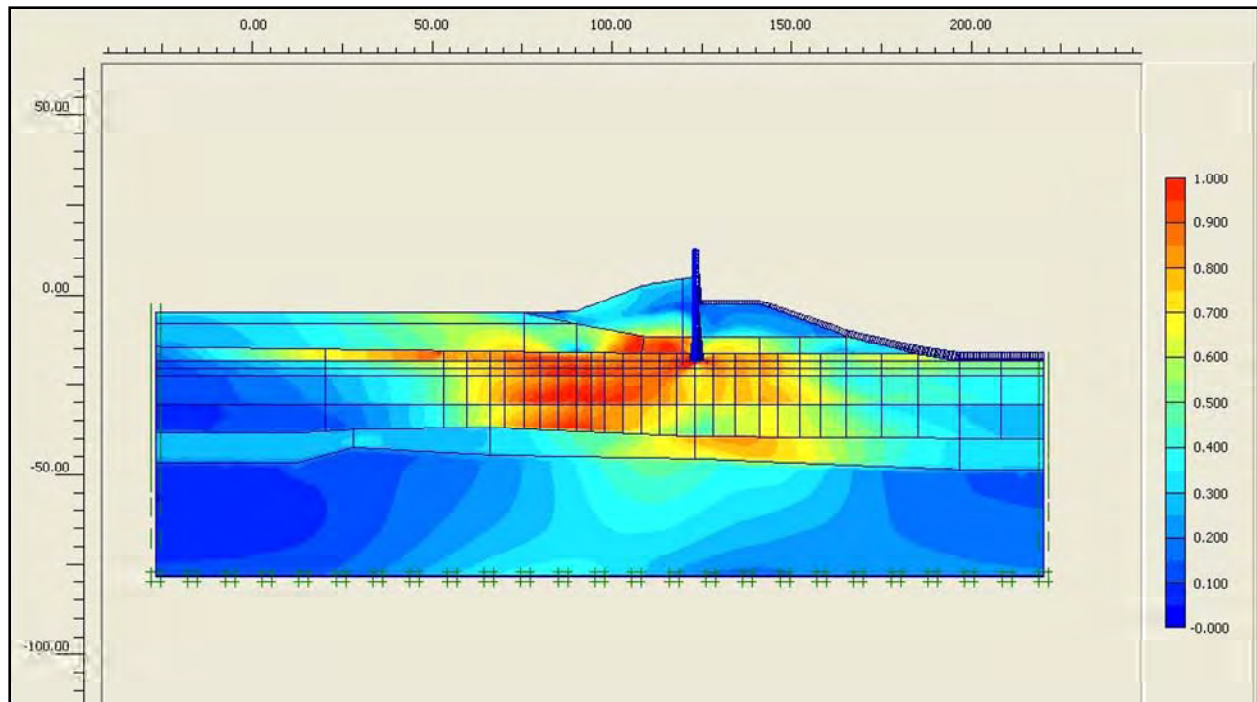
Figure 6-27. Fraction of Mobilized Shear Strength for Canal El 7.5 and Crack to El -18.5

There is no indication of a fully developed failure mechanism at this flood stage for a crack to El -16.5. However, Figure 6-28 shows that at this stage of flood loading, there are four distinct reaches of high shear strains (that may, with additional applied loadings, develop into a complete failure mechanism).
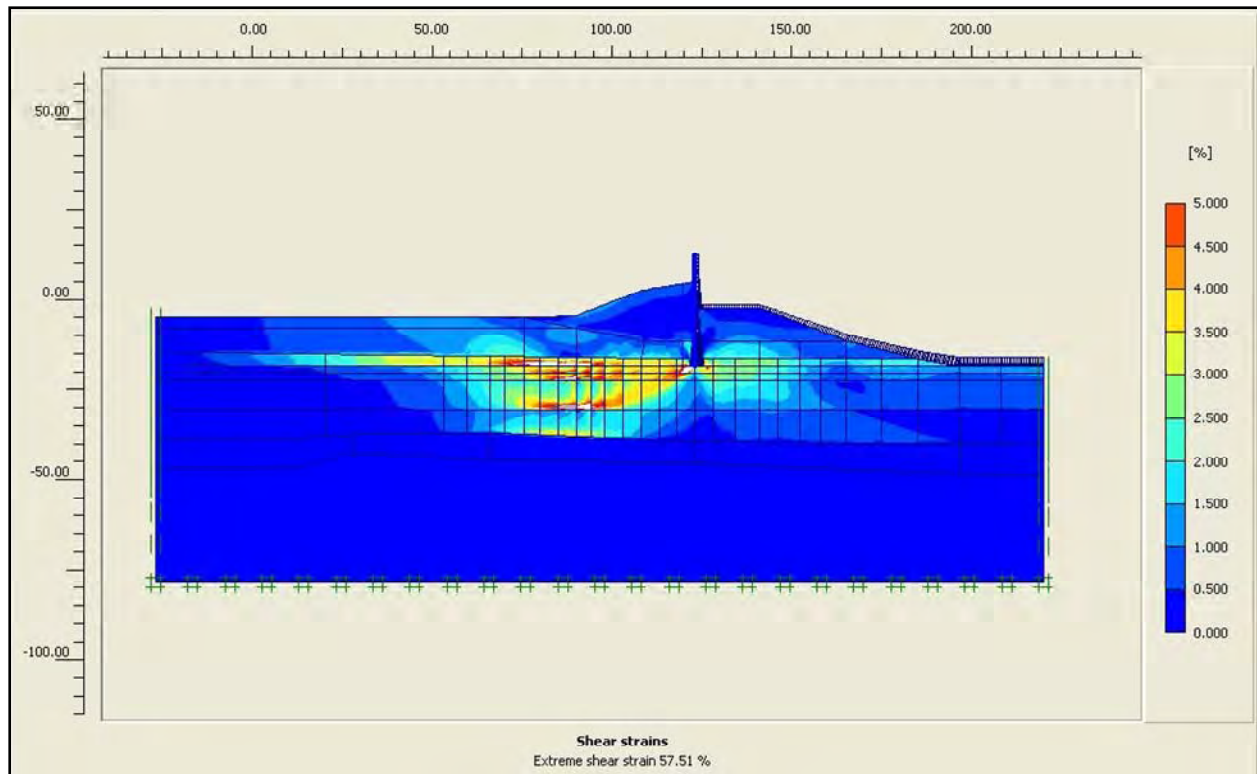
Figure 6-28. Reaches of Large Shear Strains for Canal El 7.5 and Crack to El -18.5

Figure 6-29 shows the horizontal displacements of the soil regions within the mesh, relative to their position at a canal water elevation of 1.0. This figure shows the deformation of the protected side levee, the peat below the levee, and the top layer of the lacustrine clay, all to be moving away from the canal with a displacement of between -0.7 to -1.1 ft under an El 7.5 flood loading and including a full crack.
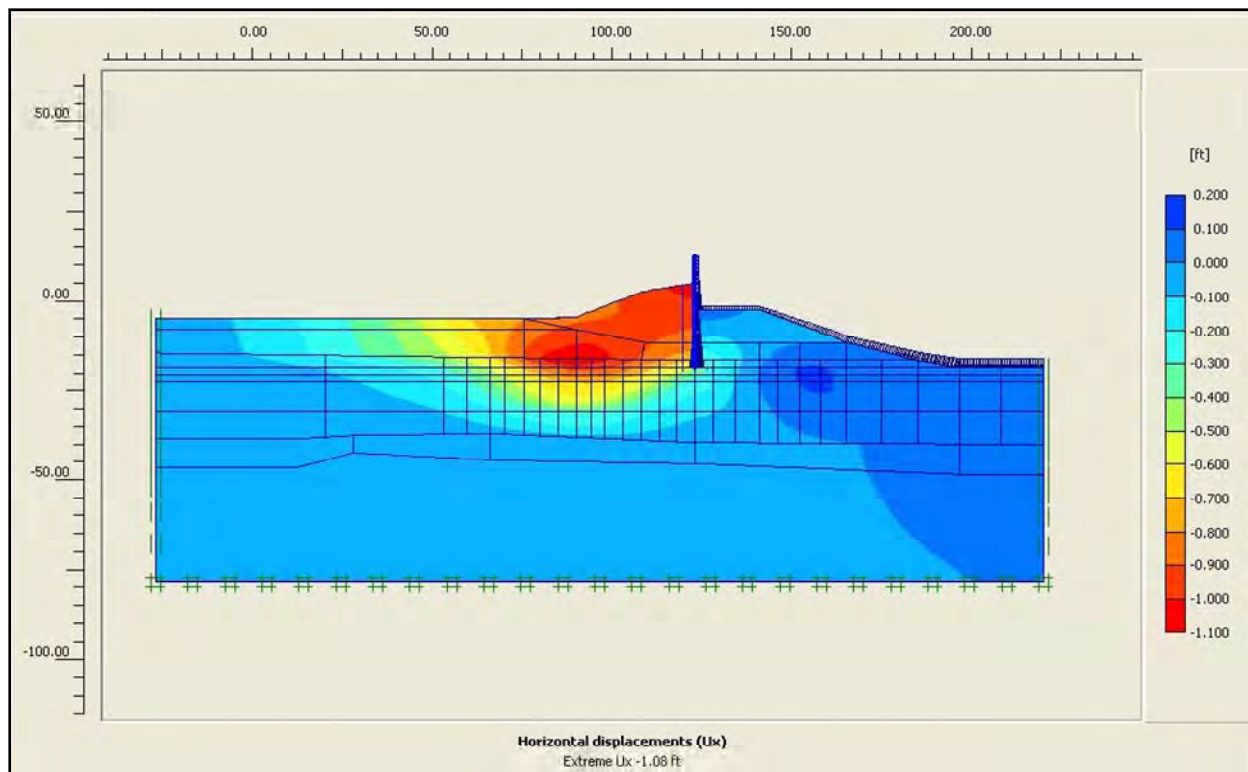
Figure 6-29. Horizontal Deformation Shadings for Canal El 7.5 and Crack to El -18.5

Figure 6-24 shows the horizontal displacements of three points within the floodwall, relative to its position at a canal water elevation of 1.0. The points monitored through the analyses are at the top of the I-wall, at El 5 (top of levee) and at sheet pile tip (El -18.5). With an open crack to sheet pile tip and with the flood loading maintained at El -7.5, the horizontal deformations at the top of the I-wall and at the base of the I-wall (El 5) are nearly identical, 1.17 ft and 1.07 ft. This implies uniform translation of the I-wall. However, the tip of the sheet pile undergoes less than half as much horizontal deformation as the I-wall, 0.64 ft.

Figure 6-30 shows the vertical displacements of the soil regions within the mesh for canal El 7.5 and with full crack, relative to its position at a canal water elevation of 1.0. This figure shows the deformation tendency of the peat to rise up (i.e., positive displacements) just beyond the toe of the levee on the protected side and the levee berm to move downwards (i.e., negative displacements).
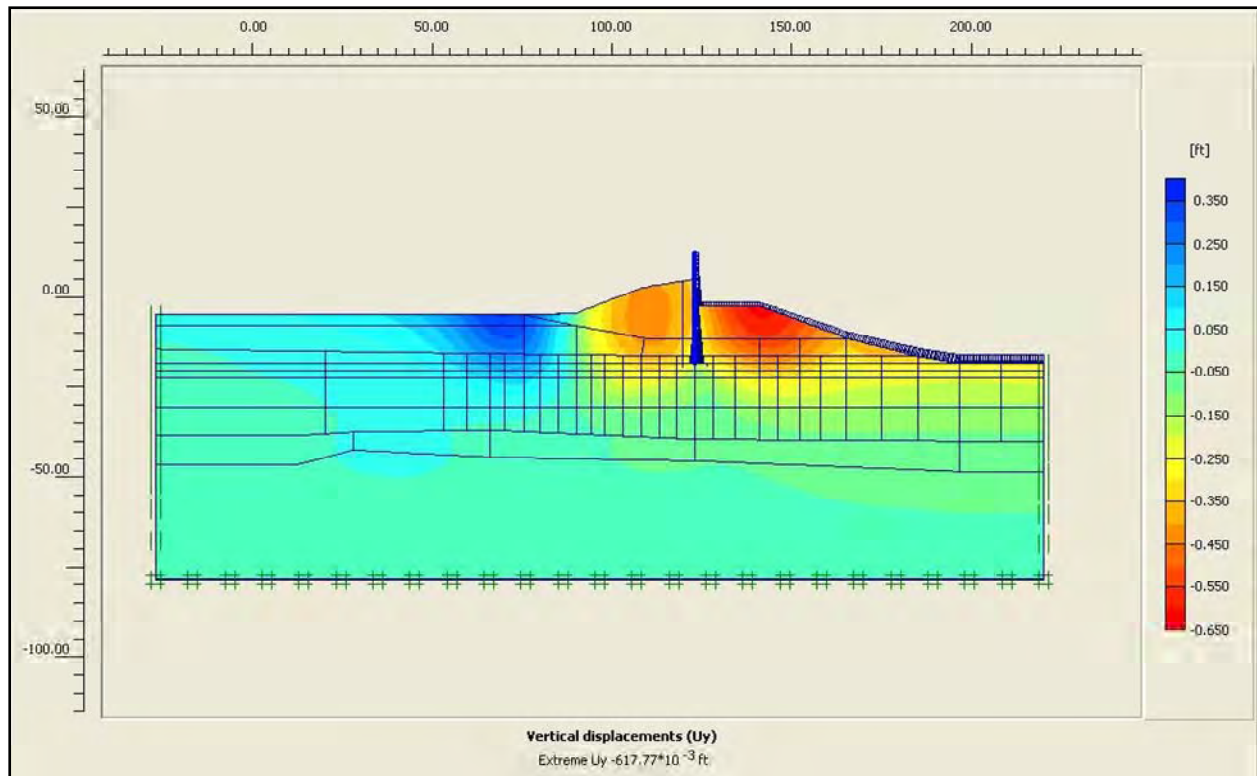
Figure 6-30. Vertical Deformation Shadings for Canal El 7.5 and Crack to El -18.5

Canal El 8.5: The tenth increment in loading, designated loading phase 23, raises the canal water to El 8.5. This is a 7.5-ft increase in canal water relative to canal steady state El 1 or, equivalently, a 1-ft increase in canal flood water elevation from canal El 7.5 of loading phase 22. The loading applied to the mesh is again solely due to hydrostatic canal water pressures applied as boundary water pressures normal to the wetted side of the I-wall, normal to the wetted exposed face of the levee and clays forming the sides and base of the canal, and normal to the sheet pile and soil that form the crack. The deformed mesh is shown in Figure 6-31. Note that the nodal deformations are increased by a factor of 7 in order to show the deformed mesh relative to its position at a canal water elevation of 1.0 (shown as a blue outline in this figure). The general trend of deformations is downward and towards the protected side due to the boundary water pressure loading applied within the canal. The maximum (relative) displacement within the mesh is 1.6 ft (19.5 in.). There is no indication of a fully developed failure mechanism occurring at this flood stage.
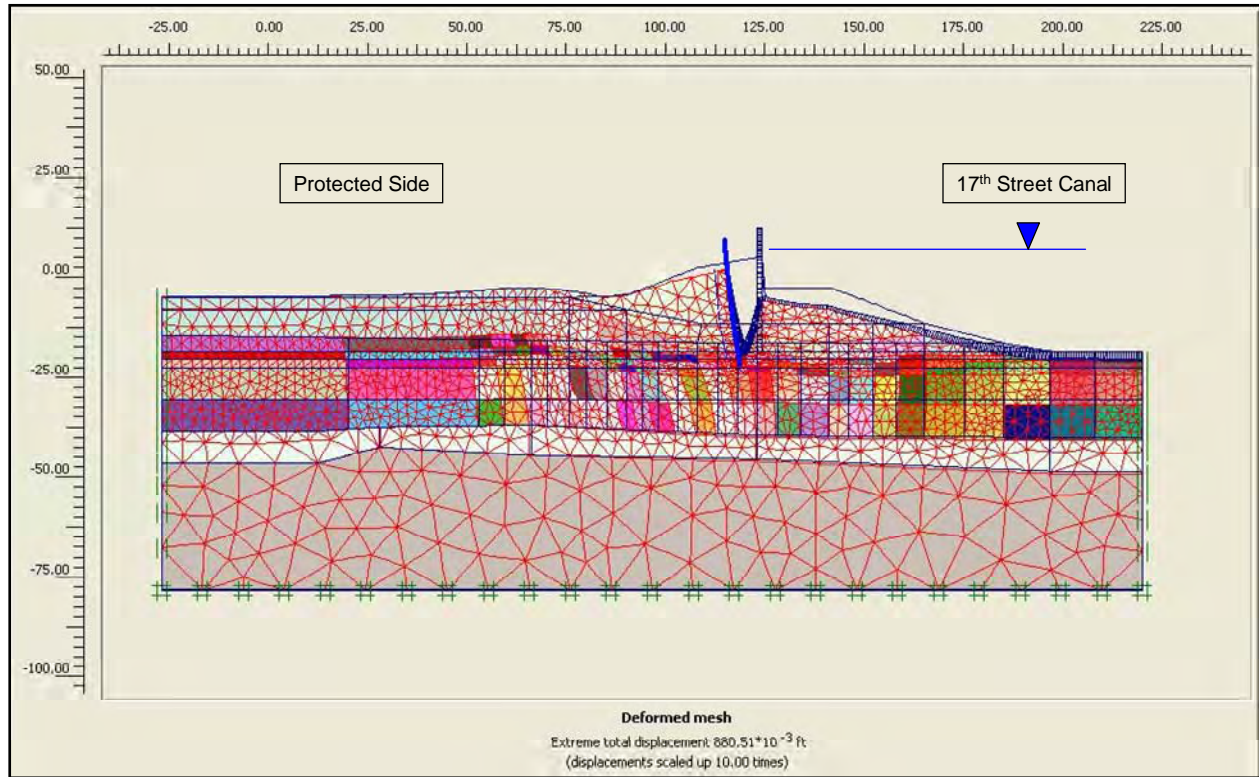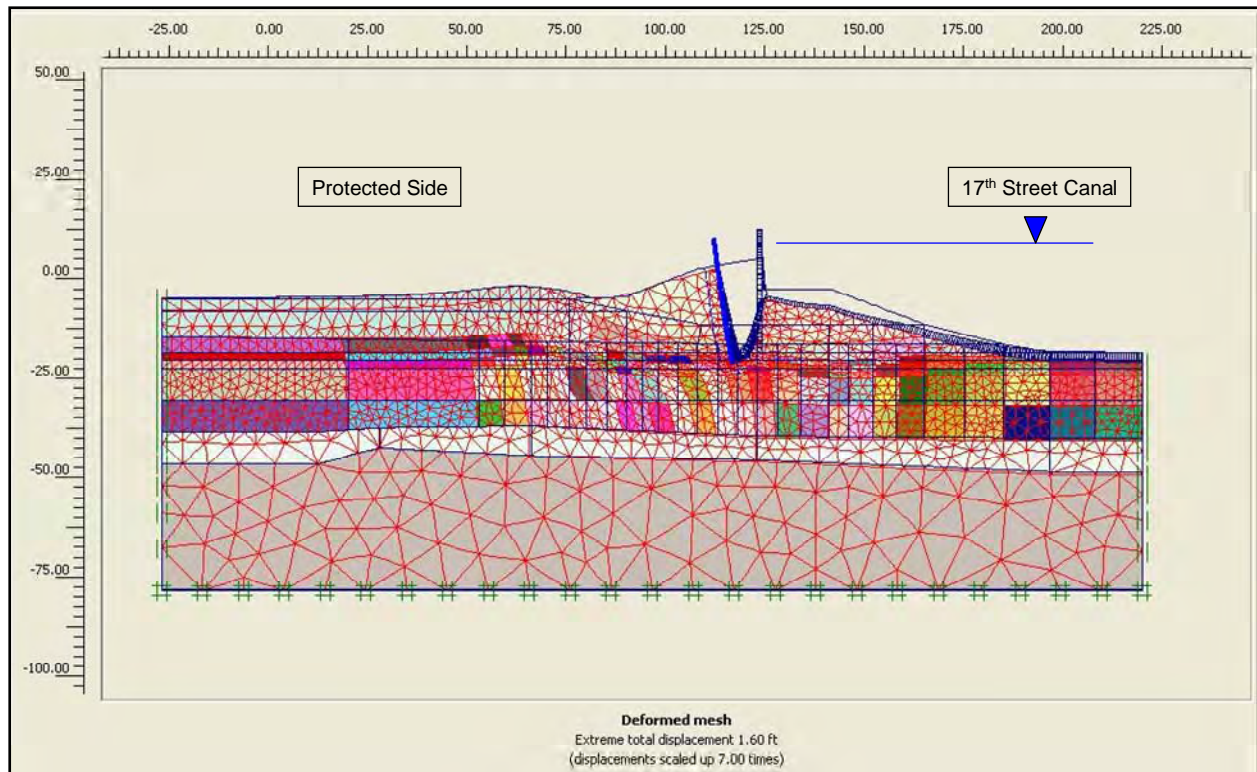
Figure 6-31. Deformed Mesh, Exaggerated by a Factor of 7, for Canal El 8.5 and Crack to El -18.5 (Note: Canal El not to scale in figure)

The mobilized shear stress at the strain integration points within the finite elements contained in the soil clusters is shown in Figure 6-32 to be less than the shear strength of the soil. The resulting computed fraction of mobilized shear strength is less than or equal to 0.96 at the stress integration points for the five soil types. Raising of canal water El 8.5 (as well as application of hydrostatic water pressures within the crack) results in more of the upper portion of the lacustrine clay layer being loaded, as indicated by comparison of Figure 6-32 fraction of mobilized shear strength results to the Figure 6-27 El 7.5 results.
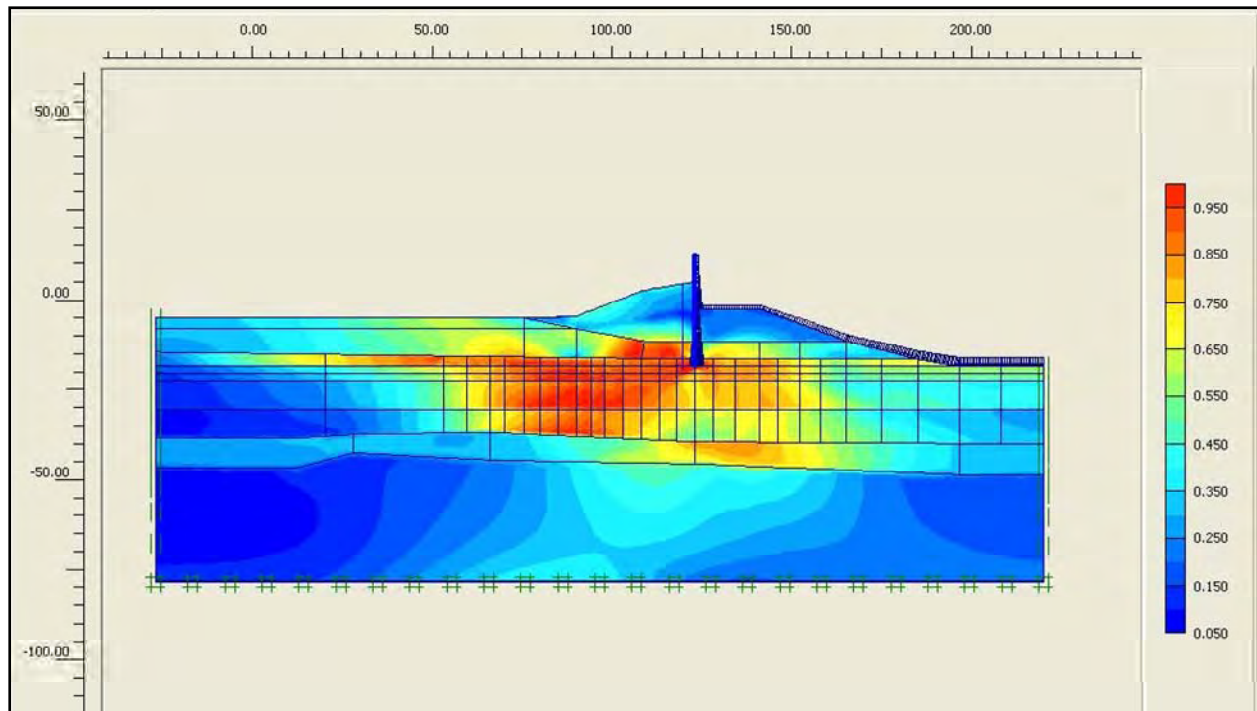
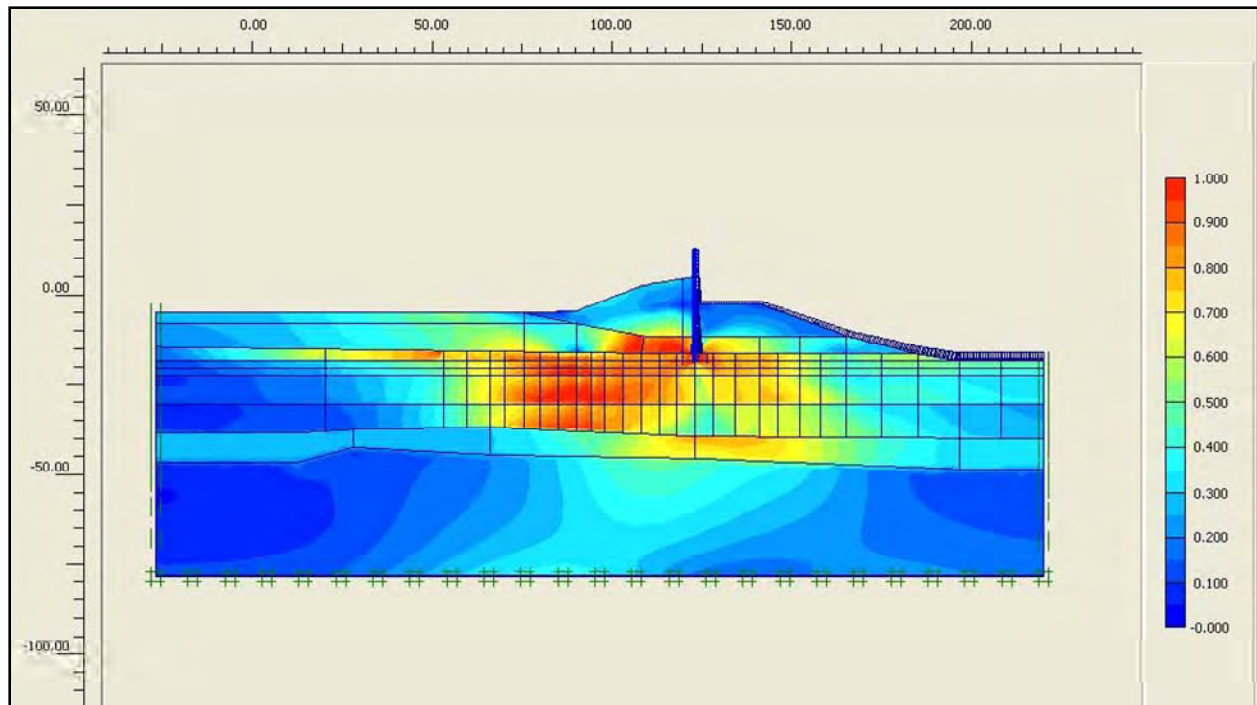Figure 6-32. Fraction of Mobilized Shear Strength for Canal El 8.5 and Crack to El -18.5

Figure 6-33 shows at this stage of flood loading the upper zone of high shear strains (beyond the toe of the levee), indicating a failure mechanism is developing.
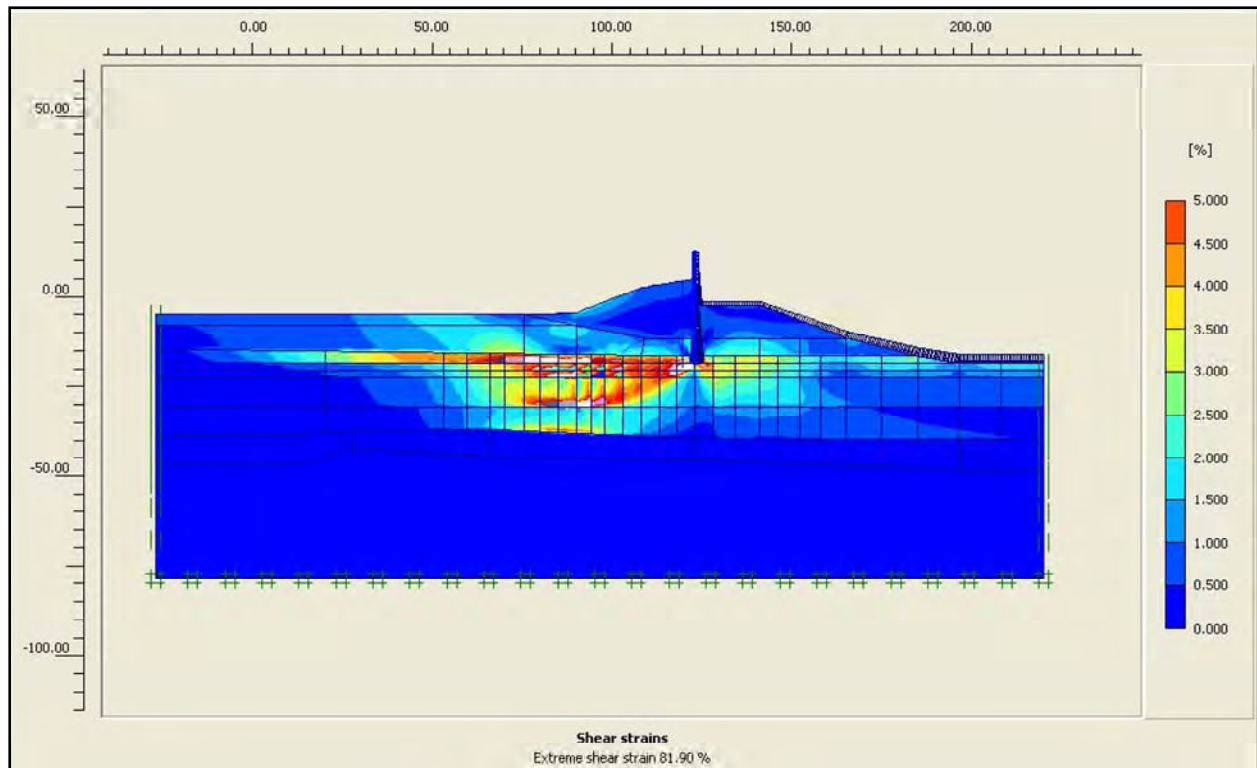
Figure 6-33. Reaches of Large Shear Strains for Canal El 8.5 and Crack to El -18.5

Figure 6-34 shows the horizontal displacements of the soil regions within the mesh, relative to their position at a canal water elevation of 1.0. This figure shows the deformation of the protected side levee, the peat below the levee, and the top layer of the lacustrine clay, all to be moving away from the canal, with a displacement of between -1.0 to -1.4 ft under an El 8.5 flood loading and including a full crack.
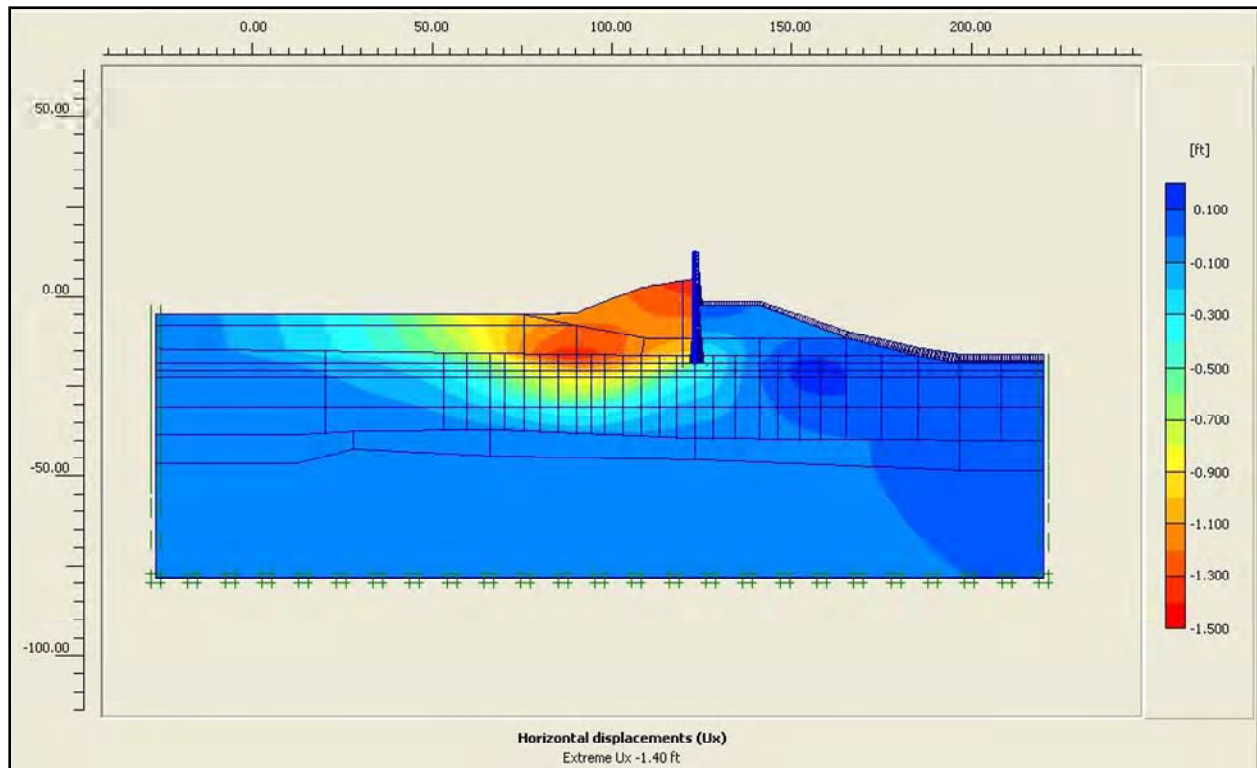
Figure 6-34. Horizontal Deformation Shadings for Canal El 8.5 and Crack to El -18.5

Figure 6-24 shows the horizontal displacements of three points within the floodwall, relative to its position at a canal water elevation of 1.0. The points monitored through the analyses are at the top of the I-wall, at El 5 (top of levee), and at sheet pile tip (El -18.5). With an open crack to sheet pile tip and with the flood loading maintained at El -8.5, the horizontal deformations at the top of the I-wall and at the base of the I-wall (El 5) are nearly identical, 1.55 ft and 1.41 ft. This implies uniform translation of the I-wall. However, the tip of the sheet pile undergoes less than half as much horizontal deformation as the I-wall, 0.84 ft.

Figure 6-35 shows the vertical displacements of the soil regions within the mesh for canal El 8.5 and with full crack, relative to its position at a canal water elevation of 1.0. This figure shows the deformation tendency of the peat to rise up (i.e., positive displacements) just beyond the toe of the levee on the protected side, and the levee berm to move downwards (i.e., negative displacements).
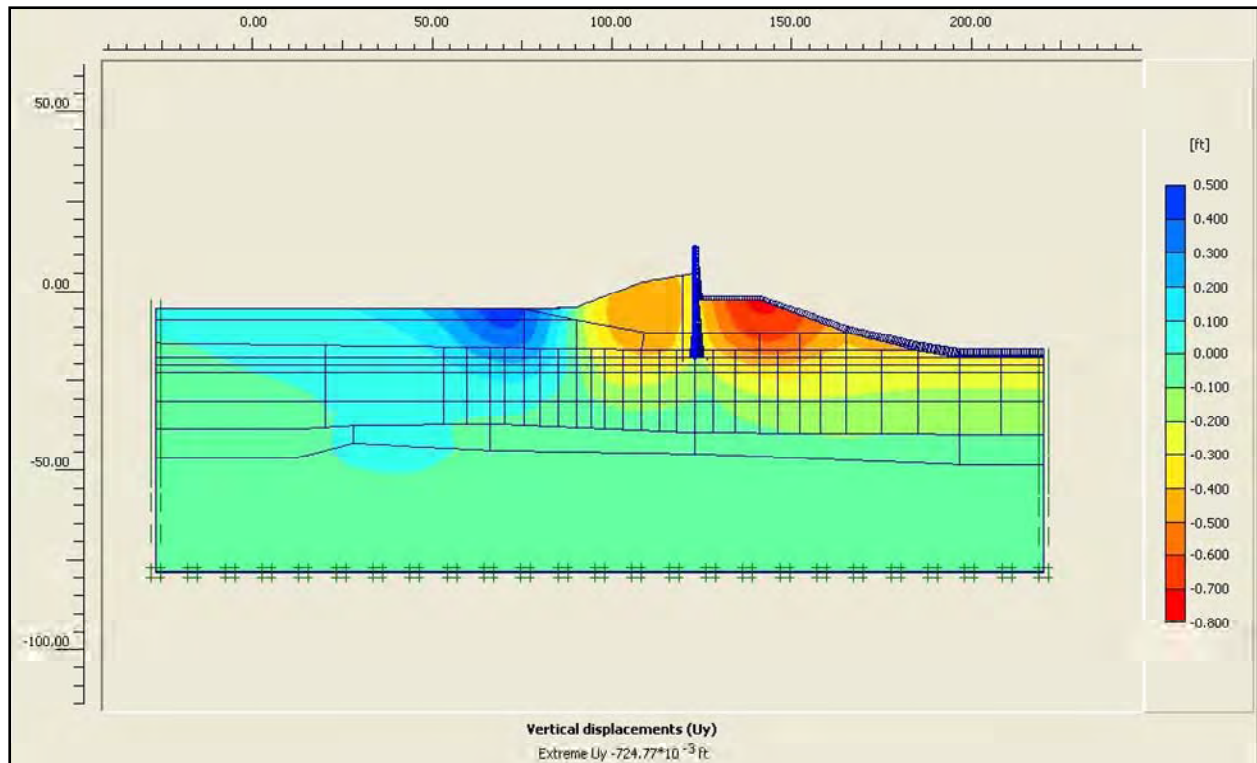
Figure 6-35. Vertical Deformation Shadings for Canal El 8.5 and Crack to El -18.5

Canal El 9: The eleventh increment in loading, designated loading phase 24, raises the canal water to El 9. This is an 8.5-ft increase in canal water relative to canal steady state El 1 or, equivalently, a 1-ft increase in canal flood water elevation from canal El 8.5 of loading phase 23. The loading applied to the mesh is again solely due to hydrostatic canal water pressures applied as boundary water pressures normal to the wetted side of the I-wall, normal to the wetted exposed face of the levee and clays forming the sides and base of the canal, and normal to the sheet pile and soil that form the crack. The deformed mesh is shown in Figure 6-36. Note that the nodal deformations are increased by a factor of 2 in order to show the deformed mesh relative to its position at a canal water elevation of 1.0 (shown as a blue outline in this figure). The general trend of deformations is downward and towards the protected side due to the boundary water pressure loading applied within the canal. The computed maximum (relative) displacement within the mesh is excessive, more than 5 ft. Note the upward bulge in the surface of the peat/marsh layer beyond the toe of the levee.
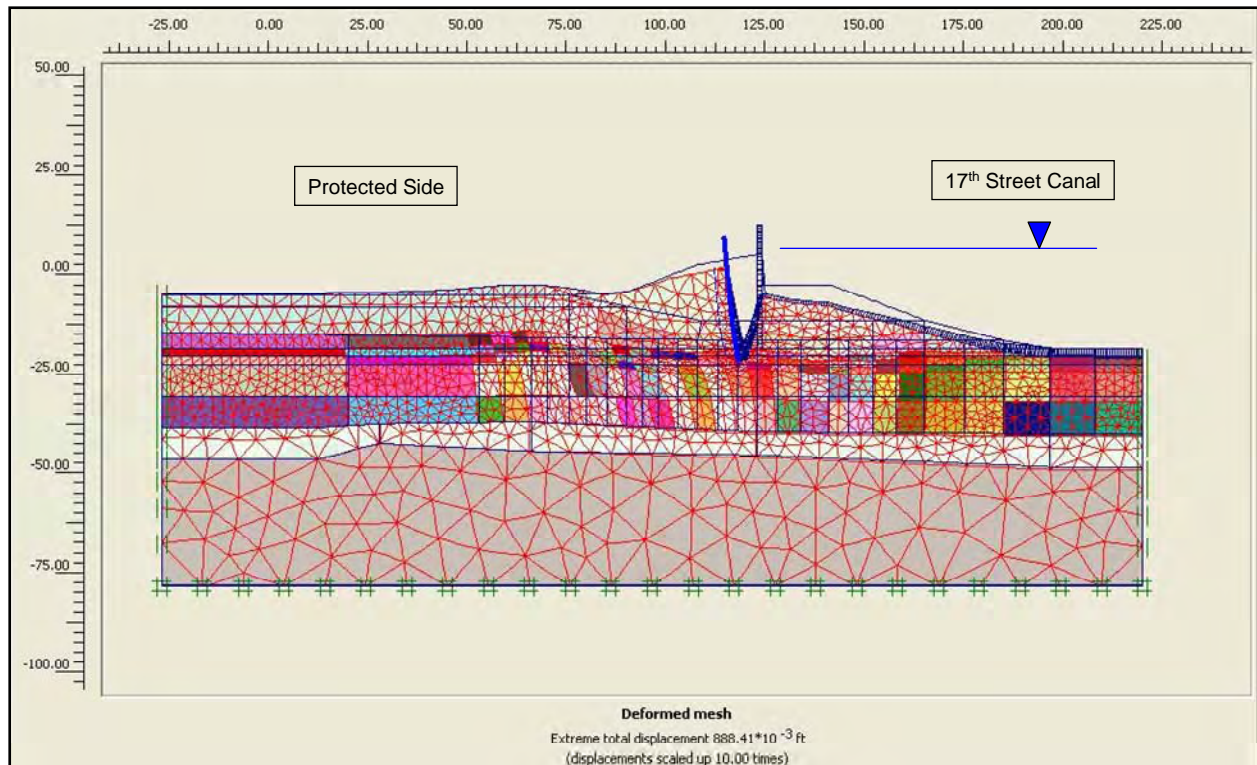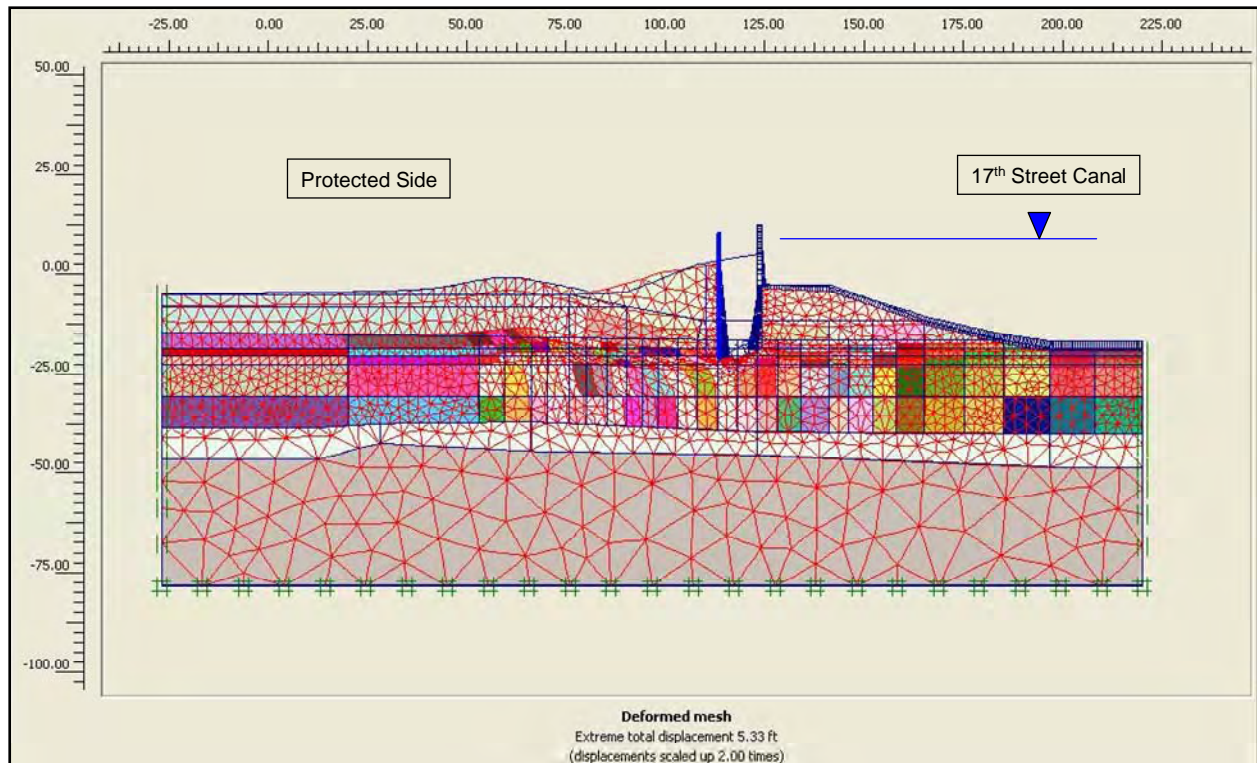
Figure 6-36. Deformed Mesh, Exaggerated by a Factor of 2, for Canal El 9 and Crack to El -18.5 (Note: Canal El not to scale in figure)

The mobilized shear stress at the strain integration points within the finite elements contained in the soil clusters is shown in Figure 6-37. Note that the zone of high values for the computed fraction of mobilized shear strength now extends to the peat/marsh region beyond the toe of the levee. These and the Figure 6-36 results indicate the formation of a failure mechanism that "daylights" beyond the toe of the levee.
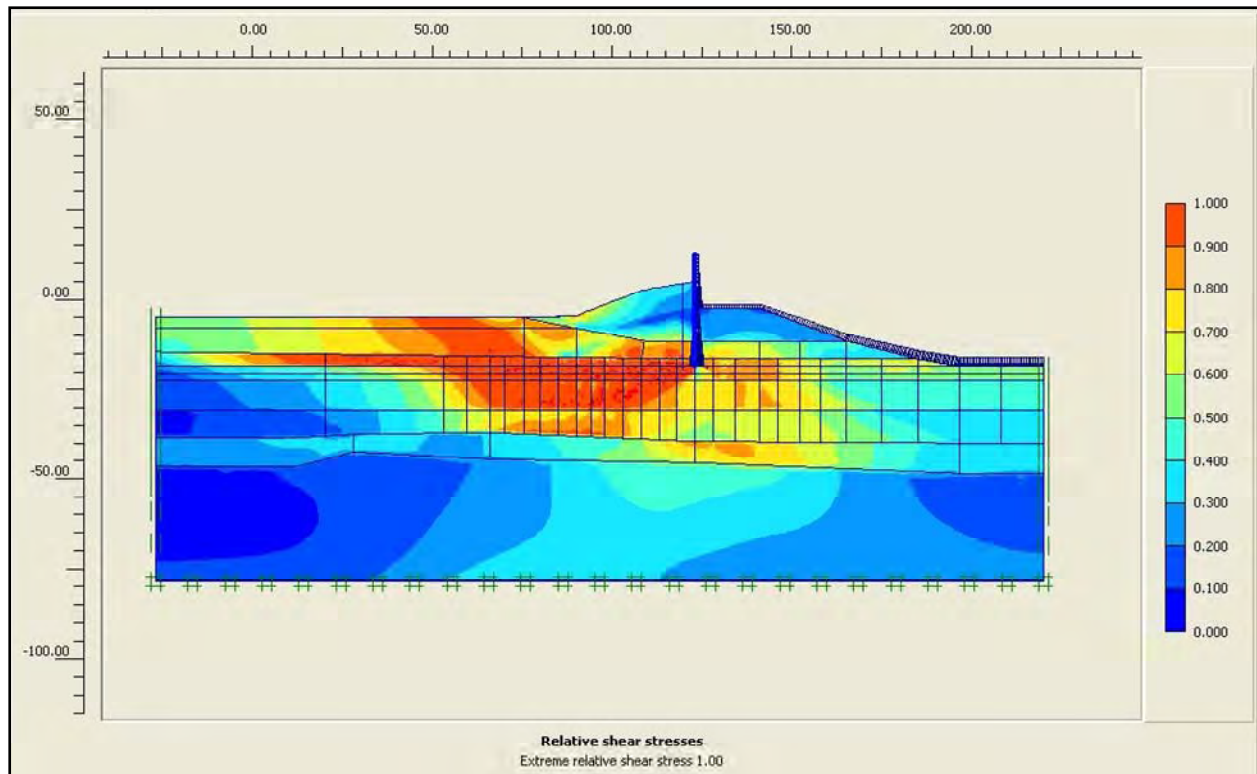
Figure 6-37. Fraction of Mobilized Shear Strength for Canal El 9 and Crack to El -18.5

Figure 6-38 shows that at this stage of flood loading, the upper reach of high shear strains also now indicate the formation of a failure mechanism up through the peat/marsh region beyond the toe of the levee.
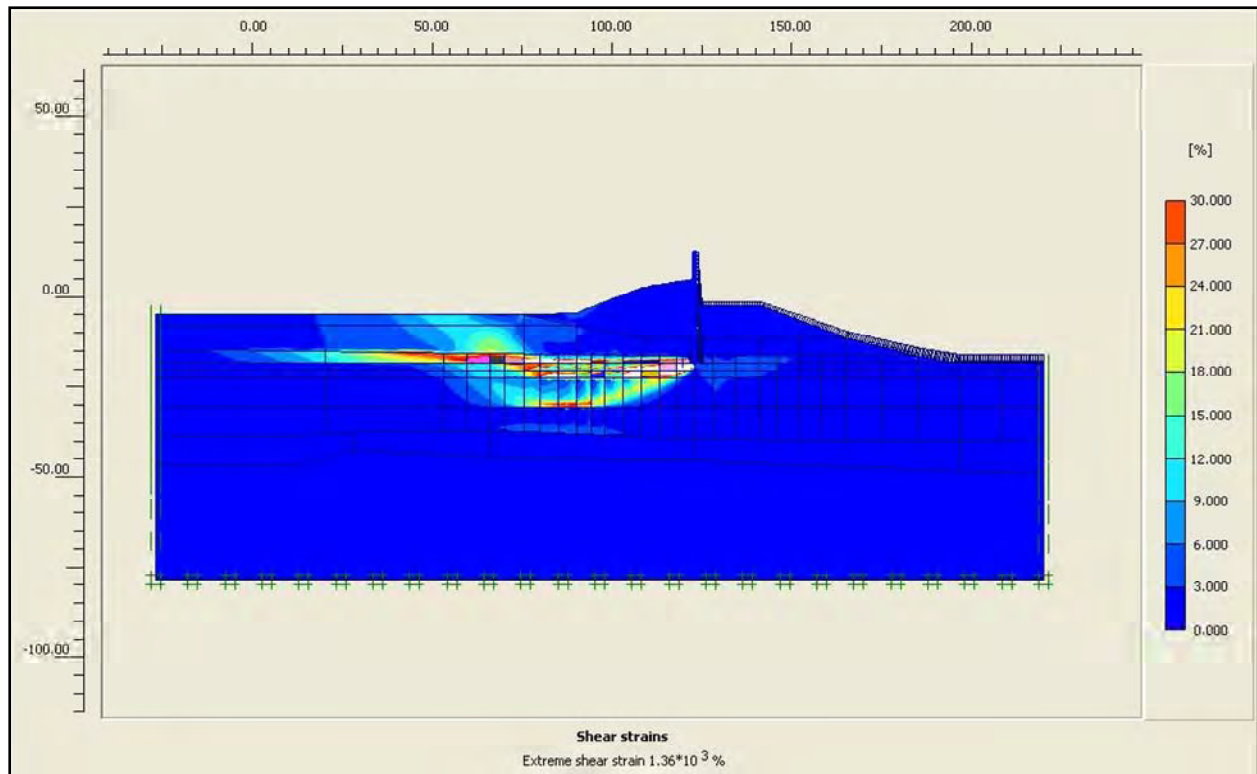
Figure 6-38. Reaches of Large Shear Strains for Canal El 9 and Crack to El -18.5

Figure 6-39 shows the failure mechanism based on a Plaxis Phi/C reduction procedure resulting in a computed factor of safety against shear failure of 0.98, while the corresponding Figure 6-40 shear strains show that the zone of higher shear strains extend to the upper layer of the lacustrine clay. Note the mechanism "daylighting" beyond the toe of the levee. This result is consistent with the Figure 6-36 displacements, showing the bulging upwards of the peat/marsh layer beyond levee toe; the zone of high values for the computed fraction of mobilized shear strength within this region in Figure 6-37; and the Figure 6-38 high shear strains also computed within this region.
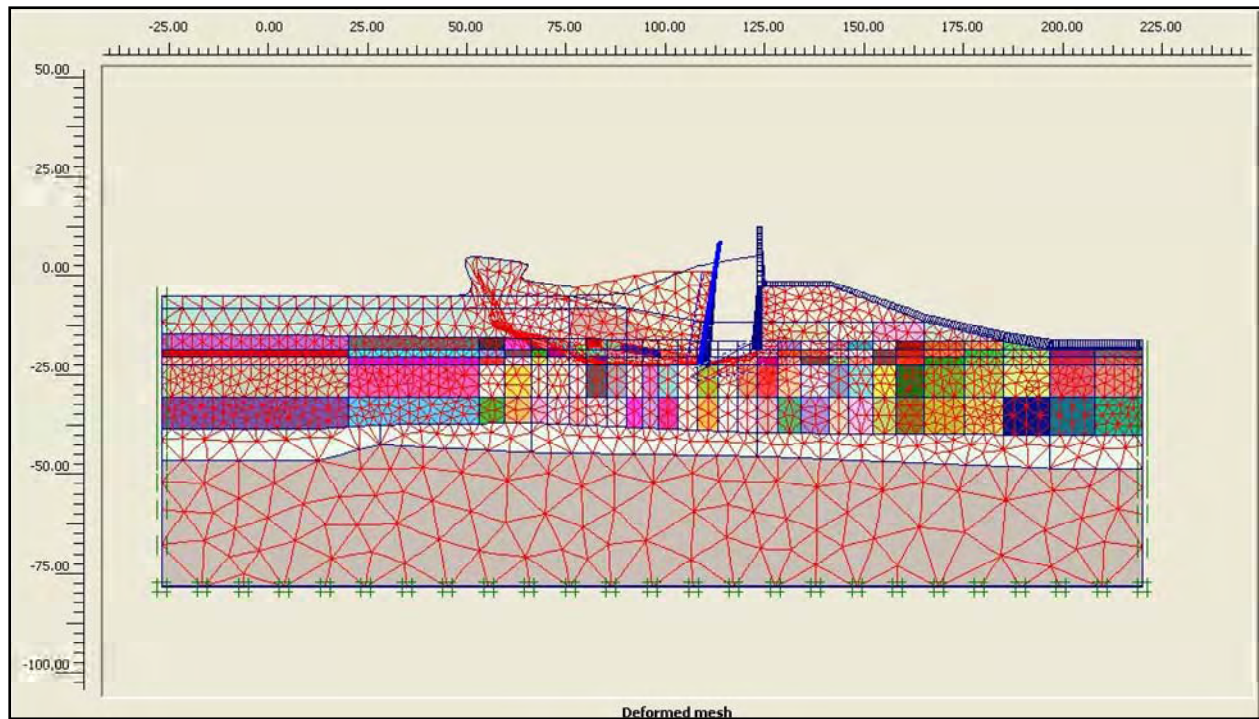
Figure 6-39. Failure Mechanism from Phi/C Reduction for Canal El 9 and Crack to El -18.5
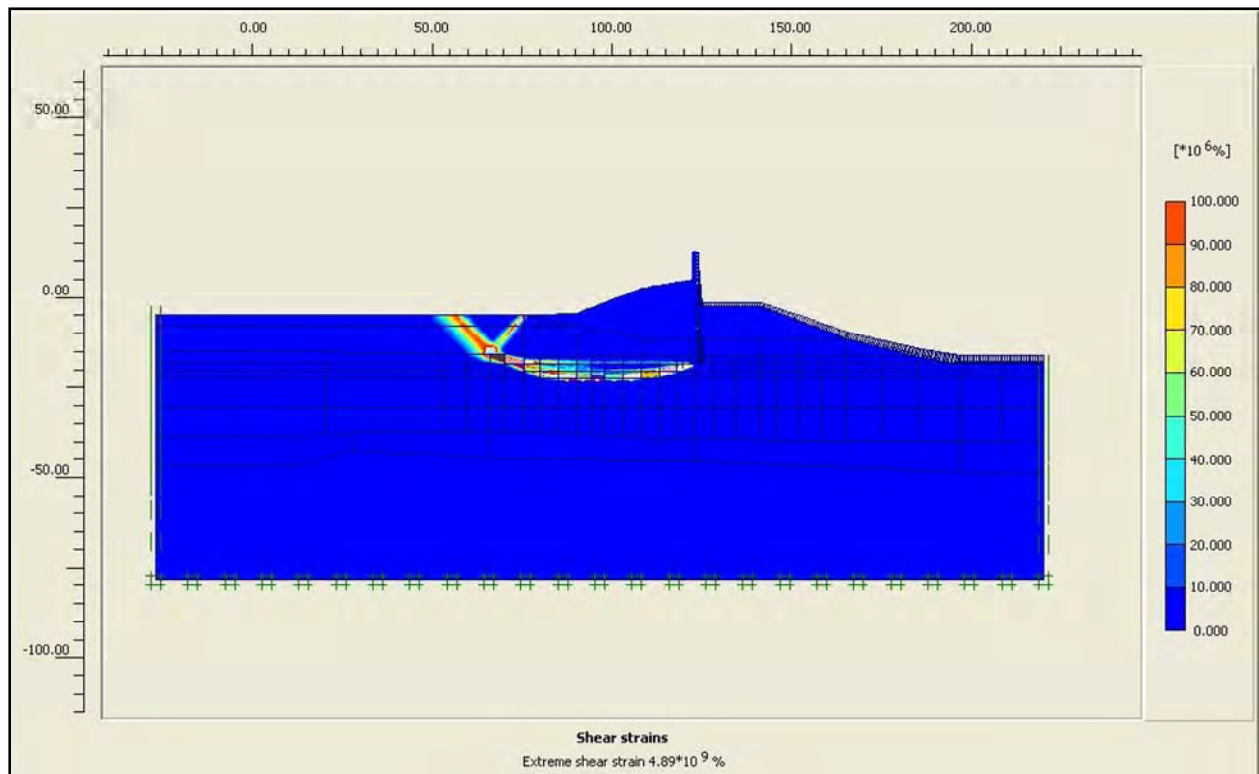
Figure 6-40. Reaches of Large Shear Strains from Phi/C Reduction for Canal El 9 and Crack to El -18.5

Subsequent complete SSI analyses are made to compute the factors of safety against shear failure for canal water less than El 9. The results summarized in Figure 6-41 indicate that the factor of safety is equal to unity for canal water El 8.8. These results demonstrate the reserve capacity of the levee/I-wall system for canal water less than El 8.8. For example, Figure 6-41 shows that at El 6.5, the factor of safety against shear failure is 1.46 prior to cracking. Figure 6-42 shows that the failure mechanism based on a Plaxis Phi/C reduction procedure, if allowed to develop, would also be "daylighting" beyond the toe of the levee, while the corresponding Figure 6-43 shear strains show that the zone of higher shear strains extend to mid-layer in the lacustrine clay. After the full crack is introduced to the sheet pile tip for canal water El 6.5, the factor of safety reduces to 1.17.

Figure 6-41. Factor of Safety Versus Canal Water El (Complete SSI results)
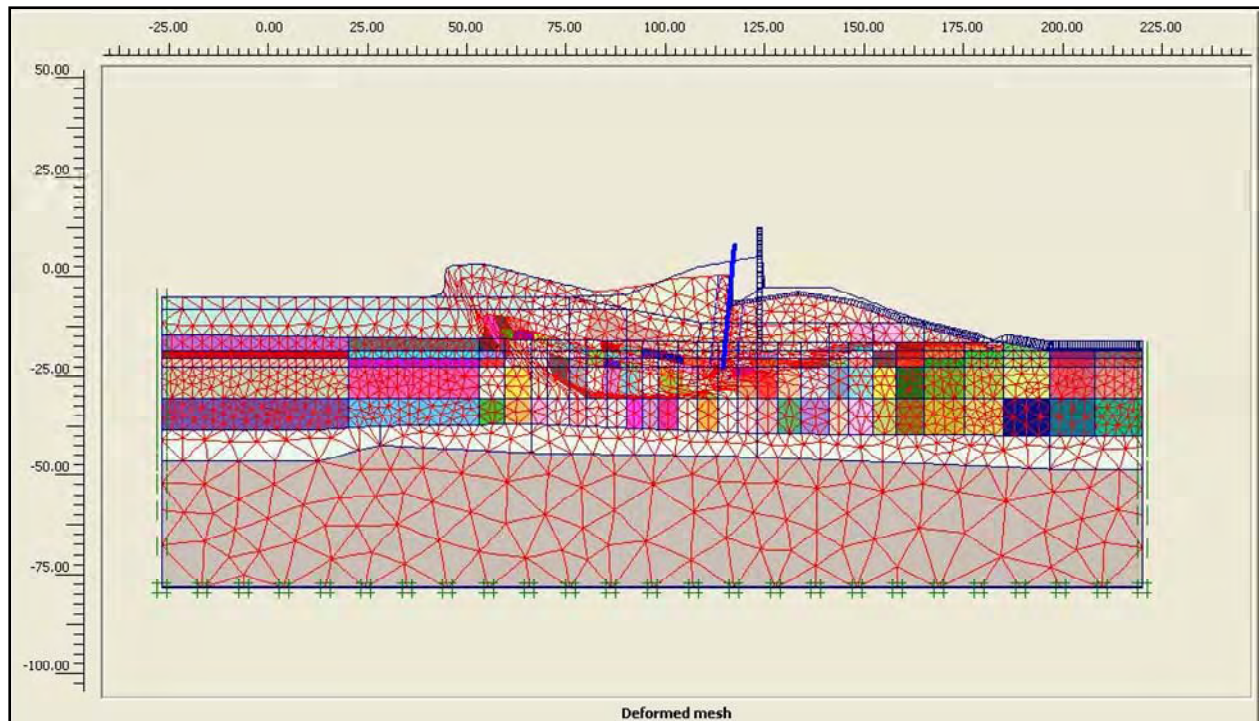
Figure 6-42. Failure Mechanism from Phi/C Reduction for Canal El 6.5 and No Crack
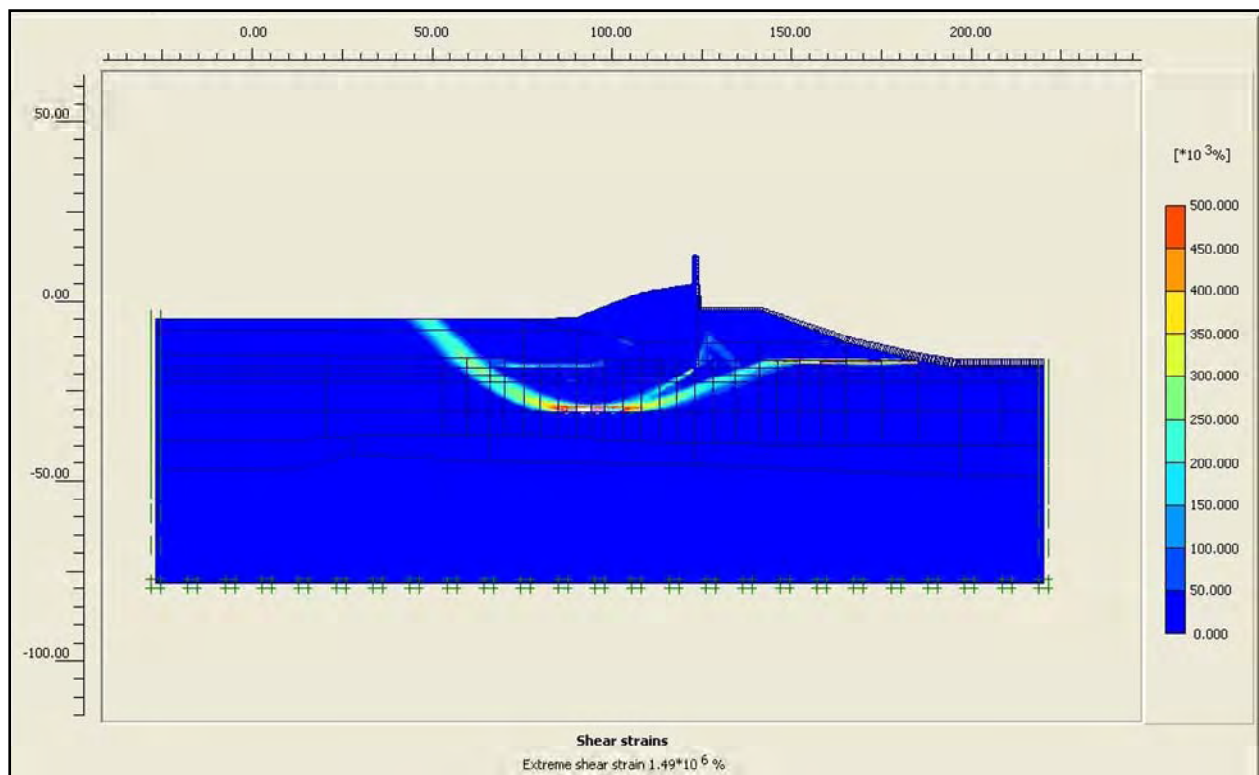
Figure 6-43. Reaches of Large Shear Strains from Phi/C Reduction for Canal El 6.5 and No Crack

References

Brinkgreve, R. B. J., Broere, W., and Waterman, D., ed. 2004. *Plaxis 2D – Version 8.* Plaxis B.V. The Netherlands: Delft University of Technology.

Kulhawy, F. H., and Mayne, P. W. 1990 (Aug). Manual on Estimating Soil Properties for Foundation Design, Research Report EL-6800, prepared for Electric Power Research Institute, Palo Alto, CA.

Potyondy, J. G. 1961. Skin Friction Between Various Soils and Construction Materials, *Geotechnique*, Vol. II, pp. 339-353.

Schmertmann, J. H. 1978. Guidelines for Cone Penetration Test, Performance and Design, Report FHWA-TS-78-209, U.S. Department of Transportation, Washington, DC, 145 p.

Skemption, A. W. 1986. Standard Penetration Test Procedures and the Effects in Sands of Overburden Pressure, Relative Density, Particle Size, Ageing and Overconsolidation, Geotechnique, Vol. 36, No. 3, pp. 425-447.

Appendix 7
Interim Data Report, London Avenue Outfall Canal

Introduction

This is an interim report that documents data collected to date for the analysis of the failure of the I-wall sections at the London Avenue Outfall Canal (north and south failures) as a result of Hurricane Katrina on August 29, 2005. London Avenue Outfall Canal and the location of the levee breaches are shown on Figure 7-1. The north is located on the west bank of the canal, south of the Robert E. Lee Blvd. Bridge and about one mile south of the outlet of the London Ave. canal. Opposite the north breach, the east I-wall experienced extreme levee distress, including landward deflection of the I-wall, cracked concrete, and the presence of several sink holes at the levee crown, and a sand boil at the levee toe. The south London or Mirabeau breach is located on the east bank, north of and adjacent to the Mirabeau Bridge.

Key data obtained for the breach sites and presented in this report include:

    a. Description of geology and soil stratigraphy
    b. Representative pre-Katrina cross section through the breach area
    c. Undrained shear strength soil profiles
    d. Piezometer data

Engineering and geologic data were obtained from a variety of sources, including the project General Design Memorandum, design documents, and surveys prepared prior to Katrina. In addition, this report contains information obtained from field and laboratory investigations and surveys conducted after the Hurricane Katrina event. This report was prepared to provide numerical and physical modelers with the information needed to build models for analyses of levee stability.
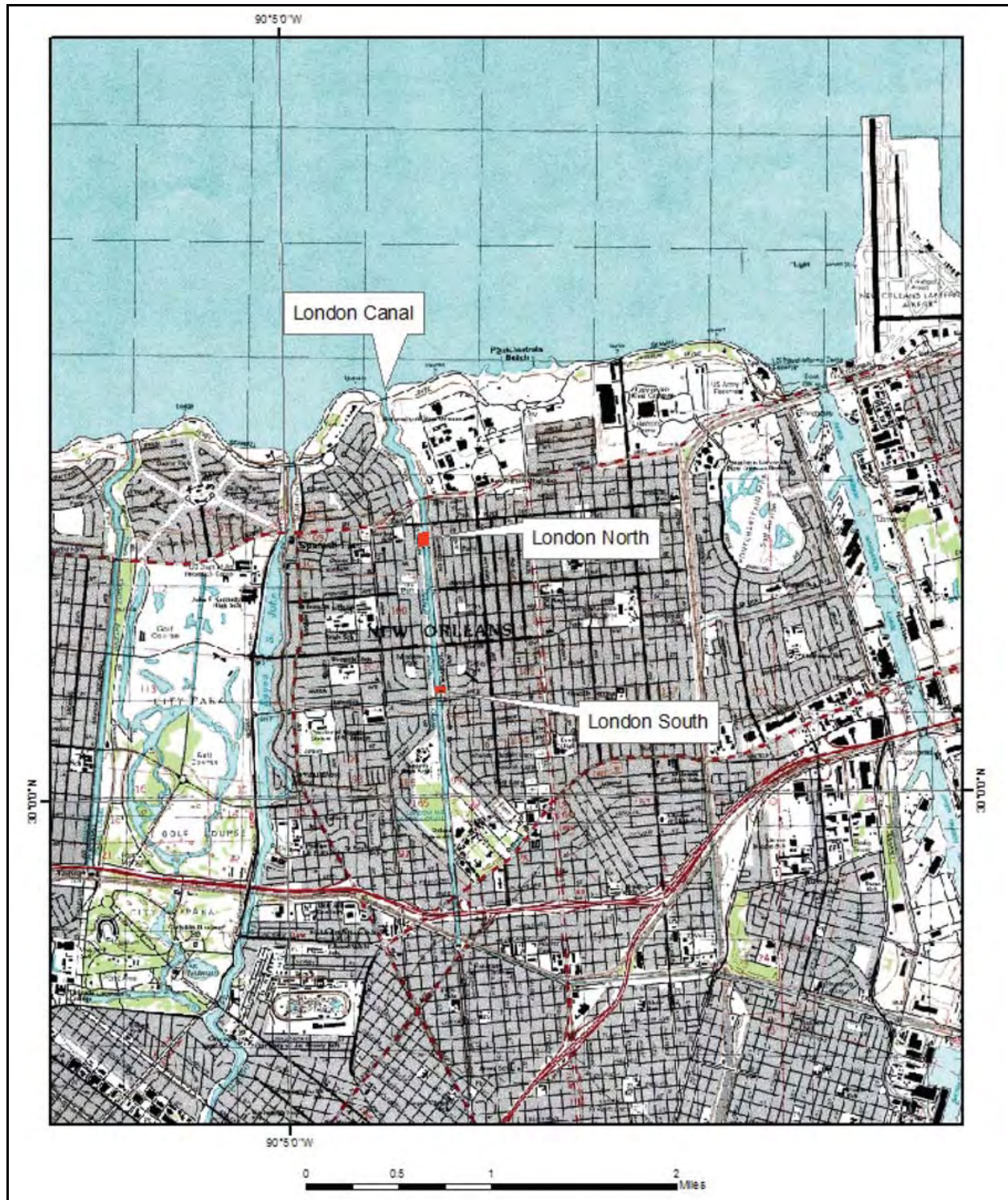
Figure 7-1. Location of the London Canal and Levee Breaches at Robert E. Lee and Mirabeau (North and South Breaches, Respectively)

Geology

Introduction

Before examining the individual failure areas at London Canal, a review of the geology is presented to familiarize the reader with the broader context of the geology of the delta plain, its stratigraphy, and the soils comprising the foundations at the different failure areas. For comparison purposes, the general geology of both the 17th Street and London Canal levee breaches is reviewed. The geology of the New Orleans area has been determined from detailed mapping studies of the Louisiana Coastal Plain (LCP), a review of the published literature, from data collection activities at each of the failure sites by an ERDC study team, and from an evaluation of preexisting and recently drilled engineering borings from each of the failure areas.

Previous Studies

A review of the past geologic literature from the New Orleans area identifies the US Army Corps of Engineers (USACE) as being actively involved with much of the regional and focused geologic studies that have been performed in the eastern LCP or deltaic plain (Dunbar and others, 1994 and 1995; Dunbar, Torrey, and Wakeley, 1999; Fisk, 1944; Kemp and Michel, 1967; Kolb, Smith, and Silva, 1975; Kolb, 1964; Kolb and Van Lopik, 1958a and 1958b; Kolb and Schultz, 1954; Kolb and Saucier, 1982; May and others, 1984; Michel, 1967; Saucier, 1963, 1984, and 1994; and Schultz and Kolb, 1950). Many of these studies and associated geologic maps are available from a USACE-sponsored website on the geology of the Lower Mississippi Valley that is accessible to the public at lmvmapping.erdc.usace.army.mil.

Geologic History and Principal Physiographic Features of the New Orleans Area

To better understand the soils beneath the 17th Street and London Canals, and the engineering properties of these soils, a brief summary of the geologic history of the New Orleans area is presented. Detailed descriptions of the geologic history are presented in Saucier (1964 and 1994), Kolb, Smith, and Silva (1975), Kolb and Saucier (1982); and Kolb and Van Lopik (1958).

The geology and stratigraphy of the New Orleans area are young in terms of its age. Generally, sediments comprising the New Orleans area are less than 7,000 years old. Formation of the present day New Orleans began with the rise in global sea level, beginning about 12,000 to 15,000 years before present. The rise in sea level was caused by melting of continental glaciers in the Northern Hemisphere and the release of ice-bound water to the oceans. At the maximum extent of continental glaciation, the eustatic sea level was approximately 300 ft (~100 m) lower than the present level. In addition, the ancestral coastal shoreline was much farther south of its current location, probably near the edge of the continental shelf.

The underlying Pleistocene surface throughout much of coastal Louisiana was subaerial, and exposed to oxidation, weathering, and erosion. These conditions led to the development of a well-developed drainage network across its surface, and created a distinct soil horizon in terms of its engineering properties. The Pleistocene horizon is easily recognizable in borings because of its distinct physical properties as compared to the overlying Holocene fill (i.e., oxidized color,

stiffer consistency, higher shear strength, lower water content, and other physical properties.).
The axis of the main valley or entrenchment of the Mississippi River was located west of New
Orleans, in the vicinity of present day Morgan City, LA (Figure 7-2). Consequently,
development of the early Holocene deltas was concentrated near the axis of Mississippi
entrenchment when sea-level rise began to stabilize sometime between 5,000 to 7,000 years
before the present. New Orleans is located on the eastern edge of this buried entrenchment or
alluvial valley.

The Pleistocene surface in the New Orleans area is variable, but generally ranges between 50
and 75 ft below sea level, as determined from detailed mapping and examination of boring data
(Kolb and Van Lopik, 1958; Kolb, Smith, and Silva, 1974; Saucier, 1994; and Dunbar and
others, 1994 and 1995). Various sea level curves for the Louisiana coast are presented and
discussed in Kolb, Smith, and Silva (1975) and Tornquist and Gonzalez (2002). These curves
generally indicate that sea level transgression in the New Orleans area generally occurred
between 6,000 to 9,000 years before the present, based on the mapped depths to the top of the
Pleistocene surface.

As the rate of sea level rise declined and stabilized, it led to the development of five, short-
lived delta complexes across the Louisiana coast by deposition of Mississippi River sediments
(Figure 7-2). Individual delta complexes are composed of numerous, branching distributary
channels. These channels transport and deposit fluvial sediments along the margin of the delta
and build land seaward into shallow coastal water. Distributary channels from the St. Bernard
delta are responsible for filling the shallow Gulf waters in the greater New Orleans area (Frazier,
1967).

Bayou Sauvage is a major distributary involved in the filling of the shallow Gulf waters in
the New Orleans area (Figure 7-3). This channel extends eastward from the Mississippi River
and is composed of Bayous Metairie, Gentilly (or Gentilly Ridge), and Sauvage. Natural levees
of this distributary channel form a pronounced physiographic feature in the northern New
Orleans area (Figure 7-3). Similarly, Mississippi River natural levees are some of the highest
land elevations found in New Orleans, and these were the first areas to be settled by the early
inhabitants in the 1700s. Distributary channels in New Orleans are pronounced physiographic
features, and are associated with the St. Bernard delta complex as determined from radiocarbon
dating of organic sediments (Frazier, 1967; Kolb and Van Lopik, 1958, McFarlan, 1961; Britsch
and Dunbar, 1999; and Smith, Dunbar, and Britsch, 1986).

Equally important to the development and filling history of the New Orleans area is the
presence of a buried, barrier beach ridge which formed approximately 4,500 to 5,000 years
before the present. This beach extends northeast in the subsurface along the southern shore of
Lake Pontchartrain (Figure 7-4). Sea level was 10 to 15 ft lower than the current level when the
beach ridge formed. A stable sea level permitted sandy sediments from the Pearl River to the east
to be concentrated by longshore drift, and formed a sandy spit or barrier beach complex in the
New Orleans area as shown by Figure 7-3 (Saucier, 1994).
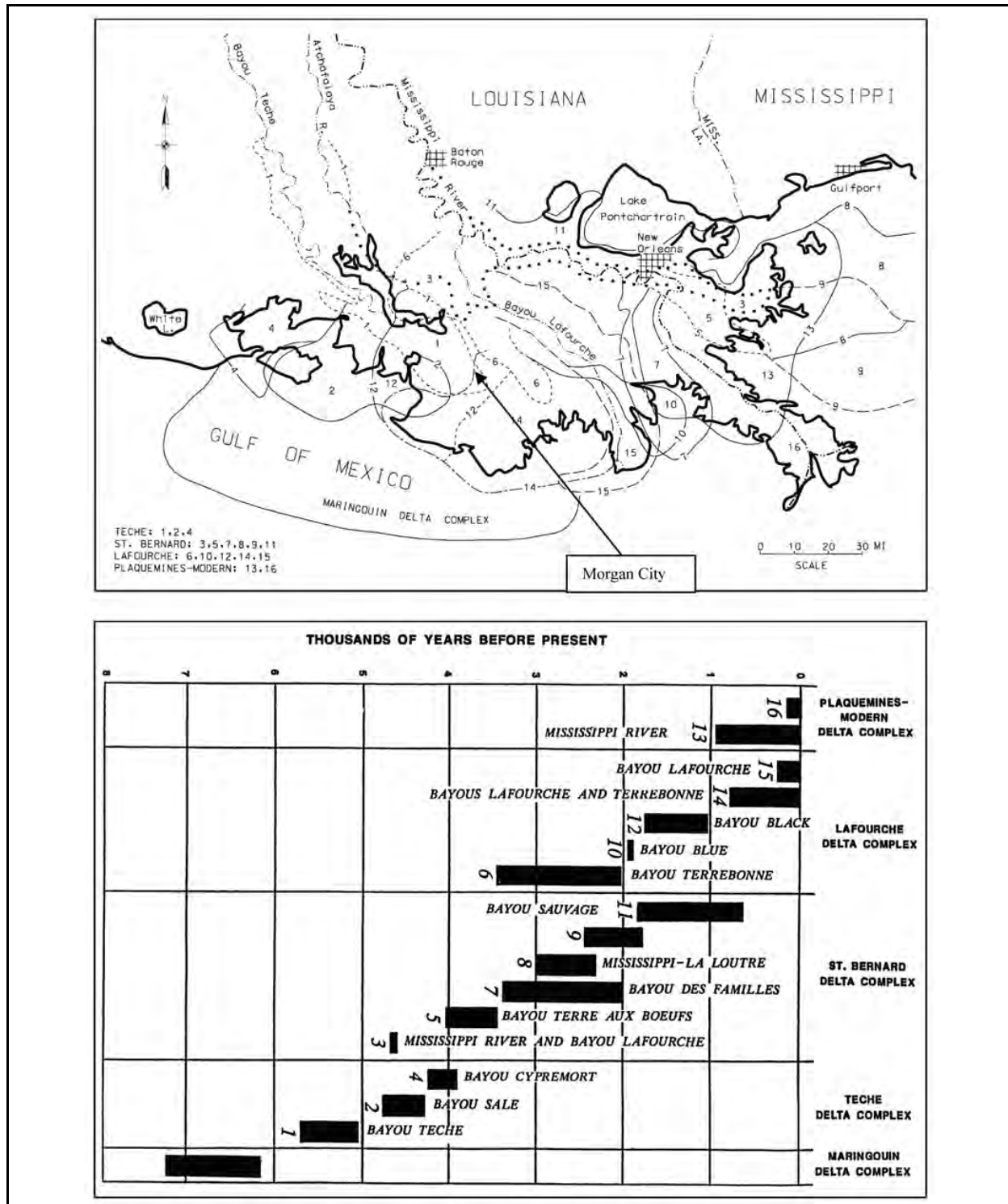
Figure 7-2. Location and Approximate Chronology of the Mississippi River Deltas, Major Distributary Channels are Numbered, Note Bayou Sauvage (No. 11) which Extends across the New Orleans Area and Forms the Bayou Metairie/Gentilly Ridge (after Frazier, 1967). Morgan City, LA, Located along Axis of Maximum Mississippi River Entrenchment.
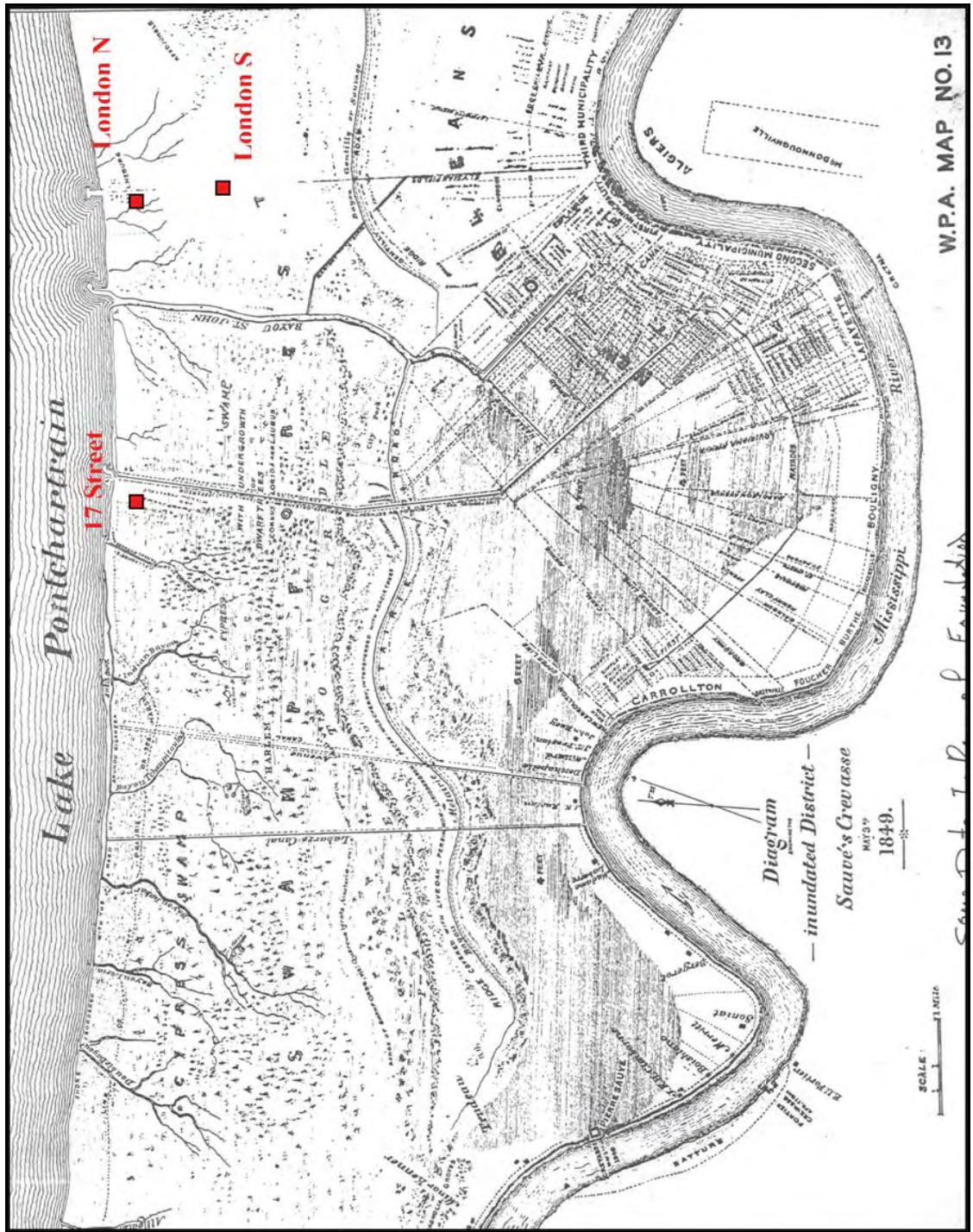
Figure 7-3. New Orleans Area Map from 1849 Showing City Limits and Topography. Note the Location of Bayous Metairie and Gentilly (i.e., Bayou Sauvage) and the Identified Cypress Swamp North of the City at this Time (Work Projects Administration, 1943).
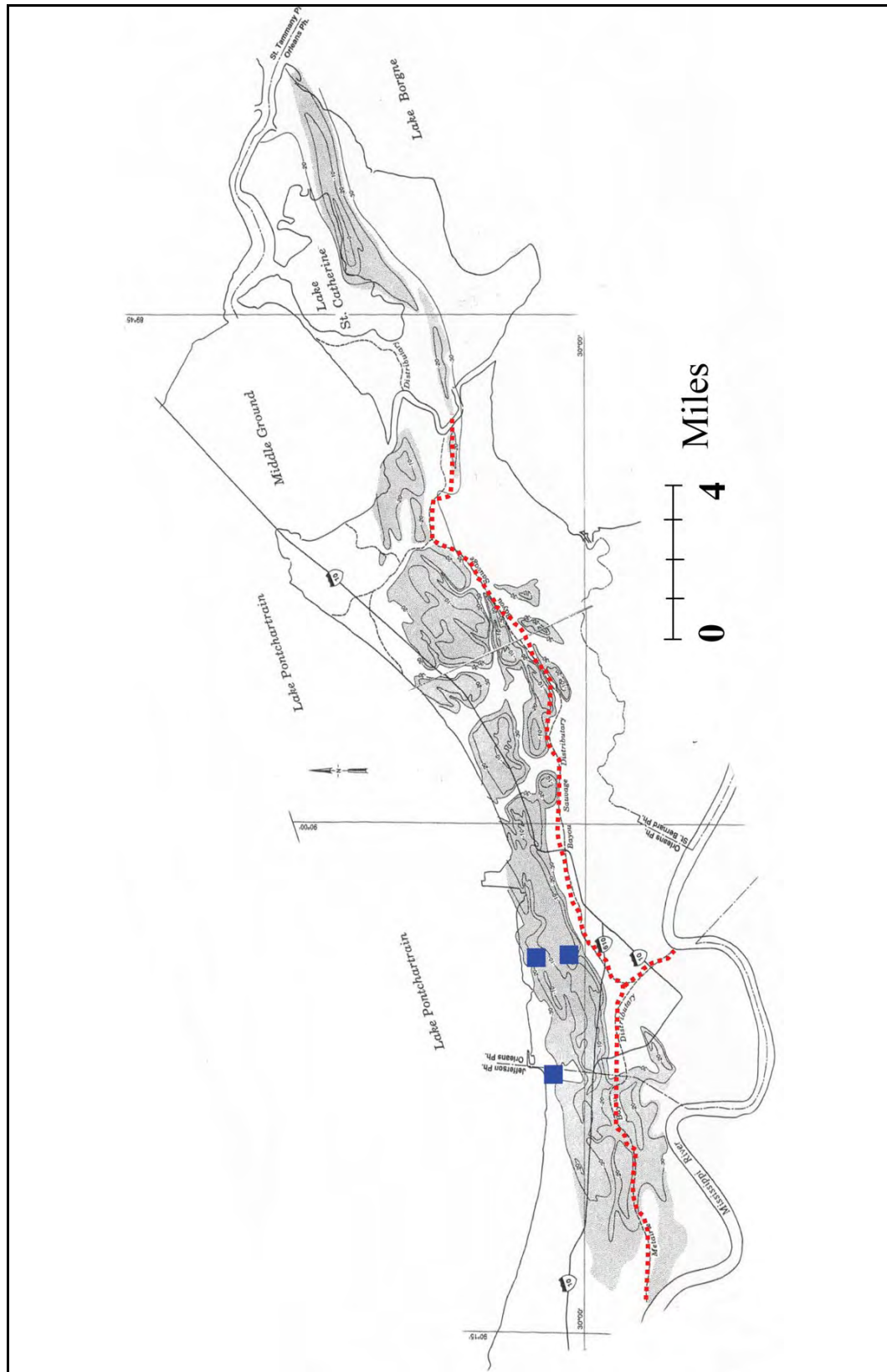
Figure 7-4a. Pine Island Buried Beach Complex in the New Orleans Area (from Saucier 1994). Course of Bayou Sauvage (I.E., Bayous Metairie and Gentilly) Identified in Red. Note the Presence of the Barrier Beach Prevented this Distributary Course from Extending Northward into Present Day Lake Pontchartrain and Filling the Lake. Canal Breaches are Identified in Blue, with 17th Street Breach Behind the Thickest Part of the Beach Ridge, while Both the London North and South Breaches are on the Axis of the Barrier. See Figure 7-4b for Close-up of Canal Areas.

Volume V The Performance – Levees and Floodwalls – Technical Appendix

V-7-7

This is a preliminary report subject to revision; it does not contain final conclusions of the United States Army Corps of Engineers.
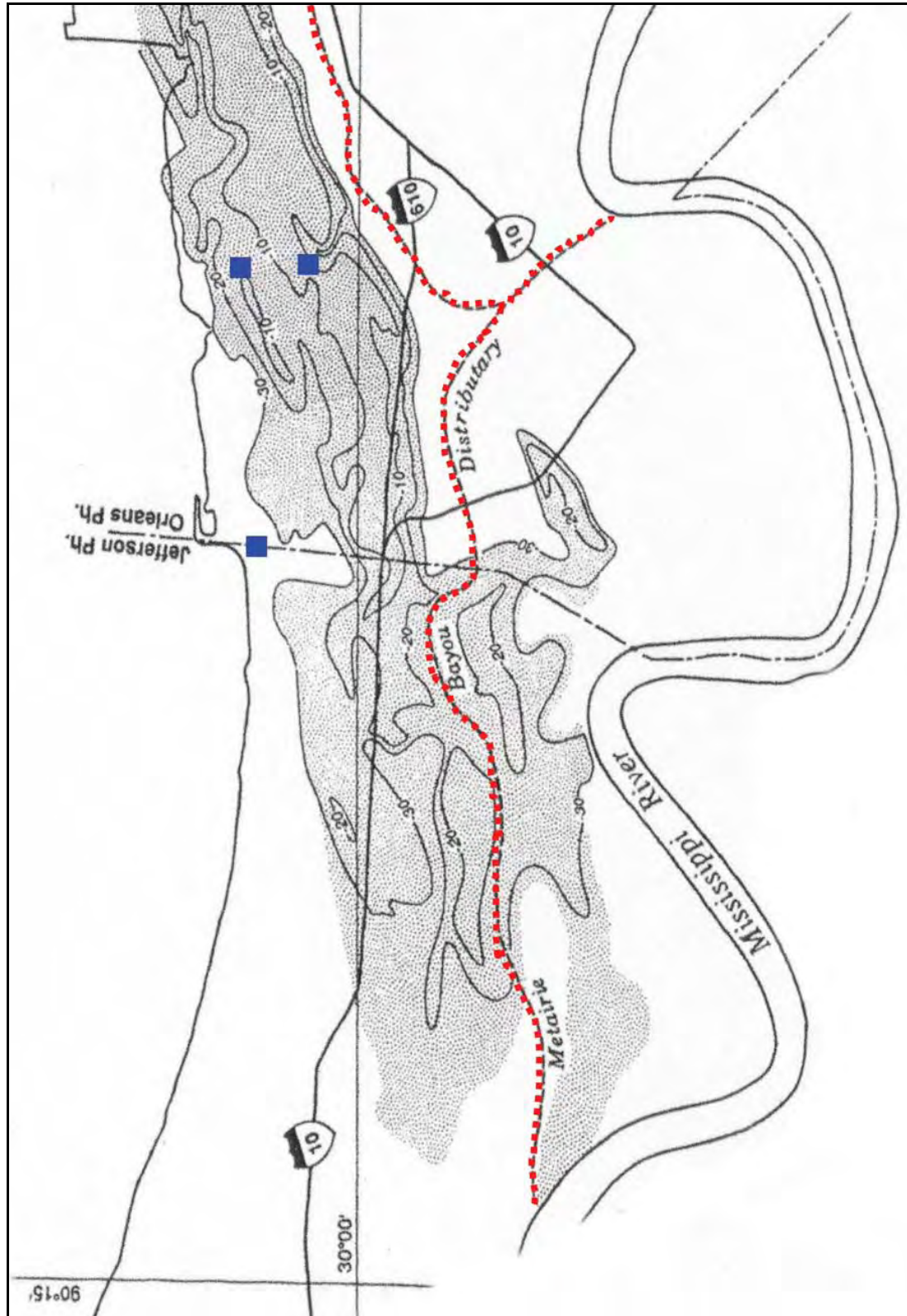
Figure 7-4b. Close-up View of the Buried Beach Ridge and the Locations of the Canal Breaches to the Buried Beach (After Saucier 1994). The 17th Street Breach is Located Behind the Axis of the Beach Ridge, while the London Canal Breaches are Located on the Axis of the Ridge. Bayou Metairie is Identified in Red and Forms the Bayou Sauvage Distributary Course (No. 11) in Figure 7-2.

The presence of the barrier beach affected sedimentation patterns and the subsequent locations for advancing distributary channels in the New Orleans area. The beach complex likely prevented the Mississippi River and later St. Bernard distributaries from completely filling Lake Pontchartrain with sediment. Consequently, foundation soils beneath the 17th and London Canal breaches are affected by their proximity to the buried beach complex. As shown by Figure 7-4, the breach at the 17th Street Canal is located on the protected or land side of the beach ridge, while both of the London Canal breaches are located over the thickest part or axis of this ridge complex.

Surface and Subsurface Geology of the New Orleans Area

A geologic map of the New Orleans area is presented in Figure 7-5 and identifies the major environments of deposition at the surface in the vicinity of the 17th Street and London Canals. Located on the surface of the New Orleans area are natural levee and point bar deposits adjacent to the Mississippi River, abandoned distributary courses (Bayou Sauvage-Metairie north of the Mississippi River and Bayou des Families south of the Mississippi River, respectively), and extensive marsh-swamp deposits at the surface (see also Figure 7-3). Land reclamation occurred in the 1920's along the shore of Lake Pontchartrain by dredging, and this area is identified as spoil deposits.

A portion of cross-section C-C from the Spanish Fort Quadrangle is presented as Figure 7-6 to identify the general subsurface stratigraphy beneath the 17th Street and London Canal breaches. Boring data from this section identify distinct depositional environments in the subsurface that are stacked vertically and form a stratigraphic record of the filling history during the Holocene. Major stratigraphic units in the subsurface, beginning with the oldest, include the Pleistocene (older fluvial and deltaic deposits), bay sound/estuarine, relic beach (Pine Island beach ridge) lacustrine/interdistributary, and marsh/swamp deposits. A summary description of the different depositional environments in the New Orleans area is presented in Appendix 2 (from Dunbar, Torrey, and Wakeley, 1999). Additionally, detailed descriptions of the different depositional environments are contained in Saucier (1994), Kolb (1962), and Kolb and Van Lopik (1958).

Besides mapping the horizontal and vertical limits of the various environments of deposition, relationships between these environments and key engineering properties of the respective soils have been developed. These relationships have been tabulated and are published in Kolb (1962), Montgomery (1974), and Saucier (1994). A summary of these engineering relationships is presented in Appendix 2. Similarly, relationships have been developed from the engineering properties and laboratory soil test data from 17th Street and London Canals. These data are presented in later sections of this summary as related to discussion of their engineering significance.

Geologic information from the New Orleans area helped focus the ERDC investigation and collection of data by the study team at the 17th Street and London canal failures. An understanding of the geology was an important first step to systematically collecting and evaluating stratigraphic and engineering data from these failures areas.
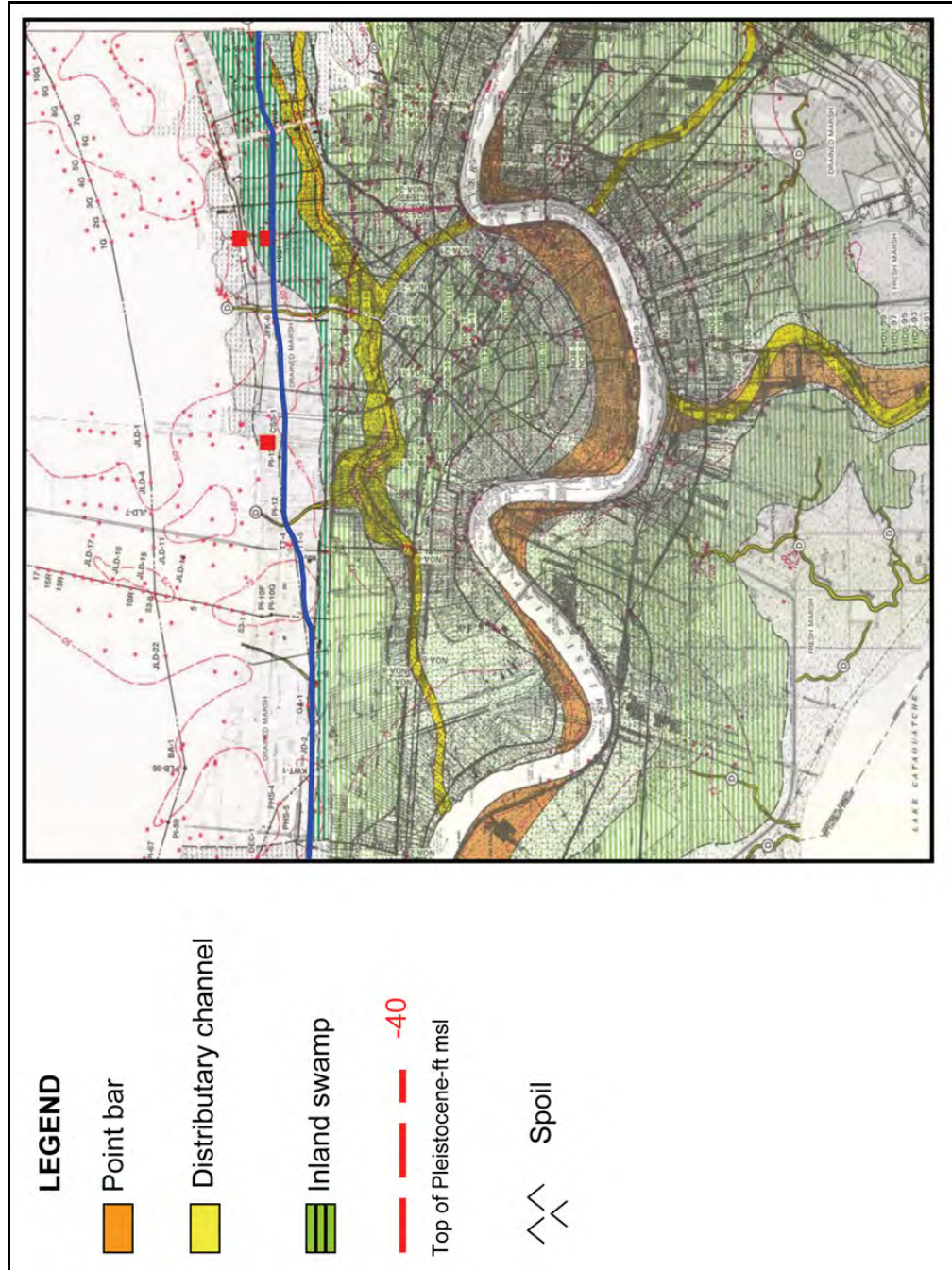
Figure 7-5. Geology Map of the New Orleans and Spanish Fort Quadrangles Showing the Distribution of Depositional Environments at Surface. Elevation of the Pleistocene Surface Shown in Red, along with Borings Used to Map this Surface. Cross-section C-C' in Blue Extends Through 17th Street and London Canal Areas (Areas Identified in Red). See Website lmvmapping.erdc.usace.army.mil for Nearby Maps and Other Cross Sections Identified. Portion of Cross-section C-C' Above is Presented as Figure 7-6 (from Dunbar and Others, 1994 and 1995).
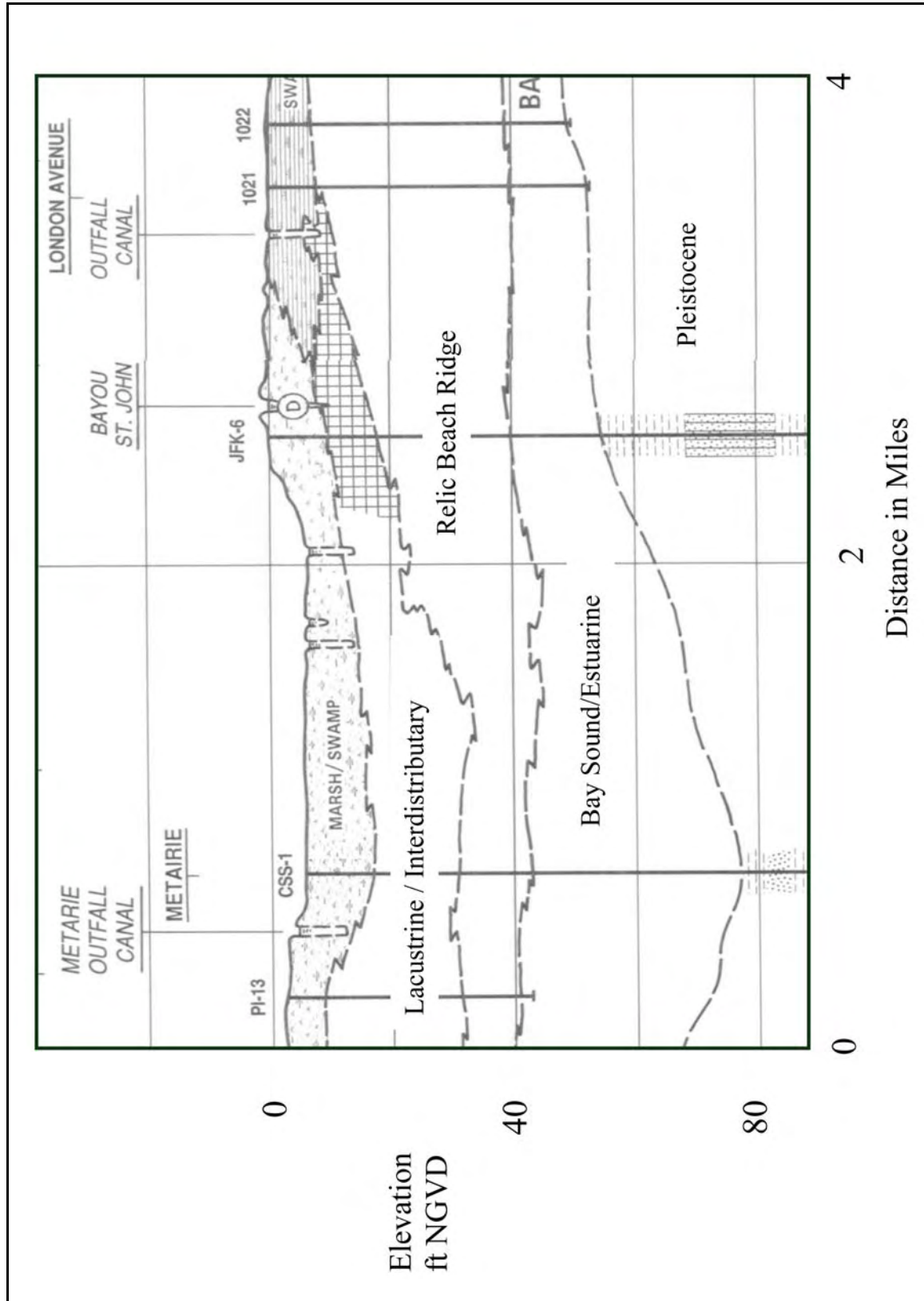
Figure 7-6. Portion of Cross-section C-C" from the Spanish Fort Quadrangle, which Extends Through the 17th and London Canal Breaches and Identifies the Sratigraphic Environments in the Subsurface (from Dunbar and Others, 1995).

Development of Cross Sections

Pre-Katrina Data

A significant amount of information was obtained from General Design Memorandum No. 19A– London Avenue Outfall Canal – Volumes I and II (USACE, 1989). This document was completed in January 1989 in preparation for upgrading the New Orleans levee system to provide increased flood protection against a stronger revised design hurricane and contains stratigraphic sections along the levee centerline. Longitudinal or centerline profiles of the west and east bank levees of the London Avenue Outfall Canal are presented as Figures 7-7 and 7-8, respectively (USACE, 1989, p. 134 and 137, respectively). These longitudinal profiles show boring locations and the USCS soil types identified during the exploration program for the project upgrade. Individual boring logs are presented in Volume II of the GDM (USACE, 1989). Foundation borings were drilled on approximately 500 ft spacing, and it is noted that odd-numbered borings are located on the west bank, and even numbered borings are located on the east bank.

Levee breach sites at London North and South have been noted on these respective sections. The northern breach is situated on the west bank of the canal according to the new levee station between Stations 8+25 and 14+00 (Figure 7-7). Opposite of this location on the east bank, between Stations 8+60 and 12+00, is an area of I-wall distress as previously noted (Figure 7-8). The southern breach (Mirabeau) is situated on the east bank of the canal between Stations 53+24 and 55+45.

Post-Katrina Data

ERDC acquired additional soil borings and cone penetrometer (CPT) borings to supplement the above cross-section data and engineering data in the London Canal breach areas (Figures 7-9 and 7-10). New borings were acquired using the U.S. Army Corps of Engineers, Vicksburg District, soil boring and CPT crews in the post-Katrina study of the New Orleans breaches during September through October 2005. Levee centerline and transverse cross sections for the London north and south areas are presented in Figures 7-11 through 7-15 (sections are in DRAFT form) and are representative of conditions before Katrina. All available elevation and geotechnical data were incorporated into the geological profiles to accurately determine the conditions at each failure site.

In the north breach area, continuous, undisturbed 5-in. soil samples were taken in borings NL-1-05U and NL-2-05U (Figure 7-9). In addition, seven CPT borings were pushed along the west side of the canal at locations NLON-1.05C, NLON-2.05C, NLON-11.05C, NLON-12.05C, NLON-13.05C, NLON-14A.05C, and NLON-15.05C (Figure 7-9). These additional borings and CPTs were needed because only two pre-Katrina borings (B26 and B27 from GDM #19A) were in the immediate vicinity of the north breach. The new borings extended the depth of the investigation in this area from an approximate elevation of -45 ft to -60 ft NGVD. Data from CPTs were used to supplement the existing soils data and better refine the stratigraphy in the
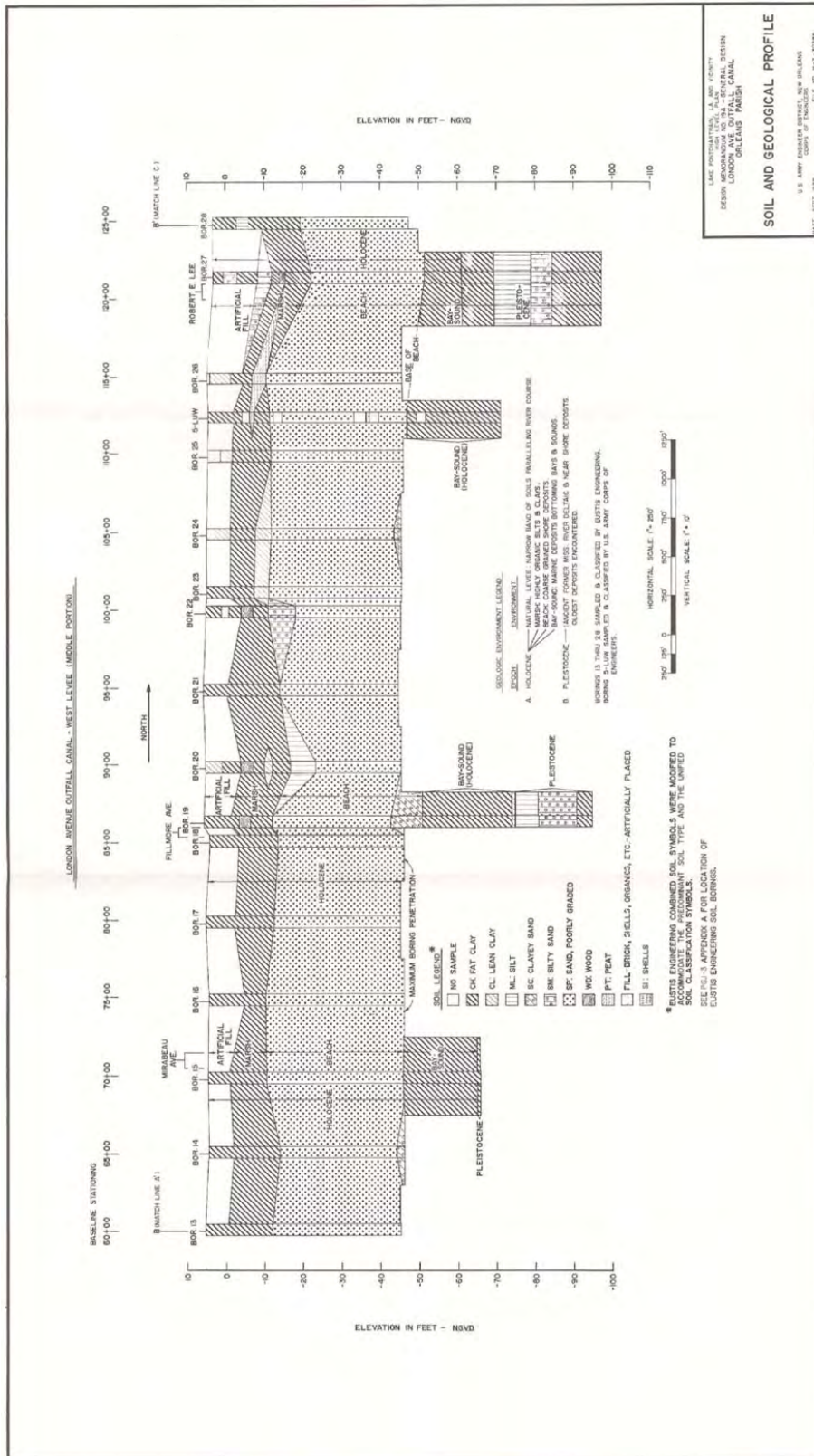
Figure 7-7. Geological Profile, along West Levee at London Canal. North London breach is South of Robert E. Lee Bridge as Shown (USACE, 1989, p. 134)

Volume V The Performance – Levees and Floodwalls – Technical Appendix

V-7-13

This is a preliminary report subject to revision; it does not contain final conclusions of the United States Army Corps of Engineers.
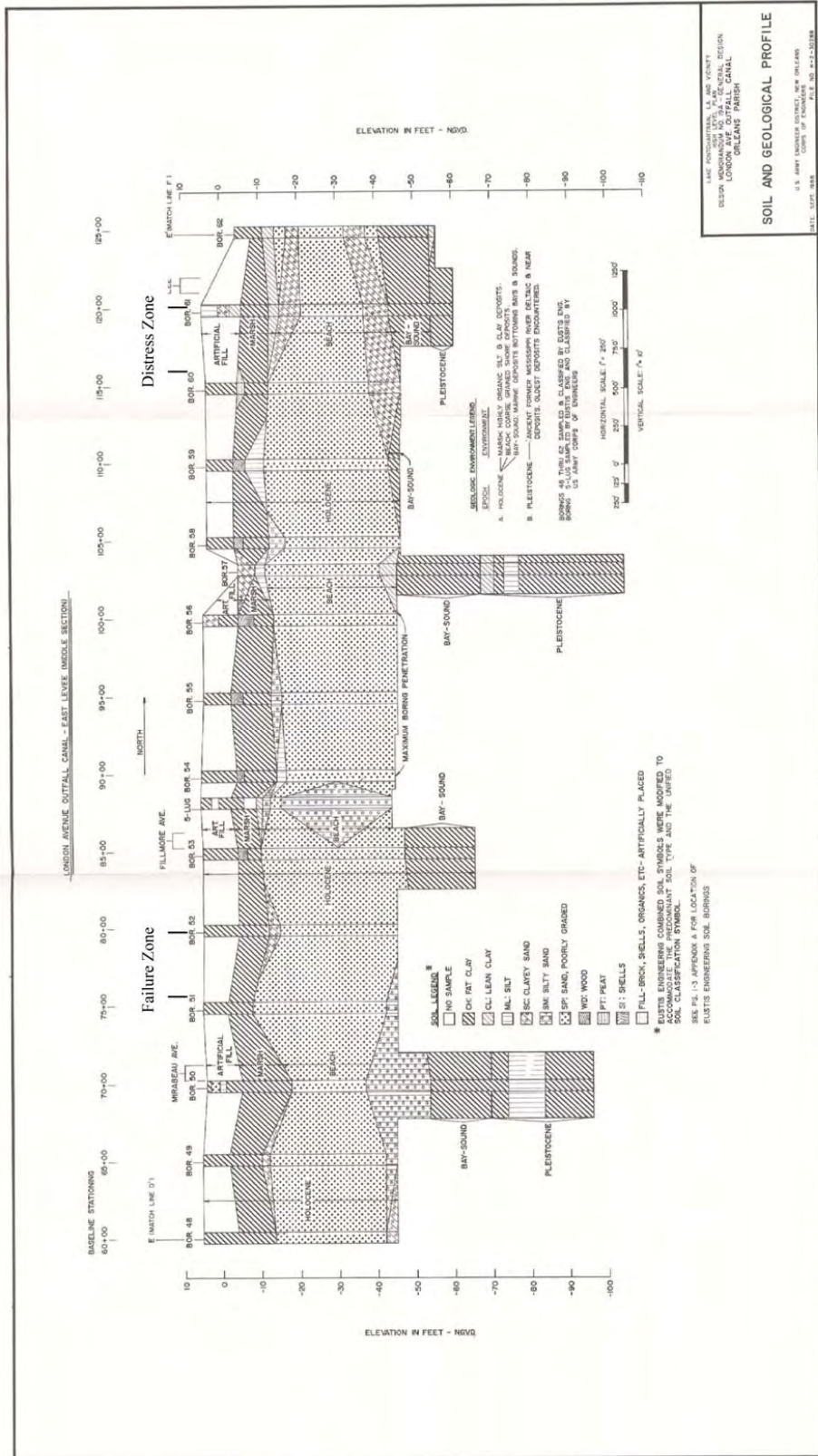
Figure 7-8. Geological Profile Along East Levee at London Canal. North London Area of Levee Distress is South of Robert E. Lee Bridge as Shown, and South London Breach Area is North of Mirabeau Bridge (USACE, 1989, p. 137).

This is a preliminary report subject to revision; it does not contain final conclusions of the United States Army Corps of Engineers.
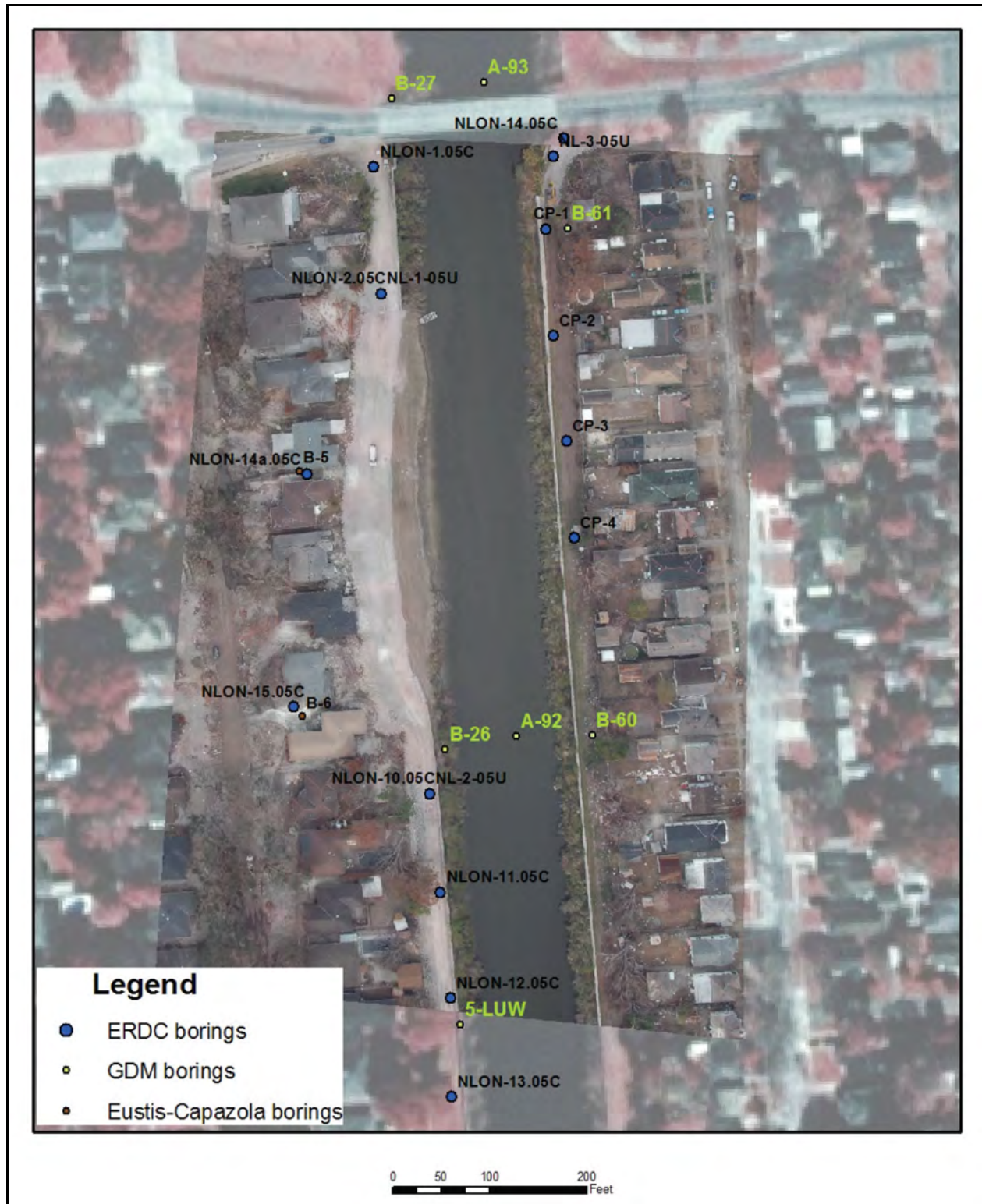
Figure 7-9. Location of all London North Borings and CPTs

Volume V The Performance – Levees and Floodwalls – Technical Appendix

V-7-15

This is a preliminary report subject to revision; it does not contain final conclusions of the United States Army Corps of Engineers.
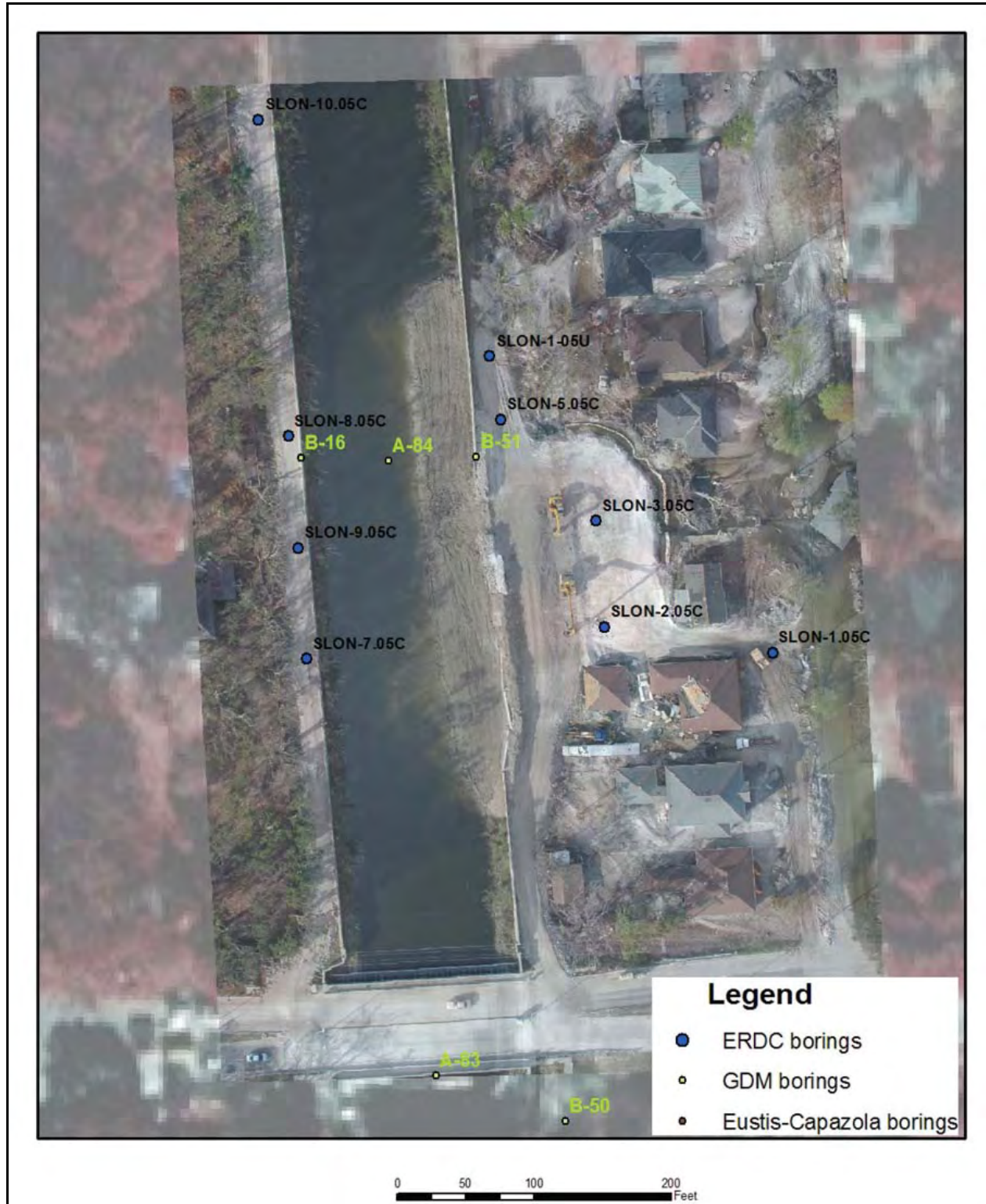
Figure 7-10.   Location of all London South Borings and CPTs

breach area. Along the east wall, borings NL3-05U and 4 CPTs (CP-1, CP-2, CP-3, and CP-4) were used to help define the stratigraphy in the area were the I-wall was in distress. Revised post-Katrina sections for the London north area are presented in Figures 7-11 through 7-13.

Additional soil borings for the south breach included borings SL-1-05U and CPTs SLON-02/2A.05C, SLON-03.05C, and SLON-05.05C (Figure 7-10). Only one existing boring (i.e., B50, GDM #19A) was in the immediate vicinity of the south breach, and additional borings were drilled as shown by Figure 7-10. Two cross sections of the south breach were prepared from these data (Figures 7-14 and 7-15).

Information from all of the soil borings and CPTs was classified into five depositional units in the cross sections in Figures 7-11 through 7-15 over the depth of the investigation (Tables 7-1 and 7-2). Classification of the subsurface into depositional environments is based on previous studies by the USACE for geotechnical purposes (see Appendix 2 for general descriptions of these environments). A summary of these different units is presented in Tables 7-1 and 7-2 for the north and south London breaches, respectively.

Table 7-1
Major Soil Groups at London Ave. Outfall Canal North Breach Site

Layer	Approximate Elevation of Top of Layer, ft		Approximate Elevation of Bottom of Layer		Soil Type	Consistency
	NGVD	NAVD 88	NGVD	NAVD 88		
Embankment (Spoil)	4	2.5	-4	-5.5	Clayey (CL's and CH)	Stiff
Swamp-Marsh	-4	-5.5	-13	-14.5	Organic/Peat	Very Soft
Beach Sand	-13	-14.5	-45	-46.5	Sand (SP, SM)	
Bay Sound/Estuarine	-45	-46.5	-60	-61.5	Clayey (CH)	Stiff to V. Stiff
Pleistocene (Undifferentiated) Prairie Formation	-60	-61.5			Clays – Generally CH with some sand	V. Stiff

Table 7-2
Major Soil Groups at London Ave. Outfall Canal South Breach Site

Layer	Approximate Elevation of Top of Layer, ft		Approximate Elevation of Bottom of Layer		Soil Type	Consistency
	NGVD	NAVD 88	NGVD	NAVD88		
Embankment (Spoil)	5	3.5	-2	-3.5	Clayey (CL's and CH)	Stiff
Swamp-Marsh	-2	-3.5	-14	-15.5	Organic/Peat	Very Soft
Beach Sand	-14	-15.5	-50	-51.5	Sand (SP, SM)	
Bay Sound/Estuarine	-50	-51.5	-78	-79.5	Clayey (CH)	Stiff to V. Stiff
Pleistocene (Undifferentiated) Prairie Formation	-78	-79.5			Clays – Generally CH with some sand	V. Stiff

In the New Orleans area, the top of the Pleistocene is an important surface for engineering purposes with foundation borings often terminating in this unit. The Pleistocene is considered to be the base of the section, and the sediments above this surface representing the Holocene fill. At the top of this Holocene fill sequence is a Swamp-Marsh unit. This unit is represented in borings as organic clay (usually CH) and a peat. Examination of the drilling logs indicates that wood is usually encountered at the top of this unit, and organic clay at the base.

Note: Tip elevation of old
sheet pile canalside of I-wall
is unkown at this time

Sheet Pile Tip @ -16(As
Builts March 1996)
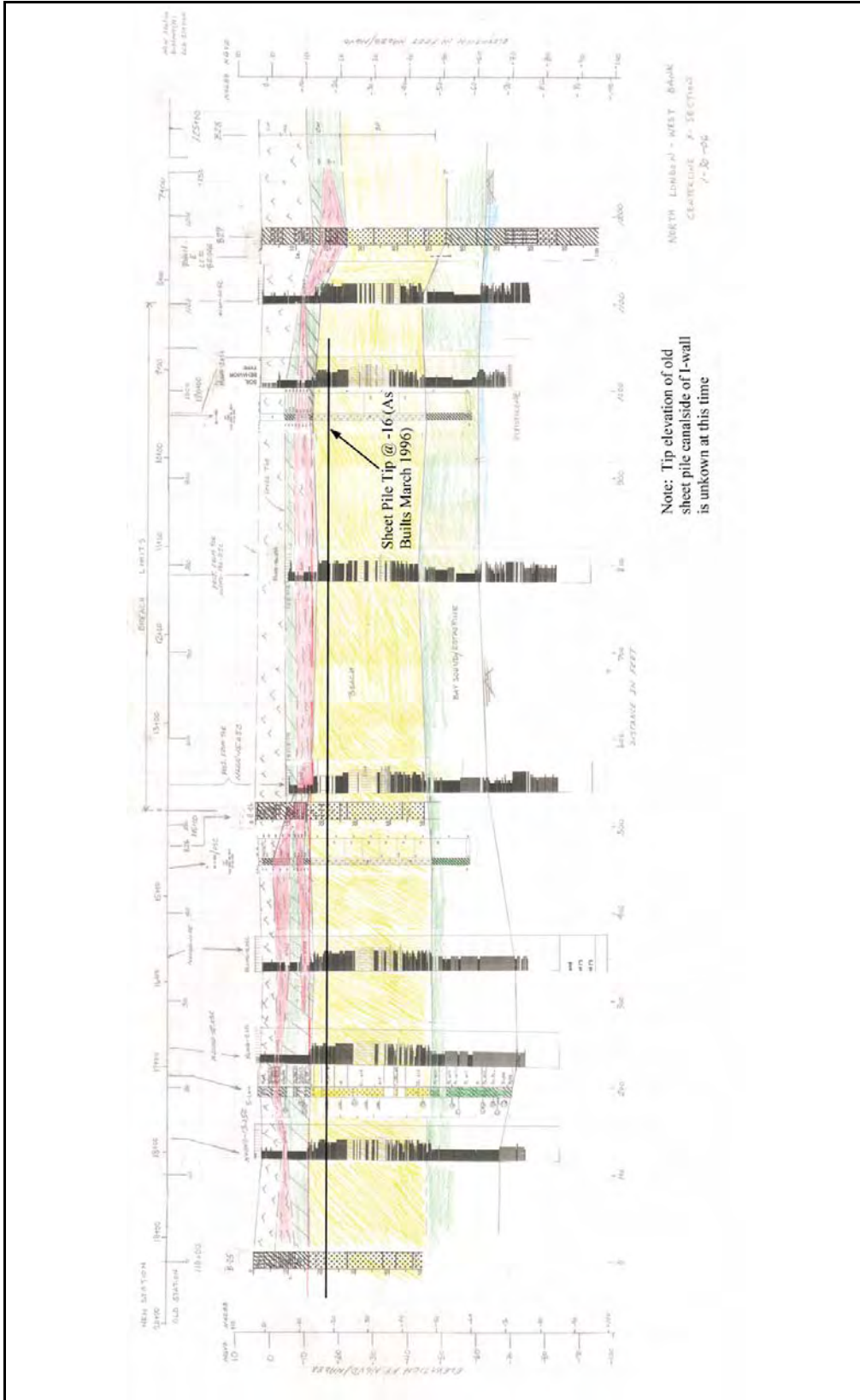
Figure 7-11.   Centerline profile along West Bank London North

Volume V The Performance – Levees and Floodwalls – Technical Appendix
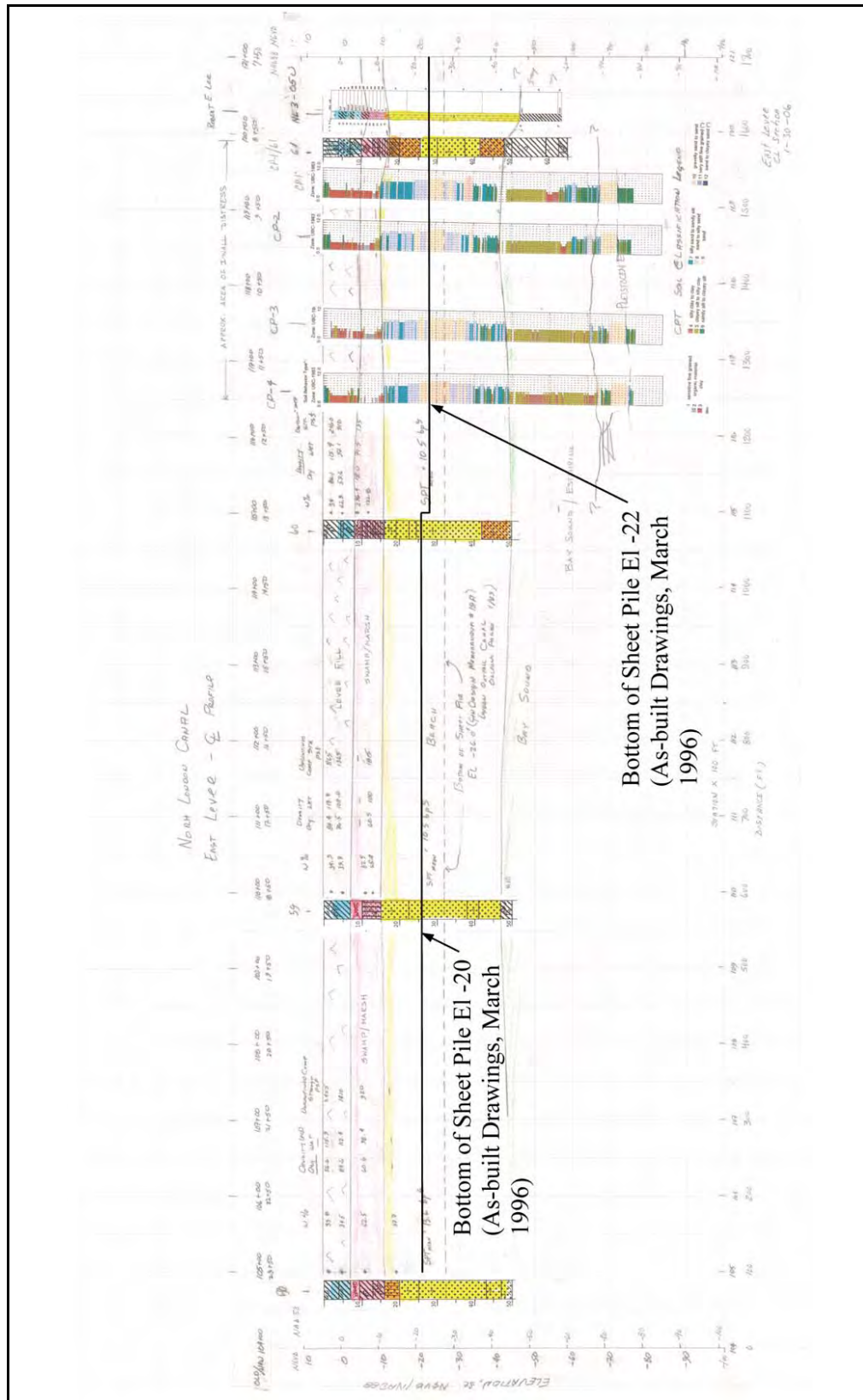
Figure 7-12. Centerline profile along East Bank London North

Volume V The Performance – Levees and Floodwalls – Technical Appendix
This is a preliminary report subject to revision; it does not contain final conclusions of the United States Army Corps of Engineers.

V-7-19
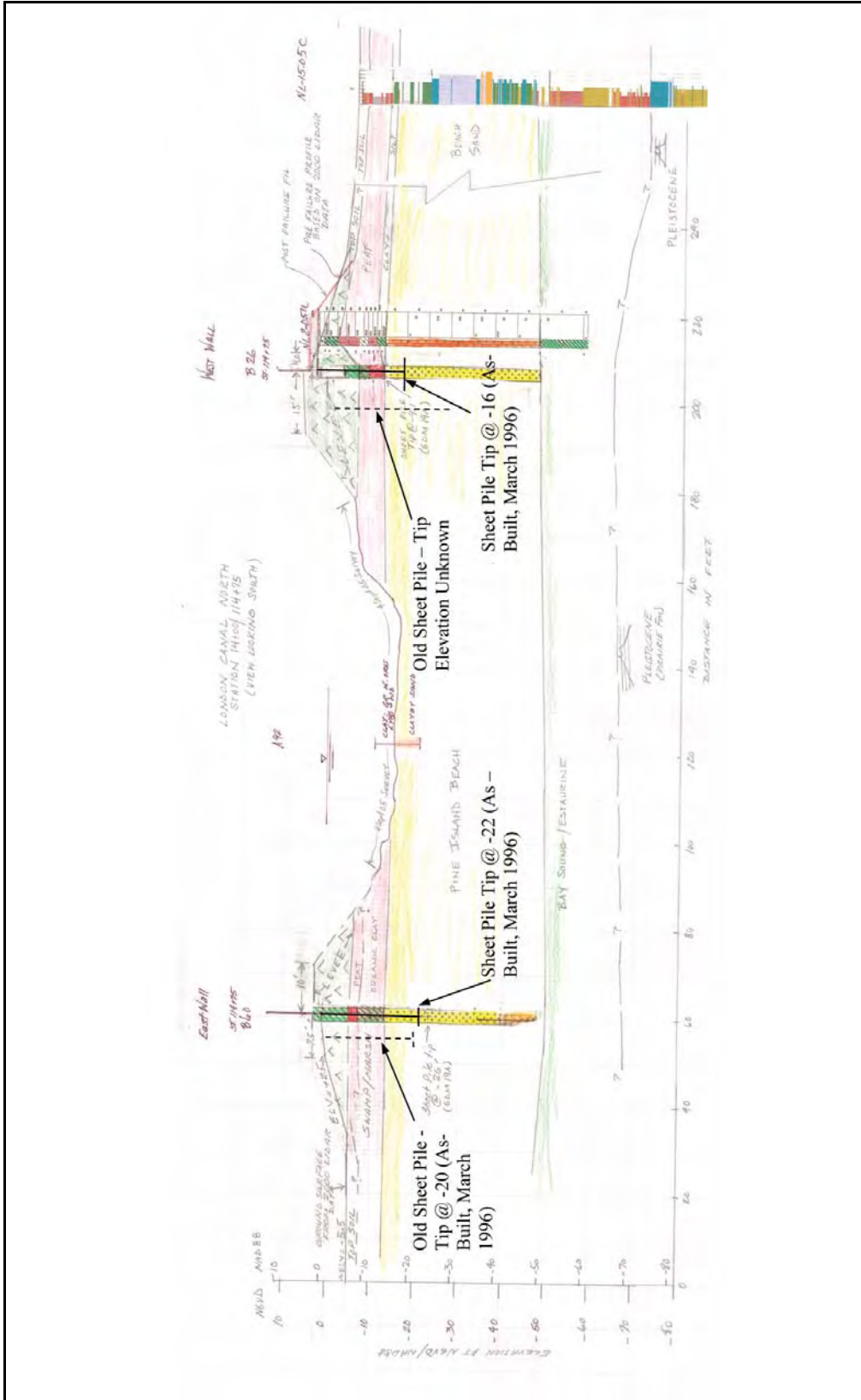
Figure 7-13.   Transverse profile at Station 14+00 (Old Station 114+75) London North

This is a preliminary report subject to revision; it does not contain final conclusions of the United States Army Corps of Engineers.
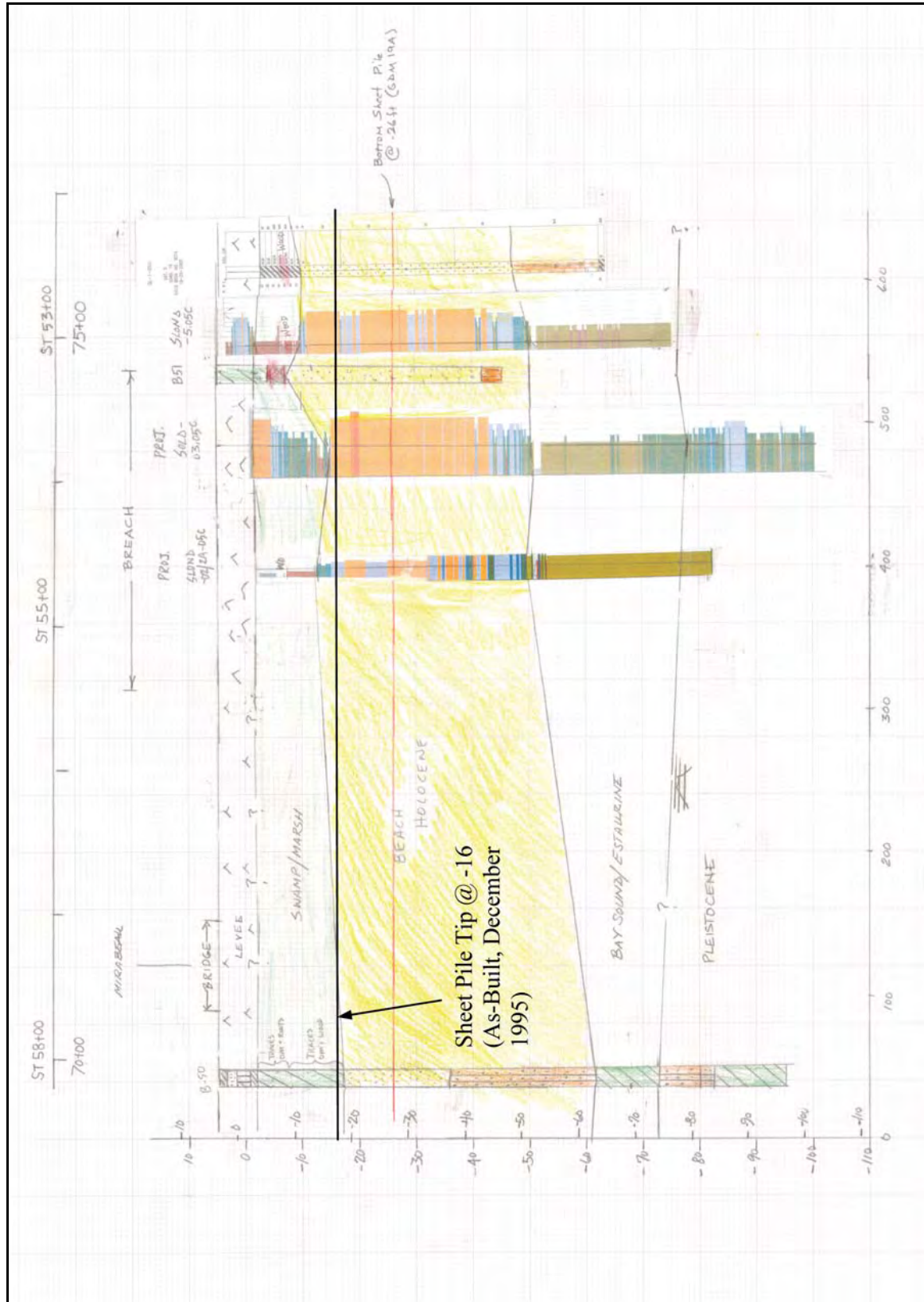
Figure 7-14.   Centerline profile along East Bank London South
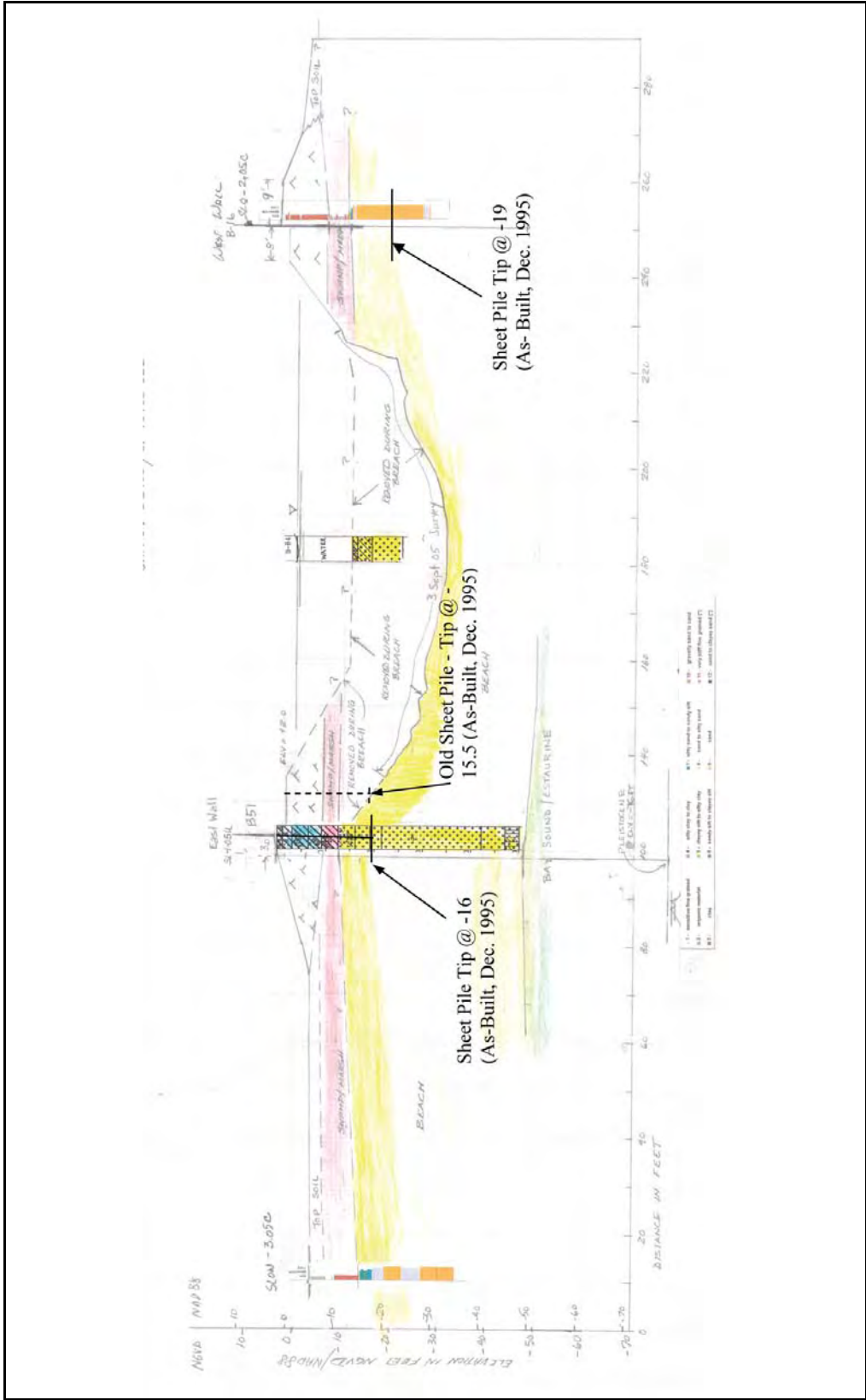
Figure 7-15.   Transverse profile at Station 53+00 (Old Station 75+00) London South

This observation is supported from a survey of the displaced peat blocks at the 17th Street area as part of the ERDC investigation of the failures. Relatively intact sections of the swamp-marsh unit were observed along the street where these blocks were eventually displaced by the flood. The swamp (woody) part of the section was at the top, graded towards a peat (fibrous) section in the middle, and an organic clay section at the base. In several instances, the displaced "peat blocks" contained the intact, underlying shallow water unit, or the entire transition representing the shallow water to a terrestrial fill sequence that occurred during the Holocene. This same environmental transition is observed at London, except the underlying unit is not cohesive. Instead, the underlying unit is sand that was easily displaced from the buried beach unit as evidenced by the volume of sand at London north and south in the nearby neighborhood.

In addition, old sheet pile that was put in before or right after Hurricane Betsy (1965) exists at the north and south London breaches. At the north breach, on the west bank, the old sheet pile is canal side of the floodwall, and the tip elevation is unknown at this time. On the east bank at the distressed area, the old sheet pile is on the protected side of the floodwall. At the south London breach, on the east bank, the old sheet pile is on the canal side of the floodwall. The tip elevations of the old sheet pile are shown on the transverse cross sections.

Transverse Cross Sections through the Breach Sites

Transverse cross sections through the London north and south breach sites (Figures 7-13 and 7-15) incorporate remotely sensed elevation and bathymetry data from in the canals. Data from a pre-Katrina airborne LIDAR (Light Detection and Ranging) survey along the New Orleans Levee System that was flown in 2000 was incorporated into the cross sections to improve the surface topography in the breach area. This 2000 LIDAR survey is the best data available for establishing the pre-Katrina surface topography of the levee embankment. LIDAR surveys generate points of X, Y, and Z data that are accurate to the nearest foot. Additionally, this LIDAR data identifies tree locations along the levee and approximate size of these trees based on the diameter of the canopies. Profiles of the levee embankments were evaluated using ArcView software to determine the elevation profiles between the vegetated areas.

Post-Katrina Bathymetric survey data were incorporated into the transverse sections to determine the canal depths and slopes in relation to the embankment geometry and stratigraphy. Survey data from September 4 and 29, 2005, were evaluated to determine the elevations of the canal bottom between the floodwalls. This early Bathymetric survey data is reflected in the cross sections. Bathymetric survey data for London South show massive scouring in the channel and are reflected by the transverse cross section in Figure 7-15, and the volume of sand deposited in the neighborhood.

Uncertainties

Many uncertainties pertaining to the subsurface in the breach area will be difficult, if not impossible, to resolve because the levee in the London north and south breach areas was destroyed and drastically changed by emergency repair efforts. Furthermore, there was a lack of subsurface information on the protected side of the levee during the 1990 levee raising project described in GDM#20. ERDC is obtaining additional information in the vicinity of the breach areas with field vane shear tests, cone penetrometer tests, and laboratory testing of samples

retrieved from existing borings to obtain data pertaining to the strength and the thickness of these layers.

Soil Properties

Introduction

The following is a summary of the current geotechnical data available in the breach areas on the London Canal. These breach areas include the north breach site, the south breach site, and the distressed area across from the north breach site. Engineering soil data from each site will include all boring, laboratory, and cone penetrometer tests (CPT) in the breach area.

North Breach Site – West Levee

New borings were taken at the centerline and toe of the levee. Centerline borings include two new borings, two borings from the GDM, and four CPTs. New borings include NL-1-05U and NL-2-05U, consisting of 5-in. undisturbed samples. The GDM borings included 5-LUW (5-in. undisturbed samples) and B-26 (3-in. undisturbed samples). The CPTs include NLON-2.05C, NLON-10.05C, NLON-11.05C, and NLON-12.05C. CPTs NLON-2.05C and NLON-10.05C were the only ones taken with pore pressure measurements.

Borings at the toe of the levee include two new borings, one boring from the GDM, and two CPTs. The new borings include B-5 and B-6, with both borings consisting of 3-in. undisturbed samples. The GDM boring includes B-27 (3-in. undisturbed samples). The CPTs include NLON-14a.05C and NLON-15.05C. NLON-14a.05c was the only CPT taken with pore pressure measurements.

Moisture Content and Unit Weights

The moisture content (%w) versus elevation (NAVD 88) for samples taken from the levee centerline and above the beach sand is shown in Figure 7-16. Generally, the borings from the levee centerline show levee fill on top of a marsh layer (which consists of peat or organic clay) and a 2-ft clay (CH) layer below the marsh layer. Boring NL-2-05 shows a 2-ft clay (CL) seam in the marsh layer from about elevation -5 to -8 (NAVD 88). However, GDM boring B-26 does not show the 2-ft clay layer at the bottom of the marsh layer.

Table 7-3 summarizes laboratory test data, showing the wet unit weights for samples taken from the levee centerline in the breach area.
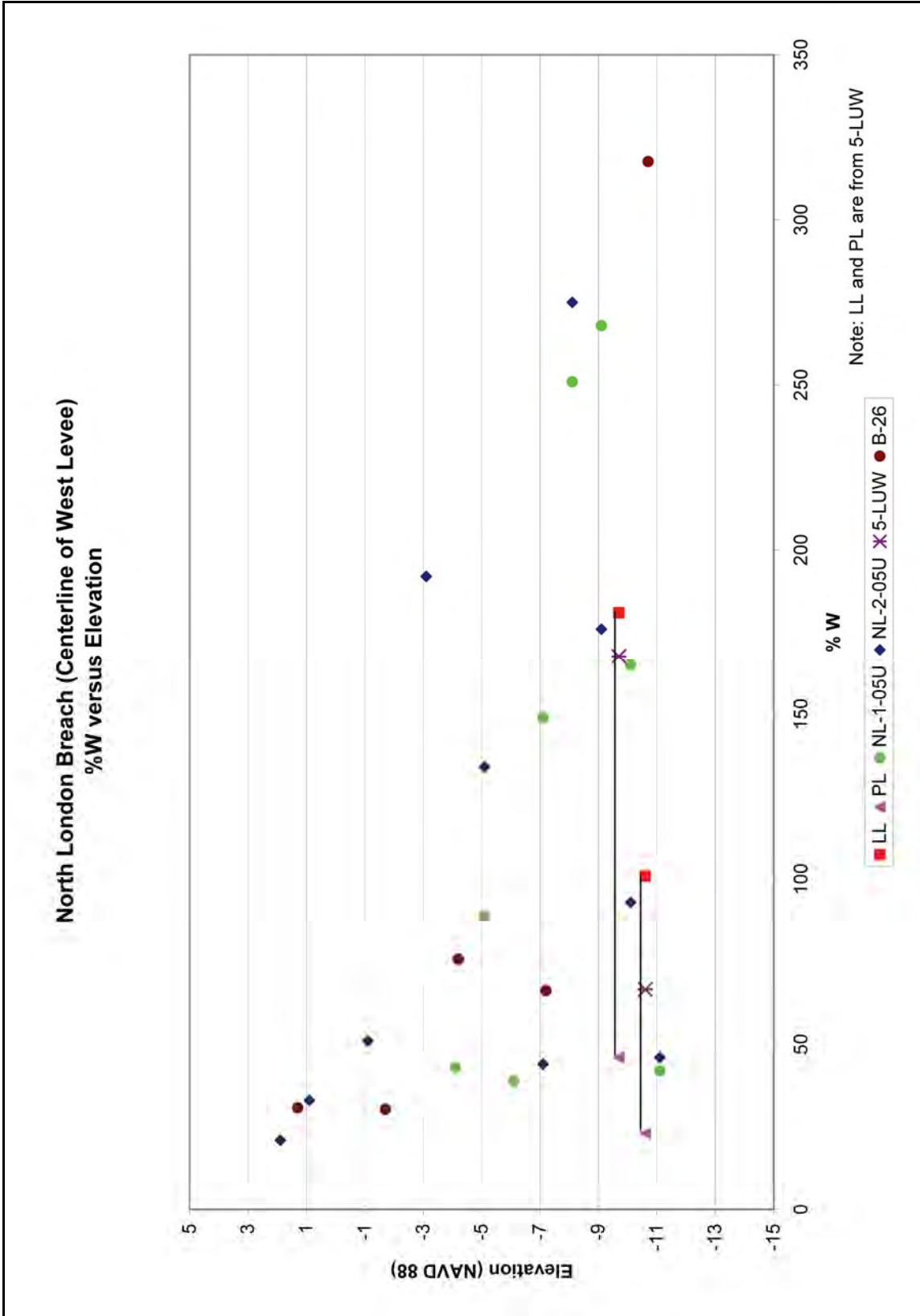
Figure 7-16.   North London Breach (Centerline of West Levee), %w versus Elevation

Table 7-3
Wet Unit Weights from Levee Centerline

Boring	Elevation (NAVD 88)	Soil Type	%w	Dry Unit Weight (pcf)	Wet Unit Weight (pcf)	Average Wet Unit Weight
Levee Embankment						
B-26	1.30	Silty Clay	30.8	79	103.4	108.1
B-26	-1.70	Silty Clay	30.4	86.5	112.8	
Marsh Layer						
B-26	-7.20	Clay	66.3	54.3	90.3	
5LUW	-9.7	CH	167.7	29	80	
5LUW	-10.6	CH	66.6	60	100	

The geologic environment for the breach area is similar to the geologic environment for the west levee between GDM Stationing 39+60 to 121+35. Therefore, the moisture content (%w) versus elevation (NAVD 88) and the wet unit weight versus elevation (NAVD 88) were plotted in Figures 7-17 through 7-20.

The moisture content (%w) versus elevation (NAVD 88) for samples taken from the levee toe and above the beach sand is shown in Figure 7-21. Generally, borings from the levee toe show a top soil layer on top of a marsh layer (which consists of peat or organic clay) and a 2-ft clay and silt layer below the marsh layer.

Below is a table showing the wet unit weights for samples taken from the levee toe in the breach area.

Boring	Elevation (NAVD 88)	Soil Type	%w	Dry Unit Weight (pcf)	Wet Unit Weight (pcf)
B-6	-4.28	CH	40	71.4	99.9
B-6	-6.78	CH	239	23.6	79.7
B-5	-6.97	CH	204	21.7	65.8
B-6	-9.28	CH	67	57.1	95.2
B-5	-9.47	CH	67	56.7	94.7
B-6	-11.78	CL	36	84.1	114.6
B-27	-14.50	Clay	70	57.8	98.2
B-27	-18.00	Organic Clay	193.4	24.5	71.8
B-27	-22.00	Organic Clay	149.2	31.3	78

Shear Strength

Shear strengths from laboratory tests of the levee embankment and marsh unit (under the centerline) are fairly sparse. Figure 7-22 shows a plot of the four shear strength data points. However, two CPTs with pore pressure measurements were taken in the breach area through the centerline. Shear strength plots of CPT NLON-2.05C using the bearing capacity method ($N_k=15$) and Mayne's method are shown in Figure 7-23. Also shown in Figure 7-23 is boring NL-1-05U, which was drilled next to the CPT. From the plot on Figure 7-23, a clay layer between
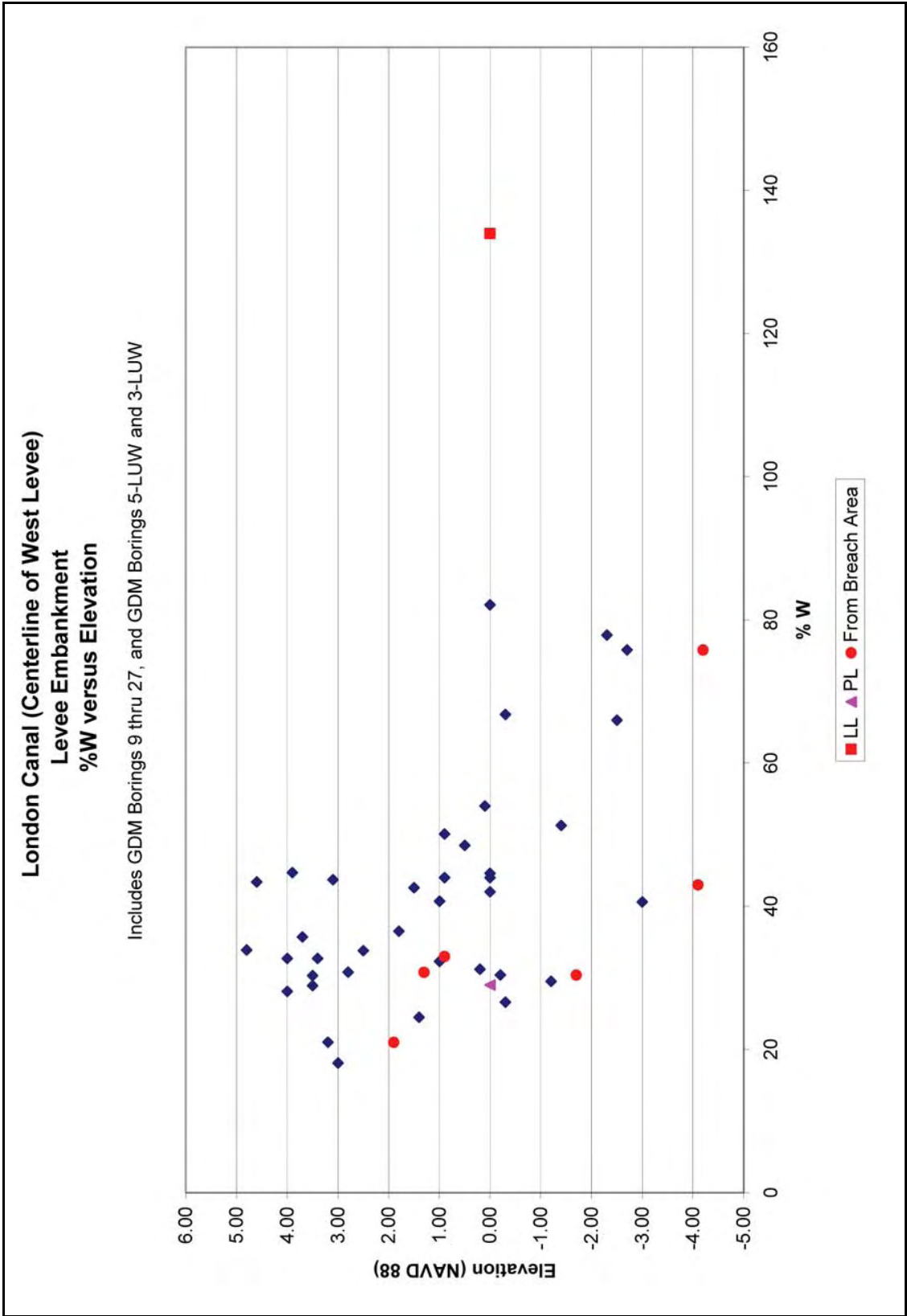
Figure 7-17.   London Canal (Centerline of West Levee), Levee Embankment, %w versus Elevation
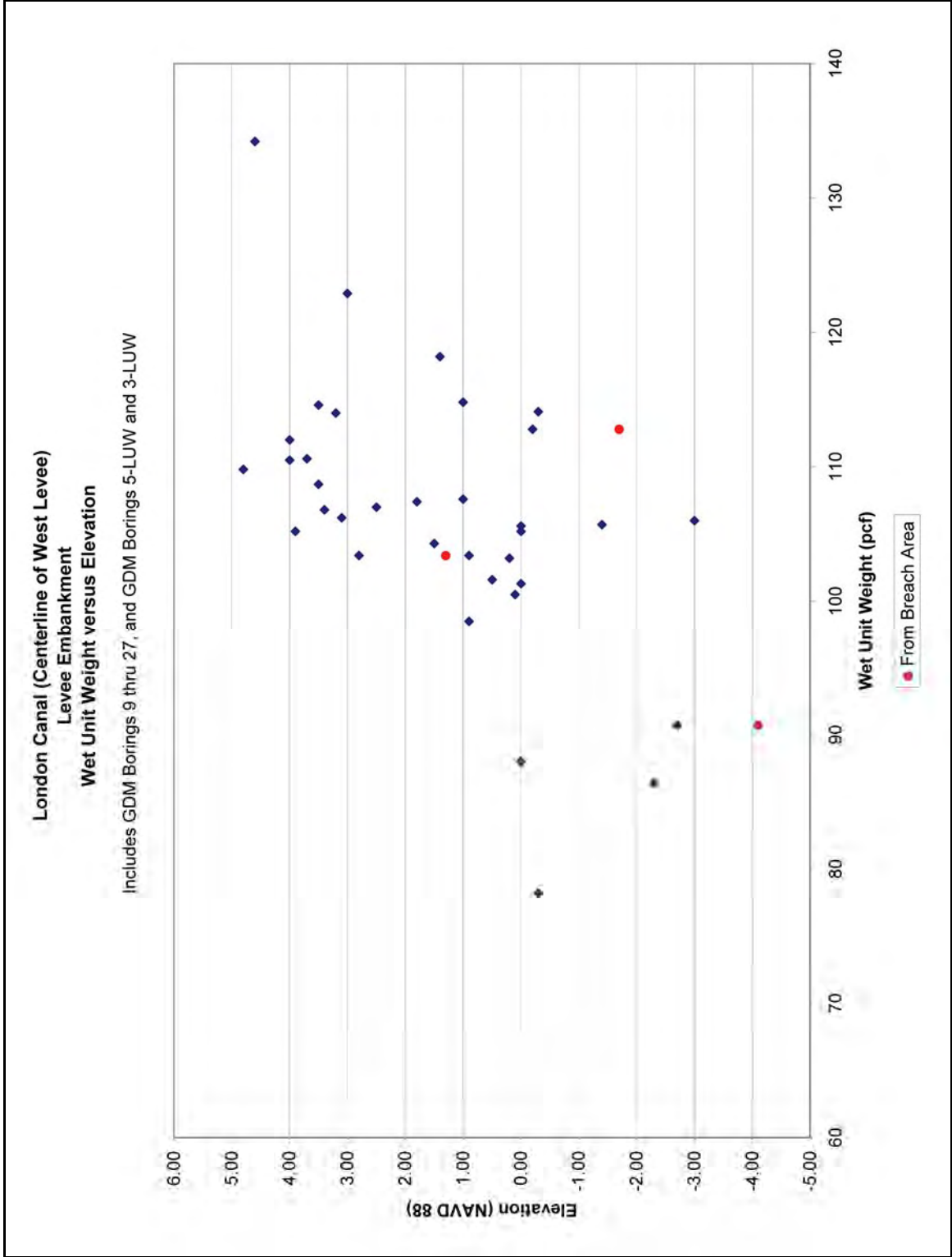
Figure 7-18.   London Canal (Centerline of West Levee), Levee Embankment, Wet Unit Weight versus Elevation
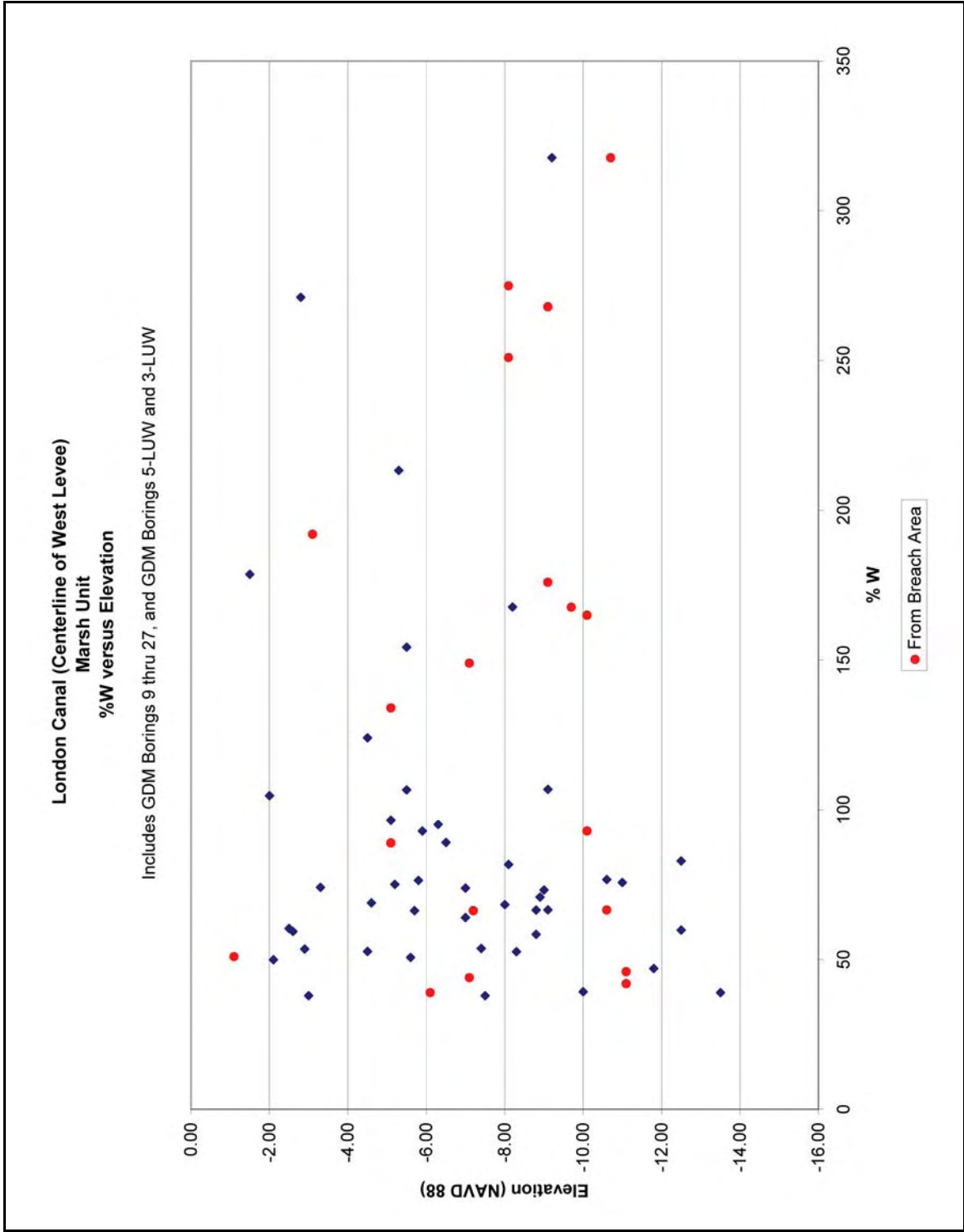
Figure 7-19.   London Canal (Centerline of West Levee), Marsh Unit, %w versus Elevation

This is a preliminary report subject to revision; it does not contain final conclusions of the United States Army Corps of Engineers.
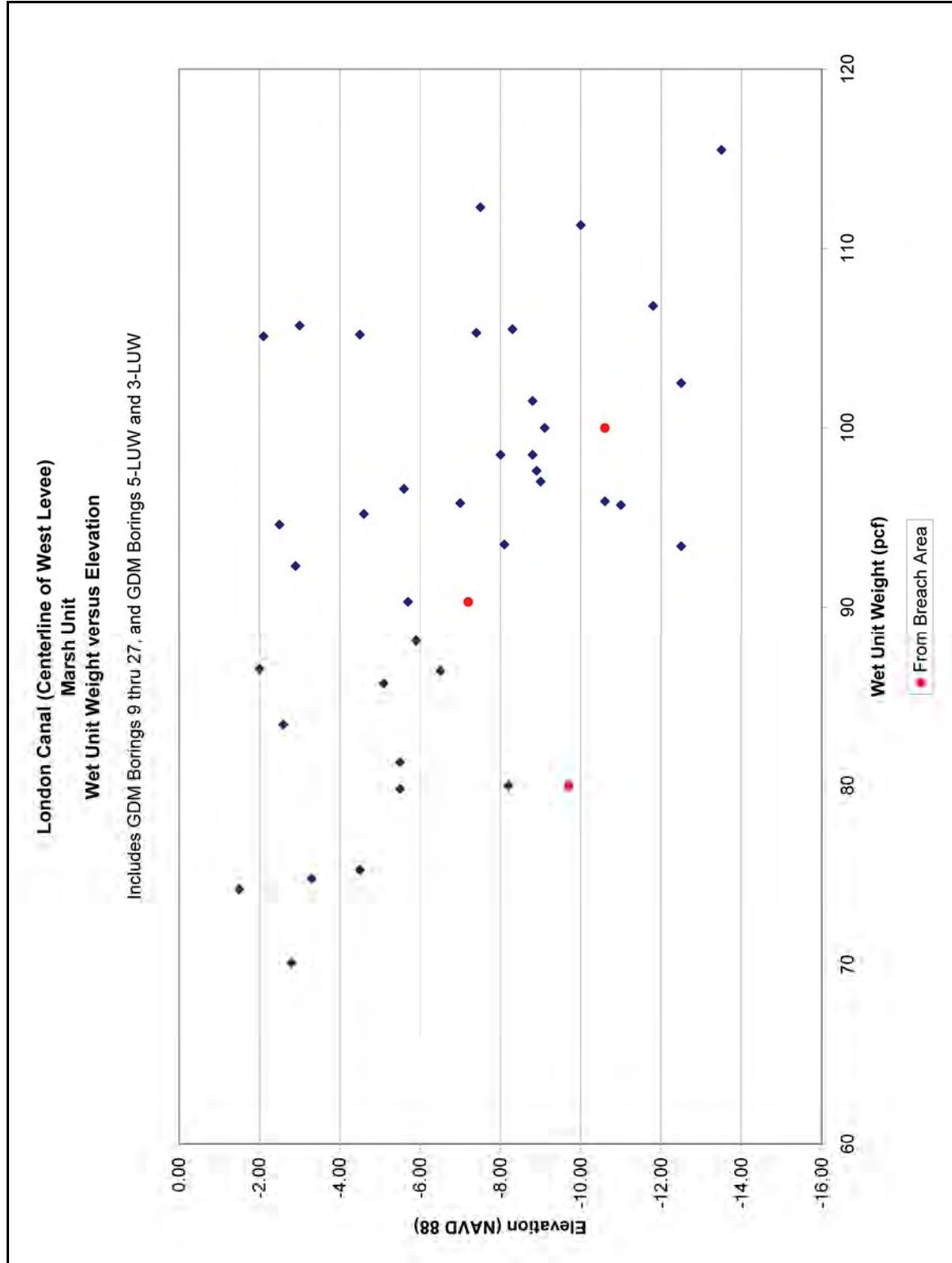
Figure 7-20.   London Canal (Centerline of West Levee), Marsh Unit, Wet Unit Weight versus Elevation
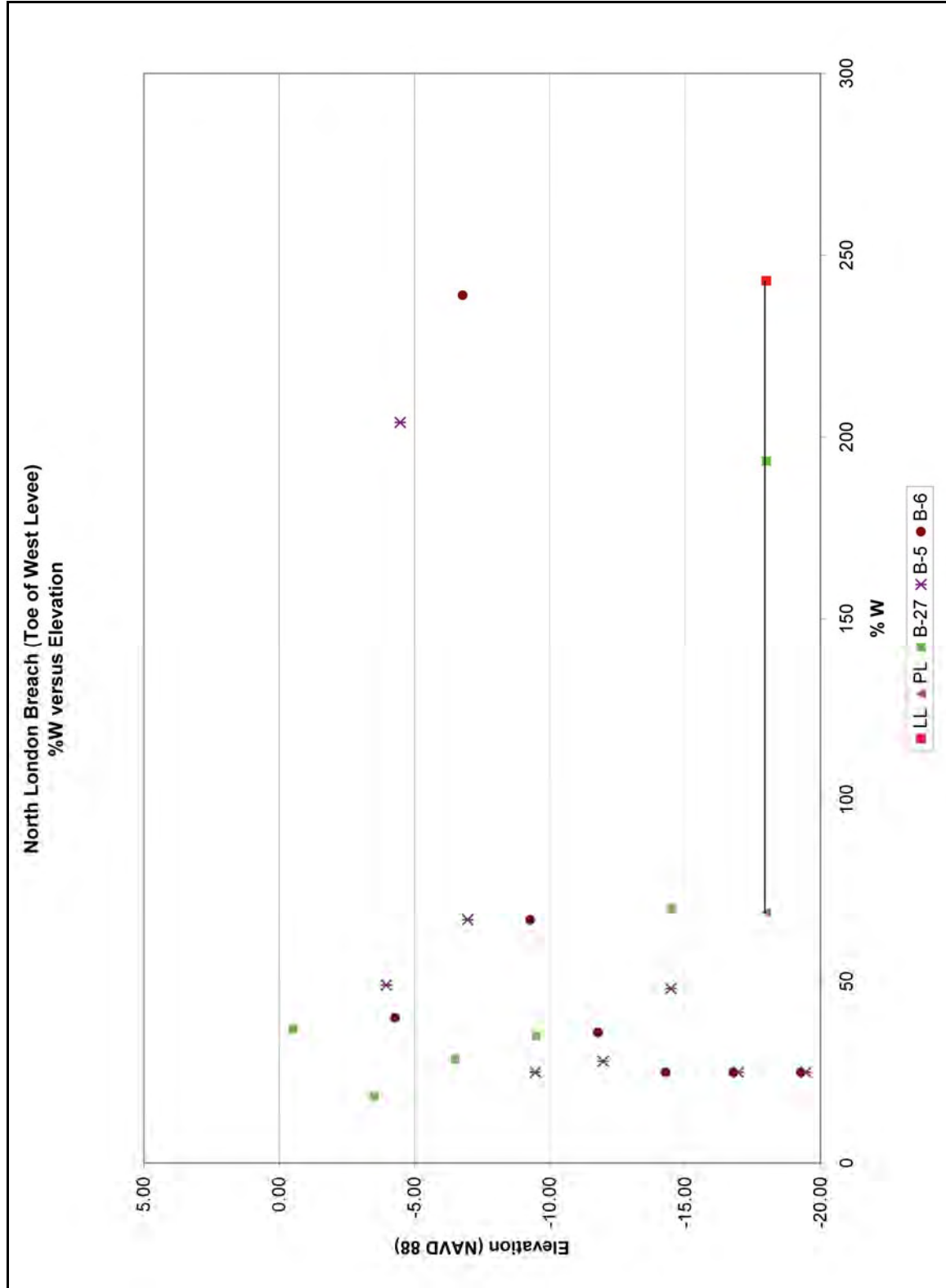
Figure 7-21.   North London Breach (Toe of West Levee), %w versus Elevation
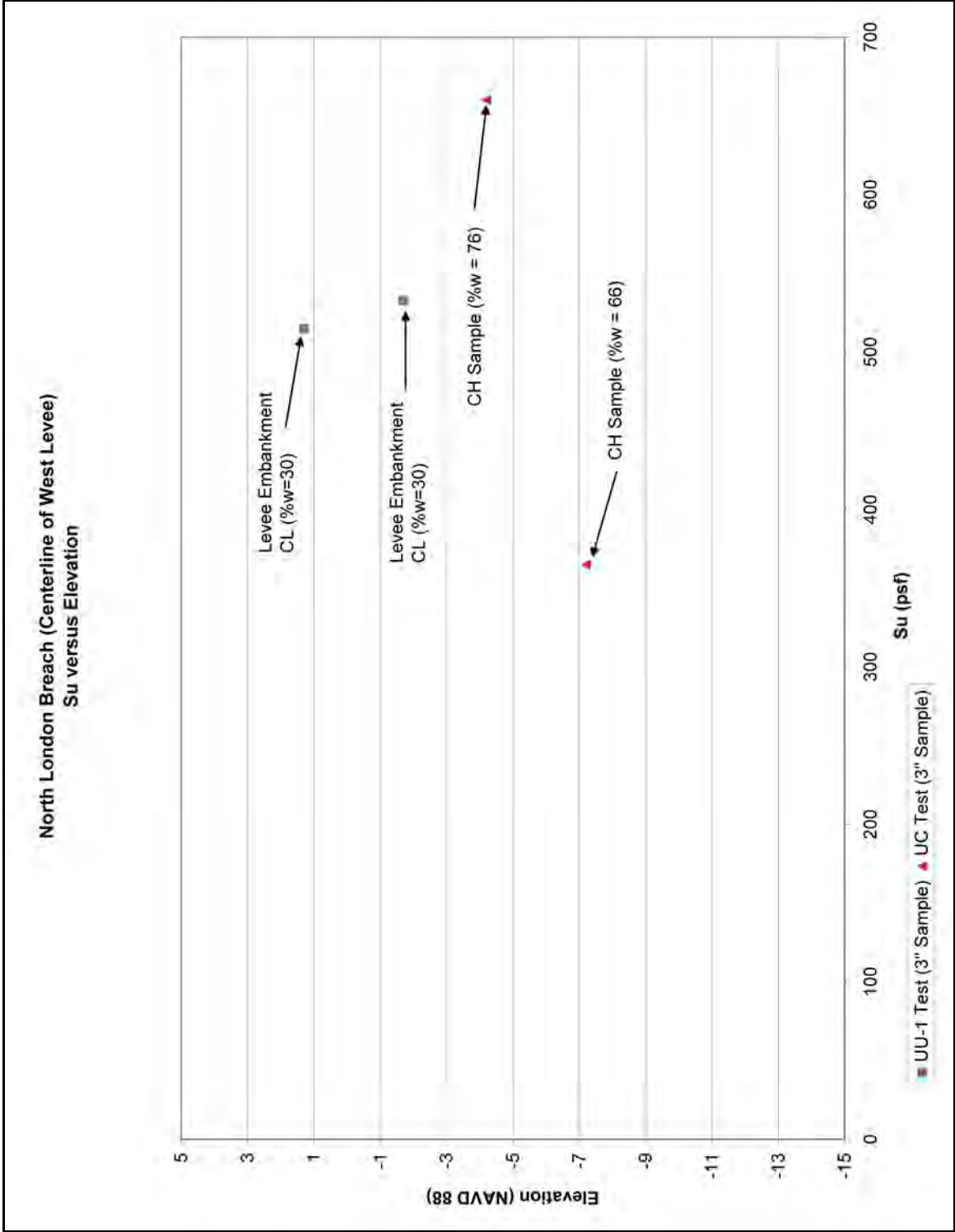
Figure 7-22.   North London Breach (Centerline of West Levee), Su versus Elevation

This is a preliminary report subject to revision; it does not contain final conclusions of the United States Army Corps of Engineers.
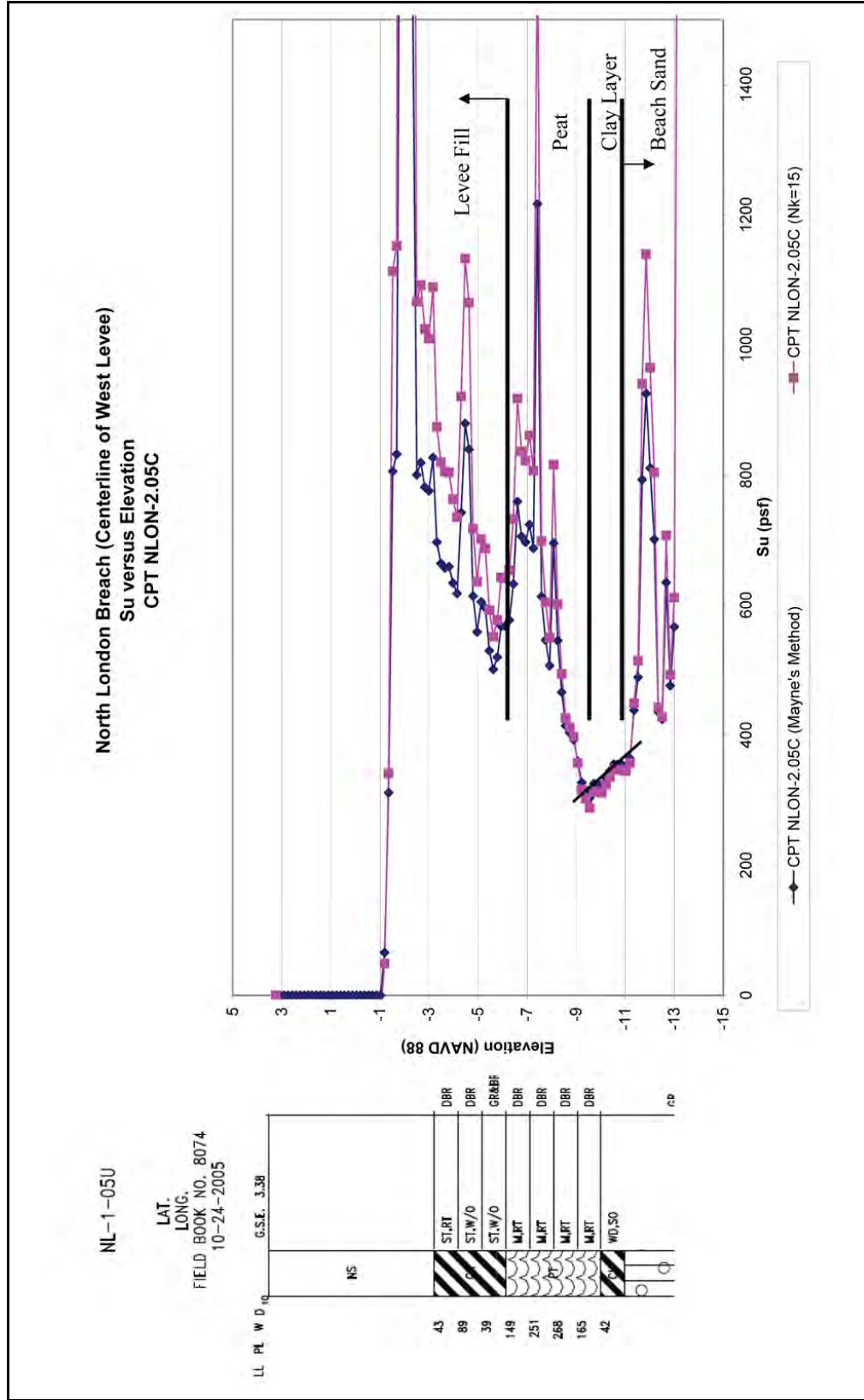
Figure 7-23. North London Breach (Centerline of West Levee), Su versus Elevation for CPT NLON-2.05C

elevations -9 and -11, which is at the top of the beach sand, is clearly detected by the CPT. The CPT shows that this clay layer has an Su/P ratio of 0.26 to 0.28.

Shear strength plots of CPT NLON-10.05C, using the bearing capacity method (N_k=15) and Mayne's method, are shown in Figure 7-24. However, an increase in strength per depth was not detected in the clay layer at the top of the beach sand. The shear strength versus elevation for both CPTs and laboratory test data is shown in Figure 7-25. Mayne's method was used to compute the shear strengths in this figure.

Shear strengths from laboratory tests of the marsh unit at the toe of the levee are shown in Figure 7-26. In addition, shear strength plots of laboratory tests and CPT data are shown in Figure 7-27. Because of equipment difficulties, CPT NLON-14a.05C was only pushed to a depth of 28 ft with pore pressure measurements. The CPT was pushed again to a depth of 80 ft, but no pore measurements were taken. Below is a table summarizing the available laboratory shear strength data from the toe.

Table 7-5
Laboratory Shear Strength Test Data for Samples taken from North London Breach Toe of Levee

Boring	Elevation (NAVD 88)	Soil Type	%w	UC Test (psf)	UU Test (psf)
6	-4.28	CH	40	540	
6	-6.78	CH	239	700	
5	-6.97	CH	204	220	
6	-9.28	CH	67	200	
5	-9.47	CH	67	110	
6	-11.78	CL	36		220
27	-14.50	Clay	70	517.5	
27	-18.00	Organic Clay	193.4	470	
27	-22.00	Organic Clay	149.2	230	

Gradation and Standard Penetration Number for Beach Sand Unit

A plot of the D_{10}, D_{30}, and D_{60} values for the Beach Sand Unit is shown on Figure 7-28. These values consist of gradation tests conducted on samples from borings B-5 and B-6. A summary of these values are presented in the table below.

Table 7-6
D10, D30, and D60 Values for the Beach Sand Unit

Boring	Elevation (NAVD 88)	Soil Type	D_{60} (mm)	D_{30} (mm)	D_{10} (mm)
5	-14.47	SM	0.21	0.175	
6	-16.78	SM	0.22	0.18	0.16
5	-19.47	SM	0.205	0.175	0.12
6	-21.78	SM	0.225	0.18	0.125
5	-24.47	SM	0.185	0.15	0.085
6	-26.78	SM	0.18	0.125	0.08
5	-29.47	SM	0.2	0.18	0.125
6	-32.78	SM	0.145	0.096	0.075
5	-34.47	SM	0.205	0.18	0.17
6	-36.78	SM	0.18	0.105	
6	-41.78	SM	0.2	0.175	0.095
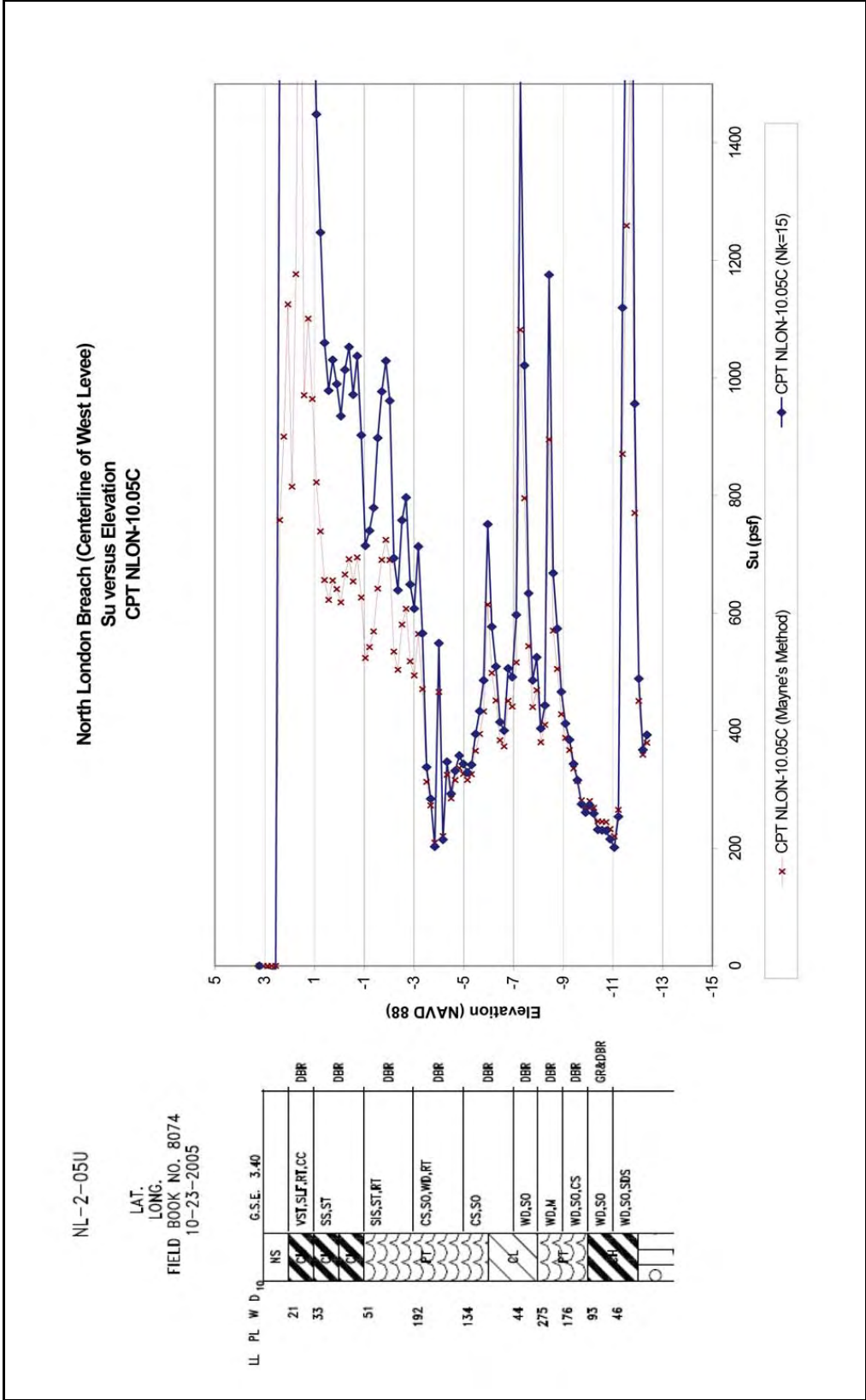
Figure 7-24. North London Breach (Centerline of West Levee), Su versus Elevation for CPT NLON-10.05C

Volume V The Performance – Levees and Floodwalls – Technical Appendix

V-7-35

This is a preliminary report subject to revision; it does not contain final conclusions of the United States Army Corps of Engineers.
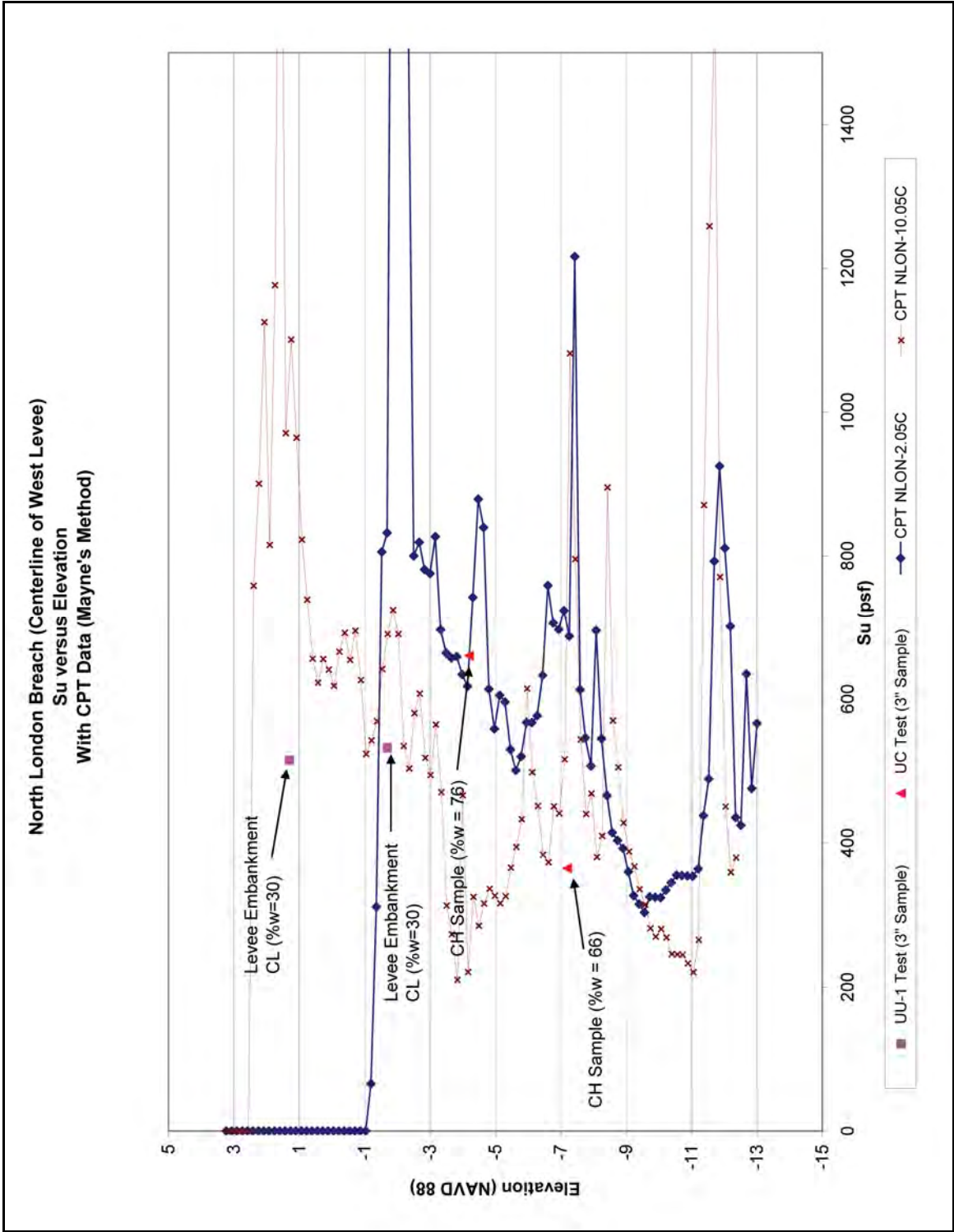
Figure 7-25. North London Breach (Centerline of West Levee), Su versus Elevation with CPT Data
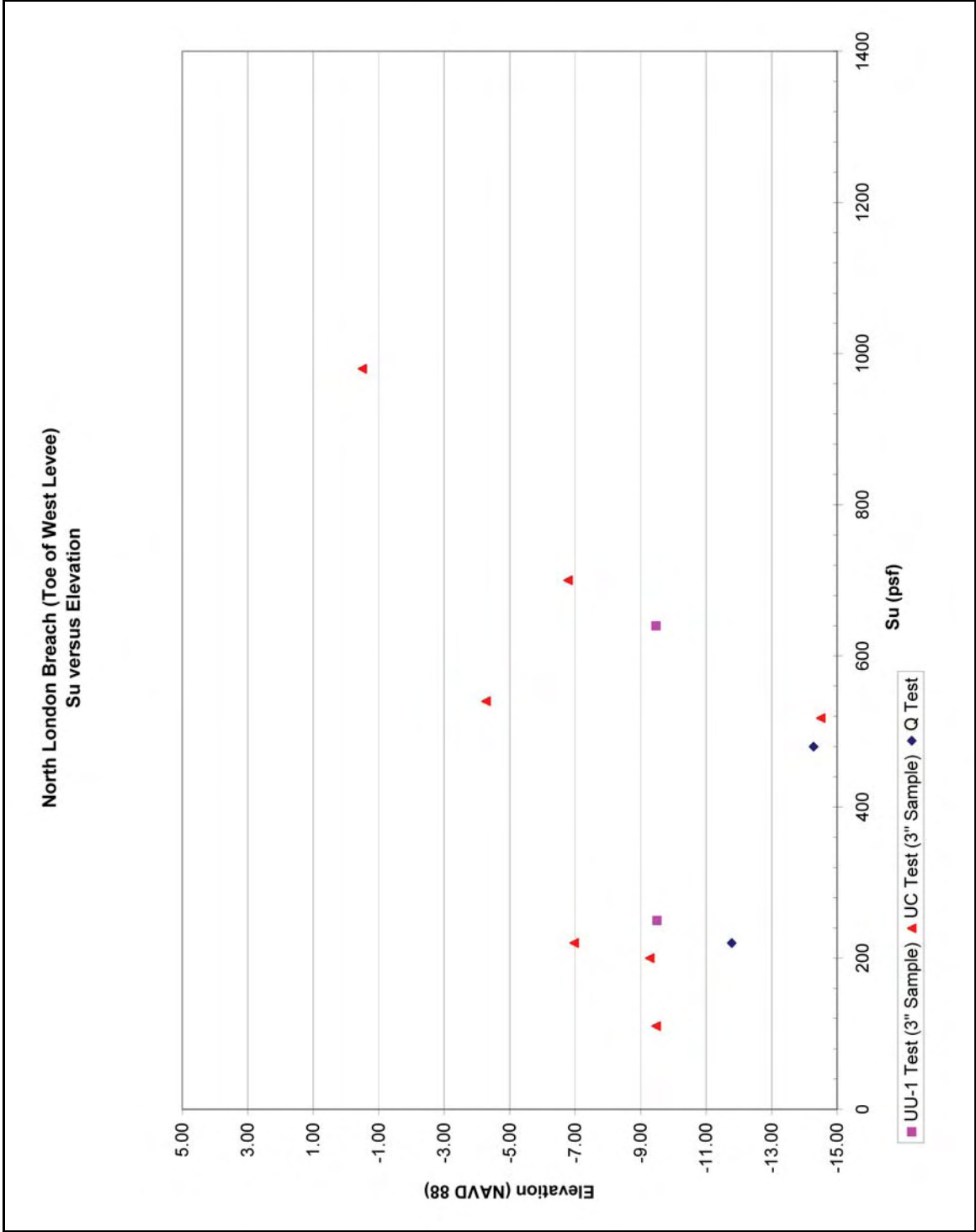
Figure 7-26. North London Breach (Toe of West Levee), Su versus Elevation
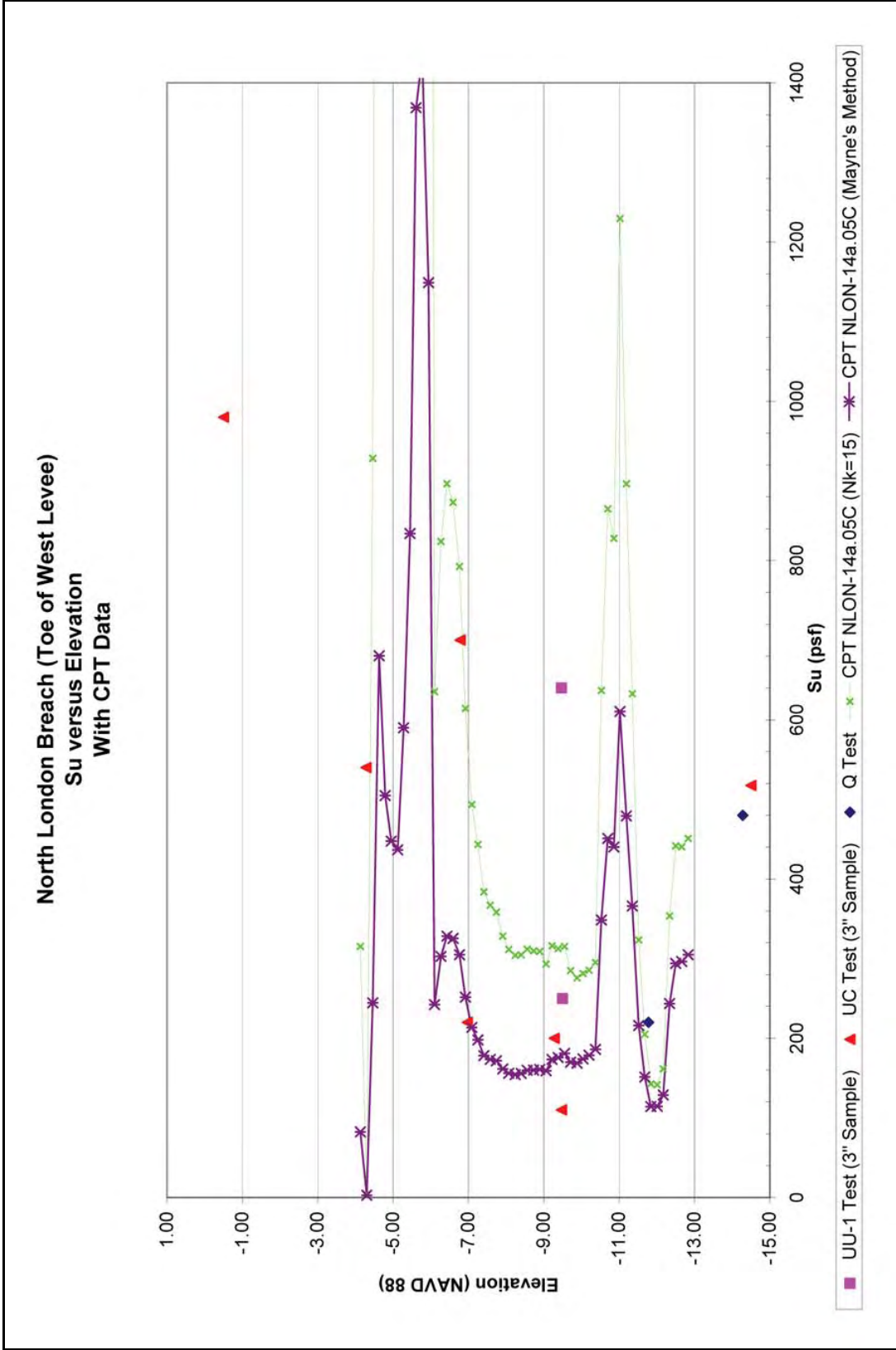
Figure 7-27. North London Breach (Toe of West Levee), Su versus Elevation with CPT Data
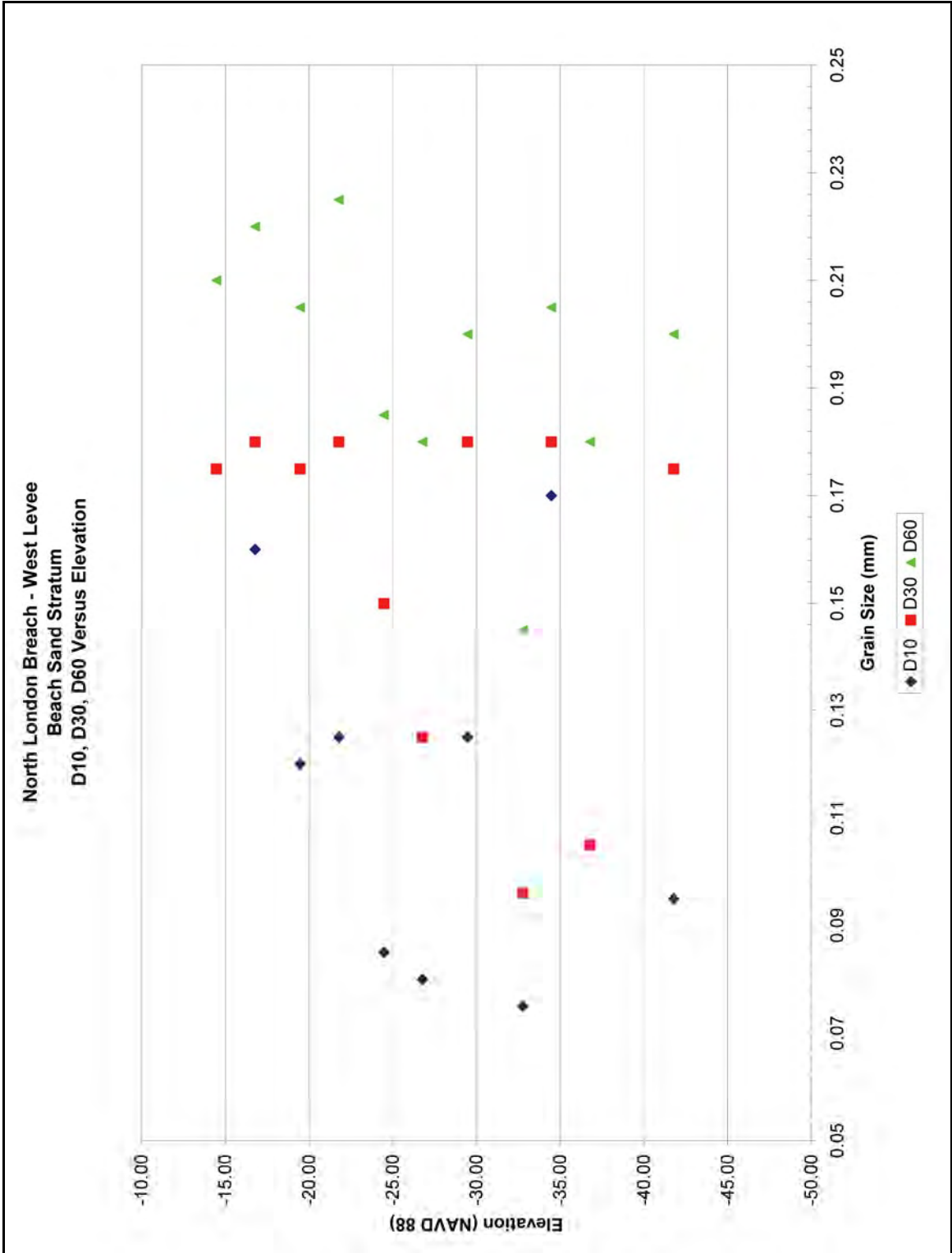
Figure 7-28. North London Breach (Beach Sand Stratum), D10, D30, and D60 versus Elevation

Figure 7-29 shows the $N_{1(60)}$ values of the beach sand under the levee determined from the CPTs. Figure 7-30 shows the $N_{(60)}$ values of the beach sand under the levee determined from the CPTs. In addition, standard penetration tests (SPT) were conducted for GDM borings B-26 and 5-LUW. However, the hammer efficiency is unknown for these borings. The blow counts are shown on Figure 7-30, and they are a fairly good comparison to the CPTs.

Figure 7-31 shows the $N_{1(60)}$ values of the beach sand at the toe of the levee determined from the CPTs. Figure 7-32 shows the $N_{(60)}$ values of the beach sand at the toe of the levee determined from the CPTs. In addition, SPTs were conducted for borings B-5 and B-6. Furthermore, the hammer efficiency is unknown for these borings, but the blow counts are also shown on Figure 7-32, and they are a fairly good comparison to the CPTs.

Pore Pressure Dissipation Tests

Pore pressure dissipation tests were conducted in the beach sand unit at CPTs NLON-2.05C, NLON-10.05c, and NLON-14a.05C. The dissipation tests with the CPTs basically consist of recording the pore pressures at a depth until the pore pressure stabilize to a constant pressure. With pervious materials such as sand, these pressures stabilize fairly quickly. The stabilized values can be assumed to be the actual pore pressure in the sand at the particular depth of the test. Below is a table summarizing the results of the dissipation tests.

Table 7-7
CPTU Pore Pressure Dissipation Tests in the Beach Sand Unit

CPT	London Canal Staff Gauge Reading (NAVD 88)	Dissipation Test Elevation (NAVD 88)	Stabilized Pressure (psi)	Computed Head (ft) (Stab. Pressure x 2.31 ft/psi)	Head Elevation (NAVD 88)
NLON-2.05c	1.04	-27.93	10	23.1	-4.83
NLON-10.05c	1.04	-25.98	9.1	21.02	-4.96
NLON-14.05c	-0.36	-32.02	13.2	30.49	-1.529

Distressed Area – Opposite of North Breach Site on East Levee

Borings in the distressed area consist of only two GDM borings (B-60, and B-61), one new boring (NL-3-05U), and four CPTUs (CP-1 through CP-4). All data are from the centerline of the levee. The boring profiles, NL-3-05U, B-60, and B-61, are shown in Figures 7-33 thru 7-35, respectively. Some of the New Orleans District personnel have stated that a slide on the canal side of the levee in this area had occurred in the past. Repairs of the area may have caused the area to have different soil conditions than adjacent levee sections. However, the exact date of this occurrence is unknown at this time, but there are efforts to obtain more information about the incident and how it was reported. For reference, the GDM borings were taken in December 1985.
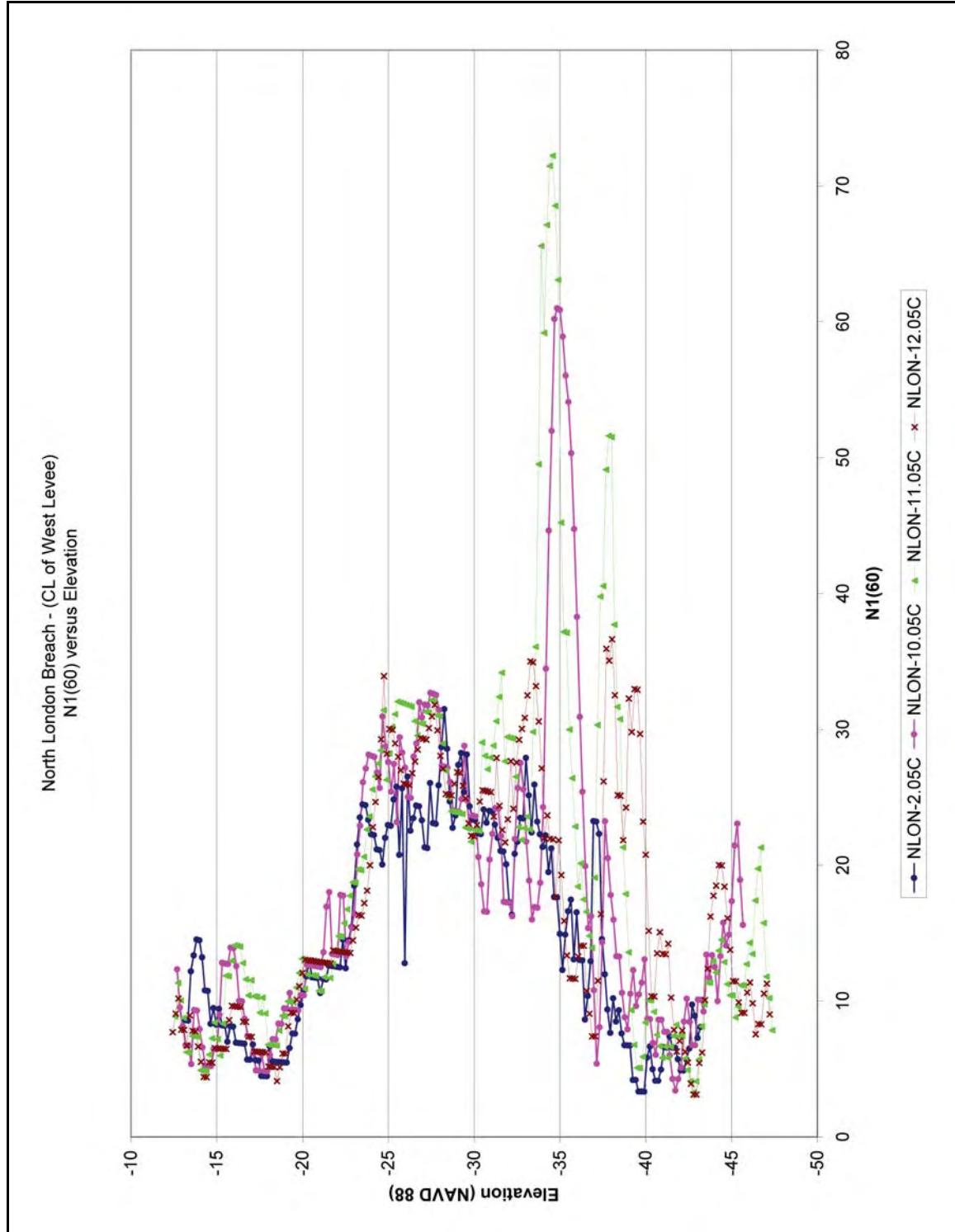
Figure 7-29. North London Breach – Beach Sand Stratum (Centerline of West Levee), N1(60) versus Elevation
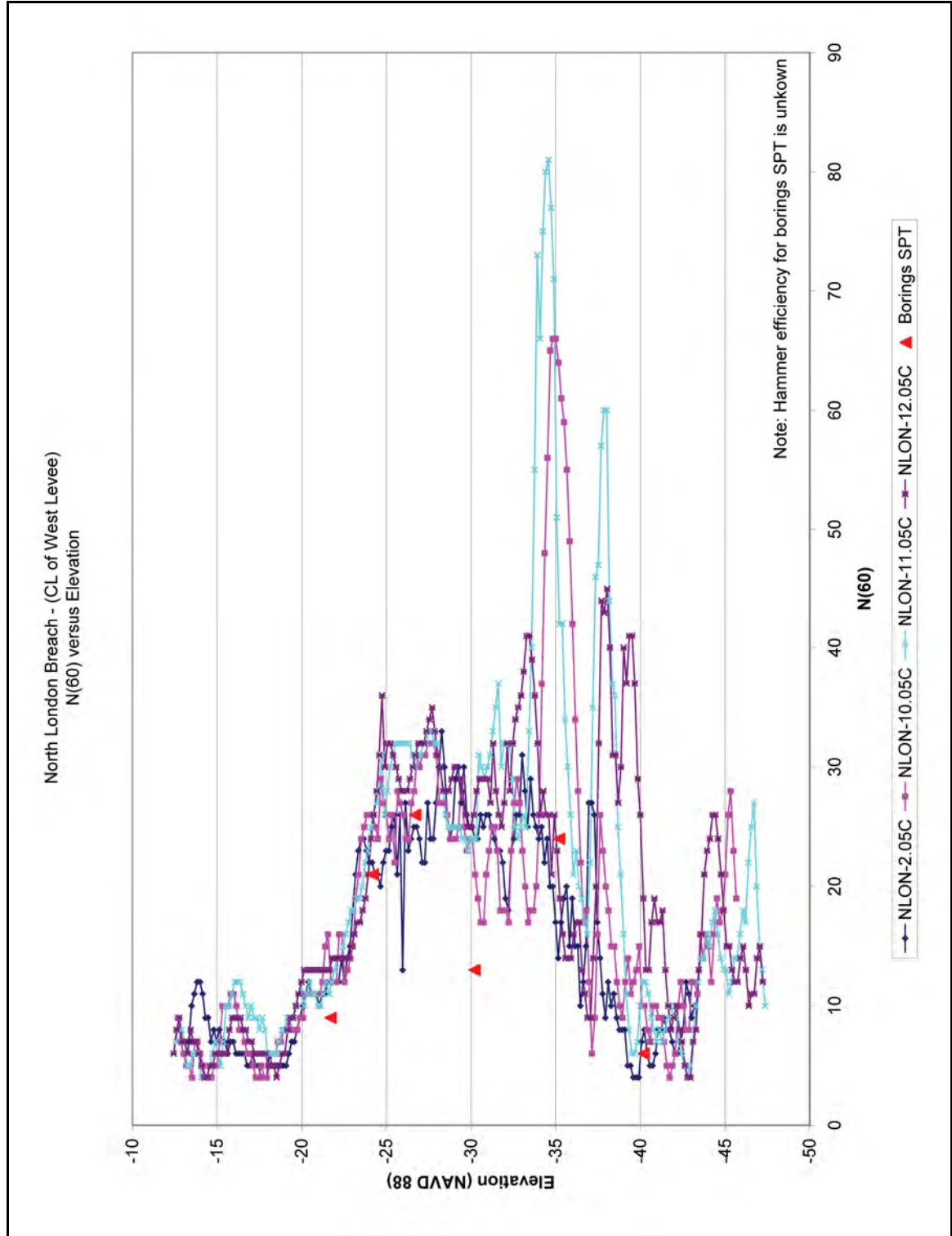
Figure 7-30. North London Breach – Beach Sand Stratum (Centerline of West Levee), N(60) versus Elevation
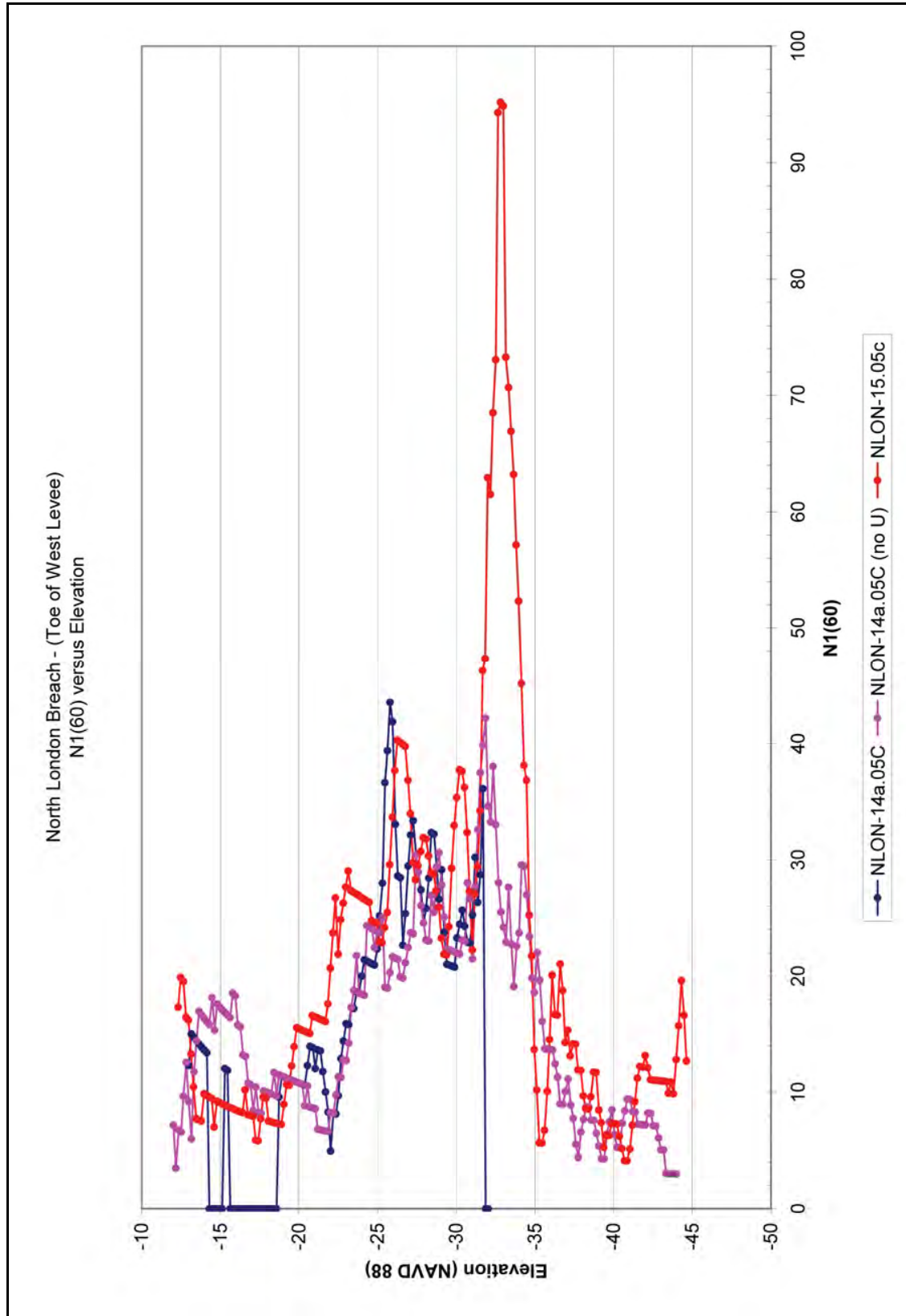
Figure 7-31. North London Breach – Beach Sand Stratum (Toe of West Levee), N1(60) versus Elevation
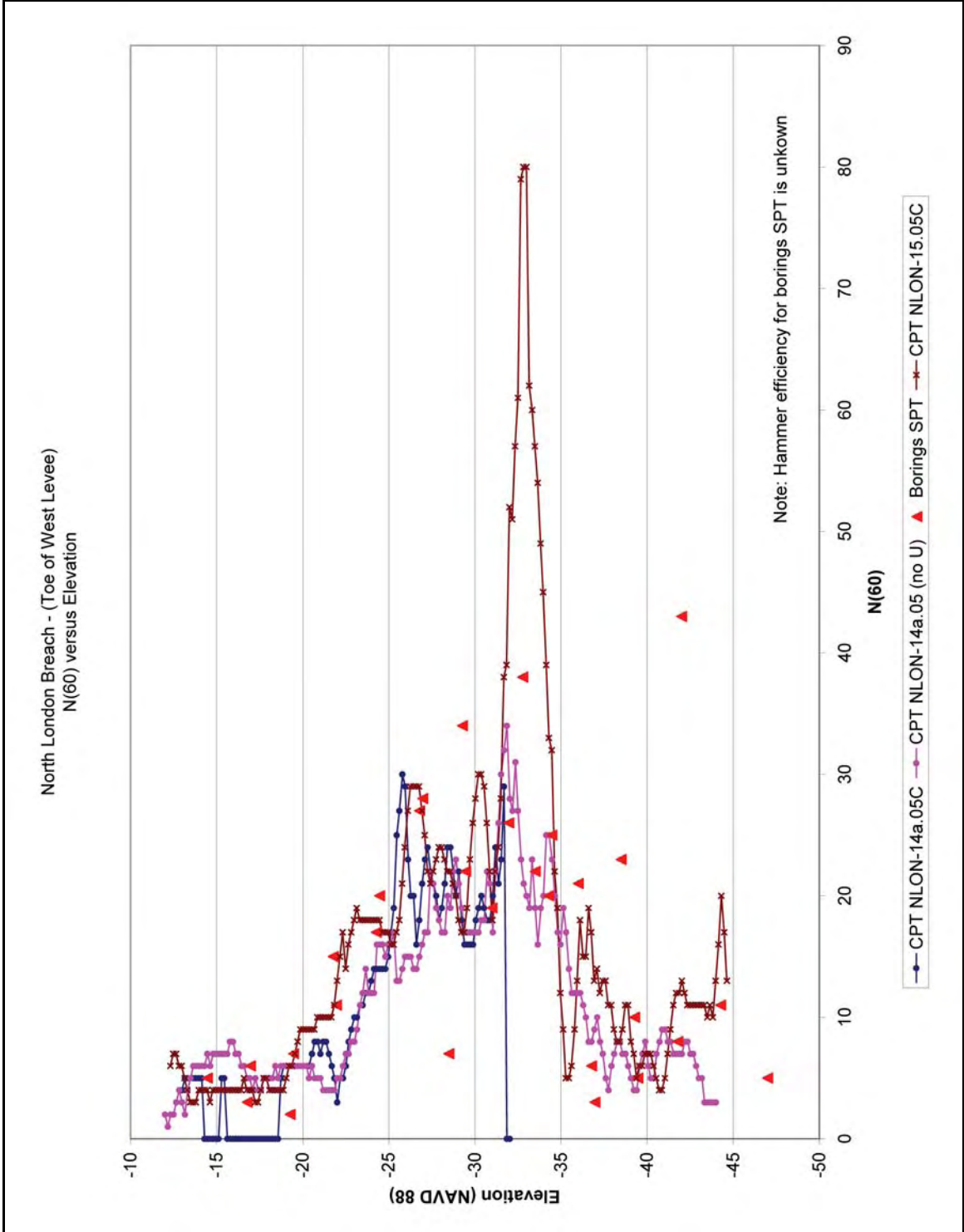
Figure 7-32. North London Breach – Beach Sand Stratum (Toe of West Levee), N(60) versus Elevation
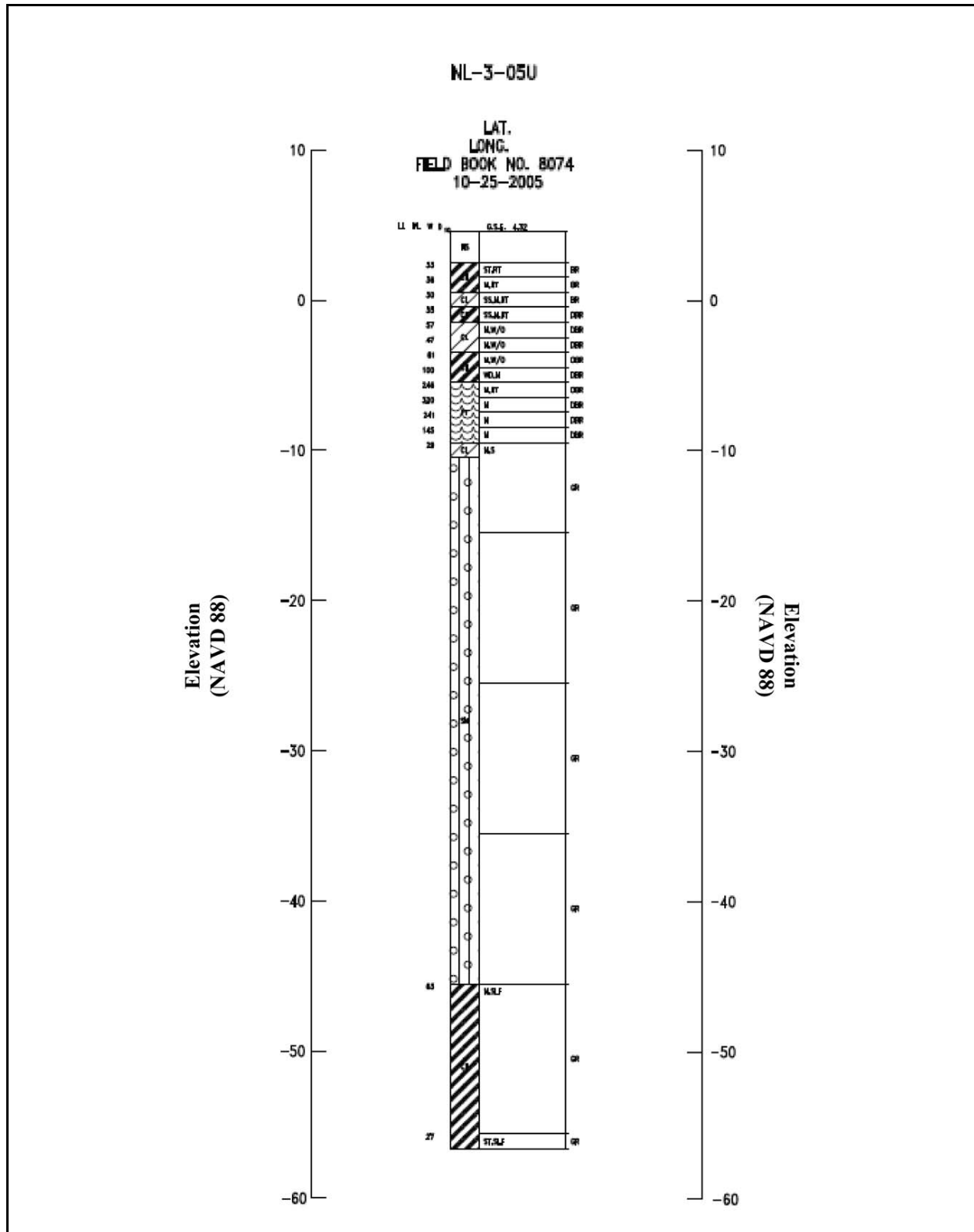
Figure 7-33. Boring NL-3-05U – Boring Profile

LOG OF BORING
EUSTIS ENGINEERING COMPANY
SOIL AND FOUNDATION CONSULTANTS
METAIRIE, LA.

Name of Project: London Avenue Canal, Levee and Floodwall Improvements

Orleans Levee Board Project No. 2049-0269, New Orleans, Louisiana

For: The Board of Levee Commissioners of the Orleans Levee District, New Orleans, La.

Burk & Associates, Inc., New Orleans, Louisiana

Boring No. 60   Soil Technician   A. J. Mayeux   Date 7 December 1985

Ground Elev. 3.50   Datum NGVD   Gr. Water Depth See Text

Sample No.	SAMPLE Depth — Feet		DEPTH STRATUM Feet		VISUAL CLASSIFICATION	*STANDARD PENETRATION TEST	
	From	To	From	To			
1	2.0	2.5	0.0	4.5	Stiff brown & gray clay w/clayey sand pockets & roots		
2	5.0	5.5	4.5	8.0	Soft gray & tan clay w/organic clay layers & roots		
3	8.0	8.5	8.0	10.0	Extremely soft brown humus w/organic clay layers & roots		
4	11.0	11.5	10.0	16.0	Soft brown organic clay w/humus layers, wood & roots		
5	17.0	17.5	16.0	19.0	Very loose gray sand w/organic matter		
6	20.0	21.5	19.0	22.5	Very loose gray sand	1	2
7	22.5	24.0	22.5	24.5	Loose gray sand	1	6
8	25.0	26.5	24.5		Medium dense gray sand w/shell fragments	2	11
9	28.5	30.0			Ditto	2	14
10	33.5	35.0			Ditto	2	11
11	38.5	40.0		42.0	Ditto	5	13
12	43.5	45.0	42.0		Very loose gray clayey sand w/shell fragments	0	2
13	49.0	49.5		50.0	Ditto		
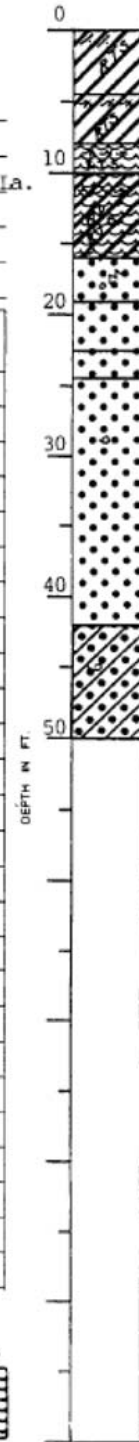
*Number in first column indicates number of blows of 140-lb. hammer dropped 30 in. required to seat 2-in. O. D. splitspoon sampler 6 in. Number in second column indicates number of blows of 140-lb. hammer dropped 30 in. required to drive 2-in. O. D. splitspoon sampler 1 ft. after seating 6 in.

WHILE THIS LOG OF BORING IS CONSIDERED TO BE REPRESENTATIVE OF SUBSURFACE CONDITIONS AT ITS RESPECTIVE LOCATION ON THE DATE SHOWN, IT IS NOT WARRANTED THAT IT IS REPRESENTATIVE OF SUBSURFACE CONDITIONS AT OTHER LOCATIONS AND TIMES.

CLAY   SILT   SAND   HUMUS

Predominant type shown heavy. Modifying type shown light.

Remarks: _____
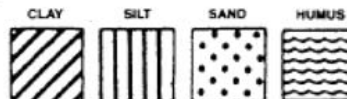
Figure 7-34. Boring B-60 – Boring Log

This is a preliminary report subject to revision; it does not contain final conclusions of the United States Army Corps of Engineers.

LOG OF BORING

EUSTIS ENGINEERING COMPANY
SOIL AND FOUNDATION CONSULTANTS
METAIRIE, LA.

Sheet 1 of 2

Name of Project: London Avenue Canal, Levee and Floodwall Improvements
Orleans Levee Board Project No. 2049-0269, New Orleans, Louisiana

For: The Board of Levee Commissioners of the Orleans Levee District, New Orleans, La.
Burk & Associates, Inc., New Orleans, Louisiana

Boring No. 61   Soil Technician A. J. Mayeux   Date 10 December 1985
Ground Elev. 3.50   Datum NGVD   Gr. Water Depth See Text

Sample No.	SAMPLE Depth — Feet		DEPTH STRATUM Feet		VISUAL CLASSIFICATION	*STANDARD PENETRATION TEST	
	From	To	From	To			
1	2.0	2.5	0.0	4.0	Very compact tan & gray clayey silt w/clay pockets & roots		
2	5.0	5.5	4.0	7.0	Dense tan & gray clayey sand w/clay lenses & roots		
3	8.0	8.5	7.0	10.0	Soft gray silty clay w/clayey sand pockets & trace of organic matter		
4	11.0	11.5	10.0	13.0	Medium stiff dark gray clay w/organic matter & wood		
5	14.0	14.5	13.0	17.5	Stiff brown organic clay w/humus layers		
6	19.0	19.5	17.5	20.0	Soft gray silty clay w/alternating clayey silt & sandy silt layers		
7	20.0	21.5	20.0		Very loose gray clayey sand	1	4
8	22.5	24.0		25.5	Ditto	0	2
9	25.0	26.5	25.5		Loose gray sand w/shell fragments	1	7
10	28.5	30.0		30.0	Ditto	2	10
11	33.5	35.0	30.0	37.5	Medium dense gray sand w/shell fragments	4	15
12	38.5	40.0	37.5	41.5	Dense gray sand	6	34
13	43.5	45.0	41.5	48.0	Loose gray clayey sand w/shell fragments	1	4
14	49.0	49.5	48.0	50.0	Soft gray clay w/clayey sand pockets & shell fragments		
15	54.0	54.5	50.0	59.0	Medium stiff gray clay w/sand pockets & & shell fragments		
16	59.0	59.5	59.0	62.5	Stiff greenish-gray & tan clay w/trace of sand		
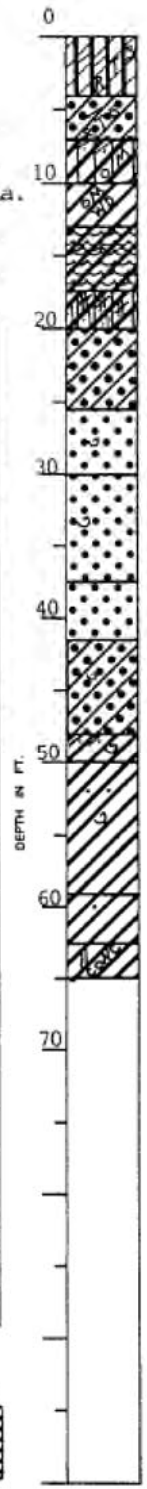
*Number in first column indicates number of blows of 140-lb. hammer dropped 30 in. required to seat 2-in. O. D. splitspoon sampler 6 in. Number in second column indicates number of blows of 140-lb. hammer dropped 30 in. required to drive 2-in. O. D. splitspoon sampler 1 ft. after seating 6 in.

WHILE THIS LOG OF BORING IS CONSIDERED TO BE REPRESENTATIVE OF SUBSURFACE CONDITIONS AT ITS RESPECTIVE LOCATION ON THE DATE SHOWN, IT IS NOT WARRANTED THAT IT IS REPRESENTATIVE OF SUBSURFACE CONDITIONS AT OTHER LOCATIONS AND TIMES.

CLAY   SILT   SAND   HUMUS

Remarks: _____
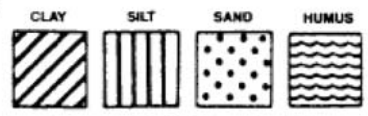
Predominant type shown heavy. Modifying type shown light.

Figure 7-35. Boring B-61 – Boring Log

Moisture Content and Unit Weights

Moisture contents (%w) and wet unit weights for samples taken from the levee centerline above the beach sand are shown in the table below.

Table 7-8
Moisture Content and Wet Unit Weights from the Levee Centerline

Boring	Elevation (NAVD 88)	Soil Type	%w	Dry Unit Weight (pcf)	Wet Unit Weight (pcf)
B-60	1.50	Clay	34	86.1	115.4
B-61	1.5	Clayey Silt	17.5	104.9	123.2
B-60	-1.50	Clay	62.9	59.6	97.1
B-61	-1.5	Clayey Sand	17	101.5	118.7
B-60	-4.50	Humus	296.4	18	71.5
B-61	-4.5	Silty Clay	39.6	79.3	110.7
B-61	-7.5	Clay	78.5	52.4	93.5
B-61	-10.5	Organic Clay	240.1	20	68.2
B-61	-15.5	Silty Clay	26.7	98.5	124.8

Shear Strength

Shear strengths from laboratory tests of the levee embankment from the GDM borings are shown in the table below.

Table 7-9
Shear Strengths Summary

Boring	Elevation (NAVD 88)	Soil Type	%w	S_u UC Test (psf)	S_u UU-1 Test (psf)
B-60	1.5	Clay	34	1080	
B-60	-1.5	Clay	62.9	455	
B-60	-4.5	Humus	296.4	97.5	
B-61	1.5	Clayey Silt	17.5		1595
B-61	-1.5	Clayey Sand	17		1012.5
B-61	-4.5	Silty Clay	39.6	337.5	
B-61	-7.5	Clay	78.5	587.5	
B-61	-10.5	Organic Clay	240.1	1860	
B-61	-15.5	Silty Clay	26.7	277.5	

Interpretation of the undrained shear strengths (using Mayne's method) of the material above the beach sand unit for CPTs CP-1 and CP-2 is shown in Figure 7-36. Also, plotted in Figure 7-36 is the shear strengths shown in Table 7-9. The shear strength plot for CP-1 shows a potential void at elevation -9 (NAVD 88). However, this void was not detected in CP-2.

Furthermore, interpretation of the undrained shear strengths for CPTs CP-3 and CP-4 is shown in Figure 7-37. CPT CP-3 shows a potential sand pocket at elevation -6.5 (NAVD 88) and CPT CP-4 also shows a potential sand pocket at elevation -4.5. Similar to CP-2, a potential void was detected in CP-4 at elevation -5.
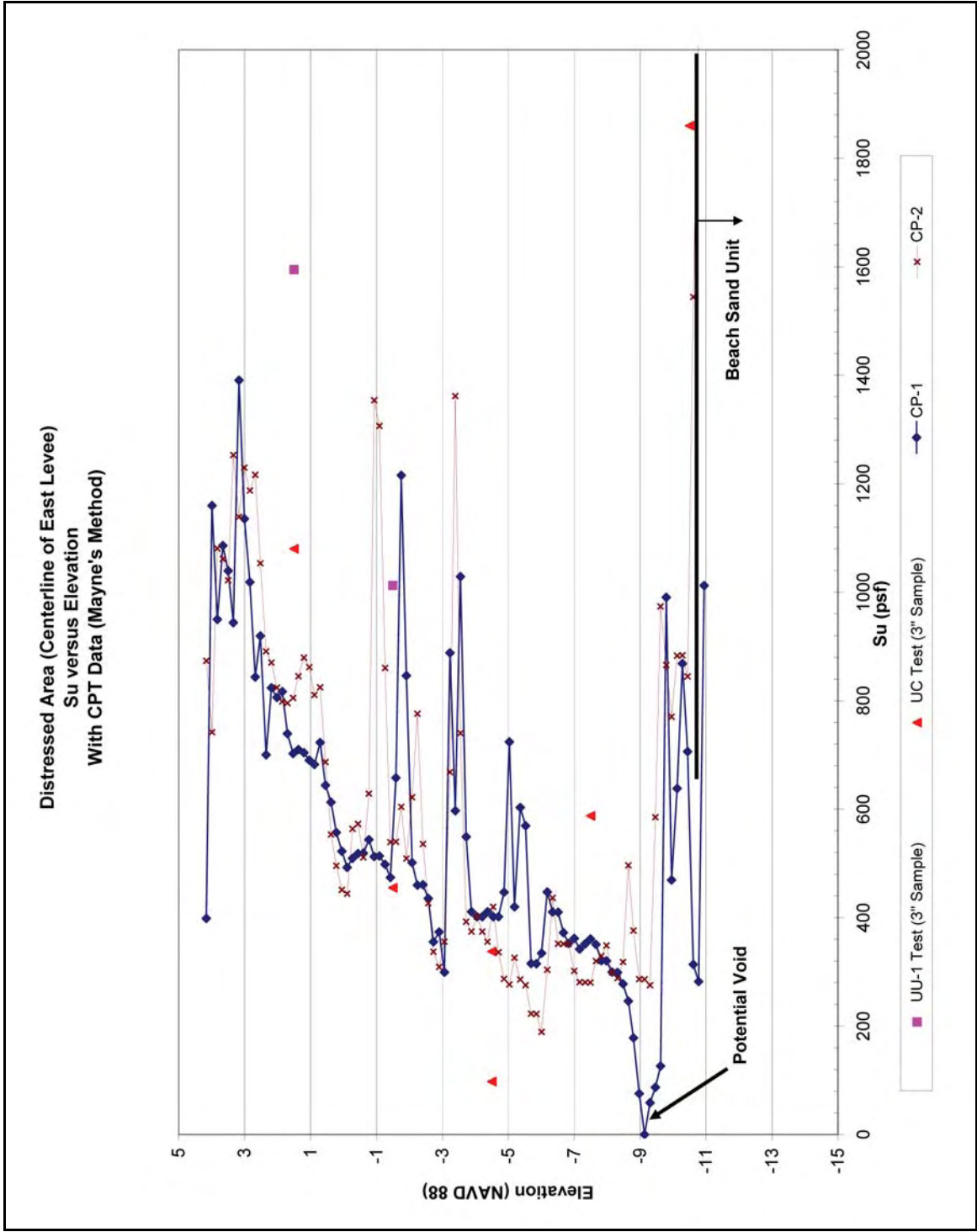
Figure 7-36. Distressed Area (Centerline of East Levee), Su versus Elevation with CPTs CP-1 and CP-2
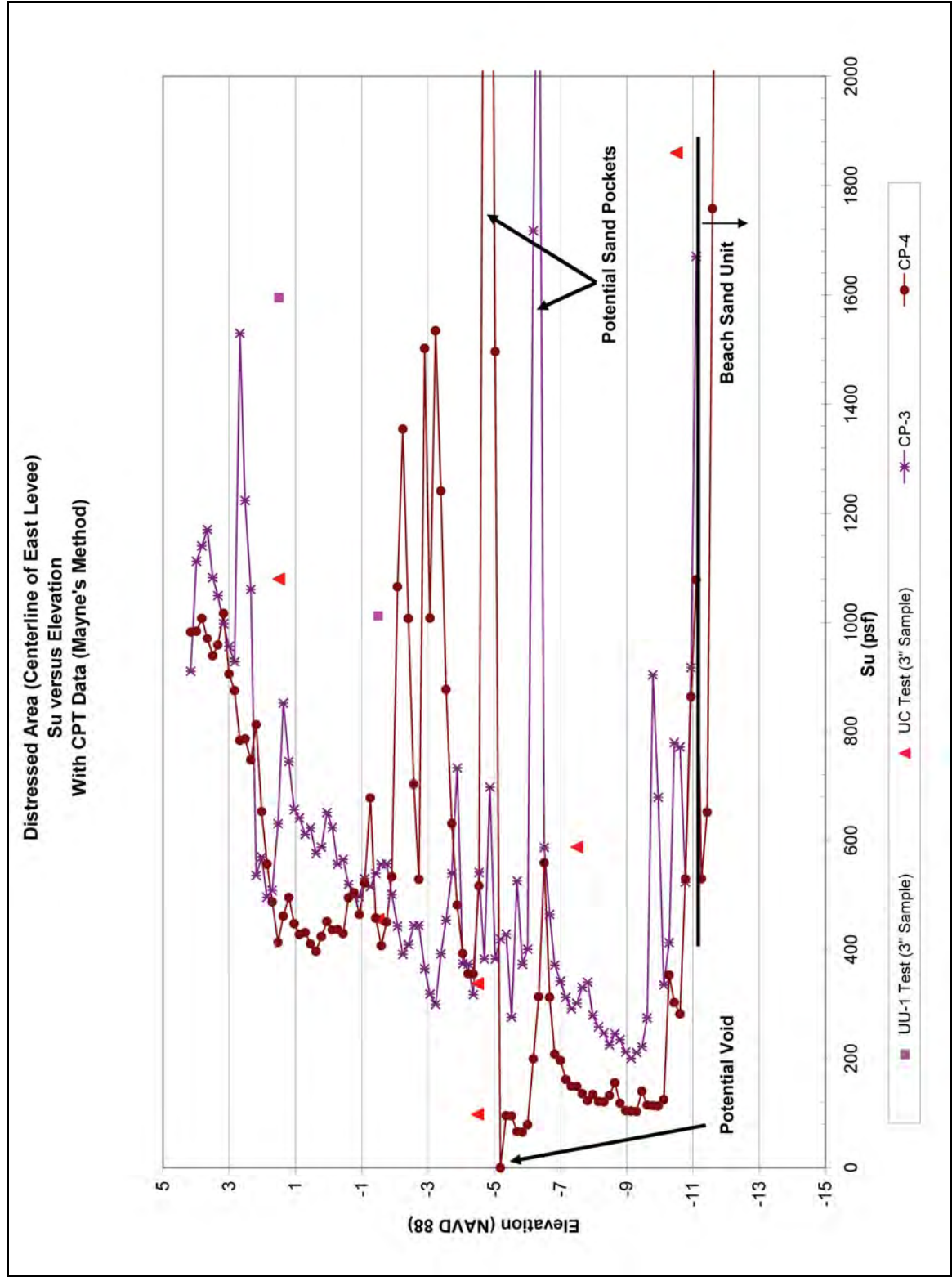
Figure 7-37. Distressed Area (Centerline of East Levee), Su versus Elevation with CPTs CP-1 and CP-2

Gradation and Standard Penetration Number for Beach Sand Unit

No gradation tests have been conducted in this area. However, SPTs were conducted in borings B-60 and B-61. The hammer efficiency is unknown for these borings, but the blow counts were also shown in Figures 7-39 and 7-40. Furthermore, $N_{1(60)}$ and $N_{(60)}$ values can be determined from the CPTs. The $N_{1(60)}$) values for CP-1 and CP-2 are shown on Figure 7-38. In addition, the $N_{(60)}$ values for CP-1 and CP-2 are plotted with the SPTs from the borings in Figure 7-39. This was repeated for CP-3 and CP-4, and Figures 7-40 and 7-41 were produced. The borings' SPT did not correlate well with the N(60) from the CPTs.

The SPTs on the east side show a similar trend as those on the west side.

South Breach Site – East Levee

The data is divided data from the centerline of the levee and from the toe of the levee. Borings from the centerline of the levee include three borings from the GDM (B-50, B-51, and B-52). GDM borings used 3-in.-diameter undisturbed samples. GDM boring B-51 was taken closest to the breach area. The boring log for this boring is shown in Figure 7-42.

Data from the toe of the levee include two new borings, and five CPTs. The new borings include LAC-1G (3-in.-diameter undisturbed samples), LAC-2G (3-in.-diameter undisturbed samples), and SL-1-05U (5-in.-diameter undisturbed samples). The CPTs include SLON-1.05C, SLON-2.05C, SLON-3.05C, and SLON-5.05C. CPT NLON-2.05c was the only CPT taken with pore pressure measurements.

Moisture Content and Unit Weights

Moisture contents (%w) and wet unit weights for samples taken from the levee centerline above the beach sand are shown in the table below.

Boring	Elevation (NAVD 88)	Soil Type	%w	Dry Unit Weight (pcf)	Wet Unit Weight (pcf)
51	3.00	Clay	22.6	90.4	110.8
52	3.00	Clay	35.9	84.3	114.5
51	0.00	Clay	42.6	72.4	103.2
52	0.00	Clay	65.2	59.8	98.7
50	-4.20	Clay	51.6	64.1	97.2
51	-3.00	Clay	52.7	68	103.8
51	-6.00	Clay	75	55.2	96.6
52	-6.00	Clay	164.2	29.1	76.8
50	-6.70	Clay	104.2	41.7	85.2
52	-9.00	Clay	91.2	48.2	92.2
52	-14.00	Clayey Sand	48.1	68.6	101.6
50	-14.20	Clay	84.3	50.6	93.2

Table 7-10
Moisture Content and Wet Unit Weights from the Levee Centerline

Not many data points exist for the marsh unit at the toe of the levee. Table 7-11 shows the moisture contents and the wet unit weights for samples taken from the levee toe in the breach area.
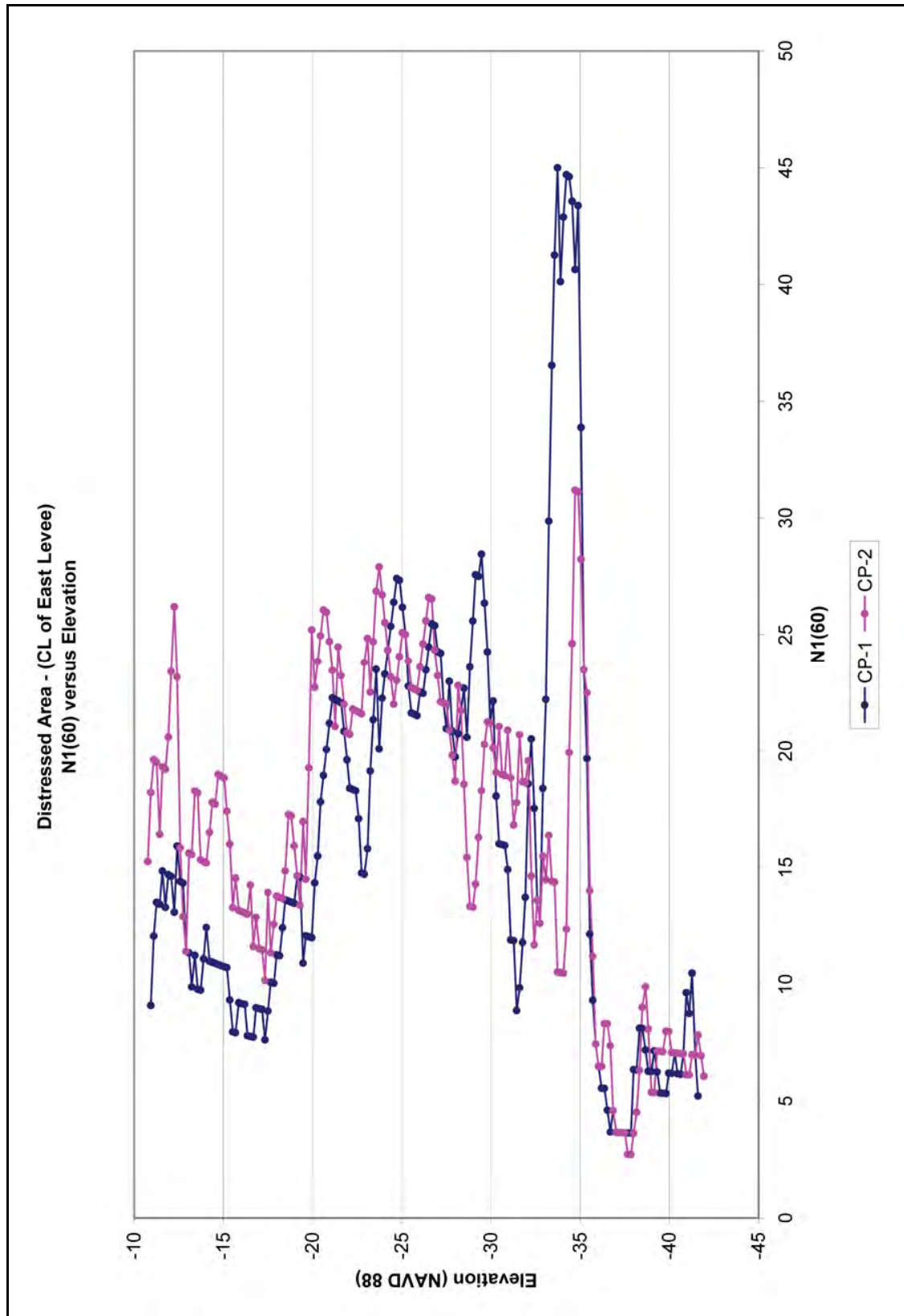
Figure 7-38. Distressed Area – Beach Sand Stratum (Centerline of East Levee), N1(60) versus Elevation for CPTs CP-1 and CP-2
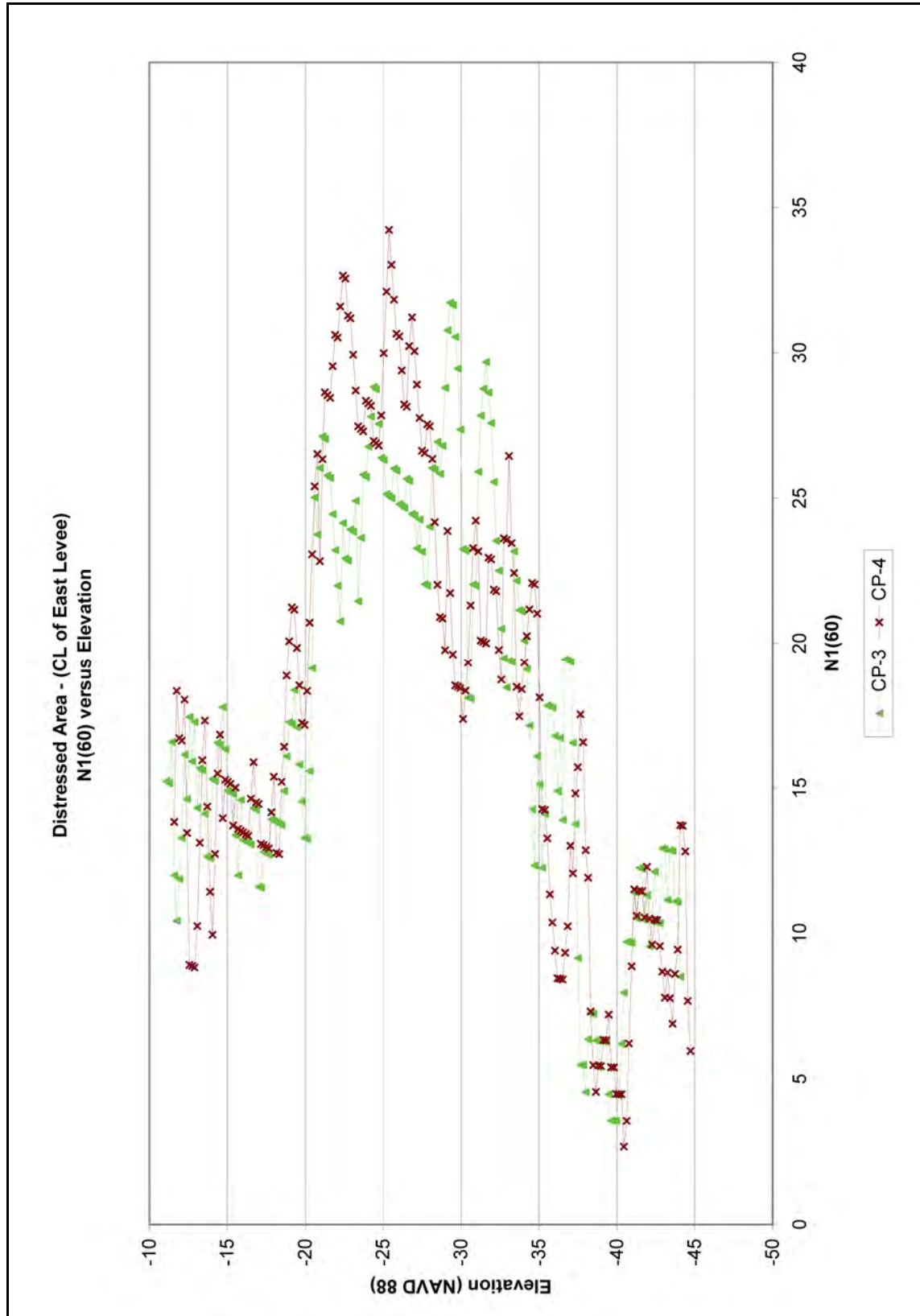
Figure 7-39. Distressed Area – Beach Sand Stratum (Centerline of East Levee), N1(60) versus Elevation for CPTs CP-3 and CP-4
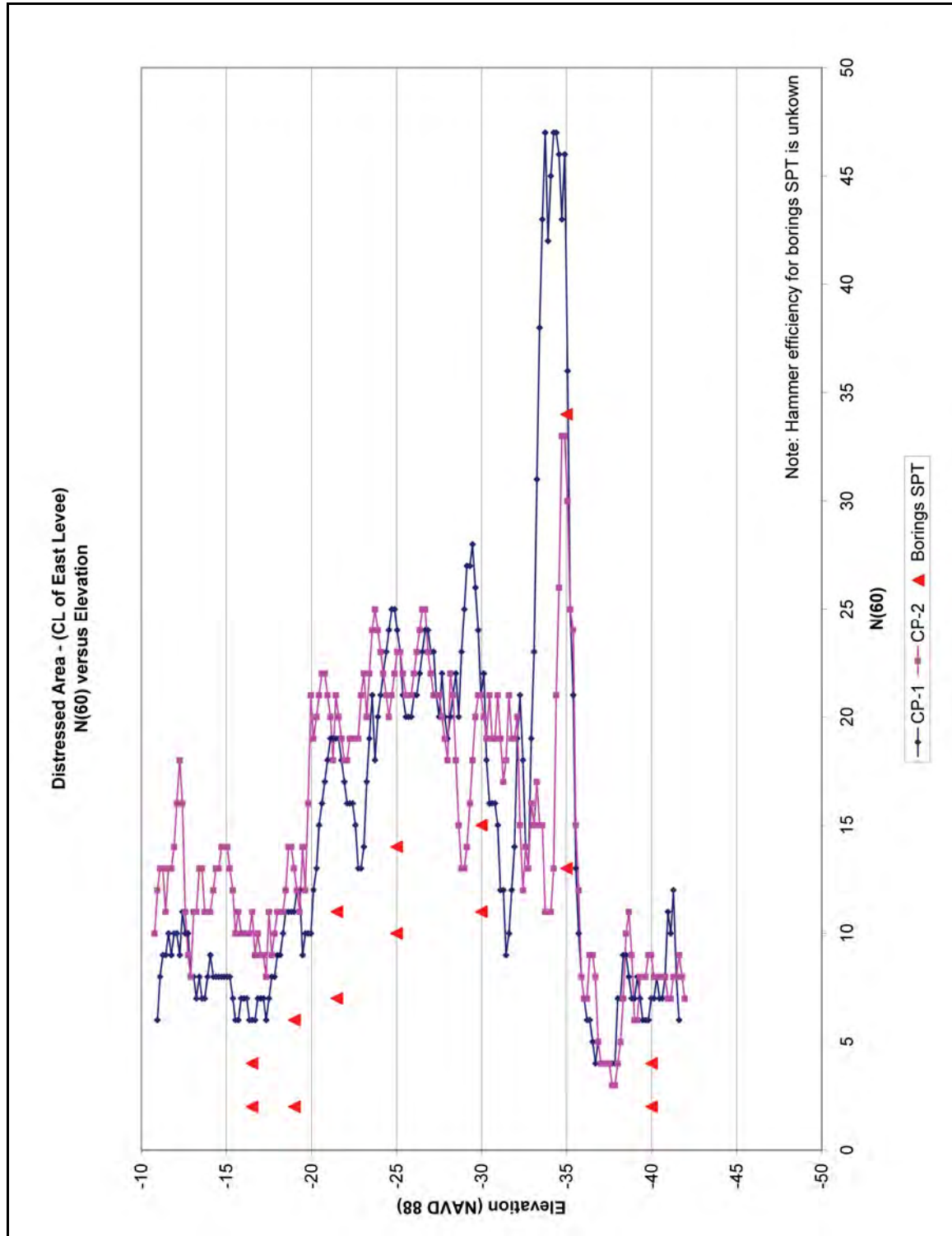
Figure 7-40. Distressed Area – Beach Sand Stratum (Centerline of East Levee), N(60) versus Elevation for CPTs CP-1 and CP-2
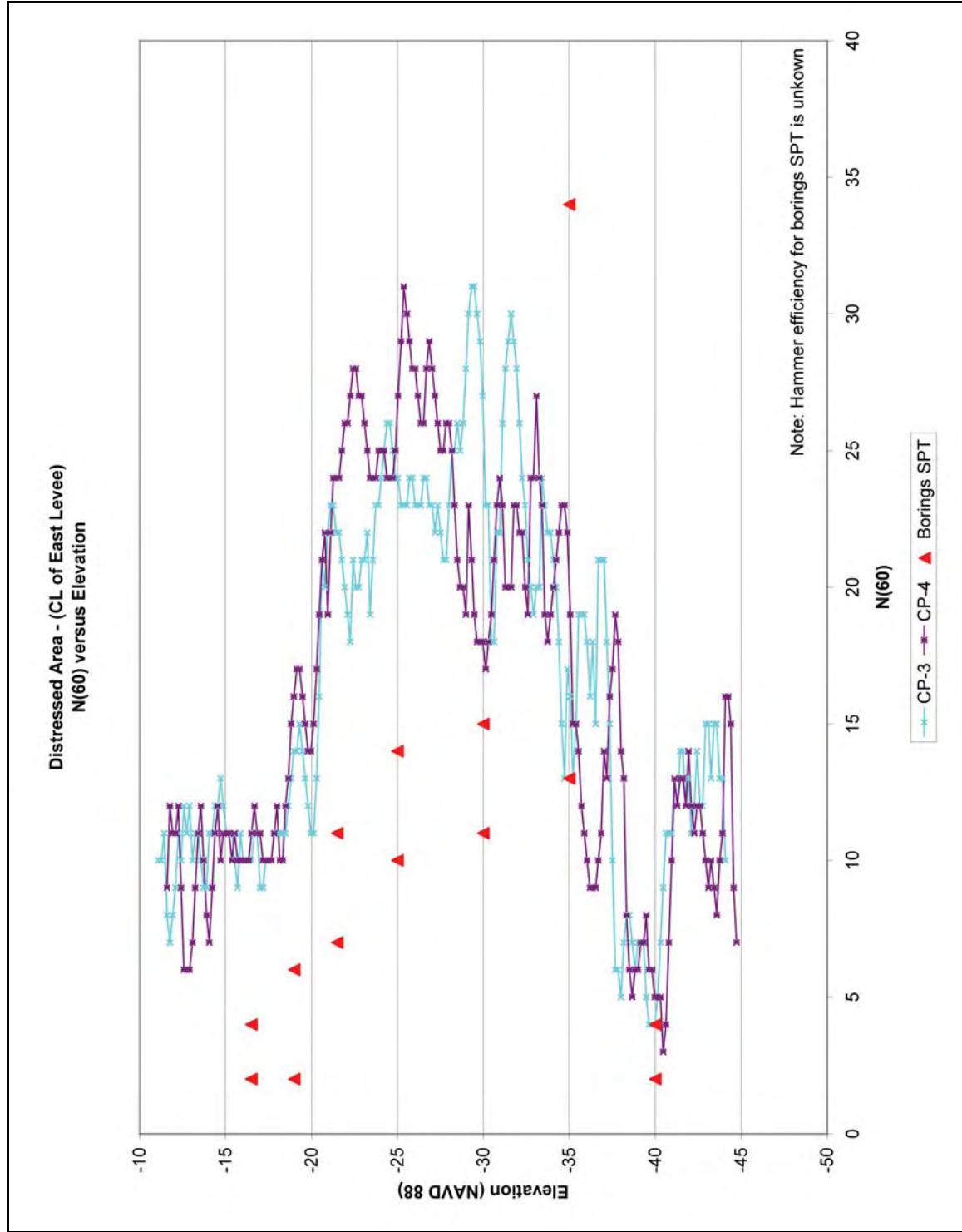
Figure 7-41. Distressed Area – Beach Sand Stratum (Centerline of East Levee), N(60) versus Elevation for CPTs CP-3 and CP-4

LOG OF BORING
EUSTIS ENGINEERING COMPANY
SOIL AND FOUNDATION CONSULTANTS
METAIRIE, LA.

Name of Project: London Avenue Canal, Levee and Floodwall Improvements

Orleans Levee Board Project No. 2049-0269, New Orleans, Louisiana

For: The Board of Levee Commissioners of the Orleans Levee District, New Orleans, La.

Burk & Associates, Inc., New Orleans, Louisiana

Boring No. 51 Soil Technician A. Croal, Jr. Date 12 November 1985

Ground Elev. 4.70 Datum NGVD Gr. Water Depth See Text

Sample No.	SAMPLE Depth — Feet		DEPTH STRATUM Feet		VISUAL CLASSIFICATION	*STANDARD PENETRATION TEST	
	From	To	From	To			
1	0.0	0.5	0.0	1.0	Stiff brown & gray clay w/shell fragments & grass roots		
2	1.7	2.5	1.0	3.0	Medium stiff tan & gray clay w/fine sand & clayey sand pockets		
3	4.7	5.5	3.0	6.5	Medium stiff black & gray clay w/roots & organic matter		
4	7.7	8.5	6.5	9.0	Medium stiff tan & gray clay w/sand layers & trace of organic matter		
5	10.7	11.5	9.0	12.5	Soft gray clay w/roots & organic matter		
6	13.7	14.5	12.5	16.0	Loose gray fine sand w/clayey sand layers, trace of organic matter & few roots		
7	16.0	17.5	16.0	19.0	Medium dense gray fine sand	2	28
8	18.5	20.0	19.0	21.5	Dense gray fine sand	4	36
9	21.0	22.5	21.5		Very dense gray fine sand	8	50=10"
10	23.5	25.0			Ditto	10	50=10"
11	26.0	27.5			Ditto	15	50=9"
12	28.5	30.0			Very dense gray fine sand w/few shell fragments	11	50=8"
13	33.5	35.0			Very dense gray fine sand	9	50=9"
14	38.5	40.0		42.0	Ditto	12	50=9"
15	43.5	45.0	42.0	47.0	Dense gray fine sand	14	41
16	48.5	50.0	47.0	50.0	Loose gray silty sand w/few clay pockets & trace of clay	2	10
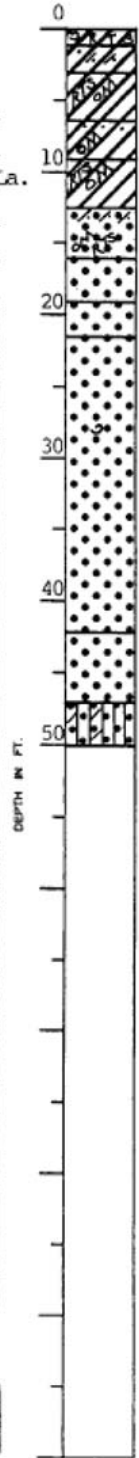
*Number in first column indicates number of blows of 140-lb. hammer dropped 30 in. required to seat 2-in. O. D. splitspoon sampler 6 in. Number in second column indicates number of blows of 140-lb. hammer dropped 30 in. required to drive 2-in. O. D. splitspoon sampler 1 ft. after seating 6 in.

WHILE THIS LOG OF BORING IS CONSIDERED TO BE REPRESENTATIVE OF SUBSURFACE CONDITIONS AT ITS RESPECTIVE LOCATION ON THE DATE SHOWN, IT IS NOT WARRANTED THAT IT IS REPRESENTATIVE OF SUBSURFACE CONDITIONS AT OTHER LOCATIONS AND TIMES.

CLAY   SILT   SAND   HUMUS

Remarks: _____
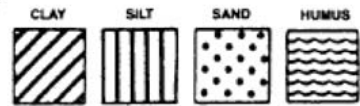
Predominant type shown heavy. Modifying type shown light.

Figure 7-42. GDM Boring B-51 – Boring Log

Table 7-11
Moisture Content and Wet Unit Weights from Levee Toe

Boring	Elevation (NAVD 88)	Soil Type	%w	Dry Unit Weight (pcf)	Wet Unit Weight (pcf)
LAC05-2G	-1.65	CL	28.7	85.3	109.8
SL-1-05U	-2.85	CH	37		
SL-1-05U	-3.85	CH	32		
LAC05-2G	-4.15	CH	148.3	30.3	75.2
SL-1-05U	-4.85	CH	43		
SL-1-05U	-5.85	CH	90		
SL-1-05U	-6.85	CH	70		
SL-1-05U	-7.85	CH	61		
SL-1-05U	-8.85	CH	43		
LAC05-2G	-9.15	CH	47.2	70.5	103.8

Shear Strength

Shear strengths from laboratory tests of the levee embankment and marsh unit (under the centerline) are fairly sparse. The table below shows the shear strength data available from the centerline of the levee.

Table 7-12
Laboratory Shear Strength Test Data for Samples taken from the Centerline of the Levee

Boring	Elevation (NAVD 88)	Soil Type	%w	UC Test (psf)	UU-1 Test (psf)
51	3.00	Clay	22.6		535
52	3.00	Clay	35.9	1127.5	
51	0.00	Clay	42.6	637.5	
52	0.00	Clay	65.2	510	
50	-4.20	Clay	51.6	402.5	
51	-3.00	Clay	52.7	605	
51	-6.00	Clay	75	360	
52	-6.00	Clay	164.2	175	
50	-6.70	Clay	104.2	350	
52	-9.00	Clay	91.2	275	
52	-14.00	Clayey Sand	48.1		172.5

Shear strengths from laboratory tests (three unconfined compression tests) taken at the toe of the levee are plotted with interpretation of the undrained shear strengths from CPT SLON-2.05c in Figure 7-43. The unconfined compression tests are from boring LAC-2G.

Gradation and Standard Penetration Number for Beach Sand Unit

A plot of the D_{10}, D_{30}, and D_{60} values of the beach sand unit are shown on Figure 7-44. These values consist of gradation tests conducted on samples from borings LAC-1G and LAC-2G. A summary of these values are presented in the table below.
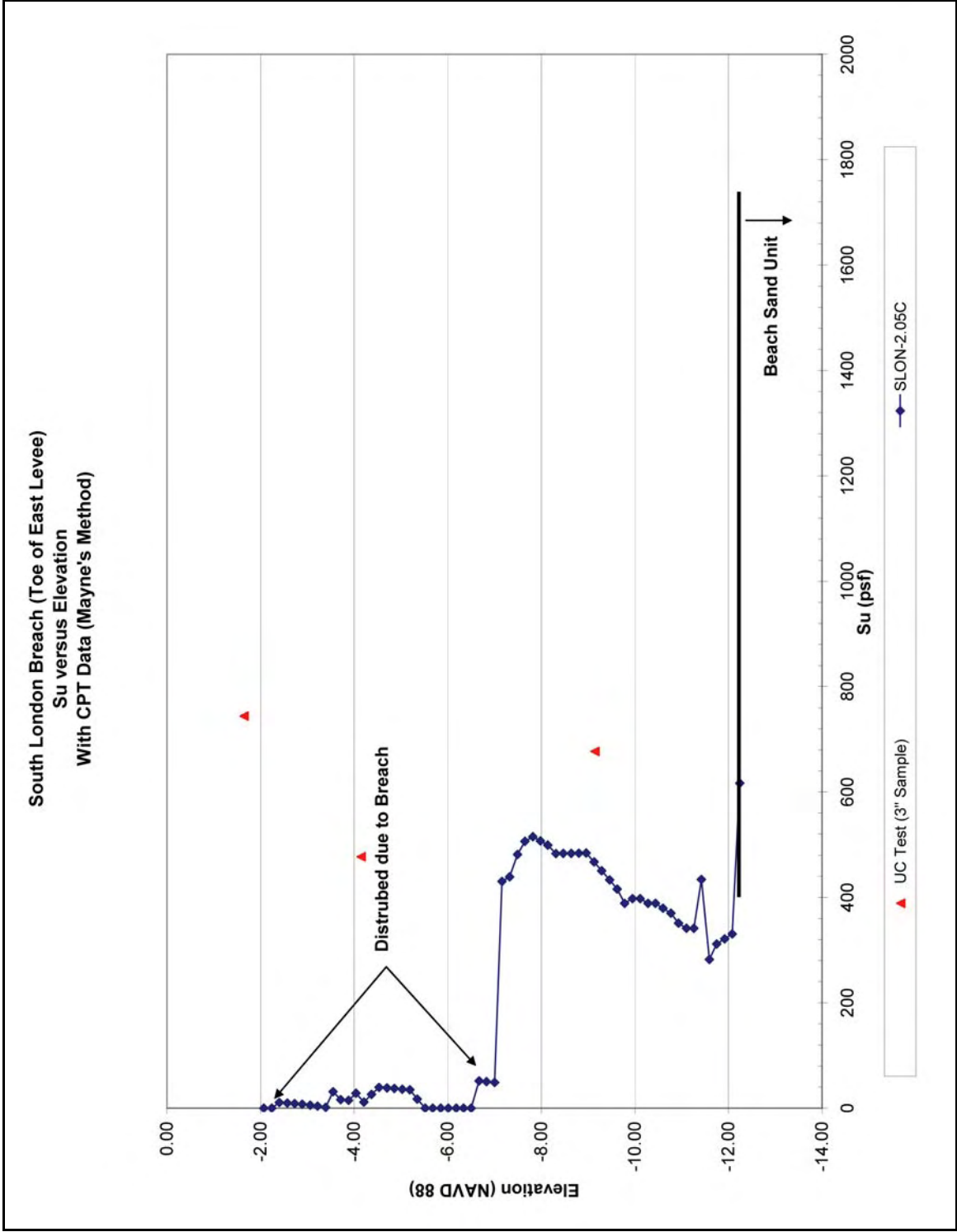
Figure 7-43. South London Breach, Su versus Elevation with CPT Data
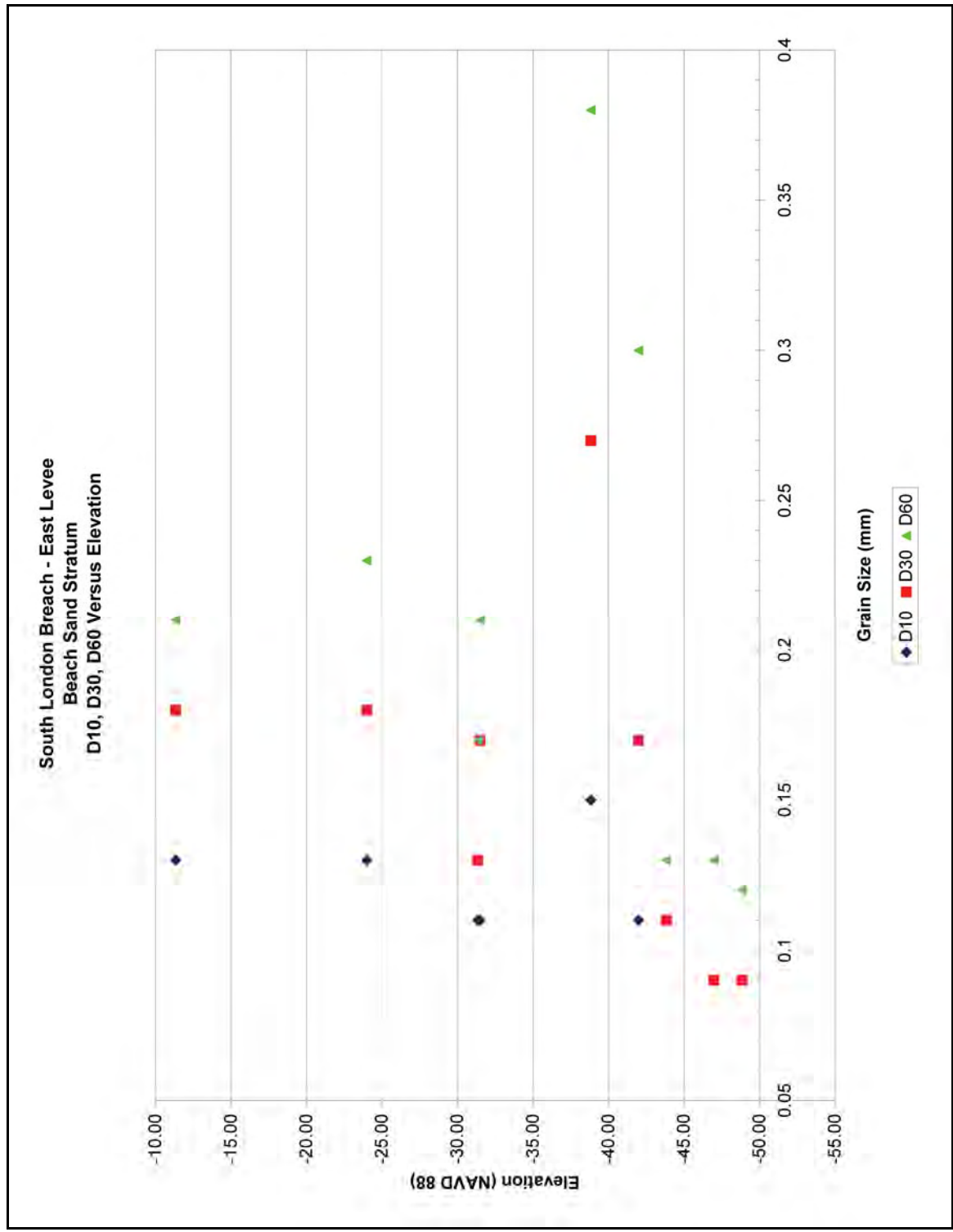
Figure 7-44. South London Breach – Beach Sand Unit, D10, D30, D60 versus Elevation

Table 7-13
D10, D30, and D60 Values for the Beach Sand Unit

Boring	Elevation (NAVD 88)	Soil Type	D_{60} (mm)	D_{30} (mm)	D_{10} (mm)
LAC05-2G	-11.35	SP	0.21	0.18	0.13
LAC05-1G	-24.00	SP	0.23	0.18	0.13
LAC05-2G	-31.35	SP	0.17	0.13	0.11
LAC05-1G	-31.50	SM1-s	0.21	0.17	0.11
LAC05-2G	-38.85	SP	0.38	0.27	0.15
LAC05-1G	-42.00	SP	0.3	0.17	0.11
LAC05-2G	-43.85	SM-1	0.13	0.11	
LAC05-1G	-47.00	SC3-s	0.13	0.09	
LAC05-2G	-48.85	SC1	0.12	0.09	

Figure 7-45 shows the SPT values obtained from the GDM borings at the breach. The hammer efficiency is unknown for these borings. Refusal was reached in some dense layers of sand between elevations -15 to -35 (NAVD 88).

Figures 7-46 and 7-47 show the N1(60) values of the beach sand unit as determined from the CPTs. CPT NLON-2.05C was first pushed with a 5-ton cone penetrometer, but because the tip loads were nearing the capacity of the device at about elevation -31, a 10-ton cone penetrometer was used. On Figure 7-46, NLON-3.05c shows a dense sand layer (N1(60) values ranging from 50 to 90) from elevations -17 to -23, and elevations -30 to -37. NLON-2.05c shows a dense sand layer (N1(60) values range from 50 to 90) from elevations -27 to -37.

On Figure 7-47, NLON-5.05c also shows a dense sand layer $N_{1(60)}$ values range from 50 to over 100) from elevations -15 to -35. Both NLON-5.05c and NLON-1.05c show $N_{1(60)}$ values over 100. This occurs because of the process in which the N1(60) values are determined. Because of shallow depths and low overburden pressures, the Cn correction factor is greater than 1; and when multiplied to the $N_{(60)}$ values, will often produce an N1(60) over 100. Liao and Whitman's (1986) relationship between Cn and vertical effective stress was used to convert the field blowcounts to their N1(60) values. However, in some cases, the $N_{(60)}$ values are already near or at 100 at overburden pressures less than 1 tsf. Usually, N values greater than 50 are accepted as refusal. NLON-1.05c shows that dense sand layer $N_{1(60)}$ values range from 50 to over 100) from elevations -13 to -35.

Pore Pressure Dissipation Test

A pore pressure dissipation test was conducted in the beach sand unit at CPT SLON-2.05C. Below is a table summarizing the results of the dissipation tests.

Table 7-14
CPTU Pore Pressure Dissipation Tests in Beach Sand Unit

CPT	London Canal Staff Gauge Reading (NAVD 88)	Dissipation Test Elevation (NAVD 88)	Stabilized Pressure (psi)	Computed Head (ft) (Stab. Pressure x 2.31 ft/psi)	Head Elevation (NAVD 88)
SLON-2.05C	0.82	-20.45	5.5	12.70	-7.7

South London Breach - (CL of East Levee) N(60) versus Elevation

50 blows first 10"
50 blows first 10"
50 blows first 9"
50 blows first 8"
50 blows first 9"
50 blows first 9"
50 blows first 11"
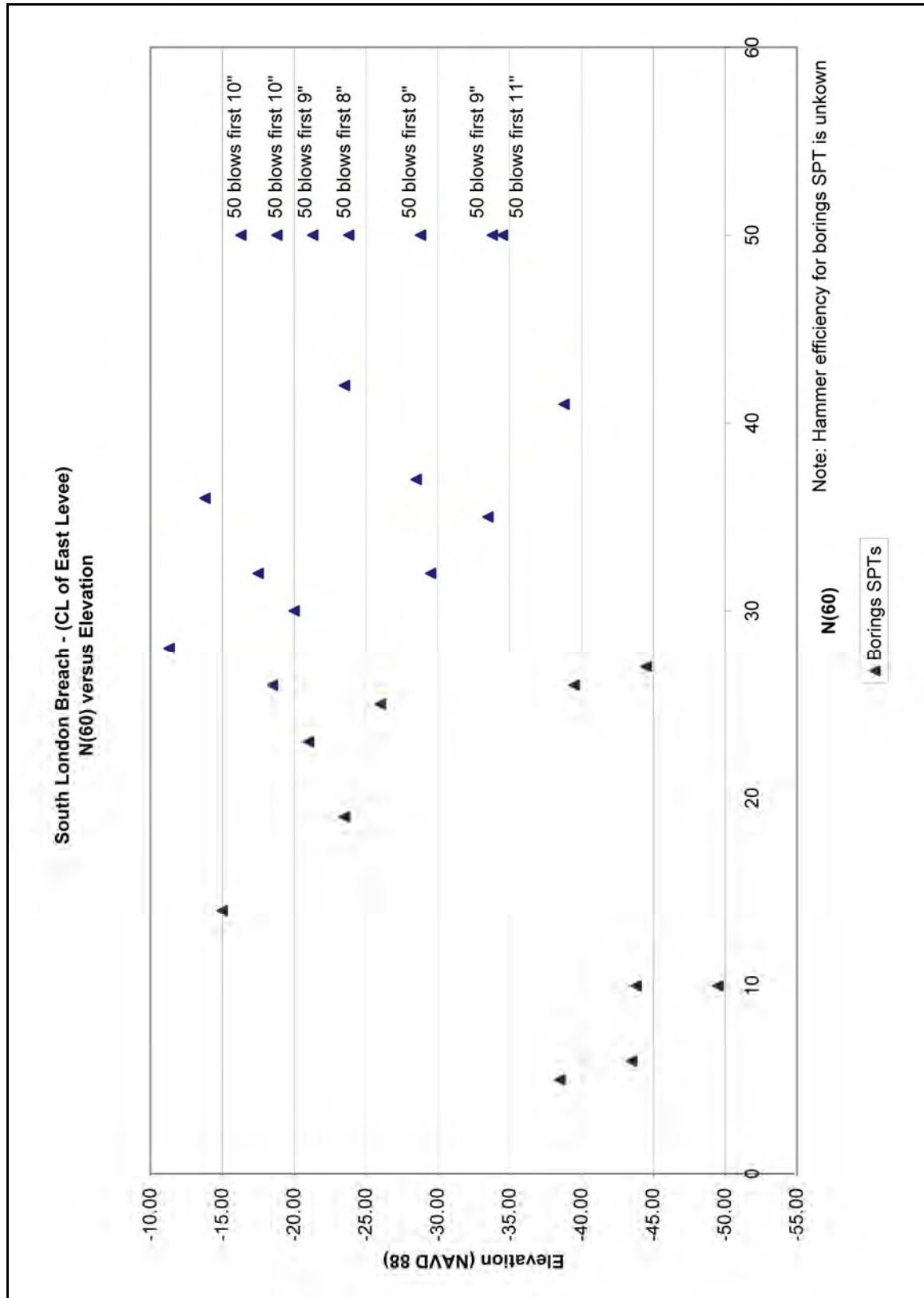
Note: Hammer efficiency for borings SPT is unkown

N(60)

▲ Borings SPTs

Figure 7-45.   South London Breach – Beach Sand Unit (CL of East Levee), SPT versus Elevation

Volume V The Performance – Levees and Floodwalls – Technical Appendix   V-7-61

This is a preliminary report subject to revision; it does not contain final conclusions of the United States Army Corps of Engineers.
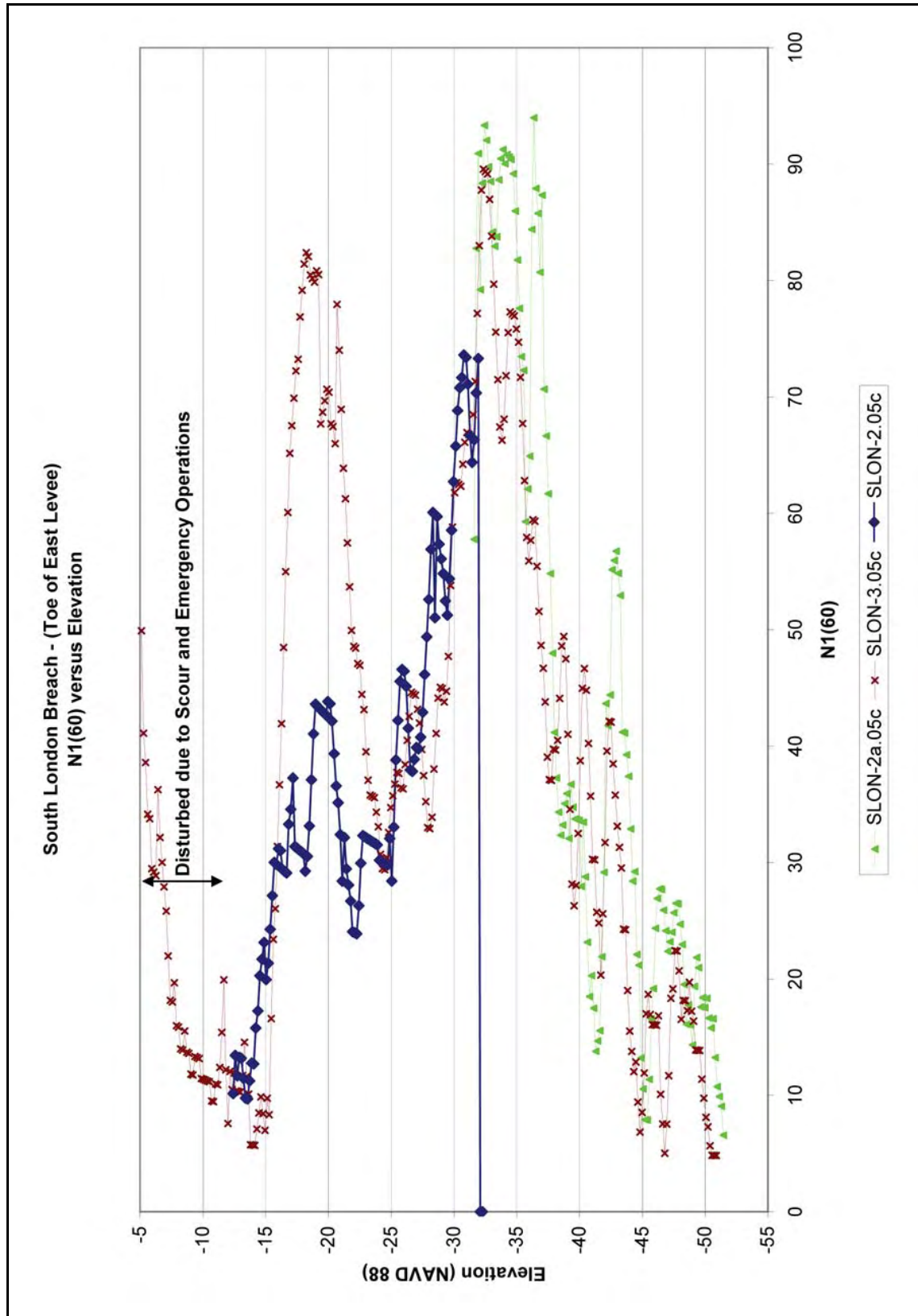
Figure 7-46. South London Breach – Beach Sand Stratum (Toe of East Levee), N1(60) versus Elevation for CPTs SLON-2.05c and SLON-3.05c
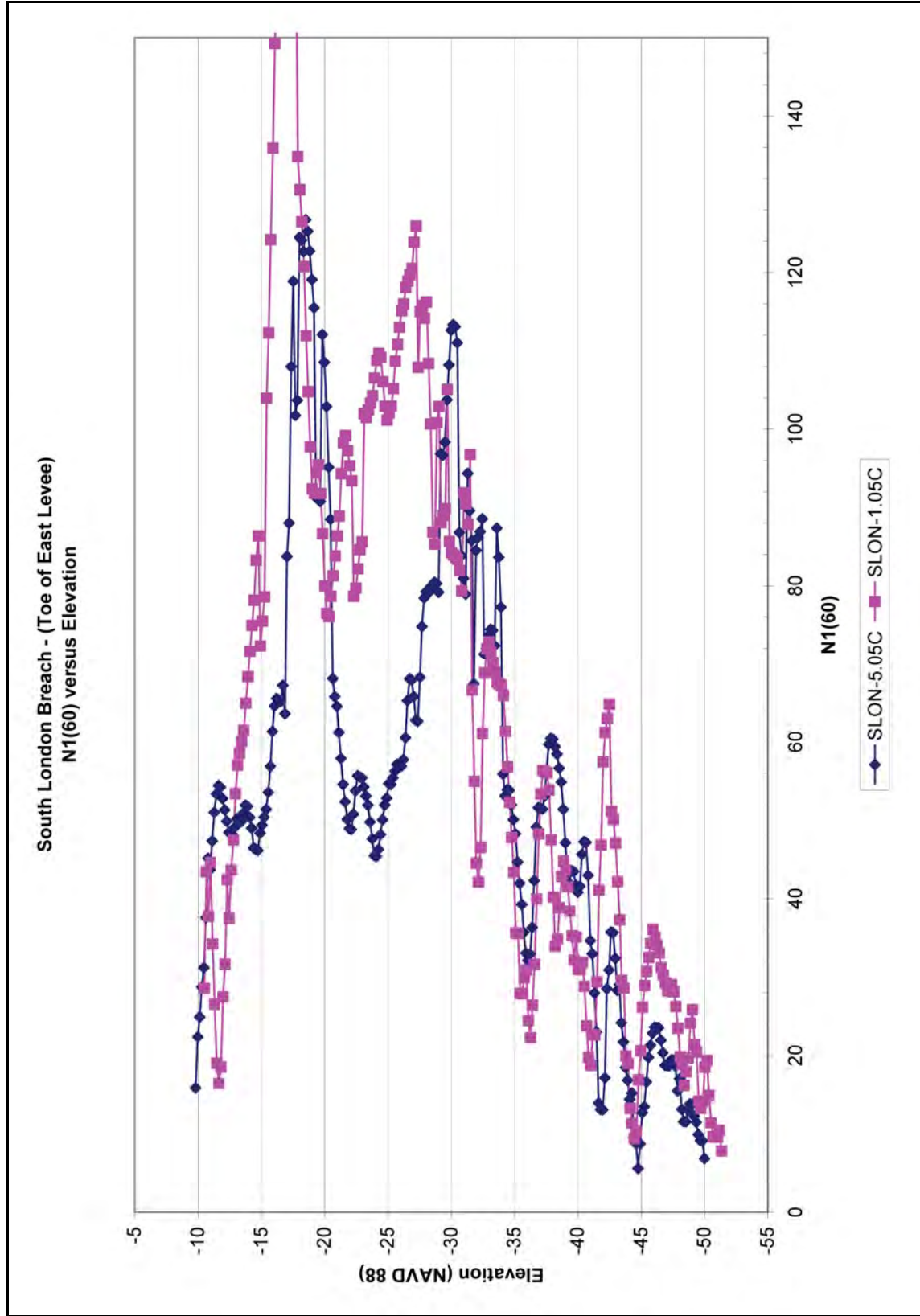
Figure 7-47. South London Breach – Beach Sand Stratum (Toe of East Levee), N1(60) versus Elevation for CPTs SLON-5.05c and SLON-1.05c

Piezometers at London Canal

Piezometer Locations

Nineteen borings with piezometers were installed along London Canal for the purpose of monitoring the piezometric response of the beach sands to changes in the water level in the canal. Figure 7-48 shows the location of these piezometers along the canal. A total of 30 piezometers are in these borings. The piezometers are located and labeled into three basic groups, depending on their location. The first group included four borings, labeled LRP1 through 4, each with two piezometers and is located near the north London Canal breach site on the west bank of the canal just south of Robert E. Lee Boulevard. The second group includes five borings, each containing two piezometers, labeled LMP1 through 5, located on the east bank of the canal in the vicinity of the South London Canal breach site near Mirabeau Avenue. The third group represents secondary borings, labeled LP, and contains a total of 13 piezometers at miscellaneous locations of interest along the canal. All piezometers were put in service by the New Orleans District after Katrina.

Tables 7-15 through 7-17 list the information pertaining to the locations of the piezometer boreholes. Identified for each borehole are the Station, offset distance from the floodwall, the ground surface elevation immediately adjacent to the hole, and an indication of which side of the canal the borehole is located on. Table 7-15 represents this data for the North London breach site; Table 7-16, the data for the South London breach site; and Table 7-17, the data for the miscellaneous group of borings.

Tables 7-18 though 7-20 give information about where the piezometers are located in each boring for the north London breach site, the south London breach site, and the miscellaneous locations, respectively. Each table lists the boring and piezometer label, ground surface elevation immediately adjacent to each boring, and the elevation that each piezometer tip is set at.

Table 7-15 Piezometer Borings in the Vicinity of the North London Breach Area near Robert E. Lee Boulevard					
Boring	Station	Offset Distance from Wall, ft	Ground Elevation, ft, NGVD88	Description of Location	Bank
LRP1	-----	-----	-4.06	Toe	West
LRP2	-----	-----	+3.54	On Levee near floodwall	West
LRP3	------	------	-1.55	Toe	West
LRP4	------	------	-5.26	Near street in neutral ground	West

Figure 7-48.   Plan View Showing Locations of the Piezometer Boreholes at London Canal

Table 7-16
Piezometer Borings in the Vicinity of the South London Breach Area near Mirabeau Avenue

Boring	Station	Offset Distance from Wall, ft	Ground Elevation, ft, NGVD88	Description of Location	Bank
LMP1	-----	-----	-1.56	In breach	West
LMP2	-----	-----	-2.16	In breach near toe	West
LMP3	------	------	-3.16	Toe near curb at Warrington Ave	West
LMP4	------	------	-4.86	At breach in the neighborhood backyard	West
LMP5	52+00	------	+0.16	At floodwall north of breach site	West

Table 7-17
Secondary Piezometer Borings at the London Canal (Miscellaneous Locations)

Boring	Station	Offset Distance from Wall, ft	Ground Elevation, ft, NGVD88	Description of Location	Bank
LP6	-----	-----	????	At the lakefront on the canal's west bank	West
LP7	-----	-----	-2.62	Near the University of New Orleans on the canal's east bank at the toe	East
LP8	------	------	Peat	At Leon C. Simon on the West side of the canal at the toe	
LP9	------	------	-0.22	Just north of Robert E. Lee Blvd bridge over canal on west bank	West
LP10	------	------	---	Just north of Robert E. Lee Blvd bridge over canal on flood side	West
LP11	-----	-----	-4.27	At bridge abutment at Robert E. Lee Blvd.	East
LP12	-----	-----	----	At Prentiss Ave. mid-way between Mirabeau and north Mirabeau breach sites on toe of levee	East
LP13	------	------	0.2	Just south of Fillmore Ave at toe of levee	West
LP14	------	------	0.66	Four blocks south of Mirabeau Ave. near Dillard University	West
LP15	------	------	----	Directly across from the Mirabeau Ave. breach site	West

Table 7-18
Piezometer Tip Elevations in the Vicinity of North London Breach Area near Robert E. Lee Boulevard

Boring	Piezometer	Ground Surface Elevation, ft NGVD88	Tip Elevation, ft NGVD88
LRP1	A	-4.06	-38.7
	B	-4.06	-23.7
LRP2	A	+3.54	-38.1
	B	+3.54	-16.1
LRP3	A	-1.55	-36.19
	B	-1.55	-18.19
LRP4	A	-5.26	-39.9
	B	-5.26	-20.9

Table 7-19
Piezometer Tip Elevations in the Vicinity of South London Breach Area near Mirabeau Avenue

Boring	Piezometer	Ground Surface Elevation, ft NGVD88	Tip Elevation, ft NGVD88
LMP1	A	-1.56	-43.2
	B	-1.56	-19.2
LMP2	A	-2.16	-43.8
	B	-2.16	-19.8
LMP3	A	-1.55	-37.8
	B	-1.55	-17.8
LMP4	A	-4.86	-46.5
	B	-4.86	-18.5
LMP5	A	+0.16	-13.48

Table 7-20
Piezometer Tip Elevations at the London Canal (Miscellaneous Locations)

Boring	Piezometer	Ground Surface Elevation, ft NGVD88	Tip Elevation, ft NGVD88
LP6	A	Not Reported (NR)	-36.36
	B	NR	-17.52
LP7	A	+2.62	-37.58
	B	NR	-8.65
LP8	A	NR	-21.95
	B	NR	-13.05
LP9	A	-0.22	-18.9
LP10	A	NR	-17.15
LP11	A	-4.27	-15.79
LP12	A	NR	-25.36
LP13	A	0.2	-15.36
LP14	A	0.66	-11.09
LP15	A	NR	-21.46

Piezometer Data

The data collected represent readings taken between the time of installation and early February 2006. Figures 7-49 though 7-67 show piezometer data for each borehole. Each plot shows the response of the piezometers to changing water levels in the canal. The location of the London Avenue staff gauge is unknown at this time. Significant events such as construction and repair activities might have an effect on the piezometer responses and are noted on these plots. In addition, placement of a clay blanket on the canal side of the repair section at Mirabeau Avenue took place between the time periods of mid-October to early November 2005. This clay blanket was placed to reduce seepage through the repair section and a significant amount of clay was also dumped into the canal.
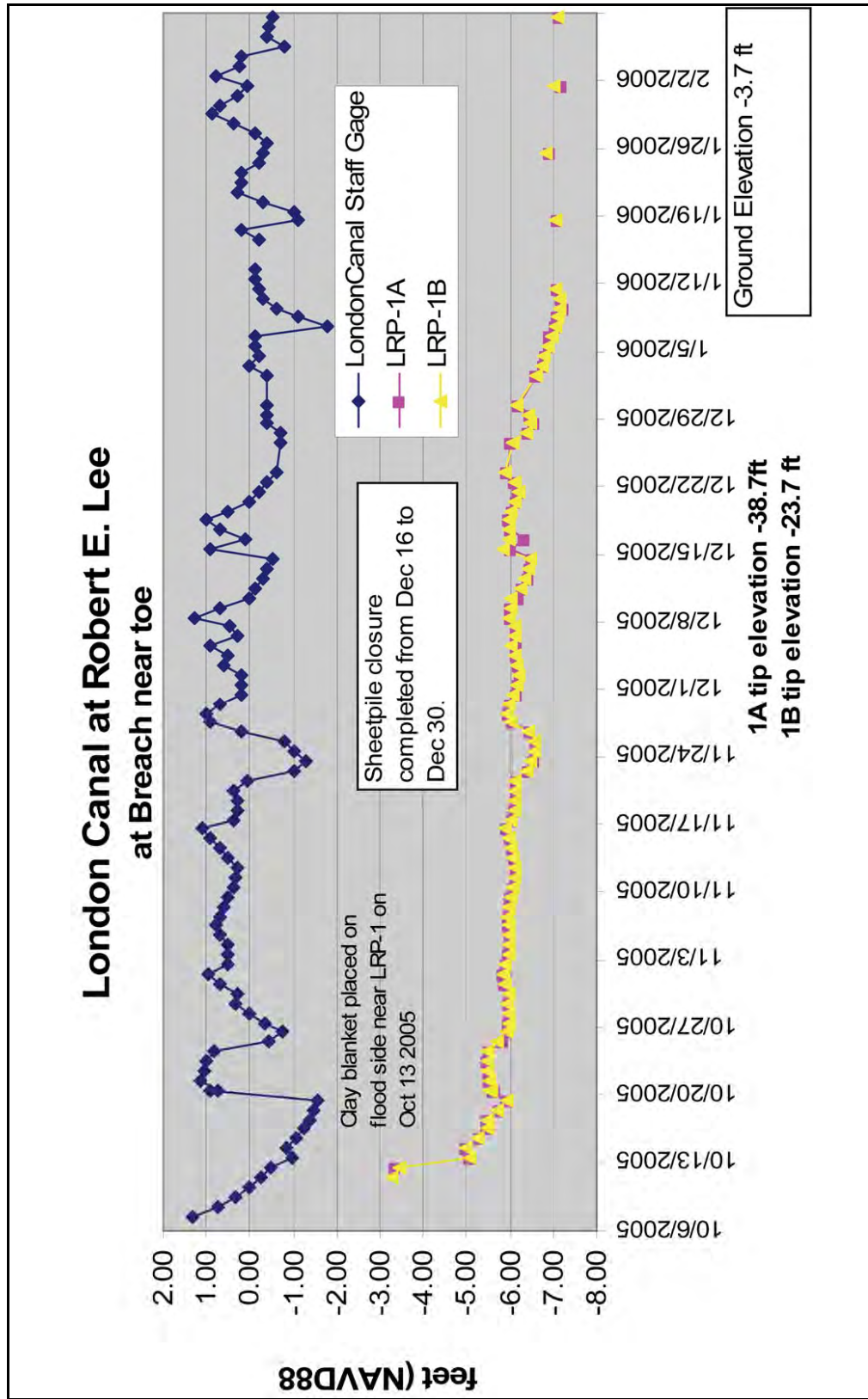
Figure 7-49. Response of Piezometers LRP-1a and LRP-1-B in the Vicinity of the North London Breach Site
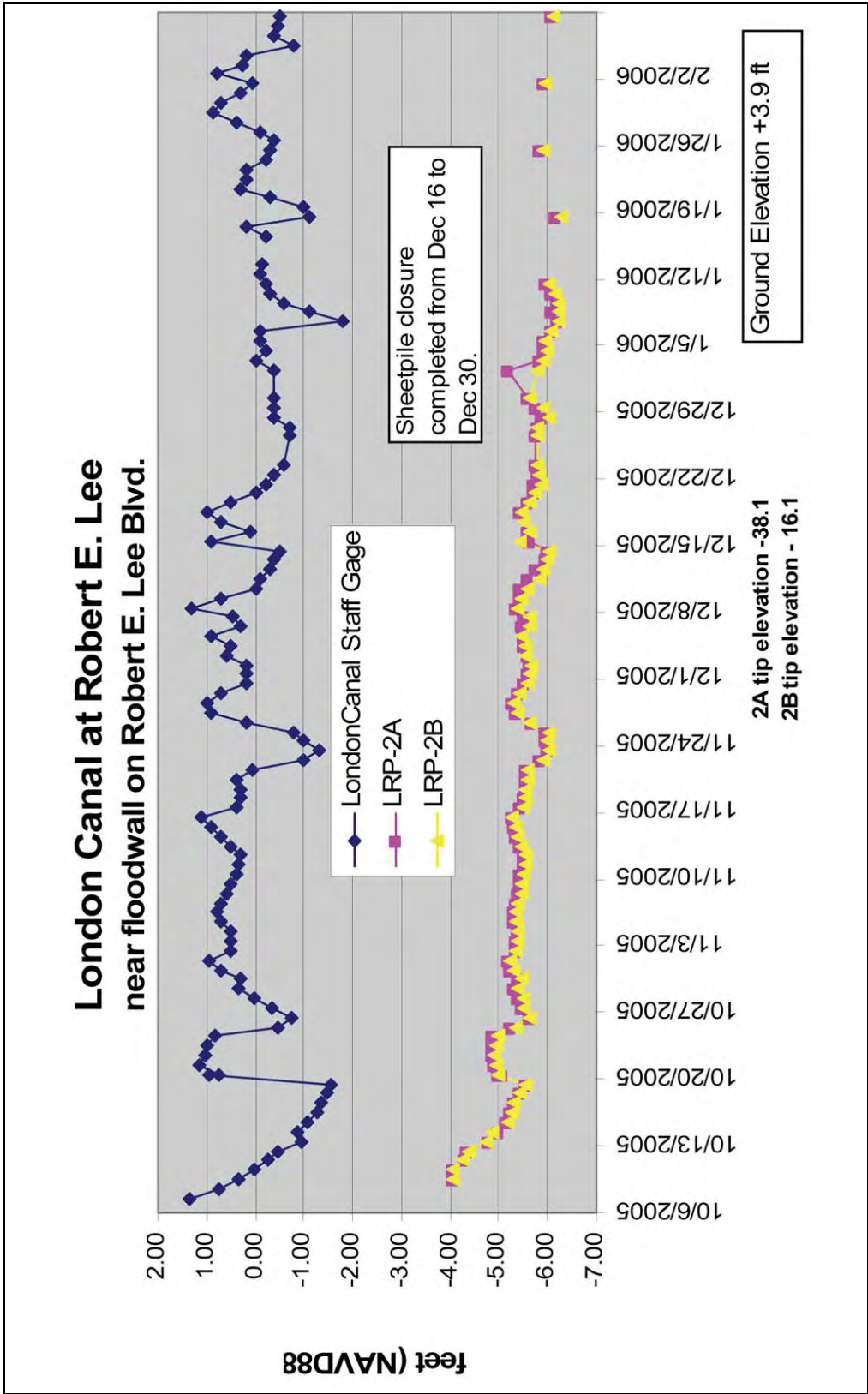
Figure 7-50. Response of Piezometers LRP-2A and LRP-2B in the Vicinity of the North London Breach Site
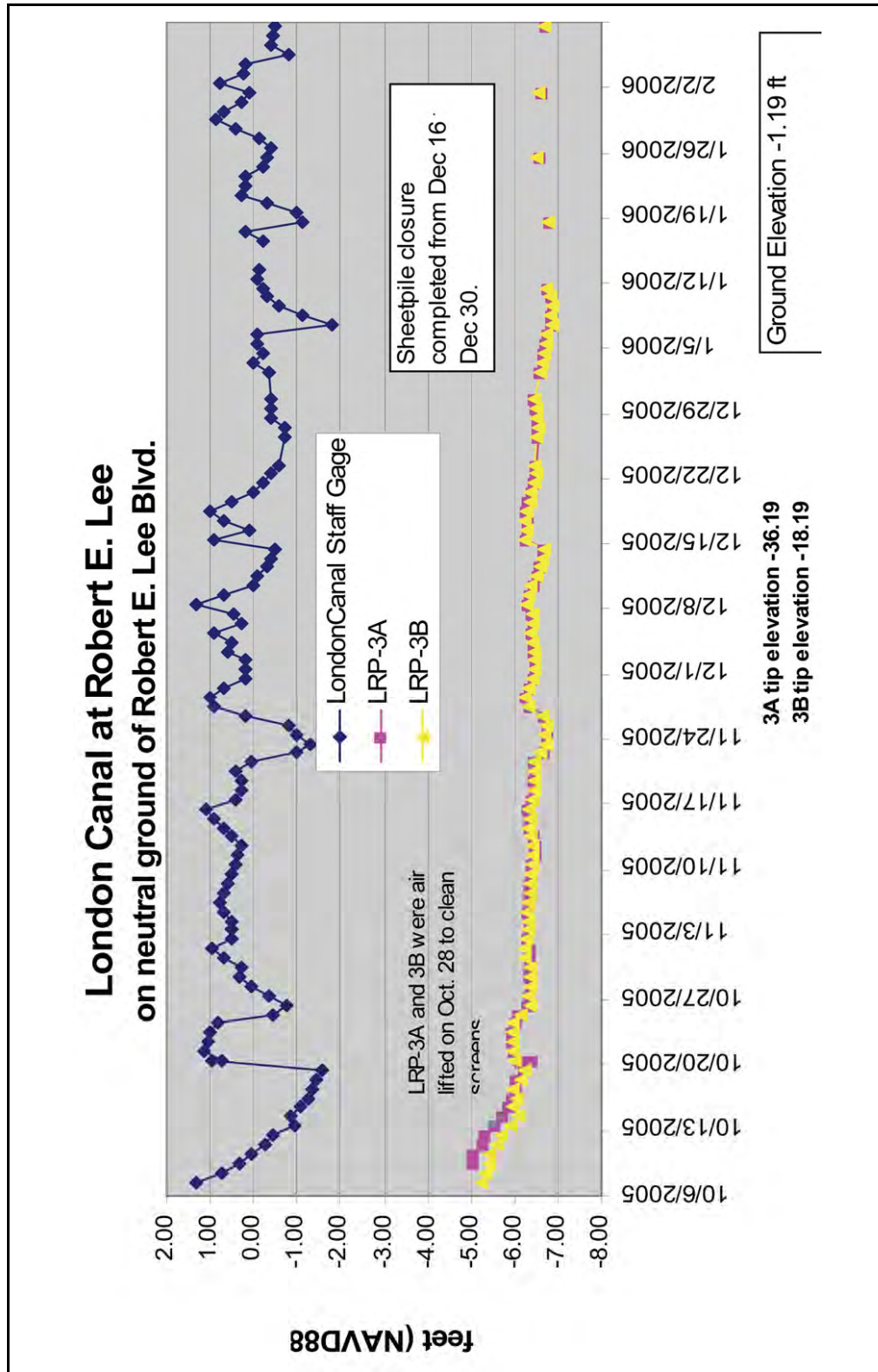
Figure 7-51. Response of Piezometers LRP-3A and LRP-3B in the Vicinity of the North London Breach Site

This is a preliminary report subject to revision; it does not contain final conclusions of the United States Army Corps of Engineers.
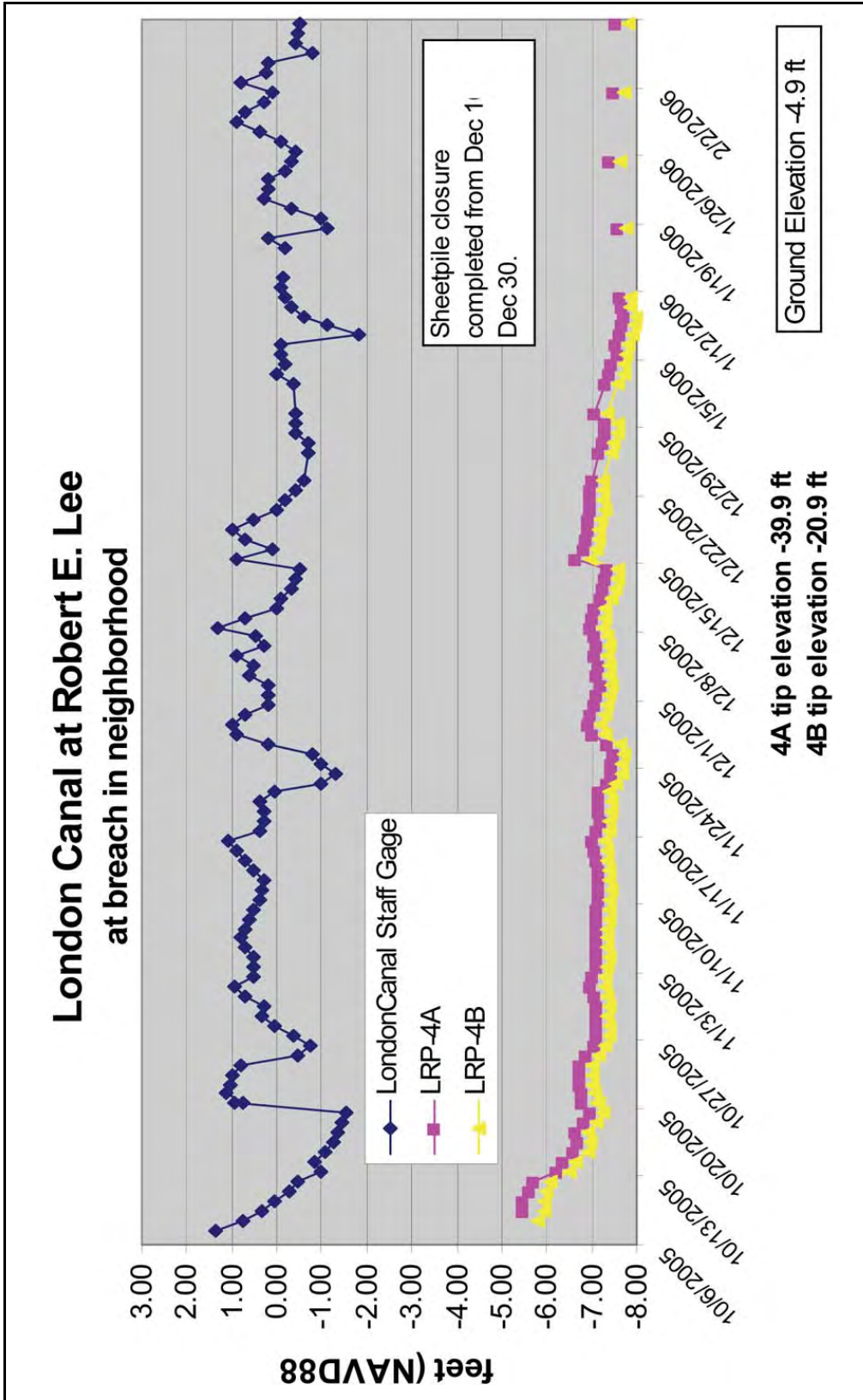
Figure 7-52. Response of Piezometers LRP-4A and LRP-4B in the Vicinity of the North London Breach Site
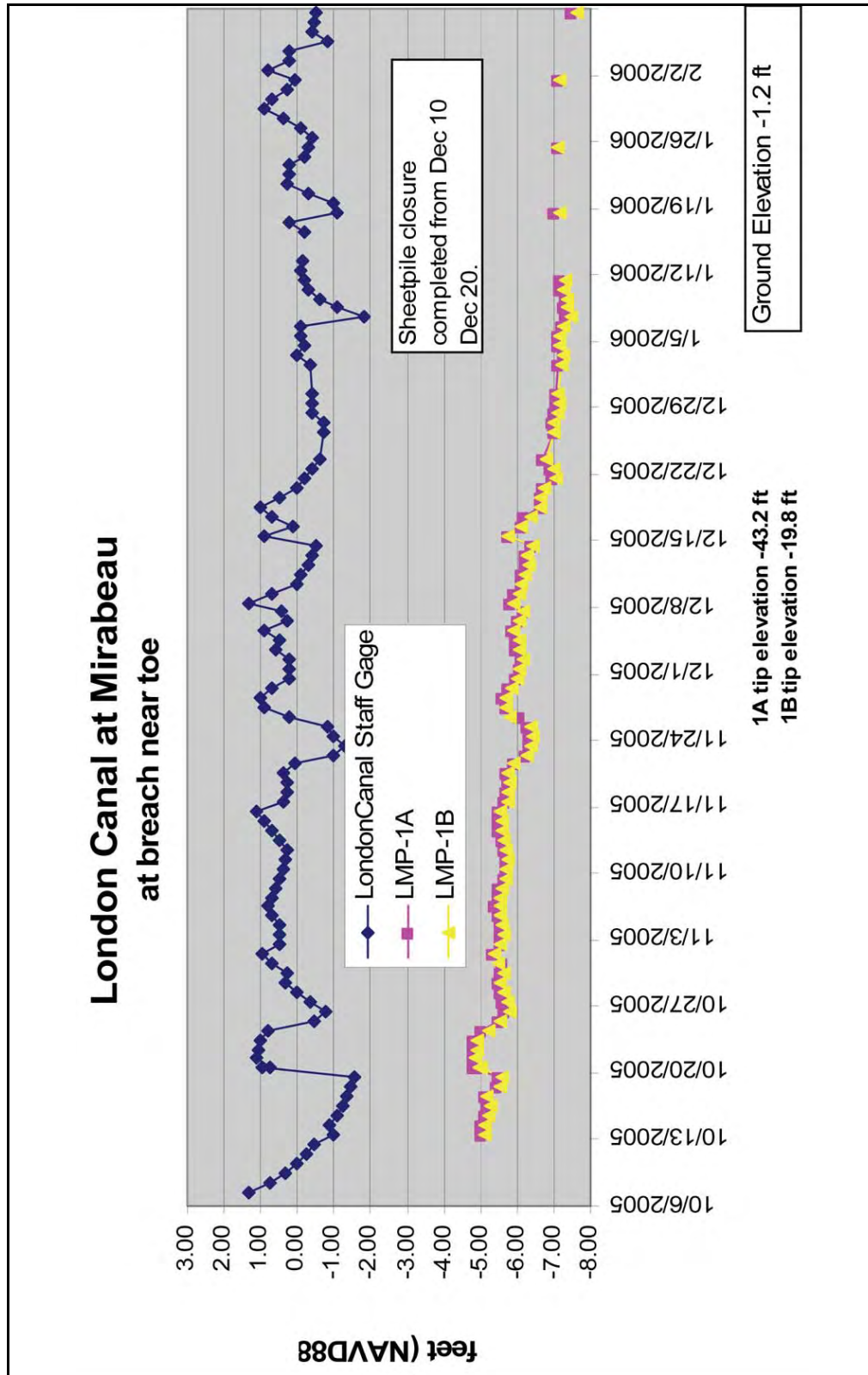
Figure 7-53. Response of Piezometers LMP-1A and LMP-1B in the Vicinity of the South London Breach Site near Mirabeau Avenue

This is a preliminary report subject to revision; it does not contain final conclusions of the United States Army Corps of Engineers.
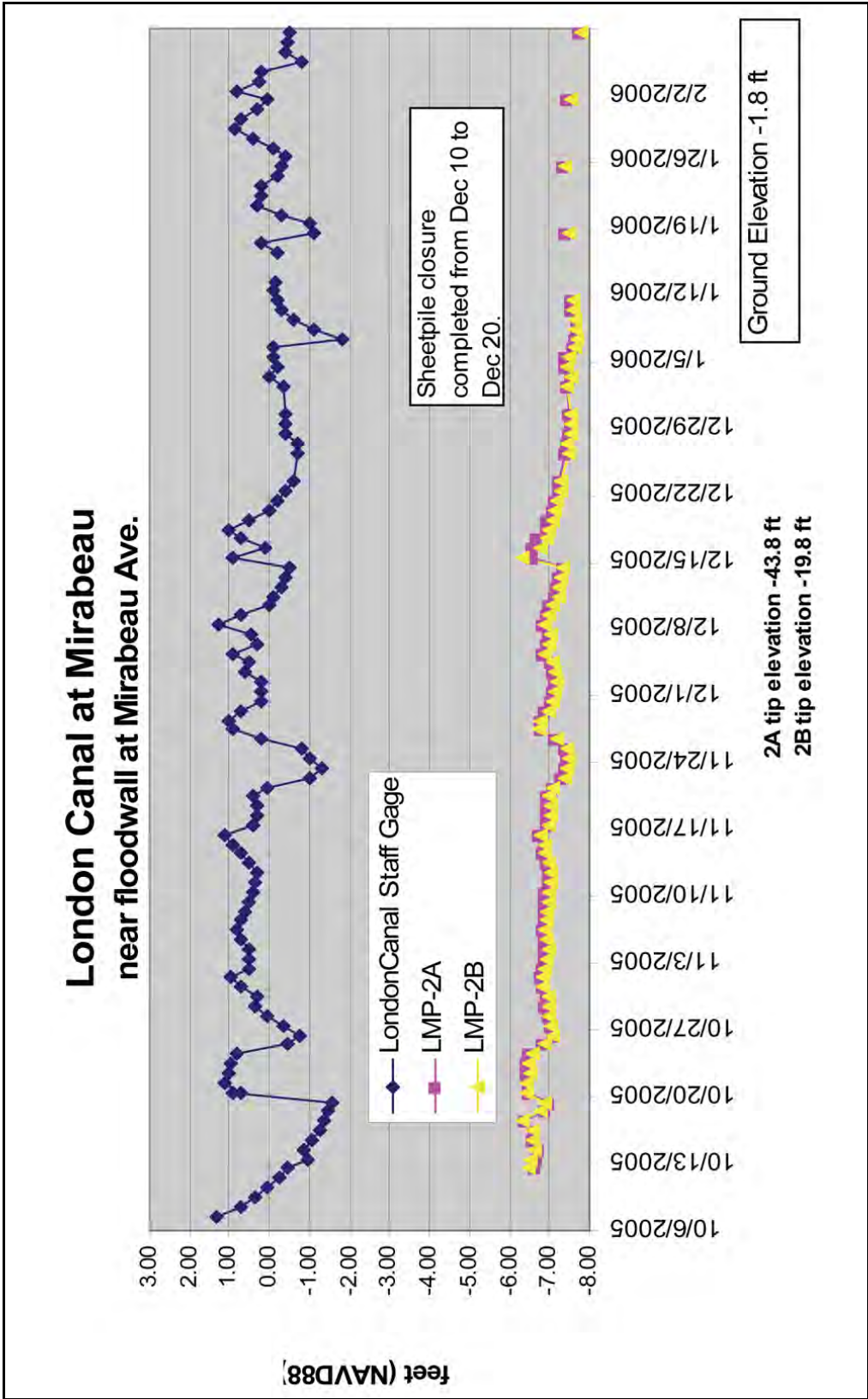
Figure 7-54. Response of Piezometers LMP-2A and LMP-2B in the Vicinity of the South London Breach Site near Mirabeau Avenue
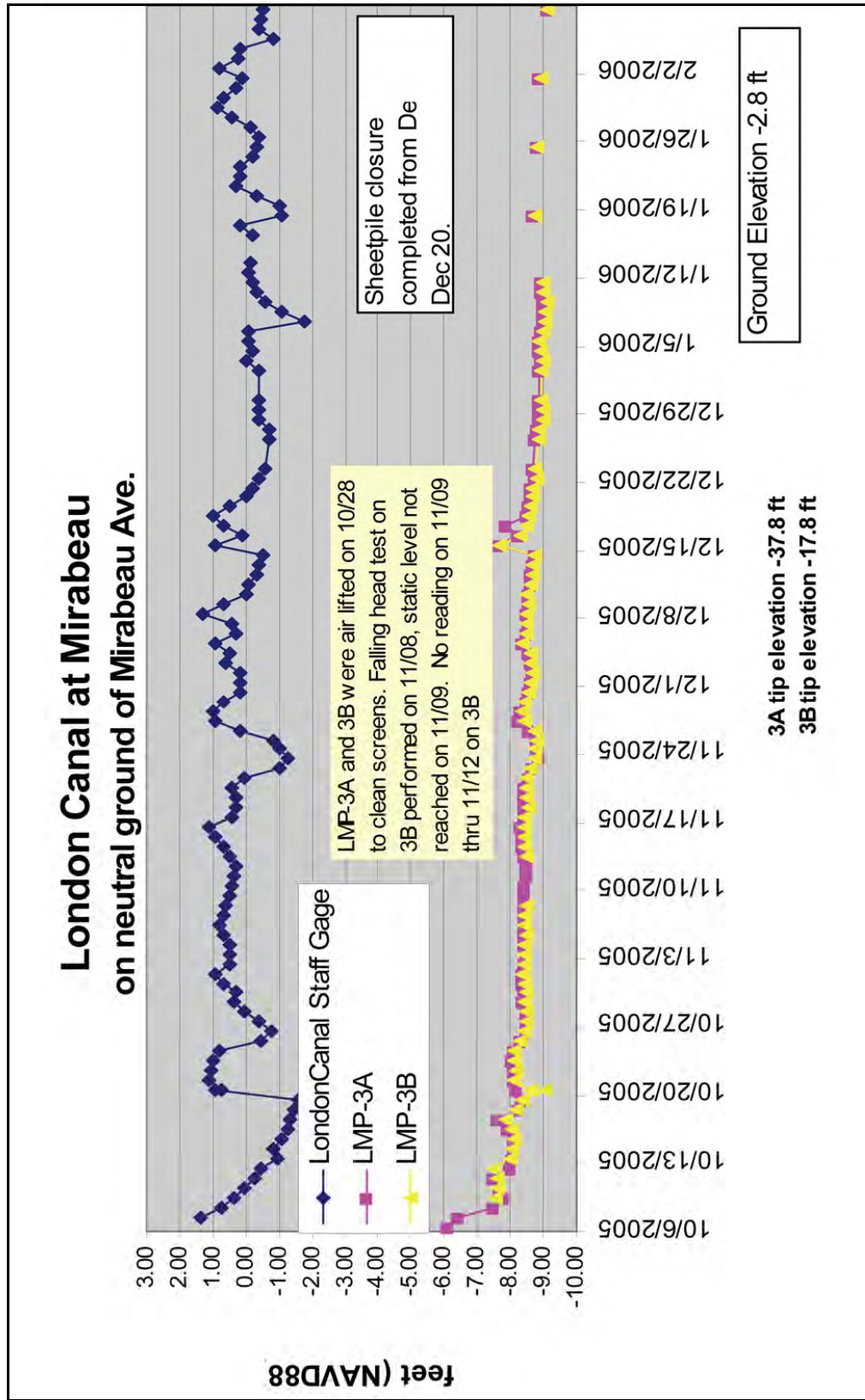
Figure 7-55. Response of Piezometers LMP-3A and LMP-3B in the Vicinity of the South London Breach Site near Mirabeau Avenue
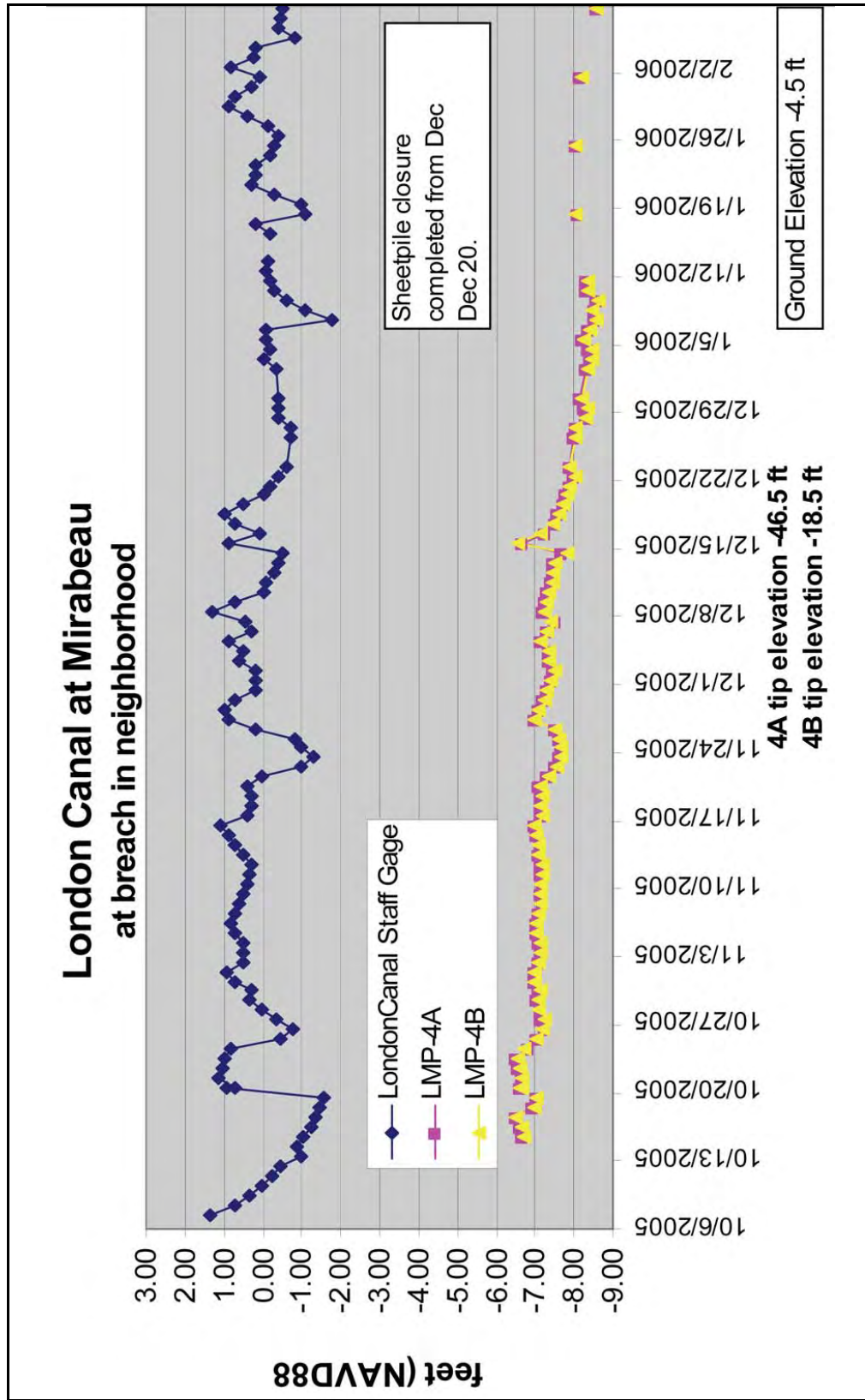
Figure 7-56. Response of Piezometers LMP-4A and LMP-4B in the Vicinity of the South London Breach Site near Mirabeau Avenue

Volume V The Performance – Levees and Floodwalls – Technical Appendix

V-7-75

This is a preliminary report subject to revision; it does not contain final conclusions of the United States Army Corps of Engineers.
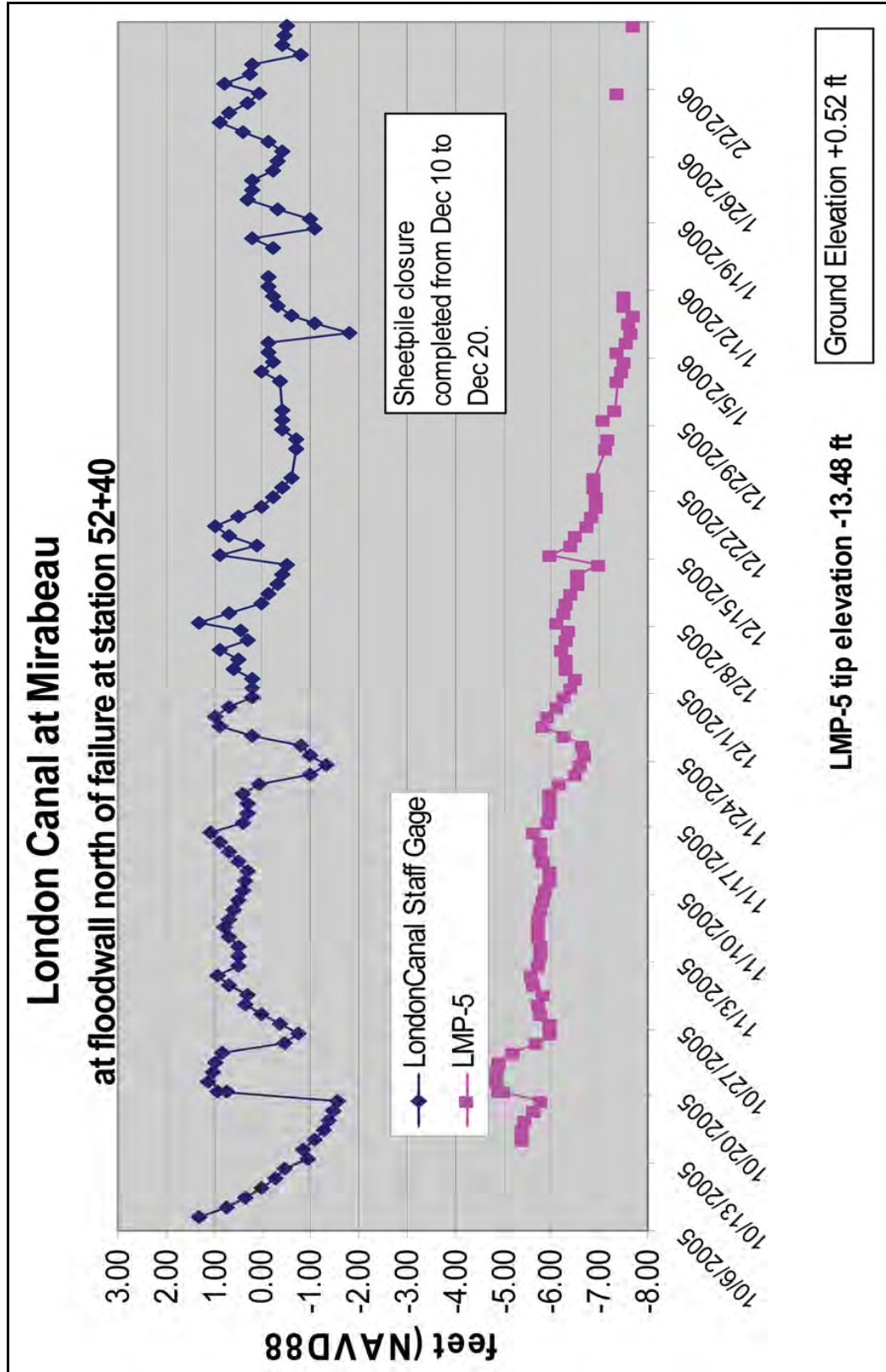
Figure 7-57. Response of Piezometer LMP5 at the South London Breach Site near Mirabeau Avenue at the Floodwall North of Breach Site at Station 52+00

    This is a preliminary report subject to revision; it does not contain final conclusions of the United States Army Corps of Engineers.
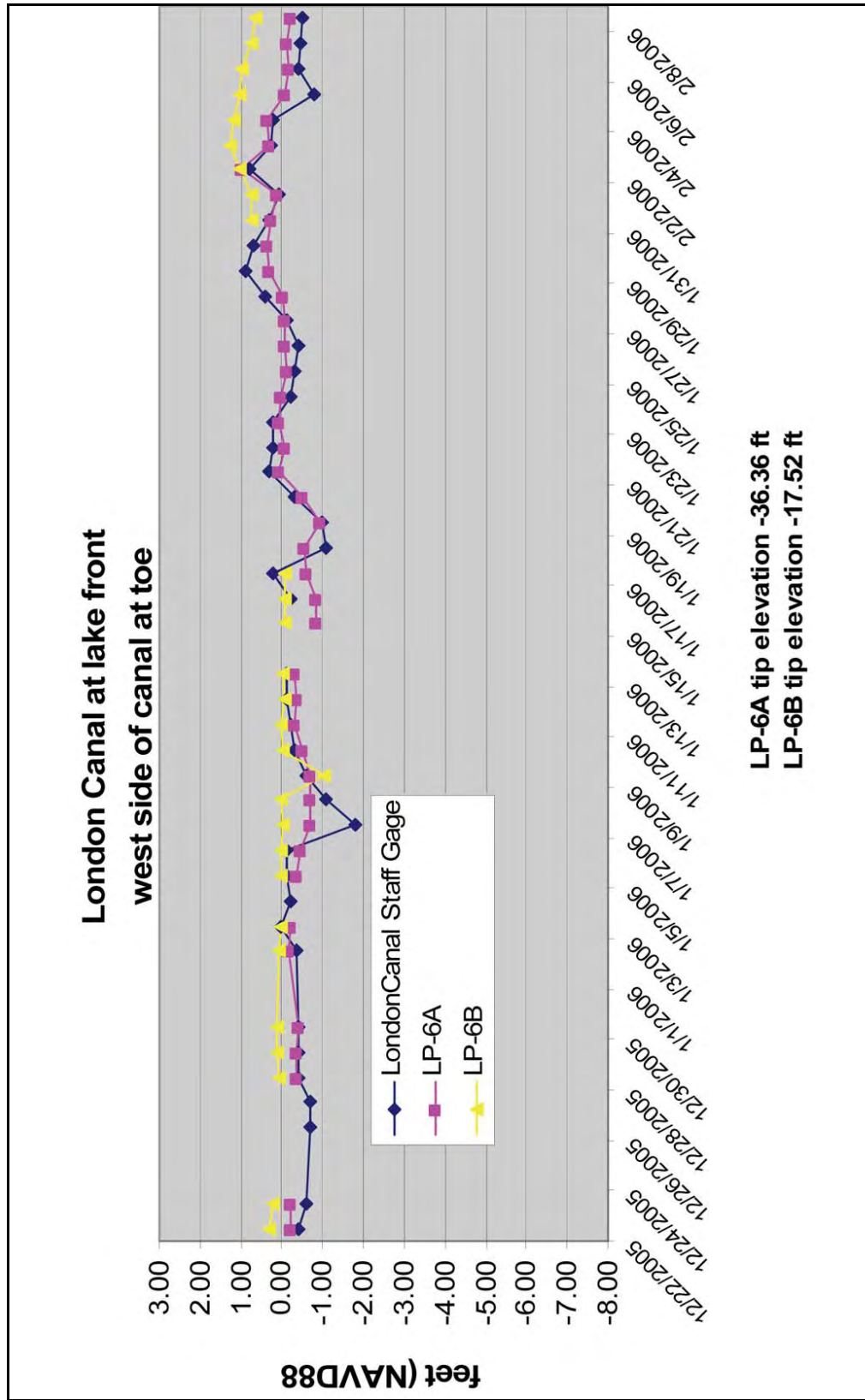
Figure 7-58. Response of Piezometer LP6A and 6B Located on the London Canal at the Lakefront at the Toe on the West Bank of the Canal

Volume V The Performance – Levees and Floodwalls – Technical Appendix

V-7-77

This is a preliminary report subject to revision; it does not contain final conclusions of the United States Army Corps of Engineers.
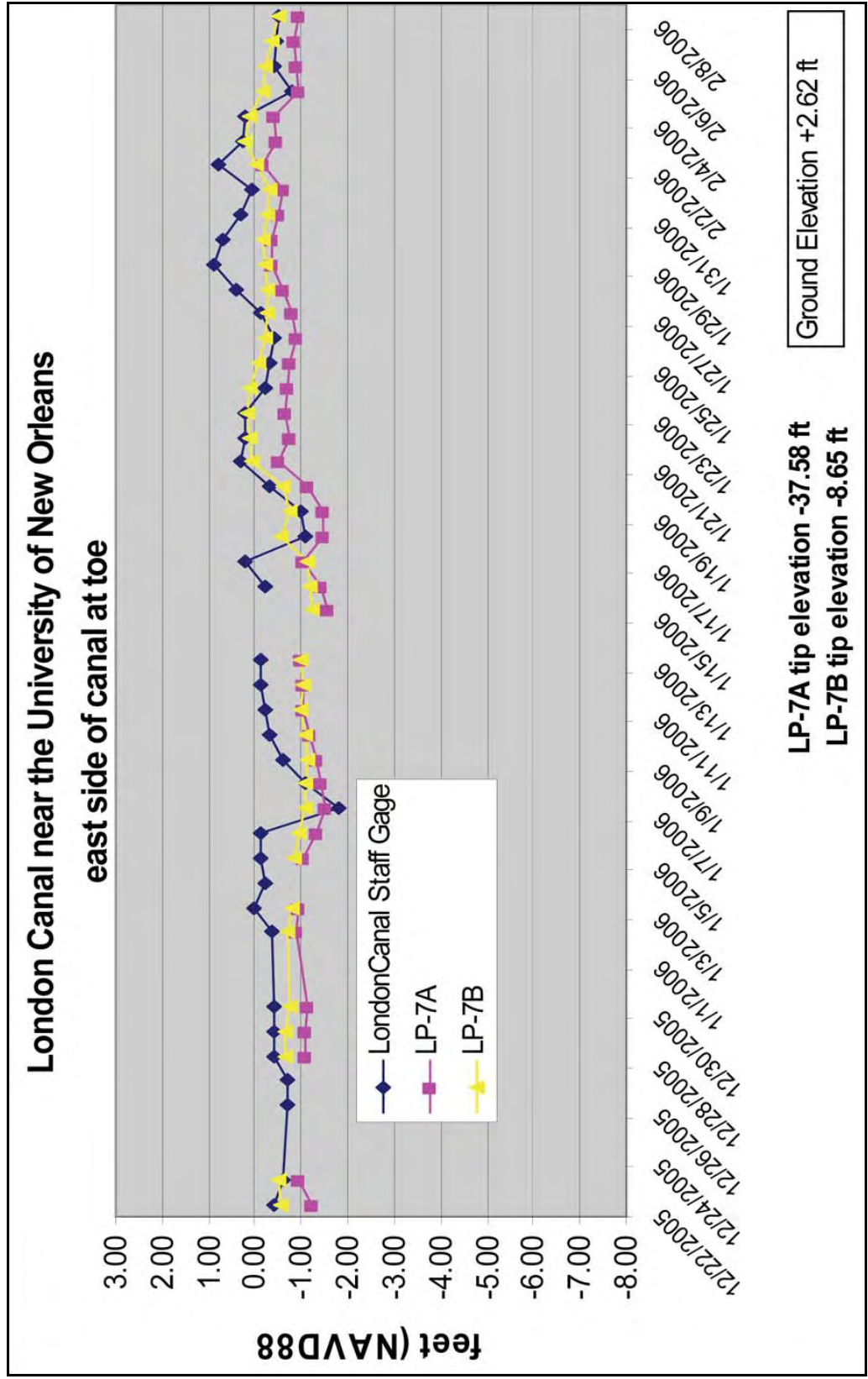
Figure 7-59. Response of Piezometers LP7A and 7B Located on the London Canal near the University of New Orleans on the East Bank of the Canal
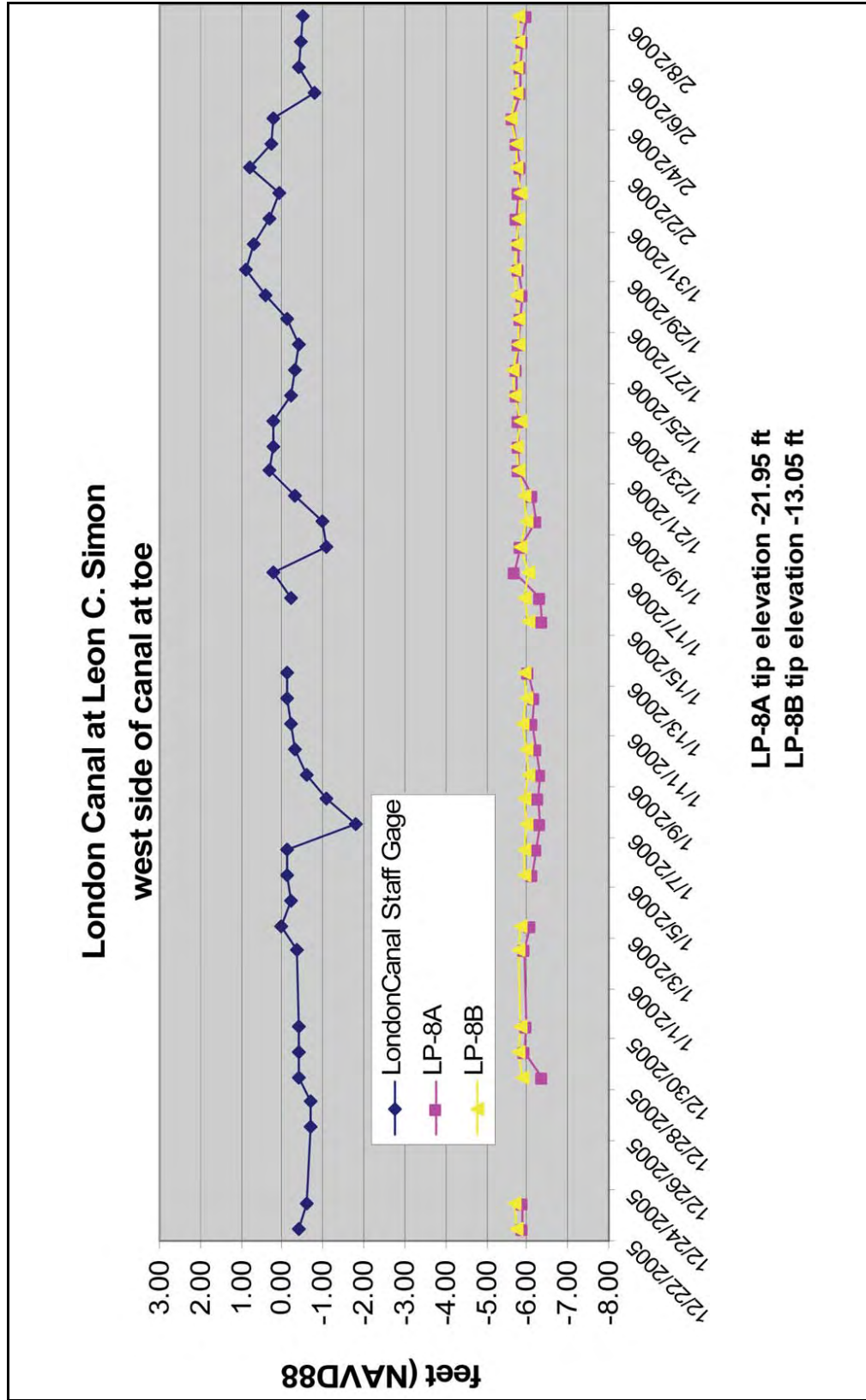
Figure 7-60. Response of Piezometers LP8A and 8B Located on the London Canal at Leon C. Simon on the Canal's West Bank
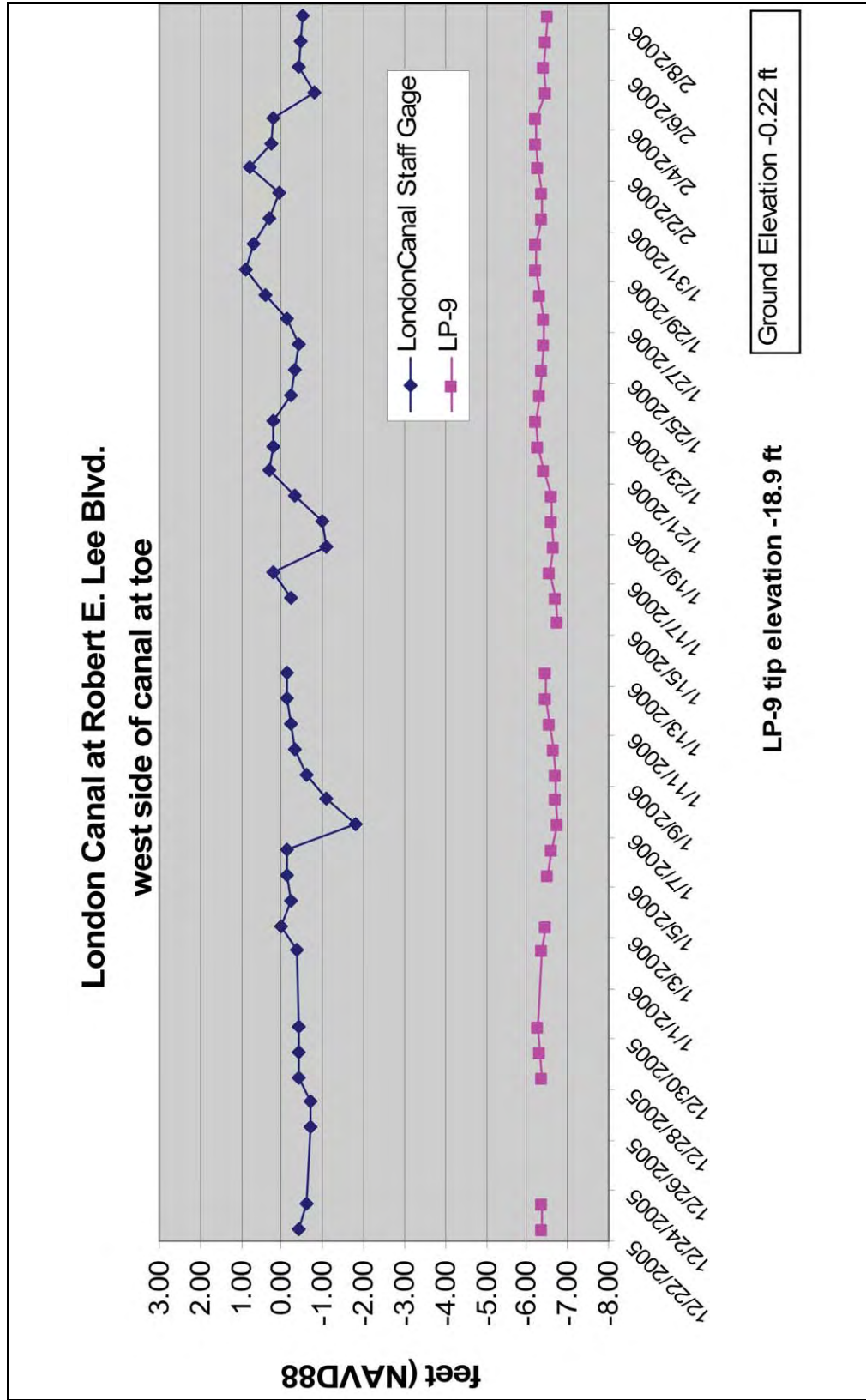
Figure 7-61. Response of Piezometer LP-9 Located on the London Canal at Robert E. Lee Boulevard on the Canal's West Bank

This is a preliminary report subject to revision; it does not contain final conclusions of the United States Army Corps of Engineers.
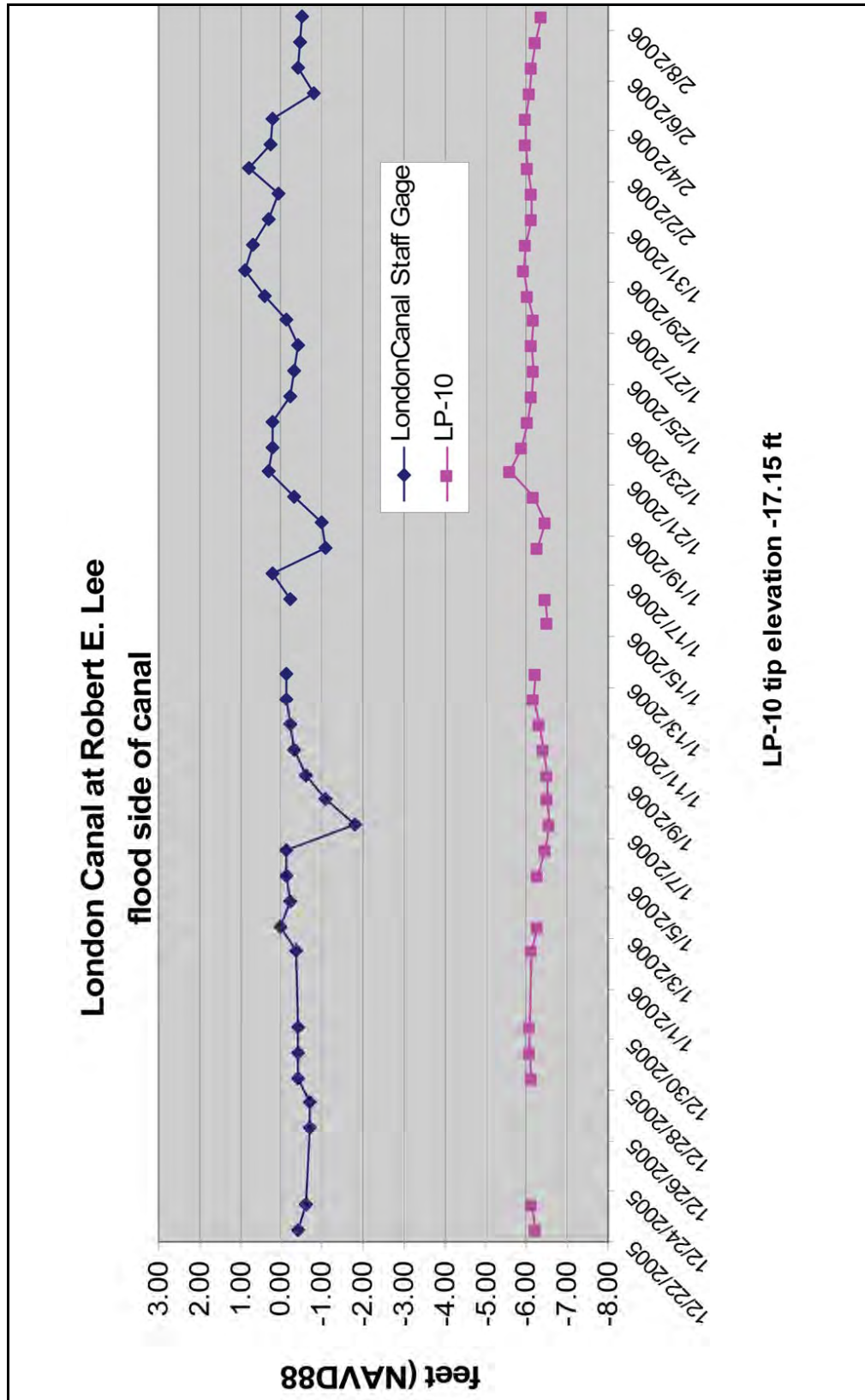
Figure 7-62. Response of Piezometer LP-10 Located on the London Canal at Robert E. Lee Boulevard on the Canal's Flood Side
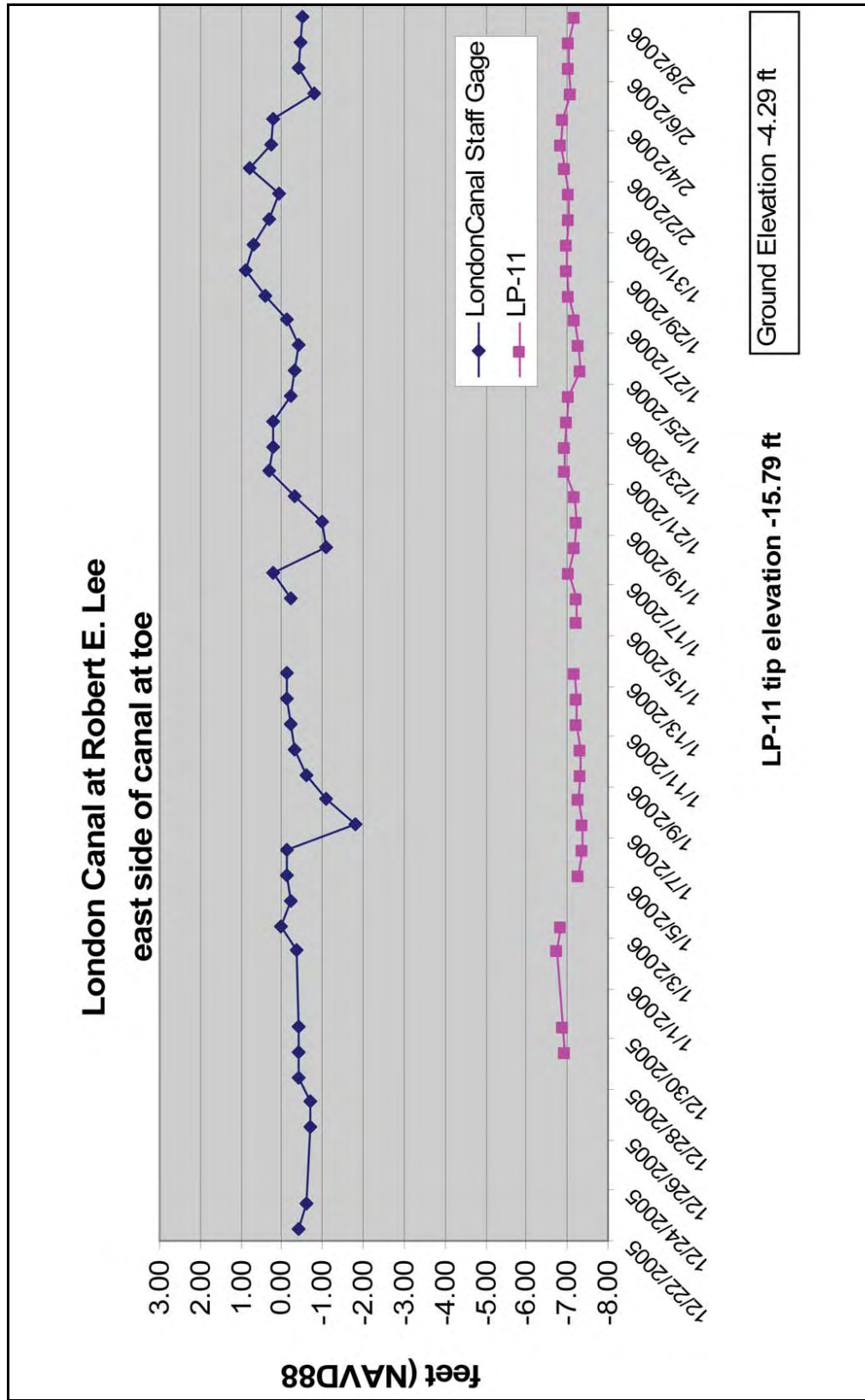
Figure 7-63. Response of Piezometer LP-11 Located on the London Canal at Robert E. Lee Boulevard on the Canal's East Side at the Toe

This is a preliminary report subject to revision; it does not contain final conclusions of the United States Army Corps of Engineers.
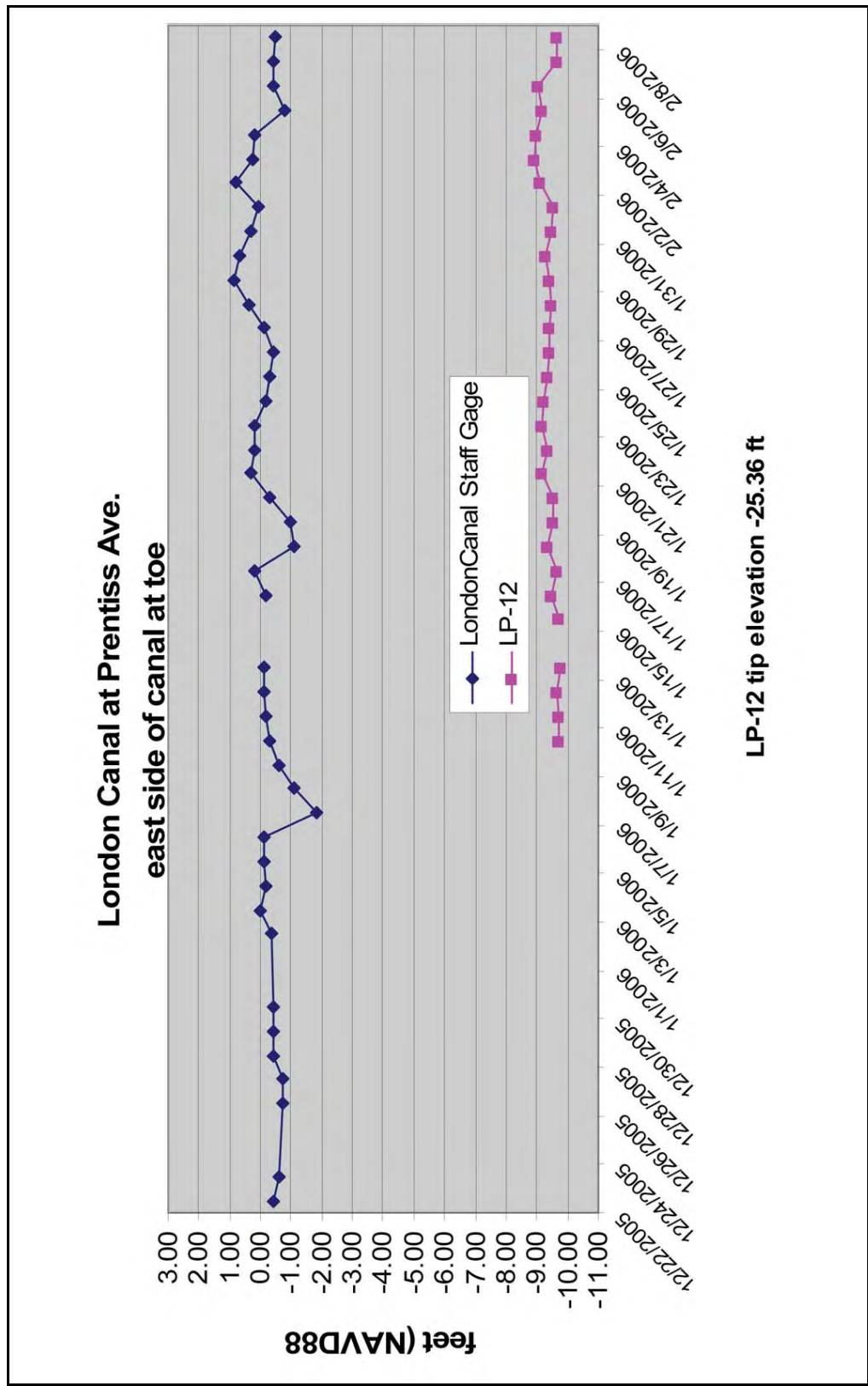
Figure 7-64. Response of Piezometer LP-12 Located at Prentiss Avenue on the Canal's East Side at the Toe

Volume V The Performance – Levees and Floodwalls – Technical Appendix

V-7-83

This is a preliminary report subject to revision; it does not contain final conclusions of the United States Army Corps of Engineers.
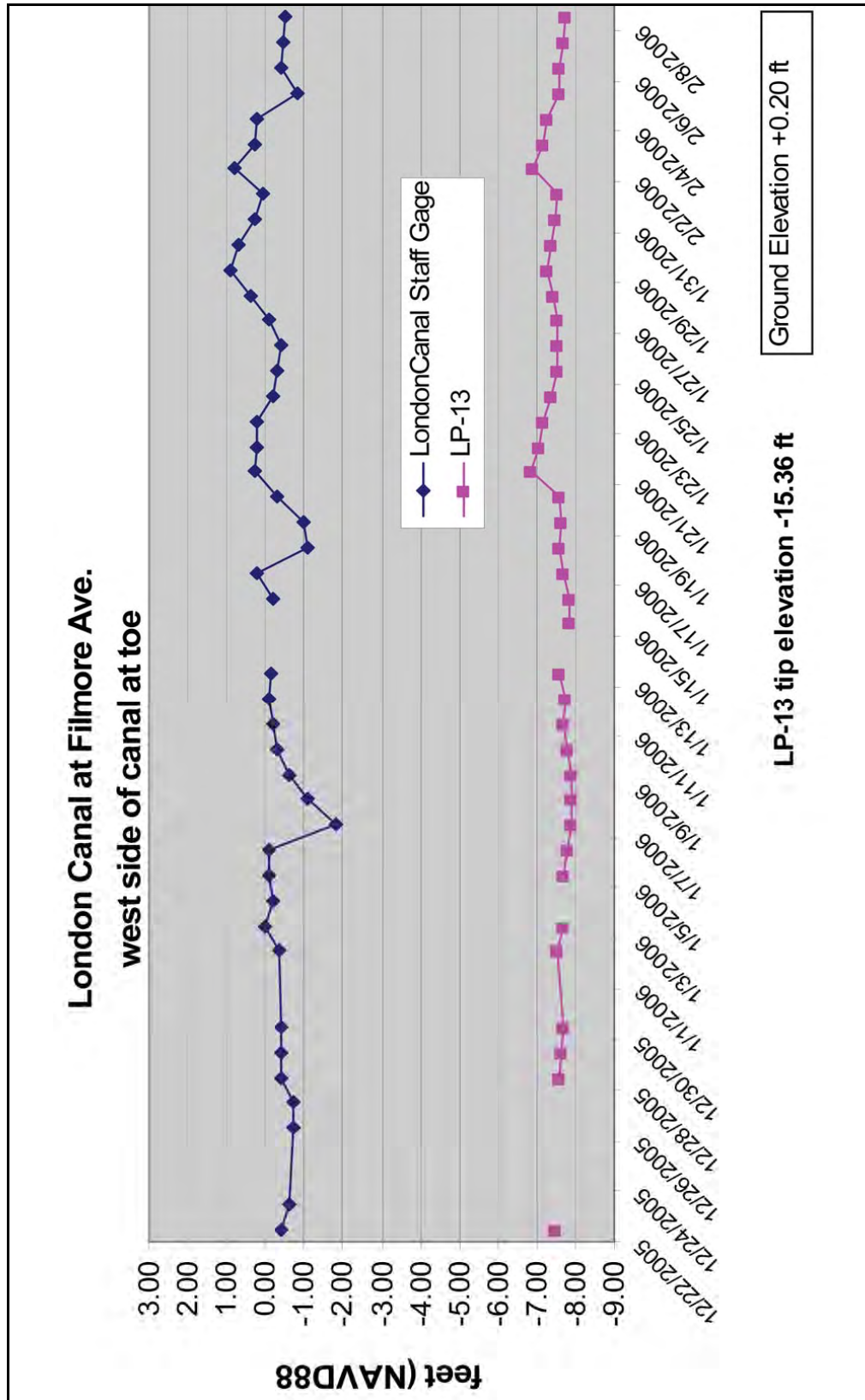
Figure 7-65. Response of Piezometers LP-13 Located at Filmore Avenue on the Canal's West Side at the Toe

V-7-84

Volume V The Performance – Levees and Floodwalls – Technical Appendix
This is a preliminary report subject to revision; it does not contain final conclusions of the United States Army Corps of Engineers.
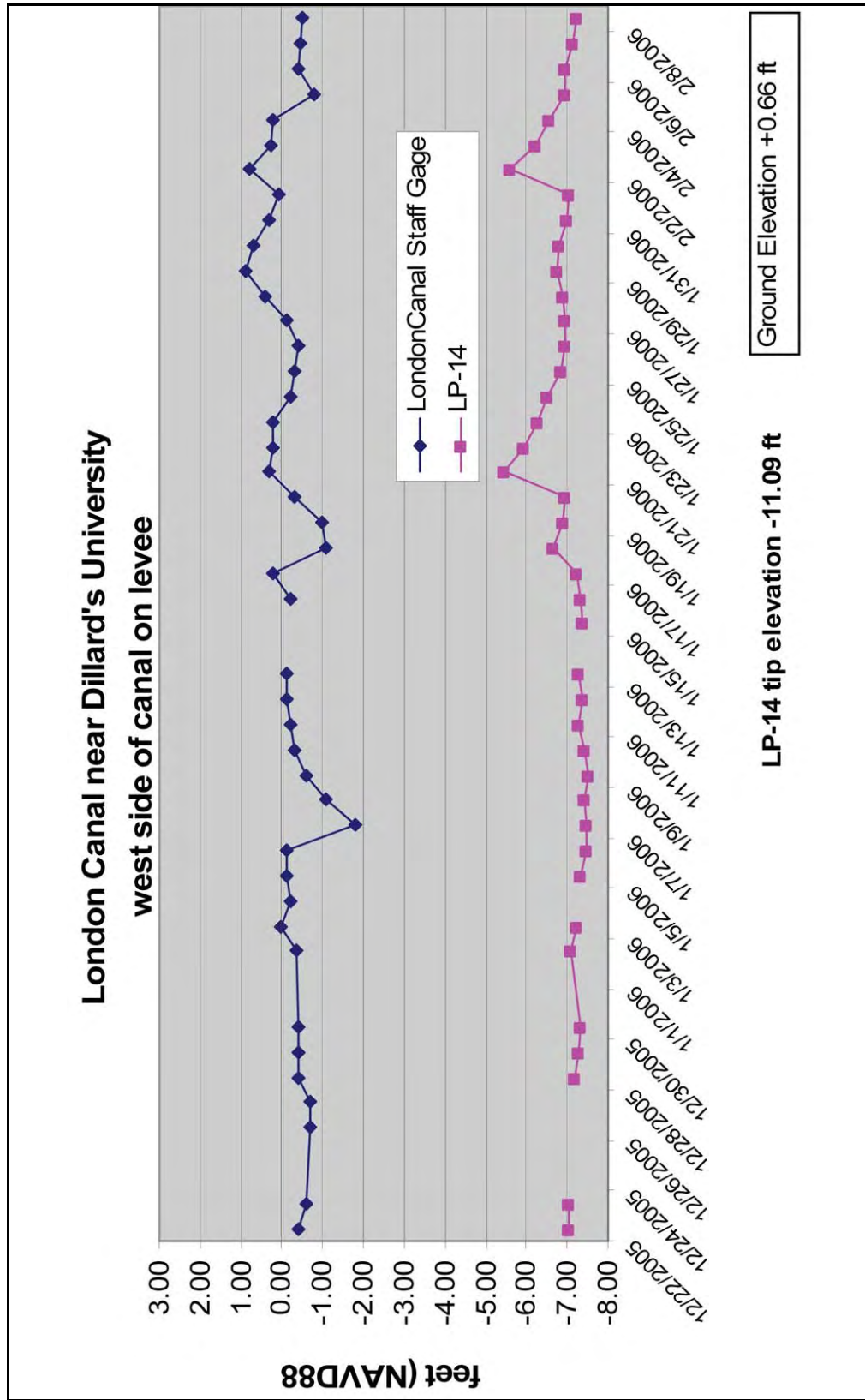
Figure 7-66. Response of Piezometer LP-14 Located near Dillard University on the Canal's West Side on the Levee
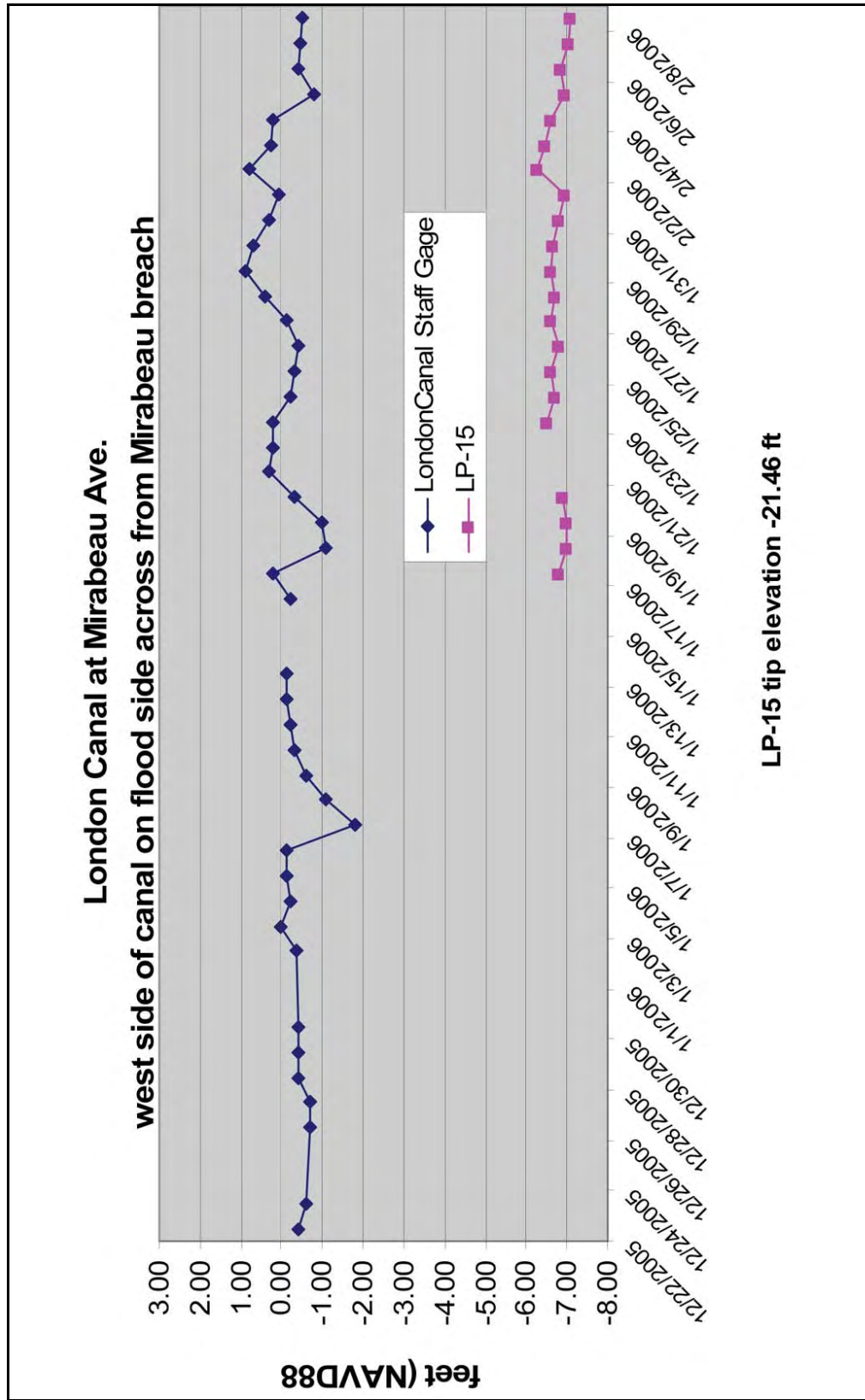
Figure 7-67. Response of Piezometers LP-15 at Mirabeau Avenue on the Canal's West Bank on the Flood Side, Directly Across from the Breach

This is a preliminary report subject to revision; it does not contain final conclusions of the United States Army Corps of Engineers.

References

Britsch, L. D., and Dunbar, J. B. 1990. "Geomorphic Investigation of Davis Pond, Louisiana," Technical Report GL-90-12, USAE Waterways Experiment Station, Vicksburg, Mississippi

Dunbar, J. B., Blaes, M. R., Dueitt, S. E., May, J. R., and Stroud, K. W., 1994. "Geological Investigation of the Mississippi River Deltaic Plain," Technical Report GL-84-15, <u>Report 2 of a Series</u>, USAE Waterways Experiment Station, Vicksburg, Mississippi

Dunbar, J. B., Blaes, M. R., Dueitt, S. E., and May, J. R., 1995. "Geological Investigation of the Mississippi River Deltaic Plain," Technical Report GL-84-15, <u>Report 3 of a Series</u>, USAE Waterways Experiment Station, Vicksburg, MS

Dunbar, J. B., Torrey, V. H., and Wakeley, L. D., 1999. "A Case History of Embankment Failure: Geological and Geotechnical Aspects of the Celotex Levee Failure, New Orleans, Louisiana," Technical Report GL-99-11, USAE Waterways Experiment Station, Vicksburg, MS

Fisk, H. N., 1944. "Geological Investigation of the Alluvial Valley of the Lower Mississippi River," Mississippi River Commission, Vicksburg, MS

Frazier, D. E., 1967. "Recent Deltaic Deposits of the Mississippi River: Their Development and Chronology," Transactions of the Gulf Coast Association of Geological Societies, Vol. 17, p. 287-315

Kemp, E. B., and Michel, U. J., Jr., 1967. Guidebook New Orleans, LA, and Vicinity Field Trip, The Geological Society of America and Associated Societies, 1967 Annual Meeting, Geological Society of America

Kolb, C. R., 1962. "Distribution of Soils Bordering the Mississippi River from Donaldsonville to Head of Passes," Technical Report No. 3-601, USAE Waterways Experiment Station, Vicksburg, MS

Kolb, C. R., and Saucier R. T., 1982. Engineering Geology of New Orleans. Reviews in Engineering Geology, Vol. V, Geological Society of America, p. 75-93

Kolb, C. R., Smith, F. L., and Silva, R. C., 1975. "Pleistocene Sediments of the New Orleans-Lake Pontchartrain Area," Technical Report S-75-6, USAE Waterways Experiment Station, Vicksburg, MS

Kolb, C. R., and Schultz, J. R., 1954. "Geological Investigation of the New Orleans Harbor Area," Technical Memorandum 3-391, USAE Waterways Experiment Station, Vicksburg, MS

Kolb, C. R., and Van Lopik, J. R., 1958a. "Geology of the Mississippi River Deltaic Plain, Southeastern Louisiana," Technical Report 3-483, two volumes, USAE Waterways Experiment Station, Vicksburg, MS

Kolb, C. R., and Van Lopik, J. R., 1958b. "Geologic Investigation of the Mississippi River Gulf Outlet Channel," Miscellaneous Paper 3-259, USAE Waterways Experiment Station, Vicksburg, MS

Liao, S.S. and Whitman, R. V. , 1986. "Overburden Correction Factor for SPT in Sand, Journal of Geotechnical Engineering, ASCE 112(3): 373-377.

May, J. R., Britsch, L. D., Dunbar, J. B., Rodriguez, J. P., and Wlosinski, L. B. 1984. "Geological Investigation of the Mississippi River Deltaic Plain," Technical Report GL-84-15, USAE Waterways Experiment Station, Vicksburg, MS

McFarlan, E., 1961. "Radiocarbon Dating of Late Quaternary Deposits, South Louisiana," Geological Society of America Bulletin, Vols. 8, 72, p. 129-158

Saucier, R. T., 1963. "Recent Geomorphic History of the Pontchartrain Basin," Coastal Studies Series Number 9, Louisiana State University Studies, Baton Rogue, LA

Saucier, R. T., 1994. "Geomorphology and Quaternary Geologic History of the Lower Mississippi Valley," In Two Volumes, Mississippi River Commission, Vicksburg, MS

Schultz, J. R., and Kolb, C. R., 1950. "Geological Investigation of the New Orleans Harbor Area," Technical Memorandum No. 3-319, USAE Waterways Experiment Station, Vicksburg, MS

Self, R. P., and Davis, D. W., 1983. "Geology of the New Orleans Area," The Compass of Sigma Gamma Epsilon, p. 29-38

Smith, L. M., Dunbar, J. B., and Britsch, L. D., 1986. "Geomorphological Investigation of the Atchafalaya Basin, Area West, Atchafalaya Delta, and Terrebonne Marsh," Technical Report GL-86-3, Volumes I and II, USAE Waterways Experiment Station, Vicksburg, MS

Tornquist, T. E., and Gonzalez, J. L., 2002. "Reconstructing Background Rates of Sea Level Rise as a Tool for Forecasting Coastal Wetland Loss, Mississippi Delta," EOS, Transactions, American Geophysical Union, Vol. 83, No. 46, p. 525, 530-531

US Army Corps of Engineers, 1989. "General Design Memorandum No. 19A, General Design, London Avenue Outfall Canal," Volumes I and II, Department of the Army, New Orleans District, Corps of Engineers, New Orleans, LA

US Army Corps of Engineers, 1990. "General Design Memorandum No. 20, General Design, Orleans Parish, Jefferson Parish, 17th St. Outfall Canal (Metairie Relief)," Volumes I and II, Department of the Army, New Orleans District, Corps of Engineers, New Orleans, LA

Work Projects Administration, 1943. <u>Foundations in New Orleans and Vicinity, Addendum</u>, Work Projects Administration, Louisiana Department of Public Works of the Mississippi River Deltas, major distributary channels are numbered, note Bayou Sauvage (No. 11) which extends across the New Orleans area and forms the Bayou Metairie/Gentilly Ridge (after Frazier, 1967). Morgan City, LA, located along axis of maximum Mississippi River entrenchment.

Appendix 8
Analysis of the London Avenue Canal I-Wall Breaches

Executive Summary

This report describes detailed assessments of the two breaches that occurred at the London Avenue Canal. The investigation of these breaches is an important step in IPET's system-wide investigation of floodwall and levee performance, and the findings illuminate a possible mechanism of failure that will be investigated system-wide for locations where sand underlies levees and floodwalls.

The breach on the London Avenue Canal near Mirabeau Avenue (the south breach) occurred at 6:00 AM to 7:00 AM on Monday, 29 August 2005. The breach on the London Avenue Canal near Robert E. Lee Boulevard (the north breach) occurred about an hour later. Field evidence, analyses, and physical model tests show that the breaches were due to the effects of high water pressures within the sand layer beneath the levee, and high water loads on the walls. The London Avenue Canal breaches had a key factor in common with the 17th Street Canal breach – formation of a gap between the wall and the levee fill on the canal side of the wall. At both the 17th Street Canal and the London Avenue Canal, formation of a gap allowed high water pressures to act on the wall below the surface of the levee, severely loading the wall. At the London Avenue Canal, an additional effect of the gap was that water flowed down through the gap into the underlying sand. High water pressures in the sand uplifted the marsh layer on the landside of the levee, resulting in concentrated flow and erosion, removing material and reducing support for the floodwall.

Analyses of the south breach showed that erosion is the most likely principal mode of failure, with sliding instability occurring after significant volumes of sand and marsh had been removed by erosion and piping. Without alteration of the south breach cross section by erosion and piping on the landside of the levee, the calculated factors of safety with respect to sliding instability are greater than 1.0, indicating that alteration of the cross section by erosion and piping probably played an essential role in the failure at this location.

Field observations at the north breach indicate that the canal-side levee crest remained intact after the breach, and a playhouse on the property adjacent to the breach was heaved upward

during the breach. The analyses presented in this report show that conditions for erosion and piping were present at the north breach, but the more likely cause of the failure was sliding instability. High uplift pressures likely resulted in a rupture through the marsh layer and the underlying thin layer of clay. At this location, however, the high pore pressures within the sand would reduce passive resistance sufficiently to result in sliding instability without significant alteration of the cross section.

Observations

Two I-wall failures resulting in breaches occurred at the London Avenue Canal during Hurricane Katrina, one on the east side of the canal at Mirabeau Avenue (the south breach), and the other on the west side of the canal at Robert E. Lee Boulevard (the north breach). At both locations the levees and I-walls were founded on a layer of marsh (peat) overlying sand. In addition, the I-wall on the east side, across the canal from the north breach, moved and tilted, but did not breach.

The south breach, shown in Figure 8-1, occurred about 6:00 AM to 7:00 AM on August 29th, when the water level in the canal was 7.1 ft to 8.2 ft NAVD88. The breach was narrower than the breach at 17th Street and the London Avenue north breach. A deep scour hole formed due to the inrush of water, and a large amount of eroded sand was deposited in the neighborhood inland of the breach. It appears that the breach was quite narrow when it formed, and subsequently widened to about 60 ft as wall panels adjacent to the initial breach were undermined by scour, and tilted into the scour hole.

The north breach, shown in Figure 8-2, occurred about 7:00 AM to 8:00 AM on August 29th, about an hour after the south breach, when the canal water level was 8.2 ft to 9.5 ft NAVD88. The breach was about 410 ft wide, approximately the same width as the breach at 17th Street. A playhouse on the property adjacent to the breach was heaved upward when the breach occurred, indicating upward movement of the ground inboard of the levee toe. The I-wall opposite the north breach (on the east side of the canal) moved and tilted significantly, presumably at about the same time as the breach occurred on the west side, but the east I-wall did not breach. A line of sinkholes was observed at the inland side of the distressed east I-wall, and a sand boil at the inboard embankment toe indicate that erosive seepage and piping had occurred beneath the levee.

Possible Modes of Failure

At both the south and north breach locations, it seems likely that underseepage and internal erosion caused or contributed to the failures.

It is not possible to establish the cause of the south breach with certainty based on the field observations made after the failure. The failed sections of the I-wall were not found, and large volumes of sand were moved by the inflow of water through the breach, covering the landscape. The failure might have resulted from underseepage erosion and piping, or from sliding instability

aggravated by seepage and uplift pressures. Analyses have been performed to examine both of these possibilities.

It has been reported that cold-rolled sheetpiles were used for the I-wall in the area of the south breach. Cold-rolled sheetpiles have lower interlock strengths than hot-rolled sheetpiles. Consequently, use of cold-rolled sheetpiles increases the likelihood that interlocks could have failed during driving, particularly because the sand in the south breach area was dense, and driving was hard. Interlock failure would result in gaps between adjacent sheets in the sheetpile wall, making it possible for water to seep through the wall as well as under the wall. Such through-flow would result in more severe seepage conditions than those reflected in the seepage analyses described here, and would make erosion and piping an even more likely mode of failure at the south breach.

Field observations at the north breach indicate that sliding instability was likely the primary mode of failure, with seepage and high pore pressures in the sand as a significant contributing factor. It seems likely that the failure and breach were the result of insufficient passive resistance to counteract the water pressure forces to which the wall was subjected. The passive resistance was likely reduced by the effects of water seeping through the foundation soils beneath the levee and the marsh layer inland, inducing uplift pressures and reducing shear strengths. Analyses have been performed to examine the likelihood of erosion and piping, and instability due to uplift and reduced shear resistance.

London South Breach Seepage and Stability Analyses

Erosion and Piping

Finite element analyses of seepage beneath the I-wall were performed using the computer program SLIDE[1]. The characteristics of the cross section analyzed are shown in Figure 8-3. The relevant materials are the sand at the base of the section, the overlying marsh (peat) layer, and the clayey levee fill. The permeability of the sand, based on field pumping tests, was $1.5x10^{-2}$ cm/sec. The permeability of the marsh layer was estimated as $1x10^{-5}$ cm/sec, and the permeability of the levee fill and the Bay Sound clay was estimated as $1x10^{-6}$ cm/sec. Thorough analyses of transient and steady seepage, described in a separate report, indicated that (a) steady seepage through the sand was established quickly, and (b) the pore pressures within the sand and the uplift pressures on the base of the marsh layer are not affected by the permeability values assigned to the marsh layer and the levee fill, provided that those materials are at least two orders of magnitude less permeable than the sand. The values of permeability of the marsh layer and the levee fill used in the seepage analyses described here were selected in accordance with these findings, and are considered to be reasonable estimates of the permeabilities of these materials.

The hydraulic boundary conditions used in these analyses are shown in Figure 8-3. The canal water level was either 7.1 ft or 8.2 ft NAVD88, a range consistent with the estimated canal water levels at the time of failure. A constant-head boundary condition was imposed at the location of the drain beneath Warrington Drive. This head value was either -8.4 ft (the normal ground water

---

[1] Available from Rocscience Inc., 31 Balsam Avenue, Toronto, Ontario, Canada M4E 3B5

level with pumps operating), or -5.1 ft NAVD88 (a higher level equal to the ground surface elevation, which might have occurred with pumps not operating). Reports indicate that the pumps stopped operating when the wall failed, severing the power line. In all, four different seepage cases were analyzed, as shown in Table 8-1.

Based on the study of the 17th Street Canal breach, it seems likely that a crack would form between the I-wall and the levee fill on the canal side of the wall. The type of crack assumed to have formed behind the 17th Street Canal I-wall, shown in Figure 8-4, does not seem feasible for the London Avenue foundation conditions, where the I-wall is driven into sand, because cohesionless sand would be unable to support a crack. A more likely condition for a wall driven into sand is shown in Figure 8-5. This "half-cracked" condition involves a crack through the levee fill and the marsh layer, down to the top of the sand. Water would fill this crack, loading the wall and introducing the canal head at the top of the sand. The part of the wall embedded in the sand would be loaded by water pressures that are somewhat lower than hydrostatic pressures, plus active earth pressures, as shown in Figure 8-5. The lower-than-hydrostatic water pressures were determined from the finite element seepage analyses. All of the seepage and stability analyses were performed based on this half-cracked condition.

Six-node triangular elements were used for the seepage analyses. The finite element mesh is shown in Figure 8-6. Computed total head contours for Case 1 are shown in Figure 8-7. It can be seen that the flow through the sand is predominantly horizontal, and that the total head on the landward side of the levee is above the ground surface, which is at elevation –5.1 ft. The head contours for the other three cases shown in Table 8-1 had similar shapes, although the values varied somewhat depending on the canal water level and the Warrington Drive water level.

Computed pore pressures, or uplift pressures, at the base of the marsh layer are shown in Figure 8-8 for the four cases analyzed, together with the total overburden pressure at the base of the marsh layer. It can be seen that in all four cases the computed pore pressures exceed the total overburden pressure at the base of the marsh layer. This result indicates that the marsh layer would be heaved off the underlying sand by the high uplift water pressures. A likely result of this heave would be rupture of the marsh layer at one or more weak points, and upward flow of water through the rupture in the marsh material. This flow would relieve the high water pressure locally, and create a new hydraulic boundary condition at the point of rupture.

Additional seepage analyses were performed to determine if the hydraulic gradients within the sand after rupture of the marsh layer would be large enough to cause erosion of the sand and begin a piping failure. The seepage boundary conditions used in theses analyses are shown in Figure 8-9, where a rupture extends upward through the marsh layer, from the top of the sand to the ground surface. The hydraulic gradients computed in these analyses were found to depend on the assumed width of the rupture in the marsh layer. While it seems clear that the marsh layer would rupture when the uplift pressures exceeded the overburden pressures, the width of the rupture would depend on factors that cannot be evaluated, and it is thus necessary to assign a width to the rupture zone based on judgment. Even so, we believe that the analytical results that follow reflect the essential aspects of the situation. The results support the view that the London south breach developed as a result of erosion and piping.

The narrower the assumed rupture zone, the higher the computed hydraulic gradient at the top of the sand below the rupture, because flow converges toward the rupture, and the flow velocities increase near the rupture. This converging flow is shown by the total head contours in the sand near the rupture in Figure 8-10. A rupture zone width equal to 1.6 ft was used in the analyses, based on a judgment of what seemed a reasonable and possible rupture zone size. Doubling the width of the rupture zone was found to reduce the computed hydraulic gradient by 23%, and cutting the width in half increased the hydraulic gradient by 33%. In the real case, flow would converge in three dimensions rather than two dimensions, as represented in these two-dimensional seepage analyses. It therefore seems likely that the actual hydraulic gradients would be higher than the values discussed in the following sections, but the magnitude of this three-dimensional effect cannot be quantified.

The changed hydraulic boundary conditions caused by the rupture through the marsh layer were computed by imposing a head at the base of the rupture that was equal to the elevation of the ground surface, simulating a condition where the water level within the ruptured zone rises to the ground surface. Values of vertical hydraulic gradient at the top of the sand for this condition are shown in Table 8-2 for the four cases analyzed. It can be seen that they range from 1.03 to 1.24.

The value of hydraulic gradient that would cause erosion of the sand is

$$i_{critical} = \frac{\gamma_b}{\gamma_w} = \frac{\gamma_s - \gamma_w}{\gamma_w}$$

where $i_{critical}$ = hydraulic gradient that would cause erosion of the sand, γ_b = buoyant unit weight of sand, γ_w = unit weight of water, and γ_s = saturated unit weight of sand. With γ_s for the sand assumed to be 120 pcf, the critical hydraulic gradient is 0.92. Thus the values of hydraulic gradient for all four cases analyzed would be large enough to cause erosion and to begin piping, as shown by the values of $F_{erosion}$ listed in Table 8-2.

Considering the variation in factor of safety caused by the uncertain landside water level, the probability of erosion was calculated as shown in Table 8-3. A simple method based on the Taylor series[2] was used for these calculations. It can be seen that the probability of erosion approaches 100% for both canal water levels, indicating a high likelihood that erosion occurred and that erosion was the cause of the failure, or an exacerbating factor in the failure.

Considering that three-dimensional concentration of flow would result in even larger hydraulic gradients, it appears that erosion and piping of the sand would be likely at the south breach. With high hydraulic gradients, backward erosion could occur rapidly, extending back to the I-wall, and leading to a catastrophic failure of the type that was observed. The analyses described here consider only the beginning of this process. Once erosion of the sand into the rupture in the marsh layer began, the situation would deteriorate quickly as seepage converged to

---

[2] Wolff, T. F. (1994). "Evaluating the reliability of existing levees." Report, Research Project: Reliability of Existing Levees, prepared for U.S. Army Engineer Waterways Experiment Station Geotechnical Laboratory, Vicksburg, Miss.

the zone of erosion, and the rate of erosion increased. Eventually, after enough sand, marsh and possibly levee fill had been eroded away, an unstable condition would develop, with the passive resistance of the materials landward of the wall becoming too small to resist the forces of the water and earth pressures pushing from the canal side of the wall.

Slope Instability

While this erosion and piping failure mechanism appears plausible based on the results of the analyses described above, it is of interest also to examine the possibility that the failure could have occurred by sliding, through a slope instability failure mechanism. To examine this possibility, slope stability analyses were performed using the computer program SLIDE[1].

The stability analyses were performed for the cross section shown in Figures 8-11, 8-12, 8-13, and 8-14. This is the same cross section as used in the seepage analyses, and the same canal water levels and landside water levels were used.

Standard Penetration Tests performed in the breach area before the breach showed that the sand had Standard Penetration Test blow counts (N_{SPT}) greater than 50, which would correspond to values of ϕ' in the range of 40 degrees to 46 degrees. Cone penetration tests performed after the breach showed high tip resistance in the sand adjacent to the breach, which correspond to similar values of ϕ'. In order not to overestimate the strength of the sand, a value of $\phi' = 40$ degrees was used in the stability analyses.

The marsh was treated as undrained, with $s_u = 300$ psf, and $\phi_u = 0$, based on the available test results. A value of $s_u = 300$ psf is considered appropriate for the areas beneath the canal-side levee slope and beyond the levee toe, where the slip circles pass through the marsh. The unit weight of the marsh was assumed to be 80 pcf.

The levee fill was also treated as undrained, with $s_u = 900$ psf, and $\phi_u = 0$. The slip circles do not intersect the levee fill, however, and the levee strength therefore has no influence on the calculated values of factor of safety. The unit weight of the levee fill was assumed to be 109 pcf.

Analyses were performed with canal water levels at 7.1 ft and 8.2 ft NAVD88, using pore pressures in the sand from the finite element seepage analyses without a rupture through the marsh layer. The non-ruptured seepage analyses were used to determine pore pressures because the rupture is conceived as a feature of very limited size, not appropriate for inclusion in a two-dimensional cross section. At the bases of the slices where the pore pressures exceeded the overburden pressures near the top of the sand on the inboard side, zero shear strength was assigned for the sand.

As discussed earlier, it was assumed in all analyses that deflection of the wall toward the land side would result in formation of a crack through the levee fill and the marsh in back of the wall, down to the top of the sand. It was assumed that the crack would not extend into the sand, because the sand is cohesionless, and would be expected to slump and fill any gap. This "half-cracked" condition was used in all stability analyses. It can be seen in Figures 8-11, 8-12, 8-13, and 8-14 that the slip circles extend to the bottom of the sheetpile wall furthest from the canal.

The factors of safety calculated in these analyses are shown in Figures 8-11 through 8-14, and in Table 8-4. For the canal water levels estimated at the time of the breach (7.1 ft to 8.2 ft) the calculated factors of safety range from a low value of F = 1.19 to a high value of F = 1.56. Thus, with this interpretation of the available data, and consistent assumptions for the seepage and stability analyses, a mechanism of failure involving erosion and piping is plausible at the south breach, but a slope stability failure mechanism is not.

An analysis was performed, with the landside water level at -8.4 ft, to determine the canal water level corresponding to a calculated factor of safety equal to 1.00. As shown in Figure 8-15, a canal water level equal to 9.7 ft would be required for a factor of safety equal to 1.00. This is 1.5 ft higher than the highest estimated water level at the time the breach occurred, indicating that instability without removal of material by erosion and piping is unlikely at the south breach.

Additional stability analyses were performed, varying the friction angle of the sand and the strength of the marsh layer, to compute the probability of slope instability. The results of these cases are shown in Table 8-5. The Taylor series approach[2] was used to compute the standard deviation of the factor of safety and the probability of failure. The most likely value of factor of safety was taken as the average of the values for the high and low inland water levels. The probability of instability was estimated assuming a log-normal distribution of factor of safety, with the results shown in Table 8-5. It can be seen that the estimated probability of instability is 1% for the lower canal water level, and 10% for the higher canal water level. Thus, while there is a small probability that failure might have occurred due to instability without erosion and piping, this mode of failure is much less likely than failure by erosion and piping.

London North Breach Seepage and Stability Analyses

The possibilities of failure due to erosion and piping, and due to instability, were also examined for the London Avenue north breach. The differences between the London south breach analyses and the London north breach analyses were:

1. The seepage boundary conditions were different. The canal water level at the time of the north breach was 8.2 ft to 9.5 ft, higher than at the south breach because the north breach occurred later. The inland seepage boundary condition ranged from -8.4 ft to -3.9 ft because Pratt Drive is at a slightly higher elevation than Warrington Drive. Four cases were analyzed, using the seepage boundary conditions shown in Figure 8-16, and summarized Table 8-6. An additional analysis was performed to determine the canal water level required for a calculated factor of safety equal to 1.00.

2. The cross sections are somewhat different. On the inland side of the wall at the north breach, there is a thin layer of lacustrine clay between the marsh layer and the sand.

3. The sand is less dense in the north breach area. Standard Penetration Test blow counts (N_{SPT}) in this area range from 2 to 14, with an average of about 10. This range of values of N_{SPT} corresponds to values of ϕ' in the range of 30 degrees to 34 degrees. Cone penetration tests performed after the breach, in the area adjacent to the breach, showed tip

resistances that correspond to about the same values of φ'. A value of φ' = 32 degrees was used in the stability analyses for the north breach area.

Erosion and Piping

Six-node triangular elements were used for the seepage analyses, as for the south breach. The finite element mesh for the north breach is shown in Figure 8-17. The same values of permeability were used as for the south breach. The lacustrine clay between the sand and the marsh layer was assumed to have a permeability of 1×10^{-6} cm/sec.

Computed total head contours for Case 1 are shown in Figure 8-18. As for the south breach, the flow through the sand is predominantly horizontal, and the total head on the landward side of the levee is above the ground surface, which is at elevation – 3.9 ft. The head contours for the other three cases that were analyzed had similar shapes, although the values varied somewhat depending on the canal water level and the Pratt Drive water level.

Water pressures at the base of the marsh layer for the north breach area are shown in Figure 8-19. As in the case of the south breach area, the uplift water pressures exceed the overburden pressures due to the weight of the marsh layer at the landside of the levee, and it would be expected that the marsh layer would be heaved upward and would rupture.

Additional seepage analyses were performed with revised boundary conditions, as was done in the south breach analyses, using the conditions shown in Figure 8-20. A rupture 1.6 ft wide, extending through the marsh layer and the lacustrine clay layer was assumed, and a hydraulic boundary condition with the water level at the ground surface was applied in the area of the rupture. Total head contours for the area around the assumed rupture through the lacustrine clay and peat are shown in Figure 8-21. The hydraulic gradients calculated for these conditions are shown in Table 8-7.

With γ_s for the sand equal to 115 pcf (5 pcf less than at the south breach where the sand was more dense), the critical hydraulic gradient is 0.84. The values of hydraulic gradient all four cases analyzed would be large enough to cause erosion and begin piping of the sand. Thus erosion and piping appears to be a plausible mode of failure for the London north breach, as well as the south breach.

Probabilities of erosion for the high and low canal water levels were calculated using the same procedure as for the south breach[2], with the results shown in Table 8-8. It can be seen that the probability of erosion exceeds 90% for both the low and the high canal water levels, and approaches 100% for the higher level. These probabilities are slightly smaller than for the south breach, where the probability of erosion approached 100% for both high and low canal water levels.

Slope Instability

While erosion and piping appears possible based on the results of the analyses described above, it is also of interest to examine the factor of safety against slope instability. To examine the possibility that the failure mechanism involved sliding, slope stability analyses were performed using the same procedures as used for the south breach. The stability analyses were performed for the cross section shown in Figures 8-22, 8-23, 8-24, and 8-25. This is the same cross section as used in the seepage analyses.

Analyses were performed for four cases, using the canal water levels and inland water levels shown in Table 8-6, and pore pressures in the sand from the same finite element seepage analyses used to compute the uplift pressures shown in Figure 8-19. As noted previously, a value of $\phi' = 32$ degrees was used for the sand. The strengths and unit weights of the marsh and the levee fill were the same as used in the south breach stability analyses described previously. The undrained strength of the lacustrine clay was assumed to be equal to 42 psf. The strength of this thin layer has a very small influence on the calculated factors of safety. At the bases of slices where the pore pressures exceeded the overburden pressures at the top of the sand on the inland side, zero shear strength was assigned for the sand.

The same half-cracked condition was used in these analyses as was used for stability analyses at the south breach. It can be seen in Figures 8-22, 8-23, 8-24, and 8-25 that the slip circles extend to the bottom of the sheetpiles. Full hydrostatic water pressure force acts on the sheetpile down to the top of the sand. From the top of the sand to the bottom of the sheetpile, the sheetpile is acted on by water pressures determined from the seepage analyses and active earth pressures.

The factors of safety for Cases 1 through 4 are shown in Figures 8-22 through 8-25, and are listed in Table 8-9. They range from a low value of F = 0.67 to a high value of F = 0.99. Thus, because the sand is considerably less dense in the north breach area, and would have a smaller friction angle, a mechanism of failure involving slope instability is plausible.

An additional analysis was performed, with the landside water level at -8.4 ft, to determine the canal water level corresponding to a calculated factor of safety equal to 1.00. As shown in Figure 8-26 and Table 8-9, a canal water level equal to 8.1 ft corresponds to a factor of safety equal to 1.00. This is very nearly equal to the lowest estimated water level at the time the breach occurred, indicating that instability is a highly likely mode of failure at the north breach.

Further analyses were performed, varying the friction angle of the sand and the strength of the marsh layer, to compute the probability of slope instability, using the Taylor series method[2]. The results of these cases are shown in Table 8-10. The most likely value of factor of safety was taken as the average of the values for the high and low inland water levels. The results of these calculations are shown in Table 8-10. It can be seen that the estimated probability of instability is 70% for the lower canal water level, and 97% for the higher canal water level. Thus, there is a very significant probability that instability could have occurred without erosion and piping. However, given the very high probability of erosion, it seems likely that both mechanisms were involved in the failure.

Design analyses

The design was divided into five reaches, designated as Reaches I, II, III, IV, and V. The south and north breaches both occurred in Reach III, which encompassed Stations 37+00 to 120+00. Seepage analyses described in paragraphs 44, 45, 47, and 52 of the geotechnical investigation report[3] were performed to evaluate the potential for erosion and piping in areas where the London Avenue Canal levee and I-wall were underlain by sand, as at the south and north breach locations. The analyses were performed using flow nets, Lane's Weighted Creep Ratio method[4], and Harr's Method.[5]

Flow net analyses were performed for the levees in Reach IV and Reach V, based on levee base width of 80 ft, 60 ft depth of pervious foundation soil, and canal water level at 10.2 ft NAVD88. The calculated values of exit gradient were found to be about 0.25. These were judged to provide a factor of safety of approximately 4.0 against erosion and piping. This factor of safety was considered acceptable, and not to require measures to cut off underseepage.

Lane's Weighted Creep Ratio values were computed for the I-walls in Reaches I, II, III, IV, and V. The results indicated that the calculated creep ratios were not acceptable for parts of Reach V where the levee and I-wall would be underlain by sand, according to Lane's empirical criteria. The required cutoff depths within this reach were subsequently evaluated using Harr's Method, and were found to require sheetpile wall penetration to elevation -14.4 ft NAVD88.

None of the seepage analyses considered the possibility that a crack might develop due to water pressures on the I-wall, resulting in flow down the canal side of the wall and into the foundation at that location.

Paragraph 45 of the design report[3] discussed the likelihood that the canal bottom would be covered with silt, which would impede seepage into the foundation in areas where the foundation soils were permeable sand. The relatively short duration of the design high water was also discussed. Based on data from field piezometer studies, it was judged that head levels on the land side of the levee would not be above the ground surface. Paragraph 46 of the report recommended that piezometers be installed and monitored periodically to provide a basis for estimating piezometric levels during floods more accurately, and for evaluating the need for landside pressure relief measures. Paragraph 47 of the report discussed the possible consequences of dredging the canal, exposing more pervious materials in the canal bottom, which could result in more adverse seepage conditions, and requested notification if dredging was planned.

---

[3] Geotechnical Investigation, Orleans Levee District, London Avenue Outfall Canal, OLB Project No. 2049-0269, New Orleans, Louisiana, Volume 1, for The Board of Levee Commissioners of the Orleans Levee District, New Orleans, Louisiana, by Eustis Engineering Company, Metairie, Louisiana, 4 March, 1986, contained in GDM86, Volume 1, Part 1, U. S. Army Corps of Engineers, New Orleans District.

[4] Lane, E. W. (1935), "Security from under-seepage – masonry dams on earth foundations," ASCE Transactions, Vol. 100, pp. 1235-1251.

[5] Harr, M. E. (1966), *Groundwater and Seepage*, McGraw-Hill, New York, 381 pp.

Stability analyses performed for Reach III did not show the failure surface entering the sand layer. All of the analyses were performed using slip surfaces within the clay layer beneath the levee and the I-wall. A minimum factor of safety of 1.30 computed by the Method of Planes[6] was required. Required depths of penetration and bending moment capacity for the I-wall were determined by cantilever analyses, as described in paragraphs 48 and 49 of the report[3].

Summary

The analyses described in the preceding sections indicate a strong likelihood that high uplift pressure on the base of the levee and the marsh layer was a key factor in the failures at both the south and the north breaches on the London Avenue Canal. At both locations these high uplift pressures probably resulted in development of a rupture through the marsh layer, and hydraulic gradients large enough to cause erosion of the sand.

At the south breach area this erosion may have been the principal mode of failure, with gross instability occurring after considerable volumes of sand, marsh and levee fill had been removed by erosion and piping. Without alteration of the south breach cross section by erosion and piping, the calculated factors of safety with respect to instability are greater than 1.0, indicating that alteration of the profile by erosion and piping probably played an essential role in the failure at this location where the sand was dense, and the sand friction angle would have been high. An additional important factor is that cold-rolled sheetpiles, with weak interlocks, were reported to have been used at this location. Loss of interlocks during driving in the dense sand would have resulted in even more severe seepage conditions than are reflected in the analyses described here, which modeled the sheetpiles as an intact seepage barrier. The south breach failure appears to have been caused principally by erosion and piping in a localized area focused in a relatively small zone where hydraulic gradients were increased by a rupture through the marsh layer overlying the sand, or by a gap in the sheetpiles due to interlock failure during driving, or both. The conclusion that the failure probably started in a small zone of intense seepage is consistent with the narrow breach that eventually developed.

At the north breach area the probability of erosion and piping is slightly less than at the south breach, although still very high. The probability of instability is higher than the probability of erosion, due to the fact that the sand was loose, and would have had a low friction angle. High uplift pressures likely resulted in a rupture through the marsh layer and the underlying thick layer of lacustrine clay. At this location, however, the high pore pressures within the sand would be sufficient to cause instability without significant alteration of the cross section by erosion. The failure at the north affected a much wider zone than the failure at the south, indicating that intense localized erosion and piping did not play a key role in the failure at the north breach. It appears that high uplift pressures and lower friction angle of the less-dense sand were key elements in the failure at the north breach.

---

[6] A study of the Method of Planes, undertaken by IPET at the request of the New Orleans District Task Force Guardian, indicates that the Method of Planes gives lower factors of safety than more accurate methods of analysis, such as Spencer's method. The magnitude of the difference between the two varies from case to case.

Table 8-1
Hydraulic Boundary Conditions for Seepage Analyses –
London Avenue South Breach

Case	Canal water level – CWL (NAVD88)	Warrington Drive water level – LWL (NAVD88)
1	7.1 ft	-8.4 ft
2	8.2 ft	-8.4 ft
3	7.1 ft	-5.1 ft
4	8.2 ft	-5.1 ft

Table 8-2
Calculated Hydraulic Gradients and Factors of Safety Against
Erosion – London Avenue South Breach

Case	CWL	LWL	i = vertical hydraulic gradient	$F_{ersosion} = i_{crit}/i$
1	7.1 ft	-8.4 ft	1.03	0.89
2	8.2 ft	-8.4 ft	1.14	0.81
3	7.1 ft	-5.1 ft	1.13	0.81
4	8.2 ft	-5.1 ft	1.24	0.74
Note: with γ_{sat} = 120 pcf, i_{crit} = 0.92				

Table 8-3
Calculated Probabilities of Erosion – London Avenue South Breach

Case	CWL	LWL	$F_{erosion}$	ΔF	σ_F	F_{MLV}	COV_F	$p_{erosion}$
1	7.1 ft	-8.4 ft	0.89	0.08	0.04	0.85	5%	> 99%
3	7.1 ft	-5.1 ft	0.81					
2	8.2 ft	-8.4 ft	0.81	0.07	0.04	0.78	4%	> 99%
4	8.2 ft	-5.1 ft	0.74					

Notes:
  F = change in F due to variation in parameter values
  $_F$ = standard deviation of factor of safety for the variations considered
F_{MLV} = most likely value of factor of safety
COV_F = coefficient of variation of factor of safety
$p_{erosion}$ = probability of erosion

Table 8-4
Factor of Safety Against Instability – London South Breach

Case	CWL	LWL	$F_{stability}$
1	7.1 ft	-8.4 ft	1.56
2	8.2 ft	-8.4 ft	1.29
3	7.1 ft	-5.1 ft	1.44
4	8.2 ft	-5.1 ft	1.19
5	9.7 ft	-8.4 ft	1.00

Table 8-5
Probability of Instability – London South Breach

Case	CWL (ft)	LWL (ft)	ϕ' (deg)	S_u (psf)	F	ΔF	σ_F	F_{MLV}	COV_F	$p_{instability}$
1	7.1	-8.4	40	300	1.56	0.12	0.25	1.50	17%	1%
3	7.1	-5.1	40	300	1.44					
1a	7.1	-8.4	44	300	1.78	0.40				
1b	7.1	-8.4	36	300	1.38					
1c	7.1	-8.4	40	200	1.42	0.28				
1d	7.1	-8.4	40	400	1.70					
2	8.2	-8.4	40	300	1.29	0.10	0.20	1.24	16%	10%
4	8.2	-5.1	40	300	1.19					
2a	8.2	-8.4	44	300	1.47	0.30				
2b	8.2	-8.4	36	300	1.17					
2c	8.2	-8.4	40	200	1.17	0.24				
2d	8.2	-8.4	40	400	1.41					

Notes:
ΔF = change in F due to variation in parameters for the two conditions
σ_F = standard deviation of factor of safety for the variations considered
F_{MLV} = most likely value of factor of safety
COV_F = coefficient of variation of factor of safety
$p_{instability}$ = probability of instability

Table 8-6
Hydraulic Boundary Conditions for Seepage Analyses – London Avenue North Breach

Case	Canal water level – (CWL) NAVD88	Pratt Drive water level – (LWL) NAVD88
1	8.2 ft	-8.4 ft
2	9.5 ft	-8.4 ft
3	8.2 ft	-3.9 ft
4	9.5 ft	-3.9 ft

Table 8-7
Calculated Hydraulic Gradients and Factors of Safety Against Erosion – London Avenue North Breach

Case	CWL	LWL	i = vertical hydraulic gradient	$F_{ersosion} = i_{crit}/i$
1	8.2 ft	-8.4 ft	0.95	0.88
2	9.5 ft	-8.4 ft	1.08	0.78
3	8.2 ft	-3.9 ft	1.12	0.75
4	9.5 ft	-3.9 ft	1.25	0.67

Note: with γ_{sat} = 115 pcf, i_{crit} = 0.84

Table 8-8
Calculated Probabilities of Erosion – London Avenue North Breach

Case	CWL	LWL	F$_{erosion}$	ΔF	σ$_F$	F$_{MLV}$	COV$_F$	p$_{erosion}$
1	8.2ft	-8.4 ft	0.88	0.13	0.07	0.82	16%	91%
3	8.2 ft	-3.9 ft	0.75					
2	9.5 ft	-8.4 ft	0.78	0.11	0.06	0.73	15%	99%
4	9.5 ft	-3.9 ft	0.67					

Notes:
ΔF = change in F due to variation in parameters for the two conditions
σ$_F$ = standard deviation of factor of safety for the variations considered
F$_{MLV}$ = most likely value of factor of safety
COV$_F$ = coefficient of variation of factor of safety
p$_{erosion}$ = probability of erosion

Table 8-9
Factor of Safety Against Instability – London North Breach

Case	CWL	LWL	F$_{stability}$
1	8.2 ft	-8.4 ft	0.99
2	9.5 ft	-8.4 ft	0.77
3	8.2 ft	-3.9 ft	0.84
4	9.5 ft	-3.9 ft	0.67
5	8.1 ft	-8.4 ft	1.00

Table 8-10
Probability of Instability – North Breach

Case	CWL (ft)	LWL (ft)	φ' (deg)	S$_u$ (psf)	F	ΔF	σ$_F$	F$_{MLV}$	C$_{OVF}$	p$_{instability}$
1	8.2	-8.4	32	300	0.99	0.15	0.17	0.92	19%	70%
3	8.2	-3.9	32	300	0.84					
1a	8.2	-8.4	36	300	1.11	0.24				
1b	8.2	-8.4	28	300	0.87					
1c	8.2	-8.4	32	200	0.89	0.20				
1d	8.2	-8.4	32	400	1.09					
2	9.5	-8.4	32	300	0.77	0.10	0.14	0.72	19%	97%
4	9.5	-3.9	32	300	0.67					
2a	9.5	-8.4	36	300	0.87	0.18				
2b	9.5	-8.4	28	300	0.69					
2c	9.5	-8.4	32	200	0.68	0.18				
2d	9.5	-8.4	32	400	0.86					

Notes:
ΔF = change in F due to variation in parameters
σ$_F$ = standard deviation of factor of safety for the variations considered
F$_{MLV}$ = most likely value of factor of safety
COV$_F$ = coefficient of variation of factor of safety
p$_{instability}$ = probability of instability

Figure 8-1. The South Breach at the London Avenue Canal Occurred at 6:00 AM to 7:00 AM on August 29, 2005. The breach, on the east side of the canal, was approximately 60 feet wide.

Figure 8-2. The North Breach at the London Avenue Canal Occurred at 7:00 AM to 8:00 AM on August 29, 2005. The breach, on the west side of the canal, is approximately 410 feet wide.
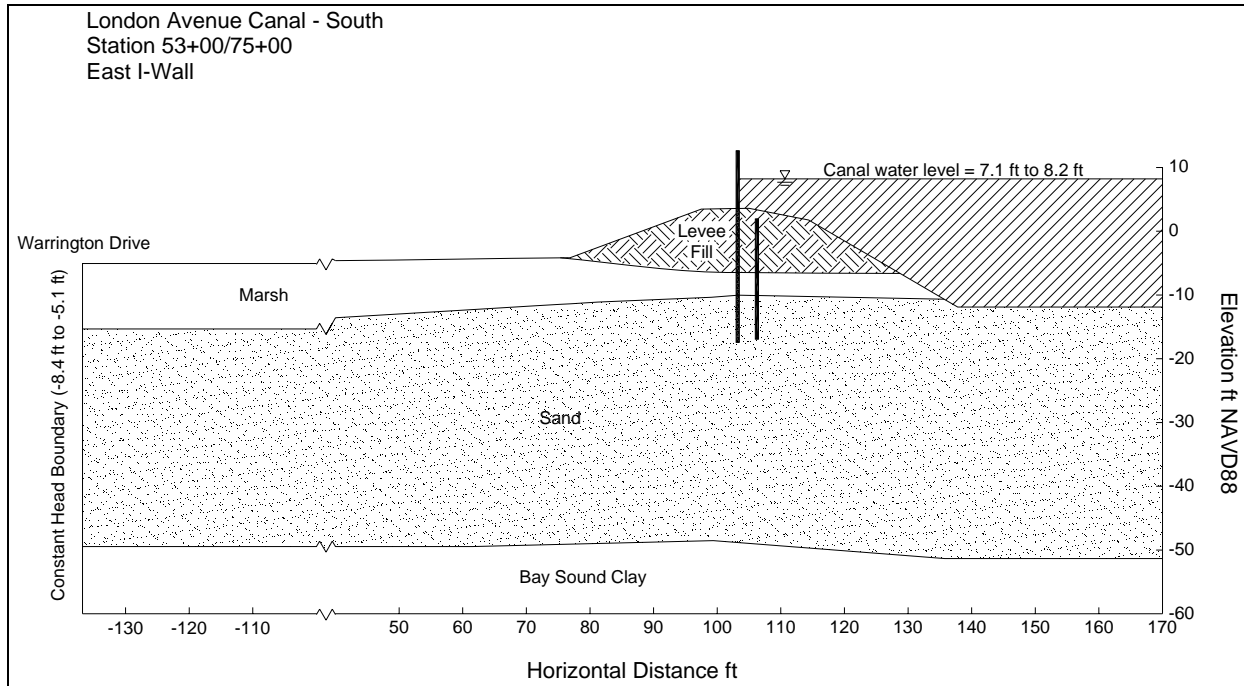
Figure 8-3. Schematic Cross Section at London South Breach, with Seepage Boundary Conditions

This is a preliminary report subject to revision; it does not contain final conclusions of the United States Army Corps of Engineers.
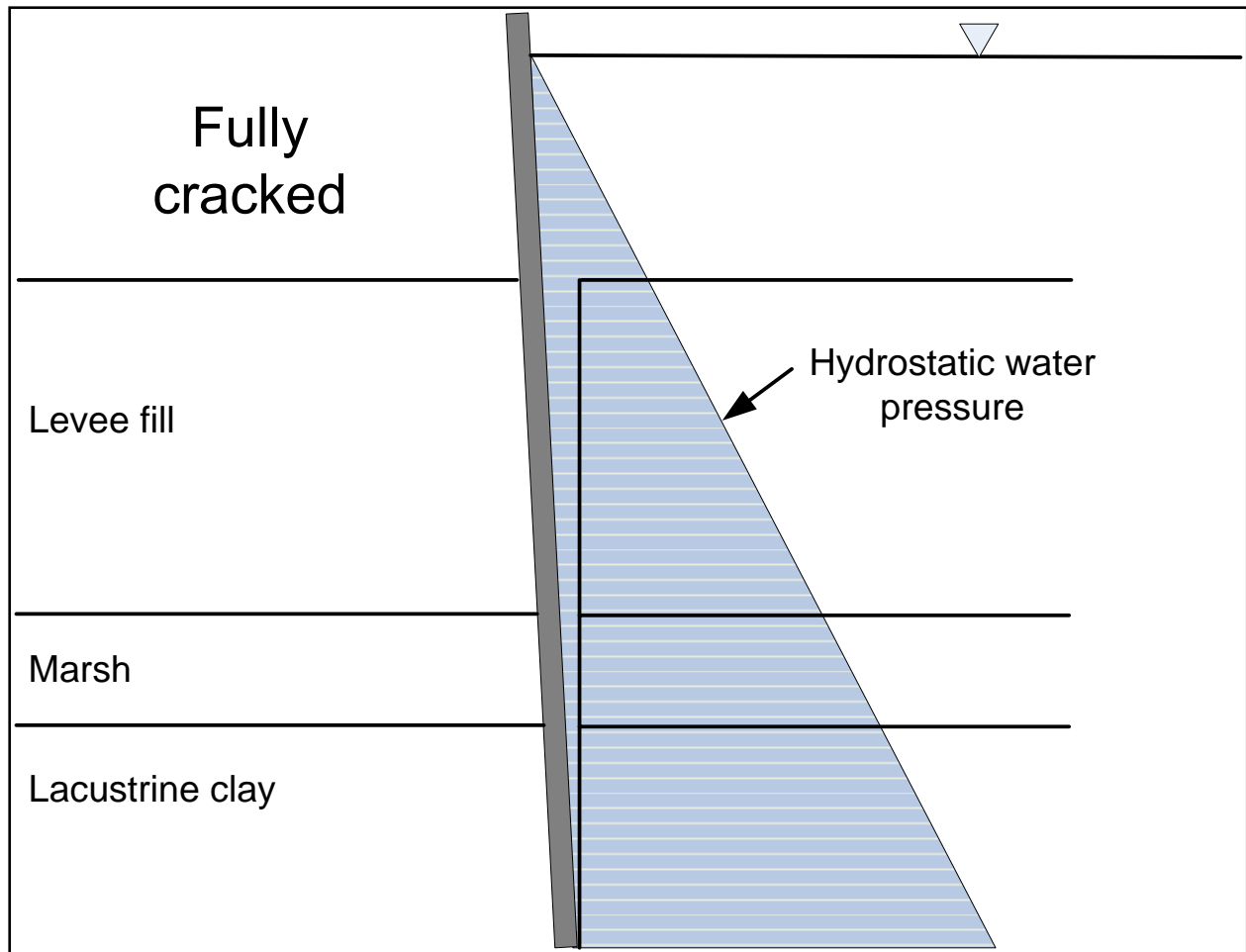
Figure 8-4. Schematic of Crack Used in 17th Street Canal Stability Analyses
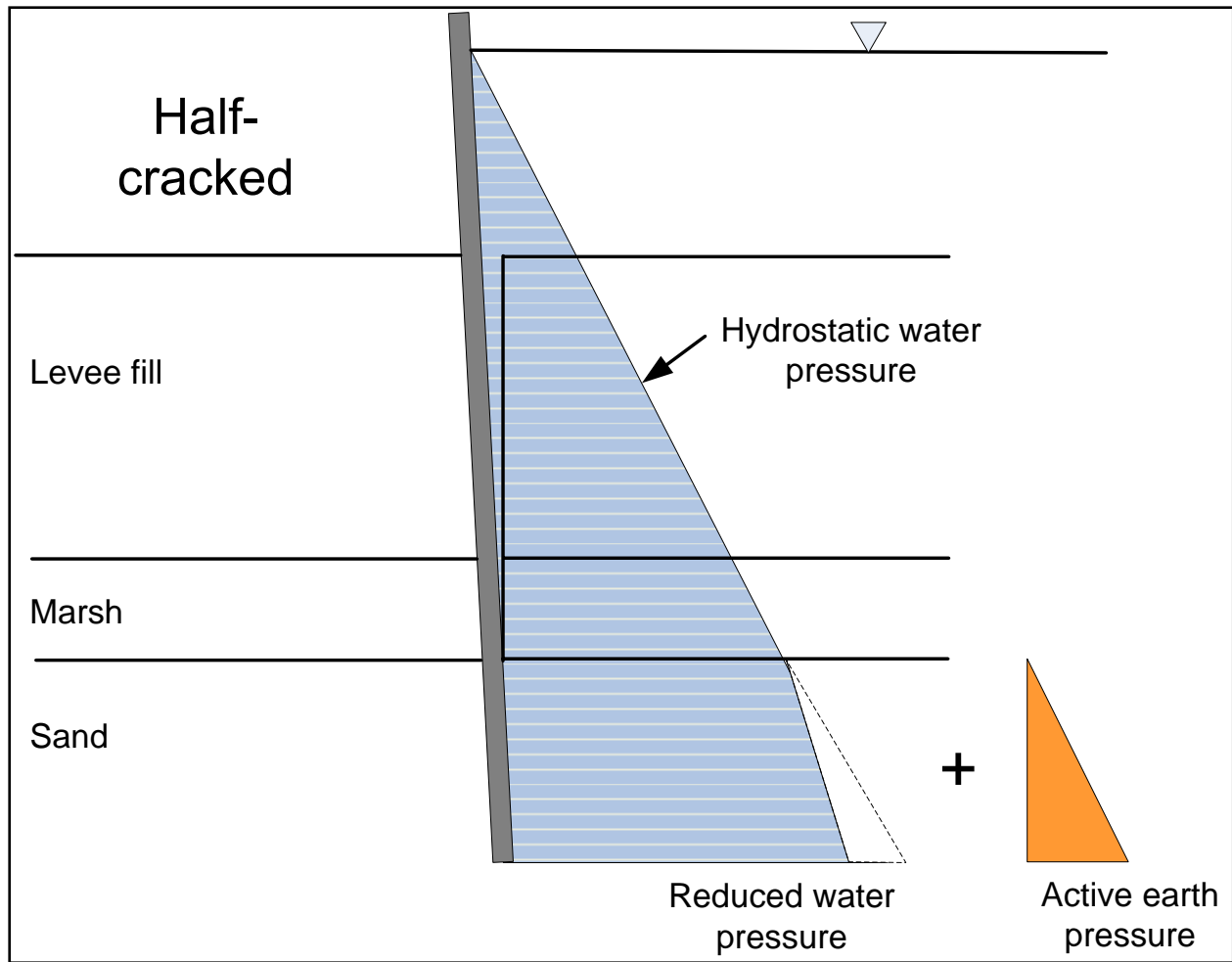
Figure 8-5. Schematic of Crack Used in London Avenue Canal Stability Analyses
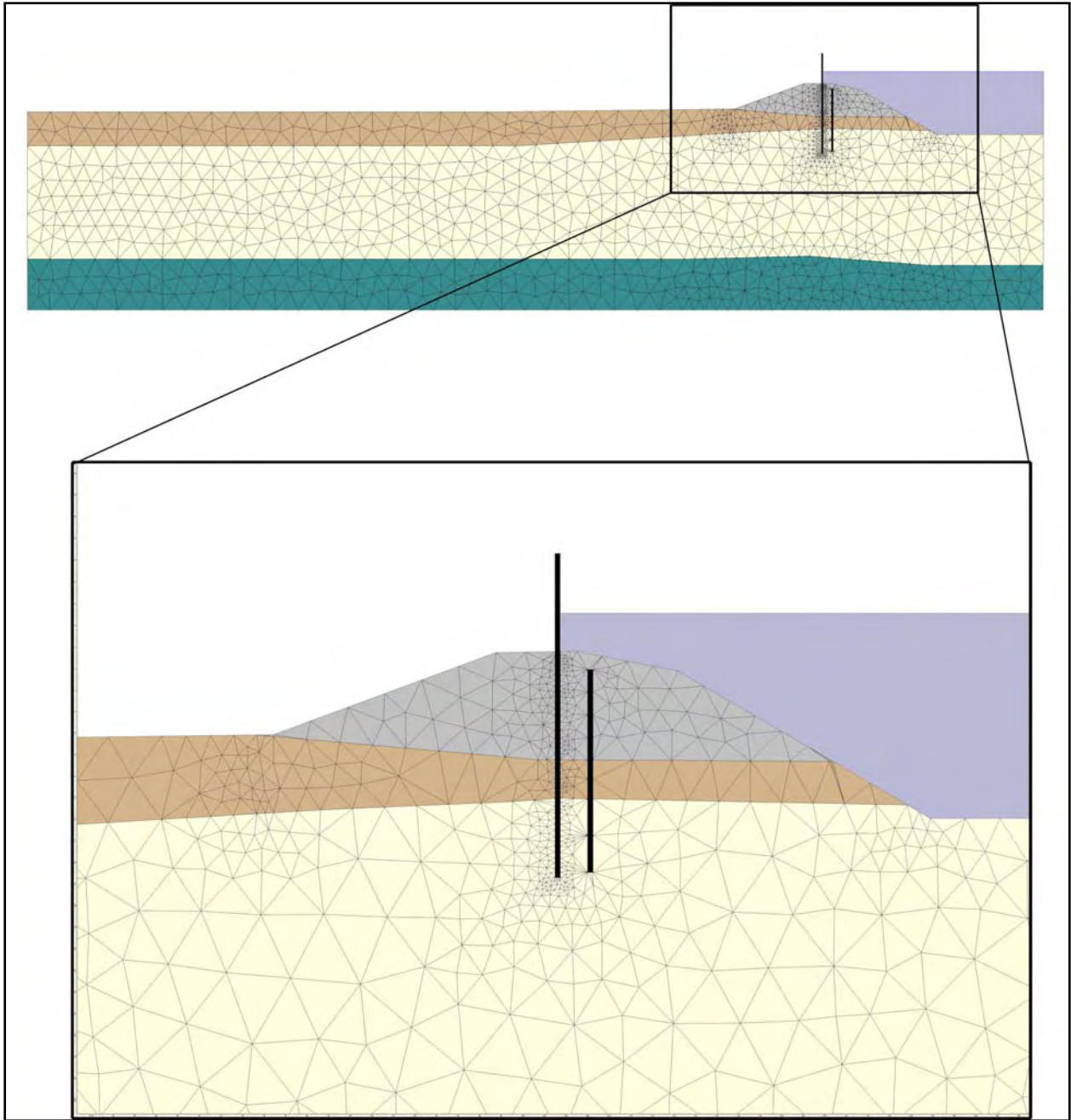
Figure 8-6. Finite Element Mesh Used for Seepage Analysis for London Avenue South Breach
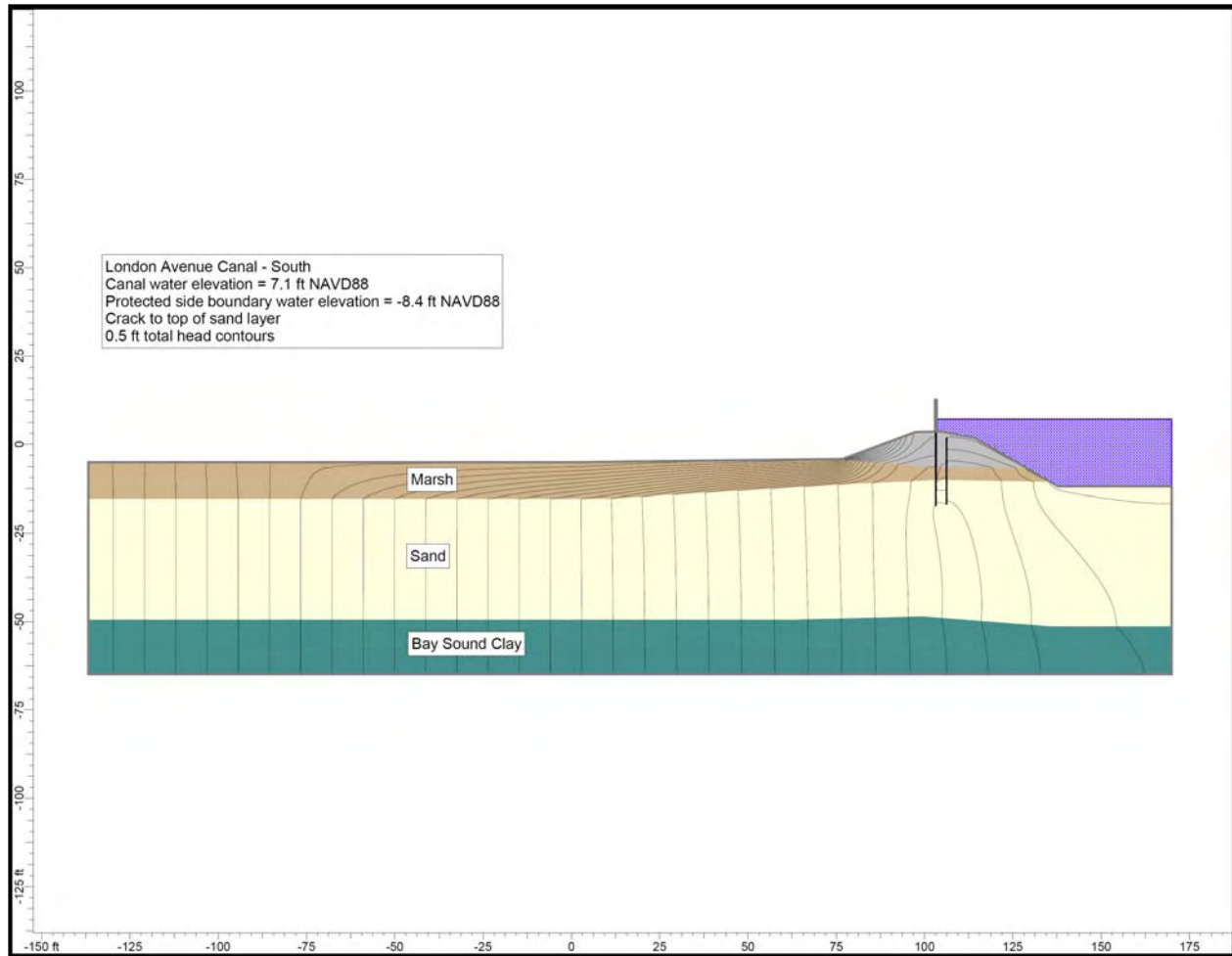
Figure 8-7. Total Head Contours Calculated for Seepage Analysis of London South Breach (Case 1)
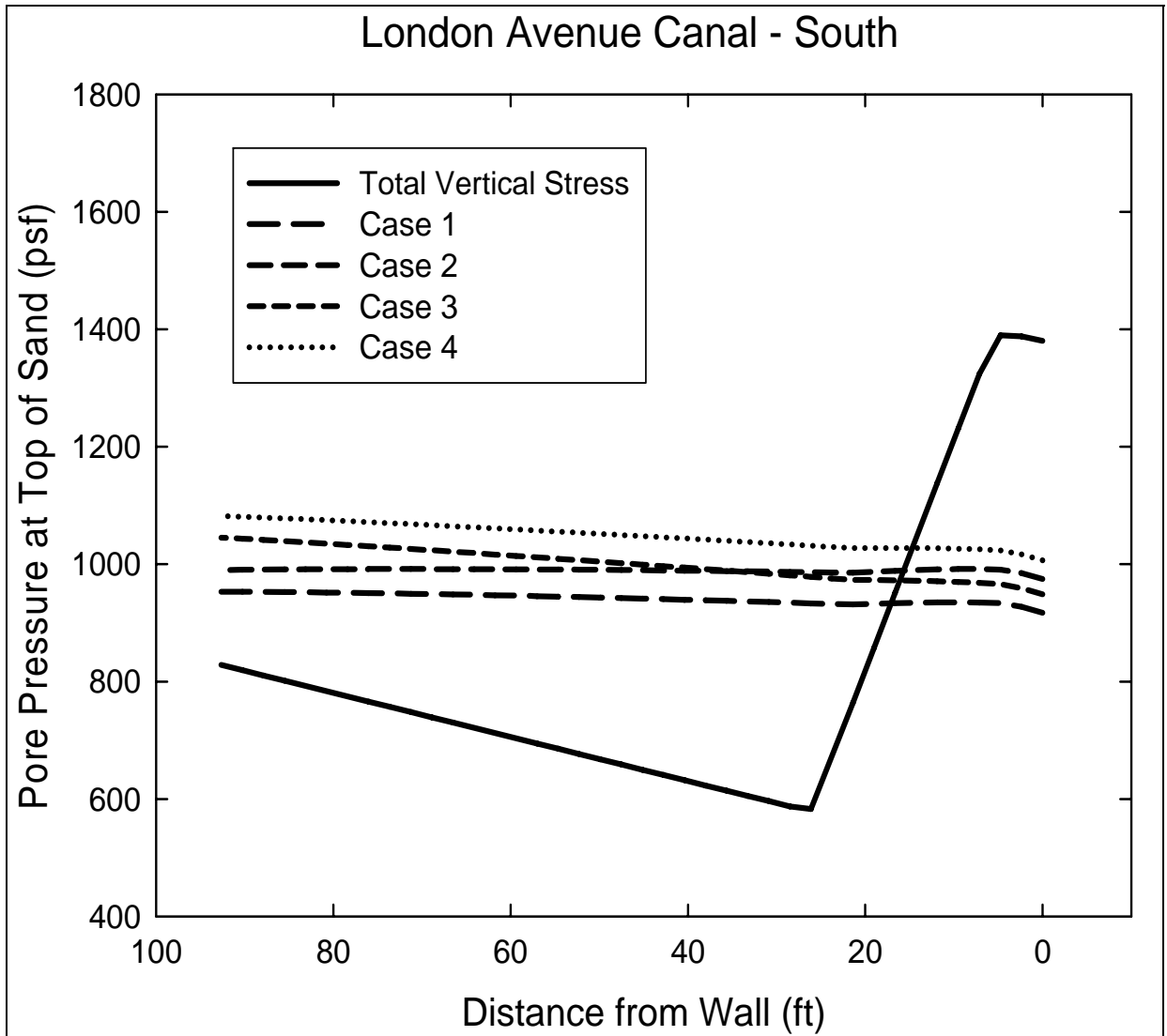
Figure 8-8. Calculated Uplift Pressures and Total Overburden Pressure for London South Breach
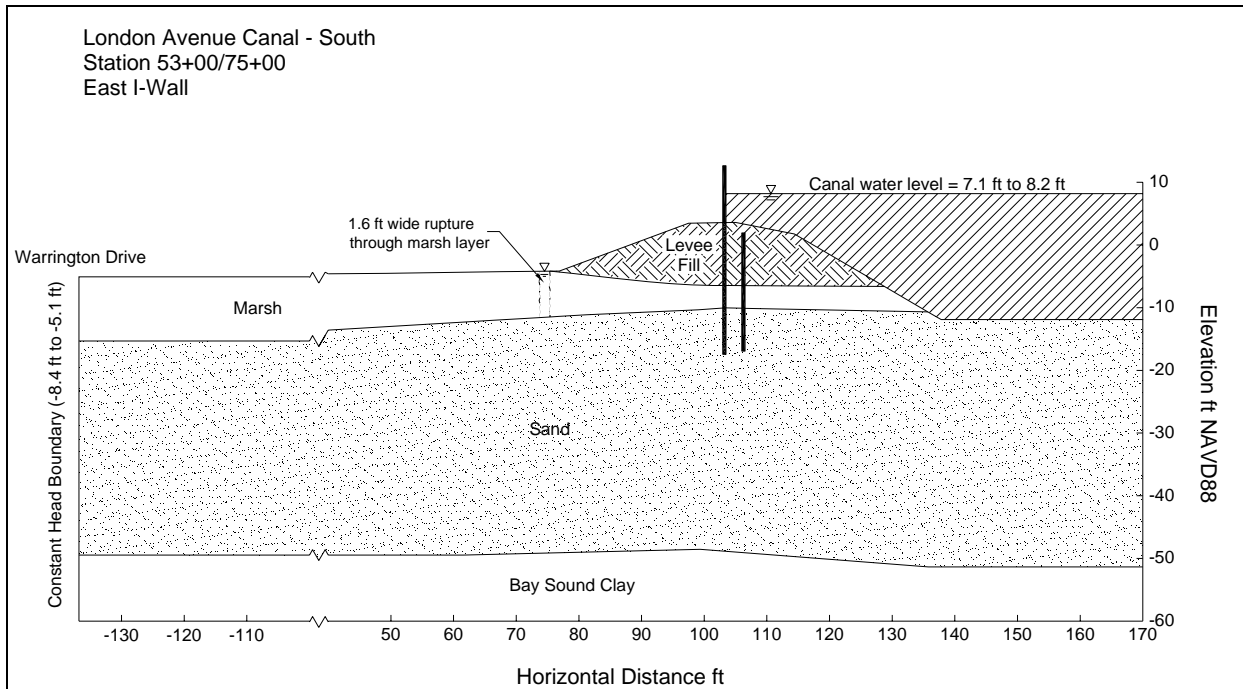
Figure 8-9. Schematic Cross Section at London South Breach, Showing Rupture Through Marsh Layer
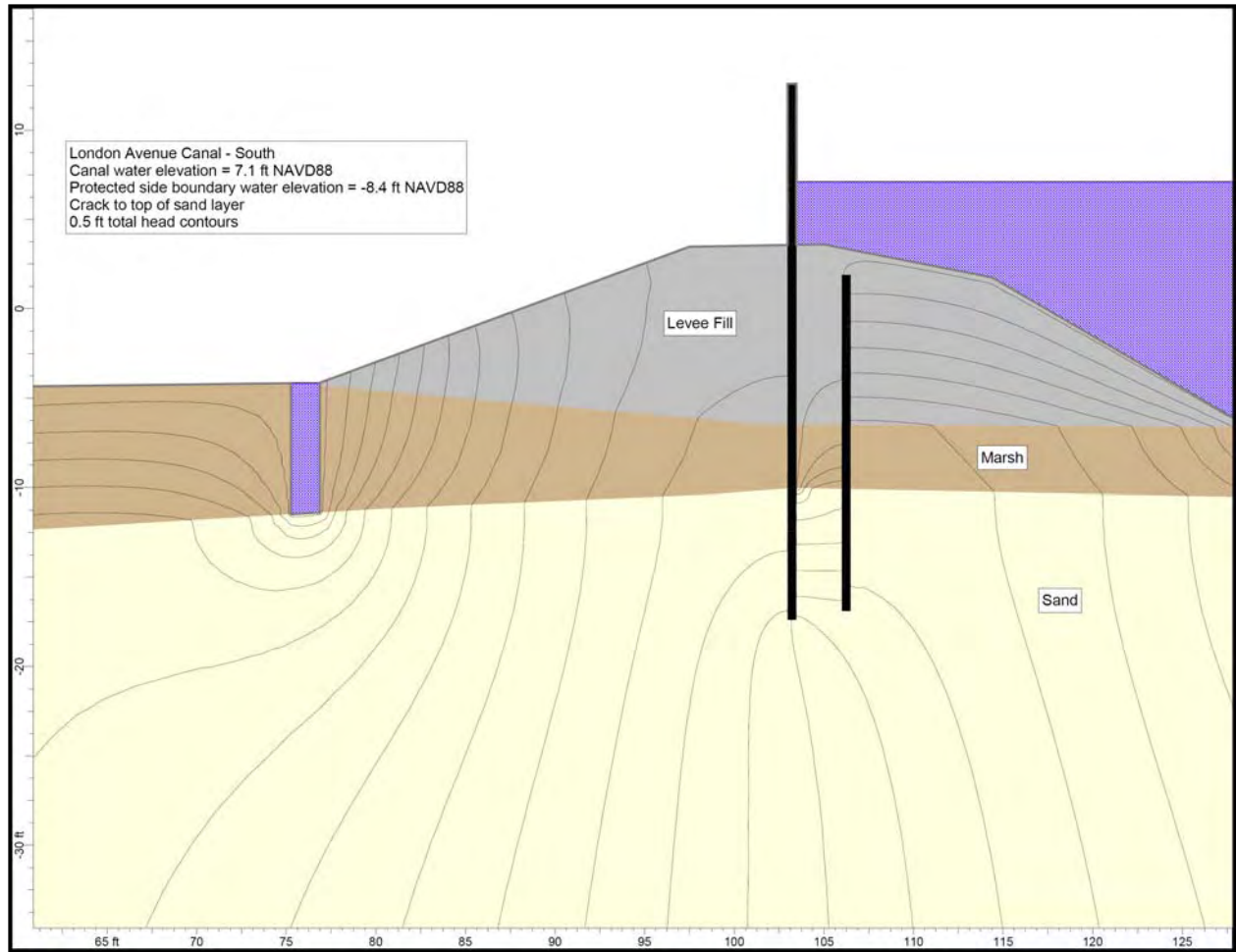
Figure 8-10.   Total Head Contours in Vicinity of Rupture for London South Breach
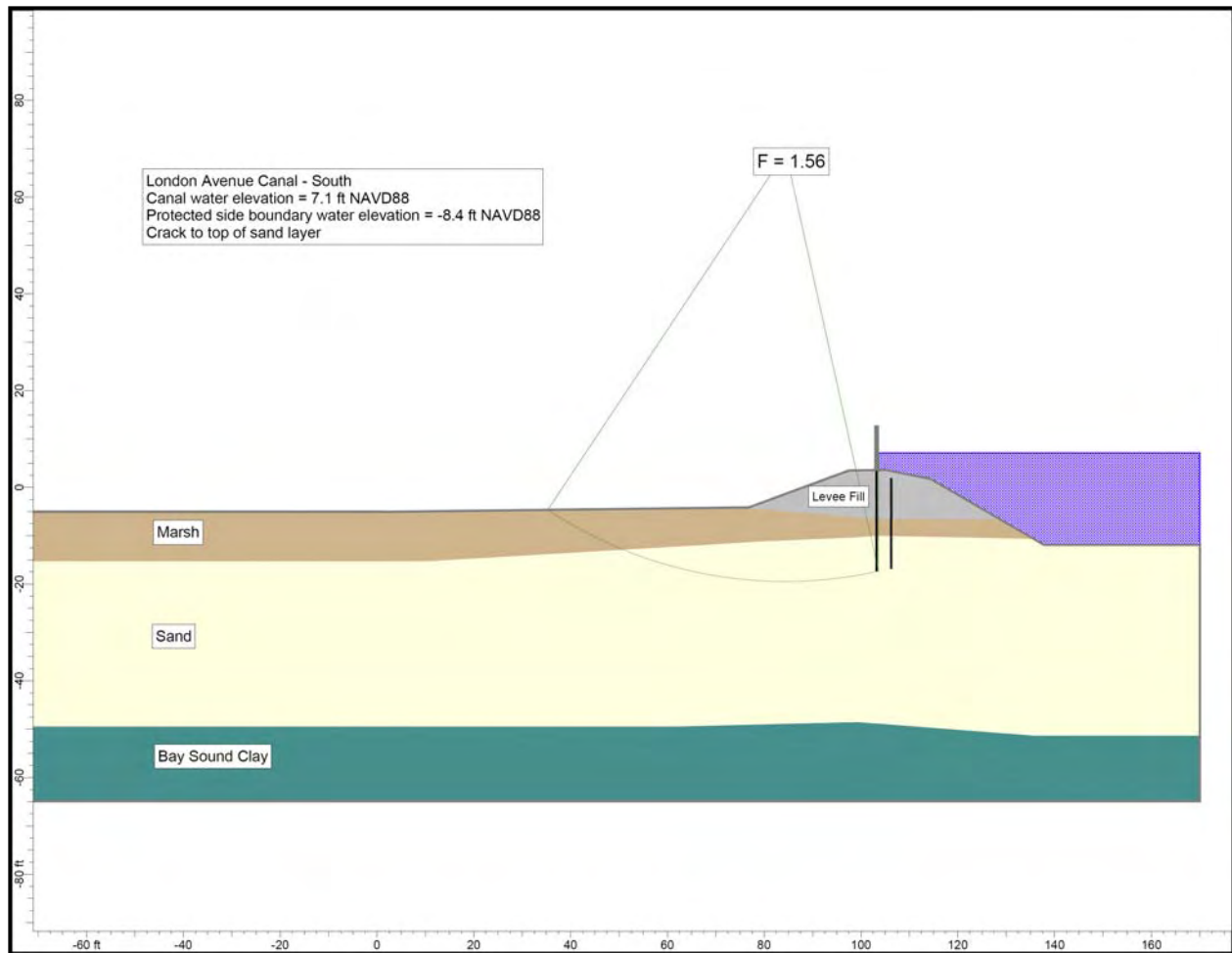
Figure 8-11.   London South Breach Case 1 Stability Analysis
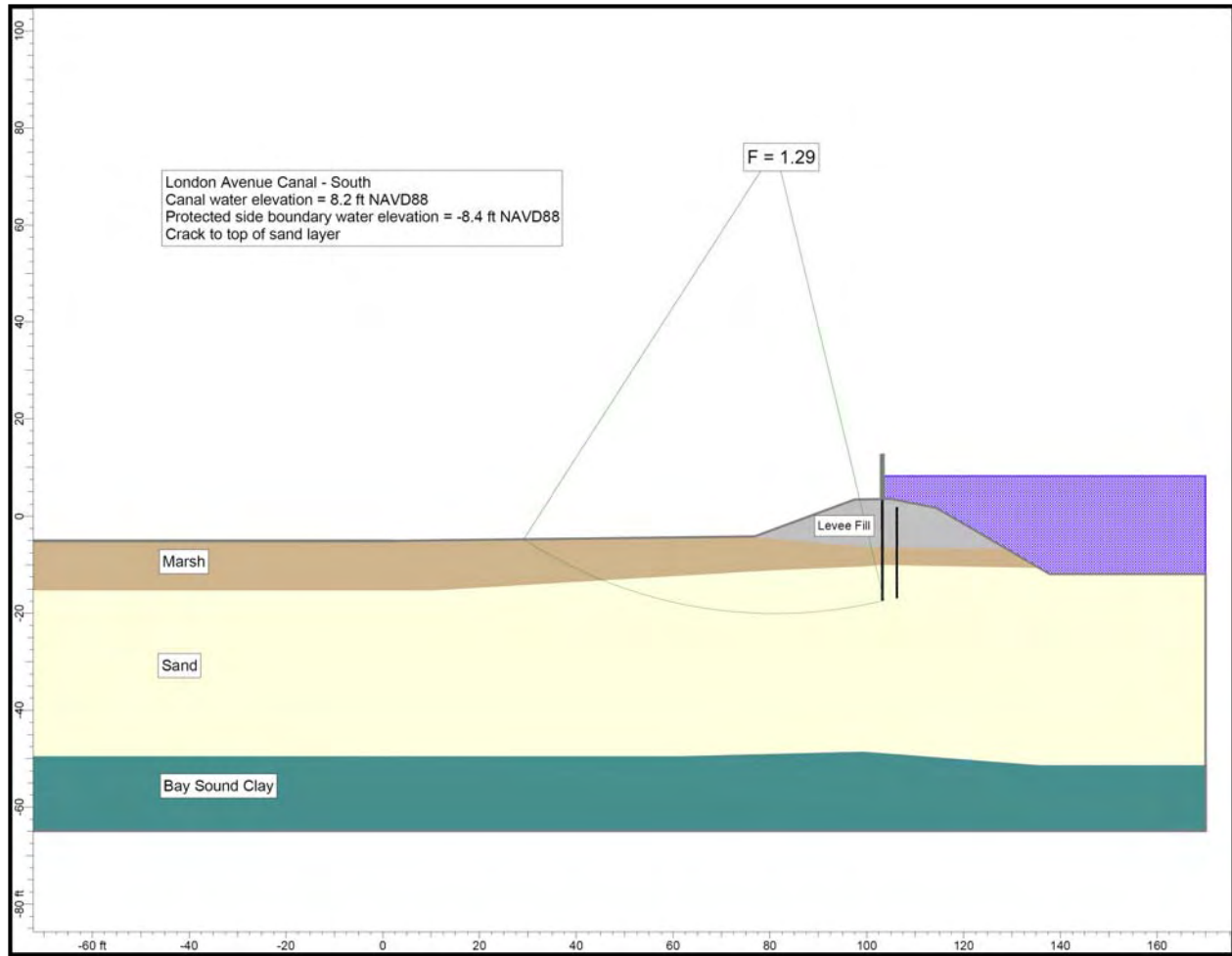
Figure 8-12.   London South Breach Case 2 Stability Analysis
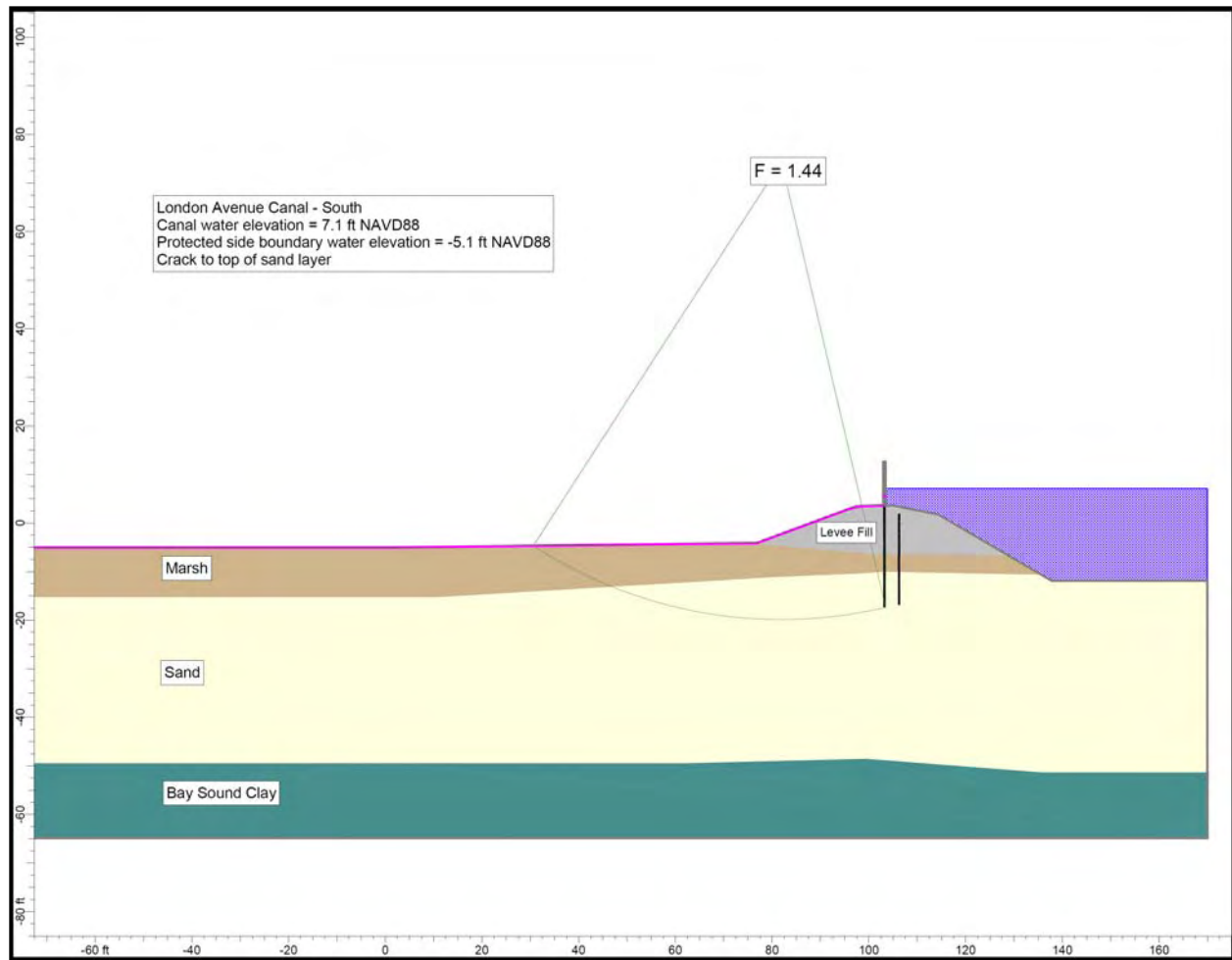
Figure 8-13.   London South Breach Case 3 Stability Analysis

The figure contains the following labels and annotations:

F = 1.19

London Avenue Canal - South
Canal water elevation = 8.2 ft NAVD88
Protected side boundary water elevation = -5.1 ft NAVD88
Crack to top of sand layer

Levee Fill

Marsh

Sand

Bay Sound Clay
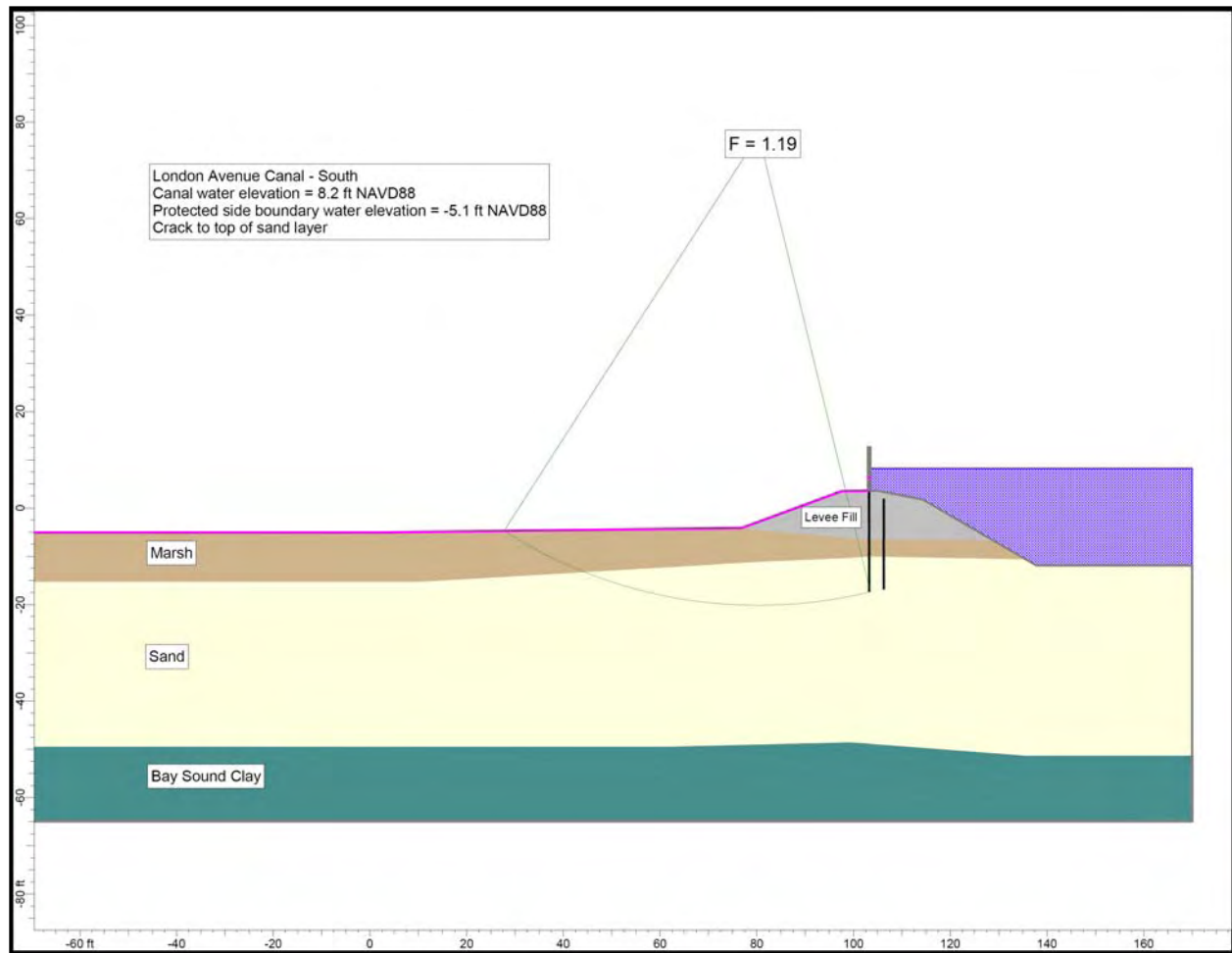
Figure 8-14.   London South Breach Case 4 Stability Analysis
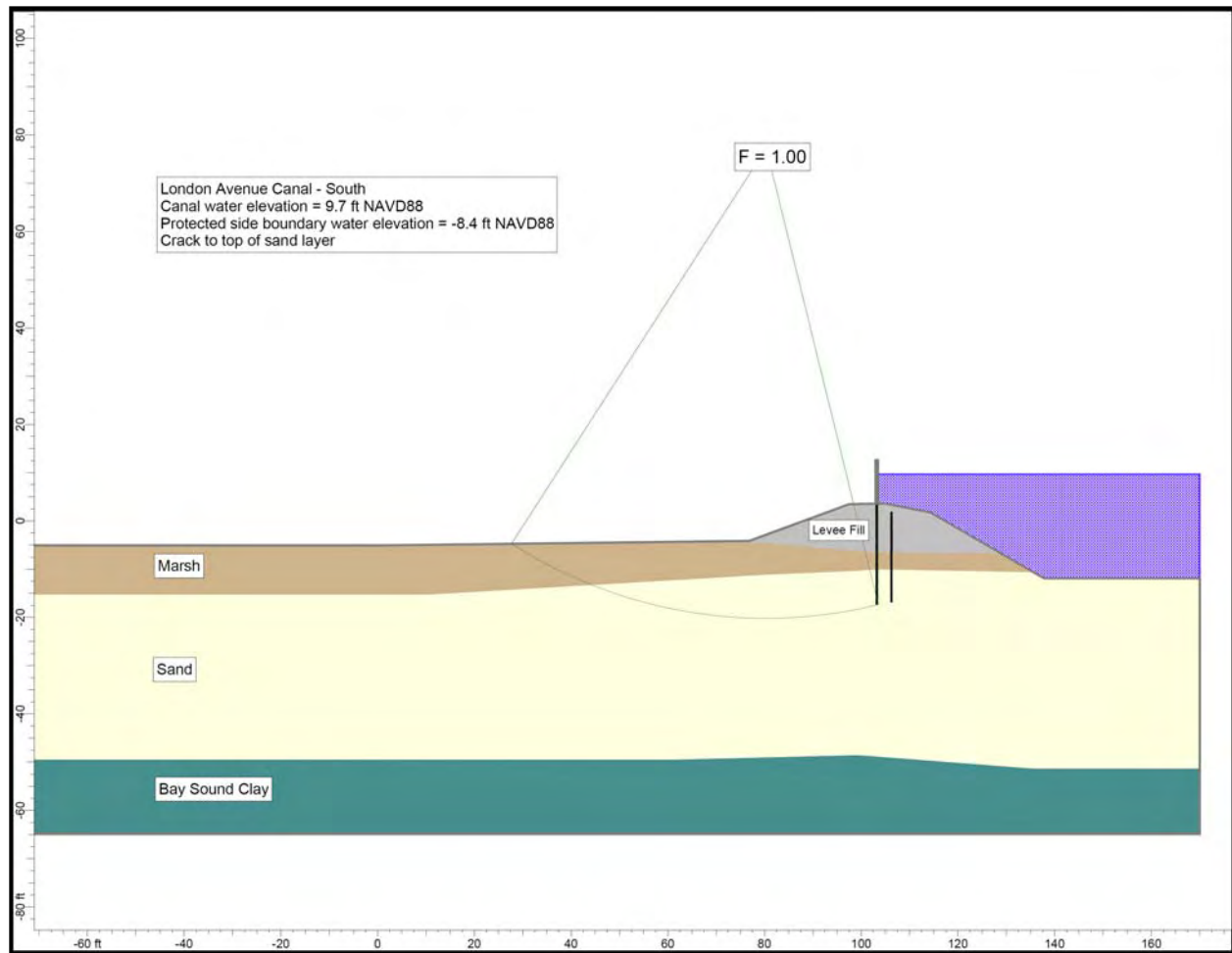
Figure 8-15.   London South Breach Case 5 Stability Analysis
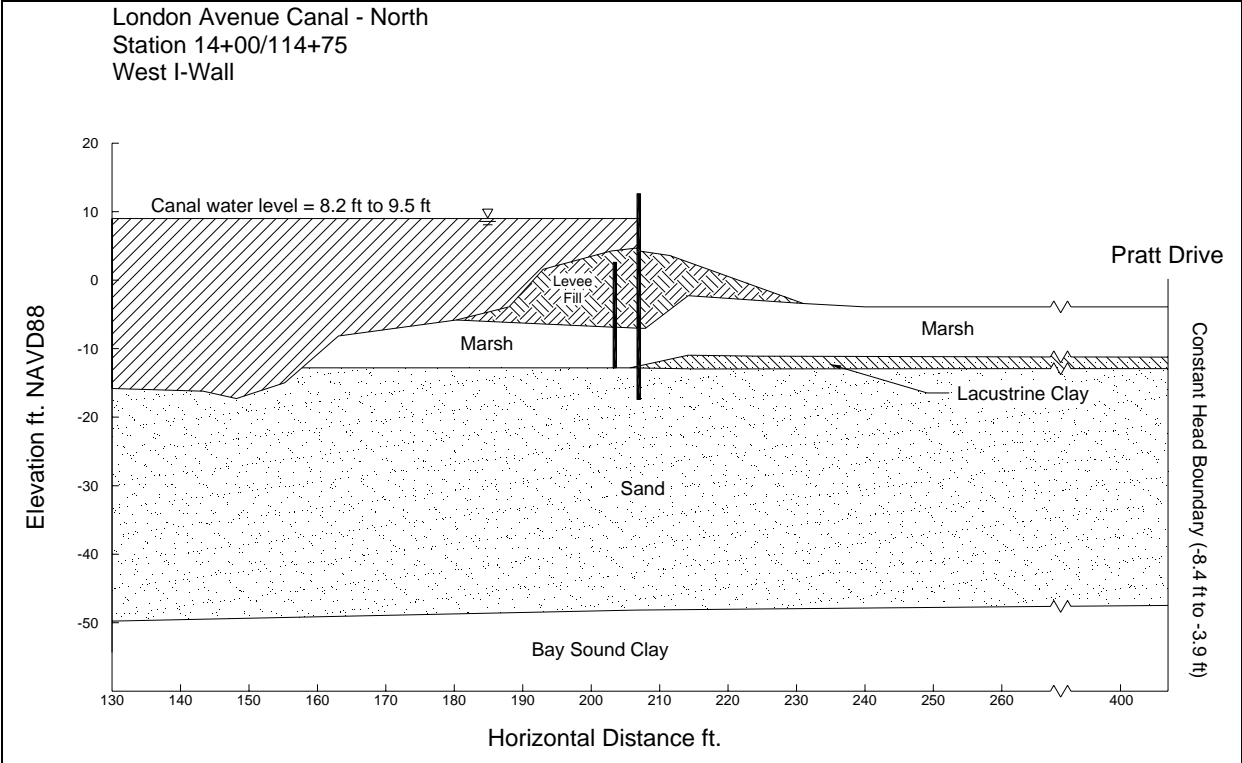
Figure 8-16.   Schematic Cross Section at London North Breach, with Seepage Boundary Conditions
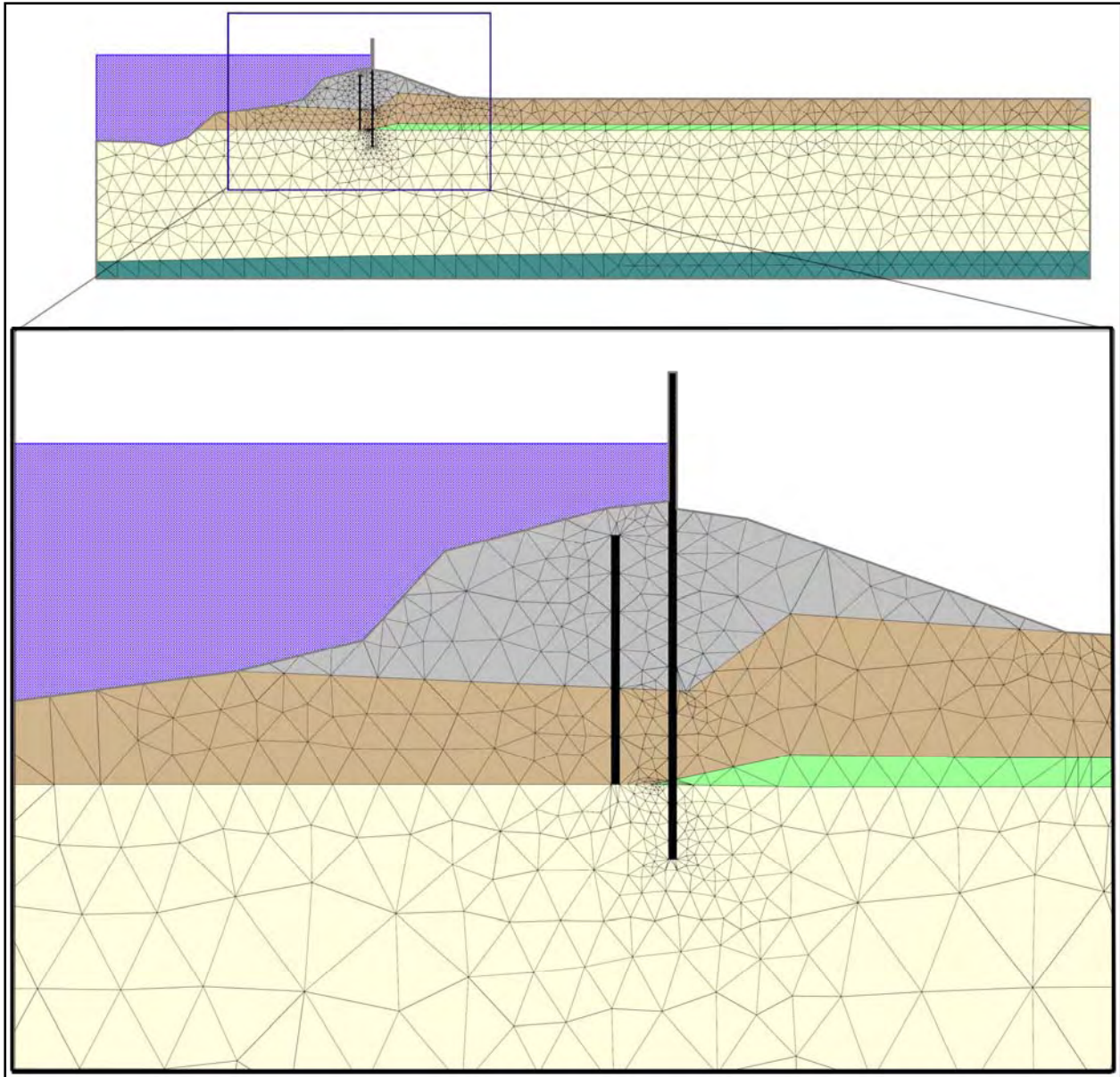
Figure 8-17.   Finite Element Mesh Used for Seepage Analysis for London Avenue North Breach
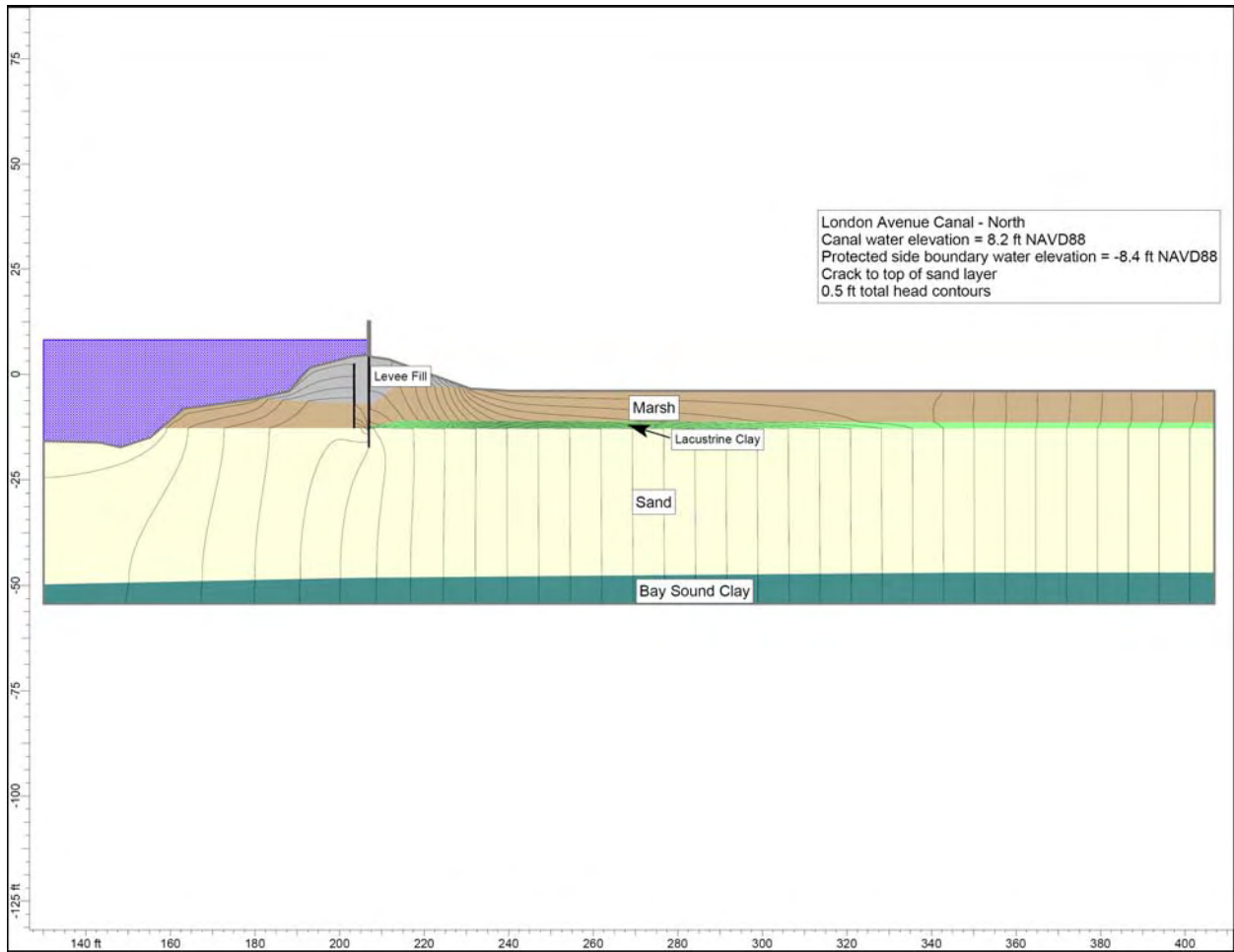
Figure 8-18.   Total Head Contours Calculated for Seepage Analysis of London North Breach (Case 1)
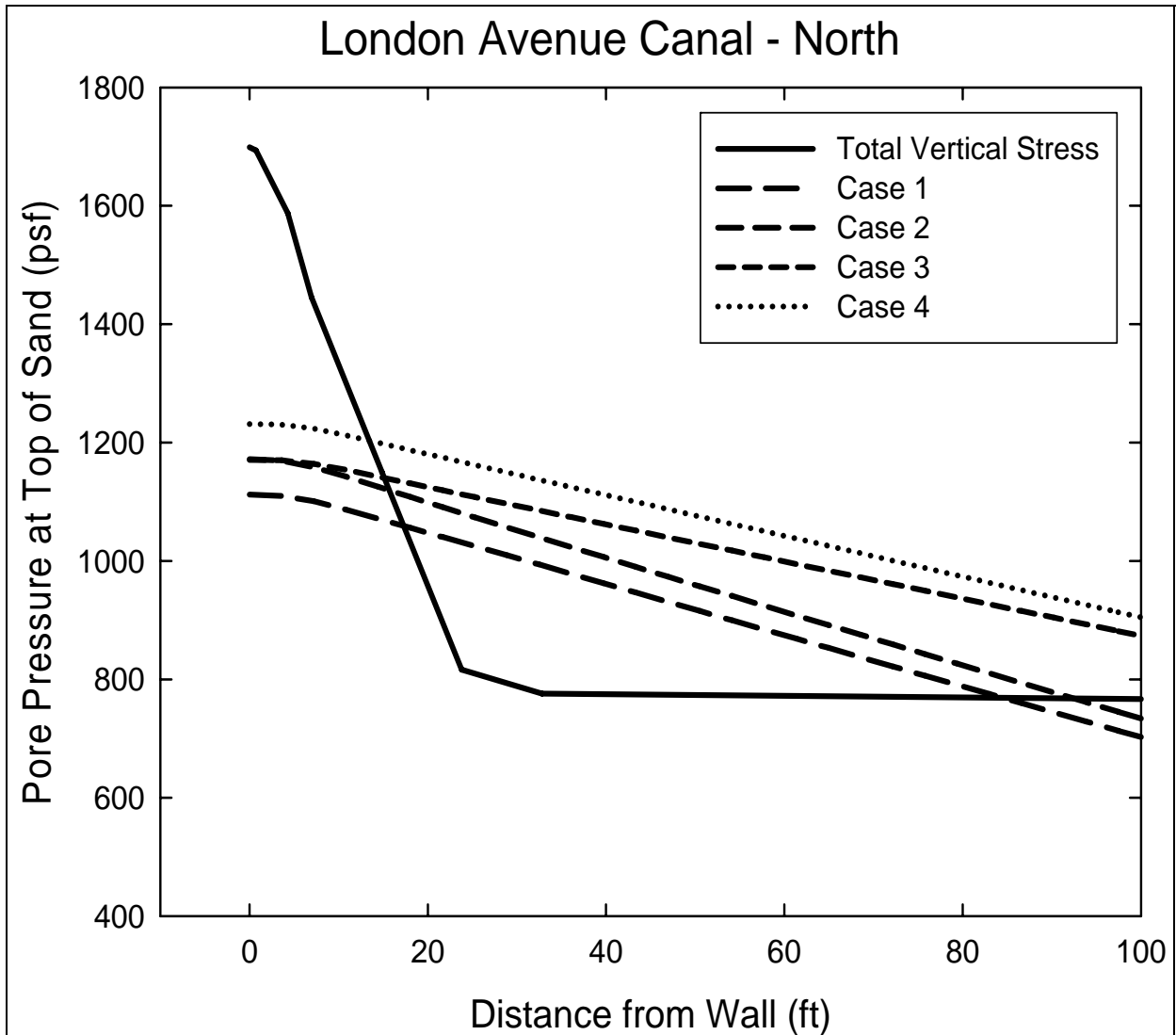
Figure 8-19.   Calculated Uplift Pressures and Total Overburden Pressure for London North Breach
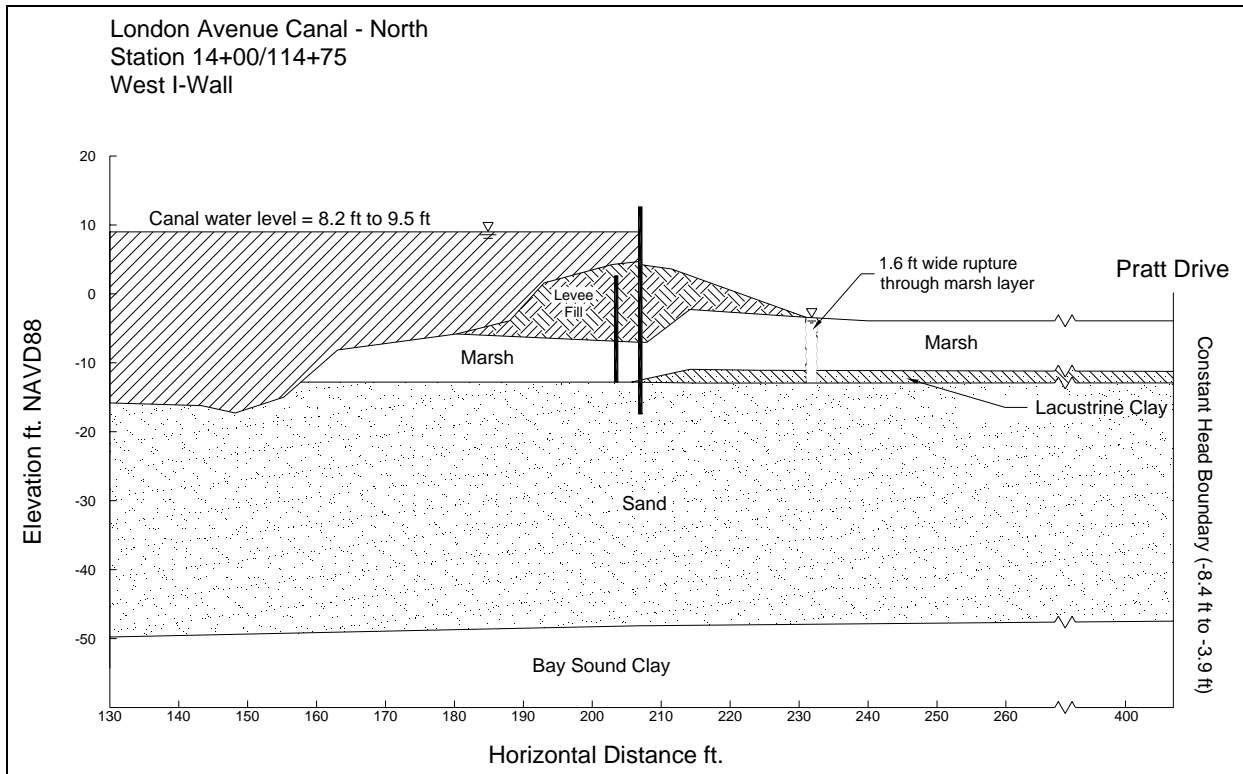
Figure 8-20. Schematic Cross Section at London North Breach, Showing Rupture Through Marsh Layer

The figure shows a cross section labeled:

London Avenue Canal - North
Station 14+00/114+75
West I-Wall

Elevation ft. NAVD88 (vertical axis, from -50 to 20)

Canal water level = 8.2 ft to 9.5 ft

Levee Fill

Marsh

1.6 ft wide rupture through marsh layer

Pratt Drive

Marsh

Lacustrine Clay

Sand

Bay Sound Clay

Horizontal Distance ft. (horizontal axis: 130, 140, 150, 160, 170, 180, 190, 200, 210, 220, 230, 240, 250, 260, 400)

Constant Head Boundary (-8.4 ft to -3.9 ft)

Figure 8-21. Total Head Contours in Vicinity of Rupture for London North Breach
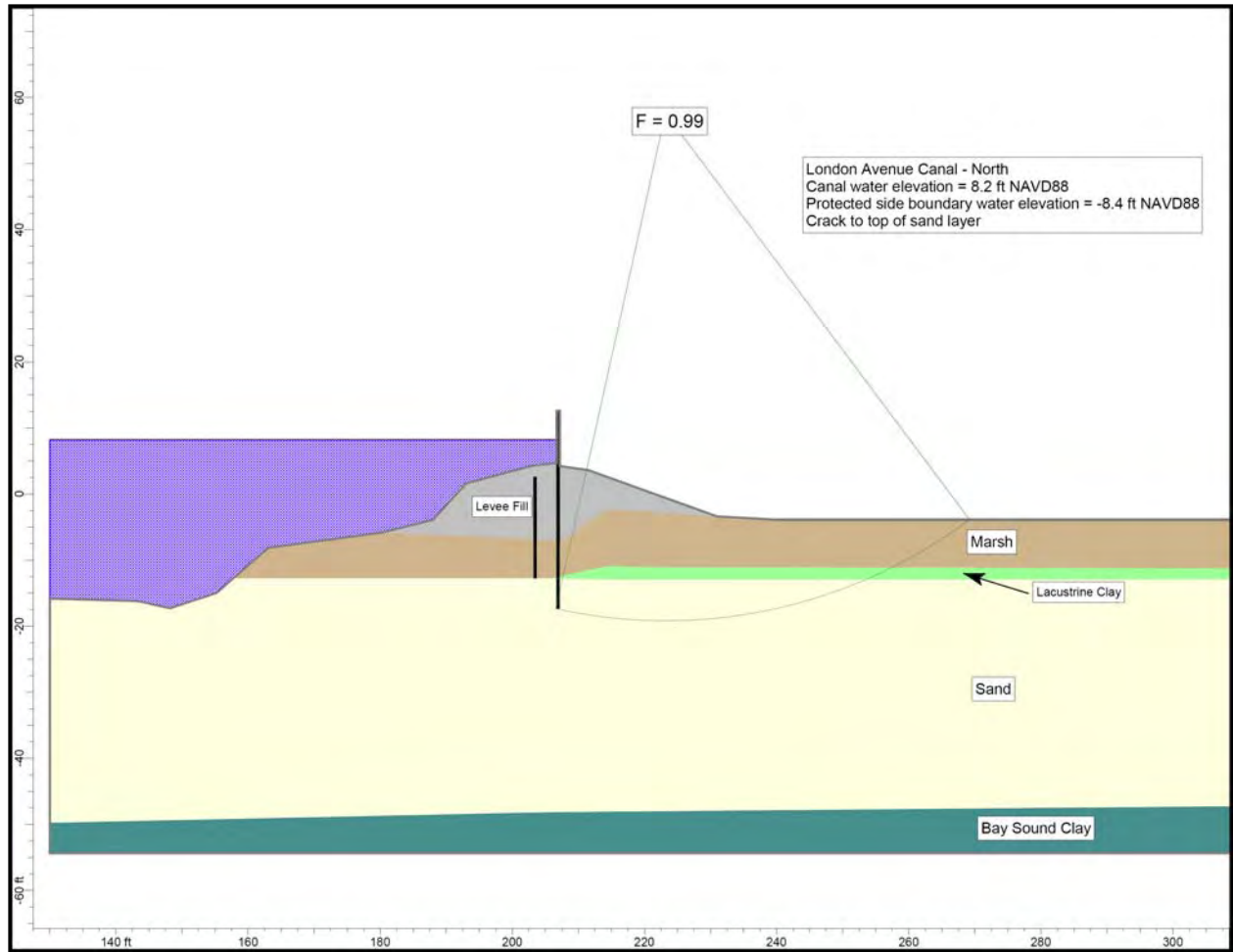
Figure 8-22.   London North Breach Case 1 Stability Analysis
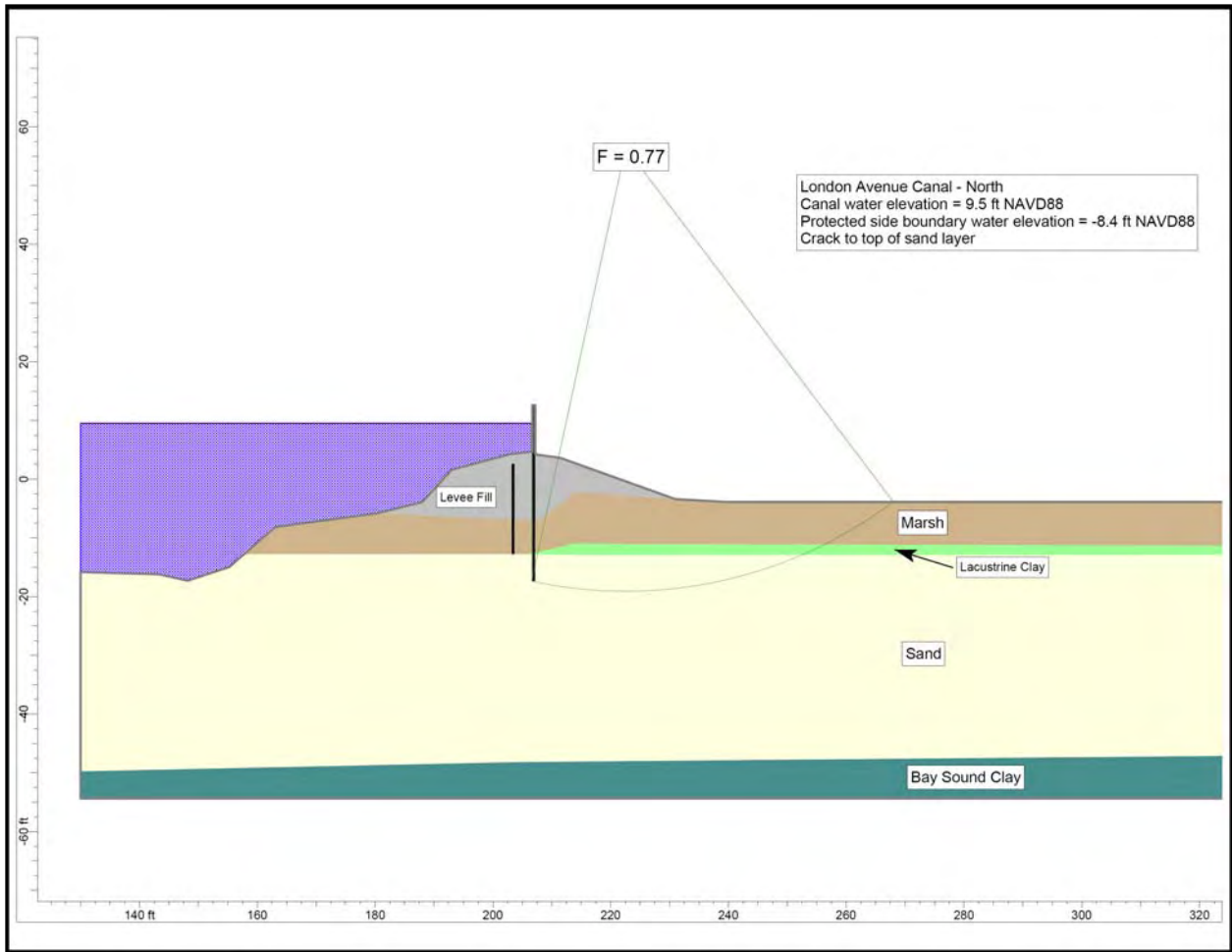
Figure 8-23.   London North Breach Case 2 Stability Analysis
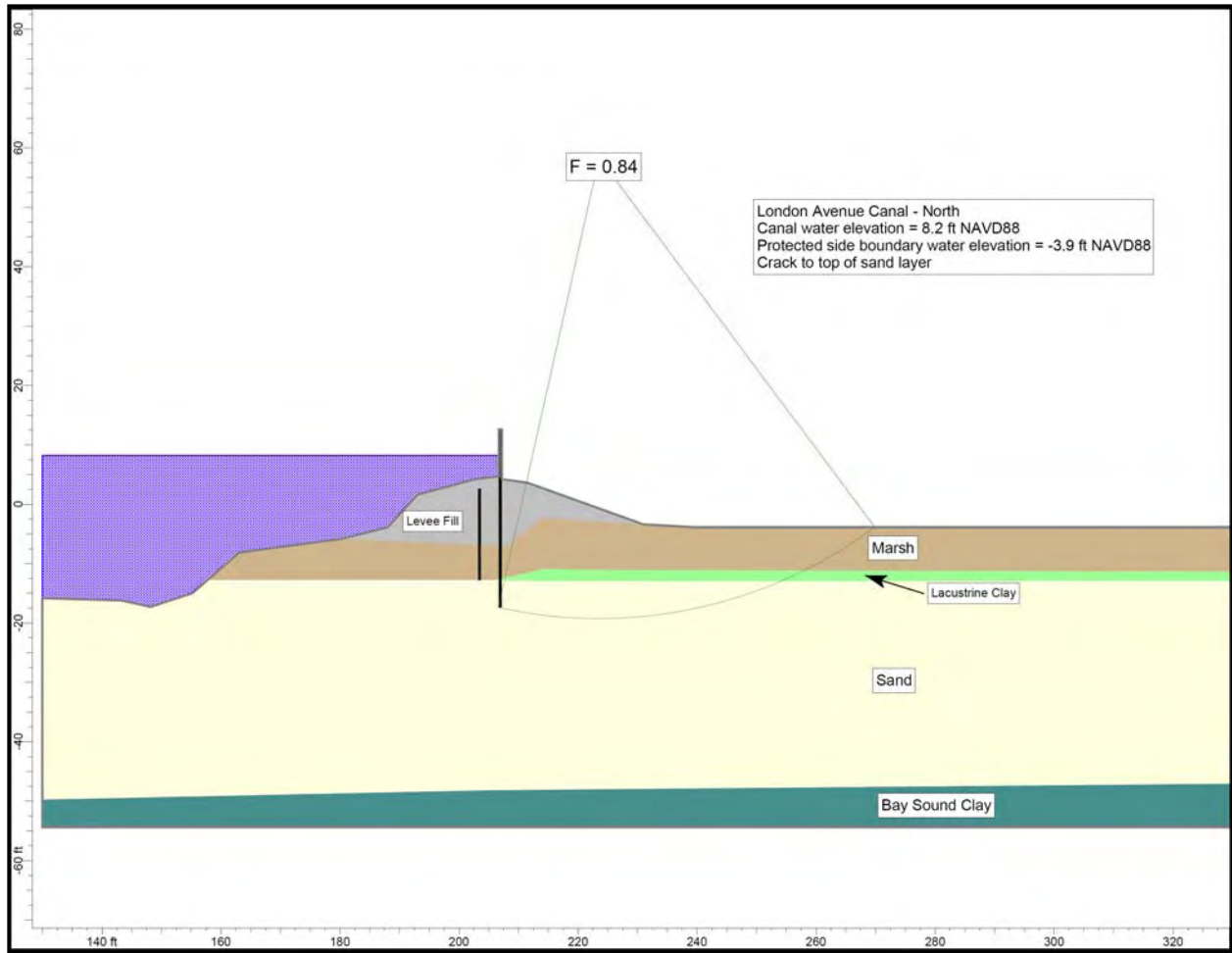
Figure 8-24.   London North Breach Case 3 Stability Analysis
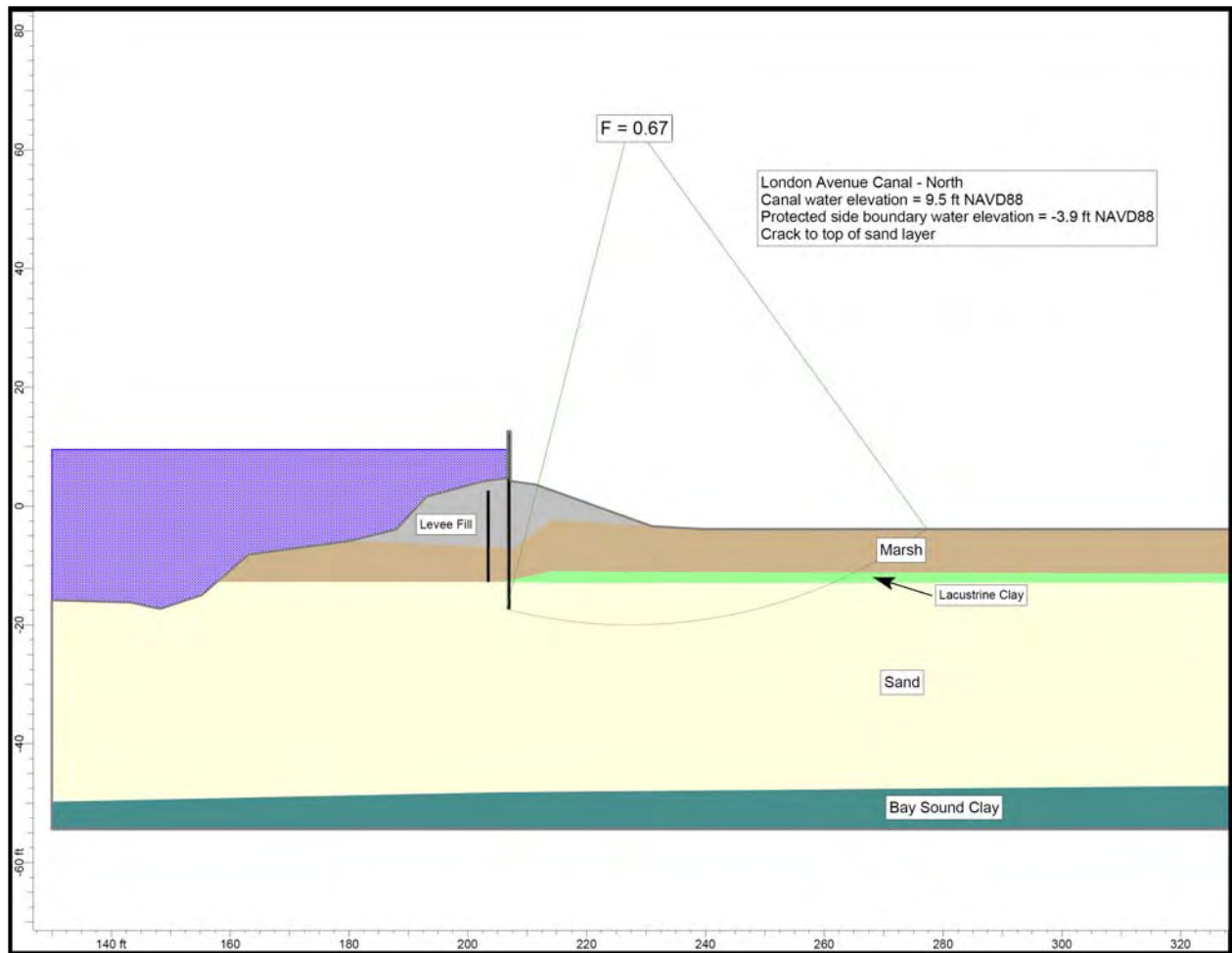
Figure 8-25.   London North Breach Case 4 Stability Analysis
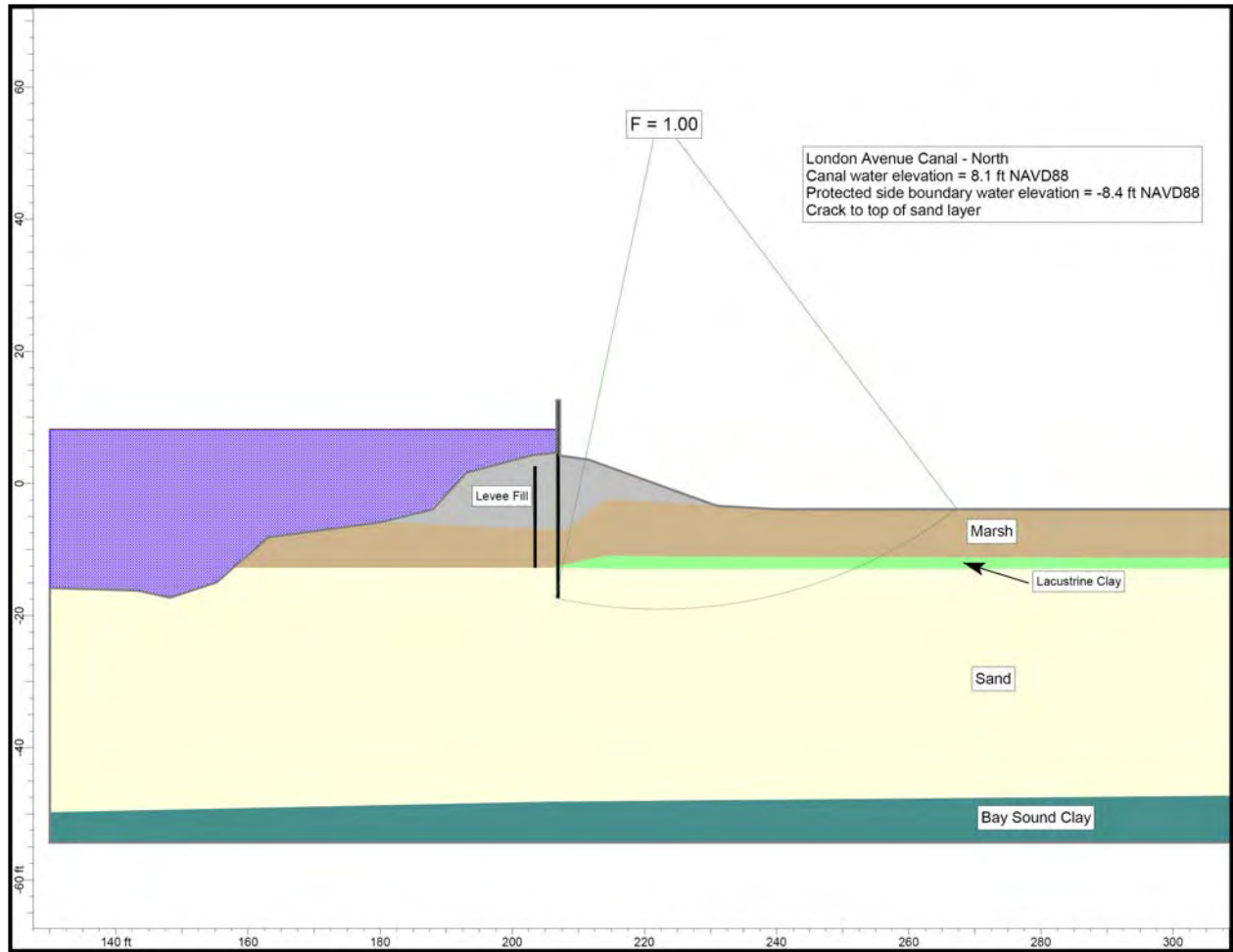
Figure 8-26.   London North Breach Case 5 Stability Analysis

Appendix 9
Soil Structure Interaction Analysis of the Floodwalls at London Avenue Canal

This interim IPET report describes detailed soil-structure interaction finite element analysis of the two breaches that occurred at the London Avenue Canal. Finite element soil-structure interaction analyses were conducted to provide a third approach to development of a complete understanding of the London Avenue Canal breach mechanisms. The investigation of these breaches is an important step in IPET's system-wide investigation of floodwall and levee performance, and the findings illuminate a possible mechanism of failure that will be investigated system-wide for locations where sand underlies levees and floodwalls.

Soil-Structure Interaction Analysis of the London Avenue Canal North Breach (West Flood Wall at London at Station 14+00)

Introduction

This section describes a complete soil-structure interaction (SSI) analysis of an existing flood wall within London Canal using the PC-based finite element program Plaxis (2004). A two-dimensional cross section within the section of the West side, at Station 14+00 of the London Canal that failed during hurricane Katrina is the subject of this evaluation. Results of a complete nonlinear finite element analysis of a two dimensional (2-D) cross section during simulated flood loading are described.

Plaxis is a complete nonlinear finite element package geared towards geotechnical engineering applications that include soil-structure interaction issues such as those that occur between a sheet pile and the soils in which it is embedded. It allows for the nonlinear response of soils to flood loading as occurred at the London canal with an I-wall along the center line of the soil-founded levee. The Plaxis PC-based software comprises a visual pre-processor, a nonlinear finite element engineering analysis module, and a visual post-processor. All software components are combined into a single package. Computed results include not only soil stresses, but also structural (e.g. sheet pile and I-wall) bending moments, interaction stresses between sheet piling and the soil in which it is embedded, as well as soil (e.g., levee) and structural deformations. A complete SSI analysis is considered to provide the most reasonable estimate for

Volume V The Performance – Levees and Floodwalls – Technical Appendix
V-9-1

This is a preliminary report subject to revision; it does not contain final conclusions of the United States Army Corps of Engineers.

deformation response of a soil-structural system involving nonlinear material behavior. In a complete SSI analysis loads exerted by the canal water acting on the soils of the levee and then onto the sheet pile wall (below the I-wall) by means of a load transfer through the levee and foundation soils are generated automatically during the analysis (i.e., predetermined earth pressure force distributions between the soil and the embedded sheet pile are not specified).

Section Analyzed

The two-dimensional cross section within the failed section of the West side of the London Canal at Station 14+00 analyzed for flood loading is shown in Figure 9-1.[1] The 2-D section is 274-ft wide and extends from the center line of the canal at x equal to 133 ft to x-coordinate equal to 407 ft. The top of the I-wall is at El 13 and sheet pile tip is at EL -17.4. An older sheet pile is embedded in the levee on the canal side of the I-wall, approximately 5 feet in front of the I-wall (centerline-to-centerline). This old sheet pile used to be part of a shorter flood wall that was removed when the existing I-wall was installed. The old sheet piling extends from the ground surface to EL -12.9 (corresponding to the elevation of the top of the Beach sand layer).

The crest of the earthen levee on the protected (West) side of the I-wall is at El 4.4, with a crest width of approximately 5 feet. Note the I-wall extends above the crest of the soil founded levee. The protected side of the levee has a 1 on 3 side slope to approximately El -3.4. The protected side ground surface is assigned El -3.4 for this section. The crest of the earthen levee on the canal side of the I-wall is also at El 4.4. The upper 3.4 feet of the levee on the canal side of the I-wall is above normal canal water elevation. From El 4.4 to EL 1.6, the levee face has a 1 on 5 side slope. Between El 1.6 and El -4.1 the face of the levee has a 1 on 1 side slope. From El -4.1 to El -7. 1 the face of the levee has a 1 on 5 side slope. From EL -7.1 to El -11.4 the peat is exposed to the canal water and has a 1 on 3 side slope. The deepest point in the canal is at canal center line (i.e., x = 133 ft in Figure 9-1), with a top of Canal bottom silt at El -12.4 at this location.

---

[1] All elevations cited are according to NAD88.
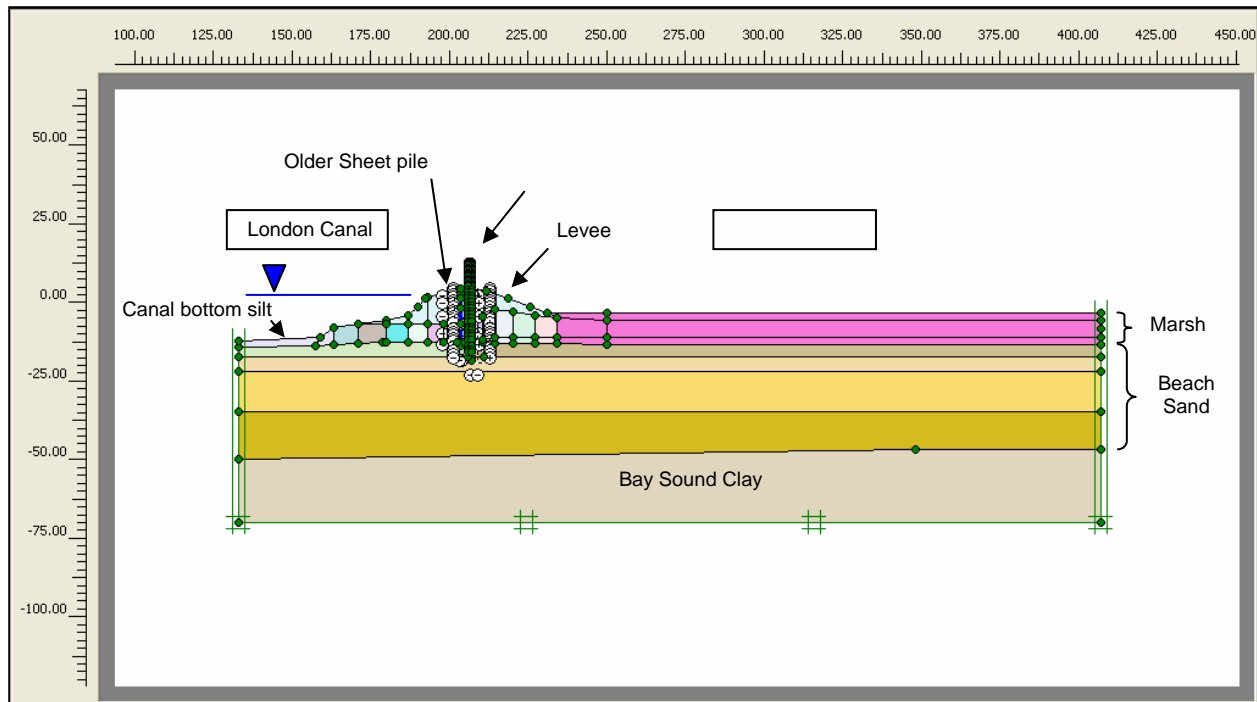
Figure 9-1. Two-Dimensional Cross Section Model used in the Complete SSI Analysis of Station 14+00 at London Canal – West Side

Proceeding from top to bottom in Figure 9-1, this cross section contains layers of Levee fill (clay), marsh (also referred to as peat), Beach sand, and Bay Sound clay. There is no Lacustrine clay contained within this cross section. The top of I-wall is at El 13 and the base of the Figure 9-1 cross-section is assigned to El -70. El -70 corresponds (approximately) to the bottom of the Bay Sound clay at Station 14+00. The soil layering is consistent with that used in the slope stability evaluations made for this cross section. The regions of uniform color in Figure 9-1 reflect the Plaxis "soil clusters" used to define the mesh and to assign soil regions with common properties.

Finite Element Mesh

Key Plaxis modeling features used in the plane strain analysis of London include the use of 15-node triangular elements to model the soil, plates (i.e., special beam elements) to model the bending of the newer I-wall/sheet pile wall as well as the older sheet pile wall, and interface elements to model soil-structure interaction between the sheet pile wall and the adjacent soil elements. A total of 33,208 nodes and 4,016 elements, containing 48,192 stress points, are used to define the Figure 9-2 mesh. Details regarding the quantity of each of the three types of plane strain elements used in the finite element model as well as select characteristics of each type of element are summarized in Table 9-1.
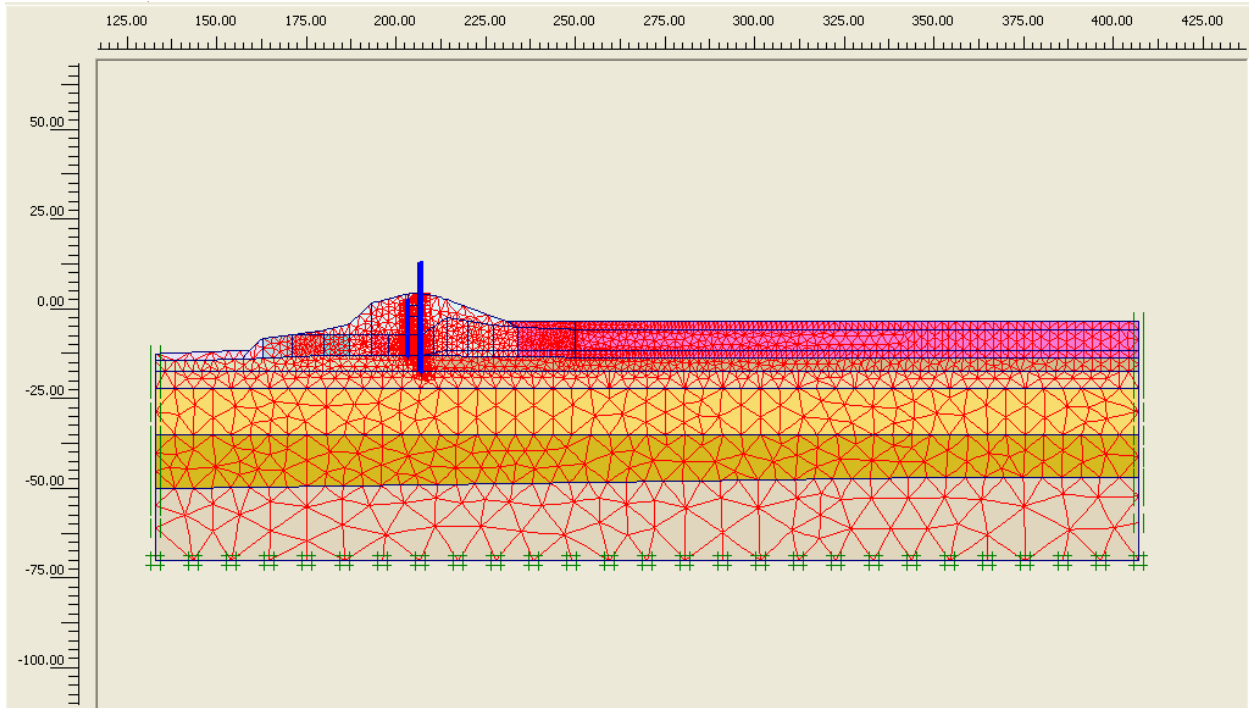
Figure 9-2. Finite Element Mesh used in the Complete SSI Analysis of Station 14+00 at London Canal – West Side

Table 9-1
Mesh Data Summary of Elements Used

Type	Type of element	Type of integration	Total no.
Soil	15-Noded	12-point Gauss	4016
Plate	5-node line	4-point Gauss	76
Interface	5-node line	4-point Newton-Cotes	144

A zero horizontal displacement is specified along the left and right hand side vertical boundaries of the Figure 9-2 finite element mesh. However, these nodes are free to displace in the vertical direction. Along the bottom boundary of the mesh zero horizontal and vertical displacements are specified at these nodes.

Material Properties for the Soils and Flood Wall in the Complete Soil-Structure Interaction Analysis

The soil material properties used in this complete SSI analysis are the same as those used in the slope stability analyses of this cross section. Figure 9-2 shows the 76 soil clusters used to define the regions of common soil properties for the four primary categories of soil within the mesh (i.e., the marsh (or peat), Lacustrine clay, Beach sand, and Bay Sound clay). Note that each soil layer comprises many clusters, each of which is designated by a different color. Spatially varying soil properties are assigned in the slope stability analyses. Accordingly, multiple soil clusters are used in the nonlinear finite element mesh to assign material properties within each

soil layer to accommodate the spatially varying (i.e., vertically as well as horizontally) soil properties. Table 9-2 summarizes the engineering material properties and the corresponding to average stiffness values in the complete SSI analysis. Note that a range in engineering soil properties is reported for the Marsh layer. Table 9-3 summarizes the engineering material properties for the complete SSI analysis with increased values for soil stiffness of the Levee clay and the Marsh. This second set of soil stiffness values are used to assess the sensitivity in computed results to the stiffness of the protected side Levee clay and Marsh (i.e., peat).

Table 9-2
Material Characterization for Soils of Average Stiffness

| Soil type | Range in Elevation, NAD88 | Total unit weight (pcf) | Constant S_u value in soil cluster (psf) | ϕ (deg) | Young's Modulus - Average | | | m | $R_{interface}$ | Hydraulic Conductivity (ft/hr) |
					E^{ref}/S_u	E^{ref} (psf)	$(E^{ref})_{ur}/E^{ref}$			
Levee clay	–	110	900	–	48	–	5	0.5	0.8	1.2E-04
Marsh (peat)	–	80	300 to 400	–	48	–	3	0.5	0.8	1.2E-04 to 1.2E-02
Beach Sand	-12 to -22	118	–	31	–	418,000	3	0.5	–	1.8
	-22 to -35	122	–	36	–	647,000	3	0.5	–	
	-35 to -47	118	–	32	–	438,900	3	0.5	–	
Bay Sound clay	–	102	779	–	68	–	3	1.0	–	1.2E-04

Note:$(E^{ref})_{50} = (E^{ref})_{oed} = E^{ref}$; ψ = 0 deg; p_{ref} = 2116 psf; v_{ur} = 0.3; R_f = 0.9

Table 9-3
Material Characterization for Soils of With Increased Stiffness

| Soil type | Range in Elevation, NAD88 | Total unit weight (pcf) | Constant S_u value in soil cluster (psf) | ϕ (deg) | Young's Modulus - Stiff | | | m | $R_{interface}$ | Hydraulic Conductivity (ft/hr) |
					E^{ref}/S_u	E^{ref} (psf)	$(E^{ref})_{ur}/E^{ref}$			
Levee clay - canal side	–	110	900	–	48	–	5	0.5	0.8	1.2E-04
Levee clay - protected side	–	110	900	–	240	–	3	0.5	0.8	1.2E-04
Marsh (peat) - canal side	–	80	300 to 400	–	48	–	3	0.5	0.8	1.2E-04 to 1.2E-02
Marsh (peat) - protected side	–	80	300 to 400	–	240	–	3	0.5	0.8	1.2E-04 to 1.2E-02
Beach Sand	-12 to -22	118	–	31	–	418,000	3	0.5	–	1.8
	-22 to -35	122	–	36	–	647,000	3	0.5	–	
	-35 to -47	118	–	32	–	438,900	3	0.5	–	
Bay Sound clay	–	102	779	–	68	–	3	1.0	–	1.2E-04

Note:$(E^{ref})_{50} = (E^{ref})_{oed} = E^{ref}$; ψ = 0 deg; p_{ref} = 2116 psf; v_{ur} = 0.3; R_f = 0.9

Levee clay: A total unit weight of 110 pcf is assigned to the Levee clay soil clusters. A smaller data base of strength and stiffness tests results are available for London Canal Levee clay, as compared with 17th Street canal Levee clay. After a careful assessment of the test data on the Levee clay at London canal, an undrained shear strength (S_u) value of 900 psf is assigned. This is the same value for Su that is assigned at 17th Street.

Stress-strain data for 17th Street canal Levee clay triaxial test specimens leads to the assignment of an average value for Young's modulus, E^{ref}, expressed in terms of (E^{ref}) normalized by S_u and equal to 48 (Table 9-2). This same value for Young's modulus is assigned to the London canal Levee clay. During the course of the complete SSI analysis of Station 14+00, an evaluation of the sensitivity in computed results to the value of Levee and Marsh stiffness is conducted. In this parametric study the protected side Levee clay E^{ref} is increased by a factor of five. It is expressed in Table 9-3 in terms of (E^{ref}) normalized by S_u and is set equal to 240 (i.e., = 5 times 48).

For the Plaxis nonlinear Hardening Soil (HS) model, the parameters $(E^{ref})_{50}$ and $(E^{ref})_{oed}$ are set equal to [E^{ref}/S_u times S_u]. Additional HS parameters assigned are reference stress for stiffness, p_{ref}, equal to 2,116 psf, failure ratio $R_f = 0.9$, the exponent m = 0.5 and v_{ur} equals 0.3. For unload reload HS parameters, $(E^{ref})_{ur}$ is set equal to 5 times $(E^{ref})_{50}$ in the average modulus complete SSI analysis and set equal to 3 times $(E^{ref})_{50}$ in the sensitivity analysis using stiff clay properties. For Casteel CZ101 cold formed steel sheet piles to levee clay, the interface strength parameter $R_{interface}$ is set equal to 0.8 for Levee clay-to-steel interfaces (by the Potyondy, 1961, data).

Marsh (or peat): A smaller data base of strength and stiffness tests results are available for London Canal Marsh (or peat), as compared with 17th Street canal peat (or marsh). After a careful assessment of the test data on the Marsh at London canal, a range in values of undrained shear strength (S_u) of 300 psf to 400 psf is assigned. This is the same range in Su values as is assigned for the 17th Street canal peat, which factored into the strength assessment made for this cross section. Below the I-wall and in the region of the greatest overburden, a value of S_u equal to 400 psf is assigned. With no overburden, the value for S_u is set equal to 300 psf in the Marsh. A shear strength value is assigned to each Marsh cluster based on the magnitude of the overburden for the center position of each Marsh cluster below the levee. There is no vertical variation in undrained shear strength for the Marsh layer. A total unit weight of 80 pcf is assigned to the Marsh soil clusters. Stress-strain data for 17th Street canal peat triaxial test specimens leads to the assignment of an average value for Young's modulus, E^{ref}, expressed in terms of (E^{ref}) normalized by S_u and set equal to 48 (Table 9-2). This same value for Young's modulus is assigned to the London canal Marsh. In the evaluation of the sensitivity in computed results to stiffness, the protected side Marsh E^{ref} is increased by a factor of five. It is expressed in Table 9-3 in terms of (E^{ref}) normalized by S_u and set equal to 240 (i.e., = 5 times 48).

For the Plaxis nonlinear Hardening Soil (HS) model the parameters $(E^{ref})_{50}$ and $(E^{ref})_{oed}$ are set equal to [E^{ref}/S_u times S_u]. Additional HS parameters assigned are reference stress for stiffness, p_{ref}, equal to 2,116 psf, failure ratio $R_f = 0.9$ and the exponent m = 0.5. For unload reload HS parameters, $(E^{ref})_{ur}$ is set equal to 3 times $(E^{ref})_{50}$ and v_{ur} equals 0.3. For Casteel CZ101 cold formed steel sheet piles to Marsh interface, $R_{interface}$ is set equal to 0.8.

Beach Sand: The results from the field investigation indicate that the Beach sand is made up of three distinct layers based on the in-situ density of the sand. The upper layer of Beach sand extends from approximately El -12 to -22 and is a loose to medium sand. The middle layer extends from El -22 to -35 and is a medium sand. The lower layer extends from El -35 to -47 and is a loose to medium sand. Proceeding from the top layer down, total unit weights of 118 pcf, 120 pcf and 118 pcf are assigned to each of the three layers of Beach Sand soil clusters.

Standard Penetration Test and cone test results in the upper Beach sand layer (i.e., El -12 to -22) indicate an average value of 10 blows per ft depth for 60 percent of free-fall energy and corrected to an effective overburden pressure of 1 ton/ft^2 [i.e., $(N_1)_{60} = 10$]. For a fine sand with an average value of $(N_1)_{60} = 10$, the relative density (D_r) is 40 percent by Skemption's (1986) correlation. A $(N_1)_{60} = 10$ results in a value of 30 deg for the effective angle of internal friction by the Peck, Hanson and Thornburn (1974) correlation. For loose sand with D_r equal to 40 percent and using the correlations of Lengkeek and Vermeer and Shanz (cited in Brinkgreve, 2005, as well as in Plaxis course notes, 2006), the value of Young's modulus E^{ref} is set equal to 418,000 psf. For the Plaxis nonlinear Hardening Soil (HS) model, the parameters $(E^{ref})_{50}$ and $(E^{ref})_{oed}$ are set equal to 418,000 psf. Additional HS parameters assigned are reference stress for stiffness, p_{ref}, equal to 2,116 psf, failure ratio $R_f = 0.9$ and the exponent $m = 0.5$. For unload reload HS parameters, $(E^{ref})_{ur}$ is set equal to 3 times $(E^{ref})_{50}$ and ν_{ur} equals 0.3. For Casteel CZ101 cold formed sheet piles to Beach sand, the interface strength parameter $R_{interface}$ is set equal to 0.8.

Standard Penetration Test and cone test results in the middle Beach sand layer (i.e., El -22 to -35) indicate an average value of 26 blows per ft depth for 60 percent of free-fall energy and corrected to an effective overburden pressure of 1 ton/ft^2 [i.e., $(N_1)_{60} = 26$]. For a fine sand with an average value of $(N_1)_{60} = 26$, the relative density (D_r) is 65 percent by Skemption's (1986) correlation. A $(N_1)_{60} = 26$ results in a value of 36 deg (approximately) for the effective angle of internal friction by the Peck, Hanson and Thornburn (1974) correlation. For medium sand with D_r equal to 65 percent and using the correlations of Lengkeek and Vermeer and Shanz (cited in Brinkgreve, 2005, as well as in Plaxis course notes, 2006), the value of Young's modulus E^{ref} is set equal to 647,000 psf. For the Plaxis nonlinear Hardening Soil (HS) model, the parameters $(E^{ref})_{50}$ and $(E^{ref})_{oed}$ are set equal to 647,000 psf. Additional HS parameters assigned are reference stress for stiffness, p_{ref}, equal to 2,116 psf, failure ratio $R_f = 0.9$ and the exponent $m = 0.5$. For unload reload HS parameters, $(E^{ref})_{ur}$ is set equal to 3 times $(E^{ref})_{50}$ and ν_{ur} equals 0.3.

Standard Penetration Test and cone test results in the lower Beach sand layer (i.e., El -35 to -47) indicate an average value of 14 blows per ft depth for 60 percent of free-fall energy and corrected to an effective overburden pressure of 1 ton/ft^2 [i.e., $(N_1)_{60} = 14$]. For a fine sand with an average value of $(N_1)_{60} = 14$, the relative density (D_r) is 46 percent by Skemption's (1986) correlation. A $(N_1)_{60} = 14$ results in a value of 32 deg (approximately) for the effective angle of internal friction by the Peck, Hanson and Thornburn (1974) correlation. For loose sand with D_r equal to 46 percent and using the correlations of Lengkeek and Vermeer and Shanz (cited in Brinkgreve, 2005, as well as in Plaxis course notes, 2006), the value of Young's modulus E^{ref} is set equal to 438,900 psf. . For the Plaxis nonlinear Hardening Soil (HS) model, the parameters $(E^{ref})_{50}$ and $(E^{ref})_{oed}$ are set equal to 438,900 psf. Additional HS parameters assigned are reference

stress for stiffness, p_{ref} , equal to 2,116 psf, failure ratio $R_f = 0.9$ and the exponent $m = 0.5$. For unload reload HS parameters, $(E^{ref})_{ur}$ is set equal to 3 times $(E^{ref})_{50}$ and ν_{ur} equals 0.3.

Bay Sound clay: A smaller data base of strength and stiffness tests results are available for London Canal Bay Sound clay, as compared with 17th Street canal Bay Sound clay. After a careful assessment of the test data on the Bay Sound clay at London canal, a value of undrained shear strength (S_u) of 779 psf is assigned. This is the same Su value assigned for the 17th Street canal Bay Sound clay, which factored into the strength assessment made for this cross section. A total unit weight of 102 pcf is assigned to the Bay Sound clay soil cluster. Stress-strain data for 17th Street canal Bay Sound clay triaxial test specimens leads to the assignment of an average value for Young's modulus, E^{ref}, expressed in terms of (E^{ref}) normalized by S_u and set equal to 68 (Tables 9-2 and 9-3). This same value for Young's modulus is assigned to the London canal Bay Sound clay.

For the Plaxis nonlinear Hardening Soil (HS) model, the parameters $(E^{ref})_{50}$ and $(E^{ref})_{oed}$ are set equal to $[E^{ref}/S_u$ times $S_u]$. Additional HS parameters assigned are reference stress for stiffness, p_{ref} , equal to 2,116 psf, failure ratio $R_f = 0.9$ and the exponent $m = 1.0$. For unload reload HS parameters, $(E^{ref})_{ur}$ is set equal to 3 times $(E^{ref})_{50}$ and ν_{ur} equals 0.3.

Hydraulic Conductivity: Values for the hydraulic conductivity of the four soil types are listed in Tables 9-2 and 9-3. The hydraulic conductivity value assigned to the Beach sand is based on field pump tests while all other values are based on typical values found in the technical literature for soils of similar engineering material characteristics. For the Marsh material, data from Weber (1969) and others leads to the assignment of hydraulic conductivity values of 1.2×10^{-2} ft/hr for regions of lower overburden pressure and 1.2×10^{-4} ft/hr for regions of higher overburden, such as below the Levee. For canal bottom silts, a hydraulic conductivity value equal to 1.2×10^{-2} ft/hr is assigned.

Flood Wall: The flood wall comprises an exposed reinforced concrete I-wall, a reinforced concrete cap and Casteel CZ101 cold formed sheet pile. The 12-inch thick reinforced concrete I-wall extends from the top of protected levee (El 4.3) to El 13. At Station 14+00, the sheet pile tip is at El -17.4. The top of the Beach sand to Marsh interface is at El -12.9. Consequently, the sheet pile extends 4.5 ft into the Beach sand. The upper reach of pile is encased in a two-foot thick reinforced concrete cap extending below the surface of the protected side of the levee. Linear elastic material response was assumed in the complete SSI analysis. Engineering properties for the I-wall, cap and sheet pile are summarized in Table 9-4 for the zero thickness plate elements used in the finite element model.

Table 9-4 Material Characterization for the Flood Wall				
Identification	EA	EI	weight	ν
	[lb/ft]	[lbft²/ft]	[lb/ft/ft]	[-]
Reinforced Concrete I-wall	4.32E8	3.6E7	150.00	0.20
Reinforced Concrete Cap	8.64E8	2.88E8	80.00	0.20
Sheet Pile (Hoesch 12)	9.77E7	1.31E7	9.15	0.30

Complete Soil-Structure Interaction Analysis

Introduction: Two sets of complete SSI analyses of the Figure 9-1 2-D cross section of Station 14+00 at London Canal are conducted in staged analysis using Plaxis. Both sets evaluate the response of the Station 14+00 cross-section to flood loading starting at canal water El 1.0 on through a series of incremental 0.6 to 3.4 feet raises in canal elevation. Table 9-5 summarizes the calculation phases of the first analysis set using average modulus values for the four soil types. More than 17 phases of calculations are used in this complete SSI analysis to a maximum canal water El 8. Table 9-6 summarizes the calculation phases of the second analysis set using stiff modulus values for the Levee clay and the Marsh on the protected side of the I-wall. More than 22 phases of calculations are used in this parametric SSI analysis to a maximum canal water El 8.

**Table 9-5
Calculation Phases of the Nonlinear Finite Element Analysis Using Average Modulus Values**

Phase	PhaseNo.	Calculation type	Load input
Initial phase	0	-	-
Place Wall & Interface	1	Plastic analysis	Staged construction
Gravity (1.0)	2	Plastic analysis	Total multipliers
Water Table El -17.4	3	Plastic analysis	Staged construction
Water Table El +1	4	Plastic analysis	Staged construction
Canal Water El +4.4	5	Plastic analysis	Staged construction
Crack to El -3	6	Plastic analysis	Staged construction
Crack to El -5	7	Plastic analysis	Staged construction
Canal Water El +5	8	Plastic analysis	Staged construction
Crack to El -6	9	Plastic analysis	Staged construction
Canal Water El +6	10	Plastic analysis	Staged construction
Crack to El -7	11	Plastic analysis	Staged construction
Crack to El -10	12	Plastic analysis	Staged construction
Canal Water El +6, Crack to El -12.9, linear phreatic surface	13	Plastic analysis	Staged construction
Canal Water El +7, linear phreatic surface	14	Plastic analysis	Staged construction
Canal Water El +7.5, linear phreatic surface	15	Plastic analysis	Staged construction
Canal Water El +8, linear phreatic surface	16	Plastic analysis	Staged construction
Phi-C Reductions	17[+]	Phi/c reduction	Incremental multipliers

Table 9-6
Calculation Phases of the Nonlinear Finite Element Analysis Using Stiff Modulus Values for the Levee Clay and the Marsh on the Protected Side

Phase	PhaseNo.	Calculation type	Load input
Initial phase	0	-	-
Place Wall & Interface	1	Plastic analysis	Staged construction
Gravity (1.0)	2	Plastic analysis	Total multipliers
Water Table El -17.4	3	Plastic analysis	Staged construction
Water Table El +1	4	Plastic analysis	Staged construction
Canal Water El +4.4	5	Plastic analysis	Staged construction
Crack to El -2	6	Plastic analysis	Staged construction
Crack to El -3	7	Plastic analysis	Staged construction
Canal Water El +5	8	Plastic analysis	Staged construction
Crack to El -4	9	Plastic analysis	Staged construction
Canal Water El +6	10	Plastic analysis	Staged construction
Crack to El -5	11	Plastic analysis	Staged construction
Crack to El -6	12	Plastic analysis	Staged construction
Canal Water El +7	13	Plastic analysis	Staged construction
Canal Water El +8	14	Plastic analysis	Staged construction
Crack to El -7	15	Plastic analysis	Staged construction
Canal Water El +8, Crack to El -12.9, linear phreatic surface	16	Plastic analysis	Staged construction
Canal Water El +4.4, Crack to El -12.9, Linear phreatic surface	17	Plastic analysis	Staged construction
Canal Water El +5, Crack to El -12.9, Linear phreatic surface	18	Plastic analysis	Staged construction
Canal Water El +6, Crack to El -12.9, Linear phreatic surface	19	Plastic analysis	Staged construction
Canal Water El +7, Crack to El -12.9, Linear phreatic surface	20	Plastic analysis	Staged construction
Canal Water El +7.5, Crack to El -12.9, Linear phreatic surface	21	Plastic analysis	Staged construction
Phi-C Reductions	22[+]	Phi/c reduction	Incremental multipliers

Loading phases 0 through 4 are used in both sets of complete SSI analyses to establish the initial total stress state condition existing prior to flooding. Loading phase 4 concludes with canal water at El 1, a steady state water elevation in the canal.

Loading phases 5 through 16 (Table 9-5) are used in the first analysis set with average modulus values for the four soil types to perform an incremental raise in the canal water to El 8, modeling the flood loading of the levee/I-wall system and the introduction of a crack along the canal-side face of the sheet pile in the Levee clay and in the Marsh/peat (eventually to the top of the Beach sand at El -12.9). The last of the loading phases (i.e., 17[+]) are used to compute the reserve capacity of the levee/I-wall system for different canal water elevations. This reserve capacity is expressed in terms of a Factor of Safety and is computed in a series of Plaxis phi/c reduction loading phases.

Loading phases 5 through 16 (Table 9-6) are used in the second analysis set with stiff modulus values assigned to the Levee clay and the Marsh on the protected side of the I-wall to perform an incremental raise in the canal water to El 8, modeling the flood loading of the levee/I-wall system and the introduction of a crack along the canal-side face of the sheet pile in the Levee clay and in the Marsh/peat (eventually to the top of the Beach sand at El -12.9). Loading phases 17 through 21 provide a data base used to determine the Factor of Safety for canal water El 8 and with a crack on the canal side of the sheet pile wall that extends from the top of the levee (El 4.4) to the top of the sand layer (El -12.9). The last of the loading phases (i.e., 22$^+$) are used to compute the reserve capacity of the levee/I-wall system for different canal water elevations by phi/c reduction.

Initial steady state condition for canal water at EL 1: Loading phases 0 through 4 are used in the complete SSI analysis to establish the initial total stress state within the finite element mesh with a steady state canal water elevation at El 1. Gravity loading is applied in a single increment, followed by an incremental rising of the water table. In the Beach sand layer, the water table is established at El -8.4 on the right-hand, protected side of the mesh, at x-coordinate 407, by analysis phase 4 and is maintained at this elevation in all subsequent computation phases. Load input for gravity loading is specified in Plaxis by means of the total multiplier method and changes in water table are accomplished by staged construction and by steady state seepage analysis, unless stated otherwise.

The initial steady-state, total stress condition for the usual canal water elevation of 1 is established by using the average stiffness modulus values given in Table 9-2 in the Mohr-Coulomb soil model for loading phases 0 through 4 for both sets of complete SSI analyses. The results from the IPET Task 7 slope stability analyses for this usual canal elevation indicate a stable cross-section with an ample Factor of Safety, i.e., above 1.5. Consequently, an important aspect of the total stress regime achieved within the Figure 9-2 finite element mesh is that the mobilized shear stress at the strain integration points within the finite elements contained in the soil clusters shown in this figure be less than the shear strength of the soil. The resulting computed fraction of mobilized shear strength (referred to as relative shear stress in Plaxis output) from the resulting initial total stress condition is shown in Figure 9-3. The fraction of mobilized shear strength is less than or equal to 0.9 at the stress integration points for the four soil types.
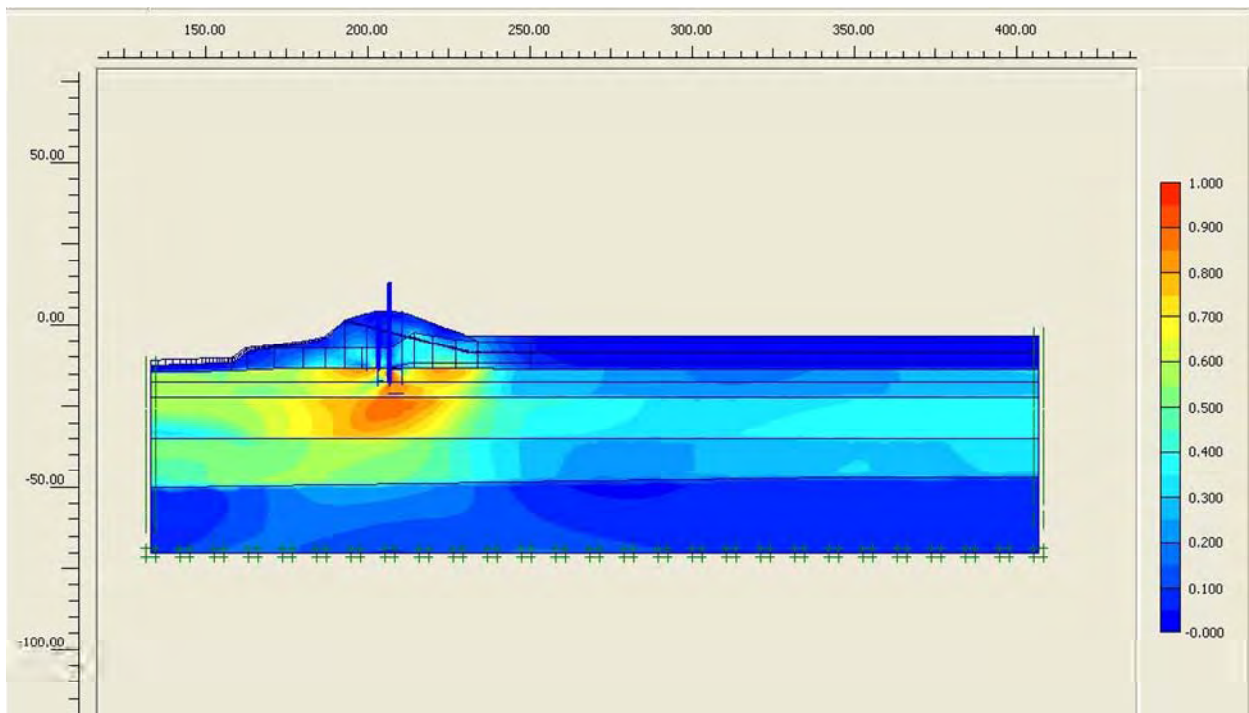
Figure 9-3. Fraction of Mobilized Shear Strength for Canal El 1

Flood loading: Modeling of flood loading commenced in the complete SSI analysis after the total initial stress state is established within the finite element mesh for steady state canal elevation (i.e., El 1). The hardening soil model with the Table 9-2 average stiffness material property values are assigned to each of the four types of soil regimes in the first complete SSI analysis set. Loading phases 5 through 16 (refer to Table 9-5) are used in the complete SSI analysis to perform an incremental raise in the canal water to El 8, modeling the flood loading of the levee/I-wall system. Load input for changes in canal water elevation is specified by staged construction. For canal water up to and including El 6 and for crack depths terminating above the top of the Beach sand layer (at El -12.9) on the canal side of the new sheet pile wall/I-wall, a steady state seepage analysis is used to establish the pore water pressure regime within the Beach sand layer for loading phases 5 through 12 (Table 9-5).

The results from first SSI set of analysis using Table 9-2 average soil stiffness values indicates that cracking commenced when Canal water reached the top of the Levee (i.e., El 4.4). Crack initiation occurs at the top of the Levee clay, on the canal side (at El 4.4) of the sheet pile wall when the total horizontal stress in the clay in less than the value for hydrostatic water pressure (i.e., γ_{water} times depth below canal water surface). This first occurs at Table 9-5 loading phase 5. Comparisons of values for hydrostatic water pressure, generated by hand computation, with the total horizontal stresses computed in the compete SSI analysis indicates a crack will extend from El 4.4 down to EL -5 in the Levee clay by loading phase 7. The line designated $E_{average}$ in Figure 9-4 summaries the Table 9-5 depth of cracking phases of analysis versus Canal water elevation. Depth of cracking to the top of Beach sand (El -12.9) occurs at Canal water El 6. Additional analyses using Table 9-2 $E_{average}$ values are conducted for Canal water El's 7, 7.5 and 8 so as to establish the variation in Factor of Safety with Canal water elevation.
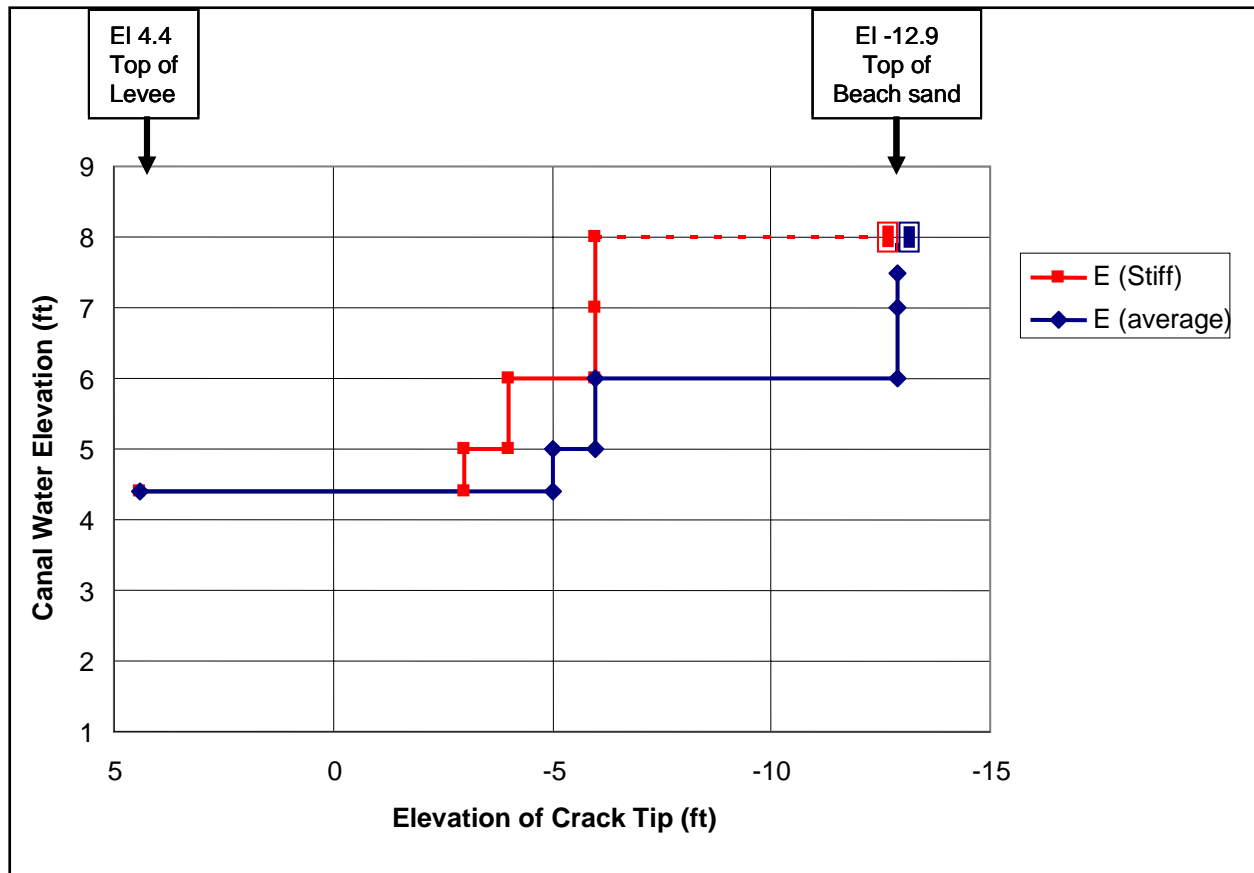
Figure 9-4. Elevation of Crack Tip Versus Canal Water Elevation

Due to numerical convergence issues, a linear phreatic surface assumption is used to establish the pore water pressures within the Beach sand for loading phases 13 through 16 (Table 9-5) of the first complete set of SSI analysis in which depth of cracking extends to the top of Beach sand layer (EL -12.9). This results in a less severe uplift pressure regime within the Beach sand below the toe of the protected side of the Levee as seen, for example, by comparing computed values and positions of equipotential lines for the Figure 9-5 steady state seepage results with the Figure 9-6 results for an analysis using a linear phreatic surface assumption. A linear phreatic surface assumption results in a less severe uplift pressure regime within the top of the Beach sand below and immediately beyond the toe of the protected side of the Levee. This results in a lower computed value for the Factor of Safety for the loading phases 13 through 16 in which this procedure is applied. Again, this compromise in accuracy is required in order to achieve convergence by Plaxis for these higher Canal water elevations with cracking to the top of the Beach sand.

Figure 9-5. Equipotential Lines from a Steady State Seepage Analysis for Canal Water El 6 and a Crack to the Top of Beach Sand (El -12.9) on the Canal Side of the New Sheet Pile Wall

Figure 9-6. Equipotential Lines Based on a Linear Phreatic Surface for Canal Water El 6 and a Crack to the Top of Beach Sand (El -12.9) on the Canal Side of the New Sheet Pile Wall

Factor of Safety: Figure 9-7 summarizes the computed Factor of Safety versus Canal water elevation for the Table 9-2 average stiffness material property values. As the canal elevation rises, the factor of safety decreases in these results labeled $E_{average}$ in this figure. Note that when the Canal water is raised to El 6, the Factor of Safety decreases from 2.5 to 1.84 with the crack tip progressing from El -6 to El -12.9 (i.e., the top of the Beach sand). With a crack tip at El -12.9 a new flow regime is established within the beach sand layer using a linear phreatic surface assumption as demonstrated in Figure 9-6 for Canal water El 6. (Note that for each subsequent rise in Canal water, a new linear phreatic surface is established based on the elevation of the Canal water in each analysis phase.) As the Canal water elevation rises to El 7, 7.5 and 8, the computed Factor of Safety decreases to 1.42, 1.25 and (approximately) 1. (Due to convergence issues in the phi/c reduction analysis, the Factor of Safety for Canal water EL 8 is established by extrapolation of the Figure 9-7 data.) Again, these computed Factors of Safety results labeled $E_{average}$ are greater than the actual values for these last four loading phases due to the linear phreatic surface assumption used within the Beach sand.
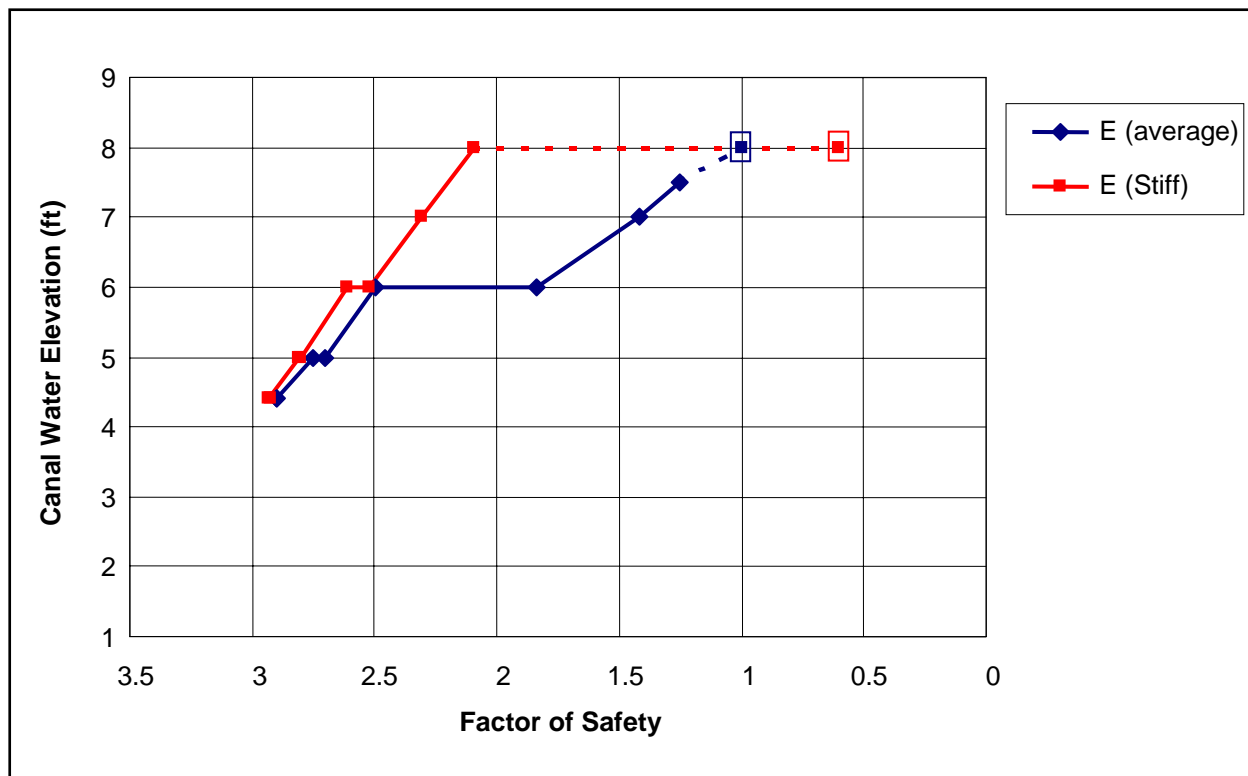
Figure 9-7. Factor of Safety Versus Canal Water Elevation

A second complete SSI analysis set with stiff modulus values (Table 9-3) assigned to the Levee clay and the Marsh on the protected side of the I-wall is conducted following the stages of loading listed in Table 9-6. Loading phases 5 through 16 (refer to Table 9-6) are used in the complete SSI analysis to perform an incremental raise in the canal water to El 8, modeling the flood loading of the Levee/I-wall system. Load input for changes in canal water elevation is specified by staged construction. For canal water up to and including El 7 in which crack depths terminate above the top of the Beach sand layer (at El -12.9) on the canal side of the new sheet pile wall/I-wall, a steady state seepage analysis is used to establish the pore water pressure regime within the Beach sand layer (i.e., loading phases 5 through 15 in Table 9-6).

The results from the second analysis set with stiff modulus values (Table 9-6) assigned to the Levee clay and the Marsh on the protected side of the I-wall indicates that cracking commenced when Canal water reached the top of the Levee (i.e., El 4.4). Crack initiation occurs at the top of the Levee clay, on the canal side (at El 4.4) of the sheet pile wall when the total horizontal stress in the clay in less than the value for hydrostatic water pressure (i.e., γ_{water} times depth below canal water surface). This first occurs at Table 9-6 loading phase 5. Comparisons of values for hydrostatic water pressure, generated by hand computation, with the total horizontal stresses computed in the compete SSI analysis indicates a crack will extend from El 4.4 down to EL -3 in the Levee clay by loading phase 7. The line designated E_{stiff} in Figure 9-4 summaries the Table 9-6 depth of cracking phases of analysis versus Canal water elevation. Depth of cracking to the top of Beach sand (El -12.9) occurs at Canal water El 8. Additional analyses using Table 9-3

Volume V The Performance – Levees and Floodwalls – Technical Appendix

E_{stiff} values are conducted for Canal water El's 4.4, 5, 6, 7 and 7.5 so as to establish the variation in Factor of Safety with Canal water elevation.

Computed results, summarized in Figure 9-4, shows that crack initiation occurs at the same Canal water EL of 4.4 in both sets of analyses. However, the progression of cracking is not as rapid in the E_{stiff} analyses set as it is for the $E_{average}$ analysis set. Additionally, the crack reached to top of Beach sand for a Canal water El 6 for the $E_{average}$ analysis set while the crack reached to top of Beach sand for a Canal water El 8 for the E_{stiff} analysis set; a difference of two feet.

Due to numerical convergence issues, a linear phreatic surface assumption is used to establish the pore water pressures within the Beach sand for loading phases 16 through 21 (Table 9-6) of the second analysis set with stiff modulus values assigned to the Levee clay and the Marsh on the protected side of the I-wall in which depth of cracking is specified to the top of Beach sand layer (EL -12.9). This results in a less severe uplift pressure regime within the Beach sand below the toe of the protected side of the Levee, as discussed previously. In turn, this results in a lower computed value for the Factor of Safety for the loading phases 16 through 21 in which this procedure is applied. Again, this compromise in accuracy is required in order to achieve convergence by Plaxis for these higher Canal water elevations with cracking to the top of the Beach sand.

Figure 9-7 also summarizes the computed Factors of Safety versus Canal water elevations for the Table 9-3 second analysis set with stiff modulus values assigned to the Levee clay and the Marsh on the protected side of the I-wall. These results are labeled E_{stiff} in this figure. This figure shows that as the canal elevation rises, the Factor of Safety decreases. Note that when the Canal water is raised to El 8, the Factor of Safety decreases from 2.09 to 0.6 (approximately) with the crack tip progressing from El -6 to El -12.9 (i.e., the top of the Beach sand). With a crack tip at El -12.9 a new flow regime is established within the beach sand layer and is computed using a linear phreatic surface assumption. The Plaxis phi/c reduction analysis for Canal water El 8, with depth of crack to EL -12.9 (i.e., top of beach sand), did not converge. In order to establish an estimate for the value of the Factor of Safety for this case, a series of phi/c reduction calculations for Canal water El's of 4.4, 5, 6, 7, and 7.5 are conducted with a fictitious depth of crack specified to EL -12.9 (i.e., top of beach sand) in each of these calculations (designated phase 17 through 21 in Table 9-6). These results are summarized in Figure 9-8. A Factor of Safety of 0.6 is estimated for Canal water El 8 by extrapolating the computed Factors of Safety results for these lower canal water elevations to canal water El 8. Additionally, this data shows that a Factor of Safety equal to unity occurs at Canal water El 7.7 (approximately). Again, recognize that these Figure 9-8 computed Factors of Safety results and the Figure 9-7 data point of Factor of Safety equal to 0.6 for Canal water El 8 on the E_{stiff} labeled curve, are greater than the actual values due to the linear phreatic surface assumption used within the Beach sand.
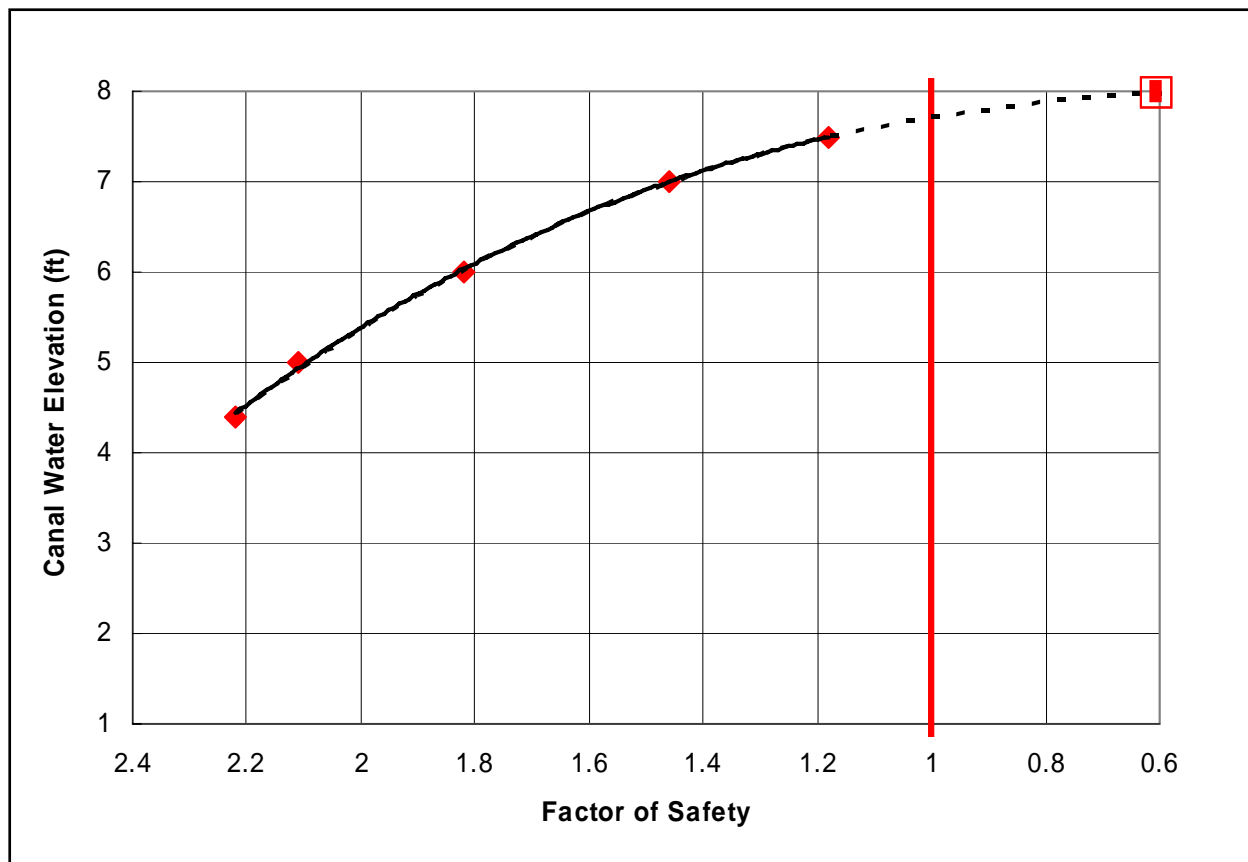
Figure 9-8. Factor of Safety Versus Canal Water Elevation, Computed With Crack to Top of Beach Sand El -12.9 and Using Stiff Modulus Values for the Levee Clay and Marsh on the Protected Side

Deformations: Figure 9-9 summarizes the computed deformations for the first analysis set with average modulus values, Canal El 6 and Crack to El -12.9 (i.e., top of Beach sand). Note the nodal deformations are magnified by a factor of 30 in order to show the deformed relative mesh relative to its position at canal water elevation of 1.0 (shown as a blue outline in this figure). The general trend is a rotational plowing of the protected side Levee clay by the I-wall/new sheet pile wall and a bulging of the Marsh beyond the toe of the Levee on the protected side. Recall that the computed Factor of Safety for this condition is 1.84 (for $E_{average}$ values).
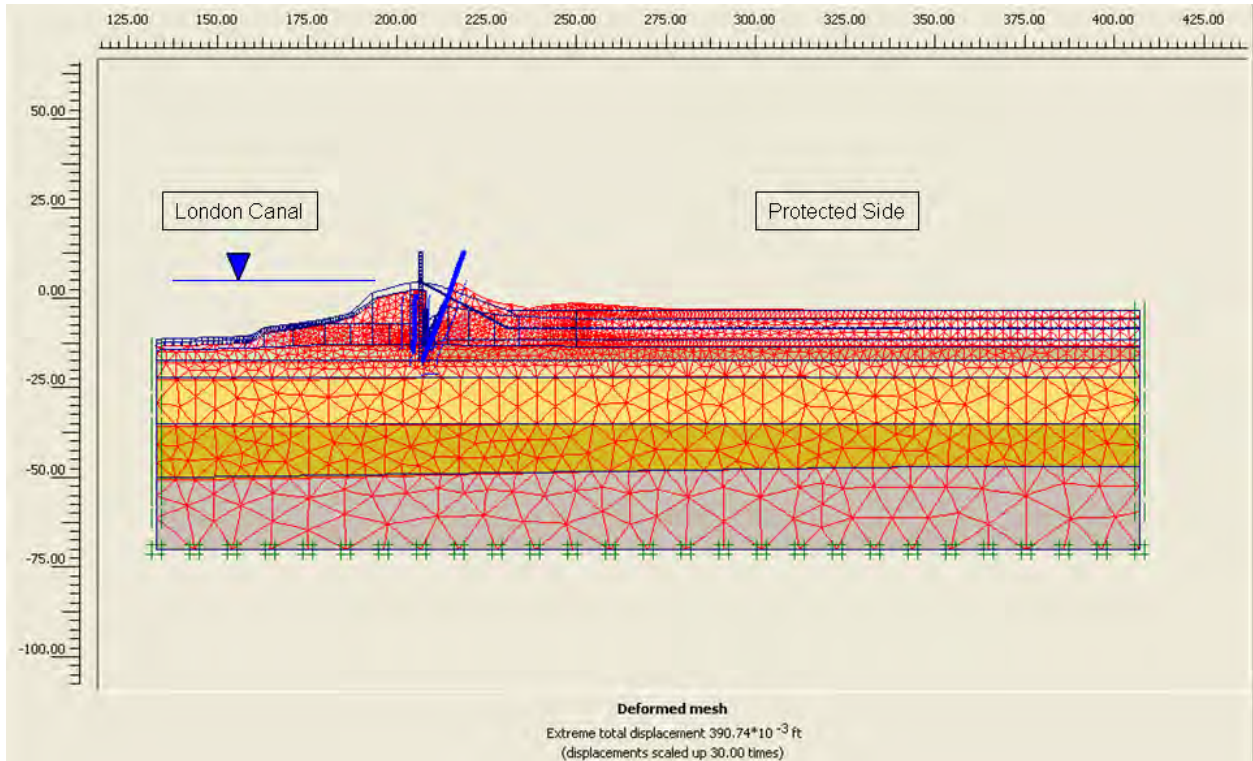
Figure 9-9. Deformed Mesh for Average Stiffness Values, Exaggerated by a Factor of 30, for Canal El 6 and Crack to El -12.9 (Note: Canal El not to scale in figure)

Figure 9-10 shows the horizontal displacements of the soil regions within the mesh, relative to their position at a canal water elevation of 1.0 for average stiffness values with Canal El 6 and Crack to El -12.9. This figure shows the horizontal deformations are concentrated within the protected region of the Levee and the Marsh immediately at the toe of the Levee on the protected side. The largest horizontal deformations are concentrated at the top of the Levee, on the protected side, approximately 0.29 ft (3½ inches).
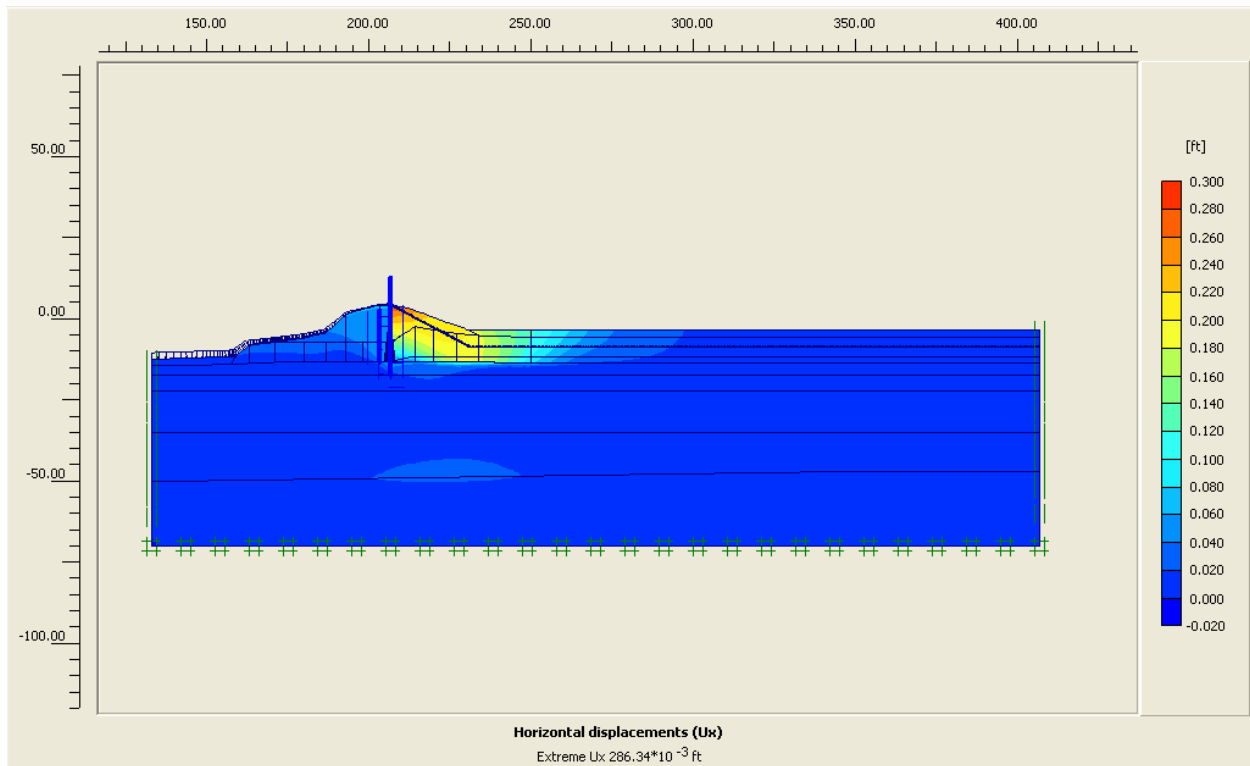
Figure 9-10. Horizontal Deformation Shadings for Average Stiffness Values with Canal El 6 and Crack to El -12.9 (Note: Canal El not to scale in figure)

Figure 9-11 shows the variation in horizontal displacements of the sheet pile versus canal water elevation for average stiffness values. These displacements are relative to their position at a canal water elevation of 1.0 for average stiffness values. This figure shows the rotational nature of the I-wall/sheet pile wall deformations, with the toe of the sheet pile "anchored" in the Beach sand.
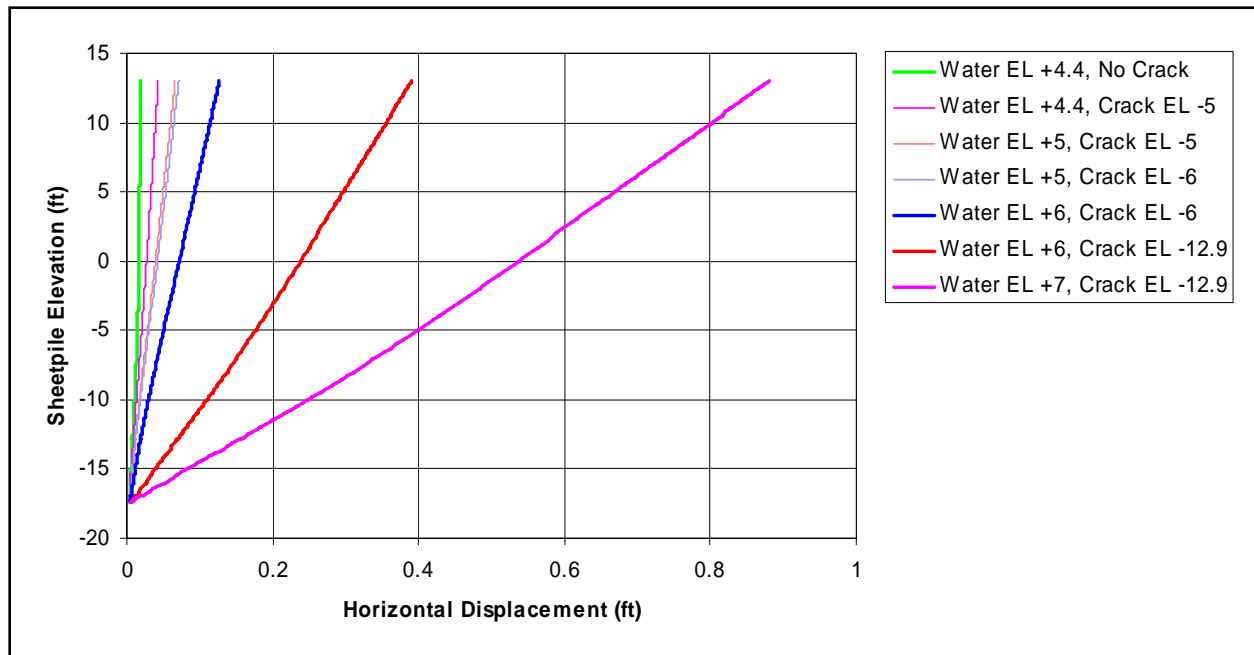
Figure 9-11. Horizontal Displacement of the I-Wall/Sheet Pile versus Canal Water El and Computed Using Average Stiffness Values

    Figure 9-12 shows the horizontal displacements of three points within the flood wall, relative to its position at a canal water elevation of 1.0 for average stiffness values. The points monitored through the analysis are at the top of the I-wall (El 13), at El 4.4 (top of Levee) and at the sheet pile tip (El -17.4). Recall for Canal water El's of 6 and higher, the crack never extends into the Beach sand layer, it terminates at the top of the Beach sand layer (i.e., El -12.9). Note that there is a significant increase in horizontal deformations of the I-wall/sheet pile wall when the crack extends to El -12.9 at Canal El 6. Results in this figure shows the Beach sand is providing enough lateral support to prevent the sheet pile tip form moving laterally, therefore the deformation of the sheet pile is mostly a rotation about the sheet pile tip. Maximum horizontal movement at the top of the I-wall is 0.88 ft (10 ½ inches) for Canal Water El 7.
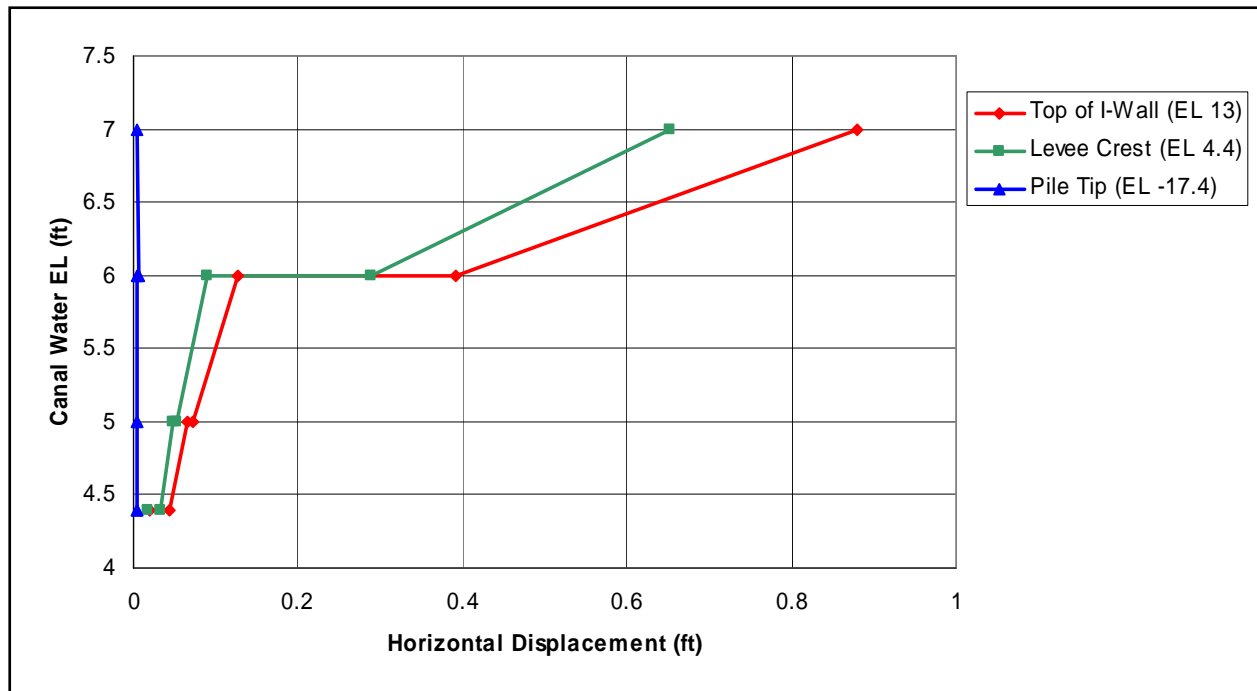
Figure 9-12. Horizontal Sheet Pile Deformations versus Canal Water El and Computed Using Average Stiffness Values

Figure 9-13 shows the vertical displacements of the soil regions within the mesh, relative to their position at a canal water elevation of 1.0 for average stiffness values with Canal El 6 and Crack to El -12.9. This figure shows the 0.07 ft (7/8 inch) uplift of the Marsh located beyond the toe of the Levee on the protected side.
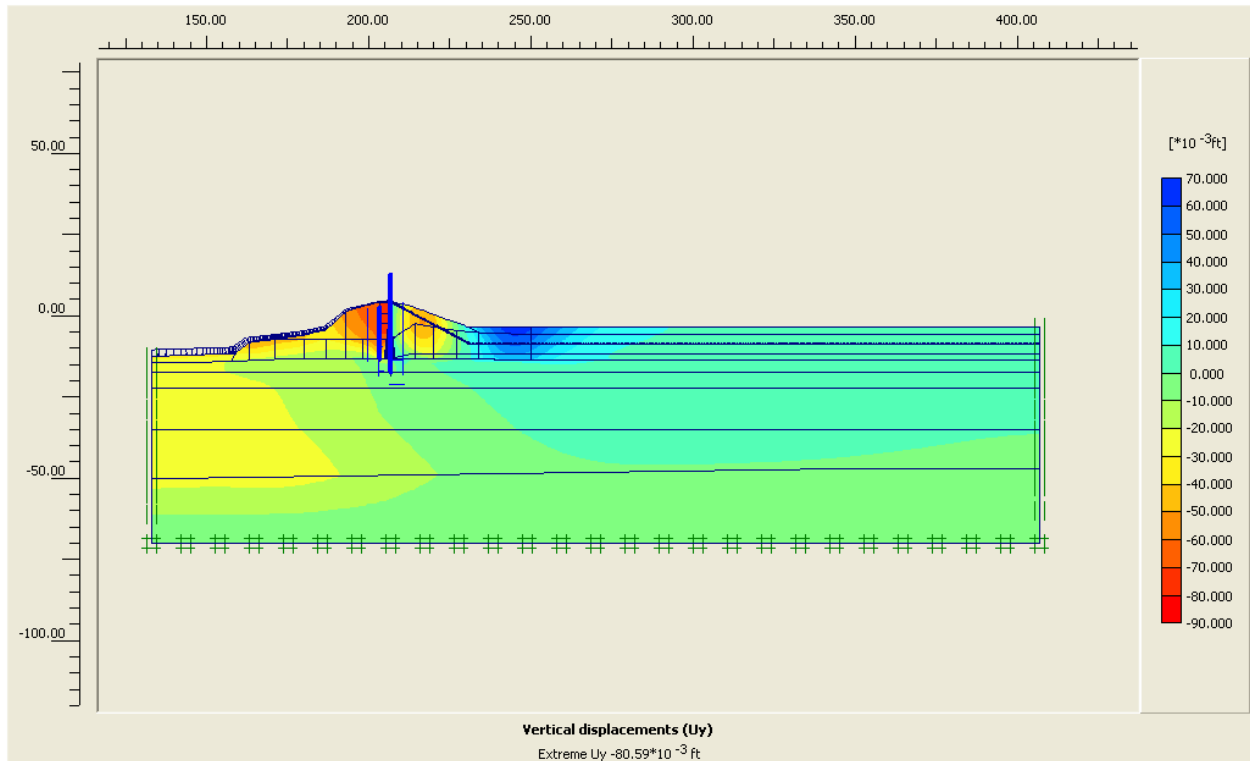
Figure 9-13. Vertical Deformation Shadings for Average Stiffness Values with Canal El 6 and Crack to El -12.9 (Note: Canal El not to scale in figure)

Figure 9-14 shows the variation in horizontal displacements of the sheet pile versus canal water elevation for the second analysis set with stiff modulus values assigned to the Levee clay and the Marsh on the protected side of the I-wall. These displacements are relative to their position at a canal water elevation of 1.0 for average stiffness values. This figure shows the rotational nature of the I-wall/sheet pile wall deformations, with the toe of the sheet pile "anchored" in the Beach sand. The shape of the deformed wall is the same for both sets of $E_{average}$ and E_{stiff} analyses. However the magnitude of the horizontal displacements in Figure 9-14 are less than the Figure 9-11 displacements for the first analysis set made using average stiffness values.
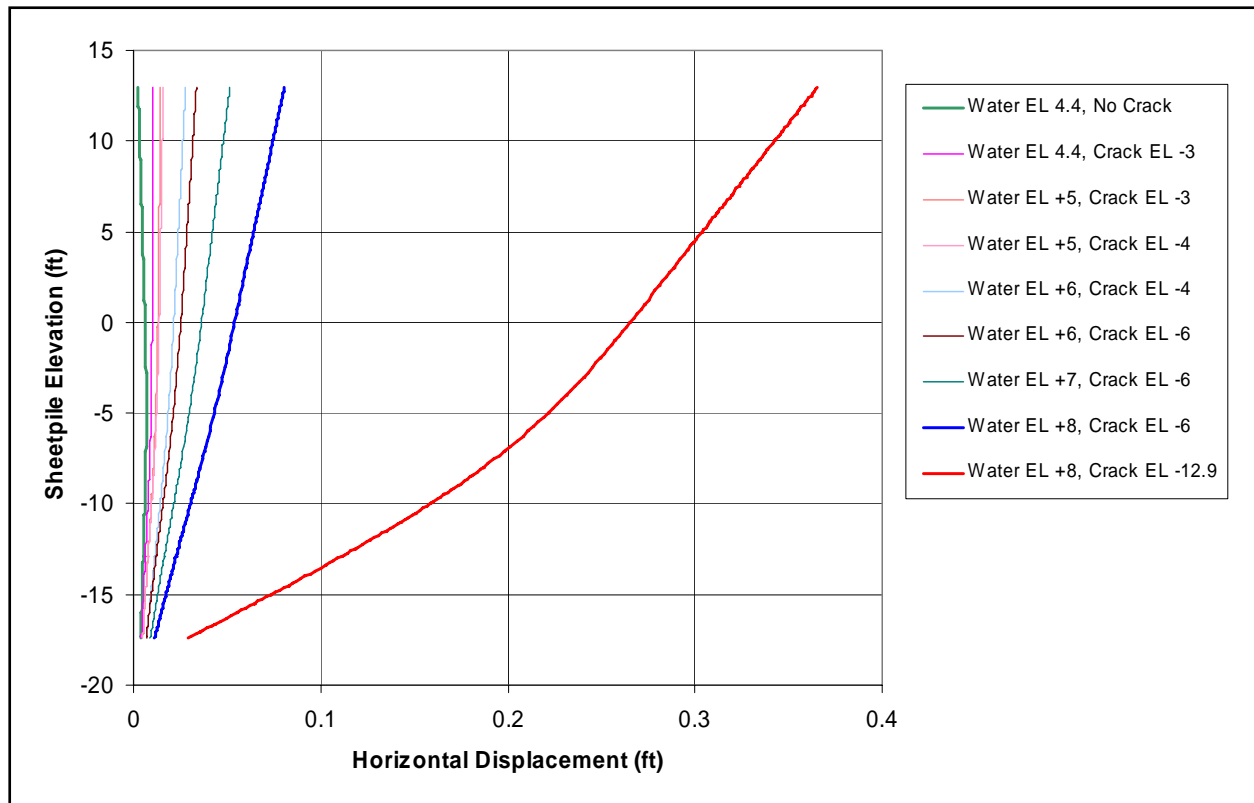
Figure 9-14. Horizontal Displacement of the Sheet Pile versus Canal Water El and Computed Using Stiff Modulus Values for the Levee Clay and Marsh on the Protected Side

Figure 9-15 shows the horizontal displacements of three points within the flood wall, relative to its position at a canal water elevation of 1.0 for average stiffness values. The points monitored through the analysis are at the top of the I-wall (El 13), at El 4.4 (top of Levee) and at the sheet pile tip (El -17.4). Recall for Canal water El 8, the crack never extends into the Beach sand layer, it terminates at the top of the Beach sand layer (i.e., El -12.9). Note that there is a significant increase in horizontal deformations of the I-wall/sheet pile wall when the crack extends to El -12.9 at Canal El 8. Results in this figure shows the Beach sand is providing enough lateral support to prevent the sheet pile tip form moving laterally, therefore the deformation of the sheet pile is mostly a rotation about the sheet pile tip for both sets of $E_{average}$ and E_{stiff} analyses. Maximum horizontal movement at the top of the I-wall is 0.36 ft (4 1/3 inches) for this analysis with Canal water El 8 and using E_{stiff} values. Contract this result with the Figure 9-12 maximum displacement at the top of I-wall is 0.88 ft (10 ½ inches) for Canal Water El 7 computed using average stiffness values. For each canal water elevation, the displacements in Figure 9-15 are less than half the Figure 9-12 displacements calculated for the first analysis set using average stiffness values.
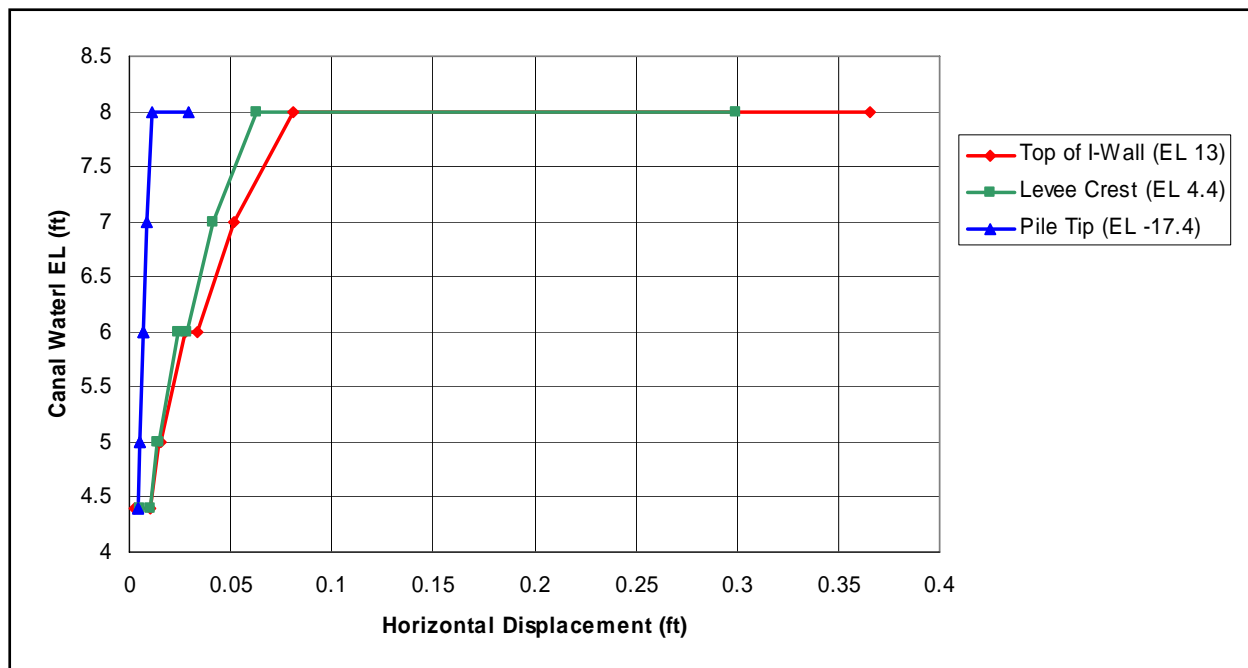
Figure 9-15. Horizontal Sheet Pile Deformations versus Canal Water El and Computed Using Stiff Modulus Values for the Levee Clay and Marsh on the Protected Side

Failure Mechanism: Figures 9-16 and 9-17 show that for the analysis using average stiffness values with Canal El 6 and Crack to El -12.9, there is a loss of effective vertical stress at the top of the Beach sand layer within the region beyond the toe of the Levee. This results in zero shear strength along the top of the Beach sand layer as demonstrated in the Figure 9-18 fraction of mobilized shear strength being equal to unity within this Beach sand region. Figure 9-19 shows that this, in turn, results in the beginning of the development of a mechanism as demonstrated by the concentration of large shear strains within this region for Canal water El 6 and crack to El -12.9. Figures 9-20 and 9-21show the development of the ultimate mechanism (i.e., the failure mechanism) computed in a phi/c reduction analysis for Canal water El 6 and crack to El -12.9, with the computed Factor of Safety of 1.84. Note the vertical "bulging" in the Marsh beyond the toe of the Levee. The reaches of large shear strain shown in Figure 9-21 shows the compete failure wedge will form along the top of the Beach sand layer and "day light" beyond the toe of the Levee. All subsequent phi/c computations for higher canal water elevations and for the E_{stiff} analyses show this same Figures 9-20 and 9-21 failure mechanism to form.
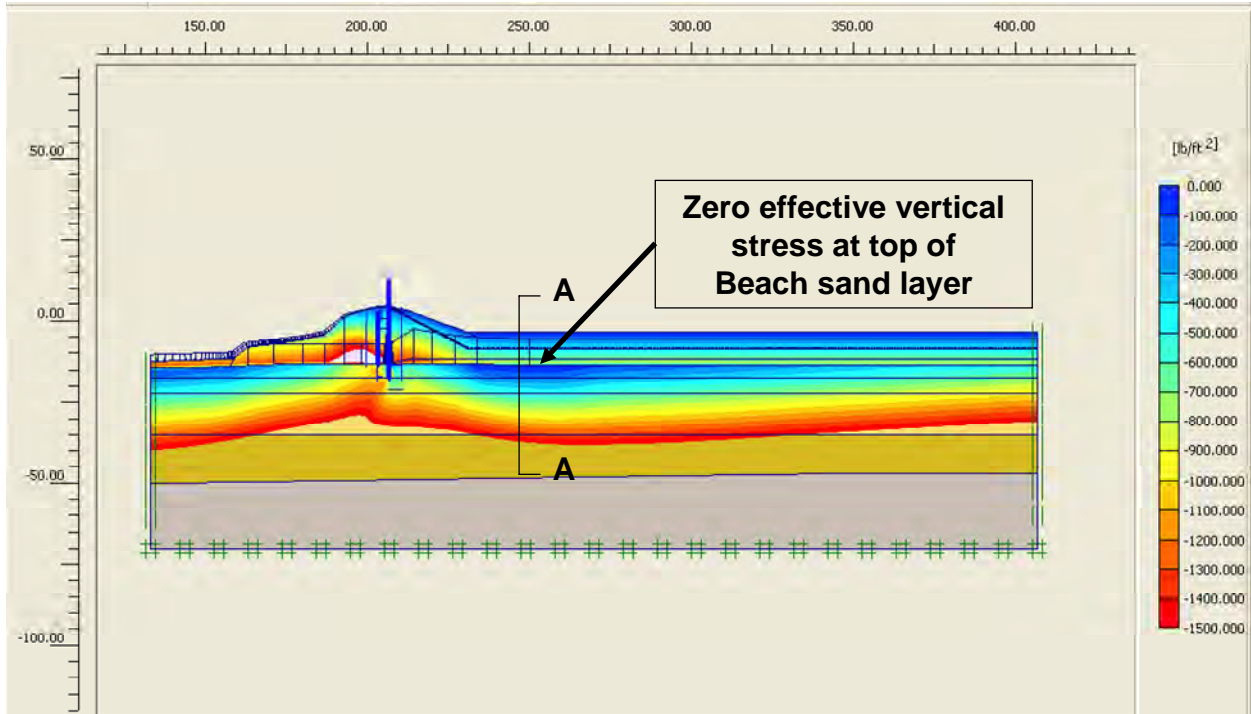
Figure 9-16. Shadings of Total Vertical Stress in the Levee Clay and Marsh and Effective Vertical Stress in the Beach Sand for the Analysis Using Average Stiffness Values with Canal El 6 and Crack to El -12.9

This is a preliminary report subject to revision; it does not contain final conclusions of the United States Army Corps of Engineers.
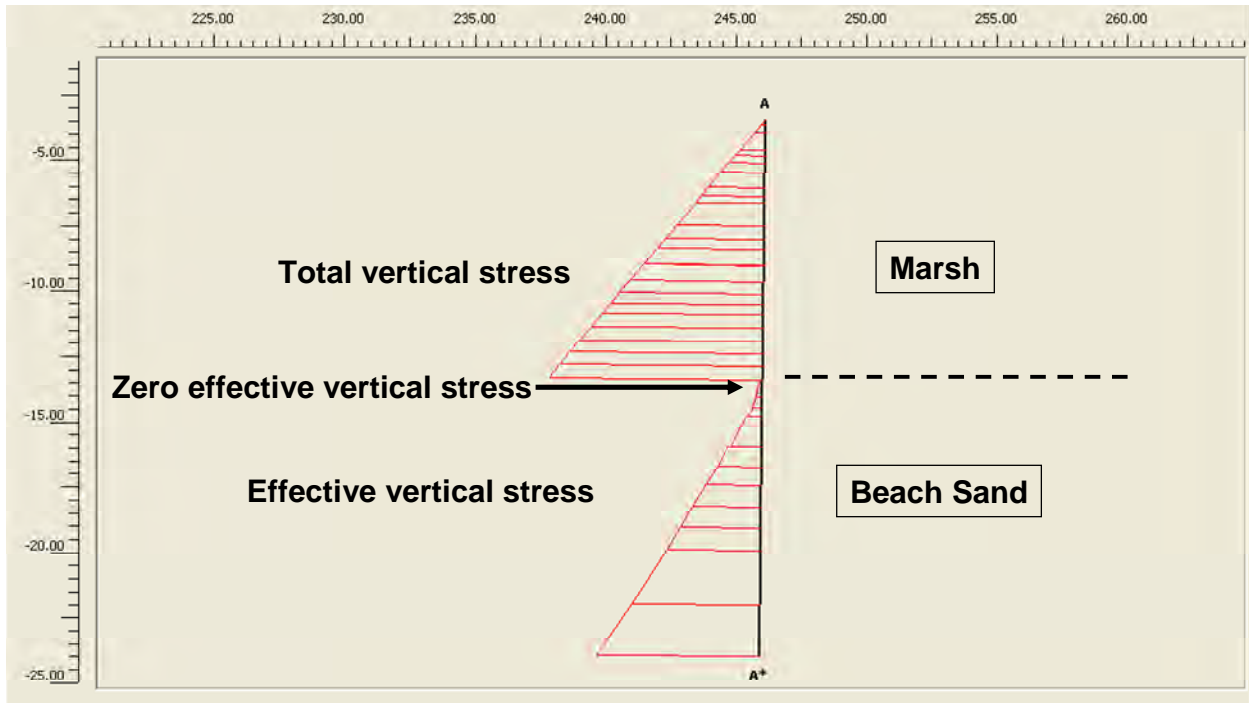
Figure 9-17. Vertical Section A-A Near the Toe of the Levee Showing Total Vertical Stress in the Marsh and Effective Vertical Stress in the Beach Sand for the Analysis Using Average Stiffness Values with Canal El 6 and Crack to El -12.9

Figure 9-18. Fraction of Mobilized Shear Strength for the Analysis Using Average Stiffness Values with Canal El 6 and Crack to El -12.9

Volume V The Performance – Levees and Floodwalls – Technical Appendix

V-9-27

This is a preliminary report subject to revision; it does not contain final conclusions of the United States Army Corps of Engineers.
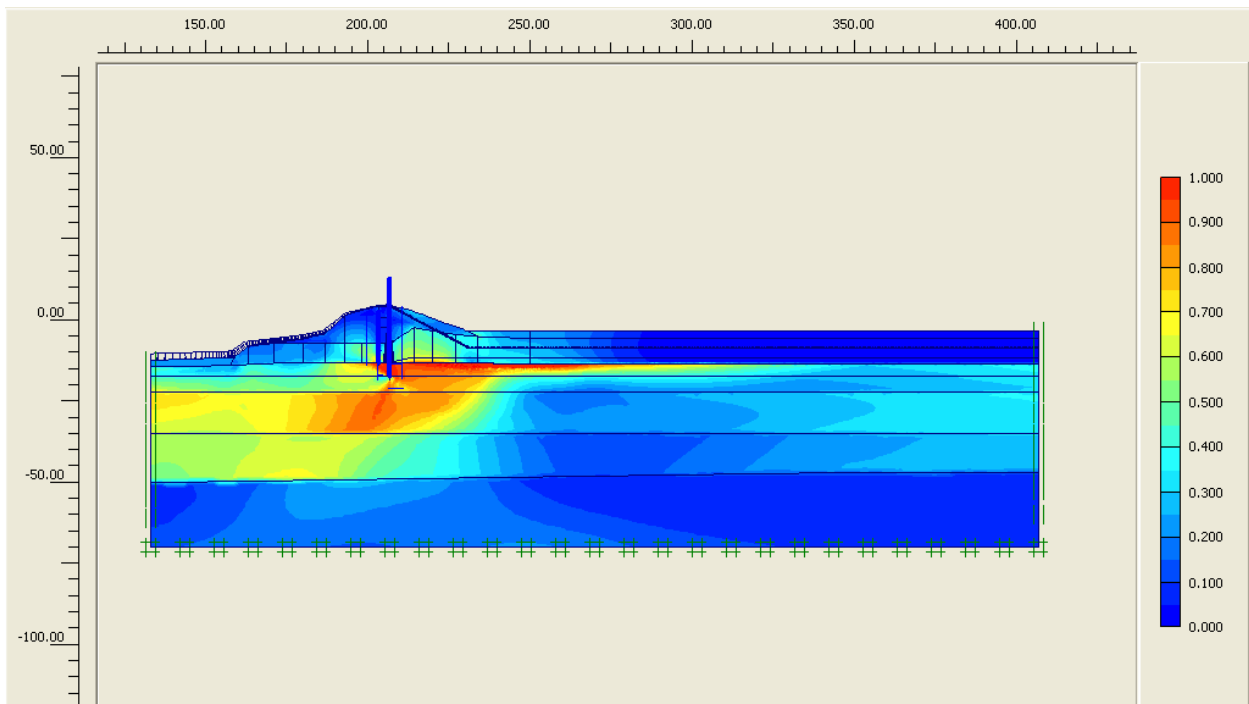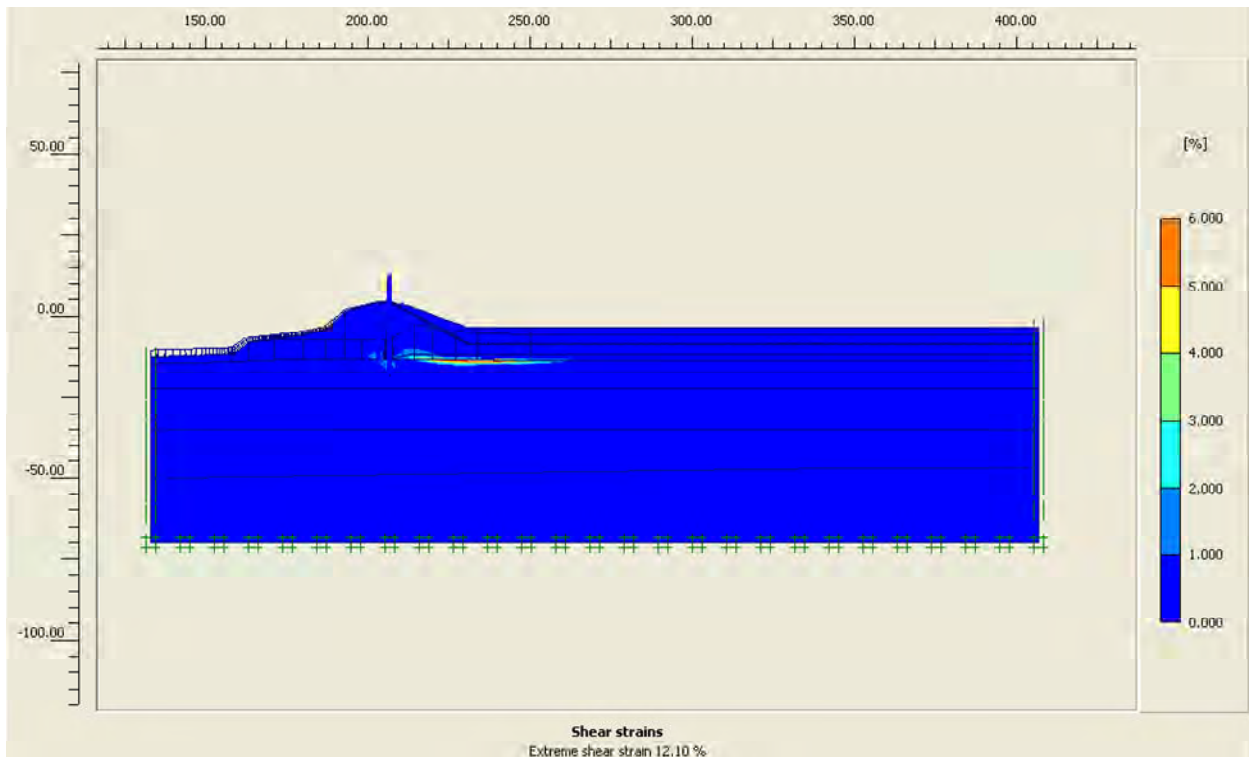
Figure 9-19. Reach of Large Shear Strains for the Analysis Using Average Stiffness Values with Canal El 6 and Crack to El -12.9
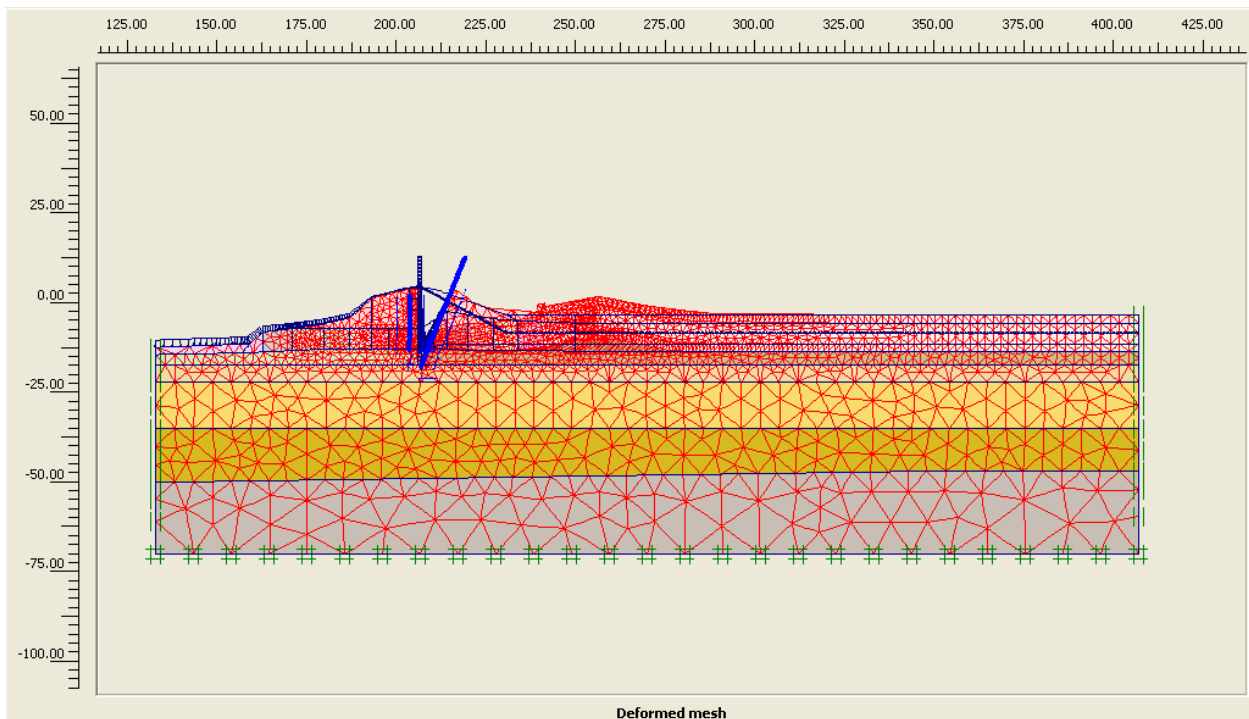
Figure 9-20. Ultimate Mechanism from Phi/C Reduction for the Analysis Using Average Stiffness Values with Canal El 6 and Crack to El -12.9
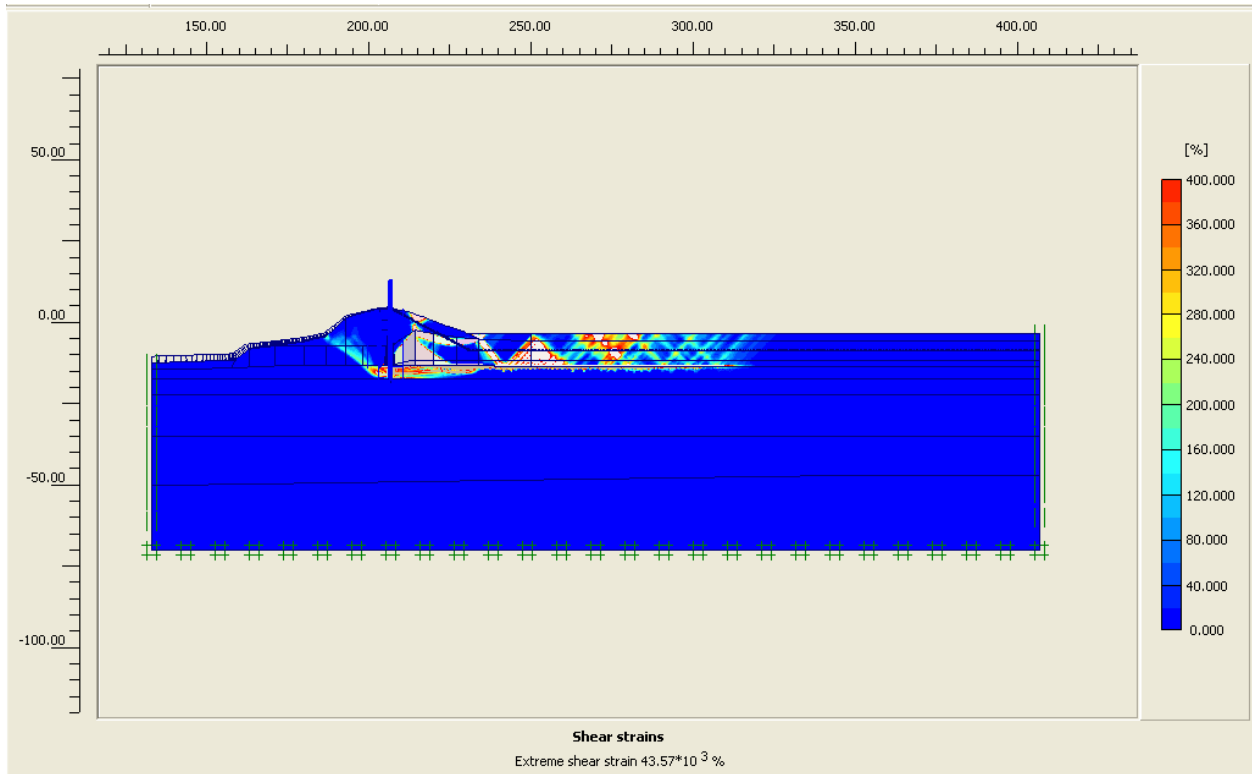
Figure 9-21. Reach of Large Shear Strains from the Phi/C Reduction Analysis Using Average Stiffness
Values with Canal El 6 and Crack to El -12.9

Soil-Structure Interaction Analysis of the London Avenue Canal South Breach (East Flood Wall at London at Station 53+00)

Introduction

This section describes a complete soil-structure interaction (SSI) analysis of an existing flood wall within London Canal using the PC-based finite element program Plaxis (2004). A two-dimensional cross section within the section of the East side, at Station 53+00 of the London Canal that failed during hurricane Katrina is the subject of this evaluation. Results of a complete nonlinear finite element analysis of a two dimensional (2-D) cross section during simulated flood loading is described.

Plaxis is a complete nonlinear finite element package geared towards geotechnical engineering applications that include soil-structure interaction issues such as those that occur between a sheet pile and the soils in which it is embedded. It allows for the nonlinear response of soils to flood loading as occurred at the London canal with an I-wall along the center line of the soil-founded levee. The Plaxis PC-based software comprise a visual pre-processor, a nonlinear finite element engineering analysis module, and a visual post-processor. All software components are combined into a single package. Computed results include not only soil stresses, but also structural (e.g. sheet pile and I-wall) bending moments, interaction stresses between sheet piling and the soil in which it is embedded, as well as soil (e.g., levee) and structural deformations. A complete SSI analysis is considered to provide the most reasonable estimate for deformation response of a soil-structural system involving nonlinear material behavior. In a complete SSI analysis loads exerted by the canal water acting on the soils of the levee and then onto the sheet pile wall (below the I-wall) by means of a load transfer through the levee and foundation soils are generated automatically during the analysis (i.e., predetermined earth pressure force distributions between the soil and the embedded sheet pile are not specified).

Section Analyzed

The two-dimensional cross section within the failed section of the East side of the London Canal at Station 53+00 analyzed for flood loading is shown in Figure 9-22.[2] The 2-D section is 307-ft wide and extends from x-coordinate equal to -137 ft to the center line of the canal at x equal to 170 ft. The top of the I-wall is at El 13 and sheet pile tip is at EL -17.4. An older sheet pile is embedded in the levee on the canal side of the I-wall, approximately 3 feet in front of the I-wall (centerline-to-centerline). This old sheet pile used to be part of a shorter flood wall that was removed when the existing I-wall was installed. The old sheet piling extends from the ground surface to within the Beach sand layer, El -16.9.

The crest of the earthen levee on the protected (East) side of the I-wall is at El 3.6, with a crest width of approximately 4 feet. Note the I-wall extends above the crest of the soil founded levee. The protected side of the levee has a 1 on 3 and 1/3 side slope to El 1.1 with a 1 on 3 side slope to El -4.1. The protected side ground surface is assigned El -3.4 for this section. The crest

---

[2] All elevations cited are according to NAD88.

of the earthen levee on the canal side of the I-wall is also at El 3.6. There is a 2-ft wide crest on the canal side of the I-wall at El 3.6. The upper 2.6 feet of the levee on the canal side of the I-wall is above normal canal water elevation. From El 3.6 to EL 1.8, the levee face has a 1 on 5 side slope. Between El 1.8 and El -11.9 the face of the levee has an approximately 1 on 1 and ¾ side slope. From EL -6.4 to El -10.4 the peat is exposed to the canal water. The deepest point in the canal is at canal center line (i.e., x = 170 ft in Figure 9-22), with a top of Canal bottom silt at El -11.9 at this location.
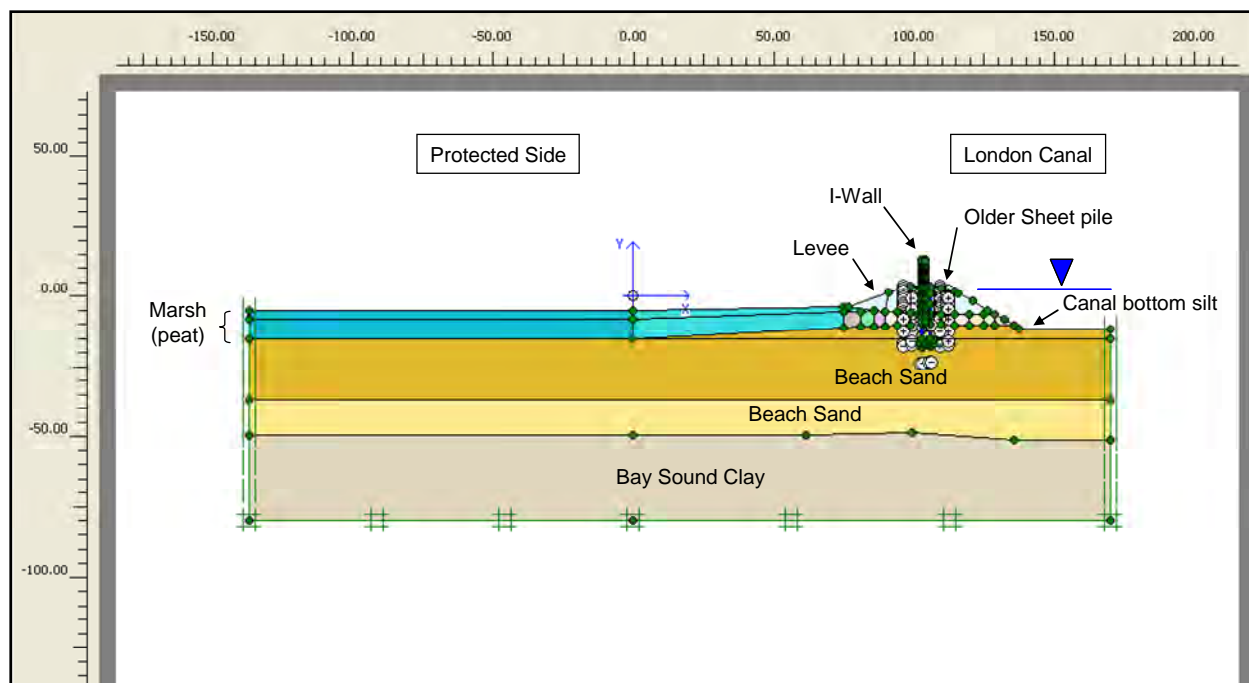
Figure 9-22. Two-Dimensional Cross Section Model used in the Complete SSI Analysis of Station 53+00 at London Canal – East Side

Proceeding from top to bottom in Figure 9-22, this cross section contains layers of Levee fill (clay), marsh (also referred to as peat), Beach sand, and Bay Sound clay. There is no Lacustrine clay contained within this cross section. The top of I-wall is at El 13 and the base of the Figure 9-22 cross-section is assigned to El -80. El -80 corresponds (approximately) to the bottom of the Bay Sound clay at Station 53+00. The soil layering is consistent with that used in the slope stability evaluations made for this cross section. The regions of uniform color in Figure 9-22 reflect the Plaxis "soil clusters" used to define the mesh and to assign soil regions with common properties.

Finite Element Mesh

Key Plaxis modeling features used in the plane strain analysis of London include the use of 15-node triangular elements to model the soil, plates (i.e., special beam elements) to model the bending of the newer I-wall/sheet pile wall as well as the older sheet pile wall, and interface elements to model soil-structure interaction between the sheet pile wall and the adjacent soil elements. A total of 31,272 nodes and 3,378 elements, containing 45,336 stress points, are used

to define the Figure 9-23 mesh. Details regarding the quantity of each of the three types of plane strain elements used in the finite element model as well as select characteristics of each type of element are summarized in Table 9-7.
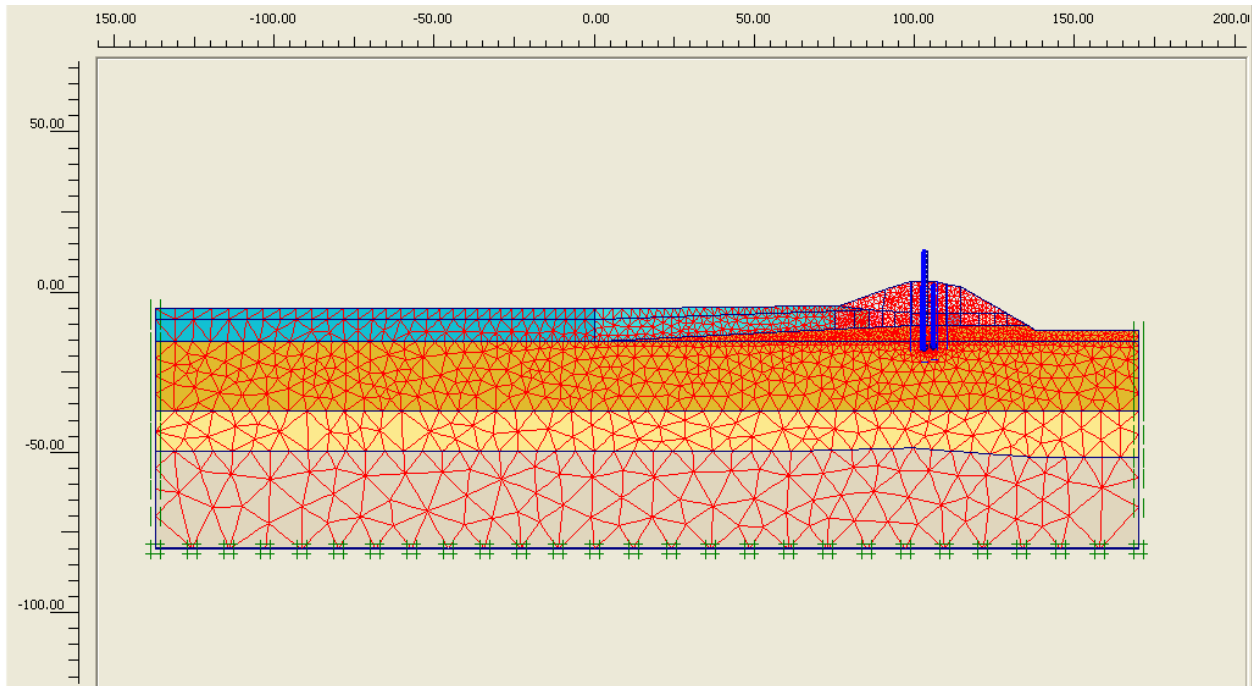
Figure 9-23. Finite Element Mesh used in the Complete SSI Analysis of Station 53+00 at London Canal – East Side

Table 9-7 Mesh Data Summary of Elements Used			
Type	**Type of element**	**Type of integration**	**Total no.**
Soil	15-Noded	12-point Gauss	3778
Plate	5-node line	4-point Gauss	75
Interface	5-node line	4-point Newton-Cotes	148

A zero horizontal displacement is specified along the left and right hand side vertical boundaries of the Figure 9-23 finite element mesh. However, these nodes are free to displace in the vertical direction. Along the bottom boundary of the mesh zero horizontal and vertical displacements are specified at these nodes.

Material Properties for the Soils and Flood Wall in the Complete Soil-Structure Interaction Analysis

The soil material properties used in this complete SSI analysis are the same as those used in the slope stability analyses of this cross section. Figure 9-23 shows the 41 soil clusters used to define the regions of common soil properties for the four primary categories of soil within the

mesh (i.e., the Levee clay, Marsh (or peat), Beach sand, and Bay Sound clay). Note that each soil layer comprises many clusters, each of which is designated by a different color. Spatially varying soil properties are assigned in the slope stability analyses. Accordingly, multiple soil clusters are used in the nonlinear finite element mesh to assign material properties within each soil layer to accommodate the spatially varying (i.e., vertically as well as horizontally) soil properties. Table 9-8 summarizes the engineering material properties and the corresponding to average stiffness values in the complete SSI analysis. Note that a range in engineering soil properties is reported for the Marsh layer. Table 9-9 summarizes the engineering material properties for the complete SSI analysis with increased values for soil stiffness of the Levee clay and the Marsh. This second set of soil stiffness values are used to assess the sensitivity in computed results to the stiffness of the protected side Levee clay and Marsh (i.e., peat).

Table 9-8
Material Characterization for Soils of Average Stiffness

Soil type	Range in Elevation, NAD88	Total unit weight (pcf)	Constant S_u value in soil cluster (psf)	ϕ' (deg)	E^{ref}/S_u	E^{ref} (psf)	$(E^{ref})_{ur}/E^{ref}$	m	$R_{interface}$	Hydraulic Conductivity (ft/hr)
					Young's Modulus - Average					
Levee clay - canal side	–	109	900	–	24	–	5	0.5	0.8	1.2E-04
Levee clay - protected side	–	109	900	–	48	–	5	0.5	0.8	1.2E-04
Marsh (peat)	–	80	300 to 400	–	48	–	3	0.5	0.8	1.2E-04 to 1.2E-02
Beach Sand	-10 to -15.5	120	–	40		1,260,000	3	0.5	–	1.8
	-15.5 to -37	120	–	40		1,260,000	3	0.5	–	
	-37 to -50	120	–	36	–	647,000	3	0.5	–	
Bay Sound clay	–	102	779	–	68	–	3	1.0	–	1.2E-04
Note:$(E^{ref})_{50} = (E^{ref})_{oed} = E^{ref}$; $\psi = 0$ deg; $p_{ref} = 2116$ psf; $\nu_{ur} = 0.3$; $R_f = 0.9$										

Soil type	Range in Elevation, NAD88	Total unit weight (pcf)	Constant S_u value in soil cluster (psf)	ϕ' (deg)	Young's Modulus - Stiff		$(E^{ref})_{ur}/E^{ref}$	m	$R_{interface}$	Hydraulic Conductivity (ft/hr)
					E^{ref}/S_u	E^{ref} (psf)				
Levee clay - canal side	–	109	900	–	48	–	5	0.5	0.8	1.2E-04
Levee clay - protected side	–	109	900	–	240	–	3	0.5	0.8	1.2E-04
Marsh (peat) - canal side	–	80	300 to 400	–	48	–	3	0.5	0.8	1.2E-04 to 1.2E-02
Marsh (peat) - protected side	–	80	300 to 400	–	240	–	3	0.5	0.8	1.2E-04 to 1.2E-02
Beach Sand	-10 to -15.5	120	–	40		1,260,000	3	0.5	–	1.8
	-15.5 to -37	120	–	40		1,260,000	3	0.5	–	
	-37 to -50	120	–	36	–	647,000	3	0.5	–	
Bay Sound clay	–	102	779	–	68	–	3	1.0	–	1.2E-04

Note:$(E^{ref})_{50} = (E^{ref})_{oed} = E^{ref}$; $\psi = 0$ deg; $p_{ref} = 2116$ psf; $\nu_{ur} = 0.3$; $R_f = 0.9$

Table 9-9
Material Characterization for Soils of With Increased Stiffness

Levee clay: A total unit weight of 109 pcf is assigned to the Levee clay soil clusters. A smaller data base of strength and stiffness tests results are available for London Canal Levee clay, as compared with 17th Street canal Levee clay. After a careful assessment of the test data on the Levee clay at London canal, an undrained shear strength (S_u) value of 900 psf is assigned. This is the same value for Su that is assigned at 17th Street.

Stress-strain data for 17th Street canal Levee clay triaxial test specimens leads to the assignment of an average value for Young's modulus, E^{ref}, expressed in terms of (E^{ref}) normalized by S_u and equal to 48 (Table 9-8) on the protected side of the I-wall. This same value for Young's modulus is assigned to the London canal Levee clay. On the canal side of the I-wall, (E^{ref}) normalized by S_u is set equal to 24. During the course of the complete SSI analysis of Station 53+00, an evaluation of the sensitivity in computed results to the value of Levee and Marsh stiffness is conducted. In this parametric study the protected side Levee clay E^{ref} is increased by a factor of five. It is expressed in Table 9-9 in terms of (E^{ref}) normalized by S_u and is set equal to 240 (i.e., = 5 times 48).

For the Plaxis nonlinear Hardening Soil (HS) model, the parameters $(E^{ref})_{50}$ and $(E^{ref})_{oed}$ are set equal to [E^{ref}/S_u times S_u]. Additional HS parameters assigned are reference stress for stiffness, p_{ref}, equal to 2,116 psf, failure ratio $R_f = 0.9$, the exponent m = 0.5 and ν_{ur} equals 0.3. For unload reload HS parameters, $(E^{ref})_{ur}$ is set equal to 5 times $(E^{ref})_{50}$ in the average modulus complete SSI analysis and set equal to 3 times $(E^{ref})_{50}$ in the sensitivity analysis using stiff clay properties. For Casteel CZ101 cold formed steel sheet piles to levee clay, the interface strength

parameter $R_{interface}$ is set equal to 0.8 for Levee clay-to-steel interfaces (by the Potyondy, 1961, data).

Marsh (or peat): A smaller data base of strength and stiffness tests results are available for London Canal Marsh (or peat), as compared with 17th Street canal peat (or marsh). After a careful assessment of the test data on the Marsh at London canal, a range in values of undrained shear strength (S_u) of 300 psf to 400 psf is assigned. This is the same range in Su values as is assigned for the 17th Street canal peat, which factored into the strength assessment made for this cross section. Below the I-wall and in the region of the greatest overburden, a value of S_u equal to 400 psf is assigned. With no overburden, the value for S_u is set equal to 300 psf in the Marsh. A shear strength value is assigned to each Marsh cluster based on the magnitude of the overburden for the center position of each Marsh cluster below the levee. There is no vertical variation in undrained shear strength for the Marsh layer. A total unit weight of 80 pcf is assigned to the Marsh soil clusters. Stress-strain data for 17th Street canal peat triaxial test specimens leads to the assignment of an average value for Young's modulus, E^{ref}, expressed in terms of (E^{ref}) normalized by S_u and set equal to 48 (Table 9-8). This same value for Young's modulus is assigned to the London Station 14+00 and the 17th Street canal Marsh. In the evaluation of the sensitivity in computed results to stiffness, the protected side Marsh E^{ref} is increased by a factor of five. It is expressed in Table 9-9 in terms of (E^{ref}) normalized by S_u and set equal to 240 (i.e., = 5 times 48).

For the Plaxis nonlinear Hardening Soil (HS) model the parameters $(E^{ref})_{50}$ and $(E^{ref})_{oed}$ are set equal to [E^{ref}/S_u times S_u]. Additional HS parameters assigned are reference stress for stiffness, p_{ref}, equal to 2,116 psf, failure ratio $R_f = 0.9$ and the exponent m = 0.5. For unload reload HS parameters, $(E^{ref})_{ur}$ is set equal to 3 times $(E^{ref})_{50}$ and ν_{ur} equals 0.3. For Casteel CZ101 cold formed steel sheet piles to Marsh interface, $R_{interface}$ is set equal to 0.8.

Beach Sand: The results from the field investigation indicate that the Beach sand is made up of three distinct layers based on the in-situ density of the sand. The upper layer of Beach sand extends from approximately El -10 to -15.5 and is a very dense sand. The middle layer extends from El -15.5 to -37 and is a very dense sand. The lower layer extends from El -37 to -50 and is a medium sand. Proceeding from the top layer down, a total unit weight of 120 pcf is assigned to each of the three layers of Beach Sand soil clusters.

Standard Penetration Test and cone test results in the upper Beach sand layer (i.e., El -10 to -15.5) indicate an average value of 46 blows per ft depth for 60 percent of free-fall energy and corrected to an effective overburden pressure of 1 ton/ft^2 [i.e., $(N_1)_{60} = 46$]. For a fine sand with an average value of $(N_1)_{60} = 46$, the relative density (D_r) is 87 percent by Skemption's (1986) correlation. A $(N_1)_{60} = 46$ results in a value of 40 deg for the effective angle of internal friction by the Peck, Hanson and Thornburn (1974) correlation. For very dense sand with D_r equal to 87 percent and using the correlations of Lengkeek and Vermeer and Shanz (cited in Brinkgreve, 2005, as well as in Plaxis course notes, 2006), the value of Young's modulus E^{ref} is set equal to 1,260,000 psf. For the Plaxis nonlinear Hardening Soil (HS) model, the parameters $(E^{ref})_{50}$ and $(E^{ref})_{oed}$ are set equal to 1,260,000 psf. Additional HS parameters assigned are reference stress for stiffness, p_{ref}, equal to 2,116 psf, failure ratio $R_f = 0.9$ and the exponent m = 0.5. For unload reload HS parameters, $(E^{ref})_{ur}$ is set equal to 3 times $(E^{ref})_{50}$ and ν_{ur} equals 0.3. For Casteel

CZ101 cold formed sheet piles to Beach sand, the interface strength parameter $R_{interface}$ is set equal to 0.8.

Standard Penetration Test and cone test results in the middle Beach sand layer (i.e., El -15.5 to -37) indicate an average value of 60 blows per ft depth for 60 percent of free-fall energy and corrected to an effective overburden pressure of 1 ton/ft^2 [i.e., $(N_1)_{60} = 60$]. For a fine sand with an average value of $(N_1)_{60} = 60$, the relative density (D_r) is 99 percent by Skemption's (1986) correlation. A $(N_1)_{60} = 60$ results in a value of 40 deg (approximately) for the effective angle of internal friction by the Peck, Hanson and Thornburn (1974) correlation. For very dense sand with D_r equal to 99 percent and using the correlations of Lengkeek and Vermeer and Shanz (cited in Brinkgreve, 2005, as well as in Plaxis course notes, 2006), the value of Young's modulus E^{ref} is set equal to 1,260,000 psf. For the Plaxis nonlinear Hardening Soil (HS) model, the parameters $(E^{ref})_{50}$ and $(E^{ref})_{oed}$ are set equal to 1,260,000 psf. Additional HS parameters assigned are reference stress for stiffness, p_{ref}, equal to 2,116 psf, failure ratio $R_f = 0.9$ and the exponent m = 0.5. For unload reload HS parameters, $(E^{ref})_{ur}$ is set equal to 3 times $(E^{ref})_{50}$ and ν_{ur} equals 0.3.

Standard Penetration Test and cone test results in the lower Beach sand layer (i.e., El -37 to -50) indicate an average value of 28 blows per ft depth for 60 percent of free-fall energy and corrected to an effective overburden pressure of 1 ton/ft^2 [i.e., $(N_1)_{60} = 28$]. For a fine sand with an average value of $(N_1)_{60} = 28$, the relative density (D_r) is 66 percent by Skemption's (1986) correlation. A $(N_1)_{60} = 28$ results in a value of 36 deg (approximately) for the effective angle of internal friction by the Peck, Hanson and Thornburn (1974) correlation. For medium sand with D_r equal to 66 percent and using the correlations of Lengkeek and Vermeer and Shanz (cited in Brinkgreve, 2005, as well as in Plaxis course notes, 2006), the value of Young's modulus E^{ref} is set equal to 647,000 psf. For the Plaxis nonlinear Hardening Soil (HS) model, the parameters $(E^{ref})_{50}$ and $(E^{ref})_{oed}$ are set equal to 647,000 psf. Additional HS parameters assigned are reference stress for stiffness, p_{ref}, equal to 2,116 psf, failure ratio $R_f = 0.9$ and the exponent m = 0.5. For unload reload HS parameters, $(E^{ref})_{ur}$ is set equal to 3 times $(E^{ref})_{50}$ and ν_{ur} equals 0.3.

Bay Sound clay: A smaller data base of strength and stiffness tests results are available for London Canal Bay Sound clay, as compared with 17th Street canal Bay Sound clay. After a careful assessment of the test data on the Bay Sound clay at London canal, a value of undrained shear strength (S_u) of 779 psf is assigned. This is the same Su value assigned for the 17th Street canal Bay Sound clay, which factored into the strength assessment made for this cross section. A total unit weight of 102 pcf is assigned to the Bay Sound clay soil cluster. Stress-strain data for 17th Street canal Bay Sound clay triaxial test specimens leads to the assignment of an average value for Young's modulus, E^{ref}, expressed in terms of (E^{ref}) normalized by S_u and set equal to 68 (Tables 9-8 and 9-9). This same value for Young's modulus is assigned to the London canal Bay Sound clay.

For the Plaxis nonlinear Hardening Soil (HS) model, the parameters $(E^{ref})_{50}$ and $(E^{ref})_{oed}$ are set equal to [E^{ref}/S_u times S_u]. Additional HS parameters assigned are reference stress for stiffness, p_{ref}, equal to 2,116 psf, failure ratio $R_f = 0.9$ and the exponent m = 1.0. For unload reload HS parameters, $(E^{ref})_{ur}$ is set equal to 3 times $(E^{ref})_{50}$ and ν_{ur} equals 0.3.

Hydraulic Conductivity: Values for the hydraulic conductivity of the four soil types are listed in Tables 9-8 and 9-9. The hydraulic conductivity value assigned to the Beach sand is based on field pump tests while all other values are based on typical values found in the technical literature for soils of similar engineering material characteristics. For the Marsh material, data from Weber (1969) and others leads to the assignment of hydraulic conductivity values of 1.2×10^{-2} ft/hr for regions of lower overburden pressure and 1.2×10^{-4} ft/hr for regions of higher overburden, such as below the Levee. For canal bottom silts, a hydraulic conductivity value equal to 1.2×10^{-2} ft/hr is assigned.

Flood Wall: The flood wall comprises an exposed reinforced concrete I-wall, a reinforced concrete cap and Casteel CZ101 cold formed sheet pile. The 12-inch thick reinforced concrete I-wall extends from the top of protected levee (El 3.6) to El 13. At Station 53+00, the sheet pile tip is at El -17.4. The top of the Beach sand to Marsh interface is at El -10.2. Consequently, the sheet pile extends 7.2 ft into the Beach sand. The upper reach of pile is encased in a two-foot thick reinforced concrete cap extending below the surface of the protected side of the levee. Linear elastic material response was assumed in the complete SSI analysis. Engineering properties for the I-wall, cap and sheet pile are summarized in Table 9-10 for the zero thickness plate elements used in the finite element model.

Table 9-10 Material Characterization for the Flood Wall				
Identification	EA	EI	weight	ν
	[lb/ft]	[lbft²/ft]	[lb/ft/ft]	[-]
Reinforced Concrete I-wall	4.32E8	3.6E7	150.00	0.20
Reinforced Concrete Cap	8.64E8	2.88E8	80.00	0.20
Sheet Pile (Hoesch 12)	9.77E7	1.31E7	8.94	0.30

Complete Soil-Structure Interaction Analysis

Introduction: Two sets of complete SSI analyses of the Figure 9-22 2-D cross section of Station 53+00 at London Canal are conducted in staged analysis using Plaxis. Both sets evaluate the response of the Station 53+00 cross-section to flood loading starting at canal water El 1.0 on through a series of incremental 0.5 to 2.6 feet raises in canal elevation. Table 9-11 summarizes the calculation phases of the second analysis set with stiff modulus values assigned to the Levee clay and the Marsh on the protected side of the I-wall. More than 13 phases of calculations are used in this parametric SSI analysis to a maximum canal water El 8. A similar set of analyses are conducted with average modulus values assigned to the four layers of soils. However, the discussion will focus on the results from the analysis set with stiff modulus values assigned to the Levee clay and the Marsh on the protected side of the I-wall.

Table 9-11
Calculation Phases of the Nonlinear Finite Element Analysis Using Stiff Modulus Values for the Levee Clay and the Marsh on the Protected Side

Phase	PhaseNo.	Calculation type	Load input
Initial phase	0	-	-
Place Wall & Interface	1	Plastic analysis	Staged construction
Gravity (1.0)	2	Plastic analysis	Total multipliers
Water Table El +1	3	Plastic analysis	Staged construction
Canal Water El +3.6	4	Plastic analysis	Staged construction
Canal Water El +5,	5	Plastic analysis	Staged construction
Canal Water El +5, Crack to El -10.2, linear phreatic surface	6	Plastic analysis	Staged construction
Canal Water El +5.5, Crack to El -10.2, linear phreatic surface	7	Plastic analysis	Staged construction
Canal Water El +6, Crack to El -10.2, linear phreatic surface	8	Plastic analysis	Staged construction
Canal Water El +6.5, Crack to El -10.2, linear phreatic surface	9	Plastic analysis	Staged construction
Canal Water El +7, Crack to El -10.2, linear phreatic surface	10	Plastic analysis	Staged construction
Canal Water El +7.5, Crack to El -10.2, linear phreatic surface	11	Plastic analysis	Staged construction
Canal Water El +8, Crack to El -10.2, linear phreatic surface	12	Plastic analysis	Staged construction
Phi-C Reductions	13[+]	Phi/c reduction	Incremental multipliers

Loading phases 0 through 3 are used in both sets of complete SSI analyses to establish the initial total stress state condition existing prior to flooding. Loading phase 3 concludes with canal water at El 1, a steady state water elevation in the canal.

Loading phases 4 through 12 (Table 9-11) are used in the analysis set with stiff modulus values assigned to the Levee clay and the Marsh on the protected side of the I-wall for the four soil types to perform an incremental raise in the canal water to El 8, modeling the flood loading of the levee/I-wall system and the introduction of a crack along the canal-side face of the sheet pile in the Levee clay and in the Marsh/peat (eventually to the top of the Beach sand at El -10.2). The last of the loading phases (i.e., 13[+]) are used to compute the reserve capacity of the levee/I-wall system for different canal water elevations. This reserve capacity is expressed in terms of a Factor of Safety and is computed in a series of Plaxis phi/c reduction loading phases. A similar set of calculation phases (not listed) are conducted with the Table 9-8 average modulus values assigned to the four layers of soils.

Initial steady state condition for canal water at EL 1: Loading phases 0 through 3 are used in the complete SSI analysis to establish the initial total stress state within the finite element mesh with a steady state canal water elevation at El 1. Gravity loading is applied in a single increment, followed by a rising of the water table. In the Beach sand layer, the water table is

established at El -8.4 on the left-hand, protected side of the mesh, at x-coordinate -137, by analysis phase 3 and is maintained at this elevation in all subsequent computation phases. Load input for gravity loading is specified in Plaxis by means of the total multiplier method and changes in water table are accomplished by staged construction and by steady state seepage analysis, unless stated otherwise.

The initial steady-state, total stress condition for the usual canal water elevation of 1 is established by using the average stiffness modulus values given in Table 9-8 in the Mohr-Coulomb soil model for loading phases 0 through 3 for both sets of complete SSI analyses. The results from the IPET Task 7 slope stability analyses for this usual canal elevation indicate a stable cross-section with an ample Factor of Safety, i.e., above 1.5. Consequently, an important aspect of the total stress regime achieved within the Figure 9-23 finite element mesh is that the mobilized shear stress at the strain integration points within the finite elements contained in the soil clusters shown in this figure be less than the shear strength of the soil. The resulting computed fraction of mobilized shear strength (referred to as relative shear stress in Plaxis output) from the resulting initial total stress condition is shown in Figure 9-24. The fraction of mobilized shear strength is less than or equal to 0.9 at the stress integration points for the four soil types.
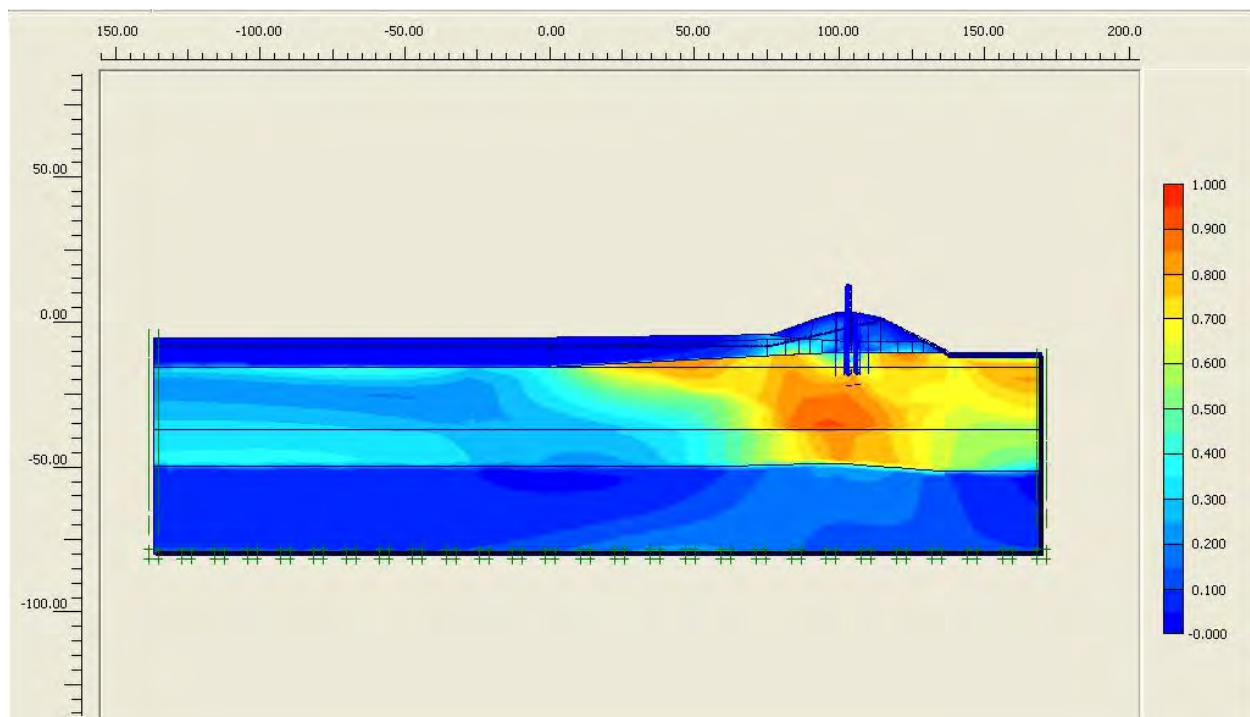
Figure 9-24. Fraction of Mobilized Shear Strength for Canal El 1

Flood loading: Modeling of flood loading commenced in the complete SSI analysis after the total initial stress state is established within the finite element mesh for steady state canal elevation (i.e., El 1). The hardening soil model with the Table 9-9 increased values for soil stiffness of the Levee clay and the Marsh are used in the analyses discussed in this section. Loading phases 4 through 12 (refer to Table 9-11) are used in the complete SSI analysis to

perform an incremental raise in the canal water to El 8, modeling the flood loading of the levee/I-wall system. Load input for changes in canal water elevation is specified by staged construction. For canal water up to and including El 5 and for crack depths terminating above the top of the Beach sand layer (at El -10.2) on the canal side of the new sheet pile wall/I-wall, a steady state seepage analysis is used to establish the pore water pressure regime within the Beach sand layer for loading phases 4 and 5 (Table 9-11).

The results from the SSI analysis set using the Table 9-9 increased values for soil stiffness of the Levee clay and the Marsh indicates that cracking commenced when Canal water reached El 5. Crack initiation occurs at the top of the Levee clay, on the canal side (at El 3.6) of the sheet pile wall when the total horizontal stress in the clay in less than the value for hydrostatic water pressure (i.e., γ_{water} times depth below canal water surface). This first occurs at Table 9-11 loading phase 5. Comparisons of values for hydrostatic water pressure, generated by hand computation, with the total horizontal stresses computed in the compete SSI analysis indicates a crack will extend from El 3.6 down to the top of the Beach sand layer (i.e., EL -10.2) in the Levee clay and Marsh in a single loading phase, phase no. 6. Subsequent analyses using Table 9-9 E_{stiff} values are conducted for Canal water El's 5.5, 6, 6.5,7, 7.5 and 8 using a crack to EL -10.2 and a linear phreatic surface within the Beach sand.

Results (not shown) from the complete SSI analysis set for the Table 9-8 $E_{average}$ analysis set indicates cracking will initiate at Canal water EL 4.5. Additionally, cracking will extend to the top of the Beach sand at this canal EL. Consequently, there is a 0.5 ft difference in Canal water elevation at which crack initiation occurs that can be directly attributed to the range in Tables 9-8 and 9-9 stiffness values.

Due to numerical convergence issues, a linear phreatic surface assumption is used to establish the pore water pressures within the Beach sand for loading phases 6 through 12 (Table 9-11) of the first complete set of SSI analysis in which depth of cracking extends to the top of Beach sand layer (EL -10.2). This results in a less severe uplift pressure regime within the Beach sand below the toe of the protected side of the Levee as discussed in the section describing the complete SSI analyses of London Canal Station 14+00. This results in a lower computed value for the Factor of Safety for the loading phases 6 through 12 in which this procedure is applied. Computed displacements are also affected in a similar fashion. Again, this compromise in accuracy is required in order to achieve convergence by Plaxis for these higher Canal water elevations with cracking to the top of the Beach sand.

Factor of Safety: The factor of safety is computed for flood loading of the I-wall/sheet pile wall using the phi/c reduction method of analysis in Plaxis by means of incremental multipliers. Problems with numerical convergence occurred in nearly all Phi/c reduction analyses of this cross-section, even for the Canal water El 5 flood loading case with a crack extending to El -10.2 (i.e., the top of the Beach sand layer). It is speculated by the authors of this document that these numerical problems stem from the change in the hydraulic boundary condition when a crack forms to the top of the Beach sand, resulting in new, higher uplift pressures at the top of the Beach sand layer, below and immediately beyond the toe of the Levee combined with the shallow (total) overburden pressure of the Marsh layer within this region. Converting from a steady state seepage analysis to a linear phreatic surface assumption with a head specified at

canal centerline as equal to the elevation of the canal was not sufficient to achieve numerical convergence as is the case for the complete SSI analyses of London Canal Station 14+00. The approach used in the Phi/c reduction analyses of this cross section with Canal water El 5 and a crack extending to the top of the Beach sand, is to maintain the Canal water El 5 but to conduct a series of Phi/c reduction analyses with different values assigned to the head within the Beach sand layer below the centerline of the canal, as depicted in Figure 9-26. Regrettably, Phi/c reduction only converged for linear phreatic surface analyses with canal centerline heads of EL 1.5 or less, as outlined in Figure 9-25. This is well below the centerline head of El 5 that would normally be assigned in a Phi/c reduction analysis. For a centerline head of El 1.5 the computed Factor of Safety is equal to 2.57. Using the data contained in Figure 9-25 it is speculated (in this figure) that for a centerline head at El 5 (corresponding to the canal water elevation), the Factor of Safety is likely to range in value from 1.0 to 2.1. Additionally, the computed Factors of Safety results shown in this figure are greater than the actual values due to the linear phreatic surface assumption used within the Beach sand (as compared to pore water pressures resulting from a steady state seepage analysis with a crack to the top of the Beach sand).
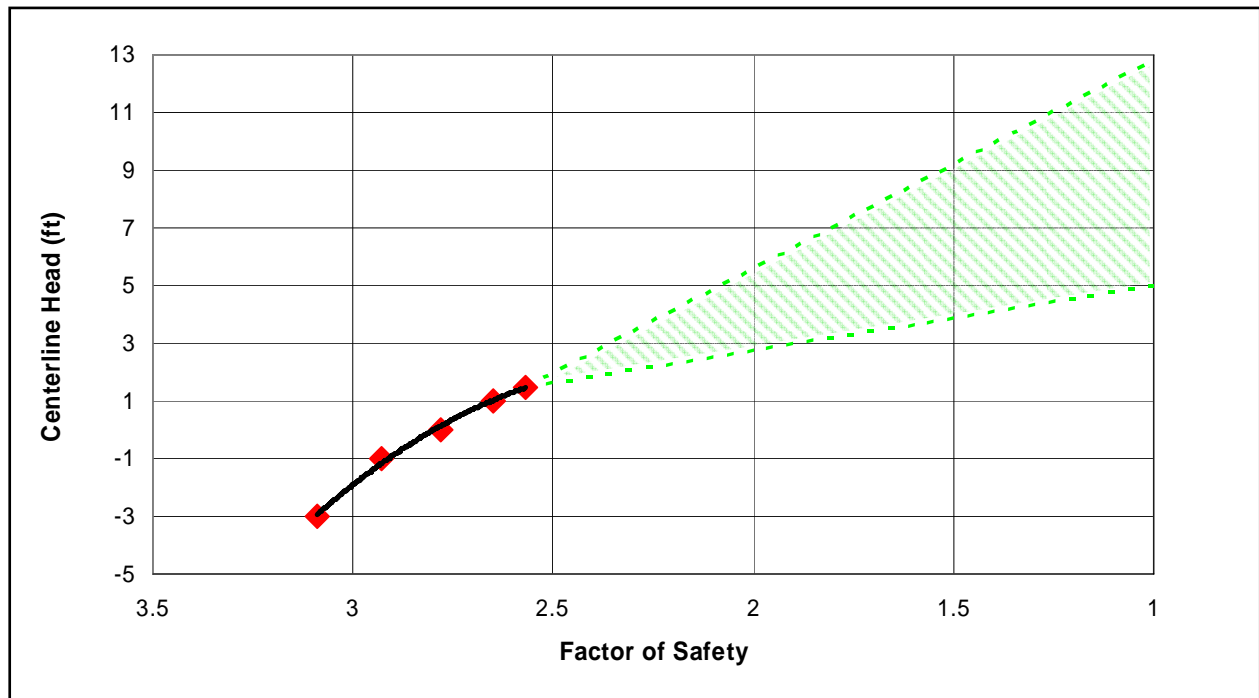
Figure 9-25. Factor of Safety Versus Centerline Head
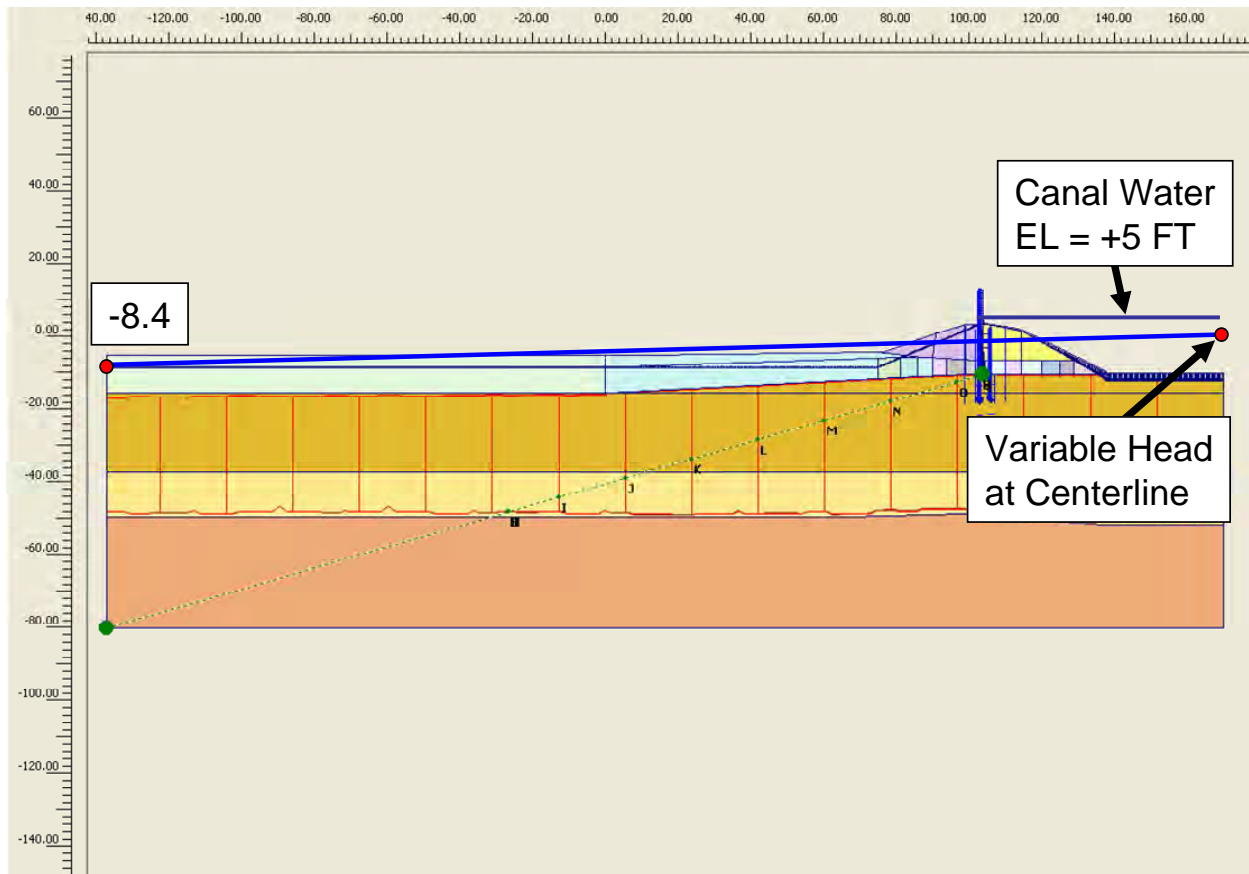
Figure 9-26. Graphical Definition of the Head at Canal Centerline for the Linear Phreatic Surface Assumption

Deformations: Figure 9-27 summarizes the computed deformations for the analysis set with stiff modulus values assigned to the Levee clay and the Marsh on the protected side of the I-wall, Canal water El 5 and crack to El -10.2 (i.e., top of Beach sand). Note the nodal deformations are magnified by a factor of 70 in order to show the deformed relative mesh relative to its position at canal water elevation of 1.0 (shown as a blue outline in this figure). The general trend is a rotational plowing of the protected side Levee clay by the I-wall/new sheet pile wall and a bulging of the Marsh beyond the toe of the Levee on the protected side.
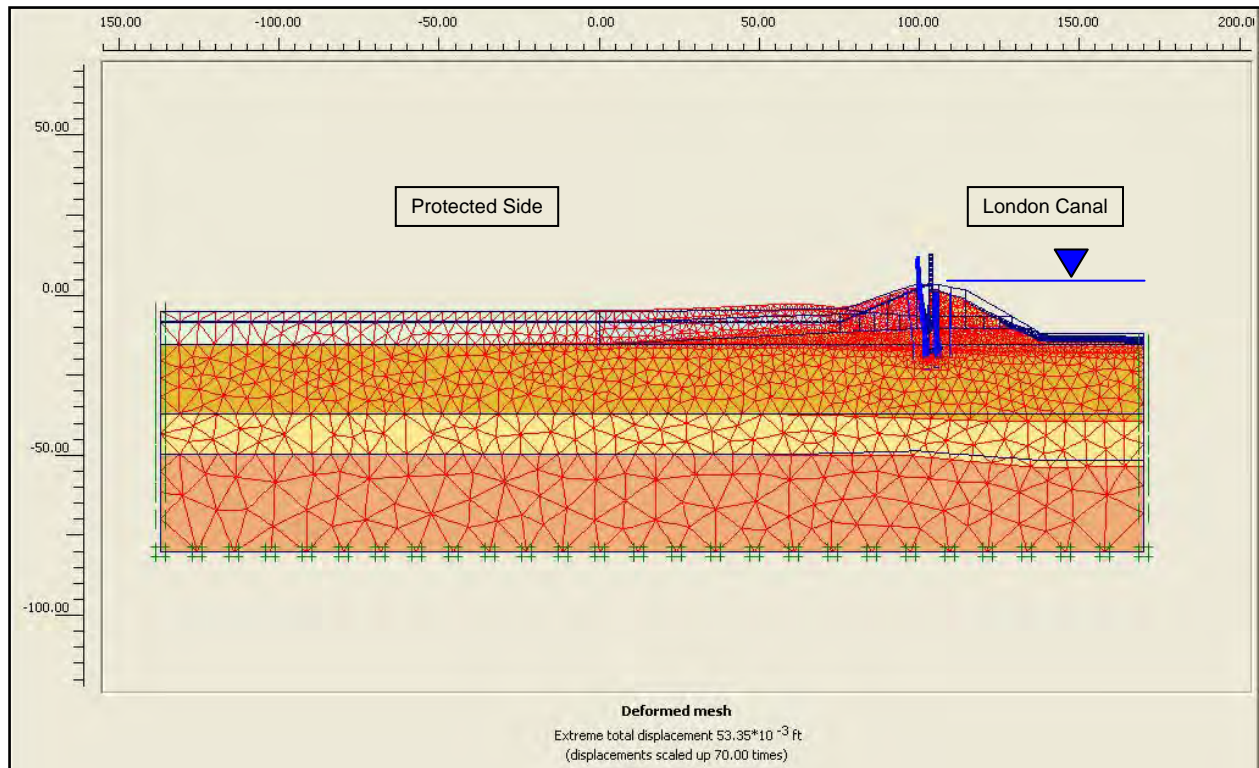
Figure 9-27. Deformed Mesh for Stiff Modulus Values for the Levee Clay and Marsh on the Protected Side, Exaggerated by a Factor of 70, for Canal El 5 and Crack to El -10.2 (Note: Canal El not to scale in figure)

Figure 9-28 shows the horizontal displacements of the soil regions within the mesh, relative to their position at a canal water elevation of 1.0 for stiff modulus values assigned to the Levee clay and the Marsh on the protected side of the I-wall with Canal water El 6 and crack to El -10.2. This figure shows the horizontal deformations are concentrated within the protected region of the Levee and the Marsh immediately at the toe of the Levee on the protected side. The largest horizontal deformations are concentrated in the Marsh, on the protected side, (approximately) equal to 0.05 ft (5/8 inch).
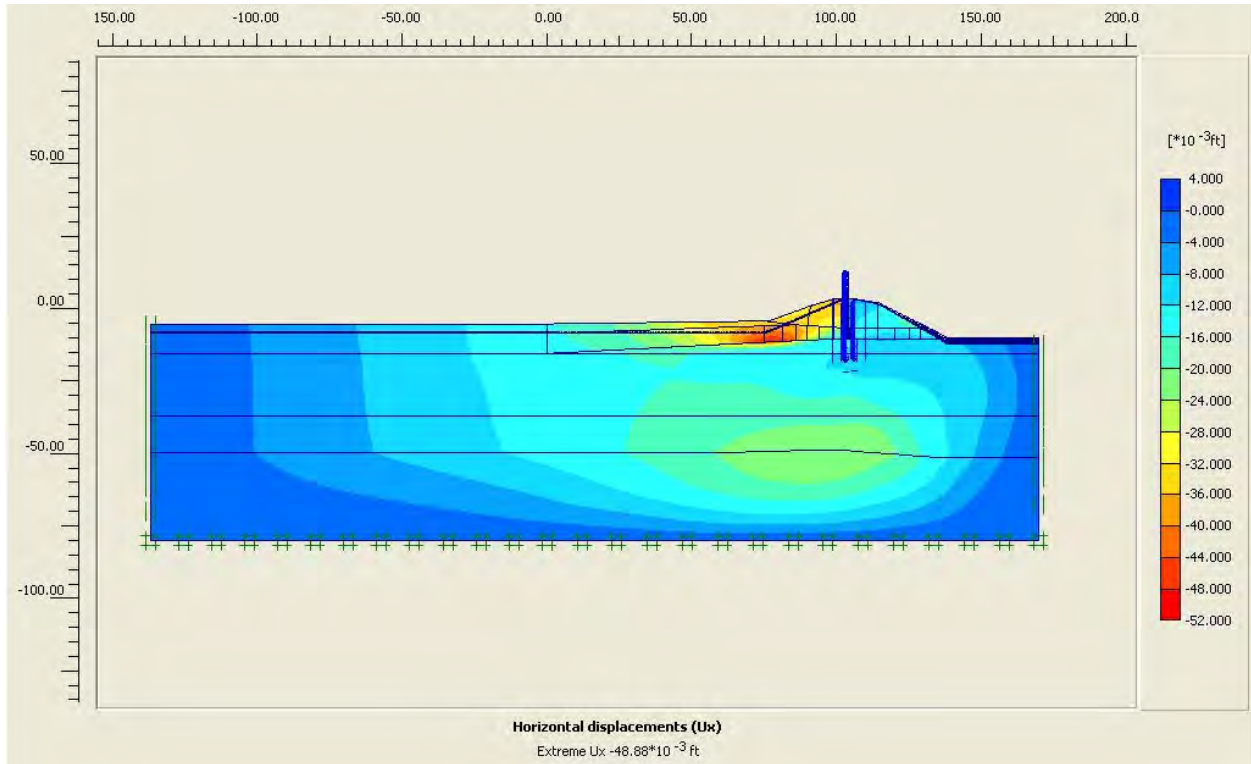
Figure 9-28. Horizontal Deformation Shadings for the Levee Clay and Marsh on the Protected Side with
Canal El 5 and Crack to El -10.2

Figure 9-29 shows the variation in horizontal displacements of the sheet pile versus canal
water elevation for the analysis set with stiff modulus values assigned to the Levee clay and the
Marsh on the protected side of the I-wall. These displacements are relative to their position at a
canal water elevation of 1.0. This figure shows the rotational nature of the I-wall/sheet pile wall
deformations, with the toe of the sheet pile "anchored" in the Beach sand.
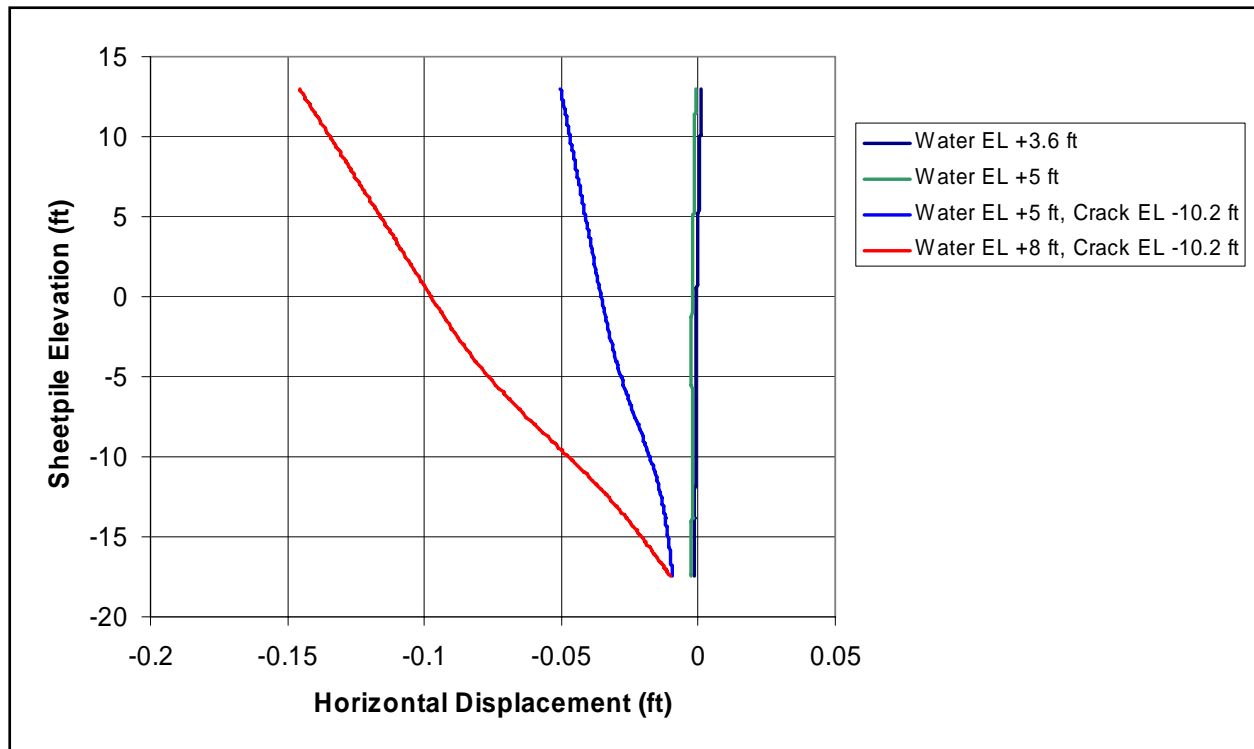
Figure 9-29. Horizontal Displacement of the I-Wall/Sheet Pile versus Canal Water El and Computed Using Stiff Modulus Values for the Levee Clay and Marsh on the Protected Side

Figure 9-30 shows the horizontal displacements of three points within the flood wall, relative to its position at a canal water elevation of 1.0 for stiff modulus values assigned to the Levee clay and the Marsh on the protected side of the I-wall. The points monitored through the analysis are at the top of the I-wall (El 13), at El 3.6 (top of Levee) and at the sheet pile tip (El -17.4). Recall for Canal water El's of 5 and higher, the crack never extends into the Beach sand layer, it terminates at the top of the Beach sand layer (i.e., El -10.2). Note that there is a significant increase in horizontal deformations of the I-wall/sheet pile wall when the crack extends to El -10.2 at Canal water El 5. Results in this figure shows the Beach sand is providing enough lateral support to prevent the sheet pile tip form moving laterally, therefore the deformation of the sheet pile is mostly a rotation about the sheet pile tip. Maximum horizontal movement at the top of the I-wall is 0.145 ft (1 ¾ inches) for Canal water El 8.
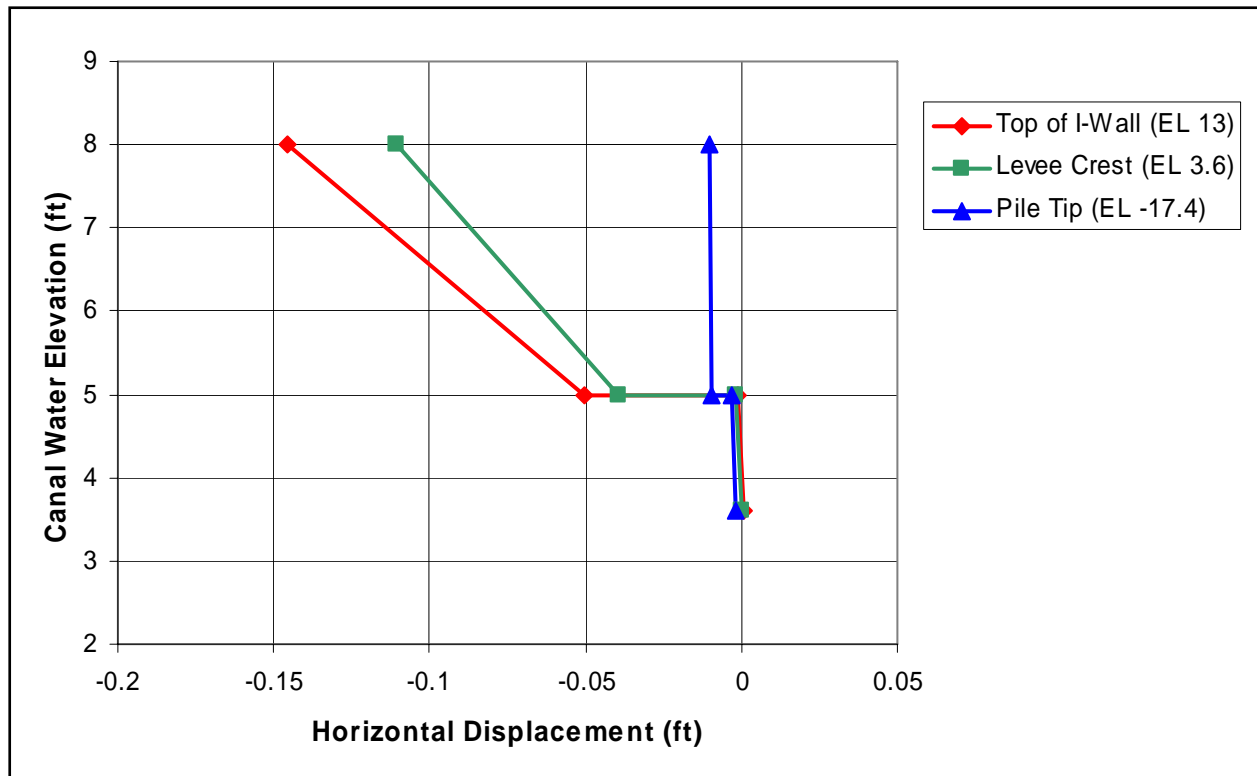
Figure 9-30. Horizontal Sheet Pile Deformations versus Canal Water El and Computed Using Stiff
Modulus Values for the Levee Clay and Marsh on the Protected Side

   Figure 9-31 shows the vertical displacements of the soil regions within the mesh, relative to
their position at a canal water elevation of 1.0 for stiff modulus values assigned to the Levee clay
and the Marsh on the protected side of the I-wall with Canal water El 5 and crack to El -10.2.
This figure shows the 0.024 ft (1/4 inch) uplift of the Marsh located beyond the toe of the Levee
on the protected side.
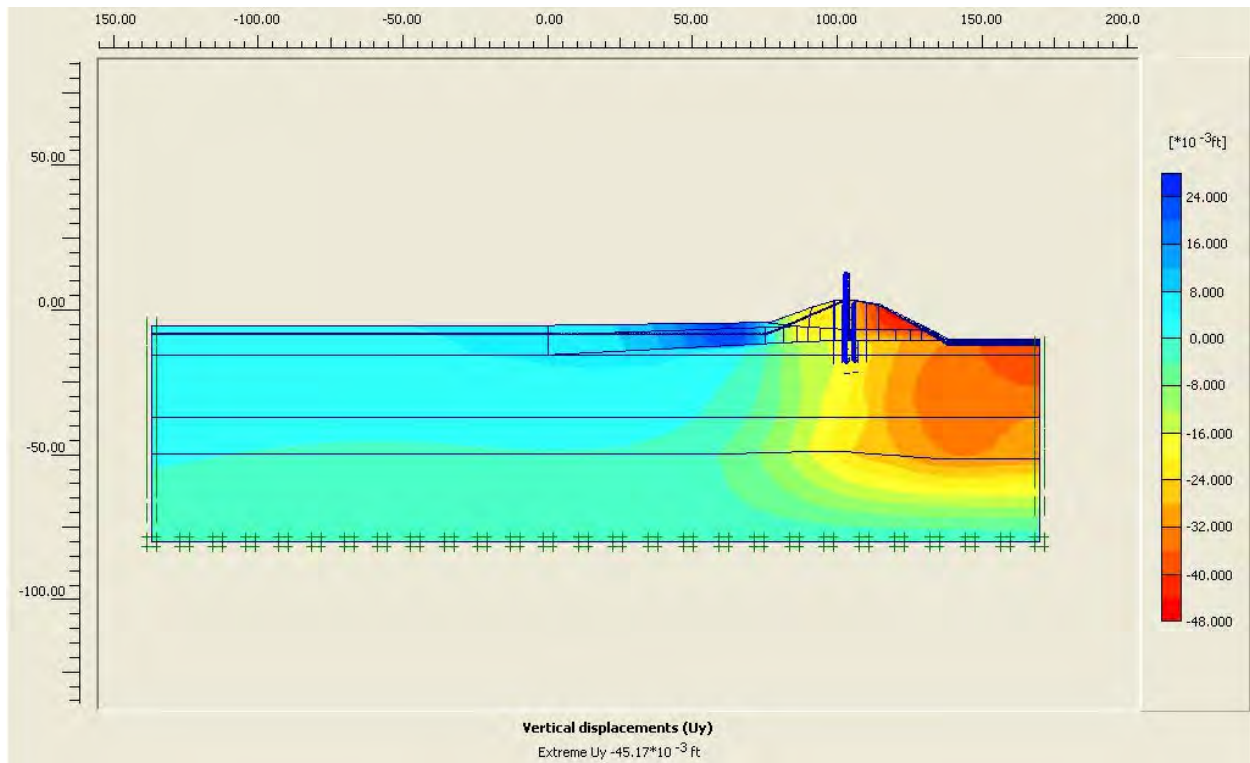
Figure 9-31. Vertical Deformation Shadings for Stiff Modulus Values for the Levee Clay and Marsh on the Protected Side with Canal El 5 and Crack to El -10.2

Failure Mechanism: Figures 9-32 and 9-33 show that for the analysis set using stiff modulus values assigned to the Levee clay and the Marsh on the protected side of the I-wall with Canal water El 5 and Crack to El -10.2, there is a loss of effective vertical stress at the top of the Beach sand layer within the region beyond the toe of the Levee. This results in zero shear strength along the top of the Beach sand layer as demonstrated in the Figure 9-34 fraction of mobilized shear strength being equal to unity within this Beach sand region. Figure 9-35 shows that this, in turn, results in the beginning of the development of a mechanism as demonstrated by the concentration of large shear strains within this region for Canal water El 5 and crack to El -10.2. Figure 9-36, with a close-up of the Levee region shown in Figure 9-37, and Figure 9-38 show the development of the ultimate mechanism (i.e., the failure mechanism) computed in a phi/c reduction analysis for Canal water El 5 and crack to El -10.2, for a linear phreatic surface Canal centerline head at El 0 with the computed Factor of Safety of 2.78 (actual value will be lower when the more realistic, larger pore water pressures are specified in an analysis). Note the vertical "bulging" in the Marsh beyond the toe of the Levee. The reaches of large shear strain shown in Figure 9-38 shows the compete failure wedge will form along the top of the Beach sand layer and "day light" beyond the toe of the Levee. All subsequent phi/c computations (that converged to a solution) for higher canal water elevations and for the E_{stiff} analyses show this same Figures 9-36, 9-37 and 9-38 failure mechanism to form.
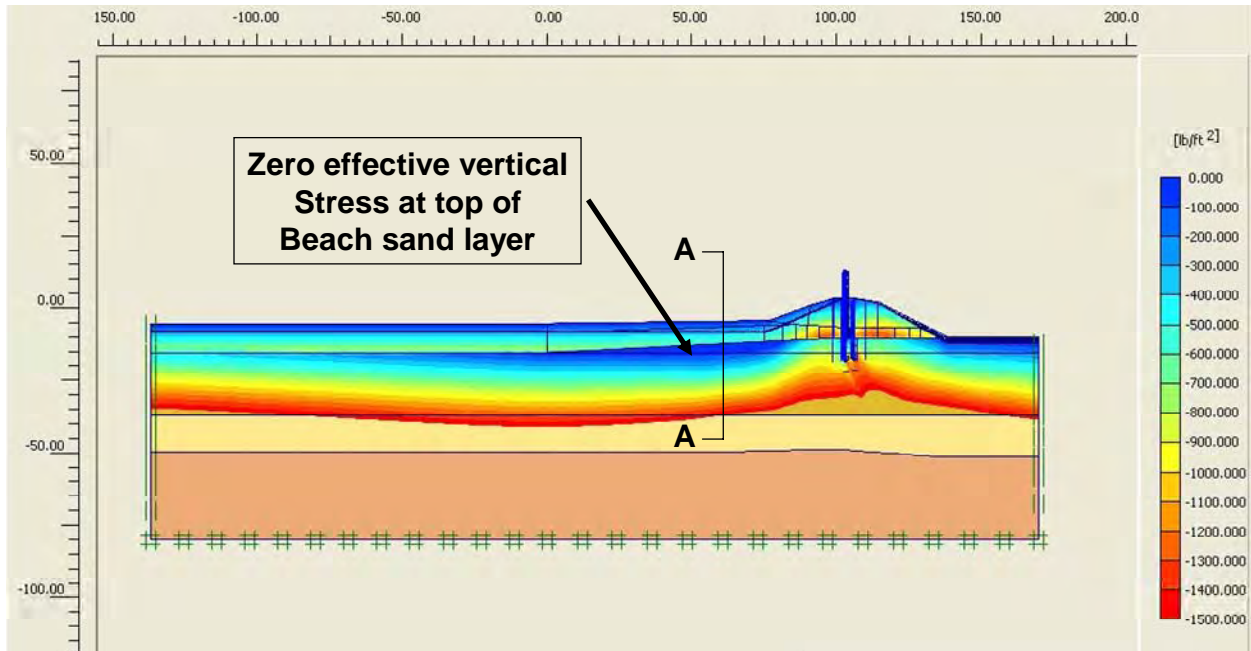
Figure 9-32. Shadings of Total Vertical Stress in the Levee Clay and Marsh and Effective Vertical Stress in the Beach Sand for the Analysis Using Stiff Modulus Values for the Levee Clay and Marsh on the Protected Side with Canal El 5 and Crack to El -10.2
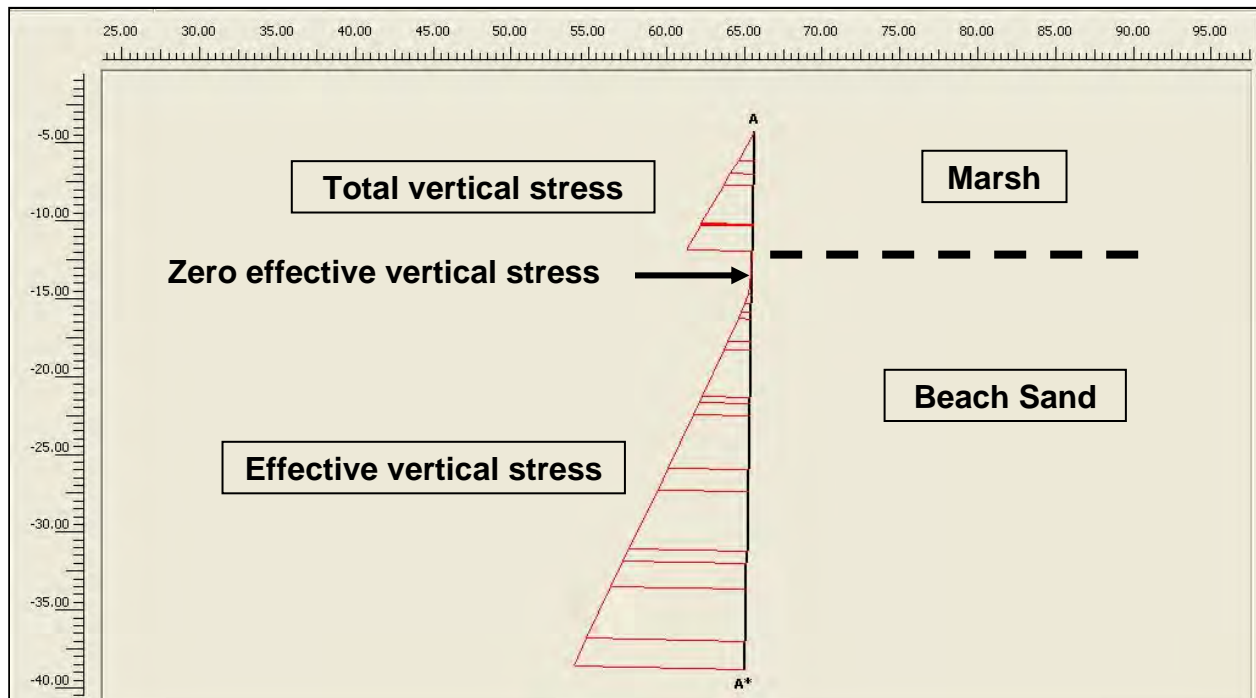
Figure 9-33. Vertical Section A-A Near the Toe of the Levee Showing Total Vertical Stress in the Marsh and Effective Vertical Stress in the Beach Sand for the Analysis Using Stiff Modulus Values for the Levee Clay and Marsh on the Protected Side with Canal El 5 and Crack to El -10.2

This is a preliminary report subject to revision; it does not contain final conclusions of the United States Army Corps of Engineers.
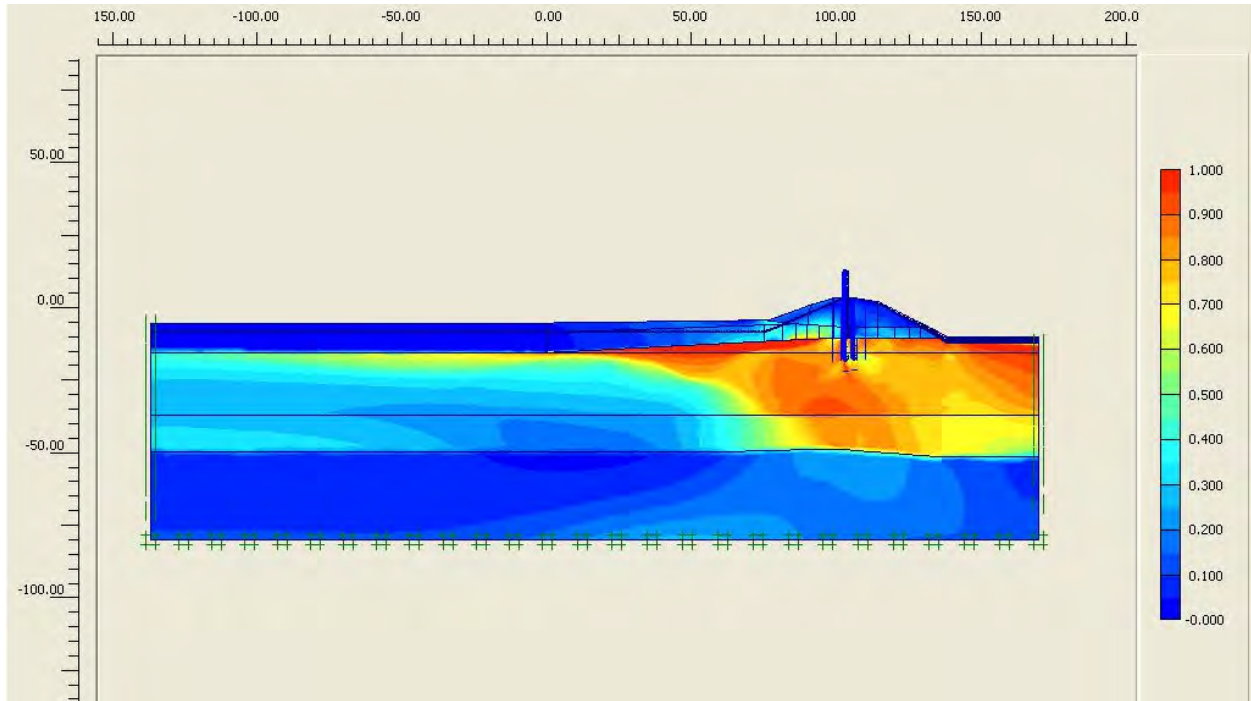
Figure 9-34. Fraction of Mobilized Shear Strength for the Analysis Using Stiff Modulus Values for the Levee Clay and Marsh on the Protected Side with Canal El 5 and Crack to El -10.2
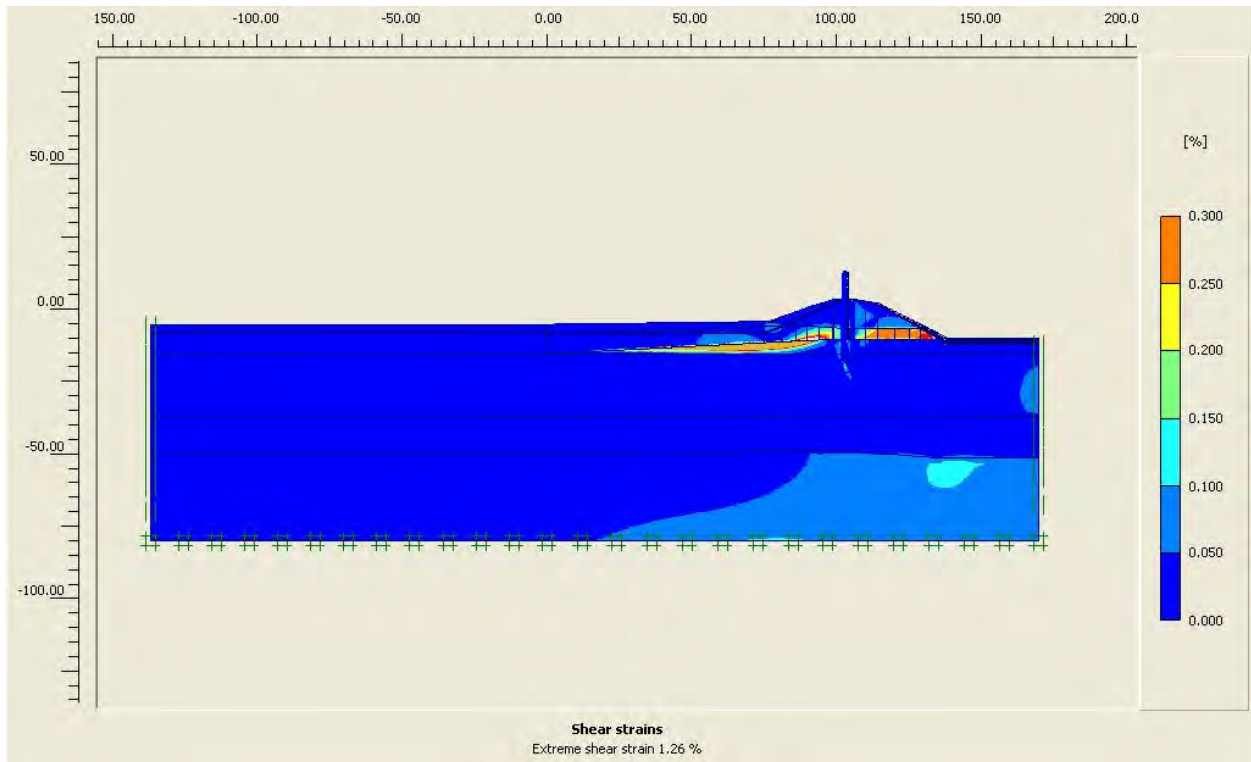
Figure 9-35. Reach of Large Shear Strains for the Analysis Using Stiff Modulus Values for the Levee Clay and Marsh on the Protected Side with Canal El 5 and Crack to El -10.2
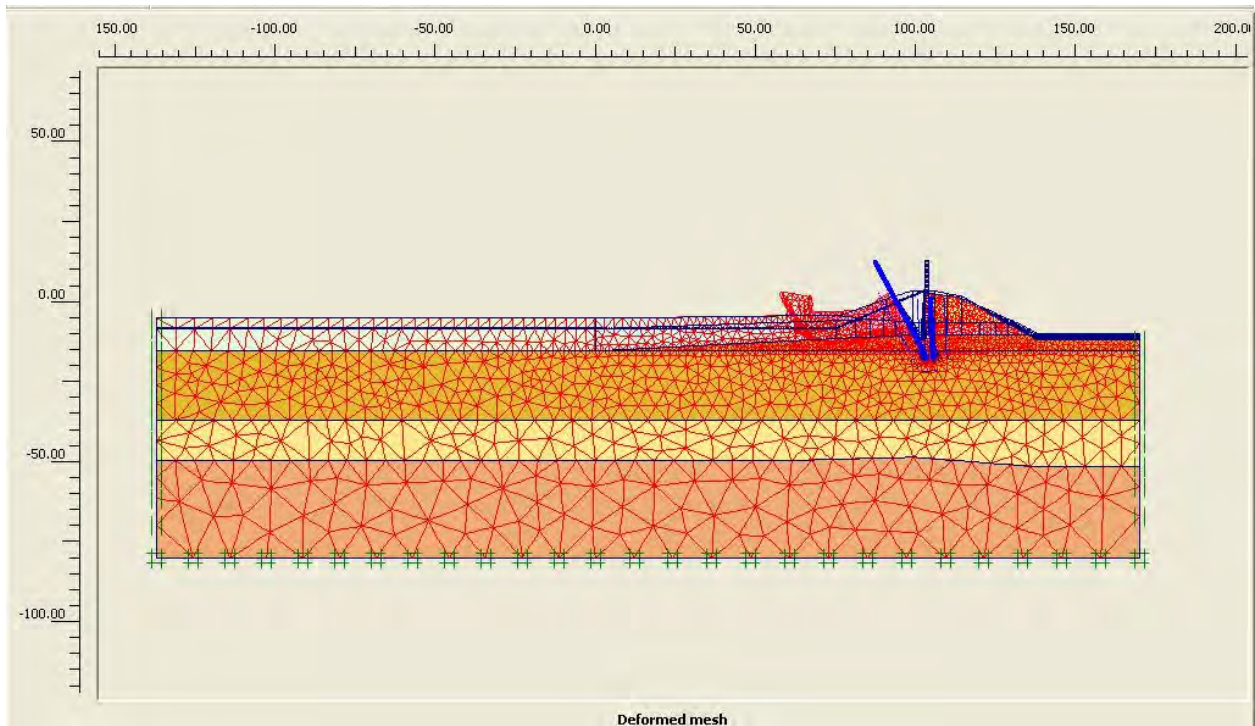
Figure 9-36. Ultimate Mechanism from Phi/C Reduction for the Analysis Using Stiff Modulus Values for the Levee Clay and Marsh on the Protected Side with Canal El 5 and Crack to El -10.2
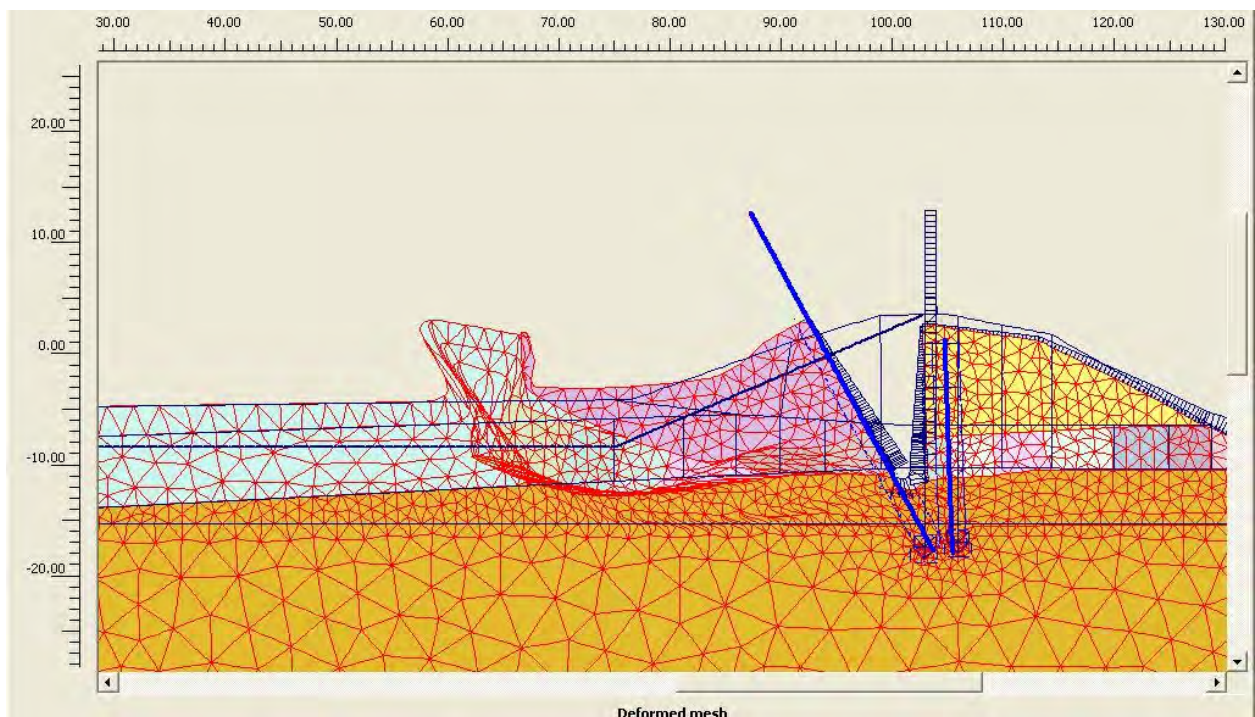
Figure 9-37. Close-up of the Ultimate Mechanism from Phi/C Reduction for the Analysis Using Stiff Modulus Values for the Levee Clay and Marsh on the Protected Side with Canal El 5 and Crack to El -10.2
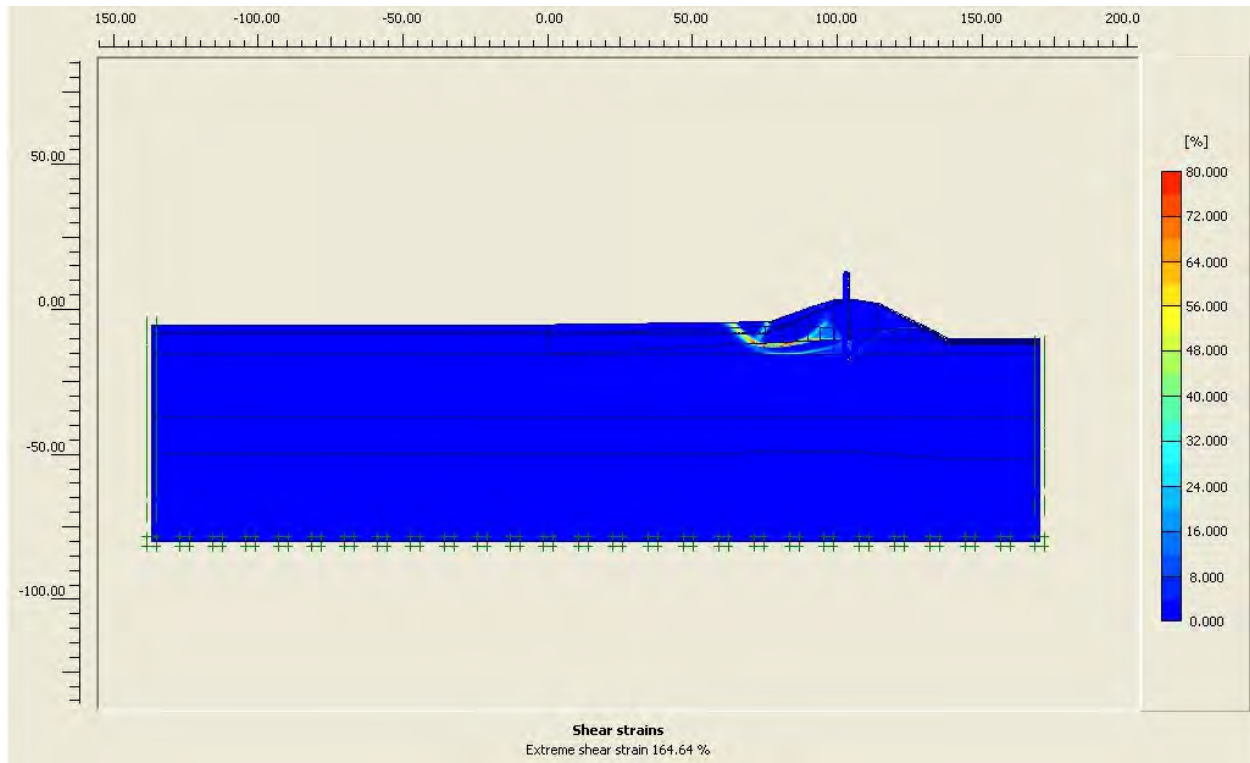
Figure 9-38. Reach of Large Shear Strains from the Phi/C Reduction Analysis Using Stiff Modulus Values for the Levee Clay and Marsh on the Protected Side with Canal El 5 and Crack to El -10.2

References

Brinkgreve, R. B. J., W. Broere, and D. Waterman, ed. 2004. *Plaxis 2D – Version 8.* Plaxis B.V. The Netherlands: Delft University of Technology.

Brinkgreve, R. B. J. 2005, Selection of Soil Models and Parameters for Geotechnical Engineering Application, ASCE Geotechnical Special Publication No. 128 Soil Constitutive Models; Evaluation, Selection, and Calibration, edited by J.A. Yamamuro and V. N. Kaliakin, pp. 69-98.

Peck, R.B., Hanson, W. E., and Thornburn, T. H. 1974. Foundation Engineering, 2nd edition, New York, John Wiley and Sons, Inc., 514 p.

Plaxis Short Course. 2006 (Jan). Computational Geomechanics and Dynamics, held at Polytechnic University Brooklyn, N.Y.

Potyondy, J. G. 1961. Skin Friction Between Various Soils and Construction Materials, Geotechnique, Vol. II, pp. 339-353.

Skemption, A. W. 1986. Standard Penetration Test Procedures and the Effects in Sands of Overburden Pressure, Relative Density, Particle Size, Ageing and Overconsolidation, Geotechnique, Vol. 36, No. 3, pp. 425-447.

Weber, W. G. 1969 (Jan). Performance of Embankments Constructed over Peat, ASCE Journal of the Soil Mechanics and Foundations Division, Vol. 95, No. SM1, pp. 53-76.

Appendix 10
Analysis of Performance of the Orleans Canal I-Walls

Purpose

The I-walls at the Orleans Canal did not fail, even though they were severely loaded. The purpose of the study described in this report was to determine if the analysis methods that indicated unstable conditions for the 17th Street Canal and London Avenue Canal I-walls, which did fail, would indicate stable conditions for the Orleans Canal I-walls, which did not fail.

The areas analyzed are shown in Figures 10-1 and 10-2. At the Orleans Canal south area (Station 8+61), the marsh layer beneath the levee is underlain by sand, as at the London Avenue breach locations. At the Orleans Canal north area (Station 64+27), the marsh layer beneath the levee is underlain by clay, as at the 17th Street Canal breach location. The geologic conditions at these two locations on the Orleans canal are thus directly comparable to the locations at the 17th Street Canal and the London Avenue Canal where breaches occurred.

Orleans South – Sand Underlying Levee and Marsh

Erosion and Piping

Steady state finite element analyses of seepage beneath the levee and I-wall were performed using the computer program SLIDE[1]. The characteristics of the cross section analyzed are shown in Figure 10-3. The relevant materials are the sand, the overlying marsh (peat) layer, and the clayey levee fill. The Bay Sound clay at the base of the section has very low permeability, and acts like an impermeable boundary beneath the sand. Similar values of permeability were used for these materials as were used for the seepage analyses at the London Avenue Canal: $k_{sand} = 1 \times 10^{-2}$ cm/sec, $k_{marsh} = 1 \times 10^{-5}$ cm/sec, $k_{levee\ fill} = 1 \times 10^{-6}$ cm sec, and $k_{Bay\ Sound\ clay} = 1 \times 10^{-6}$ cm/sec. The value of permeability for the sand was measured using a pumping test, and the other values of permeability are assumed, The most important factor governing the results of the seepage analyses is that the sand is much more permeable than the other materials in the cross section,

---

[1] Available from Rocscience Inc., 31 Balsam Avenue, Toronto, Ontario, Canada M4E 3B5

Volume V The Performance – Levees and Floodwalls – Technical Appendix

V-10-1

This is a preliminary report subject to revision; it does not contain final conclusions of the United States Army Corps of Engineers.

and the results of the seepage analyses would not be affected by moderate changes in the assumed values of permeability.

The hydraulic boundary conditions used in these analyses are shown in Figure 10-3. Two canal water levels were considered in the analyses: 11.1 ft (the highest canal water level reached on August 29th) and 13.2 ft (the elevation of the top of the I-wall). The design water elevation was 11.2 ft, essentially the same as the peak water level reached on August 29th. A constant-head boundary condition was imposed at the location of the drain beneath Marconi Drive. This head value was either -10.0 ft (the normal ground water level with pumps operating), or -3.0 ft (a higher level equal to the ground surface elevation, which might have occurred with pumps not operating).

Two possible conditions regarding cracking behind the wall are illustrated in Figure 10-4. The first involves cracking to the bottom of the wall, as considered at the 17th Street Canal. The second involves continuation of this crack below the bottom of the wall, by hydraulic fracturing of the levee fill and marsh material below the wall.

Hydraulic fracturing is possible in any location where (1) water pressures exceed the total stress on a potential fracture plane, as would be the case for a vertical plane extending below the bottom of the wall, and (2) the soil has sufficient strength for the crack to remain open, supported by the water pressure. The maximum possible depth of a hydraulic fracture, or crack, is related to the strength of the soil by the following equation:

$$ H_{\max crack} = \frac{2 s_u}{\left(\gamma_{soil} - \gamma_w \right)} \tag{10-1} $$

where $H_{\max \, crack}$ = maximum possible crack depth, s_u = undrained strength of soil, γ_{soil} = total unit weight of soil, and γ_w = unit weight of water. For the conditions at Orleans south, the levee fill and marsh are strong enough to maintain a water-filled crack extending down to the marsh-sand interface[2]. Water would fill this crack, loading the wall and the fracture plane below the wall, and introducing the canal head at the top of the sand.

Formation of a hydraulic fracture below the bottom of the wall would result in very severe loading on the wall for two reasons: (1) the crack would allow water to flow directly into the sand layer, increasing pore pressures and uplift pressures, and (2) the crack beneath the wall would extend the vertical face on which water pressures would act, thereby greatly increasing the water load acting on the plane of the wall. Although formation of a deeper crack by hydraulic fracturing has not been confirmed by field observation, it does appear to be feasible in soils as strong as the levee fill and marsh at Orleans south. Although occurrence of hydraulic fracturing is an extreme hypothesis, it is believed to be a condition that should be evaluated in this study of the performance of the Orleans south I-wall. Centrifuge model test results, and soil-structure

---

[2] The clay at the 17th Street Canal breach area is weaker than the marsh at Orleans. The clay at the 17th Street Canal is too weak to support a crack extending below the bottom of the wall.

interaction finite element analyses may help to confirm or refute the hydraulic fracturing at the Orleans Canal I-wall.

Six-node triangular elements were used for the seepage analyses. Seepage analyses were performed for eight different hydraulic boundary conditions, as shown in Table 10-1. An example finite element mesh (for Case 7) is shown in Figure 10-5. Computed total head contours for Case 7 are shown in Figure 10-6. It can be seen that the flow through the sand is predominantly horizontal, and that the total head on the landward side of the levee is above the ground surface, which is at elevation –3.0 ft. The head contours for the other cases had similar shapes, although the values of head were different, varying with the hydraulic boundary conditions.

Computed pore water pressures, or uplift pressures, at the base of the marsh layer are shown in Figure 10-7 for the eight cases analyzed, together with the total overburden pressure at the base of the marsh layer. For Cases 1 and 5, where the landside water level was -10 and the crack extended only to the bottom of the wall, the computed pore pressures are smaller than the total overburden pressure at the base of the marsh layer. In all other cases the computed pore pressures exceed the overburden pressure in some locations. This result indicates that in these cases the marsh layer would be heaved off the underlying sand by the uplift water pressures. A likely result of this heave would be rupture of the marsh layer at one or more weak points, and upward flow of water through the rupture through the marsh material. This flow would relieve the high water pressure locally, and create a new hydraulic boundary condition at the point of rupture.

Additional seepage analyses were performed to determine if the hydraulic gradients within the sand after rupture of the marsh layer would be large enough to cause erosion of the sand and begin a piping failure. For completeness, the same type of analysis was performed for Cases 1 and 5, although the uplift pressures did not exceed the overburden pressure. For these two cases the analyses correspond to existence of a pre-existing defect or void in the marsh layer, rather than a rupture caused by the uplift. The seepage boundary conditions used in theses analyses are shown in Figure 10-8, where a rupture or pre-existing void extends upward through the marsh layer, from the top of the sand to the ground surface. As for the London Avenue seepage analyses, a rupture zone width equal to 1.6 ft was used in these analyses. In the real case, flow would converge in three dimensions rather than two dimensions, as represented in these two-dimensional seepage analyses. It therefore seems likely that the actual hydraulic gradients that might develop would be higher than the values discussed in the following sections, but the magnitude of this three-dimensional effect cannot be quantified.

The effect of the changed hydraulic boundary conditions caused by the rupture or void were analyzed by imposing a head at the base of the rupture that was equal to the elevation of the ground surface, simulating a condition where the water level within the rupture or void rises to the ground surface. An example of total head contours in the sand at the base of the hypothesized rupture (for Case 6) is shown in Figure 10-9. Values of vertical hydraulic gradient in this zone are shown in Table 10-2 for the six cases analyzed. The computed values of i range from 0.20 to 1.23.

The value of hydraulic gradient that would cause erosion of the sand is:

$$i_{critical} = \frac{\gamma_b}{\gamma_w} = \frac{\gamma_s - \gamma_w}{\gamma_w} \qquad (10\text{-}2)$$

where $i_{critical}$ = hydraulic gradient that would cause erosion of the sand, γ_b = buoyant unit weight of sand, γ_w = unit weight of water, and γ_s = saturated unit weight of sand. With γ_s for the sand assumed to be 120 pcf, the critical hydraulic gradient is 0.92.

Values of $F_{erosion} = i_{crit}/i$ are shown in Table 10-2 for all eight cases analyzed. For Cases 1 and 2, with the highest observed canal water level and a crack to the bottom of the wall, the computed factors of safety against erosion are 4.60 for the lower inland water level and 1.39 for the higher inland water level. For Cases 3 and 4, with the highest observed water level and a hydraulic fracture extending to the top of the sand, the factors of safety against erosion are 1.48 for the lower inland water level, and 0.89 for the higher inland water level. Thus, for the most severe condition of the highest maximum possible inland water level and hydraulic fracturing to the top of the sand, the computed factor of safety against erosion is less than 1.0, but for all other cases it is greater than 1.0.

Cases 5 through 8 involve water levels higher than the maximum reached at the Orleans Canal. Nevertheless, it is interesting to examine the factors of safety for these conditions, to determine if the I-wall could have withstood even higher water levels. The calculated factors of safety against erosion are greater than 1.0, except for Case 8, where a hydraulic fracture to the top of the sand is assumed, and the inland water level is at the highest possible elevation.

The probability of erosion was calculated for all eight cases, considering the variation in factor of safety caused by the uncertain landside water level and the uncertain depth of cracking. A simple method based on the Taylor Series[3] was used for these calculations. The computed values of probability of erosion are shown in Table 10-3. For the canal water level at 11.1 ft, the maximum observed, the probability of erosion is 3% for a crack to the bottom of the wall, and nearly 30% for a crack down to the sand. For the canal water level at the top of the wall (13.2 ft), these probabilities of erosion are approximately twice as high.

The fact that no signs of erosion due to underseepage were reported in the Orleans south area after the flood neither confirms nor refutes these calculated probabilities. The analyses indicate a possibility of erosion, but this would not necessarily result in failure of the I-wall. Erosion, if it did occur beneath the marsh layer, might not result in visible manifestations at the ground surface, and might not move a sufficient quantity of sand to alter the cross section in any significant regard.

---

[3] Wolff, T. F. (1994). "Evaluating the reliability of existing levees." Report, Research Project: Reliability of Existing Levees, prepared for U.S. Army Engineer Waterways Experiment Station Geotechnical Laboratory, Vicksburg, Miss.

Slope Instability

Slope stability analyses were performed for Cases 1 through 8 shown in Table 10-1. The critical circles and factors of safety for these cases are shown in Figures 10-10 through 10-17. The cross section shown in theses figures is the same as that used in the seepage analyses. The analyses were performed using the computer program SLIDE[1], with Spencer's method.

Standard Penetration Tests performed in the Orleans south area showed that the sand had Standard Penetration Test blow counts (N_{SPT}) averaging about 40, which corresponds to a value of ϕ' in the range of 36 degrees to 40 degrees. Cone penetration tests in the area showed tip resistances that correspond to similar values of ϕ'. A value of $\phi' = 38$ degrees was used in the stability analyses.

The marsh layer was treated as undrained, with $s_u = 700$ psf and $\phi_u = 0$ beneath the levee crest, and $s_u = 450$ psf and $\phi_u = 0$ at the toe of the levee and beyond. These strength values, based on the available test results, are higher than the marsh strengths at the 17th Street Canal and the London Avenue Canal. The higher strengths at Orleans are likely due to the fact that the levee crest had been higher before the I-wall was constructed, and had compressed the marsh layer to a denser and stronger condition. The levee crest was degraded when the I-wall was built, and the marsh layer was overconsolidated as a result. A unit weight of 95 pcf was used for the marsh, based on available test results.

The levee fill was also treated as undrained, with $s_u = 1500$ psf, and $\phi_u = 0$. The slip circles do not intersect the levee fill, however, and the levee strength therefore has no influence on the calculated values of factor of safety. A value of unit weight = 109 pcf was used for the levee fill, based on available test results.

The analyses were performed using pore pressures in the sand from the finite element seepage analyses without a rupture or void through the marsh layer. The non-ruptured seepage analyses were used to determine pore pressures because a rupture or void would be of very limited size, not appropriate for inclusion in a two-dimensional cross section. At the bases of the slices where the pore pressures exceeded the overburden pressures near the top of the sand on the inland side, zero shear strength was assigned for the sand.

As discussed earlier, it was assumed in all analyses that deflection of the wall toward the land side would result in formation of a crack through the levee fill and the marsh in back of the wall, down to the bottom of the wall, or by hydraulic fracturing, down to the top of the sand. It was assumed that the crack would not extend below the top of the sand, because the sand is cohesionless, and would be expected to slump and fill any incipient crack. A crack to the bottom of the wall was assumed for Cases 1, 2, 5 and 6 (Figures 10-10, 10-11, 10-14 and 10-15), and a crack to the top of the sand was assumed for Cases 3, 4, 7, and 8 (Figures 10-12, 10-13, 10-16 and 10-17).

The critical circles extend to the bottom of the crack in all cases – to the bottom of the wall when the crack extends to that depth, and to the marsh/sand interface when the crack extends to

that depth. Hydrostatic water pressures act on the vertical plane of the crack, and the forces imposed by these pressures are the principal driving forces tending to cause instability.

The factors of safety calculated in these analyses are shown in Figures 10-10 through 10-17, and are summarized in Table 10-4. The values range from 1.38 to 2.71. Thus, even under the most severe conditions of water loading and possible crack formation considered here, the results of the analyses indicate that the wall would remain stable. For the highest water level observed at the Orleans south area, the lowest computed factor of safety is 1.86, which exceeds the minimum allowable for most conditions.

Probabilities of instability were computed considering uncertainties in crack depth, sand strength, and marsh strength, using the Taylor Series method[3]. The inland water level was varied from -10.0 ft to -3.0 ft, the sand friction angle was varied from 34 degrees to 42 degrees, and the marsh strength was varied by ±25% from its most likely average value. The results of the calculations are shown in Table 10-5.

For the canal water level at 11.1 ft, the calculated probability of instability is less than one in ten million for a crack extending to the bottom of the wall, and less than one in one million for a hydraulic fracture extending down to the sand. For the canal water level at the top of the wall (13.2 ft), the calculated probability of instability is less than one in one hundred thousand for a crack extending to the bottom of the wall, and less than one in one hundred for a hydraulic fracture extending down to the sand. Thus, for even the most severe conditions considered here, the calculations indicate that the probability of instability is small, and for the peak water level during the storm, it is very remote.

Orleans North – Clay Underlying Levee and Marsh

At the Orleans north area, the levee and I-wall are underlain by a marsh layer, which is in turn underlain by clay, and shown in Figure 10-18. As a consequence of the different soil conditions in this area, seepage effects are not important. The stability of the levee and I-wall are governed by the undrained shear strengths of the soils, most importantly, the clay.

The undrained strength of the clay was determined from the results of CPTU (piezocone) tests using Mayne's method[4], which is applicable to clays that are overconsolidated, as well as to clays that are normally consolidated. The undrained shear strength is related to cone tip resistance by the equation

$$s_u = 0.091\left(\sigma'_v\right)^{0.2}\left(q_t - \sigma_v\right)^{0.8} \tag{10-3}$$

where s_u = undrained shear strength, σ'_v = effective vertical stress, q_t = total cone tip resistance adjusted for pore pressure effects, and σ_v = total vertical stress.

---

[4] Mayne, P. W. (2003). "Class 'A' Footing Response Prediction from Seismic Cone Tests," Proceedings, Deformation Characteristics of Geomaterials, Vol. 1, Lyon, France.

The undrained shear strength calculated with this method is assumed to be equal to that measured using Direct Simple Shear (DSS) tests. This strength is lower than that measured by conventional triaxial compression tests and greater than that measured by triaxial extension tests. Ladd (1991)[5] suggests that this is a reasonable average value for design purposes.

Results for three CPTU tests are shown in Figure 10-19. It can be seen that the results are very consistent. Some fill was removed from the top of the levee when the I-wall was constructed, and this left the underlying marsh and clay somewhat overconsolidated. Although overconsolidation increases the value of s_u/p for a clay, and might be expected to affect the rate of increase of undrained strength with depth, it was found that the strength within the lacustrine clay depth interval could be conservatively approximated by a rate of increase of undrained strength with depth of 11 psf per ft. This is the same rate of strength increase as found for the normally consolidated clay at the 17th Street Canal. Although somewhat surprising, this result was found to be a consequence of counteracting influences – the undrained strength ratio is increased by virtue of overconsolidation, but the overconsolidation ratio decreases with depth. It was concluded that the heavy straight line shown in Figure 10-19 is a sufficiently accurate, somewhat conservative, representation of the undrained strength of the lacustrine clay. The variation of undrained shear strength horizontally and vertically beneath the levee was estimated using the equation

$$\frac{s_u}{p} = 0.24 \left(OCR^{0.8} \right) \tag{10-4}$$

where s_u = undrained shear strength, p = effective consolidation stress, and OCR = overconsolidation ratio. This equation was used to compute the undrained strength beneath the levee crest, beneath the toe, and beyond the toe of the levee. The resulting variation of undrained strength laterally and vertically within the cross section was represented in the stability analyses by means of the interpolation functions in SLIDE [1].

The marsh layer was treated as undrained, with s_u = 650 psf and ϕ_u = 0 beneath the levee crest, and s_u = 400 psf and ϕ_u = 0 at the toe of the levee and beyond. These strength values are based on the available test results. As noted above, the high strengths at Orleans are likely due to the fact that the levee crest had been higher before the I-wall was constructed, and the higher levee had compressed the marsh layer to a denser and stronger condition. A unit weight of 95 pcf was used for the marsh, based on available test results.

The levee fill was also treated as undrained, with s_u = 1500 psf, and ϕ_u = 0. The slip circles do not intersect the levee fill, however, and the levee strength therefore has no influence on the calculated values of factor of safety. A value of unit weight = 109 pcf was used for the levee fill, based on available test results.

---

[5] Ladd, C. C. (1991) "Stability Evaluation During Staged Construction," Terzaghi Lecture, ASCE Journal of Geotechnical Engineering, 117 (4), 540-615.

It was assumed in all of the Orleans north analyses that deflection of the wall toward the land side would result in formation of a crack through the levee fill and the marsh in back of the wall, down to the bottom of the wall.

The critical circles and factors of safety calculated in these analyses are shown in Figures 10-20 and 10-21, and the factors of safety are given in Table 10-6. The factors of safety are 1.62 for the highest observed water level (11.1 ft), and 1.47 for the water at the top of the wall (12.8 ft in this area). Thus, even under the most severe conditions of water loading and possible crack formation considered here, the results of the analyses indicate that the wall would remain stable. For the highest water level observed at the Orleans north area, the computed factor of safety is 1.62, which exceeds the minimum allowable for most conditions.

Probabilities of instability were computed considering uncertainties in clay strength and marsh strength, using the Taylor Series method [3]. The clay and marsh strengths were varied by ±25% from their most likely average values. The results of the calculations are shown in Table 10-7.

For the canal water level at 11.1 ft, the calculated probability of instability is less than one percent for a crack extending to the bottom of the wall. For the canal water level at the top of the wall (12.8 ft), the calculated probability of instability is 2.5%. Thus, for even the most severe conditions considered here, the calculations indicate that the probability of instability is small.

Design Analyses

The shear strengths, factor of safety criteria and stability analysis results are described in two Geotechnical Design Memoranda[6,7]. The stability analyses were performed using the Method of Planes.[8]

For Stations 0+00 to 90+50 (which includes both the south and north sections analyzed in this report) lower undrained shear strengths were used for the clay beneath the toe of the embankment and beyond the toe than were used for the clay beneath the center of the levee. For sections further to the north, from Station 90+50 to Lake Pontchartrain, the same undrained shear strengths were used at the levee centerline, and at and beyond the toe of the levee.

The GDMs[5,7] indicate a minimum acceptable factor of safety equal to 1.25 with the wall subjected to the design static water level and wave-load. The results of the stability analyses, summarized on Plate 48 for Stations 0+00 to 36+50 east (which includes to south section

---

[6] Design Memorandum No. 19, General Design Vol. 1, *Orleans Avenue Outfall Canal*, Lake Pontchartrain, LA, and Vicinity, Lake Pontchartrain High Level Plan, Department of the Army, New Orleans District, Corps of Engineers, August 1988, Serial No. 53.

[7] Design Memorandum No. 19, General Design Vol. 2, *Orleans Avenue Outfall Canal*, Lake Pontchartrain, LA, and Vicinity, Lake Pontchartrain High Level Plan, Department of the Army, New Orleans District, Corps of Engineers, August 1988, Serial No. 76.

[8] A study of the Method of Planes, undertaken by IPET at the request of the New Orleans District Task Force Guardian, indicates that the Method of Planes gives lower factors of safety than more accurate methods of analysis, such as Spencer's method. The magnitude of the difference between the two varies from case to case.

analyzed in this report), and on Plate 54 for Stations 64+00 to 90+50 east (which includes the north section analyzed in this report), show that the lowest computed factors of safety were 1.30 in both cases. No crack behind the wall was considered in the analyses.

Consideration was given by the designers to the possibility that the water pressure in the Pine Island Beach sand beneath the marsh and lacustrine clay might be elevated during periods of high water level in the canal. Such water pressures would adversely affect stability, as was the case at the London Avenue south breach. The possibility of high water pressures in the Pine Island Beach sand formation was investigated by installing three piezometers near Station 18+10. These piezometers indicated no hydraulic communication between the water in the canal and the sand. Observations of other piezometer installations, in 1970 and 1971, also indicated that the buried beach sand was not hydraulically connected to the canal. The possibility that a hydraulic connection between the canal and the sand might result from dredging or erosion of the clay in the bottom of the canal was investigated by a test section at the 17th Street Canal, where the overlying impermeable materials were dredged to expose the beach sand in the bottom of the canal. Piezometer readings taken before and after the dredging showed no significant changes in piezometric levels due to dredging. On the basis of these studies, stability analyses were performed using water pressures in the Pine Island Beach sand that reflected normal groundwater elevations, unaffected by rise in the canal water level.

Summary

The analyses described here were performed as a test of the methods of analysis that were applied previously in investigations of the failures of the 17th Street Canal and London Avenue Canal I-walls. The objective was to determine if these same methods are capable of showing that failure should not occur, in cases where failure did not occur. The Orleans Canal south area, where the levee and marsh are underlain by sand, is directly comparable to the London Avenue Canal south breach area. The Orleans Canal north area, where the levee and marsh are underlain by clay, is directly comparable to the 17th Street Canal breach area.

The same type of seepage analysis and interpretation of results that showed high hydraulic gradients, factors of safety less than 1.0, and probability of erosion greater than 99% at the London Avenue south breach showed moderate hydraulic gradients, factors of safety larger than 1.0, and probabilities of erosion of 3% and 28% for the highest water level experienced on the Orleans Canal. The fact that no signs of erosion due to underseepage were observed in the Orleans south area after the flood neither confirms nor refutes these calculated probabilities. The analyses indicate a possibility of erosion, but this would not necessarily result in failure of the I-wall. Erosion, if it did occur beneath the marsh layer, might not result in visible manifestations at the ground surface, and might not move a sufficient quantity of sand to alter the cross section in any significant regard.

The same type of stability analyses and interpretation of results that showed factors of safety less than 1.0, and probabilities of instability varying from 70% to 97% at the London Avenue north breach showed factors of safety varying from 1.9 to 2.7 for the highest water level observed at the Orleans Canal, and probabilities of instability lower than one in one million.

These results show that the methods of stability analysis applied to conditions with sand beneath the levee and marsh layer are capable of modeling instability where it occurs, and stable conditions where they occur.

The same type of stability analyses and interpretation of results that showed factors of safety from 1.0 to 1.2, and probabilities of instability from 12% to 60% for the 17th Street Canal breach, showed factors of safety from 1.5 to 1.6 for the highest water level observed at the Orleans Canal, and probabilities of instability from 1% to 3%. These results show that the methods of stability analysis applied to conditions with clay beneath the levee and marsh layer are capable of modeling instability where it occurs, and stable conditions where they occur.

Table 10-1
Hydraulic Boundary Conditions for Seepage Analyses – Orleans South

Case	Canal water level – CWL	Marconi Drive water level – LWL
1	11.1 ft	-10.0 ft
2	11.1 ft	-3.0 ft
3	11.1 ft	-10.0 ft
4	11.1 ft	-3.0 ft
5	13.2 ft	-10.0 ft
6	13.2 ft	-3.0 ft
7	13.2 ft	-10.0 ft
8	13.2 ft	-3.0 ft
Note: Elevation datum = NAVD88 Crack to bottom of wall for Cases 1, 2, 5, and 6. Crack to top of sand for Cases 3, 4, 7, and 8.		

Table 10-2
Calculated Hydraulic Gradients and Factors of Safety Against Erosion – Orleans South

Case	CWL	LWL	i = vertical hydraulic gradient	$F_{ersosion} = i_{crit}/i$
1	11.1 ft	-10.0	0.20	4.60
2	11.1 ft	-3.0	0.60	1.39
3	11.1 ft	-10.0	0.62	1.48
4	11.1 ft	-3.0	1.03	0.89
5	13.2 ft	-10.0	0.34	2.71
6	13.2 ft	-3.0	0.80	1.15
7	13.2 ft	-10.0	0.82	1.12
8	13.2 ft	-3.0	1.23	0.75
Notes: Crack to bottom of wall for Cases 1, 2, 5, and 6. Crack to top of sand for Cases 3, 4, 7, and 8. With γ_{sat} = 120 pcf, i_{crit} = 0.92				

Table 10-3
Calculated Probabilities of Erosion – Orleans South

Case	CWL	LWL	$F_{erosion}$	ΔF	σ_F	F_{MLV}	COV_F	$p_{erosion}$
1	11.1 ft	-10.0 ft	4.60	3.21	1.60	3.00	56%	3%
2	11.1 ft	-3.0 ft	1.39					
3	11.1 ft	-10.0 ft	1.48	0.59	0.30	1.19	25%	28%
4	11.1 ft	-3.0 ft	0.89					
5	13.2 ft	-10.0 ft	2.71	1.56	0.78	1.93	40%	7%
6	13.2 ft	-3.0 ft	1.15					
7	13.2 ft	-10.0 ft	1.12	0.37	0.18	0.94	19%	66%
8	13.2 ft	-3.0 ft	0.75					

Notes:
Crack to bottom of wall for Cases 1, 2, 5, and 6.
Crack to top of sand for Cases 3, 4, 7, and 8.
ΔF = change in F due to variation in parameter values
σ_F = standard deviation of factor of safety for the variations considered
F_{MLV} = most likely value of factor of safety
COV_F = coefficient of variation of factor of safety
$p_{erosion}$ = probability of erosion

Table 10-4
Factor of Safety Against Instability – Orleans South

Case	CWL	LWL	$F_{stability}$
1	11.1 ft	-10.0 ft	2.71
2	11.1 ft	-3.0 ft	2.22
3	11.1 ft	-10.0 ft	2.29
4	11.1 ft	-3.0 ft	1.86
5	13.2 ft	-10.0 ft	2.35
6	13.2 ft	-3.0 ft	1.89
7	13.2 ft	-10.0 ft	1.74
8	13.2 ft	-3.0 ft	1.38

Note:
Crack to bottom of wall for Cases 1, 2, 5, and 6.
Crack to top of sand for Cases 3, 4, 7, and 8.

Table 10-5
Probability of Instability – Orleans South

Case	CWL (ft)	LWL (ft)	ϕ' (deg)	Su marsh Crest/toe psf	F	ΔF	σ_F	F_{MLV}	COV_F	$p_{instability}$
1	11.1	-10.0	38	700/450	2.71	0.49	0.42	2.47	17%	Less than 10^{-7}
2	11.1	-3.0	38	700/450	2.22					
1a	11.1	-10.0	38	875/563	2.96	0.54				
1b	11.1	-10.0	38	525/338	2.42					
1c	11.1	-10.0	34	700/450	2.51	0.41				
1d	11.1	-10.0	42	700/450	2.92					
3	11.1	-10.0	38	700/450	2.29	0.43	0.32	2.08	15%	Less than 10^{-6}
4	11.1	-3.0	38	700/450	1.86					
4a	11.1	-3.0	38	875/563	1.97	0.24				
4b	11.1	-3.0	38	525/338	1.73					
4c	11.1	-3.0	34	700/450	1.67	0.40				
4d	11.1	-3.0	42	700/450	2.07					
5	13.2	-10.0	38	700/450	2.35	0.46	0.35	2.12	17%	Less than 10^{-5}
6	13.2	-3.0	38	700/450	1.89					
6a	13.2	-3.0	38	875/563	2.11	0.47				
6b	13.2	-3.0	38	525/338	1.64					
6c	13.2	-3.0	34	700/450	1.78	0.22				
6d	13.2	-3.0	42	700/450	2.00					
7	13.2	-10.0	38	700/450	1.74	0.36	0.25	1.53	17%	Less than 10^{-2}
8	13.2	-3.0	38	700/450	1.38					
8a	13.2	-3.0	38	875/563	1.42	0.28				
8b	13.2	-3.0	38	525/338	1.14					
8c	13.2	-3.0	34	700/450	1.18	0.22				
8d	13.2	-3.0	42	700/450	1.40					

Notes:
ΔF = change in F due to variation in parameters for the two conditions
σ_F = standard deviation of factor of safety for the variations considered
F_{MLV} = most likely value of factor of safety
COV_F = coefficient of variation of factor of safety
$p_{instability}$ = probability of instability

Table 10-6
Factors of Safety Against Instability – Orleans North

Case	CWL ft	Clay strength	Su marsh Crest/toe psf	F
1	11.1	$S_u/p = 0.24*OCR^{0.8}$	650/400	1.62
2	12.8	$S_u/p = 0.24*OCR^{0.8}$	650/400	1.47

Table 10-7
Probability of Instability – Orleans North

Case	CWL ft	Clay strength	Su marsh Crest/toe psf	F	ΔF	σ_F	F_{MLV}	COV_F	$p_{instability}$
1a	11.1	$S_u/p = 0.30*OCR^{0.8}$	650/400	1.91	0.59	0.31	1.62	19%	Less than 1 %
1b	11.1	$S_u/p = 0.18*OCR^{0.8}$	650/400	1.32					
1c	11.1	$S_u/p = 0.24*OCR^{0.8}$	813/500	1.73	0.22				
1d	11.1	$S_u/p = 0.24*OCR^{0.8}$	488/300	1.51					
2a	12.8	$S_u/p = 0.30*OCR^{0.8}$	650/400	1.73	0.52	0.28	1.47	19%	2.5%
2b	12.8	$S_u/p = 0.18*OCR^{0.8}$	650/400	1.21					
2c	12.8	$S_u/p = 0.24*OCR^{0.8}$	813/500	1.58	0.22				
2d	12.8	$S_u/p = 0.24*OCR^{0.8}$	488/300	1.36					

Figure 10-1. Aerial View of Orleans Avenue Canal – South (Station 8+61)

Volume V The Performance – Levees and Floodwalls – Technical Appendix

V-10-13

This is a preliminary report subject to revision; it does not contain final conclusions of the United States Army Corps of Engineers.

Figure 10-2. Aerial View of Orleans Avenue Canal – North (Station 64+27)

This is a preliminary report subject to revision; it does not contain final conclusions of the United States Army Corps of Engineers.

Figure 10-3. Schematic Cross Section at Orleans South, with Seepage Boundary Conditions
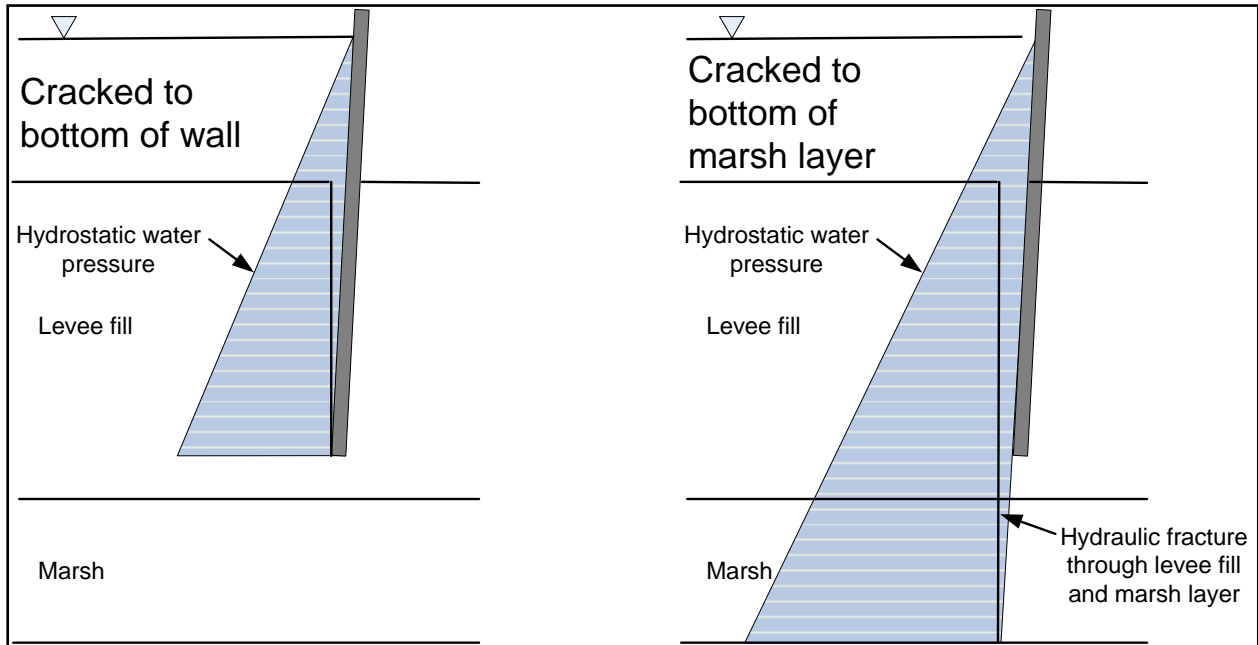
Figure 10-4. Schematic of Cracks Used in Orleans South Seepage and Stability Analyses

Volume V The Performance – Levees and Floodwalls – Technical Appendix   V-10-15

This is a preliminary report subject to revision; it does not contain final conclusions of the United States Army Corps of Engineers.
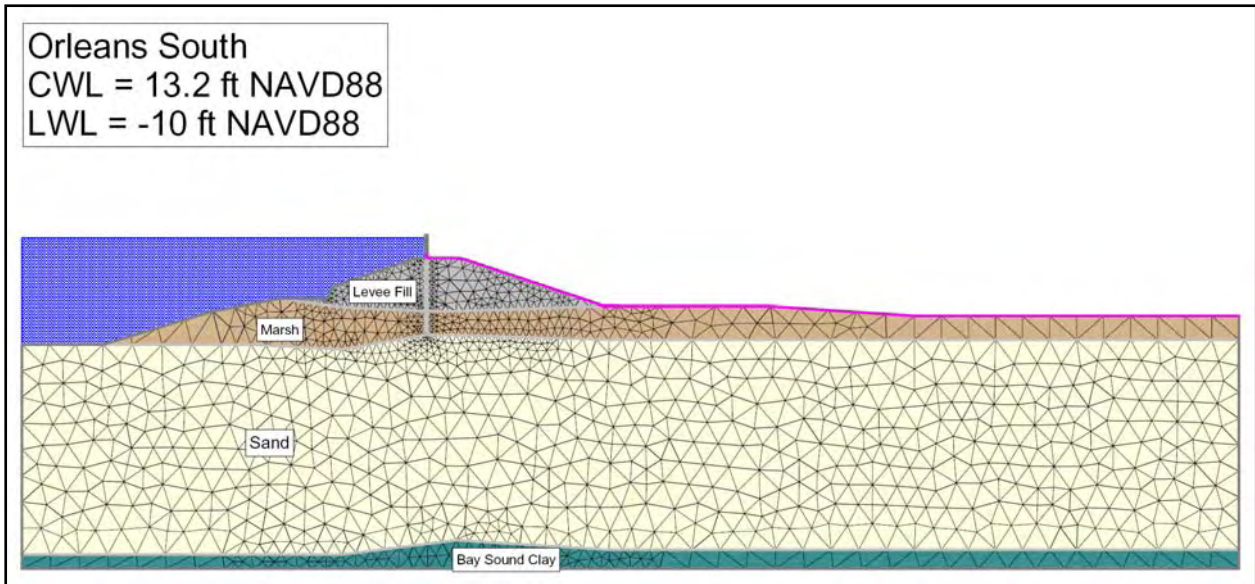
Figure 10-5. Finite Element Mesh Used for Seepage Analysis for Orleans South (Case 7)
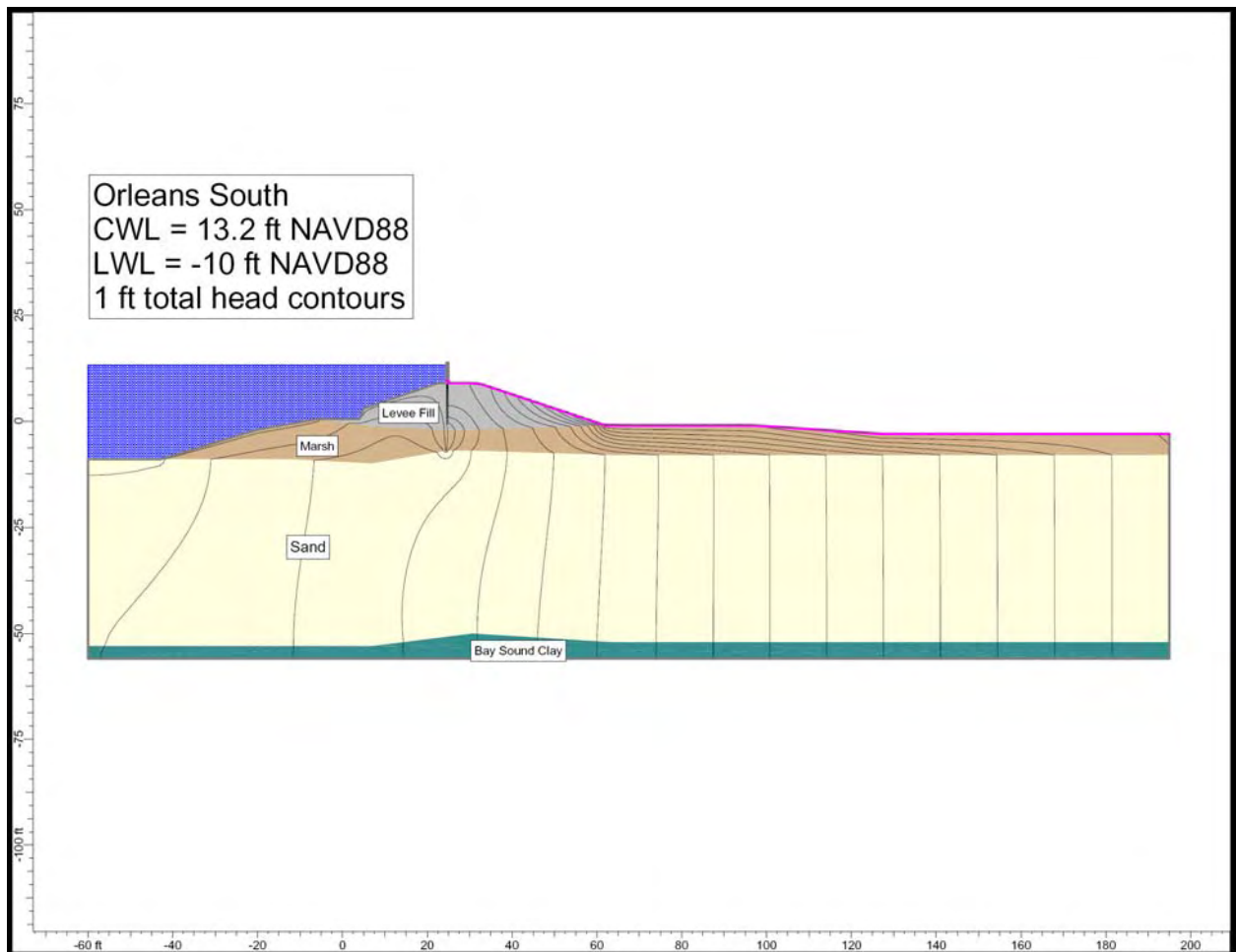
Figure 10-6. Total Head Contours for Orleans South (Case 7)

Volume V The Performance – Levees and Floodwalls – Technical Appendix
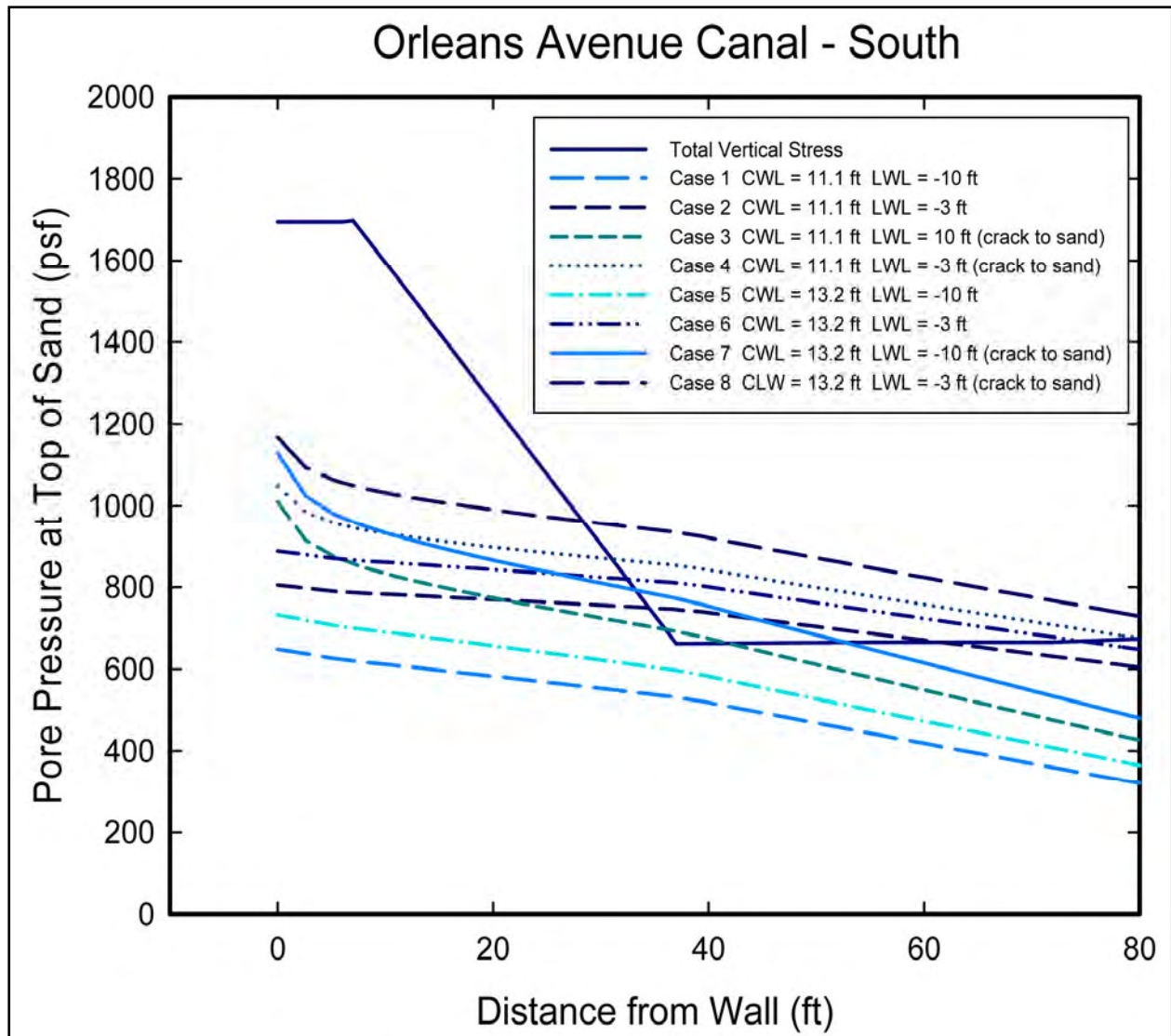
Figure 10-7. Calculated Uplift Pressures and Total Overburden Pressure for Orleans South
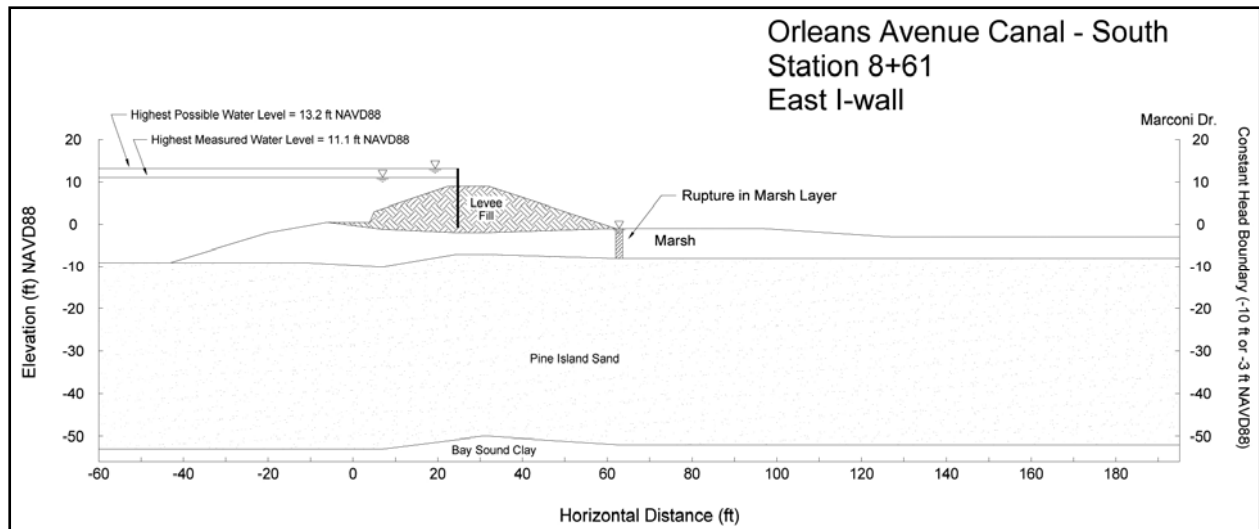
Figure 10-8. Schematic Cross Section for Orleans South, Showing Rupture Through Marsh Layer
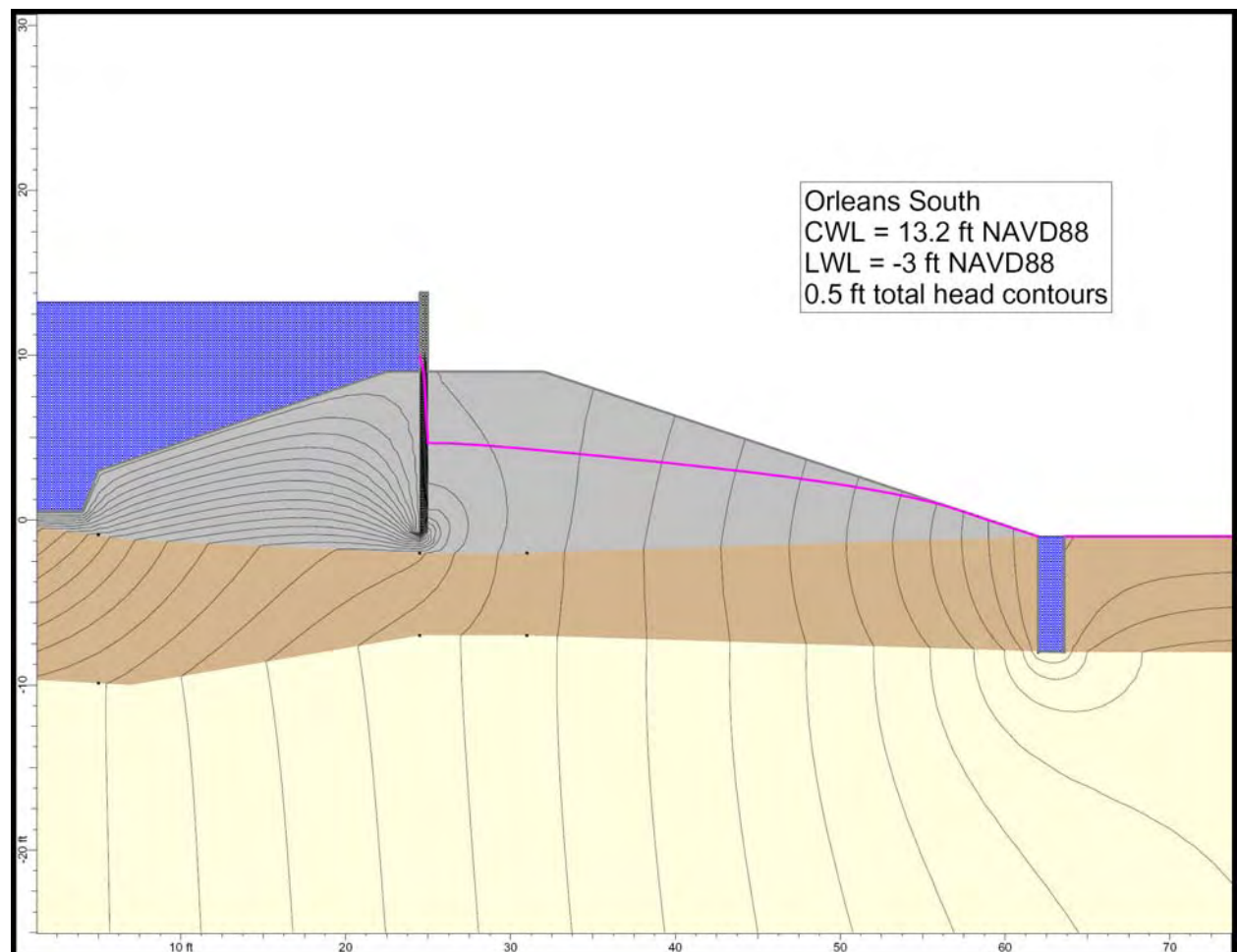
Figure 10-9. Total Head Contours in Vicinity of Rupture for Orleans South (Case 6)
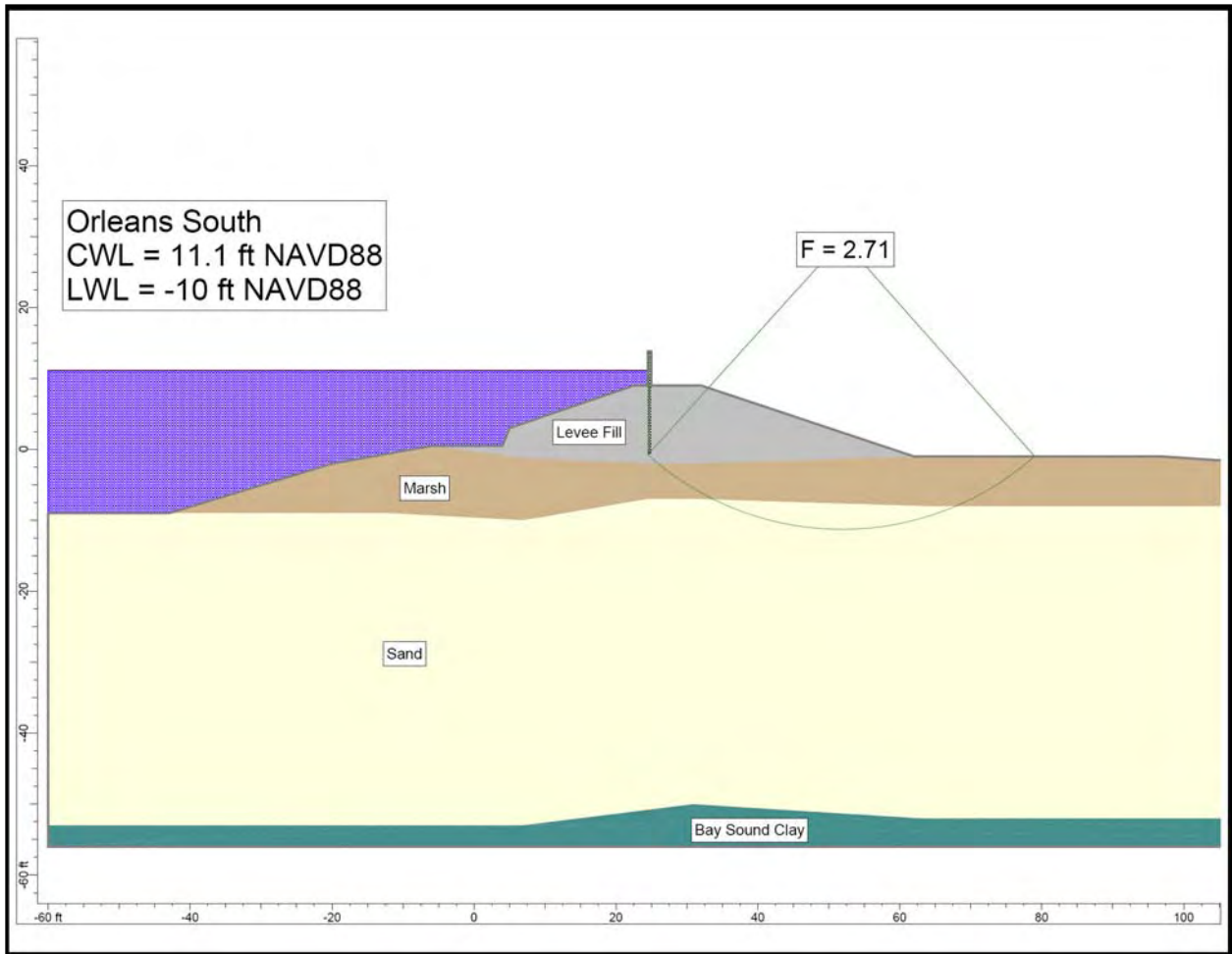
Figure 10-10. Orleans South Case 1 Stability Analysis
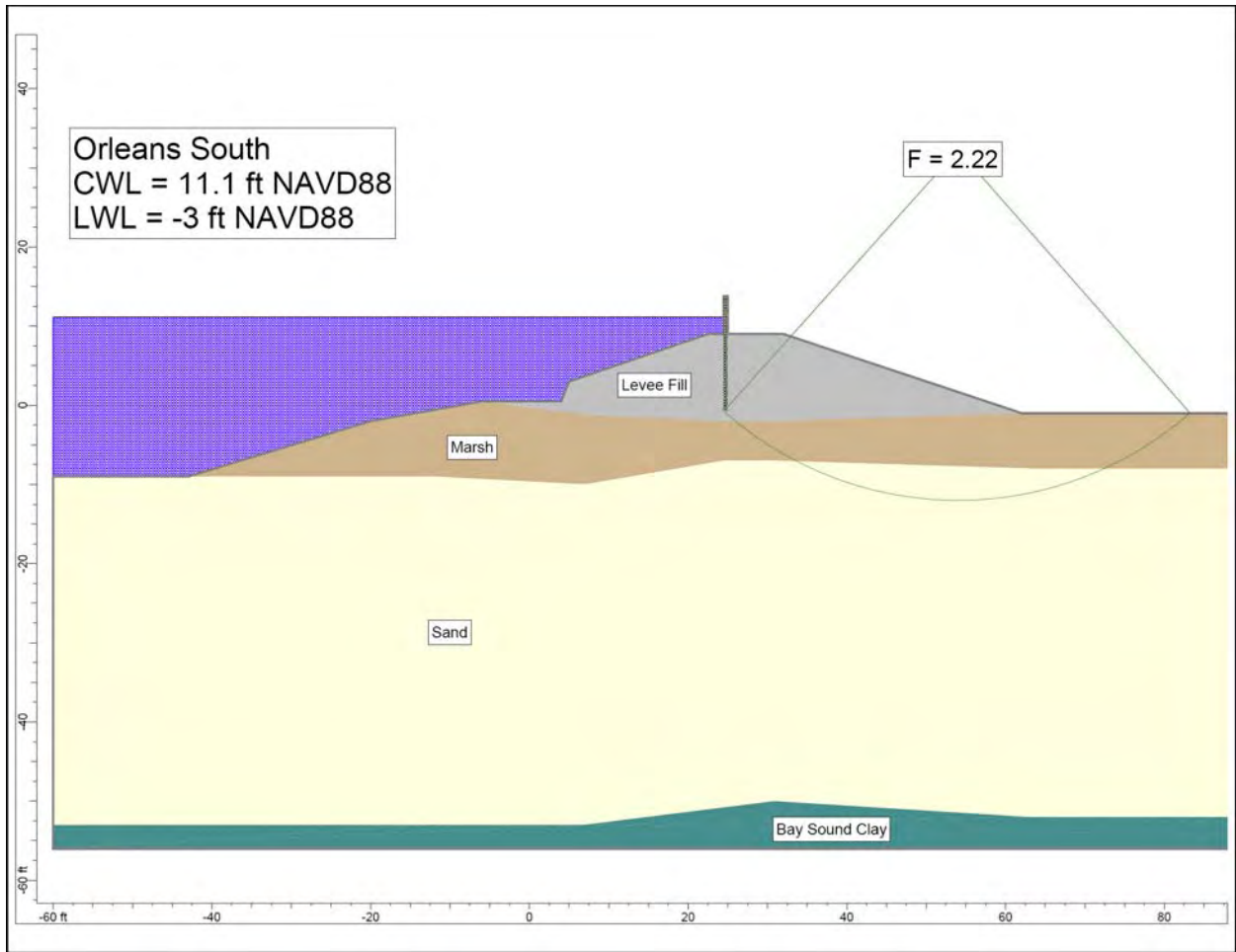
Figure 10-11. Orleans South Case 2 Stability Analysis
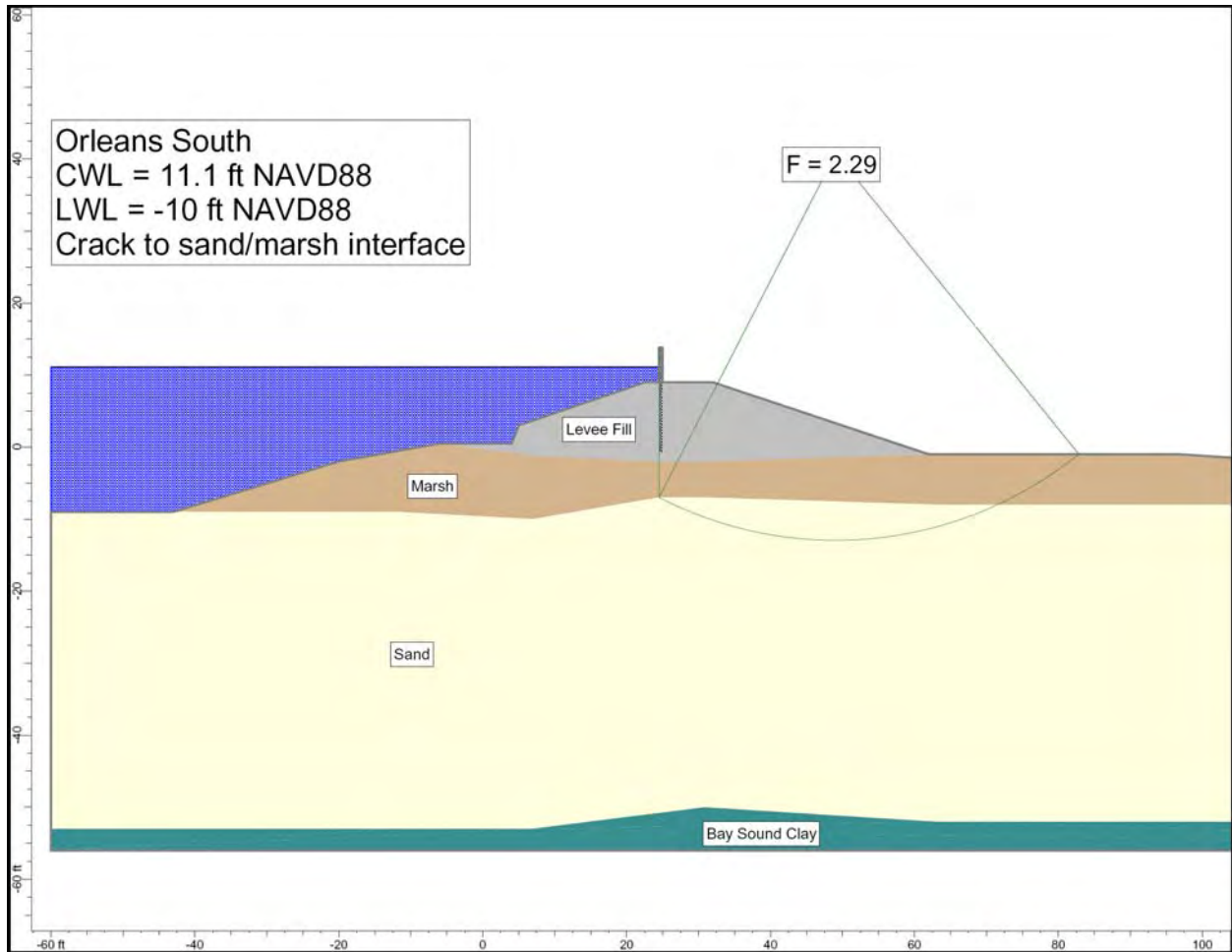
Figure 10-12. Orleans South Case 3 Stability Analysis

Volume V The Performance – Levees and Floodwalls – Technical Appendix   V-10-21

This is a preliminary report subject to revision; it does not contain final conclusions of the United States Army Corps of Engineers.
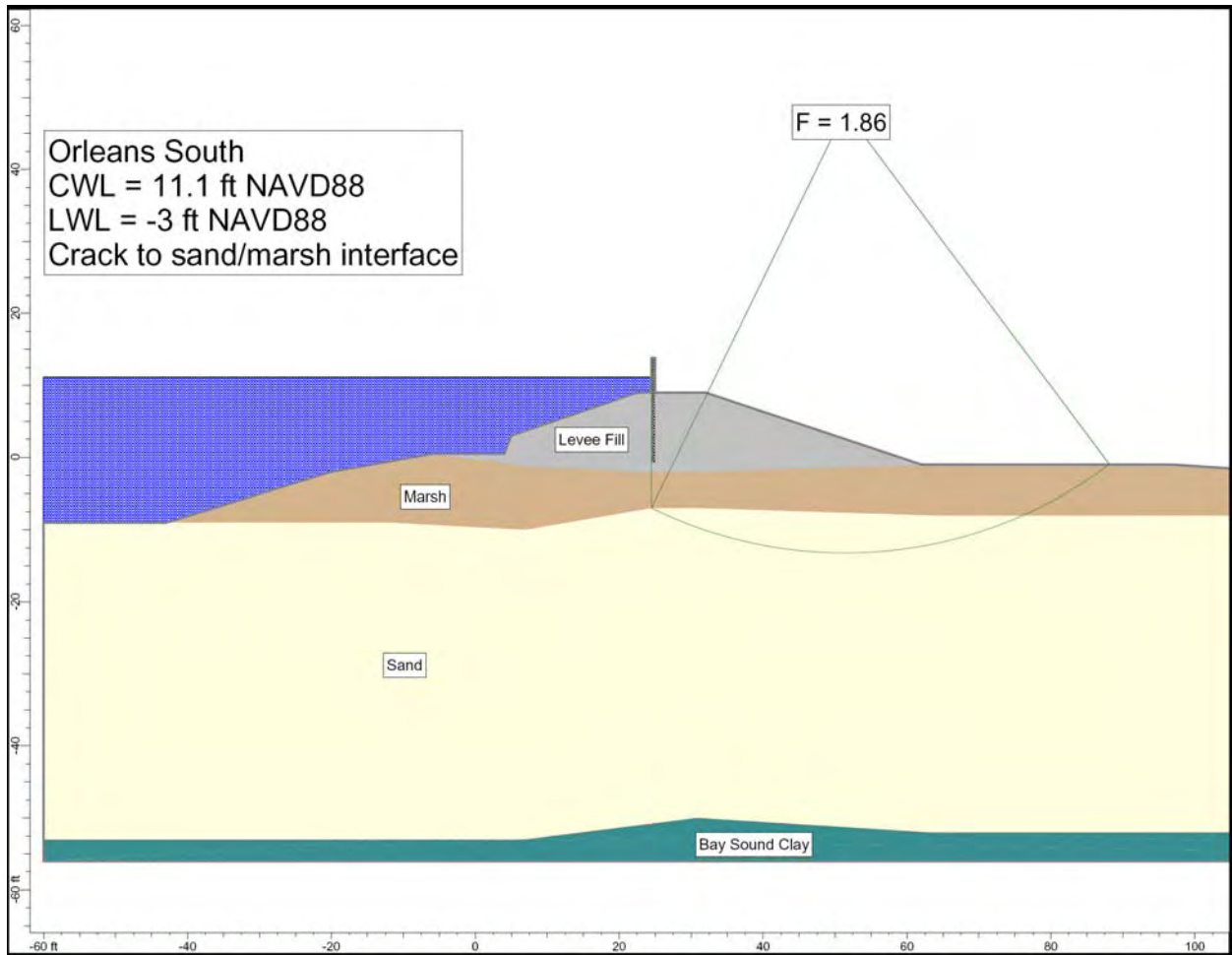
Figure 10-13. Orleans South Case 4 Stability Analysis
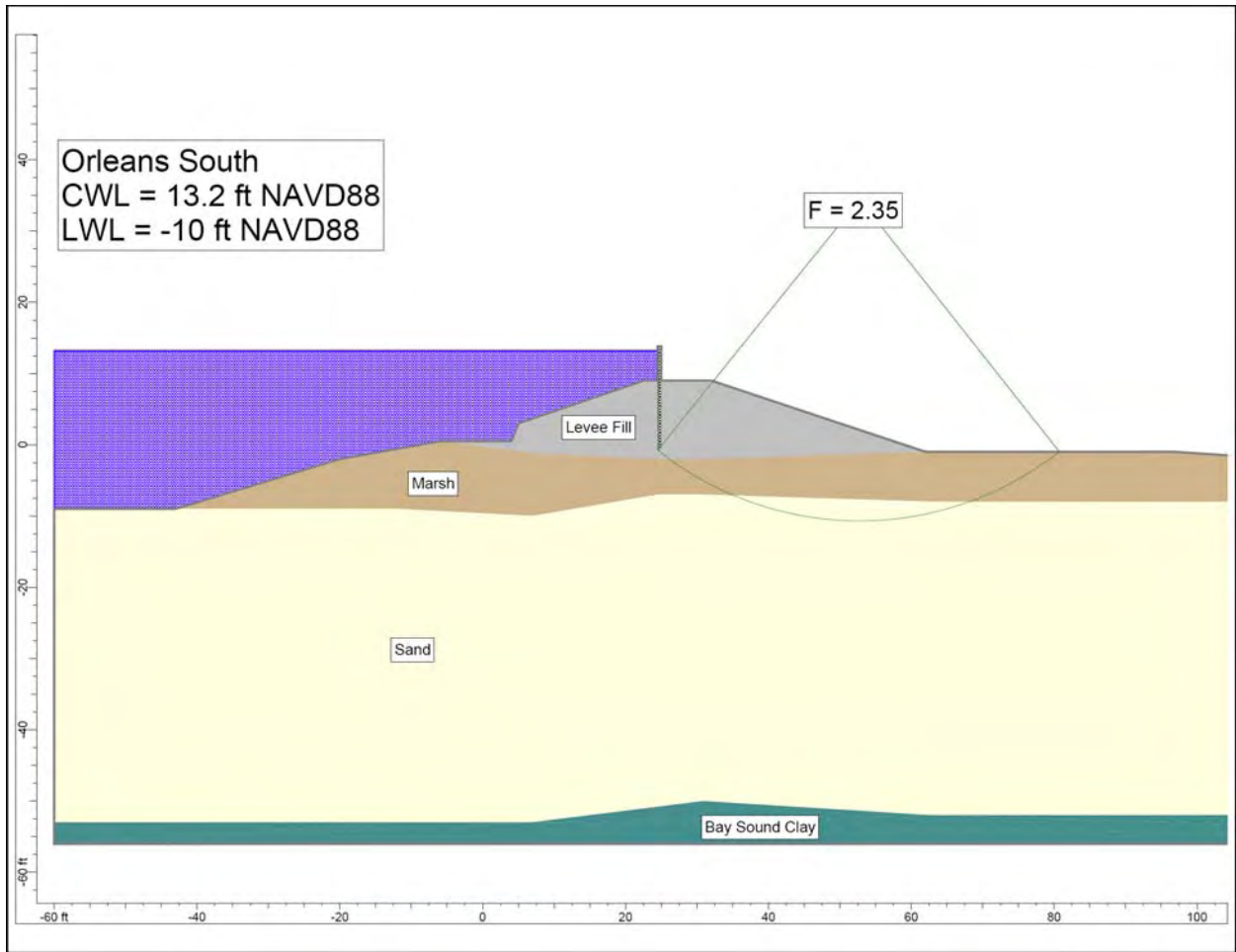
Figure 10-14. Orleans South Case 5 Stability Analysis
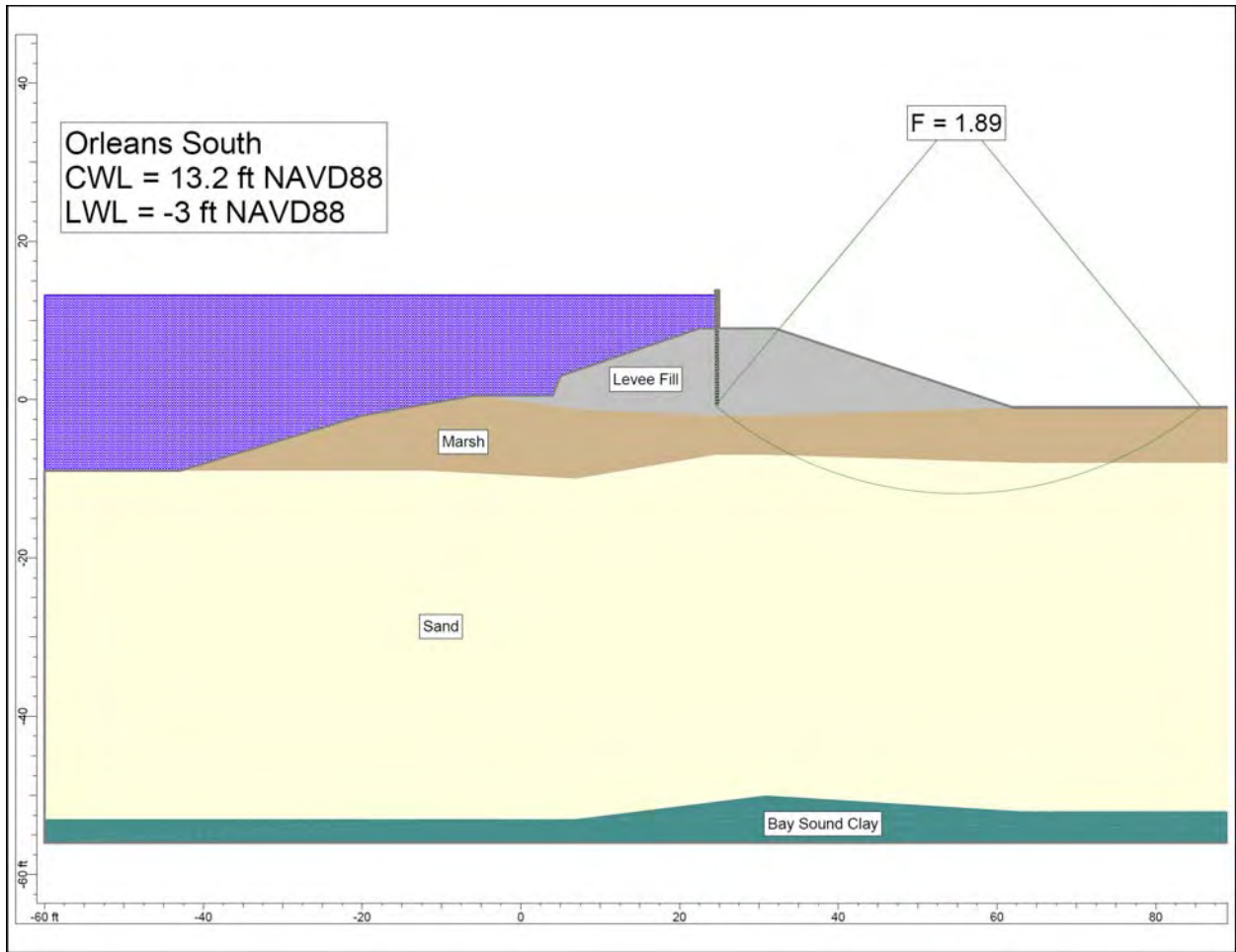
Figure 10-15. Orleans South Case 6 Stability Analysis
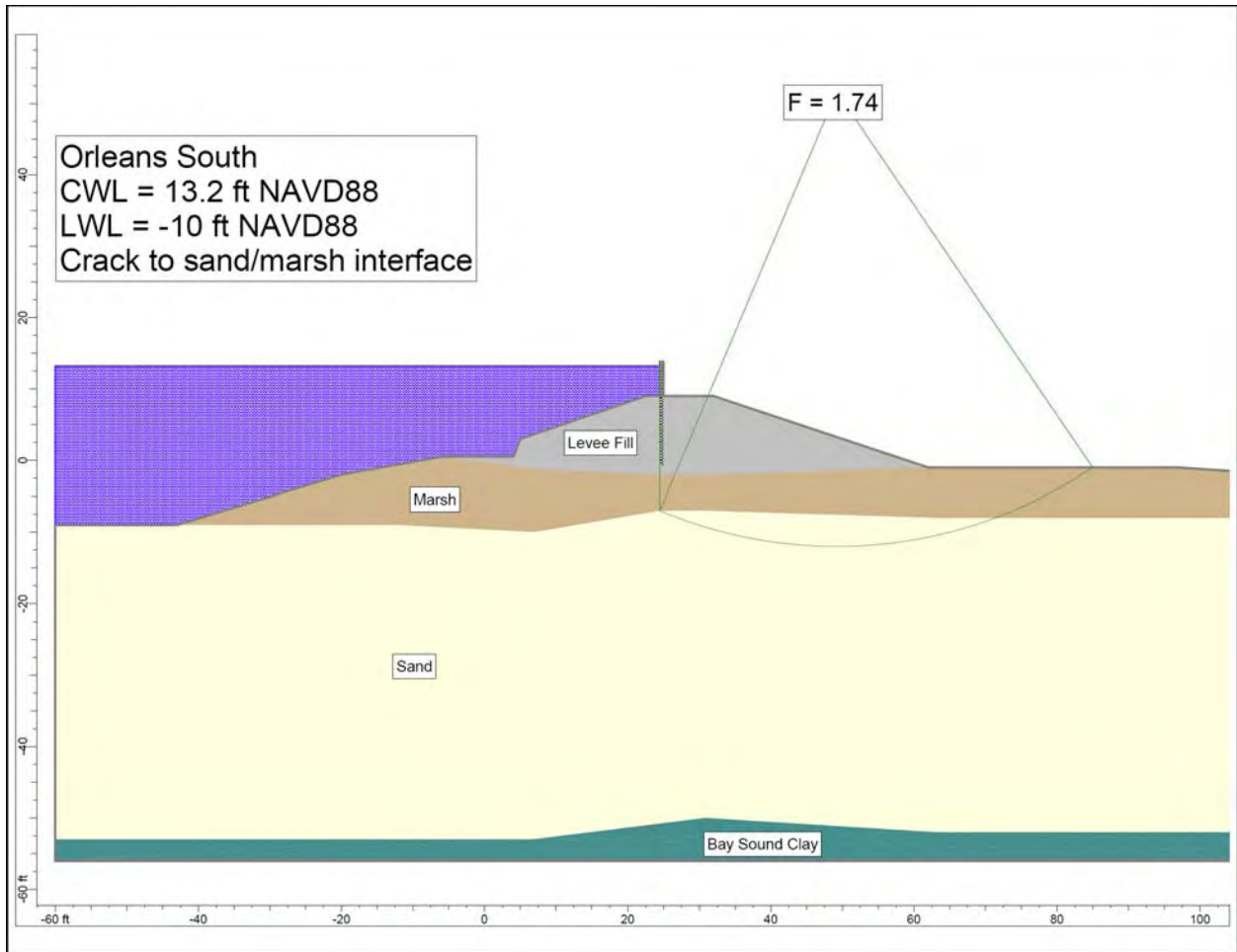
Figure 10-16. Orleans South Case 7 Stability Analysis
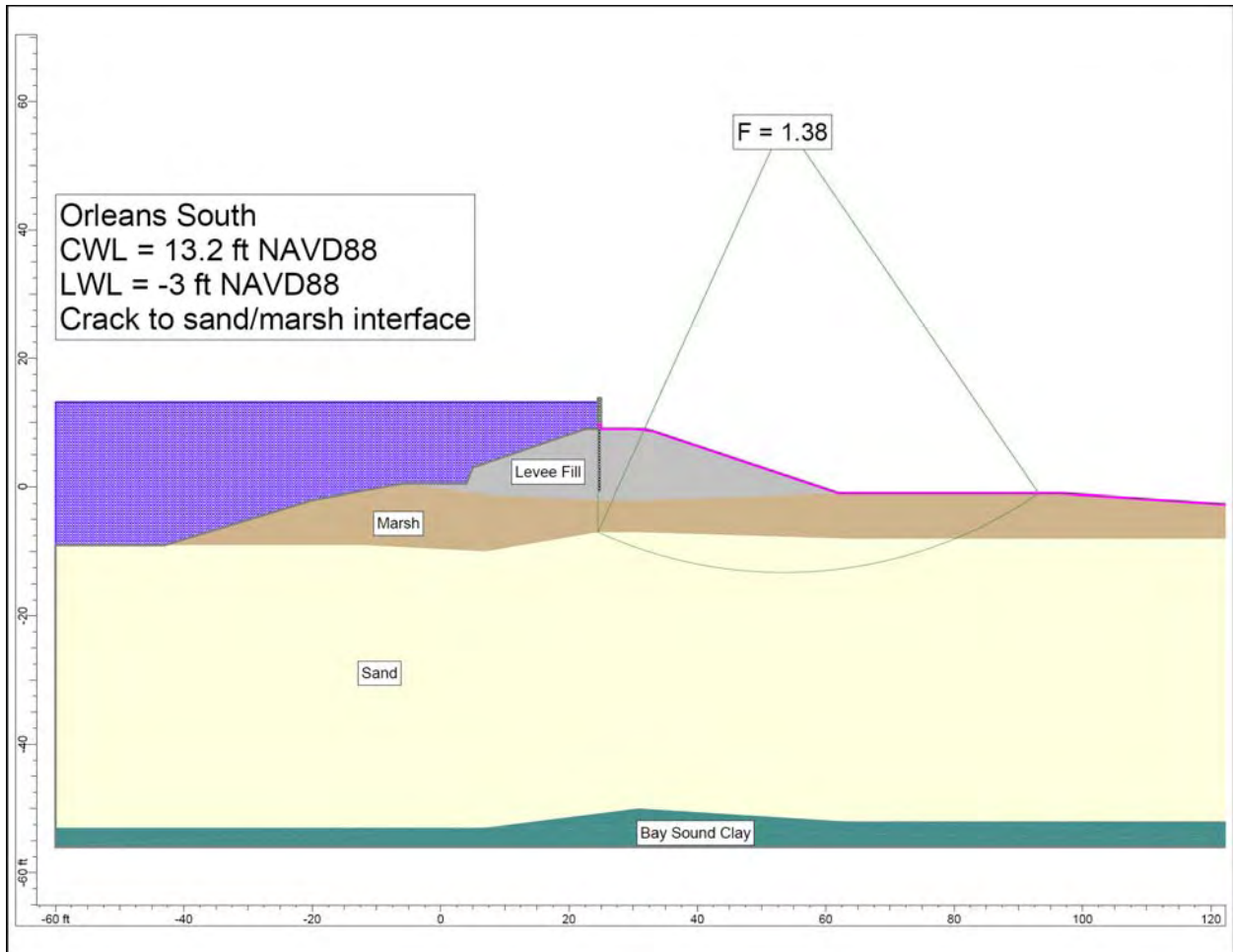
Figure 10-17. Orleans South Case 8 Stability Analysis

Orleans Avenue Canal - North
Station 64+27
East I-wall
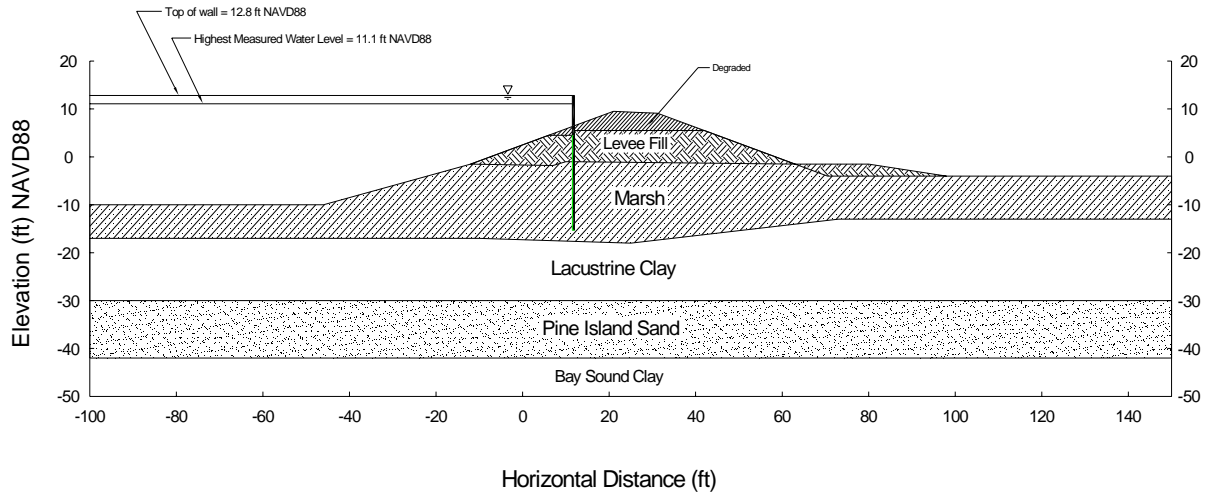
Figure 10-18. Schematic Cross Section of Orleans North
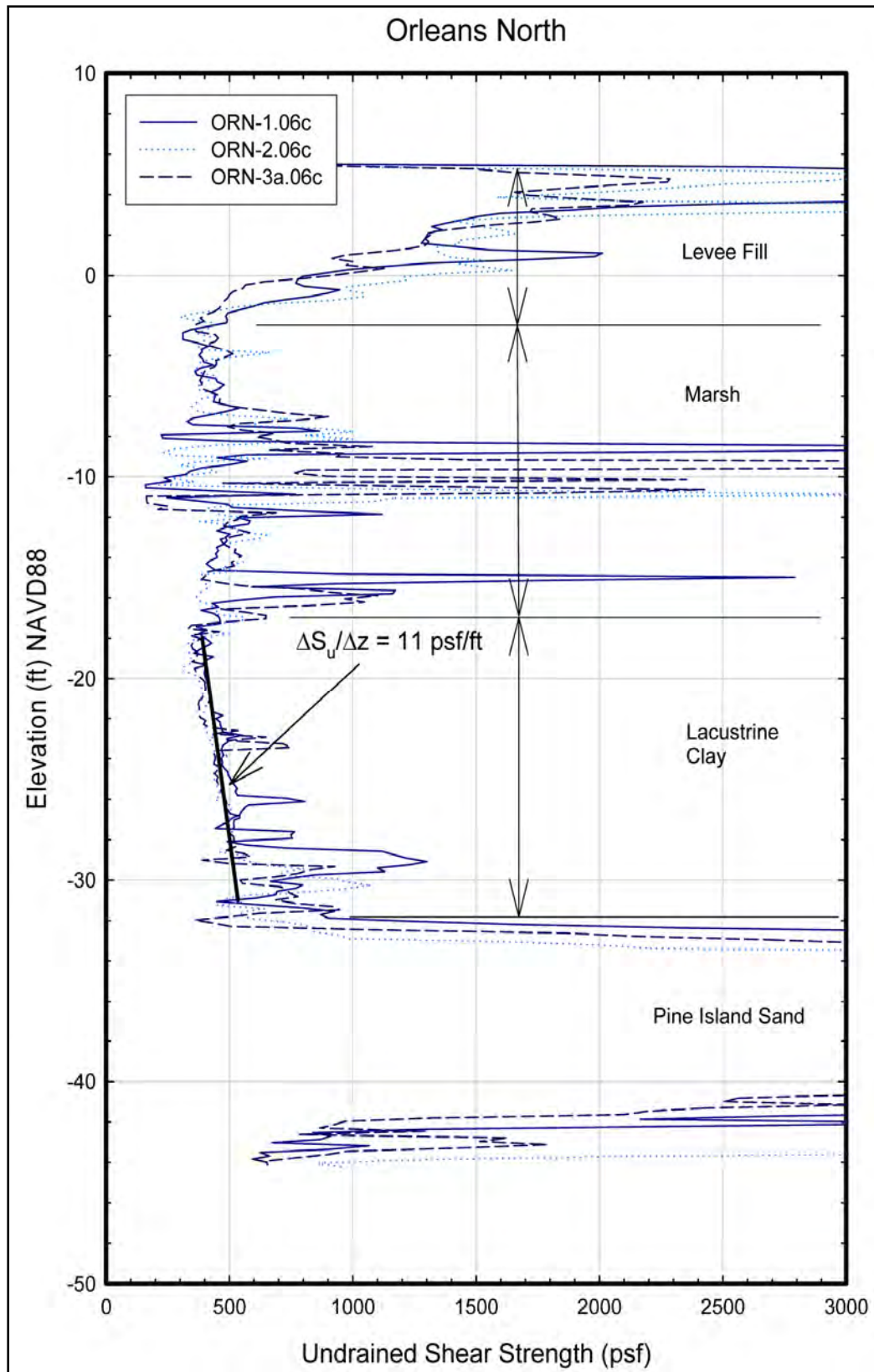
Figure 10-19. Undrained Shear Strength of Clay Calculated from CPTU Tests Using Mayne's Method
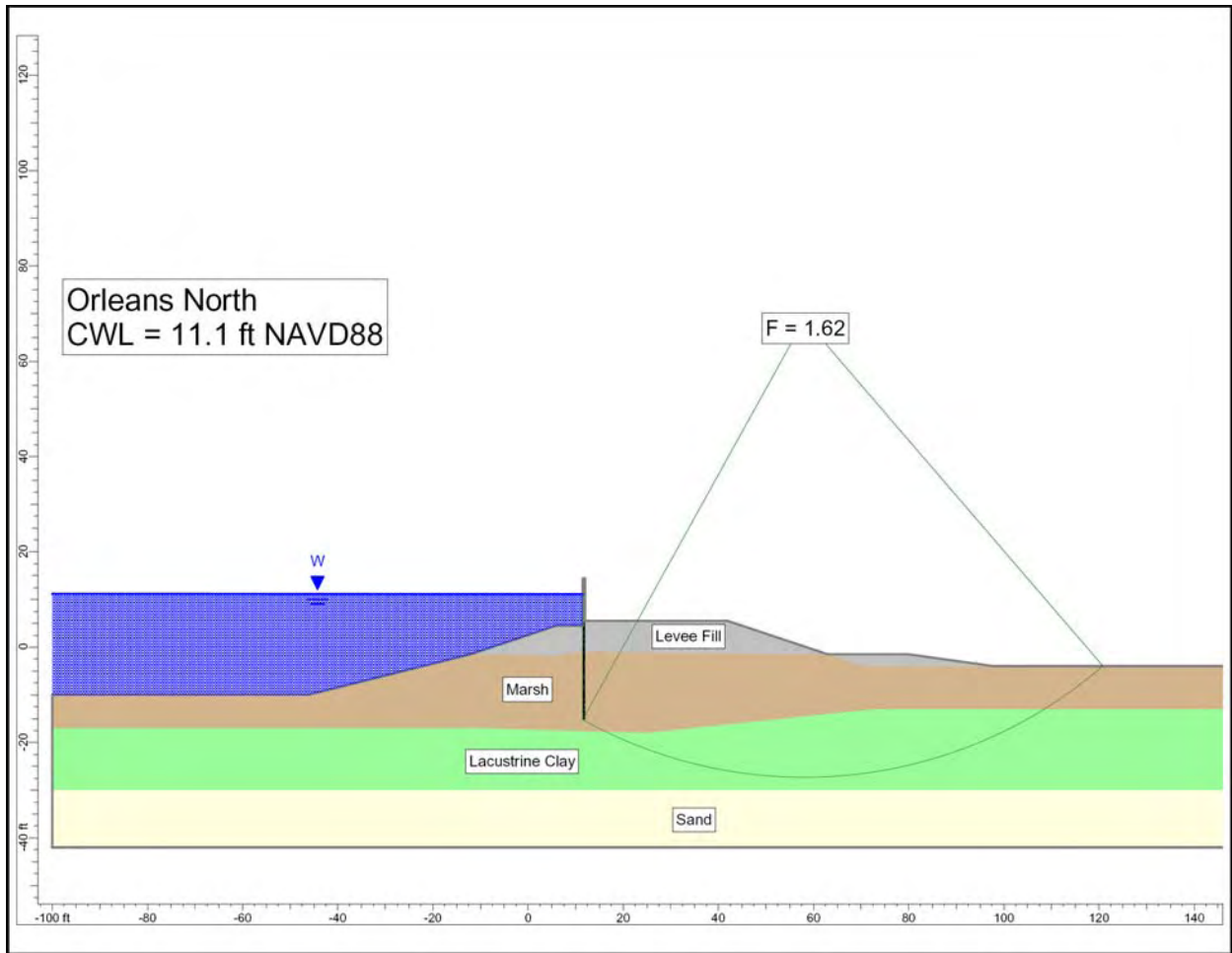
Figure 10-20. Orleans North Case 1 Stability Analysis
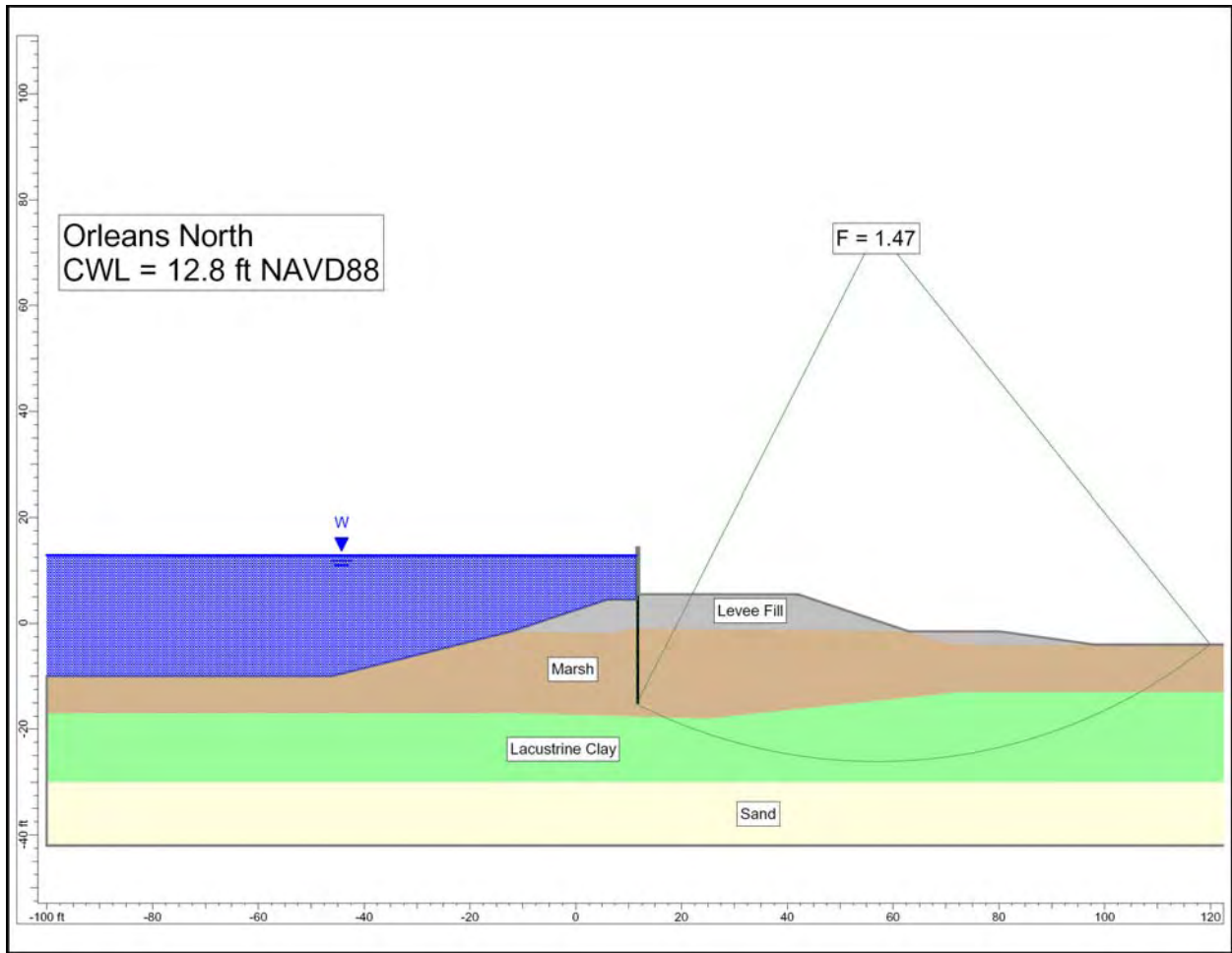
Figure 10-21. Orleans North Case 2 Stability Analysis

Appendix 11
Analysis of Performance of the Inner Harbor Navigation Canal

Executive Summary

Four breaches occurred on the Inner Harbor Navigation Canal (IHNC) during Hurricane Katrina, on the morning of August 29th. Two of the breaches occurred on the east bank between the Florida Avenue Bridge and the North Claiborne Avenue Bridge adjacent to the 9th Ward, and two on the west bank just north of the intersection of France Road and Florida Avenue (Figure 11-1). Three of the breaches involved failures of floodwalls on levees, and one involved failure of a levee.

All of the IHNC floodwalls and levees were overtopped on August 29th. The peak storm surge elevation in the IHNC was 14.2 ft[1] at 9:00 AM, about 1.7 ft above the tops of the floodwalls and levees. The reaches where the floodwalls and levees did not collapse have therefore survived water loading considerably higher than the design loading.

Water flowing over the I-walls when they were overtopped eroded trenches on the protected side of the walls as it cascaded onto the levee fill. Soil that was providing support for the walls eroded away, making the walls less stable.

Although it is clear that the walls were overtopped, and that their stability was compromised by the erosion that occurred, it is also clear that one of the east side breaches occurred before the wall was overtopped. Eyewitness reports indicate that the water level in the 9th Ward near Florida Avenue was rising as early as 5:00 AM, when the water level in the IHNC was still below the top of the floodwall. Stability analyses indicate that foundation instability would occur before overtopping at the north breach on the east side of the IHNC. This breach location is thus the likely source of the early flooding in the 9th Ward. Stability analyses indicate that the other three breach locations would not have failed before they were overtopped.

The soil immediately beneath the levees and floodwalls at all four breach locations included marsh, beneath which was clay, and beneath the clay, sand. Through most of their lengths, the

---

[1] All elevations refer to NAVD88(2004.65) datum.

critical circles passed through the marsh and clay. The critical circles did not extend to the sand layer beneath the clay.

Stability analyses of the north breach on the east side resulted in a computed factor of safety equal to 1.0 with a crack on the canal side of the wall and water in the IHNC at elevation 11.2 ft. This is about 1.0 ft higher than the average IHNC water level at the time flood water was observed in the 9th Ward. Considering that the effective water level could have been one foot higher due to wave effects, this result is consistent with the observed IHNC water level when flood water was first reported in the 9th Ward. It thus appears that the north breach occurred before overtopping, and that this breach was the source of the first influx of water into the 9th Ward.

Stability analyses of the south breach on the east side, and the north breach on the west side, resulted in computed factors of safety larger than 1.0 with the water level at the top of the wall and a crack behind the wall, indicating that the walls at those locations would have remained stable if none of the soil supporting the wall had been removed by erosion. Stability analysis of the south breach on the west side, where there was no I-wall, showed that the factor of safety there was also high, and the failure was due to overtopping erosion.

The lower computed factor of safety at the north breach on the east side is attributable to the fact that the ground elevation on the protected side is lower at that location, and as a result there was less soil on the protected side of the wall that was able to provide support for the wall.

The IPET strength model used for the north breach on the east bank, which is based on all of the data available in May 2006, agrees fairly closely with the design strengths reported in the GDM[2] under the center of the levee. Both the GDM and the IPET strength model assign lower strengths beneath the embankment toe and beyond than beneath the crest of the embankment, but the GDM strengths at this location are higher than the IPET strengths. The GDM strengths are thus reasonably consistent with the currently available data.

The design analyses were performed using the Method of Planes[3], without a crack between the wall and the levee fill on the canal side of the wall. For the canal water level at 10.5 ft (the design water level), the factor of safety computed using the Method of Planes was 1.25. The minimum factor of safety calculated for the same conditions using Spencer's method[4] was 1.45, indicating that the Method of Planes is conservative by about 14% in this case.

In summary, the failure that resulted in the north breach on the east side of the IHNC resulted from two differences between the stability analyses that were used as the basis for design and those described in this report: (1) the ground surface beyond the toe of the levee at the north breach location was lower than the landside ground surface in the design cross section, and

---

[2] Design Memorandum No. 3, General Design, Lake Pontchartrain, LA, and Vicinity, Chalmette Area Plan, U.S. Army Engineer District, New Orleans, October 1966.

[3] A study of the Method of Planes, undertaken by IPET at the request of the New Orleans District Task Force Guardian, indicates that the Method of Planes gives lower factors of safety than more accurate methods of analysis, such as Spencer's method. The magnitude of the difference between the two varies from case to case.

[4] Spencer, E. (1967) "A Method of Analysis of the Stability of Embankments Assuming Parallel Inter-Slice Forces," *Geotechnique*, Institution of Civil Engineers, Great Britain, Vol. 17, No. 1, March, pp. 11-26.

(2) the design analyses did not consider the possibility of a gap forming behind the wall, allowing water to run into the gap and increase the load on the wall. The other three breaches on the IHNC were due to overtopping and erosion.

Observations and Possible Modes of Failure

As shown by the hydrograph in Figure 11-2, the water level in the IHNC rose from elevation 1.0 ft. at 12:00 AM on August 28th to 14.2 ft. at 9:00 AM on August 29th. The peak water level was 1.7 ft. above the tops of the floodwalls and levees which were at elevation 12.5 ft. The hydrograph in Figure 11-3 shows that the water level in the 9th Ward was rising at 5:00 AM on August 29th, when the water level in the IHNC was at elevation 10.2 ft., about 2.3 ft. below the tops of the floodwalls and levees. With ground surface elevations approximately -4.0 ft., water at elevation +2.0 ft. indicates that the water was 6.0 ft. deep in the 9th Ward at 5:00 AM on August 29th.

Initial observations after the hurricane revealed that overtopping had eroded at least one section of levee along the west bank and had eroded the soil adjacent to the wall on the protected side along the east and west bank. It appeared that water flowing over the floodwall scoured and eroded the levee on the protected side of the I-wall, exposing the supporting sheet piles and reducing the passive resistance (Figure 11-4). The erosion appeared to be so severe in the breach locations that the sheet piles may have lost all of their foundation support, resulting in failure (Figure 11-5). Perhaps the best evidence of this scour can be seen along the unbreached reaches of the east bank I-walls on the Inner Harbor Navigation Canal where U-shaped scour trenches could be found adjacent to the I-walls. As the scour increased, the I-wall may have moved laterally and leaned to the protected side, causing the scour trench to grow as the water began cascading farther down the slope until sufficient soil resistance was lost and the wall was carried landward.

Other possible modes of failure are sliding instability and piping and erosion from underseepage. Piping and erosion from underseepage is unlikely because the I-walls were founded in a clay levee fill, a marsh layer made up of organics, clay and silt, and a clay layer. Because of the thickness, the low permeabilities of these materials, and the relatively short duration of the storm, this failure mode was considered not likely and was eliminated as a possible mode of failure.

It is necessary to investigate the possibility of sliding instability to determine if the I-walls could breach as a result of shear through the foundation. The foundation conditions are similar to the 17th Street Canal. As shown in Figure 11-6, no significant wall movement was found in the wall sections adjacent the south breach. However, Figure 11-7 shows significant wall movement did occur in the wall sections adjacent to the north breach.

Stratigraphy

IHNC East Bank – Lower 9th Ward

The data available to assess the stratigraphy of the area includes borings from the General Design Memorandum (GDM), borings taken after the failure, and cone penetration tests taken after the failure. The locations of these borings and cone penetration tests are shown in Figure 11-8. Note that all borings taken after the failure were at the levee toe. The GDM contains 10 borings on the levee centerline (2-U, 3, 4, 5, 6-U and 7 in the vicinity of the breach, and four at the levee toe (2-UT, 3T, 4T and 6UT). A centerline profile under the levee is represented in Figure 11-9 and is based on both pre-Katrina and post-Katrina borings. This section shows 60 to 70 ft of predominantly fine-grained Holocene (i.e., less than 10,000 years old) shallow water and terrestrial sediments overlying the Pleistocene surface (i.e., older than 10,000 years). Holocene sediments are separated into various depositional environments in Figure 11-9, based on soil texture, organic content, and other physical and engineering properties. Engineering properties of these layers are described in greater detail below.

The sections of the IHNC east bank where the north and south breaches occurred encompass Stations 54+00 to 56+00 and 22+00 to 31+00, respectively. These breaches occurred between Florida Avenue and North Claiborne Avenue. The strength evaluation focused primarily on these areas.

The GDM borings indicate the levee fill properties for the north and south breach areas are similar, consisting of compacted CL and CH materials. The average moist unit weight of the fill was estimated to be 109 pcf.

Beneath the fill is a marsh unit about 17 ft thick. The marsh layer is composed of organic material from the cypress swamp that occupied the area, together with silt and clay deposited in the marsh. Because the upper 8 to 9 ft of this unit has different material properties than the lower portion, it was divided into two layers, Marsh 1 and Marsh 2. Water contents and saturated unit weights determined from samples of marsh material taken from the toe are shown in Figures 11-10 and 11-11, respectively. These figures clearly depict the differences in the marsh layers.

Water contents, unit weights and undrained shear strengths are shown in Table 11-1, and these properties for the Marsh 2 layer are shown in Table 11-2. These properties are based on samples from post-Katrina borings at the levee toe. The average saturated unit weight of the Marsh 1 layer is about 105 pcf. Water contents of the Marsh 1 layer are as high as 80%. The average water content is approximately 49%. The average saturated unit weight of the Marsh 2 layer is about 80 pcf. Water contents of the marsh 2 layer are as high as 442%. The average water content is approximately 175%. The marsh 1 layer is mostly CH material. The Marsh 2 layer is fibrous at the top, and more amorphous near the bottom, indicating more advanced decomposition of the older organic materials at depth.

Beneath the marsh layers is a layer of interdistributary clay with an average Liquid Limit of about 79% and an average Plastic Limit of 26%. Based on consolidation test results presented in

the GDM, the clay is normally consolidated throughout its depth. The average saturated unit weight of the clay is about 100 pcf, and the average water content is approximately 60%. Water content and unit weights are summarized in Table 11-3.

Beneath the clay is a layer of Beach Sand. This layer is not involved in the observed or calculated mechanisms of instability, and its strength is therefore of little importance in stability analyses, except as a more resistant layer beneath the clay.

The unit weights measured for individual laboratory test specimens and the values used in subsequent analyses are shown in Figure 11-11.

Table 11-1
Properties of Marsh 1 Layer from Post-Katrina Borings at Toe

Marsh 1 Layer					
Number of Samples = 16					
	Mean	Standard Deviation	COV	Max	Min
%w	49	17	0.342	80.2	21.9
Saturated Unit Weight (pcf)	104	9	0.081	120.5	92.2
S_u (psf)	550	214	0.389	3195	90.0

Table 11-2
Properties of Marsh 2 Layer from Post-Katrina Borings at Toe

Marsh 2 Layer					
Number of Samples = 12					
	Mean	Standard Deviation	COV	Max	Min
%w	175	96	0.549	441.6	90.9
Saturated Unit Weight (pcf)	78.4	7	0.091	87.1	63.4
S_u (psf)	195.3	116	0.595	336	64.6

Table 11-3
Properties of Interdistributary Clay from Post-Katrina Borings at Toe

Interdistributary Clay					
Number of Samples = 45					
	Mean	Standard Deviation	COV	Max	Min
%w	60	12	0.208	77.2	25
Saturated Unit Weight (pcf)	101.1	6	0.063	125	93.6

Shear Strength - IHNC – East Bank

The sources of shear strength data include borings from the General Design Memorandum (GDM), and borings, cone penetration tests, and vane shear tests performed as part of the failure investigation. From the available sources, two GDM borings, four cone penetration tests, and three vane shear tests provide information beneath the centerline of levee. From the GDM borings (2-U and 6-U), the results of 11 Q test envelopes and 26 unconfined compression tests

were available. All laboratory tests were performed on specimens trimmed from 5-in diameter undisturbed tube samples.

Beneath the toe of the levee, the GDM contained the results of over 70 unconfined compression tests. In addition, about 100 unconfined compression tests have been conducted on test specimens obtained since Katrina. Tests were performed on 1.4-inch diameter specimens trimmed from 5-in.-diameter tube samples. Statistical analyses have been performed on the data from the post-Katrina tests to compute minimum, maximum, and average values of strength for the levee fill, the marsh layers, and the clay. The results of the statistical analyses are shown in Tables 11-1 through 11-3. Also, one cone penetration test with pore pressure measurements (CPTU) and one series of vane shear tests were performed near the area of the breaches after the failure.

Shown in Figure 11-12 are the available laboratory and vane shear test results for samples obtained beneath the crest of the levee, as well as values of undrained shear strength determined from CPTU-1 using Mayne's method[5]. Figure 11-13 presents the data available for undrained shear strength from the toe of the levee and areas beyond the toe. Plotted with these data are the results from CPTU-1T, which was performed at the toe of the levee.

Only a few strength tests for the levee fill are available from GDM borings in the breach area. The shear strength used for design (s_u =500 psf) was assumed for the levee-fill strength in the IPET strength model. As can be seen in Figure 11-12, a value of s_u = 500 psf for the levee fill seems reasonable based on the results of the CPTU tests, vane shear tests, and laboratory tests. However, the strength of the levee is not much involved in the calculated mechanisms of instability and therefore has limited importance in the stability analyses.

The marsh material is stronger beneath the levee crest where it has been compressed under the weight of the levee, and weaker at the toe of the levee and beyond, where it has not been compressed so heavily. CPTU data, vane shear tests, and unconfined compression tests conducted on test specimens trimmed from 5-in. samples were used to measure the Marsh 1 layer strengths at the toe. The measured shear strengths from the unconfined compression tests in the Marsh 1 layer scatter very widely from about 90 psf to over 800 psf, as shown in Figures 11-12 and 11-13. The vane shear test results summarized in Table 11-4 were conducted under the levee; they indicate shear strengths (corrected for strain rate effects and plasticity) ranging from 490 psf to 820 psf. Values of s_u = 650 psf beneath the levee crest, and s_u = 550 psf beneath the levee toe appear to be reasonably representative of the measured strengths for Marsh 1 layer, and these values are shown by the solid lines on Figures 11-12 and 11-13.

---

[5] Mayne, P. W. (2003). "Class 'A' Footing Response Prediction from Seismic Cone Tests," Proceedings, Deformation Characteristics of Geomaterials, Vol. 1, Lyon, France.

Table 11-4
IHNC East Bank - Results of Vane Shear Tests in Marsh 1 Layer, Beneath Levee

Vane Shear Tests	Elev. ft NAVD88	%w	PI	Corrected Peak Strength (psf)
IHNC-VST-3	-6.3	--	--	732
IHNC-VST-6	-5.8	73	56	489
IHNC-VST-6	-10.8	--	--	566
IHNC-VST-1	-3.3	--	--	818
Average				**651**

The shear strength characterization of the Marsh 2 layer was difficult because of large scatter in the data. Data obtained from post-Katrina toe borings taken between Florida Avenue and North Claiborne Avenue are presented in Table 11-2. Noting Figures 11-12 and 11-13, which include both pre-Katrina and post-Katrina strength results, the undrained shear strength of the Marsh 2 layer ranges from about 200 to 620 psf under the levee centerline, and from 90 to 500 psf beneath the levee toe. Values of s_u = 300 psf beneath the levee crest, and s_u = 200 psf beneath the levee toe appear to be reasonably representative of the measured values; these values are shown on Figures 11-12 and 11-13. These strengths are the same as were used in the GDM design analyses.

Interpretation of the undrained shear strength of the interdistributary clays was developed considering the results of all laboratory and field tests. The pore pressure results from the CPTU tests were questionable, and for this reason, less emphasis was placed on determining undrained shear strengths from the cone penetration test results. The CPTU tests did indicate that the clay deposit was normally consolidated, and that the undrained shear strength increased linearly with depth. Figure 11-12 shows the undrained shear strength with depth determined using Mayne's method[6] for CPTU-1, which was conducted under the centerline of the levee. Figure 11-13 presents the results of CPTU-1T, which was conducted at the toe of the levee.

The straight line shown in Figure 11-12, representing the average undrained shear strength in the clay, has a slope of 8.6 psf per foot of depth. This rate of strength increase with depth appears to compare reasonably well to the laboratory strength test results.

The rate of increase of strength with depth is directly related to the s_u/p' ratio for the clay and its buoyant unit weight as follows:

$$\frac{s_u}{p'} = \frac{\text{rate of increase of } s_u \text{ with depth}}{\text{rate of increase of } p' \text{ with depth}} = \frac{\Delta s_u / \Delta z}{\gamma_{buoyant}} \tag{11-1}$$

The value of $\gamma_{bouyant}$ for the clay is 100 pcf – 62.4 pcf = 37.6 pcf. Thus, the value of s_u/p' is:

---

[6] Mayne, P. W. (2003). "Class 'A' Footing Response Prediction from Seismic Cone Tests," Proceedings, Deformation Characteristics of Geomaterials, Vol. 1, Lyon, France.

$$\frac{s_u}{p'} = \frac{8.6 \ psf \ per \ ft}{37.6 \, pcf} = 0.23 \tag{11-2}$$

which is a reasonable value for this normally consolidated clay.

These values provide a good basis for establishing undrained strength profiles in the clay. The undrained strength at the top of the clay is equal to 0.23 times the effective overburden pressure at the top of the clay, and the undrained strength increases with depth in the clay at a rate of 8.6 psf per foot.

In the IPET strength model, the undrained shear strength of the clay is equal to 0.23 times the effective overburden pressure. The clay strength thus varies with lateral position, being greatest beneath the levee crest where the effective overburden pressure is greatest, and varying with depth, increasing at a rate of 8.6 psf per foot at all locations. Figure 11-13 shows the calculated undrained shear strength variation in the interdistributary clay at the toe of the levee and beyond. Based on the available test data, the IPET strength model appears to be an adequate, albeit conservative, representation of the strength beneath the toe.

The IPET strength model does not consider details of the stress distribution beneath the levee, which would result in "load spread" effects. These effects would result in rotation of principal stresses beneath the levee, and in the added stress due to the levee load that would decrease with depth. The model described in the previous paragraphs uses a simple stress distribution beneath the levee that satisfies vertical equilibrium. The consequences of this assumption are that the vertical effective stresses in the clay layer beneath the toe, and thus the undrained shear strength distribution, is underestimated. Likewise, the undrained strength distribution in the clay layer beneath the crest is overestimated using the vertical equilibrium assumption. These two effects tend to balance out, and the average shear strength on the failure plane is approximately the same as would be obtained from more complex methods of calculating the vertical effective stress in the clay layer.

It is also important to note that the ground elevation of the toe of the levee is not constant; therefore it is not possible to use the same strength versus elevation relationship for the south breach and the north breach. The decrease in elevation of the toe from the south breach to the north breach is shown in the LIDAR survey of the area in the year 2000, which is plotted in Figure 11-14. The elevation of the protected side levee toe decreases about 4 ft from the south breach to the north breach.

The drained friction angle of the sand beneath the clay was estimated to be 30 degrees for the stability analysis. As noted previously, the sand layer is not involved in observed or computed failure mechanisms, and the value of ϕ' assigned to it, therefore, has no influence on computed factors of safety.

Original Design Strengths - East Bank

The design analyses in the Chalmette Area Plan General Design Memorandum (GDM)[7] used undrained strengths for the levee fill, the marsh layers, and the clay, and a drained friction angle to characterize the strength of the sand layer beneath the clay, as does the IPET strength model described above. However, there are four marsh layers in the GDM interpretation compared to only two marsh layers for the IPET strength model. The design strengths are comparable to the IPET strengths discussed here and shown in Table 11-5 and Figure 11-15.

The values of strength for the levee fill, the marsh layers, and the clay layer that were used in the design analyses for the IHNC I-wall, Station 16+08.85 to Station 58+12.00, are shown in Table 11-5. This reach includes both breach areas on the east bank, which extends approximately from Stations 54+00 to 56+00 for the north breach and 22+00 to 31+00 for the south breach.

Table 11-5 Comparison of Strengths of Levee Fill, Marsh Layers, and Interdistributary Clay Used in Design for Stations 16+08.85 to 58+12.00 with the IPET Strengths		
Material	**Strengths used for design**	**IPET strength model**
Levee fill	$s_u = 500$ psf, $\phi = 0$	$s_u = 500$ psf, $\phi = 0$
Marsh 1a layer (uppermost marsh layer)	$s_u = 400$ psf, $\phi = 0$ beneath the levee and toe	$s_u = 650$ psf, $\phi = 0$ beneath levee $s_u = 550$ psf, $\phi = 0$ beneath toe
Marsh 1b layer (directly below uppermost marsh layer)	$s_u = 600$ psf, $\phi = 0$ beneath levee $s_u = 500$ psf, $\phi = 0$ beneath toe	
Marsh 2a layer (highly organic layer)	$s_u = 300$ psf, $\phi = 0$ beneath levee $s_u = 200$ psf, $\phi = 0$ beneath toe	$s_u = 300$ psf, $\phi = 0$ beneath levee $s_u = 200$ psf, $\phi = 0$ beneath toe
Marsh 2b layer (directly below marsh 2a layer)	$s_u = 500$ psf, $\phi = 0$ beneath levee $s_u = 300$ psf, $\phi = 0$ beneath toe	
Interdistributary Clay	12.3 psf/ft increase beneath levee (starting at 355 psf) 8 psf/ft increase beneath toe (starting at 300 psf)	Su/p' = 0.23; 8.6 psf/ft increase both beneath levee and toe (starting value depends on depth of overburden)

A comparison between the GDM and IPET strength models is presented in Figures 11-16 and 11-17 for the GDM design cross section. Shown in Figure 11-16 is the shear strength profile under the crest of the levee (horizontal coordinate of 0 ft) used in the original design, and the shear strength profile calculated using the IPET model. The IPET strength model has higher shear strengths in the Marsh 1 layer, and the GDM strength model has higher strengths in the lower portion of the Marsh 2 layer. Both models show a linear increase in undrained shear strength in the interdistributary clay layer, with the rate of increase greater for the GDM model than the IPET model. The difference in the rate of increase can be partially attributed to the difference in unit weights used in each model. The GDM strength model assumes a unit weight of the clay of 102.4 pcf for the upper portion of the clay and 107 pcf for the lower portion of the clay. The IPET model uses a unit weight of 100 pcf for the clay. The higher unit weights used in the GDM strength model would produce a larger increase in undrained shear strength per foot than the IPET model for the same undrained strength ratio. In addition, based on the assumed

---

[7] Design Memorandum No. 3, General Design, Lake Pontchartrain, LA, and Vicinity, Chalmette Area Plan, U.S. Army Engineer District, New Orleans, October 1966.

unit weights and the rate of strength increase, the GDM model corresponds to a greater undrained strength ratio, from about 0.28 to 0.31.

The difference between the GDM and IPET strength model is more pronounced for undrained strengths below the toe of the levee. Shown in Figure 11-17 is the shear strength profile under the toe of the levee (horizontal coordinate of 60 ft) used in the original design, and the shear strength profile calculated using the IPET model. The undrained shear strengths are comparable in the marsh layers, but there is about a 200 psf difference in undrained shear strength in the interdistibutary clay. The rate of increase for both models is essentially the same, but the IPET strength model produces a lower shear strength at the marsh/clay interface. As stated earlier, the IPET strength model would tend to underestimate the undrained shear strengths beneath the toe when compared to available test data.

It is interesting to note the similarity of the two strength models, particularly since the GDM strength model was developed about 40 years ago. Both models share the essential characteristics of using different strengths under the levee crest and toe, and a lateral variation of shear strengths between these points.

IHNC East Bank North and South Failures

Eighteen slope stability analyses (Cases 1 through 5, 5a, and 6 through 17 in Table 11-6) were performed for the cross section at Station 55+00 at the north breach. The cross section used for these analyses is shown in Figure 11-18. Also, 17 slope stability analyses (Cases 1 through 17 in Table 11-7) were performed for a cross section developed for Station 26+00 at the south breach. The cross section used for these analyses is shown in Figure 11-19.

In addition, four slope stability analyses (Cases 1 through 4 in Table 11-8) were performed using the cross section and strength profile shown in the GDM, and presented in this report as Figure 11-15.

Average values of saturated unit weight were used in the analyses: $\gamma_{sat} = 109$ pcf for the levee fill, $\gamma_{sat} = 105$ pcf for the Marsh 1 layer, $\gamma_{sat} = 80$ pcf for the Marsh 2 layer, and $\gamma_{sat} = 100$ pcf for the interdistributary clay beneath the marsh layers. These values are based on values measured in laboratory tests on undisturbed samples.

The critical slip surfaces found in the analyses did not extend down to the sand beneath the clay, and the sand strength and unit weight therefore did not influence the results of the analyses.

The analyses were performed for undrained conditions in the levee fill, the marsh layer, and the clay beneath the marsh layer. Based on available information, it appears that the values of permeability of all three of these materials were low enough so that dissipation of excess pore pressures during the rise of the water level in the canal would have been negligible, and would have had, at most, a minor influence on stability.

Analyses were performed for two conditions regarding contact between the I-wall and the adjacent soil on the canal side of the wall. These are indicated by "yes" or "no" in the column labeled "Crack" in Tables 11-6, 11-7 and 11-8.

- For the "no crack" analyses, it was assumed that the soil on the canal side of the wall was in intimate contact with the wall. Water pressures were applied to the surface of the levee fill, and to the I-wall where it projected above the crown of the levee, but were not applied to the face of the wall below the crown of the levee.

- For the "crack" analyses, it was assumed that the I-wall was separated from the levee fill on the canal side of the wall as the water level in the canal rose and caused the wall to deflect away from the canal. Full hydrostatic water pressures were applied to the I-wall, from the water level in the canal to the bottom of the wall.

For the north breach, stability analyses were performed for canal water elevations of 10.0, 10.5, 11.2, and 12.5 ft. Analyses were performed with water elevations of 10.0, 10.5, and 12.5 for the south breach. The elevation of the top of the wall is 12.5 ft for both the north and south cross sections.

The analyses described here were performed using the computer program UTEXAS4[8]. Critical circular slip surfaces were located for each case using the search routines available in UTEXAS4. The analyses were verified using the computer program SLIDE[9]. The analyses were performed using Spencer's method[10], which satisfies all conditions of equilibrium. Methods that satisfy all conditions of equilibrium have been shown to result in values of factor of safety that are not influenced appreciably by the details of the assumptions they involve[11].

---

[8] Available from Shinoak Software, 3406 Shinoak Drive, Austin, TX 78731
[9] Available from Rocscience Inc., 31 Balsam Avenue, Toronto, Ontario, Canada M4E 3B5
[10] Spencer, E. (1967) "A Method of Analysis of the Stability of Embankments Assuming Parallel Inter-Slice Forces," *Geotechnique*, Institution of Civil Engineers, Great Britain, Vol. 17, No. 1, March, pp. 11-26.
[11] Duncan, J. M., and Wright, S. G. (2005), *Soil Strength and Slope Stability*, John Wiley and Sons, New York, 293 pp.

Table 11-6
Results of Slope Stability Analyses for IHNC East Bank, North Breach. Note all Analyses Use Spencer's Method and Circular Slip Surfaces

Case	Water Elev. ft NAVD88	Strength Model	Crack (Yes or No)	Factor of Safety
1	10.0	IPET	Yes	1.04
2	10.5	IPET	Yes	1.03
3	10.5	IPET	No	1.22
4	11.2	IPET	Yes	1.00
5	12.5	IPET	Yes	0.96
5a	12.5	IPET	No	1.13
6	10.0	Marsh 1 + 25%	Yes	1.12
7	10.0	Marsh 1 − 25%	Yes	0.96
8	10.0	Marsh 2 + 25%	Yes	1.12
9	10.0	Marsh 2 − 25%	Yes	0.95
10	10.0	Interdistributary + 25%	Yes	1.12
11	10.0	Interdistributary − 25%	Yes	0.94
12	12.5	Marsh 1 + 25%	Yes	1.04
13	12.5	Marsh 1 − 25%	Yes	0.88
14	12.5	Marsh 2 + 25%	Yes	1.05
15	12.5	Marsh 2 − 25%	Yes	0.88
16	12.5	Interdistributary + 25%	Yes	1.03
17	12.5	Interdistributary − 25%	Yes	0.88

Table 11-7
Results of Slope Stability Analyses for IHNC East Bank, South Breach. Note all Analyses Use Spencer's Method and Circular Slip Surfaces

Case	Water Elev. ft NAVD88	Strength Model	Crack (Yes or No)	Factor of Safety
1	10.0	IPET	Yes	1.20
2	10.5	IPET	Yes	1.18
3	10.5	IPET	No	1.34
4	12.5	IPET	Yes	1.10
5	12.5	IPET	No	1.25
6	10.5	Marsh 1 + 25%	Yes	1.29
7	10.5	Marsh 1 − 25%	Yes	1.07
8	10.5	Marsh 2 + 25%	Yes	1.27
9	10.5	Marsh 2 − 25%	Yes	1.09
10	10.5	Interdistributary + 25%	Yes	1.27
11	10.5	Interdistributary − 25%	Yes	1.07
12	12.5	Marsh 1 + 25%	Yes	1.21
13	12.5	Marsh 1 − 25%	Yes	1.00
14	12.5	Marsh 2 + 25%	Yes	1.18
15	12.5	Marsh 2 − 25%	Yes	1.02
16	12.5	Interdistributary + 25%	Yes	1.18
17	12.5	Interdistributary − 25%	Yes	1.01

Formation of a crack on the canal side of the wall, allowing hydrostatic water pressure acting through the full depth of the crack, causes a very significant reduction in the value of the calculated factor of safety. Evidence that a crack did form behind the wall near the breaches can be seen in Figures 11-6 and 11-7.

For the north breach (Station 55+00), with the canal water level at elevation 12.5 ft (top of the wall), the calculated factor of safety for the cracked condition is 0.96, as compared to 1.13 for the uncracked condition (Cases 5 and 5a). A canal water elevation of 11.2 ft produces a factor of safety of unity for the cracked condition (Case 4). Figures 11-20 through 11-25 show the critical circles from UTEXAS4 analyses for the north breach for Cases 1 through 5 and Case 5a.

For the south breach (Station 26+00), the factor of safety was greater than unity for all canal water elevations analyzed using the IPET strength model. For the most extreme case of the canal water level at elevation 12.5 ft (top of the wall), the calculated factor of safety for the cracked condition is 1.10. The critical circles for the stability analyses performed on the south breach for Cases 1 through 5 are shown in Figures 11-26 through 11-30.

Analysis of GDM Cross section

An analysis of the design cross section was performed using the GDM strength model discussed earlier. This analysis allows a comparison of the Method of Planes, used in the original design, with Spencer's method using circular failure surfaces.

In the original design, a canal water level of 10.5 ft NAVD88 (13.0 ft NGVD29) was used as the design water level load condition. The Method of Planes resulted in a minimum factor of safety of 1.25 for a horizontal failure plane located in the Marsh 2 layer. Using Spencer's method with the GDM strength model, a factor of safety of 1.45 was calculated for the same canal water level. Thus, the Method of Planes is conservative by about 14% in this case.

Three other variations of the design cross section were analyzed. Introducing a crack behind the wall for the design water level decreases the factor of safety to 1.19. For a canal water elevation at the top of the wall (12.5 ft NAVD88), the factor of safety is 1.35 for the uncracked condition and 1.05 for the cracked condition. The results of all analyses performed on the GDM cross section are presented in Table 11-8. Figures 11-31 through 11-34 show the critical circles for the UTEXAS4 analysis.

Probabilities of Failure

Probabilities of failure have been estimated using an approximate technique based on the Taylor Series method. The coefficient of variation of the average clay strength and the average marsh layer strength were estimated to be 25%. The data available is sparse, and the scatter in measured values is influenced significantly by sample quality, as well as variations in properties from one location to another and systematic variations with depth over burden. The estimated values of COV = 25% is, thus, largely based on judgment. Even so, it is useful to examine what

probabilities of failure would be associated with this level of uncertainty concerning shear strengths.

The Taylor Series numerical method[12,] was used to estimate the standard deviation of the factor of safety (σ_F) and the coefficient of variation of the factor of safety (COV_F), using these formulas:

$$\sigma_F = \sqrt{\left(\frac{\Delta F_{clay\,strength}}{2}\right)^2 + \left(\frac{\Delta F_{marsh\,strength}}{2}\right)^2} \tag{11-3}$$

$$COV_F = \frac{\sigma_F}{F_{MLV}} \tag{11-4}$$

where $\Delta F_{clay\,strength}$ = difference between the values of the factor of safety calculated with the clay strength increased by one standard deviation and decreased by one standard deviation from its most likely value. $\Delta F_{marsh\,strength}$ is determined in the same way. F_{MLV} is the "most likely value" of factor of safety, computed using the IPET shear strengths.

Values of F_{MLV} and COV_F have been calculated for Station 55+00 and for Station 26+00. The results are listed in Table 11-9, together with the corresponding values of probability of instability based on an assumed lognormal distribution of factor of safety.

For Station 55+00, the calculated probabilities of instability are 42% for a water level of 10.0 ft, and 64% for the water level at the top of wall (12.5 ft, NAVD 88). For Station 26+00, the calculated probabilities of instability are 15% for the design water level of 10.5 ft, and 27% for a water level of 12.5 ft (top of wall). These values are reasonable, considering that evidence suggest that the north breach occurred before the wall overtopped and the south breach more likely failed due to overtopping.

Table 11-8
Results of Slope Stability Analyses for IHNC East Bank, Using GDM No. 3, Plate 38.
Note All Analyses Use Spencer's Method with Critical Circles

Case	Water Elev. ft. NAVD88	Strength Model	Crack (Yes or No)	Factor of Safety
1	10.5**	GDM	No	1.45
2	10.5**	GDM	Yes	1.19
3	12.5 – Top of Wall	GDM	No	1.35
4	12.5 – Top of Wall	GDM	Yes	1.05
Note: Design WL is 2.0 ft below top of wall				

---

[12]Wolff, T. F. (1994). "Evaluating the reliability of existing levees." Report, Research Project: Reliability of Existing Levees, prepared for the U.S. Army Engineer Waterways Experiment Station, Geotechnical Laboratory, Vicksburg, MS.

Table 11-9
Calculated Probabilities of Instability for IHNC East Bank

Area	Water level (ft) NAVD88	F_{MLV}	COV_F	Probability of instability
North Breach	10.0	1.04	14%	42%
North Breach	12.5	0.96	15%	64%
South Breach	10.5	1.18	15%	15%
South Breach	12.5	1.10	14%	27%
F_{MLV} = most likely value of factor of safety COV_F = coefficient of variation of factor of safety				

West Bank North and South Breaches

Observations

Two breaches occurred on the west bank of the IHNC, as shown in Figure 11-1. Both breaches occurred north of the railroad gate on France Road and just east of the France Road crossing.

The northern breach, between Stations 195+00 and 196+40[13], occurred after the I-wall at that location was overtopped, and soil supporting the wall was removed by erosion. The water elevation of the top of the wall was 12.5 ft, 1.7 ft lower than the peak elevation reached in the IHNC. A cross section through the levee and the I-wall is shown in Figure 11-35.

The southern breach, between stations 0+80 and 2+80[14], occurred when the levee at that location was overtopped and eroded. There was no I-wall in this levee reach. The elevation of the top of the levee was 12.5 ft. A cross section through the levee is shown in Figure 11-36.

The levees at both locations were founded on about 8 ft to 10 ft of fill. The fill at the north breach was clay. At the south breach the fill consisted partly of silty sand and partly of clay, as shown in Figure 11-36. At both locations the fill was underlain by a layer of marsh material, about 11 to 12 ft thick, and a layer of normally-consolidated interdistributary clay 30 to 35 ft thick.

The shear strengths used in the stability analyses of the breached sections are summarized in Table 11-10. These values are based on data from the GDMs and from post-Katrina investigations.

---

[13] Design Memorandum No. 2 – General, Supplement No. 8, Lake Pontchartrain, LA and Vicinity, Lake Pontchartrain Barrier Plan, Inner Harbor Navigation Canal Remaining Levees, Office of the District Engineer, New Orleans District, Corps of Engineers, February, 1968.

[14] Modification of Protected Alignment and Pertinent Design Information, IHNC Remaining Levees, West Levee Vicinity, France Road and Florida Avenue Containerization Complex, Office of the District Engineer, New Orleans District, Corps of Engineers, October, 1971. Note: A different stationing origin was used for the two sections in the GDMs. The location of the south section would correspond to Stations 208+00 to 210+00 in the stationing system used for the north section.

Results of Stability Analyses – West Bank – North Breach

Stability analyses of the north breach section were performed using UTEXAS4[8] for canal water elevations of 12.0 ft (the design water elevation) and 12.5 ft (the top of the wall). Analyses were performed for the cracked condition and the no-crack condition. For the cracked condition, the water-filled gap extended to the bottom of the sheetpile, elevation -12.5 ft. The factors of safety calculated in these analyses are listed in Table 11-11. It can be noted that the factors of safety for the cracked and the un-cracked conditions are the same. This occurs because, even with the crack, the critical slip circle passes beneath the tip of the sheet pile. If the slip circle is forced to intersect the gap at the bottom of the sheetpile, the calculated factor of safety increases.

These analyses show that the wall would have a considerable margin of safety against instability, even with the water at the top of the wall and a crack at the back of the wall. It thus seems highly likely that wall would have remained stable if none of the supporting soil had been removed by overtopping erosion.

Results of Stability Analyses – West Bank – South Breach

Stability analyses of the south breach section were performed using UTEXAS4[8] for a canal water elevation of 12.5 ft (the top of the levee). The factor of safety for this condition was found to be 2.08. The concept of a gap does not apply to this section since there is no sheet pile wall on or in the embankment. The high factor of safety indicates that the breach was the result of erosion of the levee.

Summary

Four breaches occurred on the IHNC, two on the east bank, and two on the west bank. Three of the breaches involved failures of floodwalls on levees, and one involved failure of a levee without a floodwall.

The peak storm surge elevation in the IHNC was 14.2 ft at 9:00 AM on August 29, about 1.7 ft above the tops of the floodwalls and levees. Water flowing over the walls when they were overtopped eroded trenches on the protected side of the walls as it cascaded onto the levee fill, and soil that was providing support for the walls was removed by this erosion, making the walls less stable.

It is clear that one of the east side breaches occurred before the wall was overtopped, because eyewitness reports indicate that the water level in the 9th Ward near Florida Avenue was rising when the water level in the IHNC was still below the top of the floodwall. Stability analyses indicate that foundation failure would occur before overtopping at the north breach on the east side of the IHNC. This breach location is thus the likely source of the early flooding in the 9th Ward. Stability analyses indicate that the other three breach locations would not have failed before they were overtopped.

The failure that resulted in the north breach on the east side of the IHNC resulted from two differences between the stability analyses that were used as the basis for design and those described in this report: (1) the ground surface beyond the toe of the levee at the north breach location was lower than the landside ground surface in the design cross section, and (2) the design analyses did not consider the possibility of a crack forming behind the wall, allowing water to run into the gap and increase the load on the wall.

Table 11-10
Shear Strength Parameters Used in Stability Analyses of North and South Breach Locations on the IHNC West Bank

Unit	Unit Weight (pcf)	Shear Strength
Levee Fill	109	$\phi = 0$ $s_u = 500$ psf
Fill (Clay)	105	$\phi = 0$ $s_u = 500$ psf
Fill (Sand)[*]	120	$\phi' = 30°$ $c' = 0$
Marsh	80	Toe: $\phi = 0$ $s_u = 200$ psf Crest: $\phi = 0$ $s_u = 300$ psf
Interdistributary Clay	100	Calculated using $s_u/p' = 0.27$
*Only present under south breach		

Table 11-11
Results of Slope Stability Analyses of the IHNC West Bank North Breach

Case	Water Elev. ft NAVD88	Strength Model	Crack (Yes or No)	Factor of Safety
1	12.0	IPET	Yes	1.75
2	12.0	IPET	No	1.75
3	12.5	IPET	Yes	1.73
4	12.5	IPET	No	1.73
Note – analyses performed using Spencer's Method with circular slip surfaces.				
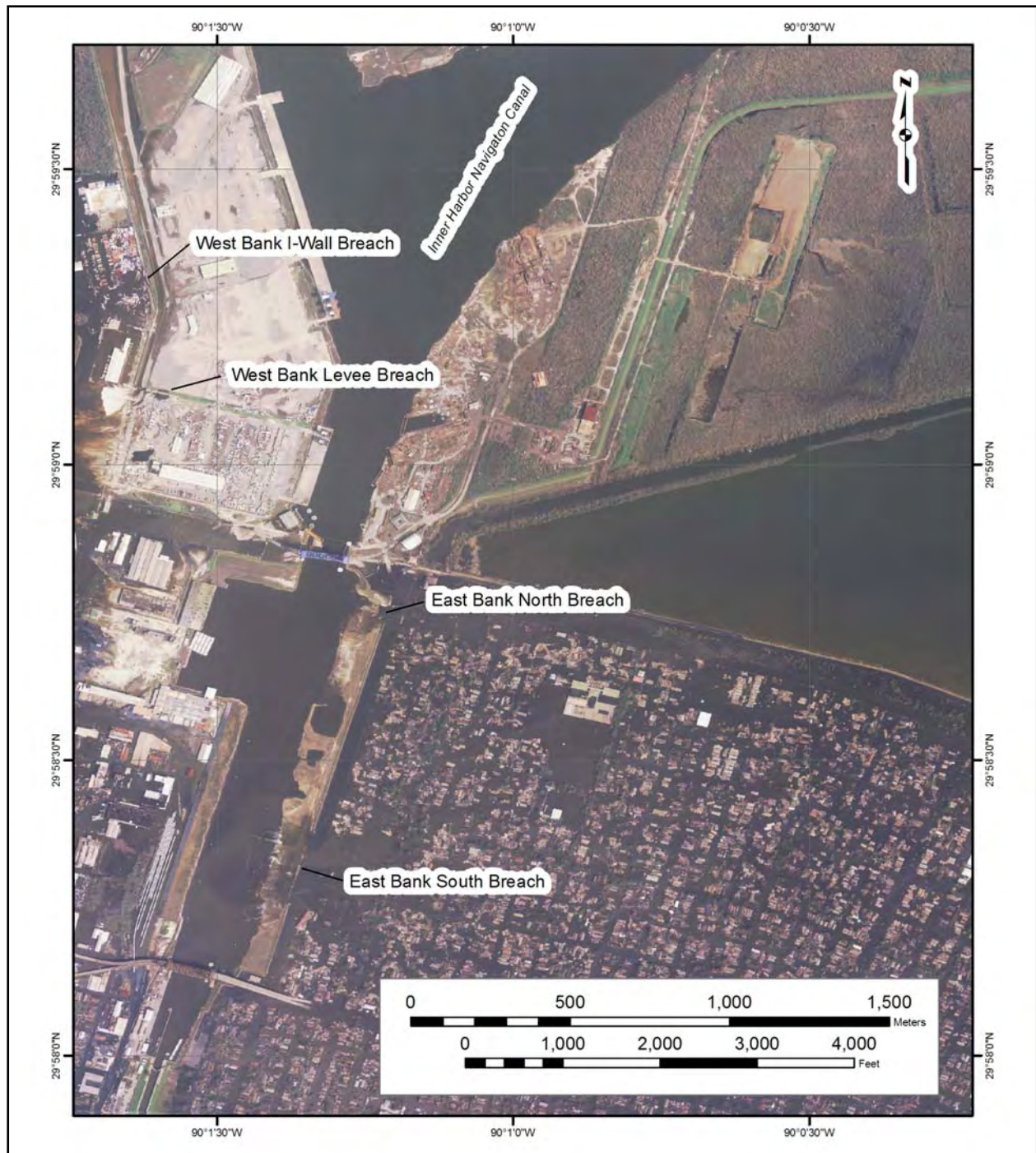
Figure 11-1. Four Breach Locations on the Inner Harbor Navigation Canal
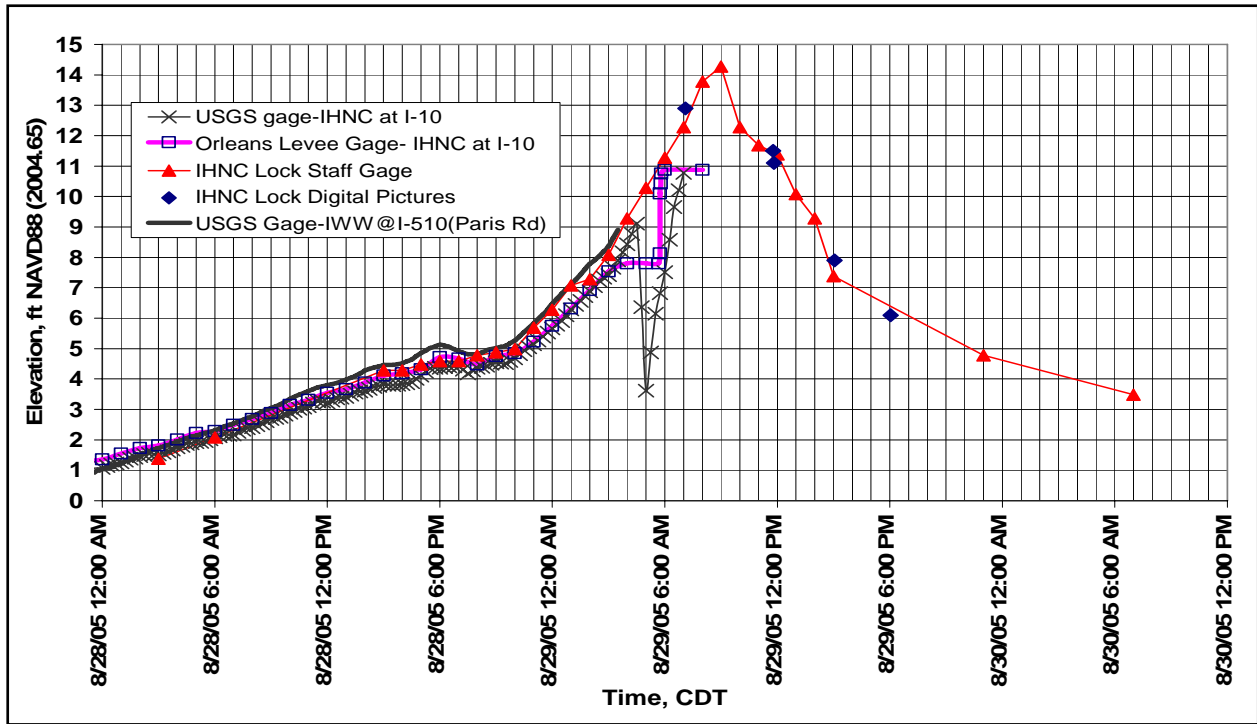
Figure 11-2. Katrina Hydrograph for the Inner Harbor Navigation Canal
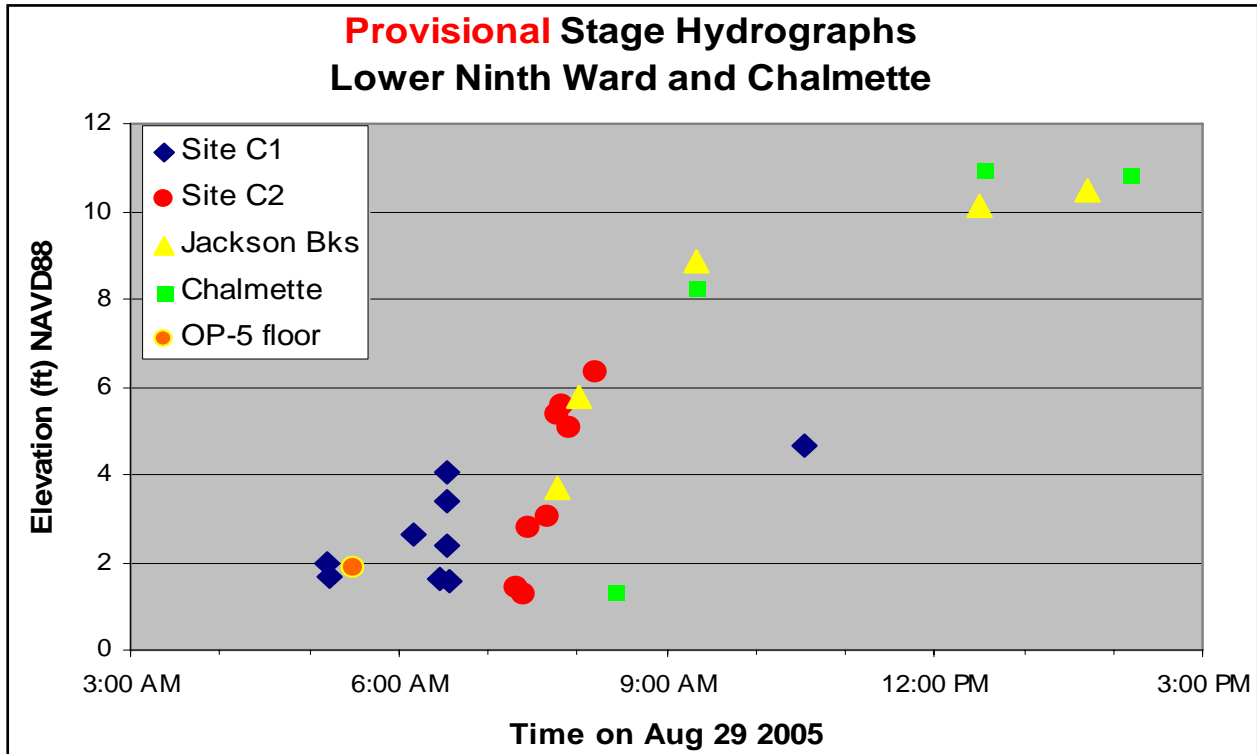
Figure 11-3. Hydrograph for the 9th Ward Inundation

Figure 11-4. Scour and Erosion on the Protected Side of the IHNC Adjacent to the Ninth Ward in the Vicinity of the South Breach

Figure 11-5. Scour and Erosion Leading to the Failure of the I-Wall on the IHNC Adjacent the South
        Breach (9th Ward)

Figure 11-6. IHNC East Bank – South Breach – Wall Movement

Figure 11-7. IHNC East Bank – North Breach – Wall Movement (View looking south)
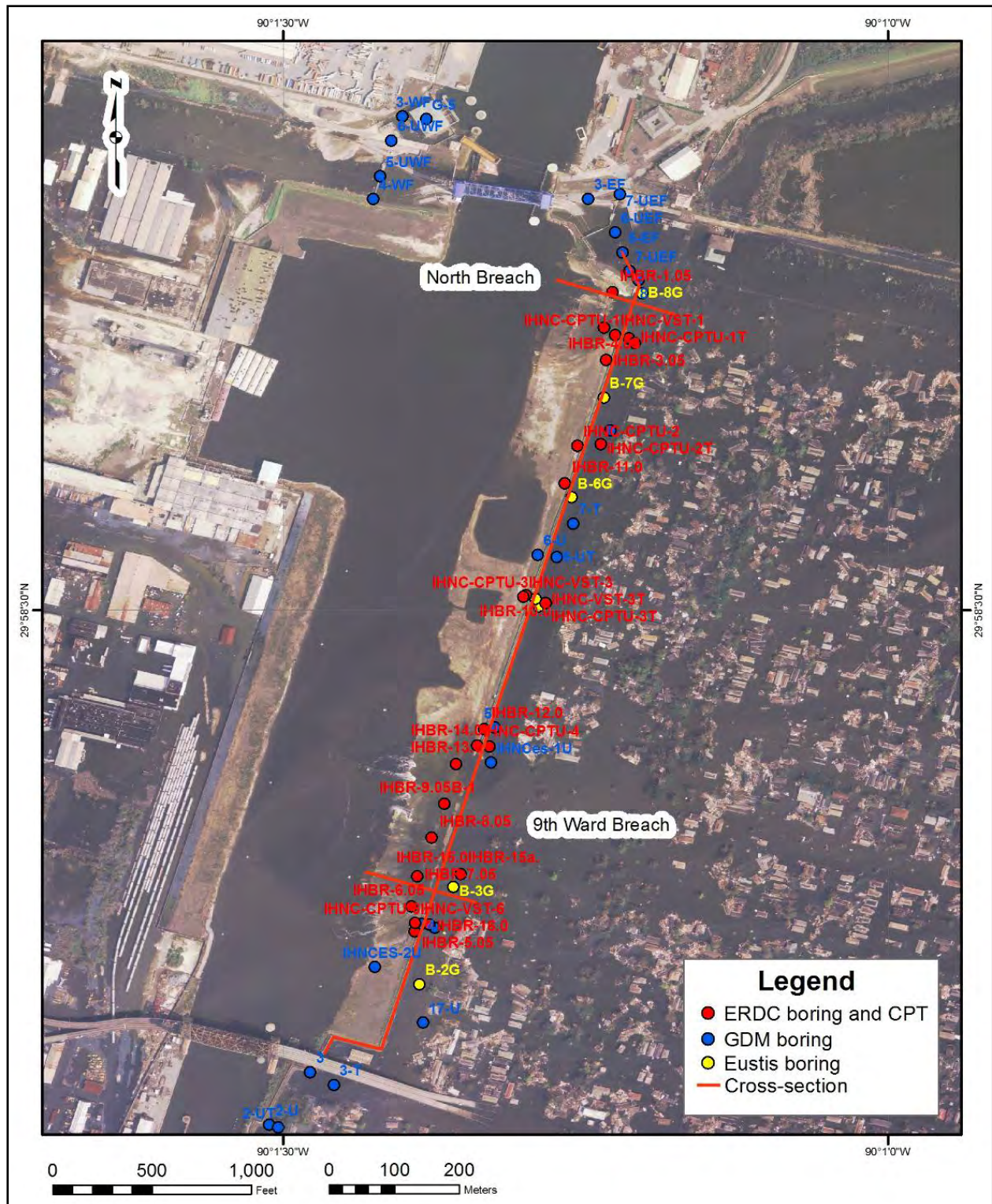
Figure 11-8. IHNC – East Bank (Between Florida Ave. and North Claiborne Ave.), Boring and CPTU Location Map

Volume V The Performance – Levees and Floodwalls – Technical Appendix

V-11-23

This is a preliminary report subject to revision; it does not contain final conclusions of the United States Army Corps of Engineers.
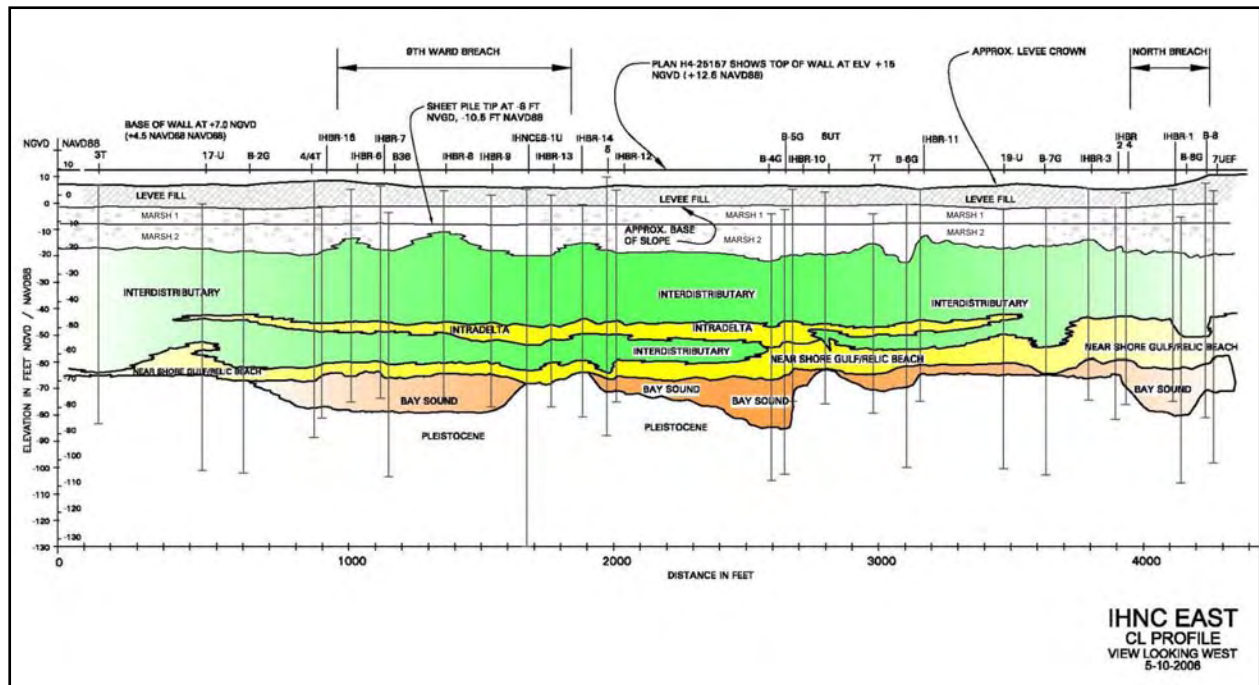
Figure 11-9. IHNC East Bank, Centerline Geologic Section Showing South (9th Ward) and North Breaches
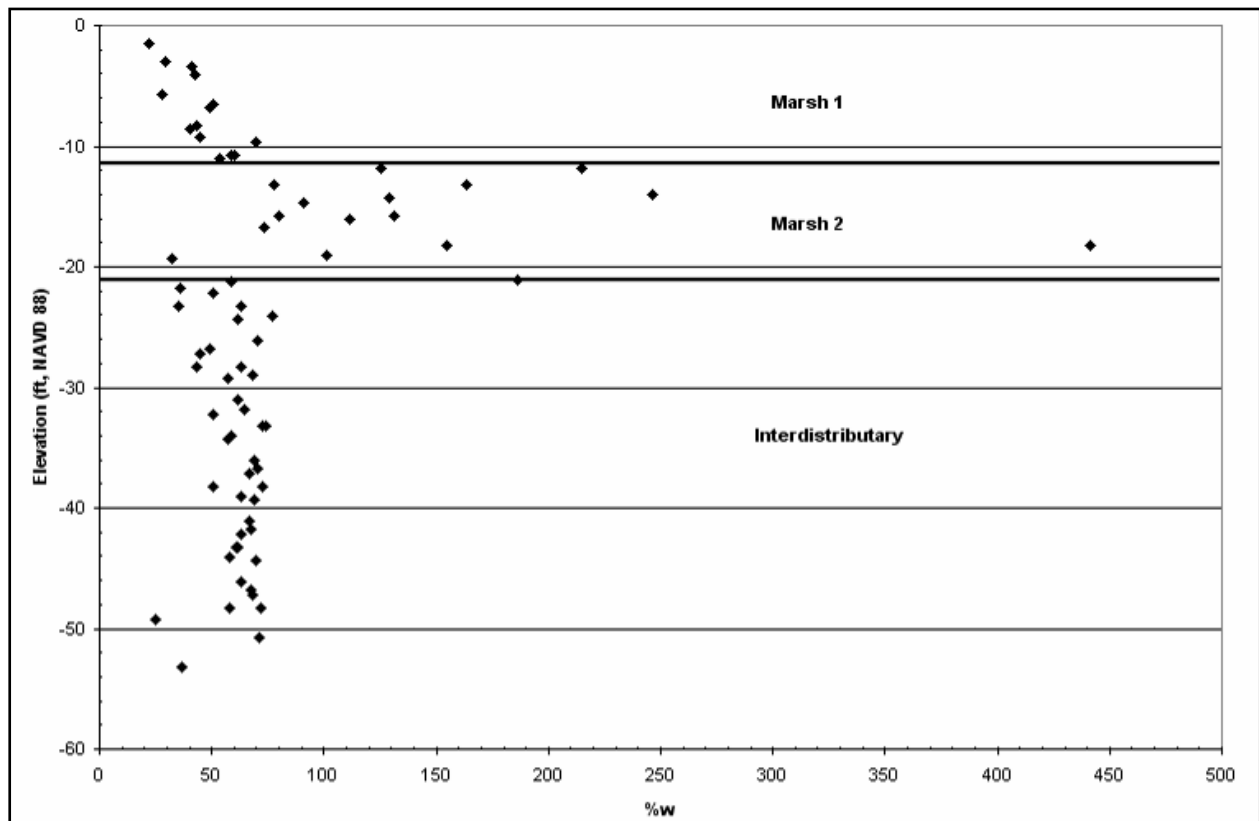
Figure 11-10. IHNC – East Bank (Between Florida Ave. and North Claiborne Ave.), % w Versus Elevation (ft, NAVD 88) from Toe Borings
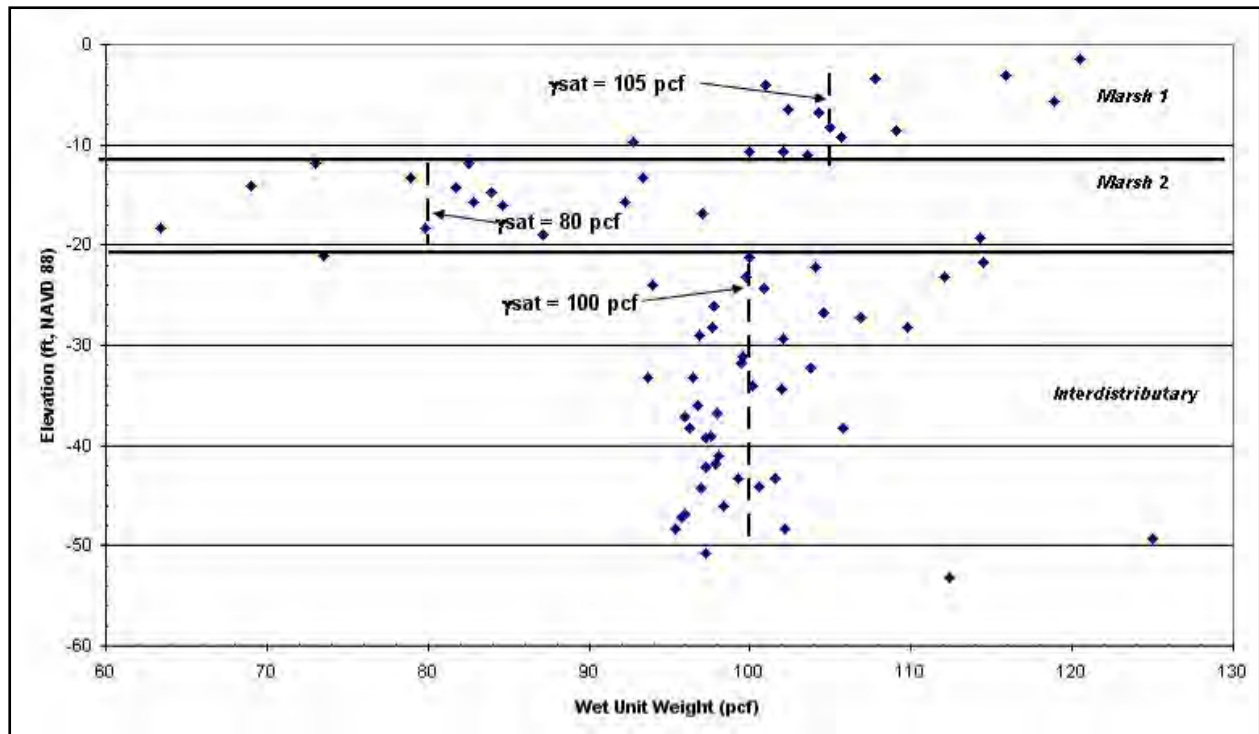
Figure 11-11. IHNC – East Bank (Between Florida Ave. and North Claiborne Ave.), Wet Unit Weight versus Elevation (ft, NAVD 88) from Post-Katrina Borings
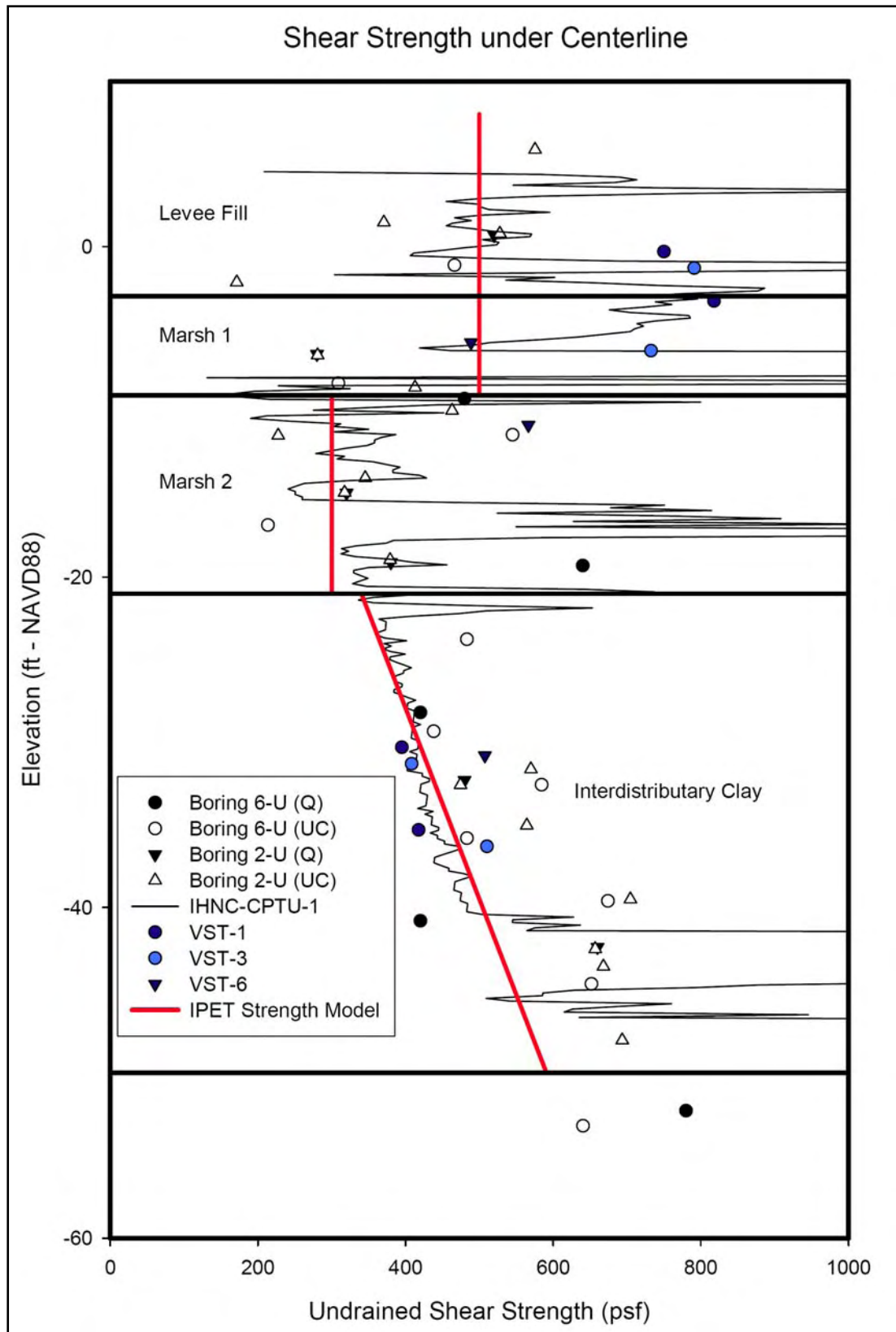
Figure 11-12. IHNC – East Bank Laboratory and Field Shear Strength Results for the Centerline of the Levee
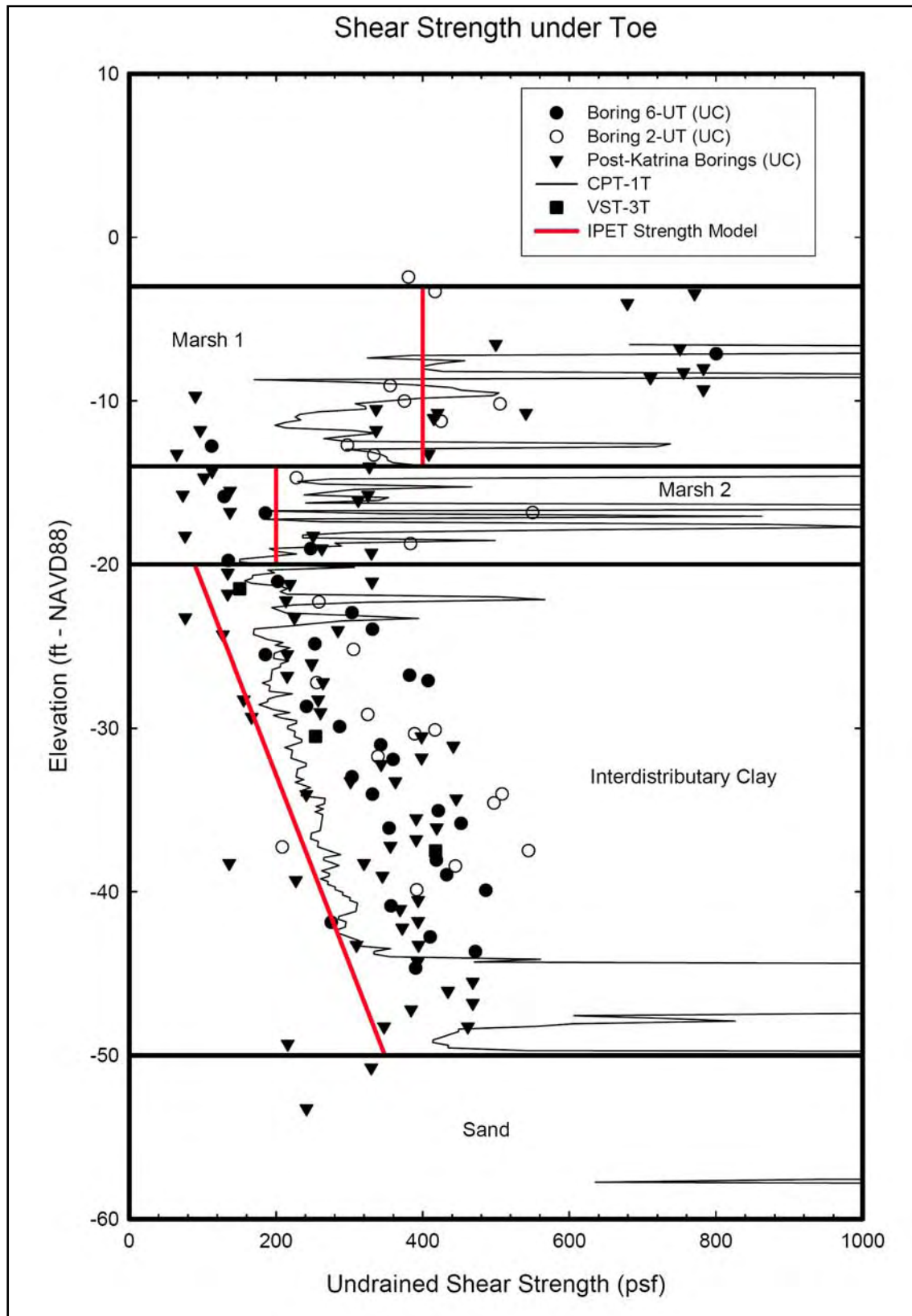
Figure 11-13. IHNC – East Bank Laboratory and Field Shear Strength Results for Toe of Levee and Beyond
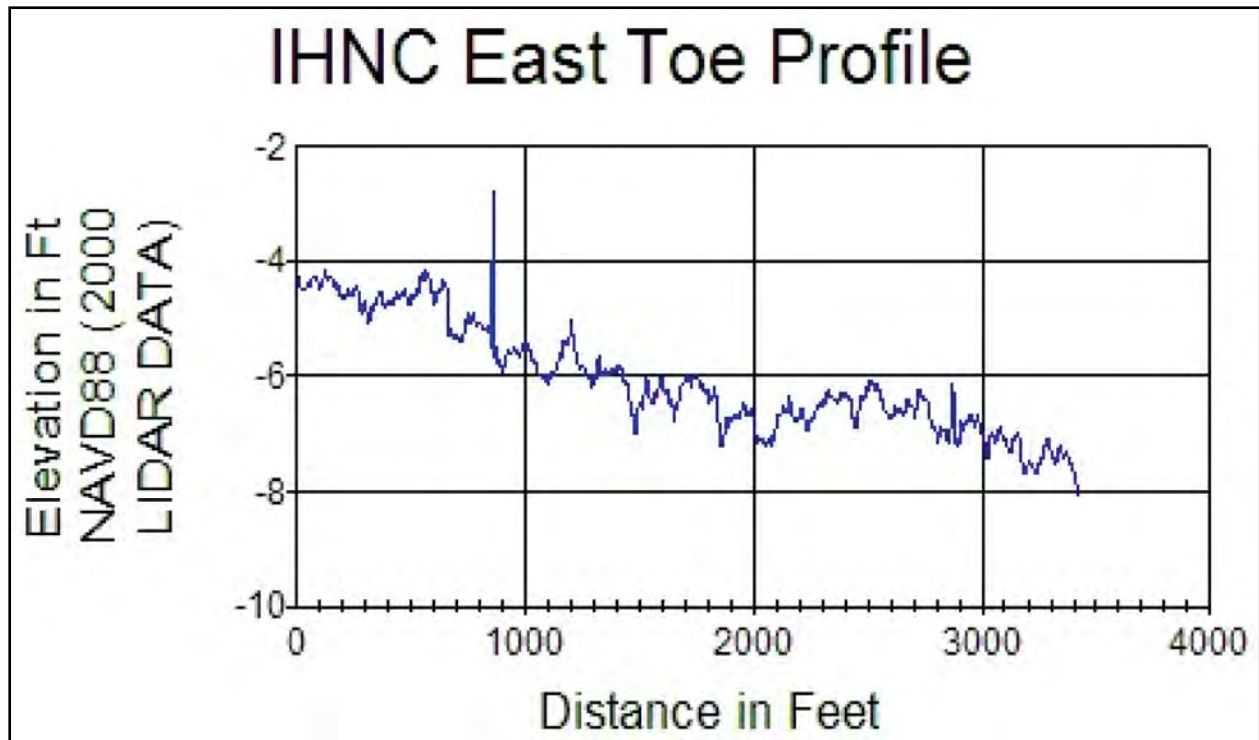
Figure 11-14. LIDAR Data at Toe of Levee
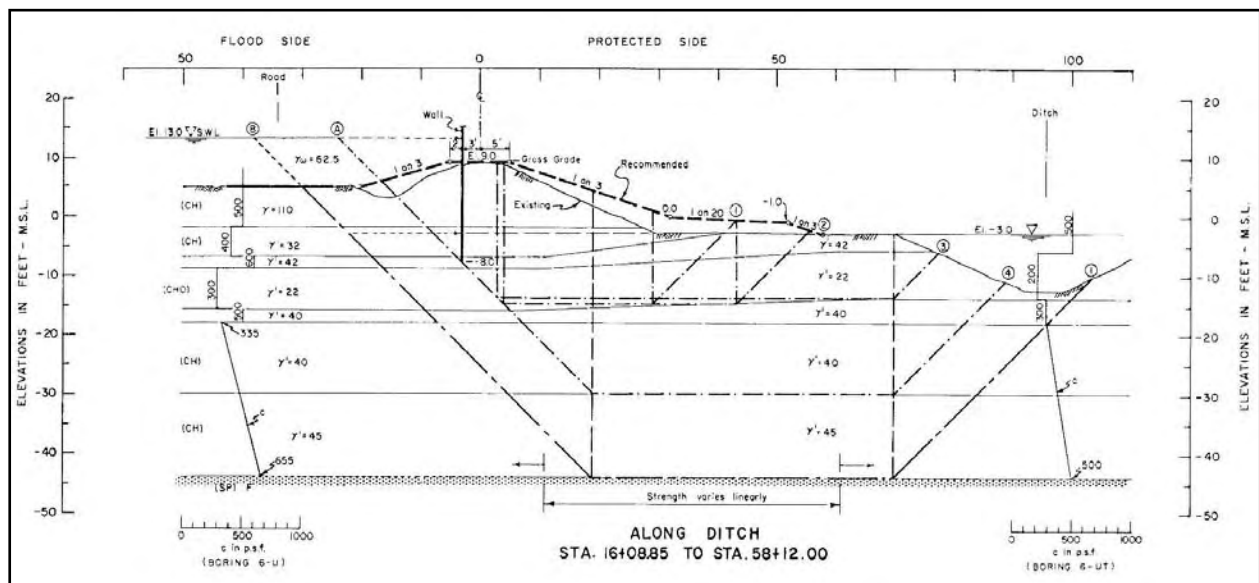
Figure 11-15. Cross Section Used for Design for Stations 16+09 to 58+12. Both East Bank Breaches Occurred Between These Two Stations

This is a preliminary report subject to revision; it does not contain final conclusions of the United States Army Corps of Engineers.
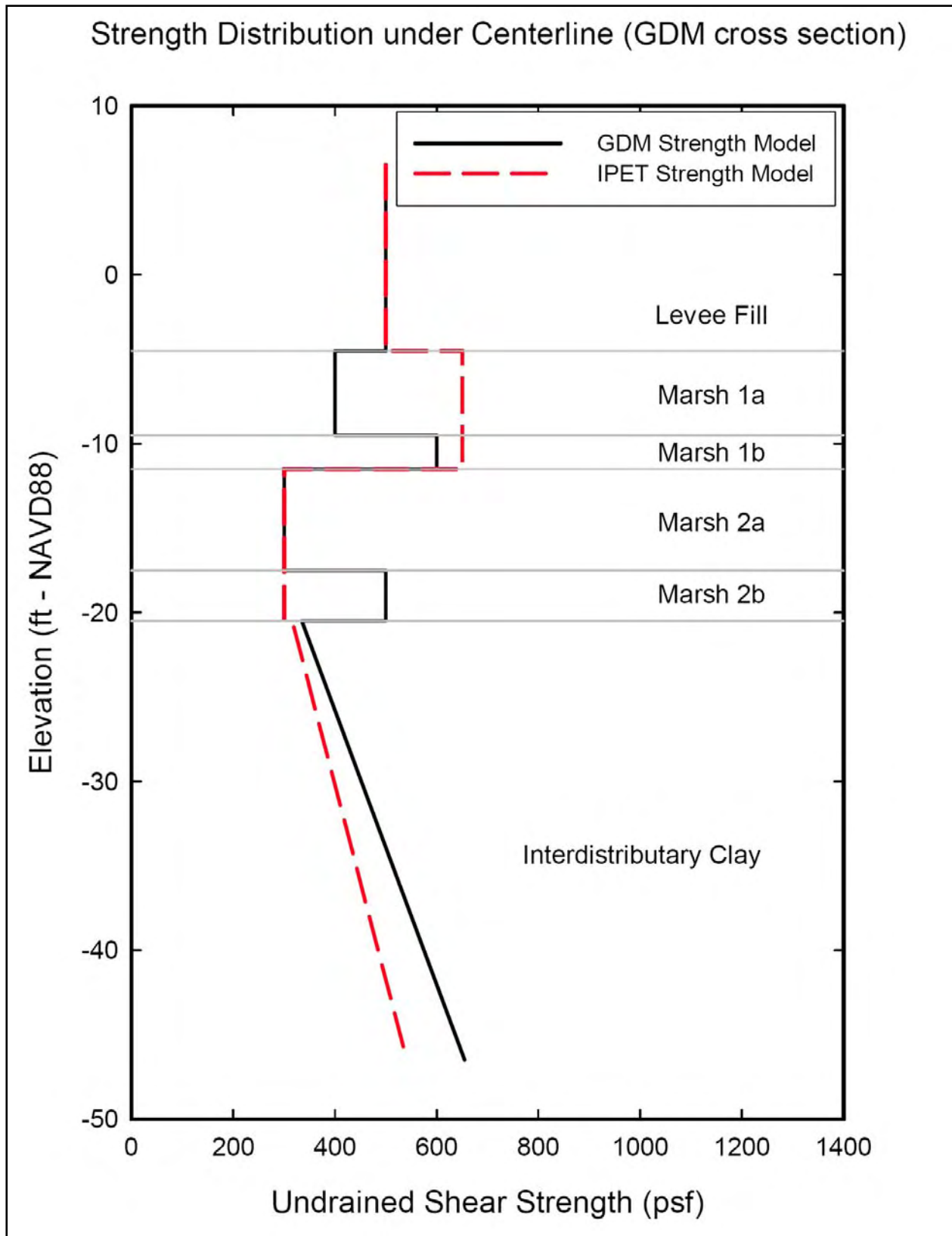
Figure 11-16. Comparison of GDM and IPET Shear Strength Models for GDM Design Cross Section at the Centerline (Horizontal Coordinate of 0 ft in Figure 11-15)
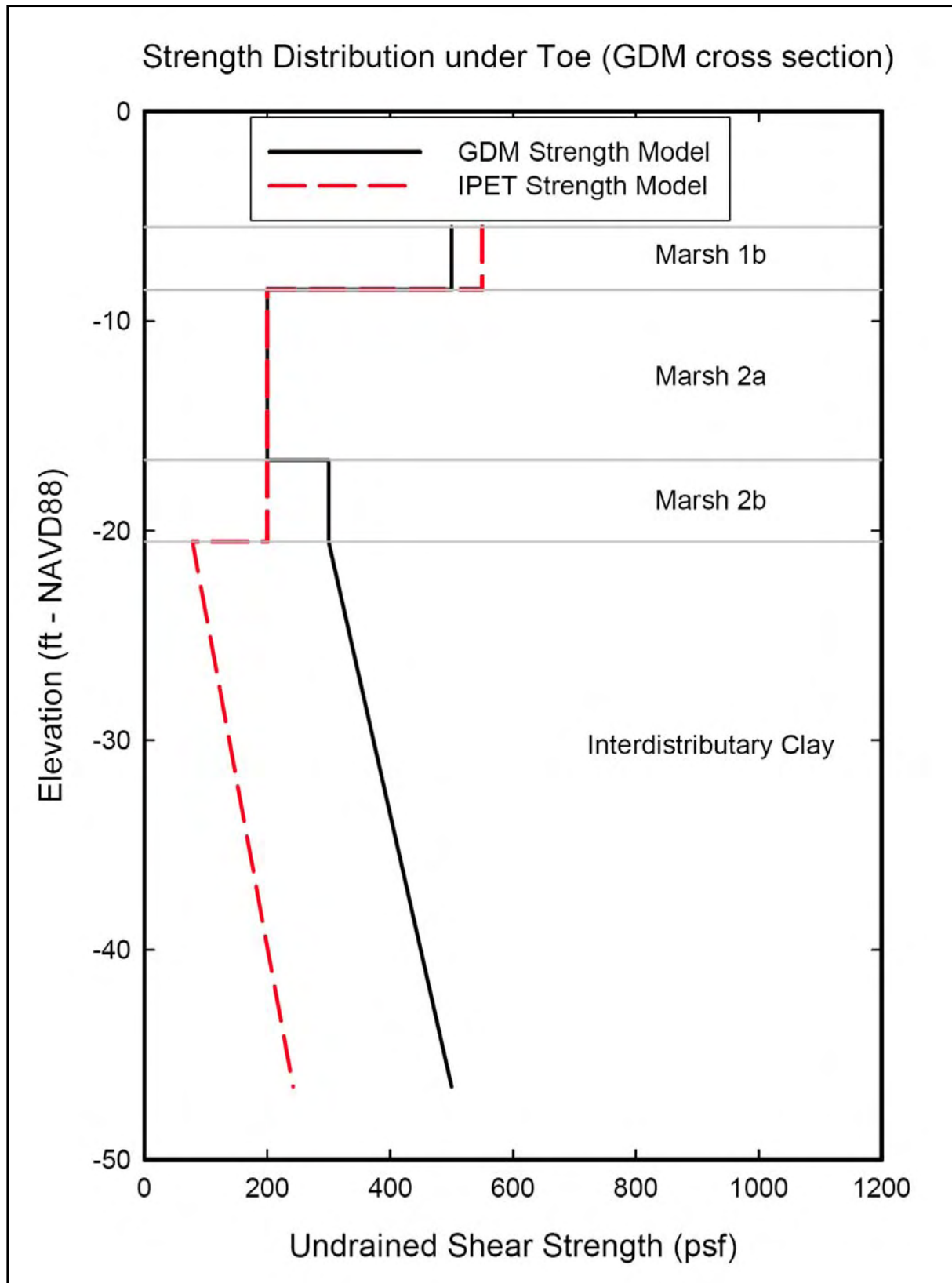
Figure 11-17. Comparison of GDM and IPET Shear Strength Models for GDM Design Cross Section at the Toe (Horizontal Coordinate of 60 ft in Figure 11-15)
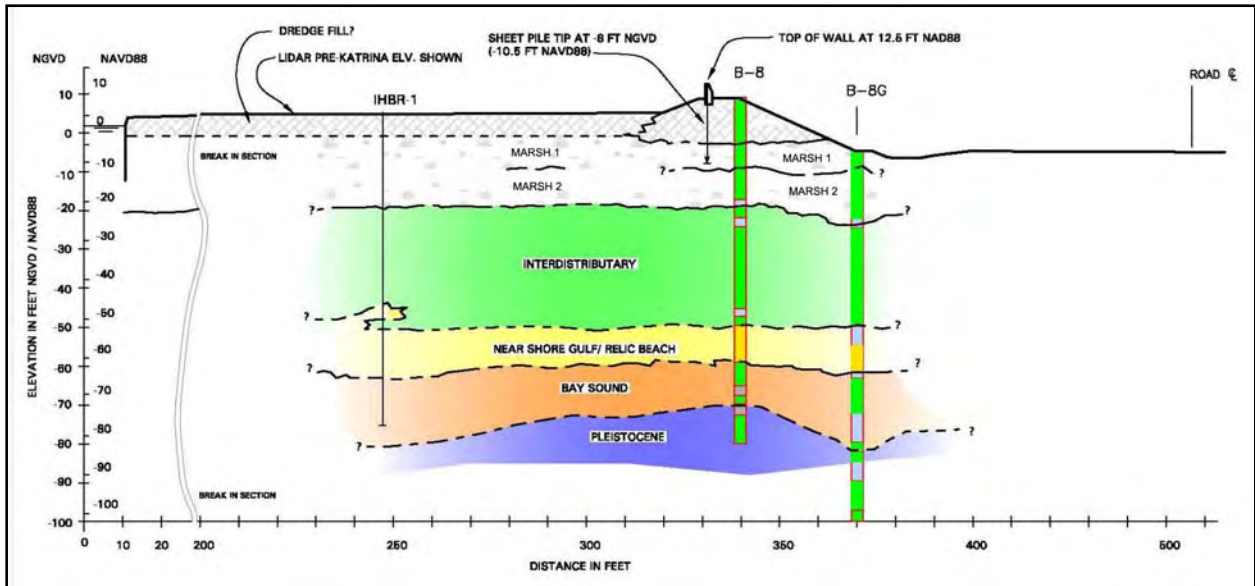
Figure 11-18. Profile of the North Breach at IHNC East bank, View Looking North
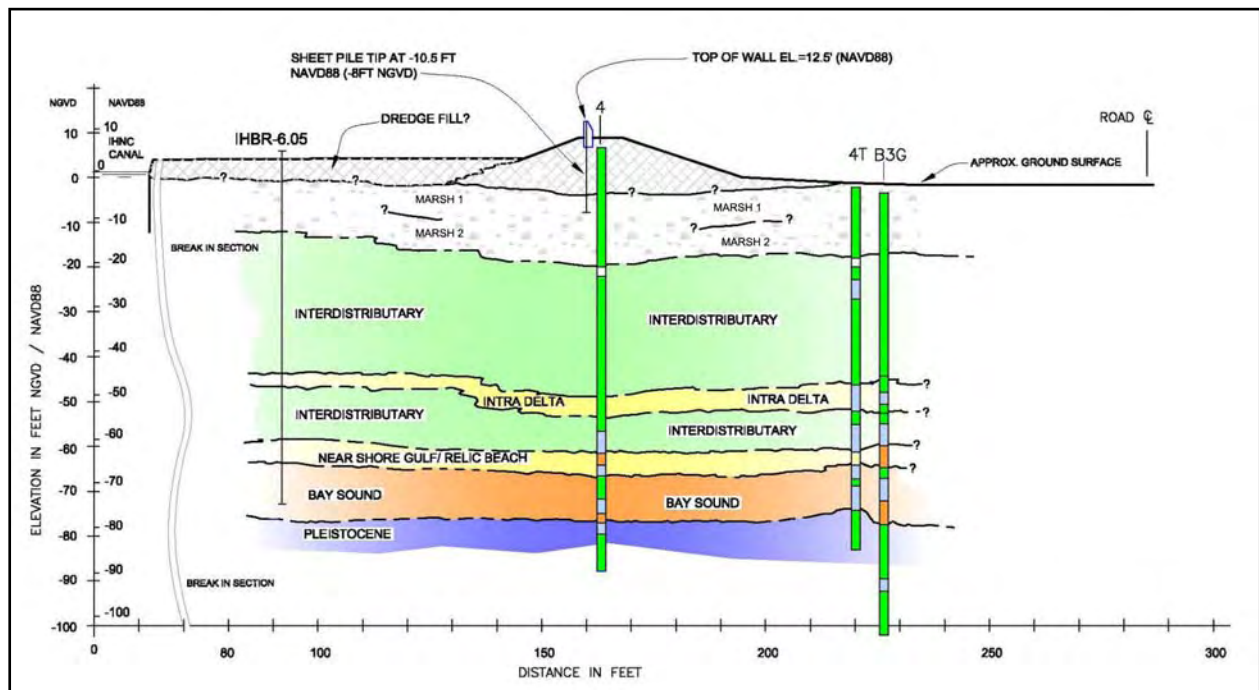
Figure 11-19. Profile of the South (9th Ward) Breach at IHNC East Bank, View Looking North
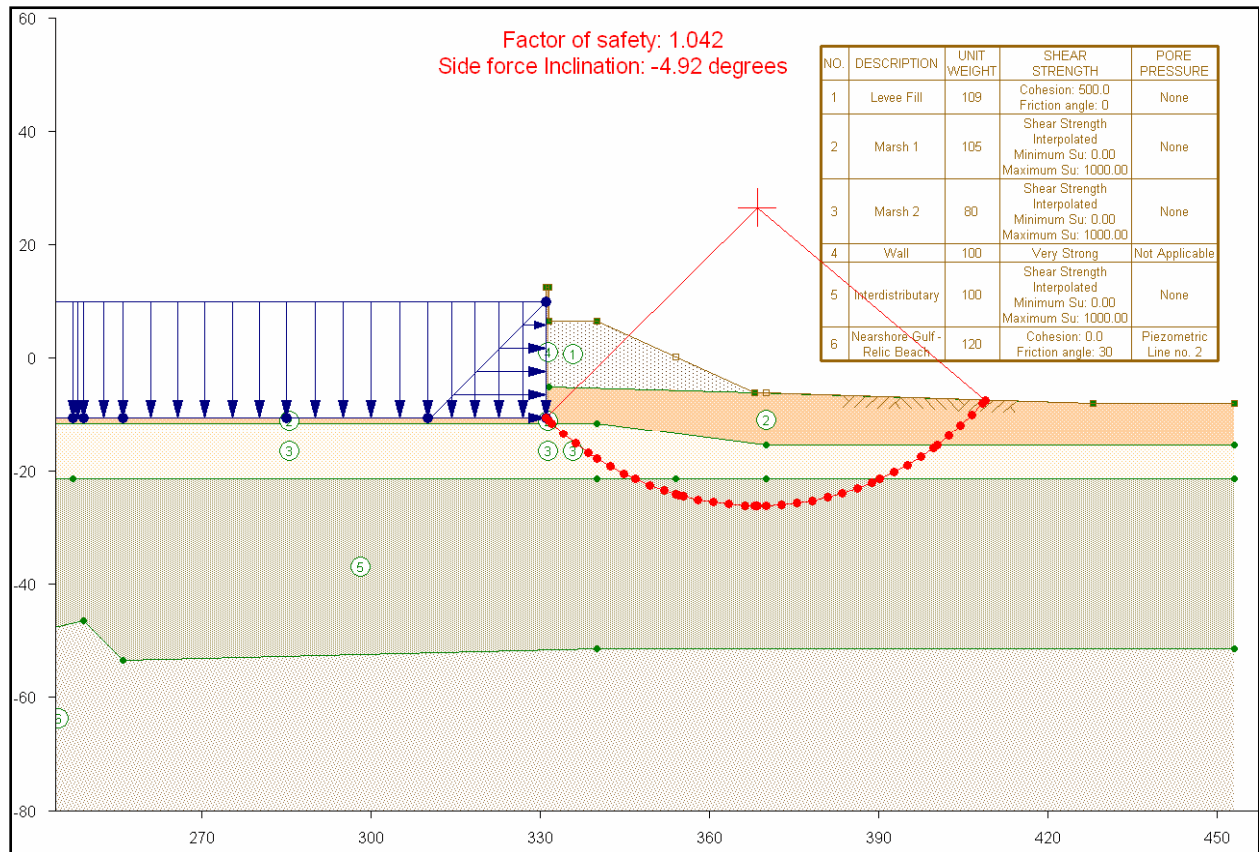
Figure 11-20. IHNC – East Bank (North Breach), Case 1, Canal Water Level = 10.0 ft (NAVD 88), with Crack
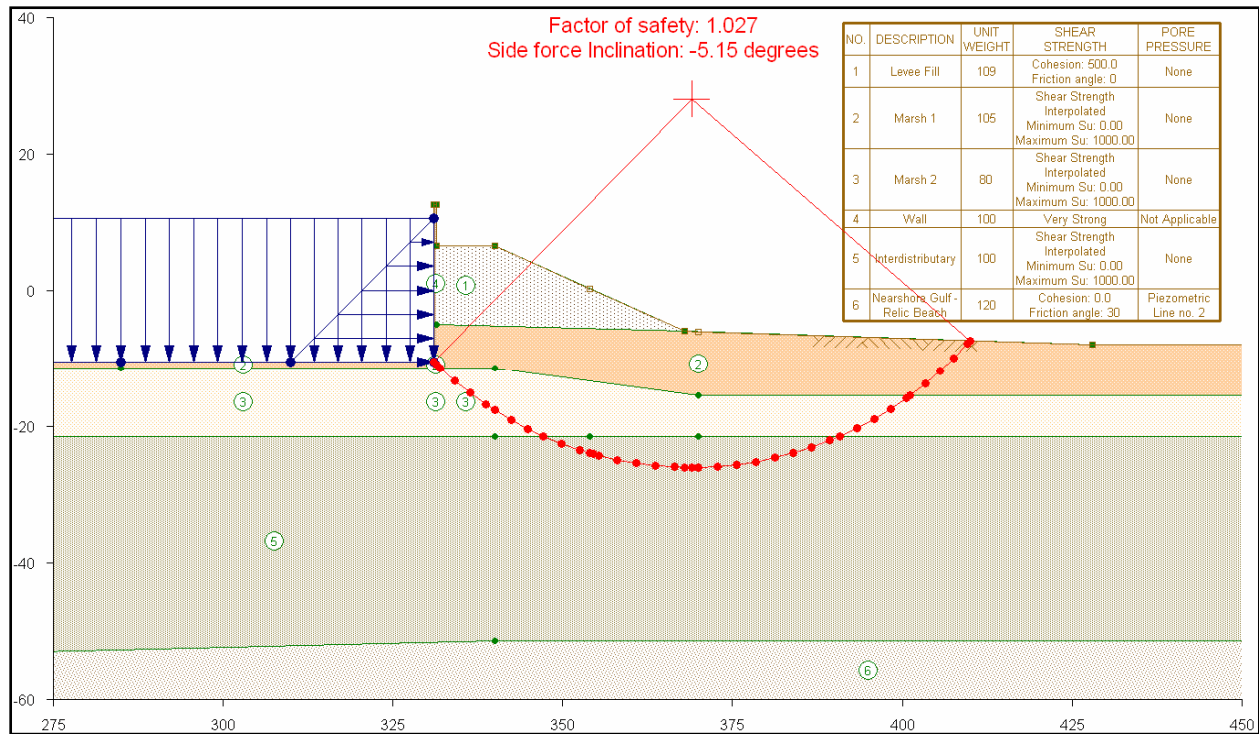
Figure 11-21. IHNC – East Bank (North Breach), Case 2, Design Canal Water Level = 10.5 ft (NAVD 88), with Crack
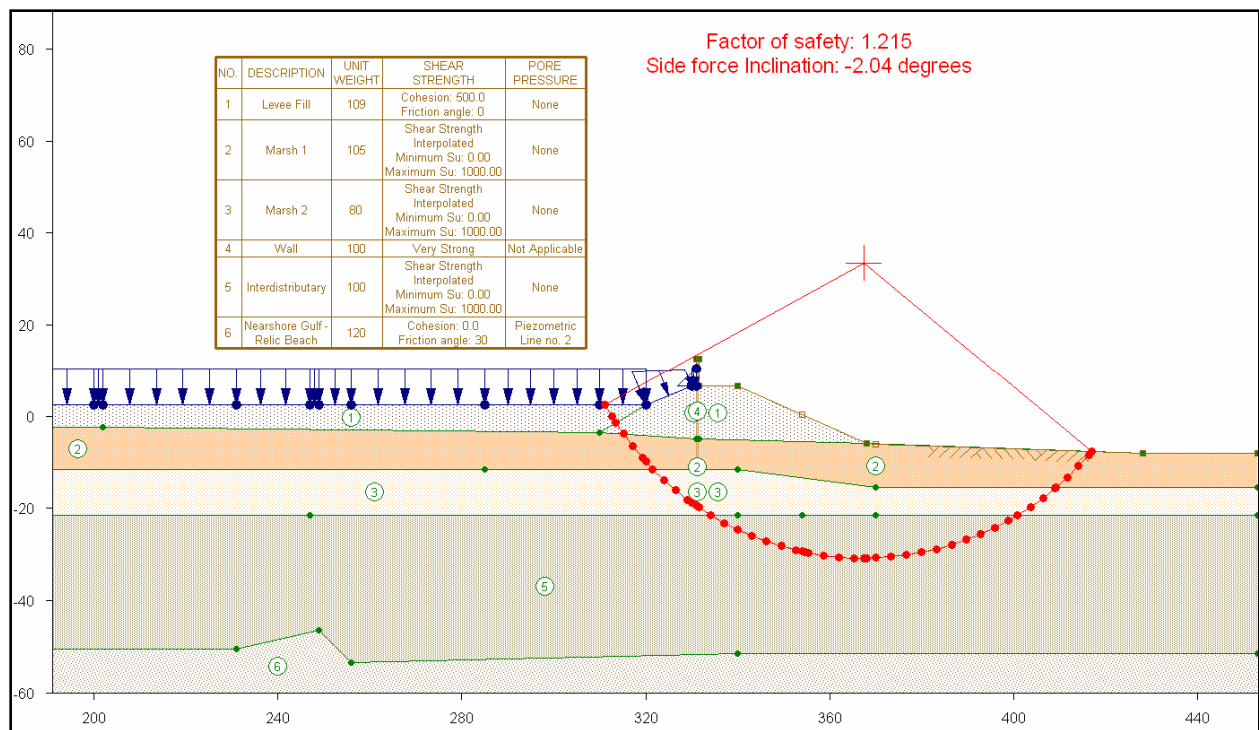
Figure 11-22. IHNC – East Bank (North Breach), Case 3, Design Canal Water Level = 10.5 ft (NAVD 88), without Crack

This is a preliminary report subject to revision; it does not contain final conclusions of the United States Army Corps of Engineers.

The figure contains the following data table:

NO.	DESCRIPTION	UNIT WEIGHT	SHEAR STRENGTH	PORE PRESSURE
1	Levee Fill	109	Cohesion: 500.0 Friction angle: 0	None
2	Marsh 1	105	Shear Strength Interpolated Minimum Su: 0.00 Maximum Su: 1000.00	None
3	Marsh 2	80	Shear Strength Interpolated Minimum Su: 0.00 Maximum Su: 1000.00	None
4	Wall	100	Very Strong	Not Applicable
5	Interdistributary	100	Shear Strength Interpolated Minimum Su: 0.00 Maximum Su: 1000.00	None
6	Nearshore Gulf - Relic Beach	120	Cohesion: 0.0 Friction angle: 30	Piezometric Line no. 2

Factor of safety: 1.005
Side force Inclination: -5.5 degrees

Figure 11-23. IHNC – East Bank (North Breach), Case 4, Canal Water Level = 11.2 ft (NAVD 88), with Crack
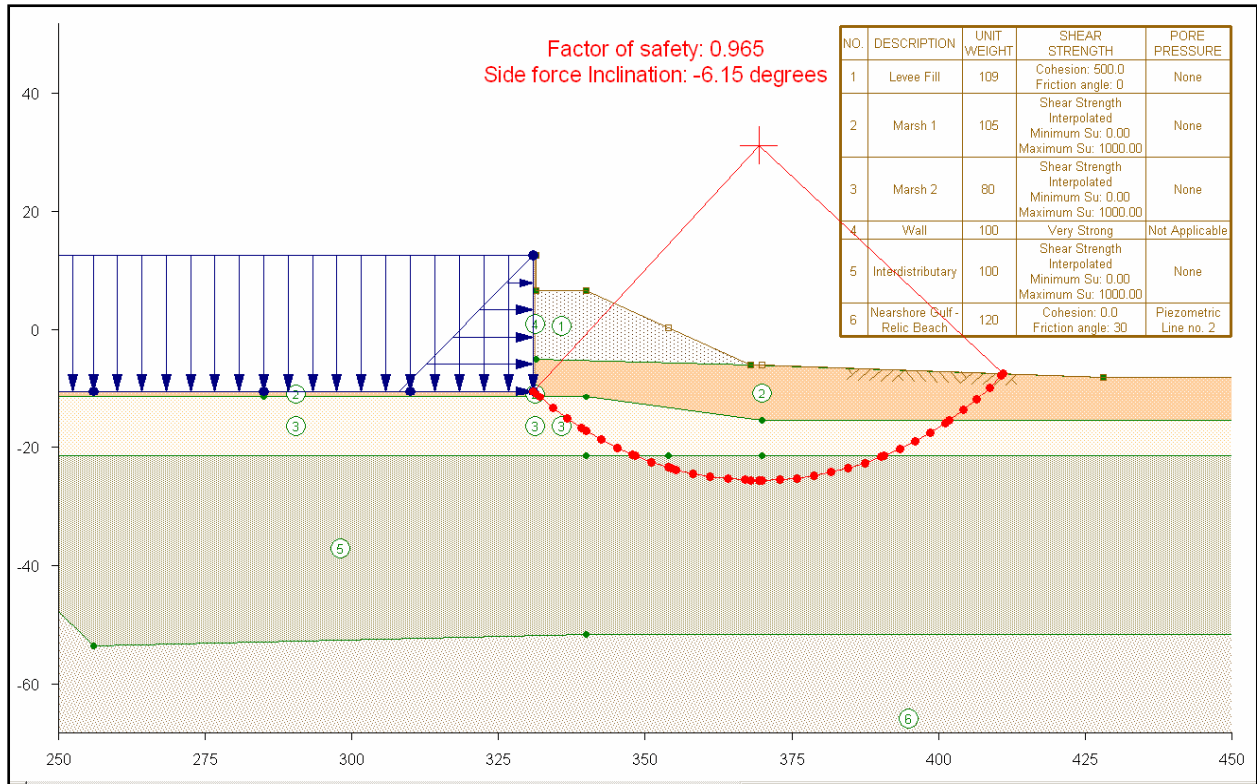
Figure 11-24. IHNC – East Bank (North Breach), Case 5, Canal Water Level = Top of Wall = 12.5 ft (NAVD 88), with Crack

Volume V The Performance – Levees and Floodwalls – Technical Appendix

V-11-35

This is a preliminary report subject to revision; it does not contain final conclusions of the United States Army Corps of Engineers.
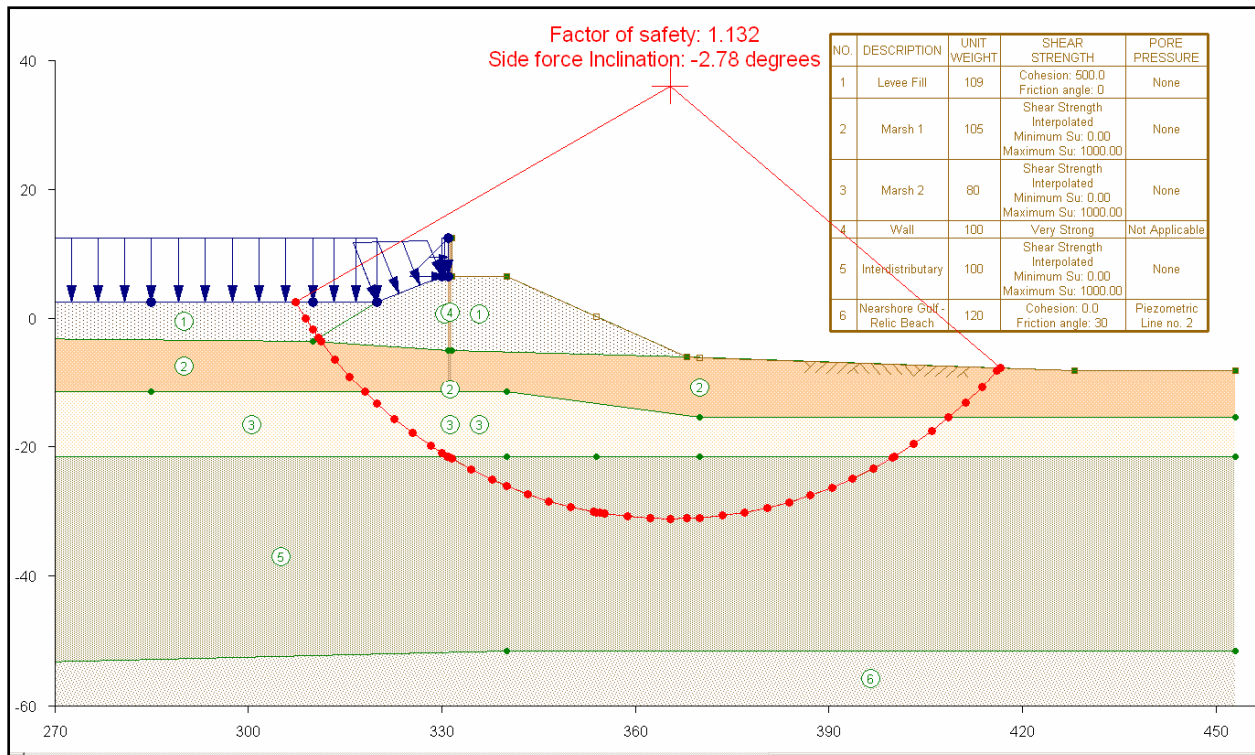
Figure 11-25. IHNC – East Bank (North Breach), Case 5a, Canal Water Level = Top of Wall = 12.5 ft (NAVD 88), without Crack
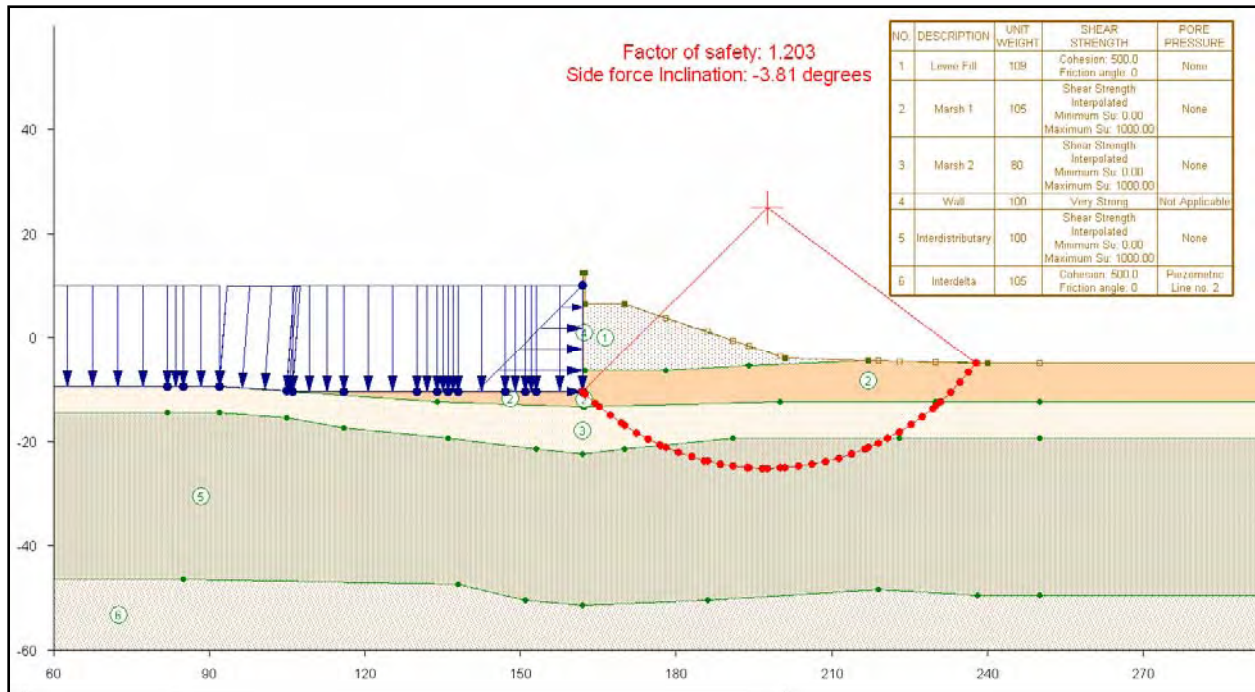
Figure 11-26. IHNC – East Bank (South Breach), Case 1, Canal Water Level = 10.0 ft (NAVD 88), with Crack
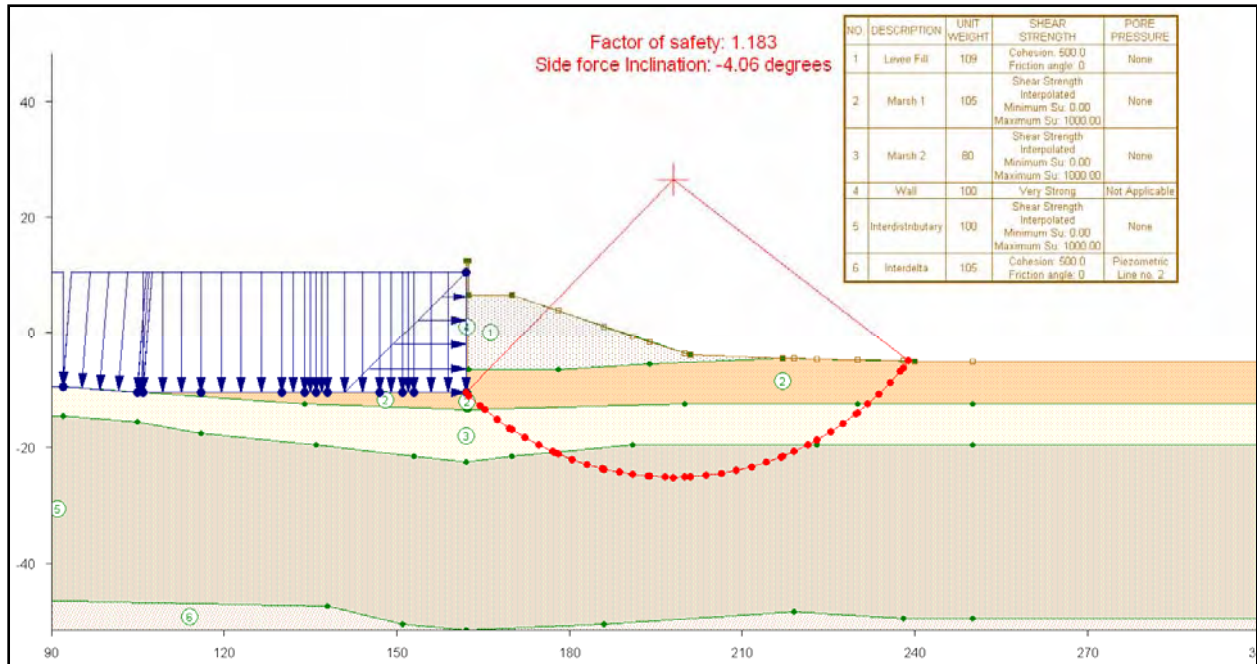
Figure 11-27. IHNC – East Bank (South Breach), Case 2, Design Canal Water Level = 10.5 ft (NAVD 88), with Crack
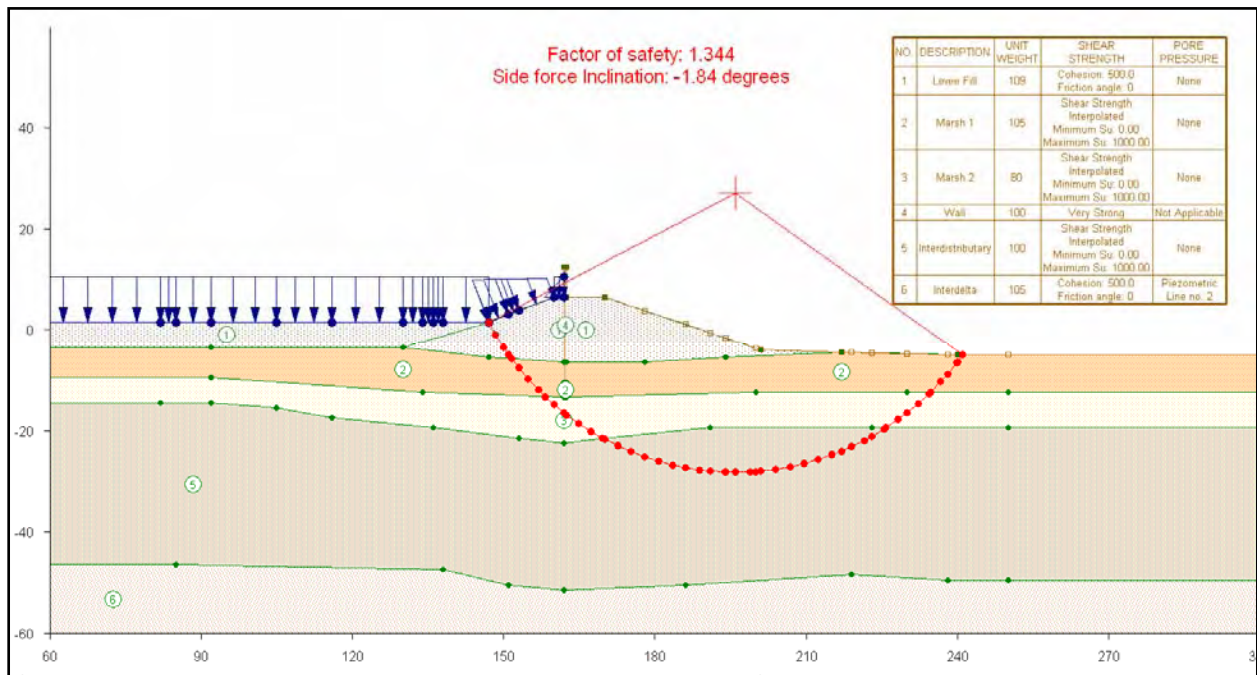
Figure 11-28. IHNC – East Bank (South Breach), Case 3, Design Canal Water Level = 10.5 ft (NAVD 88), without Crack
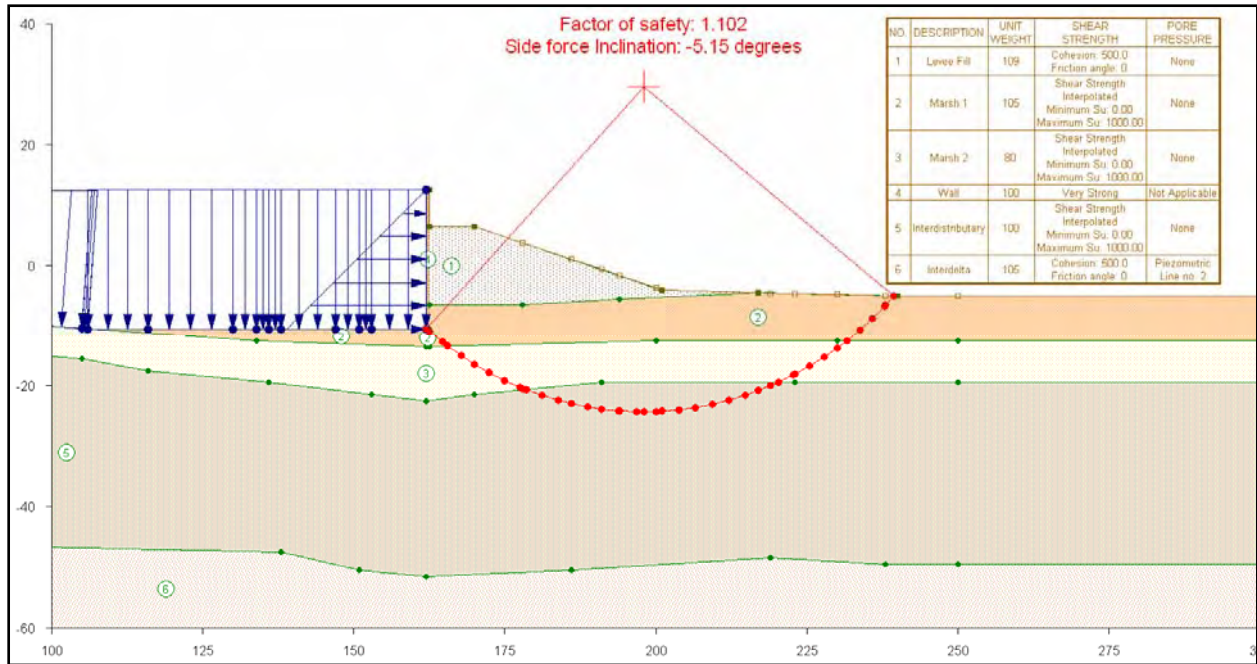
Figure 11-29. IHNC – East Bank (South Breach), Case 4, Canal Water Level = Top of Wall - 12.5 ft (NAVD 88), with Crack
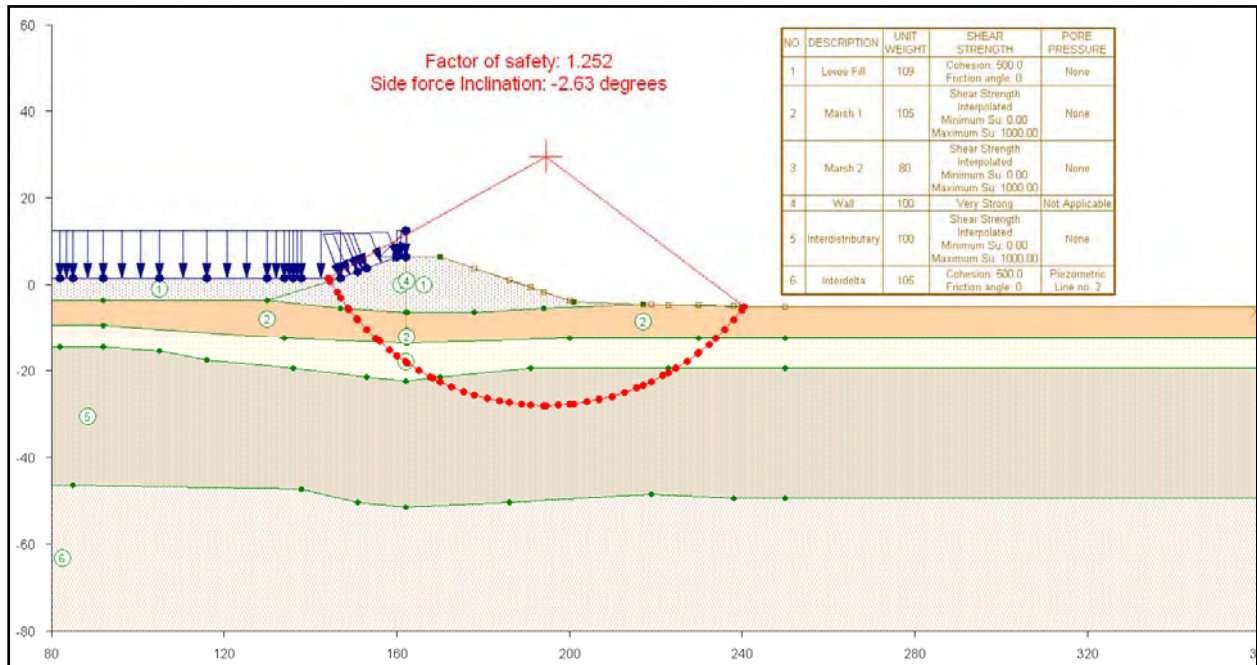
Figure 11-30. IHNC – East Bank (South Breach), Case 5, Canal Water Level = Top of Wall - 12.5 ft (NAVD 88), without Crack
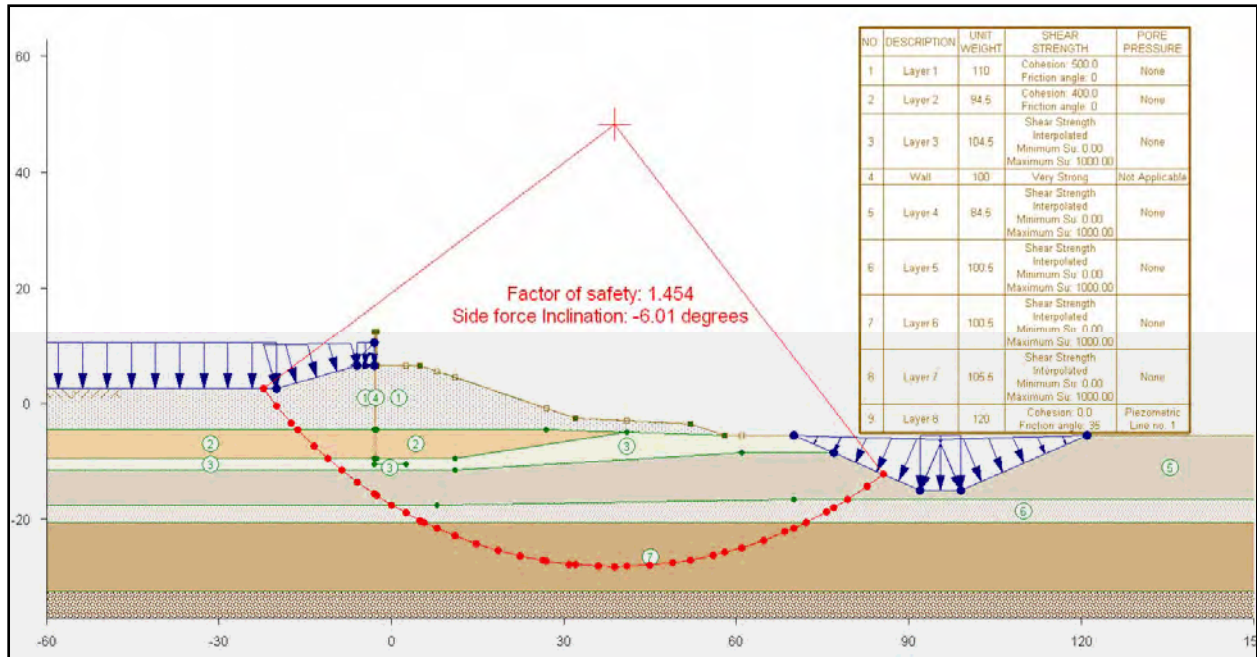
Figure 11-31. IHNC – East Bank (GDM Stability Plate), Case 1, Canal Water Level = Design - 10.5 ft (NAVD 88), without Crack
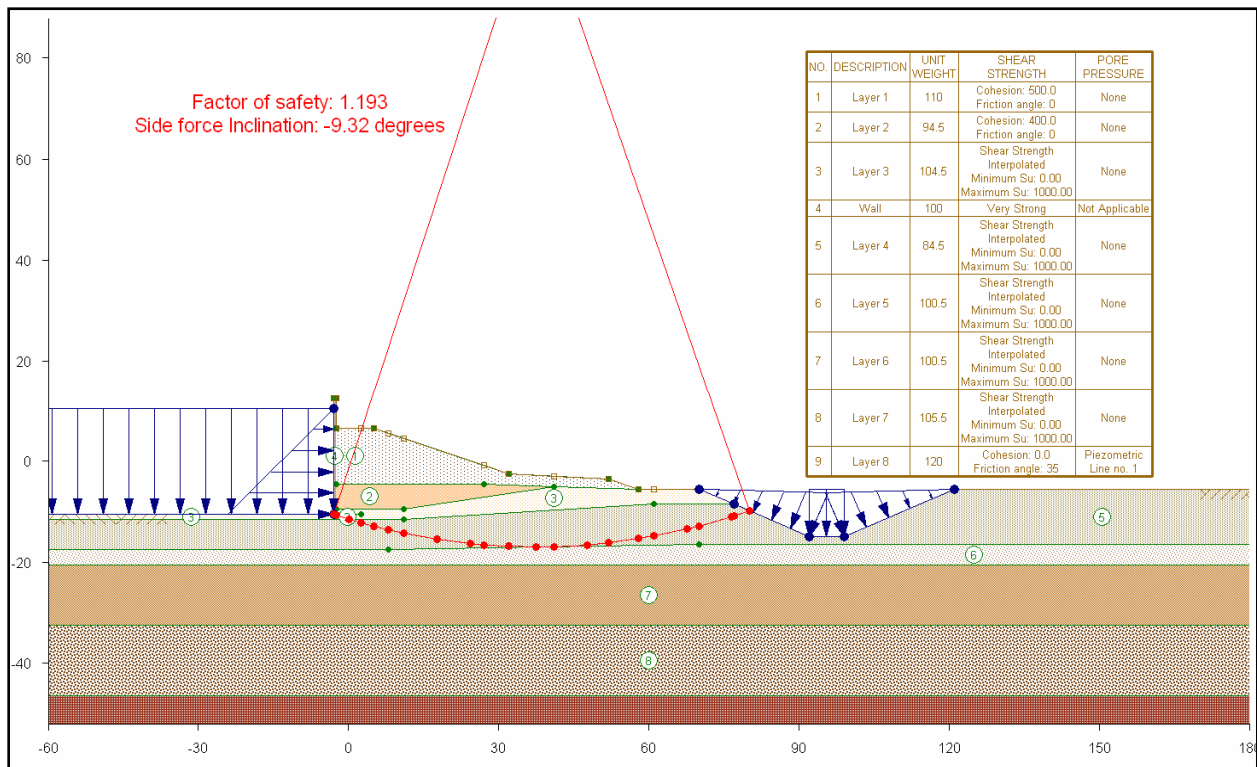
Figure 11-32. IHNC – East Bank (GDM Stability Plate), Case 2, Canal Water Level = Design - 10.5 ft (NAVD 88), with Crack
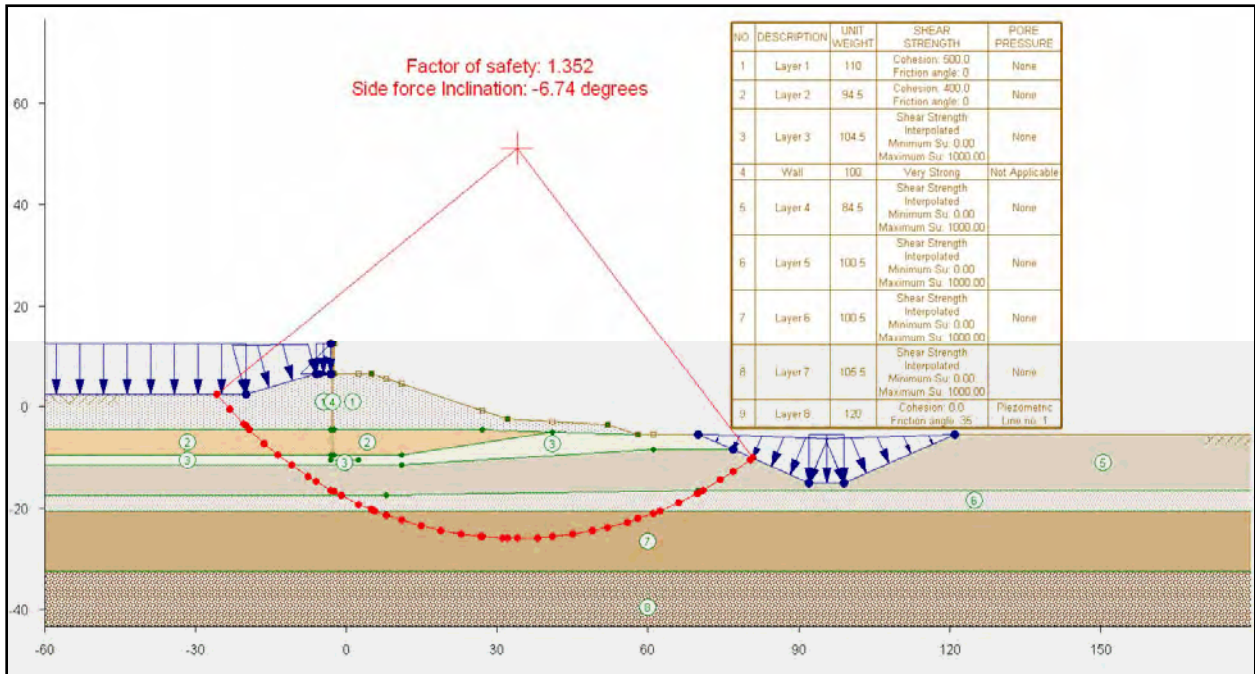
Figure 11-33. IHNC – East Bank (GDM Stability Plate), Case 3, Canal Water Level = Top of Wall - 12.5 ft (NAVD 88), without Crack
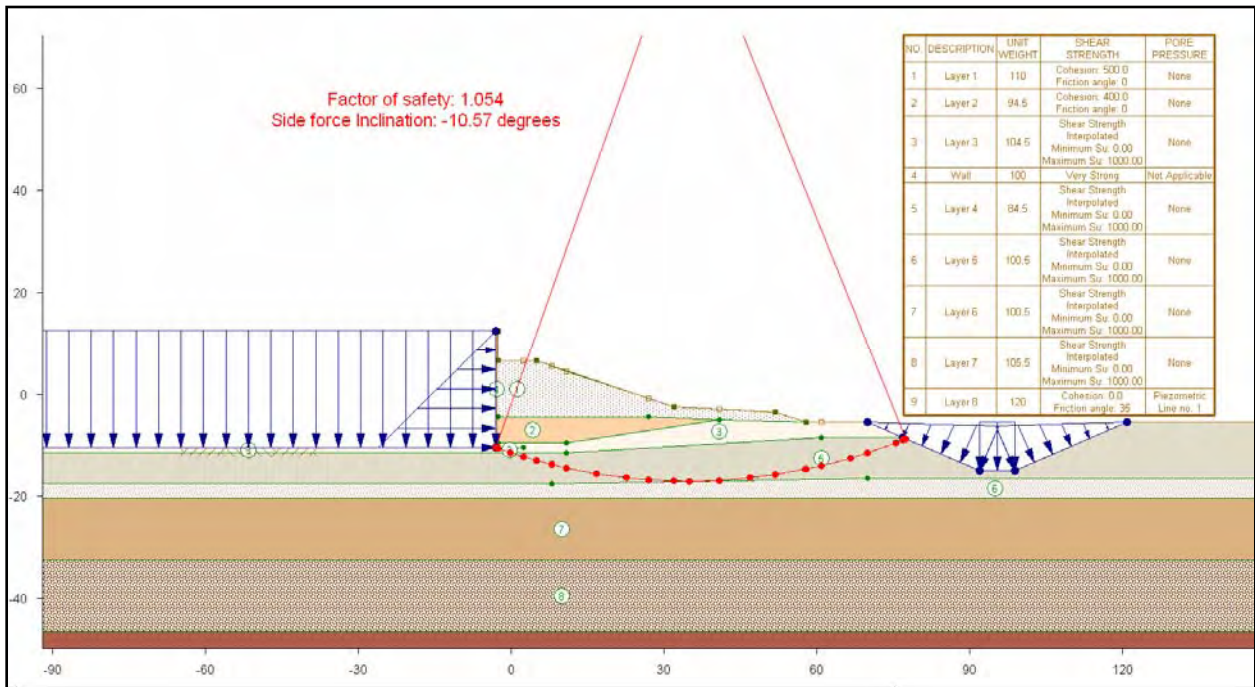
Figure 11-34. IHNC – East Bank (GDM Stability Plate), Case 4, Canal Water Level = Top of Wall - 12.5 ft (NAVD 88), with Crack
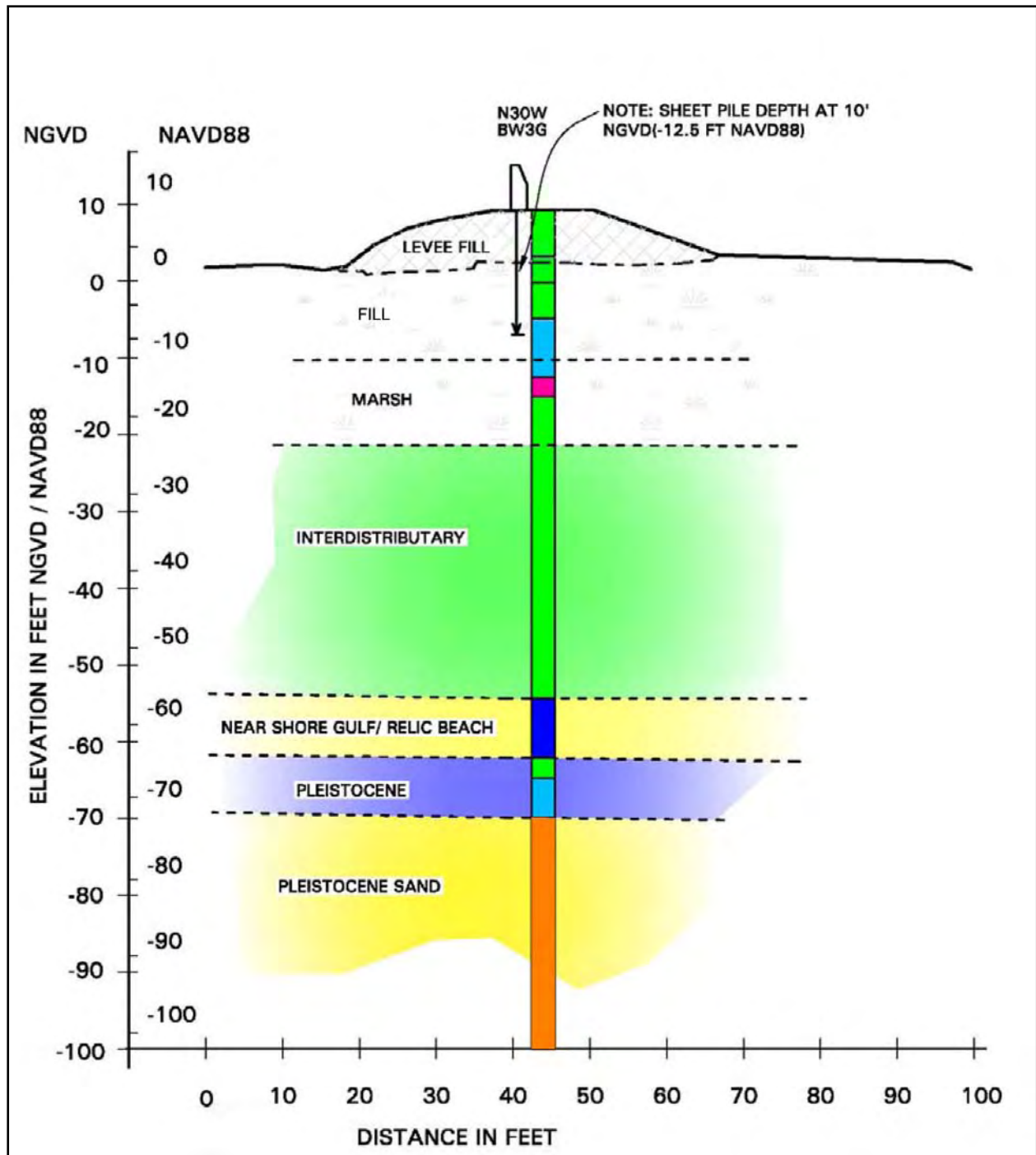
Figure 11-35. IHNC – West Bank – Cross Section of North Breach
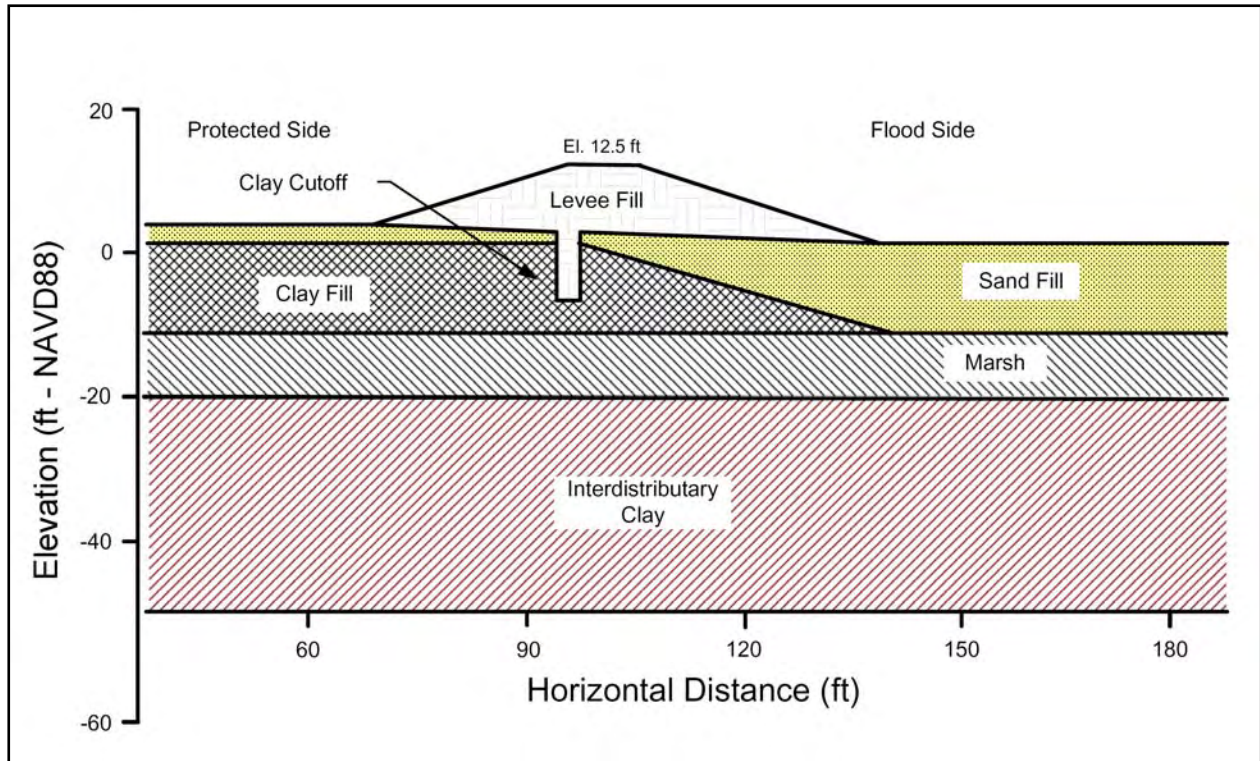
Figure 11-36. IHNC – West Bank – Cross Section of South Breach

Appendix 12
Levee Damage Report — Geotechnical Investigation — New Orleans East (Orleans Parish)

Table of Contents

Table of Figures

General Description of the New Orleans East Basin and Hurricane Protection System

The hurricane protection system for the New Orleans East (NOE) Basin was designed as part of the Lake Pontchartrain, LA and Vicinity Hurricane Protection Project. The NOE portion of the project protects 45,000 acres of urban, industrial, commercial, and industrial lands. The levee is constructed with a 10-ft crown width with side slopes of 1 on 3. The height of the levee varies from 13 to 19 ft. There are floodwall segments along the line of protection that consists of sheet-pile walls or concrete I-walls constructed on top of sheet-pile. The line of protection was designed to provide protection from the Standard Project Hurricane (category 3 hurricane).

NOE Basin Components

Figure 12-1 illustrates the boundaries and basic flood protection components within the NOE Basin. This drawing is used by the New Orleans District for planning and design, specifically because it shows as-built levee and floodwall elevations. The western border coincides with the Inner Harbor Navigation Canal (IHNC) and the eastern boundary of the Orleans Basin. It is bounded by the east bank of the IHNC, the Lake Pontchartrain shoreline (between the IHNC and Southpoint), the eastern boundary of the Bayou Savage National Wildlife Preserve, and the north side of the Gulf Intracoastal Waterway (GIWW) (between the IHNC and eastern edge of the Bayou Savage National Wildlife Preserve). The main components are described in the next section moving clockwise through the basin, beginning at the Lakefront Airport and ending at the western end of the GIWW.

Figure 12-1. NOE Basin General Components and Top of Levee/Floodwall As-Built Elevations (feet) (source USACE, New Orleans District (Wayne Naquin)

V-12-6

Volume V The Performance – Levees and Floodwalls – Technical Appendix
This is a preliminary report subject to revision; it does not contain final conclusions of the United States Army Corps of Engineers.

Hurricane Protection Features

    New Orleans East Lakefront includes the Citrus Lakefront Levee and New Orleans East Lakefront Levee consisting of 12.4 miles of earthen levee paralleling the Lakefront from the IHNC to Southpoint. It also includes floodwalls at the Lakefront Airport and Lincoln Beach.

    The New Orleans East Levee consists of 8.4 miles of earthen levee from Southpoint to the GIWW along the eastern boundary of the Bayou Savage National Wildlife Preserve.

    GIWW - The basin includes the Citrus Back Levee and New Orleans East Back Levee which consisting of approximately17.5 miles of earthen levees and concrete floodwalls along the northern edge of the GIWW.

    IHNC - The basin protection includes approximately 2.8 miles of levee and concrete floodwall along the eastern side of the IHNC. The IHNC is described in a separate report.

    Pump Stations – Eight pump stations and numerous drainage structures, pipe crossings and culverts also lay on the boundaries

Table 12-1 Summary of NOE Basin Hurricane Protection Features	
Exterior levee and floodwall (I wall)	39 miles
Drainage Structures	4
Pump Stations	8
Highway Closure Structures	2
Railroad Closure Structure	1

IPET Investigation of Hurricane Protection Project Performance

Levee/Floodwall damage categories

    The goal of Task 7 of the IPET is to characterize the adverse affects of Hurricane Katrina on the levees and floodwalls and to determine why some of these structures failed and others did not. To begin this study the levee behavior was observed from TFG reports and categorized. These categories distinguish catastrophic failure (total breach) to poor performance (scour). The categories are defined below. Figure 12-2 illustrates the spatial distribution of levee and floodwall performance along the basin boundaries. This study is not concerned with the inner levees that are not federally owned.

LEGEND
    LONB = Overtopped levees, no breaching
    WS = Overtopped floodwalls, no breaching (stable)
    LOB = Overtopped levees, breaching
    TF = Transition failure (floodwall to levee transition)
    WF = Overtopped floodwalls, breached (failure)
    WCF = Overtopped floodwalls, no breaching but came close

Figure 12-2. Generalization of Levee and Floodwall Failures in the NOE Basin

Current IPET Task 7 Scope

To determine why some of the levees/floodwalls performed well and others did not, a geotechnical investigation is being conducted. Available soil boring logs and soil tests are being collected for comparison of soil properties to levee performance. All available soil boring logs are held in the NOD boring log database. The NOE boring locations have been plotted on an aerial photo of the study area and are illustrated by Figure 12-3. The top 20 ft or so of these borings represent the levee material and possibly includes the top of the foundation. It is presumed that the soil types will correlate to levee performance. This study will focus on finding soil classification and strength data along with levee design documents.

Original test data and levee physical dimensions will be taken from the design memoranda. Additional soil data will be obtained from current drilling, sampling and cone penetration investigations in the study area. Surface geology maps will also be studied for trends in geologic environment associated with foundation scour, failure or good performance. Levee performance may be categorized as good, moderate, or poor with respect to severity of scour, length of breach, etc. This information is well defined by the TFG Project Information Reports, and other data reports. Floodwall behavior may be correlated to mode of failure or severity (sliding along foundation, rotation, minor separation from levee or embankment).

Because of the large amount of data and limited amount of time to conduct this study, this investigation will concentrate on a portion of the NOE basin; the southern border including the Citrus Back Levee and the NOE Back Levee. The entire basin will be characterized with respect to performance, but only the southern portion will be correlated to soil properties.
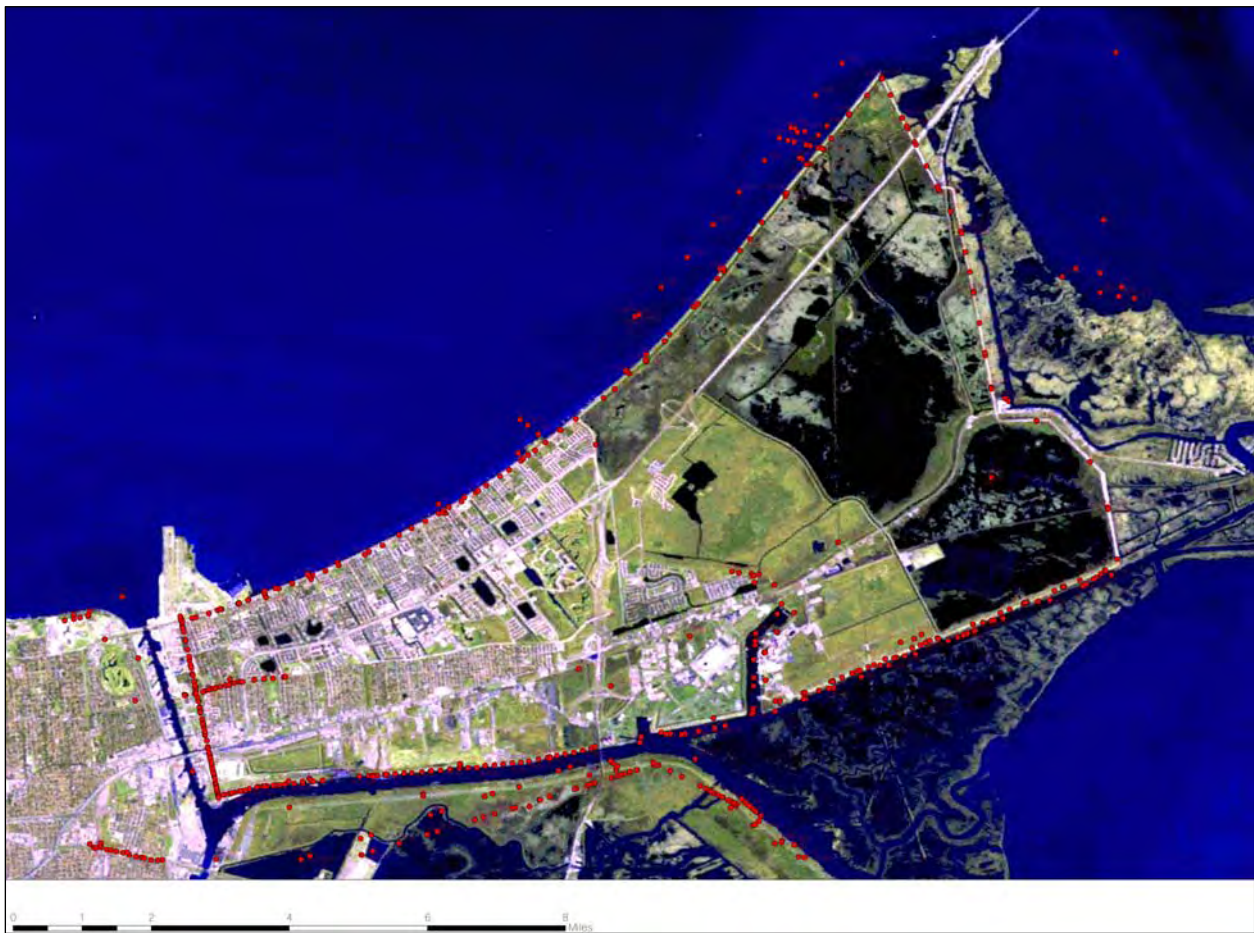
Figure 12-3. U.S. Army Corps of Engineers, New Orleans District Soil Boring Location Database (2006) New Orleans East Basin

Summary of Damages from Hurricane Katrina

Significant damages occurred mainly along the IHNC, southern end of the NOE Levee, NOE Back Levee and the Citrus Back Levee. The IHNC will be discussed in another report. Levee and floodwall damages have been documented by the Task Force Guardian in their Project Information Reports (2005) and Damage Survey Report (2005) for NOE Basin. The TFG describes the major damages as follows:

- 12,750 ft of levee breach in the NOE Back Levee between Michoud Canal along the GIWW up to the CSX Railroad crossing along the NOE Levee.
- floodwall breaches at Pump Station 15 (800 feet) near the Maxent Levee and at the Air Products Hydrogen Plant near the Michoud Canal (300 feet);
- floodgate, floodwall and adjacent levee damage at the CSX railroad;
- and 2000 feet of floodwall damage in the Citrus Back Levee along the GIWW between the IHNC and Paris Road.
- Levee and floodwall scour along the lakefront and NOE levees
- Damage to all eight pump stations.
- Note: Overtopping was generally associated with varying degrees of scour (surface erosion), generally on the levee landside.

Table 12-2 provides the gross estimated linear feet of missing levee, damaged levee and damaged floodwall.

Table 12-2 NOE Basin - Gross Linear Estimates of Damaged Features (Damage Survey Report, TFG 2005)	
Total length of levee w/o cross section	2,900 ft.
Total length of levee w/reduced cross section	3,800 ft.
Total length of damaged flood wall	24,600 ft
Total	**31,300 ft.**

Nine separate construction projects have been identified by Project Information Report (TFG 2005) to repair the damaged areas and restore flood protection to pre-hurricane Katrina conditions. These projects represent an estimated $52.4 M (not including pump stations) in construction costs. Figure 12-4 shows the linear extent of each repair contract. Table 12-3 describes the damage as light, moderate or heavy, in addition to the repair method.

Figure 12-4. NOE - Project Summary Map of Repair Contracts, Project Information Report (TFG 2005)

Table 12-3
NOE Damage Synopsis

Citrus Lakefront Levee and Floodwall			
Lakefront Airport Floodwall (Capped I-wall)	Moderate scour	the land side of the floodwall	Excavate the scour area, place flowable fill and compacted material, place bedding material and 6"-7" slope pavement
Star & Strips Bvld Floodwall	None noted		
Jancke Pumping Station Floodwall	Light Scour	the land side of the floodwall	Excavate the scour area, place flowable fill and compacted material, place bedding material and 6"-7" slope pavement
Lincoln Beach Floodwall	Light Scour	the land side of the floodwall	Excavate the scour area, place flowable fill and compacted material, place bedding material and 6"-7" slope pavement
New Orleans East Lakefront Levee			
Collins Pipeline	None noted		
South Point to GIWW Levee			
Drainage structure, N19 (400+/- lf south of South point)	Moderate scour	the lake side of levee	Excavate the scour area, place compacted material, place bedding material and gabions
Other Drainage structures	Light Scour	the lake side of levee	Excavate the scour area, place compacted material, place bedding material and gabions
Pumping Stations	None noted		
CSX Railroad gate	Heavy Scour	the land side of the floodwall	Raising the flood protection from (NAVD29) 13.5 to '88 datum Elevation 20
New Orleans Back Levee			
OP Pump Station 15	Rotation & Failure of Iwall Tie-In Walls to frontage Twalls	10'-12' Scour holes on both FS & PS of wall	Replace uncapped Iwall w/ pile founded Twalls, Raise protection from (29 datum) 17 to (88 datum) 23.
Iwall West of OPPS 15	Moderate scour	Both FS & PS	Excavate the scour area, place compacted material and graded stone
East Michoud Canal (Air Products Breach)	Rotation & Failure of Iwall Tie-In Walls to levee	10'-20' Scour holes on both FS & PS of wall; 300 lf long	Replace uncapped Iwall w/ new levee section and uncapped Iwall; Raise protection from (29 datum) 17 to (88 datum) 21.
Michoud Slip to Michoud Canal Floodwalls	Light to moderate scour	PS of floodwall	Excavate the scour area, place flowable fill and compacted material, place bedding material and 6"-7" slope pavement
Citrus Lakefront Levee and Floodwall			
IHNC to Paris Road	Light Scour	the land side of the floodwall	Excavate the scour area, place flowable fill and compacted material, place bedding material and 6"-7" slope pavement
Citrus Floodwall at Bulk Loading Facility	Rotation & Failure of Iwall	6'-10' Scour holes on both FS & PS of wall	Replace Iwall w/ new L-type wall; Raise protection from (29 datum) current 13.5 to (88 datum) 15 (as built elevation)

Details of Damages from Hurricane Katrina

This section will describe the damage associated with each of the nine repair projects, and includes all pertinent geotechnical information collected to date on the location. Discussion of NOE levee damage and repair begins at the lakefront and progresses clockwise around the polder; Lakefront, Southpoint to GIWW, Back Levee, Citrus Levee and IHNC.

Lakefront Airport Floodwall Scour Repairs

Project NOE06 consists of filling in and paving over the scour holes next to the concrete wall. It also includes filling in the scour hole and paving the damaged road section with concrete at the interface of the Floodgate L-15 concrete wall and levee. The damage in this reach was primarily scouring along the landside of the floodwall and levee sections at several distinct locations. The severity of the scouring varies from minor to severe. Scouring occurred to some degree at each of the tie-in to the closure structures located within this reach. The total quantity of materials removed by scouring along the entire Lakefront reach is estimated to be less than 5000 cys. January 31, 2006 was scheduled completion date.
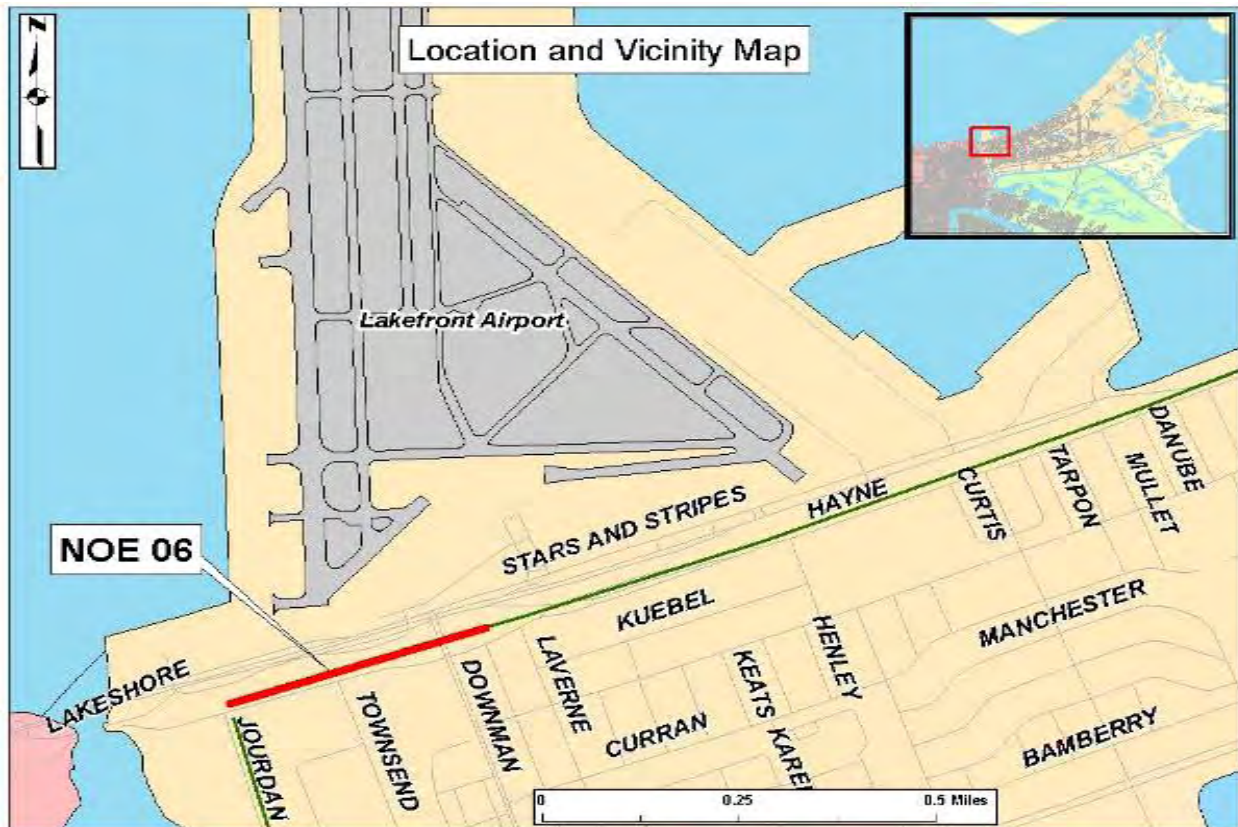
Figure 12-5. NOE6_A

Figure 12-6. NOE6_B. Scoured Section on Protected Side at Lakefront Airport Floodwall
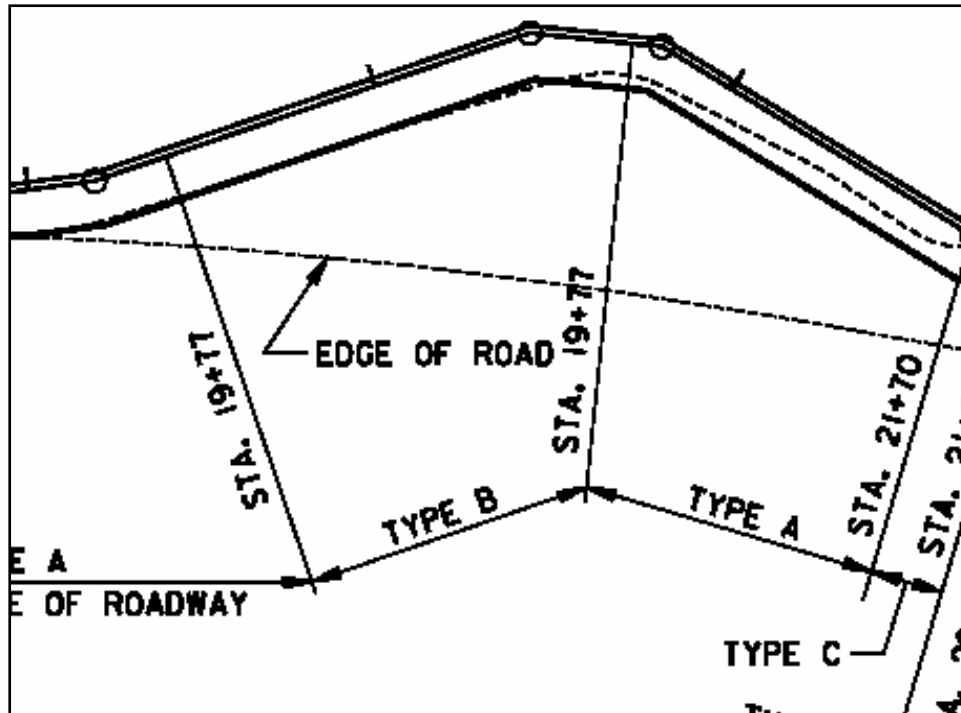
Figure 12-7. NOE6_C Rotated Plan View of Above Picture Defining Scour Extent and Type (from NOE6 Contract Solicitation drawing 4 of 9)

SCOUR DETAIL SCHEDULE

Scour Detail	Station	Scour Width (feet)	Scour Depth (feet)	Distance (feet)
A	18+16	0	0	
				54
	18+70	7	3	
				47
	19+17	11	2.5	
				60
B	19+77	12	3	
				62
	20+39	14	3	
				17
	20+56	12.5	3	
				18
A	20+74	10	3	
				96
	21+70	3	3	
C	21+70 to 21+89 No Scour			19

Figure 12-8. NOE6_D Scour Between Sta 19+17 and 19+77 in Above Picture Was 11 ft Wide and About 3 ft Deep (from dwg. sheet 5 of 9)

Volume V The Performance – Levees and Floodwalls – Technical Appendix

V-12-15

This is a preliminary report subject to revision; it does not contain final conclusions of the United States Army Corps of Engineers.

Lake Pontchartrain Lakefront Levee Scour Repair

Project NOE07 includes intermittent scour repair along approximately 19 miles of earthen levee along the Lake Pontchartrain Lakefront and the eastern boundary of the Bayou Savage National Wildlife Preserve. The work consists of filling in the scour areas with semi-compacted fill, reshaping where needed, and seeding and fertilizing. January 31, 2006 was scheduled completion date.

Figure 12-9. NOE7_A Project NOE10 Addresses Levee/Wall Repairs Near the Lakefront Airport, at Specific Locations. This project will provide scour aprons and concrete /pavement repair at less than 10 locations

Figure 12-10. NOE7_B Typical Crown and Landside Scouring

Figure 12-11. NOE7_C Floodwall Landside Scouring on Hayne Blvd. East of Downman Rd.
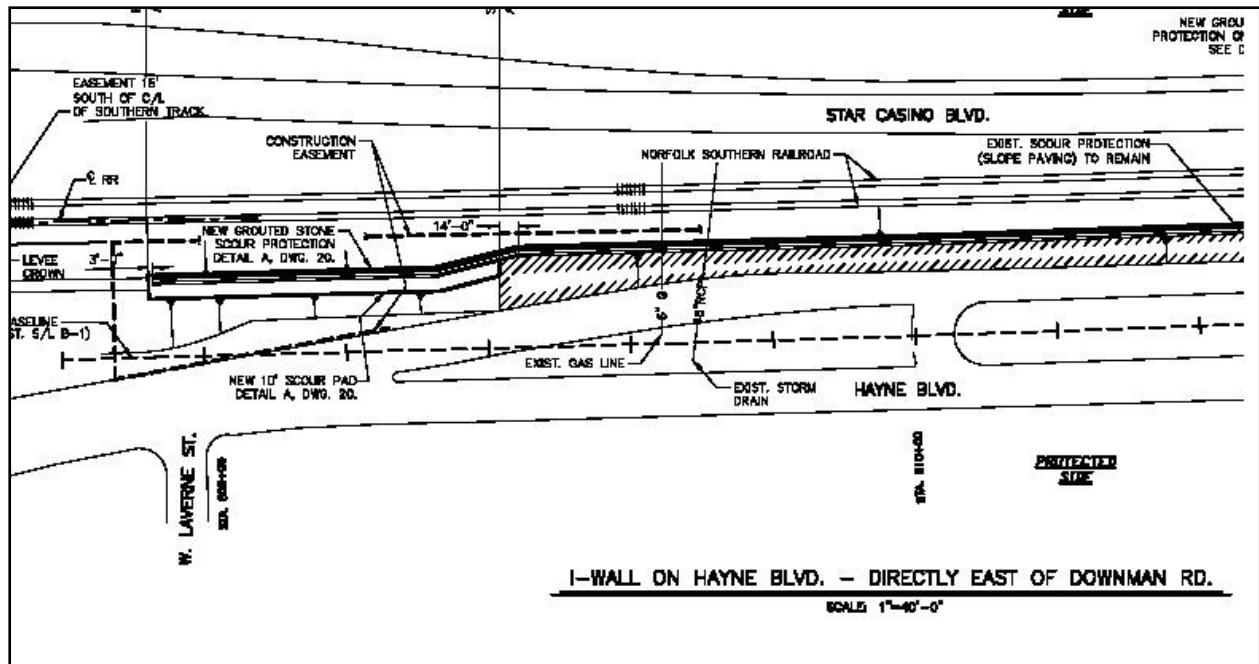
Figure 12-12. NOE7_D Above Picture Plan View from NOE10 Reconstruction Solicitation Drawings
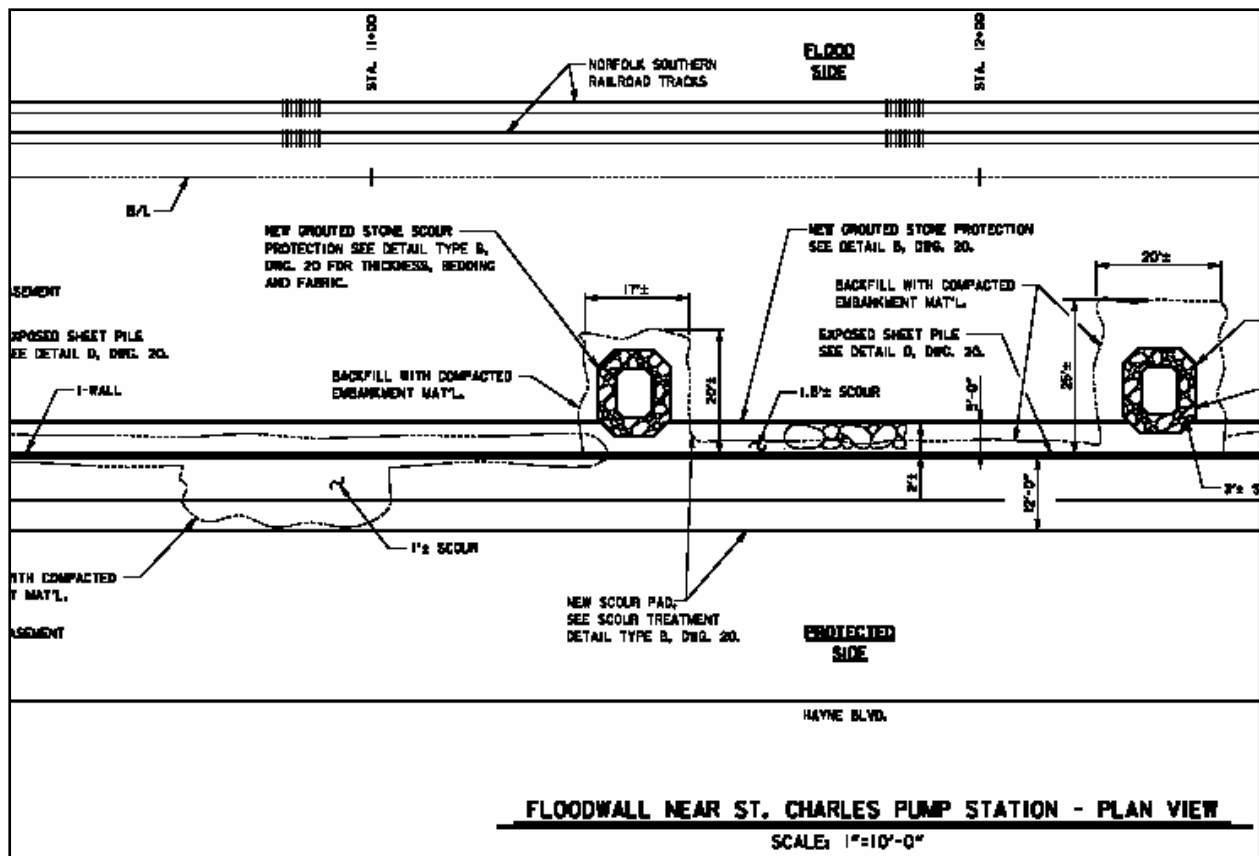
Figure 12-13. NOE7_E Scoured Areas Near St. Charles Pump Station (B/L Sta 74+00)
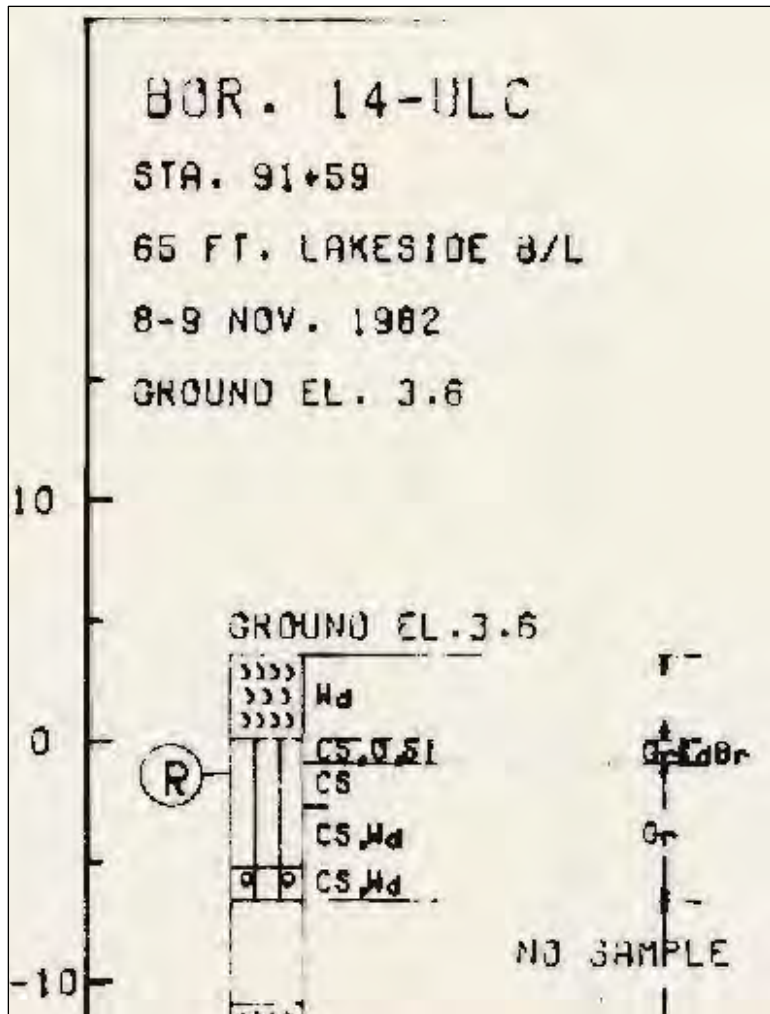
Figure 12-14. NOE7_F Pre-Levee Undisturbed Soil Boring at Sta 91+59 (from Plate 30, DM14)

Drainage and Floodgate Structures Scour Repairs From Southpoint to the GIWW

Project NOE08 includes filling in the scour holes and capping with gabion structures to prevent future erosion. The gabion structures are wire baskets filled with stone interlocked to form a surface erosion barrier. January 31, 2006 was scheduled completion date.
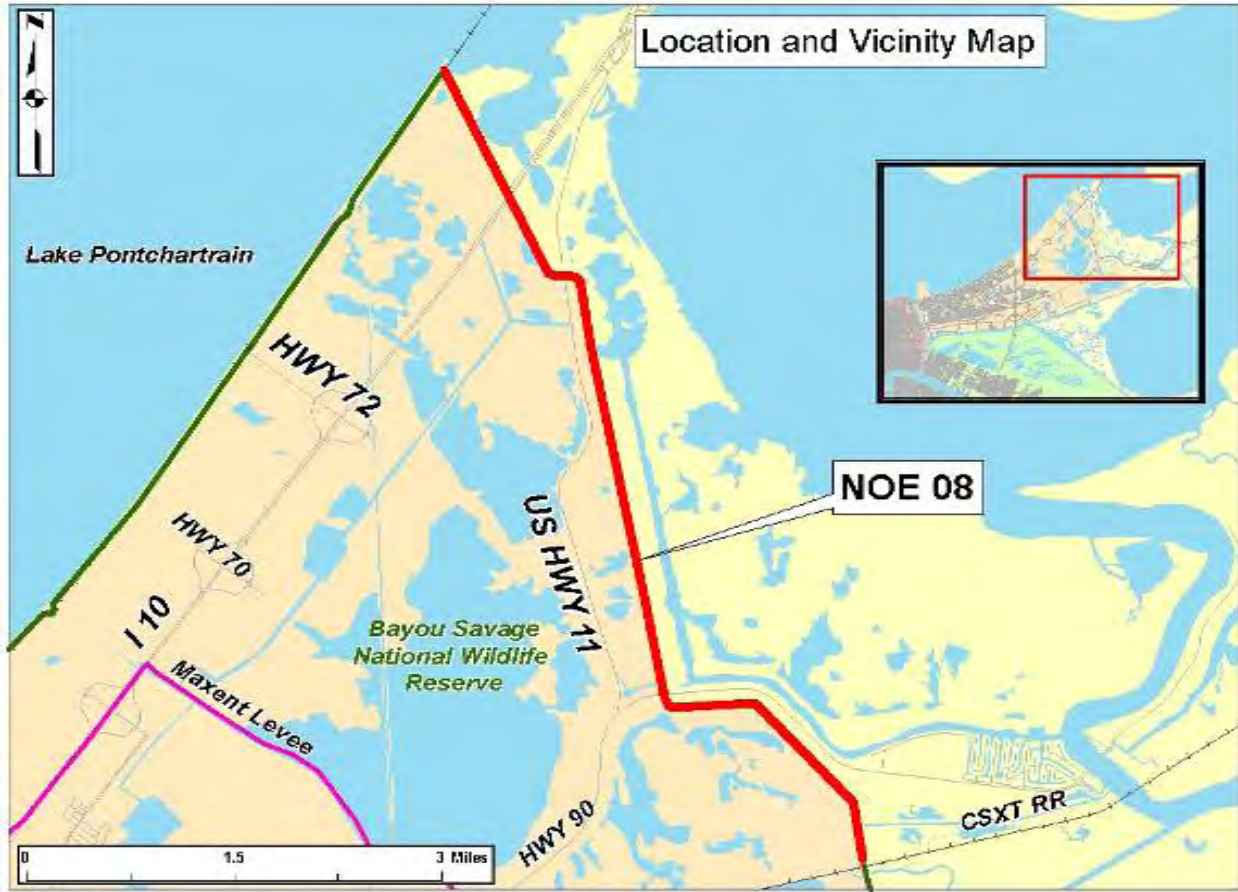
Figure 12-15. NOE8_A

Figure 12-16. NOE8_B

CSX Railroad Floodgate

Project NOE05 includes the removal of the existing concrete wall and railroad closure gate, filling the scoured areas, constructing a new closure gate and new concrete T-walls and I-walls, placement of rip rap, concrete slope paving and concrete roadway. The CSX railroad floodgate and adjacent section of the levee were damaged during the storm event. There was scour of the structural fill material resulting from overtopping of the closure gate and levee. April 1, 2006 is scheduled completion for repairs.
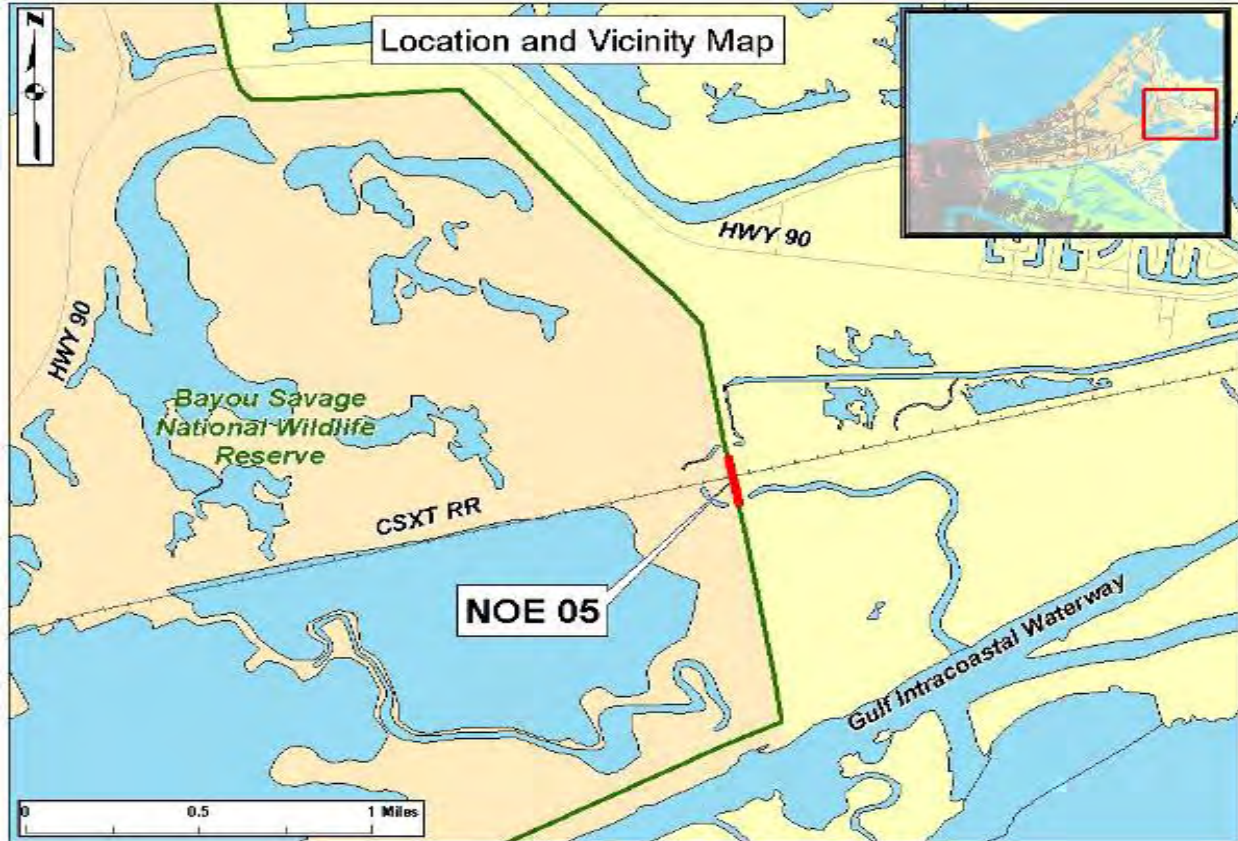
Figure 12-17. NOE5_A. Location 30 deg 03 min 24.03 sec N, 89 deg 49 min 56.76 sec W

Figure 12-18. NOE5_B

Figure 12-19. NOE5_C. View of Scour Around T-Wall

Figure 12-20. NOE5_C. Filled-In Scour Holes

Floodwall Repair at Pump Station 15

Project NOE02 includes removing the damaged steel sheet pile wall, installing a new concrete T-wall, filling in scour holes and bringing the damaged levee back up to pre-hurricane Katrina elevation. Damaged I-wall length is 900 ft (beginning at Sta 876+87 B/L). Approximately 240 ft of sheetpile failed by rotation. April 1, 2005 is scheduled completion date. (see NO East Back Levee Floodwall at Intracoastal Pumping Station.pdf for drawings). Plate 56 in DM2 Gen Design Supp 4 N.O. East Back Levee (Mar 1971).pdf shows original (pre-1977 modification) plan drawings.

Figure 12-21. NOE2_A Location of Pumpstation 15
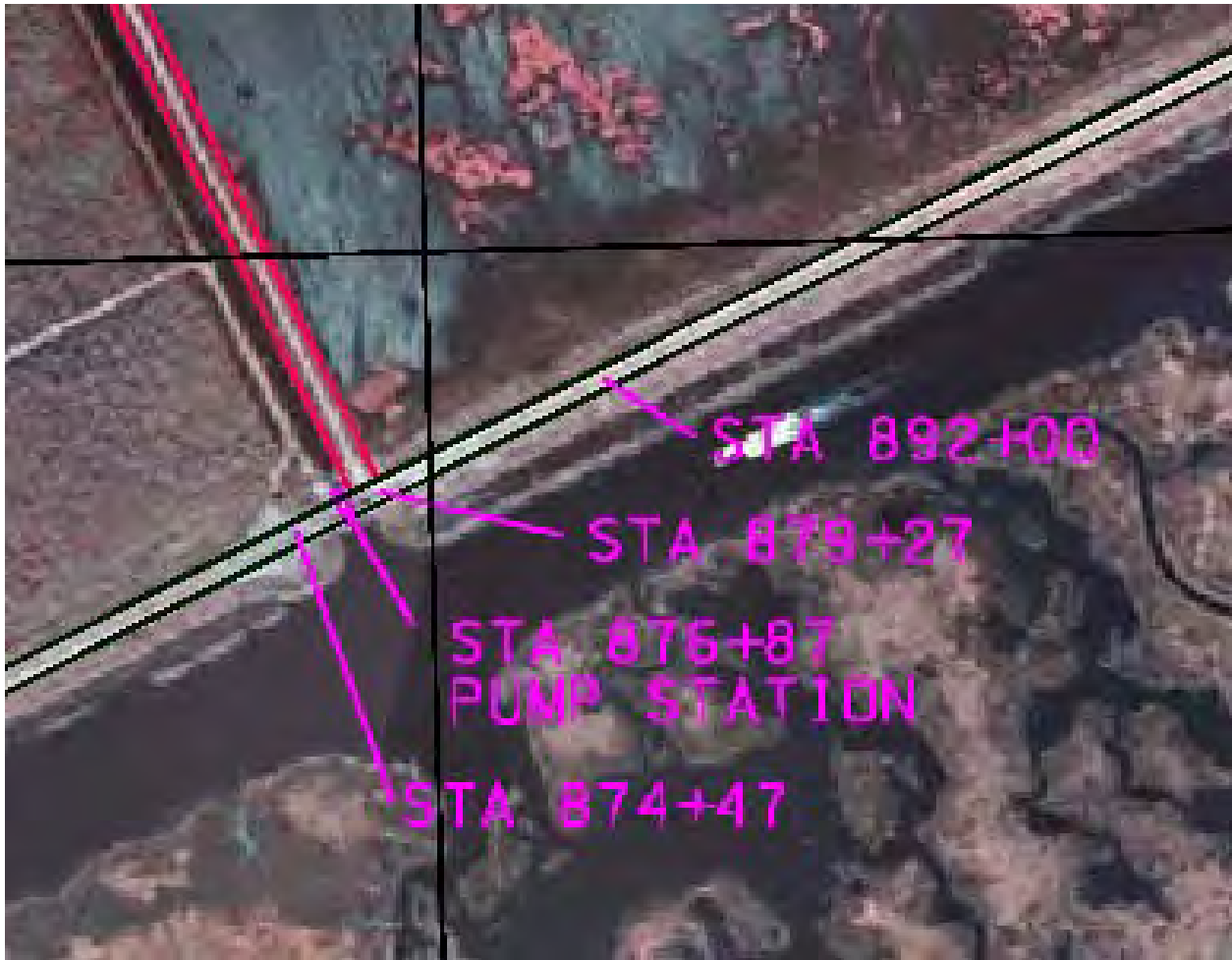
Figure 12-22. NOE2_B Pump Station 15 Coordinates are 30 deg 01 min 45.74 sec N, 89 deg 52 min 03.89 sec W (located at termination of Shell Rd)

Figure 12-23. NOE2_C Closeup of Sheet Pile Damaged by Scour/Rotation/Sliding Failure

Figure 12-24. NOE2_D View from Above

Figure 12-25. NOE2_E PS 15
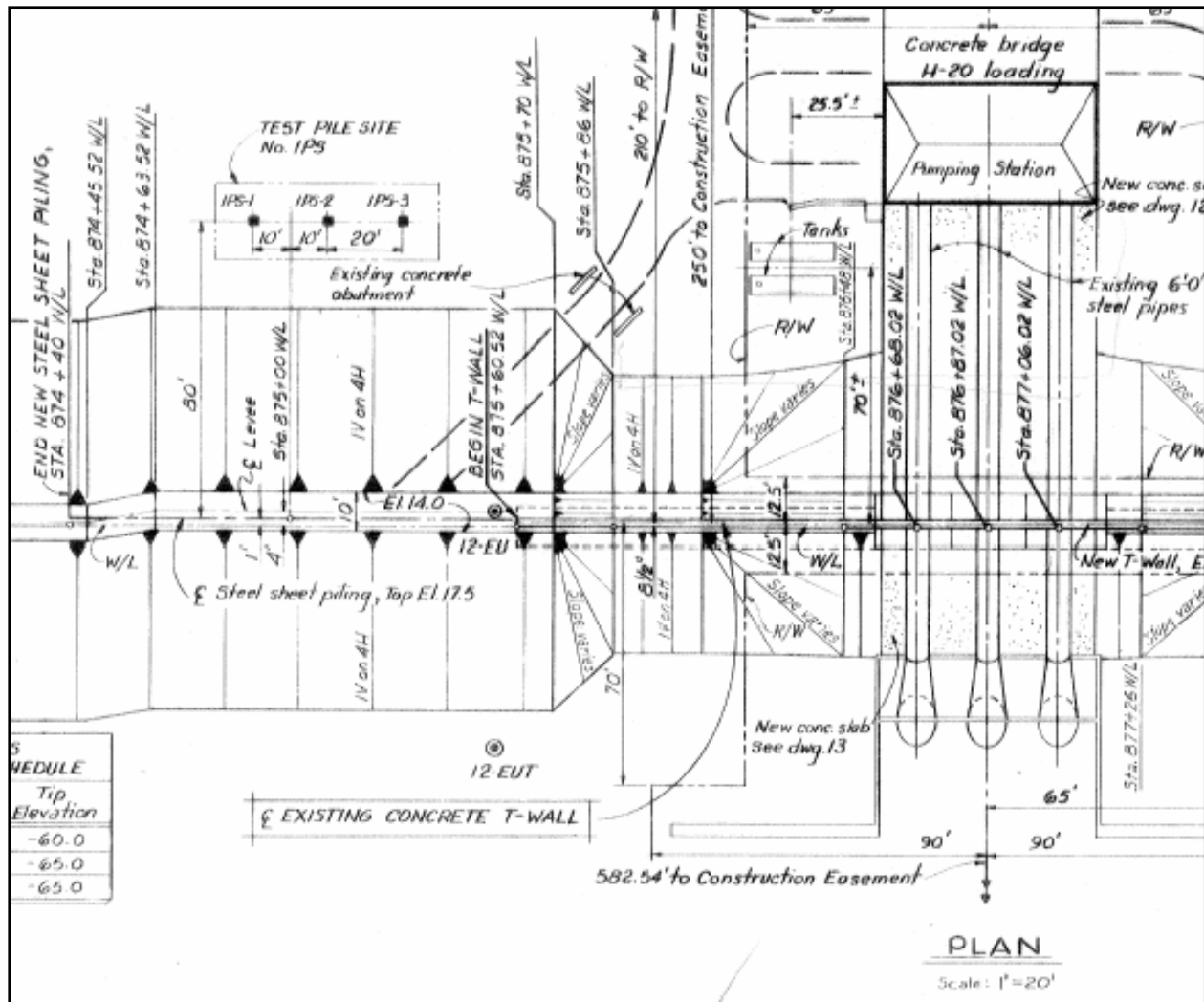
Figure 12-26. NOE2_F Failed Sheet Pile Section Between Sta 874+40 and T-Wall at Sta 875+60 (Plan view)

This is a preliminary report subject to revision; it does not contain final conclusions of the United States Army Corps of Engineers.
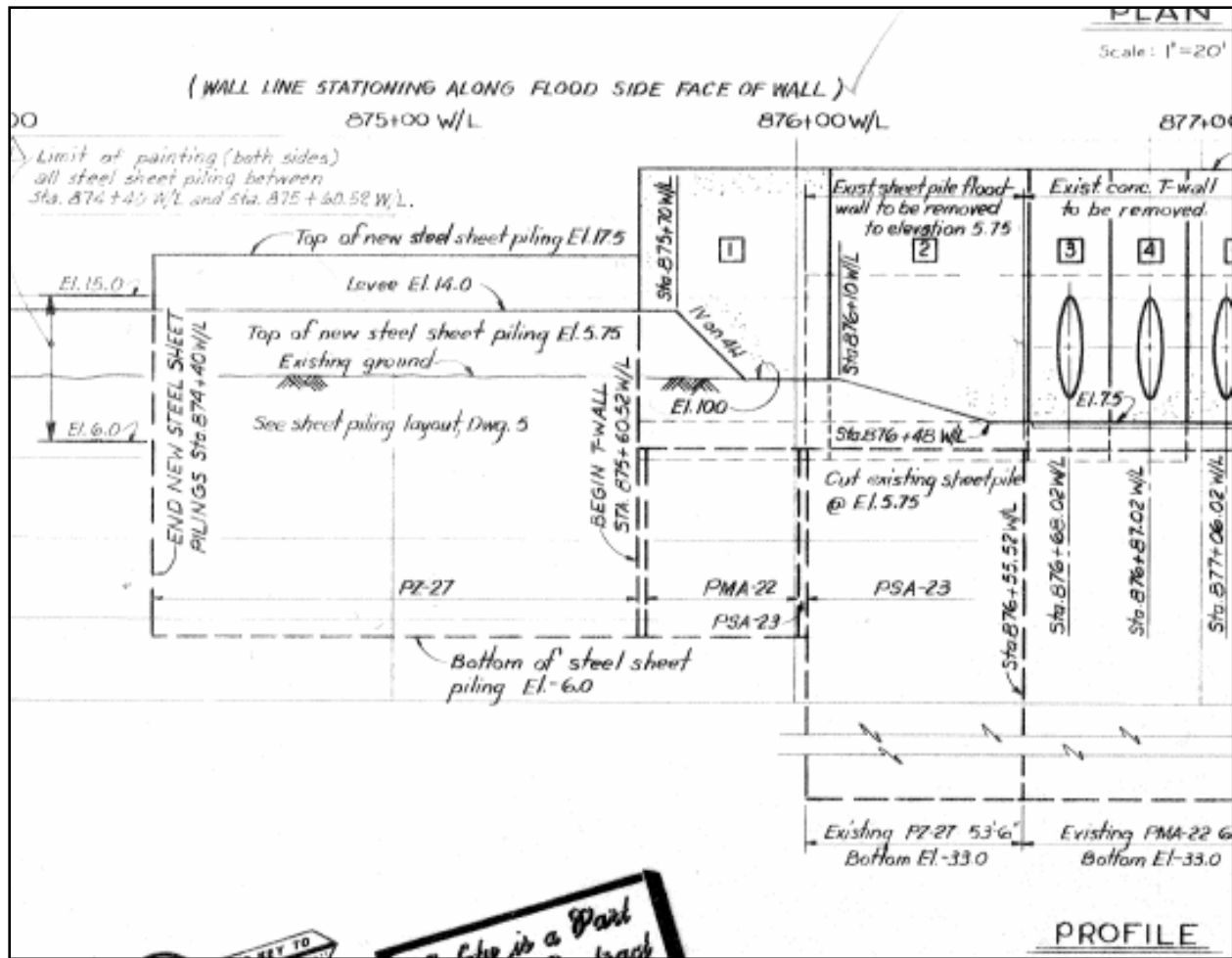
Figure 12-27. NOE2_G Profile View Showing 27' Difference Between Bottom Elevations of Existing (pre-1977) and Newer (1977 construction) Sheet Pile. Sections are from Plate 2 of 16, Mod P00001, Contract DACW29-77-C-0037
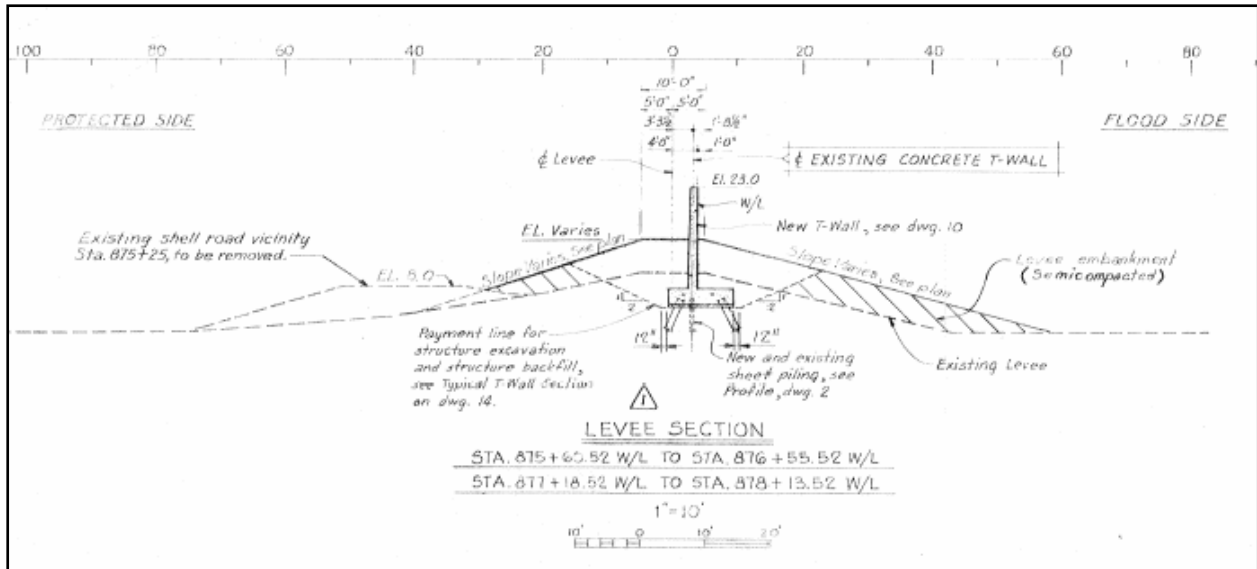
Figure 12-28. NOE2_H Newer (1977) Cut and Fill Sections for T-Wall, Same Contract as Above
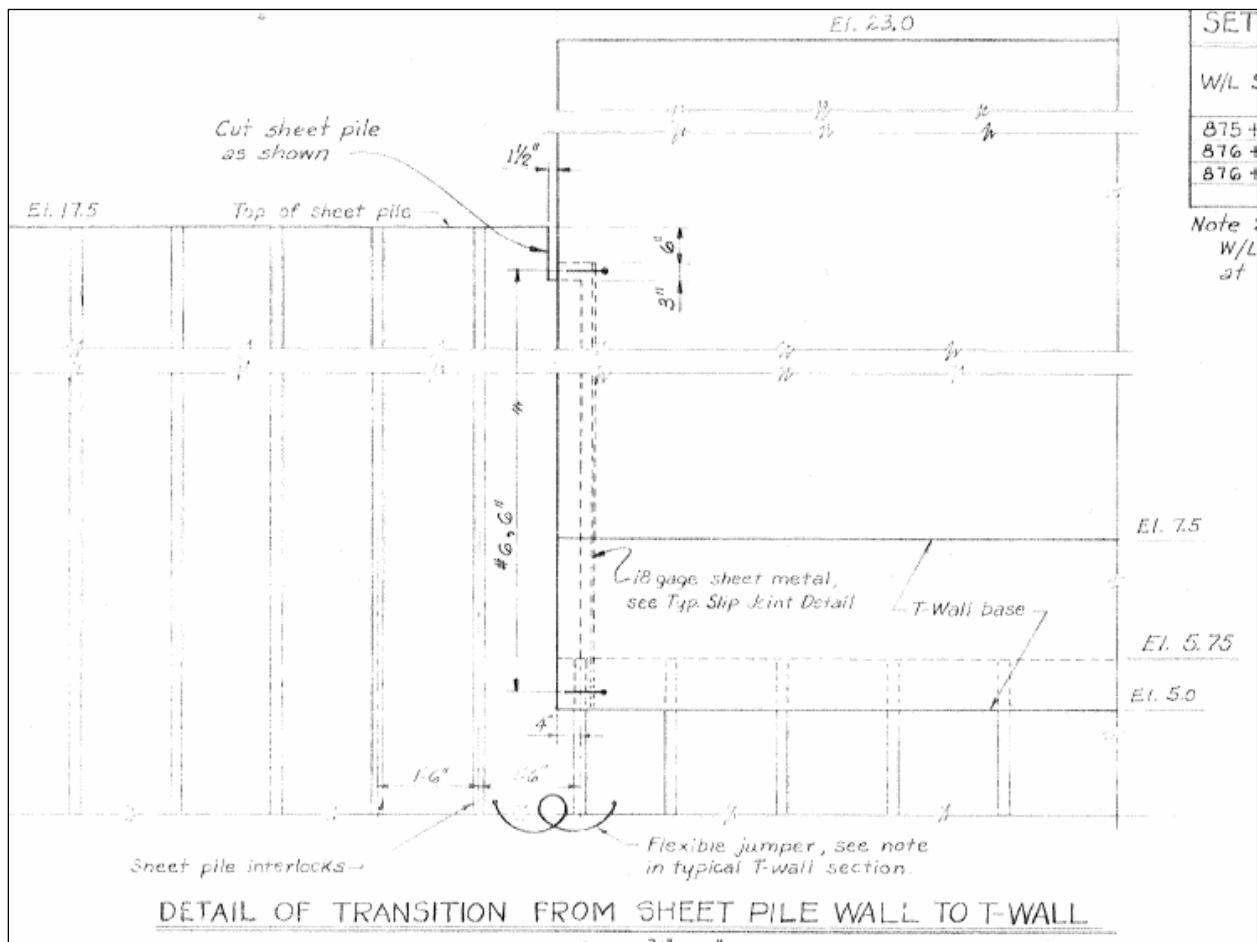
Figure 12-29. NOE2_I Top Elevation Difference of 5.5' Between Sheet Pile and T-Wall (plate 14 of 16 from above contract)

V-12-34

Volume V The Performance – Levees and Floodwalls – Technical Appendix
This is a preliminary report subject to revision; it does not contain final conclusions of the United States Army Corps of Engineers.
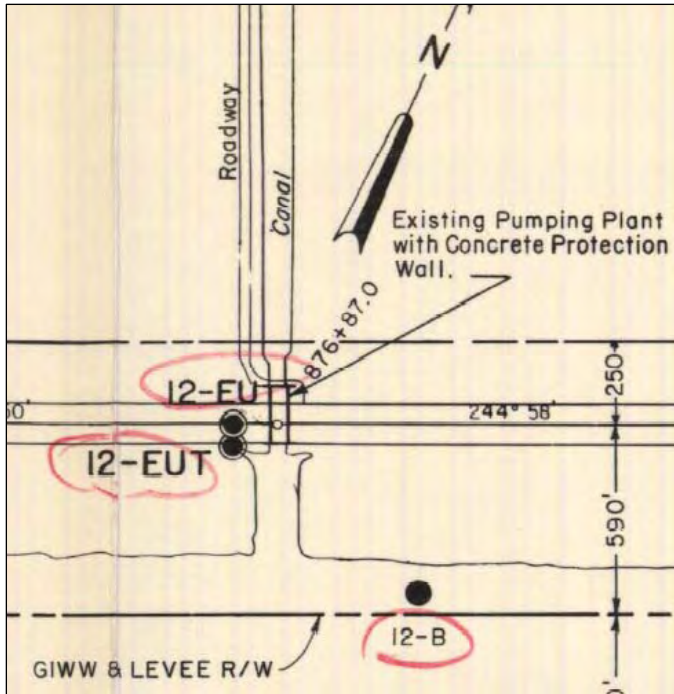
Figure 12-30. NOE2_J Soil Borings (from page 81 of 238, DM2 Gen Design Supp 4 N.O. East Back Levee (Mar 1971).pdf). Boring logs are shown on pages 88 and 89 of 238 (plates 10 and 11)
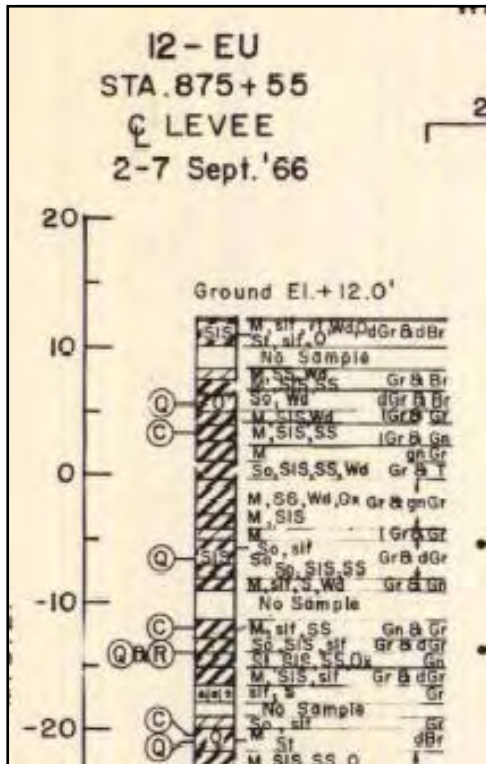
Figure 12-31. NOE2_K Nearest Boring Log (from plate 10 DM2 Sup 4) Showing Thin CL Layer in pre-1977 Levee
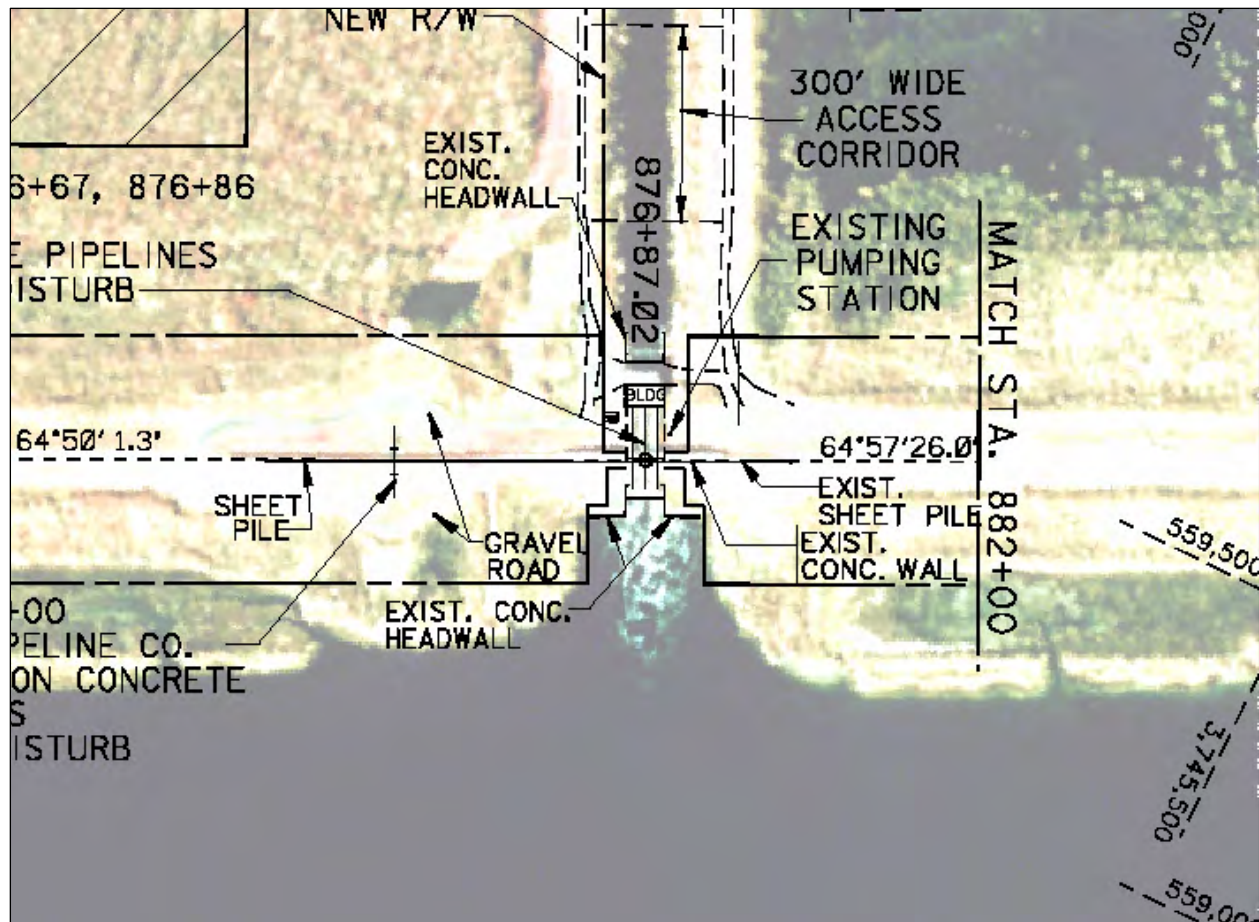
Figure 12-32. NOE2_L Plan view from Contract Solicitation NOE1 Drawing
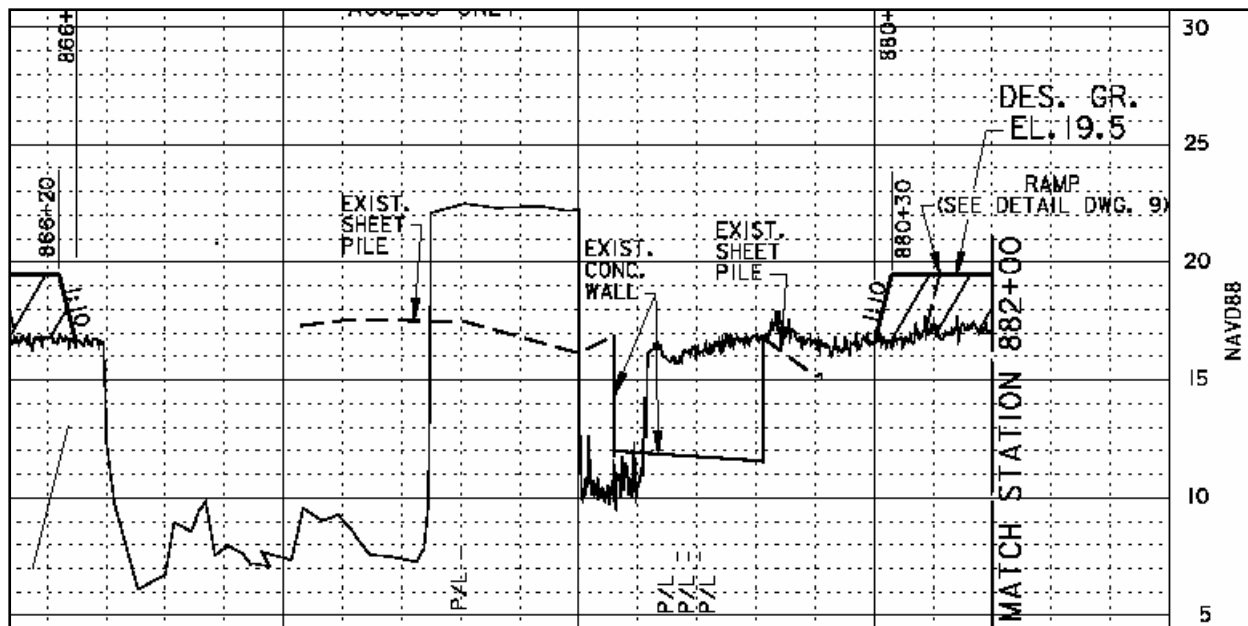
Figure 12-33. NOE2_M Plan and Post-Damage Scour Profile Immediately West of Pump Station 15 (from Contract Solicitation NOE1 drawing H-8-45594, sheet 3 of 16)

East Back Levee Repair from Michoud Canal to CSX RR

Project NOE01 consists of rebuilding approximately 4.3 miles of the existing levee back up to its constructed grade with 680,000 CY of earthen material, then seeding and fertilizing. There is 12,750 feet of levee east of Pump Station #15 that is completely degraded (Station 876+87 B/L to 1101+90 B/L). Plate 4 of DM2 Gen Design Supp 4 N.O. East Back Levee (Mar 1971).pdf shows the original soil borings and profile. The levees in the section 879+27 and 1006+59 were constructed from hydraulic fill in stages over three years (see plates 31 and 32).

West of the pump station, 9,800 feet of levee is completely degraded (approx Sta 778+00 to 876+00). Plate 3 of DM2 Gen Design Supp 4 N.O. East Back Levee (Mar 1971).pdf shows the soil borings and profile. The levees in this section were constructed from hydraulic fill in stages over three years (see plates 30 and 31).

The remaining level of protection was EL 4.0. The entire reach of levee was brought up to an interim level of protection of elevation +10 by November 15, 2005. April 1, 2006 is scheduled completion date.
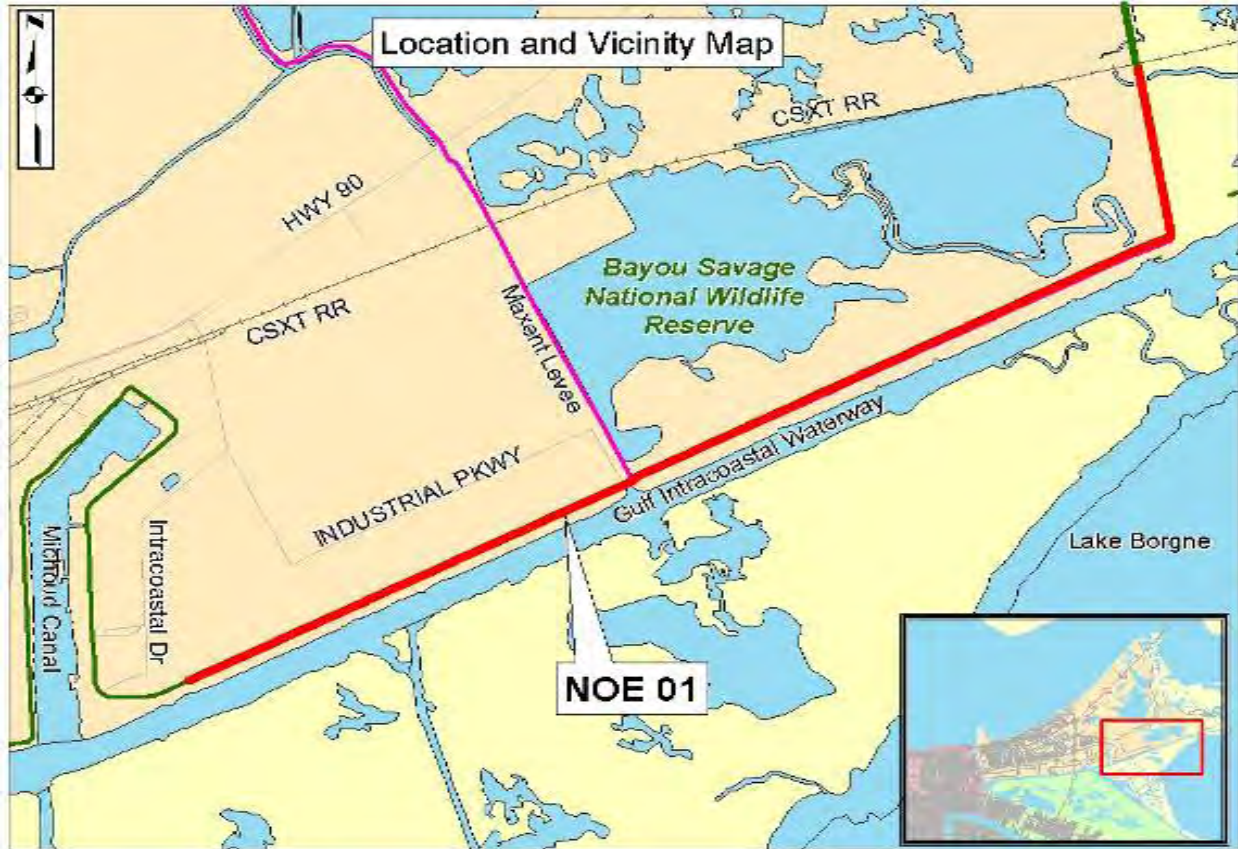
Figure 12-34. NOE1_A
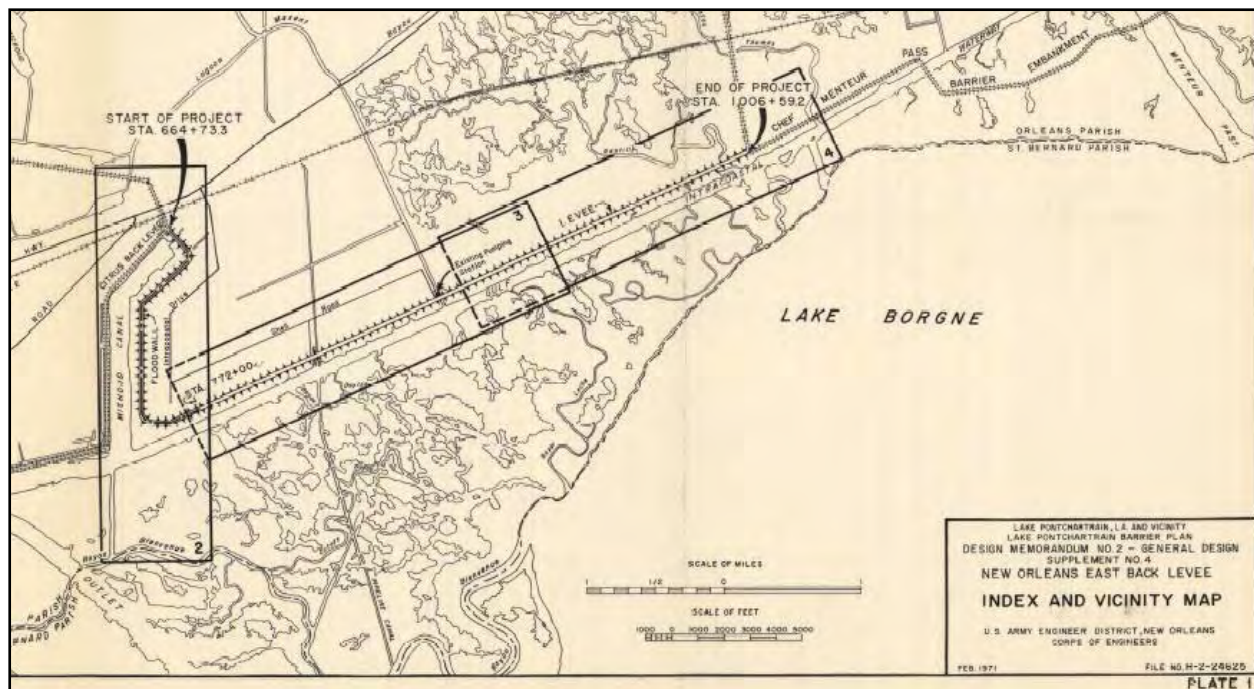
Figure 12-35. NOE1_B Page 79 of 238, DM2 Gen Design Supp 4 N.O. East Back Levee (Mar 1971).pdf

Figure 12-36. NOE1_C Complete Breach East of Pump Station 15
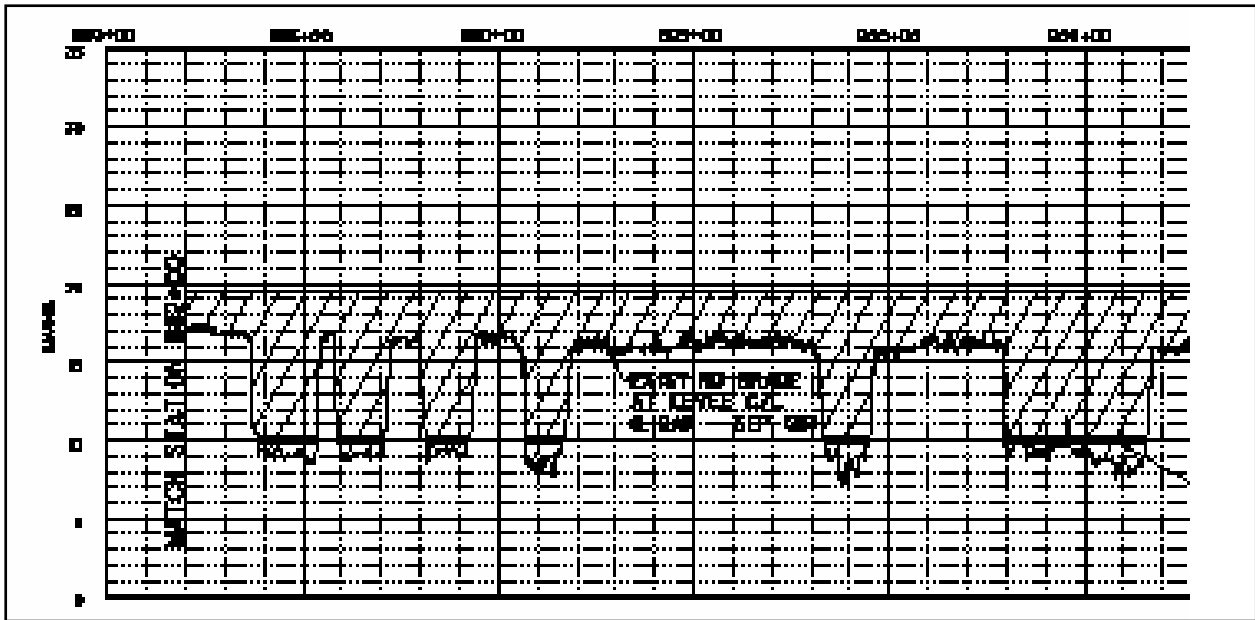
Figure 12-37. NOE1_D LIDAR Profiles of Levee East of Pump Sta 15 (from Contract Solicitation NOE1 drawings)

Volume V The Performance – Levees and Floodwalls – Technical Appendix   V-12-41

This is a preliminary report subject to revision; it does not contain final conclusions of the United States Army Corps of Engineers.

Figure 12-38. NOE1_E Partial Breach East of Pump Station 15

Figure 12-39. NOE1_F Rebuilding to Initial Elevation 10'

Figure 12-40. NOE1_G Localized Scour Typical of Several Locations

Floodwall Repair near Air Products Hydrogen Plant

Project NOE03 includes removing the damaged concrete I-wall and steel sheet pile wall, filling in scour holes, installing a new concrete I-Wall, and raising the damaged levee to pre-hurricane Katrina elevation and then seeding and fertilizing. The damaged reach was first brought up to an interim level of protection of elevation +10 by November 15, 2005 before final repairs are made. Breach length was 300' at transition between sheet pile and concrete I-wall. April 1, 2006 is scheduled completion date.
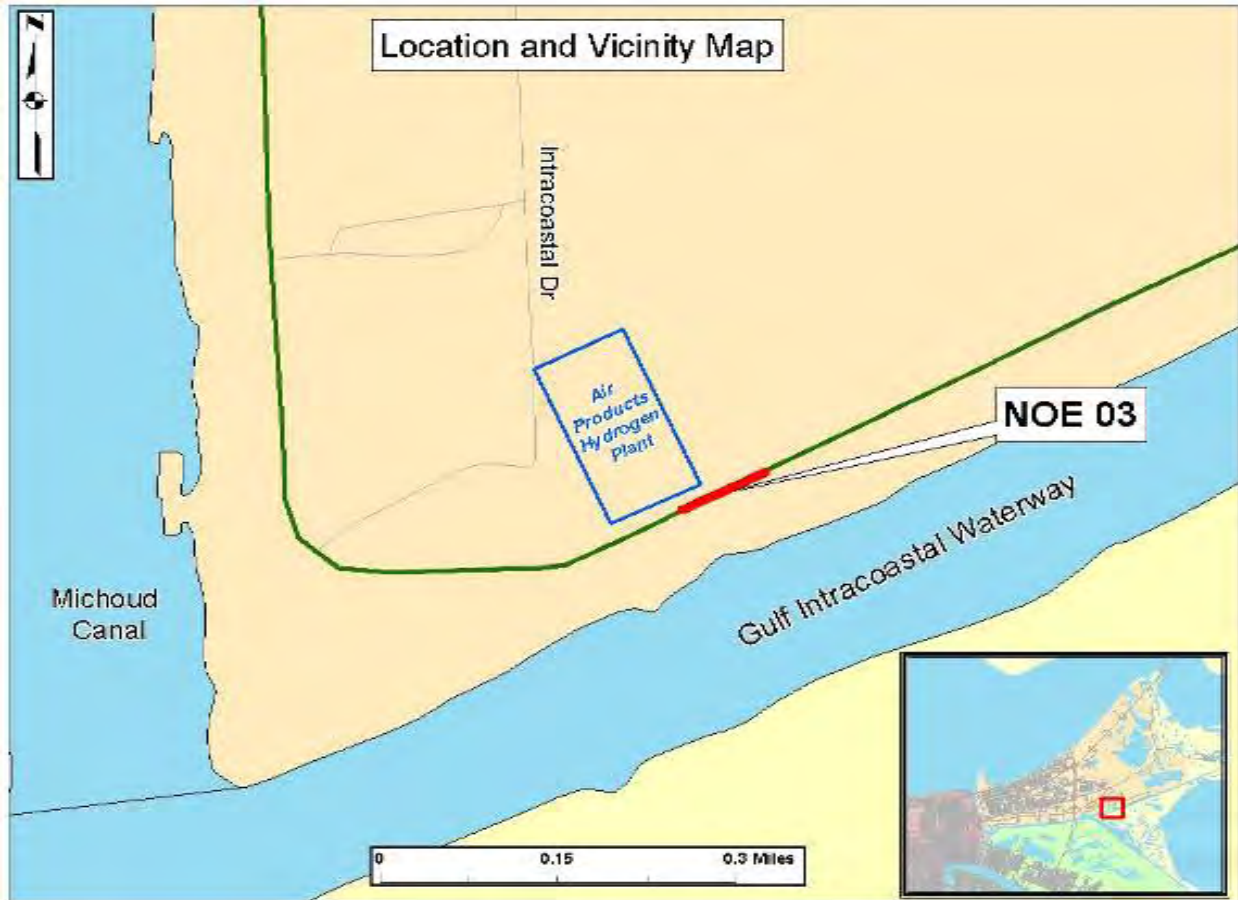
Figure 12-41. NOE3_B

Figure 12-42. NOE3_A. Page 80 of 238, DM2 Gen Design Supp 4 N.O. East Back Levee (Mar 1971).pdf
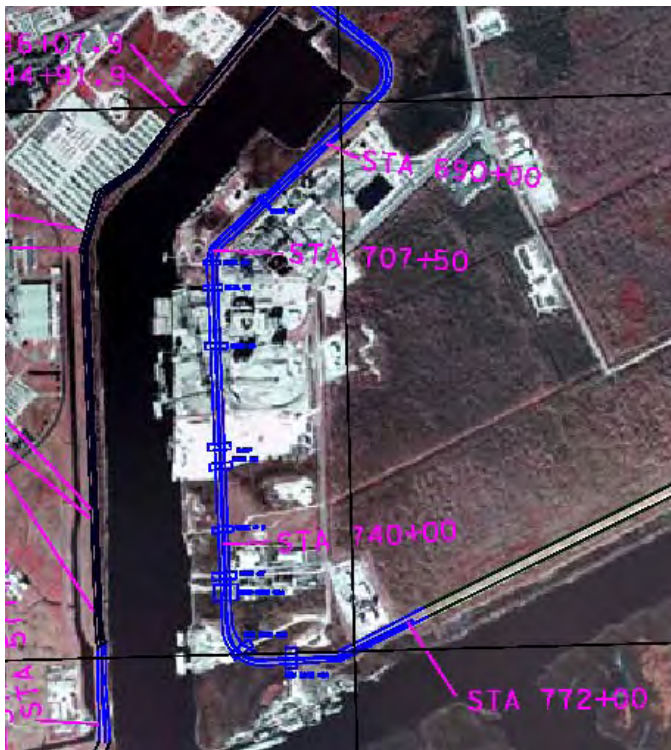
Figure 12-43. NOE3_C. Blue Color is Top of Wall Elevation 20 ft

Figure 12-44. NOE3_D Sheetpile Wall Failure (near Sta 772+00 B/L New Orleans East Back Levee)
(Coordinates 30 deg 01 min 04.30 sec N, 89 deg 53 min 49.36 sec W)

This is a preliminary report subject to revision; it does not contain final conclusions of the United States Army Corps of Engineers.
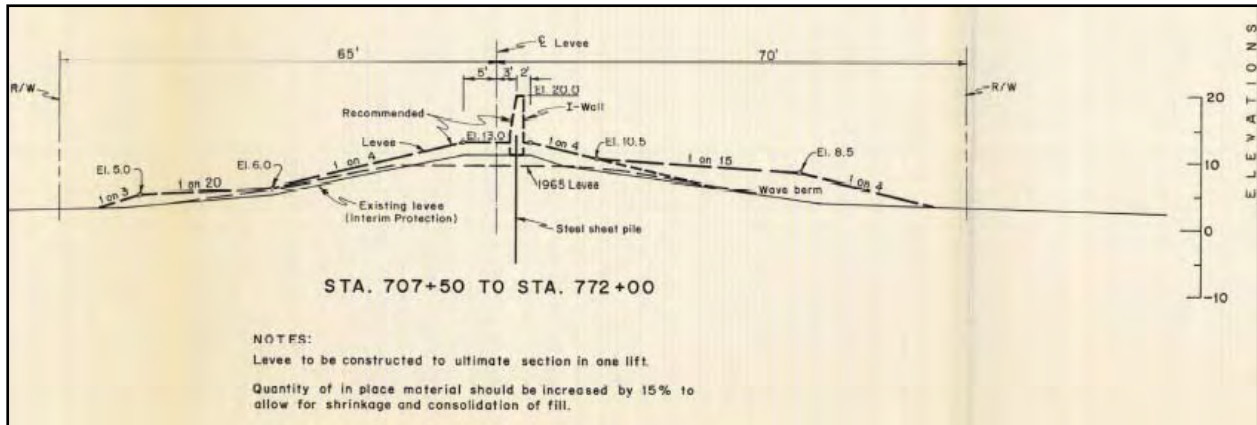
Figure 12-45. NOE3_E. Page 107 of 238, DM2 Gen Design Supp 4 N.O. East Back Levee (Mar 1971).pdf Showing Add-On to Existing Levees (1965 and interim add-on)
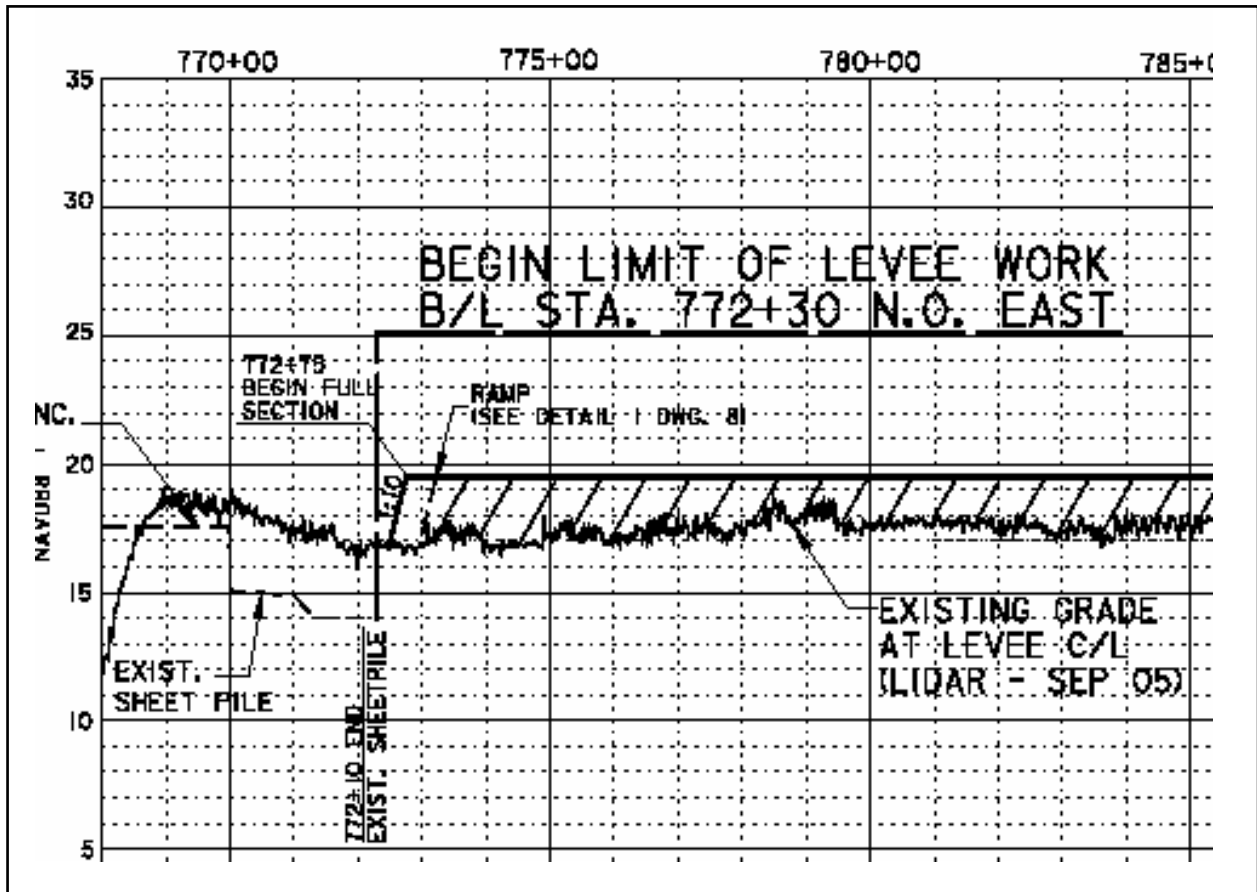
Figure 12-46. NOE3_F. Post-Damaged Lidar Elevations Show Scour Hole (approx Sta 768+00) Depth was About 8' deep (from Contract Solication NOE1 drawing H-8-45594, sheet 2 of 16)

Figure 12-47. NOE3_G. West of Failure Looking East. Drawings from NOE3 Contract Solicitation Show Scour Depth And Outline
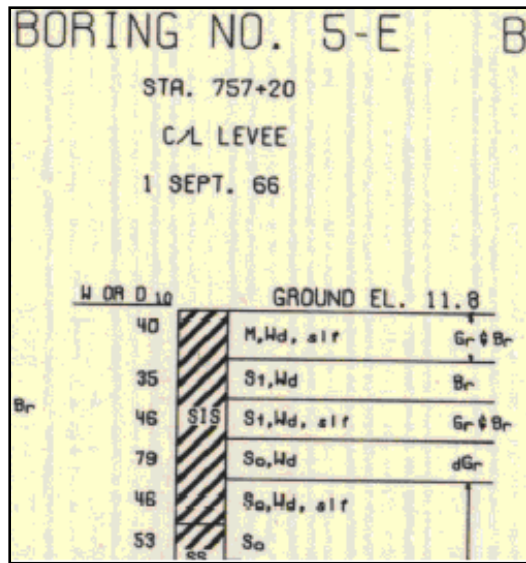
Figure 12-48. NOE3_H. Boring 5-E from plate 5, DM2 Supp 4 (March 1971) Shows CH Material in Pre-Existing 1965 Levee

This is a preliminary report subject to revision; it does not contain final conclusions of the United States Army Corps of Engineers.

Figure 12-49. NOE3_I. Repair Progress

Figure 12-50. NOE3_J. Repair Sheetpile View to the West

Floodwall Scour Repairs from Michoud Slip to Michoud Canal

Project NOE09 includes filling in the scour holes next to the wall with embankment material, installing bedding material, and concrete slope paving above the scour to prevent future erosion. Also includes adding an earthen stability berm on both flood and protected sides of the wall. The project also consists of intermittent repairs to damaged concrete and various joints and gates in the walls. April 1, 2006 is scheduled completion date.
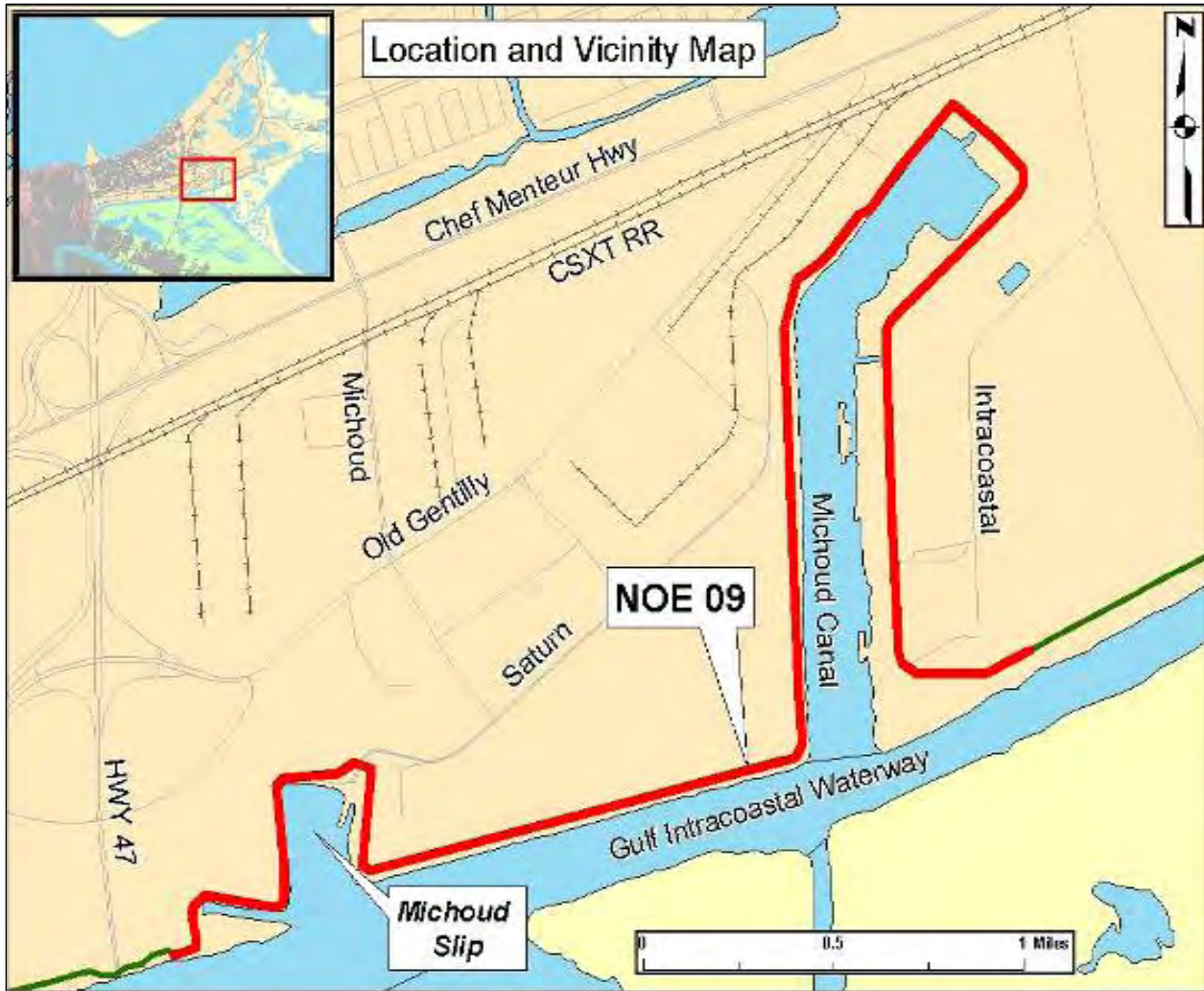
Figure 12-51. NOE9_A

Figure 12-52. NOE9_B

Figure 12-53. NOE9_C. I-Wall Damage Likely Due to Impact

Citrus Back Levee Floodwall Repair

Project NOE04 includes removing the damaged concrete I-wall sections, filling in the scour holes, regrading the damaged levee, constructing new concrete wall, and putting in an earthen stability berm on the landside of the wall. The most severe damage in this reach is a 2000 ft. section of I-wall that failed by rotation, with attendant erosion and scouring. The extend of material below the water surface that has been removed by the scouring is unknown. Localized scouring occurred at several locations along this reach. The total quantity of material removed by scouring within this reach is estimated at 150,000 cys.

The repaired levee section and stability berm will be seeded and fertilized. The damaged reach was first brought up to an interim level of protection of elevation +10 by December 1, 2005 before final repairs are made. Geotechnical analysis has determined an earthen stability berm may be required which will require additional real estate. April 1, 2006 is scheduled completion date.

Figure 12-54. NOE4_A

Volume V The Performance – Levees and Floodwalls – Technical Appendix
This is a preliminary report subject to revision; it does not contain final conclusions of the United States Army Corps of Engineers.
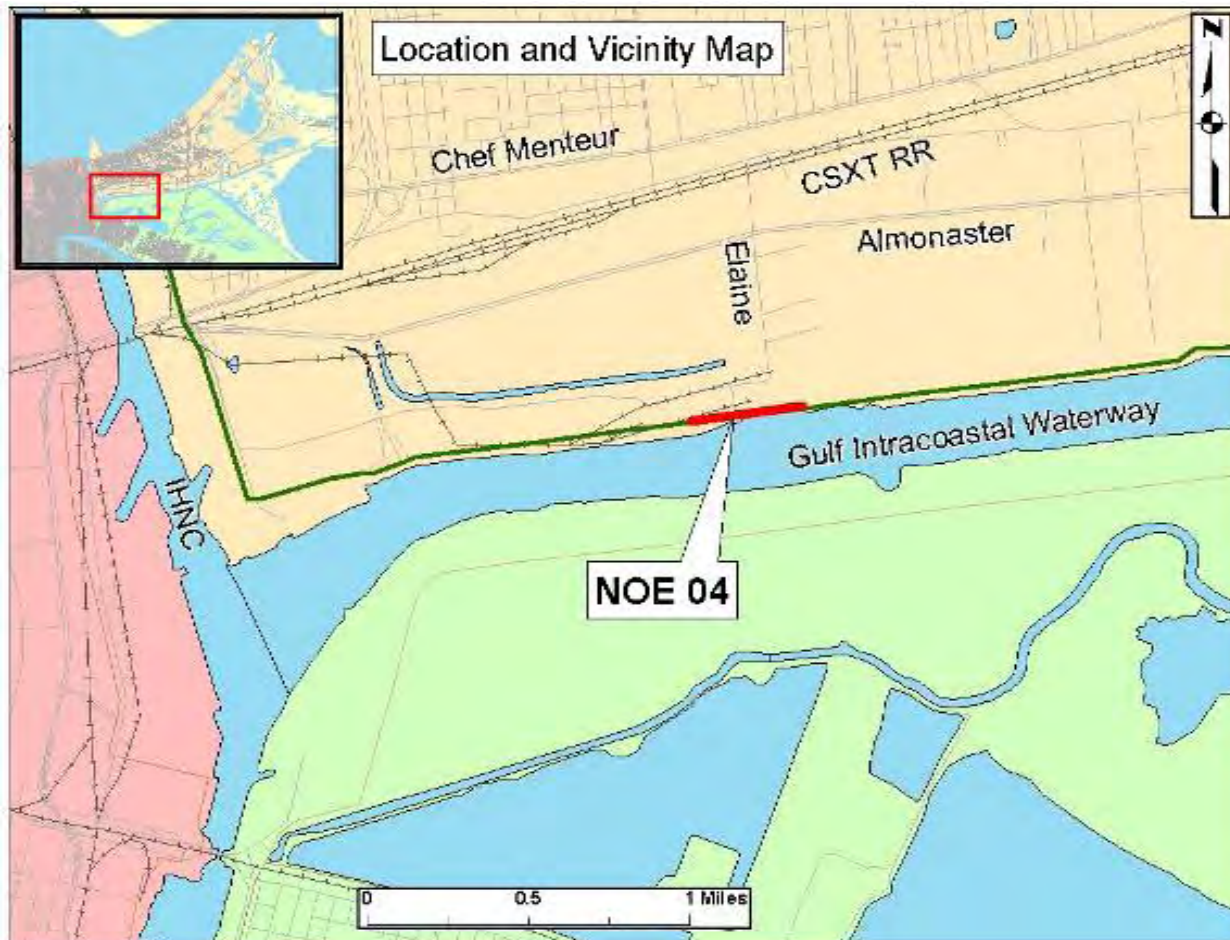
Figure 12-55. NOE4_B. Bulk Loading Terminal Facility I-Wall Failed by Rotation with Attendant Scour and Erosion (2000' near Elaine St. at GIWW), near Sta 271+55 B/L (Citrus Back Levee), Immediately Adjacent to the Tool Shed Metal Building

Figure 12-56. NOE4_C. Begin I-Wall Rotation at 30 deg 00 min 00.91 sec N, 89 deg 59 min 39.53 sec W. Pre-Existing Wall Elevation was 15 ft and Levee Elevation was 14 ft

Figure 12-57. NOE4_D. Bulk Loading Facility on the GIWW. Note Tool Shed Metal Building Location
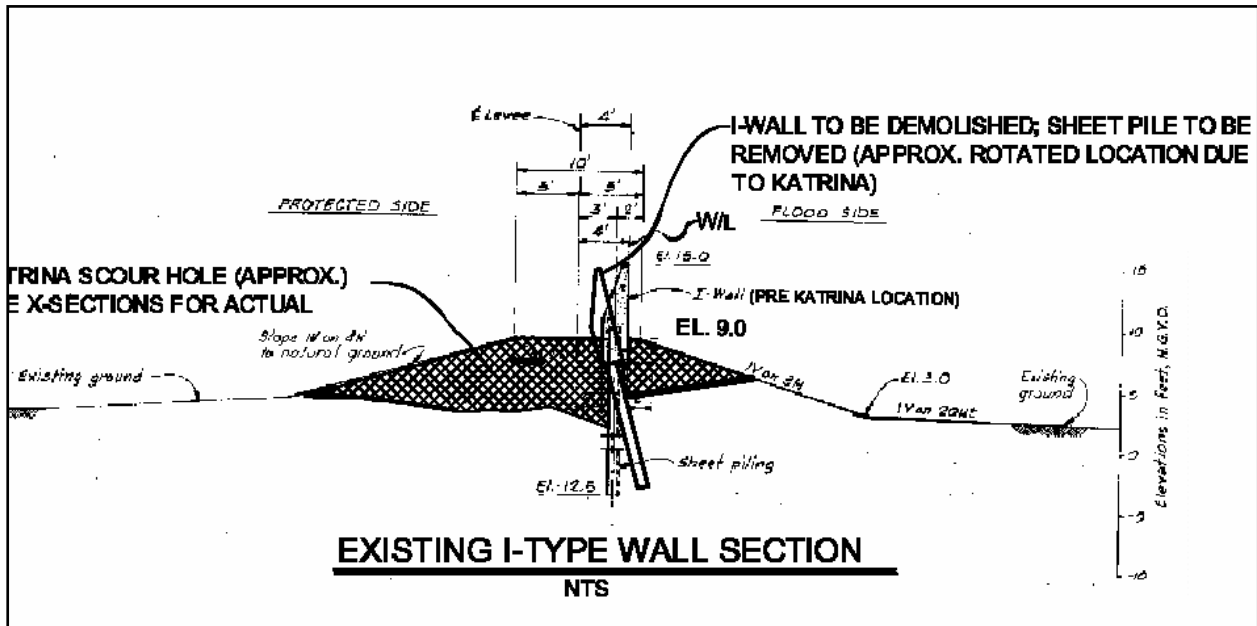
Figure 12-58. NOE4_E. Post-Katrina Condition
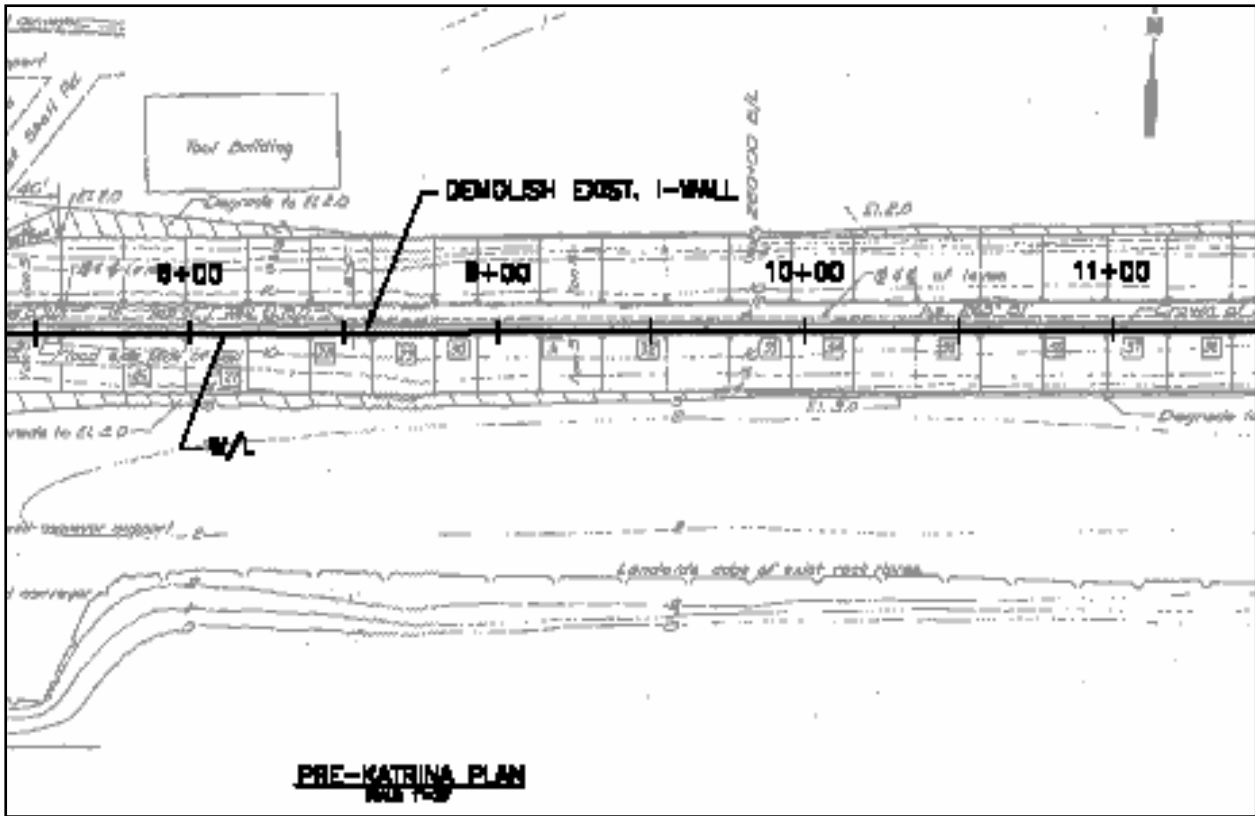
Figure 12-59. NOE4_F. Sections are from the Lake Pontchartrain, Louisiana and Vicinity, New Orleans East Area Plan Emergency Restoration, Modifications to Citrus Back Levee Floodwall Sta. 250+17.5 B/L to Sta. 279+44.50 B/L (Sta. 0+02.0 W/L to Sta. 29+41.71 W/L) Construction Contract Solicitation
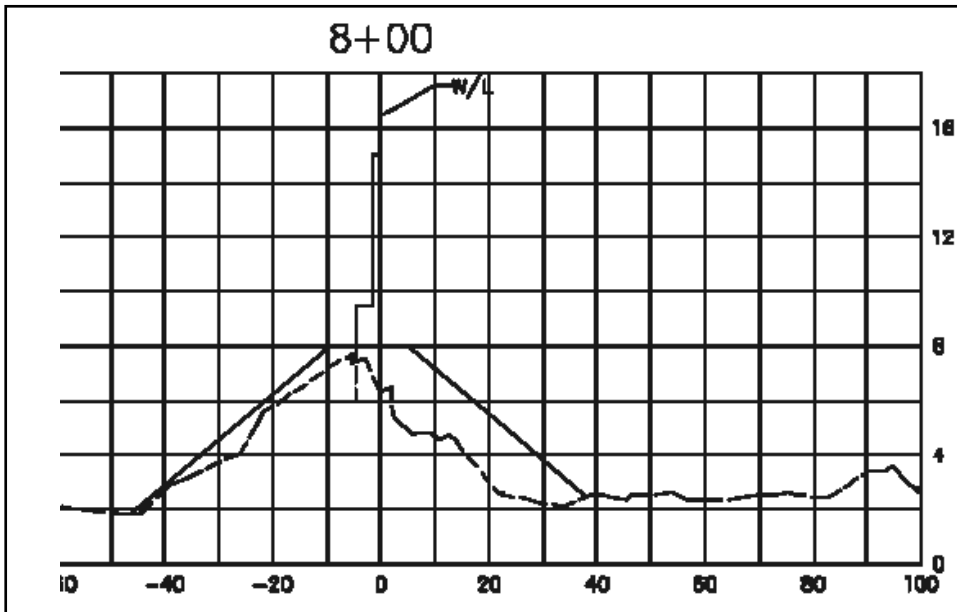
Figure 12-60. NOE4_G. Scour Pattern Along the I-Wall Immediately Adjacent to the Tool Shed Building
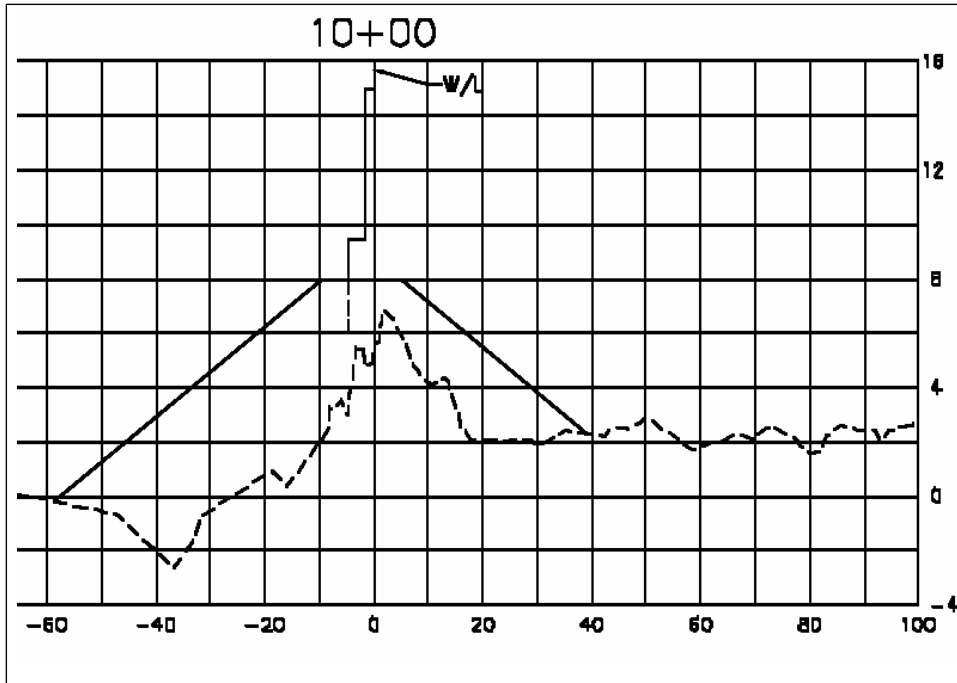
Figure 12-61. NOE4_H. Scour Pattern 200' to the East

Figure 12-62. NOE4_I. I-Wall Demolition to Replace with New "L" Wall
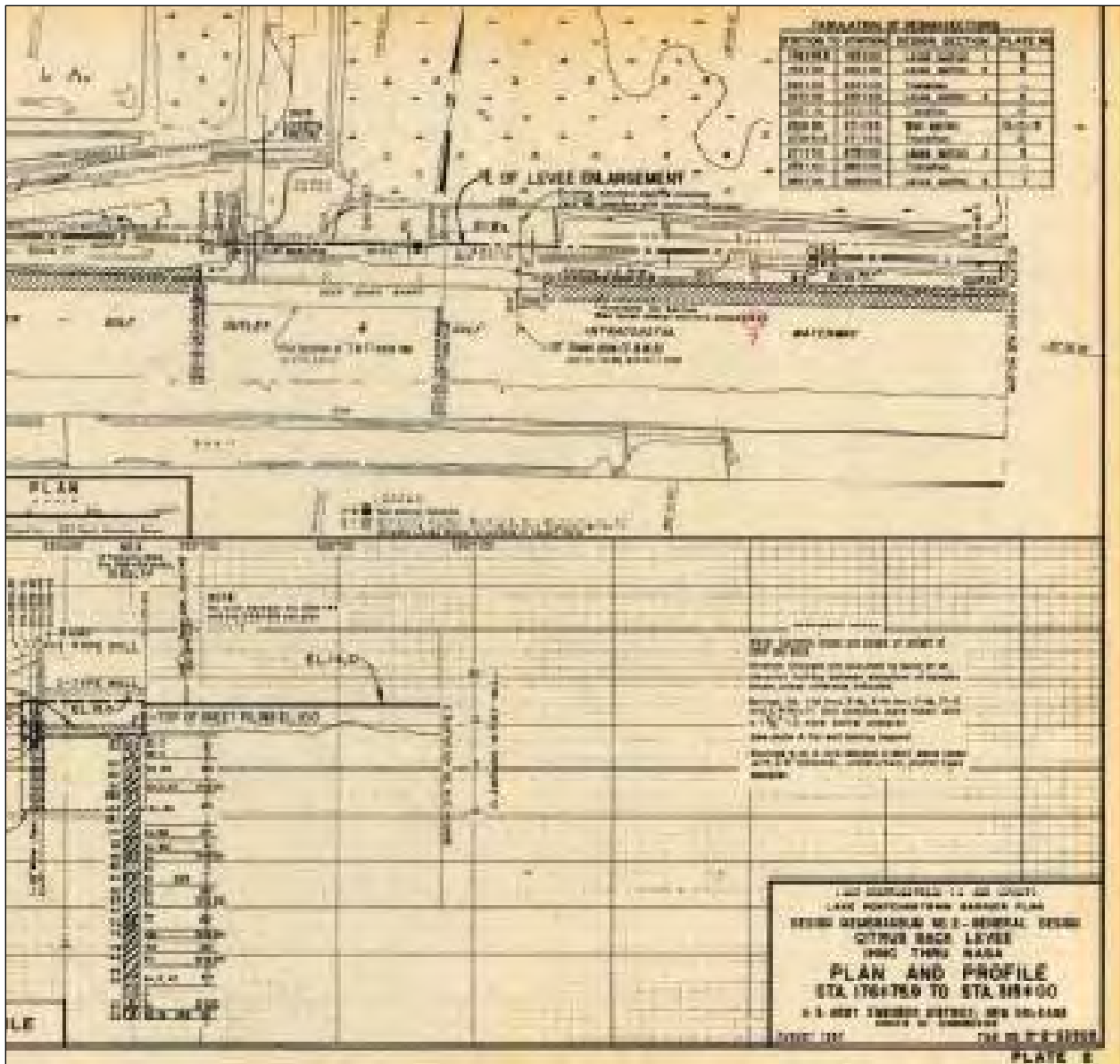
Figure 12-63. NOE4_J. Pre-Existing Condition, from Plate 2, page 104 of 161, DM2-Gen Design Citrus Back Levee (Aug 1967).pdf
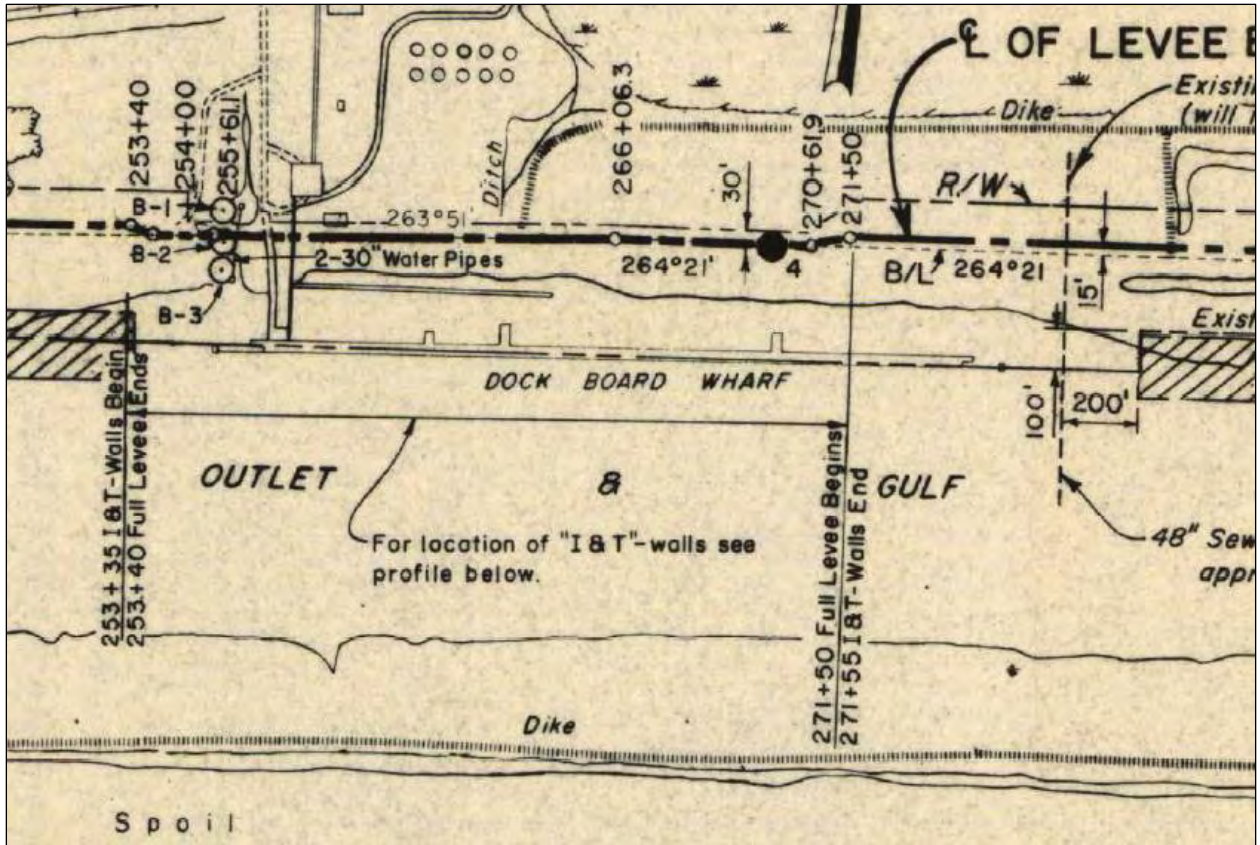
Figure 12-64. NOE4_K. Plate 2, Sta 250+ to Sta 279+
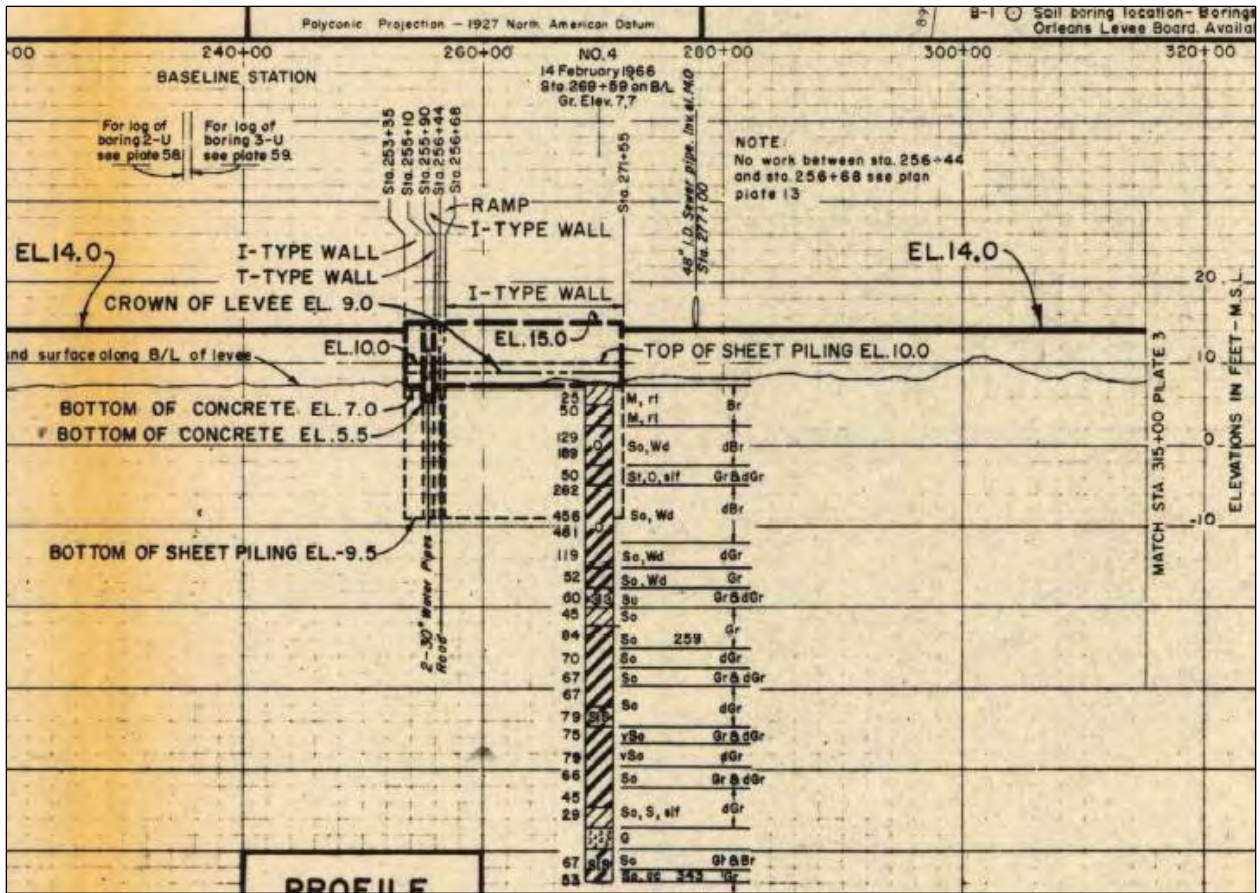
Figure 12-65. NOE4_L. Nearby Boring 4 Shows Top Layer of CL (from Plate 2 profile section)
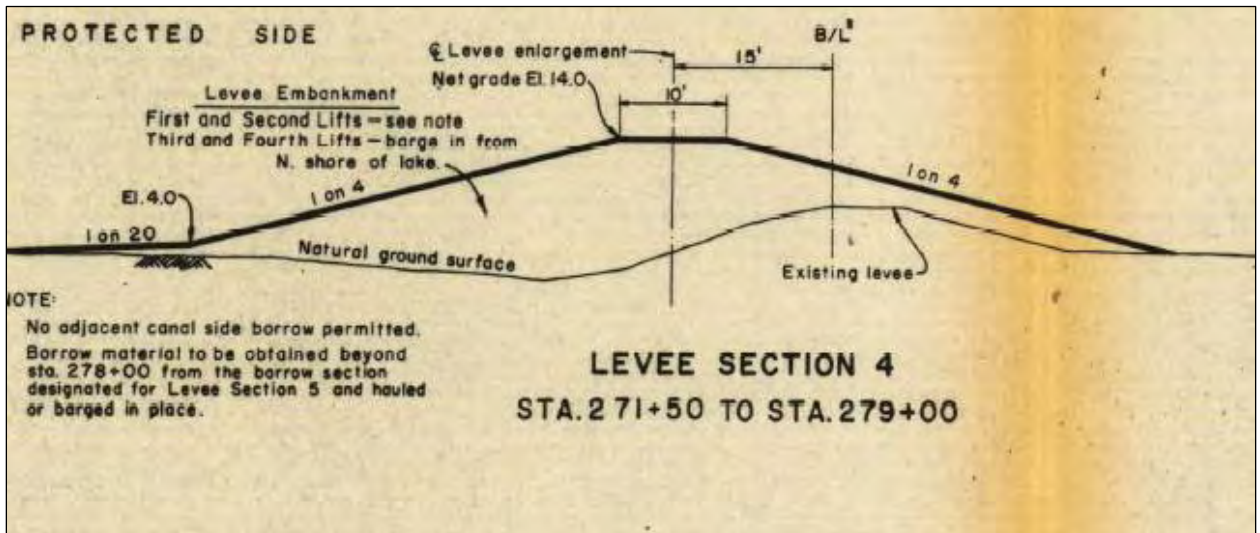
Figure 12-66. NOE4_M. Plate 6 Shows Different Borrow Source Beyond Sta 278+

Volume V The Performance – Levees and Floodwalls – Technical Appendix

V-12-65

This is a preliminary report subject to revision; it does not contain final conclusions of the United States Army Corps of Engineers.

LOCATION	El. "A"	El. "B"	El. "C" *
Sta. 253+35 to 271+55	15.0	10.0	-9.5
Sta. 431+00 to 454+80	20.0	14.0	-10.0
Sta. 571+55 to 584+236	22.0	14.0	-10.0

*Except for "T" wall sta. 255+10 to sta. 255+30 & ramp sta. 256+44 to sta. 256+68, roller gates no. 1, 2, & 3, and transit from levee to floodwall & floodwall to levee.

TYPICAL I WALL SECTION

SCALE: 3/8" = 1'-0"

Figure 12-67. NOE4_N. Plate 26 Shows Sheetpile Elevations
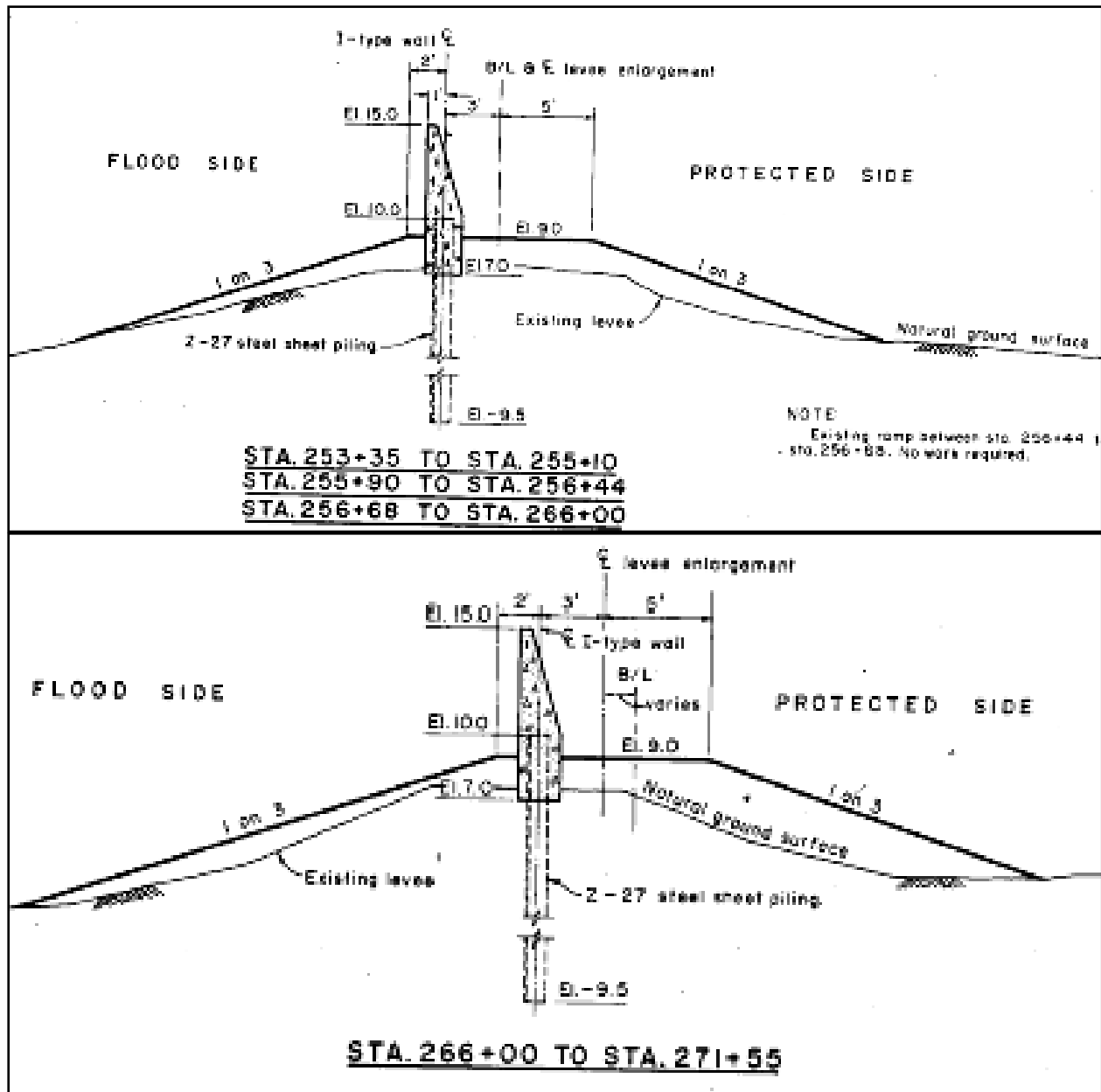
Figure 12-68. NOE4_O. Plate 28 Shows Elevations

Volume V The Performance – Levees and Floodwalls – Technical Appendix   V-12-67

This is a preliminary report subject to revision; it does not contain final conclusions of the United States Army Corps of Engineers.
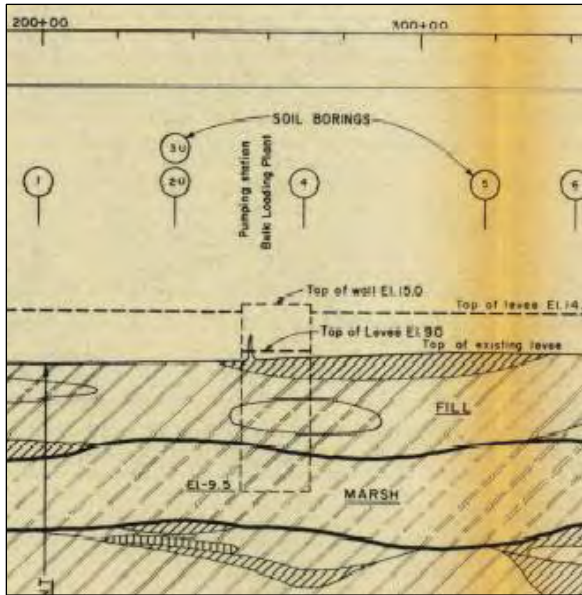
Figure 12-69. NOE4_P. Plate 35, Geology Profile. Note that Sta 240+ to Sta 300+ of the 1965 levee was approximately 5 ft of CL (lean clay) from top elevation 10' MSL down to 5' MSL. Organic clay fill lies beneath.

Citrus Back Levee, IHNC to Paris Rd

Figure 12-70. NOEX_Q. Amid Pump Station Landside Slope Erosion from Overtopping at Transition

Volume V The Performance – Levees and Floodwalls – Technical Appendix

V-12-69

This is a preliminary report subject to revision; it does not contain final conclusions of the United States Army Corps of Engineers.
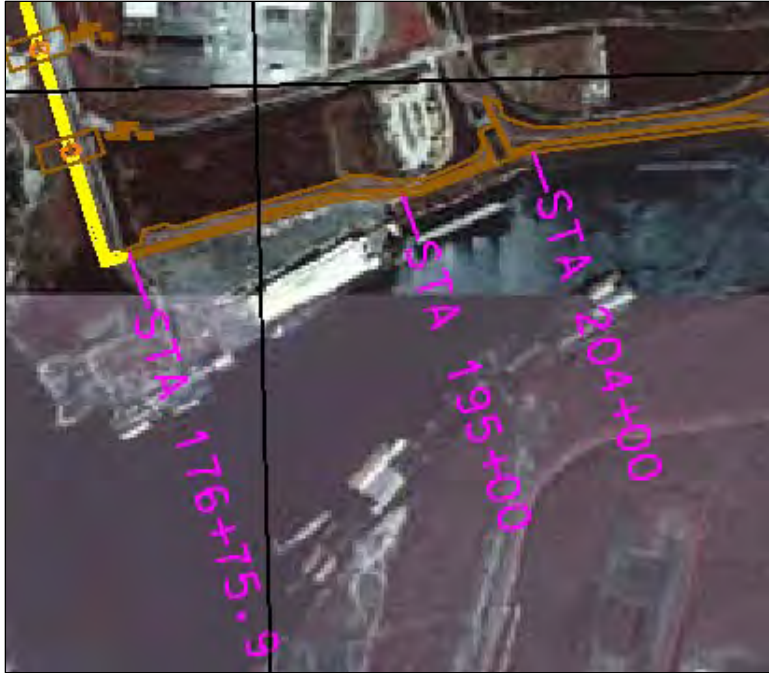
Figure 12-71. NOEX_R. Above Picture Taken Near GIWW/IHNC (coordinates 29 deg 59 min 55.37 sec N, 90 deg 00 min 41.62 sec W)

This is a preliminary report subject to revision; it does not contain final conclusions of the United States Army Corps of Engineers.

Figure 12-72. NOEX_S. Plate 2 of DM2-Gen Design Citrus Back Levee (Aug 1967) IHNC to NASA.pdf Shows Original Borings and Profile at Above Picture Location. Note that overtopping scour occurred at the intersection of the dirt road and levee crown as seen in Figure 12-NOEX-Q above

Figure 12-73. NOEX_T. Closeup of Scoured Road at Levee Crown, Amid Pump Station

Figure 12-74. NOEX_U. Overtopping Erosion on Flood Side and Land Side

Figure 12-75. NOEX_V. Narrow Localized Breach at Pre-Existing Pipeline Crossing. Coords 30 deg 00 min 10.66 sec N, 89 deg 57 min 49.31 sec W (Approximate Sta 349+00 B/L)

Figure 12-76. NOEX_W. 600' Reach of Levee with Landside Scouring

Attachment A
NOE Back Levee Design Memorandum Borings and Soil Test Data

**Attachment B
NOE Citrus Back Levee Design Memorandum Borings and Soil
Test Data**

Volume V The Performance – Levees and Floodwalls – Technical Appendix

V-12-77

This is a preliminary report subject to revision; it does not contain final conclusions of the United States Army Corps of Engineers.

Attachment C
Data Sources

Pre-existing conditions from Design Memoranda

Design Memoranda related to the NOE Basin are:

- DM 14 Citrus Lakefront Levee
- DM16 Gen Design NO East Levee South Point to GIWW (Sept 1987).pdf
- DM2 Gen Design Supp 4 N.O. East Back Levee (Mar 1971) pdf
- DM2-Gen Design Citrus Back Levee (Aug 1967) pdf

Figures C-1 thru C-4 show the geographical extent of each hurricane protection project.

Figure C-1. DM14 CitrusLakefrontLevee.pdf
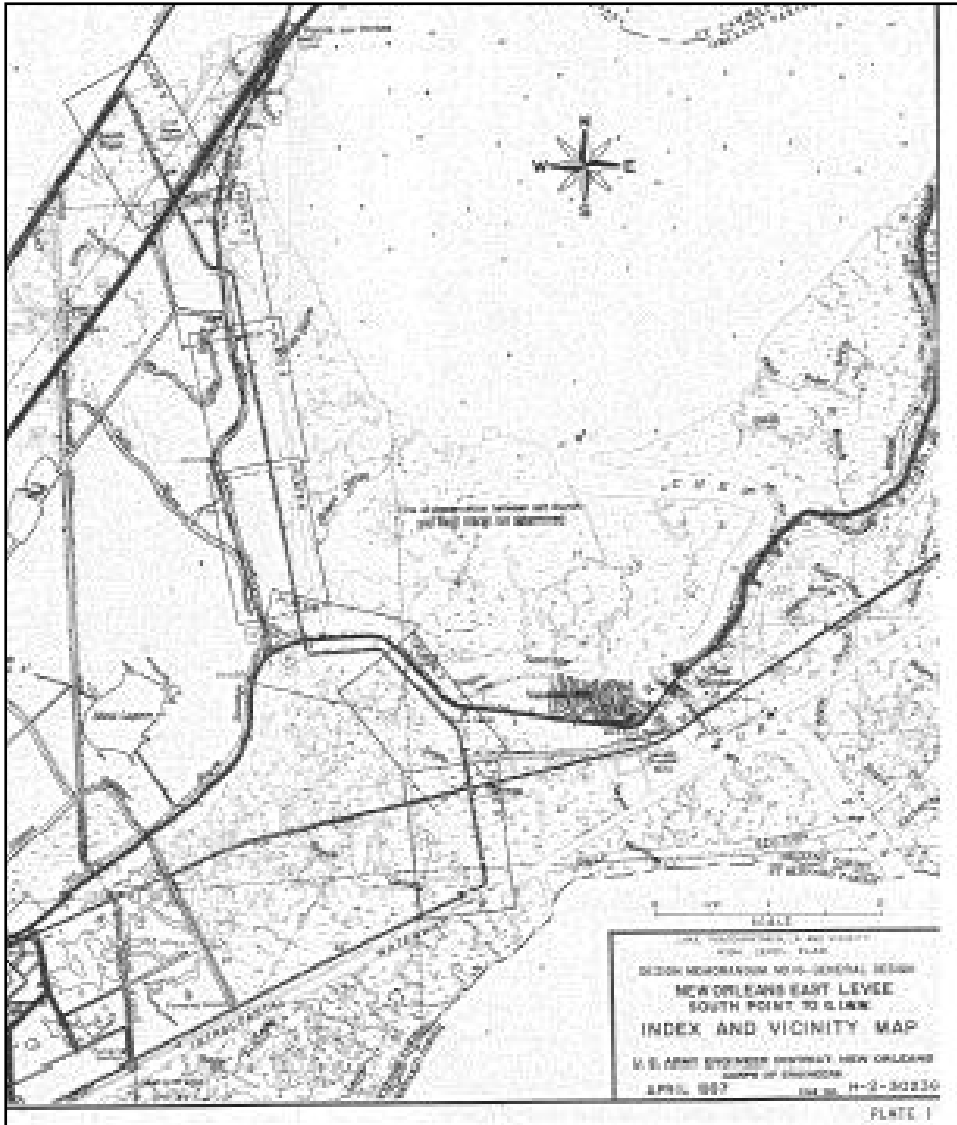
Figure C-2. DM16 Gen Design NO East Levee South Point to GIWW (Sept 1987).pdf
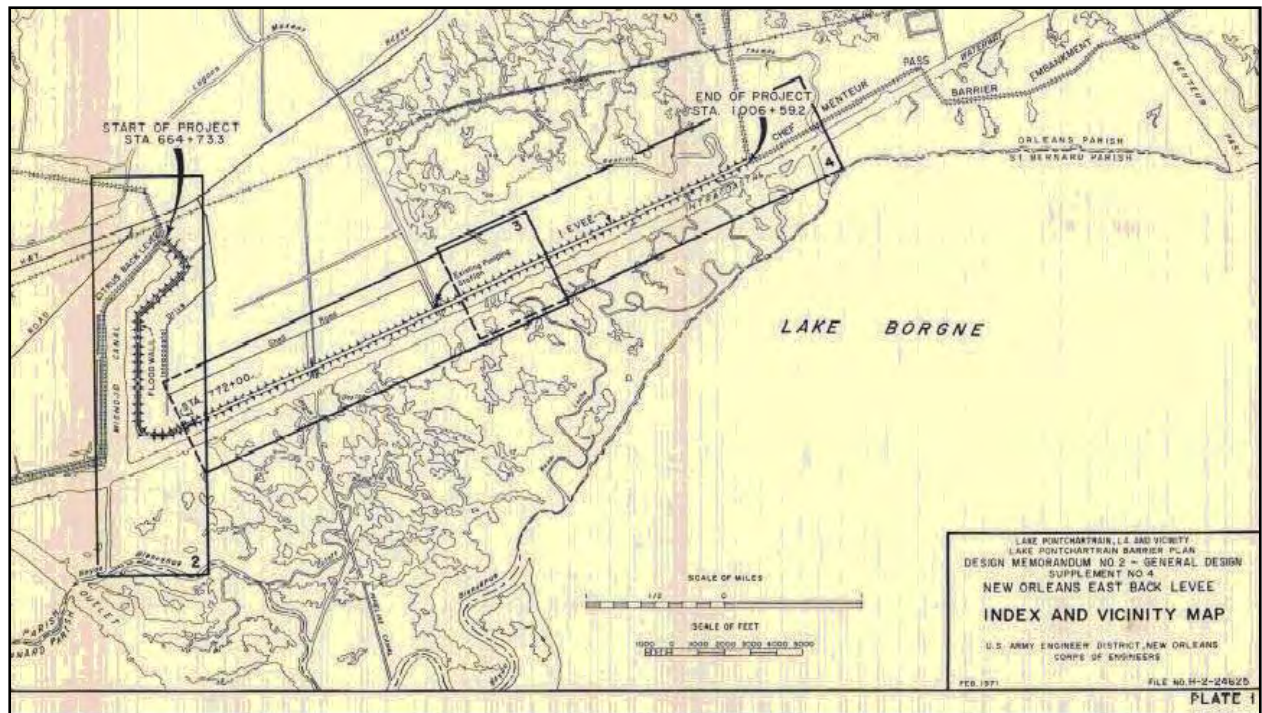
Figure C-3. DM2 Gen Design Supp 4 N.O. East Back Levee (Mar 1971) pdf
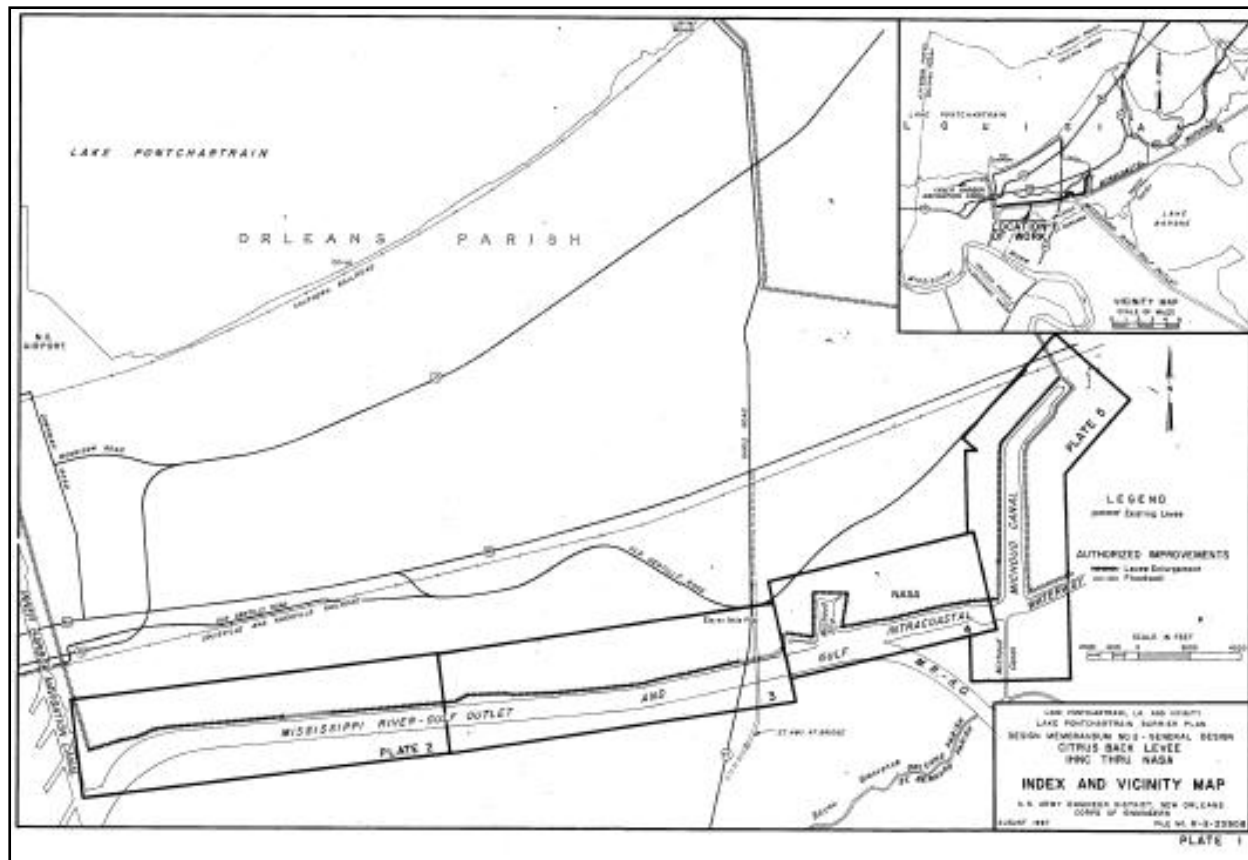
Figure C-4. DM2-Gen Design Citrus Back Levee (Aug 1967) pdf

Volume V The Performance – Levees and Floodwalls – Technical Appendix

V-12-81

This is a preliminary report subject to revision; it does not contain final conclusions of the United States Army Corps of Engineers.

Appendix 13
Levee and Floodwall Erosion and Scour from Overtopping Storm Surge

Background

Slope stability (sliding failure), underseepage and internal seepage leading to progressive failure are considered to be the primary functional failure modes for levees, and floodwalls. Water overtopping an embankment leading to surface scour and erosion has been considered as a potential failure mode for dams. Hurricane Katrina has highlighted the importance of overtopping initiating surface erosion and progressive erosion leading to breaching of the levees and floodwalls making up hurricane protection system.

The only failure modes absolutely known to have occurred during the Katrina event were overtopping and breaching, based on eyewitness accounts and forensic evidence such as high-water marks and barges resting on top of floodwalls. Lengthy reaches (miles) of earthen levees and capped levees were overtopped. Some reaches showed signs of initial erosion, others showed signs of progressive erosion, and other reaches contained significant breaching. Similar to levees, lengthy reaches of floodwall were overtopped and were left in various stages of damage ranging from minor scour at the wall base to breaches where complete floodwall sections were flattened.

In the New Orleans East, Lakeshore, and St. Bernard Parish basins, approximately 50 miles of earthen levees overtopped but did not breach; approximately 20 miles of earthen levees overtopped and contained significant breaches; approximately 7 miles of floodwall overtopped but did not breach; and approximately 2 miles of floodwall overtopped and had breaches. The majority of levees and floodwalls damaged by overtopping, but did not breach.

In Plaquemines Parish, the Mississippi River mainline levee and the back levee lengths total about 162 miles. There are about 7 miles of floodwall (I-walls and sheetpile). All of the levees in Plaquemines Parish sustained damage, and there was considerable crown and slope scour along the total length, due to overtopping. The mainline levee riverside slope pavement sustained damage from the hundreds of ships and barges that crashed into it. There were also several severe breaches, coinciding with pipeline crossings and with some floodwalls. Five of the 7 miles of floodwall were damaged beyond repair. There were major breaches at sheet pile wing

Volume V The Performance – Levees and Floodwalls – Technical Appendix

V-13-1

This is a preliminary report subject to revision; it does not contain final conclusions of the United States Army Corps of Engineers.

walls at two pump stations in the back levee. A major breach occurred at the Shell pipeline crossing near Nairn, and the West Pointe a la Hache pipeline crossing was severely damaged.

Post-Katrina evidence also indicated that progressive surface soil erosion and scour due to overtopping may have contributed to breaching. It is well known that any reduction in the cross-sectional area of a physical object will reduce the ultimate strength for which that object is capable. An earthen levee's ability to resist hydrodynamic water loading will be compromised if the cross-section geometry is altered. If water overtops the levee and washes out (erodes) the backside slope, the lateral stress-resisting ability and the underseepage force-resisting ability will be compromised, depending on the degree of erosion. Several stages of erosion and scour progression were noted along numerous levee / floodwall reaches, and although it may be too late to scientifically classify their contribution to breaching probability (due to construction repair), general observations and assumptions may be developed regarding soil erodibility and erosion progression.

Failure Patterns

Very little evidence of frontside (floodside) erosion was noted in the post-Katrina forensic evidence. Backside (landside) erosion patterns were observed along breached and unbreached levee and floodwall in Orleans, St. Bernard, and Plaquemines Parishes. The following overtopping and breaching damage patterns were observed:

a. Earthen levee backside erosion caused by: (1) wave overtopping when the surge level was below the levee crest elevation, and (2) continuous water overtopping when the surge level exceeded the levee crest elevation. Progressive erosion of unprotected soil on the protected side (backside) likely contributed to levee breaching.

b. Damage to the earthen levee on the backside of vertical floodwalls caused by wave and/or water overtopping impacting the unprotected soil. Loss of lateral soil support and progressive erosion likely contributed to wall and levee breaching.

c. Damage to transitions between earthen levees and structures such as flood gates and floodwalls. Erosion of earthen levee material and scour at the transitions was observed, and localized overtopping was most likely due to levee / wall elevation differentials.

The following pictures and descriptions show examples of the damage patterns, and available additional information such as soil borings and pre-Katrina elevations are included to provide possible explanations for scouring erosion. Figure 13-1 is a diagram of the observed general failure progression patterns.
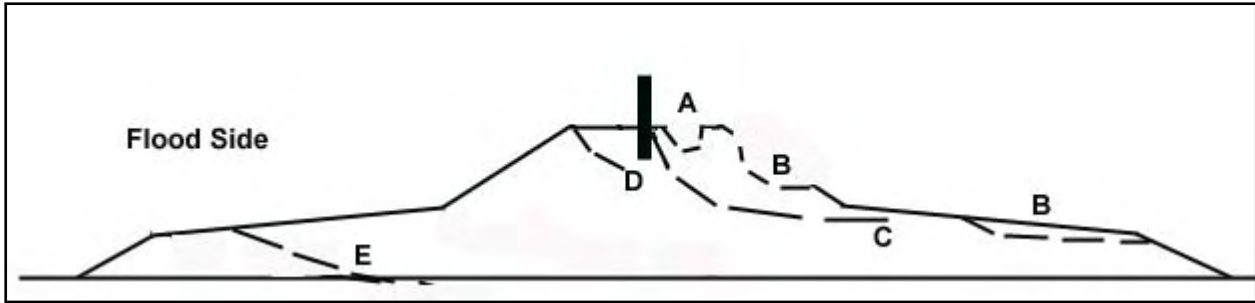
Figure 13-1. Erosion Progression Patterns for Earthen Levees, Floodwalls, and Exposed Sheetpile

Scour pattern "A" indicates scour located on the protected side levee slope (or located immediately adjacent to the floodwall or sheetpile protected side), "B" indicates erosion on the protected slopes including stabilizing transition slopes, "C" indicates erosion progressing to the levee crown and adjacent to the floodwall or sheetpile protected side, "D" indicates scour on both the flood side and the protected side of the levee or floodwall, and "E" indicates the original levee footprint has been significantly altered due to erosion and the original foundation base may have scour holes or washouts.

Concrete and Sheetpile Floodwalls

The majority of floodwalls and exposed sheetpile experienced scour pattern "A" on the backside. Figure 13-2 is a conceptual diagram illustrating the water overtopping plunging velocity and force of impact on the wall backside.
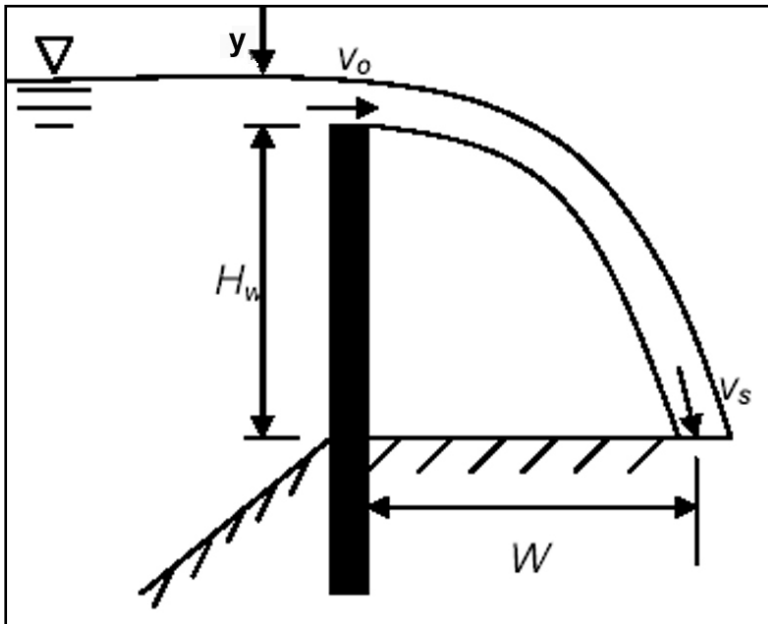
Figure 13-2. Conceptual Diagram of Water Overtopping a Floodwall or Exposed Sheetpile

Hydrodynamic analysis for floodwall overtopping assumes the floodwall acts as a weir, and the overtopping flowrate, velocity, and impact force (per unit length of floodwall) values are

derived accordingly. Figures 13-3 and 13-4 are diagrams of overtopping velocity and impact force impinging on the ground surface on the floodwall backside. These diagrams were developed from hydrodynamic relationships (Hughes 2006).
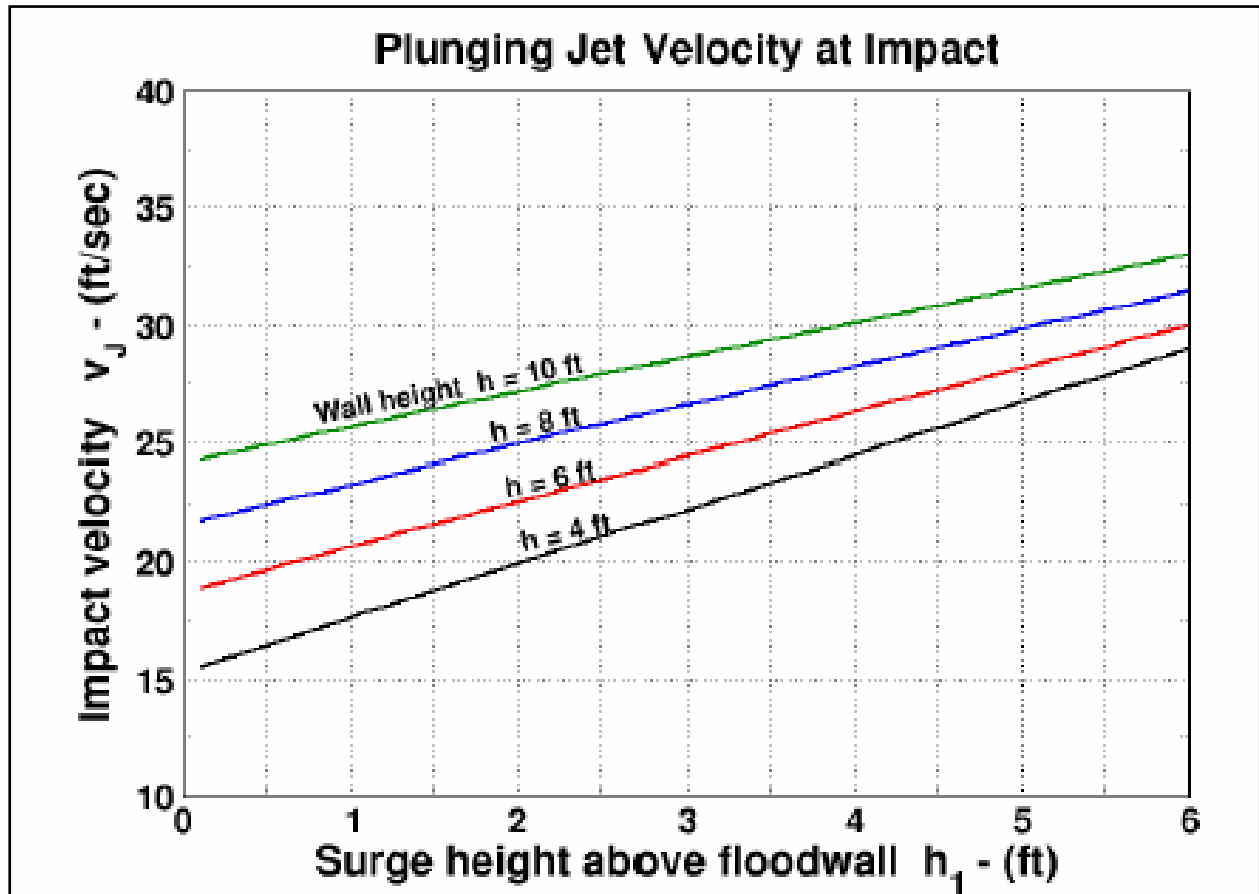
Figure 13-3. Ground Impact Velocity as a Function of Surge Height where $h_1 = y$ in Figure 13-2 (Hughes 2006)
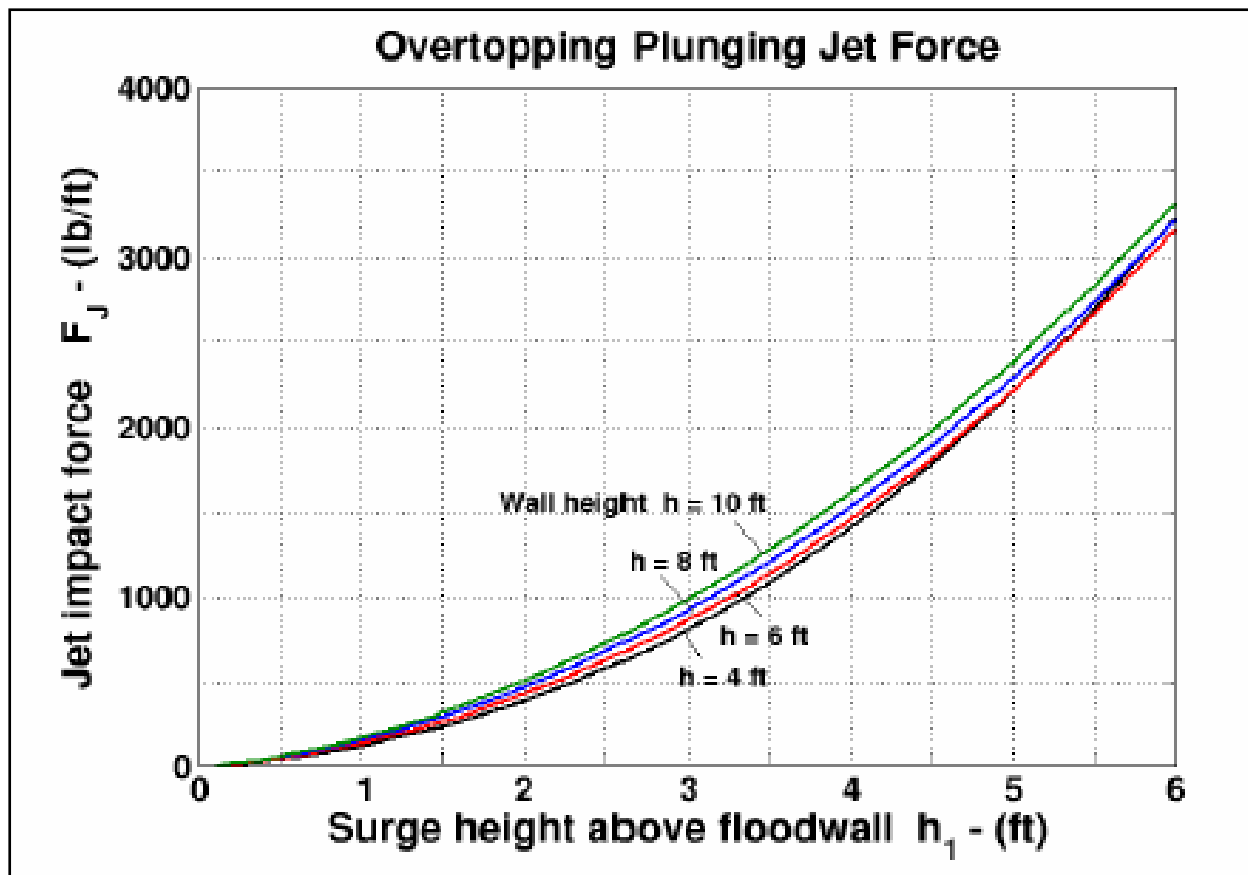
Figure 13-4. Ground Impact Force as a Function of Surge Height (Hughes 2006)

Figure 13-5 shows the I-wall along the east side of the IHNC at approximate B/L Sta 11+00 (DM3 Chalmette Area Plan), looking toward the Claiborne Avenue bridge. Depth of scour was to the bottom of the I-wall concrete cap (2 ft), and scour width was approximately 7 ft. The I-wall elevation was designed to height of 15 ft above mean sea level, the bottom of the concrete cap was elevation 7 ft, and the levee crown was elevation 9 ft . Actual wall height was reported to be 12.5 ft converted to local mean sea level, and the storm surge height was reported to be up to 15 ft. As an approximation of the overtopping water impact, a 2.5 ft crest of water cascaded from a 6-ft height onto the levee crown. Figures 13-3 and 13-4 show the estimated impact velocity was about 23 ft/sec and impact force was about 700 lb/ft. The water impact removed a portion of the levee crown, including all of the structural backfill zone adjacent to the concrete wall.

Figure 13-5. Scour Pattern "A" on East Side IHNC near N. Claiborne Ave. Bridge
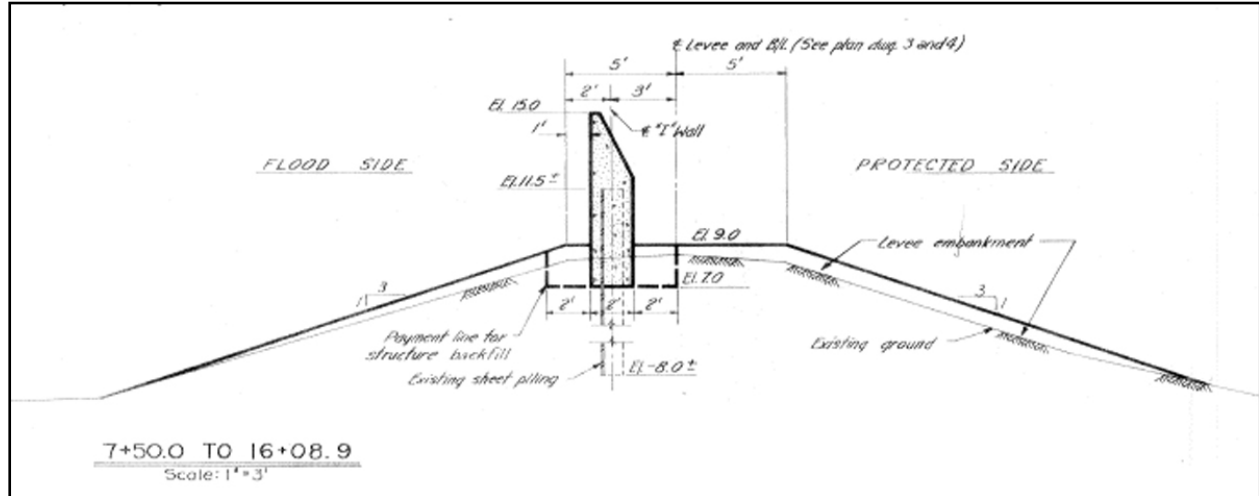
Figure 13-6. Existing Levee and I-Wall Drawing for IHNC East. Note that scoured soil included the "structure backfill" zone (from drawing file H-4-25157, IHNC East Levee from Lock to Florida Ave. Floodwall, sheet 12 of 15)
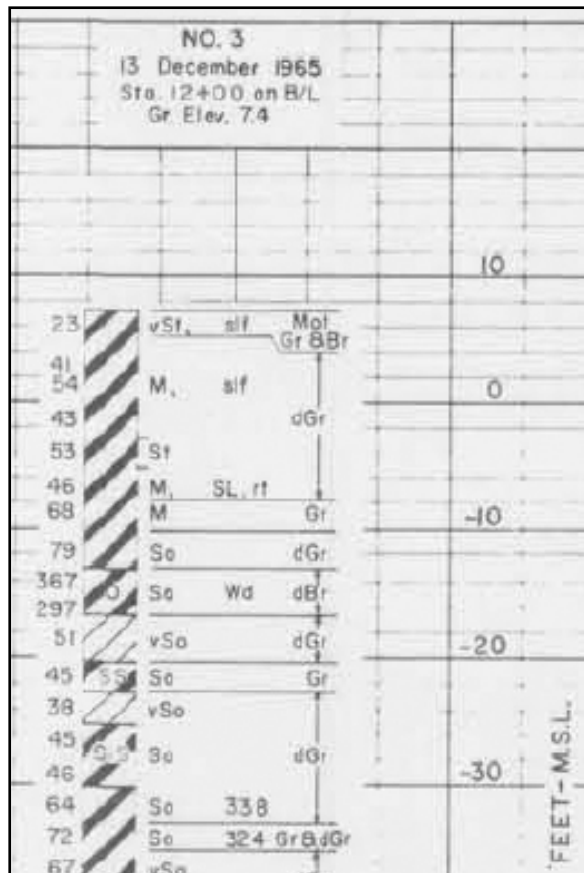
Figure 13-7. Nearest Soil Boring, No. 3, 100 ft Distant, Shows Fat Clay (CH) at Center Line Surface

Figure 13-8. IHNC East, Approximate B/L Sta 7+00 (DM3 Chalmette Area Plan), North of the Claiborne Avenue Bridge. Depth of scour was to the bottom of the I-wall concrete cap. I-wall elevation was designed 15 ft above mean sea level (MSL), bottom of concrete was elevation 7 ft (MSL), and levee crown was elevation 9 ft (MSL). Actual wall height was reported to be 12.5 ft converted to local mean sea level (LMSL), and storm surge height was reported to be up to 15 ft. As an approximation of the overtopping water impact, a 2.5 ft crest of water cascaded from a 6-ft height onto the levee crown. Nearby soil boring 2U (Figure 13-9) indicates the upper 5 ft was fat clay (CH) with sand / silt lenses
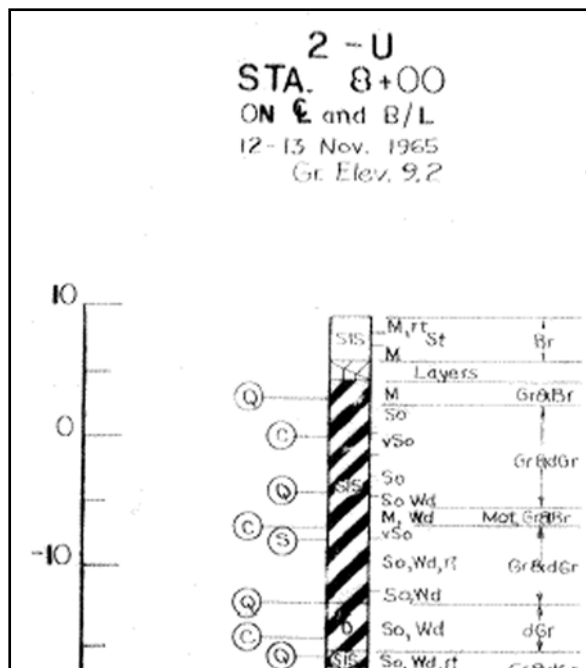
Figure 13-9. Undisturbed Boring 2U Located 100 ft to the North Shows Silt / Sand Lenses in Lean Clay in the Upper 5 ft. Undrained shear strength in the upper 3.2 ft was approximately 500 psf

Soil scour within the structure backfill zone is also evident at other locations such as the T-wall on the north side of Gate 13E on the east side of the IHNC near Lakefront Airport at approximate W/L Sta 61+38 (DM2 Supplement 8 IHNC Remaining Levees). The top of T-wall elevation is 13.25 ft (MSL) and the existing top of ground elevation was 0.1 ft (MSL), from drawing file H-2- 24111, plate IV-20. Scour depth was 30in and width was approximately 8 ft caused by a 13-ft overtopping water impact (Figure 13-10). Figures 13-3 and 13-4 show the estimated impact velocity was about 30 ft/sec and impact force was over 700 lb/ft.

Figure 13-10. T-Wall Base Scour on Backside, East IHNC Near Lakefront Airport

Volume V The Performance – Levees and Floodwalls – Technical Appendix
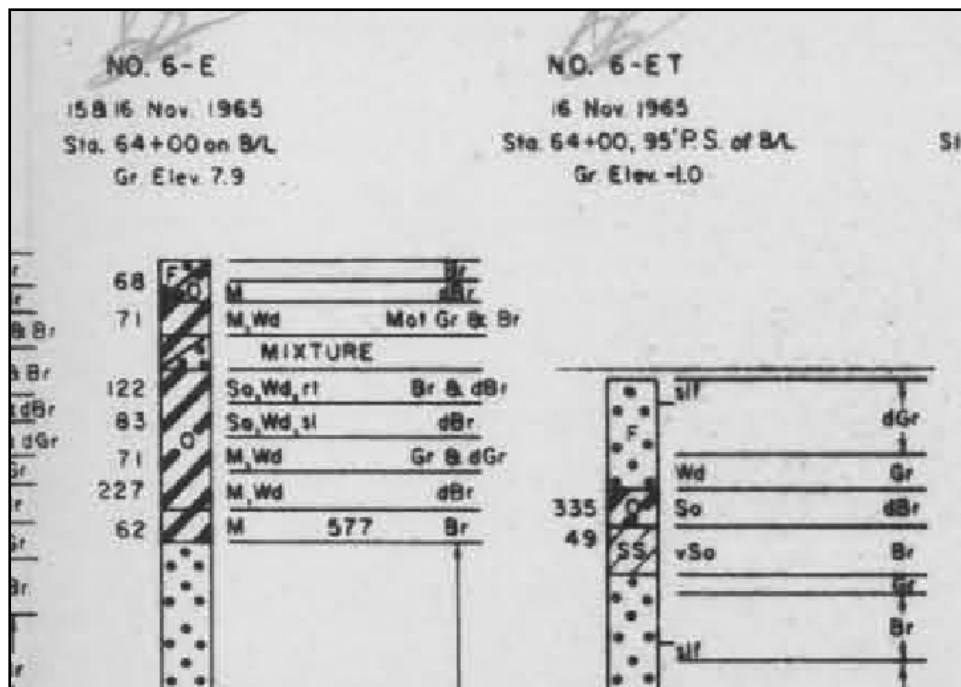
Figure 13-11. Nearest Soil Boring 6-E Shows Built-Up Levee at Elevation 7.9 ft (MSL), but Boring 6-ET, Offset 95 ft to the Protected Side of the B/L, Shows Original Ground Surface Elevation -1.0 ft (MSL) was Approximately a 10-ft Layer of Sandy Material (from drawing file H-2-24111, plate IV-34). The vertical and horizontal scour pattern indicates that the T-wall base structural backfill had lower erosion resistance than the original levee soil

Figure 13-12. Scour Along Lakefront Airport Floodwall Measures 305' (L) x 14' (w) x 48" (d). Existing levee crown appears to be composed of sandy material, based on visual observation. Nearby soil boring 1-C (5/29/1969) at Sta. 8+85, 57 ft right of B/L shows sand, silt, and lean clay lenses to 9-ft depth. Soil boring 4-A (11/3/1970) at Sta 18+00, 200 ft landside of B/L also shows sand, silt, and lean clay lenses to 9-ft depth

Figure 13-13. Lakefront Airport Floodwall. Scour is approximately 11 ft wide by 2 ft deep. Floodwall elevation is approximately 13.5 ft, ground elevation is approximately 6 ft, and wall height is approximately 7.5 ft

Figure 13-14. IHNC East, Approximate B/L Sta 101+00 (from drawing file H-2-24111, plate IV-23, DM2 Supp 8 IHNC Remaining Levees), North of Chef Menteur Hwy Bridge. Top of I-wall is elev 14.75, bottom of concrete is elev 7, and levee crown is elev 9. Nearest B/L boring is Sta 96+00 (No. 9EU), 500 feet distant. Approximate storm surge impact was a 2.5-ft water crest cascading over the 6-ft concrete wall. Note that the scour was deeper than the concrete base, indicating that the structural backfill and the original levee material eroded
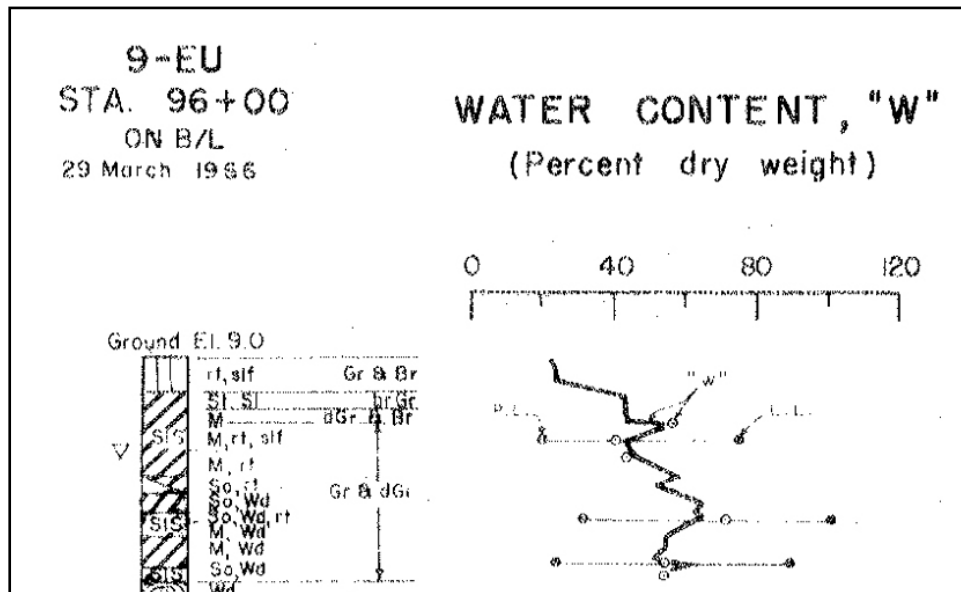
Figure 13-15. Boring 9EU (Sta 96+00 B/L, East Side IHNC) Shows a Top Layer of Silt at Levee Crown Elevation 9 ft, Possibly Explaining the Low Erosion Resistance of the Original Levee Material

Figure 13-16. IHNC West Side Between Chef Menteur Hwy. and Hayne Blvd, Approx 8400 LF. Top of I-wall elevation is 14.75 ft(MSL), bottom of concrete is elevation 7 ft (MSL), and levee crown is elevation 8 ft (MSL). Borings in this reach (B/L Sta 31+06 to Sta 109+00, borings 1W to 14W) show the top 2 ft to 3 ft layer at crown elevation is composed of sandy and/or silty soil instead of fat clay

Figure 13-17. Scour at T-Wall Base of Gate W23, West Side IHNC

Figure 13-18. IHNC West Side, View South from Benefit St. Gate Toward France Rd Ramp. Approximate W/L Sta 5+56 (B/L Sta 205+44). Top of I-wall elevation 15 ft, levee crown 9 ft, bottom of concrete 7 ft, bottom of pre-existing Z-27 sheet pile (installed by the Orleans Levee Board) at -10ft (MSL). From drawing file H-2-24111, plate IV-15. Nearest soil boring (Figure 13-19) is 30W at B/L Sta 203+00. The I-wall rotated and floodside levee deformation occurred, probably as a result of sheetpile rotation opening up a floodside tension crack. This picture represents scour pattern "C" which is a pre-breaching failure mode
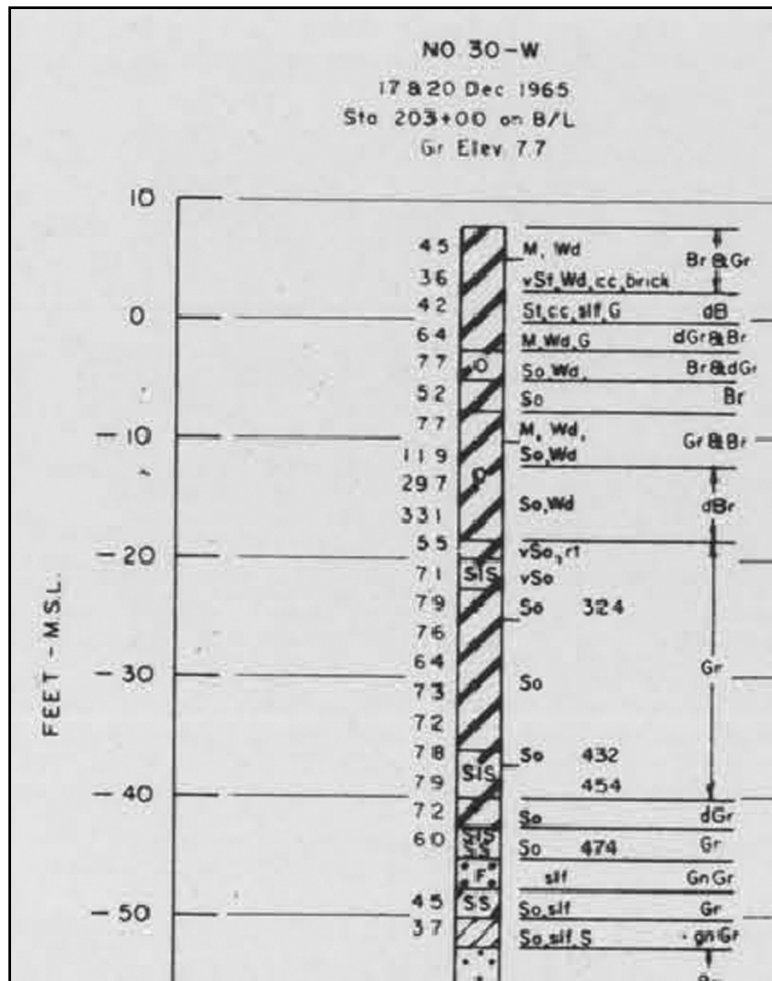
Figure 13-19. Boring 30W About 300 ft from Benefit St Gate Shows Fat Clay Soil Layers in Pre-1965 Levee

Exposed sheetpile reaches along the MRGO in St. Bernard Parish (Chalmette and Chalmette Extension Hurricane Protection Plans) experienced scouring on the backside, and several locations were breached.

Figure 13-20. View Looking Southeast from the Bayou Bienvenue Control Structure Showing Backside Scour Beyond the Structure
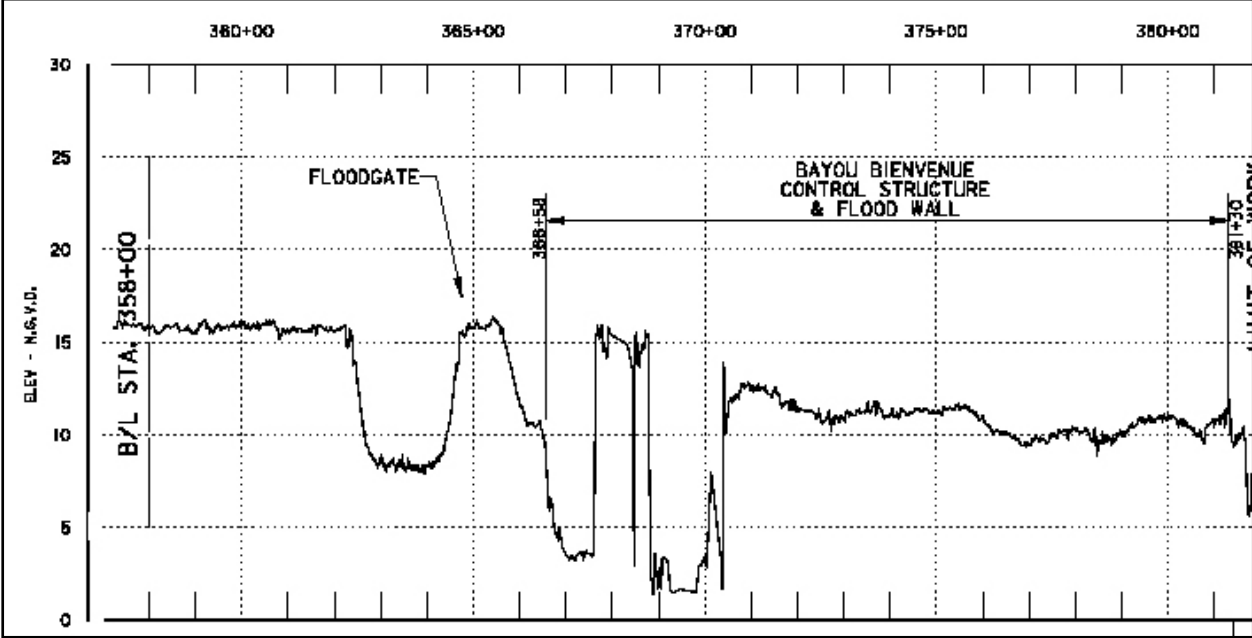
Figure 13-21. Centerline Scour Depths of Floodgate and Control Structure (from dwg 1 of 8, Emergency Restoration B/L 383+00 to 704+00 contract solicitation)
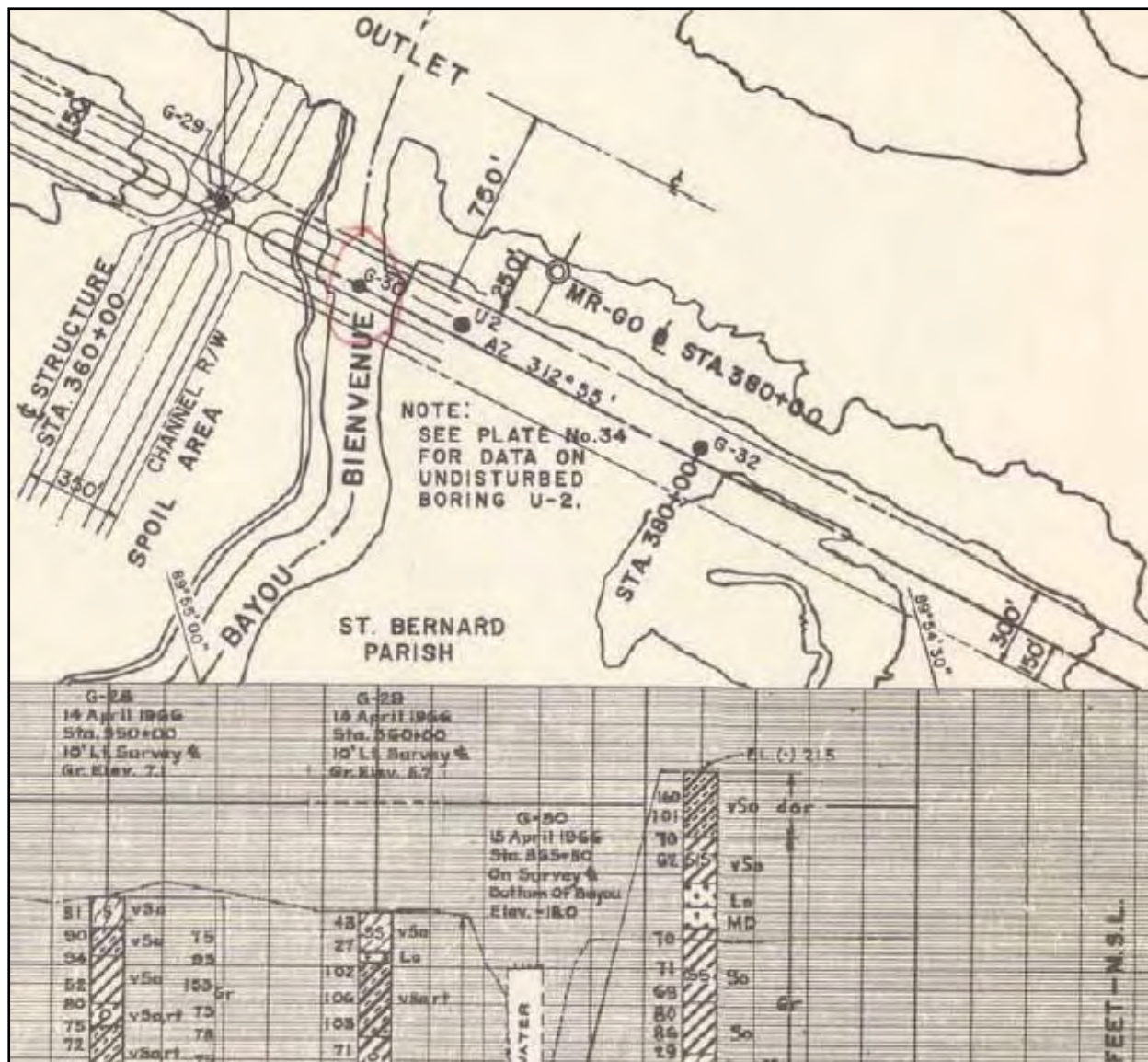
Figure 13-22. Original Ground Surface (1966) Had Sand / Silt Lenses Overlying Very Soft Organic Clay (plate 10, DM3). Note that the sheetpile east of structure (Figure 13-20 above) was driven to cut off the old Bayou channel in addition to reducing loading on the top layer of very soft organic clay seen in boring G-32.

Figure 13-23 shows a section with 4300 ft of exposed sheetpile damage along MRGO between Bayous Bienvenue and Dupre, St. Bernard Parish. The damaged sheetpile section is near utility crossings, with scour on the protected side and levee crown. B/L Sta 590+70 is centerline of the two pipelines.

Figure 13-23. Pattern "A" Scour on the Backside of Exposed Sheetpile Wall Along the MRGO South Bank in St. Bernard Parish

Volume V The Performance – Levees and Floodwalls – Technical Appendix

V-13-21

This is a preliminary report subject to revision; it does not contain final conclusions of the United States Army Corps of Engineers.
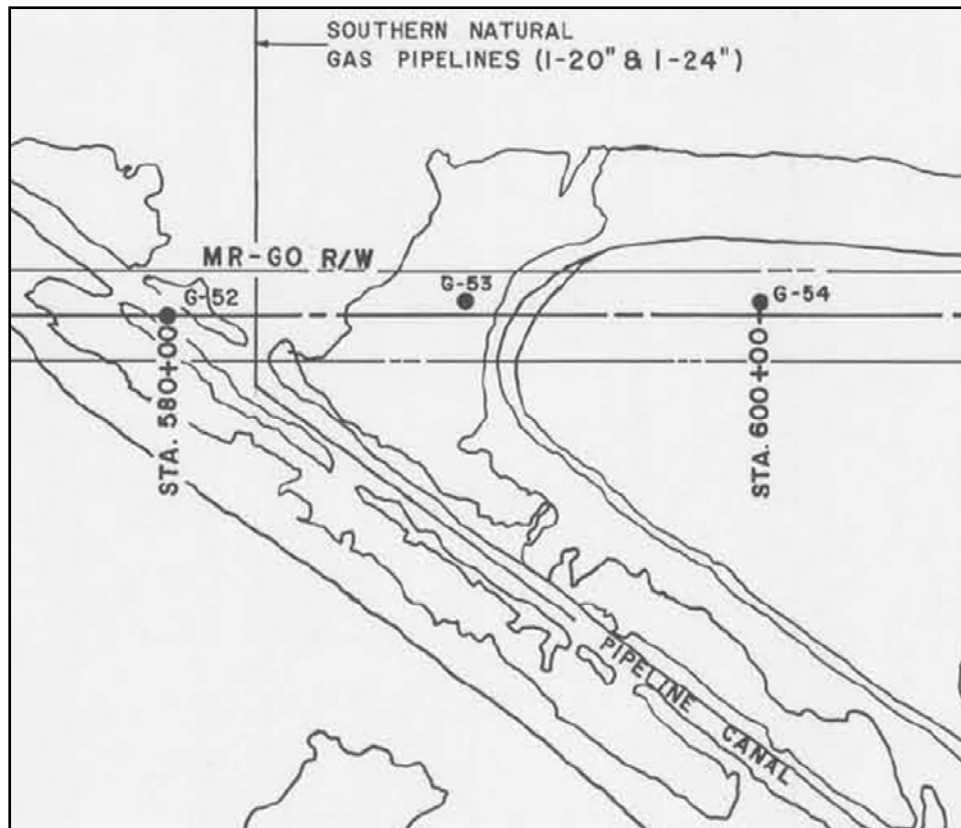
Figure 13-24. Original Pipeline Canal Prior to Backfilling and Sheetpile (from drawing file H-2-23820, plate 13)
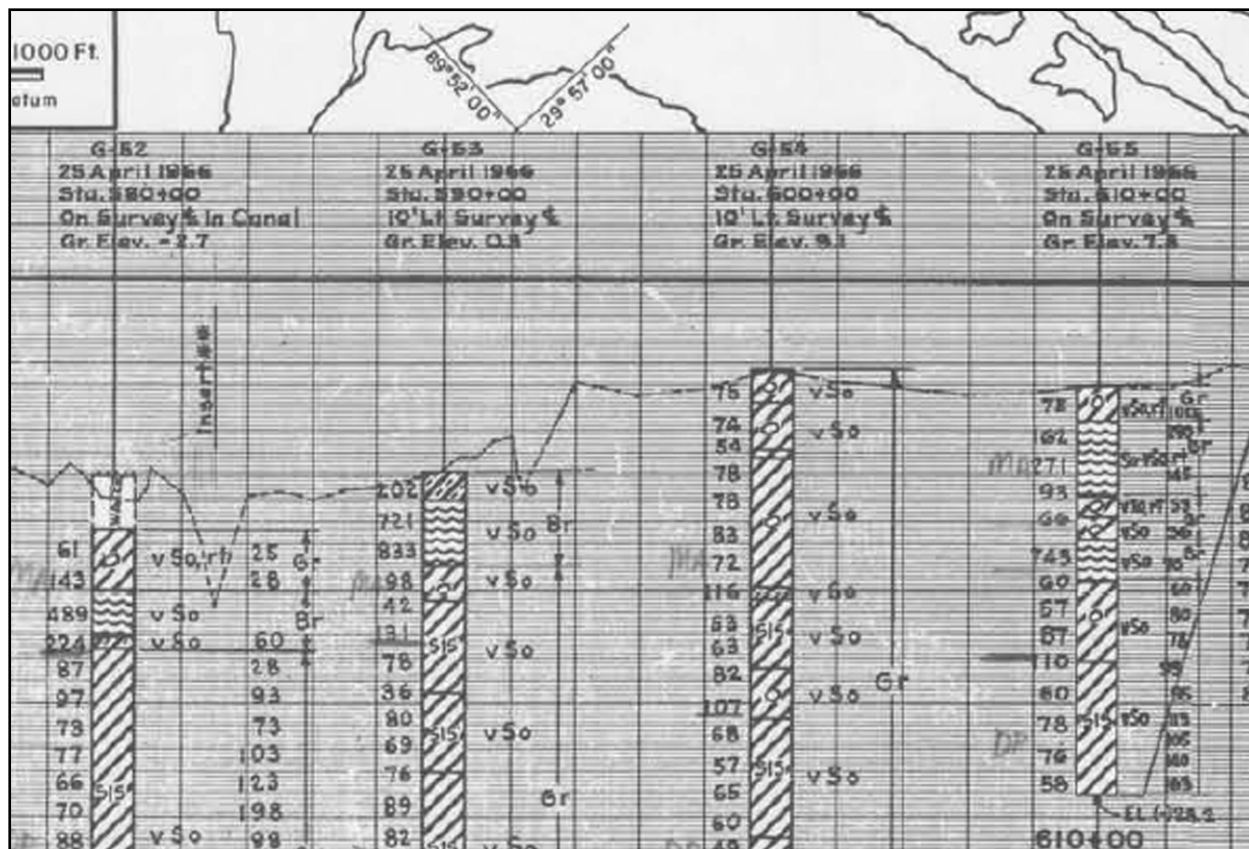
Figure 13-25. Adjacent Borings Show Very Soft Fat Clay and Peat Layer Stratification
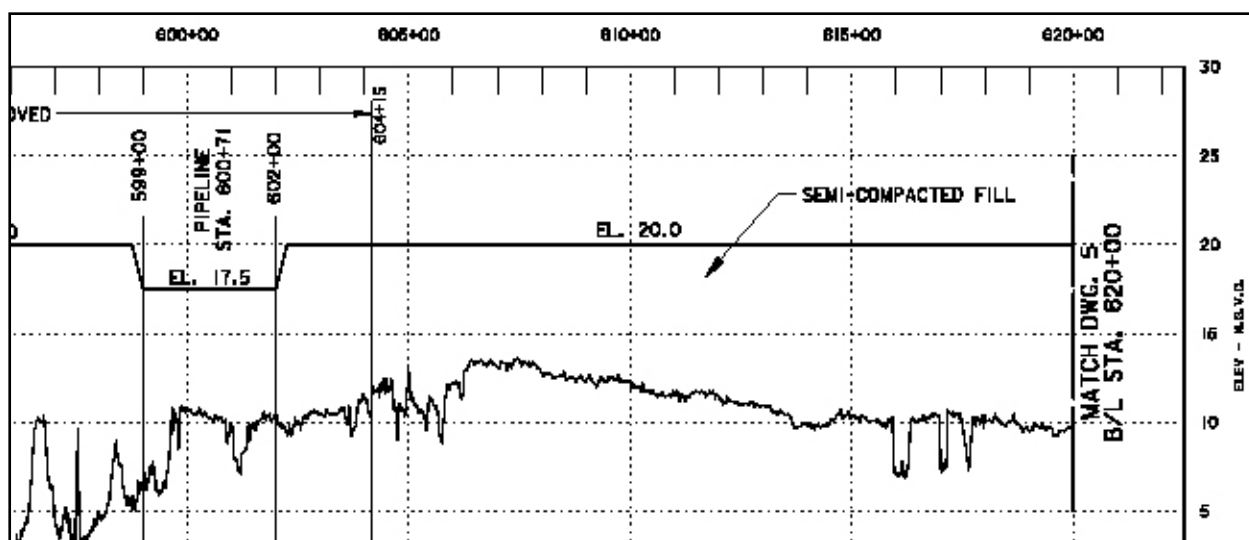
Figure 13-26. Scour Depths and Levee/Sheetpile Elevations Between B/L Sta 600+00 to 620+00 (from SB04 Contract Solicitation W912P8-05-R-0063, B/L 383+00 to 704+00 Emergency Restoration)

Figure 13-27. Closeup of Adjacent Breached Sheetpile with Backside Scour. Note the stratified layers in the soil profile representing existing hydraulic fill historically dredged from the MRGO

Figure 13-28. Sheetpile Between Bienvenue and Dupre Control Structures. Note the sheetpile elevation differences

Soil boring 18-UBD (91-02) from 1991 at B/L Sta 596+00 shows the top 5.8 ft of levee (at elevation 14.4) was composed of sandy silt (SM), with CH layers underneath. At a depth of 12 ft below the crown, a shear Q test indicated cohesion value 396 psf at 27% water content and 95 pcf dry density in a CL layer.

Figure 13-29. Sheetpile Reach Along the MRGO Southeast of Bayou Bienvenue at Approximate B/L Sta 600+00. Top of sheetpile was elevation 17 ft (MSL) and levee crown elevation was approximately 12 ft (MSL), for an exposed sheetpile height of approximately 5 ft. Storm surge on the MRGO was approximately 18 ft, resulting in approximate overtopping velocity of 20 ft per second with approximate 250 lbs/ft impact force. The end of the sheetpile section with transition to the severely eroded levee is approximate B/L Sta 604+15
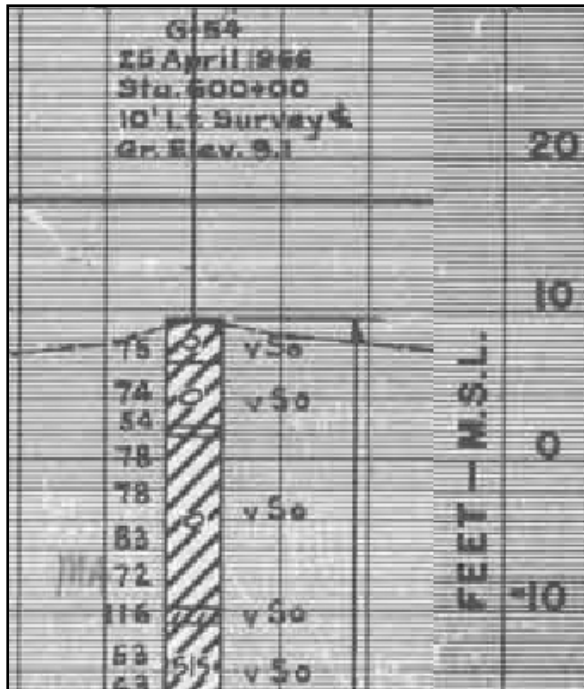
Figure 13-30. Nearest Boring at 10 ft Offset from B/L Sta 600+00 (from drawing file H-2-23820, plate 13) Shows 1966 Hydraulic Fill (dredge spoil) Surface at Elevation 10 ft Was Very Soft Fat Clay

Soil boring 13BU-CHBD (01-16834) taken in 2001 at Sta 614+00 (Martello Castle) shows the top 25 ft of levee (elevation 15.4) was composed of fat clay (CH), with organic clays and peats underneath. At a depth of 5 ft below the crown, a shear Q test indicated cohesion value 632 psf at 29% water content and 92 pcf dry density in the CH layer.

Figure 13-31. Exposed Soil Layer (final eroded surface) on Sheetpile Wall Backside Appears to be In-Situ Fat Clay with Embedded Shell Hash, Possibly an Exposed Estuarine Deposit

Large breaches along sheetpile reaches and scour patterns resembling "C" and "D" (from Figure 13-1) were evident on the north bank of the GIWW, including the Bulk Loading Facility, the Michoud Canal (Air Products plant), and pump station 15.

Figure 13-32 shows the Air Products plant breach near Sta 772+00 B/L (New Orleans East Back Levee). Scour depths were 10 to 12 ft on both floodside and protected side of the sheetpile wall. Nearest borings (Figure 13-29) on either side of the failure, 5-E and 6-E (from plate 5, DM2 Supp 4, March 1971) shows CH material with sand / silt lenses in the pre-existing (1965) levee at crown elevation ~12 ft, prior to construction of the sheetpile wall. The storm surge in the GIWW was approximate elevation 15 to 17 ft, and Figures 13-3 and 13-4 show the estimated impact velocity ranged up to about 23 ft/sec and impact force ranged up to about 700 lb/ft. Note that the breach occurred in the sheetpile reach, not along the adjacent transitions to earthen levee on the east side and connection to the T-wall on the west side.

Figure 13-32. Air Products Sheetpile Breach
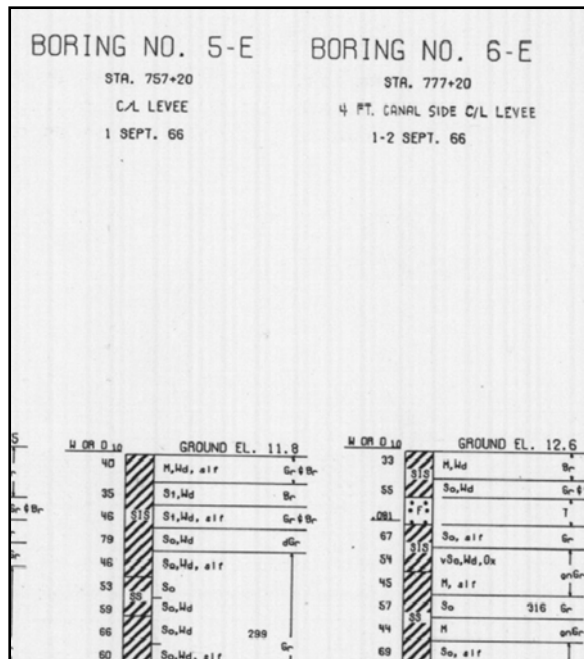
Figure 13-33. Nearest Borings on Either Side of the Breach, 5-E and 6-E (from plate 5, DM2 Supp 4, March 1971) Show CH Material With Sand / Silt Lenses in the Pre-Existing (1965) Levee at Crown Elevation ~12 ft, Prior to Sheetpile Wall. Storm surge in the GIWW was approximately 15 to 17 ft elevation

Figure 13-34. Bulk Loading Facility I-Wall Breach (2000' near Elaine St. at GIWW, near Sta 271+55 B/L, Citrus Back Levee, north bank GIWW). Scour depths were 6 to 10 ft on both floodside and protected side of the I-wall. Pre-existing wall elevation was approximately 15 ft (MSL), and levee elevation was approximately 9 ft (MSL), for an exposed wall height of approximately 6 ft. Storm surge ranged from elevation 15 to 17 ft

Figure 13-35. Nearby Boring 4 Shows Top Layer of Lean Clay (CL) (from Plate 2 profile section of DM2, General Design Citrus Back Levee, Aug 1967, drawing file H-2-23908)

Figure 13-36. New Orleans East Basin, Pump Station 15 on the North Bank GIWW. Failed sheetpile between B/L Sta 874+40 and Sta 875+60 (N.O. East Back Levee). Pre-Katrina elevations ranged from 17.5 to 19.5 ft in this reach
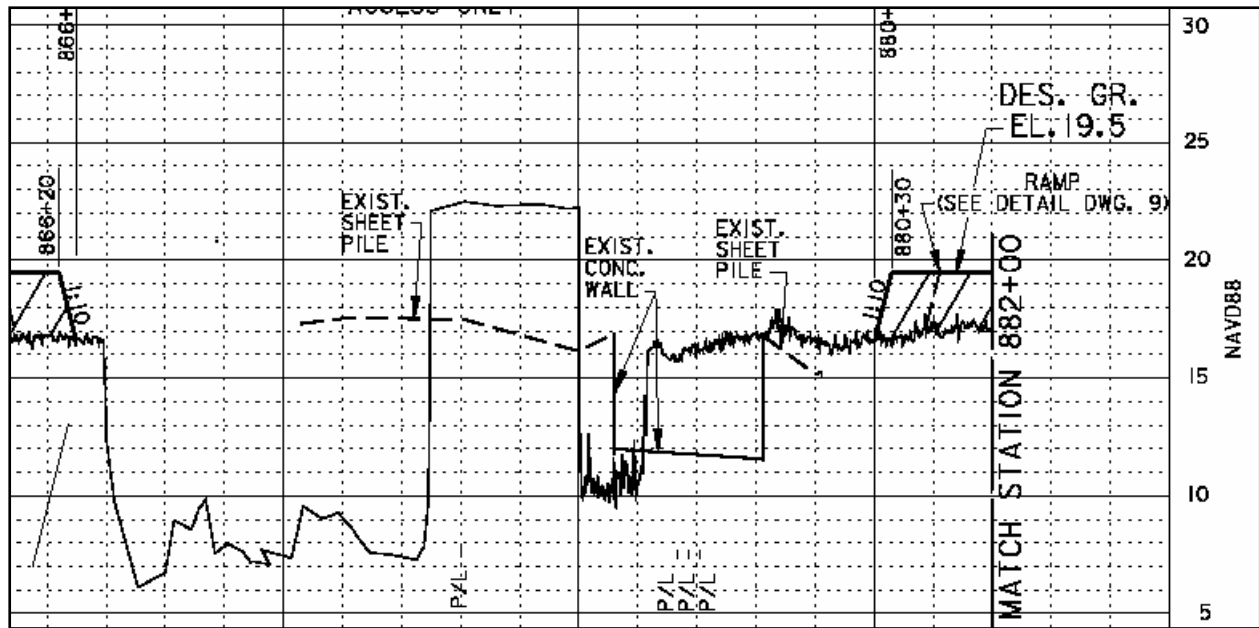
Figure 13-37. Plan and Post-Damage Scour Profile Immediately West of Pump Station 15 (from Contract Solicitation NOE1 drawing H-8-45594, sheet 3 of 16)
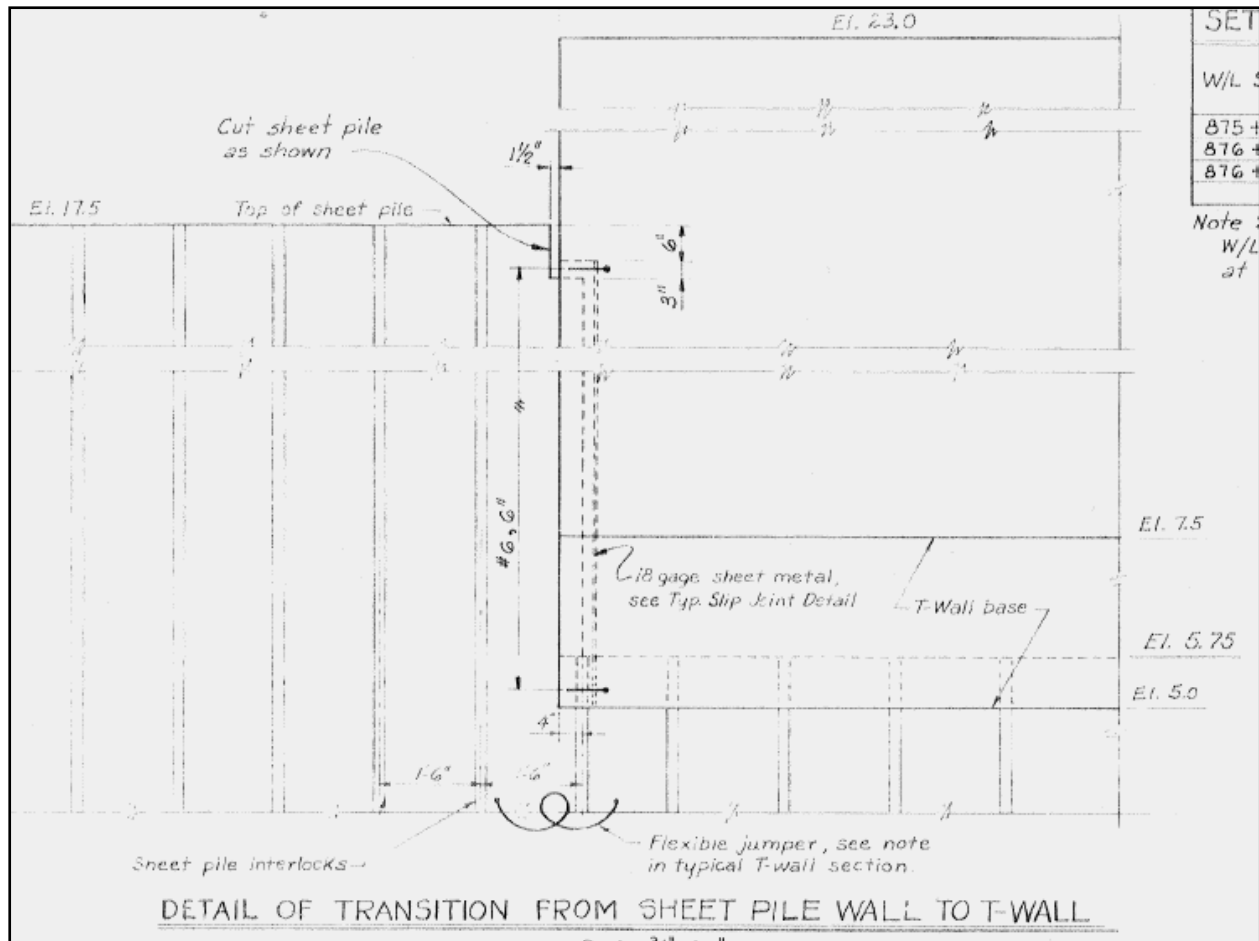
Figure 13-38. Pump Station 15 Top Elevation Difference of 5.5' Between Sheet Pile and T-Wall (plate 14 of 16 from Contract DACW29-77-C-0037, Mod P00001). If pre-Katrina sheetpile elevation was 17.5 ft and storm surge in the MRGO/GIWW was up to 18 ft, then there was minimal overtopping, and the sheetpile breach may have had contributing factors other than overtopping scour

Volume V The Performance – Levees and Floodwalls – Technical Appendix   V-13-35

This is a preliminary report subject to revision; it does not contain final conclusions of the United States Army Corps of Engineers.
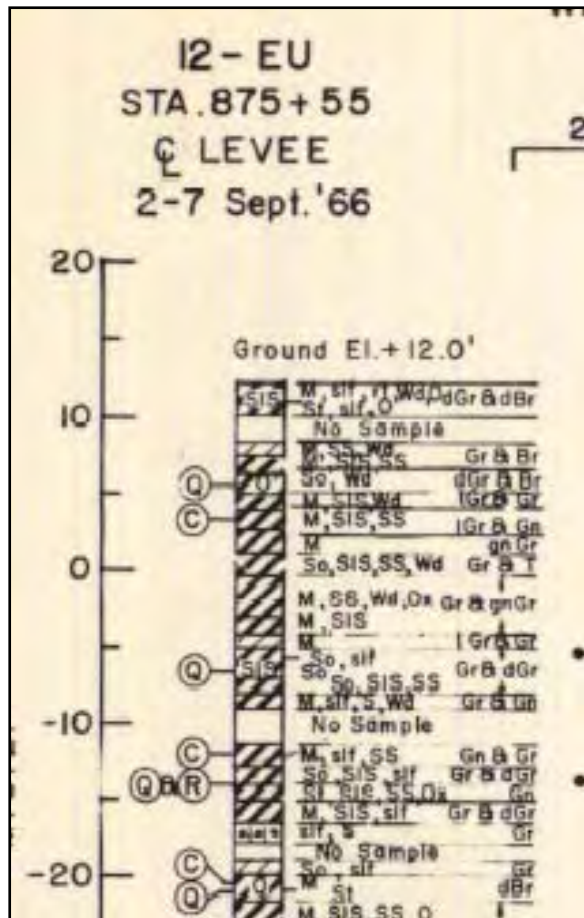
Figure 13-39. Pump Station 15 Nearest Boring 12EU Shows Levee Crown Elevation at 12 ft (MSL) with Fat Clay / Sand / Silt Lenses Overlying Lean Clay (CL) in the Upper 5 ft (from drawing file H-2-24625, plate 3)

Several floodwall (I-wall) reaches were catastrophically breached along the 17th St. and London Ave. canals and the IHNC (east and west sides). It is likely that failure modes other than erosion may have played larger roles at those locations.

Earthen Levees

Soil material properties greatly influence erodibility and erosion progression rate during overtopping. Cohesive (silt and clay) soils erode due to the formation and migration of a headcut perpendicular to the levee axis (i.e. across the levee section from the backside to the floodside). A headcut is a vertical or near-vertical elevation drop, and migrates upstream due to hydraulic stresses at the overfall, base seepage, weathering, and gravity (Hanson et al 2001). Sandy (non-cohesive) soil erosion involves a sediment transport process as the material is removed in layers. Cohesive soil erosion rates are more strongly influenced by soil material properties such as water content, density, erodibility, shear strength, and compaction effort during construction. For example, it was found that only a 5-point (5%) decrease in compaction water content caused a 100-fold increase in the breach widening rate for clay soil (Hanson et al 2003).

Figure 13-40 shows a generalized cross sectional diagram of an overtopped levee (wave dynamics are not illustrated). The water crest height (y) and mean velocity (v) impart a shear stress (τ) on the backside levee surface having a slope gradient (S). The majority of levees have slope gradients of 1V:3H (S = 0.33) or 1V:4H (S = 0.25).
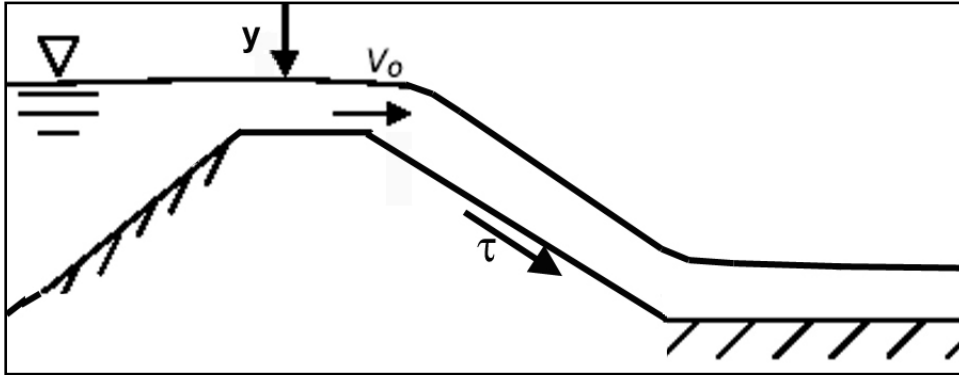
Figure 13-40. Conceptual Diagram of Water Surge (without waves) Overtopping an Earthen Levee

Overflow velocity and soil shear stress values may be estimated by making simple assumptions regarding the flow regime and using the following equations (Vennard and Street 1975). Assuming the Manning coefficient (n) for grassed levees is approximately 0.03, the friction factor (f) may be estimated as

$$f = 258 \, (0.03 \, / \, 1.49 \, y^{0.16})^2 \quad \text{where } y = \text{approximate overtopping crest depth, ft}$$

and

$$v = (258 \, / \, f)^{1/2} \, (Sy)^{1/2} \, , \text{ft/sec}$$

For example, the approximate friction factor and overtopping velocity on a 1V:3H grassed slope with crest height of 1 ft is:

$$f = 0.1$$

and

$$v = 29 \text{ ft/sec}$$

Soil shear stress (τ) is idealized by the equation

$$\tau = \gamma y S, \quad \text{where } \gamma = \text{unit weight of water}$$

For example, the idealized shear stress imposed by a water depth of 1 ft on a 1V:3H slope is:

$$\tau = \gamma y S = (63)(1)(0.33) = 21 \text{ psf}$$

These equations are listed only for the purpose of generally estimating the magnitudes of shear stress and overflow velocity for ideal flow. The actual shear stresses and overflow velocities were different due to numerous non-ideal variables (turbulence, non-uniform flow fields, and wave dynamics) present during the hurricane.
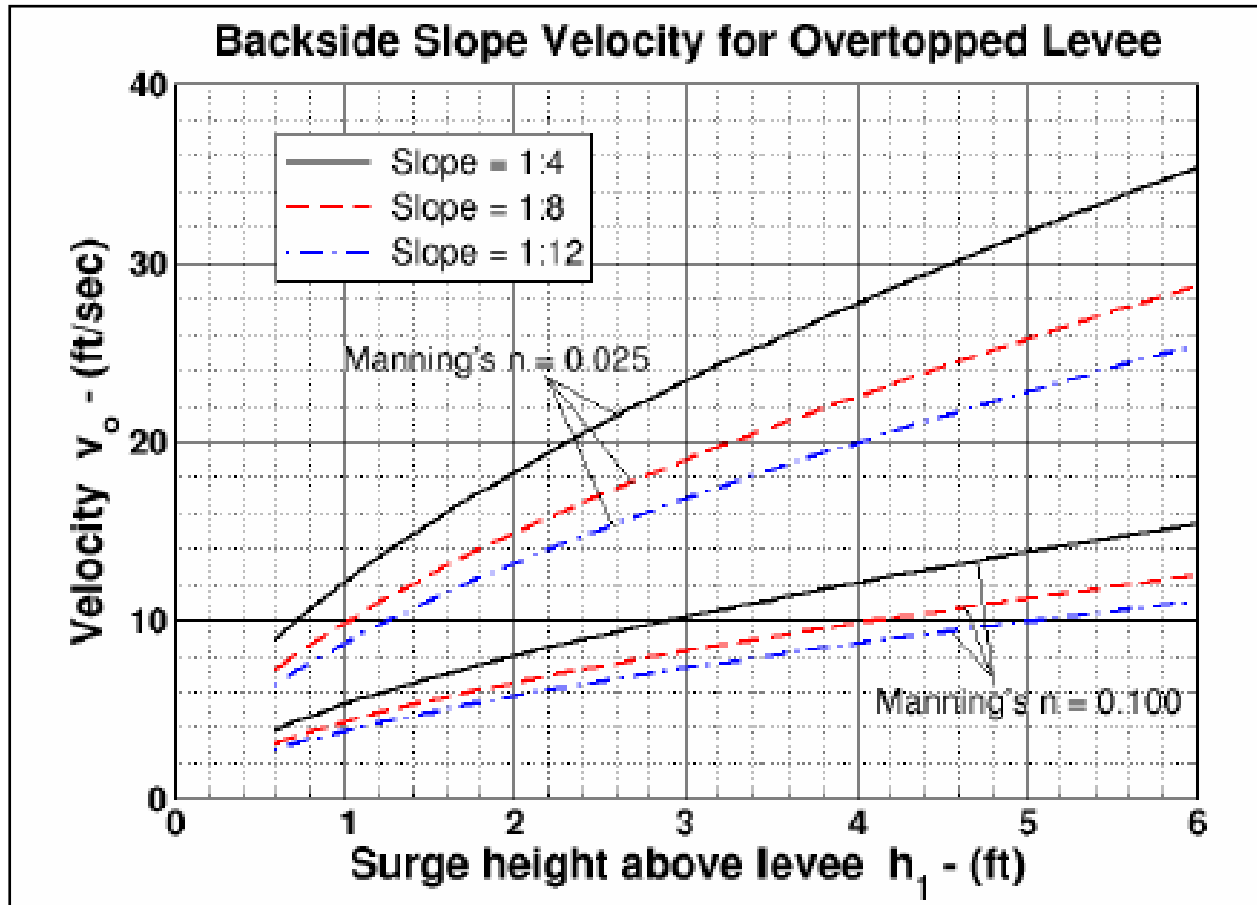
Figure 13-41. Overtopping Velocity as a Function of Surge Height (h_1 = y in above equations) (Hughes 2006)

Erosion pattern "B"

Initial overtopping causes surface sheet and rill erosion which develops into a series of cascading overfalls. The highest forces develop from the backside slope down to the backside toe, and the crown is not initially exposed to these large hydraulic forces. The cascading overfalls develop into one large headcut that migrates from the slope to the crest such that the erosion width approximately matches the overtopping width (Hanson et al 2001).

Figures 13-42 and 13-43 show examples of initial overtopping erosion on the Citrus Back Levee backside along the north bank of the GIWW in New Orleans East. The levee crown was elevation 14 to 15 ft and storm surge was 15 to 17 ft from the GIWW, so the overtopping crest

depth was approximately 1 to 2 ft. Approximate surge velocity down a 1:4 slope was 40 fps with shear stress 30 psf. Soil borings along this reach indicated non-homogeneity in the surficial layers of the levee crest and slopes, and cohesive soils with interbedded layers of silt and/or sand were typical.

Figure 13-42. Backside Levee Erosion Pattern "B" on the Citrus Back Levee, N.O. East

Figure 13-43. 600' Reach of Levee Along the North Bank of the GIWW (Citrus Back Levee, New Orleans East) Between Elaine Pump Station and Paris Road

Figure 13-44 shows a closeup of landside slope scour between the Highway 47 (Paris Rd) overpass and the Elaine Pump Station from the north bank of the GIWW protected side looking east (Citrus Back Levee, New Orleans East). Erosion damage measured 24' (length) x 13' (width) x 8" (depth). Note the headcut that developed up the slope toward the crest.

Figure 13-44. Closeup of Landside Slope Erosion at N 30deg 0 min 2.29sec W 89deg 58min 27.29sec

There is a possibility that the Figure 13-44 erosion was pre-Katrina, as seen in pre-Katrina satellite photo below (Figure 13-45).

Figure 13-45. Possible Pre-Existing Surface Erosion on Levee Slopes Along the North Bank of the GIWW (Citrus Back Levee) at N 30deg 0 min 7 sec W 89deg 58min 31 sec. (pre-Katrina image from GoogleEarth website). Possible erosion is evidenced by vegetation distress and bare spots along the levee

Figure 13-46 shows backside slope erosion and minor erosion on the stabilizing berm slope along the south bank GIWW levee between Sta. 65+008 and STA. 277+20 in St. Bernard Parish. The General Design section for the south bank GIWW indicated that the levee was built to approximate elevation +14 ft. circa 1970, and an additional lift up to elevation 19 was added circa 1985 (Figure 13-47). Post-Katrina LIDAR along the south bank GIWW shows the uneroded levee crown was up to approximate elevation 16 ft (Figures 13-48 and 13-49). Storm surge along the GIWW was approximately 15 to 17 ft, causing an estimated overtopping depth of approximately 1 to 2 ft and an approximate overtopping velocity of 40 fps. Drawing 9 of 19, New Orleans District file H-8-45533, shows several layers of hard lean clay (CL) at centerline top of levee (boring elevation 16.8 ft) from the 5/11/2000 soil boring 5A-CAU, B/L Sta 135+50 (Figure 13-51).

Figure 13-46. Scour on the Backside of the South Bank GIWW Levee Between STA. 65+008 and STA. 277+20, St. Bernard Parish, Minor Scour on the Protected Side Levee Transition Slope. The Paris Rd (I-510) high rise bridge is over approximate B/L Sta 270+00

Volume V The Performance – Levees and Floodwalls – Technical Appendix

V-13-43

This is a preliminary report subject to revision; it does not contain final conclusions of the United States Army Corps of Engineers.
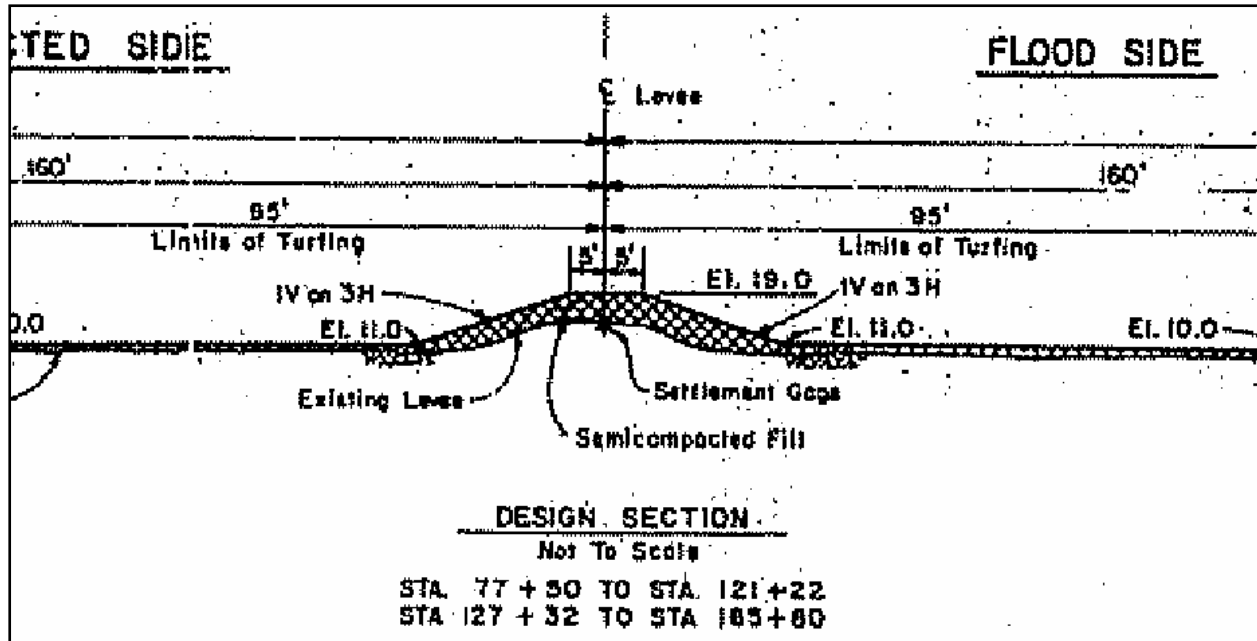
Figure 13-47. Design Section for South Bank GIWW Levee Enlargement in 1985. Levee was built to approximate elevation +14 ft. circa 1970. Additional lift up to elevation 19 was added circa 1985. Post-Katrina LIDAR along the south bank GIWW shows the unscoured levee crown was up to approximate elevation 16 ft. Storm surge along the GIWW was approximately 15 to 17 ft, causing an overtopping crest of 1 to 2 ft
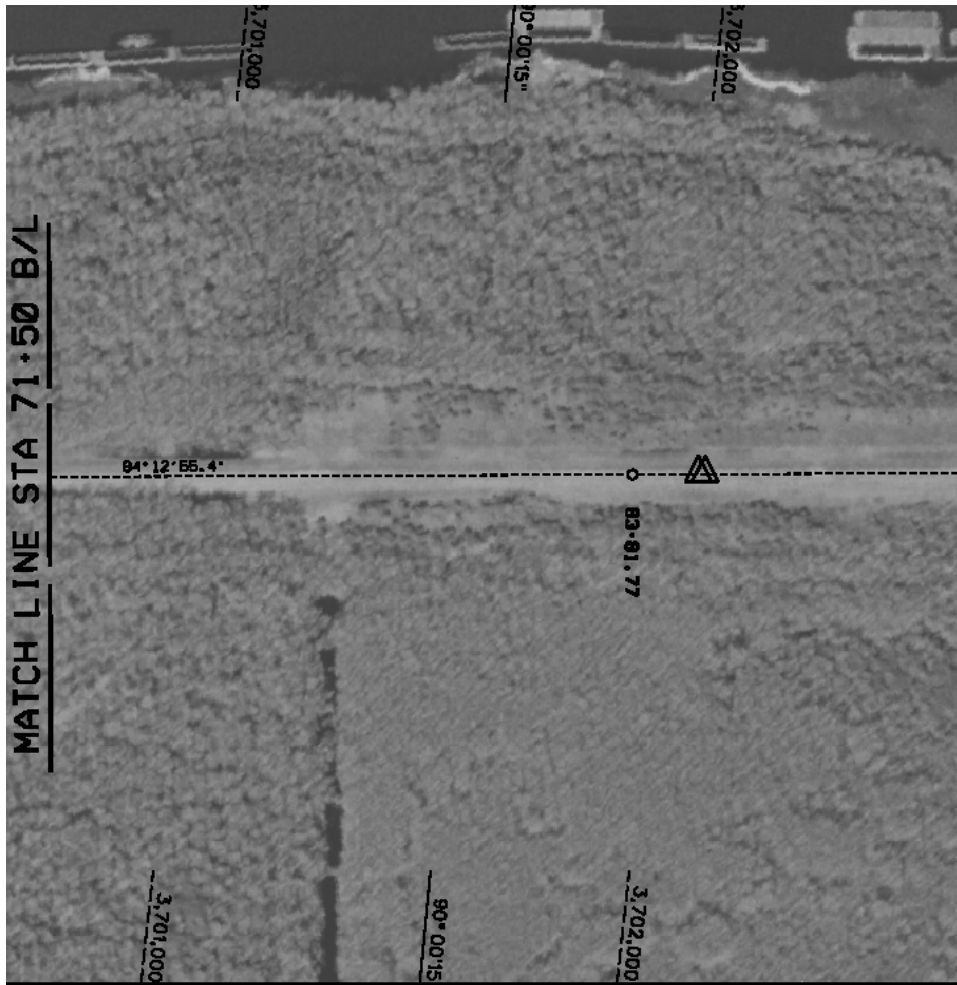
Figure 13-48. Scour Damage (Marked with Triangle) Identified East of B/L Sta 81+50 (from TFG Contract Solicitation W912PB-06-R-0022, drawing 3 of 12)
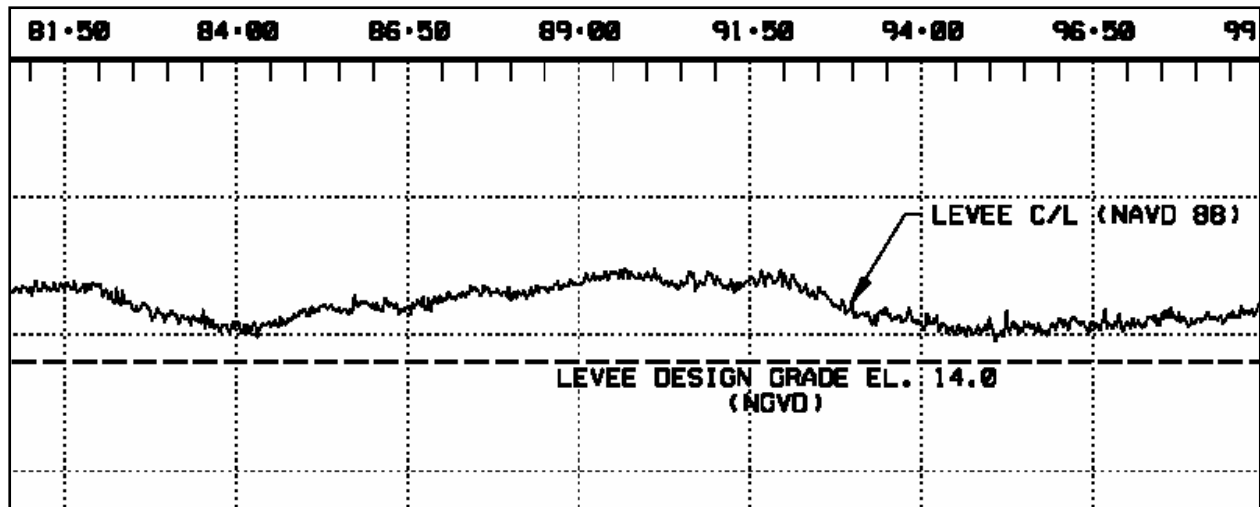
Figure 13-49. Levee Profile East of B/L Sta 81+50 (dwg 3 of 12). Note design grade elev 14 (NGVD) and lidar post-Katrina elev between 14 and 16 (NAVD 88). Also note crown grade change up to 2 ft along this 1750-ft reach
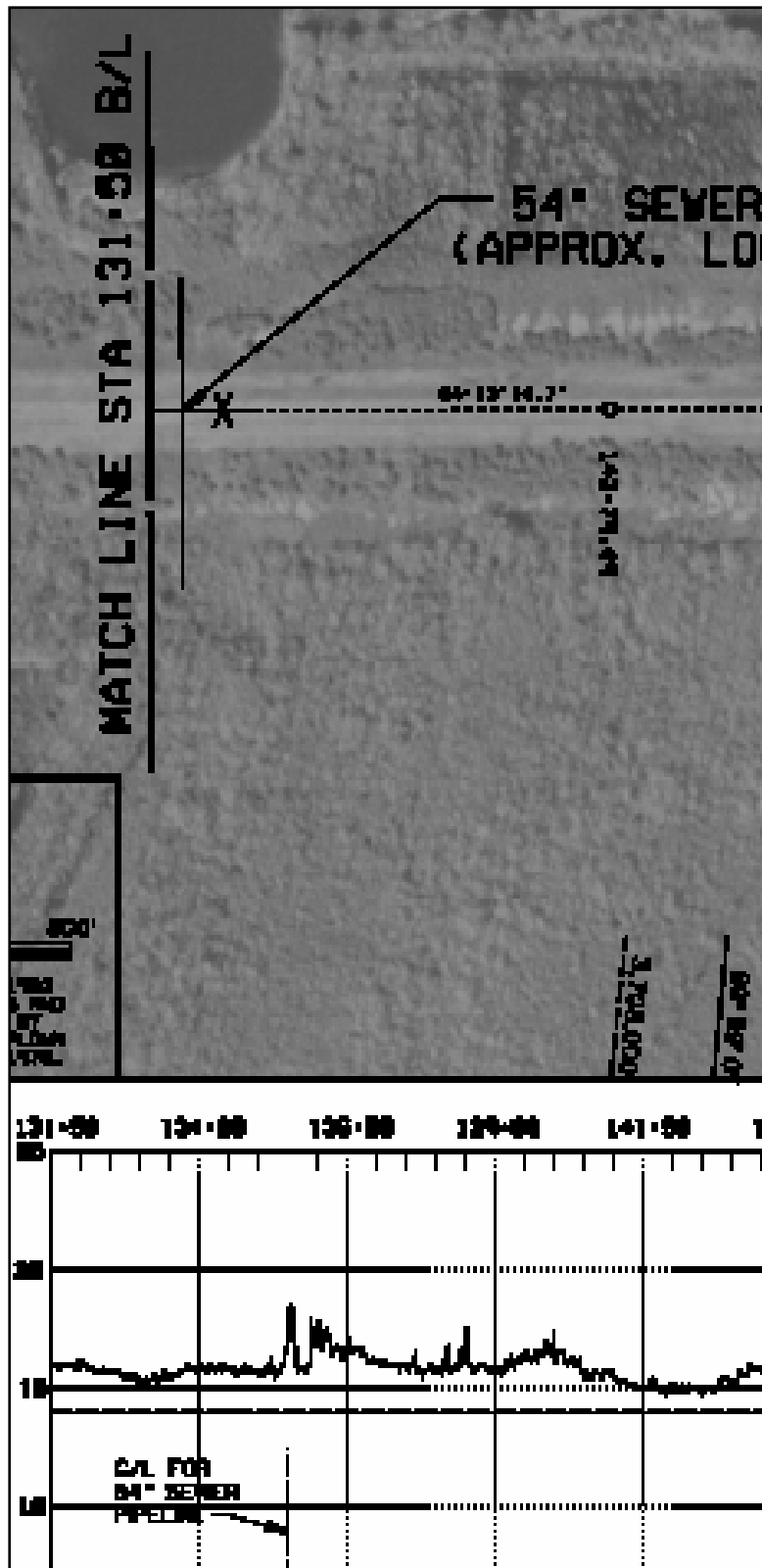
Figure 13-50. A Minor Scour Location on St. Bernard Parish South Bank GIWW Levee (marked with X) at B/L Sta 135+00 (from dwg 4 of 12, Contract Solicitation W912P8-06-R-0022)
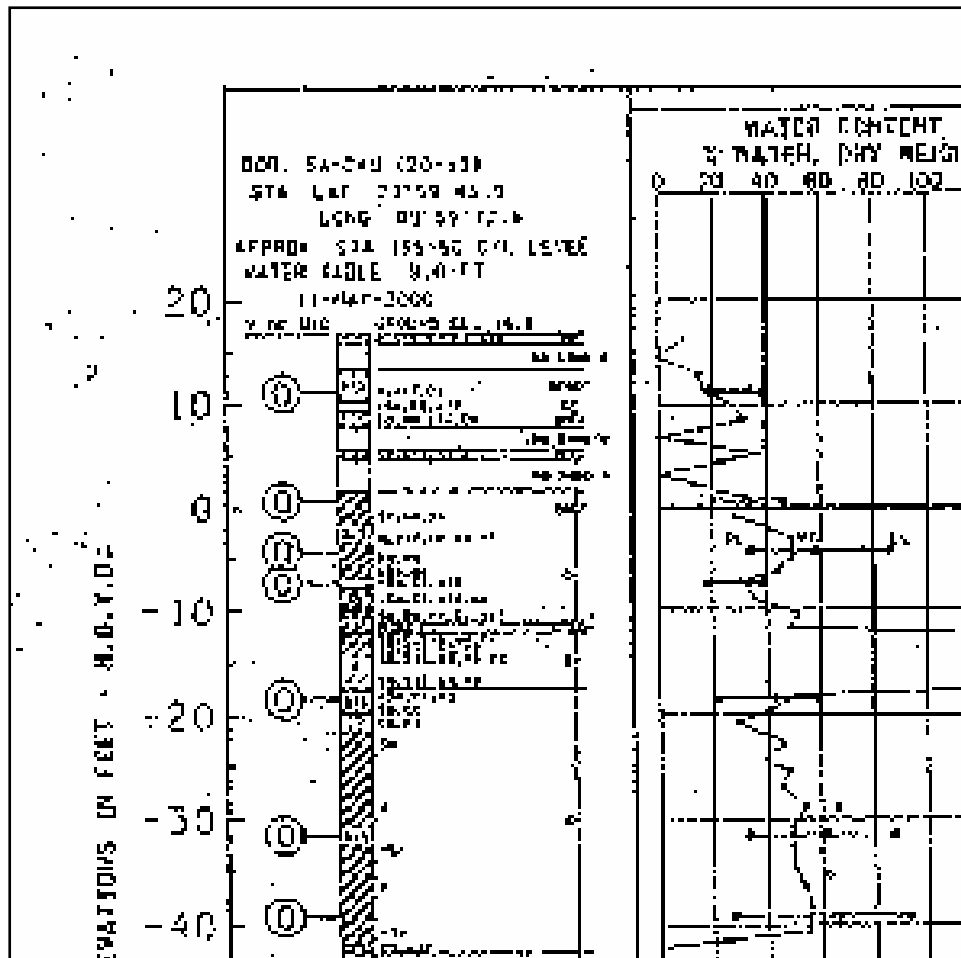
Figure 13-51. Dwg 9 of 19, New Orleans District file H-8-45533 Shows Several Layers of Hard Lean Clay (CL) at Centerline Top of Levee (boring elevation 16.8 ft) from the 5/11/2000 Soil Boring 5A-CAU, B/L Sta 135+50

Figure 13-52. New Orleans East Bank Lake Pontchartrain Floodwall Scour, 20ft long x 10ft wide x 2ft deep. GPS coords N90 deg 05min 17.3 sec, W30deg 01 min 39.3 sec

Erosion pattern "C". The headcut continues to migrate from the backside crest (crown) to the floodside crest.

Figure 13-53 shows a short levee section with progressive erosion on the west side of the IHNC protecting the container terminal between France Rd. and IHNC. The headcut extends to the top crest elevation, and was beginning to cut through the crown. Although the nearest historical boring pre-dates the levee (Figure 13-54), the unscoured soil surface appears to be a fat clay and the eroded soil visually appears to be a shell hash mixture of clay and oyster shell fragments.

Figure 13-53. Eroded Levee Crown on the IHNC West Side at Container Facility
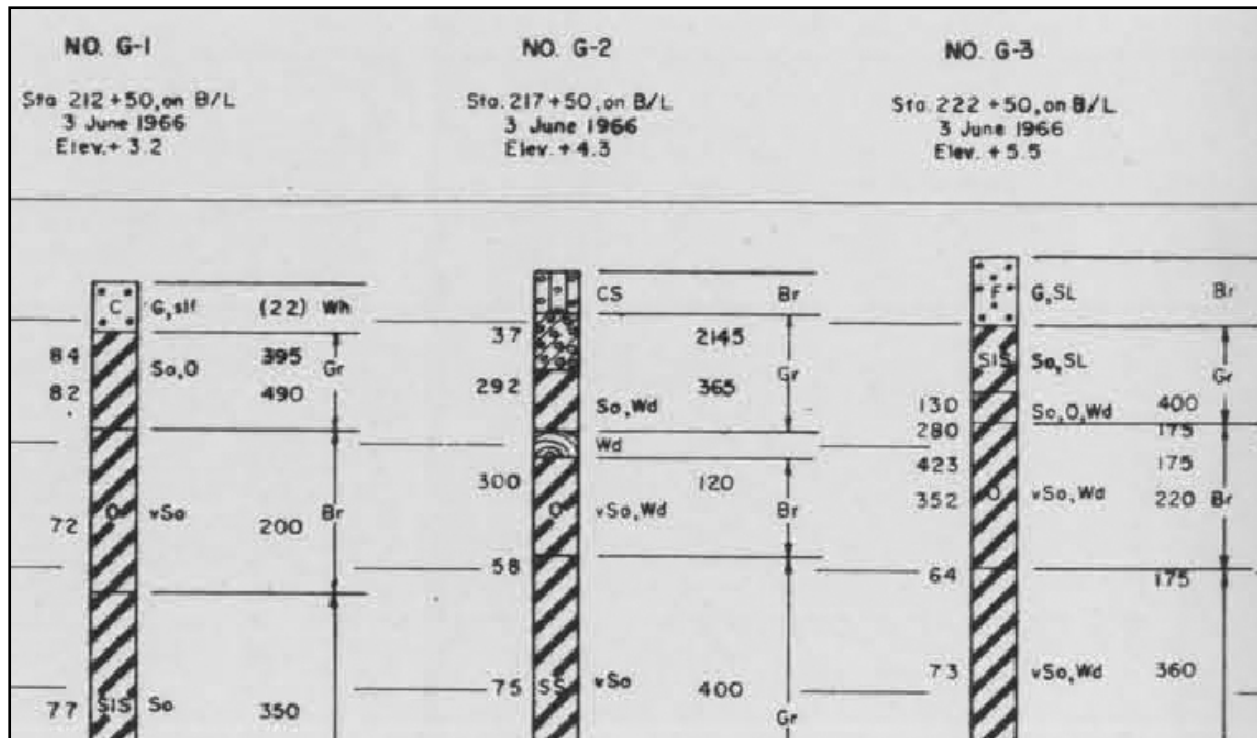
Figure 13-54. Nearest Boring, G-3, Shows Original Ground at Elev 5.5 ft is Sandy Soil

Volume V The Performance – Levees and Floodwalls – Technical Appendix V-13-51

This is a preliminary report subject to revision; it does not contain final conclusions of the United States Army Corps of Engineers.

Figure 13-55. Levee with Eroded Crown Between Bienvenue and Dupre Bayous, View South From Approximate B/L Sta 570+00. MRGO is to the Left of Photo

Soil boring 12BU-CHBD (01-16834) from 2001 at Sta 570+00 (Martello Castle) shows the top 1.4 ft of levee (elevation 16) was composed of lean clay (CL), with CH layers underneath. At a depth of 8.5 ft below the crown, a shear Q test indicated cohesion value 270 psf at 51% water content and 68 pcf dry density in a CH layer. At a depth of 16.8 ft, cohesion was slightly higher (396 psf) at 62% water content and 62 pcf dry density, also in a CH layer.

Erosion pattern "D". The crest drops as a breach begins to develop.

Figures 13-56 through 13-58 show progressive crown scour along approximate B/L Sta 1203+00 to Sta 1230+00 on the St. Bernard levee between the MRGO and the Mississippi River. Crown elevation was approximately 15 ft, but dropped to about 12 ft for about a mile in this eroded section. The levee along this reach was constructed of Mississippi River hydraulic sand fill, capped with local borrow material fat clay intebedded with silt and/or sand lenses, and shaped to grade with Mississippi River batture soil (truck-hauled fill). Similar to other levee's construction materials and history, this section contains heterogeneous soil layering probably compacted to different densities over a half-century or so timeframe.

Figure 13-56. Crown Scour Along Approximate B/L Sta 1203+00 to Sta 1230+00, St. Bernard Levee Between MRGO and Miss. River. Crown was Approximate Elevation 15 ft

This is a preliminary report subject to revision; it does not contain final conclusions of the United States Army Corps of Engineers.
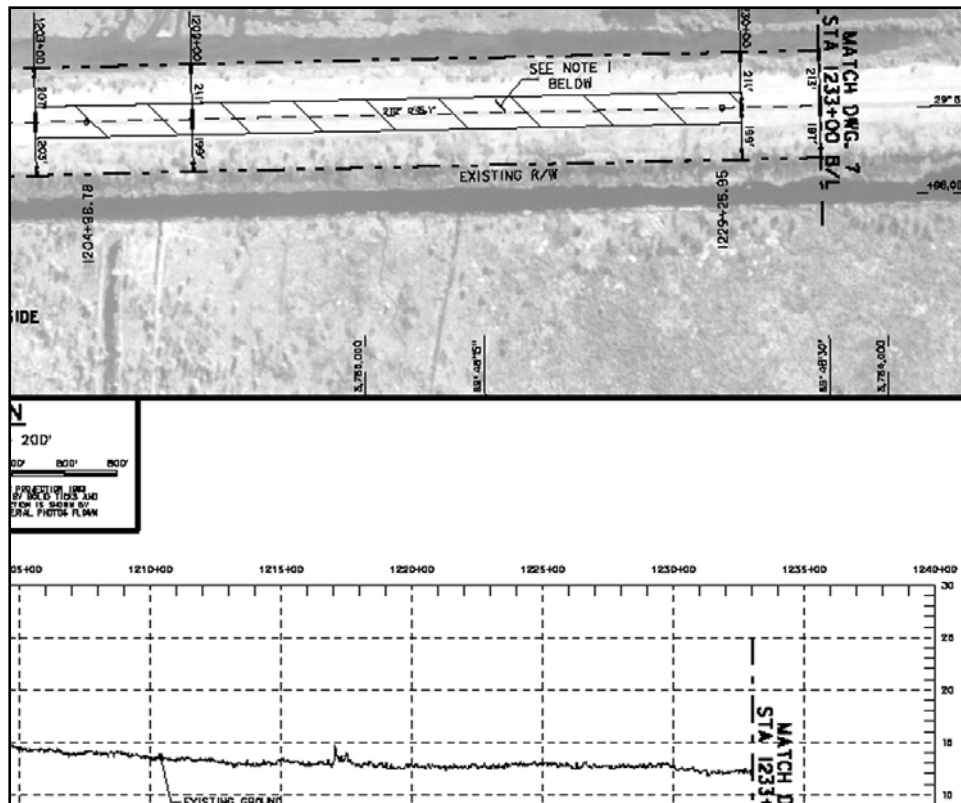
Figure 13-57. Levee Crown Elevation Drops from Elev 15 ft to Elev 12 ft in the Scour Area. Elevation 12 ft remains fairly constant along the reach for about a mile beyond the scour section. From Contract Solicitation STB08 W912P8-06-R-0094, drawing sheet C-06
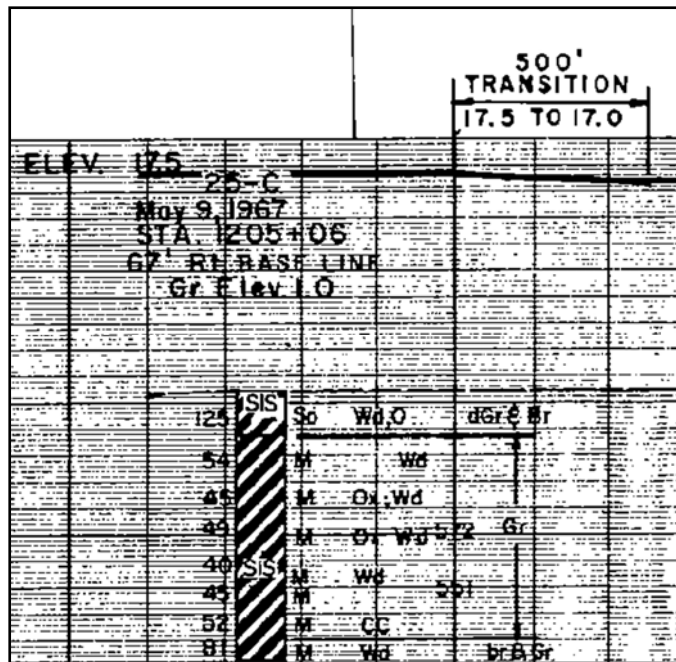
Figure 13-58. Original 1967 Boring at Ground Elevation 1 ft shows Fat Clay With Silt / Sand Lenses (from DM3 Chalmette Extension drawing file H-2- 24306, plate 7). The levee along this reach was constructed of Miss. River hydraulic sand fill, capped with local borrow clay, and shaped to grade with Miss. River batture soil (truck-hauled fill)

Figure 13-59 shows a section of Plaquemines Parish east bank back levee along Reach C (Phoenix to Bohemia, between river miles 59.3 and 44.3). Approximately 3 miles of crown erosion were noted along this 16-mile reach. This levee is approximate elevation 17 ft, and consists of a hydraulic-filled sand core with trucked-in clay blanket cap. Note the erosion has cut through the clay cap, moving clay blocks as erosion progressed downward to the sand layer.

Volume V The Performance – Levees and Floodwalls – Technical Appendix

V-13-55

This is a preliminary report subject to revision; it does not contain final conclusions of the United States Army Corps of Engineers.

Figure 13-59. Plaquemines Parish East Bank Back Levee Erosion

Erosion pattern "E". The breach opening erodes out to the toe and the breach widens.

Figure 13-60. East of Pump Station 15 (N.O. East Back Levee), North Bank of GIWW. 12,750 feet of levee east of Pump Station #15 was completely degraded (Station 876+87 B/L to 1101+90 B/L). West of the pump station, 9,800 feet of levee was completely degraded (approx Sta 778+00 to 876+00). The levees in these reaches were constructed from GIWW hydraulic fill in stages over three years
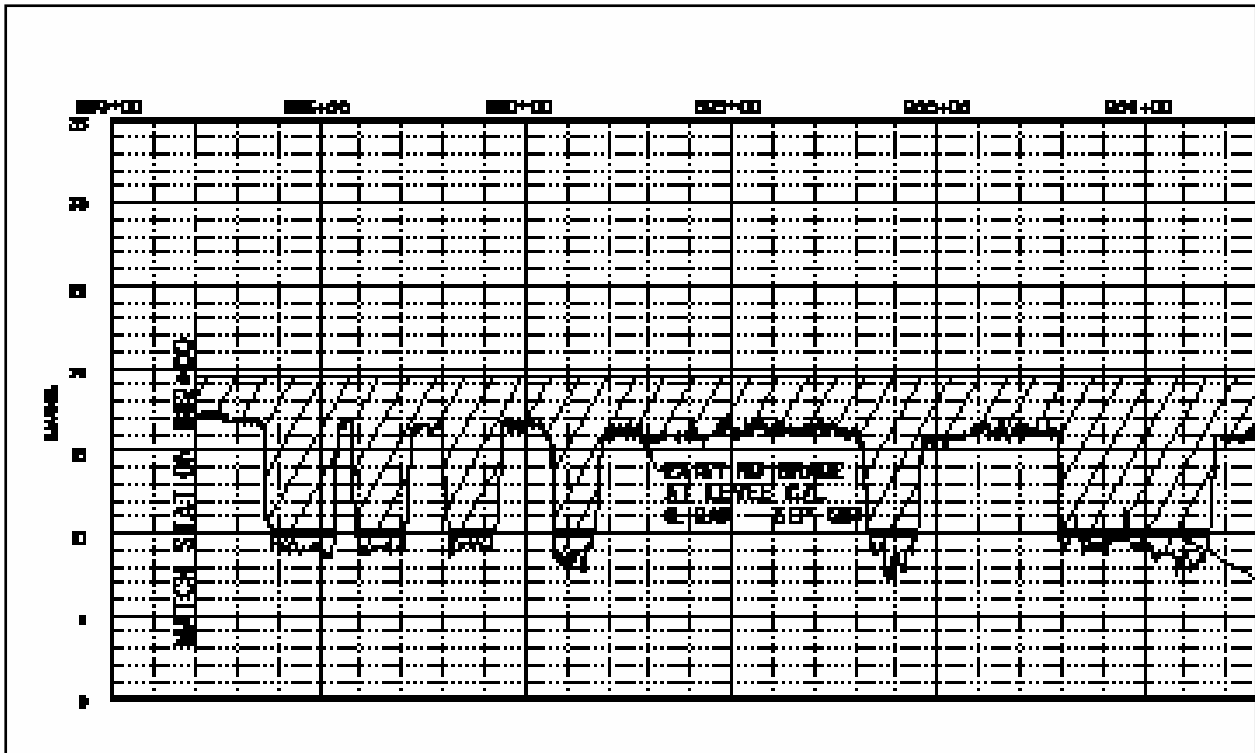
Figure 13-61. LIDAR Profiles of Levee East of Pump Sta 15 (from Contract Solicitation NOE1 drawings)

Figure 13-62. Partial Breach East of Pump Station 15

Figure 13-63. 19,000 ft. of Levee Between Bayou Bienvenue (Sta 383+00) and Bayou Dupre (Sta 704+00) Lost Approximately 12' of Levee Height From Original (design) Height 17.5 ft. Pre-Katrina elevation was approximately 12 ft, and storm surge along the MRGO was approximately 18 ft, causing an overtopping crest of up to 6 ft

Figure 13-64. 2,300 ft. of Levee Between Bayou Bienvenue (Sta 383+00) and Bayou Dupre (Sta 704+00) That Only Lost 50% of Height

Hydraulic fill from the MRGO channel formed the levee between Bienvenue and Dupre. Soil boring 9BU-CHBD (01-16834) from 2001 at Sta 445+00 shows the top 1.5 ft of the levee (elevation 18.1 ft) was composed of lean clay (CL). The underlying layers are mostly fat clay (CH) with interbedded lean clay layers. At a depth of 9.7 ft below the crown, a shear Q test indicated cohesion value 238 psf at 32% water content and 88 pcf dry density in a CH layer.

Soil boring 11BU-CHBD (01-16834) from 2001 at Sta 509+00 shows the top 2 ft of levee (elevation 17.4) was composed of fat clay (CH), but there was a 1-ft thick layer of poorly graded sand (SP) underneath. At a depth of 15.4 ft below the crown, a shear Q test indicated cohesion value 238 psf at 56% water content and 64 pcf dry density in a CH layer.

Soil boring 12BU-CHBD (01-16834) from 2001 at Sta 570+00 (Martello Castle) shows the top 1.4 ft of levee (elevation 16) was composed of lean clay (CL), with CH layers underneath. At a depth of 8.5 ft below the crown, a shear Q test indicated cohesion value 270 psf at 51% water content and 68 pcf dry density in a CH layer. At a depth of 16.8 ft, cohesion was slightly higher (396 psf) at 62% water content and 62 pcf dry density, also in a CH layer.

Soil boring 18-UBD (91-02) from 1991 at B/L Sta 596+00 shows the top 5.8 ft of levee (elevation 14.4) was composed of sandy silt (SM), with CH layers underneath. At a depth of 12 ft below the crown, a shear Q test indicated cohesion value 396 psf at 27% water content and 95 pcf dry density in a CL layer.

Soil boring 13BU-CHBD (01-16834) from 2001 at Sta 614+00 (Martello Castle) shows the top 25 ft of levee (elevation 15.4) was composed of fat clay (CH), with organic clays and peats underneath. At a depth of 5 ft below the crown, a shear Q test indicated cohesion value 632 psf at 29% water content and 92 pcf dry density in the CH layer.

Soil boring 19-UBD (91-02) from 1991 at Sta 640+00 shows the top 3 ft of levee (elevation 18.6) was composed of sandy silt (SM), with fat clay layers underneath. At a depth of 8 ft below the crown, a shear Q test indicated cohesion value 254 psf at 46% water content and 74 pcf dry density in a CH layer.

Figure 13-65. Wall / levee on the Southeast Side of Bayou Dupre Control Structure

Figure 13-66. 8,000 ft. Section of the Levee Immediately Southeast of Bayou Dupre (St. Bernard Parish) That Was Severely Damaged and Not Only Lost Approximately 12 feet of Levee Height But Also Part of the Original Levee Foundation

The storm surge depth overtopping this section of levee (Figure 13-66) was approximately 6 ft. A nearby soil boring through the crown showed the top 3 ft consisted of lean clay (CL), fat clay (CH), silt (ML or MH), and intebedded lenses of silt and/or sand. Any of these soil materials may have contributed to erosion initiation and progression. It is interesting to note in this photo that large scour pools developed on the levee backside which could possibly indicate that slope failure occurred along semi-circular slip planes on the levee backside, and the weaker soil above the slip planes eroded concurrently with the breach erosion. In other words, there may have been a slope instability failure mode in addition to overtopping erosion.
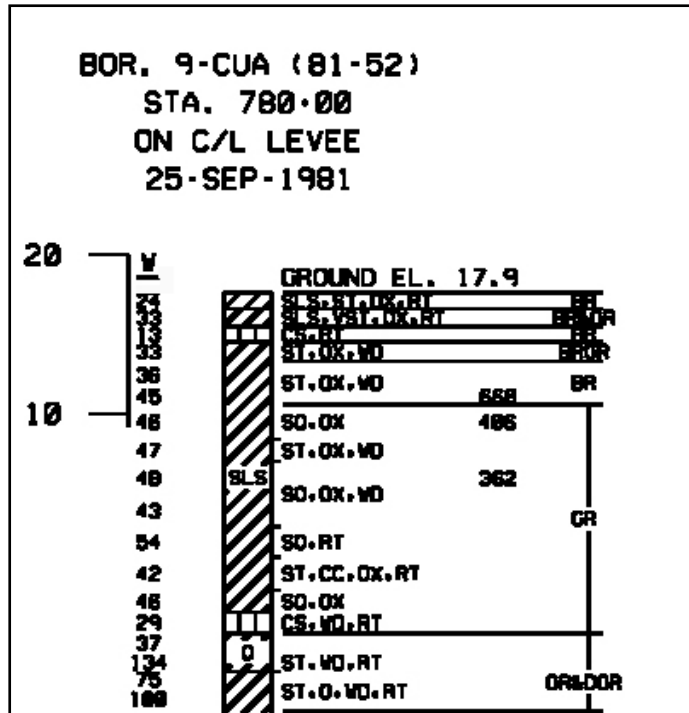
Figure 13-67. 1981 Soil Boring at Sta 780+00 Near Dupre Shows Top Layer of Lean Clay (CL) Underlain By Fat Clay (CH), Silt (ML or MH), and Silt / Sand Lenses (SLS) in the CH Material (from drawing 9 of 10, contract solicitation W912P8-06-R-0002)

Figure 13-68. 2,500 ft. of Levee Along MRGO from Bayou Dupre to STA 1007+91 That Lost
Approximately 8' of Elevation

Levee and Floodwall Transitions

Numerous transition breaches were observed post-Katrina, and they overtopped due to elevation differences. After overtopping, the soil either scoured on the backside of the vertical structure or eroded the levee. The overtopping erosion / scour followed the progressive stages for the levee and/or the impact scour pattern for the floodwall, both as described above. Figure 13-69 is a diagram of the flow patterns that develop as overtopping occurs. The backside has increased erosion due to local increases in overtopping velocity, especially if the levee crest is lower than the floodwall. As the overtopping height increases above the floodwall height, backside erosion develops along the floodwall.
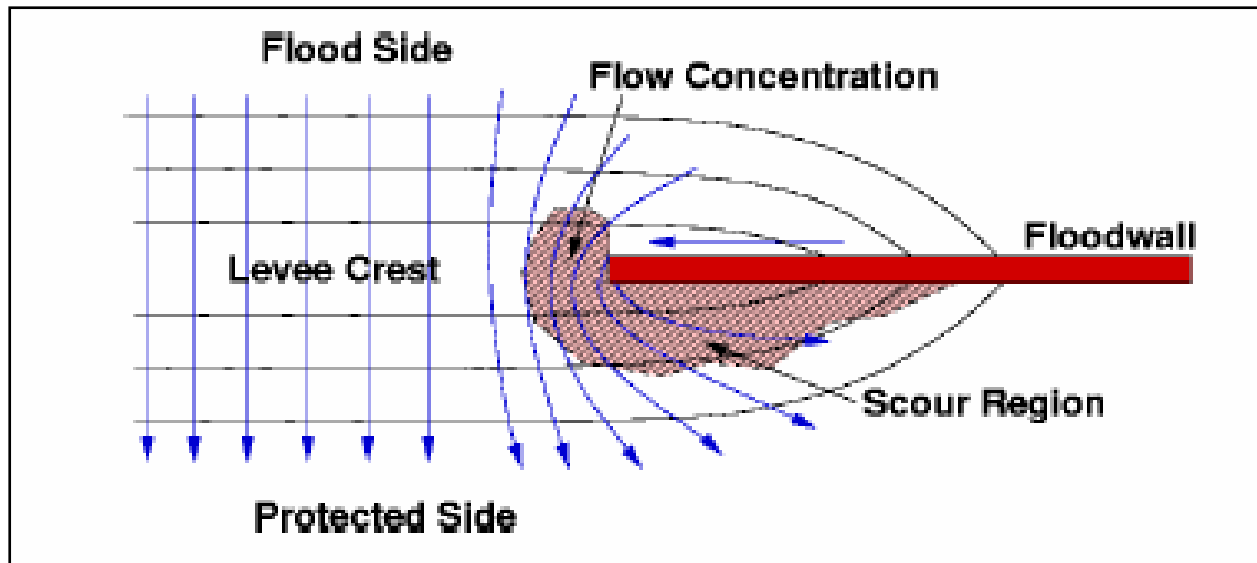
Figure 13-69. Diagram of Overtopping Erosion at Levee - Floodwall Transition (from Hughes 2006)

Figure 13-70 shows non-breaching scour caused by overtopping behind the concrete floodwall at closure gates S2 and S3 on the east side of the IHNC. Although the earthen levee abuts the concrete wall, the majority of scour occurred behind the concrete wall. Figure 13-71 depicts the scour pattern that developed along the levee slope behind the wall instead of the levee slope on the abutting earthen levee.

Figure 13-70. Southern Scrap Facility Gates S2 and S3
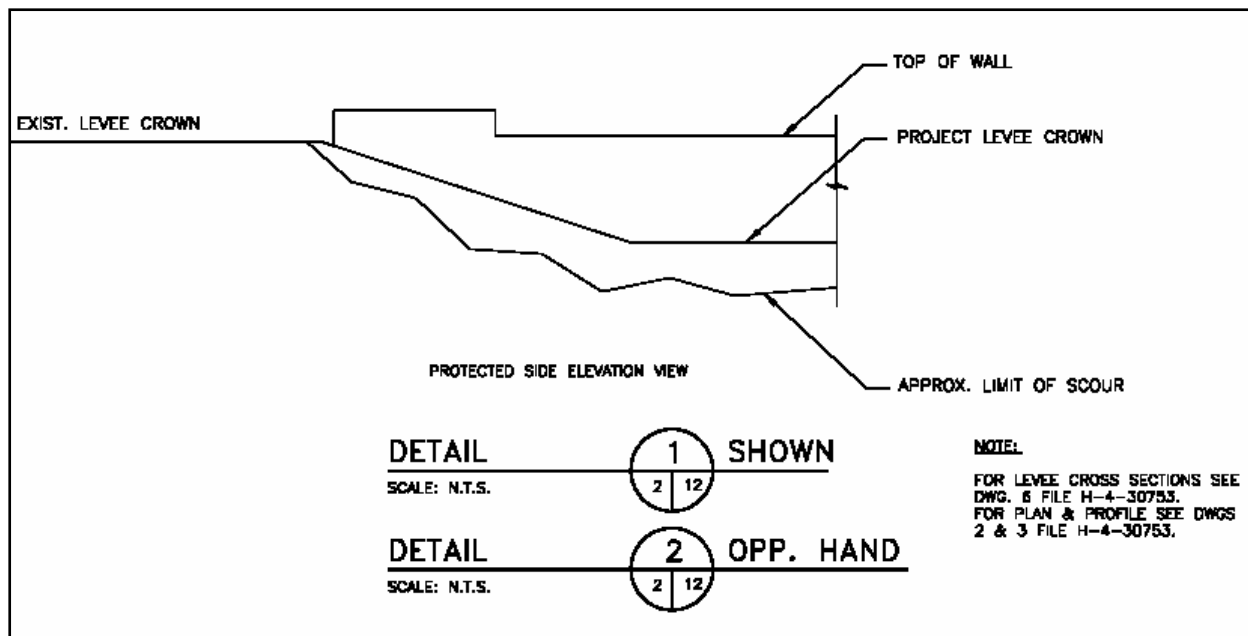
Figure 13-71. S2/S3 Erosion Pattern (From Levee Restoration, Misc. Gates and Floodwall Repairs, IHNC to Bienvenue, Chalmette Area Plan Emergency Restoration solicitation W912P8-06-R-0022, October 2005 contract drawing H-8)
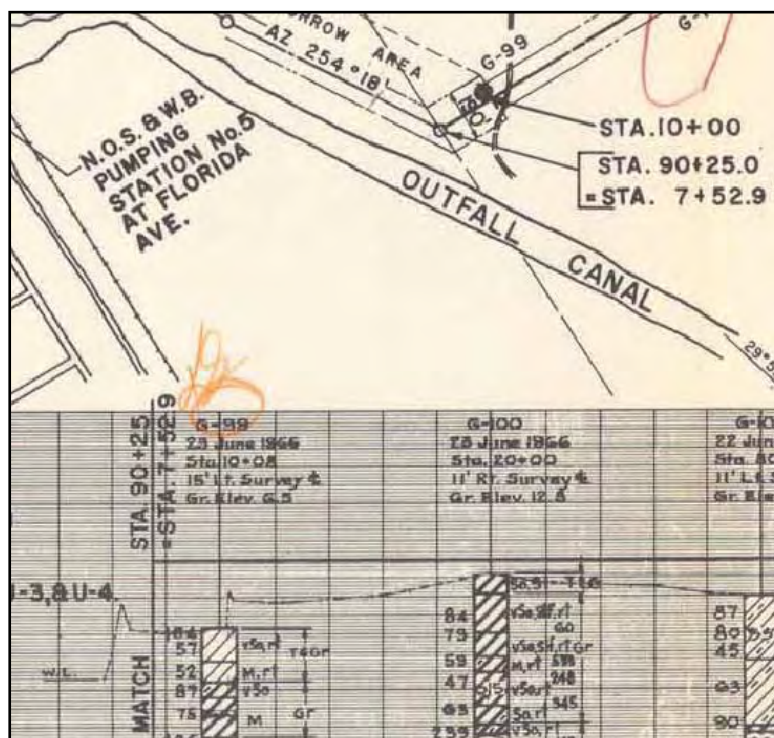
Figure 13-72. Boring G-99 Near Future Gates S2 and S3 Shows Lean Clay (CL) at Existing Ground Surface (Approximately 6' MSL). From plate 7, DM3

Figure 13-73 shows breached levee erosion at east end of floodgate structure S5, located about 100 yards west of the Bayou Bienvenue control structure. Although the levee was higher

This is a preliminary report subject to revision; it does not contain final conclusions of the United States Army Corps of Engineers.

than the wall (Figure 13-74) beyond the transition, it appears that the overtopping erosion began at the wall / levee transition where the wall was higher than the soil backfill.

Figure 13-73. Floodgate S5 Near Bienvenue Control Structure
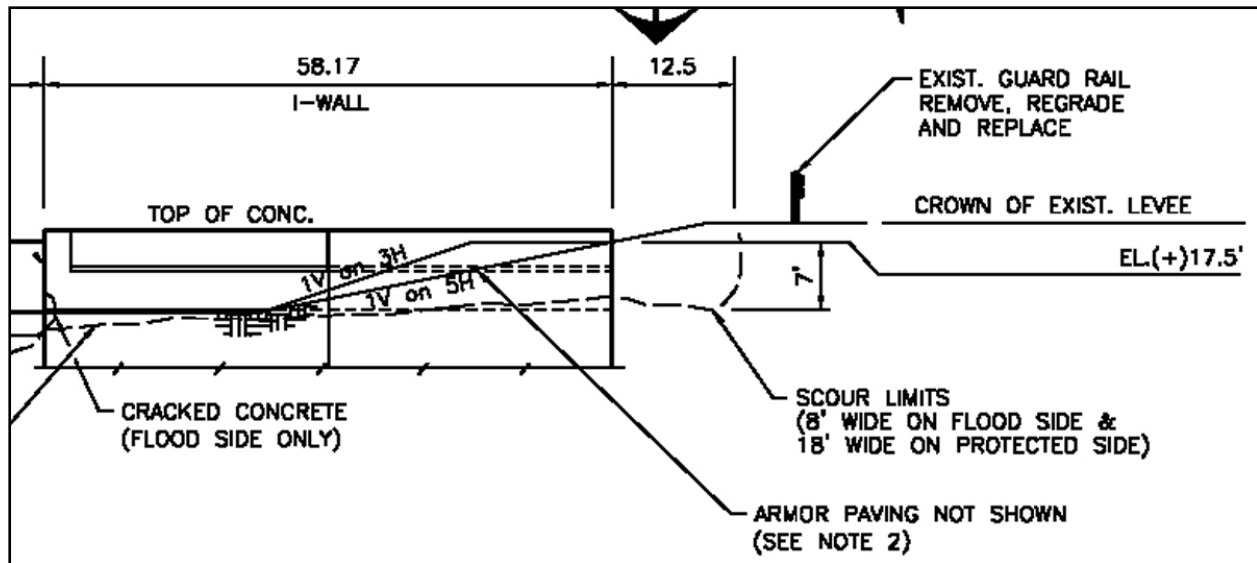
Figure 13-74. Scour pattern (From Levee Restoration, Misc. Gates and Floodwall Repairs, IHNC to Bienvenue, Chalmette Area Plan Emergency Restoration solicitation W912P8-06-R-0022, October 2005 contract drawing H-8)

Figure 13-75 shows an earthen levee breach at east side IHNC floodgate E5 looking south from inside the protected area. Scour damaged 7' (w) x 7' (d) around the adjacent flood wall. Top of wall at gate is approximate elevation 13 ft.

Figure 13-75. IHNC Floodgate E5 Transition to Levee

Figure 13-76. End of Sheetpile Wall at B/L Sta 980+58, Along the MRGO (St. Bernard Parish). Note that scour occurred along the sheetpile wall and minimally beyond the levee transition. Approximate sheetpile elevation was 17 ft and levee crown elevation was 13 ft. Beyond the transition, the levee crown elevation was approximately 17 ft. The approximate storm surge overtopping crest was 4 ft over the sheetpile and 1 ft over the transition levee

Pre-Katrina soil boring 10-CUHA (91-02) from 1991 at Sta 976+00 in the sheetpile reach shows the top 4 ft of levee (elevation 13) was composed of lean silt and clay (ML and CL) with CH layers underneath. At a depth of 4.6 ft below the crown, a shear Q test indicated cohesion value 770 psf at 45% water content and 75 pcf dry density in the uppermost CH layer.
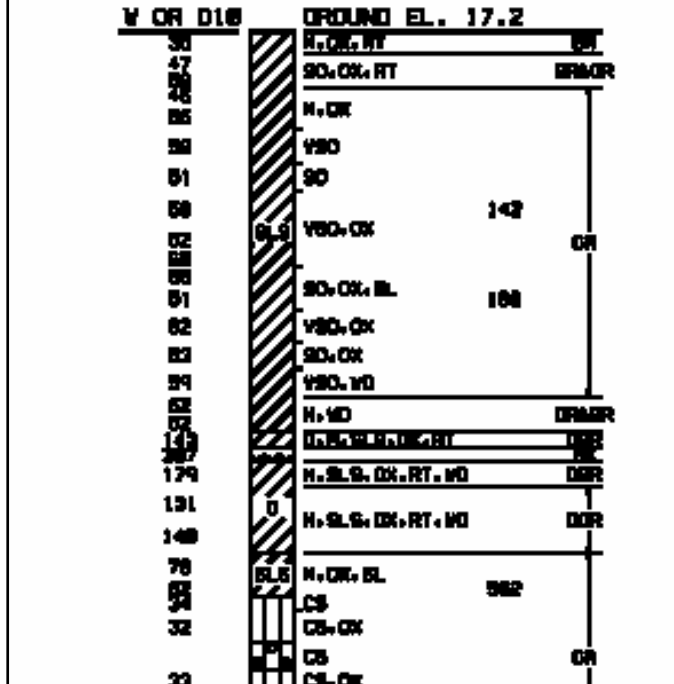
Figure 13-77. Pre-Katrina (1985) Boring at Sta 989+00 (about 800 ft beyond the sheetpile/levee transition) Shows Levee Section With Fat Clay (CH) Cap and Core, With Interbedded Silt Lenses (SLS)

Volume V The Performance – Levees and Floodwalls – Technical Appendix

V-13-73

This is a preliminary report subject to revision; it does not contain final conclusions of the United States Army Corps of Engineers.
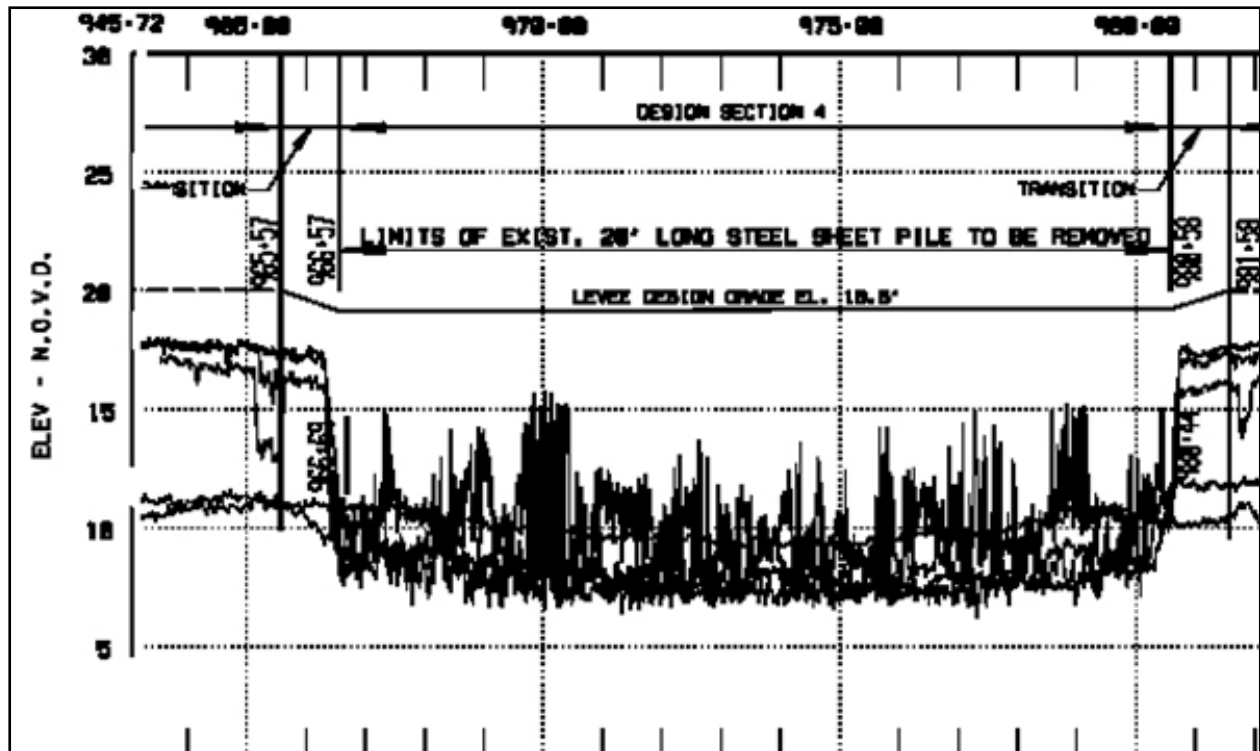
Figure 13-78. Scour Depths Along Sheetpile and at Transition to Levee. Note that scour occurred along the sheetpile reach, not at the sheetpile / levee transition (also seen in Figure 13-76), from drawing 7 of 10, contract solicitation W912P8-06-R-0002

Figure 13-79 shows the I-wall/levee transition on the east side of the IHNC at the IHNC Lock. In this case, the levee crest was about a foot lower than the I-wall top, and overtopping caused erosion and/or a scour hole on the backside. Visual observation indicates a non-cohesive surface soil type.

Figure 13-79. IHNC Lock I-wall transition to levee

Geotechnical Issues

A more erodible embankment will need a higher level of protection than a less erodible embankment to reduce or prevent backside overtopping erosion. Knowing the engineering properties of an existing embankment will help determine erodibility and allow better-informed choices for designing erosion protection. Many of the levee reaches have recently been freshly-capped with cohesive soils and compacted to specification for Katrina repair.

The rate of erosion is proportional to the applied shear stress in excess of a critical shear stress and is also proportional to an erodibility coefficient (Hanson and Simon 2001). Soils with a lower critical shear stress tend to have a higher erodibility coefficient. Levee geometry is important when analyzing erosion probability. A 1:3 side slope is steeper than a 1:4 slope, and a stabilizing berm slope acts as an overtopping energy dissipator. Water cascading down a 1:3 slope impacting a 1:20 berm slope would be more likely to initiate erosion than that on a 1:4 slope, and would also depend on slope distance between the crest and the toe, surface roughness, and water depth.

Assessing soil erodibility is a complex matter, due to spatial (horizontal and vertical) non-homogeneity and uncertainty, difficulty in selecting accurate engineering properties needed to determine erodibility, and temporal effects during erosion progression such as surface roughness changes which in turn affect the hydraulic stress and turbulence conditions. Soil properties affecting erodibility are soil classification (gravel, sand, silt, clay proportions); water content (antecedent moisture); clay mineralogy and proportion; soil structure; Atterberg limits; organic content; pore water chemistry (salinity, hardness, quality, pH); in-situ density; erodibility parameters such as the critical shear stress required to initiate soil particle detachment, hydraulic shear stress, and erodibility coefficient; in-situ shear strength, and compaction effort during construction (optimum moisture content and optimum dry density values both specified and as-built).

Answering the question of why one section of levee eroded compared to another section is difficult to do as the forensic evidence washed away during the hurricane. The pre-Katrina soil boring data (where available) was useful only for observing soil types, stratigraphy, and strength. Forensically assessing the erosion probability using the pre-Katrina soil parameters may be accomplished only in a general fashion. For example, the levees constructed of hydraulic fill along the MRGO seemed to have higher erodibility potential compared to the truck-hauled fill between the MRGO and the Mississippi River. The levees constructed with lower-plasticity (sandy or silty) surface soils instead of fat clay also appeared to have more erosion. Levees with "semicompacted" fill likely faired better than those with hydraulic fill (noncompacted).

Summary

Most erosion appeared to have occurred on the backside (landside or protected side) of both levees and floodwalls. The minor erosion / scour patterns (A and B) were the most geographically widespread. The most serious patterns (D and E) were confined to lengthy levee reaches generally located along the East Back Levee (N.O. East) and the south bank of the MRGO (Bayou Bienvenue to Bayou Dupre and southeast of Bayou Dupre). The most serious floodwall backside erosion (patterns D and E) were confined to specific relatively short reaches along the IHNC (east and west sides) and the north bank of the GIWW (East Back and Citrus Back). Localized scour contributing to failure was observed at several floodwall/levee transitions.

The environmental forcing conditions for erosion initiation (storm surge, wave height, wave period, wind velocity, etc.) are not described in the detail shown in other portions of the IPET tasks. Storm surge crest elevations are approximated for several reaches, and the overtopping waterfall heights are approximated based on available pre-Katrina levee/floodwall elevations presumably referenced to local mean sea level datum. Overtopping crest heights ranged up to about 6 ft along MRGO reaches, and waterfall cascades impacting the soil surface ranged from 1ft to about 13 ft, depending on exposed floodwall height. The most common cascade height was about 6 ft.

Erosion was initiated on soil surfaces ranging from sandy silts to fat clays, and only a limited amount of pre-Katrina soil borings were available at the eroded locations. In general, the eroded

soil surface contained sand / silt / lean clay layers, which are known to be more erodible than compacted fat clay generally specified as a levee "cap". Many of the end-of-erosion (post-Katrina) pictures showed an exposed layer of fat clay mixed with oyster shells, which is presumed to be less erodible than the missing soil.

References

Hanson, G.J., K.R. Cook, W. Hahn, and S.L. Britton. 2003. "Evaluating erosion widening and headcut migration rates for embankment overtopping tests," American Society of Agricultural Engineers Paper no. 032067.

Hanson, G.J. and A. Simon. 2001. "Erodibility of cohesive streambeds in the loess area of the midwestern USA," *Hydrological Processes*, Vol 15, pp 23 - 38.

Hanson, G.J., K.M. Robinson, and K.R. Cook. 2001. "Prediction of headcut migration using a deterministic approach," *Transactions of the American Society of Agricultural Engineers*, Vol 44(3), pp 525 - 531.

Hughes, S.A. 2006. "Protection for backside levee slopes," draft report to the New Orleans District Corps of Engineers.

Hunt, S.L., G.J. Hanson, K.R. Cook, and K.C. Kadavy. 2005. "Breach widening observations from earthen embankment tests," *Transactions of the American Society of Agricultural Engineers*, Vol 48(3), pp 1115 - 1120.

Venard, J.K. and R.L. Street. 1975. *Elementary fluid mechanics*, 5th Ed., John Wiley and Sons, New York.

Scour Damage Tabulations (from TFG Damage Reports and Restoration Contract Drawings)

DSR ID #	Type of Structure		Degrees (N)	'	"	Degrees (W)	'	"	Length	Depth	Width	Cu-yd to fill	Scour Damage Class	Type	Description

Inner Harbor Navigation Canal - West Levee
Summary of Damages

DSR ID #	Type of Structure		GPS Coordinates Degrees (N)	'	"	Degrees (W)	'	"	Scour Dimensions (Feet) Length	Depth	Width	Cu-yd to fill	Scour Damage Class	Condition of Floodwall Type	Description
Lock to Florida Avenue (West side)															
W-1	Levee with I-wall (capped)	Start/End	29	57	59.3	90	1	37.2	20				II	I-Wall	Scour adjacent to wall
W-2	Gates W2, W3 (T-wall monoliths)	Start	29	58	65.3	90	1	37.5	500	3	15	833	I	T-Wall	Scour adjacent to wall
		End	29	58	8.9	90	1	36.1							
W-3	Gates W4, W5 (T-wall monoliths)	Start	29	58	8.9	90	1	36.1	700	3	15	1,167	I	Gate monolith	Scour adjacent to wall
		End	29	58	13.6	90	1	36.2							
W-4	Wall btwn Gates W5, W6 (T-wall monoliths)	Start	29	58	13.6	90	1	36.2	1,460	3	15	2,433	I	Gate monolith	Scour adjacent to wall
		End	29	58	27.9	90	1	31.8							
W-5	Wall between Gate W6 and Namasco Bldg to Gate W13 (T-wall, I-wall monoliths)	Start	29	58	27.9	90	1	31.8	1,330	3	5	739	I	Gate monoliths, T-wall, I-wall	Scour adjacent to wall
		End	29	58	38.6	90	1	34.8							
W-6	Wall btwn Gate W14 and Gate W15 (T-wall and I-wall monoliths)	Start	29	58	40.7	90	1	33.8	300	2	5	111	I	Gate monoliths, I-wall	Scour adjacent to wall
		End	29	58	43.4	90	1	33.1							
W-7	Gate W17	Start/End	29	58	48.6	90	1	32.7	30	1	3	3	I	Gate monoliths	Scour adjacent to wall
W-8	Gate W18 to Gate W19	Start	29	58	48.6	90	1	32.3	600	2	5	222	I	I-wall	Scour adjacent to wall
		End	29	58	49.0	90	1	31.2							
W-9	Gate W19 to Gate W20	Start	29	58	49.0	90	1	31.2	200	4	5	148	I	I-wall	Scour adjacent to wall
		End	29	58	50.7	90	1	25.4							
W-10	Gate W20 to Gate W22 (adjacent to PS#19)	Start	29	58	50.7	90	1	25.4	200	2	5	74	I	I-wall	Scour adjacent to wall
		End	29	58	53.0	90	1	22.8							
Florida Avenue to Hwy 90 (West side)															
W-11	Gate W23	Start/End	29	58	56.2	90	1	27.9	30	4	15	67	II	T-wall	Scour adjacent to wall
W-12	Gate W2 to W3	Start	29	58	56.5	90	1	22.5	300	3	5	167	I	I-wall	Scour adjacent to wall
		End	29	59	4.0	90	1	19.9							
W-13	Levee	Start	29	59	4.7	90	1	23.4	150	Scour repaired			II		Scour repaired w/ aggregate
		End	29	59	4.8	90	1	25							
W-14	Gate W25B to Gate W26	Start	29	59	4.7	90	1	23.4	800	Scour repaired			III		Scour around gate W25B and on P/S of Gate W26
		End	29	59	8.0	90	1	38.2							
W-15	Gate W26 to Gate W28	Start	29	59	8.0	90	1	38.2	500	5	10	926	I	I-wall	Some scour backfilled by RR
		End	29	59	14.3	90	1	36.7							
W-16	Levee with I-wall (capped)	Start	29	59	18.7	90	1	37	200	Breach repaired			III	I-wall	I-wall rotated, breached, and scoured
		End	30	0	9.0	90	1	45.9							
W-17	Gate W29	Start	30	0	10.1	90	1	42.1	240	2	6	107	I	I-wall	Scour adjacent to wall
		End	30	0	12.3	90	1	41							
W-18	Levee with I-wall (capped)	Start	30	0	18.7	90	1	38.1	90	2	3	20	I	I-wall	Scour adjacent to wall
		End	30	0	19.6	90	1	38.3							
W-19	Gate W32 to Gate W34	Start	30	0	20.7	90	1	38.6	220	1	2	16	I	I-wall	Scour adjacent to wall
		End	30	0	26.1	90	1	40.4							

(Definition - Structural Damage is the rotation and or collapse of a floodwall or other structure.)

Floodwall/Levee	Scour type	Where	Repair methodology
Citrus Lakefront Levee and Floodwall			
Lakefront Airport Floodwall (Capped I-wall)	Moderate scour	the land side of the floodwall	Excavate the scour area, place flowable fill and compacted material, place bedding material and 6"-7" slope pavement
Star & Strips Bvld Floodwall	None noted		
Jancke Pumping Station Floodwall	Light Scour	the land side of the floodwall	Excavate the scour area, place flowable fill and compacted material, place bedding material and 6"-7" slope pavement
Lincoln Beach Floodwall	Light Scour	the land side of the floodwall	Excavate the scour area, place flowable fill and compacted material, place bedding material and 6"-7" slope pavement
New Orleans East Lakefront Levee			
Collins Pipeline	None noted		
South Point to GIWW Levee			
Drainage structure, N19 (400+/- lf south of South point)	Moderate scour	the lake side of levee	Excavate the scour area, place compacted material, place bedding material and gabions
Other Drainage structures	Light Scour	the lake side of levee	Excavate the scour area, place compacted material, place bedding material and gabions
Pumping Stations	None noted		
CSX Railroad gate	Heavy Scour	the land side of the floodwall	Raising the flood protection from (NAVD29) 13.5 to '88 datum Elevation 20
New Orleans Back Levee			
OP Pump Station 15	Rotation & Failure of Iwall Tie-In Walls to frontage Twalls	10'-12' Scour holes on both FS & PS of wall	Replace uncapped Iwall w/ pile founded Twalls, Raise protection from (29 datum) 17 to (88 datum) 23.
Iwall West of OPPS 15	Moderate scour	Both FS & PS	Excavate the scour area, place compacted material and graded stone
East Michoud Canal (Air Products Breach)	Rotation & Failure of Iwall Tie-In Walls to levee	10'-20' Scour holes on both FS & PS of wall; 300 lf long	Replace uncapped Iwall w/ new levee section and uncapped Iwall; Raise protection from (29 datum) 17 to (88 datum) 21.
Michoud Slip to Michoud Canal Floodwalls	Light to moderate scour	PS of floodwall	Excavate the scour area, place flowable fill and compacted material, place bedding material and 6"-7" slope pavement
Citrus Lakefront Levee and Floodwall			
IHNC to Paris Road	Light Scour	the land side of the floodwall	Excavate the scour area, place flowable fill and compacted material, place bedding material and 6"-7" slope pavement
Citrus Floodwall at Bulk Loading Facility	Rotation & Failure of Iwall	6'-10' Scour holes on both FS & PS of wall	Replace Iwall w/ new L-type wall Raise protection from (29 datum) current 13.5 to (88 datum) 15 (as built elevation)

	Table J-1									
	Orleans East Bank Lakefront - Summary of Damages									
	Location (GPS Coordinates)					Dimensions (feet)				
ID #	Degrees N	'	"	Degrees W	'	"	Length	Width	Depth	Cu-yd to fill	Description
L 46	90	05	17.3	30	01	39.3	20	10	2	15	Eroded levee under I-wall
L 50	90	05	10.4	30	01	36.1	10	20	1	7	Scour
L 51	90	05	7.9	30	01	35.6	20	3	1	2	Scour
L 52	90	05	7.5	30	01	35.5	10	3	1	1	Scour
L 59	90	04	59.1	30	01	33.6	20	20	3	44	Scour under bridge
L 60	90	04	59.0	30	01	34.1	20	20	1.5	22	Scour under bridge
L 67	90	04	55.4	30	01	31.1					Floodwall damage
L 72	90	04	55.3	30	01	33.7	30	20	2	44	Scour under bridge
L 73	90	04	55.4	30	01	34.6	30	20	3	67	Scour under bridge
L 83	90	03	52.6	30	01	57.2	6	4	2	2	Erosion
L 88	90	03	49.5	30	01	57.3	30	15	0.5	8	Shallow erosion
L 90	90	03	43.6	30	01	57.3					Floodwall damage
L 104	90	03	28.9	30	01	56.8	30	15	0.5	8	Degraded fill material at base of wall
L 119	90	02	15.9	30	01	52.1	10	2	2	1	Scour
L 120	90	02	15.4	30	01	52.2	10	2	2	1	Scour
L 124	90	02	19.2	30	01	53.8	20	6	2	9	Scour

(total backfill 231 cubic yards)

Scour details for levee/floodwall between Lakefront Airport and Gate L-15 along Lake Pontchartrain (New Orleans East), from dwg 5 of 9, contract solicitation NOE06W912P8-06-R-0043

Station	Scour Width (feet)	Scour Depth (feet)	Distance (feet)
18+16	0	0	
			54
18+70	7	3	
			47
19+17	11	2.5	
			60
19+77	12	3	
			62
20+39	14	3	
			17
20+56	12.5	3	
			18
20+74	10	3	
			96
21+70	3	3	
21+70 to 21+89 No Scour			19
21+89	12	2.5	
			17
22+06	12	2.5	

Volume V The Performance – Levees and Floodwalls – Technical Appendix

V-13-81

This is a preliminary report subject to revision; it does not contain final conclusions of the United States Army Corps of Engineers.

22+06 to 22+34 No Scour			28
22+34	11	3	
			45
22+79	11	2.5	
			21
23+00	11	2.5	
23+00 to 23+33 No Scour			33
23+33	10	3	
			37
23+70	10	3.5	
			55
24+25	7	2.5	
			22
24+47	15	5	
			60
25+07	14	2	
			46
25+53	15.5	5	

			120
26+73	16	4.5	
			104
27+77	16	4.5	
			50
28+27	13	4.5	
			32
28+59	11	4.5	
			36
28+95	10	3	
28+95 to 29+26 Floodgate L-14			31
29+26	10	3.5	
			46
29+72	6	3	
			44
30+16	11.5	3	
			61
30+77	14	4.5	
			7

30+84	10	3	
			72
31+56	2	2	
31+56 to 32+00 Floodgate L-15			44
32+00	See Plan	0	
			250
32+50	See Plan	6	

SEVERE SCOUR DETAILS

Location	Area (sq ft)	Depth (ft)
I	2680	6
II	3050	6
	1400	4
III	3600	5

S1, S2 & S3 - FLOOD GATES/WALL (IHNC [0 - 2+20.00'] TO STA. 23 + 04.00 W/L)

STATION	Df	Dp	Wf	Wp
0 - 220.00'	0.0	5.0	0.0	15.0
0 - 185.00'	0.0	4.0	0.0	15.0
0 - 185.00' TO 0 - 160.00'	0.0	0.0	0.0	0.0
0 - 160.00' TO 0 - 50.00'	0.0	5.0	0.0	10.0
0 - 50.00'	0.0	3.0	0.0	8.0
0 + 00.00	0.0	3.0	0.0	5.0
0 + 00.00 TO 0 + 73.00	0.0	7.0	0.0	15.0
1 + 23.00	0.0	5.0	0.0	15.0
1 + 23.00 TO 2 + 01.00	0.0	6.0	0.0	15.0
2 + 01.00	2.0	6.0	2.0	15.0
9 + 59.67 TO 11 + 20.56	1.0	6.0	2.0	15.0
20 + 00.00	0.0	3.5	0.0	10.0
20 + 43.00	0.0	5.5	0.0	9.0
21 + 15.00	0.0	2.0	0.0	9.0
21 + 80.00	1.0	2.0	6.0	9.0
21 + 84.00	0.0	4.0	0.0	10.0
22 + 61.06 TO 23 + 04.00	0.0	2.0	0.0	7.0

STATIONS INDICATED PER REFERENCE DWG: FILE NO. H-4-27147 "FLOODWALL AND LEVEE I.H.N.C. EAST - NORTH OF FLORIDA AVENUE"

Scour Stationing and Extent (feet), from Chalmette Area Plan Emergency Restoration contract drawings, October 2005:

Df = scour depth on flood side
Dp = scour depth on protected side
Wf = scour width on flood side
Wp = scour width on protected side

S4 - PARIS ROAD FLOOD GATE/WALL (STA. 267 + 00.00 C/L TO STA. 277+24.50 C/L)

STATION	Df	Dp	Wf	Wp
0 + 00.00 W/L (267 + 00.00 W/L)	0.0	8.0	0.0	8.5
0 + 50.00	0.0	3.0	0.0	25.0
0 + 83.00	0.0	10.0	0.0	35.0
1 + 29.00	0.0	4.0	0.0	40.0
1 + 29.00 TO 1 + 89.00	0.0	3.0	0.0	40.0
1 + 90.00	0.0	4.5	0.0	11.5
10 + 24.74	0.0	3.0	0.0	11.5

STATIONS INDICATED PER REFERENCE DWG:
FILE NO. H-4-29216 "PARIS ROAD FLOODWALL"

S5 - FLOOD GATE/WALL WEST OF BAYOU BIENVENUE (STA. 354 + 00 B/L TO STA. 357+00 B/L)

STATION	Df	Dp	Wf	Wp
354 + 24.83	8.0	8.0	7.0	11.0
354 + 40.00	2.0	4.0	5.0	15.0
354 + 83.00	0.5	2.0	2.0	15.0
354 + 83.00 TO 355 + 90.00	0.0	4.5	0.0	15.0
355 + 90.00	0.5	2.0	2.0	15.0
356 + 40.00	4.0	5.0	6.0	15.0
356 + 48.00	8.0	8.0	8.0	18.0

STATIONS INDICATED PER REFERENCE DWG:
FILE NO. H-8-29720 "STA. 277 + 20 TO 359 + 33
(PARIS ROAD TO BAYOU BIENVENUE) 2ND LIFT"

Scour Stationing and Extent (feet), from Chalmette Area Plan Emergency Restoration contract drawings, October 2005:

Df = scour depth on flood side
Dp = scour depth on protected side
Wf = scour width on flood side
Wp = scour width on protected side

Appendix 14
General Description of New Orleans' Basins and Damage from Hurricane Katrina

General Description of Lake Pontchartrain, LA and Vicinity and NOV, Hurricane Protection Projects Basins

The Lake Pontchartrain, LA and Vicinity Hurricane Protection Project (HPP) covers St. Bernard, Orleans, Jefferson and St. Charles Parishes in southeast Louisiana, generally in the vicinity of the city of New Orleans, and between the Mississippi River and Lake Pontchartrain. The Orleans East Bank portion of the project includes the east bank of the Mississippi River between the 17th Street Canal and Inner Harbor Navigational Canal (IHNC). Figure 14-1 is an index map showing the individual polders within the Lake Pontchartrain, LA and Vicinity HPP.

Plaquemines Parish Basin includes long, narrow strips of protected land on both sides of the Mississippi River between New Orleans and the Gulf of Mexico. The Mississippi River Levees (MRL) protect the Parish from floods coming down the river. Protection from hurricane induced tidal surges is achieved by the New Orleans to Venice (NOV) HPP. The NOV HPP is a system of levees on the gulf side of the protected lands and additional berms and floodwall on top of the MRL along the river. The NOV extends from Phoenix, LA to Venice, LA. A HPP map is not available for NOV however.
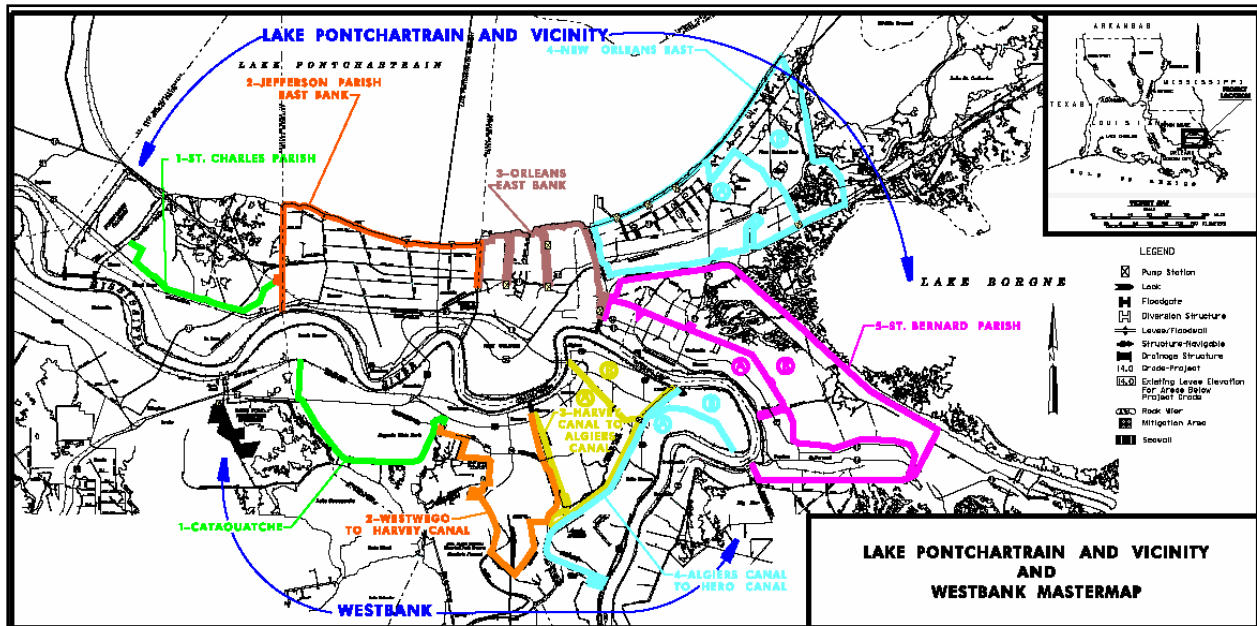
Figure 14-1. Index Map to Lake Pontchartrain, LA and Vicinity Hurricane Protection Project

This is a preliminary report subject to revision; it does not contain final conclusions of the United States Army Corps of Engineers.

Figure 14-2. Extent of NOV Hurricane Protection in Plaquemines Parish. The NOV consists of five distinct reaches; Reach C, Reach St. Jude to City Price, Reach A, Reach B-1 and Reach B-2

Orleans East Bank – HPP Features

This portion of the project that protects the city of New Orleans was designed to protect 28,300 acres of urban and industrial lands and is illustrated in detail by Figure 14-3. A series of diagrams like Figure 14-3 were developed by the New Orleans District for planning and design purposes for each of the basins and show as-built levee and floodwall elevations.

The levee portion of the New Orleans East Bank HPP is constructed with a 10-foot crown width with side slopes of 1 on 3. Along Lake Pontchartrain Lakefront the top elevation of the earthen levees range between elevation +13 and +18 ft National Geodetic Vertical Datum (NGVD). Floodwalls were designed to provide lines of protection on the east side of the 17th Street Canal, both sides of Orleans Avenue Canal and London Avenue Canal, and the west side

Volume V The Performance – Levees and Floodwalls – Technical Appendix

V-14-3

This is a preliminary report subject to revision; it does not contain final conclusions of the United States Army Corps of Engineers.

of the IHNC. Floodwalls consist of reinforced concrete T-wall floodwalls and reinforced concrete I-wall floodwalls constructed on the top of sheet-pile, and sheet piling without a concrete section. Top elevations of the floodwalls vary between elevation +13 and +15 ft.
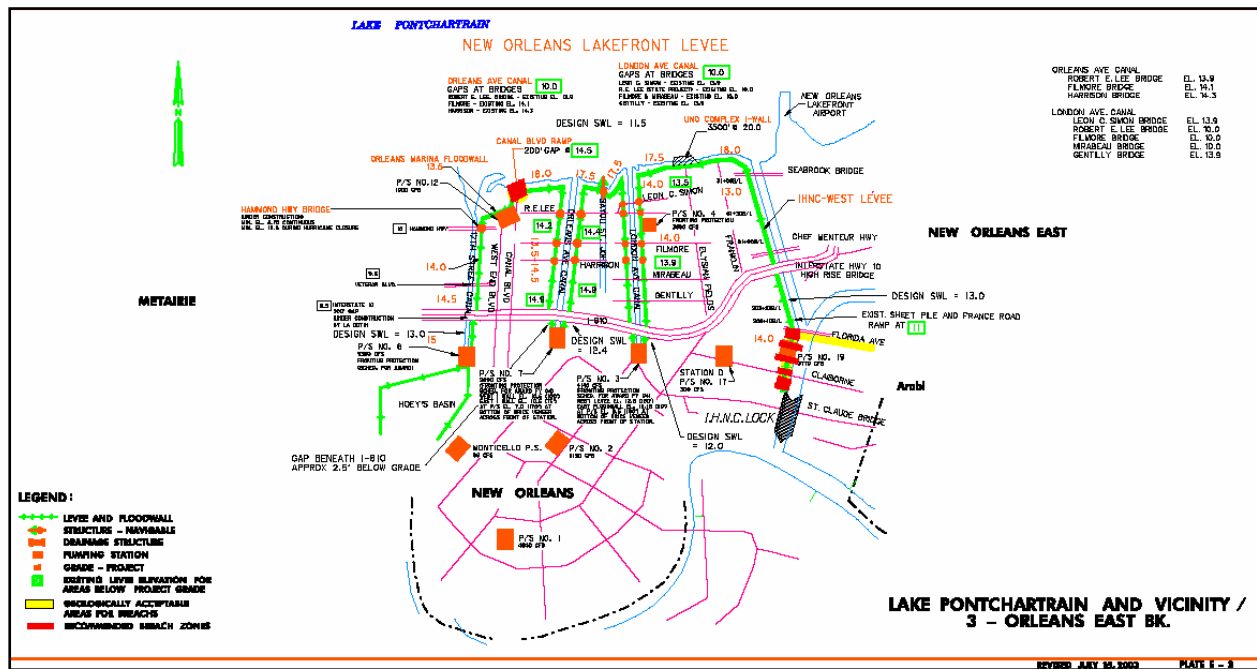
Figure 14-3. HPP features – New Orleans East Bank

Orleans East Bank Lakefront. A levee segment located in southeastern Louisiana in New Orleans and roughly parallels the shoreline of Lake Pontchartrain between the IHNC on the east and 17th Street Canal on the west. This levee segment is located in Orleans Parish.

IHNC Canal (West Bank). The Inner Harbor Navigation Canal is located in the east portion of Orleans Parish and is described in the IHNC section of this report.

17th Street Outfall Canal (Metairie Relief). The 17th Street Outfall Canal lies in Jefferson Parish immediately west of the Orleans Parish boundary line. The canal extends approximately three miles from Pump Station No. 6 near Interstate Highway 10 to its confluence with Lake Pontchartrain.

London Avenue Outfall Canal. The London Avenue Outfall Canal is located on the south side of Lake Pontchartrain in Orleans Parish. The London Avenue Outfall Canal lies to the east of 17th Street Canal and Orleans Avenue Canal.

Orleans Avenue Canal. The Orleans Avenue Canal extends about 2.4 miles from Pumping Station No.7 in the vicinity of I-610 to its mouth at Lake Pontchartrain.

Table 14-1
New Orleans East Bank Hurricane Protection System

19.2 miles	levee and floodwall
13	pump stations
15	roadway floodgates
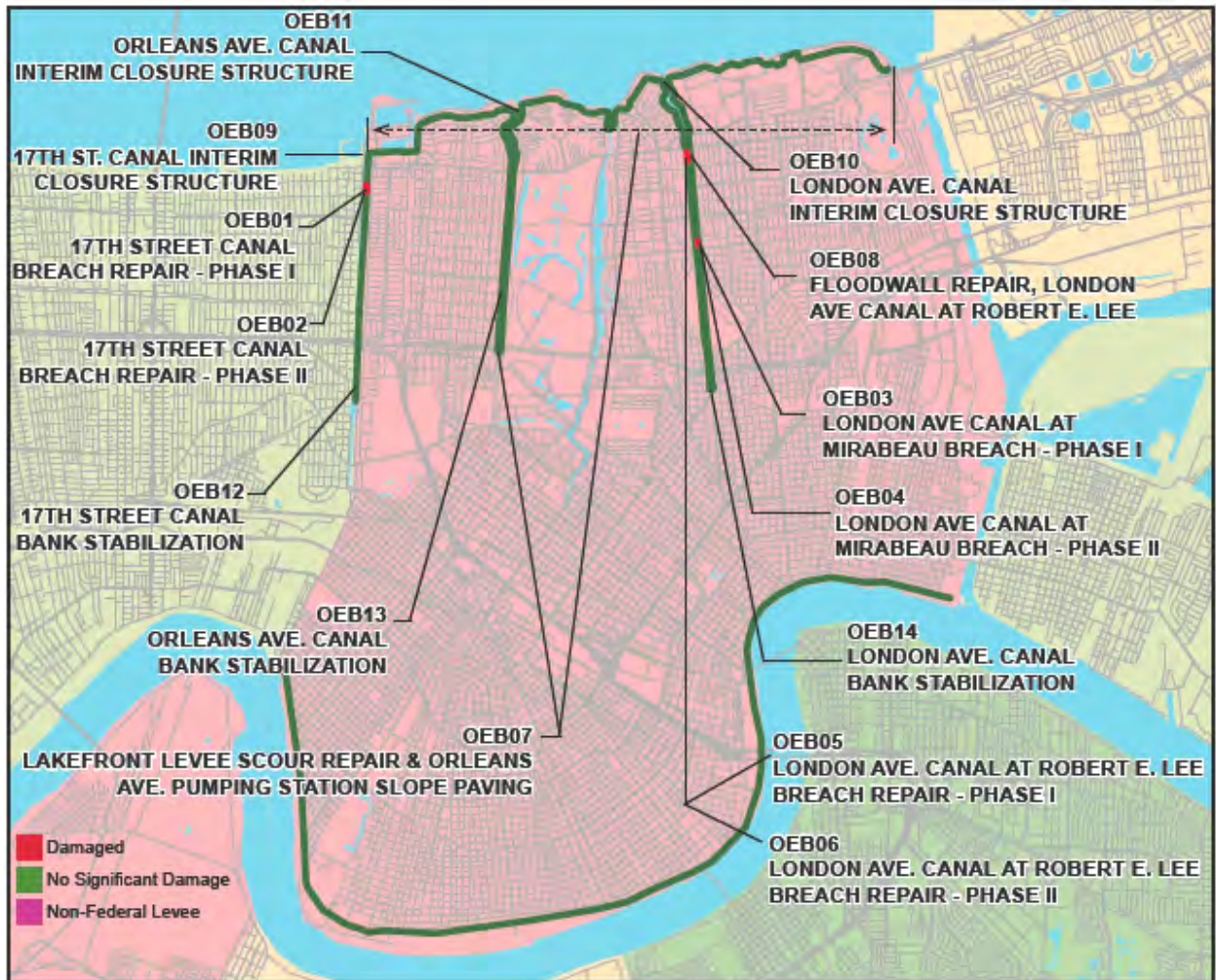
Figure 14-4. Damages and Repair Contracts – New Orleans East Bank

Primary damages to the flood protection in the Orleans East Bank basin consists of a 455- ft breach in the east side I-wall along 17th St. Canal, breaches on both the east side (425 ft) and west side (720 ft) I-wall along London Ave. Canal, breaches along the west side of IHNC floodwall and damages to all fifteen pumping stations.

New Orleans East Basin – HPP Features

The hurricane protection system for the New Orleans East (NOE) Basin was designed as part of the Lake Pontchartrain, LA and Vicinity Hurricane Protection Project. The NOE portion of the project protects 45,000 acres of urban, industrial, commercial, and industrial lands. Figure 14-5 illustrates the boundaries and basic flood protection components within the NOE Basin. The levee is constructed with a 10-ft crown width with side slopes of 1 on 3. The height of the levee varies from 13 to 19 ft. There are floodwall segments along the line of protection that consists of sheet-pile walls or concrete I-walls constructed on top of sheet-pile. The line of protection was designed to provide protection from the Standard Project Hurricane (category 3 hurricane).

Figure 14-5 is used by the New Orleans District for planning and design, specifically because it shows as-built levee and floodwall elevations. The western border coincides with the Inner Harbor Navigation Canal (IHNC) and the eastern boundary of the Orleans Basin. It is bounded by the east bank of the IHNC, the Lake Pontchartrain shoreline (between the IHNC and Southpoint), the eastern boundary of the Bayou Savage National Wildlife Preserve, and the north side of the Gulf Intracoastal Waterway (GIWW) (between the IHNC and eastern edge of the Bayou Savage National Wildlife Preserve). The main components are described in the next section moving clockwise through the basin, beginning at the Lakefront Airport and ending at the western end of the GIWW.

Figure 14-5. NOE Basin general components and top of levee/floodwall as-built elevations (feet) (source USACE, New Orleans District (Wayne Naquin)

New Orleans East Basin Components

New Orleans East Lakefront includes the Citrus Lakefront Levee and New Orleans East Lakefront Levee consisting of 12.4 miles of earthen levee paralleling the Lakefront from the IHNC to Southpoint. It also includes floodwalls at the Lakefront Airport and Lincoln Beach.

The New Orleans East Levee consists of 8.4 miles of earthen levee from Southpoint to the GIWW along the eastern boundary of the Bayou Savage National Wildlife Preserve.

GIWW - The basin includes the Citrus Back Levee and New Orleans East Back Levee which consisting of approximately 17.5 miles of earthen levees and concrete floodwalls along the northern edge of the GIWW.

IHNC - The basin protection includes approximately 2.8 miles of levee and concrete floodwall along the eastern side of the IHNC. The IHNC is described in a separate report.

Pump Stations – Eight pump stations and numerous drainage structures, pipe crossings and culverts also lay on the boundaries.

Table 14-2 is a summary of the protection features and their lengths for NOE Basin. Figure 14-6 shows the extent of damage as surveyed by the TFG. Nine repair contracts have been awarded to repair levees and floodwalls throughout the basin. The contracts are delineated on the figure.

Table 14-2 Summary of NOE Basin Hurricane Protection Features	
Exterior levee and floodwall (I wall)	39 miles
Drainage Structures	4
Pump Stations	8
Highway Closure Structures	2
Railroad Closure Structure	1
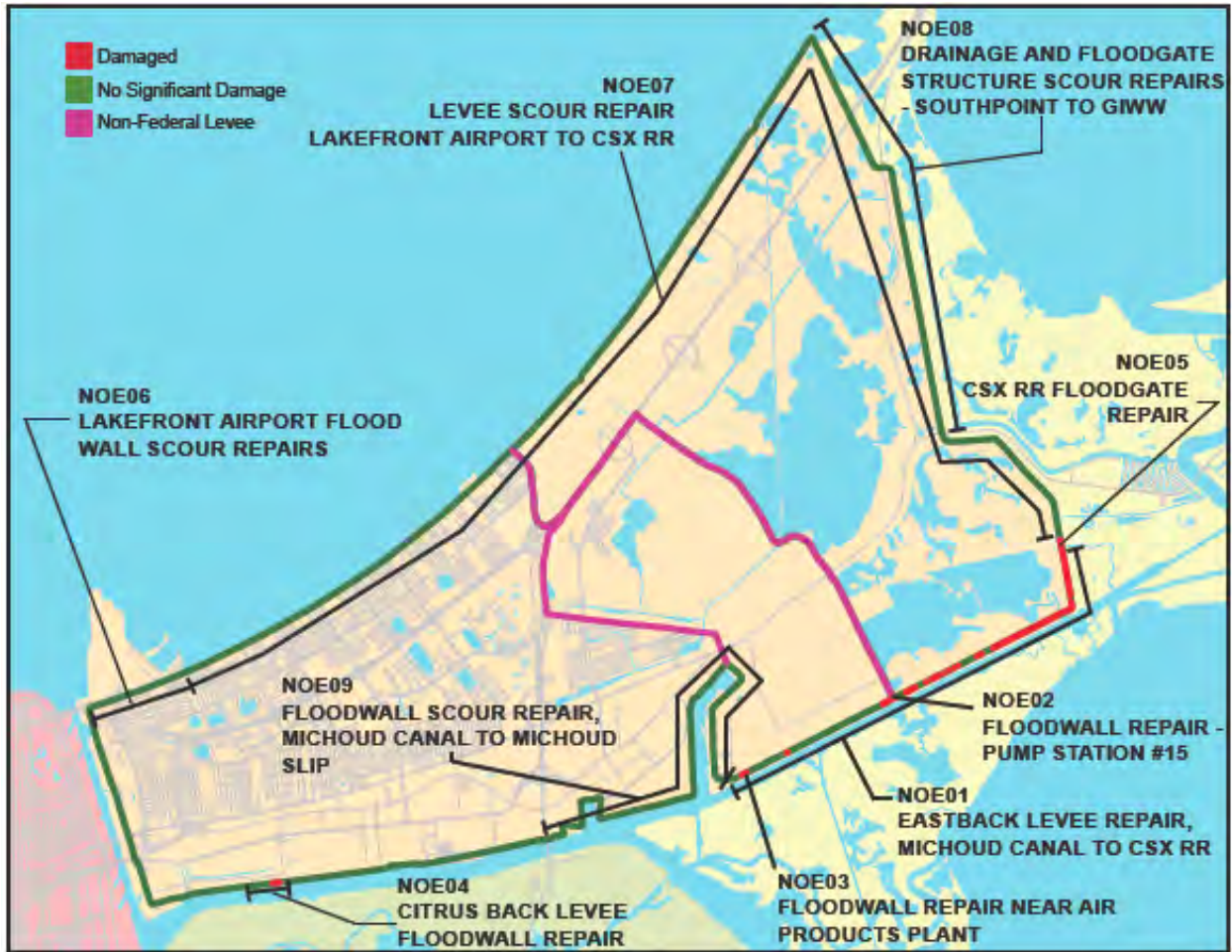
Figure 14-6. Hurricane Protection Features - New Orleans East Basin

This is a preliminary report subject to revision; it does not contain final conclusions of the United States Army Corps of Engineers.

Figure 14-7. New Orleans East IPET Characterization of Damages

West and East Sides, IHNC, Orleans Parish – HPP Features

The Inner Harbor Navigation Canal (IHNC) HPP contains approximately 12.3 miles of levee and floodwalls along the Inner Harbor Navigation Canal in a heavily industrialized area. Table 14-3 is a summary, but does not break down the floodwalls versus levees. Figure 14-8 defines some of the protection features, but was developed to show the contract repairs ongoing in the canal.

Figure 14-9 characterizes the failures with respect to IPET categories.

IPET has made six categories of levee performance to help characterize behavior. These are:

- LONB = Overtopped levees, no breaching
- WS = Overtopped floodwalls, no breaching (stable)
- LOB = Overtopped levees, breaching
- TF = Transition failure (floodwall to levee transition)
- WF = Overtopped floodwalls, breached (failure)

- WCF = Overtopped floodwalls, no breaching but came close

And have been applied to the contract maps provided by TFG as shown in

Figure 14-9.

Table 14-3 Hurricane Protection System for IHNC Hurricane Protection System	
•12.3 miles	Levee and floodwall

IHNC Damages. Overtopping of the hurricane protection by Hurricane Katrina was evident along nearly all portions of the canal. There were four breaches in the protection system, two on the east side and two on the west side. The east side breaches are both located in the lower 9th ward neighborhood and the west side breaches are both in the vicinity of France Road and Benefit Street.
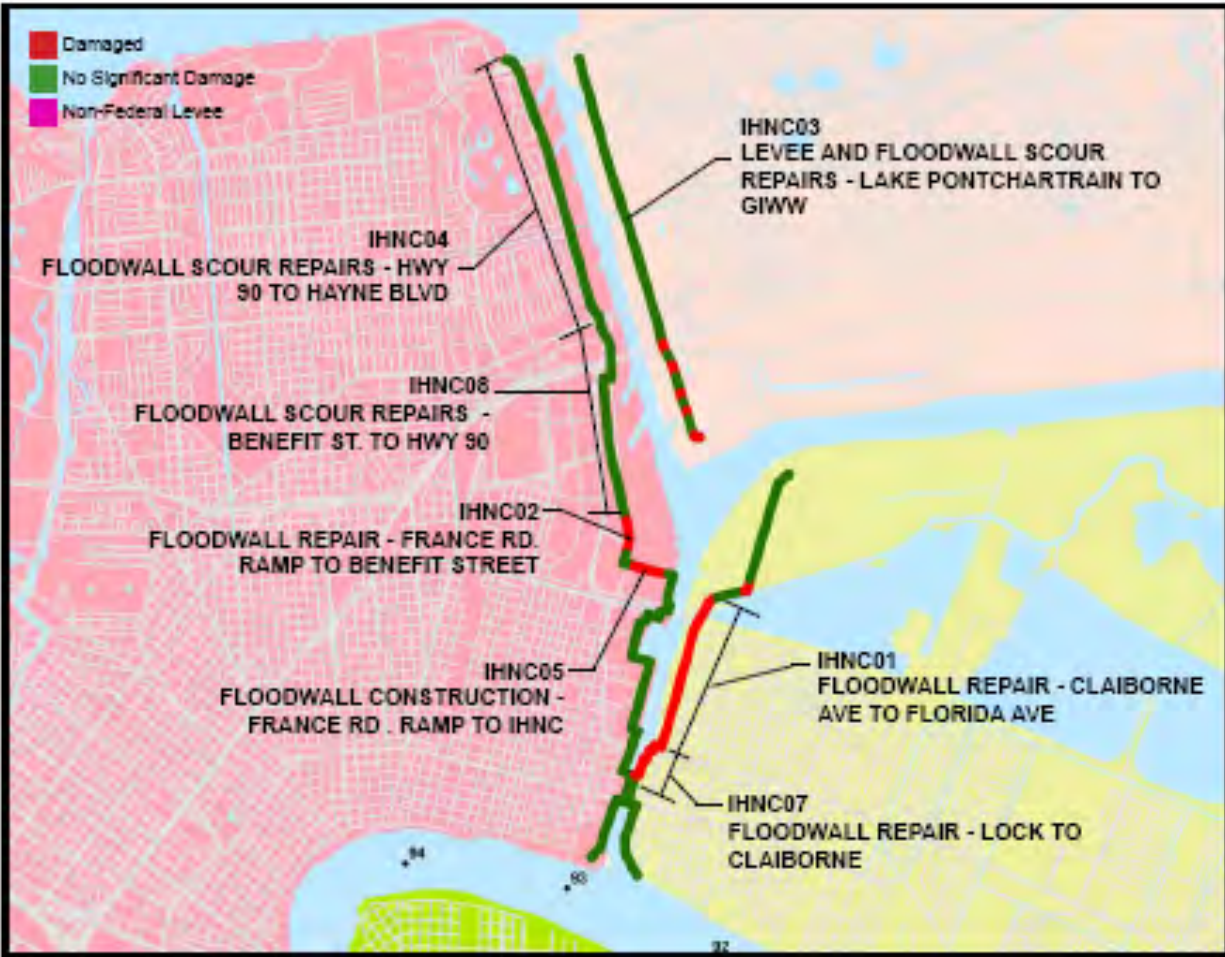
Figure 14-8. Hurricane Protection Features and Damages– IHNC
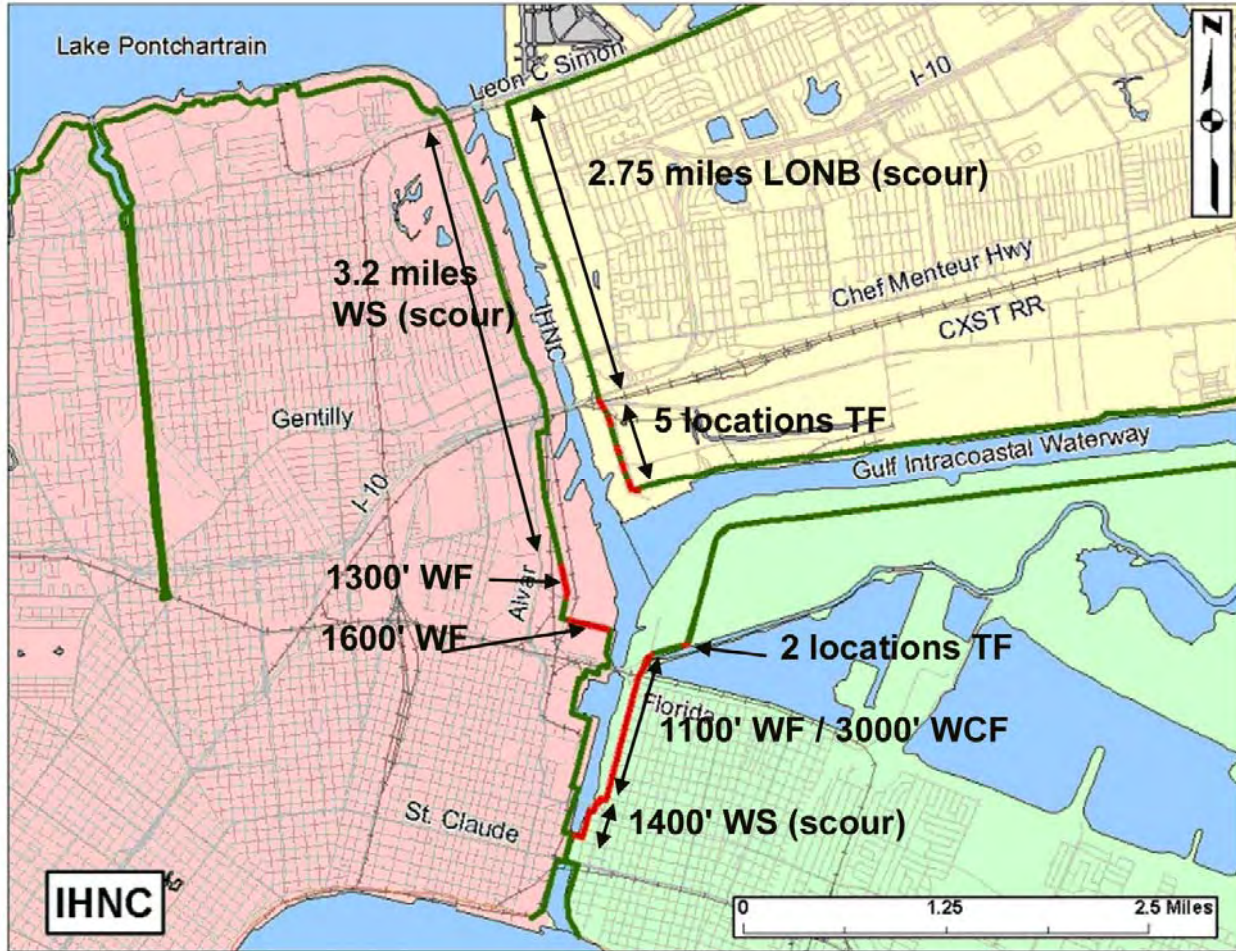
Figure 14-9. Damaged Areas Along the IHNC

St. Bernard Parish Basin – HPP Features

The St. Bernard Basin hurricane protection system includes the levee/floodwall extending from the Inner Harbor Navigation Channel (IHNC) easterly, along the Gulf Intracoastal Waterway (GIWW), to the Bayou Bienvenue Control Structure, continuing along the Mississippi River Gulf Outlet (MRGO) southeastly, then turns generally to the west, where it ties into the Mississippi River Levee at Caernarvon, as shown on the map below. A portion of the hurricane protection system in this area also provides hurricane protection to the Lower 9th Ward area in Orleans Parish. Figure 14-10 illustrates the hurricane protection components of St. Bernard Parish, while Table 14-4 summarizes their lengths. Figure 14-11 illustrates the damaged areas and the ongoing repair contracts, and

Figure 14-12 is an example of the IPET characterization of the damages.
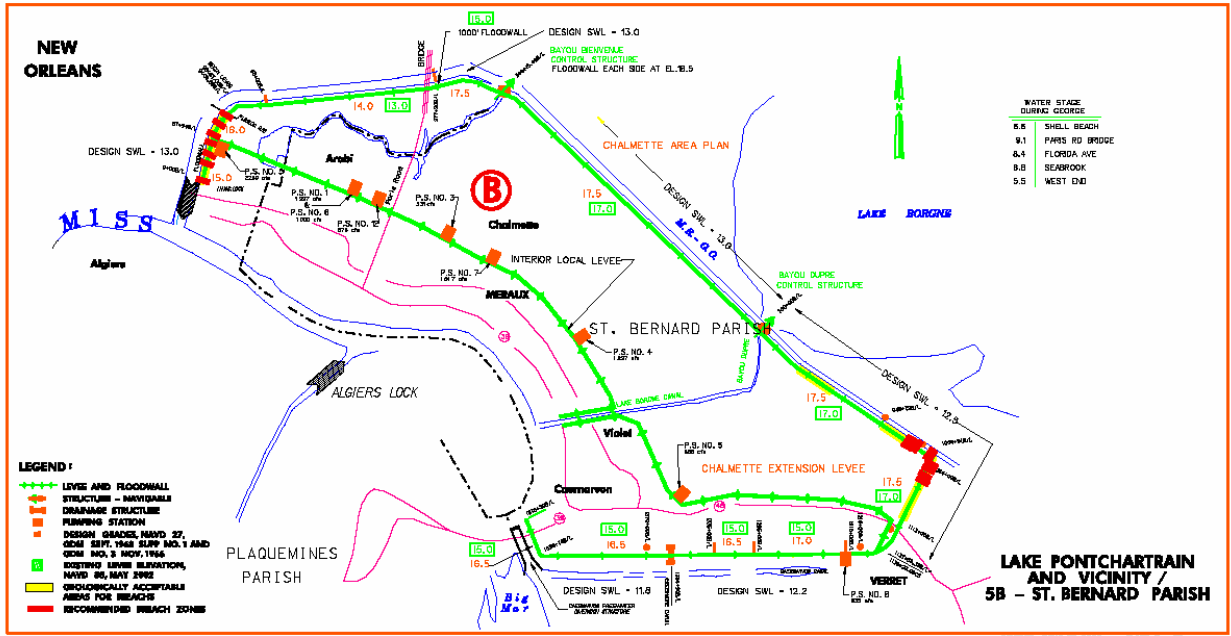
Figure 14-10. Hurricane Protection Project Features – St. Bernard

Table 14-4 Summary of St. Bernard Basin Hurricane Protection Features	
Levees and Floodwalls	157,800 ft
Road Closure Structures	6
Water Control Structures	2
Gravity Drainage Structure	1
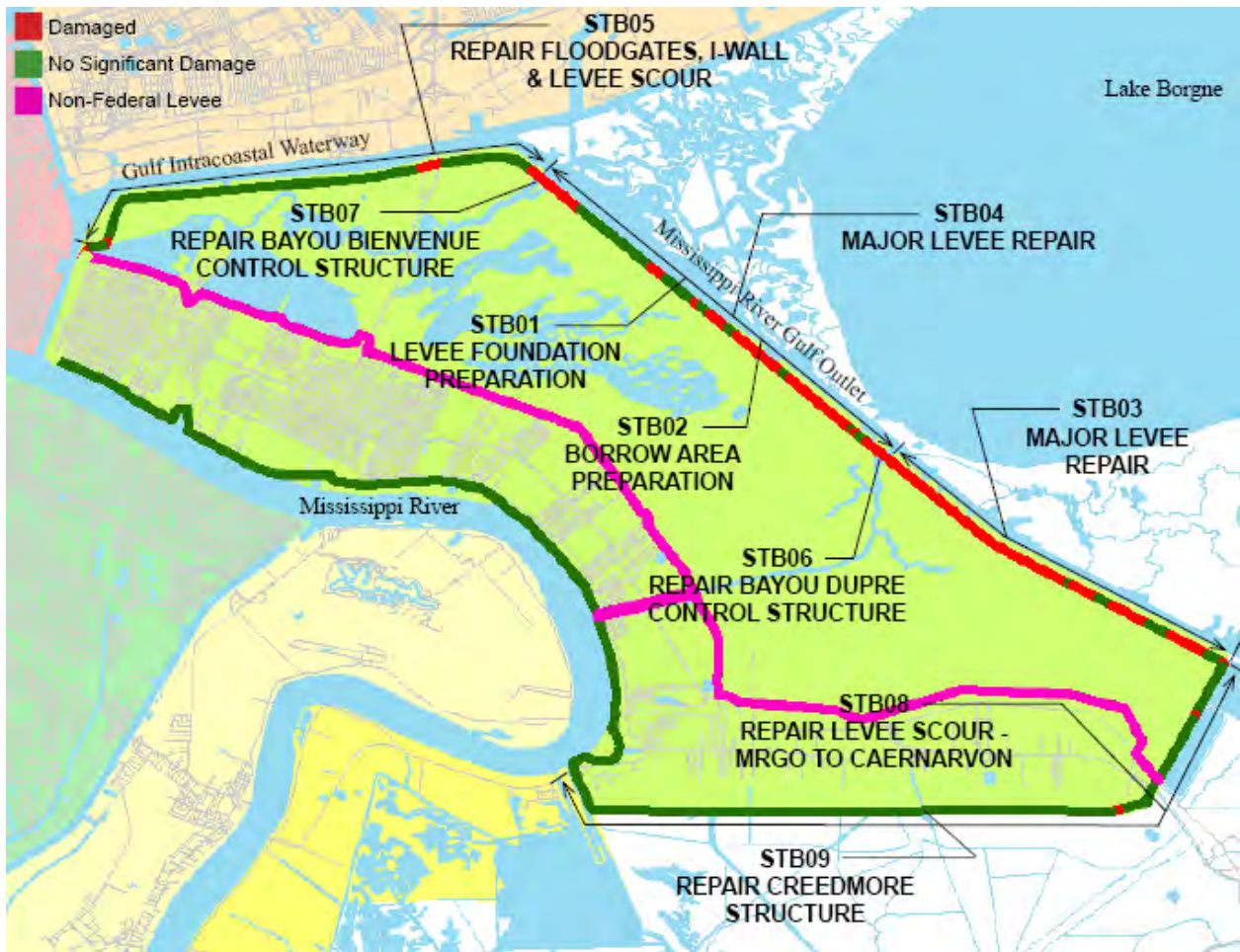
Figure 14-11. St. Bernard Damage and Contract Repair Areas
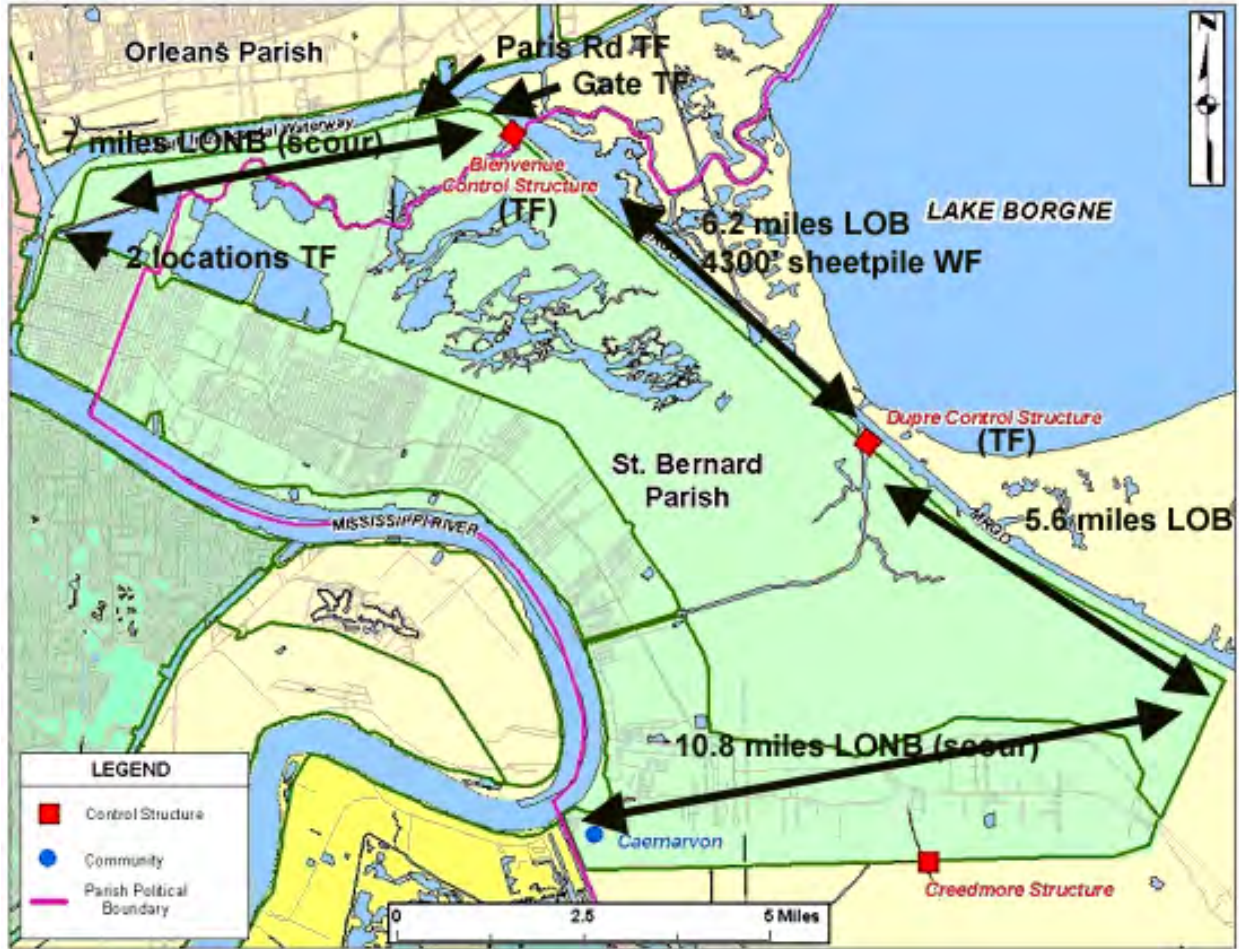
Figure 14-12. St. Bernard Parish IPET Damage Characterization

Plaquemines Parish – HPP Features

Altogether the Plaquemines Parish MRL and NOV systems include 162 miles of levee and 7 miles of floodwall. Table 14-5 summarizes the HPP components within Plaquemines Parish. Figure 14-13 illustrates the individual reaches that make up the MRL system and the NOV system. There are 19 non-federal pump stations for interior drainage. The levees are crossed by numerous pipelines, constructed in various manners. Some crossings bridge the levee without touching the embankment; some are constructed on top of the line of protection; and some pass through the line of protection with measures to prevent seepage. There is also a wicket gate closure on the back levee at Empire, where a shipping canal connects the Mississippi River to the Gulf of Mexico.

Table 14-5
Summary Plaquemines Basin Hurricane Protection Features

Mississippi River levee and floodwall	109 miles (34 miles part of NOV)
Floodwalls	6.4 miles
Hurricane Protection back levee	53 miles
Road Closure Structures	?
Numerous pipeline crossings	
Pump stations	19
Marine floodgate Empire	1
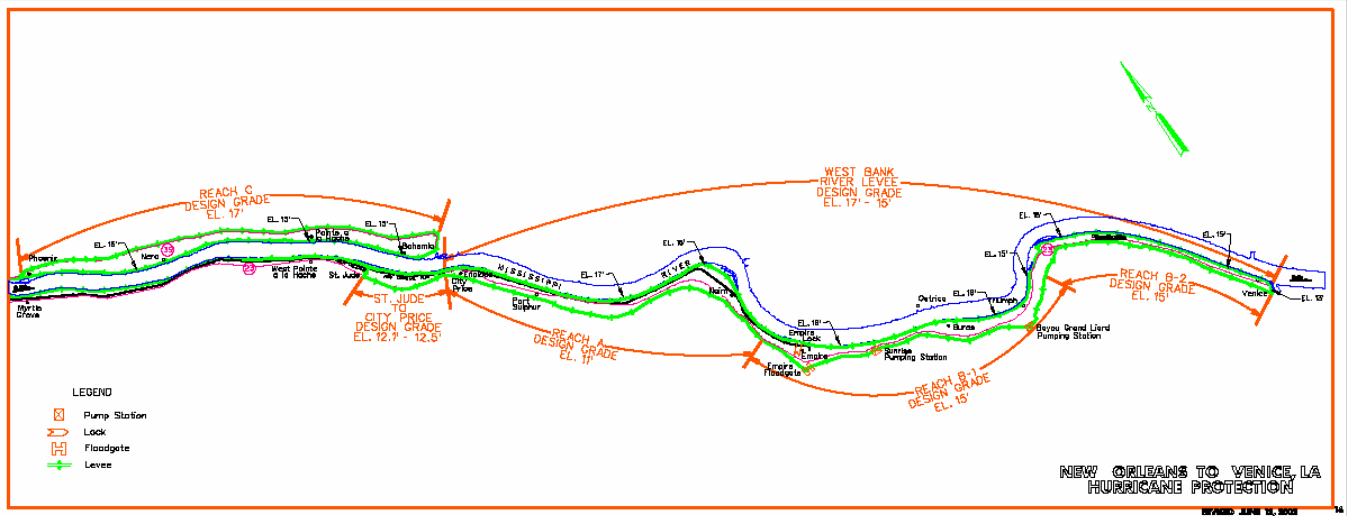
Figure 14-13. Hurricane Protection Project Features – Plaquemines Parish
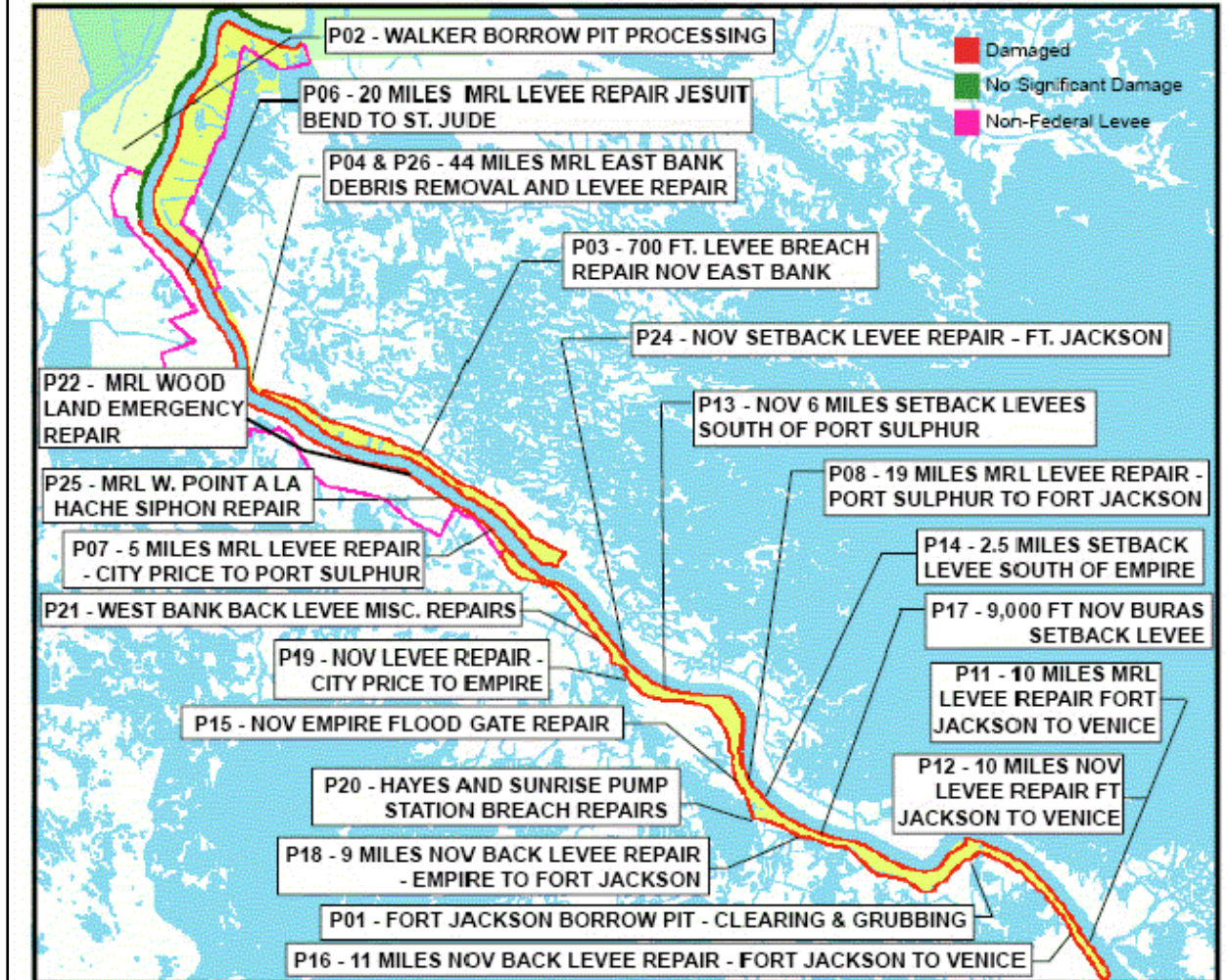
Figure 14-14. Damaged and Contract Repair Areas Along Plaquemine Parish

Table 14-6 Summary of Damages - Plaquemines Basin	
Mississippi River levee and Hurricane Protection back levee l	150 miles
Floodwalls	6.0 miles
Pump stations	
Marine floodgate Empire	1

West and East Sides, IHNC, Orleans Parish

The Inner Harbor Navigation Canal (IHNC) work area contains approximately 10 miles of levee and floodwalls along the Inner Harbor Navigation Canal in a heavily industrialized area. Lake Pontchartrain Barrier Plan Design Memorandum 2 (1968) describes pre-construction conditions and design details for the west side of IHNC and the east side north of the MRGO, up to the Seabrook Lock at the Lake. Chalmette Area Plan Design Memorandum 3 (1968) describes pre-construction conditions and design details for the east side of IHNC from the lock up to the MRGO.
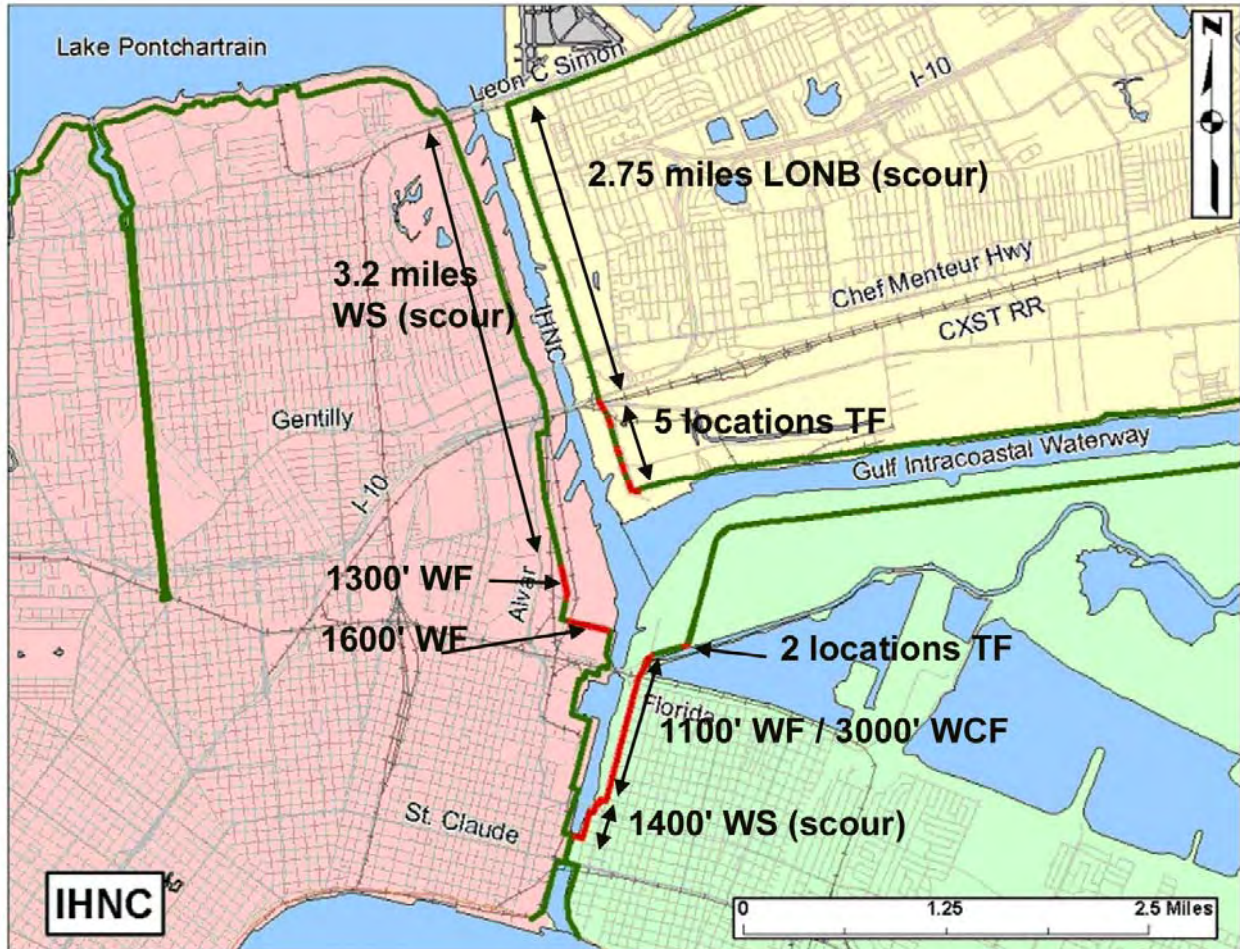
Figure 14-15. IHNC Flood Protection Damage

Damaged areas along the IHNC:

- LONB = Overtopped levees, no breaching
- WS = Overtopped floodwalls, no breaching (stable)
- LOB = Overtopped levees, breaching
- TF = Transition failure (floodwall to levee transition)
- WF = Overtopped floodwalls, breached (failure)

- WCF = Overtopped floodwalls, no breaching but came close

Overtopping was generally associated with varying degrees of scour (surface erosion), generally on the levee landside.

Figure 14-16. Photo of IHNC Area

This is a preliminary report subject to revision; it does not contain final conclusions of the United States Army Corps of Engineers.

Overtopping of the hurricane protection by Hurricane Katrina was evident along nearly all portions of the canal. There were four breaches in the protection system, two on the east side and two on the west side. The east side breaches are both located in the lower 9th ward neighborhood and the west side breaches are both in the vicinity of France Road and Benefit Street. Temporary repairs and closures have been made in these areas. Task Force Guardian will restore the protection back to pre-hurricane Katrina conditions. In the areas of the breaches, the 7 projects will replace/repair those walls back to pre-storm project authorized elevations. In the areas of scour, those walls and scour will be repaired accordingly.

The reach along the west side of the Inner Harbor Navigation Canal (IHNC) from the lock at St. Claude Avenue northward to Lake Pontchartrain consists of levee and floodwall. For the segment of this reach between the lock and Florida Avenue, damage consisted primarily of scour along the base of the floodwall. For the segment from Florida Avenue to Hwy 90, damage consisted of levee scour, scour along the base of a floodwall, and severe damage in the form of two breaches of the floodwall. For the segment of the IHNC from Hwy 90 to the lake the floodwall experienced relatively minor scour damage along its base.

In the IHNC area, seven separate construction projects have been identified to repair the damaged areas and restore flood protection to pre-hurricane Katrina conditions. These projects represent an estimated $54 million in construction costs.

Soil borings for the area north of Florida Ave to the Lake are in DM2 Supp 8 Feb 1968.pdf

"area south of MRGO (East side) are in DM3Chalmette.pdf
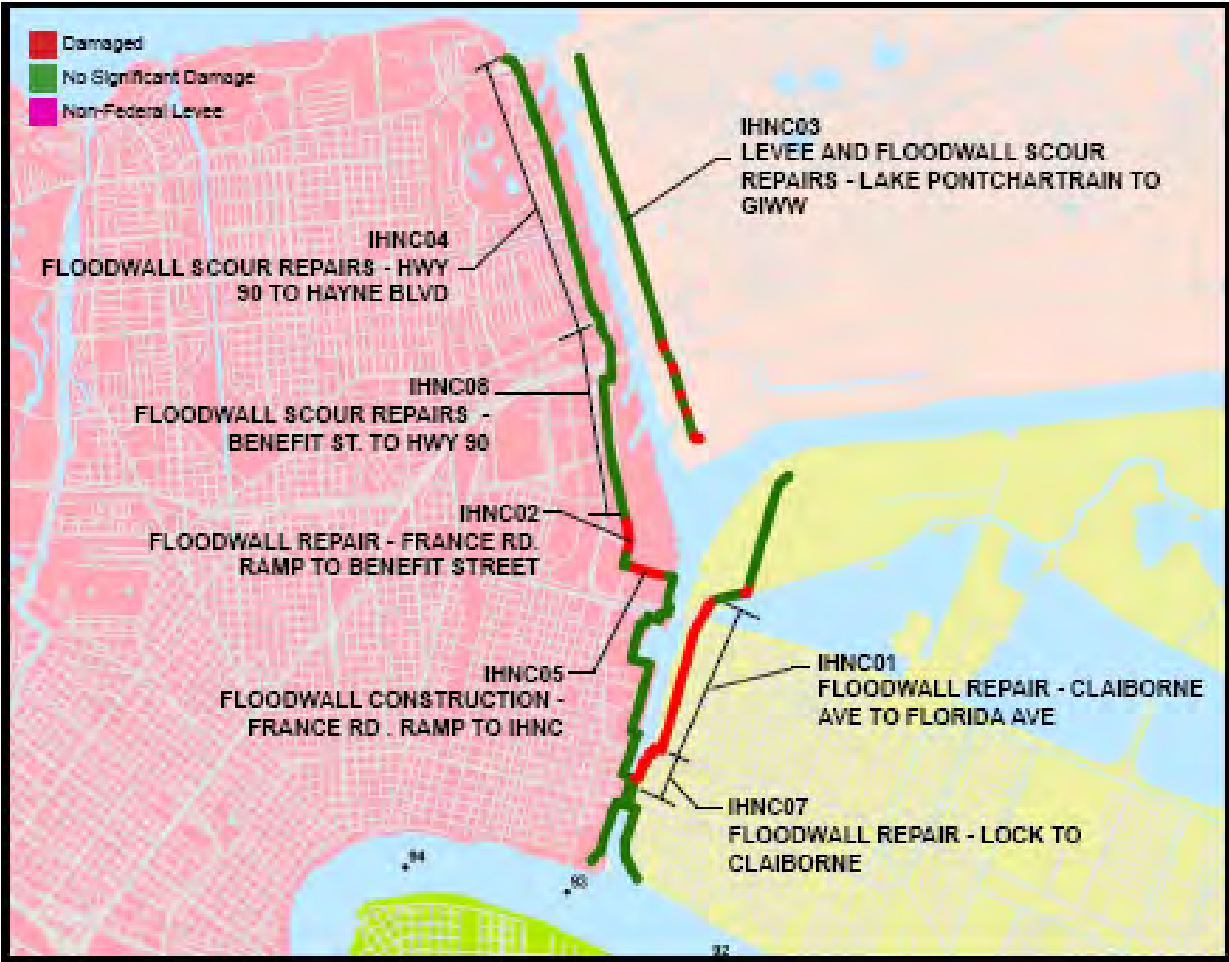
Figure 14-17. Task Force Guardian Repair Contracts
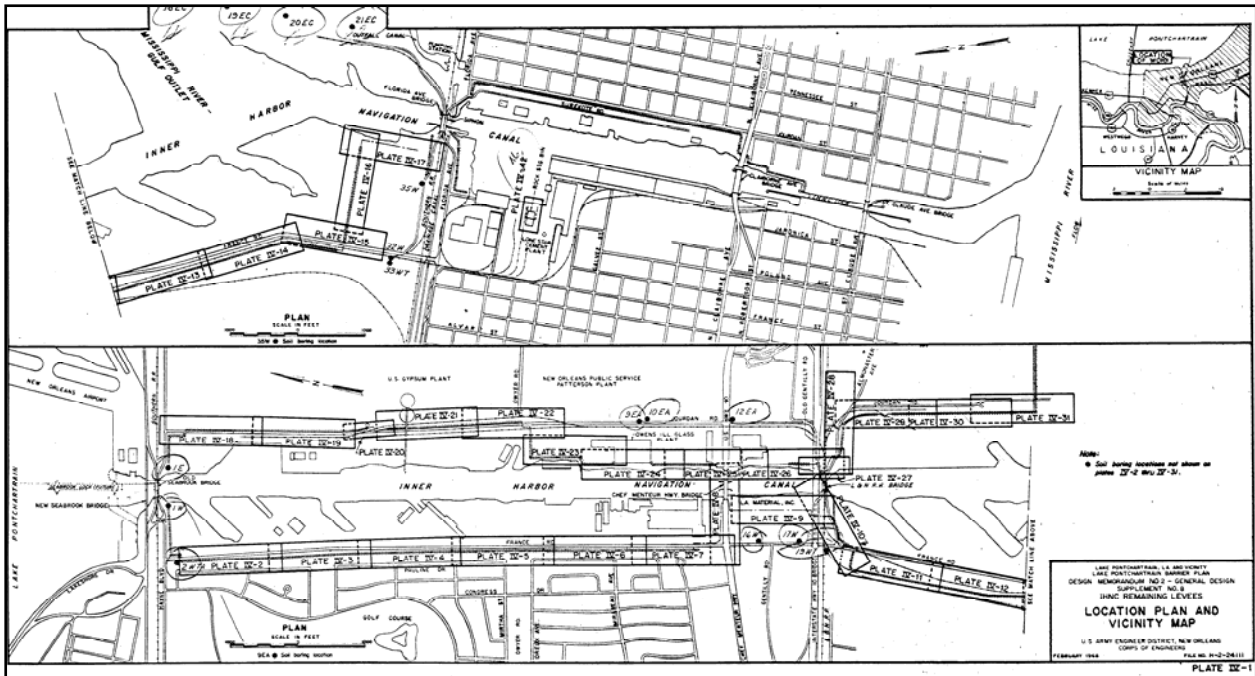
Figure 14-18. Pre-Katrina Design. Pg 154 (plate IV-1) DM2Supplement8
(GDMRemainingLeveesFeb68.pdf) shows stationing / soil borings between Fla Ave and Lake
on the IHNC west side, and between MRGO and Lake on the IHNC east side
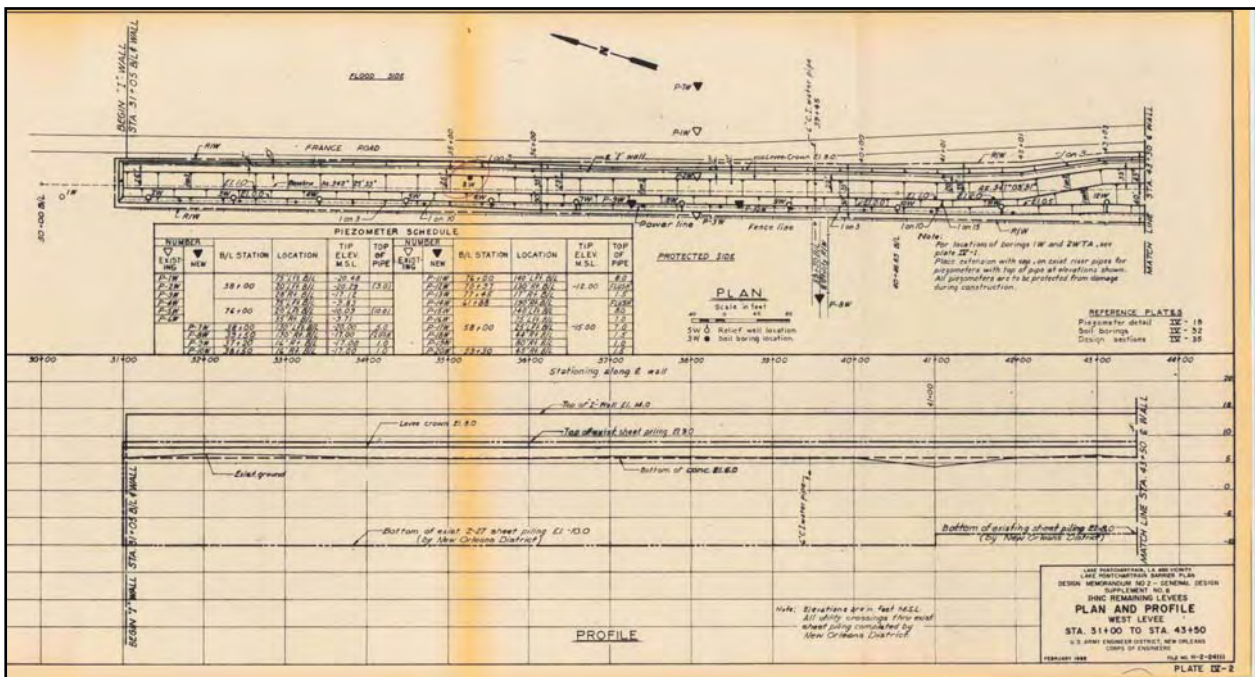
Figure 14-19. Soil Boring Layouts Begin on pg 155 (plate IV-2) of DM2Supplement8
(GDMRemainingLeveesFeb68.pdf)

IHNC EAST SIDE

Task Force Guardian (TFG) Project: IHNC01-IHNC East Side North Claiborne Avenue to Florida Avenue

Description: There is approximately 4,000 lineal feet of concrete I-wall flood barrier along the east side of the IHNC Canal between North Claiborne Avenue and Florida Avenue. The damages in this reach consisted of a breach of the floodwall immediately south of Florida Avenue (250') and one approximately 100 yards north of Claiborne Ave (850') with the remaining portions of the floodwall having areas of severe scour and tilting of the I-wall. The work includes replacement of the concrete I-wall with a concrete T-wall, supported on H-piles and sheet piling. Scheduled construction completion is 15 March 2006.

- 250' breach (WF) I-wall, south of Florida Ave
- 850' breach (WF) I-wall, 100 yds north of Claiborne Ave.
- ~3000' (WNF / WCF)

Figure 14-20. Plate 1, DM3Chalmette.pdf Showing Stationing and Soil Boring Locations for IHNC South of Fla Ave
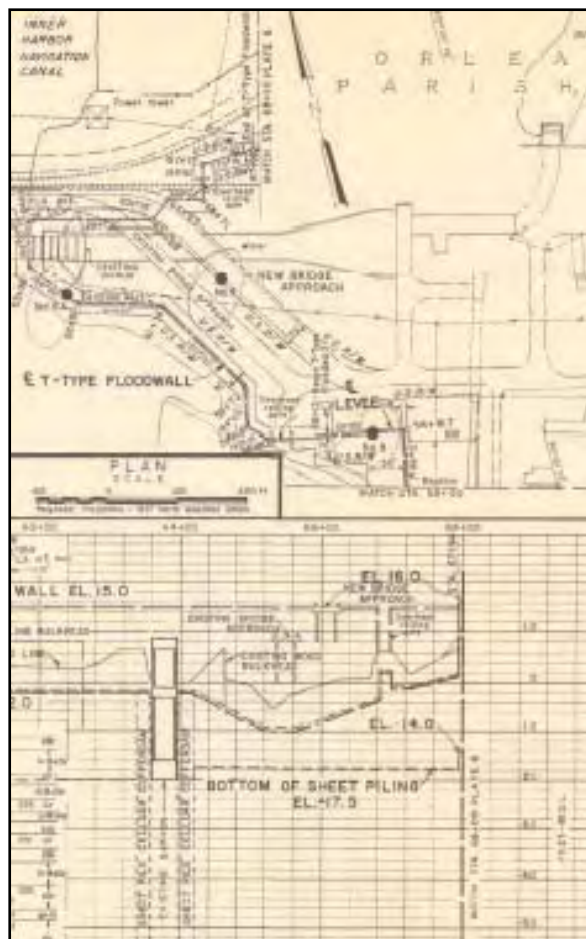
Figure 14-21. Plate 5 of DM3 Shows the Fla Ave Area, East Side IHNC
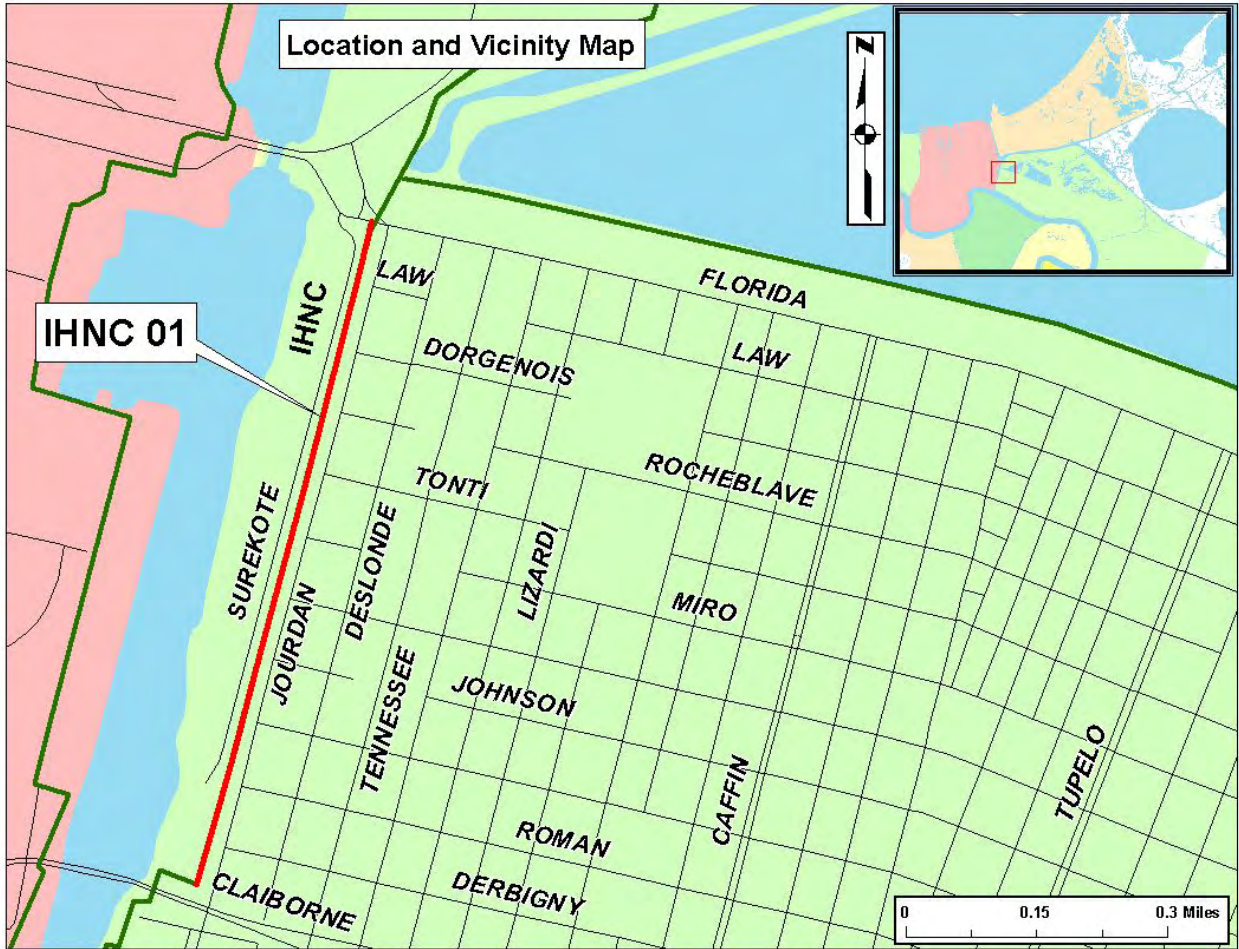
Figure 14-22. East Side IHNC Between Claiborne Ave. and Florida Ave.

Figure 14-23. During Katrina; View to East Side of IHNC South of GIWW. Breach began approximately 300 ft north of Claiborne Ave.

Volume V The Performance – Levees and Floodwalls – Technical Appendix   V-14-27

This is a preliminary report subject to revision; it does not contain final conclusions of the United States Army Corps of Engineers.

Figure 14-24. Closeup of Flattened I-Wall and Barge, View Toward Claiborne Ave.

This is a preliminary report subject to revision; it does not contain final conclusions of the United States Army Corps of Engineers.

Figure 14-25. Transition From Failed Wall to Intact Wall, View Toward Claiborne Ave.

Figure 14-26. Northernmost Transition From Failed Wall to Intact Wall

Figure 14-27. Demolishing Flattened I-Wall North of Claiborne Ave.
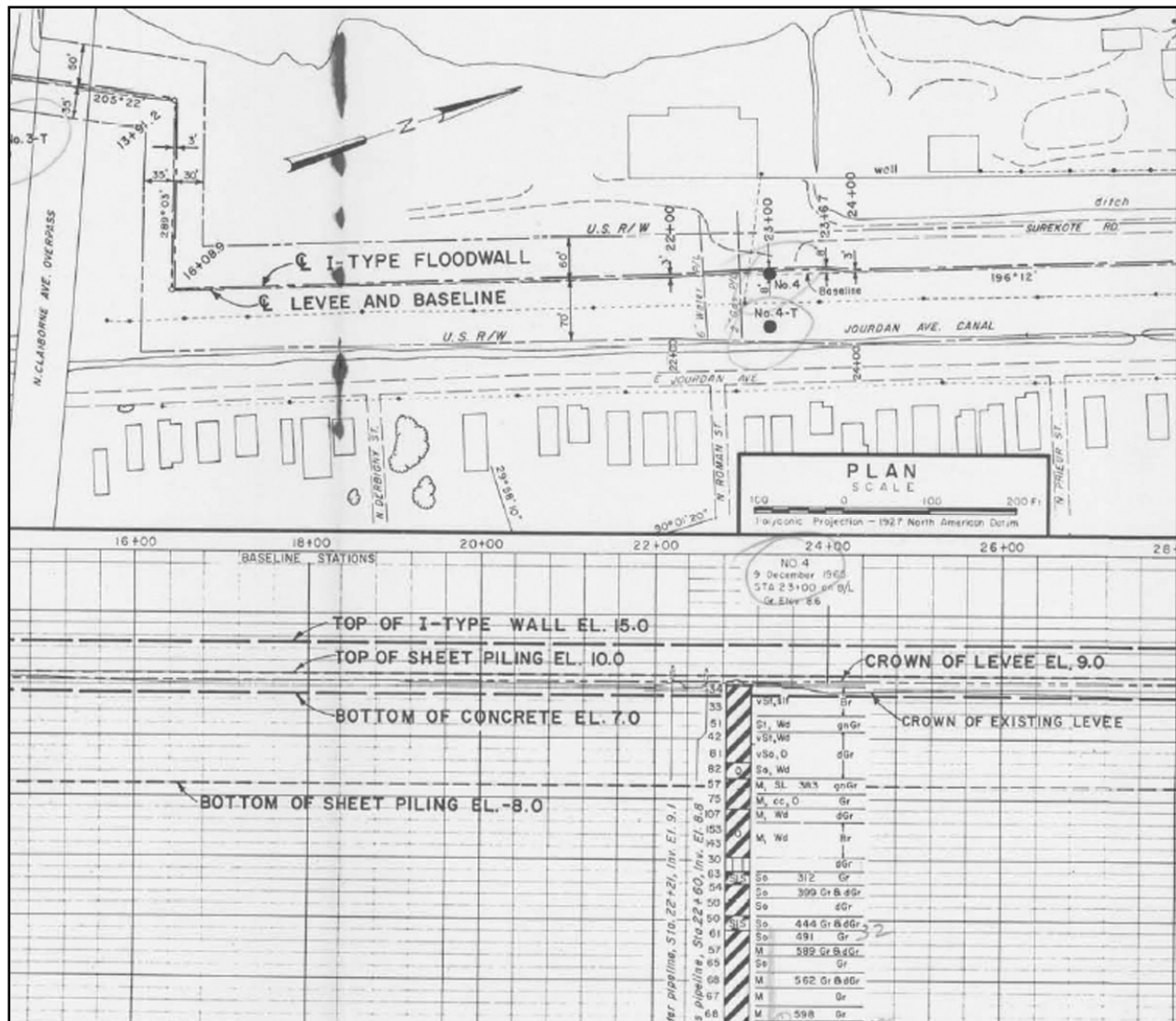
Figure 14-28. Nearby Soil Boring No. 4 Shows Existing Levee Soil and Elevations (from DM3 Chalmette drawing file H-2-23820, plate 3)

Figure 14-29. Florida Ave Bridge, View East. I-Wall Failure is Seen to Right of Bridge

Figure 14-30. Southernmost I-Wall Failure Transition Between Florida Ave and Claiborne Ave.

Figure 14-31. CPT Truck at Levee Toe on Protected Side at the Southernmost I-Wall Failure Transition Between Florida Ave and Claiborne Ave., View Toward Pump Station

Figure 14-32. Northernmost I-Wall Failure Transition Between Florida Ave and Claiborne Ave., View Toward Pump Station on the Protected Side
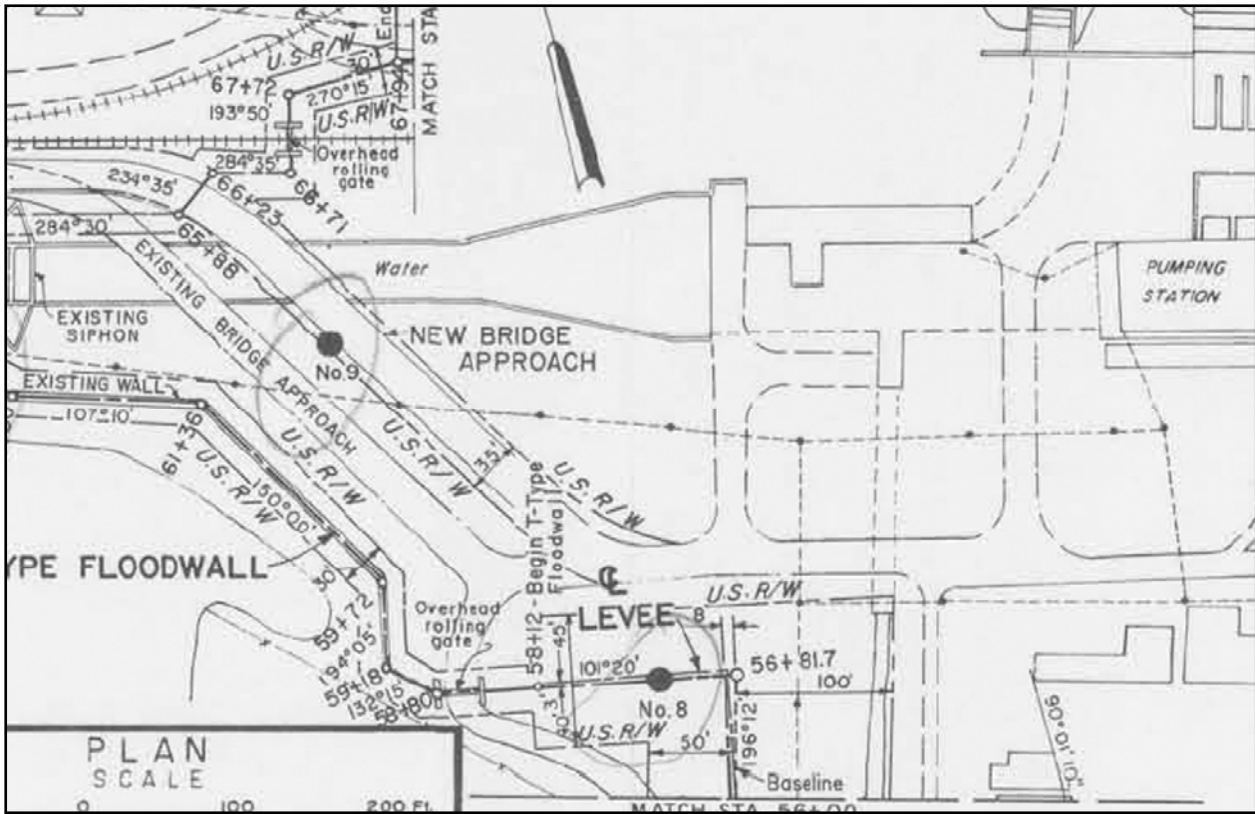
Figure 14-33. Soil boring No. 8 is Nearest to the Florida Ave Breach (from DM3 Chalmette drawing file H-2-23820, plate 5)
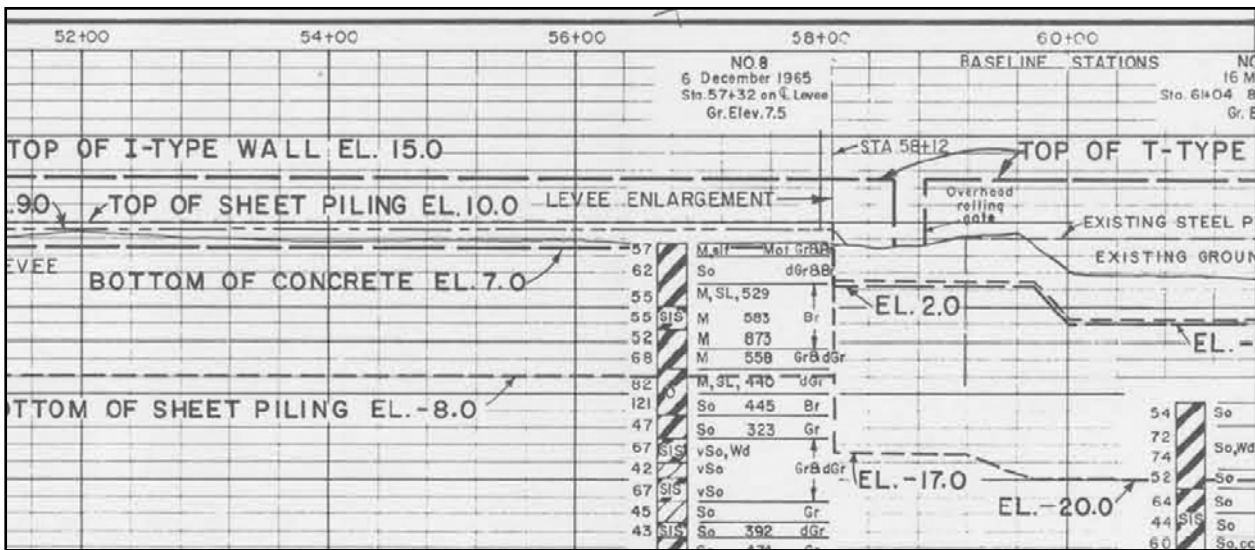
Figure 14-34. Soil Boring 8 Shows Fat Clay Soil and Sheetpile Elevation (from DM3 Chalmette drawing file H-2-23820, plate 5)
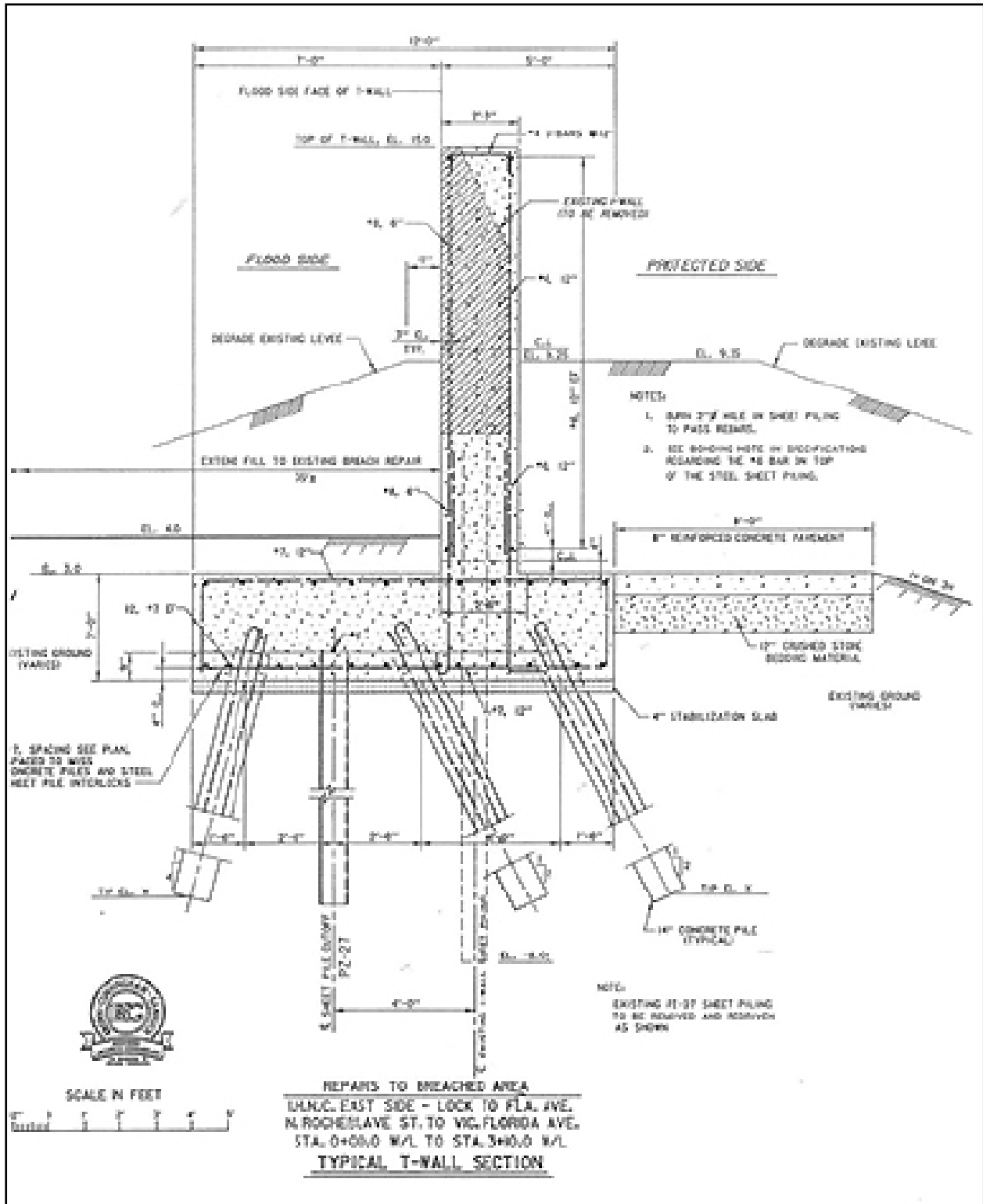
Figure 14-35. New "L" Wall ("Kicker Wall") Design for New Floodwall on IHNC East Side From Lock to Fla Ave., Sta 0+00 to 3+00

This is a preliminary report subject to revision; it does not contain final conclusions of the United States Army Corps of Engineers.

TFG Project: IHNC03 – East Side Levee and Floodwall Scour Repairs Lake Pontchartrain to the Gulf Intracoastal Waterway (GIWW)

Description: There are approximately 2.75 miles of floodwall and levee along the east side of the IHNC Canal between the Gulf Intracoastal Waterway and Lake Pontchartrain. The damages in this reach consisted of intermittent scour of the levee and scour and damage at the wall/gate closures and at the wall/levee interfaces. The repairs consist of filling in the scour areas, repairing the gate concrete sills and seals, installing new sheet piling, placing rock and ballast, and placing stone erosion protection. Scheduled completion is April 1, 2006.

~2.75 miles LONB (base scour on landside)

-5 locations WF / TF @ wall/levee transitions and wall/gate closure transitions, all south of the Twin Spans. Wall/gate and wall/levee locations (shown in picture on following page):

(A) under the I-10 high rise (Gate E9)
(B) 30 deg 00 min 15.82 sec N, 90 deg 01 min, 22.32 sec W (Gate E8)
(C) 30 deg 00 min 10.37 sec N, 90 deg 01 min, 19.55 sec W (Gate E7)
(D) " 02.39 sec N, " 16.68 sec W (Gate E6)
(E) 29 deg 59 min 55.92 sec W, " 14.39 sec W (Gate E5)
(F) " 48.84 sec W, " 11.57 sec W (RRGateE4)

All these soil boring locations south of the twin span are on plates IV-27 thru IV-30, DM2Supp8

Figure 14-36. Pre-Existing Top of Wall Elevation Along IHNC 03 Was 15 ft. Gate Top Elevations Were 14 ft

Figure 14-37. Approximate B/L Sta 101+00. Top of I-wall is elev 14.75, bottom of concrete is elev 7, and levee crown is elev 9. Nearest B/L boring is Sta 96+00 (No. 9EU), 500 feet distant
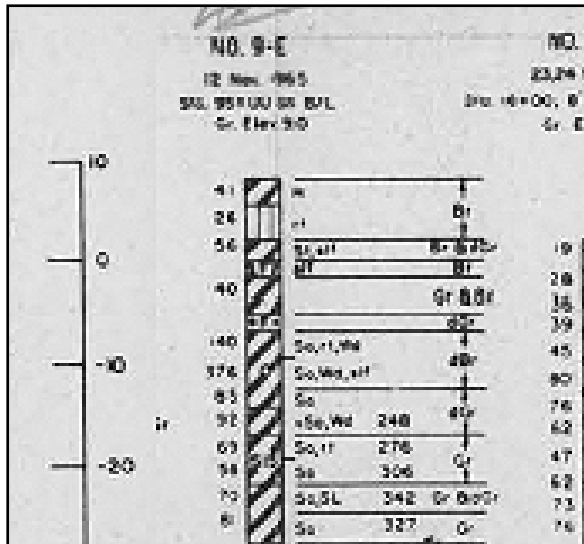
Figure 14-38. Boring 9E (Sta 95+00 B/L) Shows Approximate Depth of Fat Clay (CH) is 3 feet at Crown Elevation 9 ft
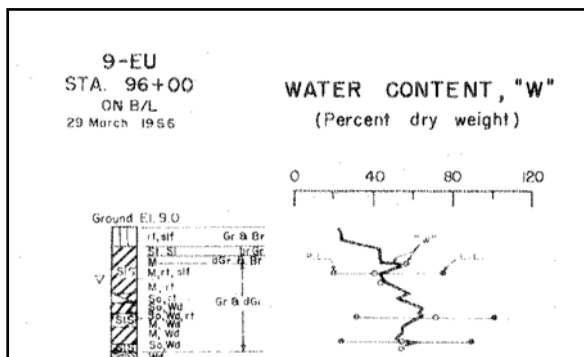
Figure 14-39. Boring 9EU (Sta 96+00 B/L) Shows Top Layer of Silt at Crown Elevation 9 ft

Figure 14-40. IHNC03 Project Repairs South of I-10 (WF / TF areas)

Figure 14-41. Scour at Gate 7E; Scour Measures 7' (w) x 30" (deep). Top of wall is at elev. 13.1 +/-

Figure 14-42. Gate E5 Looking South From Inside the Protected Area. Scour damage 7' (w) x 7' (d) around adjacent flood wall. Top of wall at gate is Elev. 13.2 +/-

Figure 14-43. Scour at Railroad Gate Closure Structure E4 at Southernmost IHNC03 Project. 29 deg 59 min 48.76 sec N, 90 deg 01 min 11.6 sec W (Sta 176+75.9)

Figure 14-44. E4 Scour Repaired

TFG Project: IHNC07 - Floodwall Repair, East Side, IHNC Lock to North Claiborne Ave.

Description: There is approximately 1,400 lineal feet of concrete I-wall flood barrier along the east side of the IHNC Canal between the IHNC lock and North Claiborne Avenue. The damages along this reach consisted of intermittent scour along the base of the floodwall. The work includes filling in the scour repairs and providing erosion protection. Contract Award NTP scheduled for early February, 2006.

1400' WNF / WS (base scour on landside)
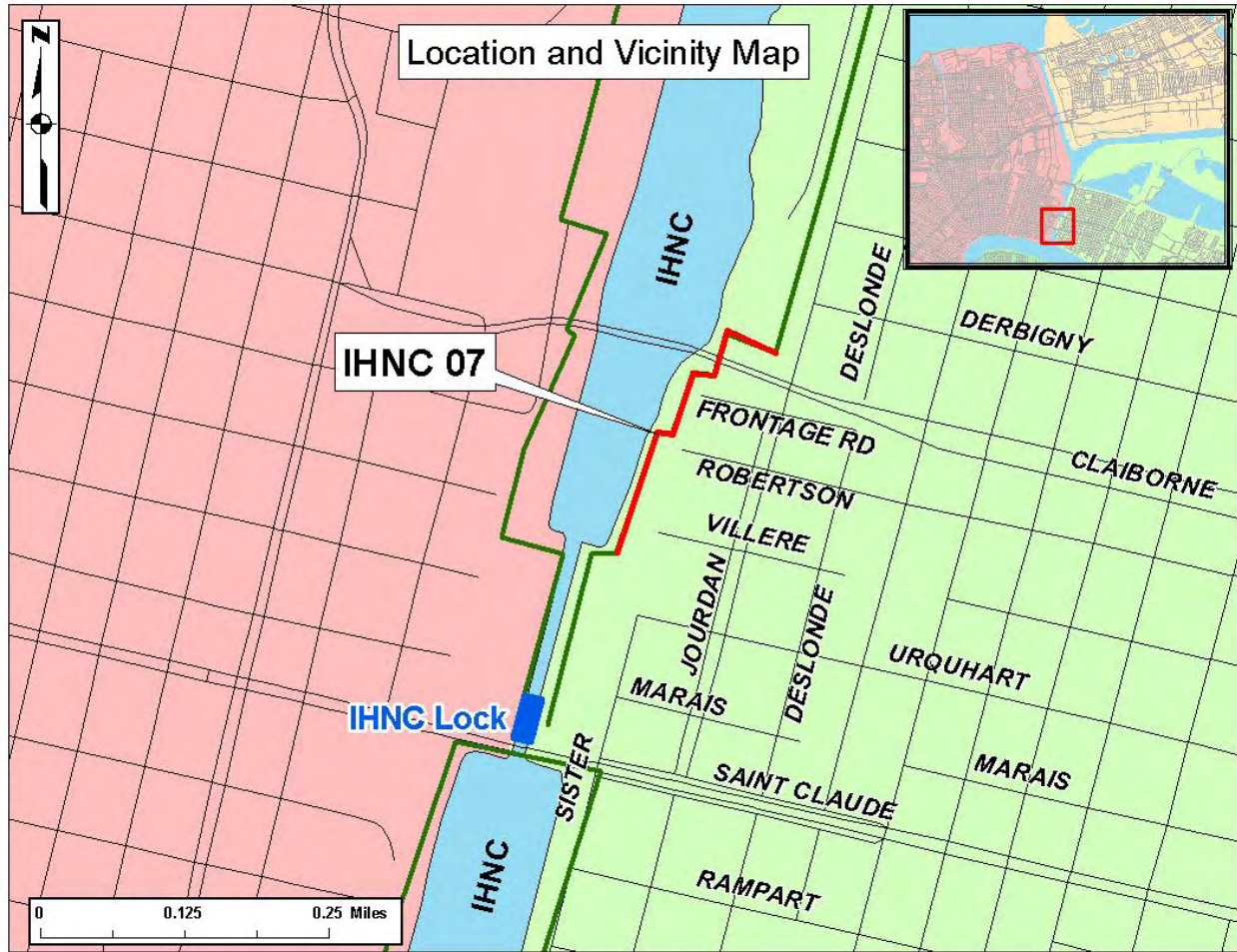
Figure 14-45.

Figure 14-46. Scour at I-Wall / Levee Transition at IHNC Lock

Figure 14-47. Approximate B/L Sta 7+00, View Toward Claiborne Ave. Bridge. Depth of scour was to the bottom of the I-wall concrete cap. Nearby soil boring 2U indicates the upper 5 ft was fat clay (CH) with sand / silt lenses
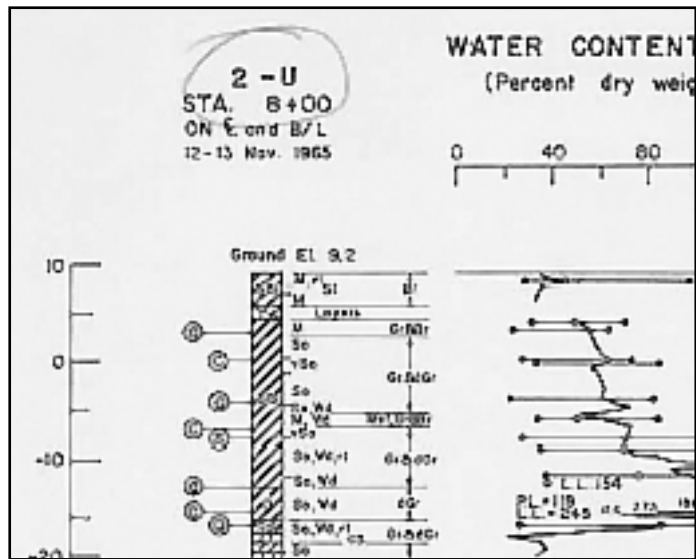
Figure 14-48. Undisturbed Boring 2U Located 100 ft Distant, Shows Fat Clay (CH) With Silt / Sand Lenses in Upper 5 ft. Undrained shear strength in upper 3.2 ft was approximately 500 psf

Figure 14-49. East Side IHNC Near N. Claiborne Ave, Approximate B/L Sta 11+00. I-wall elevation designed 15 ft (MSL), bottom of concrete elevation 7 ft (MSL), and levee crown elevation 9 ft (MSL). Nearest soil boring, No. 3, shows fat clay (CH) at surface

West Side IHNC

TFG Project: IHNC05 – IHNC West Side, Vicinity France Road Ramp to IHNC

Description: This portion of the project consists of approximately 1,600 feet of existing levee and concrete floodwall that extends from the vicinity of France Road ramp towards the IHNC. This area was breached and experienced severe scour. The repair consists of replacement with a new concrete T-Wall. Scheduled completion is April 15, 2006.

1600' WF (soil boring Plate IV-16 in DM2Supp8)

Figure 14-50.

IHNC

GIWW

Benefit

France Rd Ramp
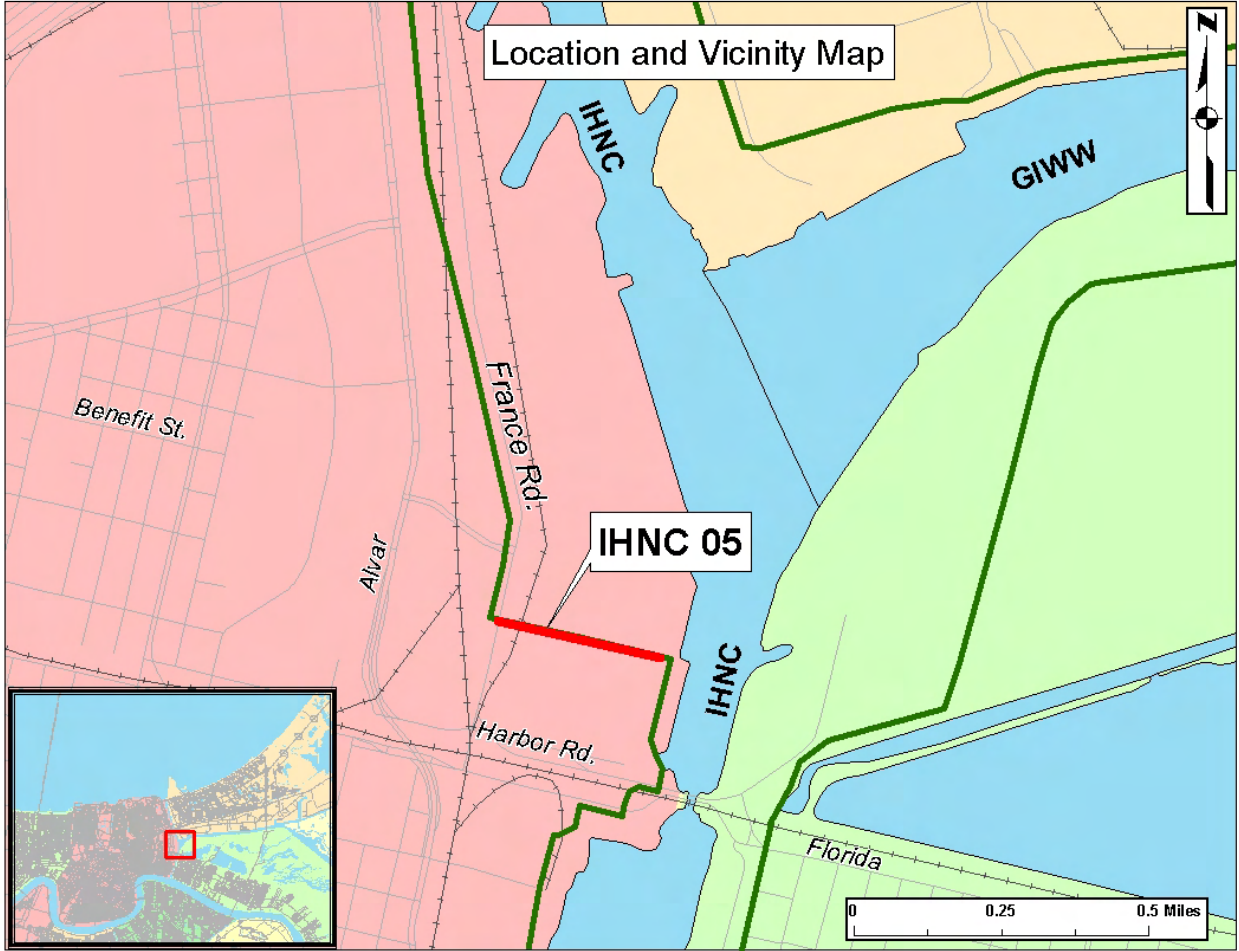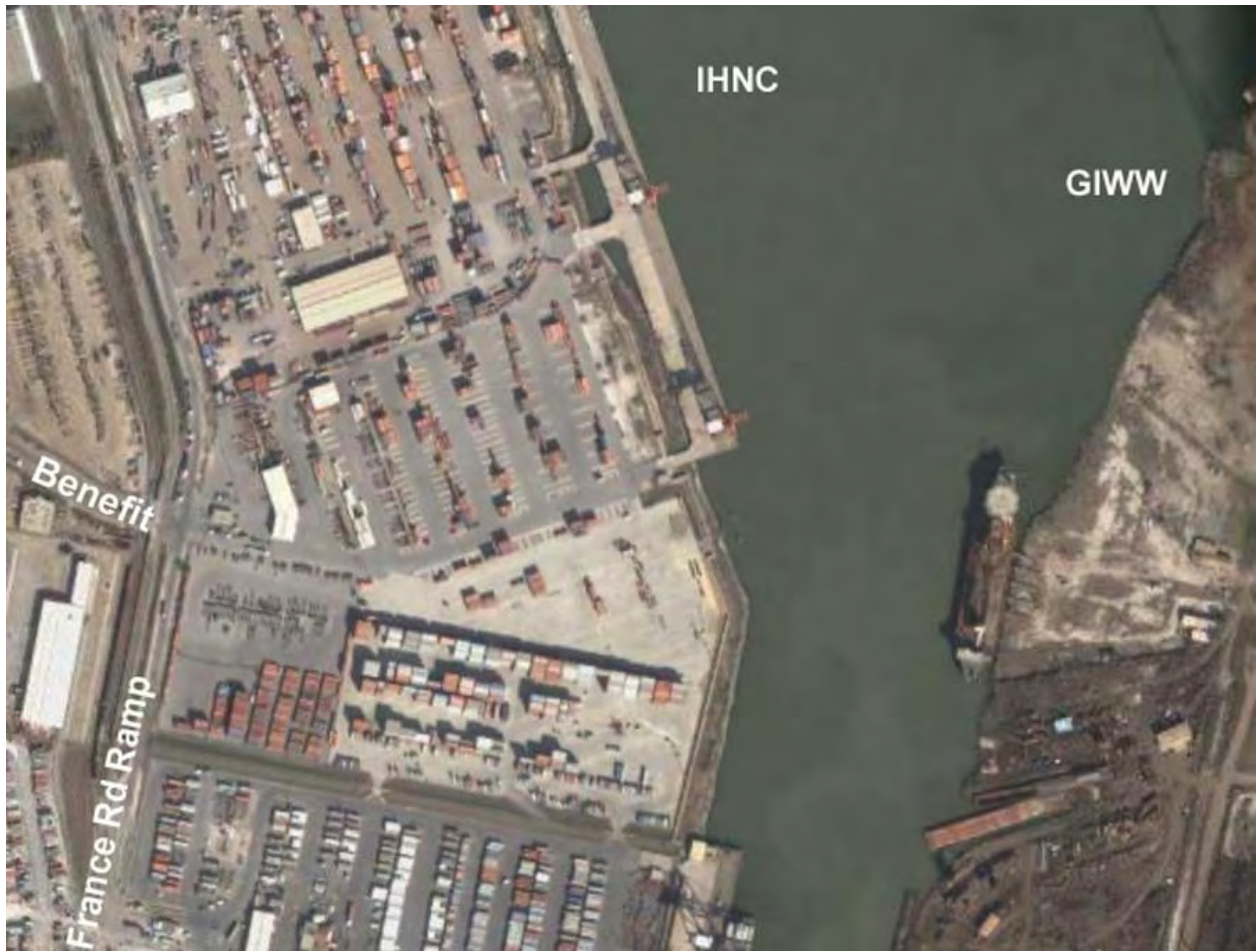
Figure 14-51. Container Terminal, West Side of IHNC Just North of Florida Ave.
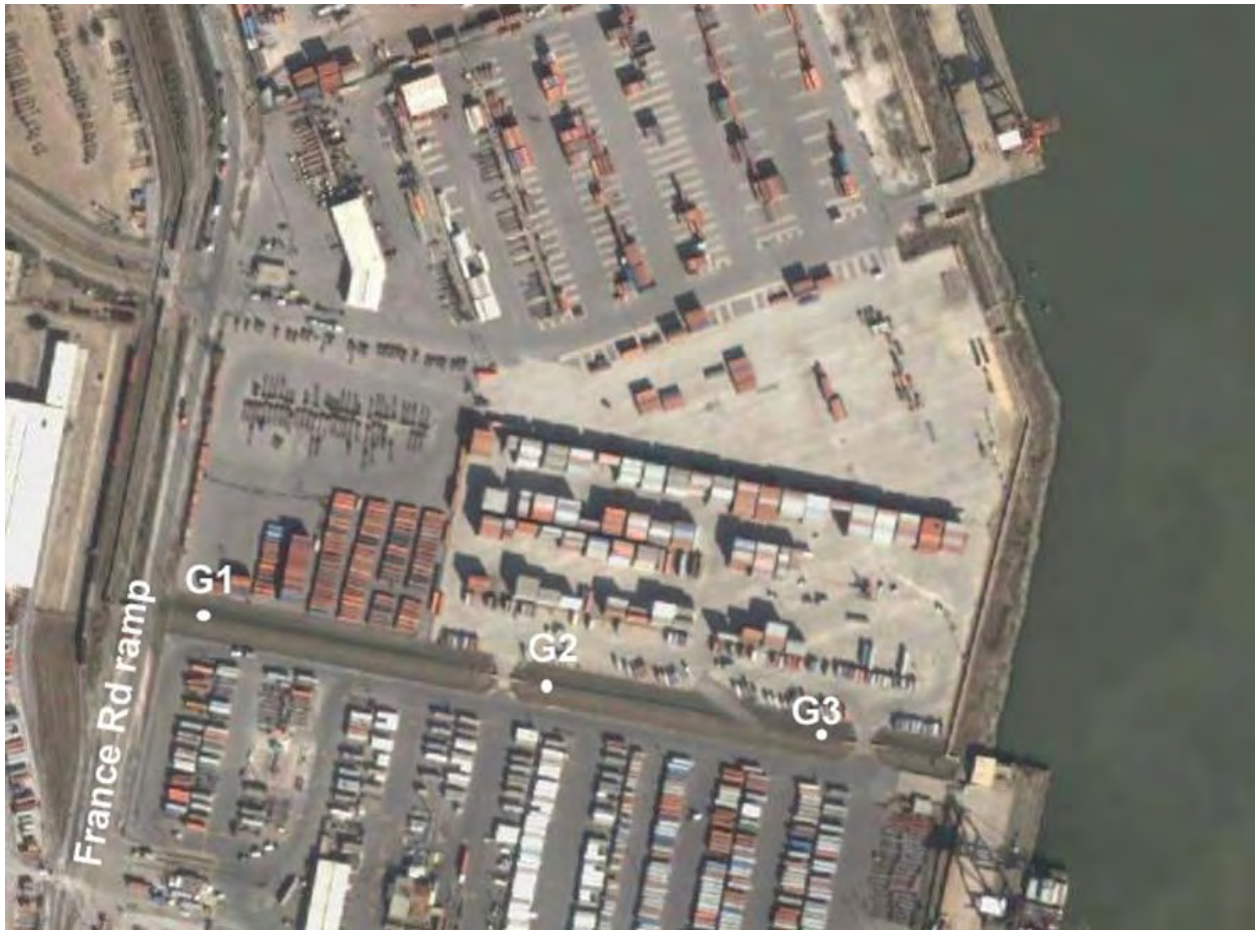
Figure 14-52. Levee / Floodwall Between IHNC and France Rd Showing Soil Boring Locations

Figure 14-53. Overtopped Levee Section With Scour. View west from approximate CL Sta 14+00, B/L Sta 222+00
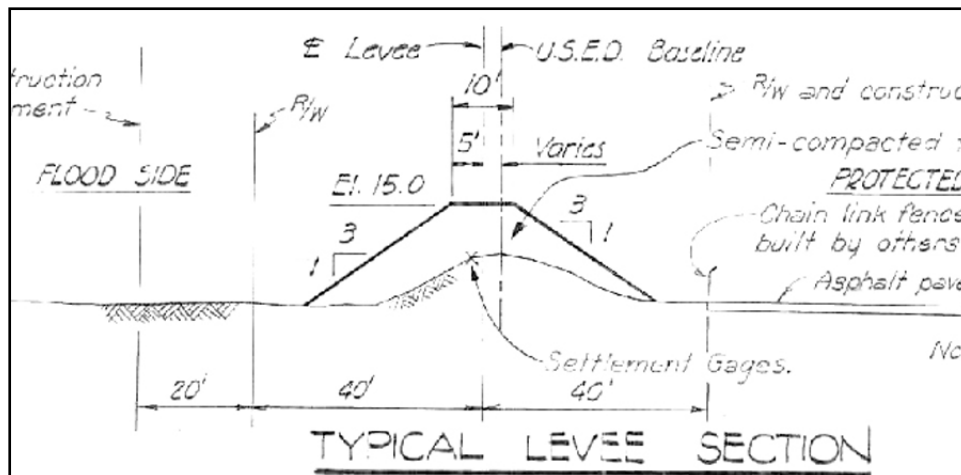
Figure 14-54. Levee Section Between IHNC and France Rd Ramp Shows Elevation 15 ft on Top of Existing Levee
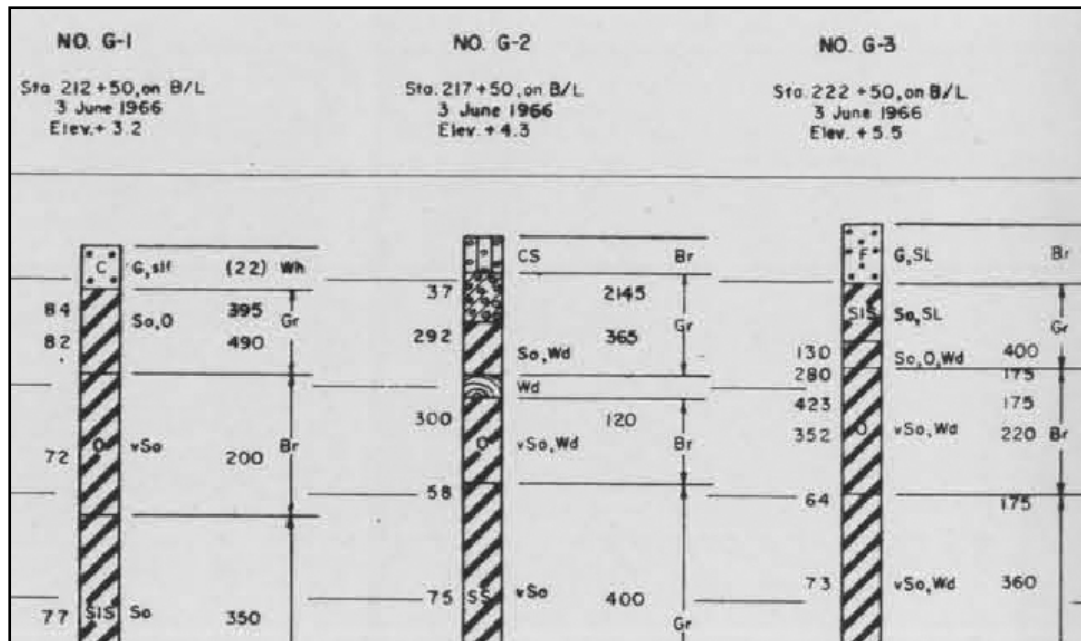
Figure 14-55. Nearest Boring G-3 Shows Original Ground Surface (elev 5.5 ft MSL) to be Sandy (from drawing file H-2-24111, plate IV-33)

Figure 14-56. View West from France Rd. Ramp (approximate B/L Sta 212+00, C/L Sta 0+00). Remaining levee covered with fresh aggregate in preparation for new concrete wall construction

Figure 14-57. Nearest Boring G-1 Shows Sandy Material at Original Ground Surface (may have provided a zone facilitating levee failure)

TFG Project: IHNC02 – IHNC west side South France Road Ramp to 770 feet North of Benefit Street

Description: – This section of the project consists of concrete I-wall. The damage in this area consisted of a breach of the floodwall at the container terminal along France Road. There was also heavy scour of the floodwall in this area. The repairs consist of removing approximately 1,300 lineal feet of the damaged concrete I-wall and replacing the damaged section of wall with new concrete L-wall. The new wall will be supported by steel H-piles and longer steel sheet piles. Scheduled completion is April 15, 2006.

1300' WF @ container terminal along France Rd.

Profile and soil boring info for this reach is found in SuppDesignInfo IHNC RemainingLevees.pdf (1969) and ModificationProtectiveAlinement IHNC Oct71.pdf (1971)

Figure 14-58.

Volume V The Performance – Levees and Floodwalls – Technical Appendix   V-14-59

This is a preliminary report subject to revision; it does not contain final conclusions of the United States Army Corps of Engineers.

Figure 14-59.

This is a preliminary report subject to revision; it does not contain final conclusions of the United States Army Corps of Engineers.

Figure 14-60. View South From Benefit St. Gate Toward France Rd Ramp. Approximate W/L Sta 5+56 (B/L Sta 205+44). Top of I-wall elevation 15 ft, levee crown 9 ft, bottom of concrete 7 ft, bottom of pre-existing Z-27 sheet pile (by Orleans Levee Board) at -10ft (MSL). From drawing file H-2-24111, plate IV-15. Nearest soil boring is 30W at B/L Sta 203+00
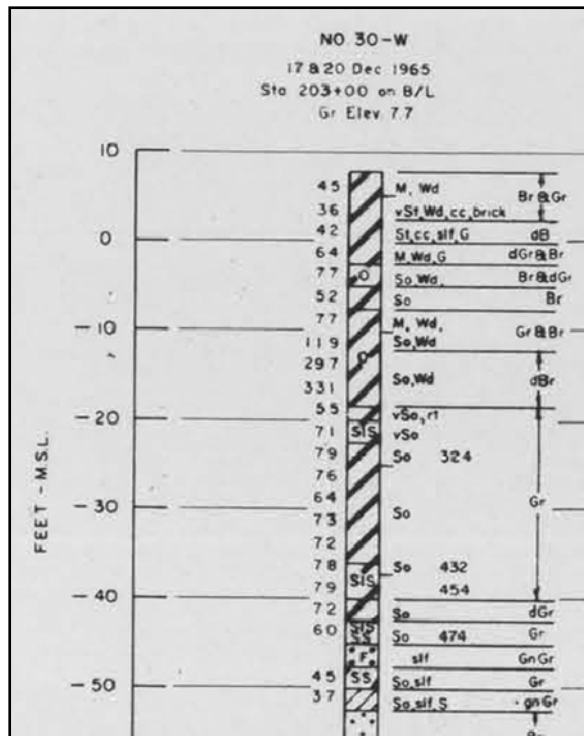
Figure 14-61. Boring 30W Near Benefit St Gate Shows Fat Clay Soil Layers

Figure 14-62.

Figure 14-63.

Figure 14-64.

Figure 14-65.
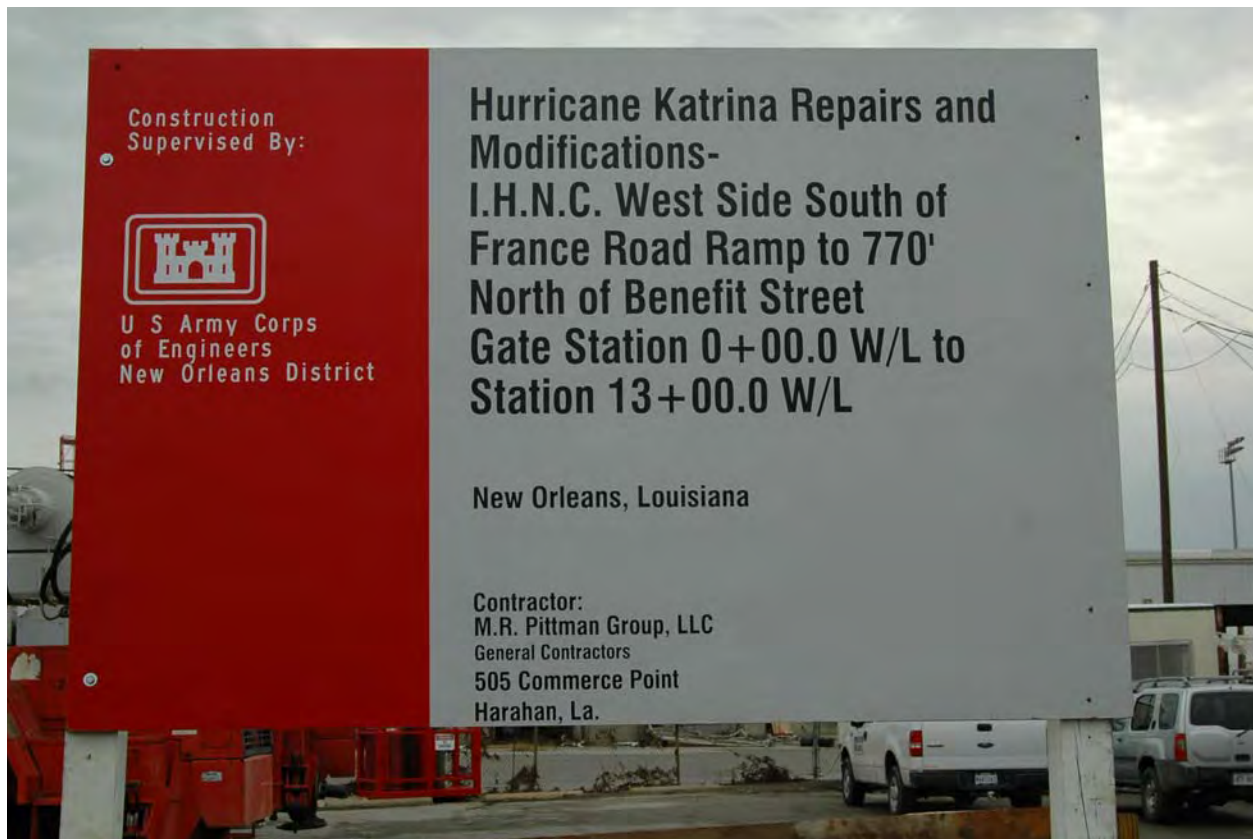
Figure 14-66.
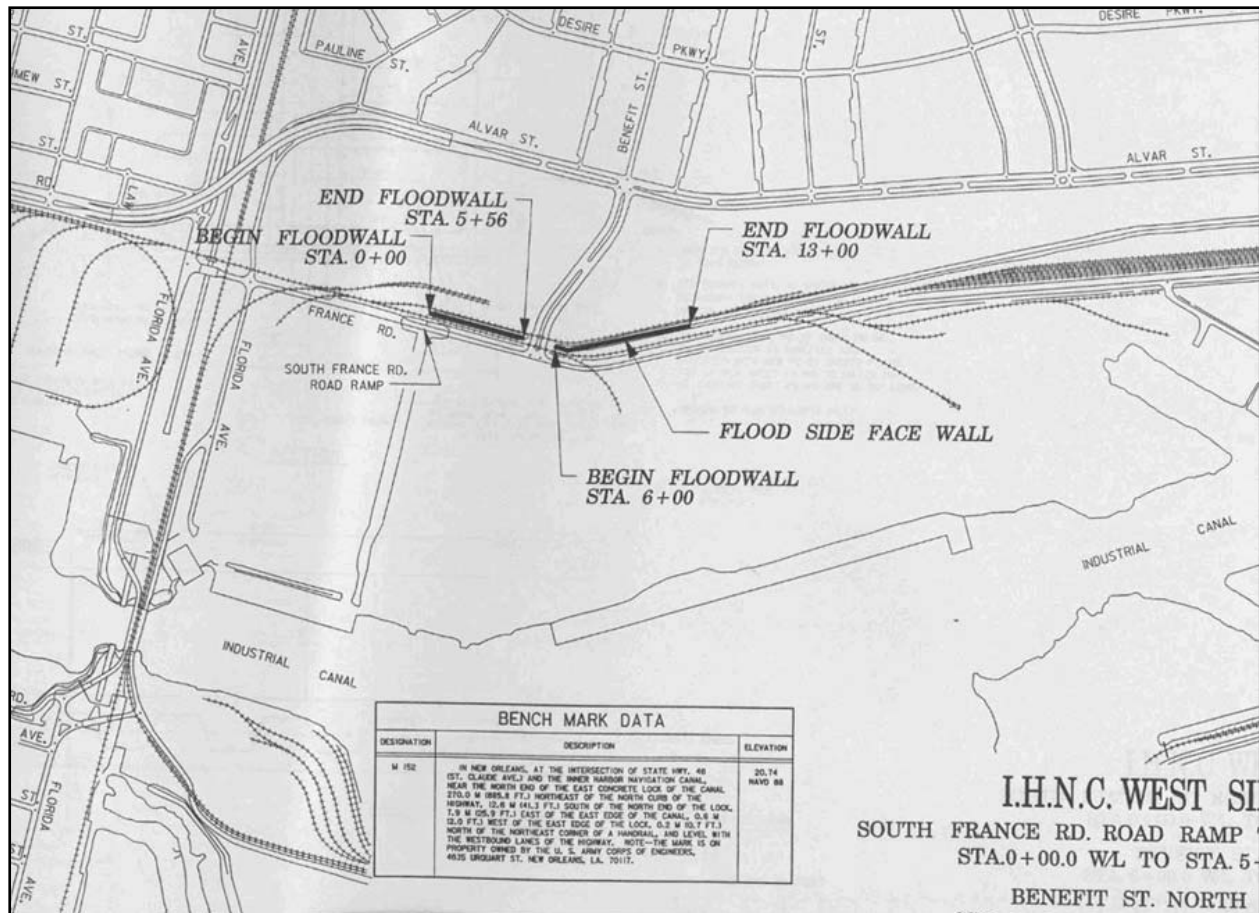
Figure 14-67. Contract Solicitation IHNC02 W912P8-05-R-0069 Layout Drawing

Volume V The Performance – Levees and Floodwalls – Technical Appendix

Figure 14-68.
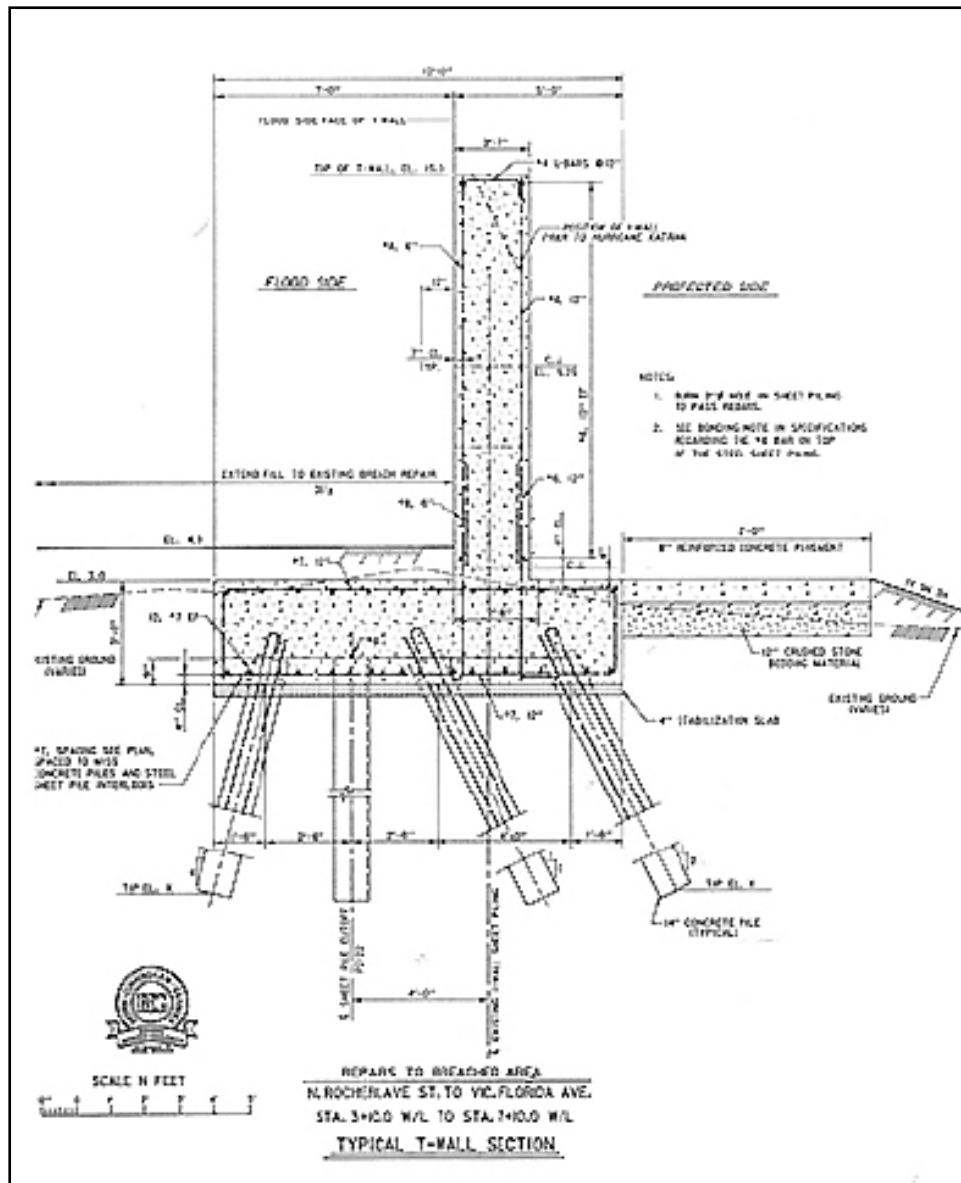
Figure 14-69.

Figure 14-70. New "Kicker Wall" Design, Sta 3+00 to 7+00

There is no IHNC06 TFG project.

TFG Project: IHNC08 – West Side 700' North of Benefit St. to Hwy 90

Description: This section of flood protection consists of concrete I-Wall embedded in compacted earthen levee embankment. The damages in this area consisted of scour along the base of the floodwall. The repairs consist of scour repair and erosion protection. Contract Award NTP scheduled for early February, 2006.

700' north of Benefit St. to Hwy 90 = ~6000' WNF / WS (base scour on landside)
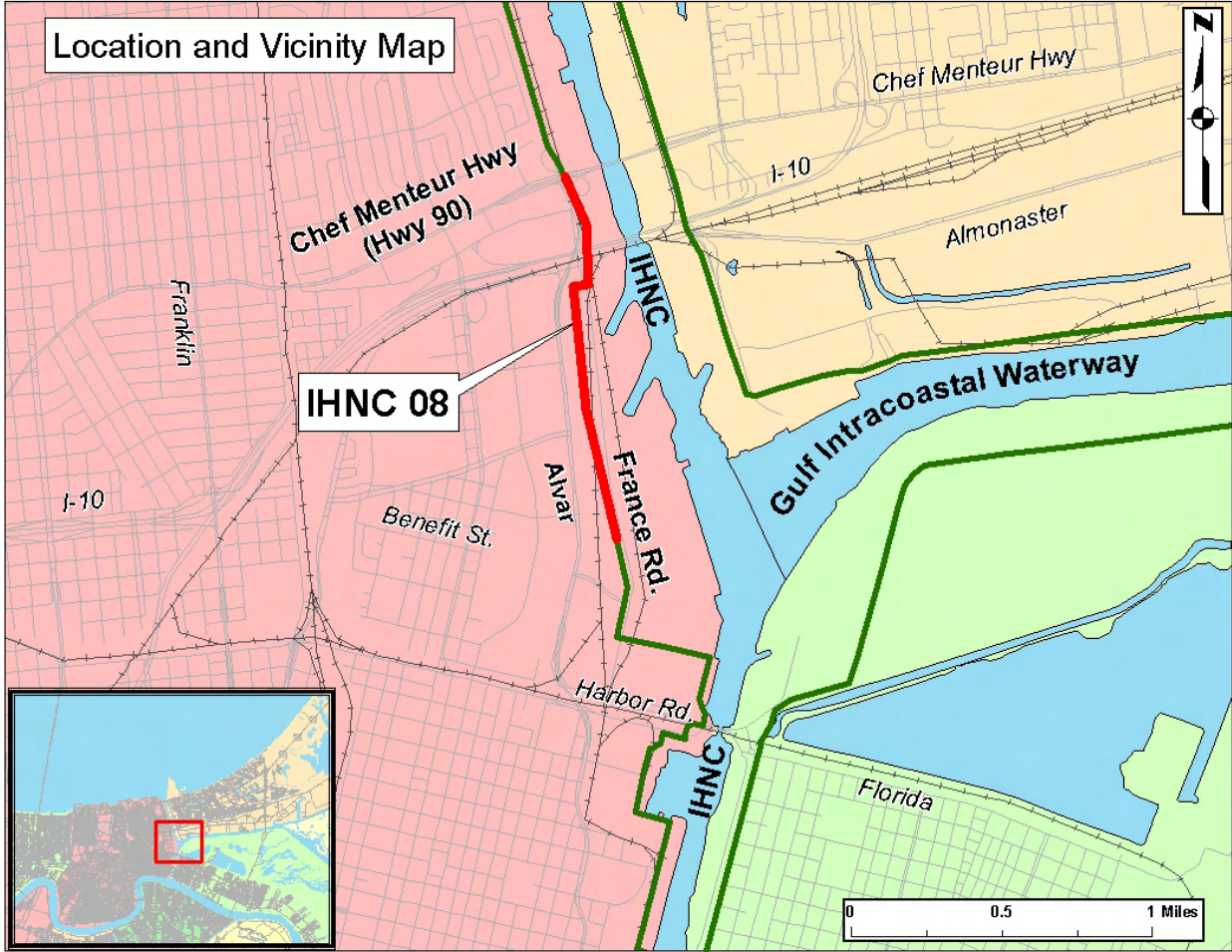
Figure 14-71.

Figure 14-72. Scour at T-Wall Base of Gate W23

TFG Project: IHNC04 – IHNC Hurricane Protection Levee Hayne Boulevard to Highway 90

Description: West Side from Hayne Blvd. to Hwy 90 - This segment of flood protection consists of concrete I-wall extending from Hwy 90 to Lake Pontchartrain. The floodwall along this segment experienced relatively minor scour damage along its base. The repairs consist of filling in the scour areas, installing steel sheet pile walls to prevent canal seepage from going beneath the wall, and cleaning existing and installing new relief wells. Scheduled completion is April 1, 2006.

8,400' WNF (base scour on landside), Hayne Blvd to Chef Menteur Hwy

Figure 14-73.

Figure 14-74.

			GPS Coordinates						Scour Dimensions (Feet)				Scour Damage Class	Condition of Floodwall	
			Degrees (N)	'	"	Degrees (W)	'	"							
DSR ID #	Type of Structure								Length	Depth	Width	Cu-yd to fill		Type	Description
Lock to Florida Avenue (West side)															
W-1	Levee with I-wall (capped)	Start/End	29	57	59.3	90	1	37.2	20				II	I-Wall	Scour adjacent to wall
W-2	Gates W2, W3 (T-wall monoliths)	Start	29	58	65.3	90	1	37.5	500	3	15	833	I	T-Wall	Scour adjacent to wall
		End	29	58	8.9	90	1	36.1							
W-3	Gates W4, W5 (T-wall monoliths)	Start	29	58	8.9	90	1	36.1	700	3	15	1,167	I	Gate monolith	Scour adjacent to wall
		End	29	58	13.6	90	1	36.2							
W-4	Wall btwn Gates W5, W6 (T-wall monoliths	Start	29	58	13.6	90	1	36.2	1,460	3	15	2,433	I	Gate monolith	Scour adjacent to wall
		End	29	58	27.9	90	1	31.8							
W-5	Wall between Gate W6 and Namasco Bldg	Start	29	58	27.9	90	1	31.8	1,330	3	5	739	I	Gate monoliths, T-wall	Scour adjacent to wall
	to Gate W13 (T-wall, I-wall monoliths)	End	29	58	38.6	90	1	34.8						I-wall	
W-6	Wall btwn Gate W14 and Gate W15 (T-wall	Start	29	58	40.7	90	1	33.8	300	2	5	111	I	Gate monoliths, I-wall	Scour adjacent to wall
	and I-wall monoliths)	End	29	58	43.4	90	1	33.1							
W-7	Gate W17	Start/End	29	58	48.6	90	1	32.7	30	1	3	3	I	Gate monoliths	Scour adjacent to wall
W-8	Gate W18 to Gate W19	Start	29	58	48.6	90	1	32.3	600	2	5	222	I	I-wall	Scour adjacent to wall
		End	29	58	49.0	90	1	31.2							
W-9	Gate W19 to Gate W20	Start	29	58	49.0	90	1	31.2	200	4	5	148	I	I-wall	Scour adjacent to wall
		End	29	58	50.7	90	1	25.4							
W-10	Gate W20 to GateW22 (adjacent to PS#19	Start	29	58	50.7	90	1	25.4	200	2	5	74	I	I-wall	Scour adjacent to wall
		End	29	58	53.0	90	1	22.8							
Florida Avenue to Hwy 90 (West side)															
W-11	Gate W23	Start/End	29	58	56.2	90	1	27.9	30	4	15	67	II	T-wall	Scour adjacent to wall
W-12	Gate W2 to W3	Start	29	58	56.5	90	1	22.5	300	3	5	167	I	I-wall	Scour adjacent to wall
		End	29	59	4.0	90	1	19.9							
W-13	Levee	Start	29	59	4.7	90	1	23.4	150	Scour repaired			II		Scour repaired w/ aggregate
		End	29	59	4.8	90	1	25							
W-14	Gate W25B to Gate W26	Start	29	59	4.7	90	1	23.4	800	Scour repaired			III		Scour around gate W25B and
		End	29	59	8.0	90	1	38.2							on P/S of Gate W26
W-15	Gate W26 to Gate W28	Start	29	59	8.0	90	1	38.2	500	5	10	926	I	I-wall	Some scour backfilled by RR
		End	29	59	14.3	90	1	36.7							
W-16	Levee with I-wall (capped)	Start	29	59	18.7	90	1	37	200	Breach repaired			III	I-wall	I-wall rotated, breached,
		End	30	0	9.0	90	1	45.9							and scoured
W-17	Gate W29	Start	30	0	10.1	90	1	42.1	240	2	6	107	I	I-wall	Scour adjacent to wall
		End	30	0	12.3	90	1	41							
W-18	Levee with I-wall (capped)	Start	30	0	18.7	90	1	38.1	90	2	3	20	I	I-wall	Scour adjacent to wall
		End	30	0	19.6	90	1	38.3							
W-19	Gate W32 to Gate W34	Start	30	0	20.7	90	1	38.6	220	1	2	16	I	I-wall	Scour adjacent to wall
		End	30	0	26.1	90	1	40.4							

Figure 14-75.

This is a preliminary report subject to revision; it does not contain final conclusions of the United States Army Corps of Engineers.

St. Bernard Parish
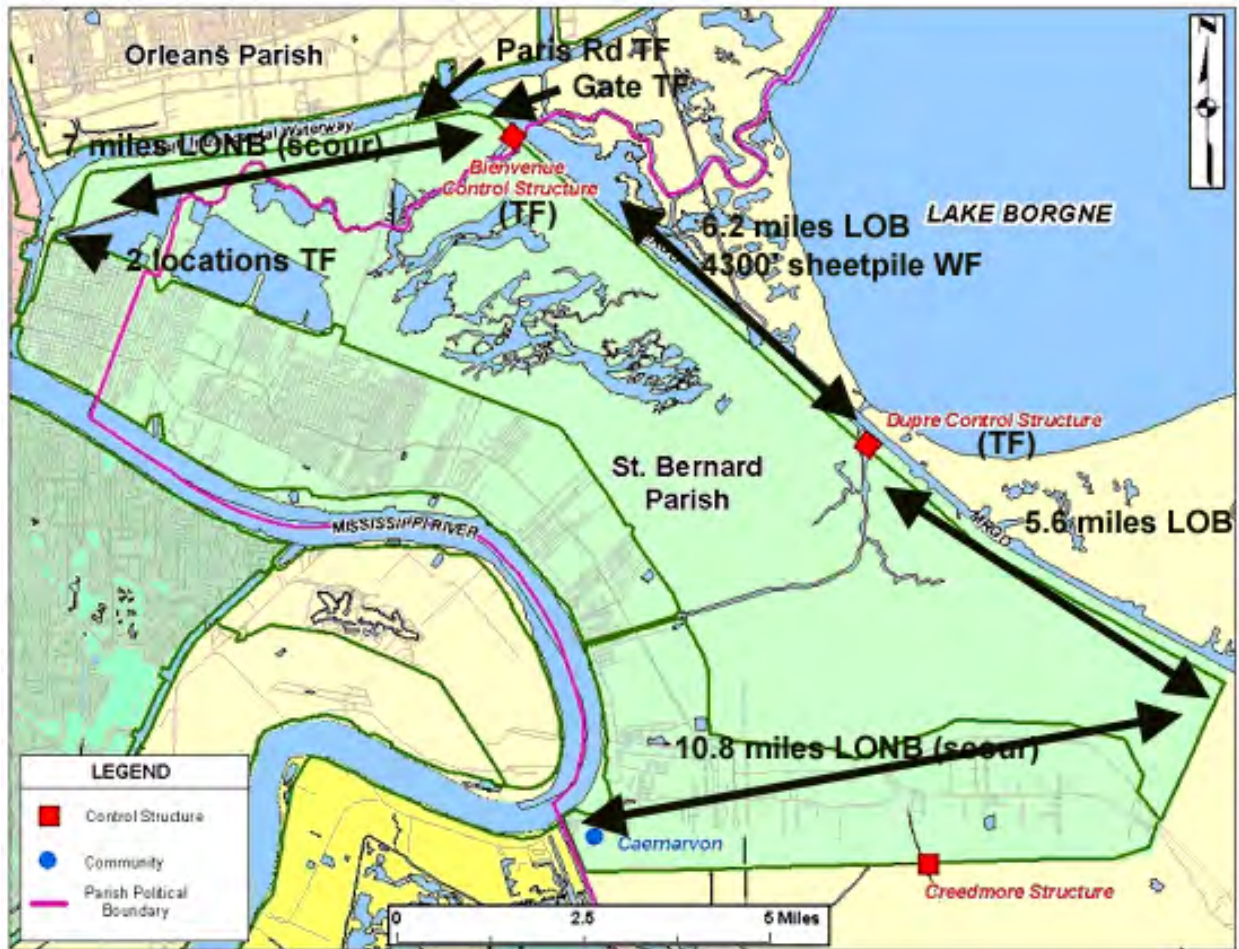
Figure 14-76. Damaged Areas in the St Bernard Basin

- LONB = Overtopped levees, no breaching
- WS = Overtopped floodwalls, no breaching (stable)
- LOB = Overtopped levees, breaching
- TF = Transition failure (floodwall to levee transition)
- WF = Overtopped floodwalls, breached (failure)
- WCF = Overtopped floodwalls, no breaching but came close

Overtopping was generally associated with varying degrees of scour (surface erosion), generally on the levee landside.

Pre-Katrina Hurricane Protection Features:

- 157,800 ft (30 miles) of Levees and Floodwalls
- 6 Road Closure Structures
- 2 Water Control Structures (Bayous Bienvenue and Dupre)

- 1 Gravity Drainage Structure (Creedmore)
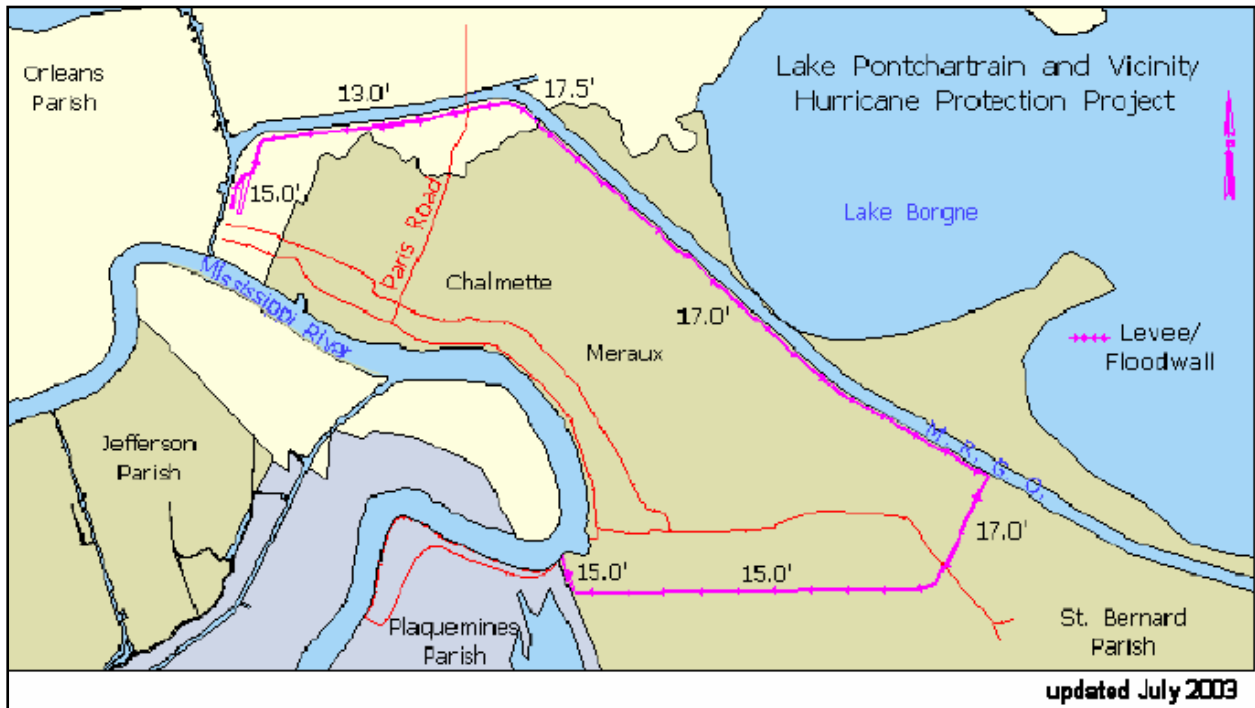
Figure 14-77. Authorized Heights. Note that St. Bernard Parish does not encompass either the IHNC East or GIWW (both of which are in Orleans Parish). However, these levee portions are geographically combined with the St. Bernard levee system

DMs:

REVIEW OF REPORTS

ST. BERNARD PARISH, LOUISIANA

DEPARTMENT OF THE ARMY
NEW ORLEANS DISTRICT, CORPS OF ENGINEERS
NEW ORLEANS, LOUISIANA

18 NOVEMBER 1969
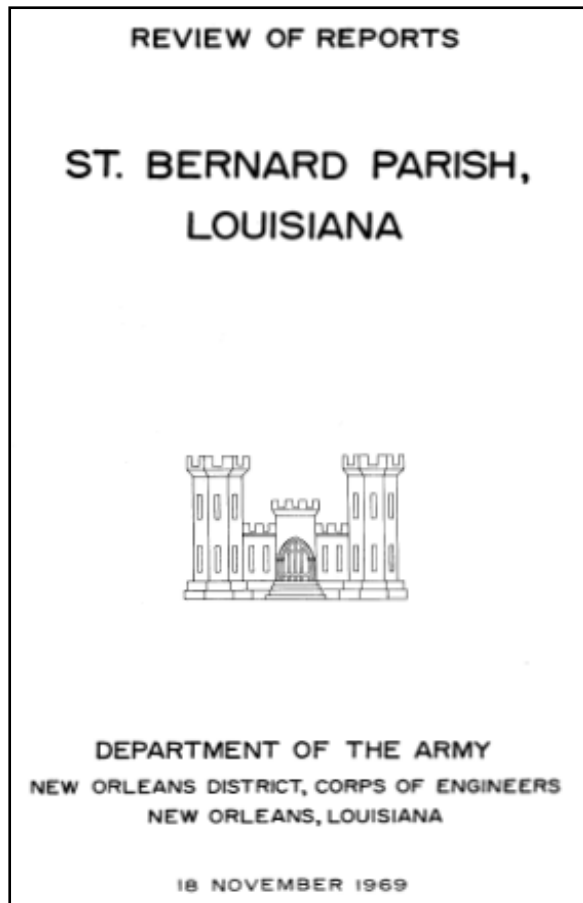
Figure 14-78. ReviewofReports.pdf provides a good background of original and modified hurricane protection authorizations for St. Bernard Parish
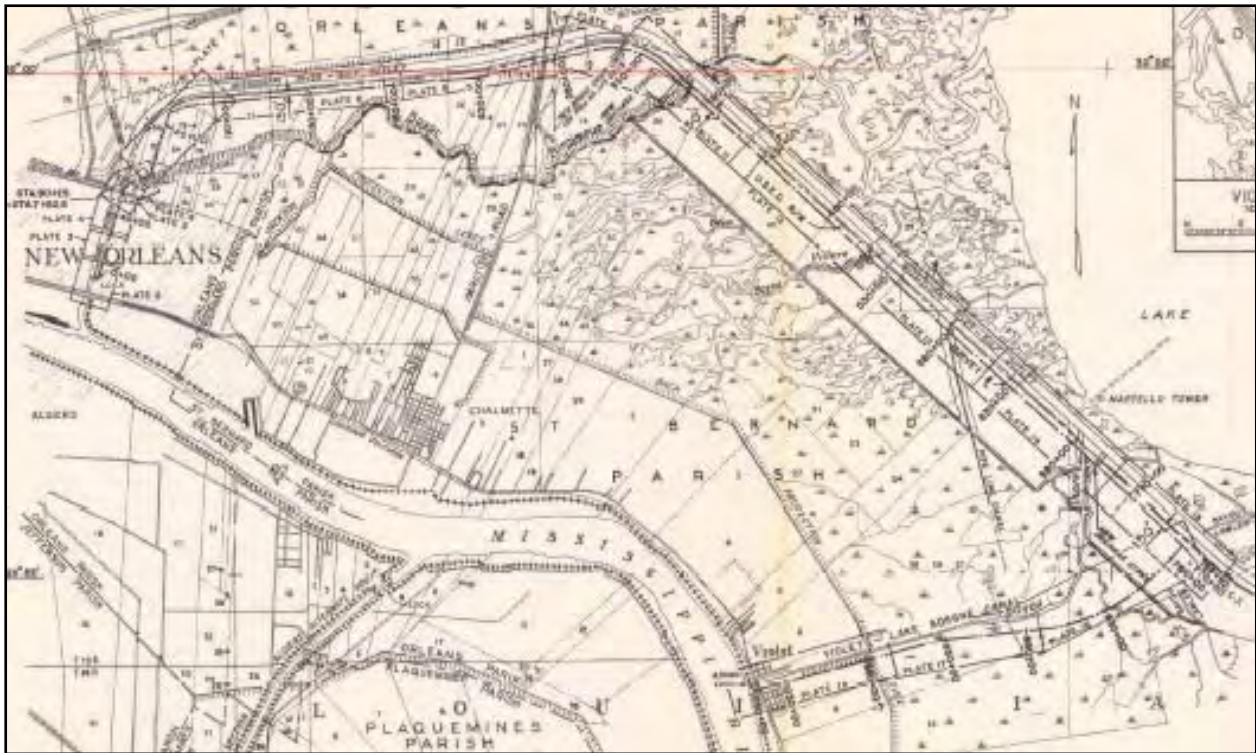
Figure 14-79. Pre-1966 Levee Sections and Soil Borings are Shown in Plates 2 thru 18 in DM3ChalmetteArea.pdf
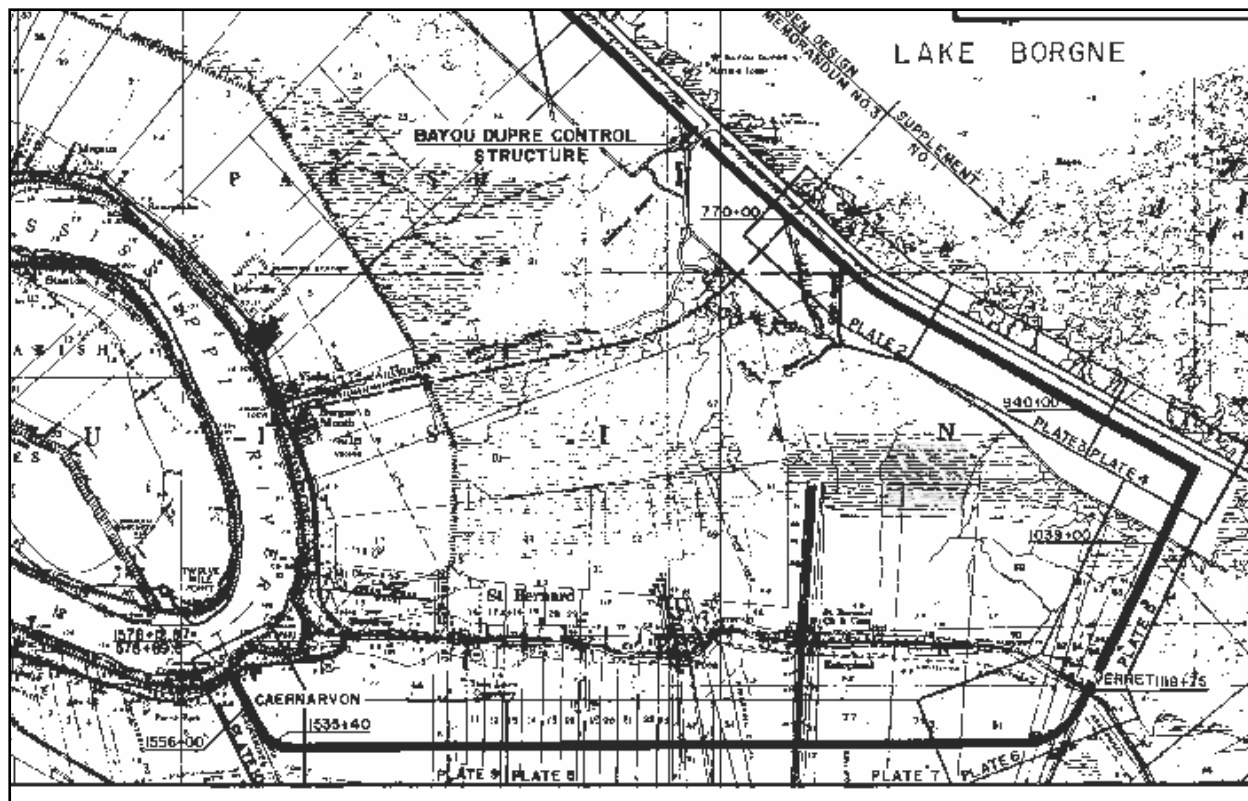
Figure 14-80. Pre-1968 Levee Sections and Soil Borings are Shown in Plates 2 thru 9, DM3ChalmetteExtension.pdf

Damages from Hurricane Katrina:

- Total Length of Levee w/o Cross Section – 27,000 ft.
- Total Length of Levee w/Reduced Cross Section – 4,800 ft.
- Total Length of Damaged Floodwall – <u>7,200 ft.</u>
- 38,000 ft.

8 miles of the 30 total miles of Federal hurricane protection levee were damaged (Non-Fed levees total 22 miles and damage isn't included herein). Most severely damaged levees are along the reach adjacent to the MRGO extending from the Bayou Bienvenue Control Structure to the southeast for 11.8 miles. Minor levee scour along GIWW in Orleans Parish. Miscellaneous scour on the levee from MRGO to Caernarvon.

- Bayou Bienvenue Control Structure – steel gate, structural, mechanical and electrical damage.
- Bayou Dupre Control Structure – structural, mechanical and electrical damage.
- Paris Road Closure Structure – structural damage and scour of floodwall backfill.
- Road Closure West of Bienvenue – scour of structural backfill.
- 2 Road Closures near Southern Scrap (STA. 67+00) – scour of structural backfill.
- Creedmore Drainage Structure – debris and damage to structure and gate hoists.

Volume V The Performance – Levees and Floodwalls – Technical Appendix   V-14-81

This is a preliminary report subject to revision; it does not contain final conclusions of the United States Army Corps of Engineers.

Nine separate construction contracts have been let to repair damaged areas and restore flood protection to pre-Katrina conditions, with approximately $47.2 million in construction costs (Task Force Guardian). These projects are labeled STB01 through STB09.
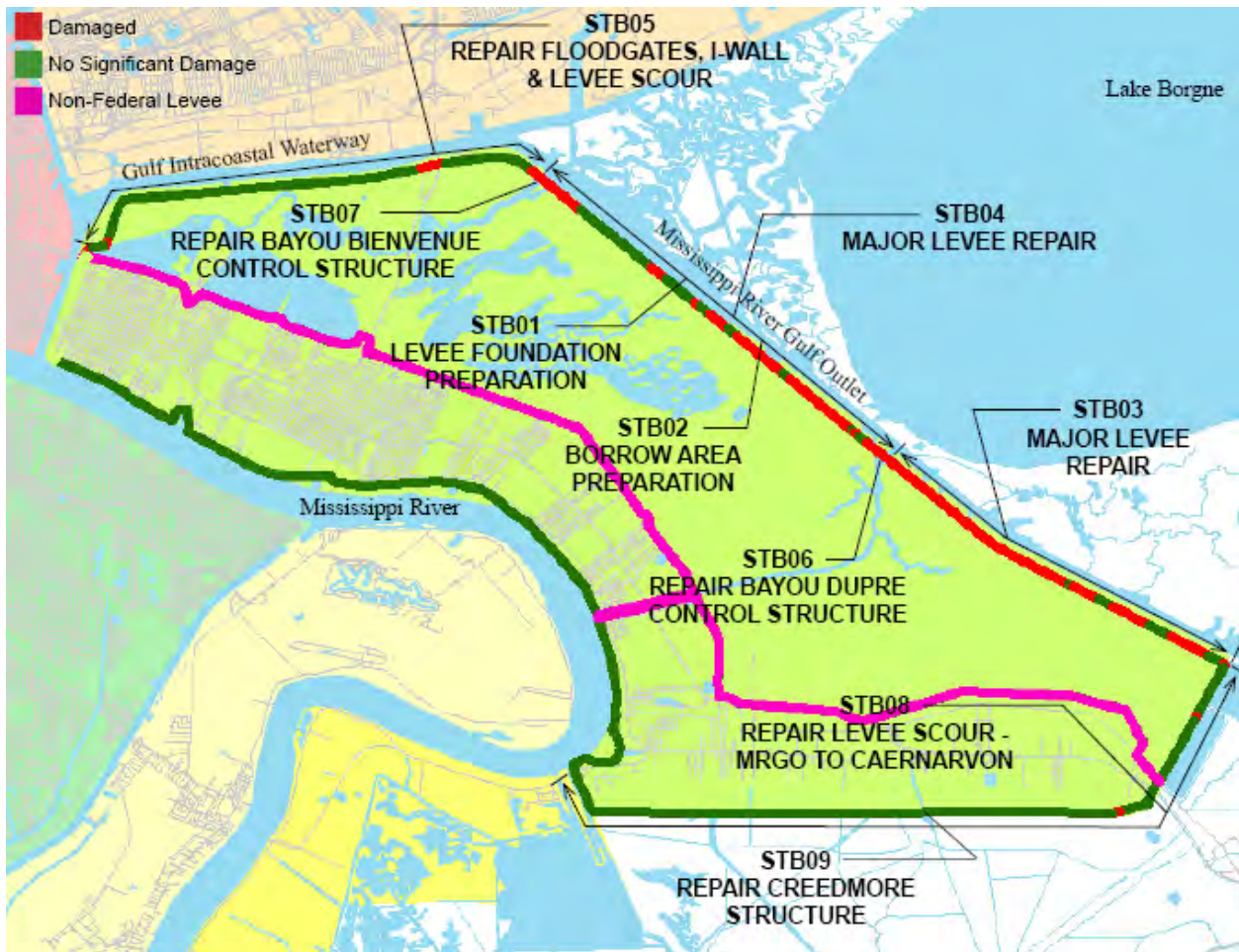
Figure 14-81. Task Force Guardian Re-Construction Contract Numbers and Locations

IHNC East Side, North of Florida Avenue (Orleans Parish) to Bayou Bienvenue. Damage in the IHNC area is detailed in the IHNC portion of Task 7 documentation. There was damage on the IHNC east side north of Florida Ave along the south side of the GIWW (all inside Orleans Parish) that is detailed in this St. Bernard documentation.

Task Force Guardian (TFG) Project **STB05** includes repair of minor scour on the backside of the levee and structural and structural backfill scour adjacent to floodwalls and four closure structures, which are located between the Bayou Bienvenue Control Structure to the GIWW (IHNC) lock. An estimated 26,000 cubic yards of fill material will be required for this work, which is being furnished by the contactor. Scheduled completion date is 1 April 2006.

Figure 14-82. Photo of St. Bernard and Orleans Parish Levee System From IHNC East (north of Florida Ave.) to Bayou Bienvenue
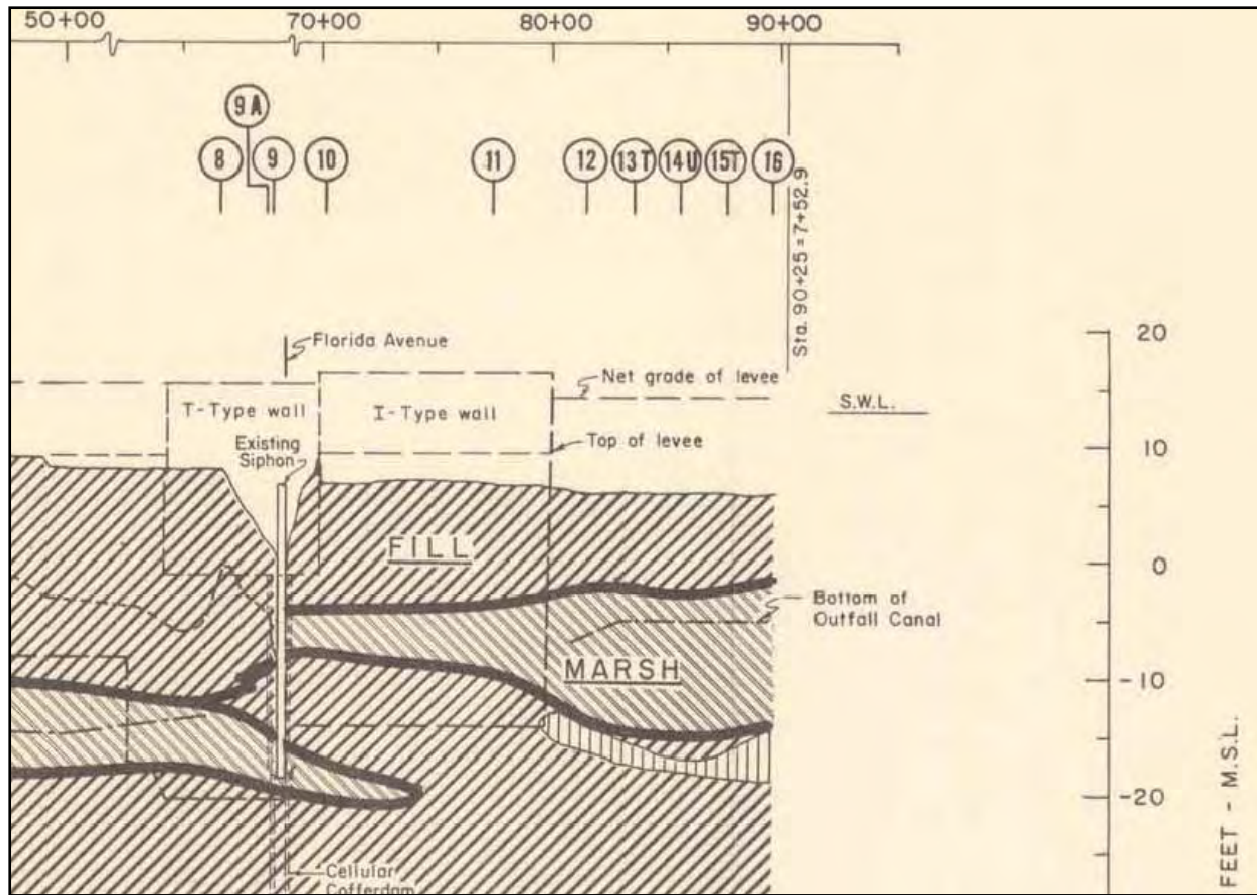
Figure 14-83. Geology Profile Between Florida Ave North to the GIWW Shows Fat Clay Layer at the Original Ground Surface

(1) Closure Structures Near Southern Scrap. There are two road closure structures that were damaged during the storm event. These closure structures are located at STA. 45+00 and STA. 67+94 at Orleans Rd. There was scour of the structural backfill resulting from overtopping of the floodwall and the closure gates.

Figure 14-84. Floodwall Between Fla Ave (IHNC East) and Southern Scrap Facility

Figure 14-85. Southern Scrap Facility Gates S2 and S3

Figure 14-86. View of Scour Outside Gates S2 and S3. IHNC/GIWW and Southern Scrap sites are on the left side of photo
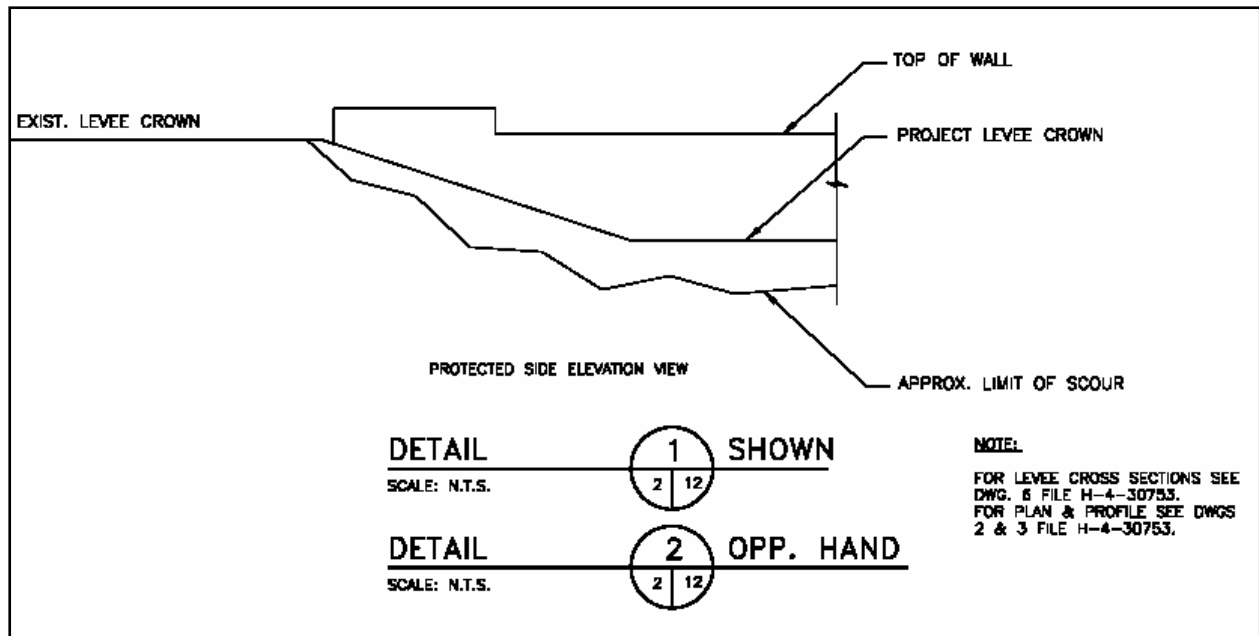
Figure 14-87. Details at Floodwall / Levee Abutments, Both Ends of Gates S2 and S3
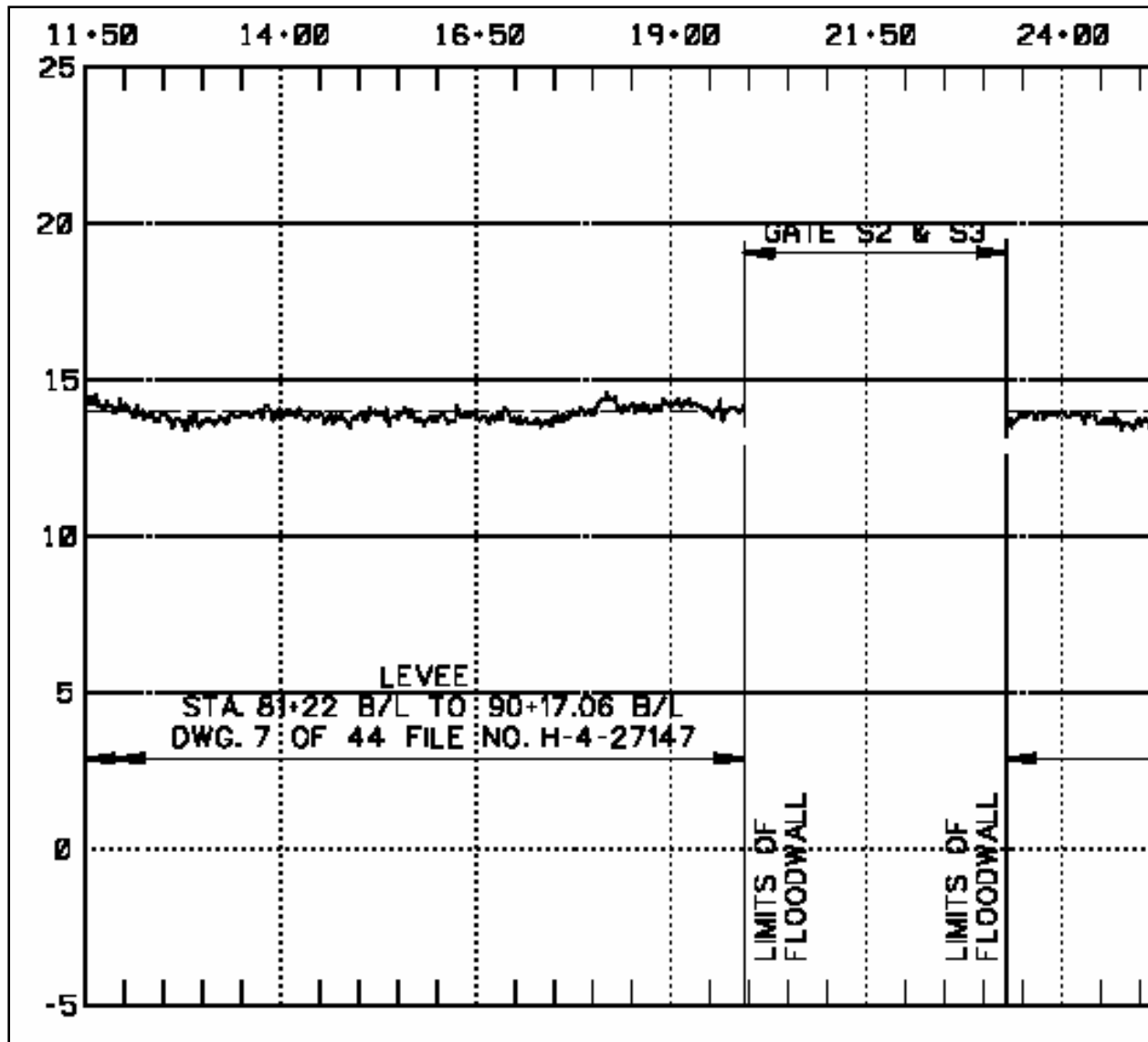
Figure 14-88. Elevations of S2, S3, and Adjacent Levee (from Chalmette Area Plan Emergency Restoration contract solicitation W912P8-06-R-0022 drawings, October 2005)

Scour Stationing and Extent (feet), from Chalmette Area Plan Emergency Restoration contract drawings, October 2005:

- Df = scour depth on flood side
- Dp = scour depth on protected side
- Wf = scour width on flood side
- Wp = scour width on protected side

S1, S2 & S3 - FLOOD GATES/WALL (IHNC [0 - 2+20.00'] TO STA. 23 + 04.00 W/L)

STATION	Df	Dp	Wf	Wp
0 - 220.00'	0.0	5.0	0.0	15.0
0 - 185.00'	0.0	4.0	0.0	15.0
0 - 185.00' TO 0 - 160.00'	0.0	0.0	0.0	0.0
0 - 160.00' TO 0 - 50.00'	0.0	5.0	0.0	10.0
0 - 50.00'	0.0	3.0	0.0	8.0
0 + 00.00	0.0	3.0	0.0	5.0
0 + 00.00 TO 0 + 73.00	0.0	7.0	0.0	15.0
1 + 23.00	0.0	5.0	0.0	15.0
1 + 23.00 TO 2 + 01.00	0.0	6.0	0.0	15.0
2 + 01.00	2.0	6.0	2.0	15.0
9 + 59.67 TO 11 + 20.56	1.0	6.0	2.0	15.0
20 + 00.00	0.0	3.5	0.0	10.0
20 + 43.00	0.0	5.5	0.0	9.0
21 + 15.00	0.0	2.0	0.0	9.0
21 + 80.00	1.0	2.0	6.0	9.0
21 + 84.00	0.0	4.0	0.0	10.0
22 + 61.06 TO 23 + 04.00	0.0	2.0	0.0	7.0

STATIONS INDICATED PER REFERENCE
DWG: FILE NO. H-4-27147 "FLOODWALL
AND LEVEE I.H.N.C. EAST - NORTH OF
FLORIDA AVENUE"

Figure 14-89. IHNC East (between Fla Ave and GIWW) Scour Stationing and Extent (feet), From Chalmette Area Plan Emergency Restoration Contract Solicitation W912P8-06-R-0022 Drawings, October 2005
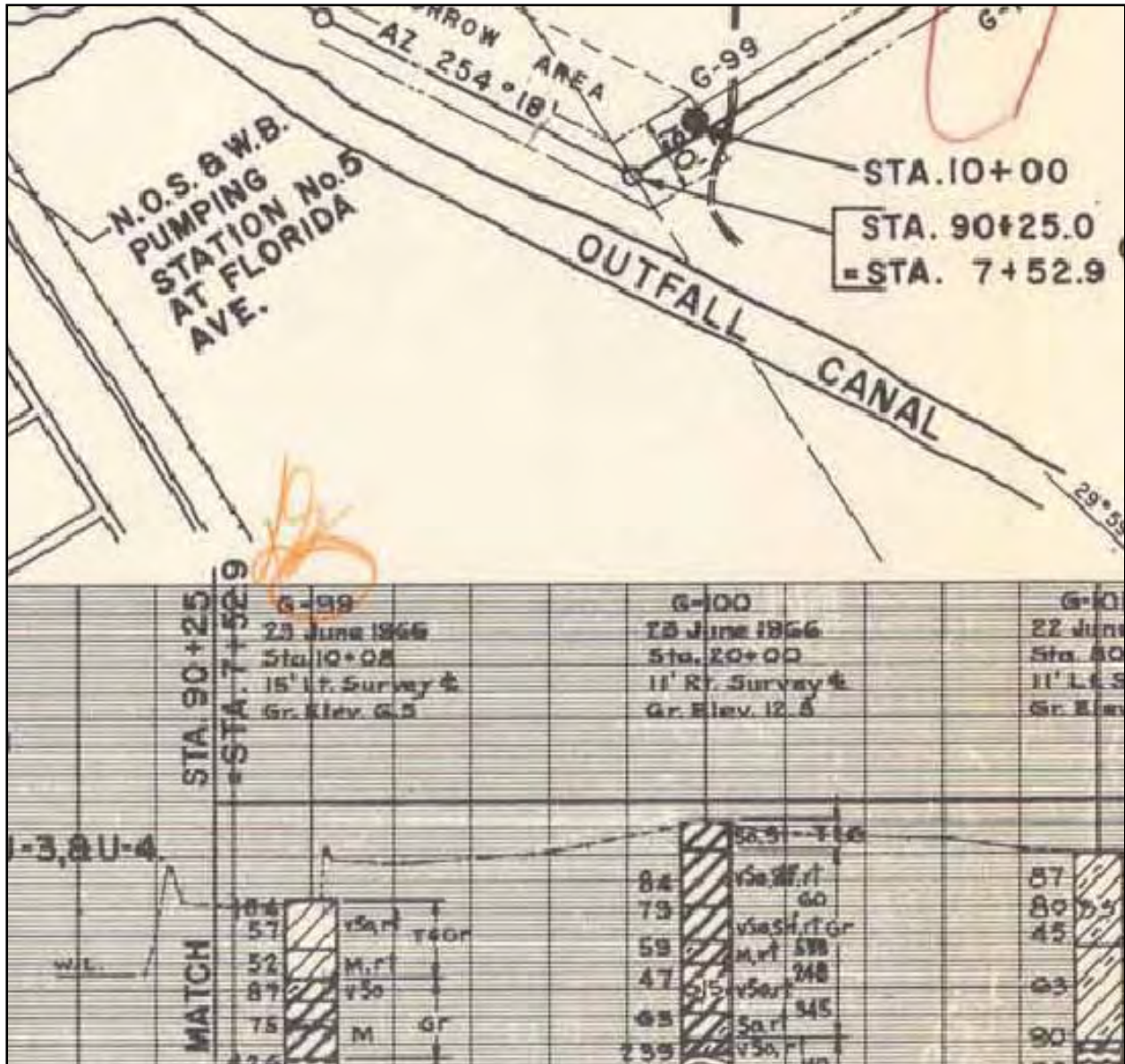
Figure 14-90. Boring G-99 Near Future Gates S2 and S3 Shows Lean Clay (CL) at Existing Ground
Surface (Approximately 6' MSL). From Plate 7, DM3

(2) Levee Damage Along Intracoastal Waterway (GIWW). There are small areas of scour on
the backside of the levee between STA. 65+008 and STA. 277+20 (the Paris Rd high rise bridge
is approximately over Sta 270+00). This scour was the result of localized overtopping of the
levees in this reach.

Figure 14-91. Localized Scour on the Levee South of the GIWW, Between IHNC and Paris Rd.
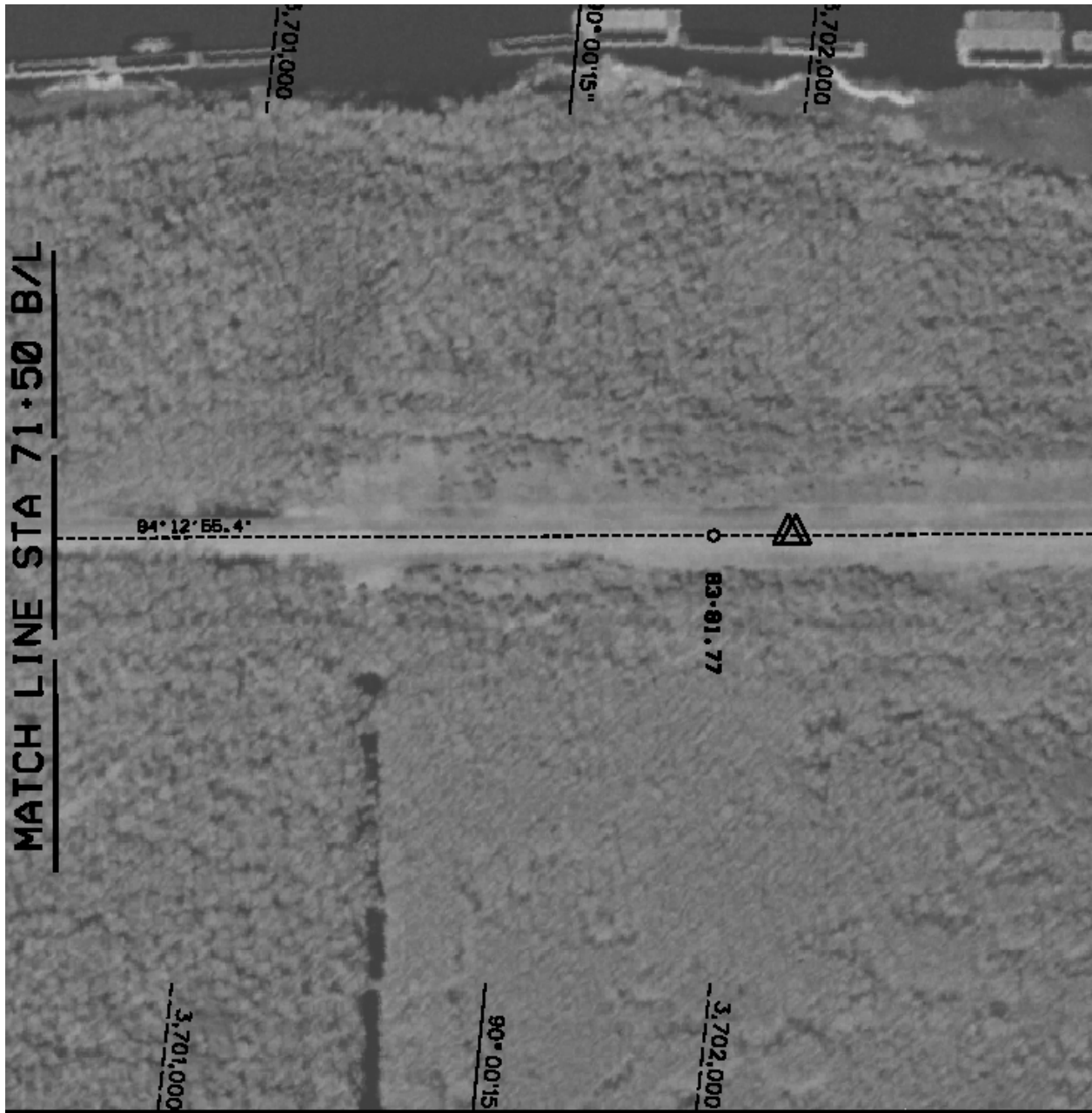
Figure 14-92. Major Scour Damage (Marked With Triangle) Identified East of B/L Sta 81+50 (From TFG Contract Solicitation W912PB-06-R-0022, Drawing 3 of 12)
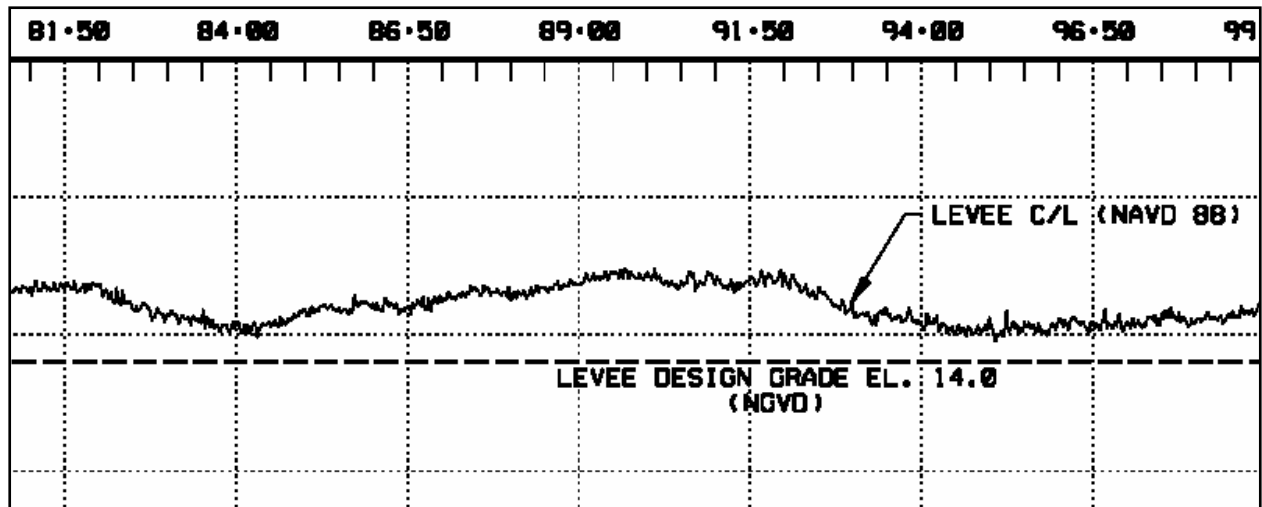
Figure 14-93. Levee Profile East of B/L Sta 81+50 (dwg 3 of 12). Note design grade elev 14 (NGVD) and lidar post-Katrina elev between 14 and 16 (NAVD 88)

Volume V The Performance – Levees and Floodwalls – Technical Appendix
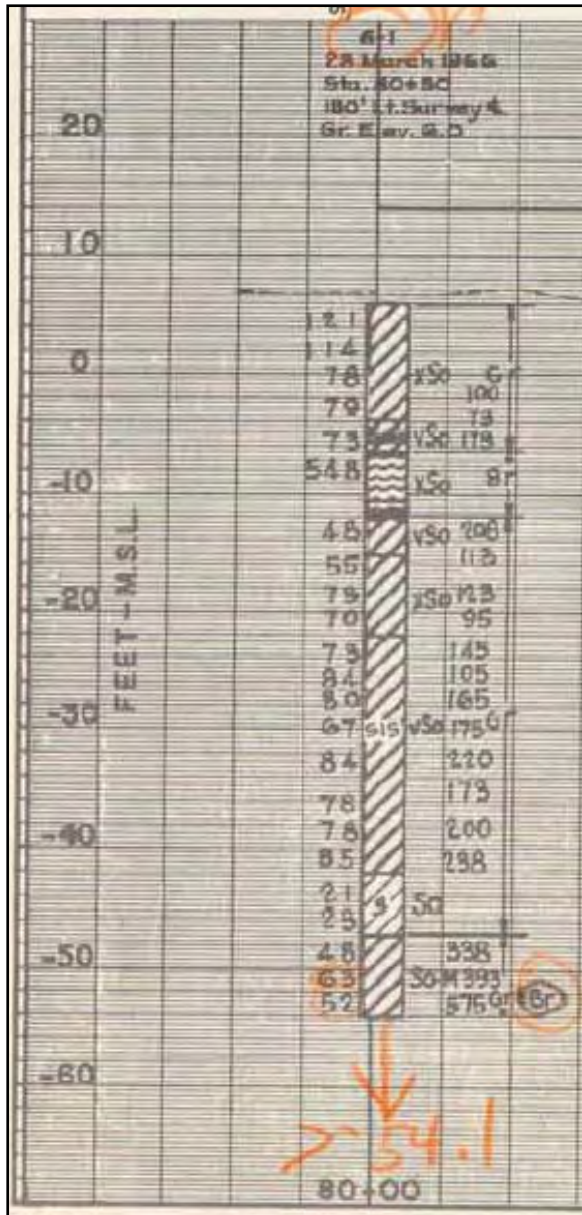
Figure 14-94. Nearest Boring at Sta 80+50, G-1, Circa 1966, From DM3, Plate 8. Original ground elevation was approximately 6 ft MSL, and surface soil was CH. Levee was built to approximate elevation +14 ft. circa 1970. Additional lift up to elevation 19 was added circa 1985

U. S. ARMY ENGINEER DISTRICT, NEW ORLEANS
CORPS OF ENGINEERS
NEW ORLEANS, LA.

LAKE PONTCHARTRAIN, LOUISIANA AND VICINITY
CHALMETTE AREA PLAN

HURRICANE PROTECTION LEVEE
STA. 65+00 TO STA. 268+00 — FIRST ENLARGEMENT
ORLEANS PARISH, LA

TYPICAL DESIGN SECTIONS
STA. 64+40 TO STA 209+35

DESIGNED:	DRAWN:	CHECKED:	DATE:	SCALE:	FILE NO.:
E.W.C.	R.t.G.	R.P.L.	FEB. 1985	AS SHOWN	H-8-29768
SUBMITTED:		SPEC NO.:			
		DACW29-85-R-00-47	DWG 4 OF 9		

Figure 14-95.
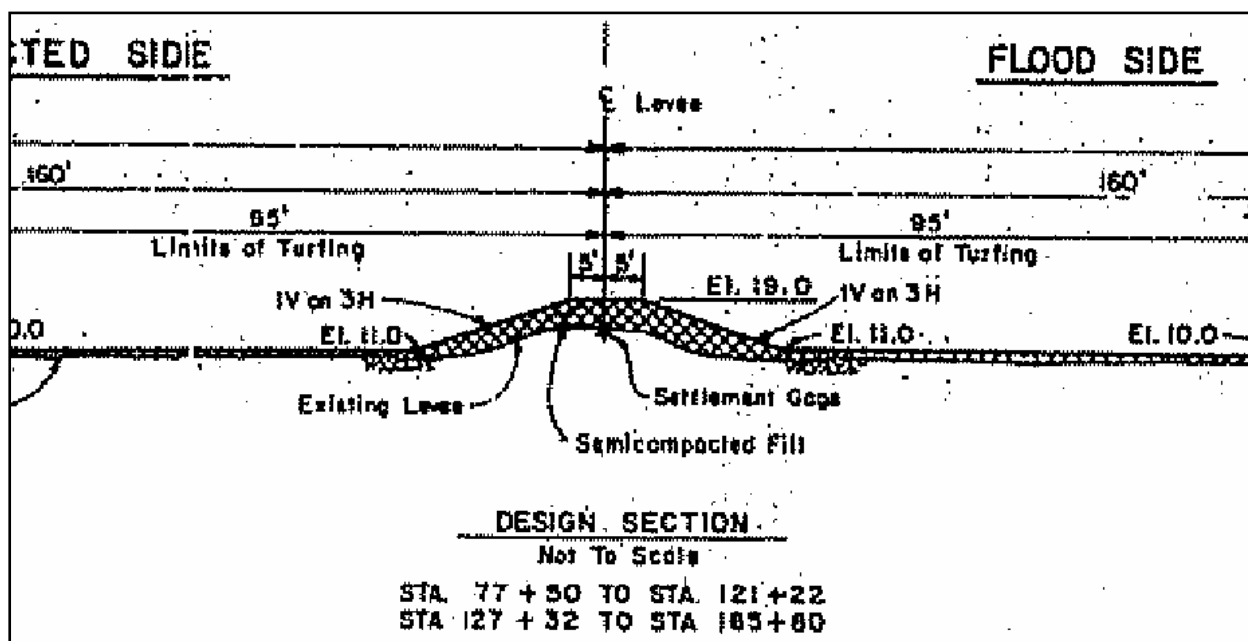
Figure 14-96. Design Section for Levee Enlargement, From Above 1985 Drawing
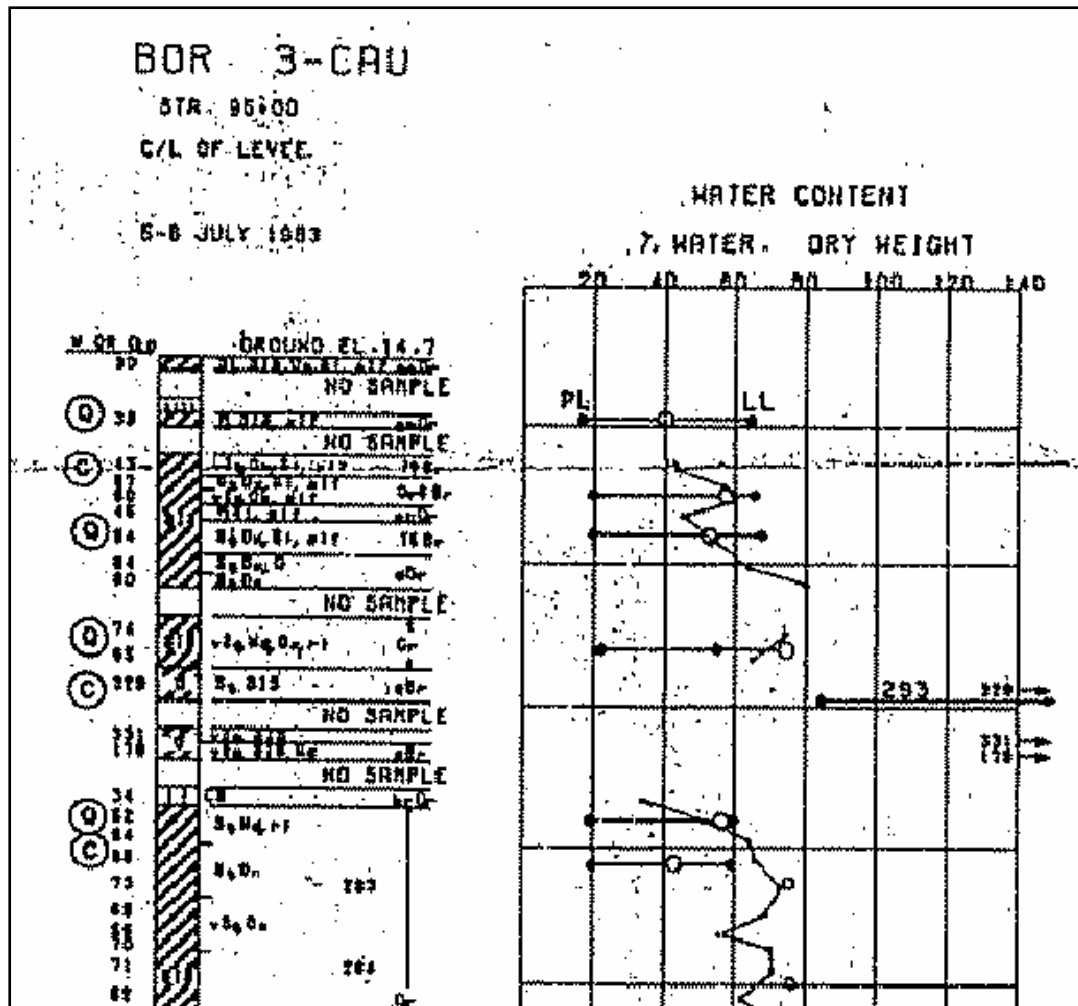
Figure 14-97. Sta 95+00 boring, 1983, shows CH soil at top of pre-existing 14' levee over a thin lense of sandy material. Note ground elevation (14.7 ft) comparison with lidar elevation (15 ft) at Sta 95+00 in Figure 14-93 above
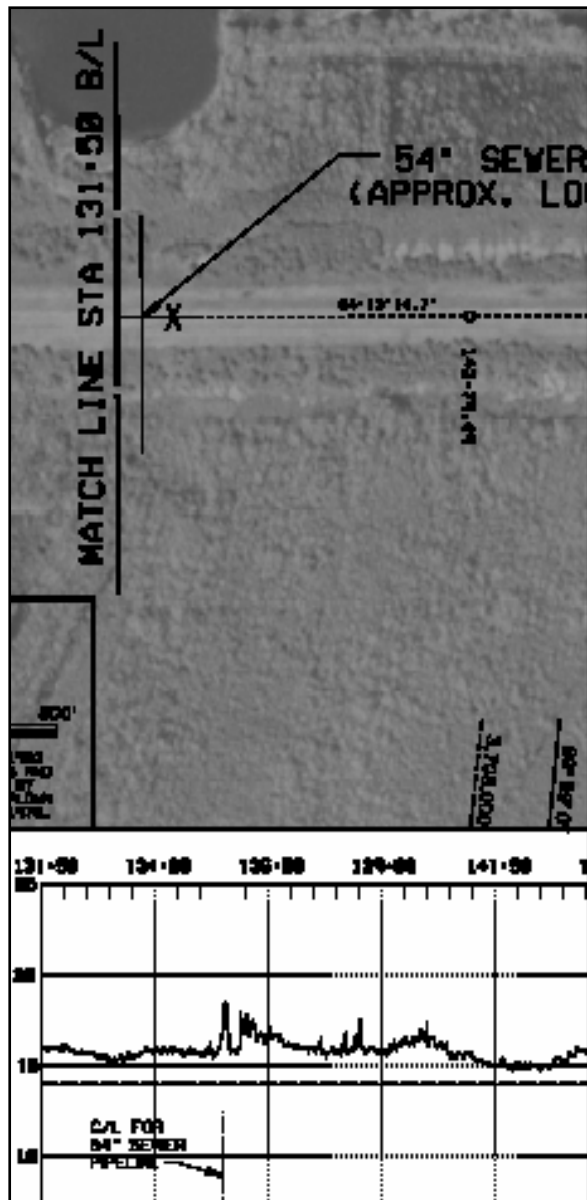
Figure 14-98. A Minor Scour Location (Marked With X) at B/L Sta 135+00 (from dwg 4 of 12, Contract Solicitation W912P8-06-R-0022)
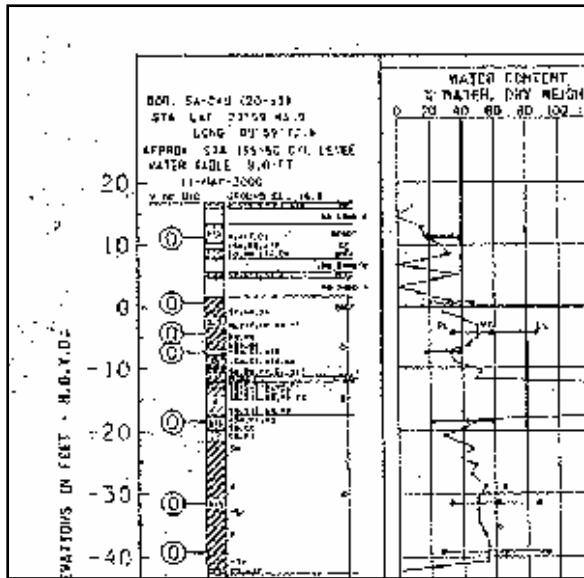
Figure 14-99. Dwg 9 of 19, New Orleans District File H-8-45533 Shows a Thin Layer of Lean Clay (CL) at Centerline Top of Levee from the 2001 Soil Boring 5A-CAU, B/L Sta 135+50
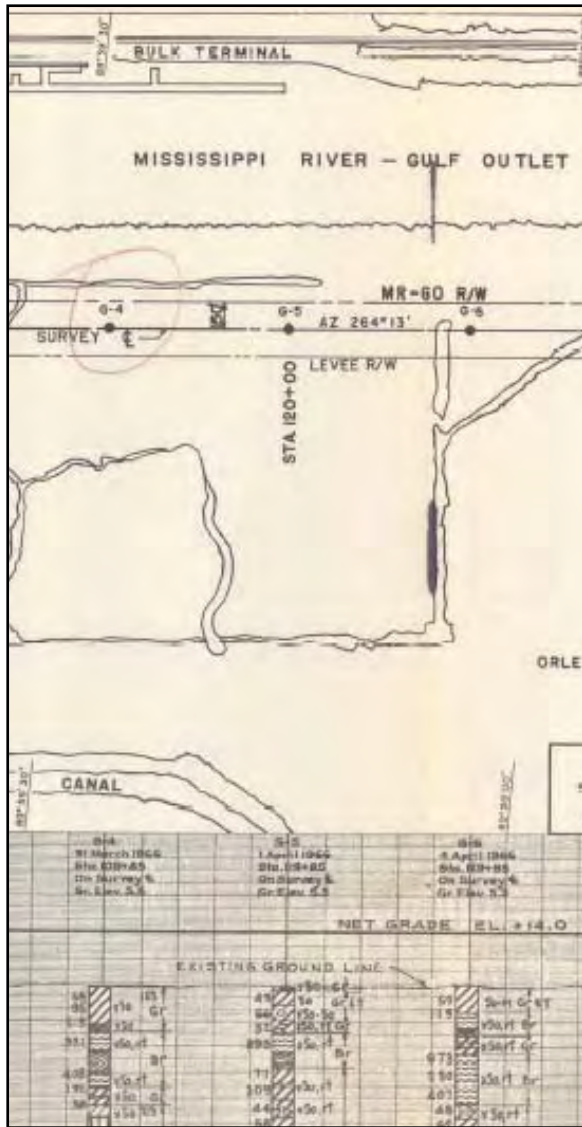
Figure 14-100. Plate 6, DM3 (1966) Soil Boring G-6 at Sta 129+80 at Levee Centerline Shows Fat Clay (CH) at Original Ground Surface

    (3) <u>Paris Road Closure Structure</u>. This closure structure was damaged during the storm event. There was scour of the structural backfill resulting from overtopping of the closure panels and additional damages due to impact from a loose barge.

STATION	Df	Dp	Wf	Wp
S4 - PARIS ROAD FLOOD GATE/WALL (STA. 267 + 00.00 C/L TO STA. 277+24.50 C/L)				
0 + 00.00 W/L (267 + 00.00 W/L)	0.0	8.0	0.0	8.5
0 + 50.00	0.0	3.0	0.0	25.0
0 + 83.00	0.0	10.0	0.0	35.0
1 + 29.00	0.0	4.0	0.0	40.0
1 + 29.00 TO 1 + 89.00	0.0	3.0	0.0	40.0
1 + 90.00	0.0	4.5	0.0	11.5
10 + 24.74	0.0	3.0	0.0	11.5

STATIONS INDICATED PER REFERENCE DWG:
FILE NO. H-4-29216 "PARIS ROAD FLOODWALL"

Figure 14-101. Scour Details for Paris Road Gate Closure Damage (From Contract Solicitation W912P8-06-R-0022)

Figure 14-102.

  This is a preliminary report subject to revision; it does not contain final conclusions of the United States Army Corps of Engineers.

Figure 14-103.

(4) Closure Structure and I-Wall West of Bienvenue. This closure structure and adjacent I-wall segments were damaged during the storm event. There was scour of the structural backfill resulting from overtopping of the closure gate and I-wall.

Figure 14-104. View Looking East Toward the Bayou Bienvenue Control Structure

Figure 14-105. Gate S5 Scour Hole (From Levee Restoration, Misc. Gates and Floodwall Repairs, IHNC to Bienvenue, Chalmette Area Plan Emergency Restoration solicitation W912P8-06-R-0022, October 2005 contract drawing H-8)

Figure 14-106. View West From Bienvenue Control Structure Toward the Unused Floodgate Structure

Figure 14-107. Scour Damage Details for Wall West of Bienvenue Structure

Bayou Bienvenue Control Structure. This control structure was damaged during the storm event. The adjacent floodwall was hit by a loose barge and the fill around the adjacent floodwalls was eroded away due to overtopping. In addition there was damage to the mechanical and electrical systems that operate the sector gates.

TFG Project **STB07** includes repair of structural damage and loss of structural backfill at the Bayou Bienvenue Control Structure. A significant scour hole is to be filled with 28,600 cubic yards of granular backfill and protected with grouted riprap. An estimated 32,100 tons of riprap and 3,400 cubic yards of embankment fill will be required for the repairs. All materials are to be furnished by the contractor, and scheduled completion is 1 April 2006.

Figure 14-108. Pre-Katrina

Figure 14-109. Post-Katrina. Note scour near guardrail shown in Figure 14-104

Figure 14-110. Barge Resting on T-Wall

Volume V The Performance – Levees and Floodwalls – Technical Appendix

Figure 14-111. View East, From Protected Side

Volume V The Performance – Levees and Floodwalls – Technical Appendix

V-14-111

This is a preliminary report subject to revision; it does not contain final conclusions of the United States Army Corps of Engineers.

Figure 14-112. View Looking East of the Bayou Bienvenue Control Structure Showing Sheetpile Damage From Scour. From this picture there is no obvious layer stratification in the scoured section profile

Figure 14-113. DM 5 Bayou Bienvenue & Bayou Dupre Ctrl Struct.pdf

Volume V The Performance – Levees and Floodwalls – Technical Appendix

V-14-113

This is a preliminary report subject to revision; it does not contain final conclusions of the United States Army Corps of Engineers.
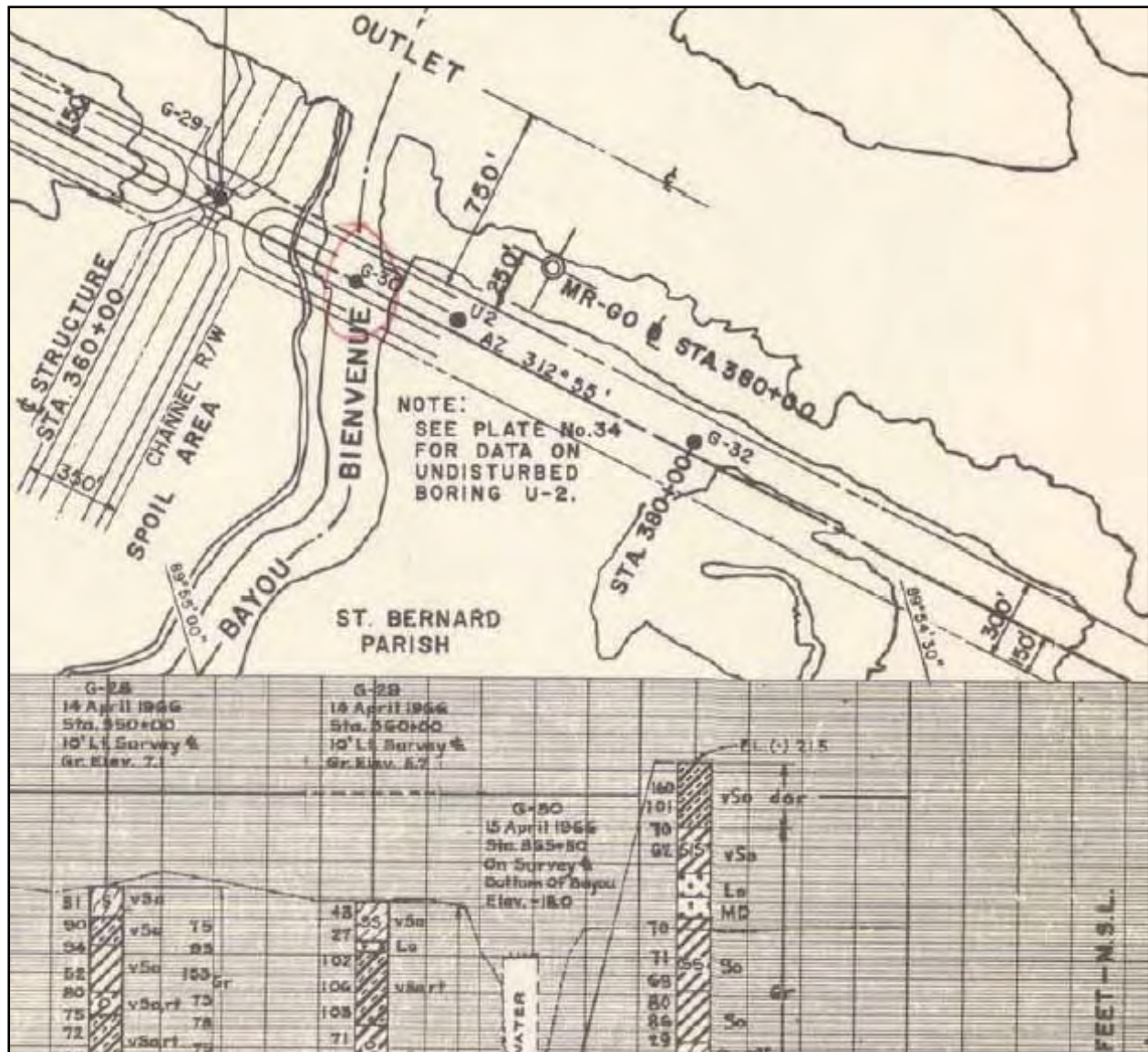
Figure 14-114. Original ground surface (1966) had sand / silt lenses overlying very soft organic clay (plate 10, DM3). Note that sheetpile east of structure (Figure 14-112) was driven to cut off old Bayou channel in addition to reduce loading on the top layer of very soft organic clay seen in boring G-32
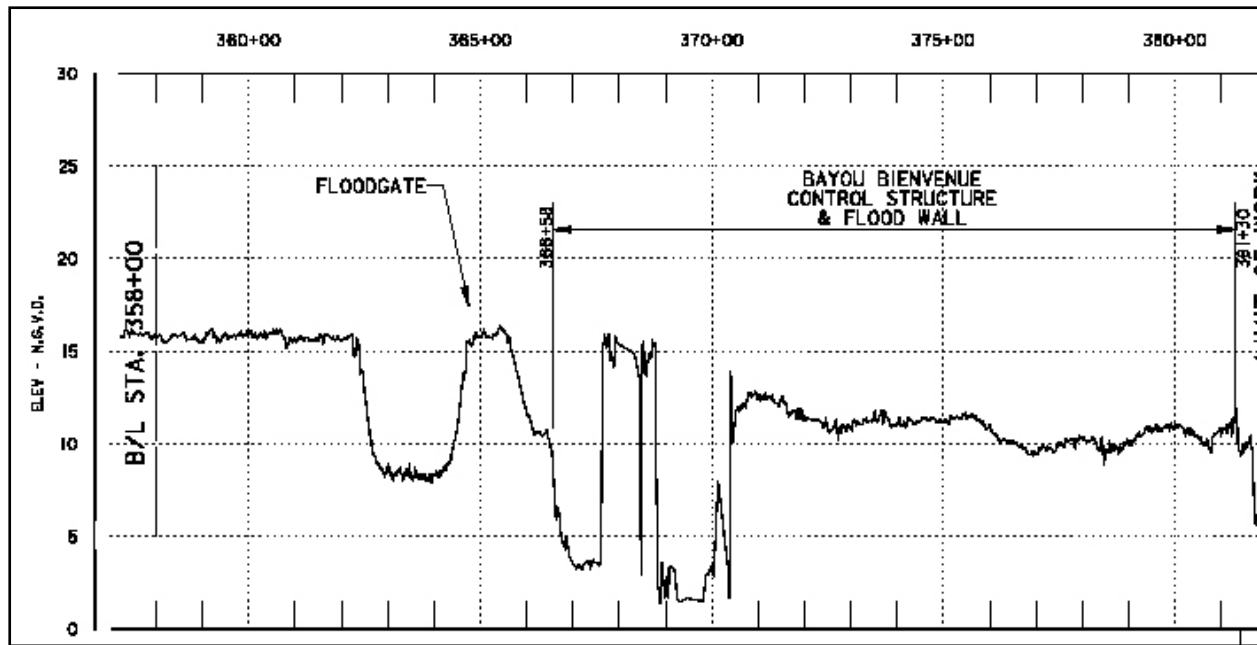
Figure 14-115. Centerline Scour Depths of Floodgate and Control Structure (From Dwg 1 of 8, Emergency Restoration B/L 383+00 to 704+00 Contract Solicitation)

Hurricane Levee Between Bayou Bienvenue and Bayou Dupre. There is 19,000 ft. of levee between Bayou Bienvenue (Sta 383+00) and Bayou Dupre (Sta 704+00) that was severely damaged from overtopping and scour, and has lost approximately 12' of levee section and was at EL 5.0.

Figure 14-116. Levee Completely Eroded Away

This is a preliminary report subject to revision; it does not contain final conclusions of the United States Army Corps of Engineers.

Figure 14-117. More Missing Levee

There is an additional 2,300 ft. of levee in this reach that has some damage (approximately 50% of the levee section was eroded away).

Figure 14-118. Partial Levee Eroded

Figure 14-119. View South From Approximate B/L Sta 570+00. MRGO is to the left of photo

The repaired levee cross section is shown below. This was the typical cross section used to estimate the required quantities.
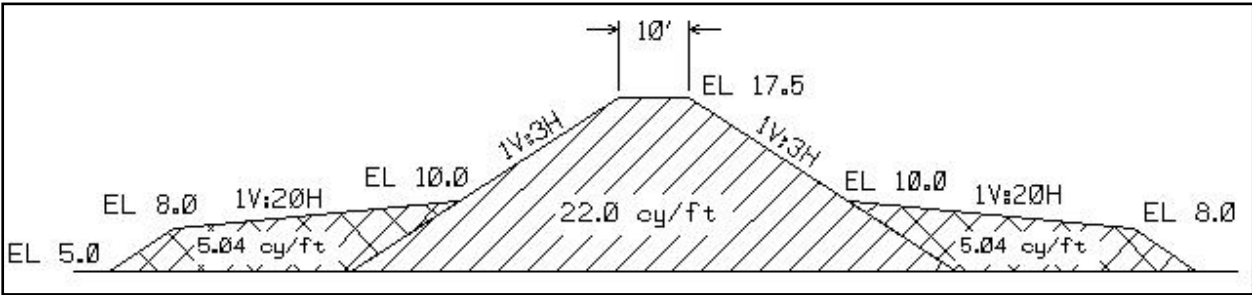
Figure 14-120.

Quantities: 660,000 cy fill – 55 acre borrow area

There is a total of 4,300 ft. of sheet pile floodwall in this reach that was badly damaged and will require replacement. There are three segments of sheetpile which makeup this quantity. These were initially planned to be replaced with 30' sheets – see section below.

Segment A: – Length – 1130 ft. Condition – badly damaged; replacement required

Segment B: – Length – 720 ft. – Condition – badly damaged; replacement required

Segment C: – Length – 2450 ft. – Condition – badly damaged; replacement required

Figure 14-121. Damaged Sheetpile Section (Utility Crossing), With Scour on the Protected Side. B/L Sta 590+70 is centerline of the two pipelines

Figure 14-122. Closeup of Damaged Sheetpile and Scour. Note stratified layers in adjacent soil profile of existing hydraulic fill from the MRGO

Volume V The Performance – Levees and Floodwalls – Technical Appendix
This is a preliminary report subject to revision; it does not contain final conclusions of the United States Army Corps of Engineers.

V-14-121

Figure 14-123. Note Sheetpile Elevation Differences

Figure 14-124. Additional Damaged Sheetpile at Utility Crossing, B/L Sta 600+00
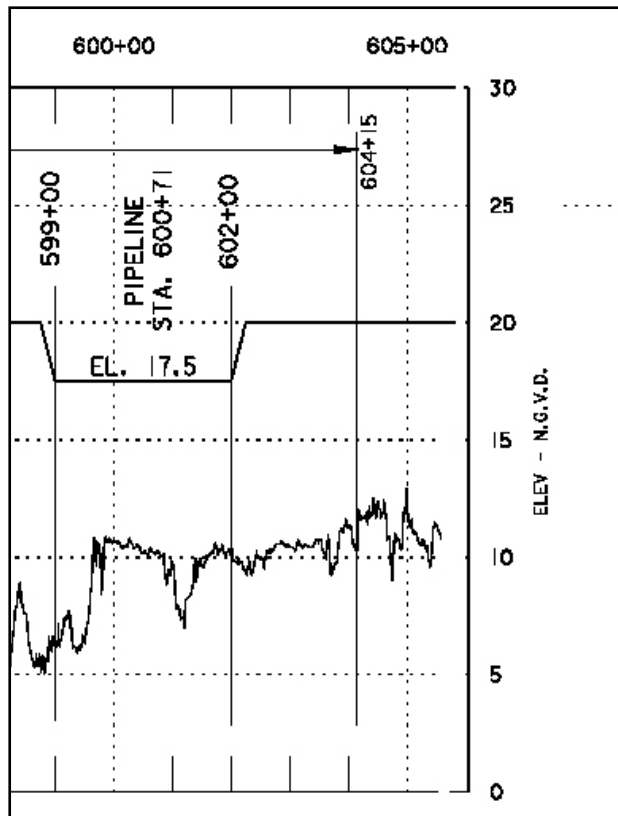
Figure 14-125. Scour Depths at Pipeline Crossing and End of Sheetpile (Sta 604+15) Transition to Levee

Figure 14-126. Exposed Soil Layer at Horizontal Scour Surface Appears to be In-Situ Fat Clay With Embedded Shell Hash, Possibly an Exposed Estuarine Deposit
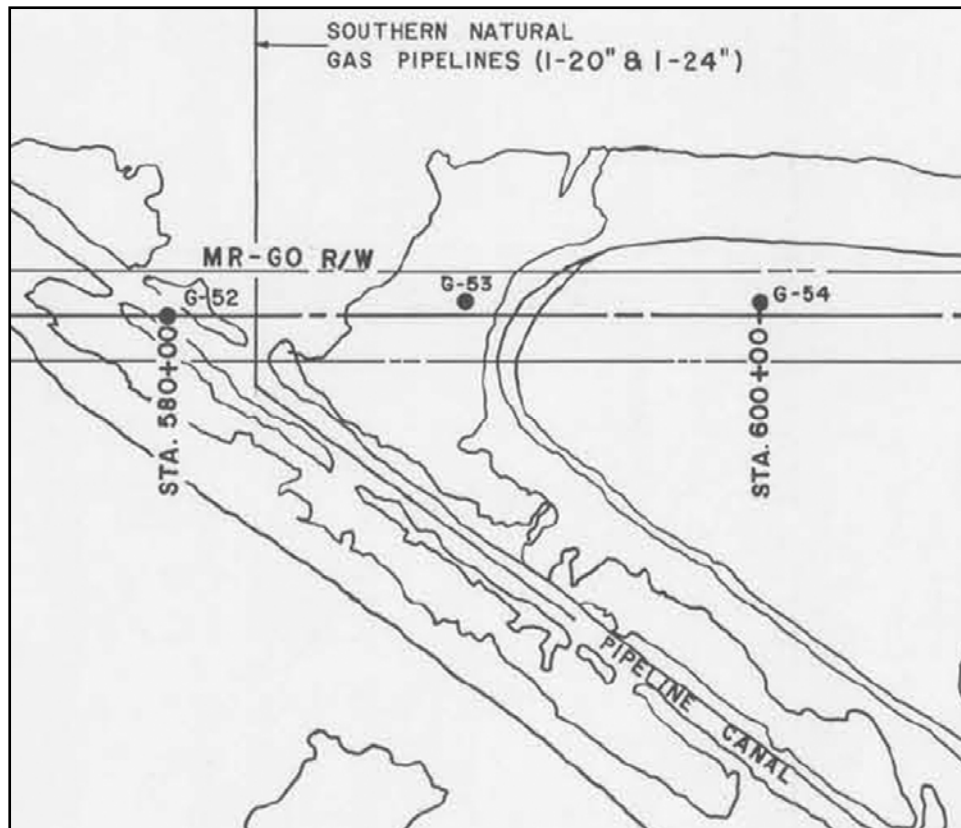
Figure 14-127. Original Pipeline Canal Prior to Backfilling and Sheetpile (From Drawing File H-2-23820, Plate 13)

Volume V The Performance – Levees and Floodwalls – Technical Appendix
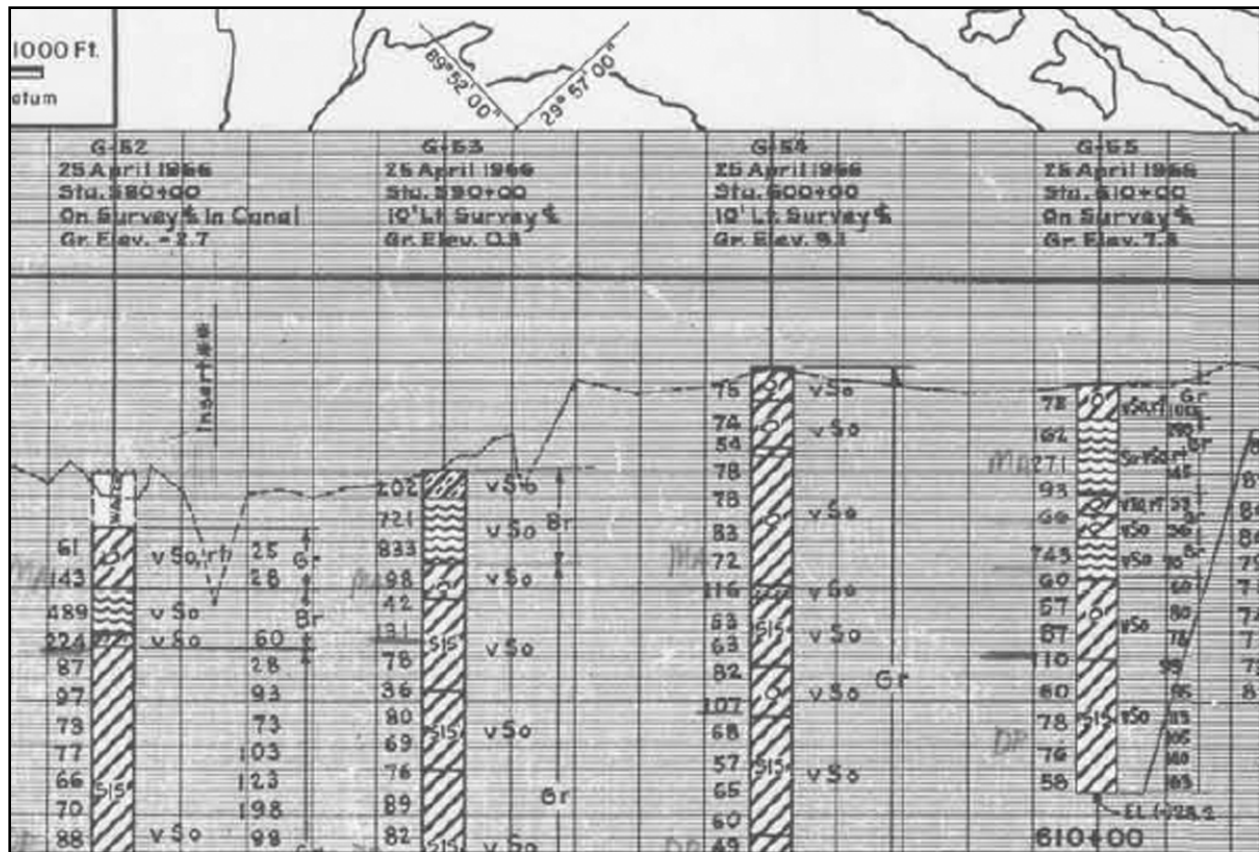
Figure 14-128. Original Borings Show Very Soft Fat Clay and Peat Layers (from drawing file H-2-23820, plate 13)

The cross section below is the cross section used to estimate repairs. The sheetpile was replaced with earthen levee to elevation 17.5'.
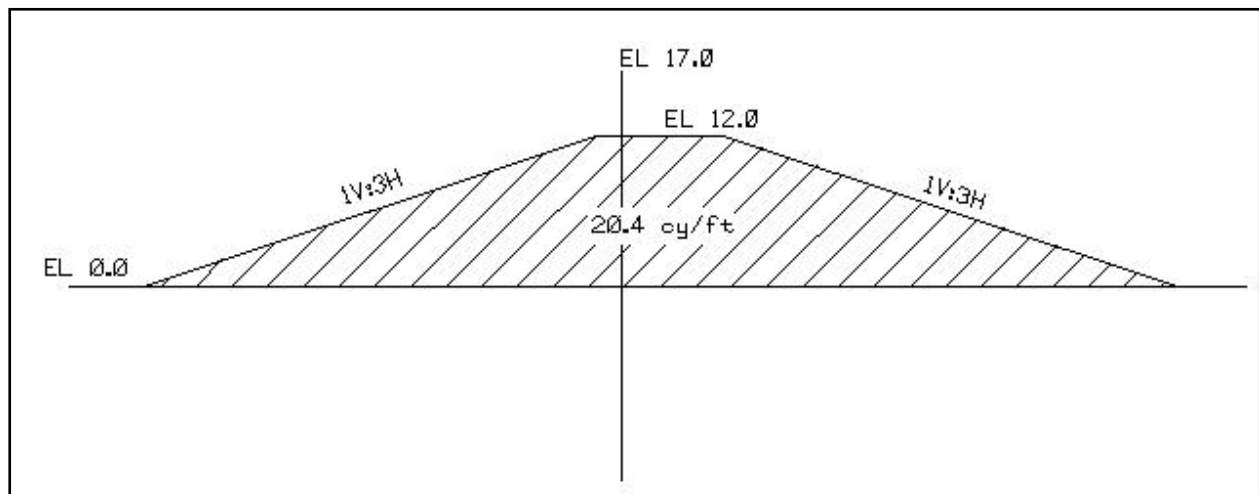
Figure 14-129.

TFG Project **STB01** included site preparation work in the areas of levee damage between the Bayou Bienvenue and Bayou Dupre Control Structures. The contracted work (rental agreement contract) is complete.

Figure 14-130. Repairs Underway, Filling Scour Holes

TFG Project **STB02** included site preparation work in the borrow areas between the Bayou Bienvenue and Bayou Dupre Control Structures. The borrow area is a strip of land adjacent to the levee, which was used as a disposal area during the construction of the MRGO canal. This rental agreement contract has not been fully utilized – some borrow area preparation work has been accomplished as part of STB01 work (same contractor). Completed contract.

TFG Project **STB04** (MRGO Baseline Station 380+00 to 705+00 - Between Bayou Depre and Bayou Bienvenue Control Structures) includes repairing a 6.2-mile reach of levee along the MRGO between the Bayou Bienvenue and the Bayou Dupre Control Structures. Several barges are located on the levee and borrow areas. The entire levee reach will be restored to the design grade elevation (17.5'), requiring the placement of an estimated 1,000,000 cubic yards of fill material. The borrow area for this fill material is a strip of land adjacent to the levee (260 acre borrow area), which was used as a dredged disposal area during the construction of the MRGO canal. Scheduled completion is 1 April 2006.

Figure 14-131. Site Map of Area Between Bienvenue and Dupre

Volume V The Performance – Levees and Floodwalls – Technical Appendix

V-14-129

This is a preliminary report subject to revision; it does not contain final conclusions of the United States Army Corps of Engineers.

Figure 14-132. Barges From the MRGO

This is a preliminary report subject to revision; it does not contain final conclusions of the United States Army Corps of Engineers.

Figure 14-133. Repair Contract Work Borrow Pit and Dragline on Protected Side Right-of-Way

Volume V The Performance – Levees and Floodwalls – Technical Appendix

V-14-131

This is a preliminary report subject to revision; it does not contain final conclusions of the United States Army Corps of Engineers.
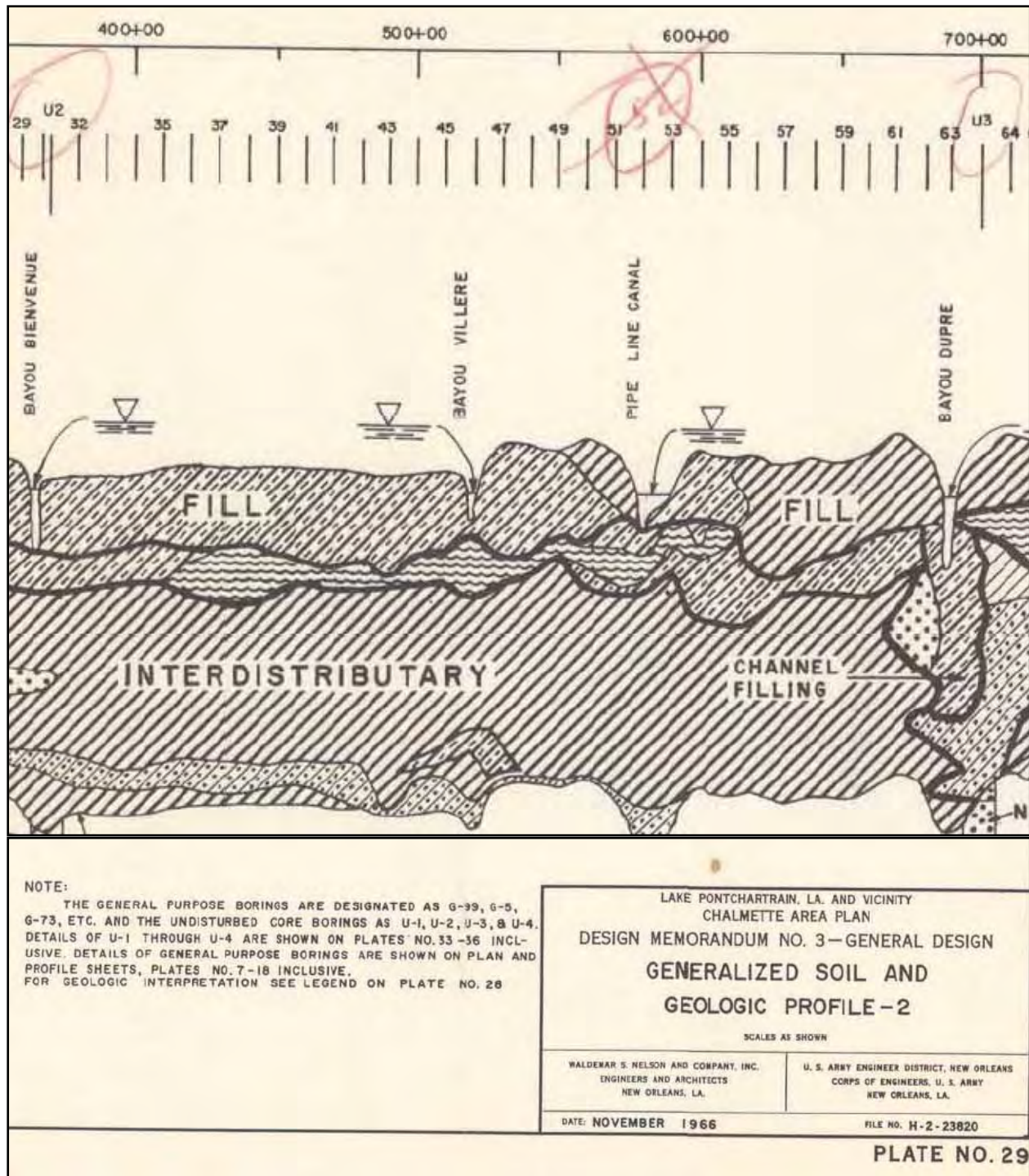
Figure 14-134. Pre-Existing Conditions Between Bienvenue and Dupre (from DM 3). The original ground surface was mostly organic clay (OH) southeast of Bayou Bienvenue. The original ground surface was fat clay (CH) between approximate Sta 612+00 and Bayou Dupre
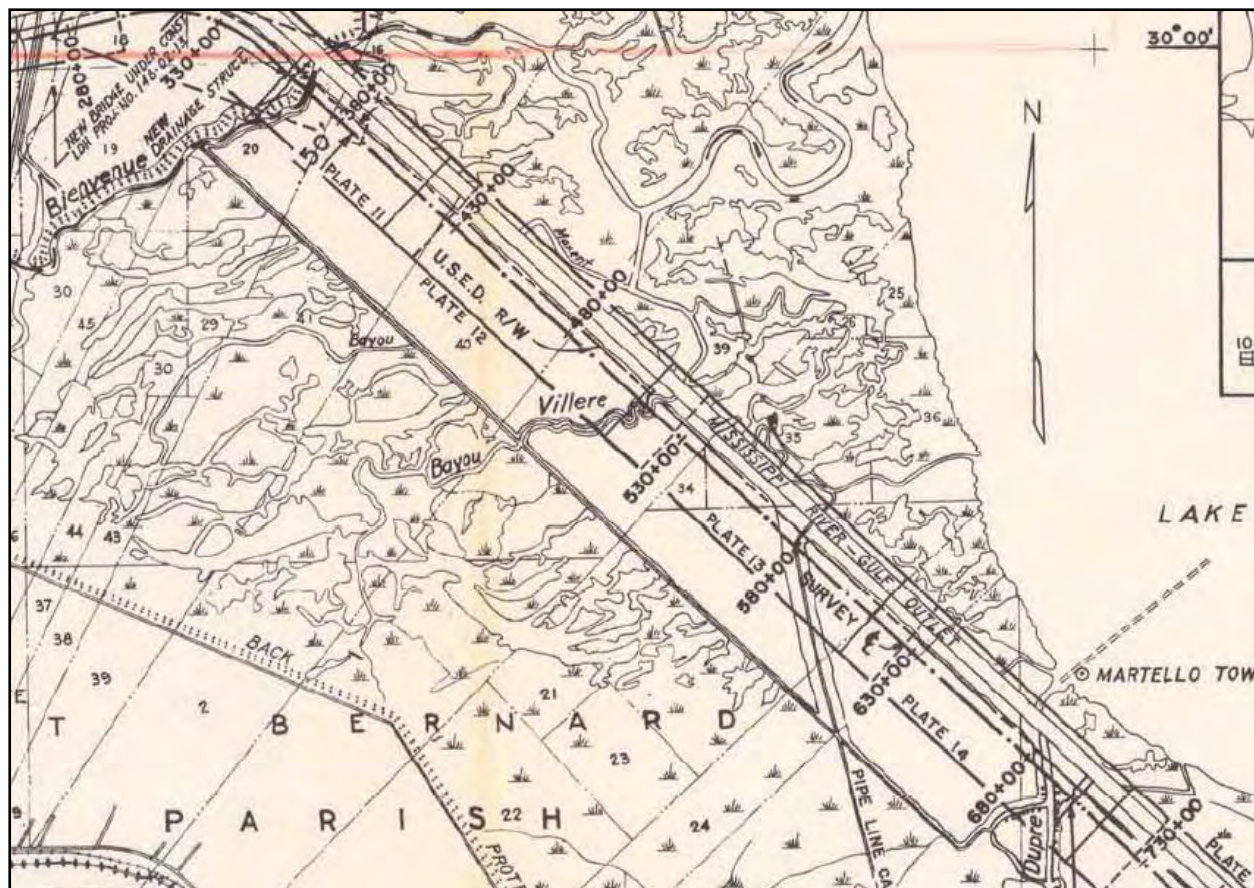
Figure 14-135. DM-3 Plates 11 thru 14 Between Bienvenue and Dupre

Volume V The Performance – Levees and Floodwalls – Technical Appendix

V-14-133

This is a preliminary report subject to revision; it does not contain final conclusions of the United States Army Corps of Engineers.
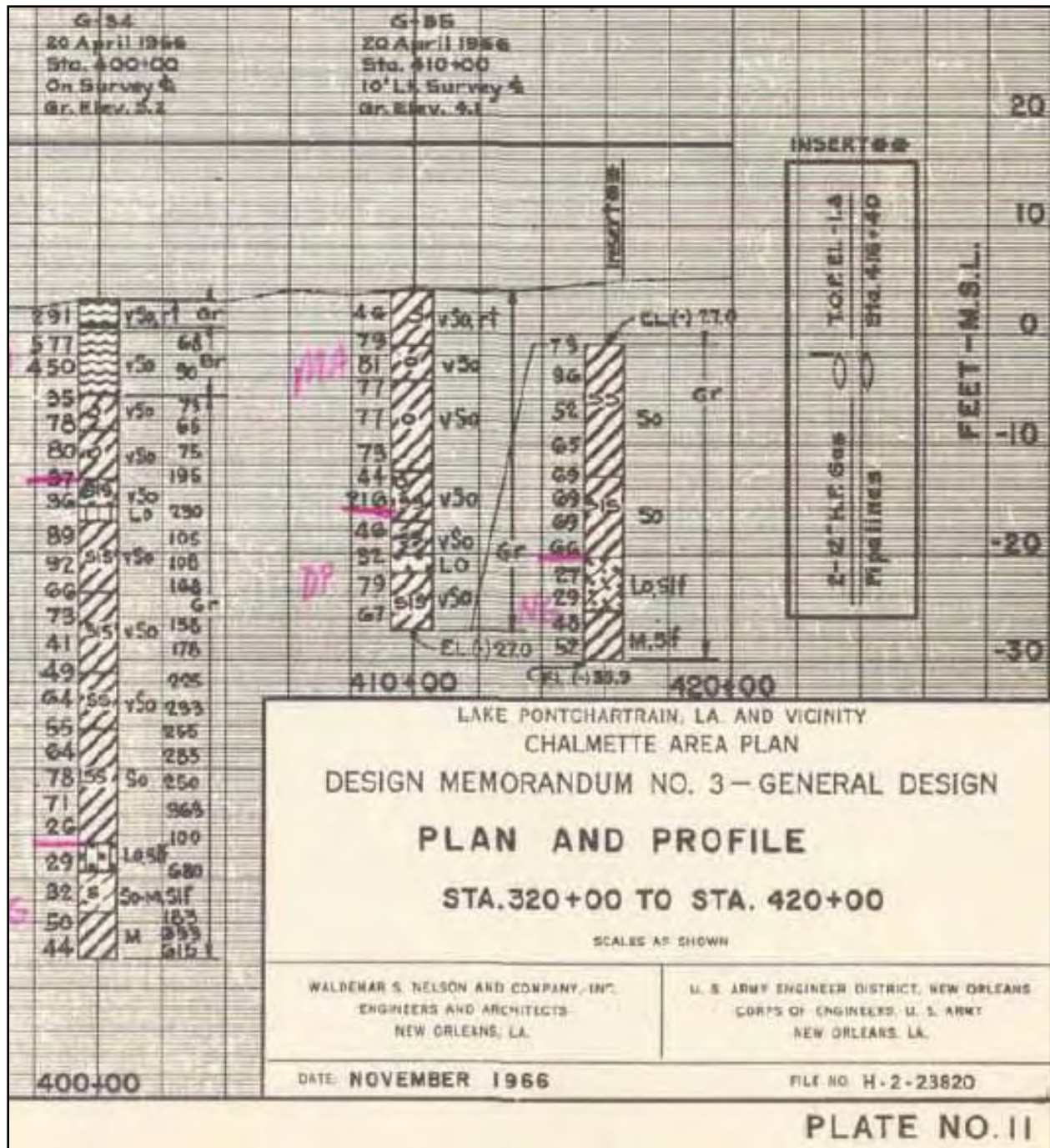
Figure 14-136. Original Ground Elevation was Approximately 5 ft Above MSL

This is a preliminary report subject to revision; it does not contain final conclusions of the United States Army Corps of Engineers.

GENERAL NOTES

1. FROM STA.7+52.5 TO 807+00, PLATES 7-16, FILL MATERIAL FOR LEVEE CONSTRUCTION IS TO BE OBTAINED FROM SELECTED BORROW AREAS ALONG THE BOTTOM OF THE MR-GO CHANNEL. BORROW AREAS FOR FILL MATERIAL STA. 807+00 TO 1020+00 AS SHOWN ON PLAN ON PLATES 16 & 17. FILL REQ'D. STA. 1020+00 TO 1050+57.7 TO BE TRUCK HAULED DRY FILL MATERIAL.

2. THERE SHALL BE A MINIMUM 100 FT. BERM BETWEEN THE TOE OF LEVEE AND THE TOP OF CUT SLOPE OF ANY BORROW AREA.

3. ± DENOTES APPROXIMATE DIMENSIONS.

4. FOR LOCATION OF CONSTRUCTION RETAINING DIKES, SEE STAGE CONSTRUCTION SECTIONS, PLATES 66 & 67.

5. FOR LIFT AND SHAPING DIMENSIONS AND CONSTRUCTION CRITERIA, SEE PLATE NO. 65.

Figure 14-137. Hydraulic Fill From MRGO Channel Formed the Levee Between Bienvenue and Dupre. Southeast of Dupre (from Sta 807+00) Utilized Other Fill Materials (from 1966 DM3)

Bayou Dupre Control Structure. This control structure was damaged during the storm event. Adjacent sections of floodwall failed and the fill around other sections of floodwalls was eroded away due to overtopping. In addition there was damage to the mechanical and electrical systems that operate the sector gates.

Figure 14-138. Bayou Dupre Control Structure, Pre-Katrina View. Note the concrete walls transitioning to earth levee on both sides of the structure

Figure 14-139. Bayou Dupre Control Structure, Post-Katrina. View toward MRGO. Note the missing levees on both sides of the structure

Volume V The Performance – Levees and Floodwalls – Technical Appendix

V-14-137

This is a preliminary report subject to revision; it does not contain final conclusions of the United States Army Corps of Engineers.

Figure 14-140. Missing Levee and Part of Wall on West Side of Control Structure

Figure 14-141. Severe Scour on East Side of Structure

Figure 14-142. Closeup of East View, End of Concrete Wall, Showing Major Scour Holes and Complete Erosion of Levee

TFG Project **STB06** includes repair of structural damage and loss of structural backfill at the Bayou Dupre Control Structure. A significant scour hole is to be filled with 17,500 cubic yards of granular backfill and protected with grouted riprap. An estimated 22,500 tons of riprap and 13,400 cubic yards of embankment fill will be required for the repairs. Scheduled completion date is 1 April 2006.
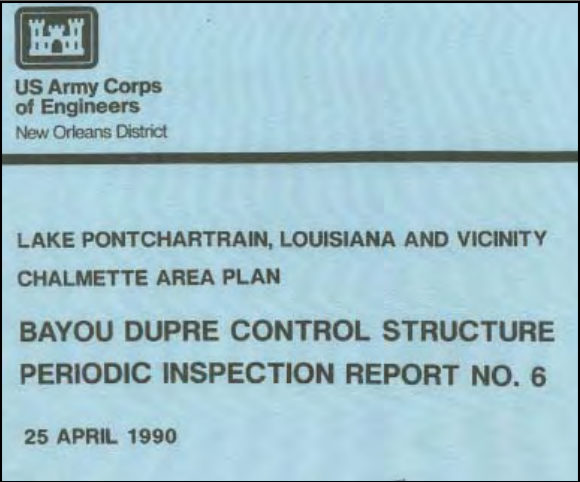
Figure 14-143. Bayou Dupre Ctrl Struct PIR No 6 25 Apr 1990.pdf Shows Pre-Katrina Condition of Structure

Hurricane Levee Between Bayou Dupre and STA. 1054+00. There is an 8,000 ft. section of the levee immediately southeast of Bayou Dupre that is severely damaged and has lost approximately 12 feet of levee section and is at approximately El. 5.0.

Figure 14-144. Major Scour on Levee Protected Side (Landside)

Figure 14-145. Scour Depths Below the Original Levee Footprint

There is 2,500 ft. of levee from Bayou Dupre to STA 1007+91 that lost approximately 8' of elevation (assume that 50% of the levee section is gone).

This is a preliminary report subject to revision; it does not contain final conclusions of the United States Army Corps of Engineers.

Figure 14-146. Scour on Landside (Protected Side) of Levee

Volume V The Performance – Levees and Floodwalls – Technical Appendix

V-14-143

This is a preliminary report subject to revision; it does not contain final conclusions of the United States Army Corps of Engineers.

Figure 14-147. Major Scour on Protected Side of Levee

The repaired levee cross section is shown below. This was the typical cross section used to estimate the required quantities.
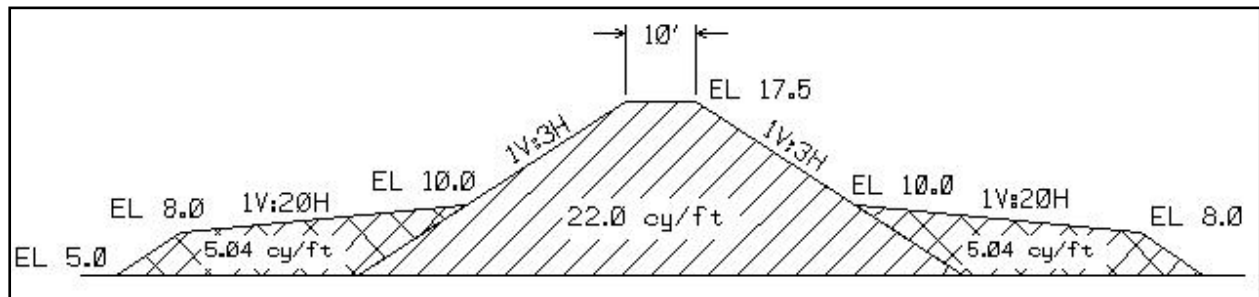
Figure 14-148.

Quantities: 650,000 cy fill – 200 acre borrow area
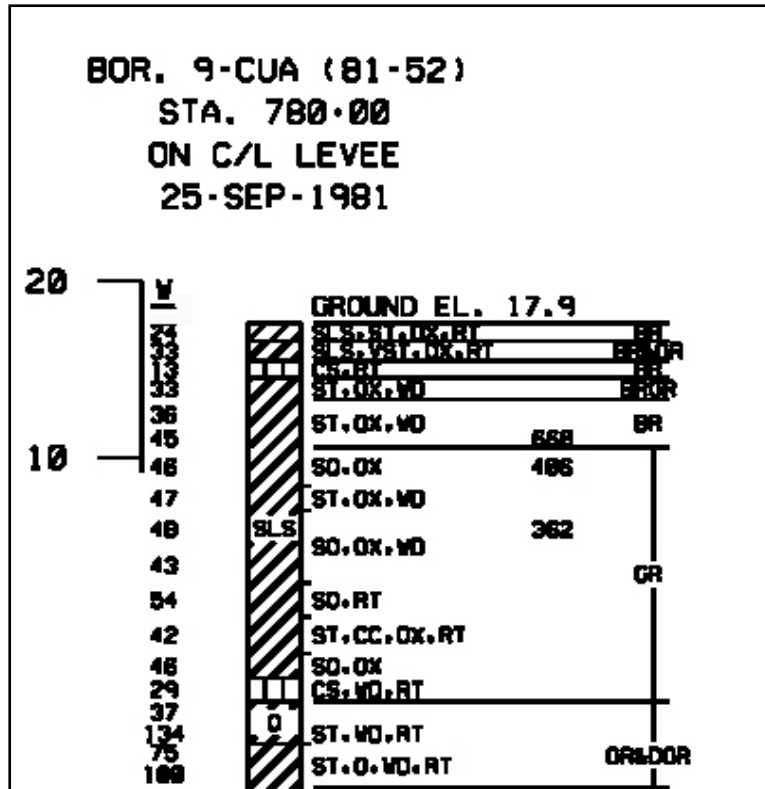
Figure 14-149. 1981 Soil Boring at Sta 780+00 Near Dupre Shows Top Layer of Lean Clay (CL) Underlain By Fat Clay (CH), Silt (ML or MH), and Silt / Sand Lenses (SLS) in the CH Material (From Drawing 9 of 10, Contract Solicitation W912P8-06-R-0002)

There is 700 ft. of this reach that is sheet pile floodwall that has been damaged and will be replaced with earthen levee. The above diagram was used to estimate required quantities.

Volume V The Performance – Levees and Floodwalls – Technical Appendix   V-14-145

This is a preliminary report subject to revision; it does not contain final conclusions of the United States Army Corps of Engineers.

Figure 14-150. Scour on Protected Side of Sheetpile Wall

Figure 14-151. End of Sheetpile Wall at B/L Sta 980+58
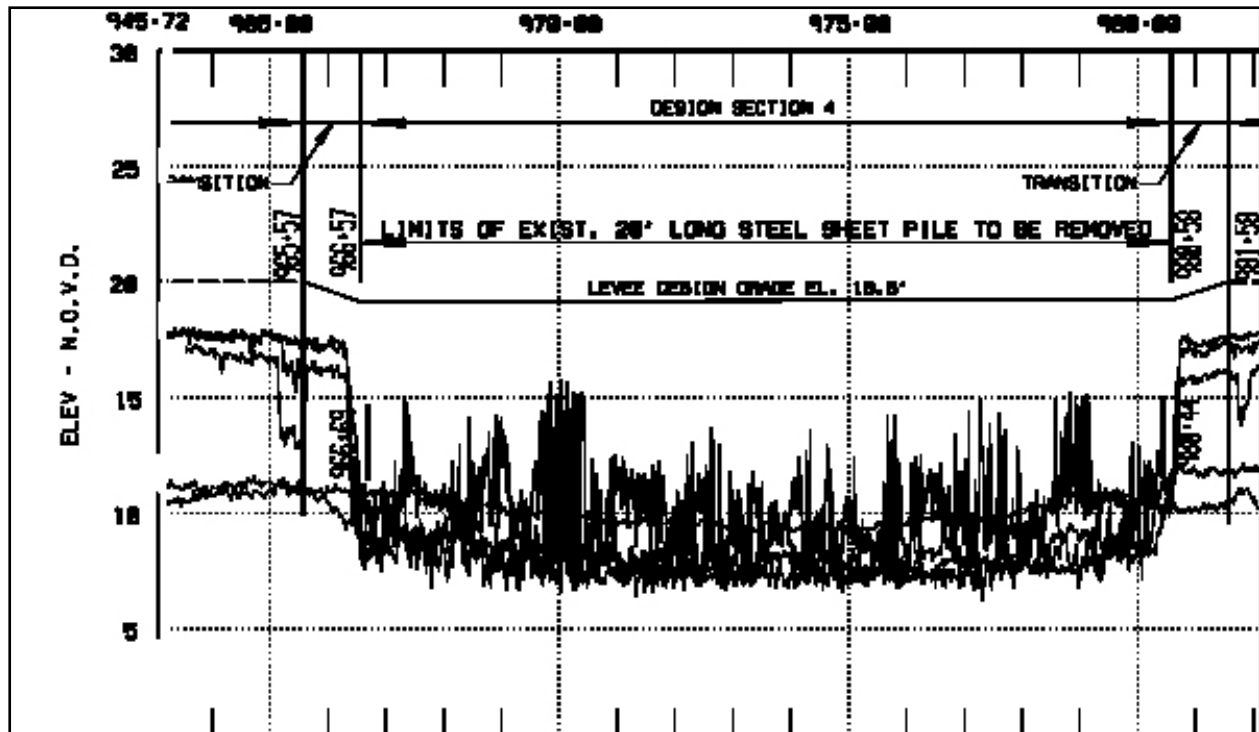
Figure 14-152. Scour Depths Along Sheetpile and at Transition to Levee. Note that scour occurred along the sheetpile reach, not at the sheetpile / levee transition (also seen in Figure 14-151), from drawing 7 of 10, contract solicitation W912P8-06-R-0002
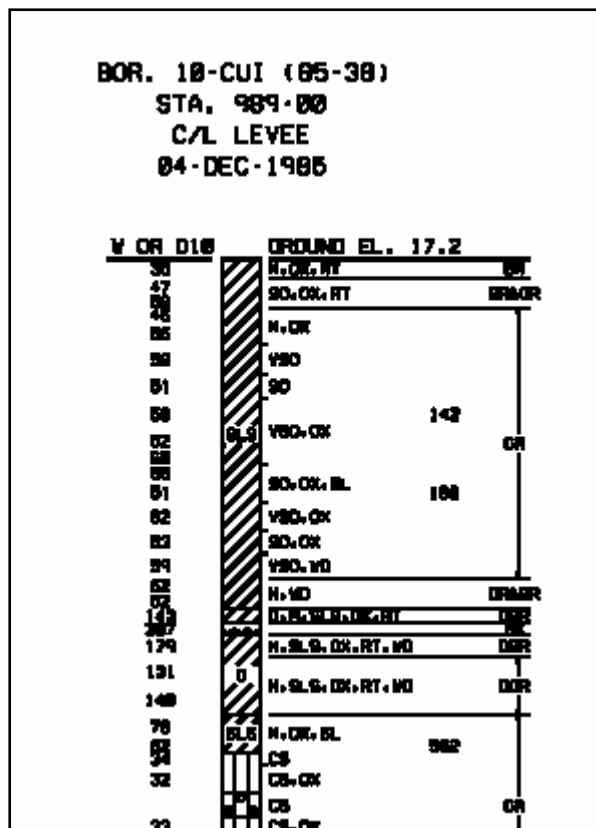
Figure 14-153. Pre-Katrina Boring at Sta 989+00 (about 800 ft beyond the sheetpile/levee transition)
Shows Levee Section with Fat Clay (CH) Cap and Core, With Interbedded Silt Lenses (SLS)

TFG Project **STB03** (Levee Restoration East of Bayou Dupre - MRGO Baseline Station 714+55 to 1007+91) includes repairing a 5.6-mile reach of levee along the MRGO extending east from the Bayou Dupre Control Structure. The entire levee reach will be restored to the design grade elevation (17.5'), requiring the placement of an estimated 1,120,000 cubic yards of fill material. The borrow area for this fill material is a strip of land adjacent to the levee, which was used as a disposal area during the construction of the MRGO canal. Scheduled completion date is 1 April 2006.

Volume V The Performance – Levees and Floodwalls – Technical Appendix

V-14-149

This is a preliminary report subject to revision; it does not contain final conclusions of the United States Army Corps of Engineers.

Figure 14-154.

MRGO to Caernarvon Levee. TFG Project **STB08** (Miscellaneous Scour Repair) includes repair of minor scour on the backside of the levee from the Mississippi River Gulf Outlet (MRGO) to Caernarvon, which is about 10.8 miles in length. An estimated 36,000 cubic yards of fill material will be required for this work Scheduled completion date is 15 April 2006.

Figure 14-155. Crown Scour Along Approximate B/L Sta 1203+00 to Sta 1230+00

Volume V The Performance – Levees and Floodwalls – Technical Appendix

V-14-151

This is a preliminary report subject to revision; it does not contain final conclusions of the United States Army Corps of Engineers.
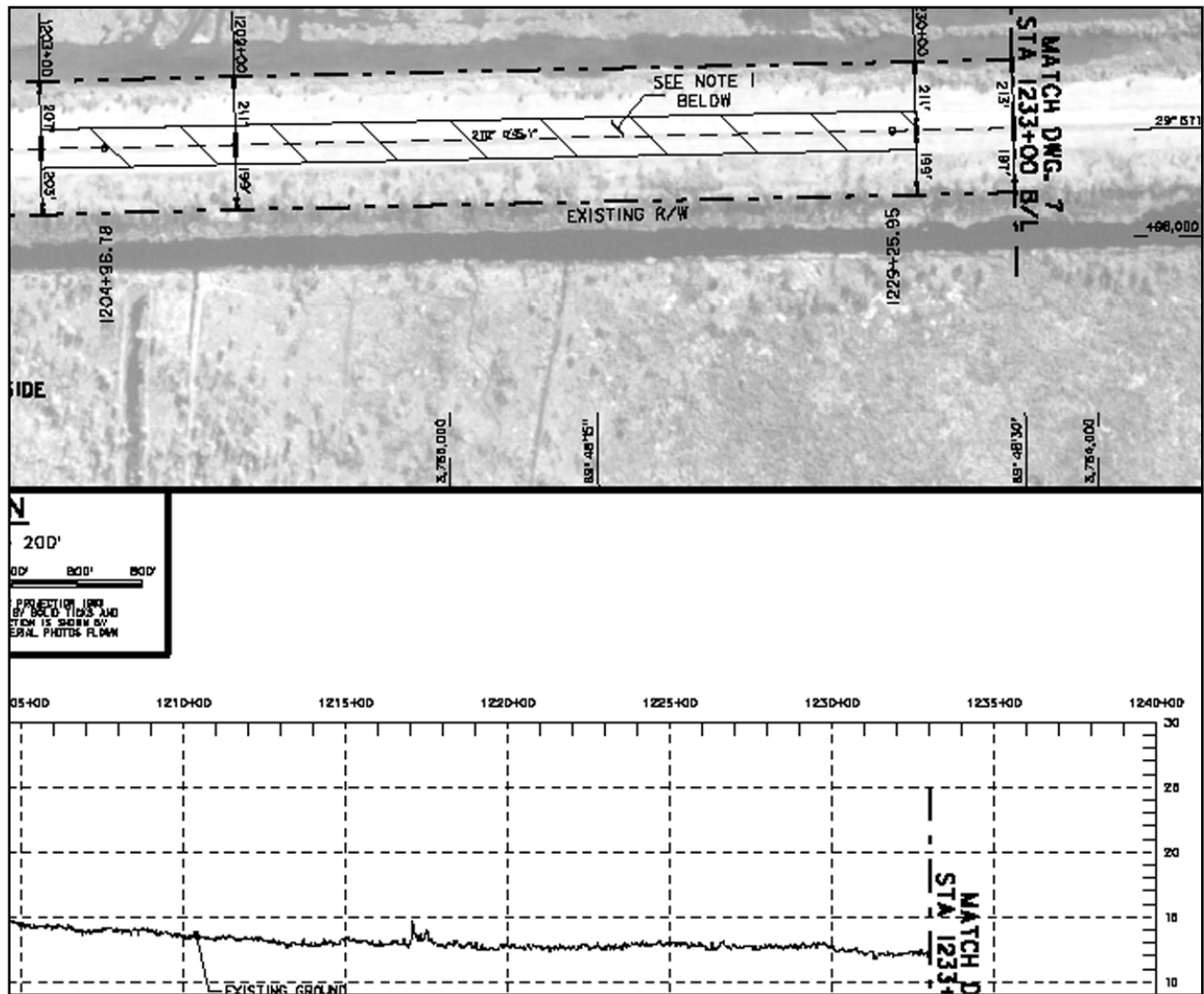
Figure 14-156. Levee Crown Elevation Drops From Elev 15 ft to Elev 12 ft in the Scour Area. Elevation 12 ft Remains Fairly Constant Along the Reach for About a Mile Beyond The Scour Section. From Contract Solicitation STB08 W912P8-06-R-0094, drawing sheet C-06

Figure 14-157. Original 1967 Boring at Ground Elevation 1 ft Shows Fat Clay With Silt / Sand Lenses (from DM3 Chalmette Extension drawing file H-2- 24306, plate 7). The levee along this reach was constructed of Miss. River hydraulic sand fill, capped with local borrow clay, and shaped to grade with Miss. River batture soil (truck-hauled fill)

Figure 14-158.

   Creedmore Gravity Drainage Structure. The levee district has been unable to fully close the two 72-inch sluice gates on drainage structure. One sluice gate is approximately 50% closed and the other is approximately 90% closed. The cause of the sluice gates being stuck is apparently debris under the gate slides. Since there are trash racks on the inlet structure to these drains the debris must have come in through the outlet structure. While attempting to close the sluice gates against this debris the gate hoists were both damaged.

Figure 14-159.

Figure 14-160.

TFG Project **STB09** (Repair Creedmore Structure) includes constructing a cofferdam and removing debris from the structure to permit closure of the gates and inspection of the structure to determine if further repairs are necessary. Scheduled completion date is 1 April 2006.

Figure 14-161.

Plaquemines Parish

Levee and Floodwall Characterization

General. The Plaquemines Parish Basin includes long, narrow strips of protected land on both sides of the Mississippi River between New Orleans and the Gulf of Mexico. The Mississippi River Levees (MRL) protect the Parish from floods coming down the river. Protection from hurricane-induced tidal surges is achieved by the New Orleans to Venice (NOV) hurricane protection system. The NOV is a system of levees on the gulf side of the protected lands and additional berms and floodwalls on top of the MRL along the river. The distance

between the gulf-side levees (back levees), and the MRL is less than a mile in most places. The extent of these protection systems is shown in ___

Figure 14-162. Plaquemine Parish Mississippi River Levees (MRL East Bank, MRL West Bank) and New Orleans to Venice Hurricane Protection Levees (St. Jude to City Price, Reach A, Reach B-1, Reach B-2, and Reach C) Project Reaches

Altogether the Plaquemines Parish MRL and NOV systems include 162 miles of levee and 7 miles of floodwall. There are fifteen non-federal pump stations for interior drainage. The levees are crossed by numerous pipelines, constructed in various manners. Some crossings bridge the levee without touching the embankment; some are constructed on top of the line of protection; and some pass through the line of protection with measures to prevent seepage. There is also a wicket gate closure on the back levee at Empire, where a shipping canal connects the Mississippi River to the Gulf of Mexico.

NOV Levees. The NOV system is a hurricane protection levee or floodwall that is built on top of the MRL or setback from the MRL. The NOV includes WAVE berms on the floodside and STABILITY berms on the protected side. Floodwalls are used where real-estate is not available to build levees. The NOV system is approximately 2 to 3 ft higher than the MRL. The NOV consists of four distinct reaches; Reach C at Phoenix to City Price, Reach A from City Price to Empire, Reach B-1 from Empire to Ft. Jackson and Reach B-2 from Ft. Jackson to Venice. Figure 14-1 illustrates the NOV levee systems in Plaquemine Parish.

MRL Levees. The Plaquemines Parish East Bank MRL system extends from the Parish line at Braithwaite 33 miles downstream to Bohemia. The flood side has concrete slope pavement from the bottom of the embankment to the design high water level. The crown is surfaced with 9 inches of crushed limestone. The freeboard and protected side slopes are grassed.

The east bank NOV back levee runs between Phoenix and Bohemia, a distance of 16 miles. It is a grass-covered earthen levee.

The West Bank Plaquemines MRL system extends from the parish line at Belle Chasse, 70 miles downstream to Venice. Its composition is similar to the East Bank MRL with concrete slope pavement, crushed limestone surface course, and the remaining slopes grassed. Below Port Sulphur (29 miles above Venice), the MRL design grade is lower than the NOV hurricane design grade, so the NOV is constructed as berms or floodwalls on top of the MRL.

The west bank NOV extends from St. Jude to Venice, a distance of 34 miles. The NOV protection along the river includes 6 miles of floodwalls in 13 distinct reaches, projecting above the MRL from 2 to 8 feet. The back levee is a grass-covered earthen embankment.
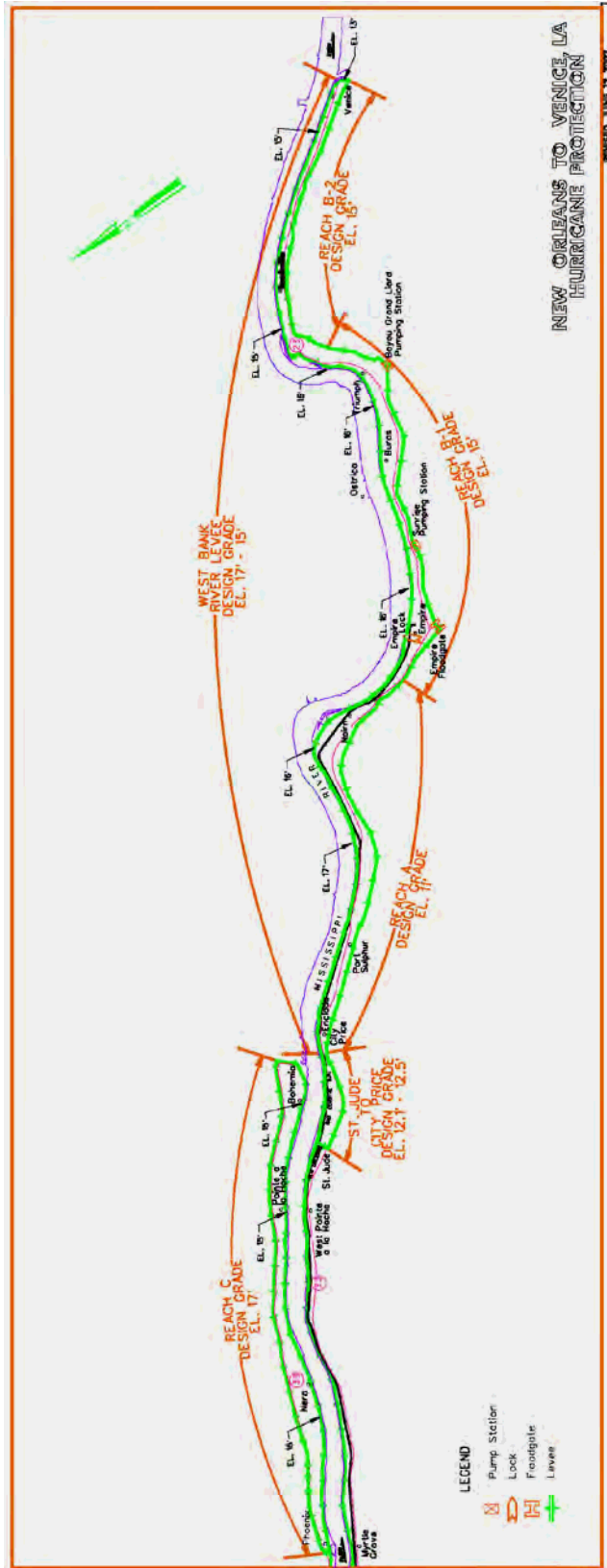
Figure 14-163. New Orleans to Venice Hurricane Protection Project

Damage from Katrina. All of the levees in Plaquemines Parish sustained damage from Hurricanes Katrina and Rita. There was considerable crown and slope scour along the total length. The MRL slope pavement sustained damage from the hundreds of ships and barges that crashed upon it. There were also several severe breaches, coinciding with pipeline crossings and with some floodwalls. Five of the six miles of NOV floodwall along the Mississippi River was damaged beyond repair. There were major breaches at sheet pile wing walls at two pump stations in the back levee. A major breach occurred at the Shell pipeline crossing near Nairn. And the West Pointe a la Hache pipeline crossing was severely damaged. Wind and water damage from Katrina and Rita severely impacted nearly every structure within the east bank area of protection and on the west bank below Myrtle Grove (50 miles above Venice).

Figure 14-3 shows the extent of contracts awarded to repair Plaquemines Parish. There are 22 projects in total that are worth approximately $107 million. Below are descriptions of contracts which relate to floodwall failures.

Code	Project	Advertise	Award	Amount	Status	Contractor
P01	Fort Jackson Borrow Pit - Clearing and Grubbing	12-Oct	19-Oct	$ 326,100	Completed	Bucktown Contractors
P02	Walker Borrow Pit Processing	2-Jan	12-Oct	$ 800,000	Awarded	MVM
P03	NOV East Bank, Reach C	19-Oct	3-Nov	$ 1,878,727	Awarded	Purnell Construction
P04	MRL East Bank Levee Repair	2-Jan	7-Oct	$ 400,300	Awarded	MVM
P06	MRL Levee Repair Jesuit Bend to St. Jude	19-Oct	26-Oct	$ 4,311,998	Completed	Wilco Industrial Service
P07	MRL Levee Repair City Price to Port Sulphur	21-Oct	26-Oct	$ 1,657,894	Completed	Grillot LLC
P08	MRL Levee Repair Port Sulphur to Fort Jackson	31-Oct	11-Nov	$ 7,968,100	Awarded	B&K Construction
P11	MRL Levee Repair Fort Jackson to Venice Shaping	2-Jan	1-Nov	$ 432,800	Completed	MVN
P12	NOV Levee Repair Fort Jackson to Venice	16-Nov	20-Nov	$ 5,586,000	Awarded	Dean Equipment
P13	NOV Setback Levees Port Sulphur Area STA 235+00 to STA 357+80				In Design	
P14	NOV Setback Levees Empire Reach STA 769+10 to STA 902+70	7-Jan	20-Jan		Award Pending	
P15	NOV Empire Flood Gate Repair	21-Dec	7-Jan		Award Pending	
P16	NOV Back Levee Repair, Reach B-2	28-Oct	18-Nov	$ 927,600	Awarded	Purnell Construction
P17	NOV Setback Levees Buras Reach STA 910+35 to STA 1002+39	14-Jan	27-Jan		In Design	
P18	NOV Back Levee Repair, Reach B-1	28-Oct	4-Nov	$ 1,175,101	Awarded	Creek Services
P19	NOV Back Levee Repair, Above City Price and Reach A	10-Nov	21-Nov	$ 7,879,958	Awarded	Shaw Environmental Serv.
P20	NOV West Bank Back Levee Floodwall Repairs	3-Nov	18-Nov	$ 4,500,000	Awarded	LL&G
P21	NOV West Bank Back Levee Miscellaneous Repairs	5-Dec	9-Jan		Award Pending	
P22	MRL Woodland Emergency Repair		21-Oct	$ 500,758	Completed	Dean Equipment
P24	NOV Setback Levees Port Sulphur Area STA 357+80 to STA 650+00	10-Jan	24-Jan		In Design	
P25	MRL West Pointe a la Hache Siphon Repair	7-Dec	14-Dec	$ 1,035,755	Awarded	Southern Services Equip.
P26	MRL Slope Pavement Repair	24-Oct	12-Nov	$ 870,550	Awarded	Bertucci Construction

Figure 14-164. Repair Project Summary for Plaquemines Parish (TFG, Jan 2006

Specific contracts to replace or repair damage to walls

P06 - Major scour at Woodlands Plantation and at a pipeline crossing at the West Pointe a la Hache (not sure if this is a sheetpile or levee failure)

P13 - Replace floodwalls with 6 miles of setback levees from station 114+57 to 426+99. Along the Port Sulphur Reach (south of Port Sulphur).

P14 - Replace floodwalls with 2.5 miles of setback levee along Empire Reach from Station 769+10 to 902+70.

P17 - Replace floodwalls with 9,000 feet of setback levee along Buras Reach Station 910+35 to 1002+39, severe scour behind wall

P20 – NOV, floodwall repair at Sunrise (next to Buras) and Hayes (next to Port Sulphur) pump stations. Emergency sheetpiling was installed at both locations.

P21 - West Bank, repair floodwalls at: Homeplace Marina (next to Port Sulphur), Gainard Wood Pump station-(south of Homeplace – 2 miles), and at Diamond Pump station (next to City Price). Floodwalls are I-walls and some are capped.

P24 - Replace floodwall from station 357+80 to 650+00. Port Sulphur Area just above Nairn

Floodwall Damage Plaquemines Parish							
Source: Task Force Guardian Project Information Report (October 2005)							
Reach and Station	length Riverside erosion	Length of Landside Erosion			floodwall damage	length of	
	Minor Top 1/4 48 sq-ft/ft	Minor Top 1/4 48 sq-ft/ft	Major Top 1/2 96 sq-ft/ft	Major Top 1/2 96 sq-ft/ft	both ends	landside	failure SP or I-wall
Reach A							
MRL							
113 to 144					40	6360	
150 to 156	2000				40	8020	
253 to 256					40	300	
273 to 276					40		
Reach b 1							
MRL							
278 to 224				5200	40	7750	4100
223 to 218					40	26282	6300
HPL							
191 to 188					40	5729	
empire					40	4583	

Appendix 15
Concrete I-Wall and Sheet Piling Material Recovery, Sampling and Testing: 17th Street Canal Levee Breach

Introduction

On Monday and Tuesday, 12-13 December 2005, samples of the concrete I-wall and sheet piling were taken at or adjacent to the 17th Street Canal levee breach. The objectives of this exercise were a:) to verify conformance of material properties of the I-wall concrete and reinforcing steel, and the sheet piling with their respective specifications; b:) to verify the as driven length of the of the sheet piling and c:) potentially validate the Parallel Seismic testing that was performed in an attempt to determine, in situ, the sheet piling tip elevation

The 17th Street Canal breach is located on the east side of the canal just south of Hammond Highway. Figure 15-1 shows the breach shortly after Hurricane Katrina. The material samples were obtained from the (relatively) undisturbed I-wall sections at the north and south end of the breach. Concrete and rebar samples were obtained on Monday, 12 December and sheet piling were extracted on Tuesday, 13 December 2005.

The I-wall is comprised of a series of concrete wall panels separated by expansion joints and is founded on sheet piling driven through the levee. A typical cross section is shown in Figure 15-2.

Material Sample Recovery

The material samples recovered from the site included two four foot square by 12 inch thick wall panel samples, two nominally six inch diameter cylindrical cores, one each from the wall panel samples, six samples of reinforcing steel from the wall panels and 14 sheet piles. All samples were marked and tagged and placed into a controlled and documented chain of custody.

Figure 15-1. 17th Street Canal Breach

The I-wall panels immediately north and south of the breach were designated H22 and H38, respectively. A four foot by four foot section was sawcut from the top of the north end of the I-wall section H38 and from the top of the south end of I-wall section H22. The contractor first drilled a six inch diameter core from the designated four foot square sample at the north end of wall panel H38. The core drill and saw are shown mounted to the wall at panel H38 at the south end of the breach in Fig 15-3. Figure 15-4 shows the core being removed from panel H38. It was marked and tagged MH38C1C01 as shown in Fig. 15-5.

Prior to drilling, the cores were considered as potential compressive strength test specimens. However the core contained rebar and was not a valid test specimen. The resulting holes were used to for rigging to support and remove the four foot by four foot wall samples as shown in Figs. 15-6 and 15-7.
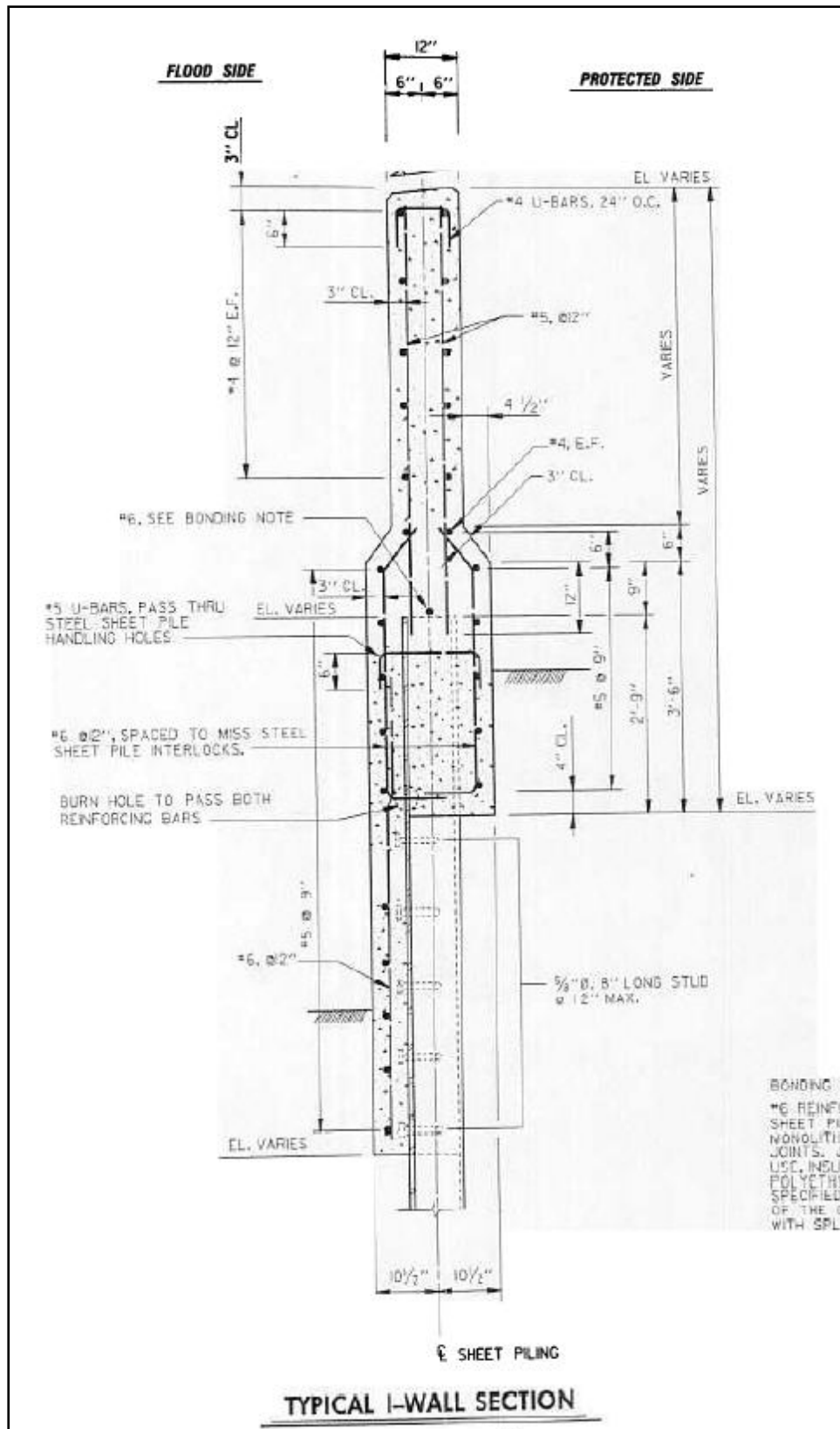
Figure 15-2. Typical I-Wall Section

Volume V The Performance – Levees and Floodwalls – Technical Appendix   V-15-3

This is a preliminary report subject to revision; it does not contain final conclusions of the United States Army Corps of Engineers.

Figure 15-3. Core Drill and Saw Mounted to Wall Panel H38

Figure 15-4. Core Being Removed from Panel H38

This is a preliminary report subject to revision; it does not contain final conclusions of the United States Army Corps of Engineers.

Figure 15-5. Core from Wall Panel H38

Figure 15-6. Sawing of Sample from Wall Panel H38

Figure 15-7. Removal of Sample from Wall Panel H38

A similar procedure was used to obtain a four foot square sample from the south end of wall panel H22 at the north end of the breach as shown in Figs. 15-8 and 15-9. The concrete core was marked and tagged MH22C1C01 as shown in Fig. 15-10. This core also contained rebar and was not suitable for testing. The wall panel sample was marked and tagged MH22C1 as shown in Fig. 15-11.

Figure 15-8. Core Drill and Saw Mounted at Panel H22

Figure 15-9. Sample Being Removed from Wall Panel H22

Figure 15-10. Cylindrical Core from Wall Panel H22

Figure 15-11. Wall Sample MH22C1

Rebar samples were then removed from the remaining sections of wall panels H38 and H22. A hoe ram was used for controlled demolition of wall panels in order to expose the rebar samples as shown in Fig. 15-12. Some of the demolition of the concrete around the rebar samples was done with a small hand held jack hammer as shown in Fig. 15-13. A portable electric bandsaw was used to cut the rebar samples as shown in Fig 15-14.

Figure 15-12. Demolition of Concrete for Rebar Sampling at Panel H22

Figure 15-13. Demolition of Concrete Around Rebar Sample at Panel H38

Volume V The Performance – Levees and Floodwalls – Technical Appendix

Figure 15-14. A Portable Electric Bandsaw is Used to Cut Rebar Samples

At wall panel H38 a two foot long sample of the following rebar were obtained: 1) A #4 horizontal bar from the east face of the wall approximately 29 inches down from the top of the wall. The north end of the sample terminated at the vertical sawcut for the wall sample MH38C1. 2) A #5 vertical approximately 76 inches from the north end of panel H38. 3) A #6 vertical from the west face of the lower section of the wall. This #6 bar was approximately 8 inches from the north end of panel H38. (This sample has the orange paint shown in Fig. 15-15.) These rebar samples were marked and tagged MH38R1, MH38R2 and MH38R3, respectively.

Figure 15-15. Number 6 Rebar Sample Being Taken from Panel H38

At wall panel H22 a two foot long sample of the following rebar were obtained: 1) A #4 horizontal bar from the west face of the wall, approximately six inches down from the top of the wall 2) A #5 vertical bar from the west face of the wall approximately 74 inches from the south end of the wall pane. 3) A #6 vertical from the west face of the lower end of the wall approximately 16 inches from the south end of the wall panel. These samples were marked and tagged MH22R1, MH22R2 and MH22R3, respectively.

Figure 15-16 shows the wall panel samples, cores, and rebar samples collected on Monday, 12 December 2005. Note that the cores were placed in sealed plastic bags and each core and the 3 rebar samples from each of the two wall panels were placed in individual latching boxes. These samples were transported to a secure area at a warehouse at the Corps of Engineers' New Orleans District Office.

Figure 15-16. Wall Panel Samples, Cores and Rebar Samples

After the cores, wall panel and rebar samples were obtained the contractor began demolition of the wall panels to expose the top of the sheet piles for extraction. A scissor concrete crusher was used to demolish the upper portion of the wall panels as shown in Fig. 15-17. A hoe ram was then used to remove the lower portion of the of the wall panel around the sheet piling (Reference

the wall cross section in Fig. 15-2.) as shown in Fig. 15-18. The same procedure was used for both wall panels H38 and H22.

Figure 15-17. Demolition of Top Portion of Wall Panel H38

Figure 15-18. Hoe Ram Demolishing Lower Portion of Wall Panel H38

On Tuesday, 13 December 2005, sheet piles were extracted. The location of the sheet piles extracted at or adjacent to wall panel H38 is schematically shown in Fig. 15-19. Starting from the north end of panel H38, the piles are designated MH38SP1, MH38SP2, …, MH38SP16 (the last number of the designation is incremented going from north to south).
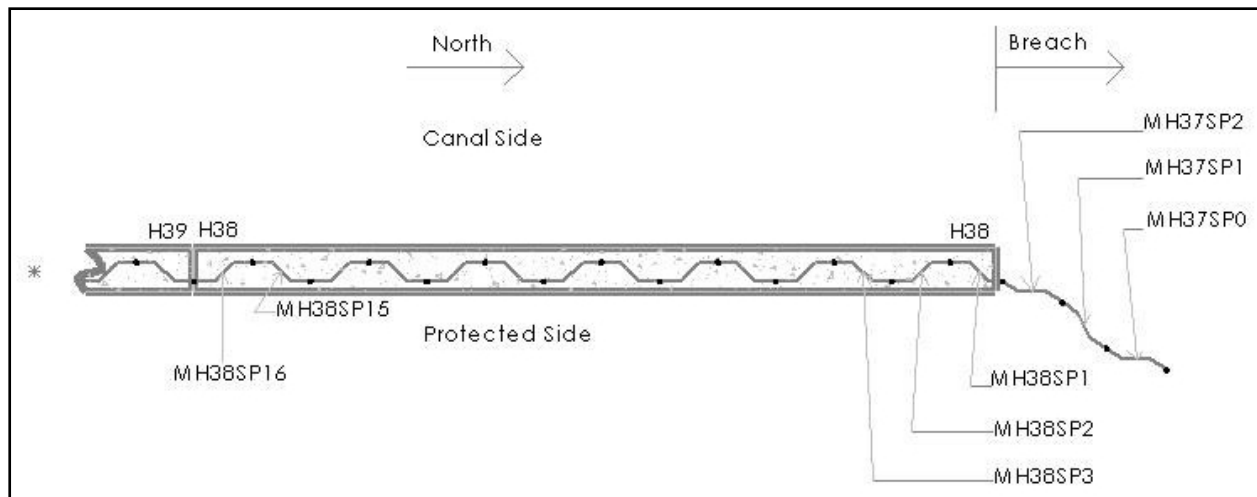
Figure 15-19. Sheet Pile Designations at Wall Panel H38

Sheet piles MH38SP2, MH38SP3 were extracted as a pair. Their lengths were approximately 23'-7" and 23'-8", respectively. MH38SP1 and MH37SP2 were then extracted as a pair. Their lengths were approximately 23'-3". The contractor then moved to the south end of wall panel H38 and extracted MH38SP15 and MH38SP16. Their lengths were approximately 23'-5". MH38SP15 and MH38SP16 were at a location corresponding to a soil boring hole where Parallel Seismic tests were conducted in an attempt to determine the length of the sheet pile in situ. The contractor then attempted to extract sheet pile MH37SP1 as a single pile, but MH37SP0 came with it. Their lengths were approximately 23'-6". Extraction of sheet piles at the south end of the breach is shown in Figs. 15-20 and 15-21. The out-of-plumb orientation (from displacement of the piling in the breach) of piles MH37SP1 and MH37SP0 is clearly evident in Fig. 15-21. Figure 15-22 shows measuring and tagging of sheet piling.

Figure 15-20. Extraction of Sheet Piles MH38SP2 and MH38SP3

Figure 15-21. Extraction of Sheet Piles MH37SP1 and MH37SP0
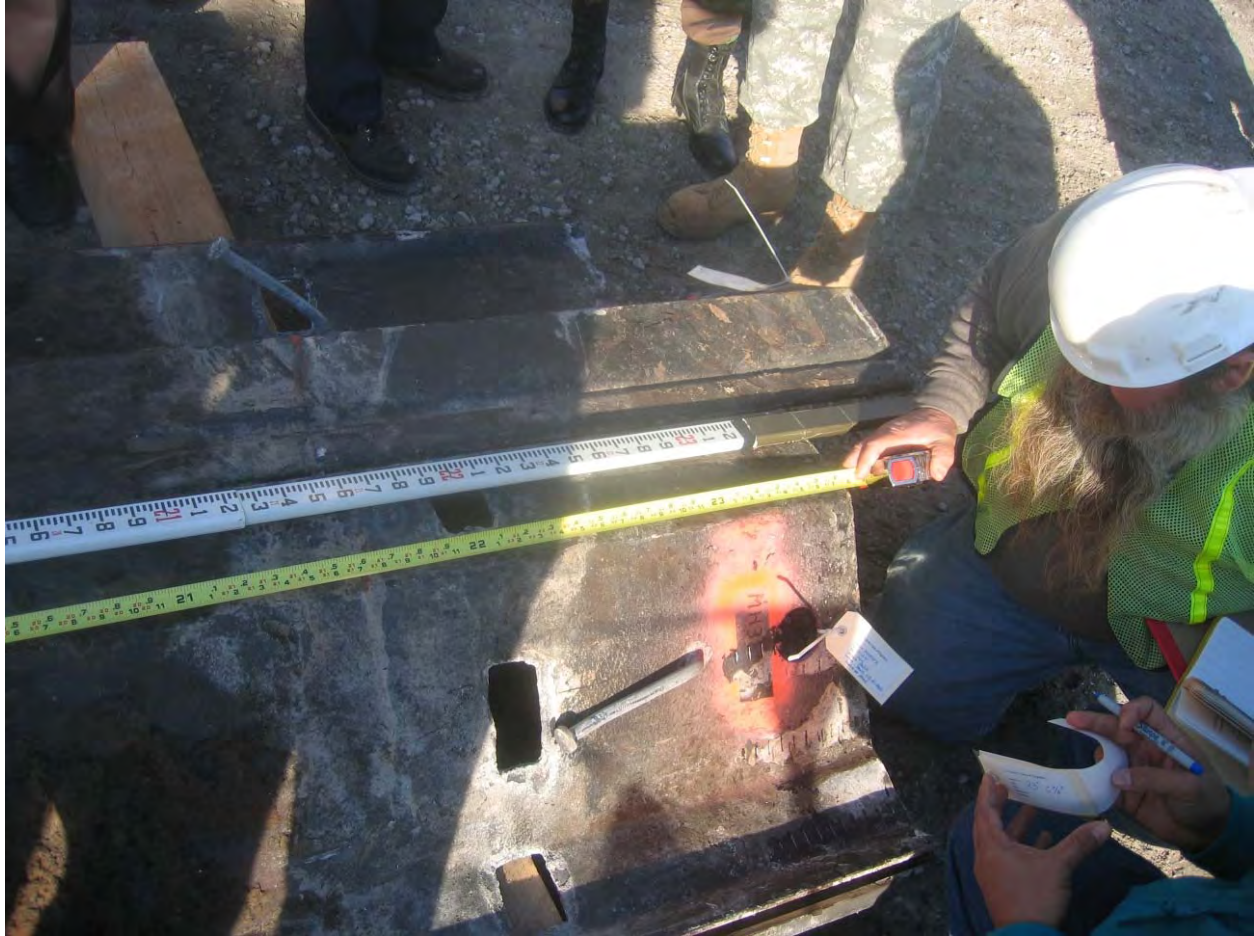
Figure 15-22. Measuring and Tagging of Sheet Piles

Sheet piles were then extracted at the location of wall panel H22, immediately north of the breach, Four sheet piles at the south end of wall panel H22 were designated MH22SP1, MH22SP2, MH22SP3 and MH22SP4. (The last number of the designation was incremented going from south to north.) Sheet piles MH22SP1 and MH22SP2 were extracted as a pair as shown in Fig. 15-23. These piles had a length of approximately 23'-7"and 23'-6", respectively. Sheet piles MH22SP3 and MH22SP4 were extracted as a pair and had a length of approximately 23'-7" and 23'-6", respectively. The contractor then pulled a pair of piles from just north of the north end of wall panel H22 at a location coincident with a boring hole where Parallel Seismic testing had been performed. These piles were designated MH21SP1 and MH21SP2. Both of these sheet piling had a length of approximately 23'-6".

Figure 15-23. Extraction of Sheet Piling MH22SP1 and MH22SP2

Volume V The Performance – Levees and Floodwalls – Technical Appendix
This is a preliminary report subject to revision; it does not contain final conclusions of the United States Army Corps of Engineers.

Figures 15-24 and 15-25 show the sheet piling extracted from the south and north ends of the breach, respectively. The sheet piles were loaded on a truck and transported to a secure location within a warehouse at the Corps of Engineers' New Orleans District Office.

Figure 15-24. Sheet Piling Extracted from South End of Breach

Figure 15-25. Sheet Piling Extracted from North End of Breach

Sheet Piling Length and Tip Elevation

The sheet piling extracted from the 17th Street Canal breach site ranged in length from 23'-3" to 23'-8". The top of the pilings were at approximately elevation 6.25 ft. (The pilings adjacent to the expansion joints between wall panels were driven slightly lower as can be seen in Fig. 15-26. This was done to improve the performance and effectiveness of the expansion joint.) A 23'-3" piling length provides for a tip elevation of -17.0 ft. Obviously, piling driven with a lower top elevation have a correspondingly lower tip elevation.

Figure 15-26. Lower Top Elevation of Sheet Piling at Expansion Joint

Material Testing

On Friday, 16 December 2005, three each, nominally six inch diameter, concrete cores were drilled from the wall panel samples MH22C1 and MH38C1. These cores were marked and tagged MH22C1-01, MH22C1-02, MH22C1-03, MH38C1-01, MH38C1-02, and MH38C1-03. A sample of steel was also flame cut from each of four sheet piling. The six cores, four steel samples and the previously obtained six samples of rebar were transferred to Beta Testing & Inspection, LLC of Gretna, LA (BTI) for testing.

The concrete cores were obtained and tested for compressive strength by BTI in accordance with ASTM C 42 and C 39. As can be seen in Table 15-1, all of the cores had a compressive strength in excess of the specified 3000 psi compressive strength. More comprehensive details of the testing are in BTI's report in Attachment A.

Table 15-1
Concrete Compressive Strength

Core	Specified Compressive Strength (psi)	Compressive Strength As Tested (psi)
MH22C1-01	3000	4000
MH22C1-02	3000	3190
MH22C1-03	3000	3940
MH38C1-01	3000	3960
MH38C1-02	3000	4360
MH38C1-03	3000	4100

Tensile tests of the sheet piling material samples were performed, in accordance of ASTM A 370, by a subcontractor to BTI. A summary of the test results and the tensile requirements of the material specification, ASTM A 328 are provided in Table 15-2. More comprehensive details of the testing are in BTI's report in Attachment A.

Table 15-2
Sheet Piling Tensile Requirements and Tests Results

Sample	Yield Strength (ksi)	Tensile Strength (ksi)	Elongation in 2 in. (%)
MH21SP1-01	58.5	80.9	33.0
MH22SP2-01	55.4	80.1	29.9
MH 37SP1-01	55.5	82.1	32.1
MH38SP16-01	57.0	80.0	32.7
ASTM A 328 Tensile Requirements	39	70	20

Tensile tests of the rebar samples, in accordance of ASTM A 370, were also performed. A summary of the test results and tensile requirements for the specified ASTM A 615 Grade 60 reinforcement is provided in Table 15-3. More comprehensive details are included in BTI's report in Attachment A.

Table 15-3
Reinforcing Steel Tensile Requirements and Test Results

Sample	Bar Size Designation No.	Yield Strength (ksi)	Tensile Strength (ksi)	Elongation in 8 in. (%)
MH22R1	4	65.0	107.5	11.7
MH22R2	5	62.9	104.5	13.2
MH22R3	6	65.9	108.1	9.3
MH38R1	4	91.0	107.5	16.2
MH38R2	5	61.3	99.7	9.8
MH38R3	6	79.5	97.7	11.4
ASTM A 615 Grade 60 Tensile Requirements	3, 4, 5 or 6	60	90	9

Attachment A
Test Report from Beta Testing & Inspection, LLC

Table C.1

Sample panel MH38C1						
Core ID	Capped Length (in.)	Diameter (in)	Area (in²)	l/d	Correction factor	Maximum load (lbs.)
MH38C1-01	11.9	5.67	25.25	2.09	1	100,000
	Compressive strength (psi)	Fracture type	Age (days)	Load application	Test date/time	Sample date/time
	3960	C	NA	vertical	12/21/05 10:00am	12/16/05 11:00am
Core ID	Capped Length (in.)	Diameter (in)	Area (in²)	l/d	Correction factor	Maximum load (lbs.)
MH38C1-02	9.19	5.65	25.12	1.62	0.97	113,000
	Compressive strength (psi)	Fracture type	Age (days)	Load application	Test date/time	Sample date/time
	4360	A	NA	vertical	12/21/05 10:00am	12/16/05 11:00am
Core ID	Capped Length (in.)	Diameter (in)	Area (in²)	l/d	Correction factor	Maximum load (lbs.)
MH38C1-03	11.8	5.66	25.15	2.08	1	103,000
	Compressive strength (psi)	Fracture type	Age (days)	Load application	Test date/time	Sample date/time
	4100	D	NA	vertical	12/21/05 10:00am	12/16/05 11:00am

Testing of 17th Street Canal
Floodwall Materials

February 14, 2006

Steel Reinforcing Bars

Six pieces of steel reinforcing bars each measuring 2' in length were secured and transported to BTI's laboratory. The steel reinforcing bar samples ranged in size from No. 4 to No. 6 bars. Mandina's Inspection a subcontractor of BTI tested the rebar specimens to failure in accordance with ASTM A-615 & A370. Section C3B-6.1.1 of the project specifications references ASTM A-615. ASTM A-615 requires a minimum tensile strength of 90,000psi for Grade 60 steel. The specimens tested tensile strength exceeds the minimum project requirements. See enclosure STEEL REINFORCING BAR TENSILES for test results.

Upon completion and acceptance of the testing program, all of the materials, tested and untested, will be sealed and returned to the New Orleans District Office of the US Army Corps of Engineers. Enclosed are copies of our laboratory accreditations and equipment calibration reports associated with the test performed. Should you have any questions regarding this letter or require additional information, please do not hesitate to contact us.

Sincerely,

Beta Testing & Inspection, LLC

Mark A. Cheek, P.E.
Vice-President

Enclosures

Volume V The Performance – Levees and Floodwalls – Technical Appendix

V-15-31

This is a preliminary report subject to revision; it does not contain final conclusions of the United States Army Corps of Engineers.

STEEL REINFORCING BAR TENSILES MH-22

MH22

MECHANICAL TESTING LABORATORY DIVISION

MTL JOB NO. _____

TENSILE NO. _____

8" Gage

SPECIMEN ID	DIA. INCHES	AREA SQ. IN.	YIELD LOAD POUNDS	YIELD STR. PSI	ULTIMATE LOAD POUNDS	TENSILE STR. PSI	ELONGATION IN 8" GAGE PERCENT	REDUCTION IN AREA PERCENT
R1	.500	.20	13,000	65,000	21500	107,500	8.935 / 11.68	.358 / .100 / 50 %

TENSILE NO. _____

SPECIMEN ID	DIA. INCHES	AREA SQ. IN.	YIELD LOAD POUNDS	YIELD STR. PSI	ULTIMATE LOAD POUNDS	TENSILE STR. PSI	ELONGATION IN 8" GAGE PERCENT	REDUCTION IN AREA PERCENT
R2	.624	.31	19,500	62,903	32400	104516	9.052 / 13.15 %	.481 / .181 / 41.6 %

TENSILE NO. _____

SPECIMEN ID	DIA. INCHES	AREA SQ. IN.	YIELD LOAD POUNDS	YIELD STR. PSI	ULTIMATE LOAD POUNDS	TENSILE STR. PSI	ELONGATION IN 8" GAGE PERCENT	REDUCTION IN AREA PERCENT
R3	.750	.44	29,000	65,909	45800	104,090	8.740 / 9.25 %	.626 / .307 / 30.2 %

TENSILE NO. _____

SPECIMEN ID	DIA. INCHES	AREA SQ. IN.	YIELD LOAD POUNDS	YIELD STR. PSI	ULTIMATE LOAD POUNDS	TENSILE STR. PSI	ELONGATION IN 8" GAGE PERCENT	REDUCTION IN AREA PERCENT

G:\WORDDATA\SIFORMS\TT505.LAB

p. 2   5043661688   David Mandina

V-15-32

Volume V The Performance – Levees and Floodwalls – Technical Appendix
This is a preliminary report subject to revision; it does not contain final conclusions of the United States Army Corps of Engineers.
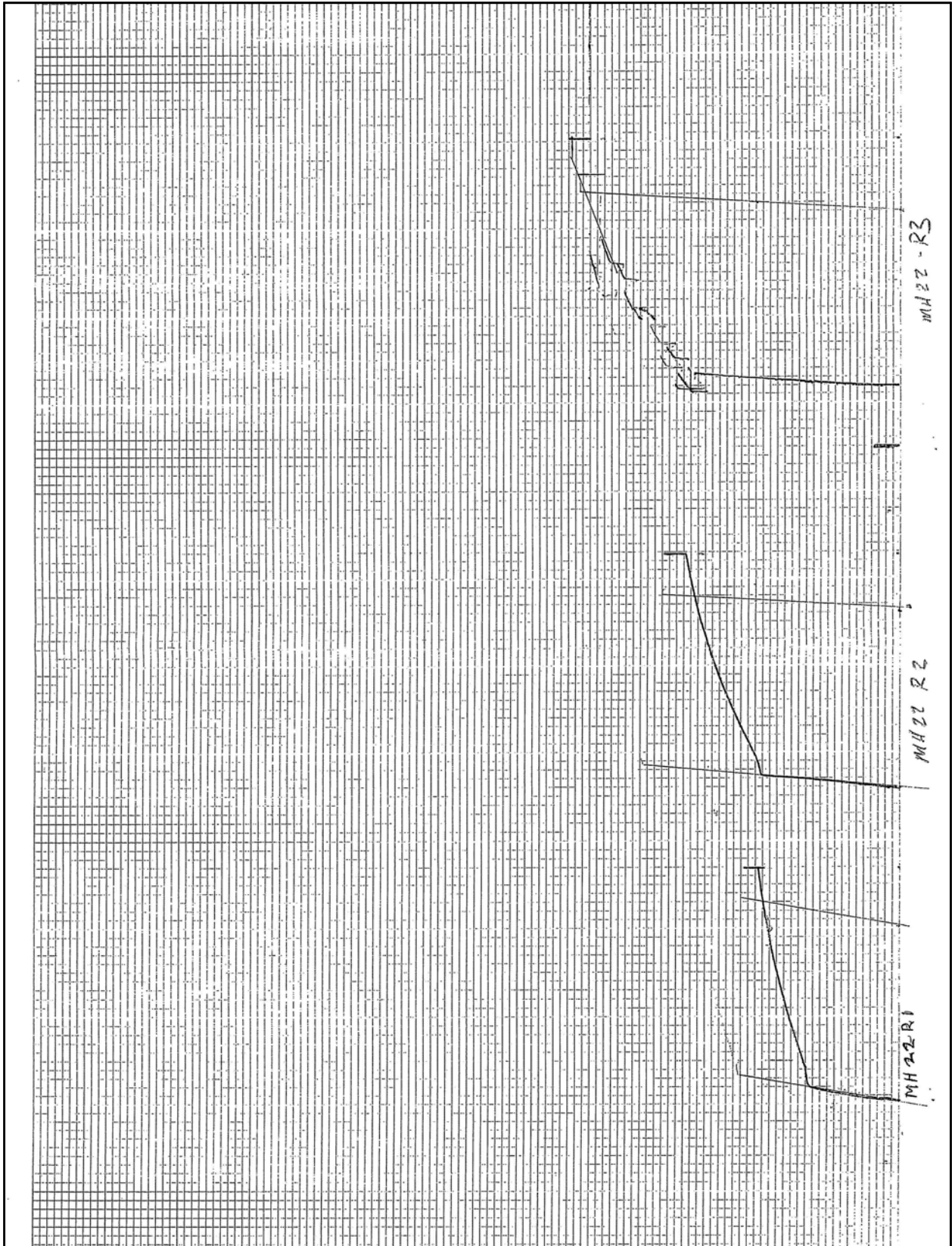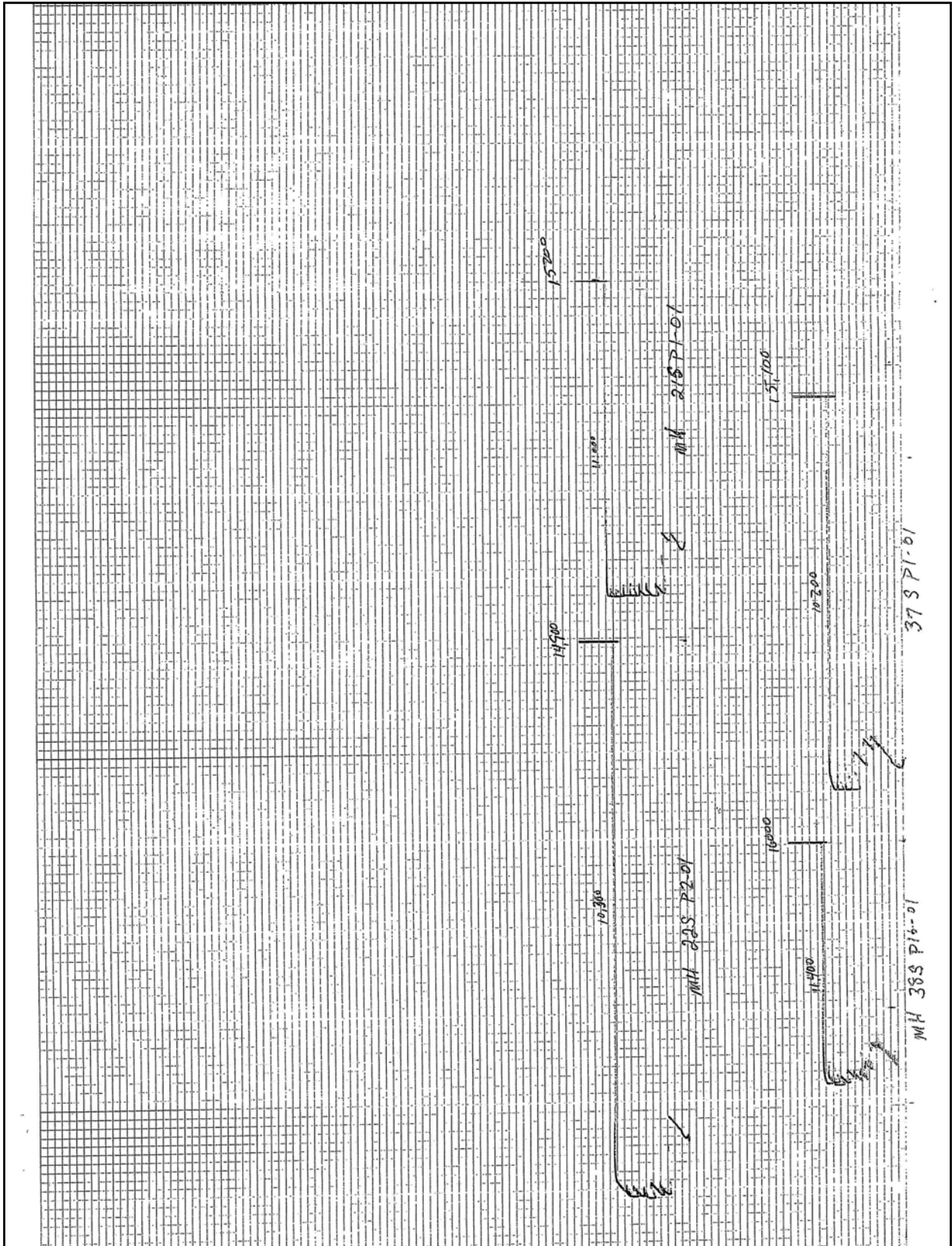
DEPARTMENT OF THE ARMY
ENGINEER RESEARCH AND DEVELOPMENT CENTER, CORPS OF ENGINEERS
GEOTECHNICAL AND STRUCTURES LABORATORY
WATERWAYS EXPERIMENT STATION, 3909 HALLS FERRY ROAD
VICKSBURG, MISSISSIPPI 39180-6199

REPLY TO
ATTENTION OF:

CEERD-GS-E (1110-1-8000c)   22 Aug 05

Memorandum For Commander, USAE District, New Orleans, ATTN: CEMVN-CD-QS/Mr. Geoff Laird,
               PO Box 60267, New Orleans, LA 70160-0267

SUBJECT: Validation of Beta Testing and Inspection, LLC, Gretna, LA

1. In reference to Military Interdepartmental Purchase Request No. W42HEM51322885, dated 13 May 05,
an inspection of the materials testing laboratory of Beta Testing and Inspection, Gretna, LA was performed
on 13 Jun 05. The results of that inspection were reported to the Commander, USAE District, New Orleans
on 20 Jun 05. The laboratory reported their deficiency corrections to the Materials Testing Center (MTC) on
19 Jul and 09 Aug 05. These corrections were compared to the ASTM Standards for compliance and were
found to be satisfactory. We also examined AMRL Inspection Report No. 994F, Dated 01 Jul 04, CCRL
Inspection Report No. J-71, dated 18 Aug 04, and the AASHTO Accredited Laboratory List dated 18 Aug 05.

2. The Quality System of the laboratory is satisfactory and we are granting a validation of the lab to perform
material tests for the U.S. Army Corps of Engineers. The material test methods that the laboratory is
validated to perform are:

   a. **Aggregate Tests:** ASTM C40, C117, C127, C128, C136, C29, C88, C131, C535, C566, C702, D75,
and D4791.

   b. **Bituminous Tests:** ASTM D2726 and D3666.

   c. **Concrete Tests:** ASTM C31, C39, C138, C143, C172, C173, C231, C1064, C42, C78, C157, C174,
C192, C293, C470, C511, C617, C1077, and C1231.

   d. **Soil Tests:** ASTM D421, D422, D558, D698, D1140, D1556, D1557, D2168, D2216, D2217, D2487,
D2488, D2922, D3017, D3740, and D4318.

3. We will add Beta Testing and Inspection, Gretna, LA to the list of commercial laboratories qualified to
conduct material tests for the U.S. Army Corps of Engineers, see the MTC homepage at
http://www.wes.army.mil/SL/MTC/mtc.htm. All Corps offices will be notified of this decision and will have the
opportunity to use their services. The laboratory will remain on our list of laboratories qualified to conduct
material tests until **13 Jun 08**, three (3) years from the date of the inspection.

DANIEL A. LEAVELL
Director, Materials Testing Center

CF:
Mr. Mark Cheek / Beta Testing and Inspection, Gretna, LA

Certificate of Calibration

and Traceability to the

United States National Institute of Standards & Technology

MODEL SST1203U2
STRAINSENSE LOAD CELL, SERIAL NO. 880305A(LO)
12,000 LBF CAPACITY, TENSION & COMPRESSION
STRAINSENSE CONAMP 20 READOUT, SERIAL NO. 900305

The above identified instrument was calibrated in accordance with section 7 of the American Society for Testing and Materials (ASTM) Specification E74-02, entitled "Standard Practice of Calibration of Force-Measuring Instruments...". This calibration is in conformance with the requirements of Morehouse QAM Rev.7, dated 12/04/00.

Calibration was performed at the following settings:
Tension Cal No: 244.84   Compression Cal No: 244.95

The result of this calibration as determined by statistical analysis according to section 8 of ASTM E74-02, is as follows:

	Uncertainty	Resolution
Tension:	2.9 Lbf	1.0 Lbf
Compression:	2.4 Lbf	1.0 Lbf

Class A Loading Range According to ASTM E74-02:
Tension: 1,160.0 Lbf to 12,000 Lbf
Compression: 960.0 Lbf to 12,000 Lbf

Calibration was performed for a temperature of 23 degrees C.

This calibration is certified traceable to the United States National Institute of Standards & Technology according to the following documentation and calibration apparatus used:

Dead Weight Force Machine   S/N M-4644   NIST Lab No. 822/255038-95

Uncertainty of Force Standard used did not exceed +/- 0.002% of applied load.

Calibrated By:

Date Calibrated:
October 05, 2004
Report No: 880305A(LO)J0504

MOREHOUSE INSTRUMENT COMPANY, INC.
FORCE CALIBRATION LABORATORY
1742 SIXTH AVENUE
YORK, PA 17403-2675 U.S.A.
PHONE: 717 / 843-0081
FAX: 717 / 846-4193
WEB : www.morehouseinst.com

This Certificate shall not be reproduced except in full, without written approval from Morehouse Instrument Company, Inc

12/16/2005 14:48 5044662826 WMEAN MOBILE CAL PAGE 03

Certificate of Calibration

and Traceability to the

United States National Institute of Standards & Technology

MODEL: SS504C
STRAINSENSE LOAD CELL, SERIAL NO. 860916A/M-8/96(HI)
500,000 LBF CAPACITY, COMPRESSION
ADMET-DC-16 INDICATOR, SERIAL NO. P16-0008081

The above identified instrument was calibrated in accordance with section 7 of the American Society for Testing and Materials (ASTM) Specification E74-02, entitled "Standard Practice of Calibration of Force-Measuring Instruments...". This calibration is in conformance with the requirements of Morehouse QAM Rev. 7, dated 12/04/00.

Calibration was performed at the following indicator settings:
Load Cell 0
Channel 1

The result of this calibration as determined by statistical analysis according to section 8 of ASTM E74-02, is as follows:

Uncertainty	Resolution
111.0 Lbf	10.0 Lbf

Class A Loading Range according to ASTM E74-02:

44,400.0 Lbf to 500,000 Lbf

Calibration was performed for a temperature of 23 degrees C.

This calibration is certified traceable to the United States National Institute of Standards & Technology according to the following documentation and calibration apparatus used:

Dead Weight Force Machine S/N M-7471 NIST Lab No. 822/268391-03
Transfer Standard   S/N   7079 NIST Lab No. 822.11/268058
Uncertainty of Applied Force from 10,000 Lbf thru 100,000 Lbf = +/-0.002% of applied load
Uncertainty of Applied Force from 150,000 Lbf thru 500,000 Lbf = 56 Lbf

Calibrated by:

Date Calibrated:
August 18, 2004
Report No:860916A/M-8/96(HI)H1804

MOREHOUSE INSTRUMENT COMPANY, INC.
FORCE CALIBRATION LABORATORY
1742 SIXTH AVENUE
YORK, PA 17403-2675 U.S.A.
PHONE: 717 / 843-0081
FAX: 717 / 846-4193
WEB : www.morehouseinst.com

Volume V The Performance – Levees and Floodwalls – Technical Appendix

V-15-37

This is a preliminary report subject to revision; it does not contain final conclusions of the United States Army Corps of Engineers.
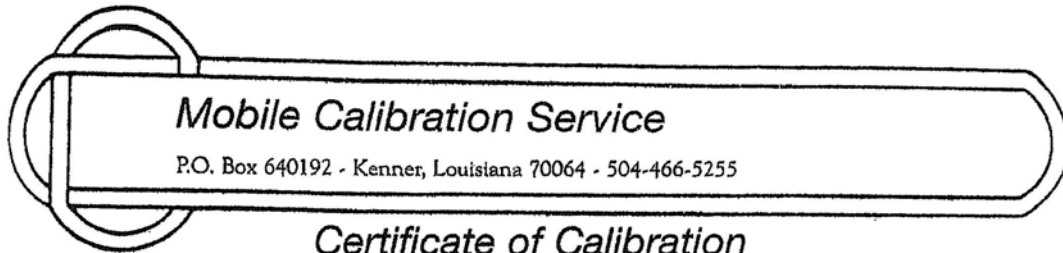
Mobile Calibration Service

P.O. Box 640192 - Kenner, Louisiana 70064 - 504-466-5255

Certificate of Calibration

This is to certify that the following described testing machine has been calibrated in accordance with ASTM E4 and found to be within a tolerance of 1%. Method of verification and pertinent data are in accordance with ASTM E-4. The testing device(s) used have been verified per ASTM E 74 and are traceable to the National Institute of Standards & Technology (N.B.S.)

CLIENT: Mandina Inspection Service   DATE: June 9, 2005
       3861 Peters Road
       Harvey, La.

MACHINE IDENTIFICATION: Tinius Olsen Universal Testing Machine
MACHINE RANGE: 0-120000 Pounds   CALIBRATED RANGE: 10000-120000 Pounds

CALIBRATION APPARATUS	CLASS A RANGE	CALIBRATED TO NIST
Strainsense Load Cell 050106	5000-50000 Pounds	1-05
Morehouse Ring 5-4537	25000-250000 Pounds	5-04

CALIBRATION RESULTS

MACHINE READING	ACTUAL LOAD LBS RUN #1	DIFFERENCE POUNDS	PERCENT ERROR	ACTUAL LOAD LBS RUN #2	DIFFERENCE POUNDS	PERCENT ERROR
10000	10030	30	-0.30	10025	25	-0.25
20000	20060	60	-0.30	20050	50	-0.25
40000	40100	100	-0.25	40060	60	-0.15
60000	60120	120	-0.20	60150	150	-0.25
80000	80190	190	-0.24	80160	160	-0.20
100000	100290	290	-0.29	100220	220	-0.22
120000	120330	330	-0.28	120290	290	-0.24

The above are as found readings. No calibration adjustments required.

MOBILE CALIBRATION SERVICE

Kevin Mevin
TECHNICIAN

OLSON
ENGINEERING, Inc.

January 6, 2006

U. S. Army Corps of Engineers
Engineering Research and Development Center
3909 Halls Ferry Rd.
Vicksburg, MS. 39180

Attn: Mr. Richard W. Haskins, ERDC-ITL-MS
Ofc: (601)634-2931
Fax: (601)634-2873
E-Mail: Richard.W.Haskins@erdc.usace.army.mil

Re: Nondestructive Testing Investigation Report No. 2
        Parallel Seismic Re-Testing Results for Sheet Pile Lengths
        New Orleans 17th Street and IHNC Levees
        New Orleans, LA
        Olson Engineering Job No. 1875C

Dear Sirs,

      We are pleased to report herein the results of re-testing with the Parallel Seismic method
of one sheet pile location at each of the 17th Street and Inner Harbor Navigational Canal (IHNC)
levees. This additional work was conducted as a result of the initial incorrect prediction of sheet
pile lengths at the North and South ends of the break at the 17th Street Levee (report dated
December 5, 2005, Olson Job No. 1875). Actual sheet pile lengths were revealed to be about
23.5 ft in USACE excavations of sheet piles conducted on December 13, 2005 (the sheet piles
were incorrectly predicted to be about 7 ft shorter in our initial report).

Discussion of Initial Sheet Pile Depth Predictions

      When we learned that the USACE removal of sheet piles at the North and South ends of
the 17th Street Levee breach for revealed actual total sheet pile lengths of about 23.5 ft, we
immediately reviewed the PS data for ground-truthing purposes to examine the data and see if
there was an indication of the actual sheet pile tips in the data or not. Our review of the data
found that there was evidence of possible weaker diffraction events in the bottom 3 ft or so of the
initial PS data that corresponded to the actual sheet pile tip depths.

      As discussed in our draft report addendum letter of December 13th, 2005 which was

transmitted to the USACE at that time, we attribute our mis-interpretation of the data to the following three factors:

1. the PS data sets contained misleading apparent ground/tube vibrations that showed apparent slower velocity and weaker signals at the incorrectly predicted 7ft short sheet pile depths. This energy is now attributed to strong energy emitting from the concrete walls in to the ground due to the horizontal impacts to the concrete walls just below the chamfers;

2. the different shape of the now apparent sheet pile diffraction events due to the spreading out of energy for the wall-shaped steel sheet piles versus our experience with previous arrowhead diffraction events measured for rod-shaped steel H-piles in research and consulting by our firm; and,

3. the single biggest problem that led to the misinterpretation of the initial data was the lack of data available to clearly identify the weak diffraction of wave energy emitting from the pile tips. This was due to the fact that the borehole casings only extended a few feet beyond the actual pile tip depths. The desired typical cased borehole depth would extend 10-15 ft beyond the suspected/hoped for maximum sheet pile depths and this was recommended in our proposal of October 22, 2005 (Olson Proposal No. 2005169.1) for the project.

Borings were also recommended to be drilled as close as practical to the foundation to be tested preferably within 3-5 ft or less horizontally of the foundation, but generally no more than 10 ft away from a foundation to be tested with the PS method. We understand that the USACE borings were initially drilled in to the levees for geotechnical sampling purposes only and that PS testing was decided upon after the borings were drilled. The 4 inch diameter PVC casings that were subsequently grouted in-place in the boreholes for the PS tests were shorter than the drilled boreholes and extended only to depths of 25 ft below the levee ground surface. Such borehole casing depths would have been deep enough for successful PS tests if the sheet piles were around 16 ft in length, but the 25 ft long casings resulted in there only being about 3 feet of casing at or below the 23.5 ft long sheet pile tips. Thus there were only 3-4 PS test records from which hydrophone PS data could be obtained at or below the pile tips. As discussed above and in the report addendum, we feel that the limited PS data from below the sheet pile tips contributed significantly to our incorrect interpretation of the weak diffraction events.

A conference call about the PS results and our draft report addendum was held with Messrs. Richard Haskins and Paul Mlakar of the USACE and Larry Olson and Dennis Sack of Olson Engineering, Inc. on December 16th. As requested by Mr. Mlakar at that time, we have updated the draft addendum letter to include not only a review of the data from the PS tests at the 17th Street Levee, but also the PS data from the London Avenue and IHNC levees that was also presented in our initial report. The final report addendum is being provided as a separate letter.

Parallel Seismic Re-Test Field Investigation Overview

We were quite concerned about the initial incorrect sheet pile length predictions and this led to our decision to gather more data on the weak diffraction events that were apparently indicative of the actual sheet pile tips for the two USACE cased boreholes at the 17th Street Levee North and South breach ends. Consequently, we decided to conduct additional PS tests at the South End of the breach at Station 20+78 which was only about 7 ft from the USACE PS boring in this area. The testing was also at the South End of the 17th Street levee breach immediately adjacent to the area where the USACE excavated sheet piles and found their total lengths to be nominally 23.5 ft on December 13, 2005. We also conducted tests at the IHNC levee adjacent to the North end of the south breach at Station 17+11 within about 10 ft north of where a cased borehole PS test had been done earlier.

This additional nondestructive investigation was conducted at no cost by Olson Engineering to the USACE with the field support of Southern Earth Sciences, Inc. (SESI) of Baton Rouge, Louisiana who also provided their services at no cost. SESI had used their Seismic Cone Penetrometer (SCPT) Geoprobe rig with a biaxial geophone to investigate sheet pile tests in PS/SCPT tests of the 17th Street and London Avenue Levees for the state of Louisiana levee investigation team and their field tests were conducted after our initial field PS tests. A photograph of the Geoprobe rig is shown in Photo 1 and the SCPT tool is shown in Photo 2.

Photo 1 - Geoprobe Rig for PS/SCPT testing at South End of Breach of 17th Street Levee at Station 17+78 where sheet piles were exposed by USACE PS Cased Borehole (white PVC cap visible)

Photo 2 - Seismic Cone Penetrometer Tool with Bearing pressure at tip followed by pore pressure ring followed by skin friction sleeve followed by bi-axial horizontal geophones

The initial SESI PS/SCPT tests were able to be conducted to greater depths and much closer horizontally (typically within 3 ft of the concrete walls) without drilling borings. As discussed with USACE, we also provided consulting services to SESI in the analysis of their initial PS/SCPT results. Analyses of their initial bi-axial geophone results showed similar sheet pile depths to our initial hydrophone PS results with their findings presented in the SESI report to the State of Louisiana.

In our joint efforts with SESI at the IHNC and 17th Street Levees on December 21 and 22, 2005, respectively, SESI conducted PS/SCPT tests with their bi-axial (two perpendicular, horizontal geophones) seismic cone penetrometer tool (Photo 2). For our comparison PS testing with a small diameter hydrophone receiver, they pushed a non-retrievable dummy tip into the levee soils. Next, SESI installed a temporary 1 inch PVC casing inside the Geoprobe hollow steel push rods which were then retrieved to leave the PVC casing in the ground. Then the hole annulus and inside of the PVC casing were filled with water so we could conduct hydrophone-based Parallel Seismic (PS) tests.

The joint effort with SESI allowed for a comparison of the data obtained from the two different types of PS test transducers, ie., the more omni-directional hydrophone receiver vs. the bi-axial horizontal geophones. In our National Cooperative Highway Research Program 21-5 and 21-5(2) research projects for Determination of Unknown Bridge Foundation Depths for scour safety studies, we compared hydrophones and tri-axial geophones in Parallels Seismic tests. Generally, the hydrophone was found to be the more sensitive receiver to the arrival of initial weak direct energy in PS tests of bridge foundations, particularly for diffraction events due to its more all-around or "omni-directional" response to wave energy emitting from the impacted bridge substructure foundation system.

Parallel Seismic Re-Test Results

The joint Olson/SESI PS re-test program was planned to evaluate both bi-axial geophones (results to be reported by SESI) and hydrophone receivers and investigate PS data results quality for impacts applied directly to sheet piles, and from horizontal to vertical impacts to the concrete walls in which the levee sheet piles are embedded. The PS re-test results of the 17th Street re-tests are presented first below followed by the IHNC results. The field effort was also made possible by USACE personnel and their subcontractors who also contributed significantly to the re-test program and assisted in the field by providing site access, excavation assistance to expose sheet piles, and testing assistance. The State of Louisiana levee investigation team also contributed their input to the re-test program and observed the field PS re-test effort as well.

17th Street PS Re-Test Results at South End of Breach - Station 20+78

Based on the stickup of the sheet piles of about 1.25 ft above the levee ground surface, the 23.5 ft long sheet piles extend to about 22.25 ft below existing grade at the south end of the 17th Street levee breach at Station 20 +78 where the 1 inch PVC casing was installed to about 30

ft deep by SESI at about 2.5 ft from the wall edge on the protected side. The locations of the impacts with a 3-lb impulse hammer with a black hard plastic tip to the sheet pile and concrete levee wall at various positions are shown in Photos 3-7 and the PVC casing is shown in Photo 8.

Photo 3 (Fig. 1) - Horizontal impact to sheet pile at 0.5 ft below concrete wall - protected levee side

Photo 4 (Fig. 2) - Horizontal impact to side of concrete wall at el. 5 about 0.5 ft below chamfer

Photo 6 (Fig. 4) - Vertical downward impact to top of wall

Photo 5 (Fig. 3) - Angled downward impact to chamfer of wall at ~ el. 5.75

Photo 8 - 3-lb Impulse Hammer with black hard plastic tip and small diameter hydrophone used in PS re-tests

Photo 7 (Fig. 5) - Angled impact to 1 inch diameter, 6 ft long steel rod held at an angle on sheet pile side at 0.5 ft below concrete - protected levee side

The PS re-test results for the impact positions shown in Photos 3-7 are respectively presented in Figures 1-5 below. The expected diffraction event should occur at a depth of about 22.25 ft from the sheet pile tip in these hydrophone-based PS results. Review of the figures shows that the weak diffraction events are now clearly evident for all of the impact locations. This is due to the increase in PS test depth 30 ft for the 1 inch diameter casing installed by the geoprobe vs. the initial grouted casing depth of only 25 ft.

The PS data presented in Figures 1-5 were produced by 5 impacts which were averaged at each 1 ft test depth interval, filtered and normalized to the largest signal strength (global maximum display) to optimize the display of the diffraction events. Review of Figure 1 shows the diffraction event at 23.0 ft deep due to direct horizontal sheet pile impacts. There is also some energy occurring in advance of the diffraction event at shallower depths. In Figure 2 the horizontal impacts to the concrete wall also show a diffraction event at 22.7 ft deep, but a little less clear with more energy emitting from the concrete wall. By comparison, the diffraction event is clear at 21.8 ft deep for the angled downward impact to the chamfer in Figure 3. Apparently the more vertical impact to the chamfer put more energy down the sheet pile with less energy emitting from the wall. In Figure 4, the impacts to the top of the wall were further away from the ground and the sheet pile, so the diffraction event is quite clear at 21.5 ft. The impacts to the angled steel rod also produced a diffraction event at 22.6 ft as shown in Figure 5, but it was comparatively weaker, likelier due to less energy being imparted by the rod impacts.
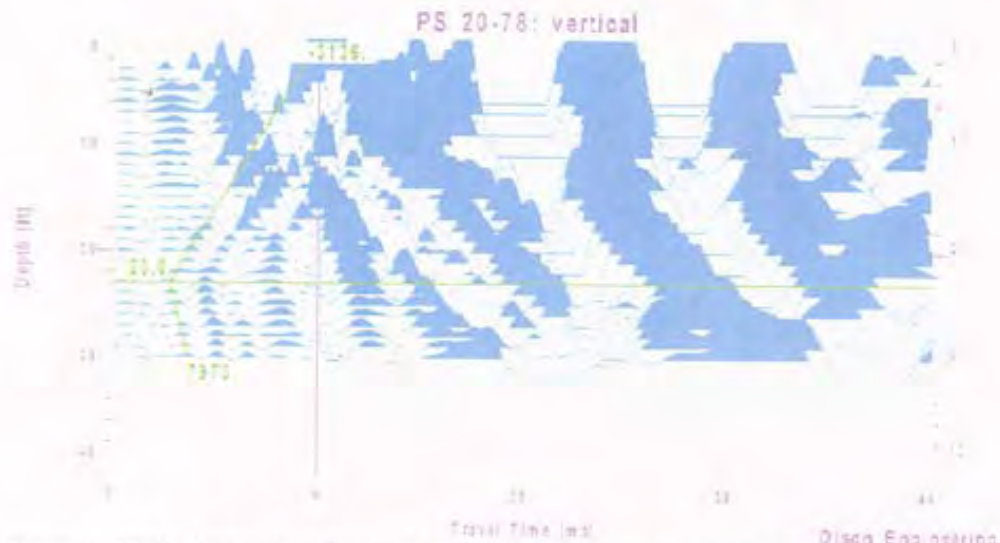
Figure 1 - 17th St. PS Results at Station 20+78 - Sheet Pile impacted at ~ el. 1.5 (0.5 ft below bottom of levee concrete wall on protected side)
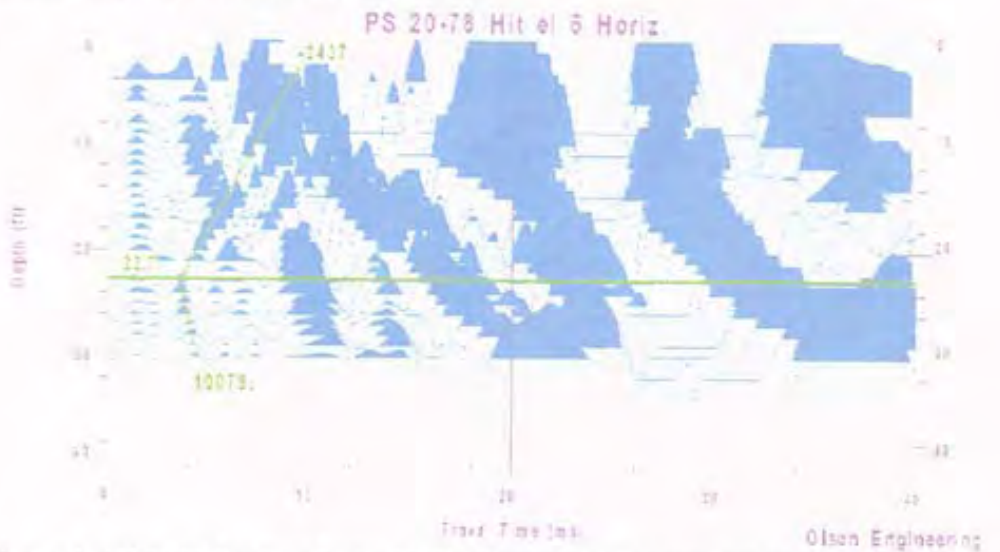
Figure 2 - 17th St. PS Results at Station 20+78 - Concrete Wall impacted horizontally at ~ el. 5 (~0.5 ft below chamfer edge on protected side)
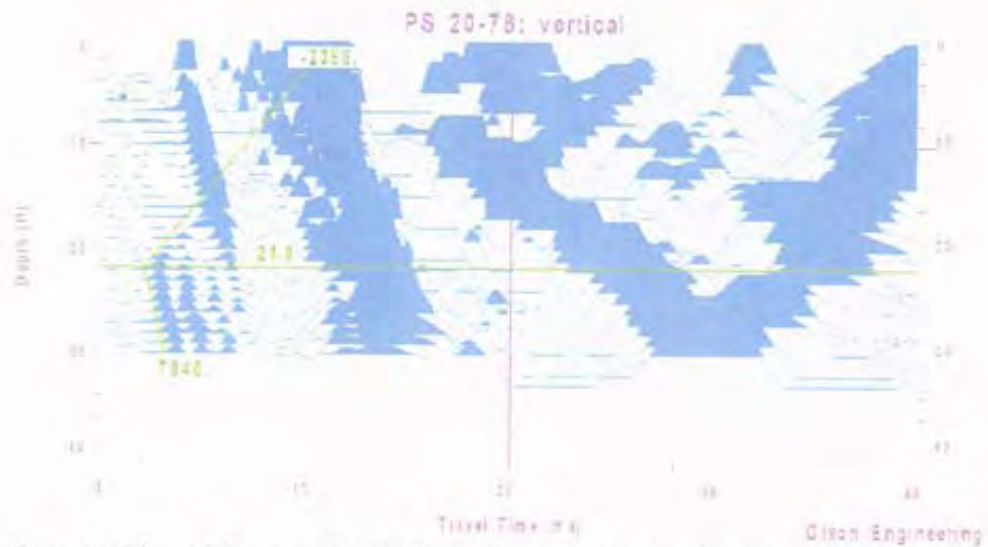
Figure 3 - 17th St. PS Results at Sta. 20+78 - Angled Impacts to Chamfer of Concrete Wall at Sta. 20+78 (~el. 5.75 on protected side)
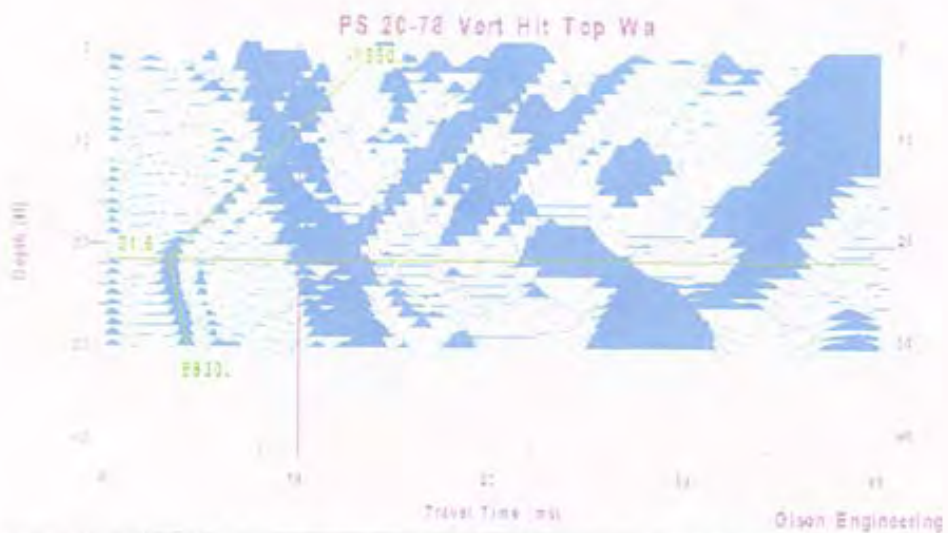
Figure 4 - 17th St. PS Results at Sta. 20+78 - Vertical Impacts to Top of Concrete Wall at Sta. 20+78

PS 20-78: vertical
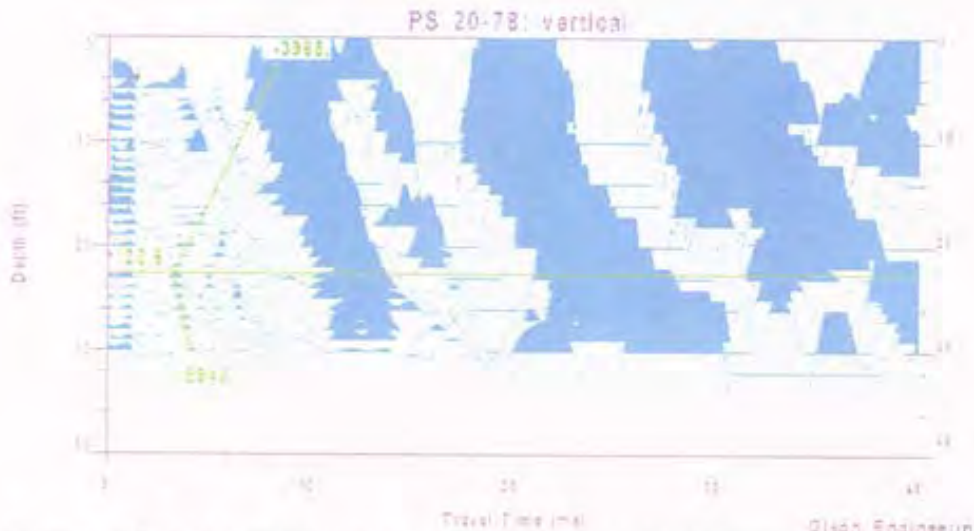
Figure 5 - 17th St. PS Results at Sta. 20+78 - Angled Impacts to 1 inch diameter, 6 ft long rod held against steel sheet pile at ~ el. 1.5 at 0.5 ft below concrete wall

IHNC PS Re-test Results at North End of South Breach - Station 17+11

The IHNC re-tests were performed in an area of the wall that had been pushed back and the levee soils dropped down to expose a sheet pile on the canal side at Station 17+11 which was about 10 ft north of the USACE cased boring in this area. Shovels were used to expose enough of the sheet pile to impact it with the 3 lb impulse hammer as shown in Photo 9. The PS tests were done using a hydrophone in the 1 inch PVC casing installed by SESI with the Geoprobe rig as shown in Photo 10.

Photo 9 - IHNC 3-lb Impulse hammer impacts to sheet pile on canal side at Station 17+11

Photo 10 - Small Hydrophone receiver on tape in 1 inch PVC casing installed by Geoprobe Rig at IHNC

Sonic Echo testing was conducted from end to end of a nearby exposed sheet pile and a compression wave velocity of about 17,000 ft/second was measured which is essentially the theoretical velocity of a steel rod of 16,600 ft/s. The Sonic Echo results did show a single clear echo from the pile tip in air, but not the multiple echoes normally measured on H-piles in air. Impulse Response analyses in the frequency did not show clear resonant echo peaks from the exposed pile tip. This is due to the spreading out of the energy in to the rest of the interlocked sheet pile wall and the lack of a resonant, rod-like shape for a sheet pile wall. When similar Sonic Echo/Impulse response tests were attempted from the exposed top of an embedded 23.5 ft long sheet pile at the South end of the 17th Street breach, no echo from the pile tip was apparent. This result was expected as the attenuation of the compression wave energy is high due to the large surface area of a steel sheet pile.

The exposed sheet pile at the north end of the south IHNC breach showed a total length of 19 ft - 6.5 inches. Of this, about 4 ft - 7 inches of the piles had been embedded in the 8 ft tall concrete wall. Thus, about 15 ft of the sheet piles are typically embedded in the levee soils. Given the 1 ft higher elevation of the top of the PVC casing on the levee soils versus the bottom of the concrete wall, the sheet pile tip is expected to be at a depth of about 16 ft in the PS hydrophone signal versus depth results which are presented below in Figures 6-8. Horizontal impacts were applied just below the concrete wall to the canal side of the exposed sheet pile (Fig. 6) and to the concrete wall at 6.5 ft below the top of the wall (Fig. 7) which was 1.5 ft above the bottom of the concrete wall while vertical impacts were applied to the top of the wall (Fig. 8).

Review of Figure 6 for the case of direct horizontal impacts to the sheet pile shows a weak direct arrival wave front that is slower below the 16 ft depth of the sheet pile. However, no diffraction events are evident in this PS-based hydrophone test data. This may be due to the evident separation of the levee soil from the canal side of the wall due to the wall being pushed back by the breach forces. This apparent lack of tight contact between the sheet pile and the levee soils may have resulted in the diffraction event energy not being well coupled into the surrounding saturated soils.

Review of Figures 7 and 8 for horizontal and vertical impacts to the concrete wall does not show clear direct arrivals when the apparent weak energy was picked as shown in the figures. No diffraction events are clearly evident in the figures either. These results further support the possibility that there is poor soil contact to the sheet pile on the canal side that dimished the diffraction effect in the IHNC re-tests.
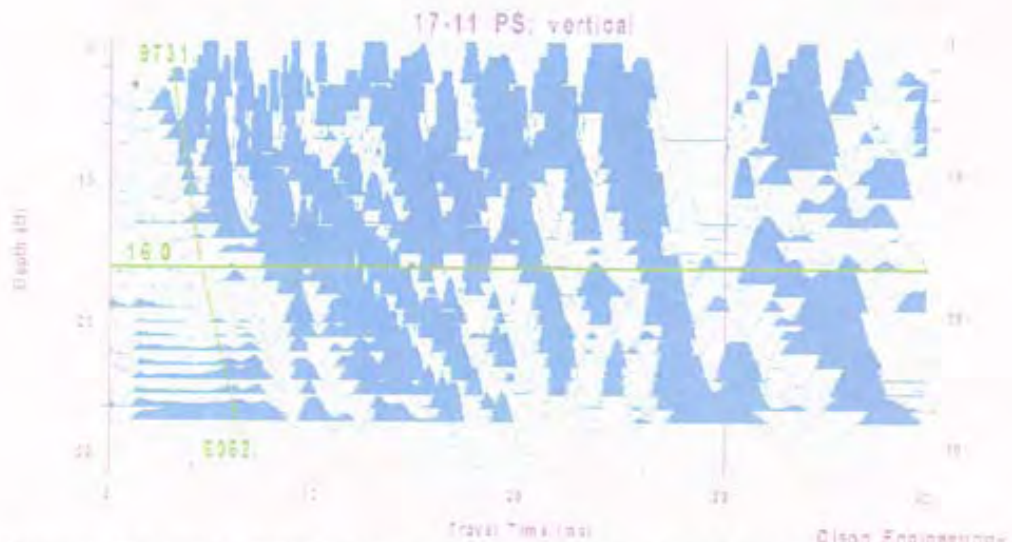
Figure 6 - PS Results at IHNC Sta. 17+11 - Impact to Sheet Pile at ~ 0.5 ft below bottom of Concrete Wall on Canal Side
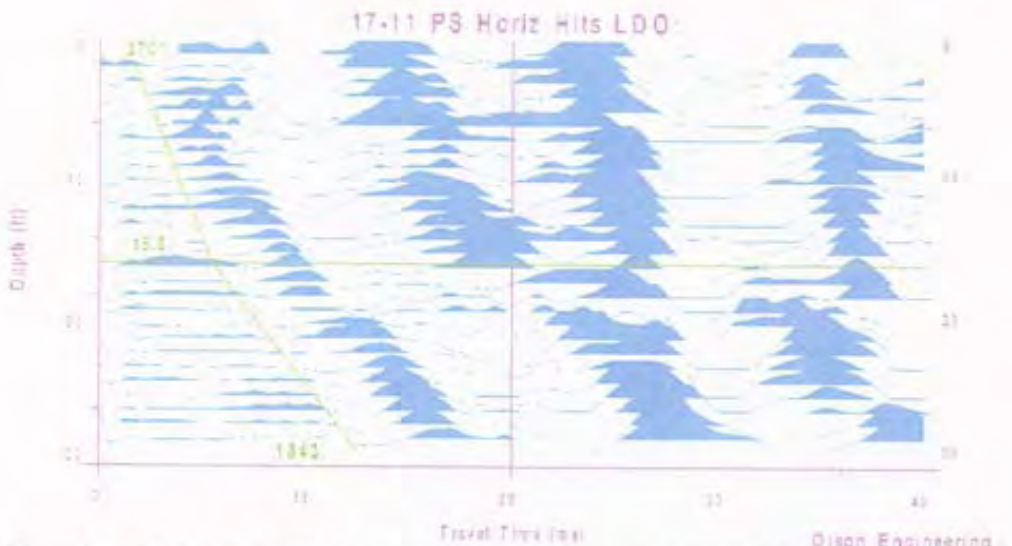
Figure 7 - PS Results at IHNC Sta. 17+11 - Horizontal Impact to Concrete Wall at ~ 6.5 ft below top of Wall on Canal Side
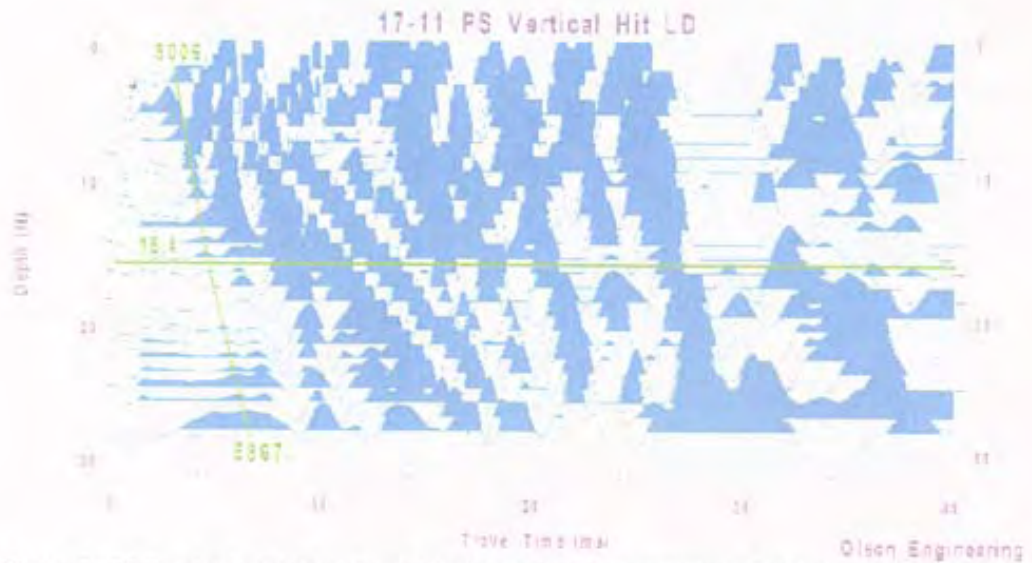
Figure 8 - PS Results for IHNC at Sta. 17+11 for Vertical Impacts to top of 8 ft tall Concrete Wall

Summary of Conclusions and Findings

17th Street Parallel Seismic (PS) Re-Test Results at Station 20+78. The hydrophone-based PS re-test results at the South End of the 17th Street breach clearly identified the pile tips within about 1 ft of the actual sheet pile depth of ~22.25 ft based on clear diffraction events at the sheet pile tip for impacts to the pile side, wall side, chamfer, wall top and even a rod held against the pile side. The results were clearest for the vertical hits on top of the wall, chamfer impacts and direct sheet pile impacts.

IHNC PS Re-Test Results at Station 17+11. The hydrophone-based PS re-test results at the North End of the south IHNC breach showed a weak direct arrival for impacts directly to the sheet pile that predicted the actual depth of 16 ft. However, only very tentative identifications of such direct arrivals were evident in PS results for either horizontal or vertical impacts to the levee concrete wall. None of the PS results at IHNC showed the clear diffraction arrival events at the pile tip depth found in all of the 17th Street PS re-test results. The lack of the diffraction arrival events may be due to the apparent lack of tight soil contact between the IHNC wall on the canal side as a result of the breach force pushing the wall back. Clear separation of the soil and wall was still evident at the surface in this area. Such lack of contact may have diminished the coupling of energy in to the soils from the diffraction event at the pile tip.

CLOSURE
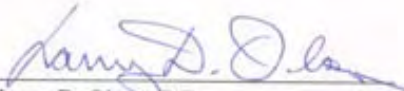
The field NDT investigation was performed in accordance with generally accepted testing procedures. If there are any questions, or further information is required, please do not hesitate to call. If any additional information is developed pertinent to this study, please contact our office.

Respectfully submitted,

OLSON ENGINEERING, INC.

Dennis A. Sack
Associate Engineer

Larry D. Olson, P.E.
Principal Engineer

(1 copy e-mailed and 2 copies mailed)

e-mail cc: Mr. Paul F. Mlakar (Paul.F.Mlakar@erdc.usace.army.mil)

V-15-52

Volume V The Performance – Levees and Floodwalls – Technical Appendix
This is a preliminary report subject to revision; it does not contain final conclusions of the United States Army Corps of Engineers.

NONDESTRUCTIVE TESTING INVESTIGATION
SHEET PILE FOUNDATION LENGTHS
NEW ORLEANS LEVEES
NEW ORLEANS, LOUISIANA

Prepared for:

U. S. Army Corp of Engineers
Engineering Research and Development Center
3909 Halls Ferry Rd.
Vicksburg, MS. 39180

Attn: Mr. Richard W. Haskins, ERDC-ITL-MS
Ofc: (601)634-2931
Fax: (601)634-2873
E-Mail: Richard.W.Haskins@erdc.usace.army.mil

Olson Engineering Job No. 1875

December 5, 2005

TABLE OF CONTENTS

This is a preliminary report subject to revision; it does not contain final conclusions of the United States Army Corps of Engineers.

1.0 INVESTIGATION SCOPE AND SUMMARY OF FINDINGS

This report presents the Nondestructive Testing (NDT) investigation results for the determination of the unknown lengths of sheet piles below concrete walls of the New Orleans levee system. The levee sheet piles were tested with the Parallel Seismic (PS) method to determine their depths. The PS tests were conducted at the 17th Street, London Avenue, and the Inner Harbor Navigational Canal (IHNC) levees in 8 cased borehole locations at undamaged levee wall locations next to breaches.

The PS results indicate the presence of piles under the concrete wall, and showed that they extended to approximately 13-15 ft below the casing top for all of the sites tested as summarized in Table I. These sheet pile depths translate to elevations of approximately 10 feet below mean sea level (range of 9.3 to 11.8 feet below mean sea level). A discussion of the PS method and the investigation results are presented below.

2.0 PARALLEL SEISMIC METHOD

The Parallel Seismic (PS) method was used to estimate the depth of the foundations. The PS test equipment used in this investigation included a 3-lb instrumented impulse hammer, single hydrophone receiver, and a dynamic signal analyzer (Olson Instruments Freedom Data PC), as illustrated in Fig. 1. When the instrumented hammer directly impacted the supported concrete wall, it (or a nearby accelerometer) triggered the PC- based signal analyzer to capture the time records. A 16-channel National Instruments digital card was used to acquire the data in an Olson Instruments portable Freedom Data PC. Photographs of the field testing are shown in Figure 2.

The PS method involves impacting the exposed portion of the foundation or substructure attached to the foundation or a location which when impacted couples sufficient energy to the pile to generate a sound or stress wave which travels down the foundation. The wave energy is tracked by a hydrophone receiver suspended in a water-filled, cased and sometimes grouted borehole drilled
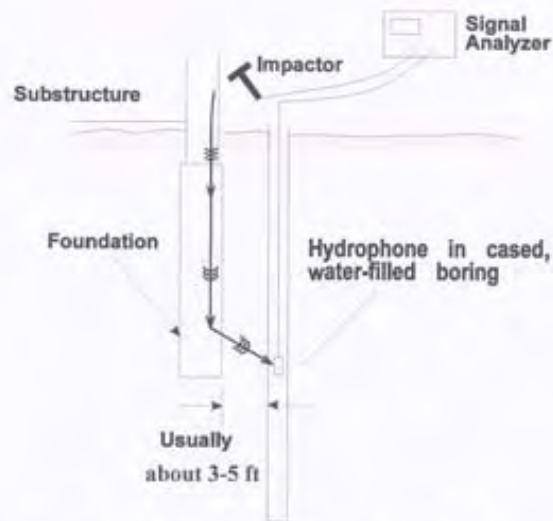
Foundation Depth Determination with the Parallel Seismic Test
Figure 1 - PS test schematic

Olson Job No. 1875   Page 2

typically within 3-5 feet of the foundation edge. Note that for this investigation, the boreholes were found to be located as far as 21.1 feet from the levee wall, resulting in poorer quality data for some tests. The PS tests typically involve lowering the hydrophone(s) to the bottom of the borehole, impacting the exposed portion of the foundation structure and recording the hydrophone(s) responses. Then the hydrophone receiver(s) is raised to the next test elevation. This test sequence is repeated until the top of the casing (or the top of the water level in the casing) is reached. The pile depth is determined by plotting the hydrophone(s) response from all depths on a single display or page. For soils of constant velocity surrounding the piles, a break in the slope of the line occurs below the bottom of the piles indicating the pile depth. For soils with varying velocities, a break often cannot be identified from the slope of the lines, but the bottom of the piles can be identified by observing the traces of the hydrophone plot to identify changes in the response, such as a reduction in signal amplitude, change in signal frequency, or diffraction/reflection of tube wave energy from the foundation bottom.

Figure 2 - Photographs of impacting Wall of IHNC Levee at South Borehole of South Breach and Freedom Data PC at Cased Borehole with Hydrophone Receiver Downhole

Olson Job No. 1875

Page 3

3.0 INVESTIGATION RESULTS AND SUMMARY

The investigation was performed on October 27, 2005 and October 28, 2005 using the Parallel Seismic (PS) method by Mr. Larry D. Olson and Ms. Hunter Yarbrough of Olson Engineering, Inc., with assistance from U. S. Army Corps of Engineers personnel Mr. Richard Haskins and Mr. Don Yule. The 3 levee locations tested were at the 17th Street, London Avenue, and Inner Harbor Navigational Channel (IHNC). The PS test site at each test area was designated by the breach location and the position of the borehole. Hammer impacting was done horizontally on the levee wall face and vertically on the wall top where possible. The Parallel Seismic tests were performed with 5 impacts (horizontal and/or vertical) to the concrete walls at each of the hydrophone receiver depth intervals of nominally 1 ft for the entire water-filled length of the boreholes, starting typically 25 ft below the top of the borehole and continuing up to the top of the borehole casing at each site.

The Parallel Seismic tests were performed using a 3-lb hard-plastic tipped instrumented impulse hammer as a source and a single Olson Instruments hydrophone as a receiver. The pile locations were chosen to obtain a length measurement at the locations adjacent to levee breaks which occurred following Hurricane Katrina. Note that the reported data in Appendix A are pile tip depths measured from top of casing and that the PS predicted pile tip depths in true elevation as well as from the bottom wall chamfer can be found in Table I. Review of this table indicates sheet pile depths of 13-15 ft below the tops of the cased boreholes which corresponds to about 10 ft below mean sea level. Given the 1 ft hydrophone receiver measurement depth intervals, the PS results are believed to be accurate to within about 1 ft of the reported depths where data quality is high.

The Parallel Seismic data and results for the 17th Street Site can be found in Figures A-1 and A-2 in the Appendix. The Parallel Seismic data and results for the London Avenue Sites can be found in Figures A-3 to A-5, where Figures A-3 and A-4 are from the North breach and Figure A-5 is from the South breach. The Parallel Seismic data and results for the IHNC can be found in Figures A-6 to A-8, where Figure A-6 is from the breach near Florida Street and Figures A-7 and A-8 are

Olson Job No. 1875

Page 4

V-15-58

Volume V The Performance – Levees and Floodwalls – Technical Appendix
This is a preliminary report subject to revision; it does not contain final conclusions of the United States Army Corps of Engineers.

from the South breach. The exposed parts of all locations consisted of concrete retaining walls which had embedded sheet piles underneath. For the eight tested sites, PS tests were performed to a depth of 25 feet below the top of the grouted, 5 inch PVC casings which were filled with water.

The PS results presented in Appendix A are from typically horizontal hammer hits (data quality was better in one location using a vertical hammer hit as presented in Figure A-3). The horizontal hammer hits were located on the thicker wall sections just below the bottommost chamfer corner and the vertical hammer hits were located on top of the approximately 7 foot concrete retaining wall. The vertical axis in Figures A-1 and A-2 represents depth below casing top, with each waveform at 1 feet intervals starting at 25 feet at the bottom of each casing. The horizontal axis represents acoustic wave travel time in milliseconds (ms).

The generally faster compressional wave velocities of the sheet piles are represented by the shallow, usually more negatively sloped data in the figures at depths near the apparent pile tips. The more gentle, usually less negatively sloped data of the first breaks of the deeper traces represent the slower soil velocities below the pile tips. This is not the case in several of the data sets due to higher soil layer velocities at depth, likely associated with the presence of ground water which results in velocities of about 5,000 ft/second. Where the boreholes could be drilled less than ten feet away from the wall/pile (preferred), such saturated faster soil layers did not have as significant of an impact on data quality.
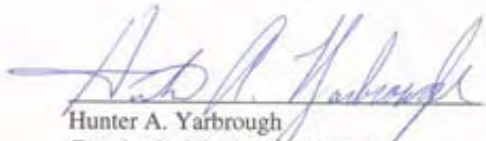
The PS measured pile tip depths for the eight locations indicate that there are piles present underneath the concrete retaining walls. Some of the results are of lower quality data due to a significant distance (17 to 22 ft) between the wall impact points to the boreholes as indicated in Table I. This is evidenced by the relatively weak signals from the piles compared to the signals from the impacted concrete walls on top of the piles, and from the relatively great depth at which the high-velocity pile signals finally start to arrive sooner than the low velocity signals being carried down the water-filled boreholes (tube waves). Accordingly, data quality was rated as high, medium and low (H, M and L) in Table I based on the distance between the wall-borehole and the signal quality.

Olson Job No. 1875

Page 5

4.0 CLOSURE

The field NDT investigation was performed in accordance with generally accepted testing procedures. If there are any questions, or further information is required, please do not hesitate to call. If any additional information is developed pertinent to this study, please contact our office.

Respectfully submitted,

OLSON ENGINEERING, INC.

Hunter A. Yarbrough
Geophysical Project Engineer

Larry D. Olson, P.E.
Principal Engineer

(1 copy faxed and 2 copies mailed)

Olson Job No. 1875

Page 6

V-15-60

Volume V The Performance – Levees and Floodwalls – Technical Appendix
This is a preliminary report subject to revision; it does not contain final conclusions of the United States Army Corps of Engineers.

Table I: Summary of Sheet Pile Tip Depths and Elevations From Parallel Seismic Testing of New Orleans Levees

Levee Site	Sheet Pile Tip Depth From Top of Casing (ft) – (Data Quality)	Sheet Pile Tip Depth From Bottom Concrete Wall Chamfer (ft)	Sheet Pile Tip Elevation (ft above sea level)*	Distance Between Borehole and Levee Wall
17th Street North End	14.4 - H	15.5	-10.6	5.5 ft
17th Street South End	14.0 - H	15.0	-9.3	6.2 ft
London Avenue North Break North End	14.6 - L	16.1	-11.2	17.8 ft
London Avenue North Break South End	13.1 - M	14.9	-9.7	7 ft
London Avenue South Break	14.3 - M	15.3	-10.6	17.2 ft
IHNC Florida Street Break	14.8 - M	16.5	-10.3	21 ft
IHNC South Break North End	13.7 – H	16.6	-10.4	9.5 ft
IHNC South Break South End	14.4 – M	16.1	-11.8	21.1 ft

H – Indicates areas where the data quality is high and the borehole is positioned within 10 feet of the sheet pile.
M – Indicates areas where the data quality is medium and/or the borehole is positioned greater than 10 feet away from the sheet pile.
L – Indicates areas where the data quality is low and/or the bore hole is positioned greater than 10 feet away from the sheet pile.

* The elevations of the borehole casing tops were provided by the US Army Corps of Engineers and are NAVD 88 Format.

**APPENDIX A
PS DATA AND RESULTS**
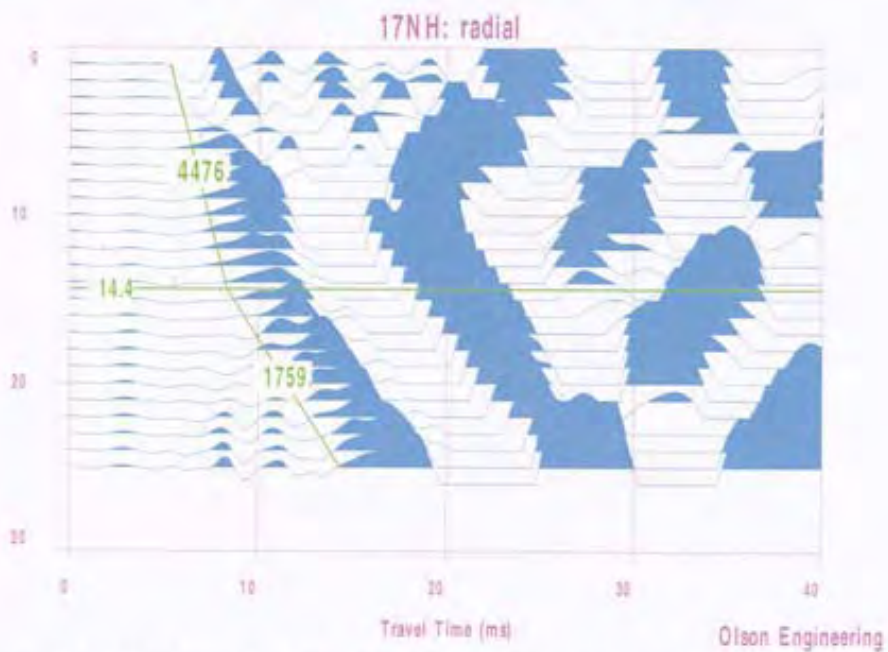
Figure A-1: 17th Street site, North borehole, depth is referenced to top of casing
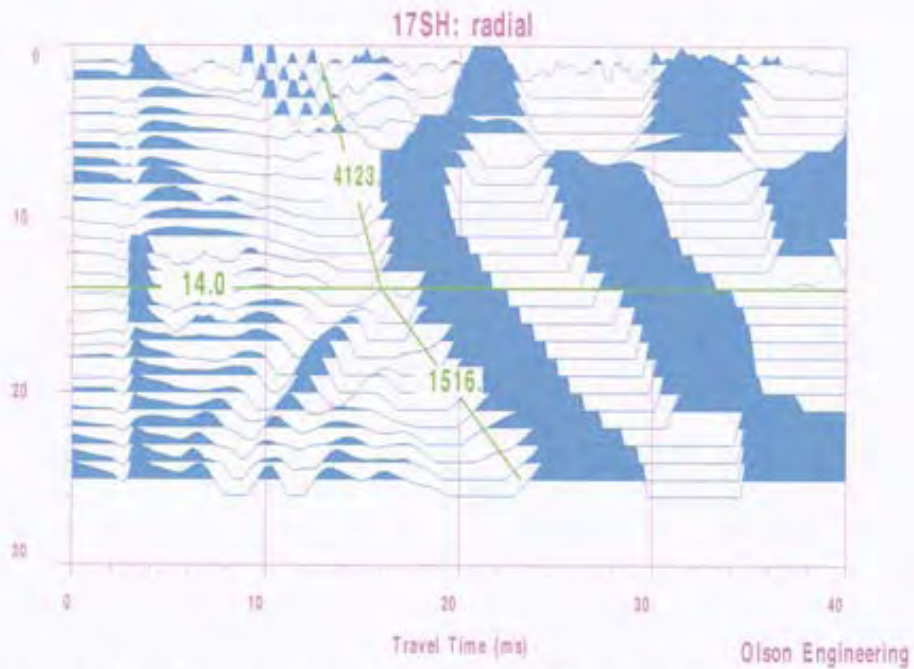
Figure A-2: 17th Street Site, South borehole, depth is referenced to top of casing
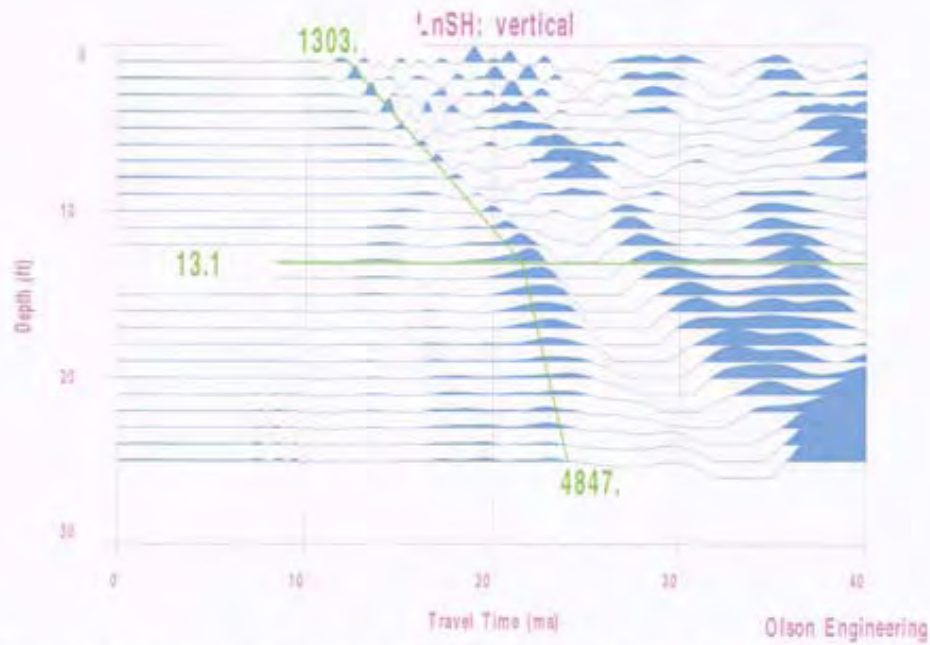
Figure A-3: London Avenue North site, North borehole, depth is referenced to top of casing
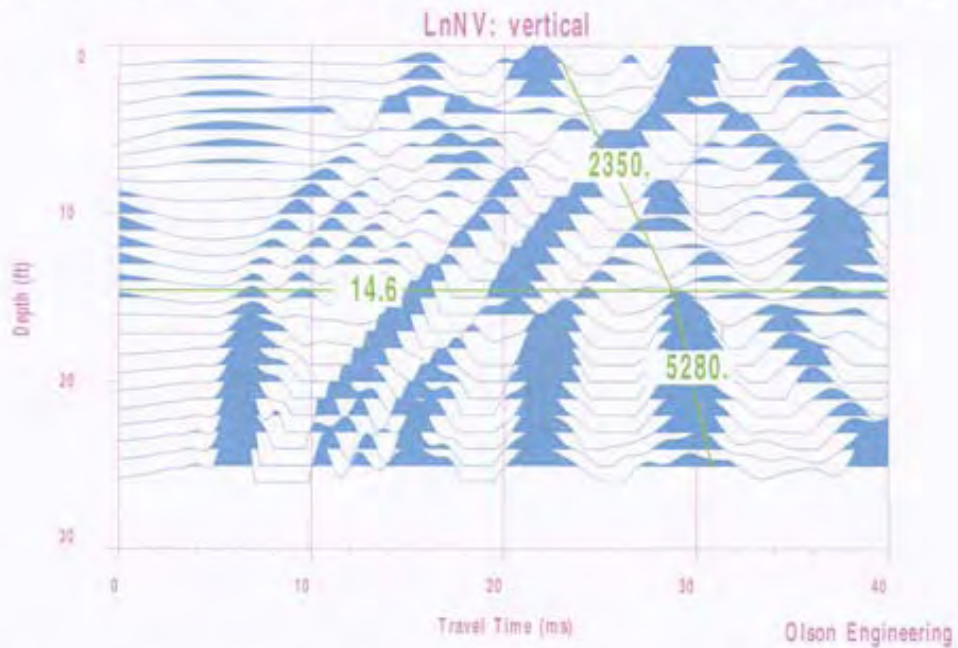
Figure A-4: London Avenue North site, South borehole, depth is referenced to top of casing
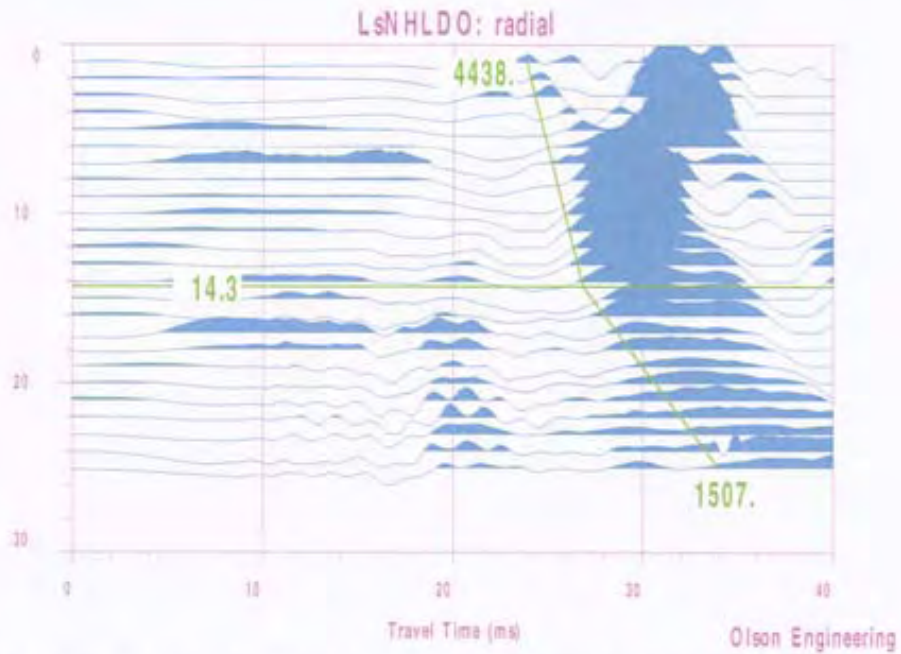
Figure A-5: London Avenue South site, North borehole, depth is referenced to top of casing
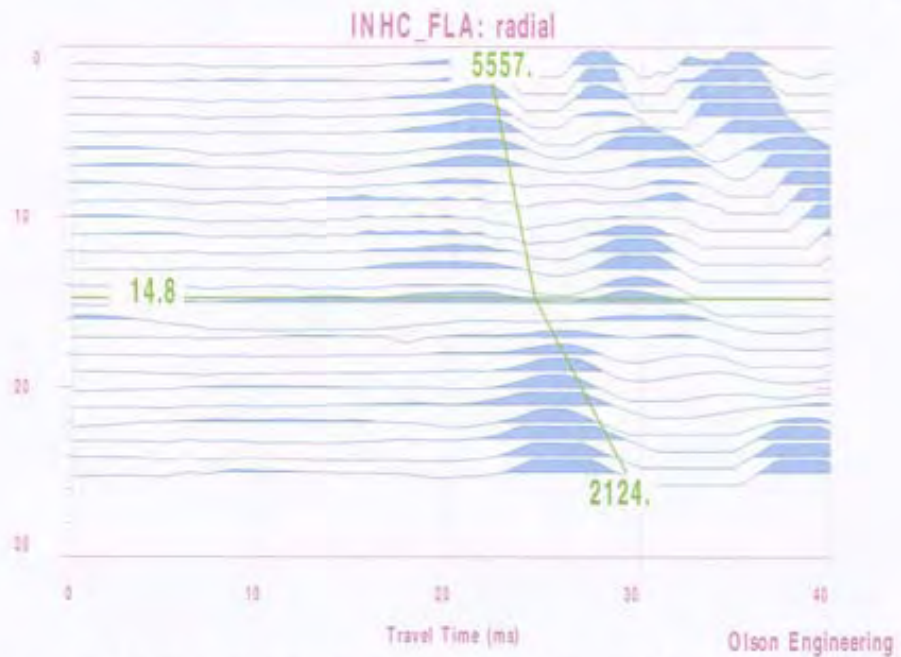
Figure A-6: IHNC Florida Street site, depth is referenced to top of casing

Volume V The Performance – Levees and Floodwalls – Technical Appendix

V-15-65

This is a preliminary report subject to revision; it does not contain final conclusions of the United States Army Corps of Engineers.
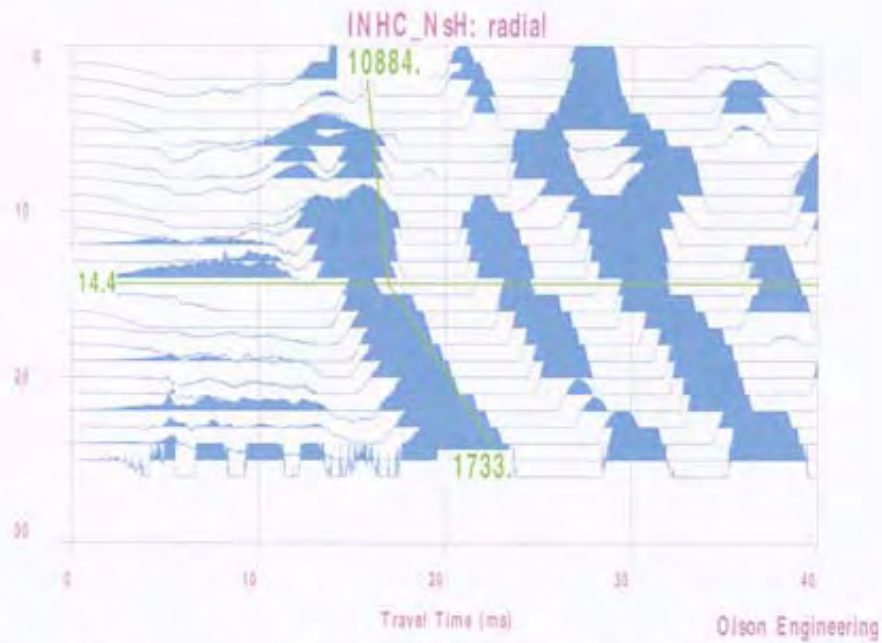
Figure A-7: IHNC South site, North borehole, depth is referenced to top of casing
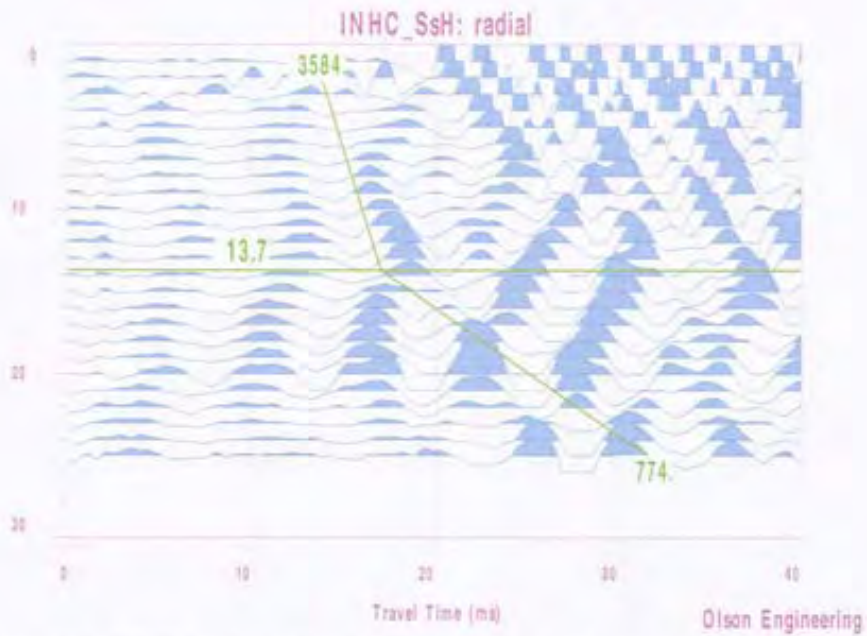
Figure A-8: IHNC South site, South borehole, depth is referenced to top of casing

OLSON
ENGINEERING, Inc.

January 9, 2006

U. S. Army Corp of Engineers
Engineering Research and Development Center
3909 Halls Ferry Rd.
Vicksburg, MS. 39180
Attn: Mr. Richard W. Haskins, ERDC-ITL-MS
Ofc: (601)634-2931
Fax: (601)634-2873
E-Mail: Richard.W.Haskins@erdc.usace.army.mil

Re: Addendum to Nondestructive Testing Investigation Report
      Sheet Pile Lengths
      New Orleans Levees
      New Orleans, LA
      Olson Engineering Job No. 1875

Dear Sirs:

This letter is being sent as an addendum to a report issued to the USACE by our office on December 5, 2005 (Olson Job No. 1875) which reported the results of an investigation conducted by our firm into the determination of the unknown length of steel sheet piles which were located beneath concrete walls and formed part of the levee structure at a number of locations in the New Orleans area. The levee sheet piles were tested with the Parallel Seismic (PS) method to determine their depths. The PS tests were conducted at the 17th Street, London Avenue, and the Inner Harbor Navigational Canal (IHNC) levees in 8 cased borehole locations at undamaged levee wall locations next to breaches.

The initially reported PS test results indicated the presence of piles under the concrete wall, and were interpreted by our firm to show that they extended to approximately 13-15 ft below the casing top for all of the sites tested. These sheet pile depths translated to elevations of approximately 10 feet below mean sea level (range of 9.3 to 11.8 feet below mean sea level).

It is our understanding that four sheet piles at the north end and 4 sheet piles at the south end of the 17th Street levee breach area have been pulled, and that the our data interpretation of nearby PS results in north and south cased borings was shown to be incorrect. The actual embedded lengths were found to be approximately 17 feet below mean sea level (20-22 feet below the casing top elevation used in our investigation) with total sheet pile lengths of 23.5 ft.

Olson Job No. 1875 Addendum   Page 1

12401 W. 49th Ave., Wheat Ridge, CO 80033-1927 USA
PHONE: 303.423.1212   FAX: 303.423.6071
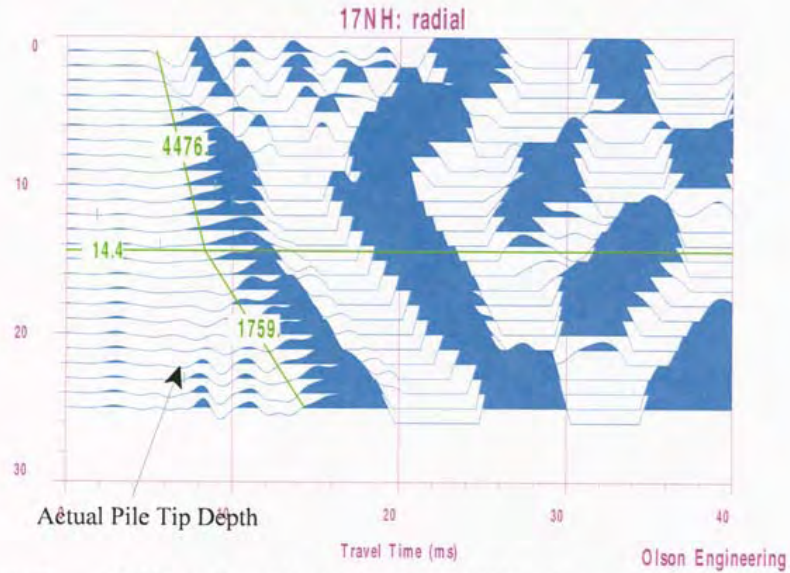
Figure 1 17th Street Levee North Site, Initial PS Data Interpretation
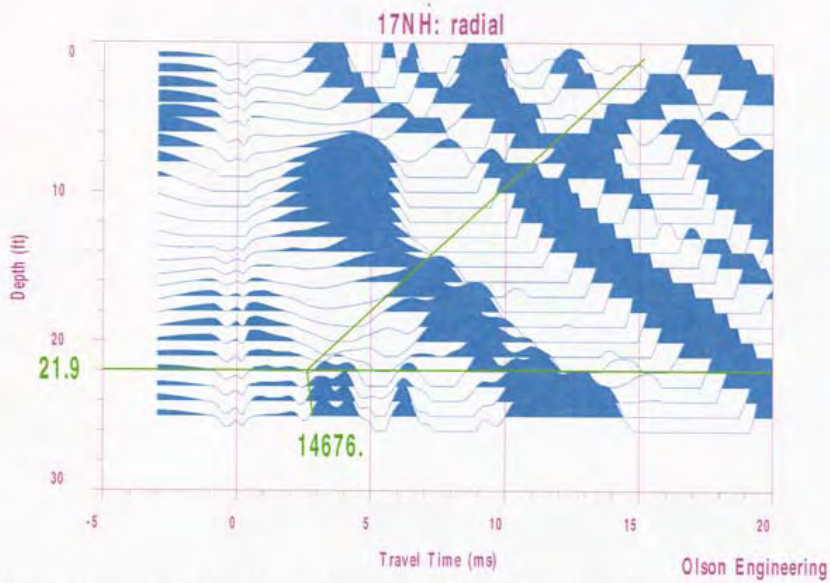
Figure 2 17th Street Levee North Site, Re-interpretation of PS Results

Olson Job No. 1875 Addendum

Page 3

V-15-68

Volume V The Performance – Levees and Floodwalls – Technical Appendix

This is a preliminary report subject to revision; it does not contain final conclusions of the United States Army Corps of Engineers.
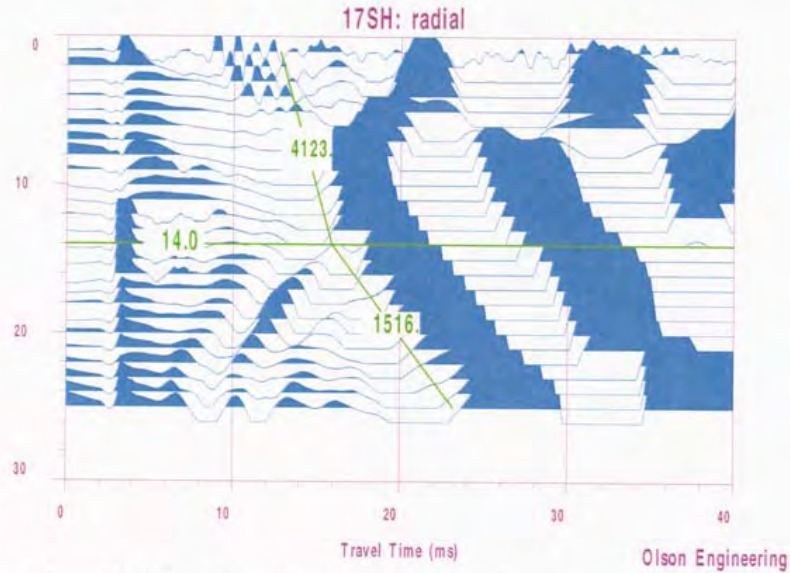
Figure 3   17th Street Levee South Site, Initial PS Data Interpretation
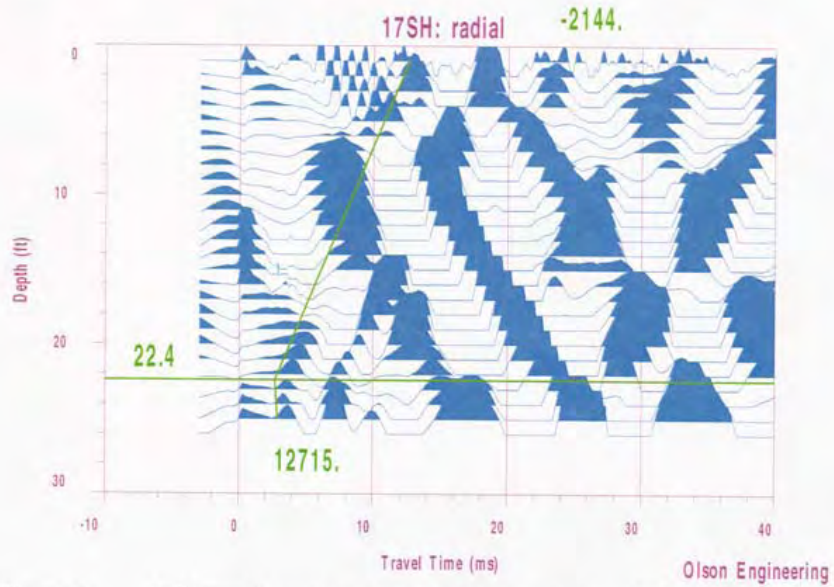
Figure 4   17th Street Levee South Site, Re-interpretation of PS Results

Olson Job No. 1875 Addendum

Page 4

Volume V The Performance – Levees and Floodwalls – Technical Appendix   V-15-69

This is a preliminary report subject to revision; it does not contain final conclusions of the United States Army Corps of Engineers.

London Avenue North Break Data Review

The data collected from the London Ave. North site was reexamined to look for tip diffraction events similar to those seen for the 17th Street site data sets. Close examination of the data sets (Figs. A-3 and A-4 in our original report on this testing) show that there is a clear but vertical diffraction event for data at the South borehole, which was located at about 7 feet from the levee wall. The diffraction event in this figure, however, appears as a near-vertical line, with no clear "break" in the slope which would be indicative of a tip depth. It would appear likely that a break would have been seen if the casing went down the recommended 10-15 feet deeper than the expected pile tip depth, since there is a small possible indication of a break visible in the very bottom data trace for this location (at about 24 feet below casing top).

The data set from the North borehole shows a very weak set of possible diffraction events, with a similar shape as the south borehole. The diffraction events in the data from this borehole, however, or very weak. This is presumably due to the almost 18 ft horizontal separation between the borehole and the levee wall at this site. This large separation would attenuate the high-frequency diffraction energy, as well as decrease the resolution of the data that is seen.

London Avenue South Break Data Review

The data set from the South Break site borehole (Fig. A-5 in our original report) shows a very weak and distorted set of possible diffraction events, but with no clear slope change in the data indicative of a tip depth. Close examination of the data shows the first arrivals of the possible diffraction energy to be nearly vertical versus depth down to the last recorded record. Again, this is likely due to the limited depth of the casing in the borehole, which limited the test range to just a few feet deeper than the pile tip. In addition, this borehole was located 17.2 feet from the levee wall, which results in attenuated, distorted, low resolution diffraction energy from the pile tip.

IHNC Florida Street Break Data Review

The data set from the IHNC Florida Street Break site borehole (Fig. A-6 in our original report) shows no indication of tip diffraction energy. Note that this borehole was located about 21 feet from the levee wall, which is a distance greater than the expected pile tip depth. This large separation would be expected to greatly distort and attenuate any energy radiating from the pile tip. Thus, it is not unexpected that there is no visible tip diffraction energy in this data set.

IHNC South Break Data Review

The data set from the two tests conducted at the IHNC South Break site were presented in Figs. A-7 and A-8 in our original report. Figure A-7 is from the north borehole, which was located 9.5 feet from the levee wall. Figure A-8 is from the south borehole, which was located 21.1 feet from the levee wall. Examination of both data sets shows no clear indication of diffraction energy from the pile tip. This may be due to the distances between the boreholes and the wall, as well as possible separation between the sheet piles and the soil in the areas near the break.

Olson Job No. 1875 Addendum

Page 5

V-15-70

Volume V The Performance – Levees and Floodwalls – Technical Appendix
This is a preliminary report subject to revision; it does not contain final conclusions of the United States Army Corps of Engineers.

Recommendations for Future Nondestructive Testing of Sheet Pile Lengths

The data presented in our original report does show the energy emitted by the sheet pile tips for most of the tests done in boreholes close to the levee walls, and can be made even clearer by re-processing the data from the 17th Street site to emphasize the higher frequency energy from the sheet piles as presented in Figs. 2 and 4 above. Based on this knowledge of how the PS test data behaves when testing these types of sheet piles in this environment, we have prepared these recommendations for any future NDT investigations of sheet pile lengths.

1. Drill Cased Borings Closer to Walls and Deeper. In our opinion, the PS method can be effectively used to measure unknown sheet pile depths with good confidence, as long as the boreholes are located and at least within 7 feet or less of the edge of the levee wall. Even closer borings will further improve the accuracy of the PS results. The borings should also be drilled and cased with PVC casings to at least 10 and preferably 15 ft below the expected pile tip depths.

2. Impact Sheet Pile Sides Directly. The PS data quality would be further enhanced by impacting the sheet piles at their exposed top just below the concrete wall directly. This will input significantly more energy in to the sheet pile and less into the concrete wall that was impacted in the initial investigation. This could be done with shallow excavations with a small backhoe in advance of the NDT. Alternatively, we have found that vertical impacts on the wall top or on the chamfer produce clearer diffraction energy traces than do horizontal impacts as discussed in our Report No. 2 for the re-test results.

3. Confirmation with complimentary NDT Methods. Magnetic metal detectors for boreholes may also be able to detect the sheet pile presence if borings are cased with plastic and able to be drilled close enough for this approach to be effective. The practicality of this can be further explored, if desired. We have already gathered some information on available equipment.
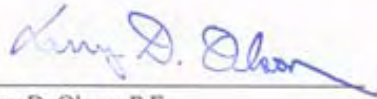
Olson Job No. 1875 Addendum

Page 6

CLOSURE

The field NDT investigation was performed in accordance with generally accepted testing procedures. If there are any questions, or further information is required, please do not hesitate to call. If any additional information is developed pertinent to this study, please contact our office.

Respectfully submitted,

OLSON ENGINEERING, INC.

_____
Dennis A. Sack
Associate Engineer

_____
Larry D. Olson, P.E.
Principal Engineer

(1 copy e-mailed and 2 copies mailed)

e-mail cc: Mr. Paul F. Mlakar (Paul.F.Mlakar@erdc.usace.army.mil)

Olson Job No. 1875 Addendum

Page 7

V-15-72

Volume V The Performance – Levees and Floodwalls – Technical Appendix
This is a preliminary report subject to revision; it does not contain final conclusions of the United States Army Corps of Engineers.

Appendix 16
Concrete I-Wall and Sheet Piling Material Recovery, Sampling and Testing: IHNC

Introduction

On Friday, 6 January 2006, samples of the concrete I-wall, reinforcing steel and sheet piling were taken from the I-wall on west bank of the Inner Harbor Navigation Canal. The location from which the materials were sampled was the west side of France Rd. near France Road Parkway. The primary objective of this exercise was to determine material properties of the I-wall concrete and reinforcing steel, and the sheet piling.

Material Sampling

An approximately eight foot long by 44 inch high section was sawcut from the top of the concrete I-wall as shown if Figure 16-1. The sample was taken from a location at approximately Station 0+44 and was labeled IPET-WE-EW 0+44.

Figure 16-1. Sawcutting Concrete Wall Sample

This sample was transported to the warehouse at the New Orleans District office. On 11 January, three six inch diameter concrete cores were taken from the wall sample by Beta Testing & Inspection for compressive testing.

An 8 by 24 inch sample was taken from the web each of two sheet piling at the site. (See Figures 16-2 and 16-3.) The pilings were labeled IHNC-SP-WS-B1 and IHNC-SP-WS-B2 and the corresponding samples were labeled IHNC-WS-B1A and IHNC-WS-B2A. The samples were provided to Beta Testing & Inspection for testing. The sheet piling was transported to the warehouse at the New Orleans District office.

Figure 16-2. Flame Cutting of Material Samples from Piling IHNC-SP-WS-B2

Figure 16-3. Flame Cutting Material Samples from Sheet Piling IHNC-SP-WS-B1

Four samples of reinforcing steel recovered from the I-wall at approximately Station 2+00 were also provided to Beta Testing and Inspection for testing. The samples were two pieces each of #4 and #6 rebar and were labeled IHNC WEST 4A, IHNC WEST 4B, IHNC WEST 6A and IHNC WEST 6B.

Test Results

Complete test results are detailed in the report by Beta Testing and Inspection included in Attachment A. The test data are summarized in Tables 16-1, 16-2, and 16-3. Material specifications for IHNC West I-wall system were not found despite extensive effort to locate them.

Table 16-1	
Concrete Compressive Strength	
Core Sample	**Compressive Strength (psi)**
IPET-WS-EW-1	5220
IPET-WS-EW-2	5850
IPET-WS-EW-3	6650

Table 16-2			
Sheet Piling Tensile Properties			
Sample	**Yield Strength (ksi)**	**Tensile Strength (ksi)**	**Elongation in 8 in. (%)**
IHNC-SP-WS-B1A	51.95	81.84	16.25
IHNC-SP-WS-B2A	61.10	89.94	15.83

The samples of the #6 rebars evidently contained small welds that were not observed during sampling. Consequently, the samples provided spurious test results and are not included here but are included in the report by Beta Testing & Inspection in Attachment A.

Sample	Bar Size	Yield Strength (ksi)	Tensile Strength (ksi)	Elongation in 8 in. (%)
IHNC-WEST-4A	4	51.00	81.00	14.12
IHNC-WEST-4B	4	48.50	79.00	14.12

Attachment A
Test Report from Beta Test & Inspection, LLC

Beta Testing & Inspection, LLC
Forensic Engineering Division

March 9, 2006

Paul F. Mlakar, Ph.D., P.E.

US Army Corps of Engineers
Engineer Research and Development Center
3909 Halls Ferry Road
Vicksburg, MS 39180

RE: **Testing of IHNC West Side South of France Rd.**
Ramp to 700' North of Benefit Street Gate
Final Report
BTI Report No.: 1054-ES010606

Dear Mr. Mlaker:

On January 6, 2006 at the referenced site, sheet pile samples and steel reinforcing bars were sampled. On January 11, 2006 concrete specimens were sampled at the US Army Corps of Engineers New Orleans District warehouse. BTI cut a total of three concrete cores from a wall section identified as IPET-WS-EW 0+44 Flood Side. Mark Cheek, P.E. of BTI witnessed the removal of 8"x 24" section from two different sheet piles and assumed responsible possession of the sheet pile samples and four reinforcing bars; two No.4 and two No.6. Representatives of BTI were informed by the Corps of Engineers that the material samples provided to BTI or obtained by BTI were portions of existing components taken from the IHNC West Side South of France Road Ramp to 700' North of Benefit Street Gate. All specimens were labeled, tagged, and secured prior to transporting. Samples were transported to Beta Testing & Inspection, LLC (BTI) laboratory for testing. Project Material data sheets and project specifications for the sampled materials were not provided. BTI has completed testing of concrete cores, steel sheet pile sections, and steel reinforcing bars.

Concrete Cores

Three cores were cut from the Flood side of sample panel IPET-WS-EW-O+44 Flood Side. The cores were obtained in accordance with procedures defined by ASTM C-42. Prior to compression testing each core was prepared in accordance with ASTM C-42, C-617, and C-39. Each core was then tested in compression to failure and the results recorded in accordance with ASTM C-39. See Table C.1 for results of the concrete core testing.

P.O. Box 2203 · Gretna, LA 70054 · (504) 227-2273 · fax (504) 227-2274
13801 Old Gentilly Road Suite #17 New Orleans, Louisiana 70129

Table C.1

Sample panel MH38C1						
Core ID	Capped Length (in.)	Diameter (in)	Area (in^2)	l/d	Correction factor	Maximum load (lbs.)
IPET-WS-EW-1	9.9	5.62	24.8	1.76	0.98	132,000
	Compressive strength (psi)	Fracture type	Age (days)	Load application	Test date/time	Sample date/time
	5220	A	NA	vertical	1/12/06 11:00am	1/11/06 10:00am
Core ID	Capped Length (in.)	Diameter (in)	Area (in^2)	l/d	Correction factor	Maximum load (lbs.)
IPET-WS-EW-2	10.25	5.62	24.8	1.82	1.0	145,000
	Compressive strength (psi)	Fracture type	Age (days)	Load application	Test date/time	Sample date/time
	5850	B	NA	vertical	1/12/06 11:00am	1/11/06 11:00am
Core ID	Capped Length (in.)	Diameter (in)	Area (in^2)	l/d	Correction factor	Maximum load (lbs.)
IPET-WS-EW-3	9.69	5.62	24.8	1.72	0.97	170,000
	Compressive strength (psi)	Fracture type	Age (days)	Load application	Test date/time	Sample date/time
	6650	B	NA	vertical	1/12/06 11:00am	1/11/06 12:00am

Average compressive strength (psi)	5907

Steel Sheet Piling

A welder provided by Pittman Construction cut one 8"x 24" specimen from each of the two-sheet pile using an acetylene cutting torch. Mandina's Inspection a subcontractor of BTI then prepared and tested each specimen in tension to failure in accordance with ASTM A-370. For test results see table SP-1 and graph SP-1

Steel Reinforcing Bars

Four pieces of steel reinforcing bars were secured and transported to BTI's laboratory. The steel reinforcing bar samples ranged in size from No. 4 to No. 6 bars. Mandina's Inspection a subcontractor of BTI tested the rebar specimens to failure in accordance with ASTM A-615 & A370. For test results see table RB-1 and graph RB-1

Upon completion and acceptance of the testing program, all of the materials, tested and untested, will be sealed and returned to the New Orleans District Office of the US Army Corps of Engineers. Enclosed are copies of our laboratory accreditations and equipment calibration reports associated with the test performed. Should you have any questions regarding this letter or require additional information, please do not hesitate to contact us.

Sincerely,

Beta Testing & Inspection, LLC

Mark A. Cheek, P.E.
Vice-President

Enclosures

Table SP-1

MECHANICAL TESTING LABORATORY DIVISION

Mardina's
Disp: 2-24-06
4405.90

MTL JOB NO. _____

TENSILE NO. _____
BTI #1054

SPECIMEN ID	WIDTH INCHES	THICKNESS SQ. IN.	AREA SQ. IN.	YIELD STR. POUNDS	YIELD STR. PSI	TENSILE STR. POUNDS	TENSILE STR. PSI	ELONGATION IN 2" GAGE PERCENT
HNC-SP-WS-B1-A	1.441	.356	.512	26600	51953	41900	81835	9.300 16.25%

TENSILE NO. _____
BTI #1054

SPECIMEN ID	WIDTH INCHES	THICKNESS SQ. IN.	AREA SQ. IN.	YIELD STR. POUNDS	YIELD STR. PSI	TENSILE STR. POUNDS	TENSILE STR. PSI	ELONGATION IN 2" GAGE PERCENT
HNC-SP-WS-B2-A	1.487	.355	.527	32200	61100	47400	89943	9.267 15.83%

G:\WORDDATA\ISIFORMS\TTFY.LAB

Volume V The Performance – Levees and Floodwalls – Technical Appendix

V-16-11

This is a preliminary report subject to revision; it does not contain final conclusions of the United States Army Corps of Engineers.
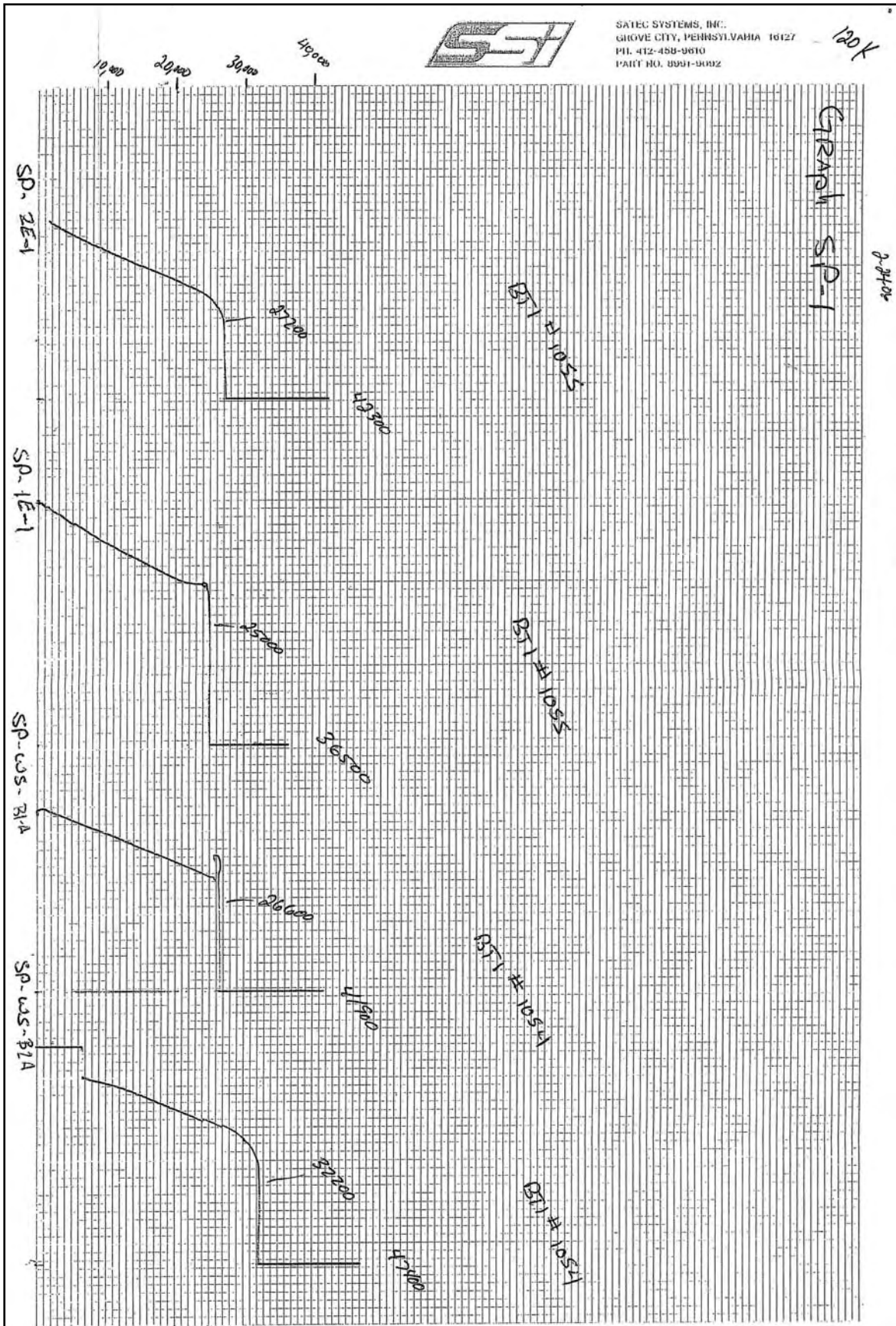
Table RB-1.

MECHANICAL TESTING LABORATORY DIVISION

2-24-06

MTL JOB NO. Mandinas ISP 4406.90

TENSILE NO. _____
BTI # 1054

8" Gage

SPECIMEN ID	DIA. INCHES	AREA SQ. IN.	YIELD LOAD POUNDS	YIELD STR. PSI	ULTIMATE LOAD POUNDS	TENSILE STR. PSI	ELONGATION IN 8" GAGE PERCENT	REDUCTION IN AREA PERCENT
IPET-RB#6A IHNC west (Pittman) ST. 2+00	.750	.44	24700	56136	39300	89318	8.715 / 8.93%	.595 .278 / 36.8%

FAILED @ WELD

TENSILE NO. _____
BTI # 1054

SPECIMEN ID	DIA. INCHES	AREA SQ. IN.	YIELD LOAD POUNDS	YIELD STR. PSI	ULTIMATE LOAD POUNDS	TENSILE STR. PSI	ELONGATION IN 8" GAGE PERCENT	REDUCTION IN AREA PERCENT
IPET-RB#6B IHNC west (Pittman) ST. 2+00	.750	.44	25000	56818	36900	83863	5.415 / 5.18%	.669 .351 / 20.2%

FAILED @ WELD

TENSILE NO. _____
BTI # 1054

SPECIMEN ID	DIA. INCHES	AREA SQ. IN.	YIELD LOAD POUNDS	YIELD STR. PSI	ULTIMATE LOAD POUNDS	TENSILE STR. PSI	ELONGATION IN 2" GAGE PERCENT	REDUCTION IN AREA PERCENT
IPET-RB-4B Pittman)(west) IHNC-west ST. 2+00	.500	.20	9700	48500	15800	79000	9.130 / 14.12%	.275 .061 / 69.5%

TENSILE NO. _____
BTI # 1054

SPECIMEN ID	DIA. INCHES	AREA SQ. IN.	YIELD LOAD POUNDS	YIELD STR. PSI	ULTIMATE LOAD POUNDS	TENSILE STR. PSI	ELONGATION IN 8" GAGE PERCENT	REDUCTION IN AREA PERCENT
IPET-RB-4A Pittman)(west) IHNC-west ST. 2+00	.500	.20	10200	51000	16200	81000	9.130 / 14.12%	.266 .055 / 72.5%

G:\WORDDATA\SIFORMS\TT505.LAB
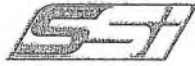
Volume V The Performance – Levees and Floodwalls – Technical Appendix

V-16-13

This is a preliminary report subject to revision; it does not contain final conclusions of the United States Army Corps of Engineers.
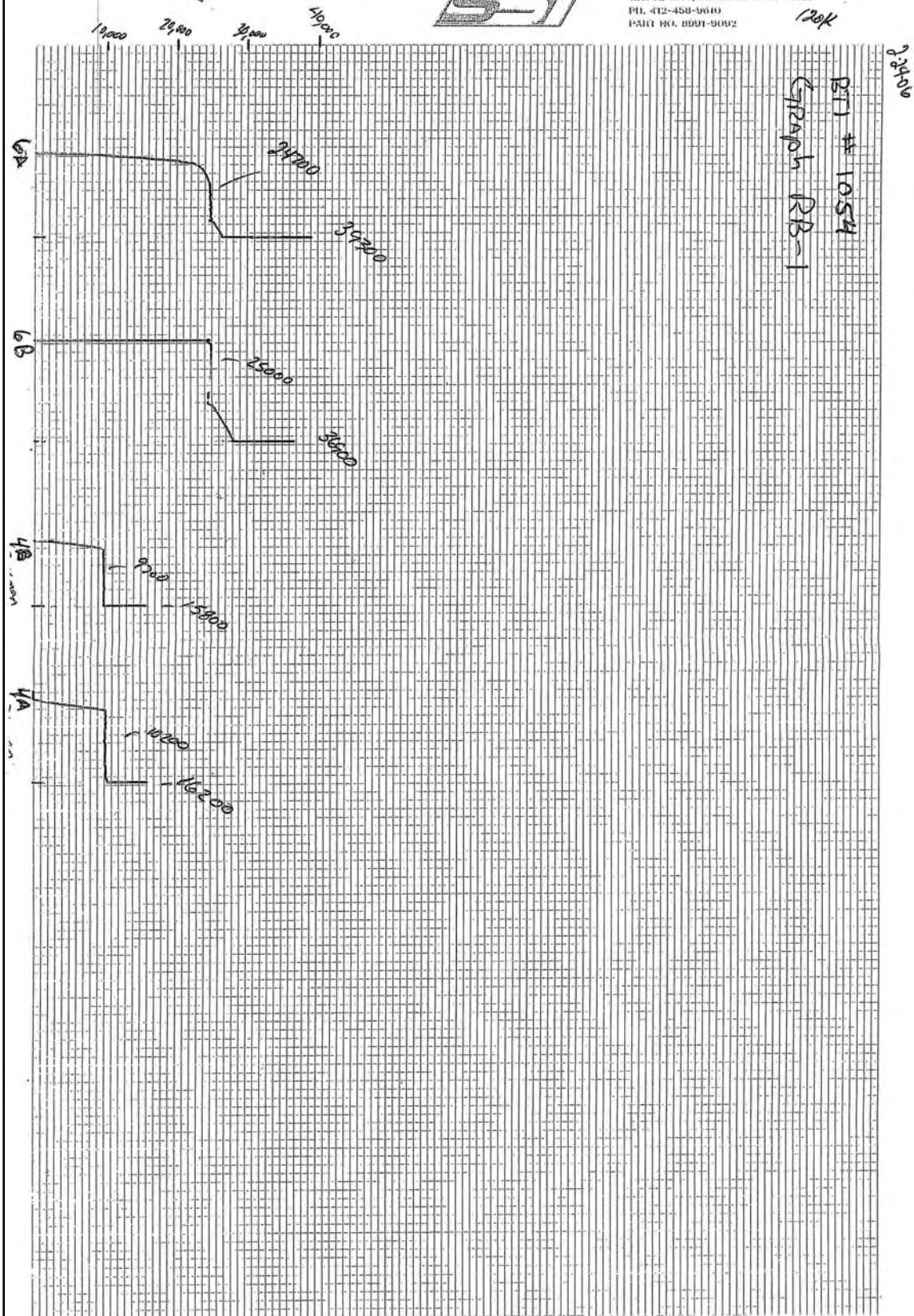
Beta Testing & Inspection, LLC
Forensic Engineering Division

March 9, 2006

Paul F. Mlakar, Ph.D., P.E.

US Army Corps of Engineers
Engineer Research and Development Center
3909 Halls Ferry Road
Vicksburg, MS 39180

RE: **Testing of IHNC East Side, North Claiborne Ave. to Florida Ave.**
Final Report
BTI Project No.: 1055
BTI Report No.: 1055-ES011306

Dear Mr. Mlaker:

On January 13, 2006 at the referenced site, sheet pile samples, steel reinforcing bars and concrete core specimens were sampled. BTI cut a total of three concrete cores from a wall section identified as IPET-IHNC-E 20+40. Mark Cheek, P.E. of BTI witnessed the removal of 9"x 25" section from two different sheet piles and assumed responsible possession of the sheet pile samples and four reinforcing bars; two No.4 and two No.7. Representatives of BTI were informed by the Corps of Engineers that the material samples provided to BTI or obtained by BTI were portions of existing components taken from the IHNC East Side, North Claiborne Ave. to Florida Ave project. All specimens were labeled, tagged, and secured prior to transporting. Samples were transported to Beta Testing & Inspection, LLC (BTI) laboratory for testing. Project Material data sheets and project specifications for the sampled materials were not provided. BTI has completed testing of concrete cores, steel sheet pile sections, and steel reinforcing bars.

Concrete Cores

Three cores were cut from the sample panel IPET-IHNC-E 20+40. The cores were obtained in accordance with procedures defined by ASTM C-42. Prior to compression testing each core was prepared in accordance with ASTM C-42, C-617, and C-39. Each core was then tested in compression to failure and the results recorded in accordance with ASTM C-39. See Table C.1 for results of the concrete core testing.

P.O. Box 2203 · Gretna, LA 70054 · (504) 227-2273 · fax (504) 227-2274
13801 Old Gentilly Road Suite #17 New Orleans, Louisiana 70129

Table C.1

Sample panel MH38C1						
Core ID	Capped Length (in.)	Diameter (in)	Area (in^2)	l/d	Correction factor	Maximum load (lbs.)
IPET-IHNC-E1	11.2	5.62	24.8	1.99	1	97,000
	Compressive strength (psi)	Fracture type	Age (days)	Load application	Test date/time	Sample date/time
	3910	A	NA	vertical	1/18/06 10:00am	1/13/06 1:30pm
Core ID	Capped Length (in.)	Diameter (in)	Area (in^2)	l/d	Correction factor	Maximum load (lbs.)
IPET-IHNC-E2	11.2	5.62	24.8	2.0	1.0	95,500
	Compressive strength (psi)	Fracture type	Age (days)	Load application	Test date/time	Sample date/time
	3850	A	NA	vertical	1/12/06 10:15am	1/13/06 2:15pm
Core ID	Capped Length (in.)	Diameter (in)	Area (in^2)	l/d	Correction factor	Maximum load (lbs.)
IPET-IHNC-E3	11.2	5.62	24.8	1.99	1.0	100,500
	Compressive strength (psi)	Fracture type	Age (days)	Load application	Test date/time	Sample date/time
	4050	A	NA	vertical	1/12/06 10:30am	1/13/06 2:30pm

Average compressive strength (psi)	3940

Steel Sheet Piling

A welder provided by Cajun Constructors cut one 9"x 25" specimen from each of the two-sheet pile using an acetylene cutting torch. Mandina's Inspection a subcontractor of BTI then prepared and tested each specimen in tension to failure in accordance with ASTM A-370. For test results see table SP-1 and graph SP-1

Steel Reinforcing Bars

Four pieces of steel reinforcing bars were secured and transported to BTI's laboratory. The steel reinforcing bar samples ranged in size from No. 4 to No. 7 bars. Mandina's Inspection a subcontractor of BTI tested the rebar specimens to failure in accordance with ASTM A-615 & A370. For test results see table RB-1 and graph RB-1

Upon completion and acceptance of the testing program, all of the materials, tested and untested, will be sealed and returned to the New Orleans District Office of the US Army Corps of Engineers. Enclosed are copies of our laboratory accreditations and equipment calibration reports associated with the test performed. Should you have any questions regarding this letter or require additional information, please do not hesitate to contact us.

Sincerely,

Beta Testing & Inspection, LLC

Mark A. Cheek, P.E.
Vice-President

Enclosures

V-16-16

Volume V The Performance – Levees and Floodwalls – Technical Appendix
This is a preliminary report subject to revision; it does not contain final conclusions of the United States Army Corps of Engineers.

Table SP-1

MECHANICAL TESTING LABORATORY DIVISION

Mandina's Insp. 2-24-06

MTL JOB NO. _____ 4405.90

TENSILE NO. _____
BTI # 1055

SPECIMEN ID	WIDTH INCHES	THICKNESS SQ. IN.	AREA SQ. IN.	YIELD STR. POUNDS	YIELD STR. PSI	TENSILE STR. POUNDS	TENSILE STR. PSI	ELONGATION IN 8" GAGE PERCENT
IPET-SP-1E-1	1.445	.321	.463	25000	53995	36500	78833	9.200 / 15.0%

TENSILE NO. _____
BTI # 1055

SPECIMEN ID	WIDTH INCHES	THICKNESS SQ. IN.	AREA SQ. IN.	YIELD STR. POUNDS	YIELD STR. PSI	TENSILE STR. POUNDS	TENSILE STR. PSI	ELONGATION IN 8" GAGE PERCENT
IPET-SP-2E-1	1.452	.358	.519	27200	52408	42300	81502	9.326 / 16.59%

TENSILE NO. _____
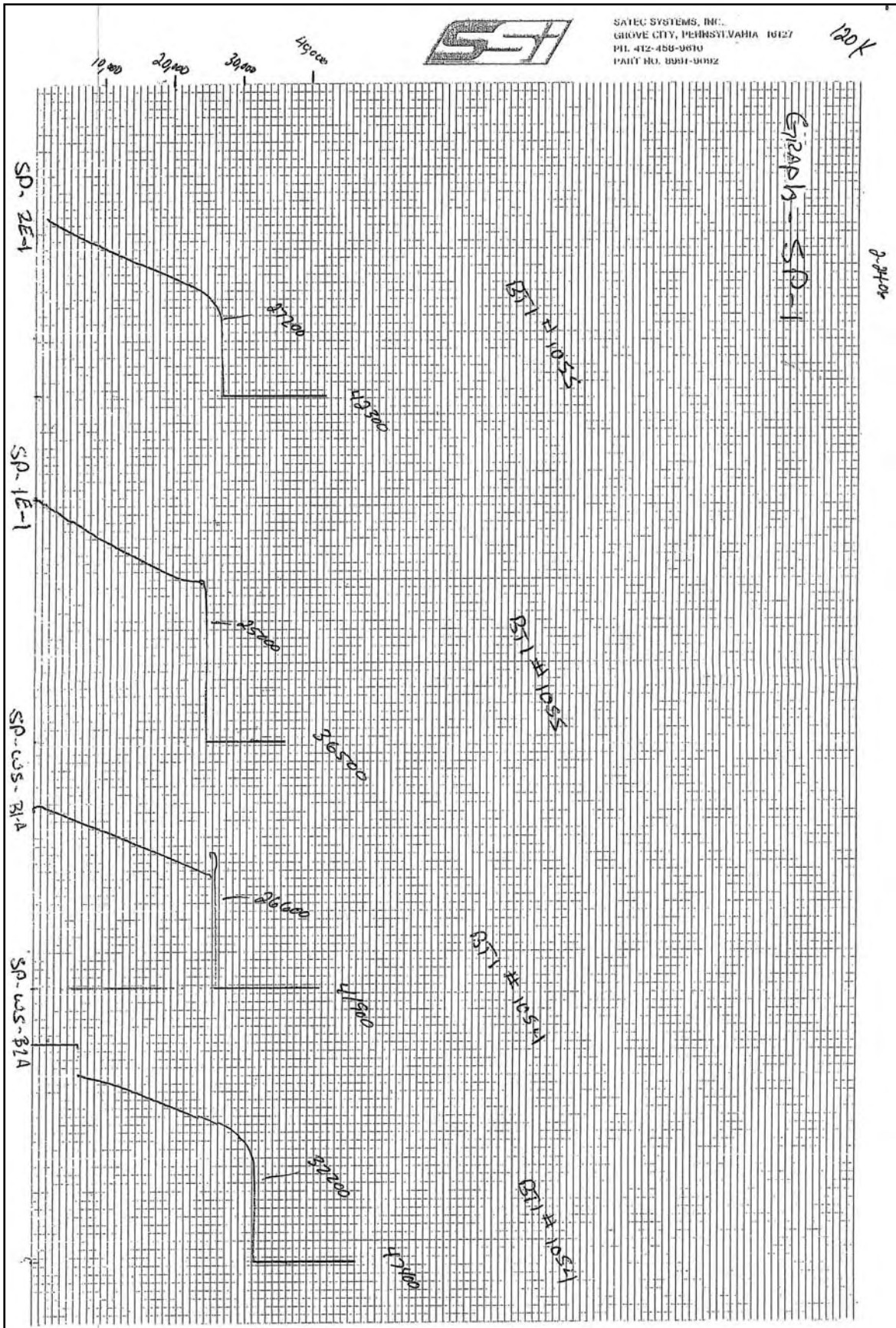
Table RB-1

MECHANICAL TESTING LABORATORY DIVISION

MTL JOB NO. _Mandina's Insp 4405.90 2-24-06_

TENSILE NO. _____
BTI # 1055

SPECIMEN ID	DIA. INCHES	AREA SQ. IN.	YIELD LOAD POUNDS	YIELD STR. PSI	ULTIMATE LOAD POUNDS	TENSILE STR. PSI	ELONGATION IN 8" GAGE PERCENT	REDUCTION IN AREA PERCENT
IPET-RB-E1 IHNC)(EAST) (CAJun)	.875	.60	39500	65833	63100	105166	8.847 10.58%	.735 .424 3.6%

TENSILE NO. _____
BTI # 1055

SPECIMEN ID	DIA. INCHES	AREA SQ. IN.	YIELD LOAD POUNDS	YIELD STR. PSI	ULTIMATE LOAD POUNDS	TENSILE STR. PSI	ELONGATION IN 8" GAGE PERCENT	REDUCTION IN AREA PERCENT
IPET-RB-E2 IHNC)(EAST) CAJun	.875	.60	38500	64166	61600	102666	8.925 11.56%	.630 .311 12.9%

TENSILE NO. _____
BTI # 1055

SPECIMEN ID	DIA. INCHES	AREA SQ. IN.	YIELD LOAD POUNDS	YIELD STR. PSI	ULTIMATE LOAD POUNDS	TENSILE STR. PSI	ELONGATION IN 8" GAGE PERCENT	REDUCTION IN AREA PERCENT
IPET-RB-E3 IHNC)(EAST) CAJun	.500	.20	9200	46000	14800	74000	9.595 19.9%	.275 .055 70.5%

TENSILE NO. _____
BTI # 1055

SPECIMEN ID	DIA. INCHES	AREA SQ. IN.	YIELD LOAD POUNDS	YIELD STR. PSI	ULTIMATE LOAD POUNDS	TENSILE STR. PSI	ELONGATION IN 8" GAGE PERCENT	REDUCTION IN AREA PERCENT
IPET-RB-E4 IHNC)(EAST) (CAJun)	.500	.20	11000	55000	15400	77000	8.650 8.1%	.389 11.8%

G:\WORDDATA\ISIFORMS\TT505.LAB

This is a preliminary report subject to revision; it does not contain final conclusions of the United States Army Corps of Engineers.
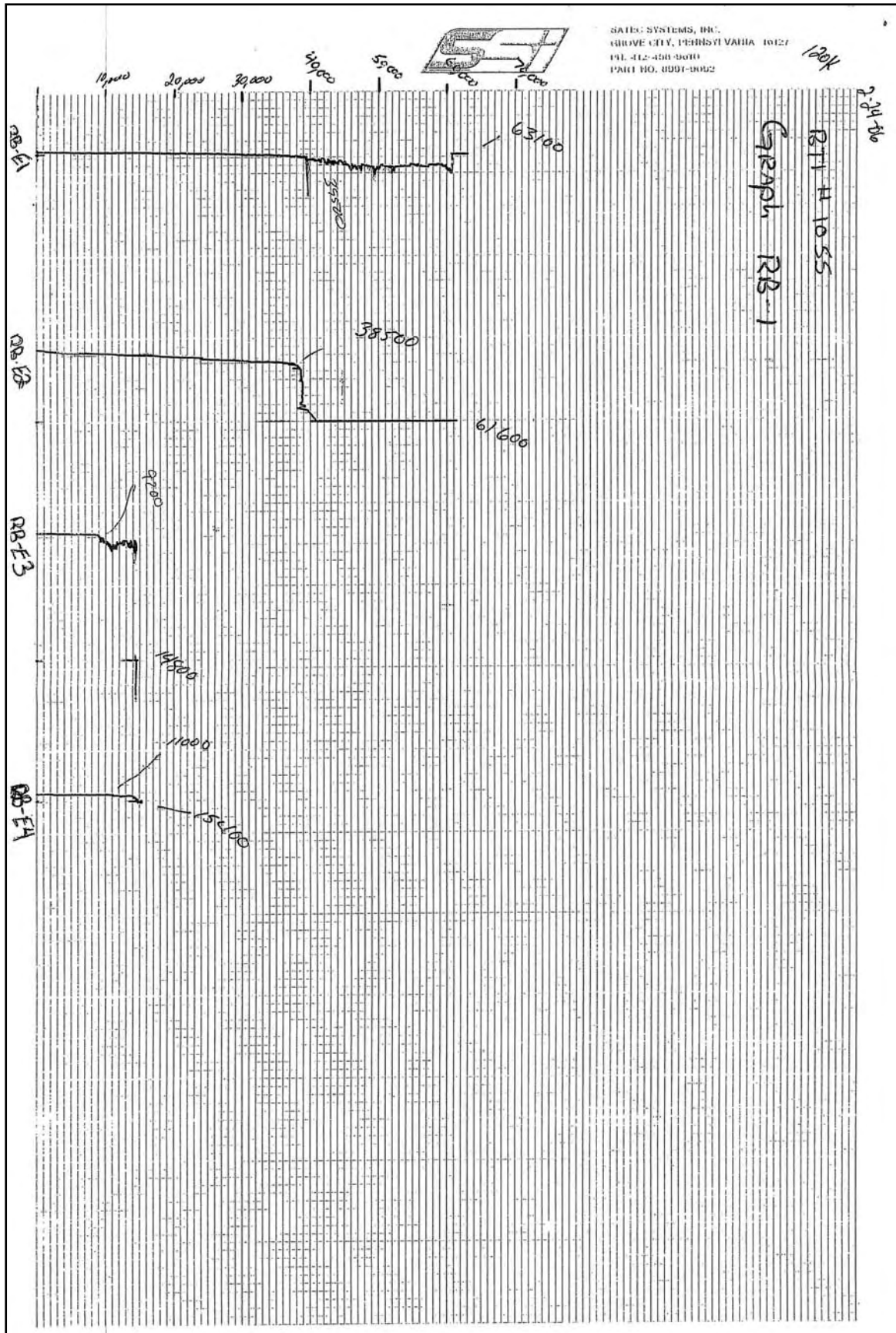
Appendix 17
Finite Element Seepage Study

(To be completed.)

Volume V The Performance – Levees and Floodwalls – Technical Appendix

V-17-1

This is a preliminary report subject to revision; it does not contain final conclusions of the United States Army Corps of Engineers.

Appendix 18
Erosion of New Orleans and St. Bernard Levees

Introduction

This document will briefly discuss the physical characteristics of the New Orleans East Back Levee (NOE BL), Orleans Parish and the Chalmette Levee (and Chalmette Extension Levee) along the MRGO in St. Bernard Parish. The purpose of this report is to examine the difference between sections of levee that performed well and sections that were catastrophically destroyed by Hurricane Katrina. Main sources of data for this study are the original design documents and post Hurricane investigations conducted mostly by the USACE Task Force Guardian (TFG) and members of the Interagency Performance Evaluation Team (IPET).

The Design Memorandum (DM) for each USACE hurricane protection project describes the local and site geology, in addition to the design of the levees and associated floodwalls. Typical geotechnical data are provided in the DM such as geologic cross sections of the levee design with associated borings, soil property tests and stability analyses. The NOE BL and the Chalmette Levee and extension were built by placing soil hydraulically in lifts over many years. At the time of the 1971 design for levee enlargement for the NOE BL the height of the existing levees were on average 10 ft above mean sea level. The 1971 proposed design elevations were 17 ft (NGVD). The levees were surveyed using LIDAR in 2001 and again in 2005 (after Katrina). The pre-storm elevations ranged from 16 to 20 ft (NAVD 88, 2004.65) and averaged 17 ft. The LIDAR surveys were adjusted by ERDC personnel (2006) and a digital elevation map (DEM) was created for the IPET. These DEM elevations were used in this study to compare storm surge and wave height to levee height. Where these data were not available the levee height was estimated from USACE, New Orleans District maps. The plots showing the damage to the levees are in Attachments A and B for NOE BL and the Chalmette Levee, respectively.

Analysis of Surge and Wave Effects on Levees

(To be completed.)

Figure 18-1. General map of NOE Basin, major levee segments are lakefront levees, NOE East Levee (South Point to GIWW), NOE Back Levee, Citrus Back Levee and IHNC levees
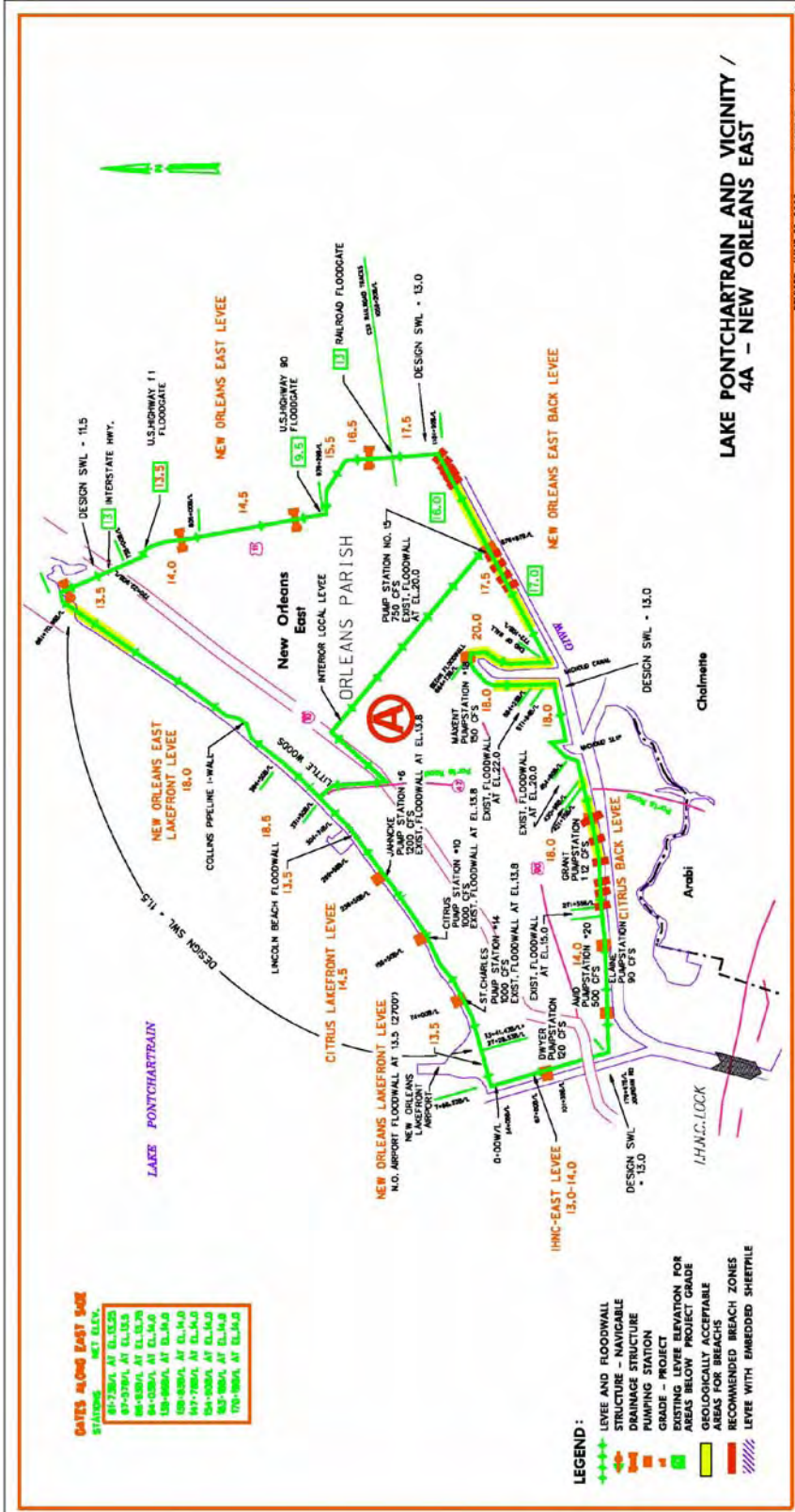
Figure 18-2. New Orleans East levee system, bounded by the South Point to GIWW levee on the east and NOE Back and Citrus Back Levees to the south

TASK FORCE GUARDIAN

New Orleans East - Project Summary

Legend:
- Damaged
- No Significant Damage
- Non-Federal Levee

NOE08
DRAINAGE AND FLOODGATE
STRUCTURE SCOUR REPAIRS
- SOUTHPOINT TO GIWW

NOE07
LEVEE SCOUR REPAIR
LAKEFRONT AIRPORT TO CSX RR

NOE05
CSX RR FLOODGATE
REPAIR

NOE06
LAKEFRONT AIRPORT FLOOD
WALL SCOUR REPAIRS

NOE09
FLOODWALL SCOUR REPAIR,
MICHOUD CANAL TO MICHOUD
SLIP

NOE02
FLOODWALL REPAIR -
PUMP STATION #15

NOE01
EASTBACK LEVEE REPAIR,
MICHOUD CANAL TO CSX RR

NOE04
CITRUS BACK LEVEE
FLOODWALL REPAIR

NOE03
FLOODWALL REPAIR NEAR AIR
PRODUCTS PLANT

Figure 18-2. TFG Damage Survey Report/ Project Information Report – for levee repair
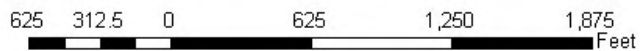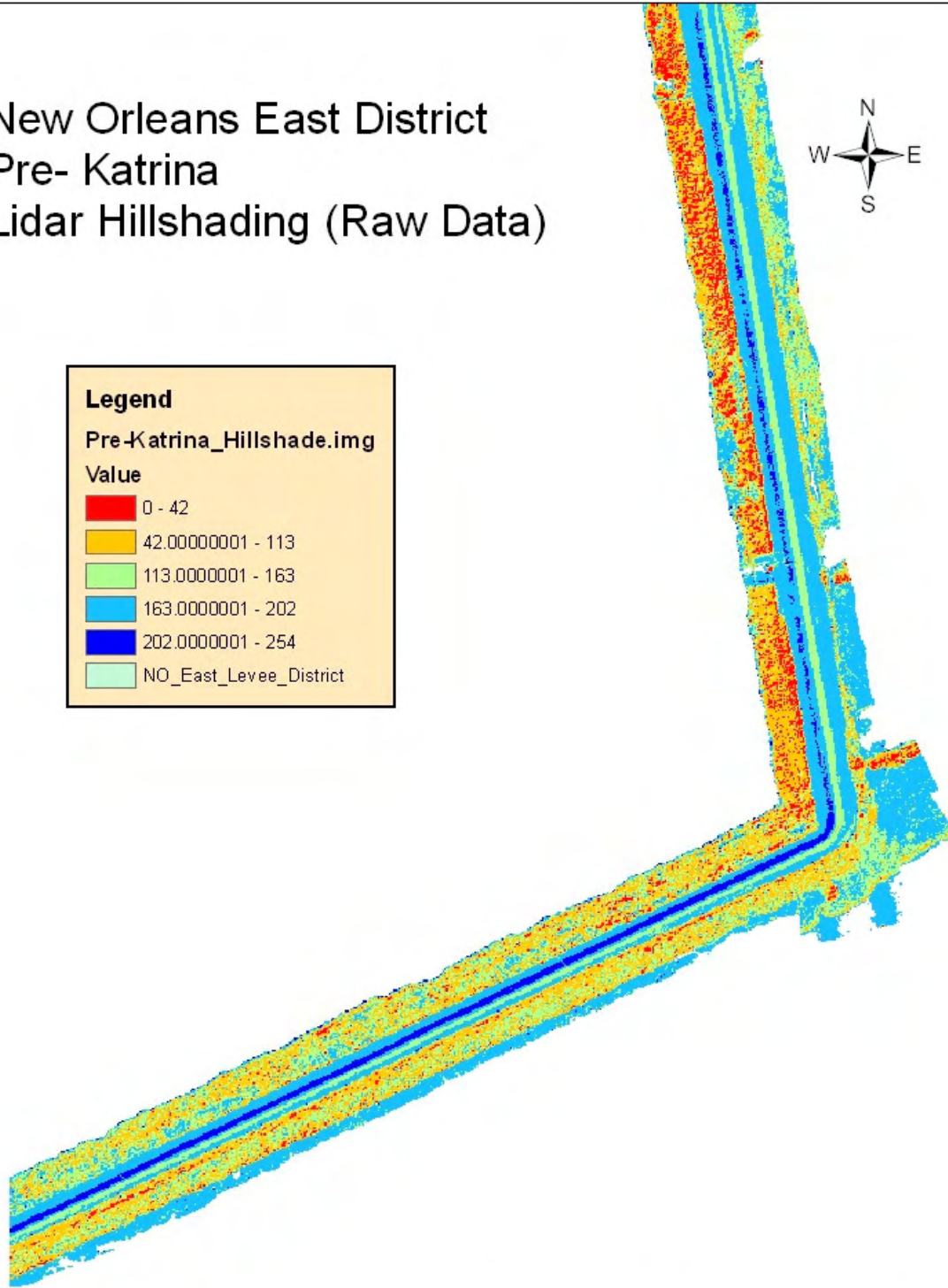
Figure 18-3. Hillshading from pre-Katrina LIDAR, southeast corner of New Orleans East Basin
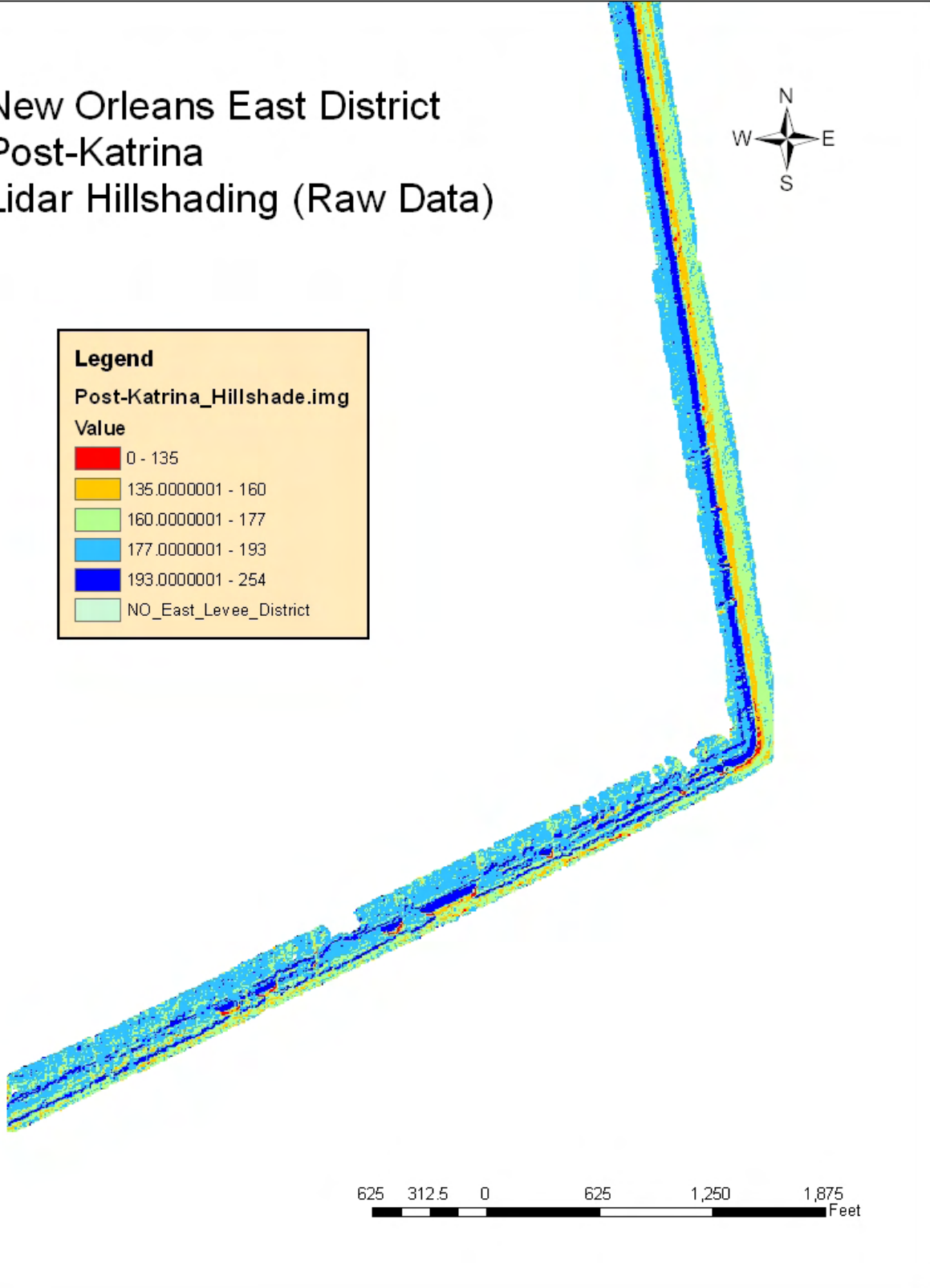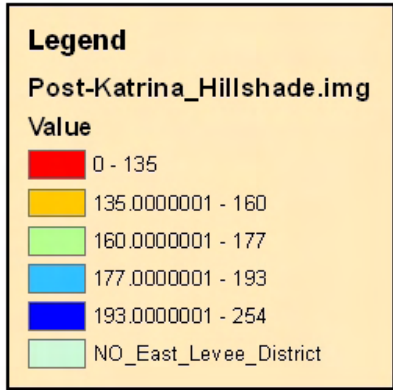
Figure 18-4. Hillshading from post-Katrina LIDAR, southeast corner of New Orleans East Basin

This is a preliminary report subject to revision; it does not contain final conclusions of the United States Army Corps of Engineers.
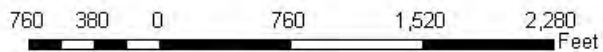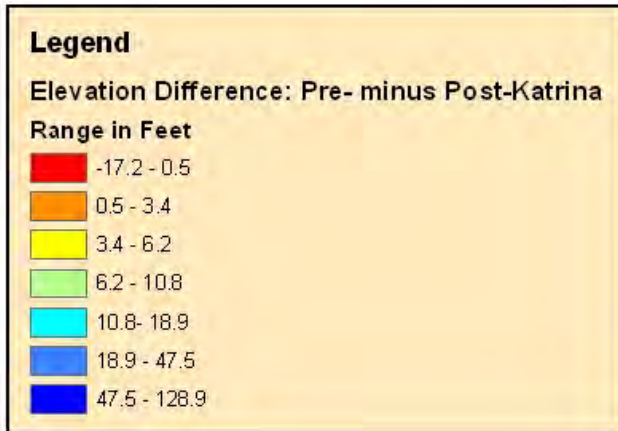
Figure 18-5. Hillshading from pre-Katrina LIDAR minus post-Katrina LIDAR, southeast corner of New Orleans East Basin. Figure created from raw LIDAR data, thus noise and outliers not removed from dataset. Red areas indicate less than 0.5 ft of scour

Figure 18-6. NOE Basin post-Katrina breaches

Figure 18-7. NOE Levee construction materials (USACE DM NOE Back Levee, Citrus Back Levee, South point to GIWW Levee, Lakefront Levees, IHNC Levees) 1971, 1969, etc.)
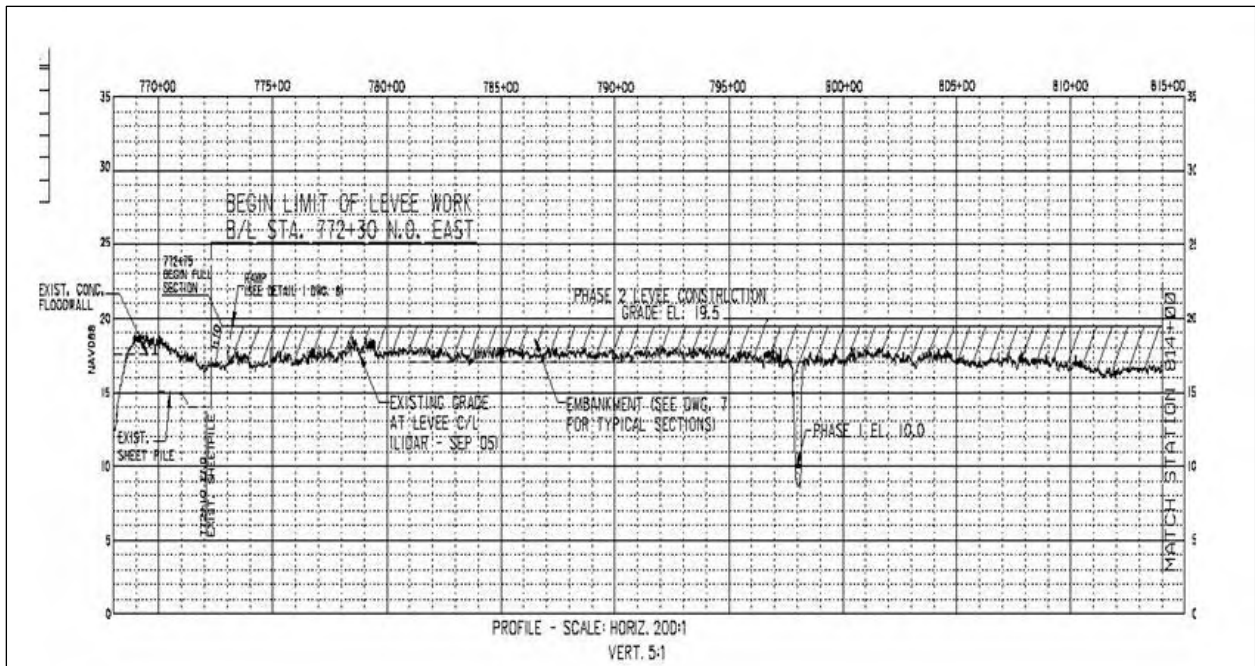
Figure 18-8. Post-Katrina profile along NOE Back Levee starting at Michoud Canal (Station 772 + 30) to Station 814 + 00 along the GIWW
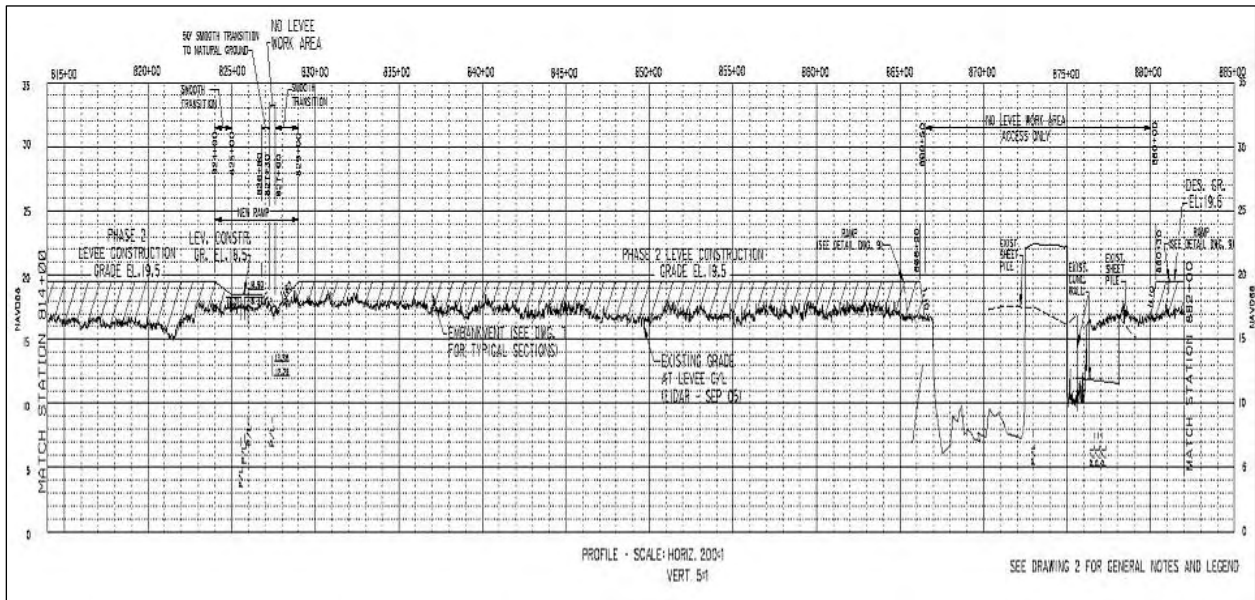
Figure 18-9. Post-Katrina profile along NOE Back Levee starting at Station 814 + 00 and ending at Station 882+00
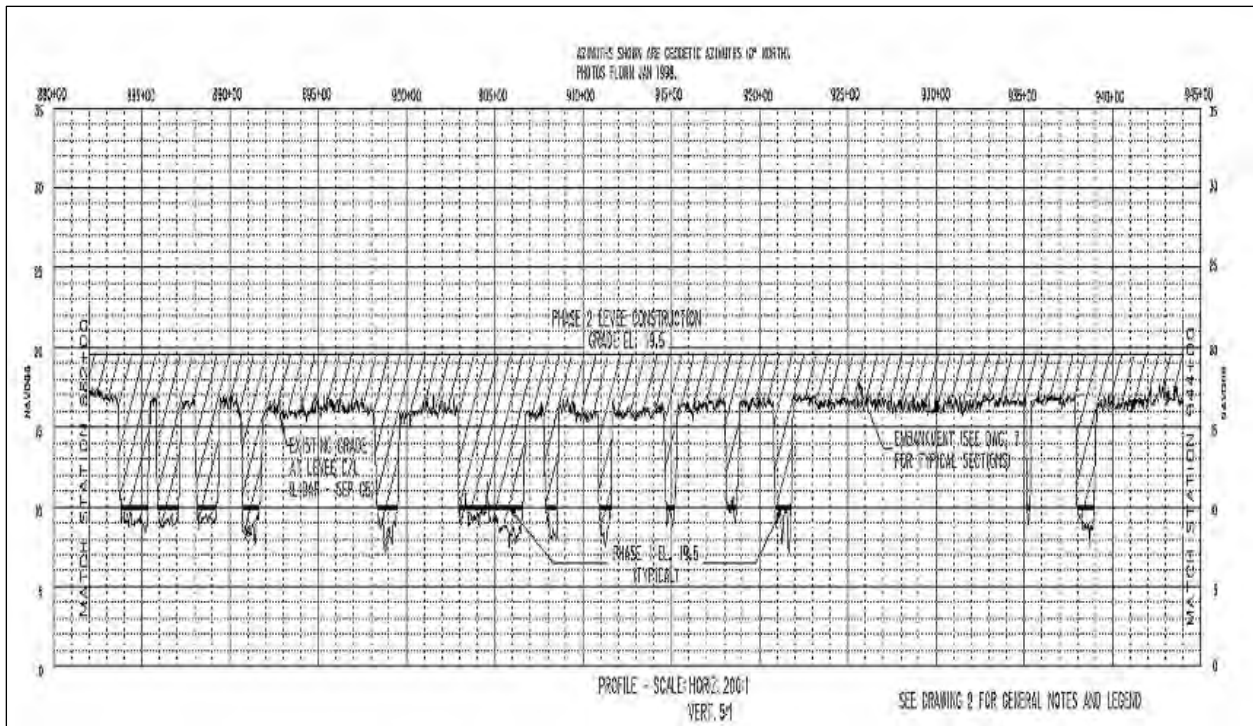
Figure 18-10. Post-Katrina profile along NOE Back Levee starting at Station 882 + 00 and ending at 944 + 00
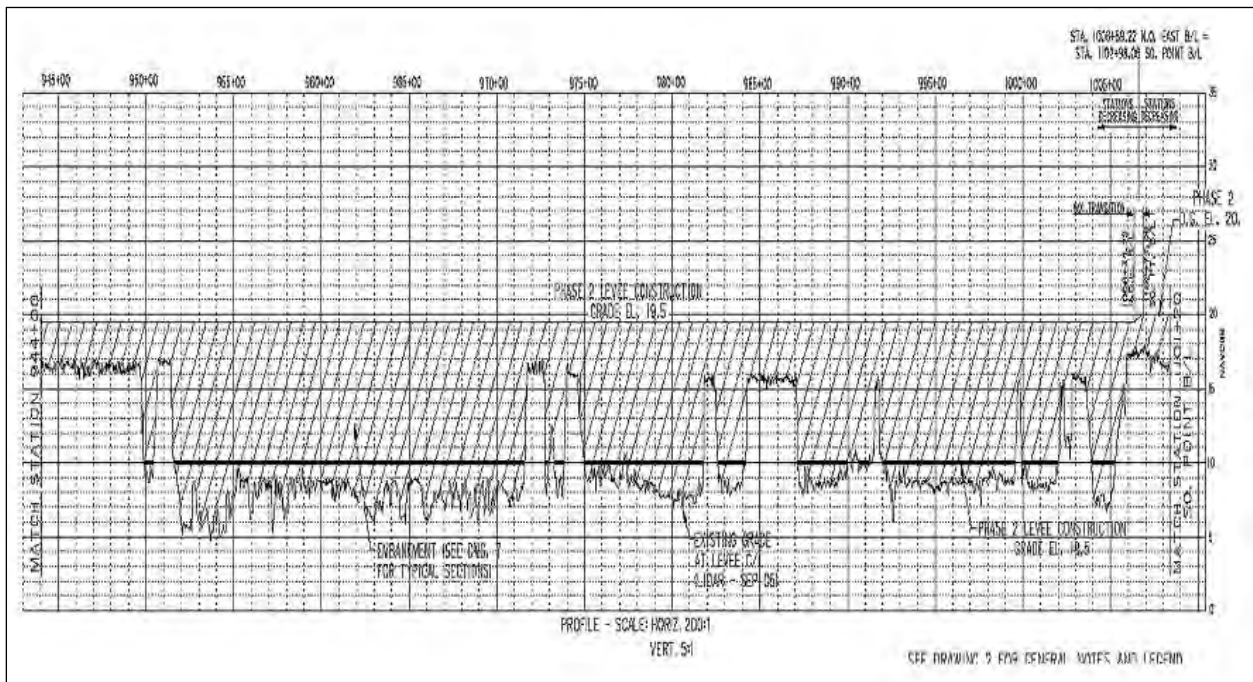
Figure 18-11. Post-Katrina profile along NOE Back Levee starting 944 + 00 and ending at station 1101 +20. Intersecting the South Point Levee
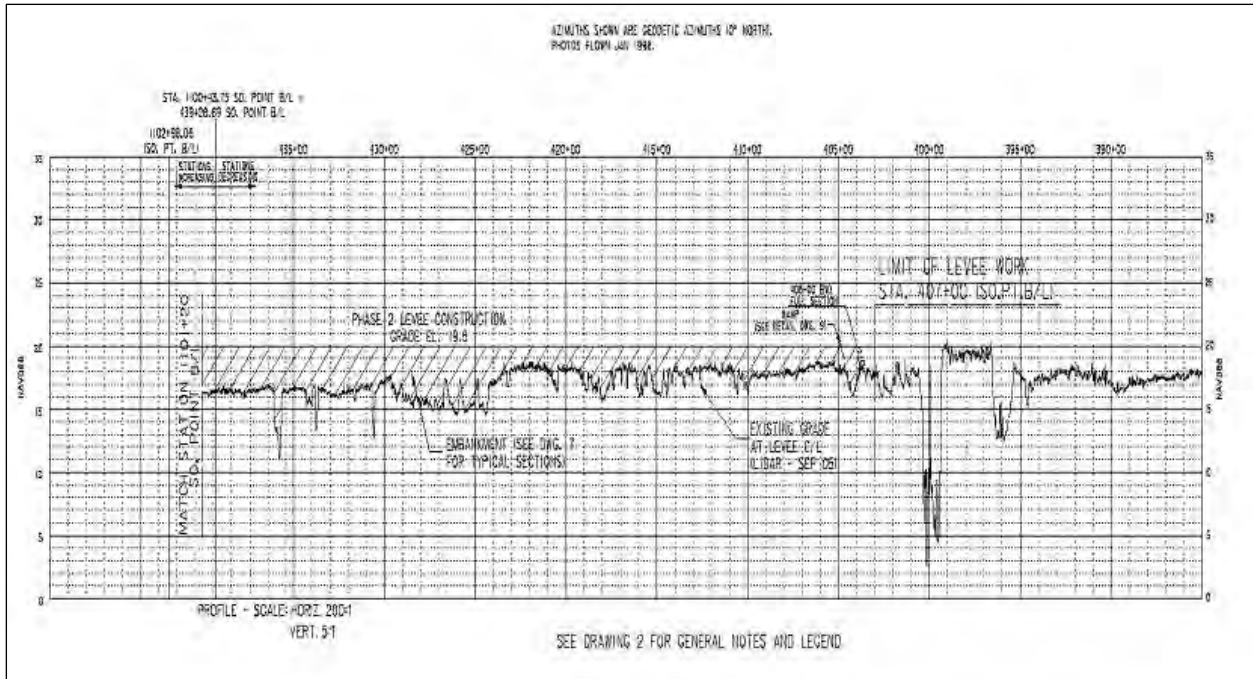
Figure 18-12. Post-Katrina profile along NOE South Point Levee starting at Station 43 + 28 (at GIWW) and ending at Station 385 + 00

Figure 18-13. Location of undisturbed borings taken in 2001 along the NOE Back Levee (42-U, 43-U, 44-U, 45-U)
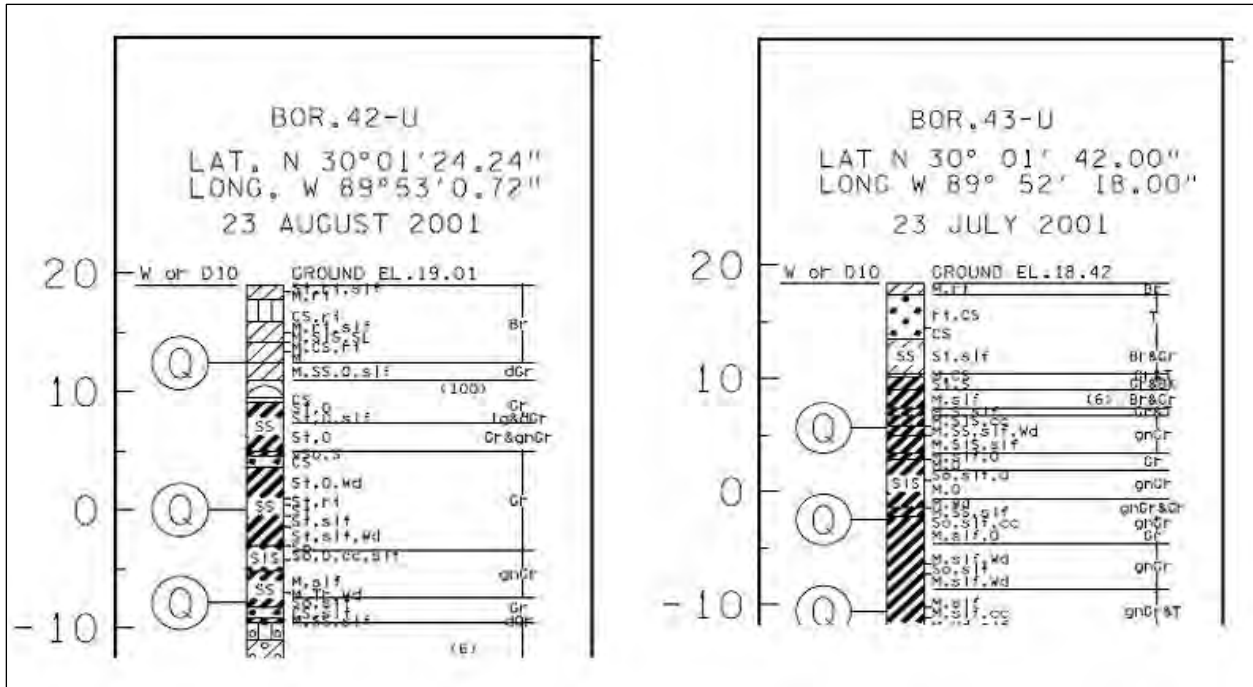
Figure 18-14. NOE Back Levee undisturbed borings 42-U and 43-U
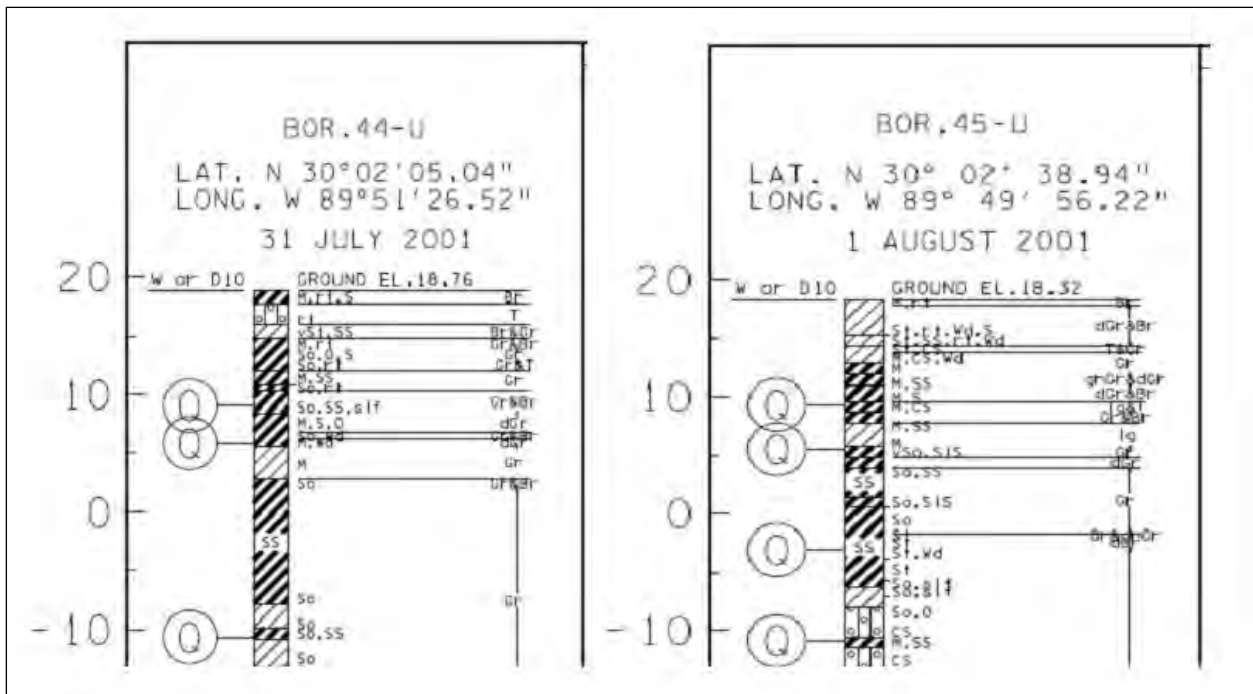
Figure 18-15. NOE Back Levee undisturbed borings 43-U and 45-U

UNIFIED SOIL CLASSIFICATION

LETTER SYMBOL	SYM BOL	TYPICAL NAMES
GW		GRAVEL,Well Graded,gravel-sand mixtures,little or no fines
GP		GRAVEL,Poorly Graded,gravel-sand mixtures,little or no fines
GM		SILTY GRAVEL,gravel-sand-silt mixtures
GC		CLAYEY GRAVEL,gravel-sand-clay mixtures
SW		SAND,Well-Graded,gravelly sands
SP		SAND,Poorly-Graded,gravelly sands
SM		SILTY SAND,sand-silt mixtures
SC		CLAYEY SAND,sand-clay mixtures
ML		SILT & very fine sand,silty or clayey fine sand or clayey silt with slight plasticity
CL		LEAN CLAY,Sandy Clay,Silty Clay,of low to medium plasticity
OL		ORGANIC SILTS,and organic silty clays of low plasticity
MH		SILT,fine sandy or silty soil with high plasticity
CH		FAT CLAY,inorganic clay of high plasticity
OH		ORGANIC CLAYS of medium to high plasticity,organic silts
Pt		PEAT,and other highly organic soil
Wd		WOOD
SI		SHELLS
NS		No Sample Retrieved

Figure 18-16. Description of boring log symbols

Figure 18-17. ERDC model points for hindcasting storm surge around NOE Levee System

Figure 18-18. Selected model data points for surge analysis

Table 18-1 Calculation of Interpreted Surge from ADCIRC Numerical Model and High Water Mark Survey for Selected Model Data Points

NOE ADCIRC Model Point	Latitude	Longitude	T_{ms} = ADCIRC Time of Maximum Surge	ADCIRC Model max surge (ft NAVD 88, 2004.65)	STWAVE Model wave height (ft) at T_{ms}	Closest HWM value (ft NAVD 88 (2004.65))	Interpreted Surge from HWM and ADCIRC (ft, NAVD 88, 2004.65)	Interpreted Surge plus wave ht at Time $_{ms}$	Levee Name
									NOE Final Table of Storm Surge Interpretation_for points along Citrus Back Levee, NOE Back Levee and South Point
596	30.004139	-89.938667	1235	15.2	2.03	15.4	15.4	17.43	Citrus Back Levee
366	30.008200	-89.923897	1235	15.2	2.13	15.4, 18.2	16.7	18.83	Citrus Back Levee
365	30.018400	-89.890984	1235	14.8	2.03	15.4, 18.2	16	18.03	NOE Back Levee
364	30.026340	-89.874229	1240	14.4	1.94	15.4, 18.2	15.6	17.54	NOE Back Levee
148	30.029604	-89.864881	1240	14.2	1.77	15.4, 15.7	15.4	17.17	NOE Back Levee
363	30.033979	-89.858070	1320	14.0	2.56	15.7	15.2	17.76	NOE Back Levee
362	30.040150	-89.843964	1355	13.7	2.59	15.7	15	17.59	NOE Back Levee
361	30.047791	-89.830162	1355	13.6	2.69	15.7	14.6	17.29	NOE Back Levee
158	30.078615	-89.848595	1655	14.2	1.31	15.7	14.2	15.51	south point
157	30.095602	-89.855300	1655	12.8	1.64	15.7	12.8	14.44	south point
351	30.121361	-89.850670	1700	12.7	2	13.4	12.6	14.6	south point
350	30.132311	-89.852409	1700	12.7	2.17	11.4	12.6	14.77	south point
349	30.144039	-89.853767	1700	12.6	1.35	11.4	12	13.35	south point
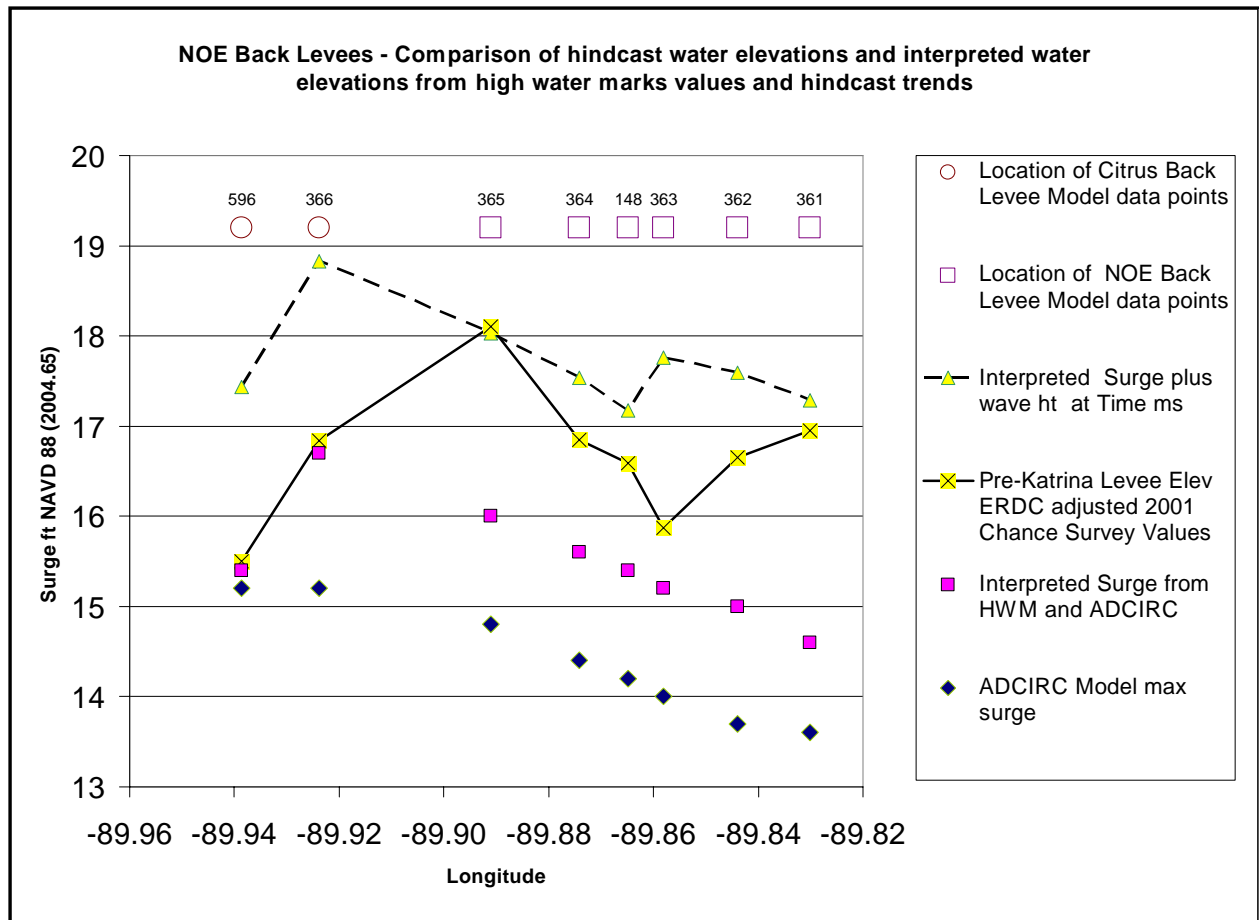
Figure 18-19. Data from Table 18-2 plotted with levee elevations derived from pre-Katrina LIDAR for Citrus Back Levee and NOE Back Levee
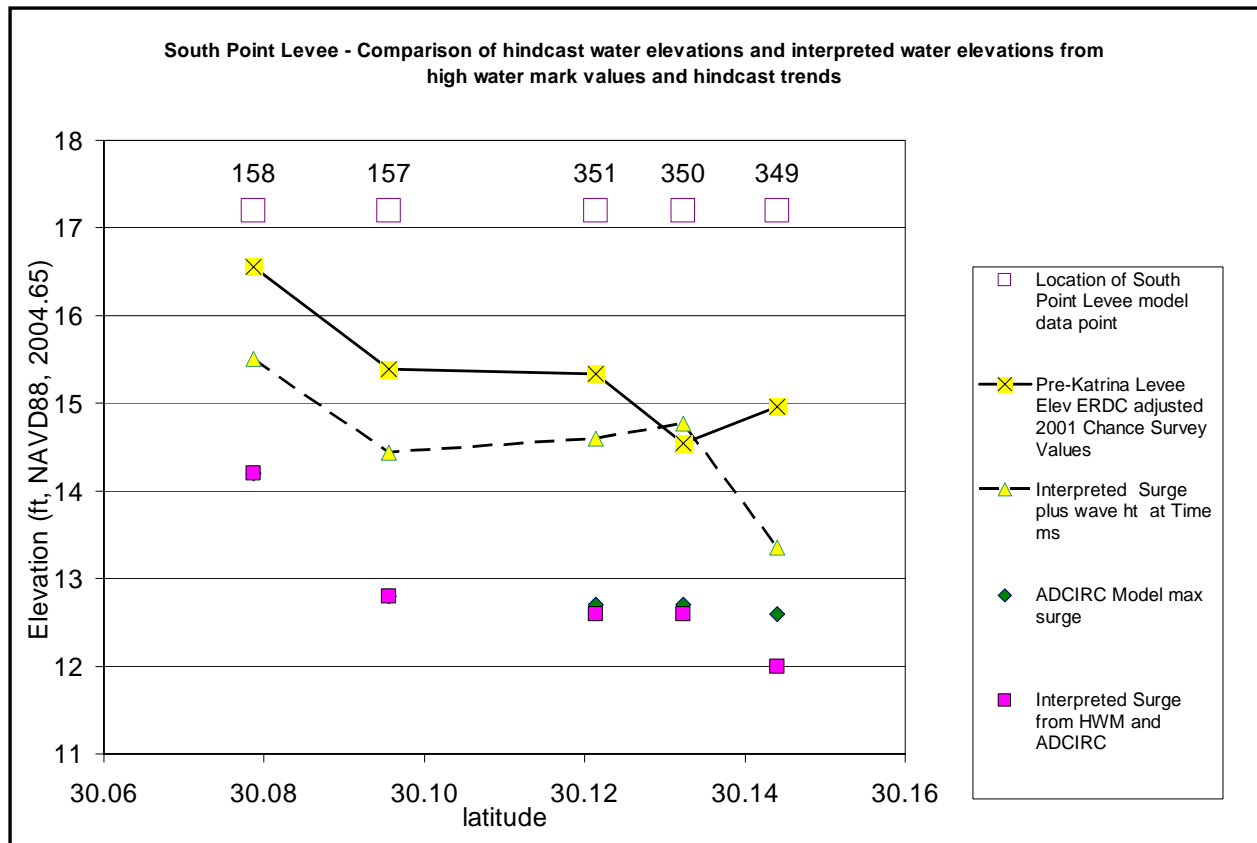
Figure 18-20. Data from Table 18-2 plotted with levee elevation derived from pre-Katrina LIDAR for Southpoint Levee

Volume V The Performance – Levees and Floodwalls – Technical Appendix

V-18-19

This is a preliminary report subject to revision; it does not contain final conclusions of the United States Army Corps of Engineers.
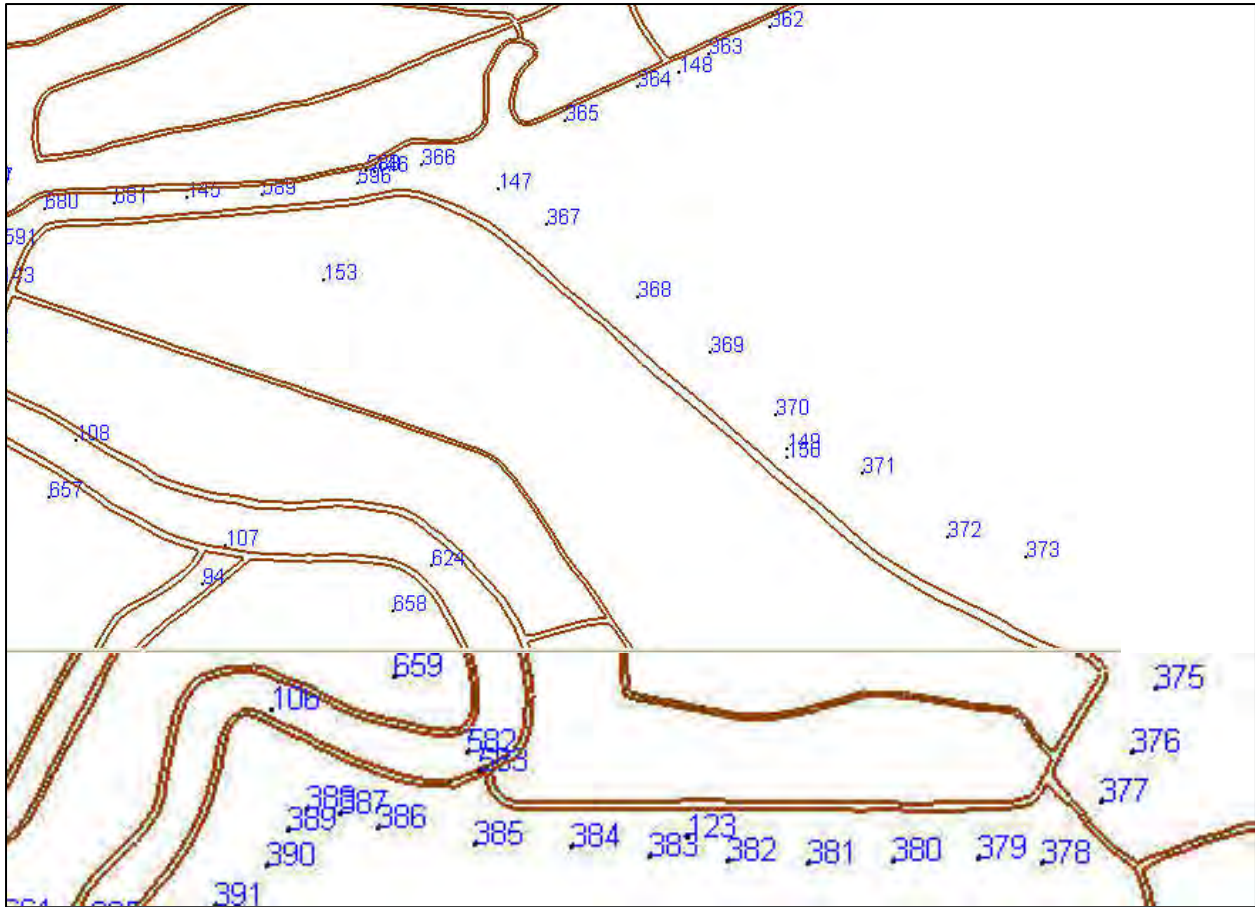
Figure 18-21. St. Bernard ADCIRC model points for hindcasting
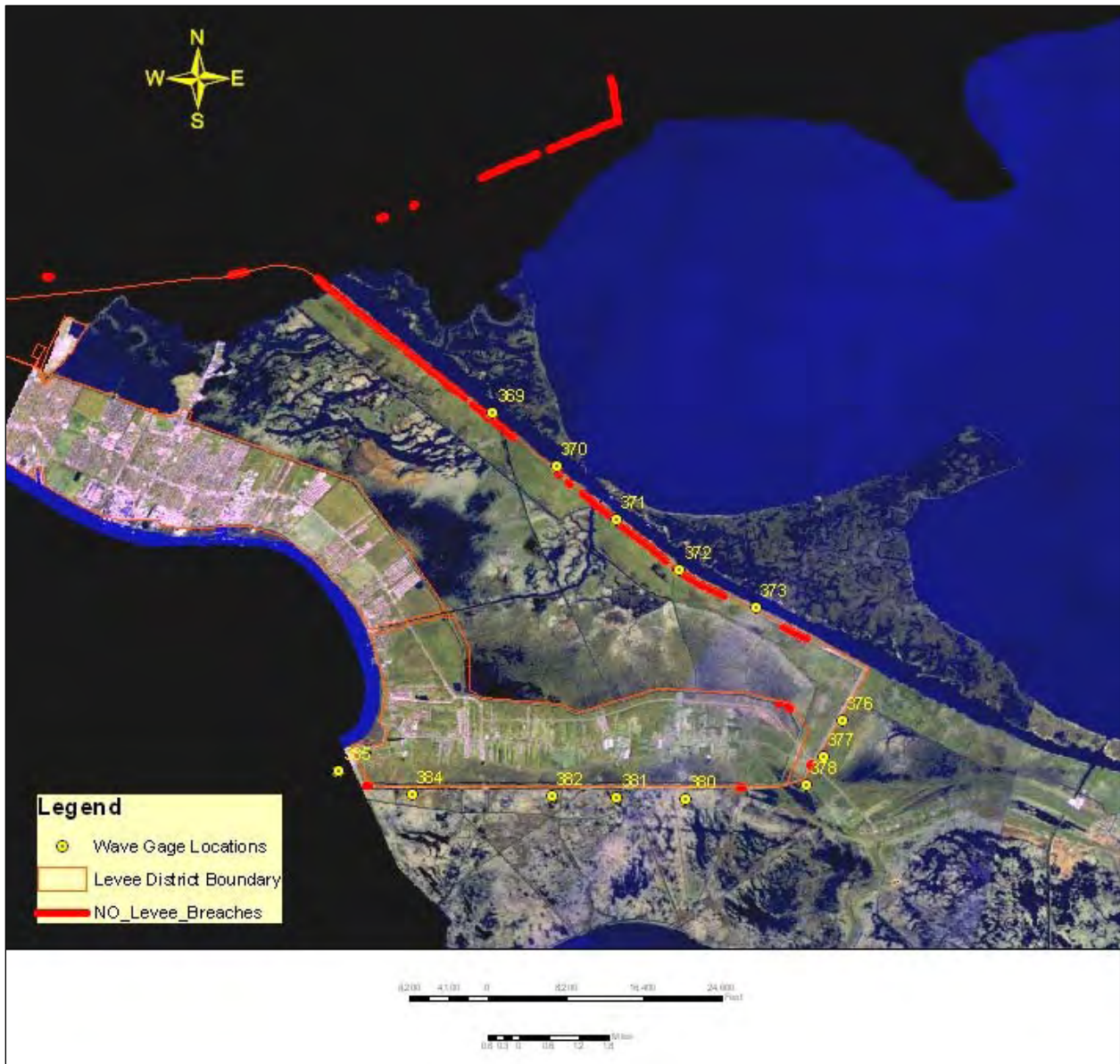
Figure 18-22. St. Bernard Parish, locations of breaches and ADCIRC model data points along MRGO and the Chalmette Extension Levees

Figure 18-23. Locations of hauled fill correlate closely with locations of breaches in Figure 18-23

Volume V The Performance – Levees and Floodwalls – Technical Appendix

Table 18-2 Calculation of Interpreted Surge Along MRGO from ADCIRC Numerical Model and High Water Mark Survey for Selected Model Data Points Shown in Figure 18-23

NOE ADCIRC Model Point	Latitude	Longitude	T ms = ADCIRC Time of Maximum Surge	ADCIRC Model max surge (ft NAVD 88, 2004.65)	STWAVE Model wave height (ft) at T ms	Closest HWM value (ft NAVD 88 (2004.65))	Interpreted Surge from HWM and ADCIRC (ft, NAVD 88, 2004.65)	Interpreted Surge plus wave ht at Time ms	Levee Name
					St. Bernard Parish -Final Table of Storm Surge Interpretation_for points along MRGO to Verret Levees				
147	29.998568	-89.915208	1240	15.4	2.2	18.2	18.0	20.2	MRGO
367	29.991980	-89.902039	1240	15.7	2.6	18.2	18.0	20.6	MRGO
368	29.975849	-89.883049	1235	16.2	3.2	18.2	18.5	21.7	MRGO
369	29.961229	-89.866470	1245	16.4	3.8	21.2, 20.8, 16.8	18.5	22.3	MRGO
370	29.945999	-89.848381	1245	16.6	1.3	21.2, 20.8, 16.8	19.5	20.8	MRGO
371	29.930630	-89.831192	1255	16.7	4.1	21.2, 20.8, 16.8	19.5	23.6	MRGO
372	29.916309	-89.812950	1255	16.9	3.9	21.2, 20.8, 16.8	19.3	23.2	MRGO
373	29.905451	-89.790939	1255	16.9	3.8	21.2, 20.8, 16.8	19.0	22.8	MRGO
375	29.881710	-89.760398	1310	16.6	1.5	18.7, 18.1	18.8	20.3	MRGO
376	29.872770	-89.766243	1310	16.4	1.7	18.7, 18.1	18.6	20.3	MRGO
377	29.862471	-89.771744	1315	16.3	1.7	18.7, 18.1	18.6	20.3	MRGO
378	29.854219	-89.776718	1325	15.7	1.8	13.7, 18.7, 18.1	15.7	17.5	MRGO
380	29.850451	-89.811249	1330	15	1.4	13.7	14.0	15.4	MRGO
381	29.850960	-89.831001	1335	14.8	1.3	12.9	13.0	14.3	MRGO
382	29.851130	-89.849548	1330	14.6	1.4	11.7, 12.0	12.0	13.4	MRGO
383	29.851129	-89.868606	1335	14.3	1.4	12.0	11.5	12.9	MRGO
384	29.851549	-89.889671	1325	13.9	1.7	11.8, 11.8	11.0	12.7	MRGO
385	29.858339	-89.910713	1340	13.3	2.0	10.5, 11.8	10.5	12.5	MRGO
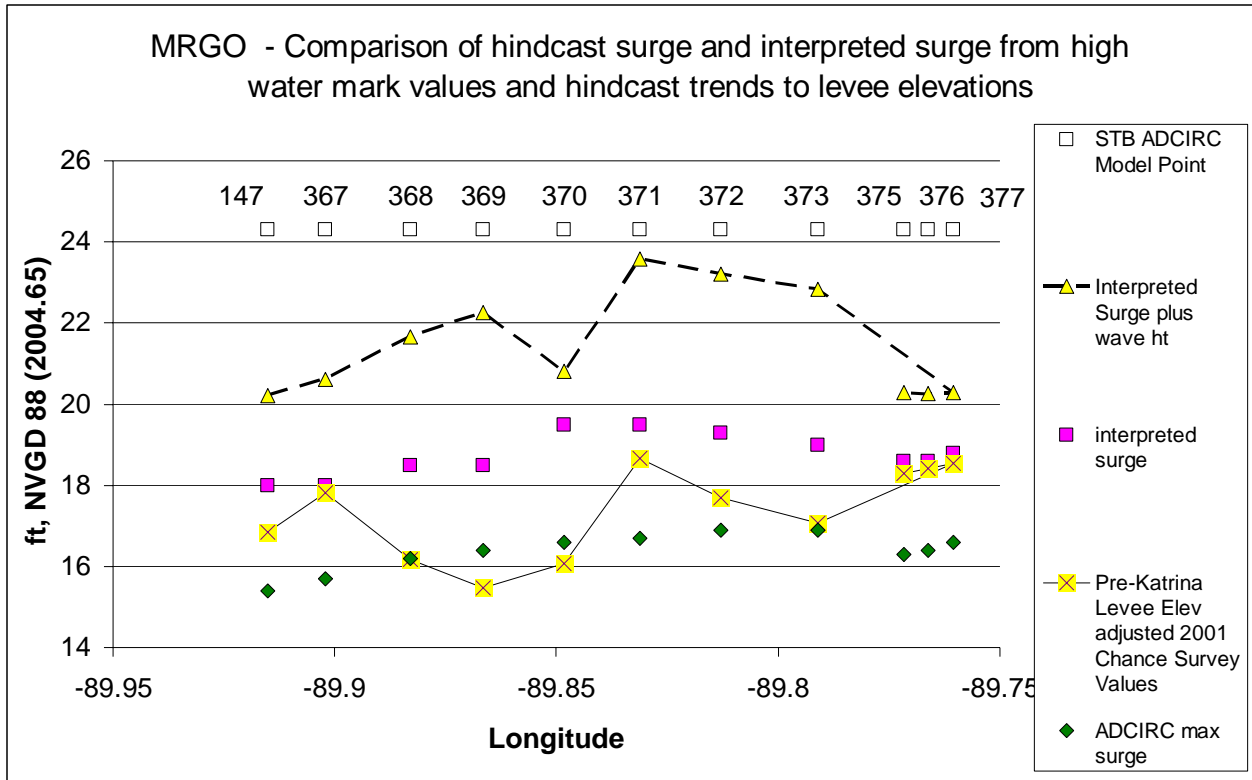
Figure 18-24. Estimated surges compared to levee heights along MRGO
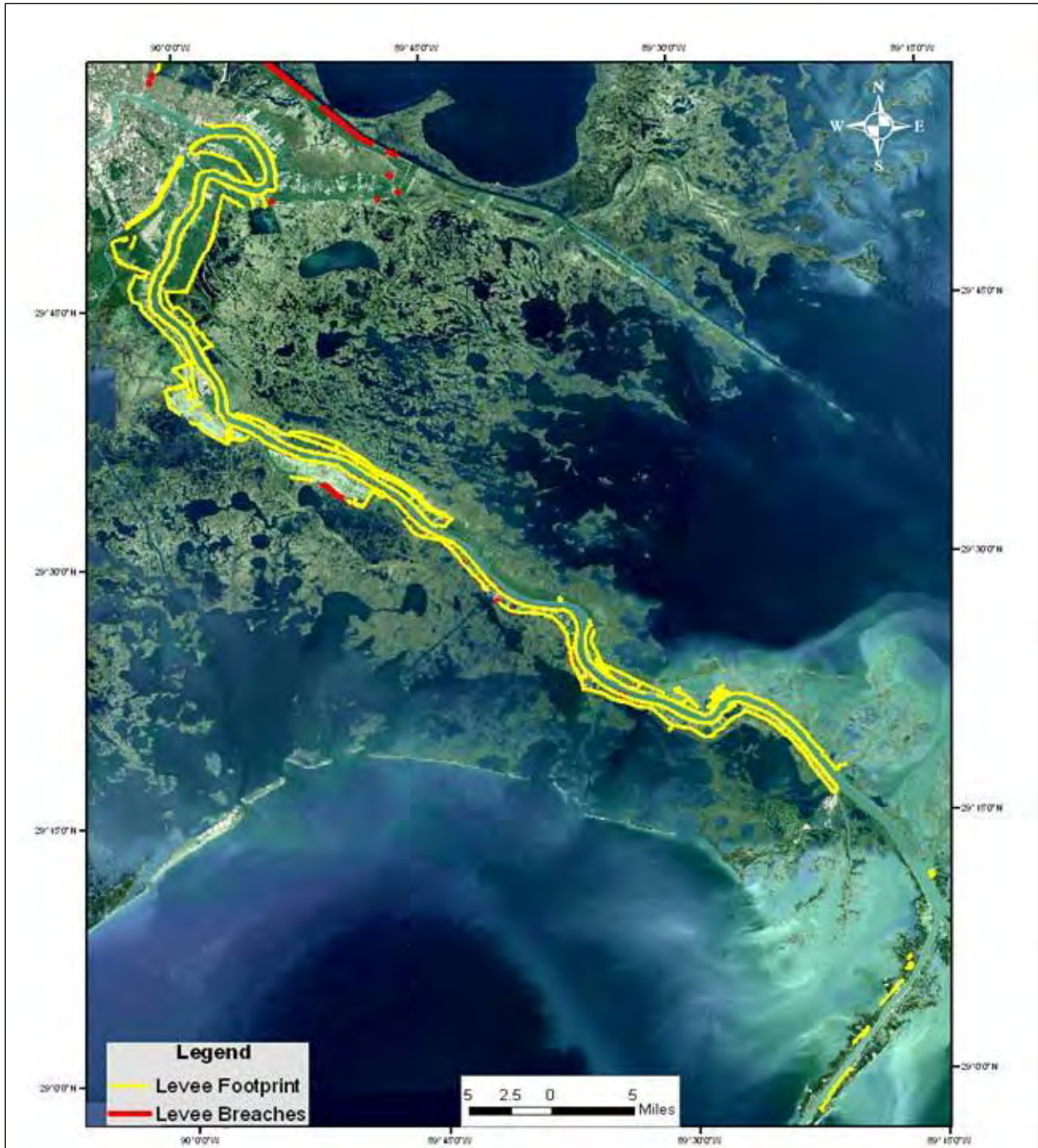
Figure 18-25. Breaches in Plaquemine Parish
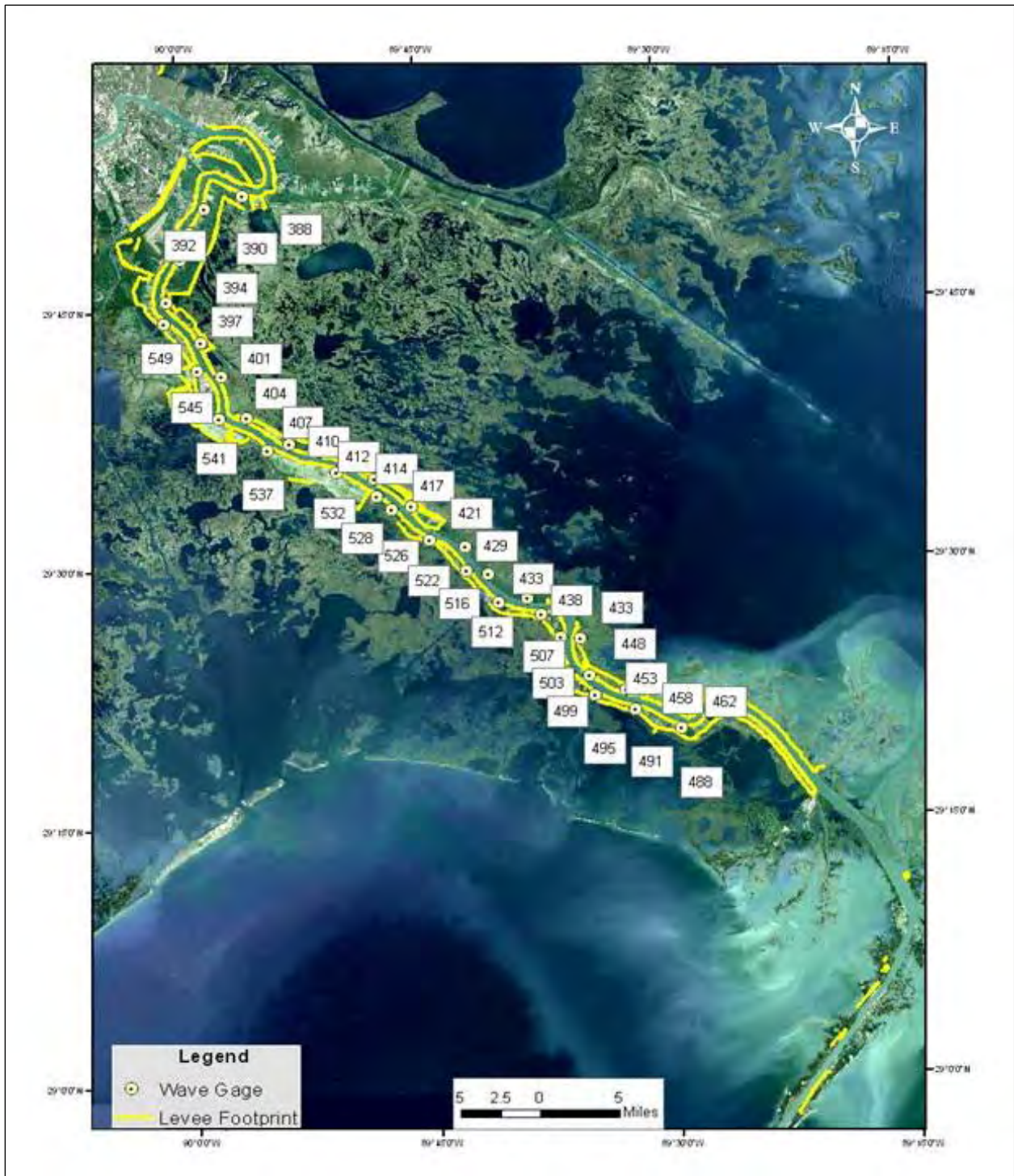
Figure 18-26. Selected ADCIRC model points for comparison of surge heights and levee heights

Attachment A
Plots Showing Damage to New Orleans East Back Levee

Volume V The Performance – Levees and Floodwalls – Technical Appendix
This is a preliminary report subject to revision; it does not contain final conclusions of the United States Army Corps of Engineers.

Volume V The Performance – Levees and Floodwalls – Technical Appendix

V-18-29

This is a preliminary report subject to revision; it does not contain final conclusions of the United States Army Corps of Engineers.

0 '
(3737932' , 599014')

3000 '
(3739611' , 601491')

Legend

Profile

0   500   1,000   1,500
                                    Feet

This is a preliminary report subject to revision; it does not contain final conclusions of the United States Army Corps of Engineers.

Legend

Profile

Elevation

+ 35 ft

- 10 ft

3000 '
(3739611' , 601491')

6000 '
(3740993' , 599949')

0	500	1,000	1,500

Feet

Volume V The Performance – Levees and Floodwalls – Technical Appendix

This is a preliminary report subject to revision; it does not contain final conclusions of the United States Army Corps of Engineers.

V-18-31

This is a preliminary report subject to revision; it does not contain final conclusions of the United States Army Corps of Engineers.

Legend

⎯⎯ **Profile**

6000 '
(3740993' , 599949')

3000 '
(3739611' , 601491')

0   500   1,000   1,500
Feet

This is a preliminary report subject to revision; it does not contain final conclusions of the United States Army Corps of Engineers.

6000 '
(3740993' , 599949')

9000 '
(3742245' , 597224')

Legend

Profile

Elevation

+ 35 ft

- 10 ft

0   500   1,000   1,500
                                    Feet

This is a preliminary report subject to revision; it does not contain final conclusions of the United States Army Corps of Engineers.

Volume V The Performance – Levees and Floodwalls – Technical Appendix

V-18-35

This is a preliminary report subject to revision; it does not contain final conclusions of the United States Army Corps of Engineers.

Legend

—— Profile

6000
(3740993' , 599949')

9000
(3742245' , 597224')

0   500   1,000   1,500
Feet

This is a preliminary report subject to revision; it does not contain final conclusions of the United States Army Corps of Engineers.

12000 '
(3743498' , 594500')

15000 '
(3745146' , 592520')

Legend

Profile

Elevation

+ 35 ft

- 10 ft

0   500   1,000   1,500
                                    Feet

This is a preliminary report subject to revision; it does not contain final conclusions of the United States Army Corps of Engineers.

12000 '
(3743498' , 594500')

15000 '
(3745146' , 592520')

Legend

Profile

0   500   1,000   1,500
Feet

Volume V The Performance – Levees and Floodwalls – Technical Appendix

V-18-39

This is a preliminary report subject to revision; it does not contain final conclusions of the United States Army Corps of Engineers.

15000⁰
(3745146' , 592520')

18000⁰
(3745670' , 589568')

Legend

Profile

Elevation

+ 35 ft

- 10 ft

0   500   1,000   1,500
Feet

Volume V The Performance – Levees and Floodwalls – Technical Appendix

This is a preliminary report subject to revision; it does not contain final conclusions of the United States Army Corps of Engineers.

V-18-41

15000
(3745146', 592520')

18000
(3745670', 589568')

Legend

Profile

| 0 | 500 | 1,000 | 1,500 |

Feet

This is a preliminary report subject to revision; it does not contain final conclusions of the United States Army Corps of Engineers.

18000⁰
(3745670' , 589568')

21000⁰
(3746190' , 586614')

Legend

Profile

Elevation

+ 35 ft

- 10 ft

0	500	1,000	1,500
			Feet

V-18-44

Volume V The Performance – Levees and Floodwalls – Technical Appendix
This is a preliminary report subject to revision; it does not contain final conclusions of the United States Army Corps of Engineers.

21000⁰
(3746190', 586614')

24000⁰
(3746727', 583664')

Legend

—— Profile

0   500   1,000   1,500
Feet

Volume V The Performance – Levees and Floodwalls – Technical Appendix

V-18-45

This is a preliminary report subject to revision; it does not contain final conclusions of the United States Army Corps of Engineers.

Legend

Profile

Elevation

+ 35 ft

- 10 ft

21000 (3746190', 586614')

24000 (3746727', 583664')

0   500   1,000   1,500
Feet

Volume V The Performance – Levees and Floodwalls – Technical Appendix

This is a preliminary report subject to revision; it does not contain final conclusions of the United States Army Corps of Engineers.

V-18-47

21000 ⁰
(3746190', 586614')

24000 ⁰
(3746727', 583664')

Legend

Profile

0   500   1,000   1,500
                          Feet

Volume V The Performance – Levees and Floodwalls – Technical Appendix
This is a preliminary report subject to revision; it does not contain final conclusions of the United States Army Corps of Engineers.

24000 0
(3746727', 583664')

27000 0
(3747252', 580713')

Legend

Profile

Elevation

+ 35 ft

- 10 ft

0   500   1,000   1,500
Feet

This is a preliminary report subject to revision; it does not contain final conclusions of the United States Army Corps of Engineers.

Legend

Profile

24000 (3746727 , 583664)

27000 (3747252 , 580713)

0   500   1,000   1,500
Feet

27000'
(3747252' , 580713')

30000'
(3747779' , 577761')

Legend

Profile

Elevation

+ 35 ft

- 10 ft

0	500	1,000	1,500

Feet

This is a preliminary report subject to revision; it does not contain final conclusions of the United States Army Corps of Engineers.

27000 ⁰
(3747252' , 580713')

30000 ⁰
(3747779' , 577761')

Legend

Profile

0   500   1,000   1,500
                                  Feet

Volume V The Performance – Levees and Floodwalls – Technical Appendix
This is a preliminary report subject to revision; it does not contain final conclusions of the United States Army Corps of Engineers.

30000 '
(3747779' , 577761')

33000 '
(3749239' , 575827')

Legend

Profile

Elevation

+ 35 ft

- 10 ft

0   500   1,000   1,500

Feet

Volume V The Performance – Levees and Floodwalls – Technical Appendix   V-18-55

This is a preliminary report subject to revision; it does not contain final conclusions of the United States Army Corps of Engineers.

33000 '
(3749239' , 575827')

36000 '
(3751990' , 575398')

Legend

Profile

0　　　　　500　　　　1,000　　　1,500
Feet

This is a preliminary report subject to revision; it does not contain final conclusions of the United States Army Corps of Engineers.

33000 '
(3749239', 575827')

36000 '
(3751990' , 575398')

Legend

Profile

0   500   1,000   1,500
Feet

This is a preliminary report subject to revision; it does not contain final conclusions of the United States Army Corps of Engineers.

36000 "
(3751990' , 575398')

39000 "
(3753996' , 573167')

Legend

Profile

Elevation

+ 35 ft

- 10 ft

0	500	1,000	1,500

Feet

This is a preliminary report subject to revision; it does not contain final conclusions of the United States Army Corps of Engineers.

36000 ⁰
(3751990' , 575398')

39000 ⁰
(3753996' , 573167')

Legend

Profile

0	500	1,000	1,500

Feet

Legend

Profile

Elevation

+ 35 ft

- 10 ft

39000 '
(3753996' , 573167')

42000 '
(3755326' , 570612')

V-18-64

Volume V The Performance – Levees and Floodwalls – Technical Appendix
This is a preliminary report subject to revision; it does not contain final conclusions of the United States Army Corps of Engineers.

Volume V The Performance – Levees and Floodwalls – Technical Appendix

This is a preliminary report subject to revision; it does not contain final conclusions of the United States Army Corps of Engineers.

V-18-65

39000 ⁰
(3753996' , 573167')

42000 ⁰
(3755326' , 570612')

Legend

Profile

0   500   1,000   1,500
Feet

This is a preliminary report subject to revision; it does not contain final conclusions of the United States Army Corps of Engineers.

42000 '
(3755326' , 570612')

45000 '
(3755825' , 567659')

Legend

Profile

Elevation

+ 35 ft

- 10 ft

0   500   1,000   1,500
Feet

This is a preliminary report subject to revision; it does not contain final conclusions of the United States Army Corps of Engineers.

This is a preliminary report subject to revision; it does not contain final conclusions of the United States Army Corps of Engineers.

42000 ⁰
(3755326' , 570612')

45000 ⁰
(3755825' , 567659')

Legend

Profile

0	500	1,000	1,500

Feet

Legend

Profile

Elevation

+ 35 ft

− 10 ft

45000 '
(3755825' , 567659')

48000 '
(3756040' , 564847')

| 0 | 500 | 1,000 | 1,500 |

Feet

This is a preliminary report subject to revision; it does not contain final conclusions of the United States Army Corps of Engineers.

Volume V The Performance – Levees and Floodwalls – Technical Appendix

V-18-71

This is a preliminary report subject to revision; it does not contain final conclusions of the United States Army Corps of Engineers.

This is a preliminary report subject to revision; it does not contain final conclusions of the United States Army Corps of Engineers.

This is a preliminary report subject to revision; it does not contain final conclusions of the United States Army Corps of Engineers.

This is a preliminary report subject to revision; it does not contain final conclusions of the United States Army Corps of Engineers.

48000 '

51000 '

Legend

Profile

| 0 | 500 | 1,000 | 1,500 |

Feet

Volume V The Performance – Levees and Floodwalls – Technical Appendix

V-18-75

This is a preliminary report subject to revision; it does not contain final conclusions of the United States Army Corps of Engineers.

This is a preliminary report subject to revision; it does not contain final conclusions of the United States Army Corps of Engineers.

This is a preliminary report subject to revision; it does not contain final conclusions of the United States Army Corps of Engineers.

3753500 3753000 3752500 3752000 3751500

563500

51000 '   54000 '

562000

562500

Legend

Profile

0   500   1,000   1,500
Feet

3753000 3752500 3752000 3751500 3751000 3750500

This is a preliminary report subject to revision; it does not contain final conclusions of the United States Army Corps of Engineers.

54000 '

57000 '

Volume V The Performance – Levees and Floodwalls – Technical Appendix

V-18-81

This is a preliminary report subject to revision; it does not contain final conclusions of the United States Army Corps of Engineers.

This is a preliminary report subject to revision; it does not contain final conclusions of the United States Army Corps of Engineers.

Volume V The Performance – Levees and Floodwalls – Technical Appendix
V-18-85

This is a preliminary report subject to revision; it does not contain final conclusions of the United States Army Corps of Engineers.

This is a preliminary report subject to revision; it does not contain final conclusions of the United States Army Corps of Engineers.

Legend

Profile

Elevation

+ 35 ft

- 10 ft

63000'

66000'

0   500   1,000   1,500
Feet

This is a preliminary report subject to revision; it does not contain final conclusions of the United States Army Corps of Engineers.

63000 '

66000 '

V-18-90

Volume V The Performance – Levees and Floodwalls – Technical Appendix
This is a preliminary report subject to revision; it does not contain final conclusions of the United States Army Corps of Engineers.

This is a preliminary report subject to revision; it does not contain final conclusions of the United States Army Corps of Engineers.

This is a preliminary report subject to revision; it does not contain final conclusions of the United States Army Corps of Engineers.

This is a preliminary report subject to revision; it does not contain final conclusions of the United States Army Corps of Engineers.

This is a preliminary report subject to revision; it does not contain final conclusions of the United States Army Corps of Engineers.

Legend

/ Profile

75000 (3733016', 555985')

72000 (3734495', 554428')

| 0 | 500 | 1,000 | 1,500 Feet |

Volume V The Performance – Levees and Floodwalls – Technical Appendix

This is a preliminary report subject to revision; it does not contain final conclusions of the United States Army Corps of Engineers.

V-18-99

75000 '
(3733016' , 555985')

78000 '
(3733051' , 558942')

Legend

Profile

Elevation

+ 35 ft

- 10 ft

0   500   1,000   1,500
Feet

Volume V The Performance – Levees and Floodwalls – Technical Appendix
This is a preliminary report subject to revision; it does not contain final conclusions of the United States Army Corps of Engineers.

75000 '
(3733016' , 555985')

78000 '
(3733051' , 558942')

Legend

Profile

0   500   1,000   1,500
                                        Feet

Volume V The Performance – Levees and Floodwalls – Technical Appendix

V-18-103

This is a preliminary report subject to revision; it does not contain final conclusions of the United States Army Corps of Engineers.

Volume V The Performance – Levees and Floodwalls – Technical Appendix

This is a preliminary report subject to revision; it does not contain final conclusions of the United States Army Corps of Engineers.

81000
(373472

78000
(3733051', 558942')

Legend

Profile

0	500	1,000	1,500

Feet

Volume V The Performance – Levees and Floodwalls – Technical Appendix

V-18-105

This is a preliminary report subject to revision; it does not contain final conclusions of the United States Army Corps of Engineers.

81000'
(3734725', 561075')

84000'
(3732620', 560357')

Legend

Profile

Elevation

+ 35 ft

- 10 ft

0   500   1,000   1,500
Feet

Volume V The Performance – Levees and Floodwalls – Technical Appendix
This is a preliminary report subject to revision; it does not contain final conclusions of the United States Army Corps of Engineers.

81000'
(3734725', 561075')

84000'
(3732620', 560357')

Legend

Profile

0	500	1,000	1,500

Feet

Volume V The Performance – Levees and Floodwalls – Technical Appendix
This is a preliminary report subject to revision; it does not contain final conclusions of the United States Army Corps of Engineers.

84000 °
(3732620' , 560357')

87000 '
(3731561' , 557785')

Legend

Profile

Elevation

+ 35 ft

- 10 ft

| 0 | 500 | 1,000 | 1,500 |

Feet

This is a preliminary report subject to revision; it does not contain final conclusions of the United States Army Corps of Engineers.

84000 ⁰
(3732620' , 560357')

87000 ⁰
(3731561' , 557785')

Legend

Profile

0   500   1,000   1,500
Feet

This is a preliminary report subject to revision; it does not contain final conclusions of the United States Army Corps of Engineers.

87000 '
(3731561' , 557785')

90000 '
(3731635' , 554786')

Legend

Profile

Elevation

+ 35 ft

- 10 ft

| 0 | 500 | 1,000 | 1,500 |
Feet

This is a preliminary report subject to revision; it does not contain final conclusions of the United States Army Corps of Engineers.

Volume V The Performance – Levees and Floodwalls – Technical Appendix

V-18-113

This is a preliminary report subject to revision; it does not contain final conclusions of the United States Army Corps of Engineers.

87000'
(3731561', 557785')

90000'
(3731635', 554786')

Legend

Profile

0   500   1,000   1,500
Feet

This is a preliminary report subject to revision; it does not contain final conclusions of the United States Army Corps of Engineers.

Legend

Profile

Elevation

+ 35 ft

- 10 ft

93000
(3730164' , 552943')

0   500   1,000   1,500
Feet

Volume V The Performance – Levees and Floodwalls – Technical Appendix   V-18-115

This is a preliminary report subject to revision; it does not contain final conclusions of the United States Army Corps of Engineers.

This is a preliminary report subject to revision; it does not contain final conclusions of the United States Army Corps of Engineers.

Legend

⟍ Profile

93000
(3730164' , 552943')

| 0 | 500 | 1,000 | 1,500 |
Feet

This is a preliminary report subject to revision; it does not contain final conclusions of the United States Army Corps of Engineers.

d

93000 '
(3730164' , 552943')

96000 '
(3727248' , 552240')

Legend

Profile

Elevation

+ 35 ft

- 10 ft

0   500   1,000   1,500
Feet

This is a preliminary report subject to revision; it does not contain final conclusions of the United States Army Corps of Engineers.

Volume V The Performance – Levees and Floodwalls – Technical Appendix

V-18-119

This is a preliminary report subject to revision; it does not contain final conclusions of the United States Army Corps of Engineers.

93000 '
(3730164' , 552943')

96000 '
(3727248' , 552240')

Legend

Profile

Elevation

+ 35 ft

- 10 ft

0	500	1,000	1,500

Feet

This is a preliminary report subject to revision; it does not contain final conclusions of the United States Army Corps of Engineers.

Attachment B
Plots Showing Damage to Chalmette Levee

Volume V The Performance – Levees and Floodwalls – Technical Appendix
This is a preliminary report subject to revision; it does not contain final conclusions of the United States Army Corps of Engineers.

Legend

⟍ Profile

Elevation

+ 35 ft

- 10 ft

0 '
(3722353' , 548727')

3000 '
(3725305' , 549258')

0   500   1,000   1,500
Feet

This is a preliminary report subject to revision; it does not contain final conclusions of the United States Army Corps of Engineers.

0'
(3722353', 548727')

3000'
(3725305', 549258')

Legend

Profile

0   500   1,000   1,500
Feet

This is a preliminary report subject to revision; it does not contain final conclusions of the United States Army Corps of Engineers.

3000 '
(3725305' , 549258')

6000 '
(3728201' , 548895')

Legend

Profile

Elevation

+ 35 ft

- 10 ft

0   500   1,000   1,500
                                          Feet

This is a preliminary report subject to revision; it does not contain final conclusions of the United States Army Corps of Engineers.

Volume V The Performance – Levees and Floodwalls – Technical Appendix

V-18-127

This is a preliminary report subject to revision; it does not contain final conclusions of the United States Army Corps of Engineers.

3000 '
(3725305' , 549258')

6000 '
(3728201' , 548895')

Legend

Profile

0   500   1,000   1,500
Feet

This is a preliminary report subject to revision; it does not contain final conclusions of the United States Army Corps of Engineers.

6000 '
(3728201' , 548895')

9000 '
(3730466' , 546937')

Legend

Profile

Elevation

+ 35 ft

- 10 ft

0   500   1,000   1,500
Feet

Volume V The Performance – Levees and Floodwalls – Technical Appendix   V-18-129

This is a preliminary report subject to revision; it does not contain final conclusions of the United States Army Corps of Engineers.

This is a preliminary report subject to revision; it does not contain final conclusions of the United States Army Corps of Engineers.

Legend

— Profile

6000 '
(372820.1', ,548895')

9000 '
(3730466' , 546937')

| 0 | 500 | 1,000 | 1,500 |
Feet

9000 '
(3730466' , 546937')

12000 '
(3732679' , 544920')

Legend

Profile

Elevation

+ 35 ft

- 10 ft

0   500   1,000   1,500
Feet

This is a preliminary report subject to revision; it does not contain final conclusions of the United States Army Corps of Engineers.

Volume V The Performance – Levees and Floodwalls – Technical Appendix

V-18-133

This is a preliminary report subject to revision; it does not contain final conclusions of the United States Army Corps of Engineers.

Legend

Profile

9000 '
(3730466' , 546937')

12000 '
(3732679' , 544920')

0   500   1,000   1,500
Feet

Volume V The Performance – Levees and Floodwalls – Technical Appendix
This is a preliminary report subject to revision; it does not contain final conclusions of the United States Army Corps of Engineers.

12000 '
(3732679' , 544920')

15000 '
(3734910' , 542917')

Legend

— Profile

Elevation

+ 35 ft

- 10 ft

0   500   1,000   1,500
Feet

This is a preliminary report subject to revision; it does not contain final conclusions of the United States Army Corps of Engineers.

12000 '
(3732679' , 544920')

15000 '
(3734910' , 542917')

Legend

Profile

0   500   1,000   1,500
                        Feet

This is a preliminary report subject to revision; it does not contain final conclusions of the United States Army Corps of Engineers.

15000 '
(3734910' , 542917')

18000 '
(3737127' , 540897')

Legend

Profile

Elevation

+ 35 ft

- 10 ft

| 0 | 500 | 1,000 | 1,500 |

Feet

This is a preliminary report subject to revision; it does not contain final conclusions of the United States Army Corps of Engineers.

This is a preliminary report subject to revision; it does not contain final conclusions of the United States Army Corps of Engineers.

15000 '
(3734910', 542917')

18000 '
(3737127', 540897')

Legend

Profile

0   500   1,000   1,500
Feet

Volume V The Performance – Levees and Floodwalls – Technical Appendix

This is a preliminary report subject to revision; it does not contain final conclusions of the United States Army Corps of Engineers.

18000 '
(3737127' , 540897')

21000 '
(3739354' , 538890')

Legend

Profile

Elevation

+ 35 ft

- 10 ft

0	500	1,000	1,500

Feet

This is a preliminary report subject to revision; it does not contain final conclusions of the United States Army Corps of Engineers.

18000 '
(3737127' , 540897')

21000 '
(3739354' , 538890')

Legend

Profile

0   500   1,000   1,500
Feet

21000 '
(3739354', 538890')

24000 '
(3741575', 536874')

Legend

Profile

Elevation

+ 35 ft

- 10 ft

0   500   1,000   1,500
Feet

V-18-144

21000 '
(3739354' , 538890')

24000 '
(3741575' , 536874')

Legend

Profile

0   500   1,000   1,500
                                Feet

This is a preliminary report subject to revision; it does not contain final conclusions of the United States Army Corps of Engineers.

24000 '
(3741575' , 536874')

27000 '
(3743800' , 534863')

Legend

Profile

Elevation

+ 35 ft

- 10 ft

0   500   1,000   1,500
Feet

Volume V The Performance – Levees and Floodwalls – Technical Appendix

This is a preliminary report subject to revision; it does not contain final conclusions of the United States Army Corps of Engineers.

Legend

⎯ Profile

24000 '
(3741575' , 536874')

27000 '
(3743800' , 534863')

0	500	1,000	1,500

Feet

This is a preliminary report subject to revision; it does not contain final conclusions of the United States Army Corps of Engineers.

Legend

⟍ Profile

Elevation

+ 35 ft

- 10 ft

27000 '
(3743800' , 534863')

30000 '
(3746036' , 532864')

0   500   1,000   1,500
Feet

This is a preliminary report subject to revision; it does not contain final conclusions of the United States Army Corps of Engineers.

Volume V The Performance – Levees and Floodwalls – Technical Appendix

This is a preliminary report subject to revision; it does not contain final conclusions of the United States Army Corps of Engineers.

V-18-151

24000 '
(3741575' , 536874')

27000 '
(3743800' , 534863')

Legend

Profile

0   500   1,000   1,500
Feet

This is a preliminary report subject to revision; it does not contain final conclusions of the United States Army Corps of Engineers.

30000 '
(3746036', 532864')

33000 '
(3748243', 530837')

Legend

Profile

Elevation

+ 35 ft

- 10 ft

0   500   1,000   1,500
                                        Feet

This is a preliminary report subject to revision; it does not contain final conclusions of the United States Army Corps of Engineers.

30000 '
(3746036', 532864')

33000 '
(3748243', 530837')

Legend

Profile

0   500   1,000   1,500
Feet

33000 '
(3748243' , 530837')

36000 '
(3750469' , 528826')

Legend

Profile

Elevation

+ 35 ft

- 10 ft

0   500   1,000   1,500
Feet

Volume V The Performance – Levees and Floodwalls – Technical Appendix
This is a preliminary report subject to revision; it does not contain final conclusions of the United States Army Corps of Engineers.

Volume V The Performance – Levees and Floodwalls – Technical Appendix

V-18-157

This is a preliminary report subject to revision; it does not contain final conclusions of the United States Army Corps of Engineers.

Legend

—— Profile

33000 '
(3748243' , 530837')

36000 '
(3750469' , 528826')

0   500   1,000   1,500
Feet

V-18-158

Volume V The Performance – Levees and Floodwalls – Technical Appendix
This is a preliminary report subject to revision; it does not contain final conclusions of the United States Army Corps of Engineers.

36000 '
(3750469' , 528826')

39000 '
(3752692' , 526812')

Legend

Profile

Elevation

+ 35 ft

- 10 ft

0   500   1,000   1,500
                                        Feet

This is a preliminary report subject to revision; it does not contain final conclusions of the United States Army Corps of Engineers.

36000'
(3750469' , 528826')

39000'
(3752692' , 526812')

Legend

Profile

0   500   1,000   1,500
Feet

This is a preliminary report subject to revision; it does not contain final conclusions of the United States Army Corps of Engineers.

39000 '
(3752692' , 526812')

42000 '
(3754916' , 524799')

Legend

⟍ Profile

Elevation

+ 35 ft

- 10 ft

| 0 | 500 | 1,000 | 1,500 |
Feet

Volume V The Performance – Levees and Floodwalls – Technical Appendix
This is a preliminary report subject to revision; it does not contain final conclusions of the United States Army Corps of Engineers.

Volume V The Performance – Levees and Floodwalls – Technical Appendix

V-18-163

This is a preliminary report subject to revision; it does not contain final conclusions of the United States Army Corps of Engineers.

Legend

⎯⎯ Profile

39000 '
(3752692' , 526812')

42000 '
(3754916' , 524799')

0   500   1,000   1,500
⎯⎯⎯⎯⎯⎯⎯⎯⎯⎯⎯⎯⎯⎯⎯⎯ Feet

V-18-164

Volume V The Performance – Levees and Floodwalls – Technical Appendix
This is a preliminary report subject to revision; it does not contain final conclusions of the United States Army Corps of Engineers.

Legend

⎯ Profile

Elevation

+ 35 ft

- 10 ft

42000 '
(3754916' , 524799')

45000 '
(3757136' , 522783')

0	500	1,000	1,500

Feet

This is a preliminary report subject to revision; it does not contain final conclusions of the United States Army Corps of Engineers.

42000 '
(3754916' , 524799')

45000 '
(3757136' , 522783')

Legend

Profile

0	500	1,000	1,500

Feet

45000 '
(3757136' , 522783')

48000 '
(3759359' , 520770')

Legend

Profile

Elevation

+ 35 ft

− 10 ft

0	500	1,000	1,500

Feet

This is a preliminary report subject to revision; it does not contain final conclusions of the United States Army Corps of Engineers.

Volume V The Performance – Levees and Floodwalls – Technical Appendix

This is a preliminary report subject to revision; it does not contain final conclusions of the United States Army Corps of Engineers.

V-18-169

45000 '
(3757136' , 522783')

48000 '
(3759359' , 520770')

Legend

Profile

0	500	1,000	1,500

Feet

This is a preliminary report subject to revision; it does not contain final conclusions of the United States Army Corps of Engineers.

Legend

—— Profile

Elevation

+ 35 ft

- 10 ft

48000 '
(3759359', 520770')

51000 '
(3761581', 518754')

0		500		1,000		1,500
Feet

Volume V The Performance – Levees and Floodwalls – Technical Appendix

V-18-171

This is a preliminary report subject to revision; it does not contain final conclusions of the United States Army Corps of Engineers.

This is a preliminary report subject to revision; it does not contain final conclusions of the United States Army Corps of Engineers.

Legend
Profile

48000 '
(3759359' , 520770')

51000 '
(3761581' , 518754')

0   500   1,000   1,500
Feet

This is a preliminary report subject to revision; it does not contain final conclusions of the United States Army Corps of Engineers.

Legend

Profile

Elevation

+ 35 ft

- 10 ft

51000 '
(3761581' , 518754')

54000 '
(3763962' , 516942')

0   500   1,000   1,500
Feet

Volume V The Performance – Levees and Floodwalls – Technical Appendix

V-18-175

This is a preliminary report subject to revision; it does not contain final conclusions of the United States Army Corps of Engineers.

Legend

Profile

51000 '
(3761581' , 518754')

54000 '
(3763962' , 516942')

0   500   1,000   1,500
                                          Feet

Volume V The Performance – Levees and Floodwalls – Technical Appendix
This is a preliminary report subject to revision; it does not contain final conclusions of the United States Army Corps of Engineers.

54000 '
(3763962' , 516942')

57000 '
(3766572' , 515466')

Legend

Profile

Elevation

+ 35 ft

- 10 ft

0	500	1,000	1,500

Feet

This is a preliminary report subject to revision; it does not contain final conclusions of the United States Army Corps of Engineers.

This is a preliminary report subject to revision; it does not contain final conclusions of the United States Army Corps of Engineers.

Legend

Profile

54000 '
(3763962' , 516942')

57000 '
(3766572' , 515466')

0   500   1,000   1,500
                              Feet

Volume V The Performance – Levees and Floodwalls – Technical Appendix

This is a preliminary report subject to revision; it does not contain final conclusions of the United States Army Corps of Engineers.

V-18-179

Legend

Profile

Elevation

+ 35 ft

- 10 ft

57000 '
(3766572' , 515466')

60000 '
(3769183' , 513988')

0   500   1,000   1,500
Feet

Volume V The Performance – Levees and Floodwalls – Technical Appendix
This is a preliminary report subject to revision; it does not contain final conclusions of the United States Army Corps of Engineers.

Volume V The Performance – Levees and Floodwalls – Technical Appendix

V-18-181

This is a preliminary report subject to revision; it does not contain final conclusions of the United States Army Corps of Engineers.

Legend

／ Profile

57000'
(3766572', 515466')

60000'
(3769183', 513988')

0   500   1,000   1,500
━━━━━━━━━━━━━━ Feet

This is a preliminary report subject to revision; it does not contain final conclusions of the United States Army Corps of Engineers.

60000 '
(3769183' , 513988')

63000 '
(3771794' , 512512')

Legend

Profile

Elevation

+ 35 ft

- 10 ft

0   500   1,000   1,500
                                    Feet

60000 '
(3769183' , 513988')

63000 '
(3771794' , 512512')

Legend

Profile

0   500   1,000   1,500
Feet

63000 '
(3771794', 512512')

66000 '
(3774406', 511037')

Legend

Profile

Elevation

+ 35 ft

- 10 ft

| 0 | 500 | 1,000 | 1,500 |
Feet

Volume V The Performance – Levees and Floodwalls – Technical Appendix
This is a preliminary report subject to revision; it does not contain final conclusions of the United States Army Corps of Engineers.

63000 '
(3771794' , 512512')

66000 '
(3774406' , 511037')

Legend

Profile

0   500   1,000   1,500
Feet

66000 '
(3774406', 511037')

69000 '
(3777017', 509562')

Legend

Profile

Elevation

+ 35 ft

- 10 ft

0   500   1,000   1,500
Feet

This is a preliminary report subject to revision; it does not contain final conclusions of the United States Army Corps of Engineers.

66000 '
(3774406' , 511037')

69000 '
(3777017' , 509562')

Legend

Profile

0   500   1,000   1,500
                              Feet

This is a preliminary report subject to revision; it does not contain final conclusions of the United States Army Corps of Engineers.

69000 '
(3777017' , 509562')

72000 '
(3779523' , 508049')

Legend

— Profile

Elevation

+ 35 ft

- 10 ft

0   500   1,000   1,500
Feet

This is a preliminary report subject to revision; it does not contain final conclusions of the United States Army Corps of Engineers.

Volume V The Performance – Levees and Floodwalls – Technical Appendix

V-18-193

This is a preliminary report subject to revision; it does not contain final conclusions of the United States Army Corps of Engineers.

69000 '
(3777017' , 509562')

72000 '
(3779523' , 508049')

Legend

Profile

0   500   1,000   1,500
Feet

Volume V The Performance – Levees and Floodwalls – Technical Appendix
This is a preliminary report subject to revision; it does not contain final conclusions of the United States Army Corps of Engineers.

72000 '
(3779523' , 508049')

75000 '
(3778239' , 505337')

Legend

Profile

Elevation

+ 35 ft

- 10 ft

0   500   1,000   1,500
Feet

Volume V The Performance – Levees and Floodwalls – Technical Appendix
This is a preliminary report subject to revision; it does not contain final conclusions of the United States Army Corps of Engineers.

V-18-195

This is a preliminary report subject to revision; it does not contain final conclusions of the United States Army Corps of Engineers.

72000 '
(3779523' , 508049')

75000 '
(3778239' , 505337')

Legend

Profile

| 0 | 500 | 1,000 | 1,500 |

Feet

Volume V The Performance – Levees and Floodwalls – Technical Appendix

This is a preliminary report subject to revision; it does not contain final conclusions of the United States Army Corps of Engineers.

V-18-197

75000 '
(3778239' , 505337')

78000 '
(3776958' , 502625')

Legend

Profile

Elevation

+ 35 ft

- 10 ft

0   500   1,000   1,500
Feet

Volume V The Performance – Levees and Floodwalls – Technical Appendix
This is a preliminary report subject to revision; it does not contain final conclusions of the United States Army Corps of Engineers.

Volume V The Performance – Levees and Floodwalls – Technical Appendix

This is a preliminary report subject to revision; it does not contain final conclusions of the United States Army Corps of Engineers.

V-18-199

75000 '
(3778239' , 505337')

78000 '
(3776958' , 502625')

Legend

Profile

0	500	1,000	1,500

Feet

This is a preliminary report subject to revision; it does not contain final conclusions of the United States Army Corps of Engineers.

78000 '
(3776958' , 502625')

81000 '
(3775679' , 499911')

Legend

—— Profile

Elevation

+ 35 ft

- 10 ft

0   500   1,000   1,500
                                              Feet

This is a preliminary report subject to revision; it does not contain final conclusions of the United States Army Corps of Engineers.

78000 '
(3776958' , 502625')

81000 '
(3775679' , 499911')

Legend

Profile

| 0 | 500 | 1,000 | 1,500 |

Feet

81000 '
(3775679' , 499911')

82825 '
(3774898' , 498260')

Legend

Profile

Elevation

+ 35 ft

- 10 ft

0	500	1,000	1,500

Feet

V-18-204

Volume V The Performance – Levees and Floodwalls – Technical Appendix
This is a preliminary report subject to revision; it does not contain final conclusions of the United States Army Corps of Engineers.

This is a preliminary report subject to revision; it does not contain final conclusions of the United States Army Corps of Engineers.

81000 '
(3775679' , 499911')

82825 '
(3774898' , 498260')

Legend

Profile

0   500   1,000   1,500
Feet

Volume V The Performance – Levees and Floodwalls – Technical Appendix
This is a preliminary report subject to revision; it does not contain final conclusions of the United States Army Corps of Engineers.
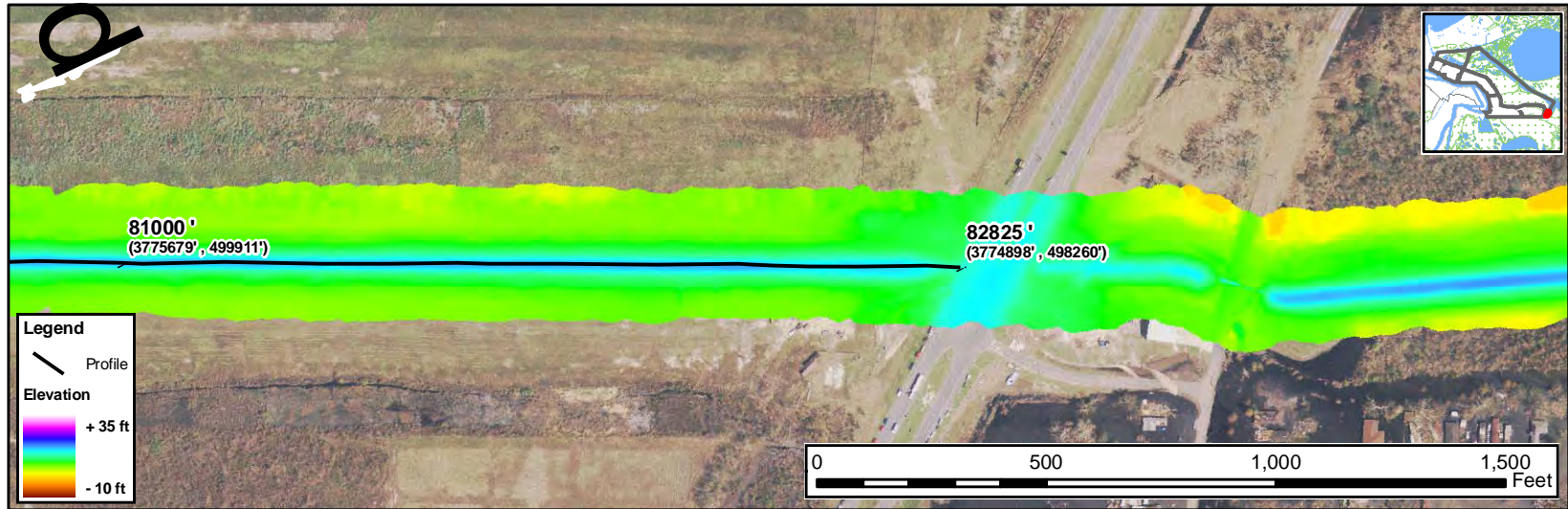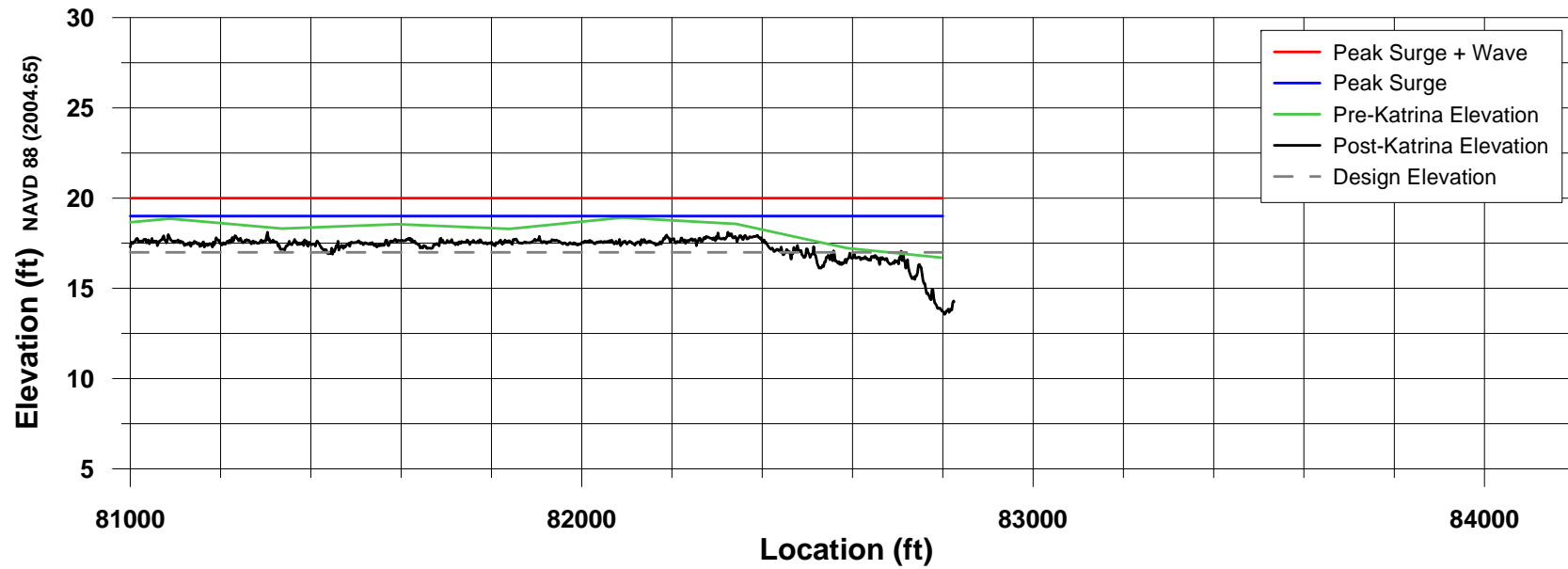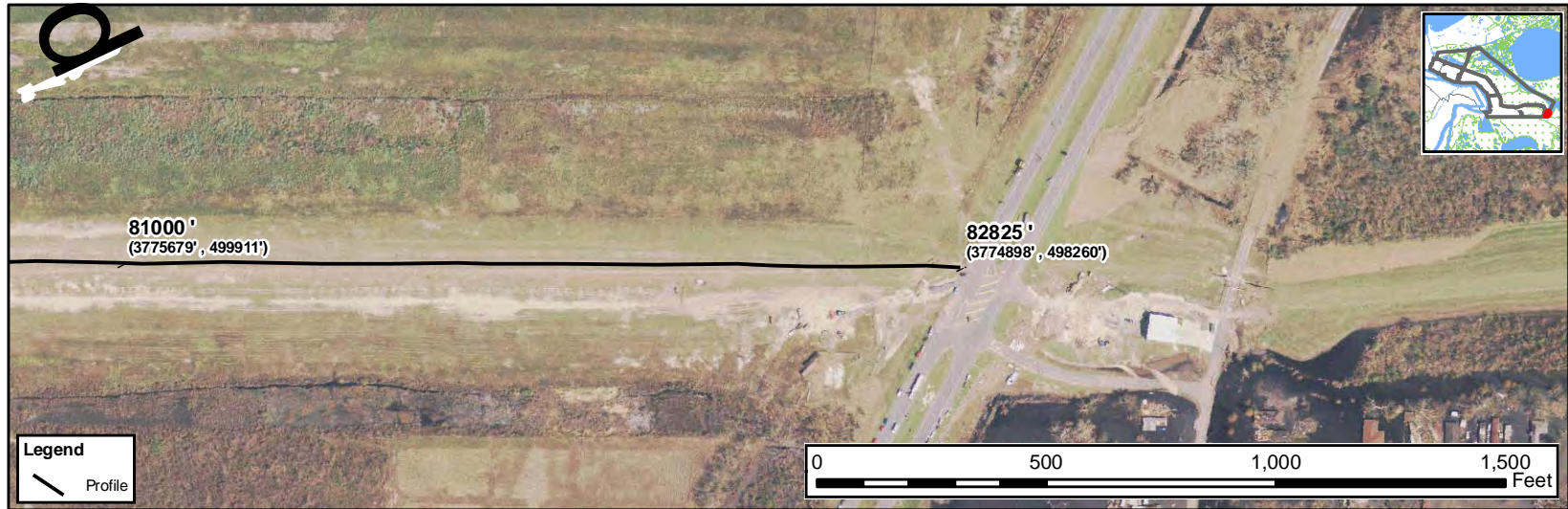
Appendix 19
FLAC Numerical Analyses of Floodwalls of New Orleans Flood Protection System

SSI Analyses of 17th St., London North, & London South Breaches

Background

A study was undertaken to analyze the performance of levees and floodwalls used in the New Orleans flood protection system to determine the most likely causes of their damage and failure from Hurricane Katrina. This study was conducted by the Interagency Performance Evaluation Task Force (IPET) and included 2D soil-structure interaction (SSI) numerical modeling. These modeling efforts support an investigation into how individual sections of the floodwall and levee system respond to the computed forces to better understand failure mechanisms and to explain phenomena observed in the field. These SSI analyses were conducted using the PC-based programs, Plaxis (Brinkgreve, 2004) and FLAC (Itasca, 1998). This report presents the results of the FLAC analyses.

Following a sequence of increasingly complex analyses provides a reasonable path when dealing with the challenging task of failure mode analysis. This is especially important since each additional step requires concomitant input data which is usually increasingly difficult to provide. Still the effort involved in SSI analyses offer potential advantages over limit equilibrium (whether or not a simple or more complex material model is used): a) better estimate of failure surface geometry, b) ability to handle strain interaction between stiff and soft materials, particularly if some of the materials may be strain softening, c) ability to obtain a relationship between deformation and safety factor, and d) ability to more easily couple the seepage and stress analyses.

Therefore, concurrent numerical analyses using Plaxis and FLAC were undertaken to provide a more thorough investigation. These coordinated but distinct analyses provided the advantage of comparing results from different numerical analysis software. The expected variations that permitted a measure of the robustness of the estimated results are the use of different model geometries, constitutive models, numerical solution schemes, and the numerical analysts. While the expected differences noted above should provide some variance among the results the

independence of this effort was necessarily constrained. All analyses relied on a common site characterization and material property assessment, system response insight provided by the prior limit equilibrium analyses, and collected field evidence on failure modes and flood water levels (IPET Stability Analyses, 2006). The analyzed sections were closely coordinated and consistent regarding section geometry control points, material properties, boundary conditions and failure mode assumptions.

The FLAC (Fast Lagrangian Analysis of Continua) numerical geotechnical analysis program was selected because it is well recognized, commercially available, and routinely used in geotechnical engineering practice. FLAC is an explicit, finite difference program that uses a Lagrangian formulation for performing large strain analyses. This program is capable of modeling two-dimensional problems in soil-structure interaction with full coupling of the stress-strain and groundwater flow components. Available constitutive models include linear elastic to non-linear plasticity-based models. FLAC also provides the capability of inputting user-defined constitutive models or making minor modifications to built-in models.

One of the distinct and significant differences between the FLAC and Plaxis programs is the method used to solve the equilibrium equations. FLAC uses an explicit solution scheme in which the dynamic equilibrium equations are solved at each of the nodal masses over a series of small timesteps. This dynamic solution process is used for static problems by ensuring enough timesteps are solved to reach equilibrium. Plaxis uses an implicit scheme which involves solution of the entire stiffness matrix of the structure. Although the equations solved in Plaxis are more computationally intensive, a solution may be achieved in significantly fewer steps.

A second key difference between the FLAC and Plaxis analyses is the formulation of the basic soil element. FLAC uses a very simple 4-noded quadrilateral element that is numerically constructed from overlaid pairs of constant strain triangular elements. Although this uncomplicated element allows for extremely fast stress-strain estimates, a relatively fine grid may be required to properly represent the variation of stress and strain within the structure. The finite element used in Plaxis is significantly more complex. In the analyses for the 17th St. Canal, 15-noded elements, each with 12 integration points, were used to model the soil.

Stability analyses were conducted with FLAC to investigate the following failure sections: 17th St. Outfall Canal breach (Station 10+00), and the two breaches on the London Outfall Canal (London North breach near the Robert E. Lee Boulevard bridge Station: 14+00 and London South breach near the Mirabeau St. bridge Station 53+00). The locations of these breached sections are show in Figures 19-1 and 19-2. These figures show two important geologic factors that were significant in the response of these floodwalls. First, the general near-surface geologic setting was mash-swamp deposits providing the possibility of low-strength clay and peat foundation soils. Secondly, a significant sand deposit that trends through the area is very shallow at London's south and north breaches, but found much deeper at 17th St. breach site. The general foundation soils stratigraphy to an approximate depth of 80 ft was idealized and modeled with material zones: levee clay, clay top soil, peat, lacustrine clay, beach sand, bay sound clay, and finally the Pleistocene clays.

A relatively brief description of each analysis is provided since much of the material and geometric description has already been provided in the other IPET reports.
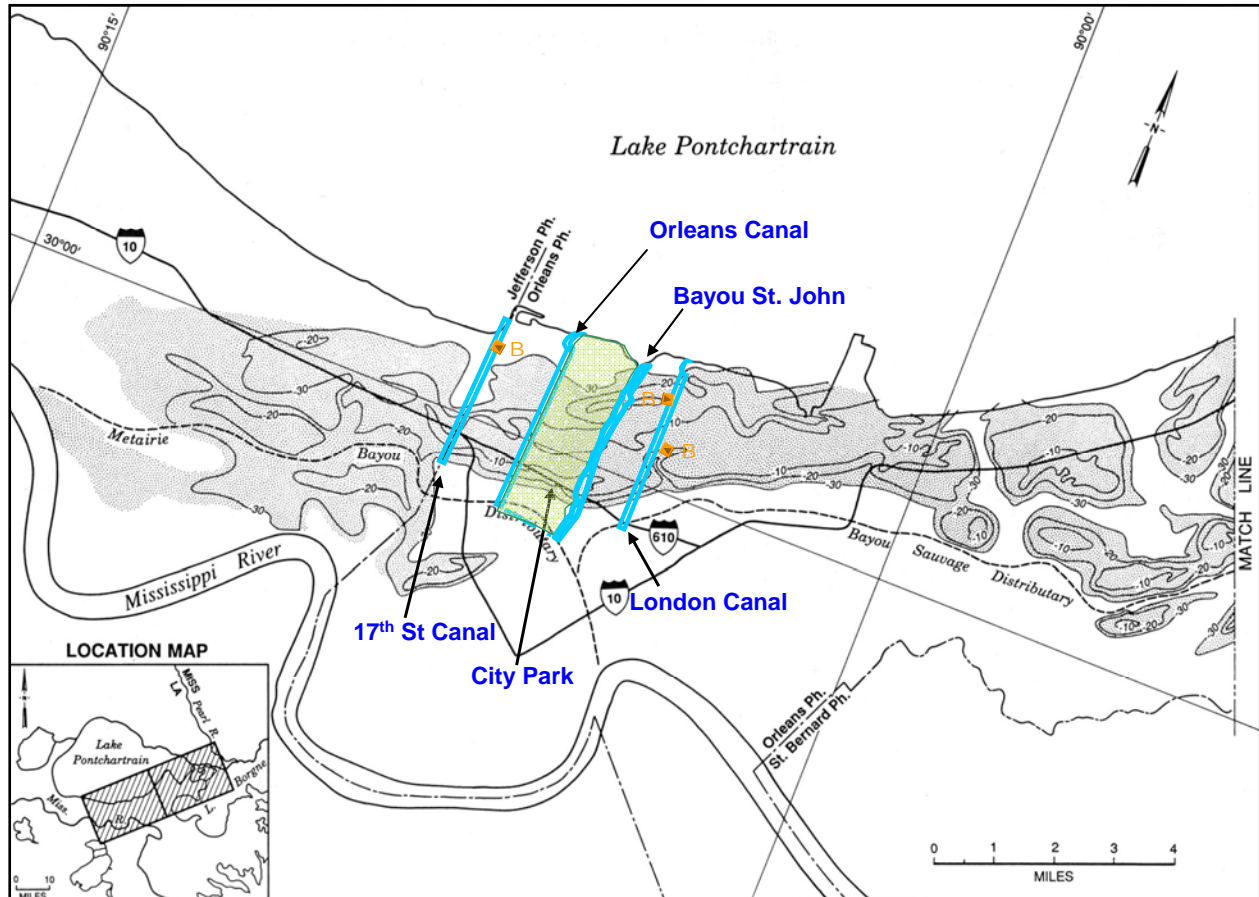

Figure 19-1. Location of breach sections analyzed plotted on a map of depth to beach sand deposit (showing why sands in foundation were important to London Canal breaches and probably not the 17th St. breach)
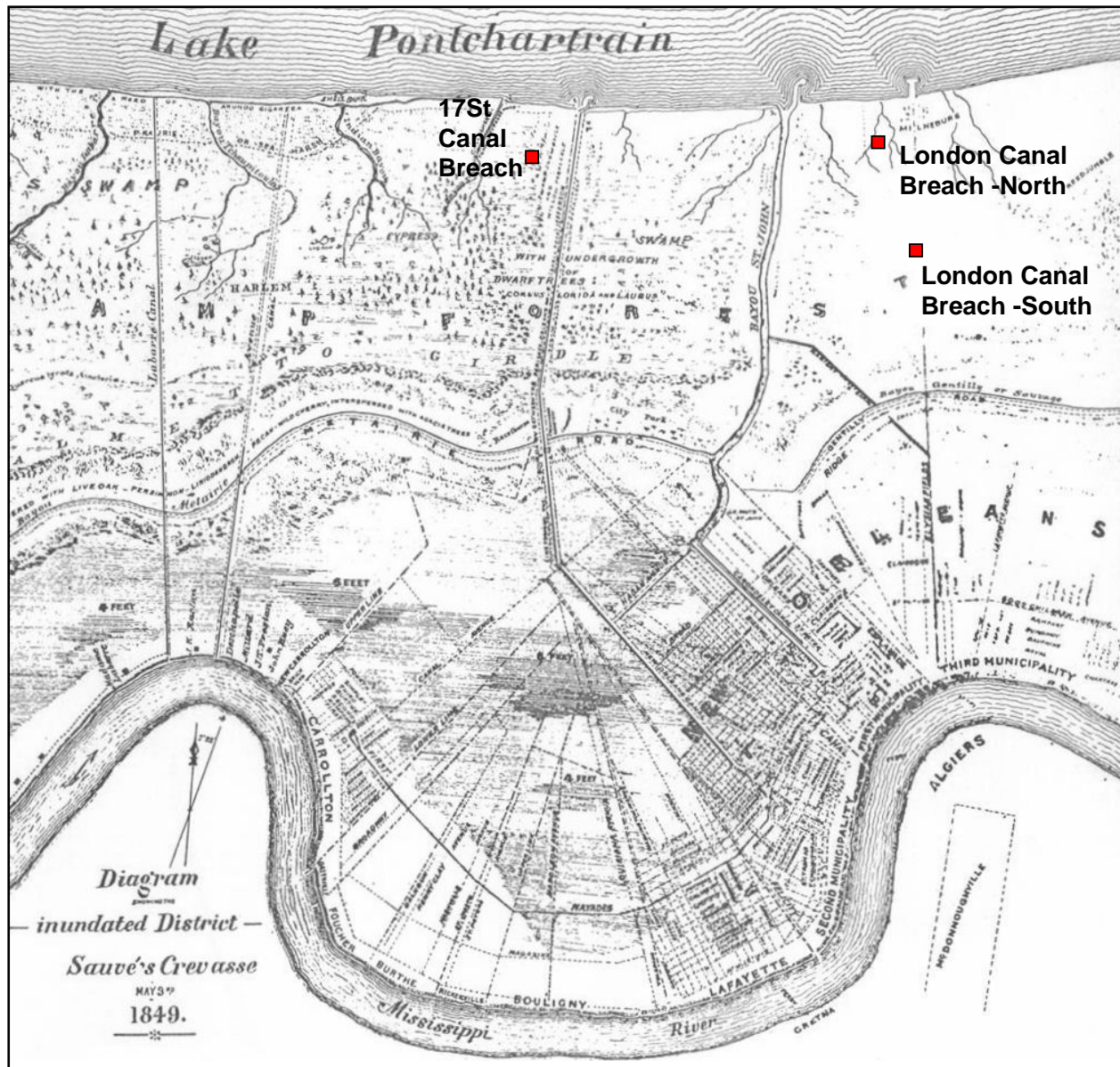
Figure 19-2. Near-surface geologic deposition environment and significant marsh-swamp peat and soft clay conditions

17th St. Outfall Canal Breach Analysis

The 17th St. Outfall Canal breach was analyzed using both a linear-perfectly plastic Mohr-Coulomb model, and a non-linear constitutive model. Both analyses used a total stress approach for representing the undrained behavior of the finer-grained soils. The canal section at Station 10+00 was used in the analysis. This section is composed of concrete and steel sheet-pile I-wall floodwall built into the centerline of the earthen levee. The findings of the limit equilibrium stability analyses showed that given the wall failure at an estimated canal water level of 6.5 ft (all elevations are referenced to NAD88 datum unless noted), introducing a full depth crack from

surface to pile tip resulted in Factor of Safety of 0.88. Without introduction of a crack, the Factor of Safety is 1.62 (IPET, 2006). This assumed crack or gap between the sheet pile wall and canal side embankment is a significant factor in these analyses. The IPET field reconnaissance study documented this condition along intact wall panels adjacent to the London North breach and along the distressed floodwall on the east side across from this breach. This response of the I-walls was also noted in places along the Inner Harbor Navigation Canal. The water level in 17th St. Canal submerged any visual evidence for this breach. The "crack" or gap between the sheet pile wall and soil embankment on the canal side was introduced into the model and its occurrence is supported with simple stress analyses.

Linear-perfectly plastic Mohr-Coulomb Analysis

This FLAC analysis uses a simple plasticity based model where the failure envelope follows the Mohr-Coulomb criterion and all stress increments below the failure envelope are considered linear elastic. The use of such a simple model can be acceptable when the strength of the material governs the behavior and other effects such as stiffness or potential strain softening are secondary. The Mohr-Coulomb model appeared suitable for this evaluation given the characterization provided for the various soil units: linearly-varying undrained strengths and average secant stiffness (E_{50}) as a simple multiple of undrained strength.

The two primary objectives of this analysis were 1) to determine if a failure consistent with the observed behavior would be predicted by FLAC using the provided site characterization, and 2) to provide a basis of comparison to other analyses performed on the same section. A thorough evaluation of the response, including sensitivity or parametric studies, was not performed.

Approach

The general development of the FLAC model was kept consistent with the Plaxis and limit equilibrium analyses by strictly adhering to the provided site interpretation. Key parameters provided for the FLAC analysis included the stratigraphic and geometric description, unit weights, undrained strength for fine grained soils, drained strength for the Beach Sand layer, and average secant elastic modulus (E_{50}) for the fine grained soils. A tensile strength was also assumed for the fine grained soils to permit the prediction of a gap adjacent to the sheet pile wall. Soil properties were assigned element by element to provide for smoothly changing properties consistent with the specified variations.

The floodwall was represented with the structural beam elements included in the FLAC program. Structural properties for the wall were input as provided. The beam element interacted with the soil grid through interface elements on each side of the structure. These interface elements were assigned zero tensile strength and assumed to have a relatively low shear strength equal to 2/3 of the adjacent soil strength.

A total stress formulation based on the undrained strengths and stiffnesses was used to evaluate the response to the flood loading.

The analysis was performed in small strain mode to eliminate the potential grid distortion caused when predicted element strains become very large. Large strain analyses can be useful when the predicted deformations have a significant influence on the stability of the section. Such changes in stability are often the result of a decrease in driving force or an increase in the resisting or buttressing force. However, the initial deformations predicted for the levee were dominated by lateral sliding with relatively little change expected in the stability. The small strain formulation is considered adequate for predicting the modest displacements related to impending failure. However, the magnitude and pattern of the very large displacements associated with failure may be influenced by this simplification.

The FLAC grid is shown in Figure 19-3. As can be seen, the model space is well sampled and uniform allowing the simple quadrilateral zone elements to accurately capture the model response.

Solution procedure

The steady state pore pressure distribution resulting from a canal water surface elevation of 1 ft was estimated using a seepage analysis. The boundary conditions were consistent with the Plaxis analysis and relative values of hydraulic conductivity were assumed. The seepage analysis produced a reasonable distribution of pore pressures across the grid as shown in Figure 19-4. The effect of the sheet pile wall on the pore pressures and flow vectors is clearly seen.

The initial state of effective stress in the model was estimated using a sequence of elastic and plastic analyses. The objective of these analyses was to establish an initial state of stress that was in equilibrium and that had values of horizontal effective stresses that reflected the geometry and strength of the material. Drained strengths were assumed during the plastic analyses to help achieve this goal. Although a more refined estimate of the initial stress state could be made using a non-linear constitutive model and imposing the loading or construction history, initial stress states are difficult to accurately estimate given the many unknowns and the stress redistribution that may occur with time. The initial stress state is shown in Figure 19-5, and contours of the fraction of mobilized shear strength are shown in Figure 19-6.

The flood analysis was performed incrementally to reduce the dynamic response related to the loading of each flood increment. Water levels were increased in the canal a maximum of 0.5 to 1.0 feet per increment. Equilibrium conditions were achieved at each increment before increasing the water surface elevation (WSE).

The development of a gap between the sheet pile wall and soil on the canal side of the levee had been identified as potentially critical prior to performing the FLAC analysis. A subroutine was added that automatically determined if a crack could occur based on the prediction of horizontal effective stress between the wall and soil. The subroutine was executed at the end of the calculations for each flood stage. This routine checked the stresses in the uppermost element against the wall. If the horizontal effective stresses were found to be compressive, then the routine assumed a crack would not propagate and the solution for the next flood increment would begin. However, if the effective stresses in the element were tensile, then the crack was assumed to propagate across that element: the interface would be removed and the full hydrostatic force

and pore pressure was applied to the edge of the soil element as well as the wall. The analysis was then stepped to equilibrium and crack propagation was evaluated across the next lower element. Pressures within the crack were updated at every flood increment.

Although the crack subroutine appeared to produce a final gap consistent with expectations, there are a couple of uncertainties with this approach. First, crack propagation depends upon accurate prediction of horizontal effective stresses. As this is not an easy task to accurately achieve, it would be reasonable to include a safety factor in the crack propagation routine. In addition, the Mohr-Coulomb model may not give the best prediction of horizontal stresses at states below failure. And second, the above routine used the effective stress in the soil element to estimate tensile conditions. This effective stress was based on the pore pressure predicted in the soil, which was typically less than the hydrostatic pressure based on the current flood stage. Because the crack propagates along the predefined interface between the wall and soil, and the opening of the crack could expose the crack tip to the full hydrostatic pressure, it seems reasonable to revise the routine so that the effective stress is based on the hydrostatic pressure rather than the predicted pore pressure.

Analysis Results and Discussion

Using the assumptions for crack formation described above, the crack was estimated to initiate during the first flood increment which had a WSE of 2.0 feet. The initial crack or gap was 5 feet deep, which gradually increased to the full 16 foot depth when the WSE reached 9.5 feet. The initiation and growth of a crack is shown to greatly increase the displacements and leads to a response indicative of impending failure. Figure 19-7 shows the predicted maximum displacements of the wall and soil as well as crack depth versus WSE. In comparison, the Plaxis analysis used a different crack initiation criteria based on hydrostatic pressure exceeding total horizontal stress. This approach has the crack initiate at WSE of 6.5 ft and extend to the marsh-lacustrine clay interface which is 2 ft above the sheet pile tip. In this analysis, the crack started at a lower flood stage but developed slower, not reaching this depth until a WSE of 8.5 ft.

The predicted response following formation of a full depth crack to the tip of the sheet pile shows a failure surface beginning at base of sheet pile and extending horizontally near the top of the Lacustrine Clay layer until turning upward and exiting the surface roughly 60 ft from wall on protected side. This is illustrated in Figures 19-8 and 19-9 which show deformed shapes and contours of maximum shear strain. The model also predicts that at a WSE of 10 ft there is sufficient wall movement, approximately 7 ft, to assume the wall section is breached. Also, although the model was in equilibrium but certainly breached for 10 ft WSE, an additional 0.5 ft rise in the water level produced additional deformations, and the modeled section could not reach equilibrium. Furthermore, the predicted wall displacements at lower flood levels such as 8.5 ft are still considerable, greater that 2 ft, Figure 19-11, which may be sufficient to separate individual wall panels and initiate a breach before the unstable condition posed by the 10.5 WSE. Accommodating over 2 feet of displacement would require a broad smooth intact deformation of a section of wall panels. The field reconnaissance documented severe distress to the wall section directly across from the London north breach that was near failure and had a gap

of approximately 2 ft at the top of soil embankment. The predicted failure surface is clearly displayed in Figure 19-9 in contour plots of maximum shear strain.
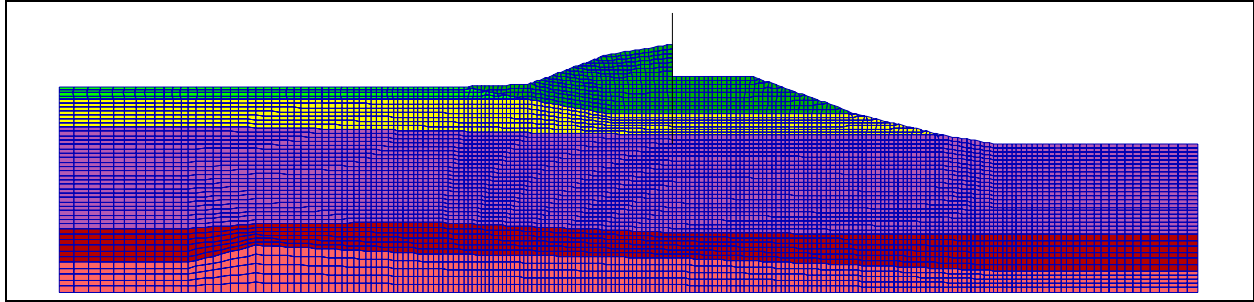
The development of the failure mode is further clarified in Figure 19-10, which shows estimated contours for the fraction of mobilized shear strength at three water levels: WSE = 4, 7, and 10.5 feet. Significant zones of the Lacustrine Clay are predicted to be highly stressed from the start of flood loading. Full instability of the section occurs as the marsh/peat and topsoil zones become highly stressed.

The representation of material properties for the soil was relatively simple. This was particularly true with respect to the assumption of linear stiffness and the relatively uniform undrained strengths. Also the numerical simplifications made in the analyses are factors which probably contributed to estimating smaller deformation than the other analyses and a higher WSE for section instability. Nevertheless, even hampered with these conservative and simplifying assumptions and approaches significant deformation is predicted for this section providing insight into the probable failure mechanism. Although a more refined modeling of soil properties and sensitivity evaluation could permit a better assessment of actual or potential response, the modeling and analysis described above appears to have been adequate to identify a critical response mode of the structure.
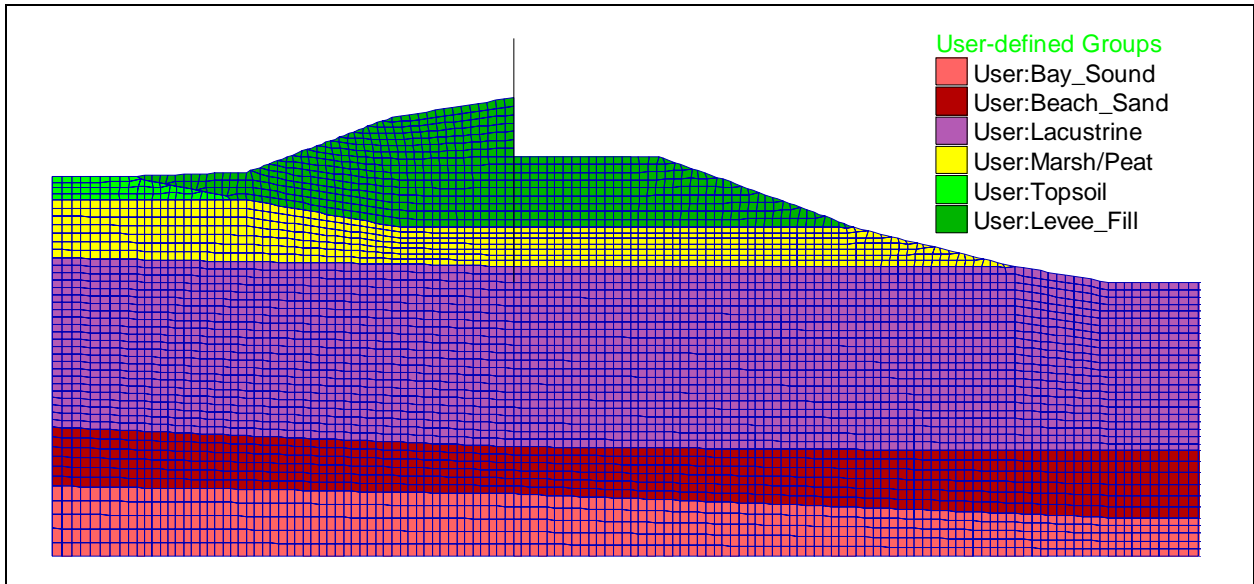
Conclusions

This analysis supports the field observations, aspects of the limit equilibrium analyses, and the Plaxis SSI analyses that a predominately translational instability breached this section at WSE less than 10.5 ft. The current model properties produce a failure surface initiating close to pile tip elevation near the top of the lacustrine clay layer. In comparison, another study being conducted by the National Science Foundation (Seed et al, 2006) report a similar failure mode, but at a higher elevation within the Marsh layer. The FLAC model also shows a kinematic response that approximately matches the field observed intact block displacement of protected side of levee embankment and heaving and over-thrusting of foundation soil layers beyond the levee toe.

The introduction of "crack" or gap between the canal side sheet pile wall and levee soil embankment was a dominant factor in inducing this failure mode. Continuing analyses involving alternative crack formation criteria support a gap formation evolution that results in failure at a WSE elevation closer to the field reported 8.5 ft. This shows the importance in this phenomenon in controlling failure behavior and should be further studied.

a. FLAC grid

User-defined Groups
User:Bay_Sound
User:Beach_Sand
User:Lacustrine
User:Marsh/Peat
User:Topsoil
User:Levee_Fill

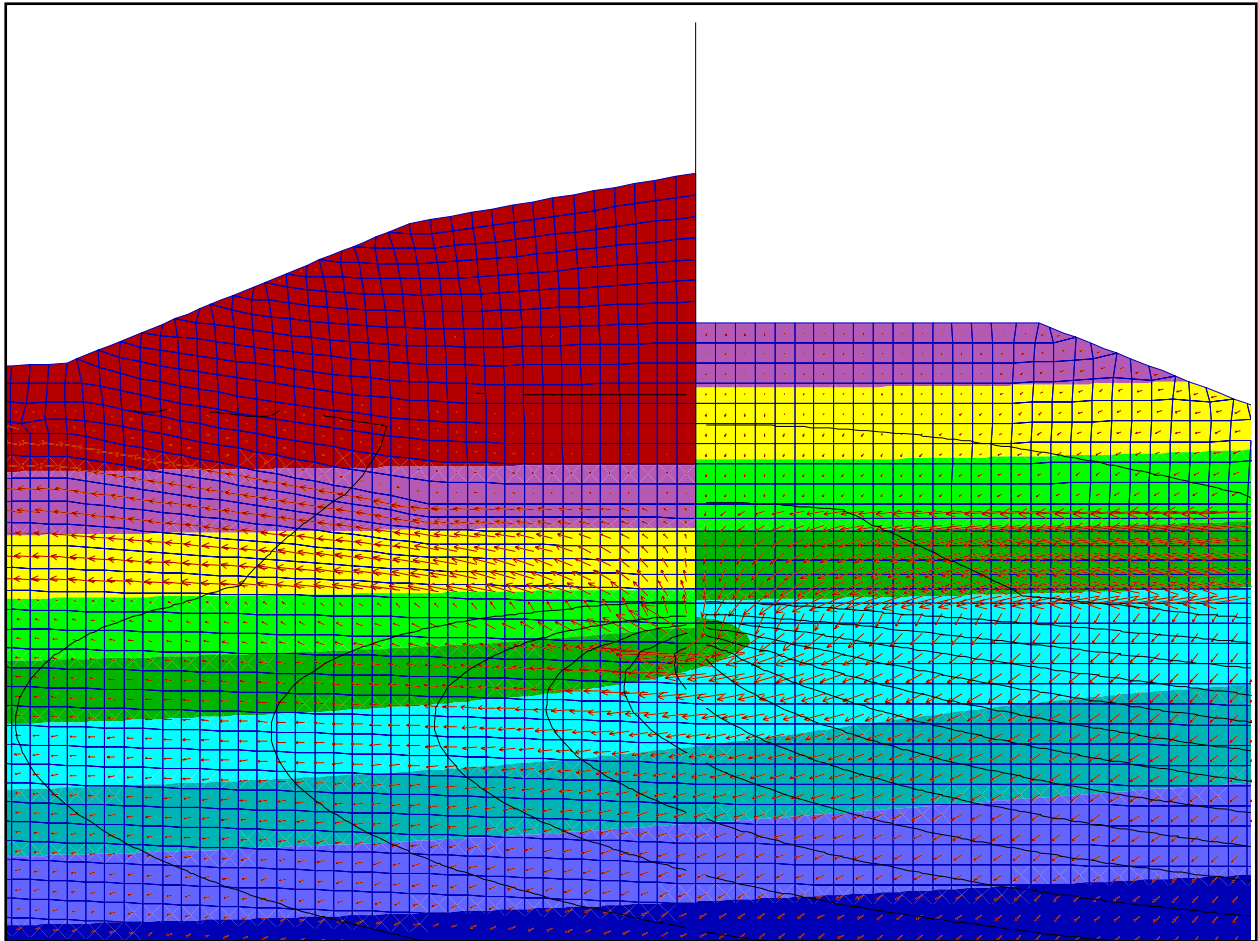b. FLAC grid at levee

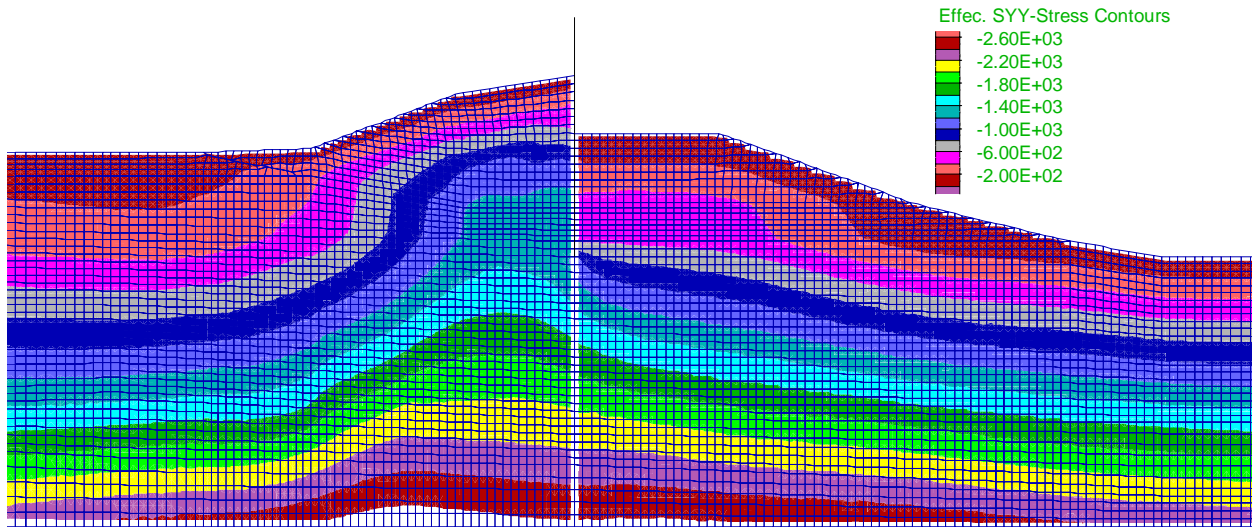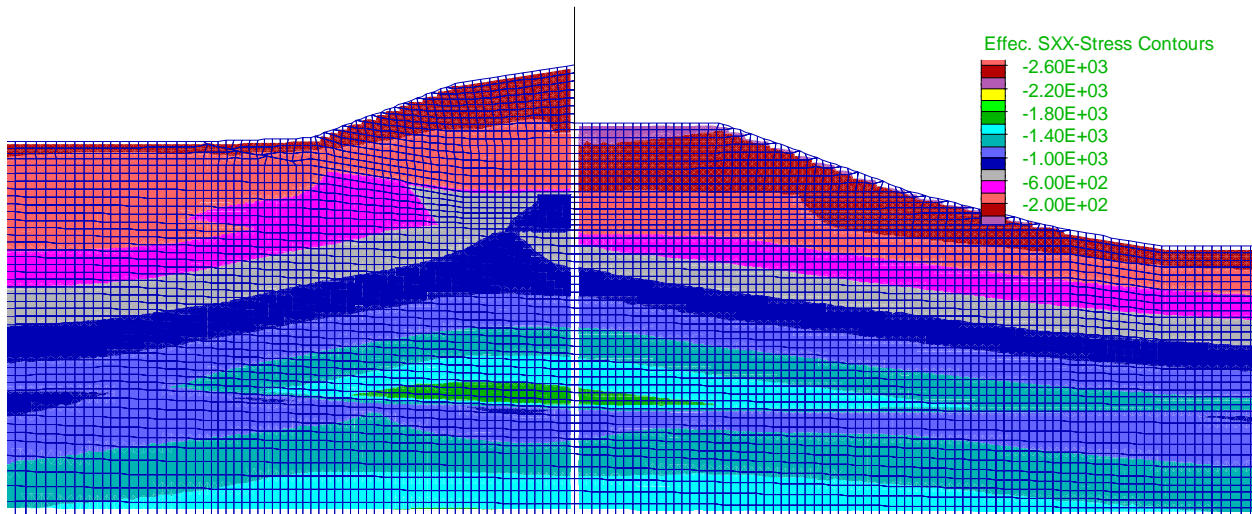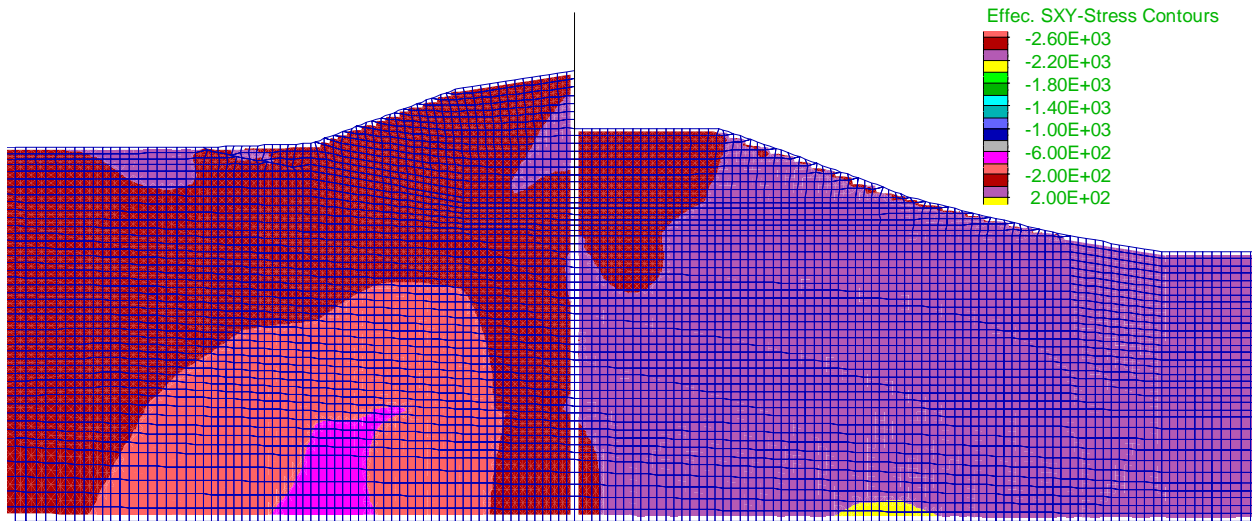Figure 19-3. FLAC model geometry for 17th St. breach

Figure 19-4. Estimated pore pressures, flow vectors, and contours of head at levee for 17th St. breach sta. 10+00

a. Vertical effective stress

b. Horizontal effective stress

Effec. SXY-Stress Contours
- -2.60E+03
- -2.20E+03
- -1.80E+03
- -1.40E+03
- -1.00E+03
- -6.00E+02
- -2.00E+02
- 2.00E+02

c. Horizontal Shear Stress

Figure 19-5. Estimated stresses for initial conditions for 17th St breach sta. 10+00

- 0.00E+00
- 1.00E-01
- 2.00E-01
- 3.00E-01
- 4.00E-01
- 5.00E-01
- 6.00E-01
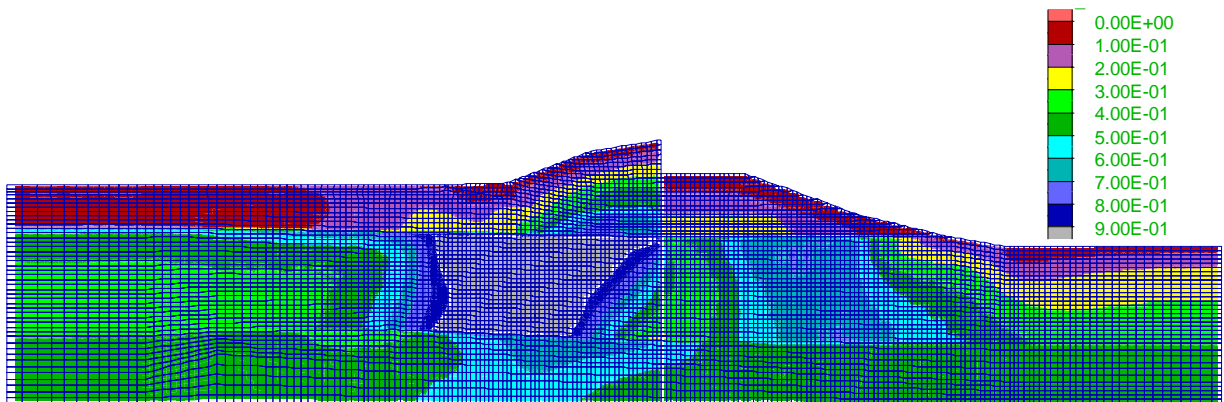- 7.00E-01
- 8.00E-01
- 9.00E-01

Figure 19-6. Fraction of mobilized shear strength for initial conditions and undrained strengths for 17th St. breach sta. 10+00
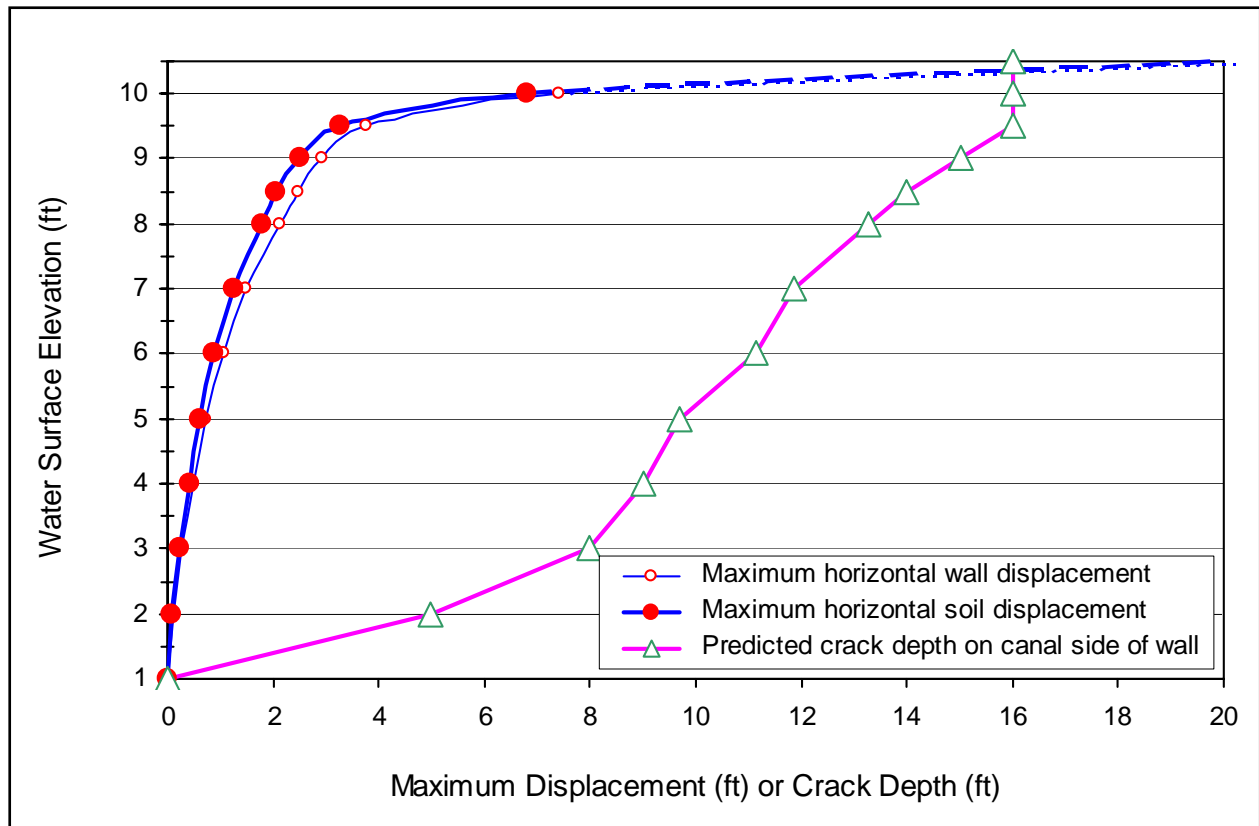
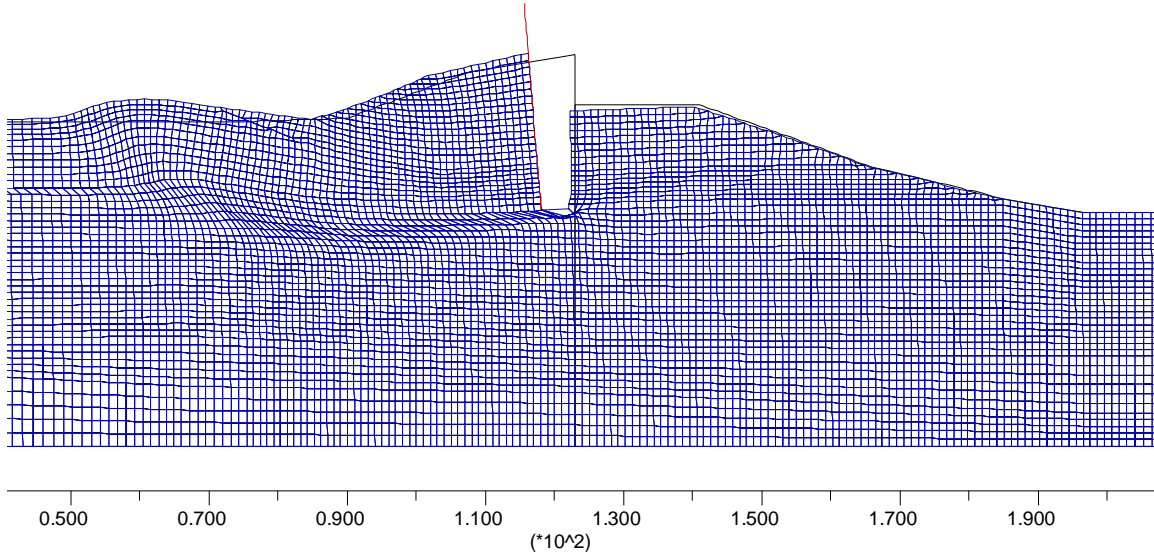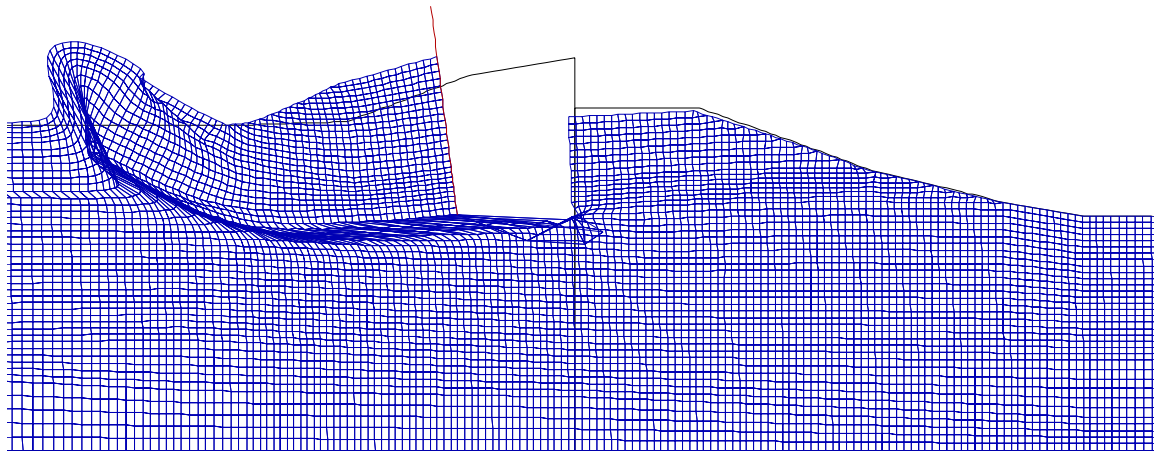Figure 19-7. Predicted maximum horizontal displacement and crack depth versus WSE for 17th St. breach sta. 10+00

Volume V The Performance – Levees and Floodwalls – Technical Appendix   V-19-13

This is a preliminary report subject to revision; it does not contain final conclusions of the United States Army Corps of Engineers.

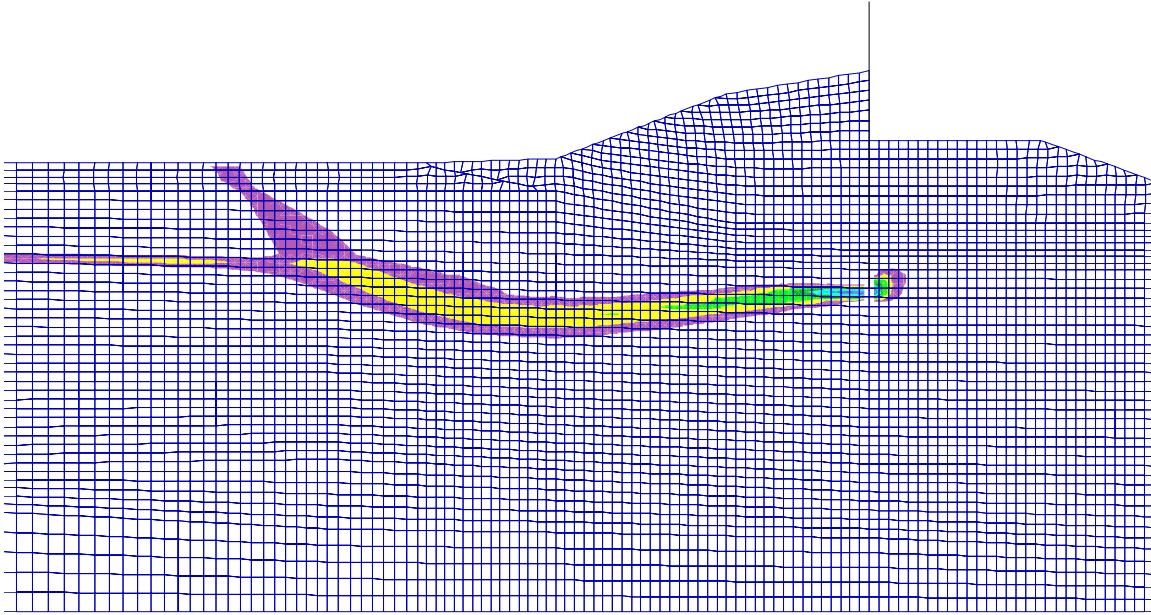0.500   0.700   0.900   1.100   1.300   1.500   1.700   1.900
(*10^2)

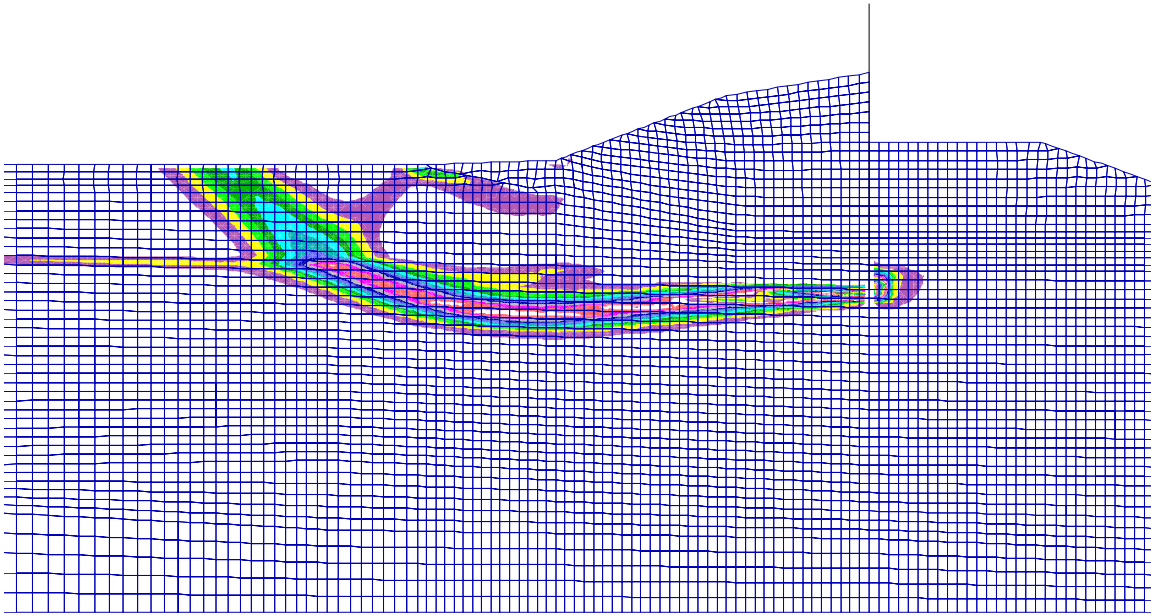a. WSE = 10.0 feet (displacement shown at true scale, model at equilibrium)

b. WES =10.5 feet (displacement shown at true scale, model NOT at equilibrium

Figure 19-8. Estimated deformed shape for 17th St. breach Sta. 10+00

a) WSE =10.0 feet (contour increment = 50% shear strain)

b) WSE = 10.5 feet (contour increment= 50% shear strain)

Figure 19-9. Estimated contours of maximum shear strain Mohr-Coulomb model for 17th St. breach sta. 10+00

Volume V The Performance – Levees and Floodwalls – Technical Appendix

V-19-15

This is a preliminary report subject to revision; it does not contain final conclusions of the United States Army Corps of Engineers.
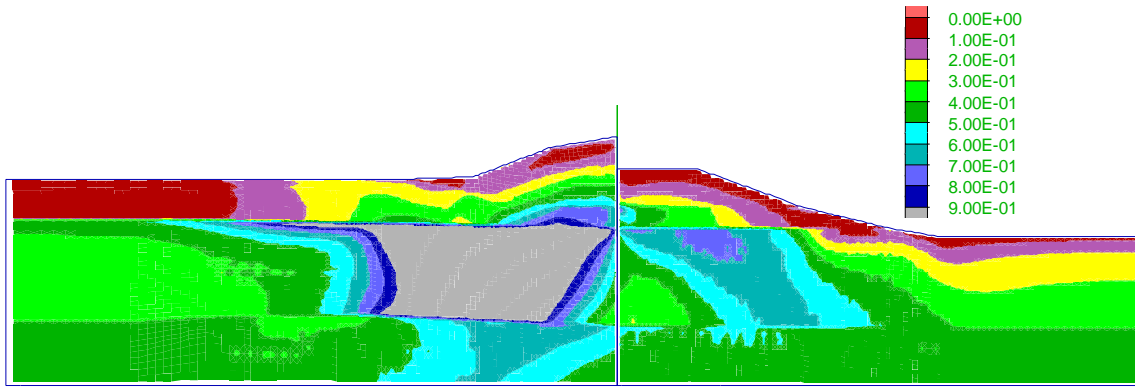
a. WSE = 4 feet
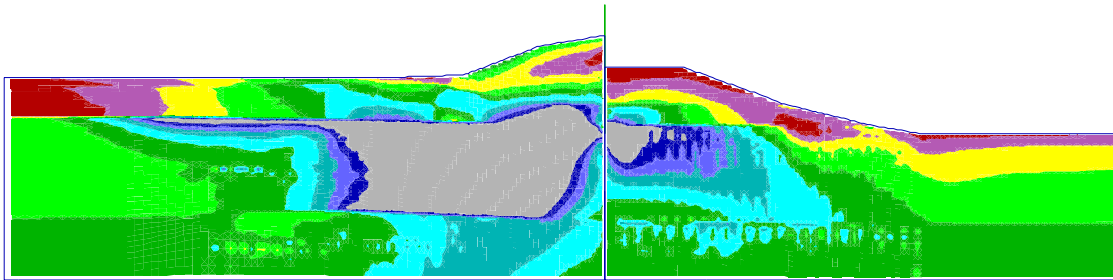
b. WES = 7 feet
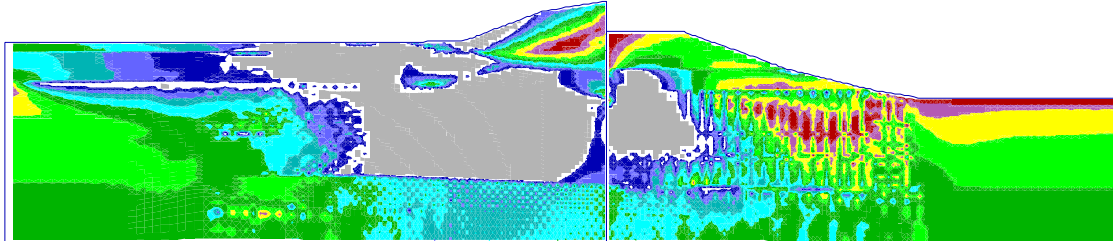
c. WSE = 10.5 feet

Figure 19-10. Estimated fraction of mobilized shear strength for 17th St breach sta. 10+00

Volume V The Performance – Levees and Floodwalls – Technical Appendix

This is a preliminary report subject to revision; it does not contain final conclusions of the United States Army Corps of Engineers.

Figure 19-11. Estimated deformed shape for WSE=8.5 for entire model (a) and near levee crest with 5x exaggeration (b) for 17th St. breach sta. 10+00

Nonlinear Constitutive Model Analysis

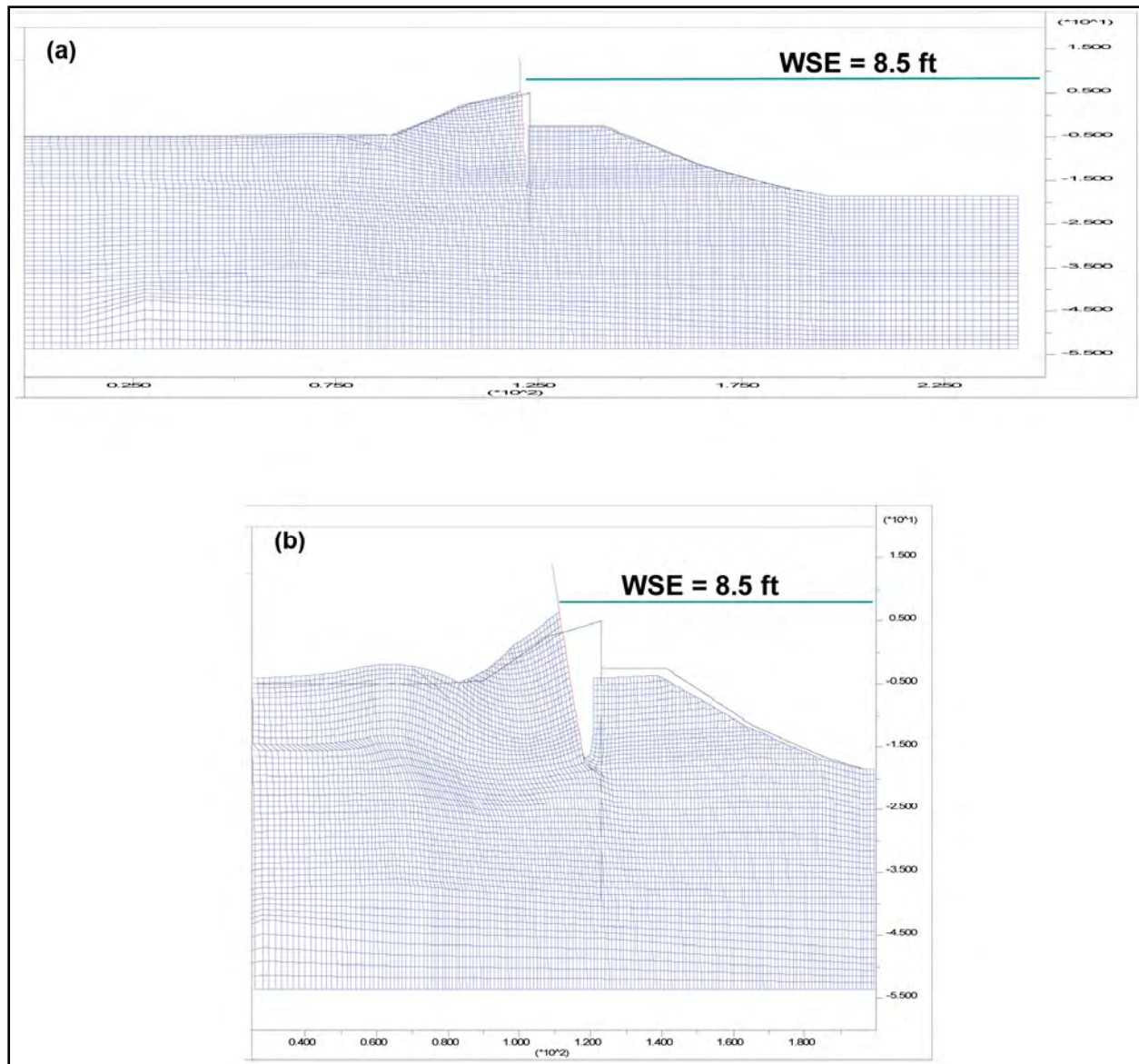**Approach.** The levee section at Station 10+00 of the 17th St. Canal in New Orleans was also analyzed using FLAC with a user-defined nonlinear soil model for the Katrina high water elevation of 8.5 ft. The geometry and undrained strengths are consistent with the Plaxis analyses. For the current analysis, a simple case was run with Young's modulus (Eu_50) of E50=92·Su for all clays (value assigned for lacustrine clay). This model is being run next for the case consistent with the Plaxis analysis which used assigned softer properties of E50=48·Su for the levee and peat clays. The nonlinear model used was developed by Wang et al, Geomatrix Consultants, Inc. (Wang 1990) and requires additional model parameters (G_{max} and h_r) for total stress analysis.

The analysis presented here used a simple relation to define these two parameters. For G_{max}, $2 \cdot G_{50} = E_{u\_50}/(2/(1+\nu))$ was used. Another parameter $h_r = 0.77$ was chosen to give a secant modulus $G = 0.5G_{max}$ at a strain level $\varepsilon = S_u/G_{max}$. The unit weight, undrained soil strength, and model parameters are presented in Table 19-1. The undrained strength of the clay for each zone was specified consistent with values used in the slope stability analyses. These strengths vary horizontally and increase with depth at the rate of 11psf/foot to account for the appropriate confining stresses.

The model profile showing the finite difference grid and the soil layers is presented in Figures 19-12 and 19-13.

Table 19-1. Soil Properties and Model Parameters for Levee Section at 17th Street Canal, Station 10+00

Description	Soil Type	gt, pcf	gt/g	Su, psf	f, deg	E50=92*su	n, Poisson	G, psf	K,psf	Gmax	hr
Fill/Top soil	1	109	3.39	900	0	82800	0.47	28163	690000	56327	0.77
Marsh (Canal side)	2	80	2.48	350	0	32200	0.47	10952	268333	21905	0.77
Marsh (Protected side)	4	80	2.48	150	0	13800	0.47	4694	115000	9388	0.77
	4	80	2.48	250	0	23000	0.47	7823	191667	15646	0.77
	4	80	2.48	300	0	27600	0.47	9388	230000	18776	0.77
	4	80	2.48	350	0	32200	0.47	10952	268333	21905	0.77
	4	80	2.48	400	0	36800	0.47	12517	306667	25034	0.77
	4	80	2.48	450	0	41400	0.47	14082	345000	28163	0.77
Lacustrine	5	109	3.39	Table	0	Table	0.47	Table	Table	Table	0.77
Beach Sand	6	120	3.73	1500		138000	0.47	46939	1150000	93878	0.77
Bay Sound	7	125	3.88	5000		460000	0.47	156463	3833333	312925	0.77

The analysis was performed in the following steps: build model and apply initial water level, estimate initial stress conditions, apply flood load, introduce crack between floodwall and soil levee, and finally introduce an interface along failure surface defined by non-interface model.

In building the model, a simple contrived construction history was implemented based on current geometry. The construction steps were first to bring soil foundation and levee embankment to canal side bench level (elevation -2.5 feet), insert sheet pile and floodwall (floodwall top elevation of 12.5 ft and sheet pile tip at elevation -18.5 ft), continue building levee embankment to final crest elevation of 5 ft on protected side. In building the numerical model the grid space was first generated and the soil was constructed layer by layer by turning on gravity for each layer. The newly added layer was a load increment for the previously constructed layers, so that the non-linear soil model can be properly invoked by simulating natural deposition and construction events to better compute the resultant static stresses within the levee embankment and foundation. The concrete I-wall and sheet piles were simulated by linear elastic beam elements using the properties assigned by the Plaxis team.

Next, the water pressures for pre-Katrina water levels were applied; a normal canal water elevation of 0.5 was used. The normal water pressures were developed based on water level of elevation -0.5 ft on the canal side levee with a tail-water level elevation -5 on the protected side.

The phreatic surface was generated using FLAC's 'Water Table' option which assigns pore pressures based on this static head in-lieu of ground water flow generated phreatic surface.

This model was then solved to equilibrium and all computed grid node displacements reset to zero. These analysis steps resulted in an estimate of pre-Katrina static effective stresses for before applying the Katrina flood loading.

The Katrina flood water level was applied in one step using FLAC's 'Water Table' option and applied water pressure to levee on the canal side to compute the displacements. The solution was obtained using FLAC's 'dynamic on' option, because the 9 feet high Katrina water (from elevation -0.5' to elevation 8.5') was simulated as an 'impact' loading while in reality such water might be raised in a few hours. The computed displacements oscillated until they reached steady values. Only the stabilized displacements were used. This loading produced a displacement of the floodwall of approximately 1 foot, but resulted in a stable section that did not predict failure. This simplified loading procedure (i.e. apply Katrina water in one step) may overly predict the levee's deformation compared with raising the water foot by foot and computing the stabilized displacement for each water increment. This conclusion for non-failure is based on the modeled single wall panel section and assumes that the wall panels can accommodate this amount of differential displacement which is beyond the scope of the current 2-D model.

Based on the results of the slope stability analyses, and the hydraulic fracturing criteria used in the Plaxis analyses, it was assumed that a crack or gap will develop next to the concrete wall and sheet pile (on the canal side), down to the elevation of the tip of the pile. The development of such a crack was verified by comparing the pore water pressure with total horizontal stress in the soil layers (as shown in Figure 19-18). For the water level at the Katrina high flood level (elevation 8.5 feet), the pore pressures in the soil profile were generally greater than the total horizontal normal stress (computed at normal pool water level at elevation -0.5 ft) down to about elevation -19 feet.

Accordingly, the soil column adjacent to the wall above the pile tip (elevation -18.5 feet) was removed (nulled). The removal of the soil (i.e., an excavation process) allows the canal water to fill the void, and boundary water pressures were then applied normal to the sheet-pile wall and the opposite side soil face as well as the base of the excavated column.

The water level is raised to the specified flood level, and the calculation is continued to compute the total wall movement as a result of the formation of the crack and the rise in the water level. Again, the crack was assumed to form in one step down to the pile tip, and the displacement induced due to the application of the water pressure in the crack was computed in the FLAC's 'dynamic on' mode. The computed displacements oscillated until they reached steady values and only the stabilized displacements were used.

In addition to the simulation of the crack formation, and before raising the water level to the specified flood level, a horizontal interface layer was included at the pile tip level (El. -18.5 feet) on the protected side, with a specified undrained shear strength equal to the strength calculated for the Lacustrine clay layer at the same elevation. This interface feature allows FLAC to

compute larger displacement along the upper portion of the weak clay layer when the water level is raised to the Katrina flood level at elevation 8.5 ft (or 10.5 ft).

Analysis Results and Discussion. The material zones, beam elements simulating the floodwall and sheet piles and the normal pool water are shown in Figure 19-12. The finite difference grid used for the FLAC analysis is shown in Figure 19-13. The computed total vertical stress and pore water pressure at normal pool water level are presented in Figure 19-14 and 19-15, respectively. The pore water pressure contours using Katrina water at elevation 8.5 ft are presented in Figure 19-16.

Computed displacements of the floodwall due to water levels associated with the high Katrina flood levels, but ignoring the effects of crack or gap formation between the floodwall and the levee berm (at the canal side) were less than 1 foot, but the levee slopes were stable with no indication of impending failure (Figure 19-17).

Pore water pressures associated with Katrina high flood water level exceeded the total horizontal normal stresses computed from normal pool water level in the clay layers down to about elevation 19 feet, indicating the potential for crack formation between the levee soil and the sheet pile wall (Figure 19-18).

The possible crack formation was simulated in the analyses. The computed deformations of the pile wall and the levee slopes when simulating the effect of cracking resulted in horizontal deformation of about 1.2 ft (Figure 19-19).

When incorporating a horizontal interface at the top of the soft lacustrine clay layer (at the elevation of pile tip), the computed deformation for the Katrina flood water level at El. 8.5 ft was about 5 to 6 ft, indicating the potential for failure (Figure 19-20).

Conclusion. The representation of material properties using a nonlinear constitutive model for the soil was more sophisticated but also more dependent on an estimate of initial stresses. The modeling and analysis described above appears to also have identified a critical failure mode for this structure.

This analysis also supports the field observations, aspects of the limit equilibrium analyses, and the Plaxis SSI analyses that a predominately translation instability breached this section at a canal water flood level at elevation 8.5 ft. The current model properties produce a failure surface initiating close to pile tip elevation near the top of the lacustrine clay layer. The FLAC model also shows a kinematic response that approximately matches the field observed intact block displacement of the protected side of levee embankment and heaving and over-thrusting of foundation soil layers beyond the levee toe.

However, the introduction of "crack" or gap between the canal side sheet pile wall and levee soil embankment and use of an interface along the failure surface were needed to induce significant displacements (5 to 6 ft) and probable failure. Continuing analyses with lower stiffnesses for the levee and marsh deposits may alter these results. Use of this non-linear soil model may be important in obtaining a better estimate of initial stresses effecting the formation of the crack or gap needed to trigger this failure mode.
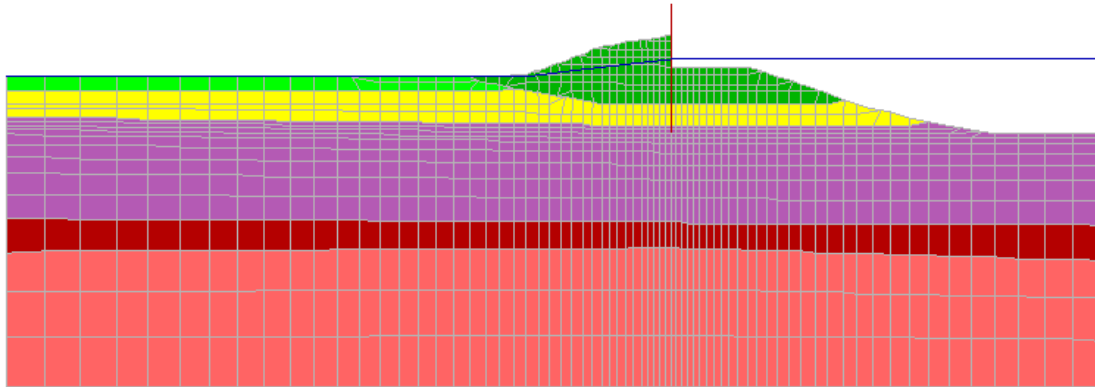
Figure 19-12. Soil zones, levee wall and sheet piles and normal Pool for 17th St. breach sta. 10+00
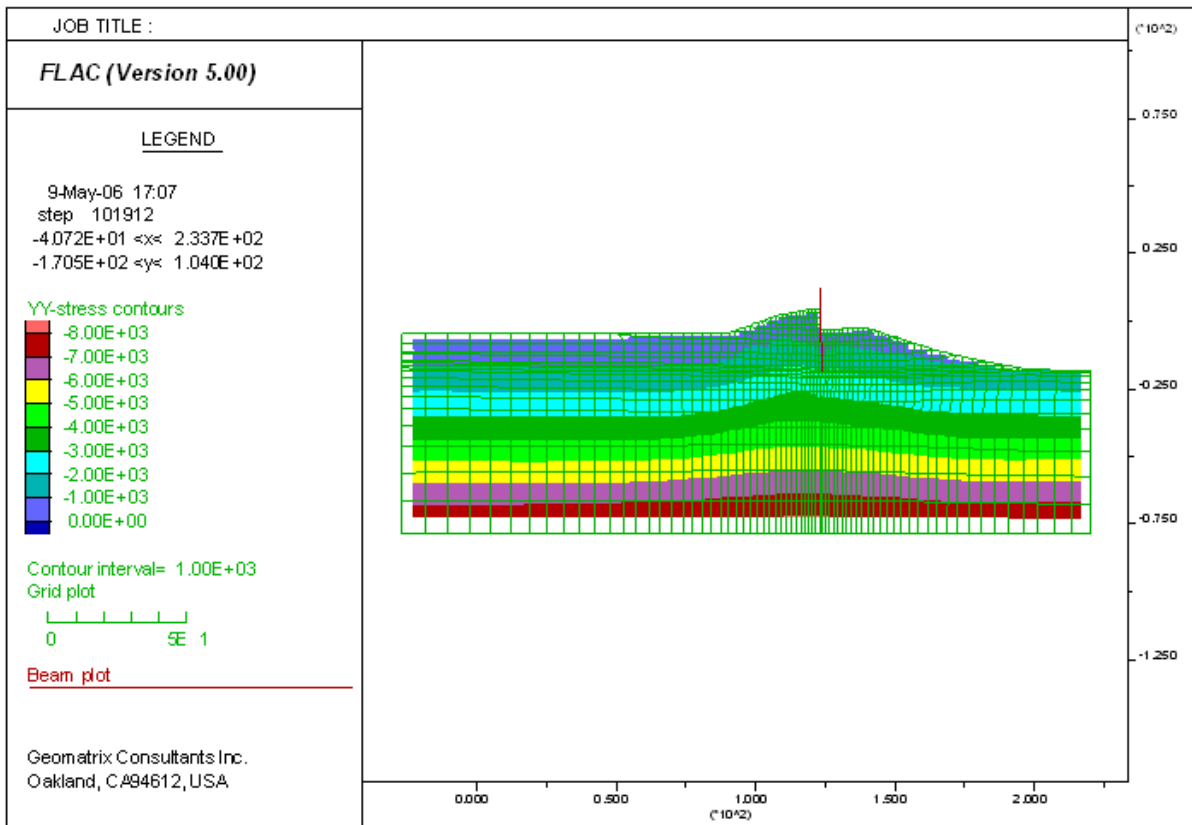

Figure 19-13. FLAC model (grid) used for the analysis of 17th St. breach sta. 10+00
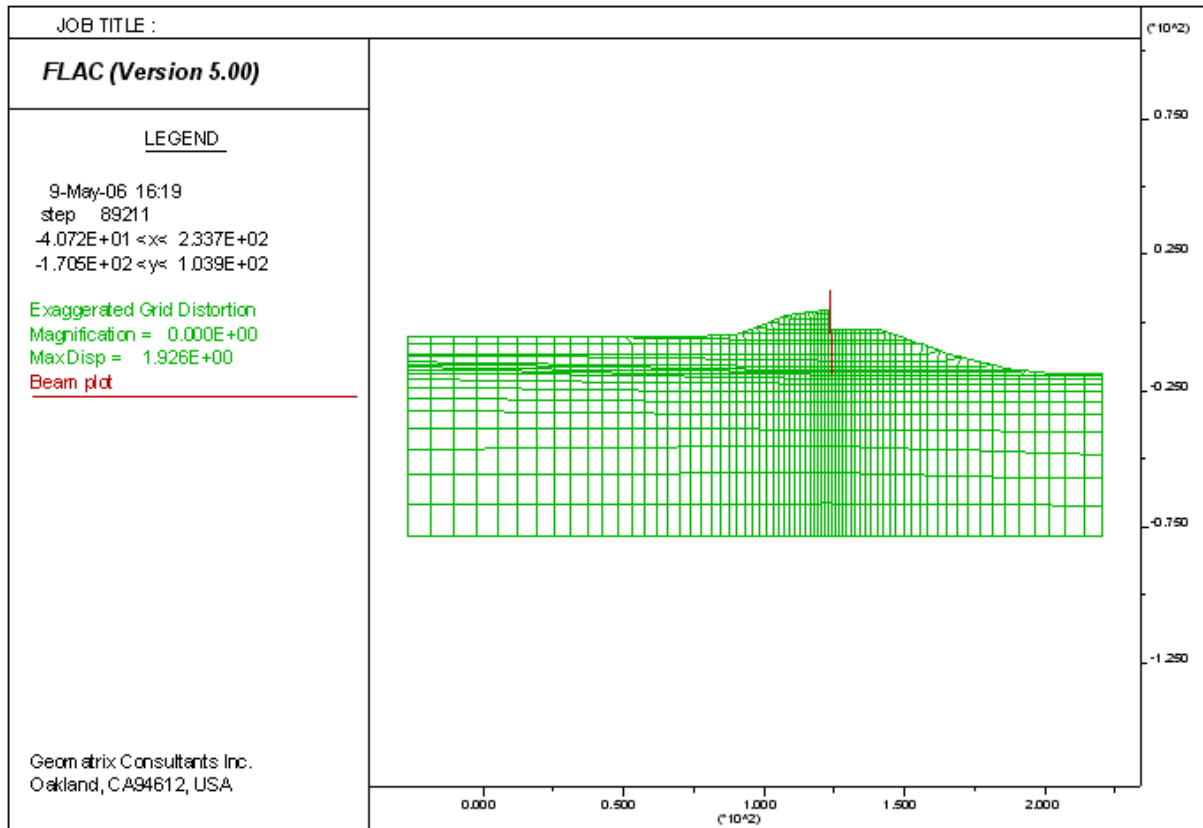
Figure 19-14. Contours of vertical total stress at normal pool water level, elevation -0.5 feet 17th St. breach sta. 10+00

This is a preliminary report subject to revision; it does not contain final conclusions of the United States Army Corps of Engineers.
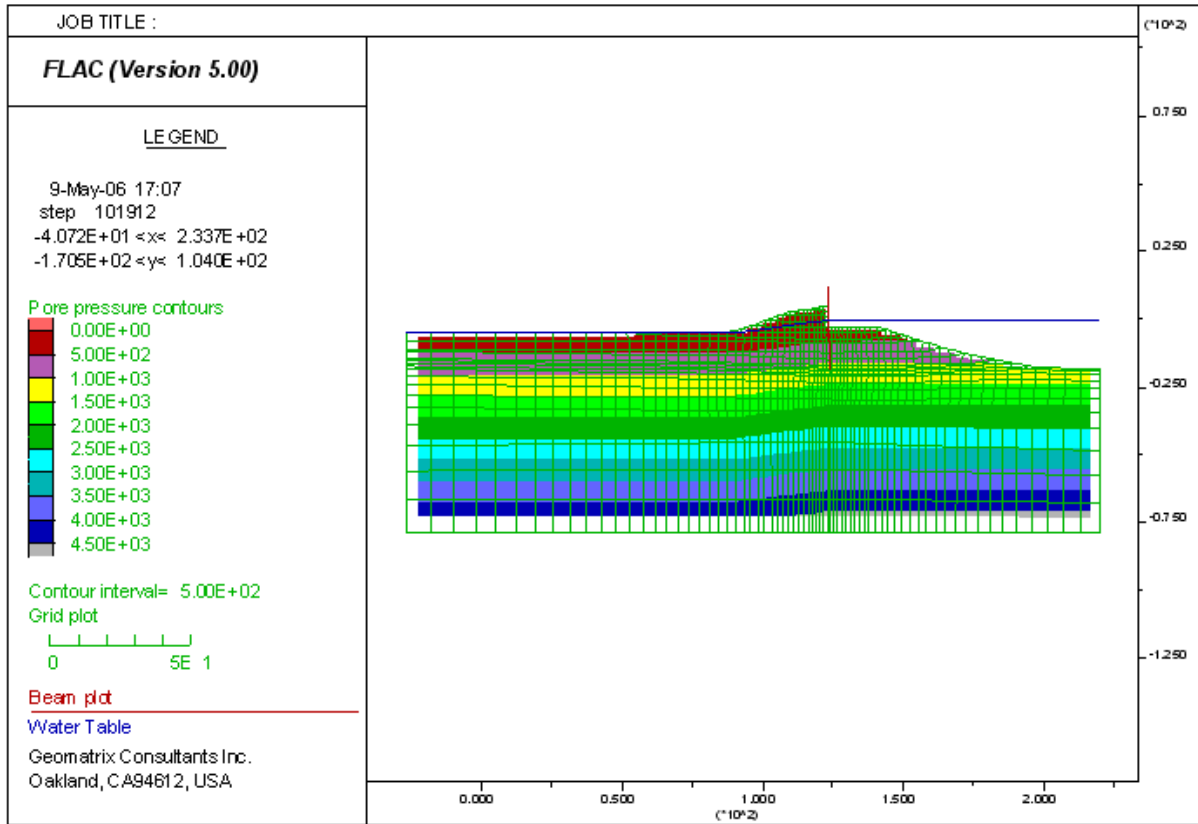
Figure 19-15. Contours of pore pressure at normal pool water at El. +0.5 feet, nonlinear model 17th St. breach sta. 10+00
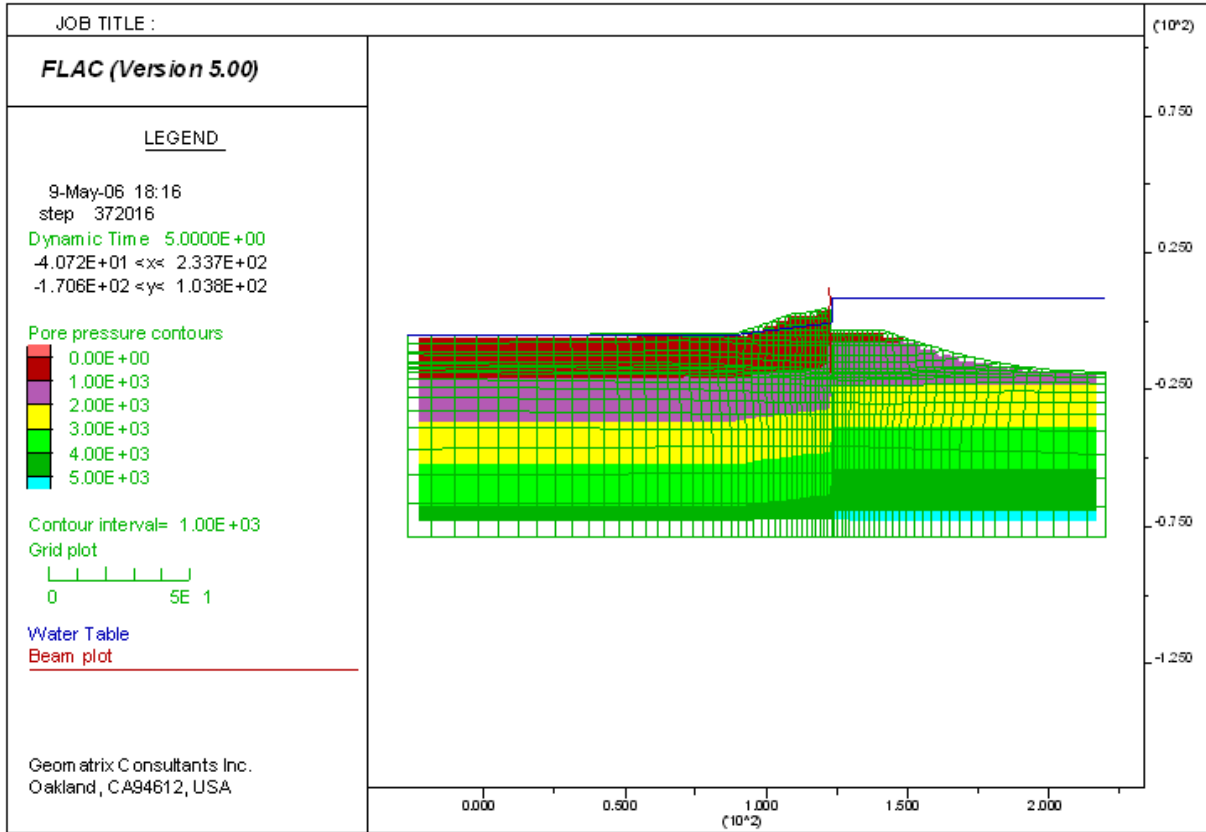
Figure 19-16. Contours of pore pressure, Katrina flood water level at El. +8.5 feet, nonlinear model 17th St. breach sta. 10+00

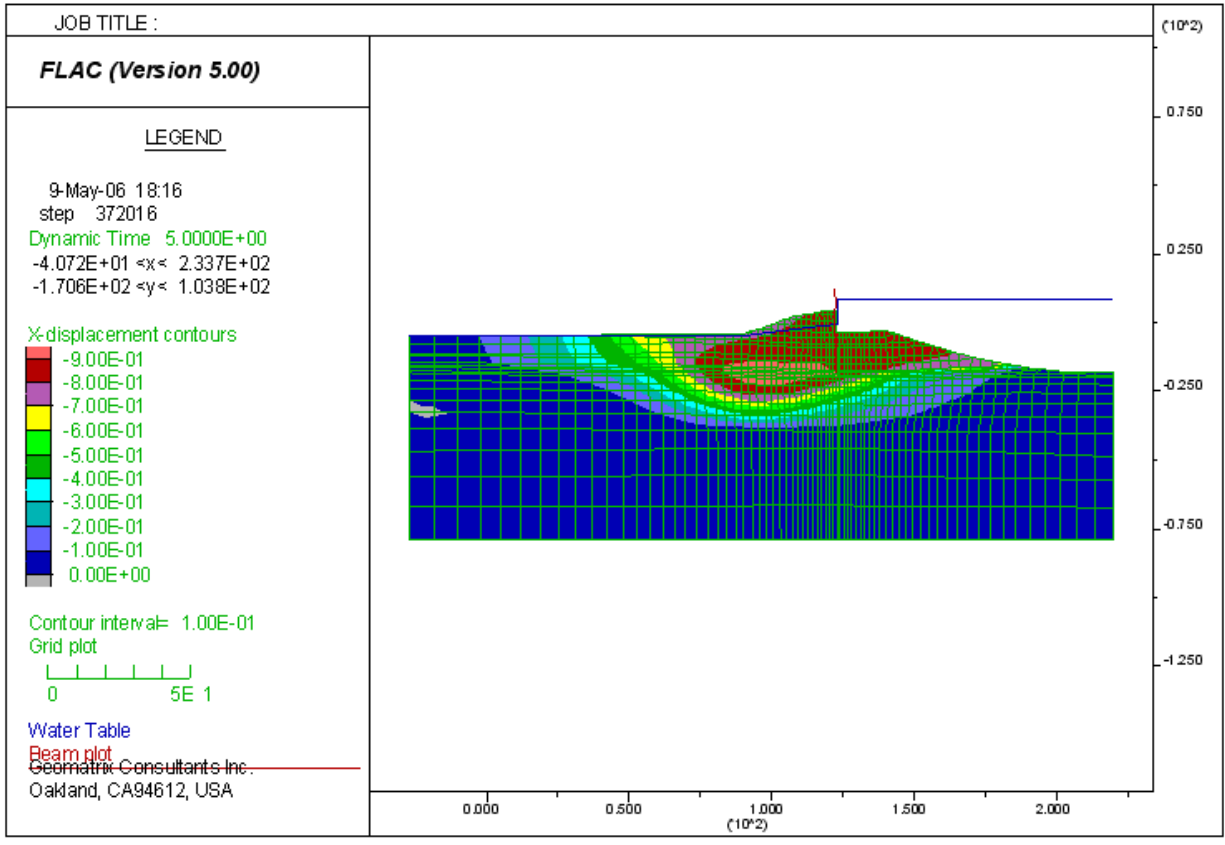Figure 19-17. Contours of horizontal displacement, Katrina flood water level at El. +8.5 feet, non-linear model 17th St. breach sta. 10+00
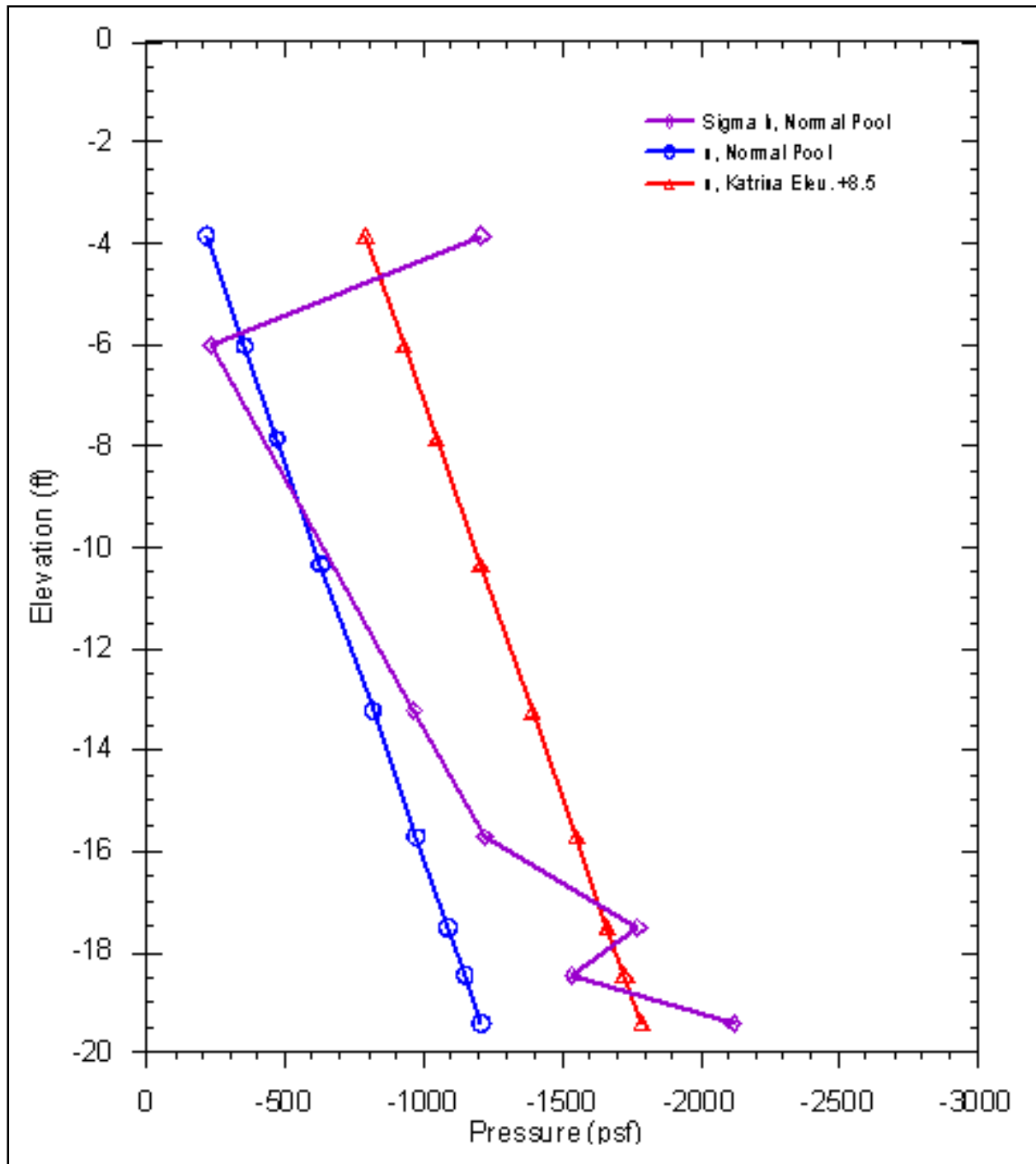
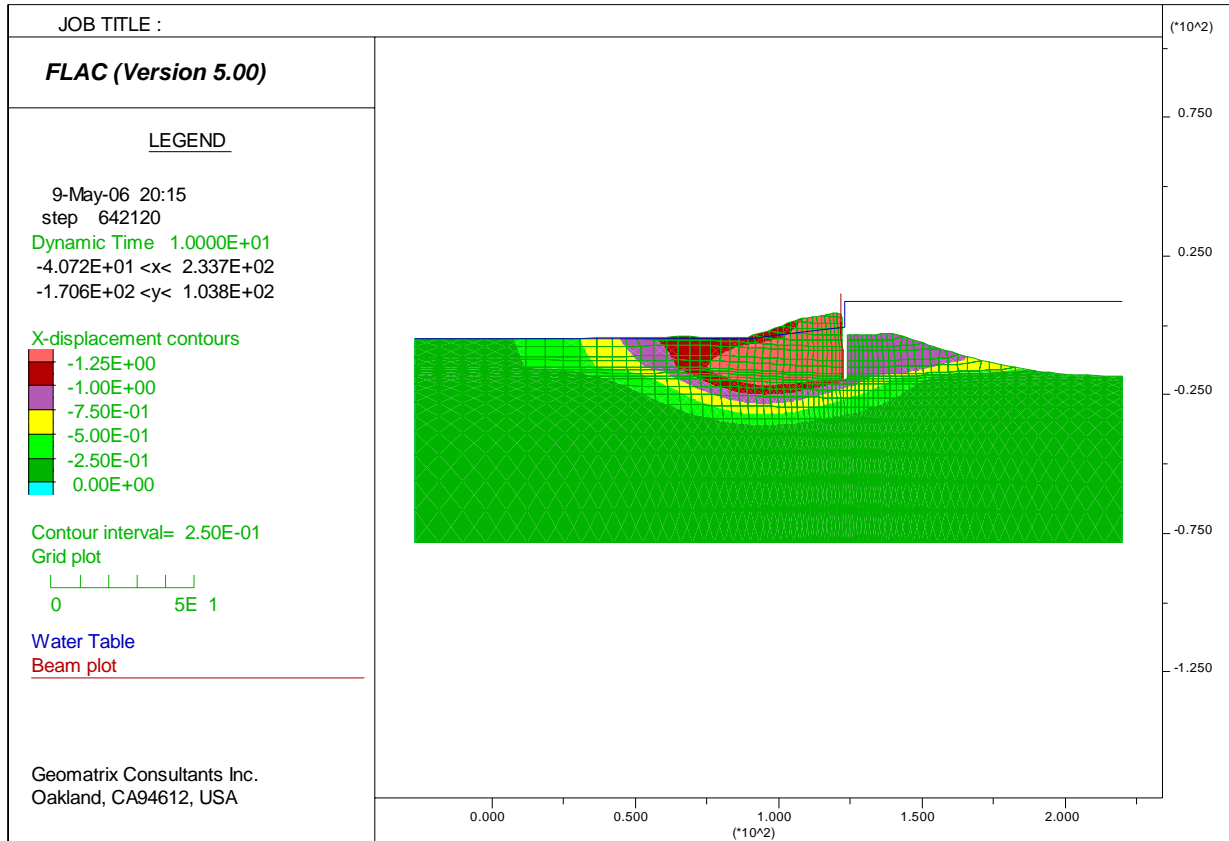Figure 19-18. Comparison of water pressure and horizontal total stress 17th St. breach sta. 10+00

Figure 19-19. Contours of horizontal displacement with crack simulation, Katrina flood water level at El. +8.5 feet, non-linear model 17th St. breach sta. 10+00
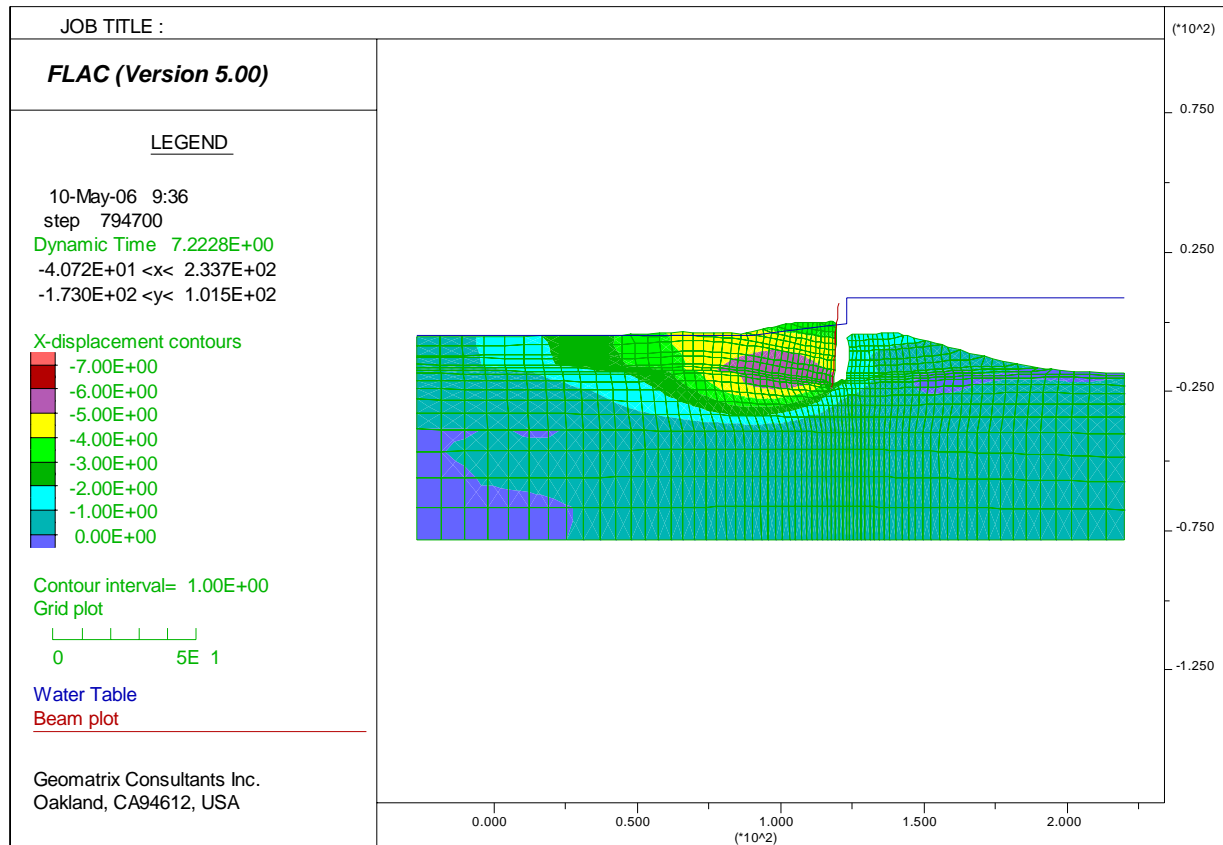
Figure 19-20. Deformed grid (with crack simulation and interface) Katrina flood water level at El. +8.5 feet, non-linear model for 17th St. breach sta. 10+00

London Canal North Levee Breach Analysis

The London Avenue Outfall Canal – North (near Robert E. Lee Bridge) was estimated to have breached around 7:00 AM to 8:00 AM, an hour later then the London South breach. This section is composed of concrete and steel sheet-pile I-wall floodwall built into the centerline of the earthen levee. The findings of the limit equilibrium stability analyses showed that the wall begun failure at canal water level between 8.2 and 9.5 ft (NAD88). One case analyzed for a water level just before the estimated breach resulted in a slope stability Factor of Safety of 1.00 for a canal water level of 8.1 ft (IPET, 2006). This report further concludes that field evidence and slope instability analyses show that the most likely mode of failure is sliding instability. Seepage studies also show that erosion and piping was another possible mode of failure. The high water pressures in the sands and the movement of the wall toward the protected side, forming a gap or crack on the canal side between the wall and earth embankment, were allowed to act directly on wall and high uplift pressures on marsh and clay deposits overlying the sands. Field evidence showed intact crest sliding and heaving at the toe.

The levee section at Station 14+00 of the London Avenue Canal (North Breach) in New Orleans was analyzed using a finite difference program, FLAC, with the Mohr –Coulomb model

and a user-defined nonlinear soil model for the Katrina high water at Elevation 9 feet. The soil profile shows that there are sand layers below the Marsh-clay layers, and the pile tip just penetrates the top sand layer. The effective stress and strength in the sand layer may be reduced due to water flow resulting from the Katrina high water load. In order to model these variations, a user-defined effective stress model (Wang, 1990) was used for the Beach Sand layer 1 (shown in yellow on the attached Figure 19-21). For other materials, the Mohr-Coulomb model was used for faster solution speed. The geometry, undrained strength and Young's modulus (Eu_50) values for the Mohr-Coulomb model are consistent with those used in the other analyses (Plaxis and limit equilibrium stability analyses). The unit weight, undrained soil strength, and model parameters are presented in Table 19-2.The nonlinear model used in this analysis requires additional model parameters (G_o , h_r, k_r, and d) for effective stress analysis. A $K_{2max} = 40$ for sandy material was estimated for $D_r = 40\%$ of Beach Sand layer 1. This $K_{2max} = 40$ was correlated with model parameter G_o. Parameter $h_r = 0.77$ was used to give a secant modulus $G = 0.5G_{max}$ at a reference strain level $\gamma = \tau_f /G_{max}$ in which τ_f is the soil strength. Two more parameters (k_r and d) are needed if excess pore water pressure generation is allowed. These parameter values were estimated for Beach Sand 1 with SPT of about 10. The unit weight and model parameters for the Beach Sand 1 layer are presented in Table 19-3 that uses the nonlinear effective stress model.

Approach

The analysis was performed using the mechanical and ground water flow modes of the FLAC program. To expedite the computational process, in the present analysis, the Mohr-Coulomb model was used in all the soil layers in the profile except for Sand Layer 1 as described above. For this layer, the non linear effective stress model was used in the analysis.

The following steps were used in the analysis:

1. Build numerical model. The grid was generated first. The soil profile was constructed layer by layer by turning on gravity for each layer. For the London Canal (North) section, 'construction' was simulated from the bottom of the profile to the crest of the levee. The newly added layer was a load increment for the previously constructed layers, so that the non-linear soil model can properly be used to compute the static stresses within the levee embankment.

2. Construct the two floodwalls (sheet pile and concrete wall), both are simulated by beam elements.

3. Apply normal pool water pressure (at El -0.5 feet) on the levee at the canal side, and develop the phreatic surface (from El. -0.5 feet on the canal side, to El. -4.4 feet on the protected side), and compute the wall deformation at the normal pool level.

4. Let FLAC balance the effective stresses as prior Katrina's static stresses and reset all computed displacement to zero (before raising the water level to specified Katrina levels).

Volume V The Performance – Levees and Floodwalls – Technical Appendix

V-19-29

This is a preliminary report subject to revision; it does not contain final conclusions of the United States Army Corps of Engineers.

5. Raise the water level to the assumed Katrina high water level at Elevation 9 feet, and apply water pressure to the levee on the canal side in one step. The new phreatic surface corresponding to the assumed Katrina water level was developed using FLAC's 'water flow on' option and assumed water level at ground surface level at the protected side. The displacement due to the Katrina high water level was computed using FLAC's 'dynamic on' option. Because the high Katrina flood water (at elevation 9') was simulated as an 'impact' loading while in reality such water might raised in a few hours, this simplified loading procedure (i.e. apply Katrina water in one step) may overly predict the levee's deformation compared with raising the water foot by foot and computing the stabilized displacement for each water increment. In the dynamic mode, the computed displacements were oscillated to reach steady values and only the stabilized displacements were used. This simplified procedure resulted in a displacement of the floodwall of approximately 3 inches, which did not cause failure.

6. Based on the results of the slope stability and seepage analyses, and the hydraulic fracturing criteria used by the Plaxis team, it was assumed that a crack will develop next to the concrete wall and sheet pile (on the canal side), and would extend down to the elevation of the top of the sand layer. The development of such a crack was verified by comparing the pore water pressure from Katrina water level at elevation 9' with the total horizontal stress computed from normal water level in the soil layers (as shown in figure below). For the water level at the Katrina High flood level (at Elevation 9 feet), the pore pressures in the clay layers were generally greater than the total horizontal normal stress down to about Elevation -13 feet.

7. Accordingly the soil column adjacent to the wall above the El. -12.9 feet was removed (nulled) to simulate the crack development. The removal of the soil (i.e., the excavation process) allows the canal water to fill the void between the levee berm and the floodwall. Thus the water pressure was then applied normal to the sheet-pile wall and to the opposite soil face, as well as at the base of the excavated soil column.

8. The water is allowed to flow through the crack into the sand layer below. The flow computation is then performed and the water flow vectors are computed and are shown on Figures 3-7 and 3-8. The increase in pore water pressure in the sand layer results in a reduction in the effective stress, and a corresponding decrease in the shear strength of this layer.

9. The flow calculation is terminated, and the mechanical calculation is continued to compute the total wall movement as a result of the formation of the crack, the rise in the water level, and the increased pore pressures in the sand layer below the tip of the sheet pile. This results in computed large movement of the wall towards the protected side. Again, the crack was assumed to form in one step down to the top of the beach sand 1, and the displacement induced due to the application of the water pressure in the crack was computed in the FLAC's 'dynamic on' mode.

Analysis Results and Discussion

The material zones, beam elements simulating the floodwall and sheet piles, and the normal pool water are shown in Figure 19-21. The finite difference grid used for the FLAC analysis is shown in Figure 19-22. The computed total vertical stress and pore water pressure at normal pool water level are presented in Figures 19-23 and 19-24, respectively. The pore water pressure contours using Katrina canal water level at elevation 9 ft are presented in Figure 19-25.

Computed displacements of the floodwall due to water levels associated with the high Katrina flood levels but ignoring the effects of crack formation between the floodwall and the levee berm (at the canal side) were of the order of 3 inches. The levee slopes were stable, with no indication of impending failure.

Pore water pressures associated with Katrina high flood water level exceeded the total horizontal normal stresses computed from normal pool water level in the clay layers down to about elevation 13 feet as shown in Figure 19-26, indicating the potential for crack formation between the levee soil and the sheet pile wall.

The possible crack formation was simulated in the analysis, and water flow into the underlying sand layer indicated significant increases in the pore pressures, and a corresponding reduction in effective stresses and shear strength. The water flow vector in the sand layers is presented in Figure 19-27. The detailed flow vectors and the simulated crack are presented in Figure 19-28.

The computed deformations of the pile wall and the levee slopes when simulating the effects of cracking and seepage flow into the underlying sand layer resulted in horizontal deformations exceeding 4 feet as shown in Figures 19-29 and 19-30. The computations were terminated at about 4 feet due to numerical problems with distorted elements, prior to reaching a stable configuration, indicating the potential for continued large movements.

The deformed shape of levee profile indicates that there was about 4 feet of upwards movement (bulging) in the top soil at the protected site, beyond the toe of the levee as shown in Figure 19-31. This is believed to be induced by the pore water pressure due to water flow into the top sand layer through the crack behind the wall. This bulging could indicate rupture of the overlying clay layer that would result in piping and possible failure.

Table 19-2
Soil Property and Mohr –Coulomb Model Parameters

Mohr Coulomb Model	Soil Type	γt pcf	Su, psf	φ, deg	E50=92*su	ν, Poisson	G psf	K psf	Vs, fps
Levee Fill	1	109	900	0	82800	0.47	28163	6.90E+05	assumed
Sheet Pile	2	125							
Silt on Bottom of Canal	3	100	100	0	9200	0.47	3129	7.67E+04	
	4	80	300	0	27600	0.47	9388	2.30E+05	
Marsh (Canal Side)	4	80	400	0	36800	0.47	12517	3.07E+05	
Clay	5	109	350	0	32200	0.47	10952	2.68E+05	
Beach Sand 2	7	122		36	0	0.47	5455901	8.91E+07	1200
Beach Sand 3	8	118		32	0	0.47	7182609	1.17E+08	1400
Bay Sound	9	125	5000	0	460000	0.47	156463	3.83E+06	

Table 19-3
Soil Property and Effective Stress Model Parameters for Beach Sand 1

Effective Stress Model	Soil Type	φ	G$_o$	h$_r$	k$_r$	d	F$_p$	ν, Poisson	b	γ$_t$, pcf
Beach Sand 1	6	31	418	1	1	2	1	0	2	118
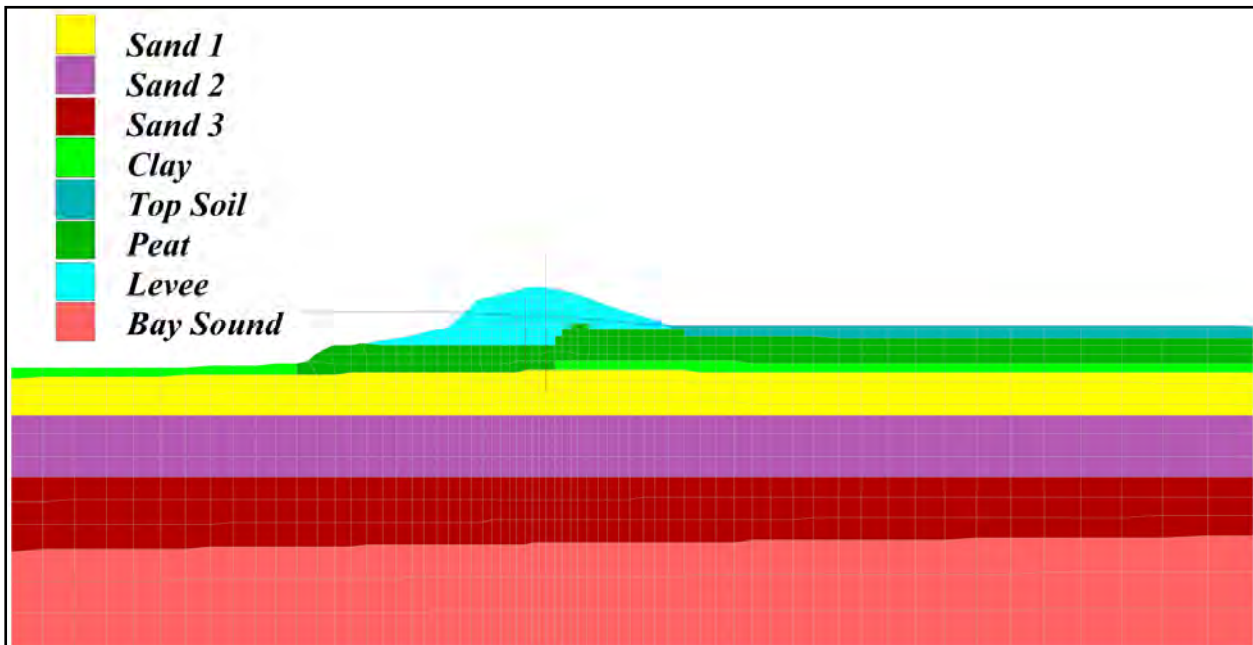
Figure 19-21. Soil zones, levee wall and sheet piles at normal pool for London north breach sta. 14+00

V-19-32

Volume V The Performance – Levees and Floodwalls – Technical Appendix
This is a preliminary report subject to revision; it does not contain final conclusions of the United States Army Corps of Engineers.
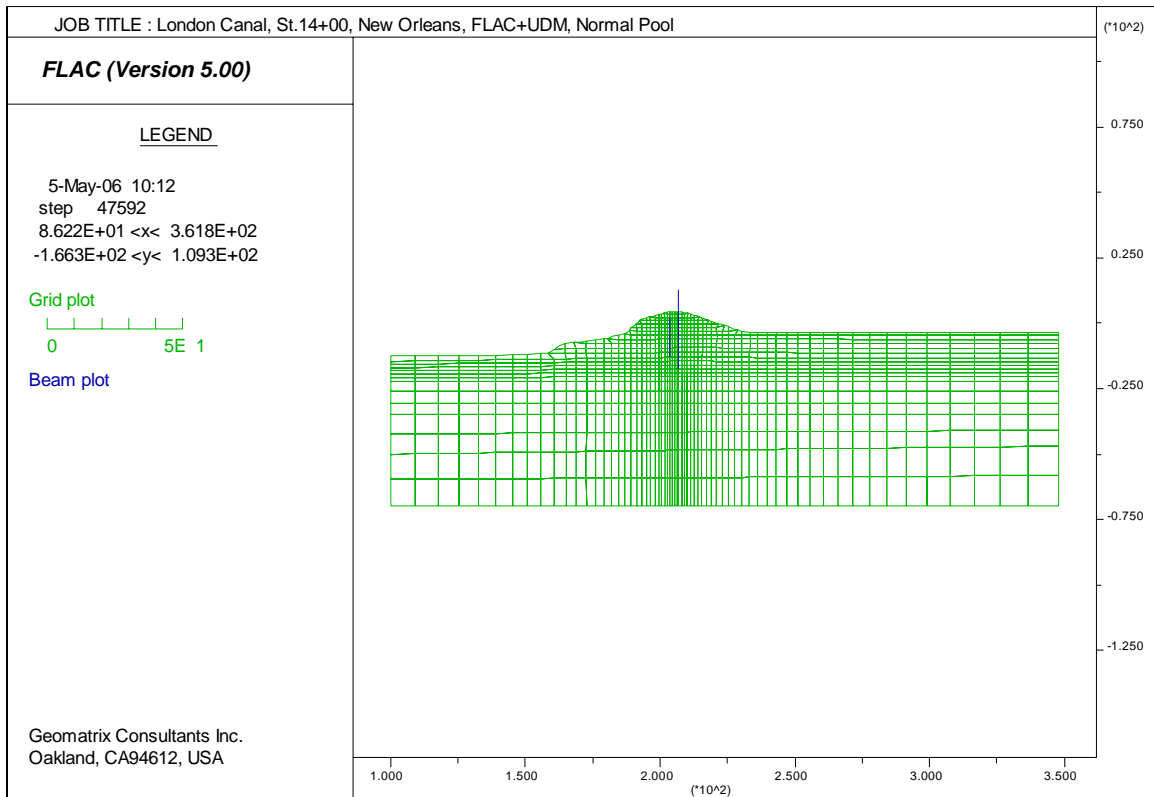
Figure 19-22. FLAC model (grid) used for analysis of London north breach sta. 14+00
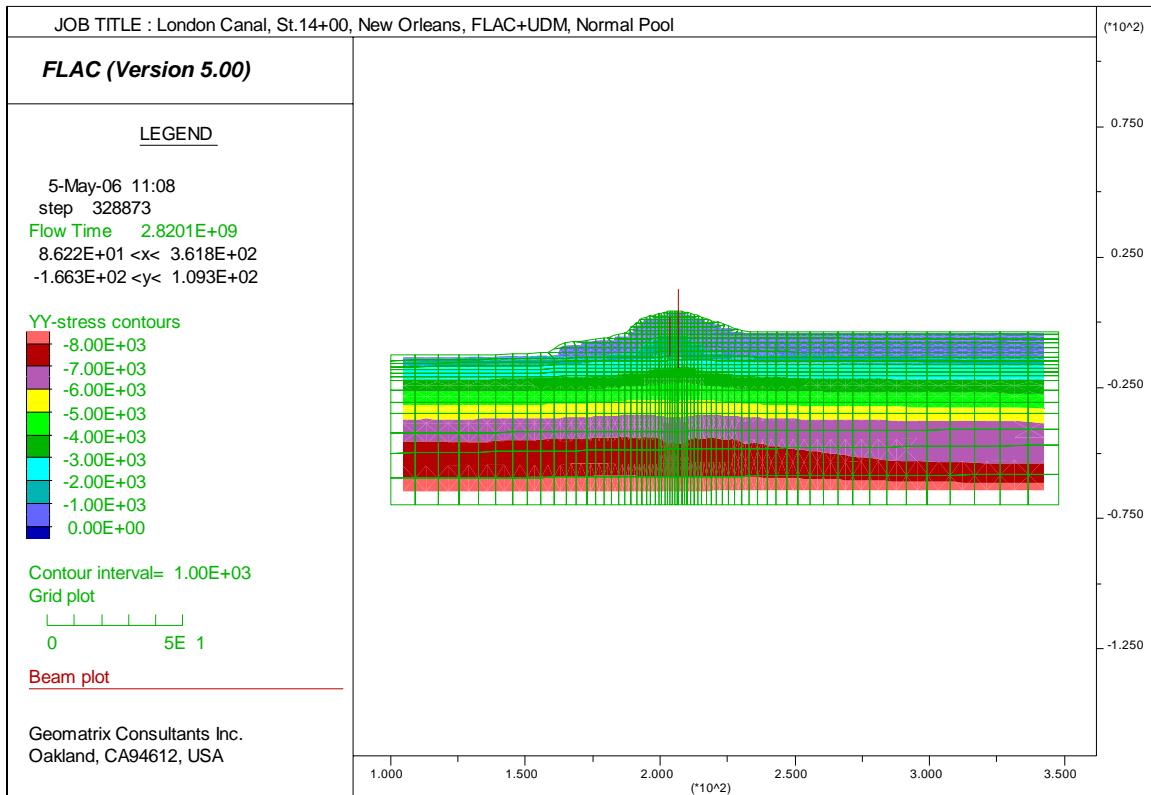
Figure 19-23. Contours of vertical total stress at normal pool water level, Elevation -0.5 feet for London north breach sta. 14+00
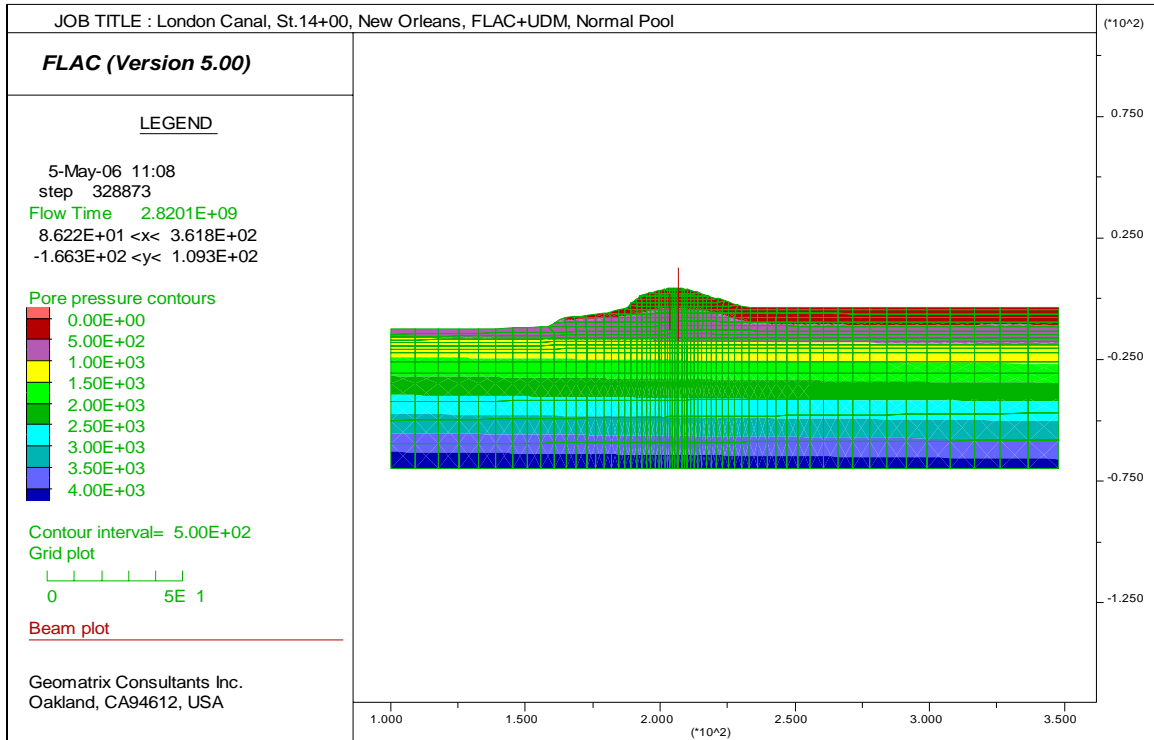
Figure 19-24. Contours of pore water pressure at normal pool water level, Elevation -0.5 feet for London north breach sta. 14+00
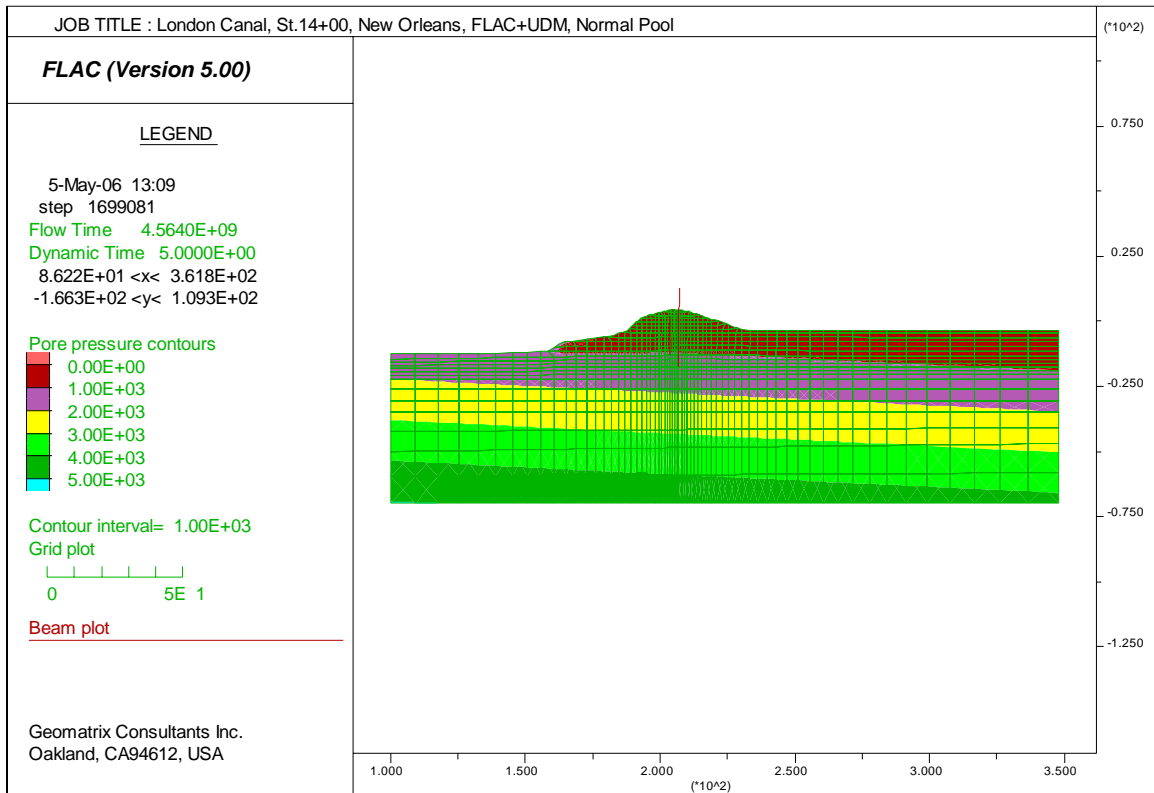
Figure 19-25. Contours of pore water pressure at Katrina Flood Water Level at Elevation 9 feet for London north breach sta. 14+00
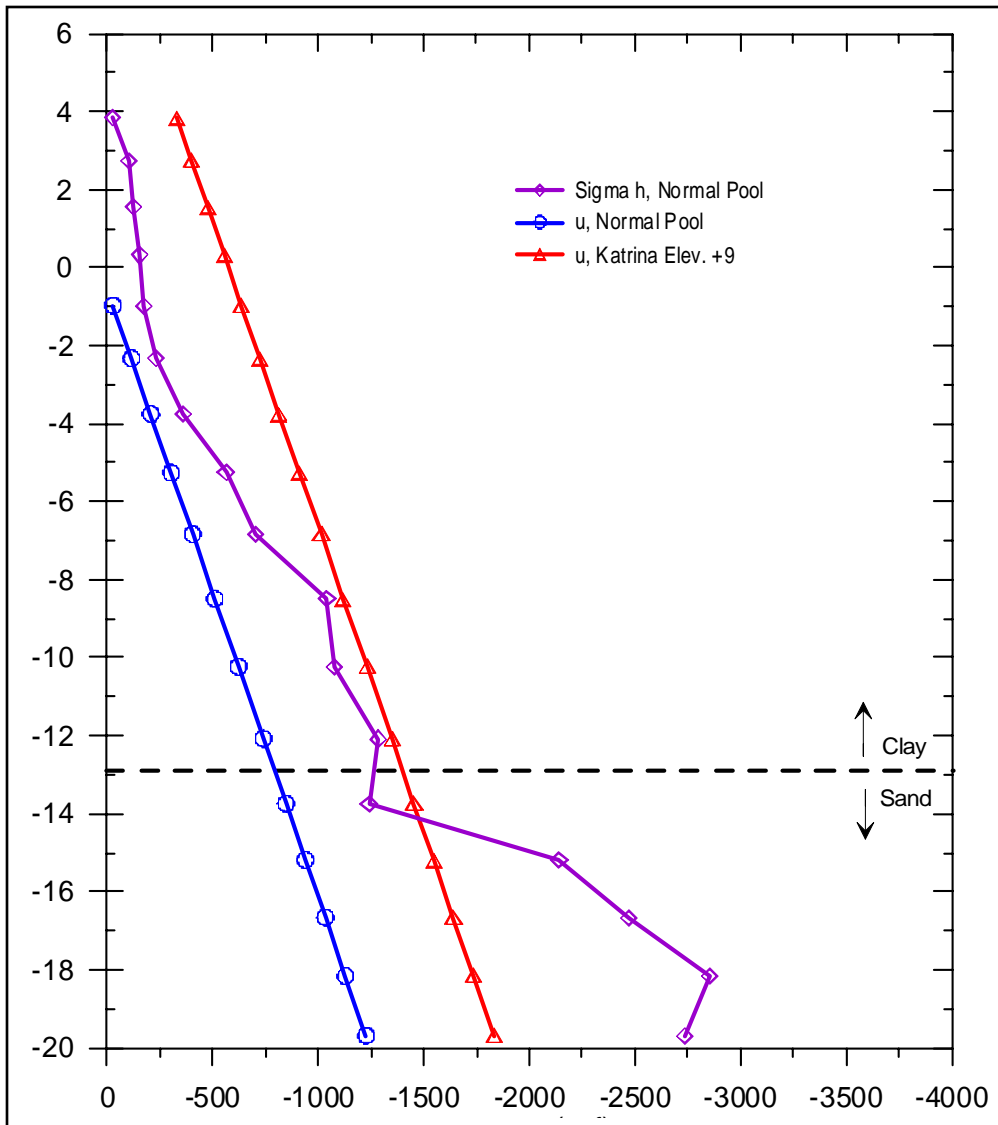
Figure 19-26. Comparison between water pressure and horizontal total stress for London north breach sta. 14+00

Volume V The Performance – Levees and Floodwalls – Technical Appendix

V-19-37

This is a preliminary report subject to revision; it does not contain final conclusions of the United States Army Corps of Engineers.
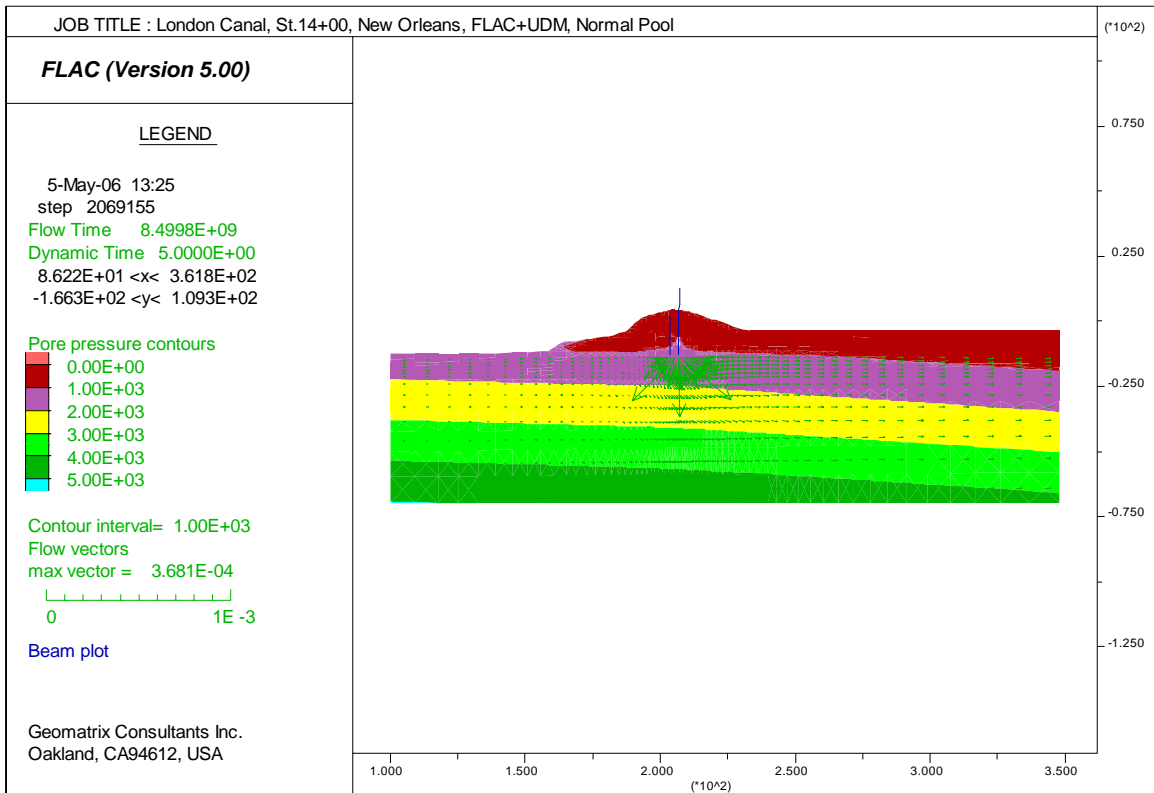
Figure 19-27. Water flow vectors through the crack (behind the wall) into sand layer for London north breach sta. 14+00
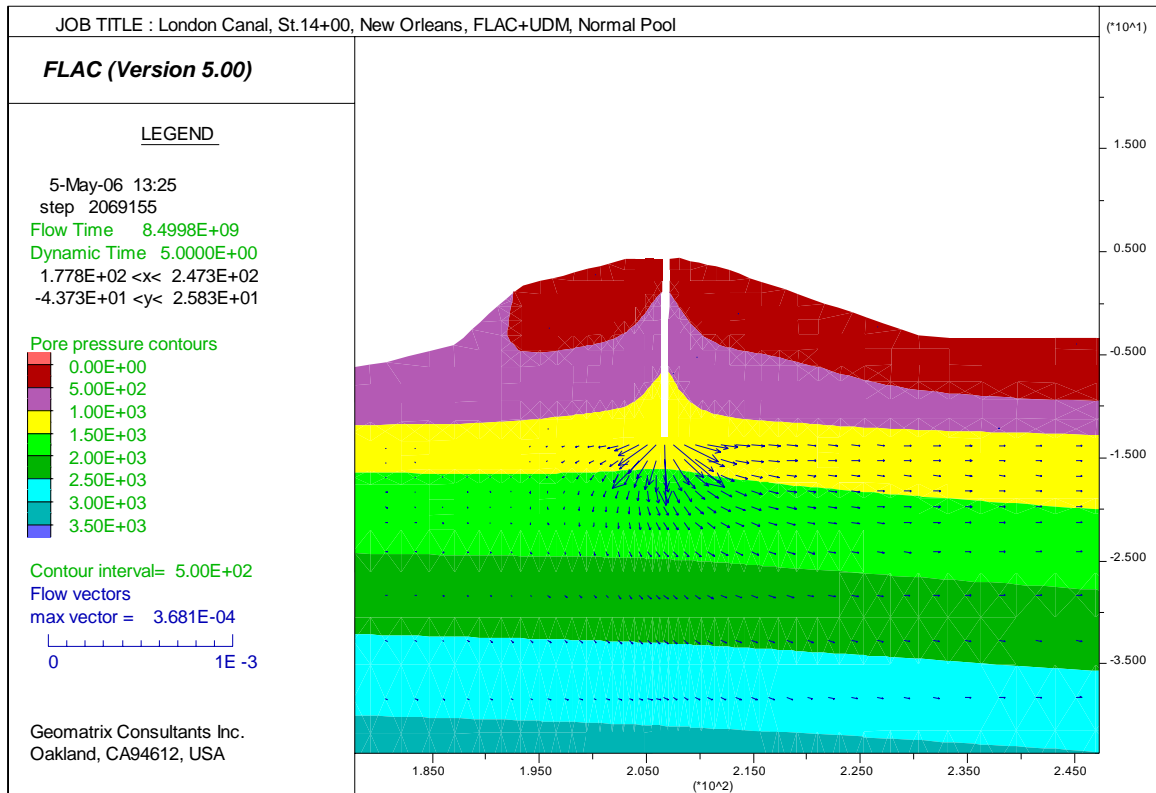
Figure 19-28. Detailed flow vectors from near tip of pile and into top sand layer for London north breach sta. 14+00

Volume V The Performance – Levees and Floodwalls – Technical Appendix

V-19-39

This is a preliminary report subject to revision; it does not contain final conclusions of the United States Army Corps of Engineers.

Figure 19-29. Wall moved two feet (computation terminated due to bad geometry at bottom of crack) for London north breach sta. 14+00
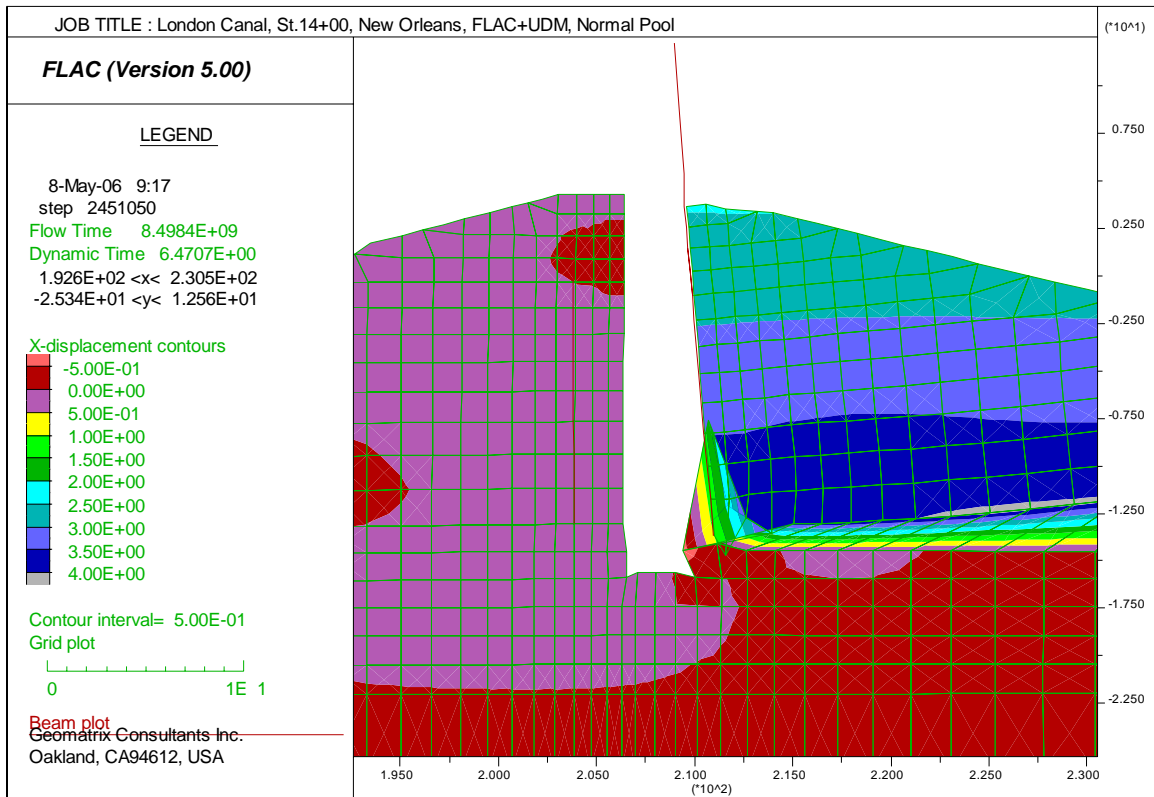
Figure 19-30. Wall moved four feet, unstable due to bad geometry at bottom of crack, (bad zones were removed to allow computation to continue) for London north breach sta. 14+00

JOB TITLE : London Canal, St.14+00, New Orleans, FLAC+UDM, Normal Pool   (*10^2)
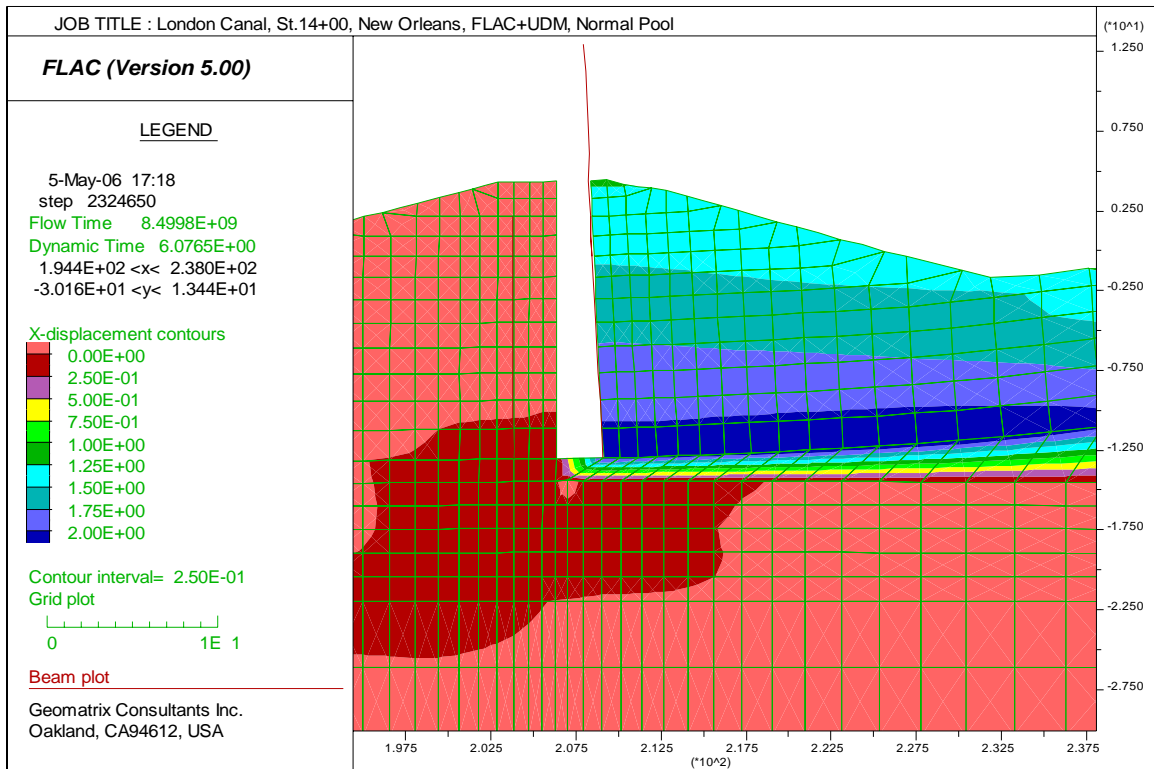
FLAC (Version 5.00)

LEGEND

8-May-06 9:17
step 2451050
Flow Time   8.4984E+09
Dynamic Time 6.4707E+00
8.622E+01 <x< 3.618E+02
-1.666E+02 <y< 1.089E+02

Grid plot

0   5E 1

Beam plot

Geomatrix Consultants Inc.
Oakland, CA94612, USA

Figure 19-31. Deformed shape at wall movement of four feet showing bulging beyond the toe (computation terminated due bad geometry) for London north breach sta. 14+00.

London South – Mirabeau Breach Analysis

Analysis Approach
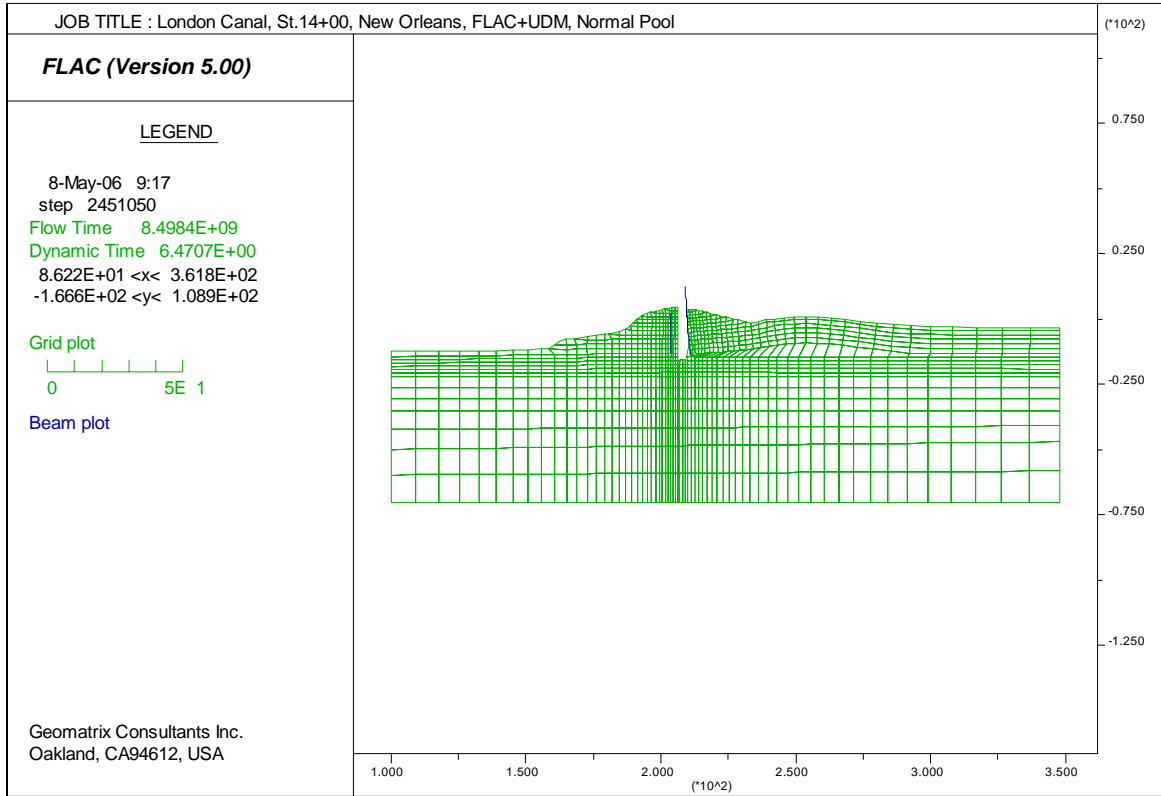
An analysis of the Mirabeau breach on the London South Canal using FLAC was performed, although the analysis had not reached a conclusion by the time of this report. The general methodology follows that described for the Mohr-Coulomb analysis performed for the 17th St. Canal breach. Geometry and material properties were provided for the analysis in an effort to maintain consistency with the Plaxis evaluation. In addition to the range of parameters supplied for the 17th St. analysis, values of hydraulic conductivity were also provided for the Mirabeau Breach section.

The simple Mohr-Coulomb model was selected because the initial analyses showed that seepage predictions and the resulting loss of effective stress in the sand were likely to be critical mechanisms. As with the 17th St. analysis, the FLAC model can be easily modified to use a nonlinear effective stress model if needed.

The FLAC model developed to analyze the Mirabeau breach is shown in Figures 19-32 and 19-33. This model includes a special wedge of material just downstream of the toe. This zone is identical to the remaining marsh-topsoil material. However, it has been isolated and connected to the remaining soil grid using interface elements. The presence of this wedge provides some additional flexibility in evaluating the effect of high pore pressures beneath the marsh deposits.

Analysis Results and Discussion

A seepage analysis using the groundwater flow capability of FLAC was performed to estimate the initial steady-state pore pressures. This analysis of steady state conditions highlighted the importance of seepage to the stability of this section of levee. The cross section provided for analysis has Beach Sand extending continuously beneath the levee section and forming the bottom of the canal. Since this layer is assigned a permeability value of 1.5×10^{-2} cm/sec, the direct connection to canal water allows for high pore pressures to be quickly transmitted beneath the levee section. The effect of this is exacerbated by the low unit weight of only 80 pcf assigned to the topsoil and marsh layer. The buoyant weight of this material is so low that it provides little effective restraining force due to dead weight on the underlying sand. Given these input parameters, the predicted pore pressures for steady state in the sand below the toe of the levee are sufficient to exceed the total overburden weight of the overlying marsh deposit.

It is likely that the steady state pore pressures were not this high in the absence of serious stability issues with this section. Assigning a vertical permeability of 10X the horizontal permeability to the sand layer was sufficient to modestly but significantly reduce the pore pressures at the toe. It may be possible that the surface of the sand exposed in the canal had become silted so that a thin layer of reduced permeability material was essentially lining the canal. A 2-ft-thick layer of material at the bottom of the canal with a permeability of 1.5×10^{-4} cm/sec was found to significantly reduce the initial pore pressures at the toe. The presence of a

silted layer would also reduce the pore pressure response during the flood loading. Unfortunately, the presence or description of this potential silted layer is not known. Although the development of such a layer appears reasonable, it may also be periodically removed by dredging. Initial pore pressures estimated using the above assumptions are shown in Figures 19-34 to 19-36.

In the analyses completed to date, instability of the section appears to begin as the pore pressures along the top of the sand exceed the buoyant weight of the overlying material. This occurrence tends to begin somewhat below the toe of the levee. Unless the seepage is restricted by a silted layer in the canal, these high pressures occur at very low flood stages. An initial deformation response due to high pore pressures is shown in Figure 19-37.

Based on the available information, the FLAC analyses clearly show that seepage is a critical issue in the behavior of this levee. These analyses have not yet identified a likely failure mechanism due to uncertainties in the actual permeability's and resulting pore pressures. A more thorough study might include an organized set of parametric studies to evaluate ranges in permeability assumptions and distributions. The likelihood of a crack between the sheet pile wall and levee fill contributing to the failure might also be evaluated as part of this study. Investigating the effect of material loss at the toe might be evaluated by systematic mining of the toe and foundation to define conditions associated with failure. The relative narrowness of the breach also suggests a potential 3D influence in the failure.
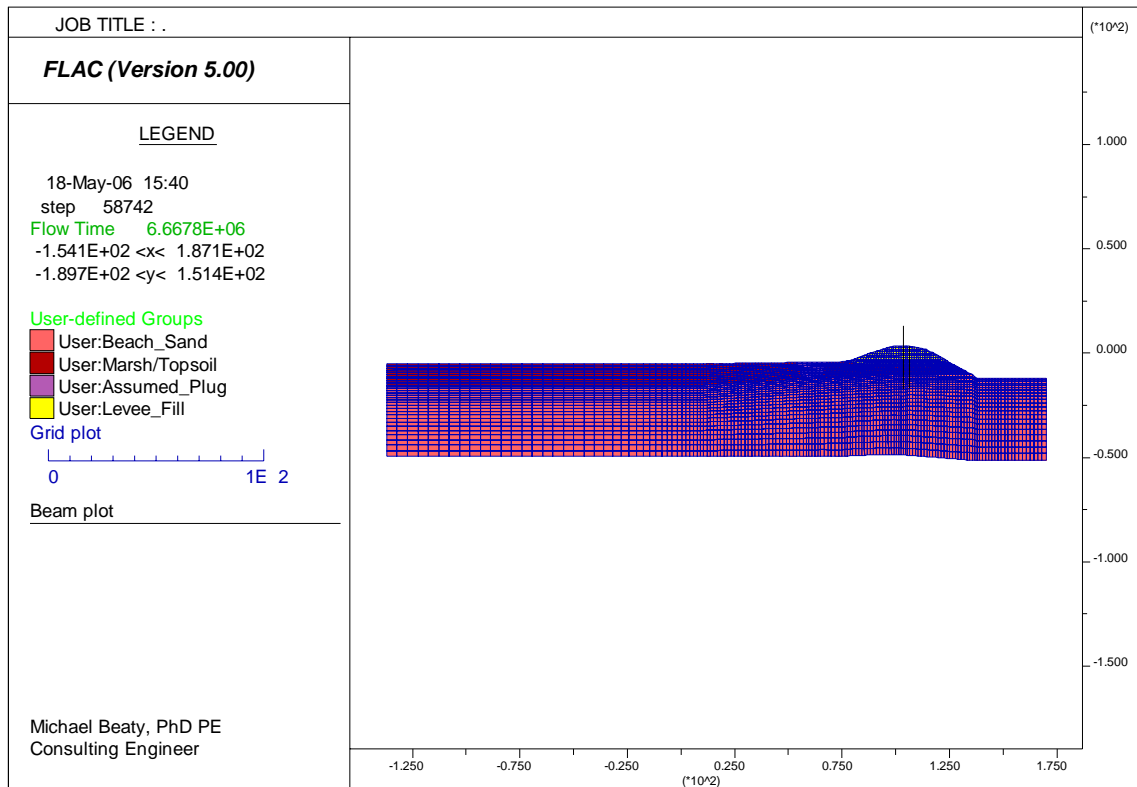
Figure 19-32. FLAC grid for London South breach sta. 53+00. (Mirabeau breach)
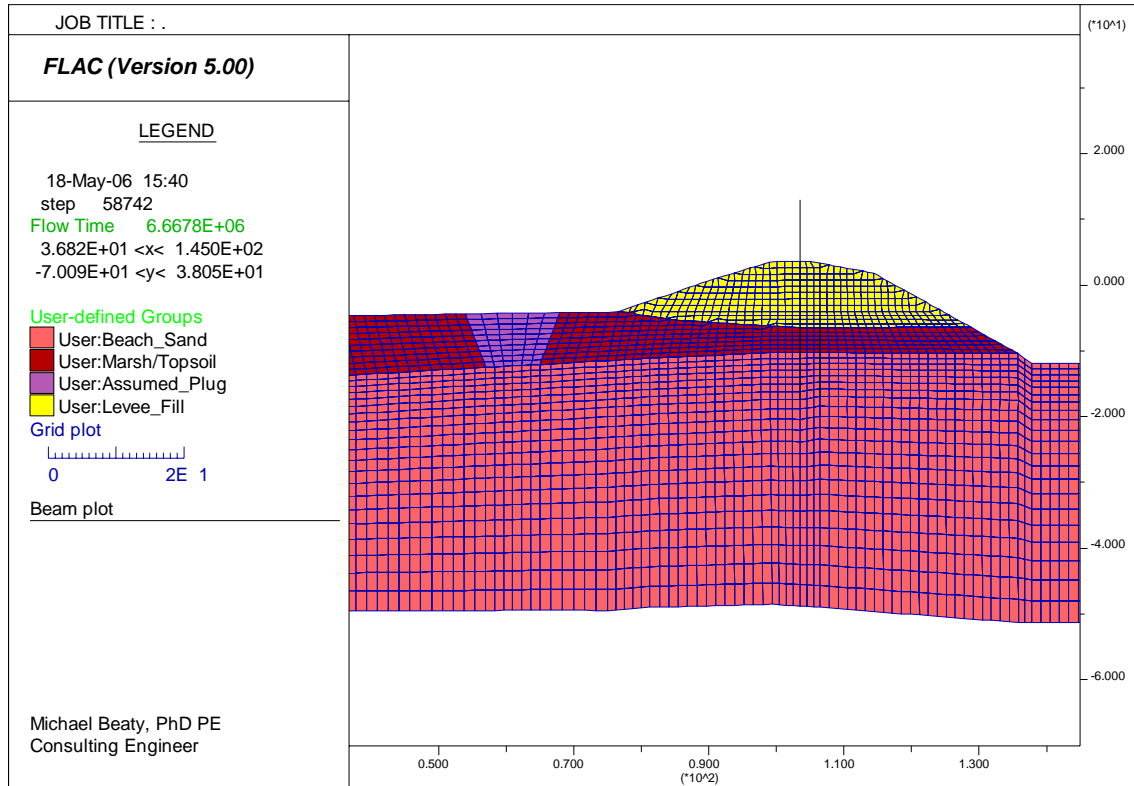
Figure 19-33. FLAC grid near levee for London South breach sta. 53+00

Volume V The Performance – Levees and Floodwalls – Technical Appendix

V-19-45

This is a preliminary report subject to revision; it does not contain final conclusions of the United States Army Corps of Engineers.
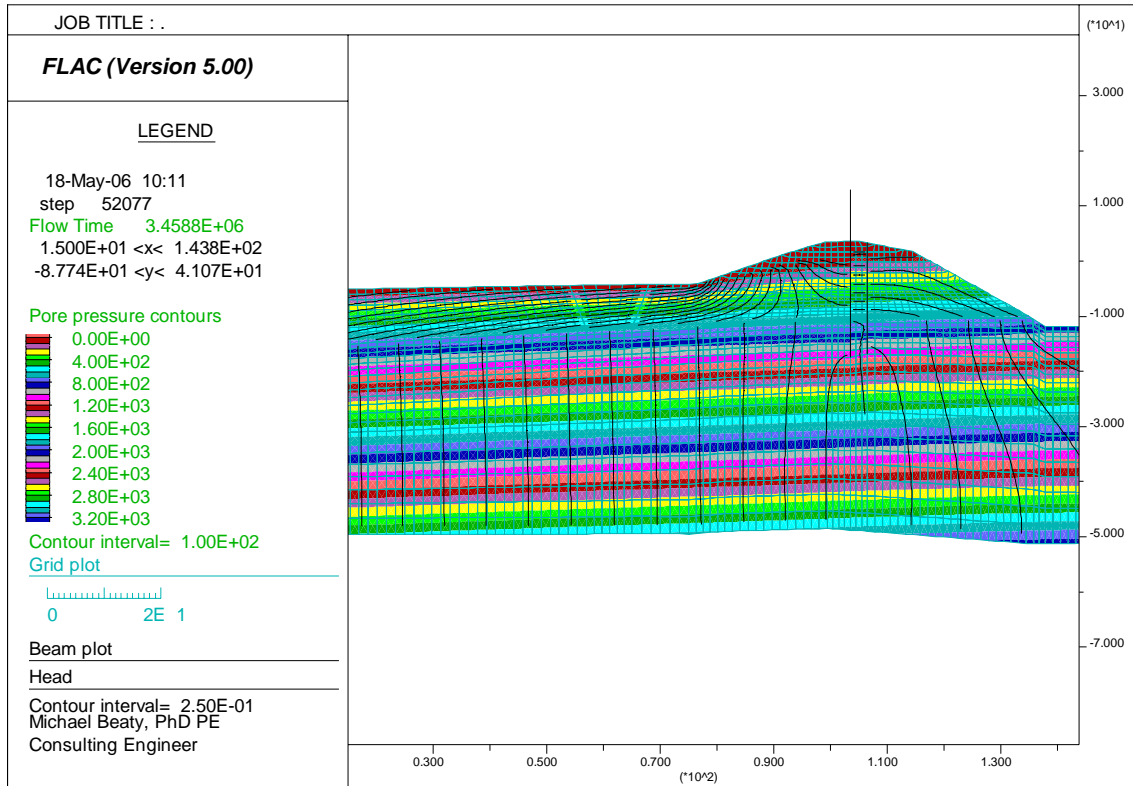
Figure 19-34. Predicted initial pore pressures for basic FLAC model for London South breach sta. 53+00

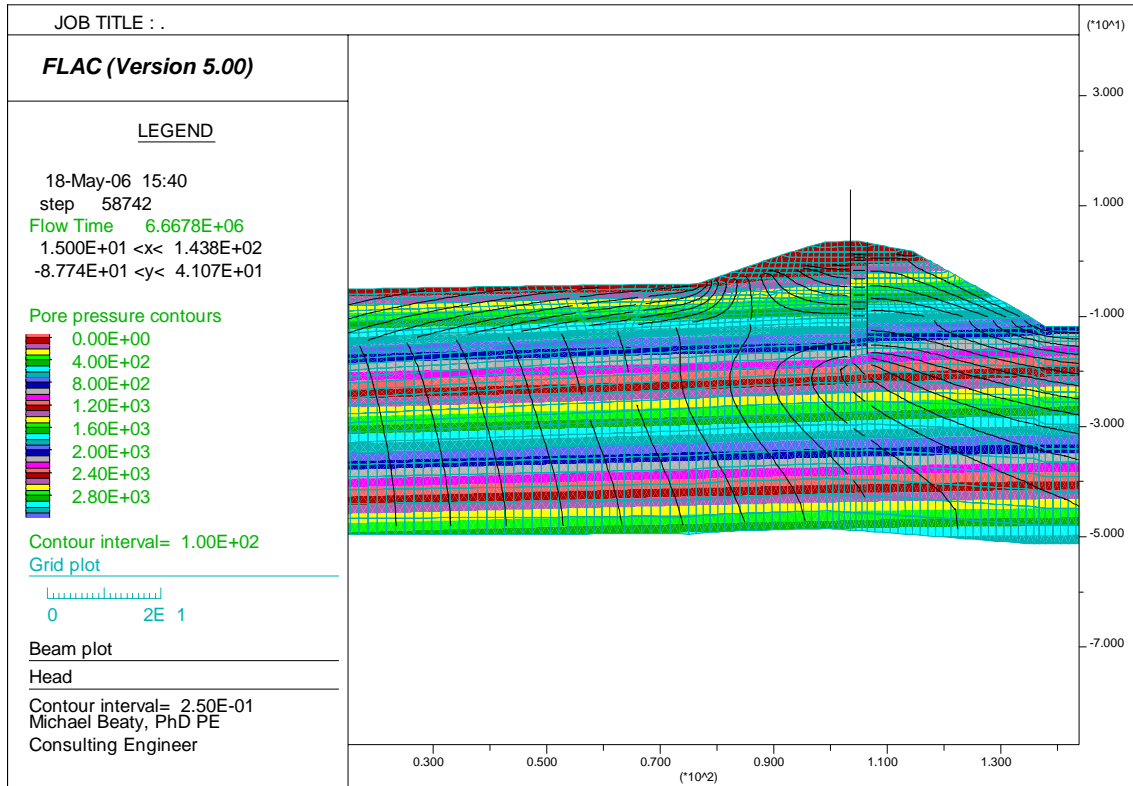Figure 19-35. Predicted initial pore pressures for Kv = 10x Kh. for London South breach sta. 53+00
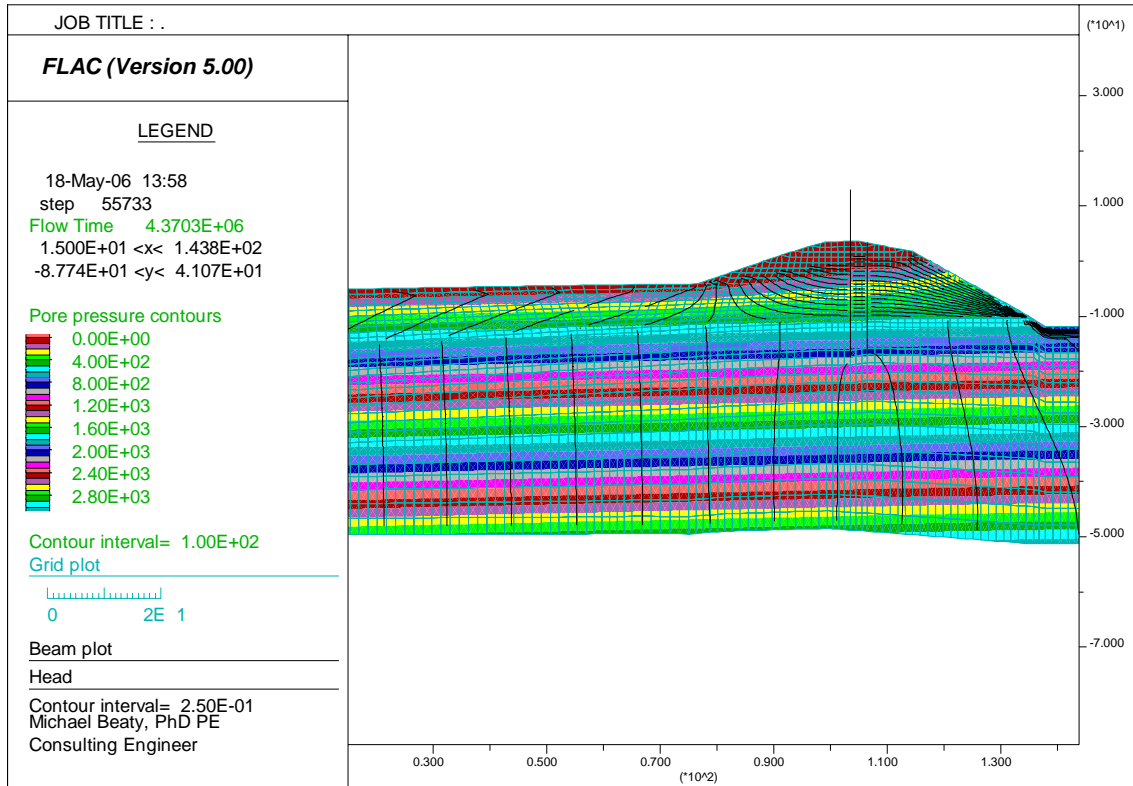
Figure 19-36. Predicted initial pore pressures for 2-foot-thick silted layer for London South breach sta. 53+00
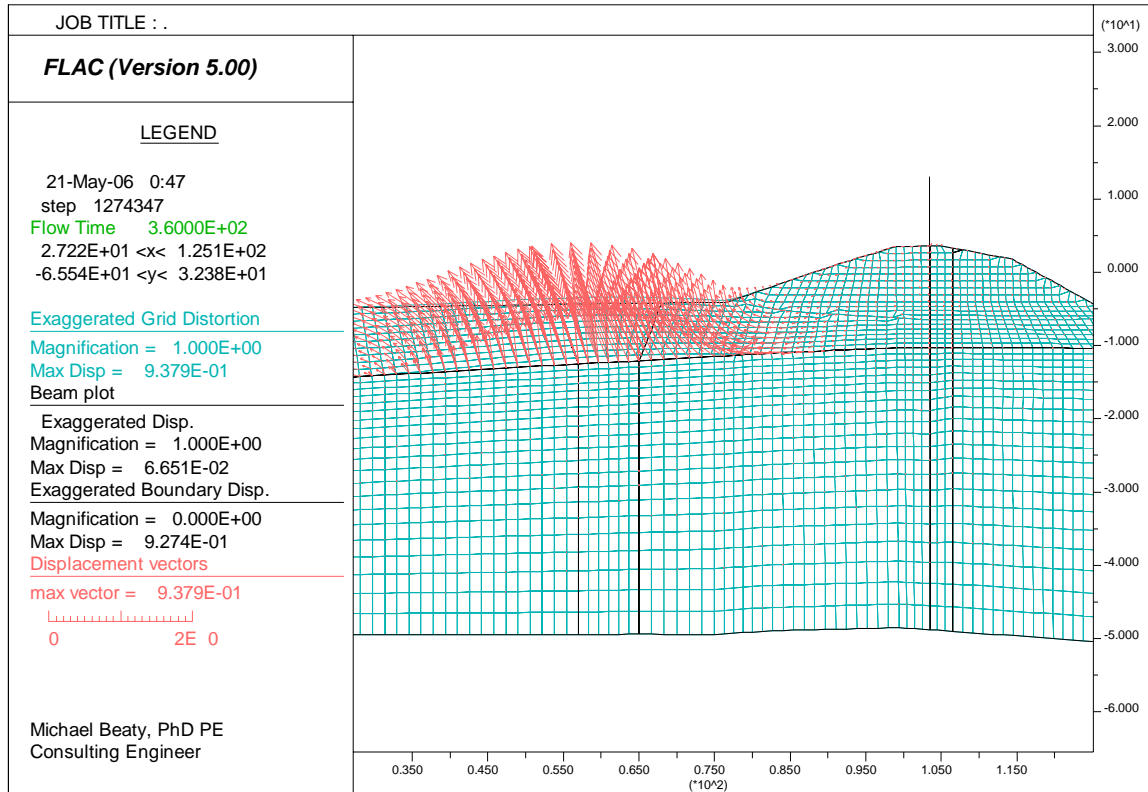
.

Figure 19-37. Estimated of initial bulge in marsh-topsoil layer due to high pore pressures in underlying sand (assumes Kv = 10x Kh in sand and WSE = 4.5 feet in canal) for London South breach sta. 53+00

.

Conclusion

Two-dimensional SSI numerical modeling analyses were conducted by IPET as part of a study undertaken to analyze the performance of levees and floodwalls used in the New Orleans flood protection system. The overall objective was to determine the most likely causes of their damage and failure from Hurricane Katrina. This report documents the findings from the analyses using the FLAC numerical geotechnical analysis program. FLAC is an explicit, finite difference program that uses a Lagrangian formulation for performing large strain analyses. This program is capable of modeling two-dimensional problems in soil-structure interaction with full coupling of the stress-strain and groundwater flow components. Available constitutive models include linear elastic to non-linear plasticity-based models. FLAC also provides the capability of inputting user-defined constitutive models or making minor modifications to built-in models.

The analysis approach considered and adopted where appropriate findings based on the field investigation and limit-equilibrium stability and seepage analyses conducted prior to these analyses. This enabled a consistent, thorough study based on site-specific field data and a progression of increasingly complex analyses, appropriately constrained by their respective assumptions and findings.

Stability analyses were conducted to investigate the following failure sections: east side 17th St. Outfall Canal breach sta. 10+00, and the two breaches on the London Outfall Canal (London North breach west side - near the Robert E. Lee Bridge Sta. 14+00 and London South breach east side - near the Mirabeau St. Bridge Sta. 53+00). Two important geologic factors that significantly contributed to the response of these floodwalls were the general near-surface geologic setting being (1) marsh-swamp deposits providing the possibility of low strength clay and peat foundation soils and the (2) shallowest sand deposit that trends through the area is very shallow at London's south and north breaches but found relatively deeper at 17th St. breach. The general foundation soils stratigraphy to an approximate depth of 80 ft was idealized and modeled by material zones: levee clay, clay top soil, peat, lacustrine clay, beach sand, bay sound clay, and finally the Pleistocene clays. The failure modes identified in these analyses involved the marsh and lacustrine clays for the 17th St. breach. For both breaches on the London canal, the shallower beach sands also played a dominant part with the overlying clays in the resulting failures.

The FLAC analyses of the 17th St. breach employing both simple to complex soil models resulted in the same general failure surface and strong dependence on formation of a gap (crack) between the floodwall sheet pile and canal side embankment to effect large wall movements and resulting failure. This gap is a triggering mechanism when coupled with the current soil model and estimated flood water level (elevation 8.5) to produce a failure that begins near the sheet pile tip near the top of the lacustrine clay layer. This analysis support the field observations, aspects of the limit equilibrium analyses, and the Plaxis SSI analyses that a predominately translation instability breached this section. The FLAC model also shows a kinematic response that approximately matches the field observed intact block displacement of protected side of levee embankment and heaving and over-thrusting of foundation soil layers beyond the levee toe. The range of computed wall deformation for the Katrina Flood water level at El. 8.5 ft was 5 to 6 feet indicating the potential for failure for the non-linear soil model and just over 2 ft for the Mohr-Coulomb model.

The FLAC analyses for the London south breach sta. 53+00 clearly show that seepage is a critical issue in the behavior of this levee. These analyses have not yet identified a likely failure mechanism due to uncertainties in the actual permeability's and resulting pore pressures. A more thorough study might include an organized set of parametric studies to evaluate ranges in permeability assumptions and distributions. In support of the Plaxis analyses the likelihood of a crack between the sheet pile wall and levee fill contributing to the failure should also be evaluated as part of further studies. Investigating the effect of material loss at the toe might be evaluated by systematic mining of the toe and foundation to define conditions associated with failure. The relative narrowness of the breach also suggests a potential 3D influence in the failure.

The FLAC analysis of the London north breach sta. 14+00 supports field evidence and slope stability analyses that concluded the most likely mode of failure is sliding instability. However, seepage studies also show that erosion and piping was another possible mode of failure or strongly coupling factor. It is interesting that this breach displays a combination of failure modes from both 17th St. and London South. The high water pressures in the sands and the movement of the wall toward the protected side forming a gap or crack on canal side between the wall and earth embankment allowed high water pressures to act directly on wall and high uplift pressures on marsh and clay deposits overlying the sands. Field evidence showed intact crest sliding and heaving at the toe which is also supported by the model response. The possible crack formation was simulated in the analysis, and water flow into the underlying sand layer indicated significant increases in the pore pressures, and a corresponding reduction in effective stresses and shear strength. The computed deformations of the pile wall and the levee slopes resulted in horizontal deformations exceeding four feet. The deformed shape of levee profile indicates that there was about 4 feet of up-wards movement (bulging) in the top soil at the protected site, beyond the toe of the levee. This is may have been induced by the pore water pressure due to water flow into the top sand layer through the gap behind the wall. This bulging could indicate rupture of the overlying clay layer that would result in piping and possible failure.

The introduction of a "crack" or gap between the canal side sheet pile wall and levee soil embankment was a dominant factor in inducing failure modes at 17th St and London North. Continuing analyses involving alternative criteria to support gap initiation and evolution that results in failure should be undertaken. Use of non-linear soil models may be important in obtaining a better estimate of initial stresses effecting the formation of the crack or gap needed to trigger this failure mode.

In summary, the FLAC analyses results were generally consistent with Plaxis results showing the same dominant failure modes for the same approximate canal water levels. This is also in agreement with the limit equilibrium stability analyses. However, these SSI analyses did not consider 3-D effects and given the relatively narrow breach zones it is possible these 2-D idealizations could over-predict the effect of lower water levels in triggering failure of the floodwall sections. Therefore the findings of these analyses may be conservative in this sense but provide important insight into the performance of the analyzed I-wall floodwalls which will be useful for improving future designs and assessments.

References

Beaty, M. H., and Byrne, P. M. (2001). "Observations on the San Fernando dams." Proc., *4th Int. Conf. on Recent Adv. in Geot. Earthquake Engrg. and Soil Dyn (CD-Rom).*, Univ. of Missouri-Rolla.

Beaty, M., and Byrne, P.M. (1998). "An Effective Stress Model for Predicting Liquefaction Behavior of Sand. In P. Dakoulas, M.Yegian, and R.D. Holts (Eds.), Geotechnical Earthquake Engineering and Soil Dynamics III, ASCE Geotechnical Special Publication No. 75 Vol.1, Proceedings of a Specialty Conference (pp 766-777). Seattle; ASCE.

Brinkgreve, R. B. J., Broere, W., and Waterman, D., ed. (2004). *Plaxis 2D – Version 8.* Plaxis B.V. The Netherlands: Delft University of Technology.

Byrne, P. M., Park, S. S., Beaty, M., Sharp, M., Gonzalez, L., and Abdoun, T. (2004). "Numerical Modeling of Liquefaction and Comparison with Centrifuge Tests," *Canadian Geotechnical Journal*, 41, 193-211.

Interagency Performance Evaluation Task Force (IPET), 2006. Interim Report on Performance of 17th St. Outfall Canal, New Orleans."

Interagency Performance Evaluation Task Force (IPET), 2006. Interim Report on Performance of London Outfall Canal, New Orleans."

Itasca Consulting Group, Inc., 2005. "FLAC – Fast Lagrangian Analysis of Continua, Version 5.0 User's Manual," Minneapolis, Minnesota: Itasca.

Seed, R. B., Abdelmalak, R. I., Athanasopoulos, A. G., Bea, R. G., Boutwell, G. P., Bray, J. D., Briaud, J.-L., Cheung, C., Collins, B. D., Cobos-Roa, D., Cohen-Waeber, J., Ehrensing, L., Farber, D., Hanenmann, M., Harder, L.F., Inamine, M. S., Inkabi, K. S., Kammerer, A. M., Karadeniz, D., Kayen, R.E., Moss, R. E. S., Nicks, J., Nimala, S., Pestana, J. M., Porter, J., Rhee, K., Riemer, M. F., Roberts, K., Rogers, J. D., Storesund, R., Thompson, A., Govindasamy, A. V., Vera-Grunauer, X., Wartman, J., Watkins, C. M., Wenk, E., and Yim, S. (2006). "Investigation of the Performance of the New Orleans Flood Protection Systems in Hurricane Katrina on August 29, 2005." Report No. UCB/CCRM – 06/01, Draft Final Report, May 22, 2006.

Wang, Z.L., 1990, "Bounding Surface Hypoplasticity Model for Granular Soils and its Applications," Ph.D. Dissertation, University of California Davis, U.M.I., Dissertation Information Service, Order No. 9110679, Ann Arbor, MI 48106.

Wang, Z.L., and Makdisi, F.I. 1999. "Implementing a Bounding Surface Hypoplasticity Model for Sand into FLAC Program," Proceedings of the FLAC Symposium on Numerical Modeling in Geomechanics, Minneapolis, Minnesota, September 1-3.

Appendix 20
Glossary for Performance of Levees and Floodwalls

Breach – The loss of the crest of a levee and/or the loss of a floodwall leading to an opening or a rupture that allows water to flow into a protected area.

Centrifuge model tests – Scale model tests conducted using a centrifuge to apply acceleration larger than the acceleration of gravity so that the stresses within the model are the same as the stresses in the full-scale prototype, resulting in behavior that closely simulates full-scale field behavior.

Clay – An aggregate of microscopic and submicroscopic particles derived from the chemical decomposition of rock constituents. Clay is cohesive and sticky over a wide range of water contents. For classification purposes, soil particles smaller than 0.002 mm.

Coefficient of variation – A measure of the dispersion of a probability distribution. It is calculated by dividing the standard deviation of a distribution by its mean value.

Cohesion – Attraction between very fine soil particles caused by intermolecular forces. Also, shear strength of soil at zero normal stress.

Cohesionless – Describes a soil with no cohesion, and no tendency for particles to stick together.

Cone Penetration Test (CPT) – An in-situ test in which an instrumented cone-tipped rod is pushed into the ground at a constant rate, while measuring tip resistance, side friction, and in some cases pore pressure.

COV – Coefficient Of Variation.

CPT – Cone Penetration Test.

CPTU – A cone penetration test in which pore pressures are measured during penetration.

Crest – The top of the levee.

Critical slip surface – The potential slip surface with the lowest factor of safety.

Cross-section – A view as seen in a plane cutting through a structure. The levee cross sections used in the analyses described here are vertical, at right angles to the levee axes.

Crown – The top of a levee.

Elevation – The height of a point above a known reference level or datum.

Erosion – Dislodgement and transportation of soil by flowing water.

Factor of safety – A measure of the stability of a slope – the shear strength of the soil divided by the shear stress required for equilibrium.

Finite element analysis – A method for numerical analysis of stresses and deformations.

Friction angle (ϕ) – A parameter used to characterize the shear strengths of soils.

Harr's Method – A method for analyzing groundwater flow.

Head – See hydraulic head.

Hydraulic gradient – Change in hydraulic head divided by the distance over which the change occurs.

Hydraulic head – A measure of the amount of energy in groundwater, often expressed in ft = ft-lb/lb.

Hydrostatic water pressure – The pressure exerted by water that is not moving.

IPET – Interagency Performance Evaluation Task Force.

I-wall – A type of flood wall consisting of sheetpiles embedded within a levee, and projecting above the levee crest. In cross section view, the wall is "I" shaped.

Lacustrine clay – Clay formed by deposition of soil particles in a lake.

Lane's Weighted Creep Ratio – The ratio of the length of flow, measured along the base of a hydraulic structure, divided by the net hydraulic head across the structure. The length of flow is weighted by dividing horizontal flow distances by 3.0.

Lognormal distribution – In probability and statistics, the probability distribution of a random variable whose logarithm is normally distributed.

Marsh – An organic soil formed in marshy areas – contains mineral as well as organic matter.

Method of Planes – A method of slope stability analysis used by the New Orleans District of the Corps of Engineers. It involves calculation of factors of safety based on a wedge mechanism consisting of three planes.

Overburden pressure – The vertical stress on the ground resulting from the weight of overlying soil.

Passive resistance – Resistance of the ground to horizontal or sub-horizontal forces.

Peat – A fibrous or amorphous aggregate of macroscopic and microscopic fragments of partially decayed vegetable matter.

Permeability – A measure of the ease with which water flows through soil.

Piezometer – An instrument for measuring hydraulic head and water pressure.

Piping – A phenomenon involving erosion due to groundwater flow, resulting in formation of an eroded pipe-like feature in the ground.

Pore pressure – The pressure in water in the voids of a soil.

Pressure – Force divided by the area over which it acts.

Probability of failure – A number that indicates the likelihood of failure.

Progressive failure – A type of failure involving a sequence of events; a progressively worsening condition leading eventually to failure.

Sand – A cohesionless soil, consisting predominantly of soil particles ranging in size from 0.074 mm to 4.76 mm.

Sand boil – A feature resulting from upward flow of groundwater, transporting sand to the ground surface.

Scour – Erosion of soil particles by flowing water.

Seepage – Flow of water through the ground.

Shear strength – The maximum shear stress that a soil can sustain.

Sheetpile – One of a series of interlocking thin steel members – sheetpiles are driven into the ground to form a wall for retaining soil or for reducing the flow of water through the ground.

Silt – A fine-grained soil consisting predominantly of particles ranging in diameter from 0.002 mm to 0.074 mm.

Sinkhole - A depression in the ground surface caused by collapse of the roof of an underground hole, often associated with underground erosion and piping.

Slope stability analysis – An analysis performed to determine the degree of stability of a slope.

Spencer's Method – An accurate numerical method of slope stability analysis.

SPT – Standard Penetration Test.

Standard deviation – A measure of statistical dispersion of values of a variable.

Standard Penetration Test (SPT) – An in-situ dynamic penetration test designed to provide information on the geotechnical properties of soils. In this test, a thick-walled soil sampler is driven 18 inches into the ground by consecutive blows from a 140 lb. hammer dropped from a height of 30 inches. The number of blows required to advance the sampler 12 inches (after it has already been advanced 6 inches) is the blow count N. The value of N provides information about the density and strength of the soil, and is used in many empirical geotechnical engineering correlations.

Station – A location along a line, frequently expressed in terms of hundreds of feet plus feet. For example, Station 8+30 indicates a point 830 ft from the reference point.

Taylor Series – A mathematical relationship that can be used to represent a wide range of mathematical functions by a power series.

Toe – The lowest part of an embankment, levee, or dam, where the slope merges with the adjacent ground surface.

T-wall – A type of flood wall that looks like an inverted "T" in cross section, usually supported on deeply penetrated bearing piles, and usually with a sheet pile wall beneath it to cut off seepage.

Underseepage – Flow of water beneath a structure, through the ground.

Undrained conditions – The condition under which there is no flow of water into or out of a mass of soil in the length of time that the soil is subjected to a change in load.

Unit weight – The weight of soil per unit volume, often expressed in pounds per cubic foot.

Uplift pressure – Upward water pressure exerted on a structure or lower permeability soil layer by water pressure in the ground beneath.

Vane shear test – An in-situ shear test involving rotation around a vertical axis of an x-shaped device to measure the shear strength of soil.

Wave effect – An increase in pressure, above hydrostatic pressure, caused by waves.